THE UNIVERSITY
of ADELAIDE

TECTONIC EVOLUTION AND PALAEOGEOGRAPHY OF THAILAND

ROMANA E.C. DEW

Earth Sciences
School of Physical Sciences
University of Adelaide

This thesis is submitted in fulfilment of the requirements for the degree of Doctor of Philosophy

June 2019

TABLE OF CONTENTS

Thesis abstract v
Thesis declaration vi
Acknowledgements vii
Publications during the course of this thesis viii

Chapter 1: Introduction and Thesis Outline 1
Introduction to the tectonic evolution and palaeogeography of Thailand 2
Thesis outline 4
References 6

Chapter 2: 11
A: Probing into Thailand's basement: New insights from U–Pb geochronology, Sr, Sm–Nd, Pb and Lu–Hf isotopic systems from granitoids 18
Abstract 18
1. Introduction 18
2. Methodology 23
3. Results 27
4. Timing of magmatism for Thailand's granitoids 40
5. Isotopic characteristics of Thailand 41
6. Implications for terrane evolution 46
7. Conclusion 49
Acknowledgements 49
References 50
B: Data analysis of the isotopic systems for the granitoids of Thailand 56
Abstract 56
Value of the data 56
1. Data 56
2. Experimental design, materials and methods 56
Specifications Table 57
Acknowledgements 70
References 71

Chapter 3: A detrital provenance story from Gondwana to northwest Thailand 77
Abstract 80
1. Introduction 80
2. Geology of the Sibumasu Terrane 81
3. Methodology 86
4. Results 89
5. Discussion 94
6. Conclusion 101
Acknowledgements 101
References 102

Chapter 4: The Permo-Triassic tectonic geography of Thailand deduced from terrane-based sediment provenance **113**
Abstract 116
1. Introduction 116
2. Geology of Permo-Triassic Thailand 117
3. Methodology 125
4. Results 127
5. Discussion 134
6. Conclusion 140
Acknowledgements 140
References 141

Chapter 5: Age and provenance of the Chaung Magyi Group, Yeywa Dome, Myanmar, based on U–Pb dating of detrital zircons **151**
Abstract 154
1. Introduction 154
2. Geological background 156
3. Methodology 159
4. Results 162
5. Discussion 163
6. Conclusion 164
References 165

Chapter 6: Stratigraphy of deformed Permian carbonate reefs in Saraburi Province, Thailand **167**
Abstract 170
1. Introduction 170
2. Geological setting of the Saraburi region of Thailand 173
3. The Saraburi locality and methodology 178
4. Fauna of the Khao Khwang carbonate platform 178
5. Facies of the Permian Saraburi carbonate sequence 181
6. Correlation of the stratigraphic sections from the Khao Khwang Platform 182
7. Tectonic juxtaposition of facies 183
8. Palaeogeography 185
9. Conclusion 187
Acknowledgements 187
References 187

Chapter 7: Discussion and Conclusion - Updated tectonic evolution and palaeogeography of Thailand **191**
Thesis summary 192
Tectonic and palaeogeographic evolution of Thailand 194
References 203

TABLE OF CONTENTS

Appendix I: Other publications during the course of this thesis **211**
Harvey *et al.* (2017) – Land Use Policy 212
Harvey and Dew (2016) – Journal of Coastal Research 223
Collins and Dew (2018) – The Conversation 228
Dew *et al.* (2018) – International Sedimentological Congress 2018 231
Dew *et al.* (2017) – Puzzling Out Gondwana 2017 232
Dew *et al.* (2015) – The 4th IGCP 589 Symposium 234
Dew (2016) – The 4th IGCP 589 Symposium for TAG Magazine 237
Dew (2016) – Memoir of Endeavour Australia Fellowship 238

Appendix II: Supplementary material for Chapter 2 **239**
Tables 240

Appendix III: Supplementary material for Chapter 3 **273**
Figures 274
Data references 276
Tables 277

Appendix IV: Supplementary material for Chapter 4 **313**
Figures 312
Tables 315

Appendix V: Supplementary material for Chapter 5 **351**
Tables 352

Appendix VI: Supplementary material for Chapter 6 **359**
Figures 360
Table 369
Dew (2014) – Honours thesis 372

THESIS ABSTRACT

The tectonic evolution and palaeogeography of Thailand requires refinement, especially the origin and nature of the basement, the relative position of the three main Thai terranes from their genesis to their amalgamation, the location of the terrane boundaries and the exact timing of the amalgamation of Thailand. This thesis endeavours to better unravel the tectonic evolution and palaeogeography of the three major Thai terranes: Indochina, Sukhothai and Sibumasu. But, it aims to do this by coupling disparate geological disciplines from palaeontology and sedimentology of the SW margin of Indochina to igneous geochemistry and detrital geochronology; Thailand-wide. Magmatic zircon Lu–Hf and whole-rock Sm–Nd data and model ages illustrate that the Indochina Terrane is relatively juvenile and distinct from the Sibumasu Terrane. The latter is composed of considerable Archean–Paleoproterozoic material. The granitoids of the Sukhothai Terrane are syn-collisional and are isotopically intermediate between Indochina and Sibumasu. I interpret this to reflect juvenile magmatism that is contaminated by evolved crustal material, which is likely to be from the leading edge of the Sibumasu Terrane as it enters the subduction zone during the closure of the Palaeo-Tethys Ocean.

Detrital zircon analysis from Neoproterozoic–Triassic sequences from the Sibumasu Terrane track the terrane's evolution from the Australian margin of Gondwana to its collision with the terranes of present-day Asia. The detrital record in conjunction with other palaeontological and stratigraphic evidence, indicates that during the early Permian, Sibumasu was still connected with Australia. In contrast, analysis of the biostratigraphy of the Khao Khwang Platform demonstrates this region of the Indochina Terrane was part of a tropical shallow marine environment from the Yakhtashian–Midian (Tethyan equivalents to middle Cisuralian to late Guadalupian). This biostratigraphic analysis revealed the presence of several separate carbonate platforms dominated by four major middle Permian facies: peritidal, platform interior, algal reef and basin slope, which are dated using foraminifera and algae.

The comparison of the detrital zircon population spectra from Permo-Triassic sandstones across Thailand provides further evidence for the shared and separate parts of their tectonic histories. Primarily, the ages found in the Sibumasu Terrane are typical of provenance within Gondwana and contain both juvenile and evolved Hf signatures. In contrast, in the Sukhothai Terrane, the predominant age peak is 296–207 Ma and contains $\varepsilon Hf_{(t)}$ values that correspond to the isotopic signatures of the synchronous Sukhothai granitoids. Detrital data from the Triassic Huai Hin Lat Formation of the Indochina Terrane contain zircon age populations and characteristics similar to those of the South China Terrane.

These results have implications for research on the Tethys Oceans, not only within Thailand but also for research conducted on greater Southeast Asian tectonics. Additionally, this study unearths information on the origin of the Thai terranes and their potential positions within Gondwana during the Neoproterozoic to early Paleozoic.

THESIS DECLARATION

I, Romana Elysium Carthew Dew, certify that this work contains no material, which has been accepted for the award of any other degree or diploma in my name in any university or other tertiary institution and, to the best of my knowledge and belief, contains no material previously published or written by another person, except where due reference has been made in the text. In addition, I certify that no part of this work will, in the future, be used in a submission in my name for any other degree or diploma in any university or other tertiary institution without the prior approval of the University of Adelaide and where applicable, any partner institution responsible for the joint award of this degree.

The author acknowledges that copyright of published works contained within this thesis resides with the copyright holder(s) of those works.

I give permission for the digital version of my thesis to be made available on the web, via the University's digital research repository, the Library Search and also through web search engines, unless permission has been granted by the University to restrict access for a period of time.

I acknowledge the support I have received for my research through the provision of an Australian Government Research Training Program Scholarship.

Romana Elysium Carthew Dew

ACKNOWLEDGEMENTS

Alan. Thank you for being a helpful and supportive primary supervisor. The Haighs, the GnTs, the fairy bread too on top of the geology.

Ros, our scheduled fortnightly meeting were so helpful to keep my routine and momentum going. Even when the half hour was a discussion about life goals, lifestyle balancing and doggos rather than specific research questions — it all helped!

Stijn, thanks for your persistence, drive and granitoid samples, my research has greatly benefitted from all three!

Thanks to Chris Morley not only for his valuable geological and monetary contributions but also for his restaurant and music advice, my stomach and ears are forever grateful.

To Diew, Pîi Man, Kan and Niti for breaking up the long car rides with colourful non-geological discussions about the Thai language, politics, netball, weddings and family. Also thanks to Pîi Man for the countless motorcycle lifts to and from *Mɔɔ Chɔɔ* and ensuring I did not have dengue fever. Additionally, to the Viriyasuksing extended family for the banana whiskey and Absolut vodka post-field experience of Chiang Rai hospitality.

Pîi Roj from Chiang Mai University Lapidary for conceding to let a *farang* girl use the rock saw and finally after a month of a practice reaching the dexterity of a *sŭai* thin section.

Morgan, thanks for braving the multiple yoga trials, medical emergencies and daily breakdowns, you are the best friendship partner and PT motivational speaker a gal could ask for. And to the PhD cohort who often would help me escape the hallowed gloomy Mawson halls, including Rachel, Briony, Bo and B. Big collective thank you to the members of the Gondwana/Tectonics & Earth Systems Research Group also.

To Xiaofang He for insightful discussions about U–Pb geochronology and whole-rock geochemistry techniques and assistance in the interpretation of Mandarin publications.

To my parents and extended family, I have been forever certain of your love and support no matter the distance, even when we were all unsure of what my research was about! Especially the young members of the family, Abbi Paige and Billy Con who are always curious about Nahna's life, rocks and map making.

To my dear Maddie, Rosie, Drakes and Stephie, thank you for being there for me in your own special ways no matter which town or hemisphere you were in.

To my various housemates during this time, Charlie, Luke, Kris, Dan, Mark, Erin, Martin, Shannon, Xiaofang, Hannah and Sam, listed chronologically not order of helpfulness, some were more hindrance but should be acknowledged for their effect on the overall experience.

Also unclear the effect of copious alcohol consumption, disrupted circadian rhythms and failed relationships on the timely completion of my PhD candidature, that would require further research and sounds like the topic for someone else's doctorate!

PUBLICATIONS DURING THE COURSE OF THIS THESIS

Peer-reviewed journal publications:

Dew, R.E.C., Collins, A.S., Glorie, S., Morley, C.K., Blades, M.L., Nachtergaele, S., King, R., Foden, J., De Grave, J., Kanjanapayont, P., Evans, N.J., Alessio, B.L. & Charusiri, P. 2018. Probing into Thailand's basement: New insights from U–Pb geochronology, Sr, Sm–Nd, Pb and Lu–Hf isotopic systems from granitoids. *Lithos*, 320-321, 332-354, doi: 10.1016/j.lithos.2018.09.019.

Dew, R.E.C., King, R., Collins, A.S., Morley, C.K., Arboit, F. & Glorie, S. 2018. Stratigraphy of deformed Permian carbonate reefs in Saraburi Province, Thailand. *Journal of the Geological Society*, 175, 163-175, doi: 10.1144/jgs2017-035.

Dew, R.E.C., Nachtergaele, S., Collins, A.S., Glorie, S., Foden, J., De Grave, J., Blades, M.L., Morley, C.K., Evans, N.J., Alessio, B.L., Kanjanapayont, P., King, R. & Charusiri, P. 2018. Data analysis of the U–Pb geochronology and Lu–Hf system in zircon and whole-rock Sr, Sm–Nd and Pb isotopic systems for the granitoids of Thailand. *Data in Brief*, 21, 1794-1809, doi: 10.1016/j.dib.2018.10.176.

Dew, R.E.C., Morley, C.K., Tin Aung Myint & Collins, A. (in review). Age and provenance of the Chaung Magyi Group, Yeywa Dome, Myanmar, based on U–Pb dating of detrital zircons. *Journal of Asian Earth Sciences*.

Harvey, N., **Dew**, R.E.C. & Hender, S. 2017. Rapid land use change by coastal wind farm development: Australian policies, politics and planning. *Land Use Policy*, 61, 368-378, doi: 10.1016/j.landusepol.2016.11.031.

Harvey, N. & **Dew**, R.E.C. 2016. Coastal Impact of Onshore Wind Farms in Australia. In: Vila-Concejo, A., Bruce, E., Kennedy, D.M. & McCarroll, R.J. (eds.) Proceedings of the 14th International Coastal Symposium. *Journal of Coastal Research*, Sydney, Australia, 992-996.

Conference presentations:

Dew, R.E.C., Collins, A.S., King, R., Morley, C., Evans, N. & Glorie, S. 2018. A detrital provenance story from Gondwana to northwest Thailand. *20th International Sedimentological Congress*, August 2018.

Dew, R.E.C., Collins, A.S., Glorie, S., King, R., Morley, C.K., Foden, J., De Grave, J., Alessio, B.L., Kanjanapayont, P., Charusiri, P. & Evans, N.J. 2017. Zircon Probes and Provenance: New insights in the palaeogeography of Southeast Asia. *Puzzling out Gondwana 16*, Bangkok, Thailand, November 2017, 155-156.

Dew, R.E.C., Collins, A.S., King, R., Arboit, F. & Glorie, S. 2015. Stratigraphy of deformed Permian carbonate reefs in Saraburi Province of Thailand. *The 4th International Symposium of the International Geosciences Programme (IGCP) Project 589*, Bangkok, Thailand, October 2015, 14-16.

PUBLICATIONS DURING THE COURSE OF THIS THESIS

Science communication:

Collins, A. & **Dew**, R. When Thailand and Australia were closer neighbours, tectonically speaking, October 19 2018, *The Conversation*, http://theconversation.com/when-thailand-and-australia-were-closer-neighbours-tectonically-speaking-100824.

Dew, R. (2016) The 4th IGCP 589 Symposium and Field Trip. *The Australian Geologist* (TAG) Magazine.

Dew, R. (2016, September). Memoir of Awardee, Endeavour Australia Cheung Kong Research Fellowship, Adelaide, Australia, p.83.

CHAPTER 1

Introduction and Thesis Outline

1. Introduction to the tectonic evolution and palaeogeography of Thailand

The progressive development and destruction of the Tethys Oceans, with the northward movement of Gondwana-derived terranes in the Phanerozoic, resulted in the landmasses of Southeast Asia that we recognise today (Audley-Charles et al. 1988; Burrett et al. 2014; Cocks and Torsvik 2013). The complex tectonic history of the region has led to controversy over when and where fragments separated from Gondwana and when and where they docked in Southeast Asia (Domeier and Torsvik 2014; Li et al. 2004; Loydell and Aung 2017; Seton et al. 2012; Yan et al. 2018; Zhang et al. 2018). Various attempts have been made to unravel the tectonic history of Southeast Asia, resulting in the subdivision of the region into different terranes. However, there is still little known about the precise location of the boundaries, the nature of the basement and source region characteristics of the associated sediments. This thesis focuses on three main terranes; the Sibumasu, Sukhothai and Indochina (Fig. 1), which amalgamated during the Permo-Triassic Indosinian Orogeny to form modern-day Thailand.

The Sibumasu Terrane is a ribbon-like continent that is equivalent to the South Qiangtang Terrane in Tibet, and the Baoshan and Tengchong terranes in southwest China (Ali et al. 2013; Jiang et al. 2017; Morley 2018). The word Sibumasu is a combination of its constituents: *Si*am-Thailand and *Si*no-China-*Bu*rma-*Ma*laysia-*Su*matra. Paleozoic sedimentary rocks from the Sibumasu Terrane, including lower Permian glaciomarine diamictites, show Gondwanan faunal affinities (Metcalfe, 1984; 2013; Schwartz et al., 1995; Sevastjanova et al., 2011). Triassic continental collision S-type granites are common in the Sibumasu Terrane and are host to economic tin and tungsten mineralisation (Dew et al. 2018; Gardiner et al. 2016; Hutchison 2014; Schwartz et al. 1995; Searle et al. 2012). There is published evidence from southwest China, Myanmar, Malaysia and peninsula Thailand for Hadean–Mesoproterozoic-aged crustal material within the Sibumasu Terrane (Gardiner et al. 2016; Jiang et al. 2017; Li et al. 2015; Liew and McCulloch 1985; Lin et al. 2013; Sevastjanova et al. 2011; Sevastjanova et al. 2016). Sevastjanova et al. (2016) interpreted that the Archaean zircons identified in the Burmese section of the Sibumasu Terrane were derived from the Western Australian Yilgarn and/or Pilbara cratons.

The Sukhothai Terrane contains the remnants of an arc system and its associated short-lived basin, known as the Nan basin in northern Thailand (e.g. Sone and Metcalfe, 2008; Metcalfe, 2013). This terrane is thought to be equivalent to the Chanthaburi Terrane in southwest Thailand and the Lincang Terrane of southern China (Fig. 1; Sone and Metcalfe, 2008). Permo-Triassic deformed fore-arc basin sequences and overlying late Permian–Triassic shallow marine molasse-type sedimentary rocks predominant the Sukhothai Terrane's stratigraphy (Chaodumrong 1992; Hara et al. 2017). The Sukhothai Terrane also includes Permo-Triassic metaluminous granitoids with an I-type affinity (Sone and Metcalfe 2008; Sone et al. 2012). Previously published granitoid model ages (T_{DM}) from northern Thailand region of the Sukhothai Terrane range from 1.95 to 0.96 Ga, with peaks at 1.90 Ga and 1.10 Ga from northwest Thailand (Hansen

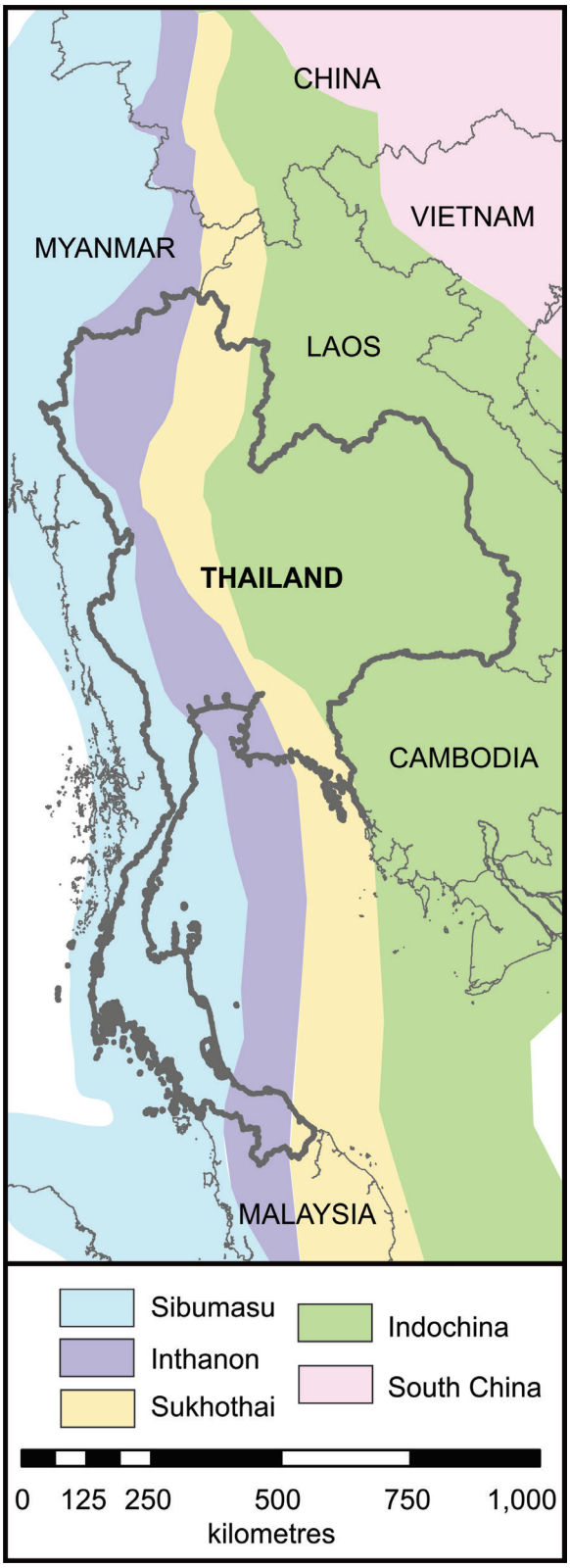

Fig. 1. Regional map showing major tectonic subdivisions of Southeast Asia, Thailand country border in bold. Tectonic boundaries adjusted from Metcalfe (2013).

et al. 2014; Wang et al. 2016b). Model ages from granitoids of the southern Chanthaburi Terrane are Neoproterozoic to Silurian in age (Qian et al. 2017).

The Indochina Terrane extends across large expanses of Laos, Vietnam, Cambodia, Malaysia and Thailand (Fig. 1). There is evidence that it may be a composite terrane comprised of multiple micro-terranes, potential sutures, metamorphic complexes and mylonitic fault zones (Arboit et al. 2016; Lepvrier et al. 2004; Sone and Metcalfe 2008). Within Thailand, the Indochina Terrane encompasses all of Thailand east of the Sukhothai Terrane. Metaluminous I-type granitoids are commonly found in the Indochina Terrane and host economic Cu–Fe–Au–Sb mineralisation (Charusiri et al. 1993; Salam et al. 2014; Zaw et al. 2014). Mesozoic and Cenozoic sediments cover the Indochina Terrane throughout most of Thailand, however, basement rocks, up to granulite-facies, are exposed in Vietnam, Laos and Cambodia (Nakano et al. 2018; Shi et al. 2015; Wang et al. 2016a). Inherited zircons and model ages suggest that the Indochina Terrane formed between Paleoproterozoic and Mesoproterozoic times (Lan et al. 2003; Shi et al. 2015; Wang et al. 2016a). There is evidence that the high grade metamorphism of basement rocks, such as the Kontum Massif and the Truong Son Belt, were caused by the multi-phased Indosinian Orogeny, often specifically attributed to the oblique collision of the Indochina and South China terranes (see Faure et al. 2018; Halpin et al. 2016; Lan et al. 2003; Lepvrier et al. 2004; Nagy et al. 2001; Nakano et al. 2018).

The evolution of these three terranes form a principal component in the history of the Tethys and the development of Southeast

Asia. However, their tectonic evolution and palaeogeography are not entirely constrained. It is well established that the Indochina and Sibumasu terranes were once part of the Gondwana supercontinent (Audley-Charles et al. 1988; Burrett et al. 2014; Cocks and Torsvik 2013). However, there are various models on their placement within this supercontinent and the timing of separation (Li et al. 2004; Loydell and Aung 2017; Yan et al. 2018; Zhang et al. 2018). Proterozoic to early Paleozoic palaeogeographic reconstructions for the Sibumasu Terrane are often oversimplified with the terrane commonly appearing off the northwest margin of Australia in the Gondwanan supercontinent (Burrett et al., 2014; Cocks and Torsvik, 2013; Usuki et al., 2013). The Sukhothai Terrane is rarely included in models of Gondwana since there has been much historical debate on its origins, whether it is an oceanic (e.g. Sone and Metcalfe 2008) or continental arc system (Hara et al. 2017; Sevastjanova et al. 2011). In palaeogeographic reconstructions of Gondwana, the Indochina Terrane is often positioned in varying configurations outboard of the Sibumasu Terrane adjacent to South China, India and Iran (Burrett et al. 2014; Cocks and Torsvik 2013; Metcalfe 2013; Usuki et al. 2013).

The terranes of Thailand amalgamated during the Indosinian Orogeny, with the timing of the collision between Indochina and Sibumasu yet to be detailed, and current constraints range from latest Permian to late Triassic (Barber et al. 2011; Cai et al. 2017; Hara et al. 2012; Metcalfe 2013; Wakita and Metcalfe 2005). Since this collision, the Thai terranes have had a tectonically and structurally complicated history with vast amounts of later sedimentation and fault reactivation obscuring the basement and older Paleozoic sequences (Hansen and Wemmer 2011; Kanjanapayont et al. 2013; Minezaki et al. 2018; Morley et al. 2013). As basement exposures are sparse, little is known about the nature of the underlying basement in Thailand. Therefore, granitoids are used in this study as probes to identify the isotopic characteristics of the three terrane basements. This study also examines the provenance of the sediments to elucidate source region characteristics and help to unravel the tectonic evolution of the terranes that make up modern-day Thailand.

2. Thesis Outline

Three distinct tectonic terranes amalgamated during the Permian–Triassic to form present day Thailand. Therefore, this thesis endeavours to unravel the tectonic evolution and palaeogeography of the main Thai terranes: Indochina, Sukhothai and Sibumasu. Prior to their Triassic amalgamation, these three terranes have different tectonic histories therefore each chapter of this thesis aims to provide further information on their origin, relative position, separation/ collision with other blocks and past environments. Understanding the evolution of the terranes of Thailand not only has implications for the palaeogeographic history of Southeast Asia, but can provide information on the formation of petroleum-hosted basins to the genesis of arc-related mineral resources. This thesis uses zircon isotopic systematics in detrital and granitoid rocks in conjunction with whole-rock granitoid geochemistry to characterise the nature of Thailand's development from Gondwana to Southeast Asia today.

Chapter 2

Chapter 2a is published in *Lithos* as:
Dew, R.E.C., Collins, A.S., Glorie, S.,

Morley, C.K., Blades, M.L., Nachtergaele, S., King, R., Foden, J., De Grave, J., Kanjanapayont, P., Evans, N.J., Alessio, B.L. & Charusiri, P. 2018. Probing into Thailand's basement: New insights from U–Pb geochronology, Sr, Sm–Nd, Pb and Lu–Hf isotopic systems from granitoids. *Lithos*, **320-321**, 332-354, doi: https://doi.org/10.1016/j.lithos.2018.09.019.

Chapter 2b is published in *Data in Brief* as:
Dew, R.E.C., Nachtergaele, S., Collins, A.S., Glorie, S., Foden, J., De Grave, J., Blades, M.L., Morley, C.K., Evans, N.J., Alessio, B.L., Kanjanapayont, P., King, R. & Charusiri, P. 2018. Data analysis of the U–Pb geochronology and Lu–Hf system in zircon and whole-rock Sr, Sm–Nd and Pb isotopic systems for the granitoids of Thailand. *Data in Brief*, **21**, 1794-1809, doi: https://doi.org/10.1016/j.dib.2018.10.176.

This chapter focuses on the granitoids of Thailand and their isotopic signatures of the underlying basement. The aim of this chapter is to use granites as a probe to further develop our understanding of the unexposed basement in Thailand. To understand the isotopic characteristics of Thailand's basement we use an integrated zircon (U–Pb and Lu–Hf) and whole-rock (Rb–Sr, Sm–Nd and Pb) isotopic dataset from granitoids across Thailand. The U–Pb age, $\varepsilon Hf_{(t)}$, $\varepsilon Nd_{(t)}$, $^{87}Sr/^{86}Sr_{(t)}$ and Pb isotopic signatures assist in characterising the underlying basement and highlight the variance in the history of the three tectonic domains. Part 2a of this chapter focusses on the overall granitoid isotopic data, the regional trends and the implications of the tectonic evolution. Part 2b thoroughly describes the granitoid samples' petrography, experimental design, methodology and parameters, the reasoning and determination of interpreted ages.

Chapter 3
Chapter 3 is written for publication in *Gondwana Research* as:

Dew, R.E.C., Collins, A.S., King, R., Morley, C.K., Evans, N.J. & Glorie, S. A detrital provenance story from Gondwana to northwest Thailand.

Chapter 3 involves a coupled detrital zircon U–Pb and Lu–Hf provenance study from northwest Thailand. These detrital samples are Cambrian to Triassic in age and were taken from the Sibumasu Terrane. This study enhances our understanding of the evolution of Sibumasu and neighbouring terranes, which are often oversimplified in palaeogeography reconstructions. Additionally, this study unearths information on the shared margin of Sibumasu, northern India and northwestern Australia during the Proterozoic to early Paleozoic.

Chapter 4
Chapter 4 is written for publication in the *Geological Journal* as:

Dew, R.E.C., Collins, A.S., King, R., Morley, C.K., Evans, N.J. & Glorie, S. The Permo-Triassic tectonic geography of Thailand deduced from terrane-based sediment provenance.

Chapter 4 focuses on the provenance of Permo-Triassic siliciclastic rocks throughout Thailand. This study integrates detrital zircon U–Pb and Lu–Hf isotopic systems to better constrain and compare the provenance across the three terranes, with a particular emphasis on the potential source rocks in the adjoining terranes of Southeast Asia.

Chapter 5
Chapter 5 is in review for publication in the *Journal of Asian Earth Sciences* as:

Dew, R.E.C., Morley, C.K., Collins, A.S. & Tin Aung Myint. Age and provenance of the Chaung Magyi Group, Yeywa Dome, Myanmar, based on U–Pb dating of detrital zircons.

Chapter 5 focuses on the Neoproterozoic–Cambrian Chaung Magyi Group of Myanmar. This sedimentary sequence is part of the Sibumasu Terrane and has historically had little constraints on the depositional age. This study analyses the U–Pb geochronology of the Chaung Magyi Group and compares it to the equivalent sequences in northwest Thailand. This study enhances our understanding of the Sibumasu Terrane and can be used as evidence that this ribbon continent has similar sediment sources in both Myanmar and northwest Thailand indicating it is a cohesive terrane. Additionally, this study unearths information on the shared margin of Sibumasu, northern India and northwestern Australia during the Proterozoic to early Paleozoic.

Chapter 6
Chapter 6 is published in the *Journal of the Geological Society* as:

Dew, R.E.C., King, R., Collins, A.S., Morley, C.K., Arboit, F. & Glorie, S. 2018. Stratigraphy of deformed Permian carbonate reefs in Saraburi Province, Thailand. Journal of the Geological Society, **175**, 1, 163-175, doi: http://dx.doi.org/10.1144/jgs2017-035.

Chapter 6 focuses on carbonate biostratigraphy of the Khao Khwang Platform on the southern margin of the Indochina Terrane. This platform sequence has been structurally complicated during the amalgamation of Thailand and now forms a fold-thrust belt. This study aims to reconstruct the Permian carbonate palaeogeography using foraminiferal biostratigraphy and detailed microfacies analysis in light of the recent structural cross-sections (e.g. Arboit et al. 2014).

Chapter 7
Chapter 7 provides a summary for the findings within this study. To provide a clear overview, we highlight the new insights from this study to the overall understanding of the tectonic evolution and palaeogeography of Southeast Asia from the terrane origins in the Precambrian through to the Triassic amalgamation of Thailand.

References

Ali, J.R., Cheung, H.M.C., Aitchison, J.C. & Sun, Y. 2013. Palaeomagnetic re-investigation of Early Permian rift basalts from the Baoshan Block, SW China: constraints on the site-of-origin of the Gondwana-derived eastern Cimmerian terranes. Geophysical Journal International, 193, 650-663, doi: 10.1093/gji/ggt012.

Arboit, F., Collins, A.S., King, R., Morley, C.K. & Hansberry, R. 2014. Structure of the Sibumasu–Indochina collision, central Thailand: A section through the Khao Khwang Fold and thrust belt. Journal of Asian Earth Sciences, 95, 182-191, doi: http://dx.doi.org/10.1016/j.jseaes.2014.06.016.

Arboit, F., Collins, A.S., Morley, C.K., King, R. & Amrouch, K. 2016. Detrital zircon analysis of the southwest Indochina terrane, central Thailand: Unravelling the Indosinian orogeny. Geological Society of America Bulletin,, 128, 1024-1043.

Audley-Charles, M.G., Ballantyne, P.D. & Hall, R. 1988. Mesozoic-Cenozoic rift-drift sequence of Asian fragments from Gondwanaland. Tectonophysics, 155, 317-330.

Barber, A.J., Ridd, M.F. & Crow, M.J. 2011. The origin, movement and assembly of the pre-Tertiary tectonic units of Thailand. In: Ridd, M.F., Barber, A.J. & Crow, M.J. (eds.) The

Geology of Thailand. The Geological Society, London, 507-537.

Burrett, C., Khin, Z., Meffre, S., Lai, C.K., Khositanont, S., Chaodumrong, P., Udchachon, M., Ekins, S. & Halpin, J. 2014. The configuration of Greater Gondwana—Evidence from LA ICPMS, U–Pb geochronology of detrital zircons from the Palaeozoic and Mesozoic of Southeast Asia and China. Gondwana Research, 26, 31-51, doi: http://dx.doi.org/10.1016/j.gr.2013.05.020.

Cai, F., Ding, L., Yao, W., Laskowski, A.K., Xu, Q., Zhang, J.e. & Sein, K. 2017. Provenance and tectonic evolution of Lower Paleozoic–Upper Mesozoic strata from Sibumasu terrane, Myanmar. Gondwana Research, 41, 325-336, doi: 10.1016/j.gr.2015.03.005.

Chaodumrong, P. 1992. Stratigraphy, sedimentology and tectonic implications of the Lampang Group, central north Thailand. Doctorate of Philosophy, University of Tasmania.

Charusiri, P., Clark, A.H., Farrar, E., Archibald, D. & Charusiri, B. 1993. Granite belts in Thailand: evidence from the 40Ar/39Ar geochronological and geological syntheses. Journal of Southeast Asian Earth Sciences, 8, 127-136, doi: http://dx.doi.org/10.1016/0743-9547(93)90014-G.

Cocks, L.R.M. & Torsvik, T.H. 2013. The dynamic evolution of the Palaeozoic geography of eastern Asia. Earth-Science Reviews, 117, 40-79, doi: http://dx.doi.org/10.1016/j.earscirev.2012.12.001.

Dew, R.E.C., Collins, A.S., Glorie, S., Morley, C.K., Blades, M.L., Nachtergaele, S., King, R., Foden, J., De Grave, J., Kanjanapayont, P., Evans, N.J., Alessio, B.L. & Charusiri, P. 2018. Probing into Thailand's basement: New insights from U–Pb geochronology, Sr, Sm–Nd, Pb and Lu–Hf isotopic systems from granitoids. Lithos, 320-321, 332-354, doi: 10.1016/j.lithos.2018.09.019.

Domeier, M. & Torsvik, T.H. 2014. Plate tectonics in the late Paleozoic. Geoscience Frontiers, 5, 303-350, doi: http://dx.doi.org/10.1016/j.gsf.2014.01.002.

Faure, M., Nguyen, V.V., Hoai, L.T.T. & Lepvrier, C. 2018. Early Paleozoic or Early-Middle Triassic collision between the South China and Indochina Blocks: The controversy resolved? Structural insights from the Kon Tum massif (Central Vietnam). Journal of Asian Earth Sciences, 166, 162-180, doi: https://doi.org/10.1016/j.jseaes.2018.07.015.

Gardiner, N.J., Searle, M.P., Morley, C.K., Whitehouse, M.P., Spencer, C.J. & Robb, L.J. 2016. The closure of Palaeo-Tethys in Eastern Myanmar and Northern Thailand: New insights from zircon U-Pb and Hf isotope data. Gondwana Research, 39, 401-422, doi: 10.1016/j.gr.2015.03.001.

Halpin, J.A., Tran, H.T., Lai, C.-K., Meffre, S., Crawford, A.J. & Zaw, K. 2016. U–Pb zircon geochronology and geochemistry from NE Vietnam: A 'tectonically disputed' territory between the Indochina and South China blocks. Gondwana Research, 34, 254-273, doi: https://doi.org/10.1016/j.gr.2015.04.005.

Hansen, B.T. & Wemmer, K. 2011. Age and evolution of the basement in Thailand. In: Ridd, M.F., Barber, A.J. & Crow, M.J. (eds.) The Geology of Thailand. The Geological Society, London, 19-32.

Hansen, B.T., Wemmer, K., Putthapiban, P., Kleinhanns, I.C. & Wilsky, F. 2014. Do U/Pb-SHRIMP Dating and Pb Stepwise Leaching (PbSL) Analyses Confirm the Lack of Precambrian Basement Outcrops in Thailand? Open Journal of Geology, Vol.04No.10, 13, doi: 10.4236/ojg.2014.410037.

Hara, H., Kunii, M., Hisada, K.I., Ueno, K., Kamata, Y., Srichan, W., Charusiri, P., Charoentitirat, T., Watarai, M., Adachi, Y. & Kurihara, T. 2012. Petrography and geochemistry of clastic rocks within the Inthanon zone, northern Thailand: Implications for Paleo-Tethys subduction and convergence. Journal of Asian Earth Sciences, 61, 2-15, doi: 10.1016/j.jseaes.2012.06.012.

Hara, H., Kunii, M., Miyake, Y., Hisada, K.I., Kamata, Y., Ueno, K., Kon, Y., Kurihara, T., Ueda, H., Assavapatchara, S., Treerotchananon, A., Charoentitirat, T. & Charusiri, P. 2017. Sandstone provenance and U–Pb ages of detrital zircons from Permian–Triassic forearc sediments within the Sukhothai Arc, northern Thailand: Record of volcanic-arc evolution in response to Paleo-Tethys subduction. Journal of Asian Earth Sciences, 146, 30-55, doi: 10.1016/j.jseaes.2017.04.021.

Hutchison, C.S. 2014. Tectonic evolution of Southeast Asia. Bulletin of the Geological Society of Malaysia, 60, 1-18.

Jiang, H., Li, W.-Q., Jiang, S.-Y., Wang, H. & Wei, X.-P. 2017. Geochronological, geochemical and Sr-Nd-Hf isotopic constraints on the petrogenesis of Late Cretaceous A-type granites from the Sibumasu Block, Southern Myanmar, SE Asia. Lithos, 268–271, 32-47, doi: http://dx.doi.org/10.1016/j.lithos.2016.11.005.

Kanjanapayont, P., Kieduppatum, P., Klötzli, U.,

Klötzli, E. & Charusiri, P. 2013. Deformation history and U–Pb zircon geochronology of the high grade metamorphic rocks within the Klaeng fault zone, eastern Thailand. Journal of Asian Earth Sciences, 77, 224-233.

Lan, C.Y., Chung, S.L., Van Long, T., Lo, C.H., Lee, T.-Y., Mertzman, S.A. & Shen, J.J.-S. 2003. Geochemical and Sr–Nd isotopic constraints from the Kontum massif, central Vietnam on the crustal evolution of the Indochina block. Precambrian Research, 7-27.

Lepvrier, C., Maluski, H., Van Tich, V., Leyreloup, A., Truong Thi, P. & Van Vuong, N. 2004. The Early Triassic Indosinian orogeny in Vietnam (Truong Son Belt and Kontum Massif); implications for the geodynamic evolution of Indochina. Tectonophysics, 393, 87-118, doi: http://dx.doi.org/10.1016/j.tecto.2004.07.030.

Li, G., Wang, Q., Huang, Y., Chen, F. & Dong, P. 2015. Discovery of Hadean–Mesoarchean crustal materials in the northern Sibumasu block and its significance for Gondwana reconstruction. Precambrian Research, 271, 118-137, doi: https://doi.org/10.1016/j.precamres.2015.10.003.

Li, P., Rui, G., Junwen, C. & Ye, G. 2004. Paleomagnetic analysis of eastern Tibet: implications for the collisional and amalgamation history of the Three Rivers Region, SW China. Journal of Asian Earth Sciences, 24, 291-310, doi: http://dx.doi.org/10.1016/j.jseaes.2003.12.003.

Liew, T.C. & McCulloch, M.T. 1985. Genesis of granitoid batholiths of Peninsular Malaysia and implications for models of crustal evolution: Evidence from a Nd–Sr isotopic and U–Pb zircon study. Geochimica et Cosmochimica Acta, 49, 587-600, doi: https://doi.org/10.1016/0016-7037(85)90050-X.

Lin, Y.-L., Yeh, M.-W., Lee, T.-Y., Chung, S.-L., Iizuka, Y. & Charusiri, P. 2013. First evidence of the Cambrian basement in Upper Peninsula of Thailand and its implication for crustal and tectonic evolution of the Sibumasu terrane. Gondwana Research, 24, 1031-1037, doi: http://dx.doi.org/10.1016/j.gr.2013.05.014.

Loydell, D.K. & Aung, K.P. 2017. The "Panghkawkwo graptolite bed" (Llandovery, Silurian), Myanmar and the location of the Sibumasu (or Sibuma) Terrane in the Silurian. Palaeogeography, Palaeoclimatology, Palaeoecology, 469, 1-17, doi: https://doi.org/10.1016/j.palaeo.2016.12.028.

Metcalfe, I. 2013. Gondwana dispersion and Asian accretion: Tectonic and palaeogeographic evolution of eastern Tethys. Journal of Asian Earth Sciences, 66, 1-33, doi: http://dx.doi.org/10.1016/j.jseaes.2012.12.020.

Minezaki, T., Hisada, K.-i., Hara, H. & Kamata, Y. 2018. Tectono-stratigraphy of Late Carboniferous to Triassic successions of the Khorat Plateau Basin, Indochina Block, northeastern Thailand: Initiation of the Indosinian Orogeny by collision of the Indochina and South China blocks. Journal of Asian Earth Sciences, doi: https://doi.org/10.1016/j.jseaes.2018.10.020.

Morley, C.K. 2018. Understanding Sibumasu in the context of ribbon continents. Gondwana Research, doi: https://doi.org/10.1016/j.gr.2018.07.006.

Morley, C.K., Ampaiwan, P., Thanudamrong, S., Kuenphan, N. & Warren, J. 2013. Development of the Khao Khwang fold and thrust belt; implications for the geodynamic setting of Thailand and Cambodia during the Indosinian Orogeny. Journal of Asian Earth Sciences, 62, 705-719, doi: http://dx.doi.org/10.1016/j.jseaes.2012.11.021.

Nagy, E.A., Maluski, H., Lepvrier, C., Schärer, U., Truong Thi, P., Leyreloup, A. & Van Thich, V. 2001. Geodynamic Significance of the Kontum Massif in Central Vietnam: Composite 40Ar/39Ar and U-Pb Ages from Paleozoic to Triassic. The Journal of Geology, 109, 755-770.

Nakano, N., Osanai, Y., Nam, N.V. & Tri, T.V. 2018. Bauxite to eclogite: Evidence for late Permian supracontinental subduction at the Red River shear zone, northern Vietnam. Lithos, 302-303, 37-49, doi: https://doi.org/10.1016/j.lithos.2017.12.023.

Qian, X., Feng, Q., Wang, Y., Zhao, T., Zi, J.-W., Udchachon, M. & Wang, Y. 2017. Late Triassic post-collisional granites related to Paleotethyan evolution in SE Thailand: Geochronological and geochemical constraints. Lithos, 286, 440-453, doi: http://dx.doi.org/10.1016/j.lithos.2017.06.026.

Salam, A.A., Zaw, K., Meffre, S., McPhie, J. & Lai, C.-K. 2014. Geochemistry and geochronology of the Chatree epithermal gold-silver deposit: Implications for the tectonic setting of the Loei Fold Belt, central Thailand. Gondwana Research, 26, 198-217.

Schwartz, M.O., Rajah, S.S., Askury, A.K., Putthapiban, P. & Djaswadi, S. 1995. The Southeast Asian tin belt. Earth-Science Reviews, 38, 95-293, doi: https://doi.org/10.1016/0012-8252(95)00004-T.

Searle, M.P., Whitehouse, M.J., Robb, L.J., Ghani, A.A., Hutchison, C.S., Sone, M., Ng, S.W.P., Roselee, M.H., Chung, S.L. & Oliver, G.J.H. 2012. Tectonic evolution of the Sibumasu-Indochina terrane collision zone in Thailand and Malaysia: Constraints from new U-Pb zircon chronology of SE Asian tin granitoids. Journal of the Geological Society, 169, 489-500, doi: 10.1144/0016-76492011-107.

Seton, M., Müller, R.D., Zahirovic, S., Gaina, C., Torsvik, T., Shephard, G., Talsma, A., Gurnis, M., Turner, M., Maus, S. & Chandler, M. 2012. Global continental and ocean basin reconstructions since 200 Ma. Earth-Science Reviews, 113, 212-270, doi: http://dx.doi.org/10.1016/j.earscirev.2012.03.002.

Sevastjanova, I., Clements, B., Hall, R., Belousova, E.A., Griffin, W.L. & Pearson, N. 2011. Granitic magmatism, basement ages, and provenance indicators in the Malay Peninsula: Insights from detrital zircon U–Pb and Hf-isotope data. Gondwana Research, 19, 1024-1039, doi: 10.1016/j.gr.2010.10.010.

Sevastjanova, I., Hall, R., Rittner, M., Paw, S.M.T.L., Naing, T.T., Alderton, D.H. & Comfort, G. 2016. Myanmar and Asia united, Australia left behind long ago. Gondwana Research, 32, 24-40, doi: https://doi.org/10.1016/j.gr.2015.02.001.

Shi, M.F., Lin, F.C., Fan, W.Y., Deng, Q., Cong, F., Tran, M.D., Zhu, H.P. & Wang, H. 2015. Zircon U-Pb ages and geochemistry of granitoids in the Truong Son terrane, Vietnam: Tectonic and metallogenic implications. Journal of Asian Earth Sciences, 101, 101-120, doi: 10.1016/j.jseaes.2015.02.001.

Sone, M. & Metcalfe, I. 2008. Parallel Tethyan sutures in mainland Southeast Asia: New insights for Palaeo-Tethys closure and implications for the Indosinian orogeny. Comptes Rendus - Geoscience, 340, 166-179, doi: 10.1016/j.crte.2007.09.008.

Sone, M., Metcalfe, I. & Chaodumrong, P. 2012. The Chanthaburi terrane of southeastern Thailand: Stratigraphic confirmation as a disrupted segment of the Sukhothai Arc. Journal of Asian Earth Sciences, 61, 16-32, doi: 10.1016/j.jseaes.2012.08.021.

Usuki, T., Lan, C.-Y., Wang, K.-L. & Chiu, H.-Y. 2013. Linking the Indochina block and Gondwana during the Early Paleozoic: Evidence from U–Pb ages and Hf isotopes of detrital zircons. Tectonophysics, 586, 145-159, doi: http://dx.doi.org/10.1016/j.tecto.2012.11.010.

Wakita, K. & Metcalfe, I. 2005. Ocean Plate Stratigraphy in East and Southeast Asia. Journal of Asian Earth Sciences, 24, 679-702, doi: http://dx.doi.org/10.1016/j.jseaes.2004.04.004.

Wang, S., Mo, Y., Wang, C. & Ye, P. 2016a. Paleotethyan evolution of the Indochina Block as deduced from granites in northern Laos. Gondwana Research, 38, 183-196, doi: https://doi.org/10.1016/j.gr.2015.11.011.

Wang, Y., He, H., Cawood, P.A., Srithai, B., Feng, Q., Fan, W., Zhang, Y. & Qian, X. 2016b. Geochronological, elemental and Sr-Nd-Hf-O isotopic constraints on the petrogenesis of the Triassic post-collisional granitic rocks in NW Thailand and its Paleotethyan implications. Lithos, 266-267, 264-286, doi: https://doi.org/10.1016/j.lithos.2016.09.012.

Yan, Y., Huang, B., Zhang, D., Charusiri, P. & Veeravinantanakul, A. 2018. Paleomagnetic Study on the Permian Rocks of the Indochina Block and Its Implications for Paleogeographic Configuration and Northward Drifting of Cathaysialand in the Paleo-Tethys. Journal of Geophysical Research: Solid Earth, 0, doi: 10.1029/2018jb015511.

Zaw, K., Meffre, S., Lai, C.-K., Burrett, C., Santosh, M., Graham, I., Manaka, T., Salam, A., Kamvong, T. & Cromie, P. 2014. Tectonics and metallogeny of mainland Southeast Asia — A review and contribution. Gondwana Research, 26, 5-30, doi: http://dx.doi.org/10.1016/j.gr.2013.10.010.

Zhang, X., Chung, S.-L., Lai, Y.-M., Ghani, A.A., Murtadha, S., Lee, H.-Y. & Hsu, C.-C. 2018. Detrital Zircons Dismember Sibumasu in East Gondwana. Journal of Geophysical Research: Solid Earth, 123, doi: 10.1029/2018jb015780.

CHAPTER 2

Part A of this chapter is published as:

Dew, R.E.C., Collins, A.S., Glorie, S., Morley, C.K., Blades, M.L., Nachtergaele, S., King, R., Foden, J., De Grave, J., Kanjanapayont, P., Evans, N.J., Alessio, B.L. & Charusiri, P. 2018. Probing into Thailand's basement: New insights from U–Pb geochronology, Sr, Sm–Nd, Pb and Lu–Hf isotopic systems from granitoids. *Lithos*, **320-321**, 332-354, doi: 10.1016/j.lithos.2018.09.019.

Part B of this chapter is published as:

Dew, R.E.C., Nachtergaele, S., Collins, A.S., Glorie, S., Foden, J., De Grave, J., Blades, M.L., Morley, C.K., Evans, N.J., Alessio, B.L., Kanjanapayont, P., King, R. & Charusiri, P. 2018. Data analysis of the U–Pb geochronology and Lu–Hf system in zircon and whole-rock Sr, Sm–Nd and Pb isotopic systems for the granitoids of Thailand. *Data in Brief*, **21**, 1794-1809, doi: 10.1016/j.dib.2018.10.176.

Statement of Authorship

Title of Paper	Probing into Thailand's basement: New insights from U–Pb geochronology, Sr, Sm–Nd, Pb and Lu–Hf isotopic systems from granitoids
Publication Status	☑ Published ☐ Accepted for Publication ☐ Submitted for Publication ☐ Unpublished and Unsubmitted w ork w ritten in manuscript style
Publication Details	Dew, R.E.C., Collins, A.S., Glorie, S., Morley, C.K., Blades, M.L., Nachtergaele, S., King, R., Foden, J., De Grave, J., Kanjanapayont, P., Evans, N.J., Alessio, B.L. & Charusiri, P. 2018. Probing into Thailand's basement: New insights from U—Pb geochronology, Sr, Sm—Nd, Pb and Lu—Hf isotopic systems from granitoids. *Lithos*, **320-321**, 332-354, doi: https://doi.org/10.1016/j.lithos.2018.09.019.

Principal Author

Name of Principal Author (Candidate)	Romana E.C. Dew		
Contribution to the Paper	Performed majority of sample analysis, interpreted data, wrote manuscript and acted as corresponding author.		
Overall percentage (%)	70		
Certification:	This paper reports on original research I conducted during the period of my Higher Degree by Research candidature and is not subject to any obligations or contractual agreements with a third party that would constrain its inclusion in this thesis. I am the primary author of this paper.		
Signature		Date	14/12/2018

Co-Author Contributions

By signing the Statement of Authorship, each author certifies that:

i. the candidate's stated contribution to the publication is accurate (as detailed above);
ii. permission is granted for the candidate in include the publication in the thesis; and
iii. the sum of all co-author contributions is equal to 100% less the candidate's stated contribution.

Name of Co-Author	Alan S. Collins		
Contribution to the Paper	Primary supervisorial role, conception and design of the project, helped in data interpretation and manuscript construction and editing		
Signature		Date	14/12/2018

Name of Co-Author	Stijn Glorie		
Contribution to the Paper	Co-supervisorial role, conception and design of the project, sample collection (NT and ST samples), helped in data interpretation and manuscript evaluation		
Signature		Date	30/11/2018

Name of Co-Author	Christopher K. Morley		
Contribution to the Paper	Assistance with data interpretation and manuscript editing		
Signature	Dr. Christopher Morley	Date	10/01/2019

Name of Co-Author	Morgan L. Blades		
Contribution to the Paper	Interpretation of U–Pb crystallisation ages and manuscript evaluation		
Signature		Date	10/01/2019

Name of Co-Author	Simon Nachtergaele		
Contribution to the Paper	Performed the petrographic analysis, zircon sample preparation (KM, ST and NT samples) and manuscript evaluation		
Signature		Date	13/12/2018

Name of Co-Author	Rosalind King		
Contribution to the Paper	Co-supervisorial role, conception and design of the project		
Signature		Date	28/11/2018

Name of Co-Author	John Foden		
Contribution to the Paper	Whole-rock geochemistry interpretation and formatting		
Signature		Date	14/01/2019

Name of Co-Author	Johan De Grave		
Contribution to the Paper	Conception and design of the project, sample collection (KM, NT and ST samples)		
Signature		Date	13 DEC 2018

Name of Co-Author	Pitsanupong Kanjanapayont		
Contribution to the Paper	Sample collection (Th11/01 and Th11/02) and manuscript evaluation		
Signature		Date	18 DECEMBER 2018

Name of Co-Author	Noreen Evans		
Contribution to the Paper	Hafnium data reduction and manuscript editing		
Signature		Date	28-11-18

Name of Co-Author	Brandon Alessio		
Contribution to the Paper	Hafnium data collection (NT-09, NT-10, NT-11, NT-12, RDT15_076A, ST-16, ST-49A, Th11/01, Th11/02) and manuscript evaluation		
Signature		Date	14/12/2018

Name of Co-Author	Punya Charusiri		
Contribution to the Paper	Financial contribution to the majority of field expeditions and manuscript evaluation		
Signature		Date	18 Dec 2018

Statement of Authorship

Title of Paper	Analysis of the U-Pb geochronology and Lu-Hf system in zircon and whole-rock Sr, Sm-Nd and Pb isotopic systems for the granitoids of Thailand
Publication Status	☑ Published ☐ Accepted for Publication ☐ Submitted for Publication ☐ Unpublished and Unsubmitted w ork w ritten in manuscript style
Publication Details	Dew, R.E.C., Nachtergaele, S., Collins, A.S., Glorie, S., Foden, J., De Grave, J., Blades, M.L., Morley, C.K., Evans, N.J., Alessio, B.L., Kanjanapayont, P., King, R., & Charusiri, P. (2018) Analysis of the U-Pb geochronology and Lu-Hf system in zircon and whole-rock Sr, Sm-Nd and Pb isotopic systems for the granitoids of Thailand. *Data in Brief,* doi: https://doi.org/10.1016/j.dib.2018.10.176.

Principal Author

Name of Principal Author (Candidate)	Romana E.C. Dew		
Contribution to the Paper	Performed majority of sample analysis, interpreted data, wrote manuscript and acted as corresponding author.		
Overall percentage (%)	70		
Certification:	This paper reports on original research I conducted during the period of my Higher Degree by Research candidature and is not subject to any obligations or contractual agreements with a third party that would constrain its inclusion in this thesis. I am the primary author of this paper.		
Signature		Date	14/12/2018

Co-Author Contributions

By signing the Statement of Authorship, each author certifies that:

i. the candidate's stated contribution to the publication is accurate (as detailed above);

ii. permission is granted for the candidate in include the publication in the thesis; and

iii. the sum of all co-author contributions is equal to 100% less the candidate's stated contribution.

Name of Co-Author	Simon Nachtergaele		
Contribution to the Paper	Performed the petrographic analysis, zircon sample preparation (KM, ST and NT samples) and manuscript evaluation		
Signature		Date	13/12/2018

Name of Co-Author	Alan S. Collins		
Contribution to the Paper	Primary supervisorial role, conception and design of the project, helped in data interpretation and manuscript construction and editing		
Signature		Date	14/12/2018

Name of Co-Author	Stijn Glorie		
Contribution to the Paper	Co-supervisorial role, conception and design of the project, sample collection (NT and ST samples), helped in data interpretation and manuscript evaluation		
Signature		Date	30/11/2018

Name of Co-Author	Christopher K. Morley		
Contribution to the Paper	Assistance with data interpretation		
Signature	Dr. Christopher Morley	Date	10/01/2019

Name of Co-Author	Morgan L. Blades		
Contribution to the Paper	Interpretation of U–Pb crystallisation ages and manuscript evaluation		
Signature		Date	10/01/2019

Name of Co-Author	Rosalind King		
Contribution to the Paper	Co-supervisorial role, conception and design of the project		
Signature		Date	28/11/2018

Name of Co-Author	John Foden		
Contribution to the Paper	Whole-rock geochemistry interpretation and formatting		
Signature		Date	14/01/2019

Name of Co-Author	Johan De Grave		
Contribution to the Paper	Conception and design of the project, sample collection (KM, NT and ST samples)		
Signature		Date	13 DEC 2018

Name of Co-Author	Pitsanupong Kanjanapayont		
Contribution to the Paper	Sample collection (Th11/01 and Th11/02) and manuscript evaluation		
Signature		Date	18 DECEMBER 2018

Name of Co-Author	Noreen Evans		
Contribution to the Paper	Hafnium data reduction and manuscript editing		
Signature		Date	28-11-18

Name of Co-Author	Brandon Alessio		
Contribution to the Paper	Hafnium data collection (NT-09, NT-10, NT-11, NT-12, RDT15_076A, ST-16, ST-49A, Th11/01, Th11/02)		
Signature		Date	14/12/2018

Name of Co-Author	Punya Charusiri		
Contribution to the Paper	Financial contribution to the majority of field expeditions		
Signature		Date	18 Dec 2018

ABSTRACT

The evolution of the Thai terranes: Indochina, Sibumasu and Sukhothai, form a principal component in the history of the Tethys Ocean and the development of Southeast Asia. These terranes have not always been connected, and the premise for this study is to use intrusions as isotopic probes to determine the origin and nature of their terrane basement. Here, we present an integrated zircon (U–Pb and Lu–Hf) and whole-rock (Rb–Sr, Sm–Nd and Pb) isotopic dataset from granitoids across Thailand. The U–Pb age, $\varepsilon Hf_{(t)}$, $\varepsilon Nd_{(t)}$, $^{87}Sr/^{86}Sr_{(t)}$ and Pb isotopic signatures assist in characterising the underlying basement and highlight the variance in the history of the three tectonic domains. Magmatic zircon Lu–Hf and whole-rock Sm–Nd data and model ages from this study illustrate that the Indochina Terrane is relatively juvenile and distinct from the Sibumasu Terrane that is composed of considerable Archean–Paleoproterozoic components. The geochemical signature of the Inthanon Zone implies a shared history with the Sibumasu Terrane. As a result of the mixing of juvenile and evolved material, the isotopic systems in the Sukhothai Terrane are similar to the bulk silicate earth creating a CHUR-like signature. This study demonstrates that the granitoids of the Sukhothai Terrane are syn-collisional and are sourced from a juvenile magma that is contaminated by evolved crustal material, which is likely to have originated from the Sibumasu Terrane during the closure of the Palaeo-Tethys Ocean. These results have implications for research on the Tethys Oceans, not only within Thailand but also in the greater Southeast Asian region.

1. Introduction

The terranes that form Thailand are key to understanding the palaeogeography of Greater Gondwana, the Tethys Oceans and the development of present-day Southeast Asia. In attempts to unravel the tectonic history of Southeast Asia, the region has been divided into various terranes, although there is no consensus on their number, the nature and location of their boundaries, the sources and characteristics of the basement, their global affinities or tectonic models for their amalgamation (Barr et al. 2006; Metcalfe 2013). This problem is accentuated by the lack of basement exposure due to the vast cover of younger sedimentary sequences, extensive jungle cover and deep lateritic weathering. Therefore, on a regional scale, the nature of the basement within Thailand is mostly unknown. The available basement data is limited to the three main regions of exposure: northern, southeast and on the peninsula (Hansen and Wemmer 2011). The 'basement' rocks in Thailand, most of which are medium to high grade regional metamorphic rocks, were described as 'Pre-Permian' by Javanaphet (1969). In recent years, radiometric dating yielded basement ages ranging from Cambrian to Paleogene (Kanjanapayont et al. 2012; Kawakami et al. 2014; Lin et al. 2013).

While there are sparse basement exposures, granitoid plutons are common throughout Thailand, and are useful for understanding the nature of the unexposed basement (Charusiri et al., 1993; Cobbing, 2011). These granitoids formed during the stages of subduction and orogenesis (Ng et al., 2015a; Ng et al., 2015b; Searle et al., 2012) and also are part of the Southeast Asian Tin Belt, one of the world's most productive and largest sources of metallic mineral deposits, especially Sn and Cu (Cobbing et al., 1992; Schwartz et al., 1995; Searle et al., 2012).

There are two main events that led to this granite emplacement: the Permo-Triassic closure of the Palaeo-Tethys Ocean (and the resultant Indosinian Orogeny) and the Mesozoic–Paleogene closure of the Neo-Tethys Ocean (Gardiner et al., 2016; Searle et al., 2012; Sone and Metcalfe, 2008). The Indosinian Orogeny currently encompasses all late Paleozoic to early Mesozoic orogenesis throughout Asia: from China (Gao et al., 2017; Li et al., 2004), Vietnam (Halpin et al., 2016; Lepvrier et al., 2004), to Thailand (e.g. Barr and Macdonald, 1991; Metcalfe, 2013; Sone and Metcalfe, 2008). However, the precise timing of the individual collisional events that make up the Indosinian Orogeny remains uncertain. The earliest events of the Indosinian Orogeny are latest Permian to Lower Triassic in age and include the collision of South China with Indochina (e.g. Faure et al., 2014). However, the collision of Indochina and Sukhothai terranes with Sibumasu is controversial, and may possibly have been diachronous, with the proposed timing of collision ranging all throughout the Triassic (e.g. Barber et al., 2011; Faure et al., 2014; Hara et al., 2013; Morley et al., 2013; Sone and Metcalfe, 2008).

Isotopic systems provide important information on the crust's evolution and can be spatially modelled to highlight reworked continental crust and juvenile material (Kemp et al., 2006; Liew and McCulloch, 1985). The aim of this study is to use granites as a probe to further develop our understanding of the underlying basement in Thailand. To do this, we use zircon U–Pb geochronology and Lu–Hf isotopic signatures and whole-rock Sr, Pb and Nd geochemistry of granitoids. Together, these signatures assist in unravelling Thailand's complex evolution and help strengthen our understanding of Southeast Asian tectonics.

1.1 Terranes of Thailand

Throughout Thailand, the main tectonic terranes (Sibumasu, Sukhothai and Indochina; Fig. 1) predominantly trend north–south. This trend is not just visible in the main terranes but also in the suture zones, including the Inthanon Zone, coloured purple in Fig. 1.

The Sibumasu Terrane has been variably defined in the past (Audley-Charles et al., 1988; Hisada et al., 2004; Metcalfe, 1984), but here will be defined as the basement of Peninsula Thailand, which extends north into eastern–central Myanmar, east to the Chiang Rai Line and south through the western Malay Peninsula as defined by Gardiner et al. (2016). The name, Sibumasu, is a combination of its constituents: *Si*am-Thailand and *Si*no-China-*Bu*rma-*Ma*laysia-*Su*matra. The Sibumasu Terrane is a ribbon-like continent that is equivalent to the South Qiangtang Terrane in Tibet, and the Baoshan and Tengchong terranes in southwest China (Ali et al., 2013; Jiang et al., 2017). It contains tin-bearing, continental collision S-type granites emplaced between 220–200 Ma (Gardiner et al., 2016; Schwartz et al., 1995; Searle et al., 2012). Paleozoic sedimentary rocks, including early Permian glaciomarine diamictites, from the Sibumasu Terrane show Gondwanan biogeographic affinities (Metcalfe, 1984; 2013; Schwartz et al., 1995; Sevastjanova et al., 2011).

The Inthanon Zone represents the convergence zone between the Sukhothai, Indochina and Sibumasu terranes (Hara et al., 2013; Sone and Metcalfe, 2008). It contains deep-water sequences (thought to be remnants of the Palaeo-Tethys Ocean) that have been caught up in an

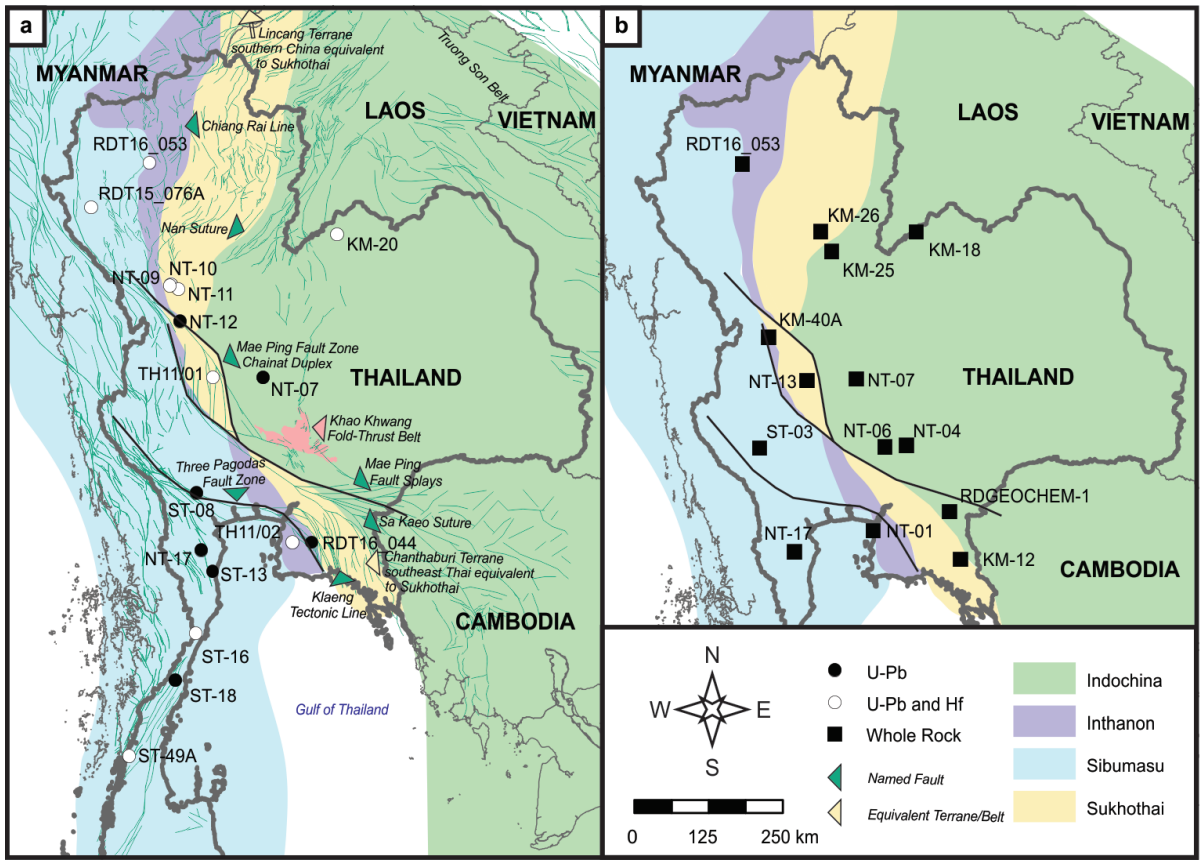

Fig. 1. a (left): Regional map showing the major tectonic subdivisions and the granitoid sample localities for zircon U–Pb and Hf analyses. Structure and tectonic domains discussed in text are highlighted with arrows. b (right): Regional map showing major terranes and the granitoid sample localities for whole-rock analyses.

accretionary prism and was subsequently thrust westwards onto the eastern margin of the Sibumasu Terrane (Barber et al., 2011; Barr and Macdonald, 1991; Hara et al., 2012). The Inthanon Zone also contains deformed sequences from the continental margin of the Sibumasu Terrane including metamorphic rocks of unknown age, Cambrian sandstone, Ordovician limestone and Silurian–Carboniferous sedimentary rocks (Hara et al., 2012; Ueno and Charoentitirat, 2011). Barr and Macdonald (1991) introduced the term 'Inthanon Zone' to describe the high grade metamorphic rocks of the Doi Inthanon and Doi Suthep areas, including the detached Paleozoic cover rocks of the Sibumasu Terrane. Usage of this term has since distorted, instead referring to a region containing relics of the Palaeo-Tethys oceanic domain (see Fig. 1).

The Sukhothai Terrane is thought to be equivalent to the Chanthaburi Terrane in southeast Thailand and the Lincang Terrane of southern China (Fig. 1; Sone and Metcalfe, 2008). This region contains the remnants of an arc and its associated short-lived basin (e.g. Sone and Metcalfe, 2008; Metcalfe, 2013). The Sukhothai Terrane is dominated by a Permo-Triassic deformed fore-arc basin sequence and overlying late Permian–Triassic shallow marine molasse-type sedimentary rocks (Chaodumrong, 1992; Hara et al., 2017). The Sukhothai Terrane also includes

Permo-Triassic metaluminous granitoids with an I-type affinity (Sone and Metcalfe, 2008; Sone et al., 2012). Indosinian-aged deformation occurred in the "Sukhothai Fold Belt", with the resultant cleavage giving a K–Ar age between 220–188 Ma (Ahrendt et al., 1993). During the Carboniferous and Permian, the Nan basin has been interpreted to have separated the Sukhothai and Indochina terranes (Barr and Macdonald, 1987; Qian et al., 2016; Sone and Metcalfe, 2008; Ueno and Hisada, 2001). This, supposedly, short-lived back-arc basin, is preserved as a narrow N–S trending and discontinuous ophiolite belt known as the Nan–Uttaradit Suture in northern Thailand and Sa Kaeo Suture in the southeast of the country (Fig. 1; Sone and Metcalfe, 2008; Ueno and Hisada, 2001). This suture zone is a mélange complex of gabbro (zircon U–Pb age of 311 ± 10 Ma), tholeiitic meta-basalt (zircon U–Pb age of 316 ± 3 Ma), andesite and radiolarian chert lithologies (Barr and Macdonald, 1987; Sone et al., 2012).

The Indochina Terrane extends across large expanses of Laos, Vietnam, Cambodia, Malaysia and Thailand (Fig. 1). There is evidence that it may be a composite terrane comprised of multiple micro-terranes, potential sutures, metamorphic complexes and mylonitic fault zones (Lepvrier et al., 2004; Sone and Metcalfe, 2008). Within Thailand, the Indochina Terrane encompasses all of Thailand east of the Sukhothai Terrane. The granitoids from the Indochina Terrane are mostly metaluminous I-type granitoids that are related to Cu–Fe–Au–Sb mineralisation (Charusiri et al., 1993; Salam et al., 2014; Zaw et al., 2014). Mesozoic and Cenozoic sediments cover the Indochina Terrane throughout most of Thailand, however basement rocks, up to granulite-facies, are exposed in Vietnam, Laos and Cambodia (Nakano et al., 2018; Shi et al., 2015; Wang et al., 2016b). Model ages and inherited zircons suggest that the main crust of the Indochina Terrane formed in the Paleoproterozoic to Mesoproterozoic (Lan et al., 2003; Shi et al., 2015; Wang et al., 2016b). There is evidence that the high grade metamorphism of basement rocks such as the Kontum Massif and the Truong Son Belt were caused by the multi-phased Indosinian Orogeny, often specifically attributed to the oblique collision of the Indochina and South China terranes (see Halpin et al., 2016; Lan et al., 2003; Lepvrier et al., 2004; Nakano et al., 2018). However, no data are available on the nature of the buried Indochina basement that underlies eastern Thailand.

1.2 Proterozoic to Triassic tectonic evolution

Previous studies have located the Indochina and Sibumasu terranes within the Gondwana supercontinent during the Proterozoic to early Paleozoic, with Sibumasu off the margin of northern Australia and Indochina further outboard (Bunopas, 1981; Burrett et al., 2014; Cocks and Torsvik, 2013; Usuki et al., 2013). In the past, there has been much debate on the origin of Sukhothai Terrane, however, it is now acknowledged to be an arc system built on older continental material (Hara et al., 2017; Sevastjanova et al., 2011).

The northern Gondwana margin was tectonically dynamic in the Cambro-Ordovician, when strike-slip faulting caused Indochina and South China to begin moving eastwards (Cocks and Torsvik, 2013). Indochina, South China and northern Tibet separated from Sibumasu and other remnants of Gondwana as the southern Palaeo-Tethys Ocean opened in the Lower Devonian (Cocks and Torsvik, 2013; Hara et al.,

2012; Metcalfe, 2013). This ocean covered the equatorial region from the Devonian to the Triassic, where carbonates and pelagic chert were deposited (Cocks and Torsvik, 2013; Hara et al., 2012; Metcalfe, 2013). The preserved Palaeo-Tethyan rocks are characterised by ocean plate stratigraphy, and were later subducted during the Permian–Triassic under the Indochina Terrane (Cai et al., 2017; Metcalfe, 2013; Wakita and Metcalfe, 2005).

Previously published plate-tectonic models (e.g. Li et al., 2004; Metcalfe, 2013) suggest that by the Carboniferous, the South China and Indochina terranes were located in equatorial to low northern palaeolatitudes. The Indochina Terrane became a stable carbonate shelf in the middle Carboniferous (Ueno and Charoentitirat, 2011). By the late Carboniferous, carbonate platforms developed along the margin of the Indochina Terrane (Dew et al., 2018; Ueno and Charoentitirat, 2011; Wielchowsky and Young, 1985). Rift-grabens filled with glacial-marine sediments derived from Gondwana, indicate that during the early Permian, the Sibumasu Terrane rifted from the Himalayan-Australian margin of Gondwana (Burrett et al., 2014; Metcalfe, 2013). This northward movement of the Sibumasu Terrane is thought to have opened the Meso-Tethys Ocean (Burrett et al., 2014). The late Carboniferous–early Permian sparked the start of the destruction of the main Palaeo-Tethys Ocean, with subduction northwards beneath the Indochina Terrane (Li et al., 2004; Metcalfe, 2013; Sone et al., 2012). In this model, as subduction continued, slab rollback caused the Nan back-arc basin to open between the Indochina and the Sukhothai terranes (Metcalfe 2013). Subduction of the Palaeo-Tethys Ocean formed an accretionary wedge of "ocean plate stratigraphy" and caused the arc magmatism of the Sukhothai Terrane (Barr et al., 2006; Qian et al., 2016).

The Indosinian Orogeny led to granite emplacement throughout much of Thailand, often described as the Central/Main Range and Eastern Granitoid Provinces (Cobbing, 2011; Searle et al., 2012). The timing of the collision between Indochina and Sibumasu is yet to be detailed, and current constraints range from latest Permian to late Triassic (Barber et al., 2011; Cai et al., 2017; Hara et al., 2012; Metcalfe, 2013; Wakita and Metcalfe, 2005). The early stage of this orogenic event is thought to be driven by the collision of northern margin of the Indochina Terrane with the South China Terrane (Arboit et al., 2014; Lepvrier et al., 2004; Metcalfe, 2013; Morley et al., 2013). Contemporaneously, or following the South China–Indochina terrane collision, the Nan basin closed and subsequently thrust the Sukhothai Terrane over the Indochina Terrane (Lepvrier et al., 2004; Morley et al., 2013). On the southern margin of the Khorat continental fragment of the Indochina Terrane, the Khao Khwang Platform was deformed resulting in the Khao Khwang Fold and Thrust Belt (Arboit et al., 2016; Dew et al., 2018; Morley et al., 2013; Sone and Metcalfe, 2008). The age of this collision, which was possibly related to the closure of a small oceanic basin between different Indochina Terrane fragments, is marked by granite emplacement at a peak age of ~241 Ma (Meffre et al., 2008). In the Khorat Plateau of central Thailand, the end of this early Indosinian event (sometimes known as Indosinian I) is defined by an unconformity whereby the deformed Permian and older units are overlain by late Triassic (~220 Ma) Kuchinarai Group rift-related sediments (Booth and

Sattayarak, 2011). The later Indosinian Orogeny (referred to as the Indosinian II event) is thought to be related to the collision of the Sibumasu Terrane to the Sukhothai and Indochina terranes (Booth and Sattayarak, 2011; Morley et al., 2013). The sediments of the Sibumasu Terrane were thrust underneath the accretionary complex of the Sukhothai Terrane with the closure of the subduction zone (Sone and Metcalfe, 2008).

2. Methodology

2.1 Sample acquisition

Twenty-eight granitoid samples in total are used for this study. The sampling strategy for this study was to collect granitoids from all three terranes and across major faults and sutures to better delineate tectonic boundaries. Representative samples of granitoids, and therefore also their underlying basement, were collected from widespread localities within Thailand. The individual sample locations and lithology and analysis method for each sample are outlined in Table 1. For further details on the sample preparation and petrographic descriptions see Dew et al. (2018b).

2.2 U–Pb zircon geochronology

Eighteen granitoid rock samples were used for zircon analyses. Details of the preparatory methods and analytical conditions are summarised by Dew et al. (2018b). All cathodoluminescence (CL) imagery and laser ablation inductively coupled plasma mass spectrometry (LA–ICP–MS) was completed at Adelaide Microscopy, Adelaide, South Australia. The GEMOC zircon standard GJ-1 ($^{206}Pb/^{238}U$ TIMS age of 600.7 ± 1.1 Ma) was run as the primary standard every 10–20 unknown analyses, to correct for isotopic drift and down-hole fractionation. Across all analytical sessions, analyses of GJ-1 yielded a $^{206}Pb/^{238}U$ weighted average age of 601.61 ± 0.47 Ma (n=556, MSWD=1.10). For further information on the zircon standards, analytical parameters and reduction techniques, see Dew et al. (2018b).

2.3 Zircon Lu–Hf isotope analysis

After the U–Pb zircon geochronology analyses, ten of these granitoid samples were selected for further zircon Lu–Hf isotope analysis. A subset of the zircon grains for each sample were then analysed for their hafnium isotopic composition (the specific grains analysed and their concordance percentage are highlighted in Appendix A). The number of Hf analyses for each sample was determined by the variability in the age data and the amount of interpreted inheritance. For individual zircon U–Pb ages that were interpreted to be indicative of the overall granitoid crystallization age, the weighted average age of the granitoid was used to calculate the initial $^{176}Hf/^{177}Hf$. For interpreted inherited zircons the age of the individual analysis was used to calculate the initial $^{176}Hf/^{177}Hf$. Ten samples used for Hf and Lu isotopic analyses (all samples except KM-20) were analysed using a Resonetics S-155-LR 193nm excimer laser ablation system connected to a Nu Plasma II multi-collector ICP–MS in the GeoHistory Facility, John de Laeter Centre, Curtin University, Perth, Western Australia. Hafnium analysis for one sample (KM-20) was undertaken using a Neptune Plus multi-collector ICP–MS at the University of Wollongong, New South Wales. For further information on standards, analytical parameters, correction and reduction techniques, see Dew et al. (2018b).

2.4 Sm–Nd, Sr and Pb whole-rock geochemistry

Sm–Nd and Sr isotopic whole-rock

Table 1. Descriptions and localities for samples in this study. Mineral abbreviations are as follows: quartz (Qtz), plagioclase (Pl), K-feldspar (Kfs), microcline (Mc), pyroxene (Px), clinopyroxene (Cpx), orthopyroxene (Opx), hornblende (Hbl), biotite (Bt), muscovite (Mu), garnet (Gt), chlorite (Chl), sillmanite (Sill), tourmaline (To), epidote (Ep), sphene (Sp) and fluorite (Fl).For further petrographic information, see in-table references and Chapter 2B. All age uncertainties where given are 2σ.

Sample Number	*Latitude*	*Longitude*	*Lithology*	*Mineralogy*	*Previous description or affinity*	*Interpreted U–Pb Age (Ma)*	*Age Source*	*Lu–Hf*	*Sr, Sm–Nd*	*Pb*
KM-12	12°54'38.52"N	102°14'29.58"E	granodiorite	Holocrystalline, Qtz + Pl + Kfs + Bt + Mu + Chl	Eastern Province Late Triassic I-type granite (on Kawakami et al. 2014 map)	217 ± 3	Nearby granite Th 18/95 (Hansen and Wemmer, 2011)		✔	
KM-18	17°47'12.18"N	101°34'34.08"E	qtz-diorite	Holocrystalline, equigranular Qtz + Pl + Hbl + Px	Mapped as a granodiorite by Intasopa and Dunn (1994) Eastern Granitoid Province	229.9 ± 1.7	Nearby U–Pb data KM-20		✔	
KM-20	17°43'53.34"N	101°47'4.14"E	granodiorite	Holocrystalline, Qtz + Pl + Kfs	Eastern Granitoid Province	229.9 ± 1.9	Weighted average $^{206}Pb/^{238}U$ age This Study	✔		
KM-25	17°29'40.08"N	100°18'7.20"E	tonalite	Holocrystalline, Qtz + Pl + Kfs + Bt + Chl + Mu + Sill + Ep	Eastern Granitoid Province	296 ± 20	Nearby U–Pb age by (Meffre et al., 2008b)		✔	✔
KM-26	17°47'31.98"N	100° 7'48.30"E	tonalite	Holocrystalline, Qtz + Pl + Bt + Chl + Cpx + Mu + Sill + Sp	Eastern Granitoid Province	296 ± 20	Nearby U–Pb age by (Meffre et al., 2008b)		✔	✔
KM-40A	16°12'57.18"N	99°16'42.84"E	granite	Holocrystalline, Qtz + Kfs + Pl + Bt + Chl + Mu		238.0 ± 2.9	Nearby U–Pb data NT-12		✔	✔
NT-01	13°20'22.50"N	100°55'28.80"E	biotite granite	Holocrystalline, Bt + Qtz + Kfs + Pl + Chl + Mu	Main Range Granitoid Province	229 +21/−27	Nearby sample Th 22/95 (Hansen and Wemmer, 2011)		✔	✔
NT-04	14°36'29.50"N	101°25'21.90"E	quartz diorite	Holocrystalline, Qtz + Pl + Kfs + Sp + Hbl + To	Eastern Granitoid Province	241 ± 6	Nearby Pak Chong granodiorite age quoted by Arboit et al. (2016)		✔	
NT-06	14°34'56.40"N	101° 6'13.40"E	amphibolitic gabbro-diorite	Holocrystalline, Hbl + Pl + Kfs + Chl + Sp	Eastern Granitoid Province	241 ± 6	Nearby Pak Chong granodiorite age quoted by Arboit et al. (2016)		✔	

Table 1 (continued). Descriptions and localities for samples in this study. Mineral abbreviations are as follows: quartz (Qtz), plagioclase (Pl), K-feldspar (Kfs), microcline (Mc), pyroxene (Px), clinopyroxene (Cpx), orthopyroxene (Opx), hornblende (Hbl), biotite (Bt), muscovite (Mu), garnet (Gt), chlorite (Chl), sillmanite (Sill), tourmaline (To), epidote (Ep), sphene (Sp) and fluorite (Fl).For further petrographic information, see in-table references and Chapter 2B. All age uncertainties where given are 2σ.

Sample Number	*Latitude*	*Longitude*	*Lithology*	*Mineralogy*	*Previous description or affinity*	*Interpreted U–Pb Age (Ma)*	*Age Source*	*Lu–Hf*	*Sr, Sm–Nd*	*Pb*
NT-07	15°35'57.10"N	100°40'9.80"E	quartz diorite	Holocrystalline, porphyritic-phaneritic Qtz + Pl + Hbl + Kfs + Chl + Mu	Eastern Granitoid Province	273.5 ± 3.9	Weighted average $^{206}Pb/^{238}U$ age This Study		✔	
NT-09	16°59'32.90"N	99°16'34.90"E	diorite - monzonite	Holocrystalline, Pl + Kfs + Hbl + Qtz + Chl + Bt + Mu	Tak Batholith	226.5 ± 1.8	Weighted average $^{206}Pb/^{238}U$ age This Study	✔		
NT-10	16°59'32.90"N	99°16'34.90"E	(leuco) granite	Holocrystalline, Qtz + Kfs + Pl + Bt + Chl	Tak Batholith	236.2 ± 2.9	Discordia lower intercept This Study	✔		
NT-11	16°55'16.10"N	99°23'19.00"E	granite	Holocrystalline, Qtz + Kfs + Bt + Sp + Ep	Tak Batholith	228.7 ± 2.1	Weighted average $^{206}Pb/^{238}U$ age This Study	✔		
NT-12	16°26'12.20"N	99°24'49.80"E	granodiorite	Holocrystalline. Qtz + Pl + Kfs + Chl + Bt + Mu + Gt	Tak Batholith	238.0 ± 2.9	Discordia lower intercept This Study			
NT-13	15°34'28.20"N	99°55'0.80"E	granite-adamellite	Holocrystalline, Qtz + Kfs + Pl + Bt + Mu + Gt		227.9 ± 1.9	Nearby U–Pb data Th11/01		✔	✔
NT-17	13° 1'23.00"N	99°44'11.30"E	granite	Holocrystalline, porphyritic-phaneritic, Qtz + Kfs + Mu + Pl	Mogok–Mandalay–Mergui Belt	214.15 ± 0.87	Concordant (<20% discordant) zircon rims weighted average $^{206}Pb/^{238}U$ age This Study		✔	✔
RDT15_076A	18° 9'5.00"N	98° 4'7.00"E	altered granodiorite	Holocrystalline, Pl + Qtz + Mu + Fl	Similar to Mae Lama pluton	No crystallisation identified	Inherited ages only	✔		
RDT16_044	13°10'12.00"N	101°24'2.00"E	migmatite	Holocrystalline, banded, Qtz + Pl + Mu + Gt	Mylonitic gneiss (on Kawakami et al. 2014 map)	73.3 ± 3.7	$^{206}Pb/^{238}U$ age of youngest near concordant zircon This Study			
RDT16_053	18°48'4.00"N	98°56'47.48"E	adamellite	Holocrystalline, Qtz + Pl + Kfs + Bt + Chl		204.1 ± 1.6	Weighted average $^{206}Pb/^{238}U$ age This Study	✔	✔	✔

Table 1 (continued). Descriptions and localities for samples in this study. Mineral abbreviations given on previous page. For further petrographic information, see in-table references and Chapter 2B. All age uncertainties where given are 2σ.

Sample Number	*Latitude*	*Longitude*	*Lithology*	*Mineralogy*	*Previous description or affinity*	*Interpreted U–Pb Age (Ma)*	*Age Source*	*Lu–Hf*	*Sr, Sm–Nd*	*Pb*
RDGEOCHEM-1	13°37'05"N	102°4'47"E	granodiorite	Holocrystalline, perthitic textures Qtz + Kfs + Pl + Mc + opaques	Late Triassic I-type granite (on Kawakami et al. 2014 map) Eastern Granitoid Province	203 ± 8	Nearby U–Pb data by Muller *et al.* (1999) collated by Zaw et al. (2014)		✔	
ST-03	14°34'5.10"N	99°12'13.90"E	granodiorite with tourmaline pegmatite	Holocrystalline, Pl + Kfs + Qtz + Bt + Hbl + Chl + Mu	Mogok–Mandalay–Mergui Belt	213.6 ± 2.9	Nearby U–Pb data ST-08A		✔	
ST-08A	13°52'32.60"N	99°39'50.70"E	*(grano)diorite*	Holocrystalline, phaneritic, Pl + Kfs + Qtz + Bt + Hbl + Chl + Mu	Mogok–Mandalay–Mergui Belt	213.6 ± 2.9	Weighted average $^{206}Pb/^{238}U$ age This Study			
ST-13	12°42'27.40"N	99°54'7.60"E	*granite*	Holocrystalline, Kfs + Qtz + Pl + Bt	Hub Kapong (on Kawakami et al. 2014 map)	210.9 ± 1.1 (magmatic) 80.72 ± 0.79 (metamorphic)	Weighted average $^{206}Pb/^{238}U$ age This Study			
ST-16	11°47'23.60"N	99°38'56.10"E	*granite*	Holocrystalline, Kfs + Qtz + Pl + Bt + Chl + Mu	Mogok–Mandalay–Mergui Belt (DeClerq 2016)	501 ± 15	Weighted average $^{206}Pb/^{238}U$ age This Study	✔		
ST-18	11° 5'5.00"N	99°20'20.00"E	*granodiorite*	Holocrystalline, Qtz + Pl + Kfs	Mogok–Mandalay–Mergui Belt (DeClerq 2016)	76.26 ± 0.82	Weighted average $^{206}Pb/^{238}U$ age This Study			
ST-49A	9°57'32.80"N	98°38'37.20"E	*granite*	Holocrystalline, Kfs + Qtz + Mu + Pl + Chl + Mu + Gt	Mogok–Mandalay–Mergui Belt	81.4 ± 1.1	Weighted average $^{206}Pb/^{238}U$ age This Study	✔		
TH11/01	15°36'2.52"N	99°54'49.91"E	*granite*	Holocrystalline, Kfs + Pl + Qtz		227.9 ± 1.9	Weighted average $^{206}Pb/^{238}U$ age This Study	✔		
TH11/02	13° 8'49.66"N	101° 6'43.01"E	*granite*	Holocrystalline, Kfs + Qtz + Mu + Pl	Main Range Granitoid Province	207.1 ± 1.3	Weighted average $^{206}Pb/^{238}U$ age (±20% discordance) This Study	✔		

analyses were conducted for fourteen granitoid samples and one duplicate run for Sm–Nd analyses (NT-13) at the University of Adelaide's Isotope Geochemistry Facility (see Table 1). Eight samples and one duplicate (NT-13) were used for whole-rock Pb isotope measurements (see Table 1). These samples were chosen due to their spatial distribution across the main tectonic terranes in Thailand (see Fig. 1), and also containing Nd, Sr and Pb elemental concentrations above the detection limits of the x-ray fluorescence spectrometer (XRF) at Franklin and Marshall College, U.S.A. Details of analytical conditions, standards and sample preparation are summarised in Dew et al. (2018b).

3. Results

3.1 U–Pb zircon geochronology

The age of the granitoids in Thailand is mostly well constrained (Cobbing, 2011; Hansen and Wemmer, 2011; Salam et al., 2014; Searle et al., 2012). Additional granitoid ages have been determined in this study, specifically to better constrain the isotopic data collected (Lu–Hf, Sr, Sm–Nd and Pb) for their age, and to target any inherited components.

The morphologies and internal structure of the zircons analysed using LA–ICP–MS are documented in Fig. 2. Concordia plots were created using Isoplot (Ludwig, 1998), and are displayed in Fig. 3. The crystallisation ages are interpreted from data within ±5% discordance using the ($^{206}Pb/^{238}U$ age)/ $^{207}Pb/^{235}U$ age) calculation. Some analyses clearly show the effects of radiogenic lead loss with anomalously young apparent $^{206}Pb/^{238}U$ ages. Crystallisation ages from these samples were also determined using regression techniques where appropriate. Outliers were rejected after subsequent examination, if the laser beam traversed cracks or overlapped with multiple zircon domains within the grain. For further information on the U–Pb LA–ICP–MS data see Dew et al. (2018b).

3.1.1 Sibumasu Terrane

Crystallisation ages for granitoids from the Sibumasu Terrane vary from the Cambrian to the Cretaceous. The interpreted crystallisation age for ST-16 was the weighted average age of the cluster of concordant analyses yielding a $^{206}Pb/^{238}U$ age of 501 ± 15 Ma (n=4, MSWD=1.4; Fig. 3, Dew et al. (2018b) Table 4). Analyses from ST-16 that were younger than Cambrian in age had very low Th:U, suggesting that the large Th ion has diffused from the zircon during a subsequent thermal event. The observation that young $^{206}Pb/^{238}U$ age zircons have low Th:U suggests that both Pb and Th have been lost from the zircon. This is supported by petrographic observations of igneous garnet breaking down to muscovite, chlorite and biotite (Dew et al. (2018b), Fig. 1—mm, nn). The interpreted crystallisation age for NT-17 is the weighted average of the cluster of concordant (±5%) analyses yielding a $^{206}Pb/^{238}U$ age of 214.15 ± 0.87 Ma (n=10, MSWD=0.89; Fig. 3). For ST-08A, concordant (±5%) analyses all with Th:U>0.19 yielded a weighted average $^{206}Pb/^{238}U$ age of 213.6 ± 2.9 Ma (n=9, MSWD=3.1; Fig. 3). The crystallisation age of ST-13 was determined from the concordant (±5%) analyses all with Th:U>0.1, which yielded a weighted average $^{206}Pb/^{238}U$ age of 210.9 ± 1.1 Ma (n=23, MSWD=1.2). A younger cluster of data with low Th:U was interpreted to be the age of metamorphic resetting, yielding a weighted average $^{206}Pb/^{238}U$ age of 80.72 ± 0.79 Ma (n=5, MSWD=0.58). The crystallisation age of ST-49A was

Fig. 2. Representative cathodoluminescence images for all granitoid rocks sampled in Thailand. U–Pb laser, Hf spots shown. The age given for each spot is the $^{206}Pb/^{238}U$ age, unless marked with an asterisk (*) indicating that the $^{207}Pb/^{206}Pb$ age is given. Individual spot $\varepsilon Hf_{(t)}$ values are given.

determined from the cluster of concordant (±5%) data analyses yielding a $^{206}Pb/^{238}U$ age of 81.4 ± 1.1 Ma (n=6, MSWD=0.37). The interpreted crystallisation age for ST-18 was determined by the weighted average of concordant (±5%) zircon analyses, yielding a $^{206}Pb/^{238}U$ age of 78.26 ± 0.82 Ma (n=10, MSWD=1.5; Fig. 3).

Analyses from RDT15_076A included many inherited ages with no crystallisation age evident in the data collected (see Fig.

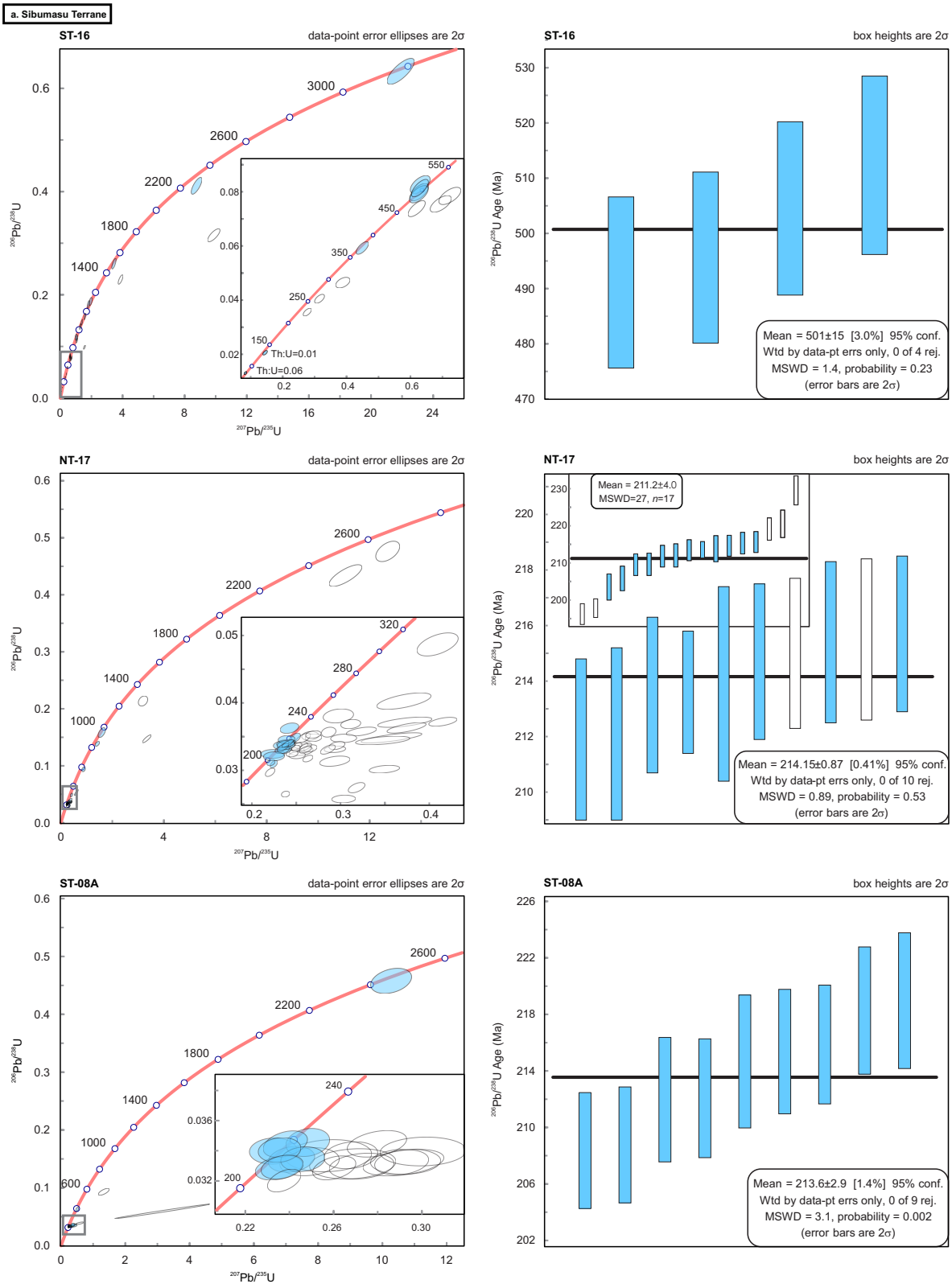

Fig. 2. Concordia diagrams and weighted averages for each U–Pb sample, grey box indicates extent of expanded concordia diagram where applicable. All age uncertainties are quoted at the two sigma level and MSWDs are quoted for each calculated age. Data with Th:U<0.1 are coloured white on weighted average plots. **a:** U–Pb data for samples from the Sibumasu Terrane, coloured blue.

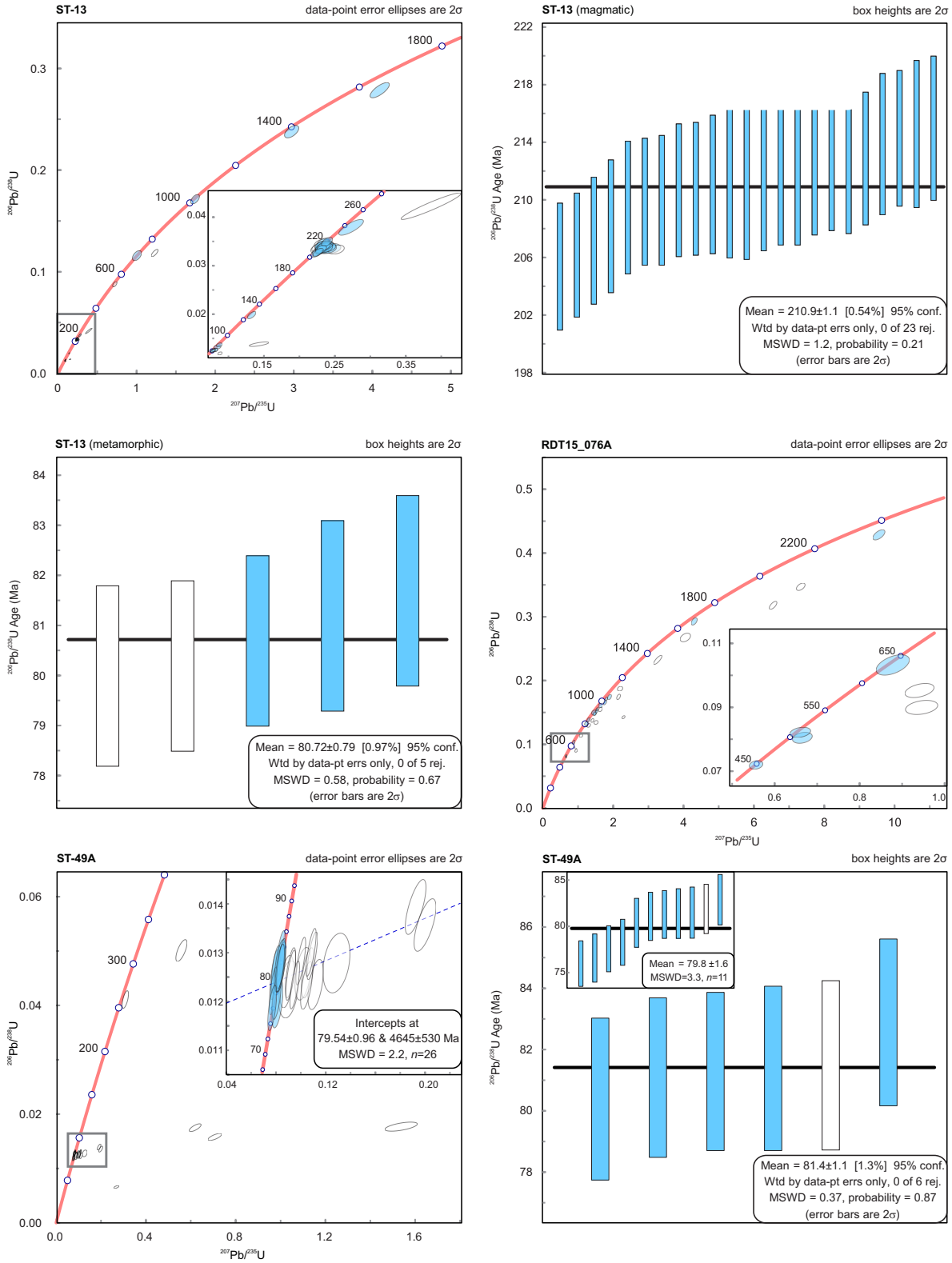

Fig. 2. Concordia diagrams and weighted averages for each U–Pb sample, grey box indicates extent of expanded concordia diagram where applicable. All age uncertainties are quoted at the two sigma level and MSWDs are quoted for each calculated age. Data with Th:U<0.1 are coloured white on weighted average plots. **a:** U–Pb data for samples from the Sibumasu Terrane, coloured blue.

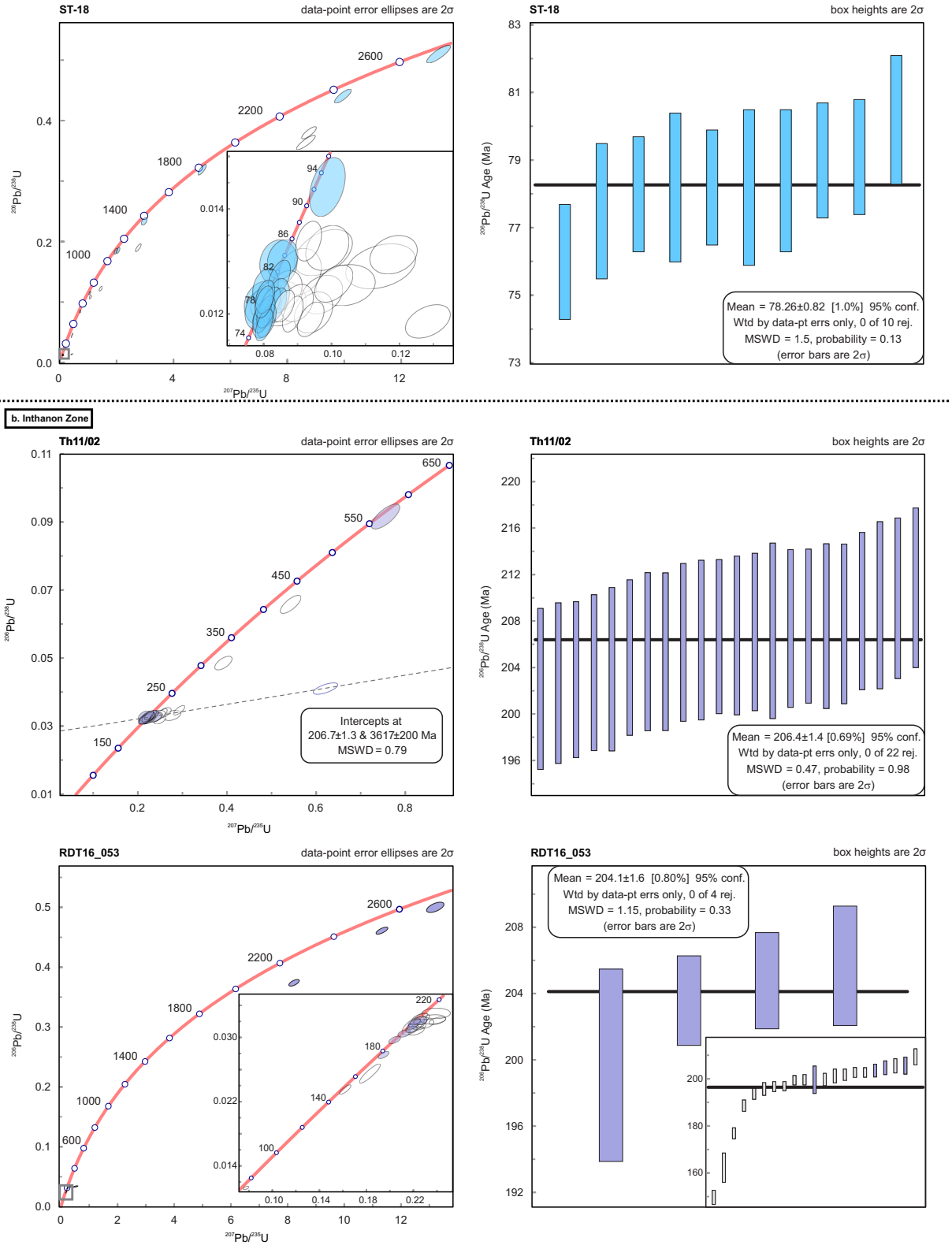

Fig. 2. Concordia diagrams and weighted averages for each U–Pb sample, grey box indicates extent of expanded concordia diagram where applicable. All age uncertainties are quoted at the two sigma level and MSWDs are quoted for each calculated age. Data with Th:U<0.1 are coloured white on weighted average plots. **a:** U–Pb data for samples from the Sibumasu Terrane, coloured blue. **b:** U–Pb data for samples from the Inthanon Zone, coloured purple.

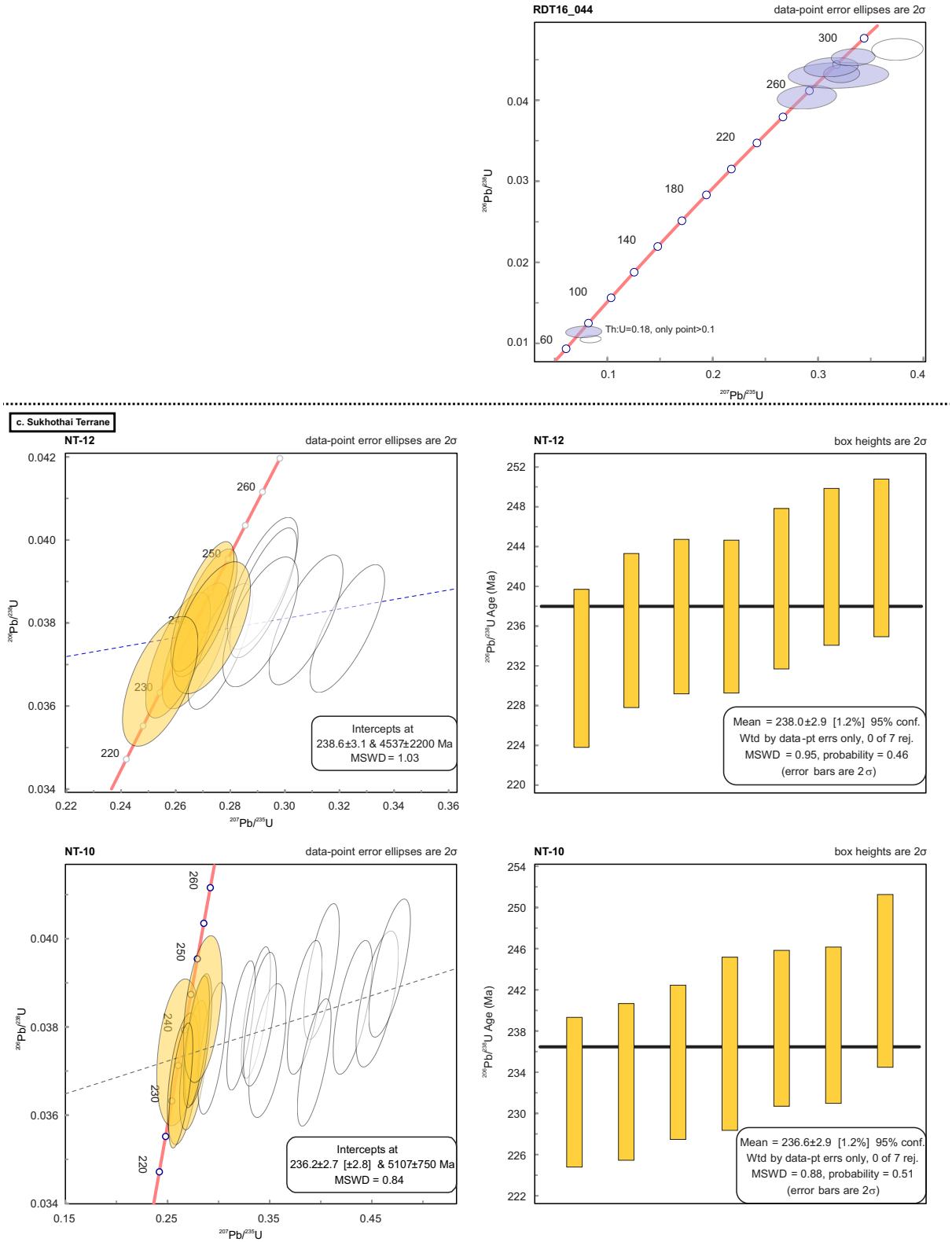

Fig. 2. Concordia diagrams and weighted averages for each U–Pb sample, grey box indicates extent of expanded concordia diagram where applicable. All age uncertainties are quoted at the two sigma level and MSWDs are quoted for each calculated age. Data with Th:U<0.1 are coloured white on weighted average plots. **b:** U–Pb data for samples from the Inthanon Zone, coloured purple, **c:** U–Pb data for samples from the Sukhothai Terrane, coloured yellow-orange.

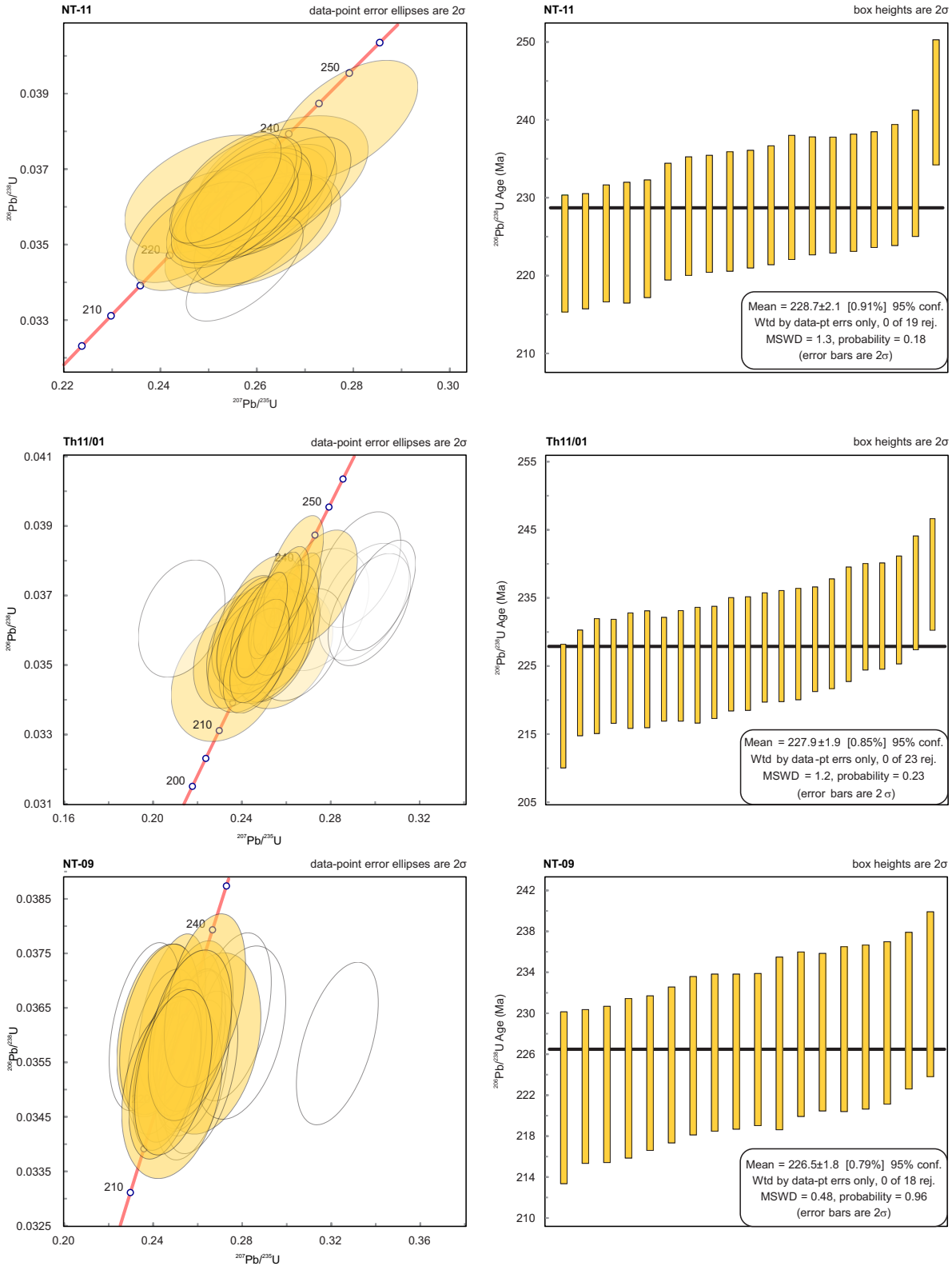

Fig. 2. Concordia diagrams and weighted averages for each U–Pb sample, grey box indicates extent of expanded concordia diagram where applicable. All age uncertainties are quoted at the two sigma level and MSWDs are quoted for each calculated age. Data with Th:U<0.1 are coloured white on weighted average plots. **c:** U–Pb data for samples from the Sukhothai Terrane, coloured yellow-orange.

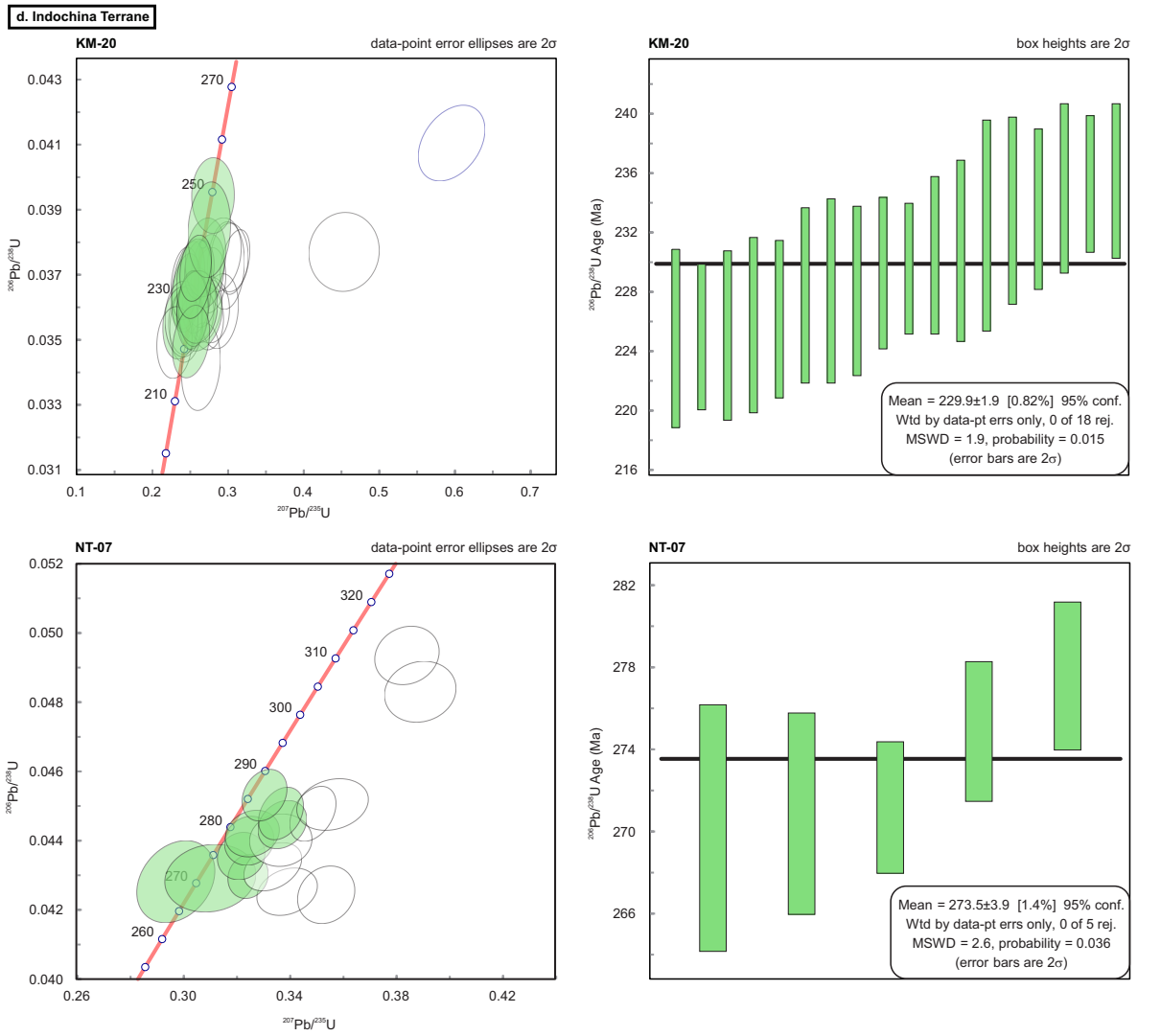

Fig. 2. Concordia diagrams and weighted averages for each U–Pb sample, grey box indicates extent of expanded concordia diagram where applicable. All age uncertainties are quoted at the two sigma level and MSWDs are quoted for each calculated age. Data with Th:U<0.1 are coloured white on weighted average plots. **d:** U–Pb data for samples from the Indochina Terrane, coloured green.

2 and 3). Interpreted inherited zircon analyses from the Sibumasu Terrane ranged in age from $^{207}Pb/^{206}Pb$ age of 3189.3 ± 17.8 Ma to $^{206}Pb/^{238}U$ age of 371.5 ± 5.8 Ma, with age peaks at 2725 Ma, 2491 Ma, 1360 Ma, 1090 Ma, 940 Ma, 840 Ma, 700 Ma and 500 Ma (see Fig. 3). For further details on the age determination, please see Dew et al. (2018b).

3.1.2 Inthanon Zone

Three samples from the Inthanon Zone were analysed for U–Pb zircon geochronology. Concordant (±5%) zircon analyses from Th11/02 with Th:U>0.1 yield a tightly constrained age magmatic age of 206.4 ± 1.4 Ma (n=22, MSWD=0.47, Fig. 3). The interpreted crystallisation age for RDT16_053 is the weighted average of all concordant (±5%) analyses with Th:U>0.1, yielding a $^{206}Pb/^{238}U$ age of 204.1 ± 1.6 Ma (MSWD=1.15, n=4). The interpreted crystallisation age for RDT16_044 is the youngest concordant grain yielding a $^{206}Pb/^{238}U$ age of 73.3 ± 3.7 Ma. The Th:U of this zircon is >0.1

however, the majority of the analyses from this sample have low Th:U indicating that both Pb and Th have been lost from the zircon during subsequent thermal events. The interpreted inherited analyses ranged from a $^{207}Pb/^{206}Pb$ age of 2746 ± 29 Ma to a $^{206}Pb/^{238}U$ age of 258.8 ± 4.2 Ma (see Fig. 3). There is a concentration of middle Permian ages from interpreted inherited ages from the Inthanon Zone samples with an age peak at 270 Ma.

3.1.3 Sukhothai Terrane

All five samples taken from the Sukhothai Terrane yielded magmatic ages within 15 Ma, between 238 and 224 Ma. No concordant inherited zircons were found from any of these samples (coloured yellow in Fig. 3). The interpreted crystallisation age for NT-12 is the weighted average of all seven concordant (±5%) analyses yielding a $^{206}Pb/^{238}U$ age of 238.0 ± 2.9 Ma (MSWD=0.95; Fig. 3). The interpreted crystallisation age for NT-10 is the weighted average of all seven concordant (±5%) zircon analyses yielding a $^{206}Pb/^{238}U$ age of 238.6 ± 2.9 Ma (n=7, MSWD = 0.88; Fig. 3). Nineteen concordant (±5%) analyses from NT-11 have Th:U>0.1 and yield a $^{206}Pb/^{238}U$ weighted average age of 228.7 ± 2.1 Ma (MSWD=0.48; Fig. 3). The magmatic age of Th11/01 is interpreted to be the weighted average of the ±5% concordant analyses with Th:U>0.1 yielding a $^{206}Pb/^{238}U$ age of 227.9 ± 1.9 Ma (n=23, MSWD=1.2; Fig. 3). Concordant (±5%) analyses with Th:U>0.1 from sample NT-09 yielded a weighted average $^{206}Pb/^{238}U$ age of 226.5 ± 1.8 Ma (n=18, MSWD=0.48; Fig. 3). This range of Triassic magmatic ages are common in the "Eastern Granitoid Province" within the Sukhothai and Indochina terranes (Charusiri et al., 1993; Searle et al., 2012).

3.1.4 Indochina Terrane

KM-20 contains $^{206}Pb/^{238}U$ ages within ±5% discordance for the entire first half of the Triassic period, from 249.4 ± 5.9 Ma to 221.5 ± 5.7 Ma. All zircons analyses contained Th:U more than 0.4. We interpret that the ages older than 235.5 Ma are inherited and the crystallisation age was calculated from the weighted average of all concordant (±5%) zircon analyses younger than 235.5 Ma, yielding a $^{206}Pb/^{238}U$ age of 229.9 ± 1.9 Ma (n=18, MSWD=1.9). All zircons analyses from NT-07 contained Th:U more than 0.61. The weighted average of 273.5 ± 3.9 Ma (n=5, MSWD=2.6) is the interpreted crystallisation age of NT-07. NT-07 also included earliest Permian and latest Carboniferous ages that were interpreted as inherited analyses. This sample yielded a spread of analyses that may suggest limited post-crystallisation disturbance of the isotopic system that is supported by the sericitisation of feldspars seen in thin section (Dew et al. (2018b), Fig 1—u, v).

3.2 Zircon Lu–Hf isotope analysis

The $^{176}Hf/^{177}Hf$ and $^{176}Lu/^{177}Hf$ isotopes were measured and used to interpret the isotopic differentiation of the mantle and crustal reservoirs (Patchett and Tatsumoto, 1980). They reflect the separation time of the parental magma from the mantle (Gardiner et al., 2016; Kemp et al., 2006). Hafnium data were plotted in epsilon Hf (εHf) versus age space, displayed in Fig. 4, to highlight the similarities and differences in crustal evolution of similar aged zircon grains (Kemp et al., 2006). For the interpreted magmatic ages, the U–Pb weighted average age was used to calculate $\varepsilon Hf_{(t)}$ where possible. For older inherited zircons, the individual U–Pb age for that analyses was used to calculate $\varepsilon Hf_{(t)}$ values.

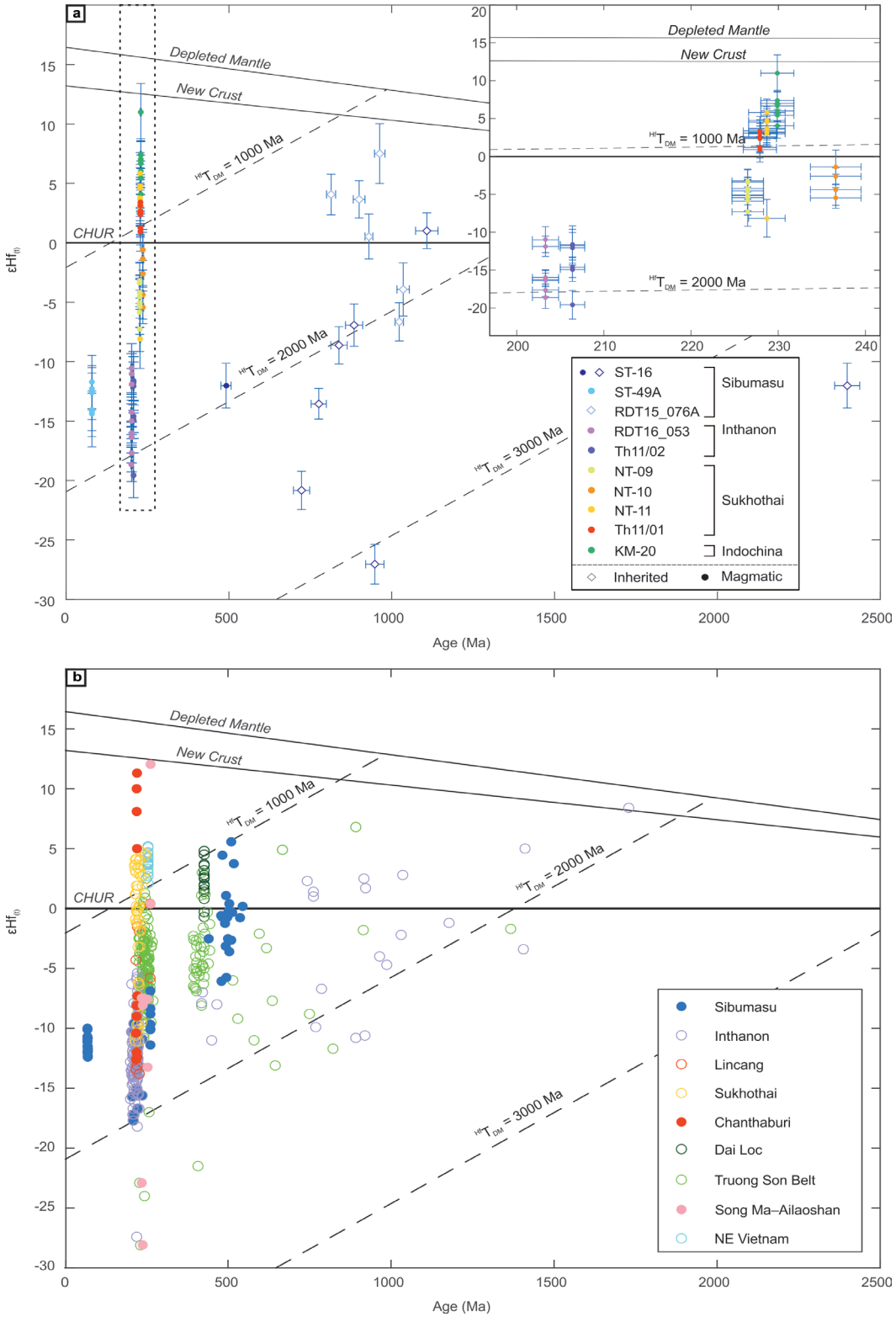

Fig. 4. a (top): Hafnium isotope diagram for the sampled granitoids, displayed as $\varepsilon Hf_{(t)}$ against the interpreted sample age. Interpreted crystallisation ages used the weighted average age. For interpreted inherited zircons, individual zircon spot U–Pb ages are used to calculate $\varepsilon Hf_{(t)}$. Both horizontal and vertical error bars are 2σ. The dashed rectangle indicates the extent of the inset. b (bottom): Hafnium isotope diagram for published granitoid data (see Dew et al., (2018b) for further details) displayed as $\varepsilon Hf_{(t)}$ against the age. The $^{Hf}T_{DM}$ crustal evolution lines are based on a $^{176}Lu/^{177}Hf$ ratio of 0.015 (Griffin et al. 2004).

3.2.1 Sibumasu Terrane

The analysis of magmatic zircons from ST-49A for hafnium yielded $\varepsilon Hf_{(t)}$ values between −14.42 and −11.73 (Fig. 4). For ST-16, Hf analyses were conducted on one magmatic zircon ($\varepsilon Hf_{(t)}$ of −4.82) and seven interpreted inherited zircons yielding $\varepsilon Hf_{(t)}$ values between −27.12 and +0.98 (Fig. 4). The Hf analyses were conducted on six interpreted inherited zircons for RDT15_076A yield $\varepsilon Hf_{(t)}$ values between −6.69 and +9.03 (Fig. 4).

3.2.2 Inthanon Zone

Magmatic $\varepsilon Hf_{(t)}$ values from RDT16_053 range between −18.60 and −10.49 (Fig. 4). The hafnium isotopic analyses of magmatic zircons from Th11/02 yielded $\varepsilon Hf_{(t)}$ values between −19.58 and −11.62. The zircons from RDT16_053 and Th11/02 have a similar crystallisation age and yield a similar range of negative $\varepsilon Hf_{(t)}$ values.

3.2.3 Sukhothai Terrane

All Hf analyses from the Sukhothai Terrane were taken from magmatic zircons (Fig. 4). The analysis of nine zircons from NT-09 yielded $\varepsilon Hf_{(t)}$ values between −7.31 and −3.23. The hafnium analysis of five magmatic zircons from the NT-10 sample yielded $\varepsilon Hf_{(t)}$ values between −5.47 and −0.61 (Fig. 4). The hafnium analysis of seven magmatic zircons from the Th11/01 sample yielded $\varepsilon Hf_{(t)}$ values between +0.89 and +3.37. The analysis of nine zircons from NT-11 for hafnium yielded $\varepsilon Hf_{(t)}$ values between −8.12 and +5.85, but, eight of the zircons analysed contained positive $\varepsilon Hf_{(t)}$ values between +3.00 and +5.81, however, one magmatic zircon from this sample yielded a negative $\varepsilon Hf_{(t)}$ value of −8.71.

3.2.4 Indochina Terrane

Seven magmatic analyses from KM-20 yielded positive $\varepsilon Hf_{(t)}$ values ranging from +4.06 to +10.99 as shown in Fig. 4.

3.3 Sm–Nd, Sr and Pb whole-rock geochemistry

The whole-rock geochemistry of granitoid rocks from Thailand was used to infer the petrogenetic and tectonic history of the region. The Sm–Nd isotopic system was used, in a similar way to the Lu–Hf isotopic system in zircon, to interpret the isotopic differentiation of the mantle and crustal reservoirs. The Sm–Nd whole-rock technique is advantageous compared to the zircon Lu–Hf isotopic system since it can be used for zircon-poor lithologies and for smaller sample sizes. The Sm–Nd system was plotted firstly in Epsilon Nd (εNd) - age space shown in Fig. 5a, with interpreted depleted mantle model ages in Fig. 5b. Epsilon Nd ($\varepsilon Nd_{(t)}$) was also displayed with the initial $^{87}Sr/^{86}Sr$ ratios ($^{87}Sr/^{86}Sr_{(t)}$) in Fig. 5c to indicate the nature of the magmatic source for granitoids and assist in the discrimination of S- and I-type granitoids (Chappell and White, 1992, 2001; Ng et al., 2015a).

Lead isotopes help establish the nature and origin of mixing components in the mantle due to the linear mixing relationship between the four Pb isotopes: the radiogenic ^{206}Pb, ^{207}Pb and ^{208}Pb and the non-radiogenic ^{204}Pb (Taylor et al., 2015). The ratios of $^{206}Pb/^{204}Pb$ and $^{207}Pb/^{204}Pb$ are displayed in Fig. 5d with the Stacey and Kramers (1975) terrestrial Pb evolution model and the Northern Hemisphere Reference Line (NHRL), outlined by Hart (1984), for comparison.

3.3.1 Sibumasu Terrane

The two samples from the Sibumasu terranes have negative $\varepsilon Nd_{(t)}$ values of −13.69 (ST-03) and −12.80 (NT-17) as displayed in Fig. 5. These strongly

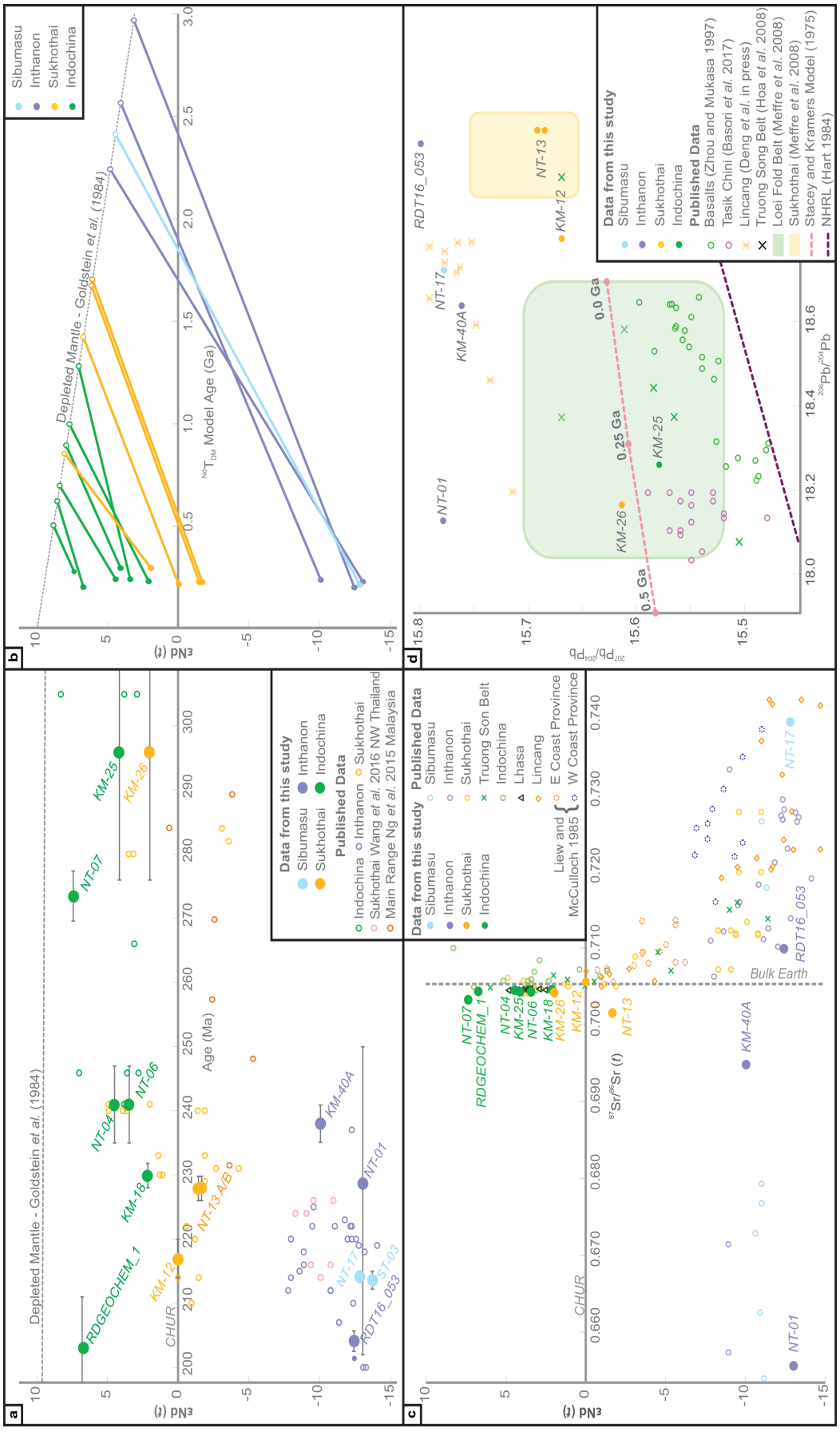

Fig. 5. a (top left): $\varepsilon Nd_{(t)}$ against age. Depleted Mantle assumes the linear depletion of the mantle as per Goldstein et al., (1984). Error bars show 2σ age uncertainties. b (top right): Plot of $\varepsilon Nd_{(t)}$ with depleted mantle model ages ($^{Nd}T_{DM}$) using assumed values from Goldstein et al. (1984). c (bottom left): $\varepsilon Nd_{(t)}$ against initial Sr. d (bottom right): Lead isotope ratio plot for granitoid analysed in this study with published Pb data. Reference lines from (Hart (1984) and Stacey and Kramers (1975). References for published data tabulated in Dew et al., (2018b).

negative $\varepsilon Nd_{(t)}$ values indicate the remelting of pre-existing continental crust. ST-03 contained anomalously low Nd concentrations (see Tables 6 and 7 of Dew et al. (2018b)), therefore we cannot be confident in the reliability of this value, although it is similar to the $\varepsilon Nd_{(t)}$ value found in the other Sibumasu sample, NT-17. The $^{87}Sr/^{86}Sr_{(t)}$ value of 0.739474 from NT-17 is an enriched upper continental crust signature (see Fig. 5c). In contrast, the $^{87}Sr/^{86}Sr_{(t)}$ value measured for ST-03 is highly anomalous at 1.476070, this may be due to the low Sr concentration of this sample at 23 ppm and its very high Rb/Sr ratio (Rb ppm is 904.4), which has been previously suggested by Romer et al. (2012) to create remarkably large uncertainties of the initial $^{87}Sr/^{86}Sr$ ratios. NT-17 is enriched in all three radiogenic Pb isotopes with ratios of $^{206}Pb/^{204}Pb$ 18.723486, $^{207}Pb/^{204}Pb$ 15.777563 and $^{208}Pb/^{204}Pb$ 38.819131 (Fig. 5d). The enriched radiogenic Pb isotopes measured in this sample suggests the involvement of recycled continental material.

3.3.2 Inthanon Zone

All three samples from the Inthanon Zone have strongly negative $\varepsilon Nd_{(t)}$ values (RDT16_053 −12.40, KM-40A −10.04 and NT-01 −13.01) indicating remelting of pre-existing continental crust (Fig. 5). The $\varepsilon Nd_{(t)}$ value of RDT16_053 of −12.40 is within the range of the $\varepsilon Hf_{(t)}$ values found from the zircons within this sample ($\varepsilon Hf_{(t)}$ between −18.60 to −10.49; Fig. 4). The Permo-Triassic $\varepsilon Hf_{(t)}$ values found within the zircons from Sibumasu and Inthanon samples also display strong negative values. Similarly, negative $\varepsilon Nd_{(t)}$ values were also calculated for the two samples from the Sibumasu Terrane (Fig. 5a).

The $^{87}Sr/^{86}Sr_{(t)}$ values for the Inthanon Zone have a wide variance from 0.655385 and 0.704255 (Fig. 5c). It is unreasonable for the initial $^{87}Sr/^{86}Sr$ ratios to be lower than values of Basaltic Achondrite Best Initial (0.69897 ± 0.00003). The anomalously low $^{87}Sr/^{86}Sr_{(t)}$ value from NT-01 of 0.655385 could be a result of a post-crystallisation shift in the Rb/Sr isotopic system (high Rb 753.8 ppm and low Sr 52 ppm). The $^{87}Sr/^{86}Sr_{(t)}$ for KM-40A (0.694704) could have also experienced minor resetting within the Rb–Sr system. The enriched $^{87}Sr/^{86}Sr_{(t)}$ value of 0.704255 for RDT16_053 suggests a lower crustal source for this granitoid.

The initial Pb ratios for RDT16_053 were $^{206}Pb/204Pb$ 19.026140, $^{207}Pb/^{204}Pb$ 15.799454 and $^{208}Pb/^{204}Pb$ 39.397697. The Pb ratios for KM-40A were $^{206}Pb/^{204}Pb$ 18.642169, $^{207}Pb/^{204}Pb$ 15.762181 and $^{208}Pb/^{204}Pb$ 38.999662. The Pb ratios for NT-01 were $^{206}Pb/^{204}Pb$ 18.127639, $^{207}Pb/^{204}Pb$ 15.778859 and $^{208}Pb/^{204}Pb$ 35.393159. The enriched radiogenic Pb isotopes measured in these sample suggests that it was sourced from continental material that has experienced multiple recycling events. NT-17, the only sample for Pb isotopic analyses from the Sibumasu Terrane, is within the isotopic range of the samples from the Inthanon Zone (Fig. 5d).

3.3.3 Sukhothai Terrane

The duplicate runs of NT-13 contained similar $\varepsilon Nd_{(t)}$ values of −1.66 and −1.45. The older KM-26 sample from further north also located in the Sukhothai Terrane was more juvenile in nature with an $\varepsilon Nd_{(t)}$ value of +1.97. KM-12, located further south gave a $\varepsilon Nd_{(t)}$ value of −0.00. These four $\varepsilon Nd_{(t)}$ values from Sukhothai sit very close to the CHUR line (Fig. 5a). The Sukhothai samples gave $^{87}Sr/^{86}Sr_{(t)}$ values of 0.701347 (NT-13), 0.705499 (KM-12)

and 0.704083 (KM-26). Although the $^{87}Sr/^{86}Sr_{(t)}$ data sit within the bulk earth range, $\varepsilon Nd_{(t)}$ values are slightly enriched compared to the observable silicate earth (Fig. 5c). These results indicate a relatively undepleted mantle source or a depleted mantle source, which has been contaminated by crustal material with an enriched isotopic signature. These data, like the $\varepsilon Hf_{(t)}$ results (Fig. 4), support a hypothesis where the Sukhothai arc was built on older continental material (Hara et al., 2017). The duplicate runs of NT-13 gave Pb ratios of $^{206}Pb/^{204}Pb$ 19.057330 (A) and 19.058107 (B), $^{207}Pb/^{204}Pb$ 15.685211(A) and 15.691958 (B) and $^{208}Pb/^{204}Pb$ 38.608086 (A) and 38.624095 (B). The Pb ratios for KM-26 ($^{206}Pb/^{204}Pb$ 18.168563, $^{207}Pb/^{204}Pb$ 15.614036 and $^{208}Pb/^{204}Pb$ 36.9956861) are very close to the Stacey and Kramers (1975) terrestrial lead evolution model (see Fig. 5d). The Pb ratios of KM-12 are $^{206}Pb/^{204}Pb$ 18.801927, $^{207}Pb/^{204}Pb$ 15.669479 and $^{208}Pb/^{204}Pb$ 38.391281 are slightly enriched in radiogenic lead. Overall the Pb isotopes from the Sukhothai Terrane closely follow the Stacey and Kramers (1975) terrestrial lead evolution model, although KM-12 and NT-13 are slightly more enriched in radiogenic Pb. The whole-rock data from this study are within the range of the published data from the Sukhothai Terrane, although KM-26 appears to have more isotopic affinity to the Indochina Terrane (see Fig. 5).

3.3.4 Indochina Terrane

All $\varepsilon Nd_{(t)}$ values from the six samples from the Indochina Terrane are positive, ranging between +2.11 to +7.40, reflecting juvenile sources, with minimal continental crust involvement. The samples from the Indochina Terrane have $^{87}Sr/^{86}Sr_{(t)}$ values ranging from 0.703140 to 0.704491. These values are within the range expected for primitive Bulk Earth. The Pb ppm concentration within all samples from Indochina, besides KM-25, which was below the 1 ppm detection limit of the XRF, therefore, whole-rock TIMS analyses were not completed on these samples. The Pb ratios for KM-25 were $^{206}Pb/^{204}Pb$ 18.263816, $^{207}Pb/^{204}Pb$ 15.579570 and $^{208}Pb/^{204}Pb$ 37.462045. This plots in $^{206}Pb/^{204}Pb$, $^{207}Pb/^{204}Pb$ space between the crustal evolution model and the MORB-like reservoir of the NHRL (see Fig. 5d; Hart, 1984; Stacey and Kramers, 1975).

4. Timing of magmatism for Thailand's granitoids

In this study, latest Triassic magmatism is observed only in samples from the Sibumasu Terrane and the Inthanon Zone (see Fig. 3). These ages are consistent with published data from Sibumasu and Inthanon with ages spanning 240–200 Ma (Ahrendt et al., 1993; Charusiri et al., 1993; Gardiner et al., 2016; Kawakami et al., 2014; Ng et al., 2015a; Searle et al., 2012; Wang et al., 2016c). These are thought to be supra-subduction zone granitoids, forming coeval with the closure of the Palaeo-Tethys Ocean (i.e. the older granites from the Sukhothai Terrane) and the subsequent collision of Sibumasu with the Sukhothai and Indochina terranes during the Upper Triassic (Searle et al., 2012).

Unlike the exclusively Permo-Triassic crystallisation ages found in this study from Indochina and Sukhothai, the Sibumasu and Inthanon granitoids contained concordant data of other ages. The weighted average age from ST-16 and inherited zircons from samples in the Sibumasu and Inthanon regions are Cambrian in age (see Fig. 3). Cambrian-aged crystalline basement has been found

previously in the Sibumasu Terrane and was associated with arc-related magmatism along the Gondwanan Indo-Australian margin (Lin et al., 2013). Cretaceous crystallisation ages found in samples from Sibumasu and Inthanon are also represented in published data from these terranes and are synchronous with the closure of the Neo-Tethys Ocean (Jiang et al., 2017; Kanjanapayont et al., 2012; Metcalfe, 2013). U–Pb data from samples ST-16 and ST-13 suggest limited isotopic disturbance at this time, consistent with a thermal overprint in this terrane at this time. Additionally the samples from Sibumasu and Inthanon contain abundant Precambrian inherited zircon grains (3200–600 Ma, see Fig. 3), studies such as Wang et al. (2016c) have also found inherited zircon grains ranging from 2545 to 400 Ma.

In this study, only early Ladinian (final stage of the Middle Triassic) crystallisation ages are found in the samples from the Sukhothai Terrane (see Fig. 3). Magmatic ages ranging from 296 to 200 Ma are found in the Sukhothai Terrane (This study; Beckinsale et al., 1979; Charusiri et al., 1993; Cobbing, 2011; Hansen and Wemmer, 2011; Meffre et al., 2008; Ng et al., 2015b; Qian et al., 2017; Singharajwarapan and Berry, 2000; Sone et al., 2012; Wang et al., 2016c; Zaw et al., 2014). The ages from the Indochina Terrane express prolonged Permo-Triassic magmatism compared to the later Triassic ages seen in the samples from the Inthanon Zone and Sibumasu Terrane (see Fig. 3 and 5). Published data from the Indochina Terrane are consistent with this study's dataset and indicate ages spanning from 310 to 203 Ma (Arboit et al., 2016; Charusiri et al., 1993; Halpin et al., 2016; Kamvong et al., 2014; Ng et al., 2015b; Salam et al., 2014; Zaw et al., 2014). The Ladinian (late Middle Triassic) ages found in the Sukhothai and Indochina granitoids are likely to be as a result of the early stages of the South China and Cathaysia collision with Vietnam and Indochina (Halpin et al., 2016; Lepvrier et al., 2004), or the similarly timed collision between Indochina and Sukhothai (Morley et al. 2013).

5. Isotopic characteristics of Thailand

The data collected in this study shows that the three main terranes in Thailand (Sibumasu, Sukhothai and Indochina) that show distinctions in their basement isotopic characteristics (see Fig 4 and 5).

5.1 Sibumasu and Inthanon terranes

The Sibumasu and Inthanon terranes exhibit similar age patterns and isotopic characteristics, suggesting a similar history. Both terranes generally contain evolved recycled crust, which is a consistent feature of the Hf, Sm–Nd, Sr and Pb isotopic signatures of the Cambrian–Cretaceous samples from this region (see Fig 4 and 5). The inherited zircon domains from the Sibumasu samples also have evolved signatures, seen in the negative $\varepsilon Hf_{(t)}$ values for ages ranging from 2400 to 600 Ma, providing further evidence for multiple recycling events (Fig. 4). The elevated $^{207}Pb/^{204}Pb$ ratios measured in the samples from the Sibumasu Terrane and the Inthanon Zone suggest the involvement of recycled continental material in these terranes (Taylor et al., 2015). Evolved isotopic signatures are also evident in published Sibumasu and Inthanon studies from Thailand, Malaysia and Myanmar (see Fig. 4–5; Gardiner et al., 2016; Jiang et al., 2017; Kanjanapayont et al., 2012; Lin et al., 2013; Ng et al., 2015a; Wang et al., 2016a).

A wide range of $\varepsilon Hf_{(t)}$ signatures are observed in the older inherited grains from RDT15_076A and ST-16 from Sibumasu (see Fig. 4). This is consistent with the isotopic signatures of S-type granitoids that can have more heterogeneous source material (Chappell and White, 2001; Cobbing et al., 1992). The granitoids from Inthanon and Sibumasu have been previously identified to have peraluminous S-type characteristics indicating that their source rocks had been through an earlier sedimentary cycle (Charusiri et al., 1993; Cobbing et al., 1992; Liew and McCulloch, 1985; Qian et al., 2017; Searle et al., 2012; Yokart et al., 2003). Petrographic investigations confirmed the peraluminous characteristics of ST-16 in which we found the disintegration of garnet crystals, typical for S-type granitoids (see Fig. 1 of Dew et al. (2018b).

Granites from the Sibumasu Terrane have been previously interpreted to be syn-collisional granitoids formed during the final stages of the Permo-Triassic Indosinian Orogeny and the closure of the Palaeo-Tethys Ocean (Beckinsale et al., 1979; Bunopas, 1981; Charusiri et al., 1993; Cobbing et al., 1992; Metcalfe, 2013; Pour et al., 2017; Searle et al., 2012; Yokart et al., 2003). The crustal thickening and melting of the Sibumasu Terrane during the Indosinian Orogeny is a possible mechanism for the formation of these S-type granitoids seen both in the Sibumasu Terrane and the Inthanon Zone (Bunopas, 1981; Charusiri et al., 1993; Mitchell, 1992; Searle et al., 2012).

5.2 Sukhothai Terrane

The isotopic values from the Sukhothai and Chanthaburi samples in this study are similar to values expected for the Bulk Silicate Earth or undifferentiated chondrite models (see Fig. 4 and 5). Similar isotopic values have been found in previous studies (e.g. Barr et al., 2006; Du et al., 2016; Ng et al., 2015b; Qian et al., 2017). In this study, the granitoids from the Sukhothai Terrane form a continuum from more juvenile metaluminous I-type granitoids in the east through to more crustally evolved granitoids in the west. These data are within the range found in previous studies from Sukhothai and its equivalent terranes (Cobbing, 2011; Mahawat et al., 1990; Qian et al., 2017; Singharajwarapan and Berry, 2000). The petrogenesis causing these characteristics has been previously attributed to a hybridised source of a juvenile mafic magma with an ancient meta-sedimentary component (Ng et al., 2015b; Qian et al., 2017; Wang et al., 2016c). Further evidence for this origin is from a detrital study by Hara et al. (2017), which concluded that the Sukhothai arc system was built on older continental material.

5.3 Indochina Terrane

Data from the Thailand sector of the Indochina Terrane are predominantly from its western margin due to thick sedimentary cover in the Khorat Plateau further east. The combination of data from this study with isotopic data from published works indicates that the Thai part of the Indochina Terrane is relatively juvenile (Fig. 5; Arboit et al., 2016; Intasopa and Dunn, 1994; Kamvong et al., 2014; Qian et al., 2016; Wang et al., 2016b). The granitoids from the Indochina Terrane are metaluminous with an I-type affinity (See Fig. 5; Charusiri et al., 1993; Salam et al., 2014). Kamvong et al. (2014) found adakites in the Loei and Truong Son Belts suggesting their petrogenesis from mantle-modified slab melts. Similarly, Salam et al. (2014) suggests arc-derived magma origins produced by the

interaction between the depleted mantle wedge and subduction-derived melts and fluids. There are few available data on the granitoids within the Cambodian sector of the Indochina Terrane. However, one study based on magnetic susceptibility and major and trace elements by Kong et al. (2012) implies that I-type granitoids are also found in this southeastern domain of the Indochina Terrane.

5.4. Spatial distribution of the isotopic signatures in Thailand and neighbouring regions

Vervoort et al. (1999) used Archean to recent samples from a wide range of depositional environments to demonstrate the behaviour of Lu–Hf and Sm–Nd isotopic systems in the global sedimentary system. The crustal array define this isotopic relationship as $\varepsilon Hf = 1.34\varepsilon Nd + 2.82$ (Vervoort et al. 1999). For this study, all the available published $\varepsilon Nd_{(t)}$ and recalculated $\varepsilon Hf_{(t)}$ data from Thailand and neighbouring regions of Myanmar, Laos, China and Vietnam were used to create an $\varepsilon Nd_{(t)}$ grid, to be used as a visualisation tool to highlight any trends in the isotopic characteristics.

The $\varepsilon Nd_{(t)}$ model was generated using the "natural neighbor" analyst tool in ArcGIS, to place the data into a spatial context. The grid was then clipped to the coastline and manually buffered around the outermost data points. The resultant model is shown in Fig. 6. Although in some regions the density of the $\varepsilon Nd_{(t)}$ and recalculated $\varepsilon Hf_{(t)}$ data is relatively low and no external constraints were used, the interpolation model highlights the different terranes and their boundaries. It also emphasises faults and major sutures, including the Three Pagodas Fault, the Klaeng Tectonic Line in SE Thailand and the complex Mae Ping Fault system including the Chainat Duplex and splays further east (see Fig. 6).

From this grid, a definable eastwards trend towards increasing juvenile characteristics occurs in Thailand (Fig. 6). The data in Fig. 6 clearly differentiates the juvenile nature of the Indochina Terrane from the more evolved Sibumasu and Inthanon. Additionally, the grid accentuates the isotopic difference between juvenile western Indochina to the more evolved Truong Son Belt of northwest Vietnam near the boundary zone between Indochina and South China (Liu et al., 2012; Wang et al., 2016b).

Fig. 6 also illustrates that the Sukhothai Terrane is less juvenile than the Indochina Terrane. The mixed isotopic characteristics of the Sukhothai Terrane require a relatively undepleted mantle source or a depleted mantle source that has been contaminated with old crust carrying an enriched isotopic signature. From this study's isotopic data and previously published studies, the most likely explanation is that a juvenile magma was mixed with evolved crustal material to produce the Sukhothai granitoids. The spatial position of the Sukhothai Terrane between the juvenile Indochina Terrane and the evolved Sibumasu Terrane and the trend of increasing juvenility eastwards through the Sukhothai Terrane implies that Sukhothai was a juvenile arc derived from Indochina, but incorporated evolved continental crust, similar to the Sibumasu Terrane, prior to or during granitoid emplacement.

5.5 Model ages for Thailand's basement

Barovich and Patchett (1992) demonstrated the overall insensitivity of the Nd and Hf isotopic systems in granitoids to extreme deformational events, lending confidence

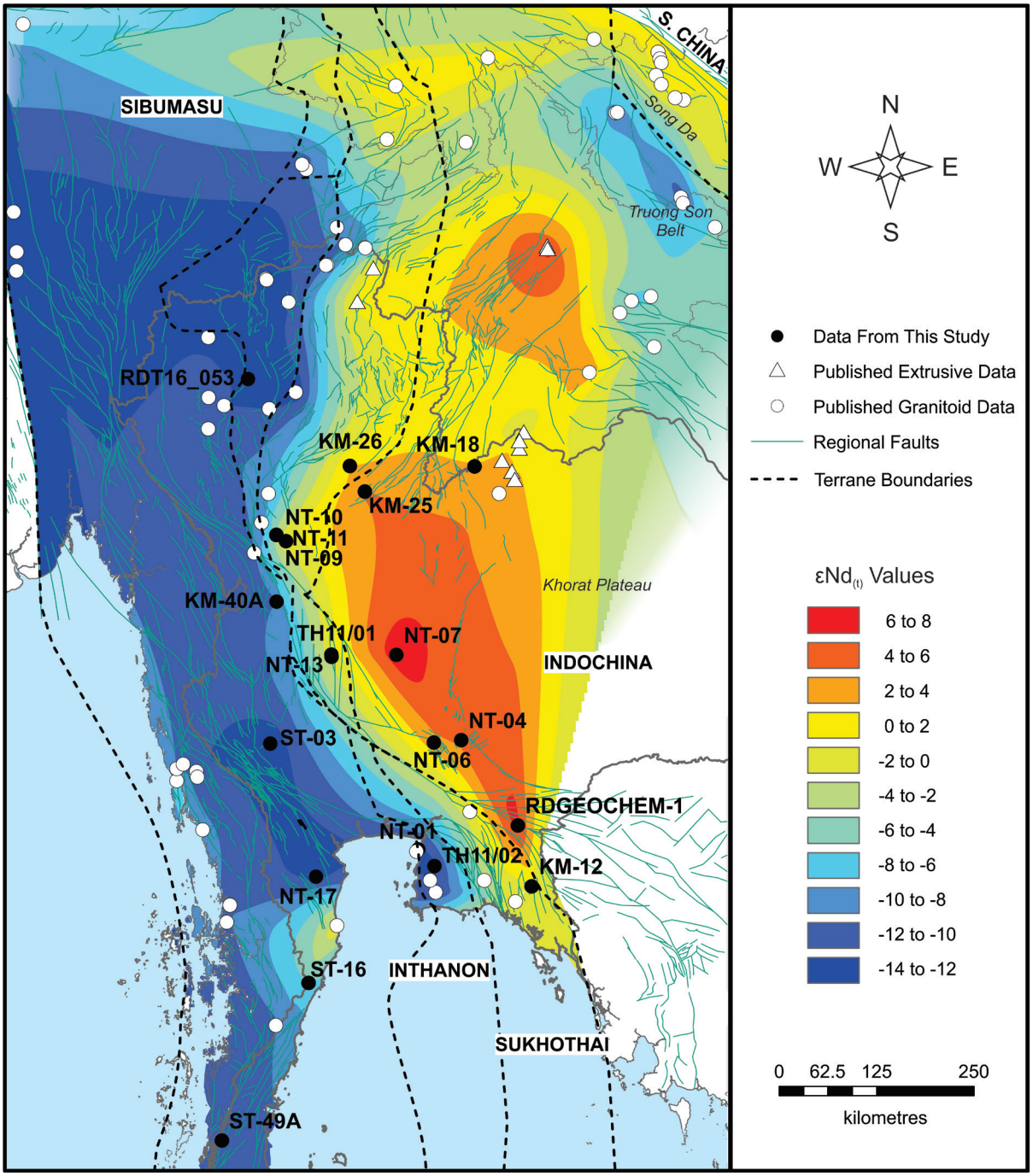

Fig. 6. A map collating all available $\varepsilon Nd_{(t)}$ and $\varepsilon Hf_{(t)}$ data from Thailand and neighbouring regions, references for published data tabulated in Dew et al., (2018b). The data have been scaled by colour and gridded in ArcGIS using the "nearest neighbor" analyst tool, to assist in visualising the data in a spatial context. Data clearly differentiates the juvenile Indochina Terrane from the other more evolved terranes, showing a trend of increasing juvenility to the east in Thailand, with the dark blue highly negative $\varepsilon Nd_{(t)}$ values in the Sibumasu Terrane moving eastwards into the orange to red positive $\varepsilon Nd_{(t)}$ values in the more juvenile Indochina Terrane.

to the use of Nd and Hf isotopic systems, and hence model ages, in crustal evolution studies. Hafnium crustal depleted mantle model ages ($^{Hf}T_{DM}$, shown in Fig. 4) denote a minimum formation age for the source material of the zircon's parental magma

(Gardiner et al., 2016; Kemp et al., 2006; Sevastjanova et al., 2011). These model ages were calculated for each zircon assuming the zircon grain growth reservoir was average continental crust with $^{176}Lu/^{177}Hf$ values of 0.0015 (Griffin et al., 2002). The Nd depleted mantle model ages ($^{Nd}T_{DM}$, shown in Fig. 5b) similarly reflect the time of the differentiation of the crust from the mantle but is a representation for the whole rock rather than individual zircons. However, since $^{Nd}T_{DM}$ samples the whole rock, if it is inhomogeneous in age and the material has been extracted from the mantle at various times, then the model age then represents an "average continental crustal residence time" (Arndt and Goldstein, 1987). Together, these model ages, when supported by other geological constraints i.e. zircon U–Pb inheritance, can be used to infer the rock's journey from the mantle to crust (Arndt and Goldstein, 1987; Gao et al., 2017; McCulloch, 1987).

5.5.1 Sibumasu Terrane

The depleted mantle model ages ($^{Hf}T_{DM}$) from the magmatic zircon Hf analyses in this study range between 2.02 Ga to 1.73 Ga with an average of 1.92 Ga. One Sm–Nd model age ($^{Nd}T_{DM}$) was calculated from the Sibumasu Terrane (NT-17) yielding an age of 2.41 Ga. This range of older heterogeneous T_{DM} values observed in the Sibumasu granitoids suggests that these granitoids were formed by assimilating or remelting older crustal material, which is consistent with the isotopic signatures analysed in this study. The $^{Hf}T_{DM}$ model ages found in this study are consistent with zircon inheritance found in this study (Fig. 2 and 3) and other published studies from the Sibumasu Terrane (Gardiner et al., 2016; Jiang et al., 2017; Liew and McCulloch, 1985; Lin et al., 2013; Sevastjanova et al., 2011). Although the older Sm–Nd model age from this study is in agreement with the zircon inheritance ages (see Fig. 2, 3, 4 and 5), this age is not commonly reported in the literature. A minor model age peak of 2.8–2.5 Ga was mentioned in Sevastjanova et al. (2011).

5.5.2 Inthanon Zone

The corresponding $^{Hf}T_{DM}$ model ages from the magmatic $\varepsilon Hf_{(t)}$ data in this study are between 2.44 Ga and 1.87 Ga (Fig. 4). The $^{Nd}T_{DM}$ from this study range between 2.97 Ga to 2.24 Ga with an average of 2.60 Ga. The U–Pb zircon inheritance ages are consistent with these model ages (Fig. 3). These values suggest that these granitoids were produced by assimilating or remelting 2.44–1.87 Ga crustal material. These model ages correspond to values for other rocks in the Sibumasu and Inthanon terranes along with their equivalents throughout Asia (Hansen and Wemmer, 2011; Qian et al., 2017; Sevastjanova et al., 2011; Wang et al., 2016c).

5.5.3 Sukhothai Terrane

The solely magmatic data from the Sukhothai Terrane yielded Lu–Hf model ages between 1.74 and 0.86 Ga, with an average of 1.27 Ga. The Sm–Nd model ages were within a similar age range (1.71 to 0.85 Ga with an average of 1.42 Ga). The $^{Nd}T_{DM}$ from KM-26, close to the Indochina Terrane (0.85 Ga), affects the range of model ages seen in the Sukhothai Terrane since this value is 570 Ma younger than the next youngest model age from this terrane. This age is more comparable with model ages found in Indochina. The T_{DM} ages for the Sukhothai samples in this study are within the range of previously published T_{DM} values (1.95 to 0.96 Ga, with peaks at 1.90 Ga and 1.10 Ga) from northwest Thailand (Wang et al., 2016c).

5.5.4 Indochina Terrane

The corresponding $^{Nd}T_{DM}$ model ages from the Nd data are between 1.28 and 0.50 Ga with an average of 0.83 Ga (Fig. 4). One sample from the Indochina Terrane was used for zircon Hf analyses (KM-20), giving corresponding $^{Hf}T_{DM}$ model ages between 0.97 and 0.53 Ga. These values suggest that the source material is largely juvenile, with minimal crustal input. Similar model ages have been published from the Khao Khwang Fold-Thrust Belt of Indochina's western margin (location is shown in Fig. 1a; Arboit et al., 2016). Previous studies have highlighted that there is little evidence of the existence of the western Thai sector of the Indochina Terrane prior to the middle Silurian (Cocks and Torsvik, 2013; Ridd, 2011). However, published detrital zircon studies from the Indochina Terrane suggest that the protoliths of the metasedimentary basement rock formed during the Neoproterozoic–early Paleozoic (Burrett et al., 2014). The model ages calculated for the Indochina Terrane in this study are much younger than the previous published source estimates from equivalent regions in Vietnam and Malaysia of greater than 3.7 Ga to 1.88 Ga (Sevastjanova et al., 2011; Usuki et al., 2013).

6. Implications for terrane evolution

This study indicates that western Indochina is relatively juvenile with middle Mesoproterozoic to Cambrian $^{Nd}T_{DM}$ model ages. Regions that conceivably have similar-aged material to the Indochina Terrane are the west coast of Australia (Collins, 2003), and northeast margin of India (Ghosh et al., 2005), both are locations where the Pinjarra Orogen crops out. The Neoproterozoic–Cambrian Pinjarra Orogen forms part of a much larger orogenic belt that can be traced along Western Australia and through eastern Antarctica (Burrett et al., 2014; Collins, 2003; Ghosh et al., 2005). Published $^{Nd}T_{DM}$ ages of 1.18 to 1.08 Ga from southwestern Australia are consistent with the older Mesoproterozoic model ages for the Indochina Terrane in this study (Fletcher and Libby, 1993; McCulloch, 1987; Wilde, 1999). Other possible neighbouring domains could be northwest India (Wang et al., 2017), along with other localities where the East African Orogen intersects the northern Gondwanan margin i.e. the Arabian Nubian Shield (Blades et al., 2015).

Previous detrital zircon work on Paleozoic–Mesozoic sediments demonstrates that the Thai parts of the Indochina Terrane had U–Pb and Lu–Hf affinities to the rest of Indochina (including Central Vietnam and the Truong Son Belt), South China, Qiangtang and Lhasa terranes during the early Paleozoic (Burrett et al., 2014; Usuki et al., 2013). Published granitoid geochemistry from the Lhasa Terrane is juvenile, similar to the Indochina data from our study (Fig. 5b; Ma et al., 2017). However, the data from this study, when integrated with published works in Fig. 6, highlights a distinct isotopic contrast between juvenile western Indochina and the evolved Truong Son Belt, which are both part of the composite Indochina Terrane. Previous studies in the northern Truong Son Belt (see Fig. 6; Liu et al., 2012; Wang et al., 2016b) produced $\varepsilon Hf_{(t)}$ and $\varepsilon Nd_{(t)}$ values that were generally negative and had corresponding T_{DM} ages dated to the Paleoproterozoic and backed up by zircon U–Pb inheritance ages. Further south in the Truong Son Belt, the $\varepsilon Nd_{(t)}$ values from Hoa et al. (2008) range from +6.0 for in extrusive rocks from Dak Lin to −13.3 for the peraluminous granite from Hai Van Complex. Hoa et

al. (2008) stated that the model ages for the Permo-Triassic granites in this study were late Paleoproterozoic (2.23 to 1.80 Ga). Although these model ages are older than the T_{DM} for the Indochina Terrane determined in this study, much of the isotopic data from the Truong Son Belt is comparable (see Fig. 5b and c). The main isotopic difference is that along with the juvenile signature observed in both Indochina and Truong Son, Truong Son also has a more evolved component, which is coincidentally similar to values seen in the Sukhothai Terrane. A more comprehensive study of Indochina, its western margin, the Truong Son Belt and the regions through Cambodia and Laos, is required to further understand this relationship.

South China and Indochina have been shown in a previous detrital U–Pb zircon provenance study to be statistically similar with Gondwanan elements, common sediment sources and palaeo-proximity (Burrett et al., 2014). In the South China Terrane, Permo-Triassic granitoids with $\varepsilon Nd_{(t)}$ values of –11 to –8 and T_{DM} values of 2.0 to 1.6 Ga, have been interpreted to be derived from Neoproterozoic sedimentary and igneous rocks based on zircon inheritance and the spatial relationship to adjacent Neoproterozoic material (Gao et al., 2017). This supports the idea that Indochina was spatially linked with South China in the Neoproterozoic, possibly part of the geodynamic system involving South China, Madagascar, NW India and Seychelles presented by Wang et al. (2017). This study produced new isotopic data and has incorporated all the available published $\varepsilon Nd_{(t)}$ and recalculated $\varepsilon Hf_{(t)}$ data from Thailand and neighbouring regions of Myanmar, Laos, China and Vietnam to visualise and highlight trends in the isotopic characteristics. However, more analysis of the separate components of the composite Indochina and South China terranes, would be beneficial in order to constrain their affinities and palaeo-positions more closely.

The young and juvenile Indochina Terrane contrasts with the Sibumasu Terrane, which is more conceivably part of ancient cratonic Australia. The T_{DM} ages of the Sibumasu Terrane are within the range of values also seen in Western Australia through the Kimberley, Pilbara and Yilgarn regions (McCulloch, 1987; Wilde, 1999). For example, Sibumasu may have originated outboard of northwest Australia, in association with the Barramundi and older orogens (Ali et al., 2013; Bunopas, 1981; Burrett et al., 2014; McCulloch, 1987; Sevastjanova et al., 2016).

In this study, we demonstrate that the Sukhothai arc system involved pre-Paleozoic continental crust, contrary to models where Sukhothai represents a Carboniferous oceanic arc system (Sone and Metcalfe, 2008). Possible explanations for these observations include: 1) The Sukhothai arc would have been located outboard of Sibumasu on the northwest Australian margin of Gondwana (see Fig. 7). In this model, the Inthanon Zone would represent the back-arc basin between Sibumasu and Sukhothai and the main Palaeo-Tethys suture would separate Sukhothai and Indochina (the Nan Suture). 2) The Sukhothai arc was derived from Indochina, but contains relict Precambrian signatures, similar to those signatures observed in the Truong Son Belt to the northeast. This would require a zone of weakness between the more juvenile western Thai Indochina Terrane and the evolved Sukhothai Terrane crust to have been exploited by the back-arc

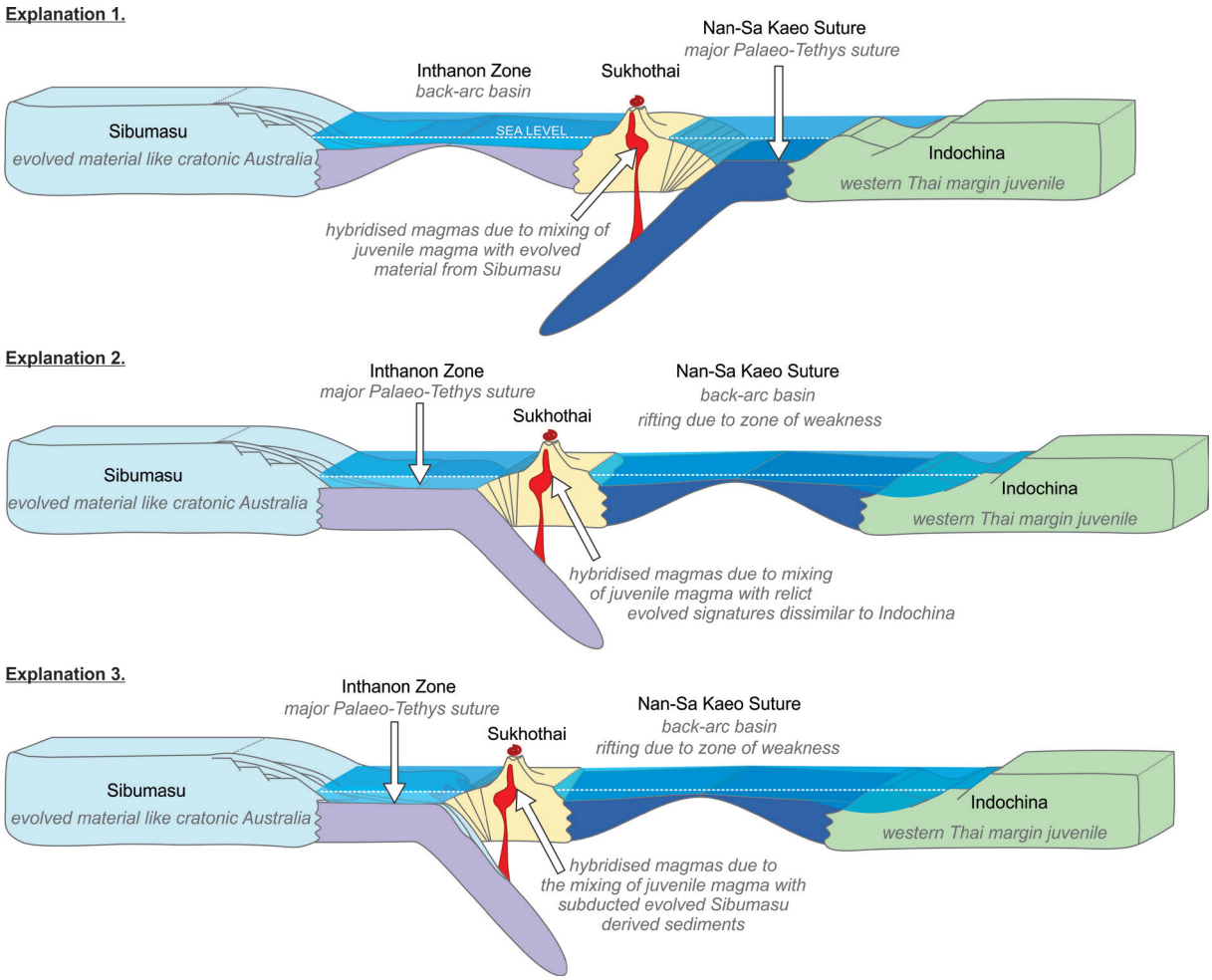

Fig. 7. Diagrams for the potential tectonic development of the Thai terranes. a: Explanation 1) The Sukhothai arc would have sat outboard of Sibumasu on the northwest Australian margin of Gondwana. In this model, the Inthanon Zone would represent the back-arc basin between Sibumasu and Sukhothai and the main Palaeo-Tethys suture separates Sukhothai and Indochina (the Nan Suture). b. Explanation 2) The Sukhothai arc was derived from Indochina, but contains relict Precambrian signatures. This would require a zone of weakness between the more juvenile western Thai Indochina Terrane and the evolved Sukhothai Terrane crust to have been exploited by the back-arc extension that separated these terranes. c. Explanation 3) The hybridised nature of the mid-Triassic granitoids in the Sukhothai Terrane may be due to the incorporation of evolved distal passive margin sequences of the Sibumasu Terrane as they approached the subduction zone.

extension that separated these terranes (see Fig. 7). For example, analogue modelling by Corti et al. (2013) has shown how the boundary zone between colder, more rigid cratonic (i.e. Archean-type) crust, and less rigid mobile belts tends to localise rifting.

Explanation 1) is contrary to popular models where the Inthanon Zone represents the main Palaeo-Tethys suture. These models are based on the presence of long-lived Devonian–Triassic highly condensed deep marine cherts, allochthonous limestone-capped seamounts and the continuation of the zone into the Changning–Menglian zone of Yunnan (see reviews in Sone and Metcalfe, 2008; Metcalfe 2013; Gardiner et al., 2015). Explanation 2) adheres

to the currently accepted consensus regarding the origin of the terranes, but requires a coincidence of circumstances to explain the lack of similarity between the Sukhothai and Indochina terranes. However, there is a third possibility that may reconcile these two contradictory explanations. The hybridised nature of the mid-Triassic granitoids in the Sukhothai Terrane may be due to the incorporation of evolved distal passive margin sequences of the Sibumasu Terrane as they approached the subduction zone (see illustration in Fig. 7). A similar manner of arc contamination is observed in the Sunda Arc (Handley et al., 2011). In this third model, the Sukhothai Terrane could still be part of the Indochina Terrane and the Inthanon Zone could still represent the major Palaeo-Tethys suture, coinciding with the evidence from the long-lived deep basin sedimentary sequences. It also broadly follows the geochemical data from the Sukhothai Terrane that appears to spatially distinguish between the I-type and hybrid granites, with more juvenile granitoids closer to the margin with Indochina and more crustal contamination in the granites further west, closer to the Inthanon Zone boundary. Nevertheless, further analyses and data collation on a regional scale is required to visualise a more complete history of the founding components of Southeast Asia.

7. Conclusion

This study used granites as a probe to further develop our understanding of the unexposed basement in Thailand. From the investigation of zircon U–Pb geochronology and Lu–Hf isotopic systems and whole-rock Sm–Nd, Sr and Pb geochemistry of granitoids, we determined:

- The Indochina Terrane is isotopically juvenile
- The Sukhothai Terrane has a hybridised isotopic signature indicating that juvenile material was contaminated with evolved continental crust
- The Sibumasu Terrane and associated Inthanon Zone contain relatively evolved, recycled crust
- $\varepsilon Hf–Nd_{(t)}$ model highlights a trend from evolved granitoid source material in the west of Thailand (Sibumasu and Inthanon) through to juvenile affinities in the east (Indochina)

Contrary to a number of previous hypotheses, the Indochina Terrane is built on relatively juvenile crust that formed primarily in the Neoproterozoic. There is no evidence for older crust in the western part of the Indochina Terrane. This contrasts with the Sibumasu and Sukhothai terranes that preserve evolved crustal material. We suggest that the hybridised isotopic nature of the mid-Triassic granitoids in the Sukhothai Terrane is due to the integration of evolved material from the Sibumasu Terrane during the progressive subduction of the Palaeo-Tethys Ocean.

Acknowledgements

Fieldwork was conducted with the kind assistance of staff and students from Chulalongkorn University and Chiang Mai University. Other field expeditions were conducted with great thanks to Liviu Matenco and Ernst Willingshofer from Utrecht University, Thamfatt Ng and Diew. Pîi Roj from Chiang Mai University Lapidary for training and permission to use facilities. We would like to acknowledge Ann-Eline Debeer from Ghent University for the zircon mount preparation for the KM, ST and NT samples. Many thanks to David Bruce from the University of Adelaide's Isotope Geochemistry Facility for his support in

the whole-rock geochemistry component of this project along with Sarah Gilbert and Aoife McFadden at Adelaide Microscopy for their help with the zircon analyses. Also thanks to Stanley Mertzman at Franklin and Marshall College for analysing the major and trace elements for this research. Thank you to Brad McDonald at the GeoHistory Facility at Curtin University for instrument setup for the Hf analyses. Appreciation to Sheree Armistead for conducting the Hf analysis for the KM-20 sample and assistance with MATLAB.

This work was supported by Australian Research Council [#DP150101730, #DP120101460 and #FT120100340]. R.E.C. Dew is also funded by a University of Adelaide Research Training Program Stipend and some of the fieldwork conducted was funded on an Endeavour Australia Cheung Kong Fellowship. P. Kanjanapayont is funded by the Ratchadaphiseksomphot Endowment Fund, Chulalongkorn University. S. Nachtergaele is funded by a PhD fellowship of the Research Foundation Flanders (FWO). GeoHistory Facility instruments were funded via an Australian Geophysical Observing System grant provided to AuScope Pty Ltd. by the AQ44 Australian Education Investment Fund program. The NPII multi-collector was obtained via funding from the Australian Research Council LIEF program [#LE150100013]. This is a contribution to IGCP projects #589 (Development of the Asian Tethyan Realm) and #628 (The Gondwana Map). This publication forms TRaX Record #411.

References

Ahrendt, H., Chonglakmani, C., Hansen, B.T., Helmcke, D., 1993. Geochronological cross section through northern Thailand. Journal of Southeast Asian Earth Sciences 8, 207-217.

Ali, J.R., Cheung, H.M.C., Aitchison, J.C., Sun, Y., 2013. Palaeomagnetic re-investigation of Early Permian rift basalts from the Baoshan Block, SW China: constraints on the site-of-origin of the Gondwana-derived eastern Cimmerian terranes. Geophysical Journal International 193, 650-663.

Arboit, F., Collins, A.S., Jourdan, F., King, R., Foden, J., Amrouch, K., 2016. Geochronological and geochemical study of mafic and intermediate dykes from the Khao Khwang Fold-Thrust Belt: Implications for petrogenesis and tectonic evolution. Gondwana Research 36, 111-128.

Arboit, F., Collins, A.S., King, R., Morley, C.K., Hansberry, R., 2014. Structure of the Sibumasu–Indochina collision, central Thailand: A section through the Khao Khwang Fold and thrust belt. Journal of Asian Earth Sciences 95, 182-191.

Arndt, N.T., Goldstein, S.L., 1987. Use and abuse of crust-formation ages. Geology 15, 893-895.

Audley-Charles, M.G., Ballantyne, P.D., Hall, R., 1988. Mesozoic-Cenozoic rift-drift sequence of Asian fragments from Gondwanaland. Tectonophysics 155, 317-330.

Barber, A.J., Ridd, M.F., Crow, M.J., 2011. The origin, movement and assembly of the pre-Tertiary tectonic units of Thailand, in: Ridd, M.F., Barber, A.J., Crow, M.J. (Eds.), The Geology of Thailand. The Geological Society, London, pp. 507-537.

Barovich, K.M., Patchett, P.J., 1992. Behavior of isotopic systematics during deformation and metamorphism: a Hf, Nd and Sr isotopic study of mylonitized granite. Contributions to Mineralogy and Petrology 109, 386-393.

Barr, S.M., Macdonald, A.S., 1987. Nan River suture zone, northern Thailand. Geology 15, 907-910.

Barr, S.M., Macdonald, A.S., 1991. Toward a late Palaeozoic–early Mesozoic tectonic model for Thailand. Journal of Thai Geoscience 1, 11-22.

Barr, S.M., Macdonald, A.S., Ounchanum, P., Hamilton, M.A., 2006. Age, tectonic setting and regional implications of the Chiang Khong volcanic suite, northern Thailand. Journal of the Geological Society 163, 1037-1046.

Beckinsale, R.D., Suensilpong, S., Nakapadungrat, S., Walsh, J.N., 1979. Geochronology and geochemistry of granite magmatism in Thailand in relation to a plate tectonic model. Journal of the Geological Society 136, 529-537.

Blades, M.L., Collins, A.S., Foden, J., Payne, J.L., Xu, X., Alemu, T., Woldetinsae, G., Clark, C., Taylor, R.J.M., 2015. Age and hafnium isotopic

evolution of the Didesa and Kemashi Domains, western Ethiopia. Precambrian Research 270, 267-284.

Booth, J., Sattayarak, N., 2011. Subsurface Carboniferous - Cretaceous geology of NE Thailand, in: Ridd, M.F., Barber, A.J., Crow, M.J. (Eds.), The Geology of Thailand. The Geological Society, London, pp. 185-222.

Bunopas, S., 1981. Paleogeographic history of western Thailand and adjacent parts of Southeast Asia - A plate tectonics interpretation. Paleogeographic History of Western Thailand and Adjacent Parts of Southeast Asia - A Plate Tectonics Interpretation.

Burrett, C., Khin, Z., Meffre, S., Lai, C.K., Khositanont, S., Chaodumrong, P., Udchachon, M., Ekins, S., Halpin, J., 2014. The configuration of Greater Gondwana—Evidence from LA ICPMS, U–Pb geochronology of detrital zircons from the Palaeozoic and Mesozoic of Southeast Asia and China. Gondwana Research 26, 31-51.

Cai, F., Ding, L., Yao, W., Laskowski, A.K., Xu, Q., Zhang, J.e., Sein, K., 2017. Provenance and tectonic evolution of Lower Paleozoic–Upper Mesozoic strata from Sibumasu terrane, Myanmar. Gondwana Research 41, 325-336.

Chaodumrong, P., 1992. Stratigraphy, sedimentology and tectonic implications of the Lampang Group, central north Thailand, Geology. University of Tasmania, Hobart, p. 230.

Chappell, B.W., White, A.J.R., 1992. I- and S-type granites in the Lachlan Fold Belt, in: Brown, P.E., Chappell, B.W. (Eds.), The Second Hutton Symposium on the Origin of Granites and Related Rocks. Geological Society of America.

Chappell, B.W., White, A.J.R., 2001. Two contrasting granite types: 25 years later. Australian Journal of Earth Sciences 48, 489-499.

Charusiri, P., Clark, A.H., Farrar, E., Archibald, D., Charusiri, B., 1993. Granite belts in Thailand: evidence from the 40Ar/39Ar geochronological and geological syntheses. Journal of Southeast Asian Earth Sciences 8, 127-136.

Cobbing, E.J., 2011. Granitic Rocks, in: Ridd, M.F., Barber, A.J., Crow, M.J. (Eds.), The Geology of Thailand. The Geological Society, London, pp. 443-457.

Cobbing, E.J., Pitfield, P.E.J., Darbyshire, P.D.F., Mallick, D.I.J., 1992. Thailand, The granites of the South-east Asian tin belt. HMSO, London.

Cocks, L.R.M., Torsvik, T.H., 2013. The dynamic evolution of the Palaeozoic geography of eastern Asia. Earth-Science Reviews 117, 40-79.

Collins, A.S., 2003. Structure and age of the northern Leeuwin Complex, Western Australia: Constraints from field mapping and U–Pb isotopic analysis. Australian Journal of Earth Sciences 50, 585-599.

Corti, G., Iandelli, I. & Cerca, M. 2013. Experimental modeling of rifting at craton margins. Geosphere, 9, 138-154, doi: 10.1130/GES00863.1.

Dew, R.E.C., King, R., Collins, A.S., Morley, C.K., Arboit, F., Glorie, S., 2018a. Stratigraphy of deformed Permian carbonate reefs in Saraburi Province, Thailand. Journal of the Geological Society 175, 163-175.

Dew, R.E.C., Nachtergaele, S., Collins, A.S., Glorie, S., Foden, J., De Grave, J., Blades, M.L., Morley, C.K., Evans, N.J., Alessio, B.L., Kanjanapayont, P., King, R., Charusiri, P., 2018b. Data analysis of the U–Pb geochronology and Lu–Hf system in zircon and whole-rock Sr, Sm–Nd and Pb isotopic systems for the granitoids of Thailand. Data in Brief.

Du, B., Wang, C., He, Z., Yang, L., Chen, J., Shi, K., Luo, Z., Xia, J., 2016. Advances in research of bulk-rock Nd and zircon Hf isotopic mappings: Case study of Sanjiang Tethyan Orogen. Acta Petrologica Sinica 32, 2555-2570.

Faure, M., Lepvrier, C., Nguyen, V.V., Vu, T.V., Lin, W., Chen, Z., 2014. The South China block-Indochina collision: Where, when, and how? Journal of Asian Earth Sciences 79, 260-274.

Fletcher, I.R., Libby, W.G., 1993. Further isotopic evidence for the existence of two distinct terranes in the southern Pinjarra Orogen, Western Australia, Professional Papers. Geological Survey, Western Australia, pp. 81-83.

Gao, P., Zheng, Y.-F., Zhao, Z.-F., 2017. Triassic granites in South China: A geochemical perspective on their characteristics, petrogenesis, and tectonic significance. Earth-Science Reviews 173, 266-294.

Gardiner, N.J., Searle, M.P., Morley, C.K., Whitehouse, M.P., Spencer, C.J., Robb, L.J., 2016. The closure of Palaeo-Tethys in Eastern Myanmar and Northern Thailand: New insights from zircon U-Pb and Hf isotope data. Gondwana Research 39, 401-422.

Ghosh, S., Fallick, A.E., Paul, D.K., Potts, P.J., 2005. Geochemistry and Origin of Neoproterozoic Granitoids of Meghalaya, Northeast India: Implications for Linkage with Amalgamation of Gondwana Supercontinent. Gondwana Research 8, 421-432.

Goldstein, S.L., O'Nions, R.K., Hamilton, P.J.,

1984. A Sm-Nd isotopic study of atmospheric dusts and particulates from major river systems. Earth and Planetary Science Letters 70, 221-236.

Halpin, J.A., Tran, H.T., Lai, C.-K., Meffre, S., Crawford, A.J., Zaw, K., 2016. U–Pb zircon geochronology and geochemistry from NE Vietnam: A 'tectonically disputed' territory between the Indochina and South China blocks. Gondwana Research 34, 254-273.

Handley, H.K., Turner, S., Macpherson, C.G., Gertisser, R., Davidson, J.P., 2011. Hf–Nd isotope and trace element constraints on subduction inputs at island arcs: Limitations of Hf anomalies as sediment input indicators. Earth and Planetary Science Letters 304, 212-223.

Hansen, B.T., Wemmer, K., 2011. Age and evolution of the basement in Thailand, in: Ridd, M.F., Barber, A.J., Crow, M.J. (Eds.), The Geology of Thailand. The Geological Society, London, pp. 19-32.

Hara, H., Kon, Y., Usuki, T., Lan, C.Y., Kamata, Y., Hisada, K.I., Ueno, K., Charoentitirat, T., Charusiri, P., 2013. U-Pb ages of detrital zircons within the Inthanon Zone of the Paleo-Tethyan subduction zone, northern Thailand: New constraints on accretionary age and arc activity. Journal of Asian Earth Sciences 74, 50-61.

Hara, H., Kunii, M., Hisada, K.I., Ueno, K., Kamata, Y., Srichan, W., Charusiri, P., Charoentitirat, T., Watarai, M., Adachi, Y., Kurihara, T., 2012. Petrography and geochemistry of clastic rocks within the Inthanon zone, northern Thailand: Implications for Paleo-Tethys subduction and convergence. Journal of Asian Earth Sciences 61, 2-15.

Hara, H., Kunii, M., Miyake, Y., Hisada, K.I., Kamata, Y., Ueno, K., Kon, Y., Kurihara, T., Ueda, H., Assavapatchara, S., Treerotchananon, A., Charoentitirat, T., Charusiri, P., 2017. Sandstone provenance and U–Pb ages of detrital zircons from Permian–Triassic forearc sediments within the Sukhothai Arc, northern Thailand: Record of volcanic-arc evolution in response to Paleo-Tethys subduction. Journal of Asian Earth Sciences 146, 30-55.

Hart, S.R., 1984. A large-scale isotope anomaly in the Southern Hemisphere mantle. Nature 309, 753-757.

Hisada, K.-i., Sugiyama, M., Ueno, K., Charusiri, P., Arai, S., 2004. Missing ophiolitic rocks along the Mae Yuam Fault as the Gondwana–Tethys divide in north-west Thailand. Island Arc 13, 119-127.

Hoa, T.T., Anh, T.T., Phuong, N.T., Dung, P.T., Anh, T.V., Izokh, A.E., Borisenko, A.S., Lan, C.Y., Chung, S.L., Lo, C.H., 2008. Permo-Triassic intermediate–felsic magmatism of the Truong Son belt, eastern margin of Indochina. Comptes Rendus Geoscience 340, 112-126.

Intasopa, S., Dunn, T., 1994. Petrology and Sr□Nd isotopic systems of the basalts and rhyolites, Loei, Thailand. Journal of Southeast Asian Earth Sciences 9, 167-180.

Javanaphet, C., 1969. Geological Map of Thailand; Scale 1 : 1 000 000, with explanation. Department of Mineral Resources, Bangkok.

Jiang, H., Li, W.-Q., Jiang, S.-Y., Wang, H., Wei, X.-P., 2017. Geochronological, geochemical and Sr-Nd-Hf isotopic constraints on the petrogenesis of Late Cretaceous A-type granites from the Sibumasu Block, Southern Myanmar, SE Asia. Lithos 268–271, 32-47.

Kamvong, T., Khin, Z., Meffre, S., Maas, R., Stein, H., Lai, C.-K., 2014. Adakites in the Truong Son and Loei fold belts, Thailand and Laos: Genesis and implications for geodynamics and metallogeny. Gondwana Research 26, 165-184.

Kanjanapayont, P., Klötzli, U., Thöni, M., Grasemann, B., Edwards, M.A., 2012. Rb–Sr, Sm–Nd, and U–Pb geochronology of the rocks within the Khlong Marui shear zone, southern Thailand. Journal of Asian Earth Sciences 56, 263-275.

Kawakami, T., Nakano, N., Higashino, F., Hokada, T., Osanai, Y., Yuhara, M., Charusiri, P., Kamikubo, H., Yonemura, K., Hirata, T., 2014. U-Pb zircon and CHIME monazite dating of granitoids and high-grade metamorphic rocks from the Eastern and Peninsular Thailand — A new report of Early Paleozoic granite. Lithos 200–201, 64-79.

Kemp, A.I.S., Hawkesworth, C.J., Paterson, B.A., Kinny, P.D., 2006. Episodic growth of the Gondwana supercontinent from hafnium and oxygen isotopes in zircon. Nature 439, 580-583.

Kong, S., Watanabe, K., Imai, A., 2012. Magnetic susceptibility and geochemistry of granitic rocks in Cambodia. ASEAN Engineering Journal Part C 2, 113-132.

Lan, C.Y., Chung, S.L., Van Long, T., Lo, C.H., Lee, T.-Y., Mertzman, S.A., Shen, J.J.-S., 2003. Geochemical and Sr–Nd isotopic constraints from the Kontum massif, central Vietnam on the crustal evolution of the Indochina block. Precambrian Research, 7-27.

Lepvrier, C., Maluski, H., Van Tich, V., Leyreloup,

A., Truong Thi, P., Van Vuong, N., 2004. The Early Triassic Indosinian orogeny in Vietnam (Truong Son Belt and Kontum Massif); implications for the geodynamic evolution of Indochina. Tectonophysics 393, 87-118.

Li, P., Rui, G., Junwen, C., Ye, G., 2004. Paleomagnetic analysis of eastern Tibet: implications for the collisional and amalgamation history of the Three Rivers Region, SW China. Journal of Asian Earth Sciences 24, 291-310.

Liew, T.C., McCulloch, M.T., 1985. Genesis of granitoid batholiths of Peninsular Malaysia and implications for models of crustal evolution: Evidence from a Nd□Sr isotopic and U□Pb zircon study. Geochimica et Cosmochimica Acta 49, 587-600.

Lin, Y.-L., Yeh, M.-W., Lee, T.-Y., Chung, S.-L., Iizuka, Y., Charusiri, P., 2013. First evidence of the Cambrian basement in Upper Peninsula of Thailand and its implication for crustal and tectonic evolution of the Sibumasu terrane. Gondwana Research 24, 1031-1037.

Liu, J., Tran, M.-D., Tang, Y., Nguyen, Q.-L., Tran, T.-H., Wu, W., Chen, J., Zhang, Z., Zhao, Z., 2012. Permo-Triassic granitoids in the northern part of the Truong Son belt, NW Vietnam: Geochronology, geochemistry and tectonic implications. Gondwana Research 22, 628-644.

Ludwig, K.R., 1998. On the Treatment of Concordant Uranium-Lead Ages. Geochimica et Cosmochimica Acta 62, 665-676.

Ma, X., Xu, Z., Meert, J.G., 2017. Syn-convergence extension in the southern Lhasa terrane: Evidence from late Cretaceous adakitic granodiorite and coeval gabbroic-dioritic dykes. Journal of Geodynamics 110, 12-30.

Mahawat, C., Atherton, M.P., Brotherton, M.S., 1990. The Tak Batholith, Thailand: the evolution of contrasting granite types and implications for tectonic setting. Journal of Southeast Asian Earth Sciences 4, 11-27.

McCulloch, M.T., 1987. Sm-Nd isotopic constraints on the evolution of Precambrian crust in the Australian continent, in: Kröner, A. (Ed.), Proterozoic lithospheric evolution. American Geophysical Union, Washington, D.C., pp. 115-130.

Meffre, S., Khin, Z., Khositanont, S., Halpin, J., Cumming, G., 2008. 'Tectonic evolution of SE Asia', 'Ore Deposits of SE Asia' - Annual Report to Sponsors. CODES, Hobart, Australia.

Metcalfe, I., 1984. Stratigraphy, palaeontology and palaeogeography of the Carboniferous of Southeast Asia. Memoires de la Societe Geologique de France 147, 107-118.

Metcalfe, I., 2013. Gondwana dispersion and Asian accretion: Tectonic and palaeogeographic evolution of eastern Tethys. Journal of Asian Earth Sciences 66, 1-33.

Mitchell, A.H.G., 1992. Late Permian-Mesozoic events and the Mergui Group Nappe in Myanmar and Thailand. Journal of Southeast Asian Earth Sciences 7, 165-178.

Morley, C.K., Ampaiwan, P., Thanudamrong, S., Kuenphan, N., Warren, J., 2013. Development of the Khao Khwang fold and thrust belt; implications for the geodynamic setting of Thailand and Cambodia during the Indosinian Orogeny. Journal of Asian Earth Sciences 62, 705-719.

Nakano, N., Osanai, Y., Nam, N.V., Tri, T.V., 2018. Bauxite to eclogite: Evidence for late Permian supracontinental subduction at the Red River shear zone, northern Vietnam. Lithos 302-303, 37-49.

Ng, S.W., Chung, S.L., Robb, L.J., Searle, M.P., Ghani, A.A., Whitehouse, M.J., Oliver, G.J.H., Sone, M., Gardiner, N.J., Roselee, M.H., 2015a. Petrogenesis of Malaysian granitoids in the Southeast Asian tin belt: Part 1. Geochemical and Sr-Nd isotopic characteristics. Bulletin of the Geological Society of America 127, 1209-1237.

Ng, S.W., Whitehouse, M.J., Searle, M.P., Robb, L.J., Ghani, A.A., Chung, S.L., Oliver, G.J.H., Sone, M., Gardiner, N.J., Roselee, M.H., 2015b. Petrogenesis of Malaysian granitoids in the Southeast Asian tin belt: Part 2. U-Pb zircon geochronology and tectonic model. Bulletin of the Geological Society of America 127, 1238-1258.

Patchett, P.J., Tatsumoto, M., 1980. Hafnium isotope variations in oceanic basalts. Geophysical Research Letters 7, 1077-1080.

Pour, A.B., Hashim, M., Park, Y., 2017. Gondwana-Derived Terranes Structural Mapping Using PALSAR Remote Sensing Data. Journal of the Indian Society of Remote Sensing, 1-14.

Qian, X., Feng, Q., Wang, Y., Chonglakmani, C., Monjai, D., 2016. Geochronological and geochemical constraints on the mafic rocks along the Luang Prabang zone: Carboniferous back-arc setting in northwest Laos. Lithos 245, 60-75.

Qian, X., Feng, Q., Wang, Y., Zhao, T., Zi, J.-W., Udchachon, M., Wang, Y., 2017. Late Triassic post-collisional granites related to Paleotethyan evolution in SE Thailand: Geochronological

and geochemical constraints. Lithos 286, 440-453.

Ridd, M.F., 2011. Lower Palaeozoic, in: Ridd, M.F., Barber, A.J., Crow, M.J. (Eds.), The Geology of Thailand. The Geological Society, London, pp. 33-51.

Romer, R.L., Förster, H.-J., Hahne, K., 2012. Strontium isotopes — A persistent tracer for the recycling of Gondwana crust in the Variscan orogen. Gondwana Research 22, 262-278.

Salam, A.A., Zaw, K., Meffre, S., McPhie, J., Lai, C.-K., 2014. Geochemistry and geochronology of the Chatree epithermal gold-silver deposit: Implications for the tectonic setting of the Loei Fold Belt, central Thailand. Gondwana Research 26, 198-217.

Schwartz, M.O., Rajah, S.S., Askury, A.K., Putthapiban, P., Djaswadi, S., 1995. The Southeast Asian tin belt. Earth-Science Reviews 38, 95-293.

Searle, M.P., Whitehouse, M.J., Robb, L.J., Ghani, A.A., Hutchison, C.S., Sone, M., Ng, S.W.P., Roselee, M.H., Chung, S.L., Oliver, G.J.H., 2012. Tectonic evolution of the Sibumasu-Indochina terrane collision zone in Thailand and Malaysia: Constraints from new U-Pb zircon chronology of SE Asian tin granitoids. Journal of the Geological Society 169, 489-500.

Sevastjanova, I., Clements, B., Hall, R., Belousova, E.A., Griffin, W.L., Pearson, N., 2011. Granitic magmatism, basement ages, and provenance indicators in the Malay Peninsula: Insights from detrital zircon U–Pb and Hf-isotope data. Gondwana Research 19, 1024-1039.

Sevastjanova, I., Hall, R., Rittner, M., Paw, S.M.T.L., Naing, T.T., Alderton, D.H., Comfort, G., 2016. Myanmar and Asia united, Australia left behind long ago. Gondwana Research 32, 24-40.

Shi, M.F., Lin, F.C., Fan, W.Y., Deng, Q., Cong, F., Tran, M.D., Zhu, H.P., Wang, H., 2015. Zircon U-Pb ages and geochemistry of granitoids in the Truong Son terrane, Vietnam: Tectonic and metallogenic implications. Journal of Asian Earth Sciences 101, 101-120.

Singharajwarapan, S., Berry, R., 2000. Tectonic implications of the Nan Suture Zone and its relationship to the Sukhothai Fold Belt, Northern Thailand. Journal of Asian Earth Sciences 18, 663-673.

Sone, M., Metcalfe, I., 2008. Parallel Tethyan sutures in mainland Southeast Asia: New insights for Palaeo-Tethys closure and implications for the Indosinian orogeny. Comptes Rendus - Geoscience 340, 166-179.

Sone, M., Metcalfe, I., Chaodumrong, P., 2012. The Chanthaburi terrane of southeastern Thailand: Stratigraphic confirmation as a disrupted segment of the Sukhothai Arc. Journal of Asian Earth Sciences 61, 16-32.

Stacey, J.S., Kramers, J.D., 1975. Approximation of terrestrial lead isotope evolution by a two-stage model. Earth and Planetary Science Letters 26, 207-221.

Taylor, R.N., Ishizuka, O., Michalik, A., Milton, J.A., Croudace, I.W., 2015. Evaluating the precision of Pb isotope measurement by mass spectrometry. Journal of Analytical Atomic Spectrometry 30, 198-213.

Ueno, K., Charoentitirat, T., 2011. Carboniferous and Permian, in: Ridd, M.F., Barber, A.J., Crow, M.J. (Eds.), The Geology of Thailand. The Geological Society, London, pp. 71-136.

Ueno, K., Hisada, K., 2001. The Nan-Uttaradit-Sa Kaeo Suture as a main Paleo-Tethyan suture in Thailand: Is it real? . Gondwana Research, 804-805.

Usuki, T., Lan, C.-Y., Wang, K.-L., Chiu, H.-Y., 2013. Linking the Indochina block and Gondwana during the Early Paleozoic: Evidence from U–Pb ages and Hf isotopes of detrital zircons. Tectonophysics 586, 145-159.

Vervoort, J.D., Patchett, P.J., Blichert-Toft, J., Albarède, F., 1999. Relationships between Lu–Hf and Sm–Nd isotopic systems in the global sedimentary system. Earth and Planetary Science Letters 168, 79-99.

Wakita, K., Metcalfe, I., 2005. Ocean Plate Stratigraphy in East and Southeast Asia. Journal of Asian Earth Sciences 24, 679-702.

Wang, L., Long, W., Zhou, D., Xu, W., Jin, X., 2016a. Late Triassic zircon U-Pb ages and Sr-Nd-Hf isotopes of Darongshan granites in southeastern Guangxi and their geological implications. Geological Bulletin of China 35, 1291-1303.

Wang, S., Mo, Y., Wang, C., Ye, P., 2016b. Paleotethyan evolution of the Indochina Block as deduced from granites in northern Laos. Gondwana Research 38, 183-196.

Wang, W., Cawood, P.A., Zhou, M.-F., Pandit, M.K., Xia, X.-P., Zhao, J.-H., 2017. Low-δ18O Rhyolites From the Malani Igneous Suite: A Positive Test for South China and NW India Linkage in Rodinia. Geophysical Research Letters 44, 10,298-210,305.

Wang, Y., He, H., Cawood, P.A., Srithai, B., Feng, Q., Fan, W., Zhang, Y., Qian, X., 2016c. Geochronological, elemental and Sr-Nd-Hf-O isotopic constraints on the petrogenesis of the

Triassic post-collisional granitic rocks in NW Thailand and its Paleotethyan implications. Lithos 266-267, 264-286.

Wielchowsky, C.C., Young, J.D., 1985. Regional facies variations in Permian rocks of the Phetchabun fold and thrust belt, Thailand., in: Thanvarachorn, P., Hokjaroen, S., Youngme, W. (Eds.), Conference on Geology and Mineral Resources Development of the North-east Thailand, Khon Kaen, pp. 41-55.

Wilde, S.A., 1999. Evolution of the Western Margin of Australia during the Rodinian and Gondwanan Supercontinent Cycles. Gondwana Research 2, 481-499.

Yokart, B., Barr, S.M., Williams-Jones, A.E., Macdonald, A.S., 2003. Late-stage alteration and tin–tungsten mineralization in the Khuntan Batholith, northern Thailand. Journal of Asian Earth Sciences 21, 999-1018.

Zaw, K., Meffre, S., Lai, C.-K., Burrett, C., Santosh, M., Graham, I., Manaka, T., Salam, A., Kamvong, T., Cromie, P., 2014. Tectonics and metallogeny of mainland Southeast Asia — A review and contribution. Gondwana Research 26, 5-30.

ABSTRACT

This article provides zircon U–Pb and Lu–Hf isotopic information along with whole-rock Sm–Nd, Sr and Pb isotopic geochemistry from granitoids in Thailand. The U–Pb ages are described and the classification of crystallisation and inherited ages are explained. The petrography of the granitoid samples is detailed. The data presented in this article are interpreted and discussed in the research article entitled "Probing into Thailand's basement: New insights from U–Pb geochronology, Sr, Sm–Nd, Pb and Lu–Hf isotopic systems from granitoids" (Dew et al. 2018).

Value of the data

- Assists in the understanding of the basement of Thailand, which is mostly covered by thick sequences of younger sediment
- This combination of isotopic data is an innovative approach to investigate the buried rock systems that make up this key part of Southeast Asia.
- This approach and methodology can be implemented for future studies to further understand the evolution of this part of the world.
- Can be compared with other isotopic data from Southeast Asia for further insight into the tectonic history of the region
- Provides information about Thailand's history and its links to Australia

1. Data

In this article, we report isotopic data from Thai granitoids of the Southeast Asian Granitoid Belts. This data includes U–Pb geochronology and Lu–Hf analyses from over 480 zircons and Sm–Nd, Sr and Pb isotopic geochemistry from fourteen whole-rock granitoid samples.

U–Pb data were obtained during nine sessions along with common zircon reference materials (e.g. GJ-1, Plešovice and 91500). Lu–Hf data were obtained during three sessions along with common zircon reference materials (e.g. Mudtank and Plešovice). The zircon dataset contains the LA–ICP–MS raw and processed data. Each of the four whole-rock isotopes were measured for all samples in one TIMS analytic run. The mass fractionation for Sm–Nd, Sr and Pb was controlled by the G-2 standard (Flanagan 1976), with the BHVO-2 standard (Wilson 1997) was also used for the Sm and Nd analyses.

2. Experimental design, materials and methods

2.1 Model ages for Thailand's basement

Twenty-nine granitoid samples in total are used for this study. For detailed preparatory methodology of the KM, ST and NT samples see De Grave et al. (2015) and De Clercq (2016). The individual sample locations, lithology, associated granitoid belt where applicable and analysis method for each sample are outlined in Table 1 of Dew et al. (2018). Details of the petrography including mineralogy, textures and degree of deformation are outlined in Table 1. Hand specimen and thin section imagery of the analysed samples are displayed in Fig. 1. Some of the analysed granitoids are associated with named batholiths or specific plutons whose petrography and petrogenesis has been previously described, for further information see Table 1 of Dew et al. (2018). The sampling strategy for this study was to collect granitoids from all three terranes and across major faults and sutures to

Specifications Table

Subject area	*Geology*
More specific subject area	*Geochronology, isotope geochemistry, zircon, granitoid*
Type of data	*Tables, images (photographs and microscopy)*
How data was acquired	*Petrography and Thin Section Imagery: Zeiss AxioScope A1 microscope with a AxioCam MRc5 camera* *Cathodoluminescence:* FEI Quanta600 Scanning Electron Microscope with the Mineral Liberation Analysis *U–Pb geochronology: Agilent 7900x with a New Wave NW213 laser ablation system with a TwoVol2 sample chamber (Adelaide Microscopy)* *Lu–Hf isotope analyses: Resonetics S-155-LR 193nm excimer laser ablation system connected to a Nu Plasma II multi-collector ICP–MS (Perth) and a Neptune Plus multi-collector ICP–MS (Wollongong)* *Whole-rock geochemistry: Isotopix Phoenix thermal ionization mass spectrometer (University of Adelaide Isotope Geochemistry Facility)*
Data format	*The 2015 U–Pb data were collected, corrected and filtered in the GLITTER version 3.0 software package (Van Achterbergh et al. 2001). The 2017* U–Pb *data and all* Lu–Hf analyses *were reduced using Iolite software (Paton et al. 2011).* *Corrected individual analyses are given in .xlsx format*
Experimental factors	*Zircons were extracted from bulk rock granitoid samples through the conventional magnetic and heavy liquid separation procedures.* *Whole-rock geochemistry samples were prepared with standard milling equipment.*
Experimental features	*Separated zircon grains were mounted in epoxy resin, polished and mapped by cathodoluminescence.* *Major and trace elemental compositions were determined prior to whole-rock isotopic analyses using an x-ray fluorescence spectrometer.*
Data source location	*Granitoid belts of Thailand, specific coordinates for each sample tabulated.*
Data accessibility	*Data is with this article and/or the below related research article*
Related research article	Dew, R.E.C., Collins, A.S., Glorie, S., Morley, C.K., Nachtergaele, S., Blades, M.L., King, R., Foden, J., De Grave, J., Kanjanapayont, P., Evans, N.J., Alessio, B.L. and Charusiri, P. Probing into Thailand's basement: New insights from U–Pb geochronology, Sr, Sm–Nd, Pb and Lu–Hf isotopic systems from granitoids. *Lithos*. **320-321**, 332-354, https://doi.org/10.1016/j.lithos.2018.09.019.

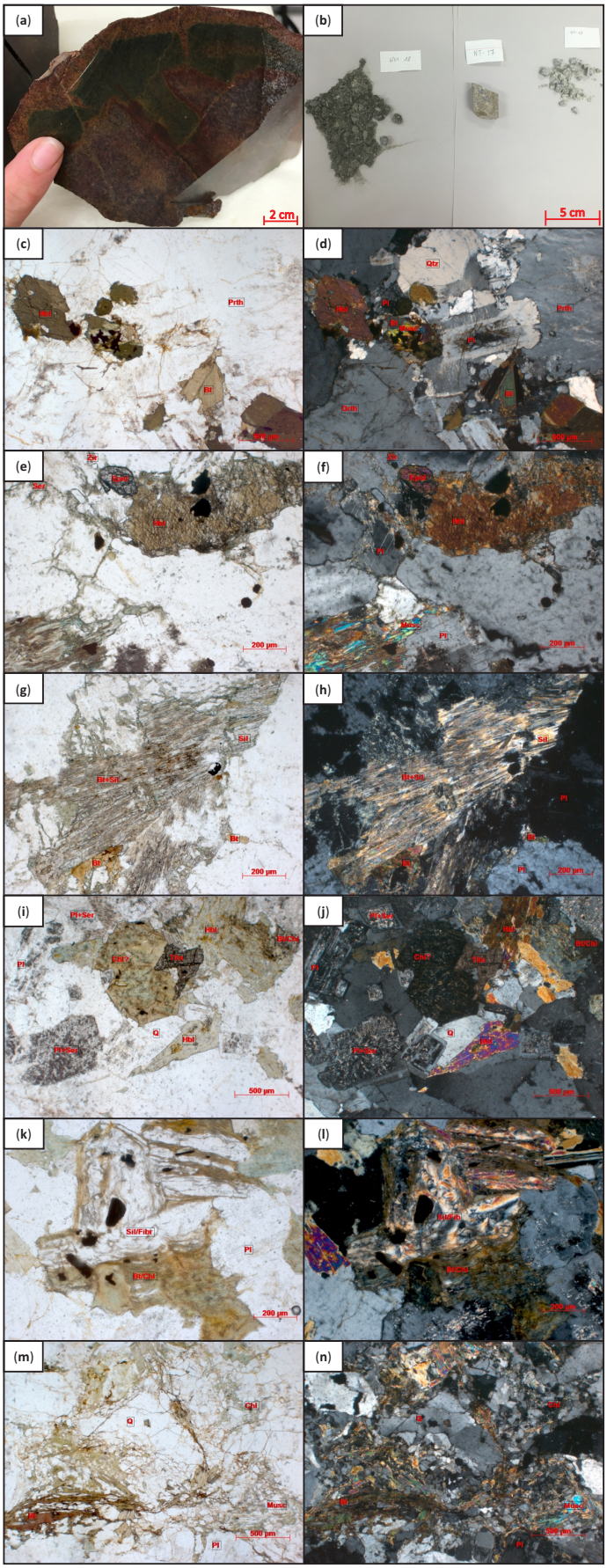
(a)
2 cm
(b)
5 cm
(c)
(d)
(e)
(f)
(g)
(h)
(i)
(j)
(k)
(l)
(m)
(n)

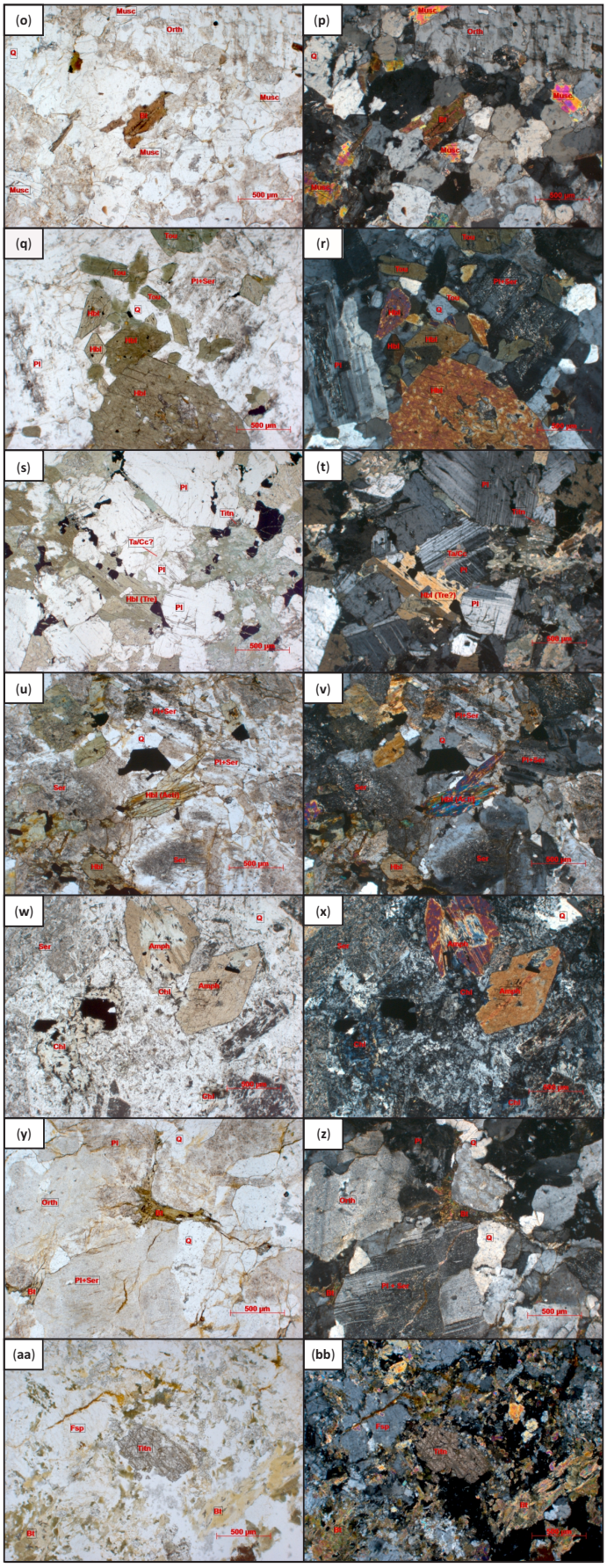
(o)
(p)
(q)
(r)
(s)
(t)
(u)
(v)
(w)
(x)
(y)
(z)
(aa)
(bb)

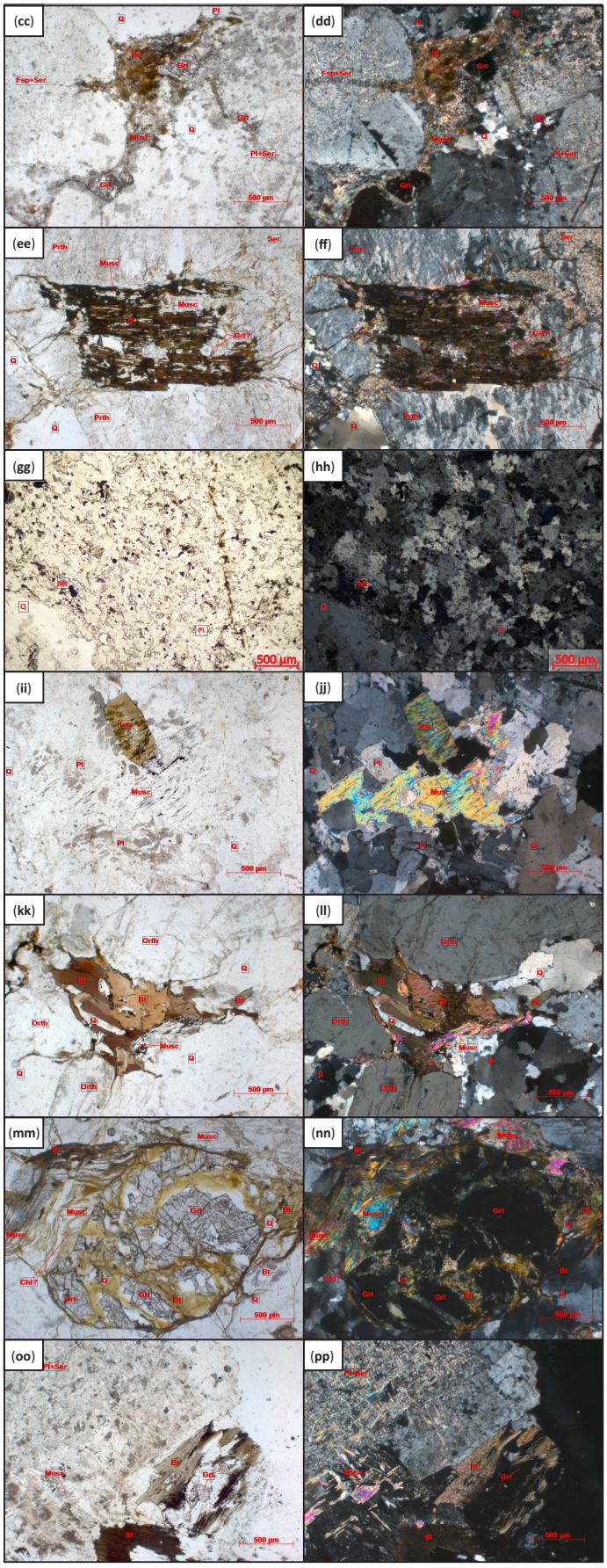
(cc)
(dd)
(ee)
(ff)
(gg)
(hh)
(ii)
(jj)
(kk)
(ll)
(mm)
(nn)
(oo)
(pp)
500 µm

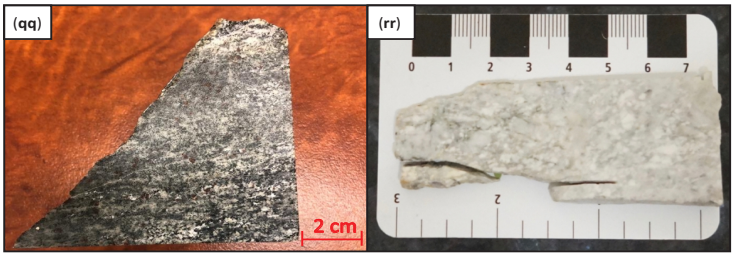

Fig. 1. Thin sections, outcrop and hand specimens of granitoid samples. Minerals present are labelled where: Qtz is quartz; Bt is biotite; Mu is muscovite; Am is amphibole mainly hornblende in these samples); Pl is plagioclase; Mc is microcline and Px is pyroxene. (a) Hand specimen of RDT15_076A altered granodiorite (b) From left to right: rock chips of KM-18, NT-17 and ST-03 (c) KM-12 overview thin section image in Plane Polarised Light (PPL) 10x (d) KM-12 overview thin section image in Cross Polarised Light (XPL), (e) KM-25 overview thin section image in PPL, (f) KM-25 overview thin section image in XPL, (g) KM-25 overview thin section image showing sillimanite mineral growth in PPL, (h) KM-25 overview thin section image showing sillimanite mineral growth in XPL, (i) KM-26 overview thin section image in PPL, (j) KM-26 overview thin section image in XPL, (k) KM-26 overview thin section image showing sillimanite mineral growth in PPL, (l) KM-26 overview thin section image showing sillimanite mineral growth in XPL, (m) KM-40A overview thin section image in PPL, (n) KM-40A overview thin section image in XPL, (o) NT-01 overview thin section image in PPL, (p) NT-01 overview thin section image in XPL, (q) NT-04 overview thin section image in PPL, (r) NT-04 overview thin section image in XPL, (s) NT-06 overview thin section image in PPL, (t) NT-06 overview thin section image in XPL, (u) NT-07 overview thin section image in PPL, (v) NT-07 overview thin section image in XPL, (w) NT-09 overview thin section image in PPL, (x) NT-09 overview thin section image in XPL, (y) NT-10 overview thin section image in PPL, (z) NT-10 overview thin section image in XPL, (aa) NT-11 overview thin section image in PPL, (bb) NT-11 overview thin section image in XPL, (cc) NT-12 overview thin section image in PPL, (dd) NT-12 overview thin section image in XPL, (ee) NT-13 overview thin section image in PPL, (ff) NT-13 overview thin section image in XPL, (gg) RDGEOCHEM-1 overview thin section image in PPL, (hh) RDGEOCHEM-1 overview thin section image in XPL, (ii) ST-03 overview thin section image in PPL, (jj) ST-03 overview thin section image in XPL, (kk) ST-08A overview thin section image in PPL, (ll) ST-08A overview thin section image in XPL, (mm) ST-16 overview thin section image in PPL, (nn) ST-16 overview thin section image in XPL, (oo) ST-49A overview thin section image in PPL, (pp) ST-49A overview thin section image in XPL, (qq) RDT16_044 hand specimen, (rr) RDT16_053 hand specimen.

better delineate tectonic boundaries. Representative samples of granitoids, and therefore also their underlying basement, were collected from widespread localities within Thailand.

The three main tectonic domains in Thailand: Sibumasu, Sukhothai and Indochina, are associated with three large granites provinces: Western Thailand/ Myanmar, North Thailand–West Malaya Main Range and East Malaya (for further information and locations see Cobbing et al. 1992; Gardiner et al. 2016; Searle et al. 2012). The Western Thailand–Myanmar/Burma Province also known as the Mogok–Mandalay–Mergui Belt extends from eastern Myanmar (Burma) southwards to Phuket Island. The Mogok–Mandalay–Mergui Belt and the Western Thailand North Thailand–West Malaya Main Range broadly correlate with the Sibumasu Terrane and Inthanon Zone respectively although this correlation depends on the delineation of the terrane boundaries, which are have been variably defined in the past (Audley-Charles et al. 1988; Gardiner et al. 2016; Hisada et al. 2004; Metcalfe 1984). The mineralogy consists of hornblende–biotite I-type granodiorite–granites and felsic biotite–K-feldspar (± garnet ±

tourmaline) S-type granites (Searle et al. 2012; Sone and Metcalfe 2008). These granitoids are associated with abundant tin mineralisation in greisen type veins (Searle et al. 2012). Recent U–Pb dating of Western Thailand granitoids in Phuket displays zircons with Triassic cores (e.g. 212 ± 2 Ma and 214 ± 2 Ma) and Cretaceous rims (81.2 ± 1.2 and 85–75 Ma) (Searle et al. 2012).

The North Thailand–West Malaya or Main Range Province occurs northward from West Malaya towards to the Doi Inthanon range of north Thailand. This province is characteristically is composed of biotite–K-feldspar S-type granites although also contains subordinate I-type granitoids (Cobbing et al. 1992; Searle et al. 2012). Searle et al. (2012) suggests that they are more likely to be evolved felsic I-types rather than the S-type granites proposed by Cobbing et al. (1992). The ages of this province range from early late Triassic to late early Jurassic (Sone and Metcalfe 2008). The sheer batholithic proportions of this province suggest crustal anatexis as the potential source (Searle et al. 2012). It is suggested that these granitoids are orogenic, forming as a result of the crustal thickening following the closure of the Palaeo-Tethys and the collision of Sibumasu and Sukhothai–Indochina in the late Triassic (Searle et al. 2012; Sone and Metcalfe 2008). The boundary between the Western Province and the West Malaya Main Range Province has been historically defined as the Paleogene Khlong Marui fault (e.g. Cobbing et al. 1992). However, Searle et al. (2012) suggests that the nature of the boundary is not as clear as stated by Cobbing et al. (1992) due to the presence of S-type granite either side of the Khlong Marui fault, which also formed later than the granite emplacement.

The Eastern or East Malaya Province is mostly Permo-Triassic I-type granites, granodiorites and tonalities but with subordinate S-type plutons and A-type syenite–gabbros (Cobbing et al. 1992; Searle et al. 2012). The I-type granitoids of the East Malaya Province are distributed throughout the Sukhothai and Indochina terranes (Gardiner et al. 2016; Sone and Metcalfe 2008). These granitoids are thought to originate from arc magmatism caused by the subduction of the Palaeo-Tethys under Indochina (Searle et al. 2012; Sone and Metcalfe 2008). However, the genesis of the S-type granitoids associated with the Loei-Phetchabun Volcanic Belt is unlikely to be subduction-induced arc magmatism. Instead, it is suggested by Sone and Metcalfe (2008) to be associated to the crustal thickening of western Indochina that was induced by back-arc compression and later emphasised by the Sibumasu collision. The East Malaya Province granitoids range primarily from the early Permian to end of the Triassic with occasional Cretaceous magmatism, which is shared with the Western Thailand–Myanmar/Burma Province (Searle et al. 2012; Sone and Metcalfe 2008).

2.2 Zircon sample preparation

Eighteen granitoid rock samples were crushed and sieved for collecting zircon grains through the conventional magnetic and heavy liquid separation procedures. About 50 randomly selected zircon grains were set in epoxy resin and polished for U–Pb zircon age analysis. In order to characterise the textural and chemical-zoning features within each zircon (Table 2), cathodoluminescence (CL) images for zircon were obtained using the FEI Quanta600 Scanning Electron Microscope with the Mineral Liberation

Analysis (MLA) at Adelaide Microscopy, Adelaide, South Australia. Each mount was carbon coated prior to CL imaging to increase the conductivity of the sample and to retrieve higher quality images.

For each sample, 20–30 magmatic grains were selected for laser ablation inductively coupled plasma mass spectrometry (LA–ICP–MS) at Adelaide Microscopy, Adelaide, South Australia. All assumed inherited grains or distinct zircon domains were also ablated using LA–ICP–MS. The analyses were conducted on an Agilent 7900x with a New Wave NW213 laser ablation system with a TwoVol2 sample chamber. A 30 μm spot size was used where possible, however, one analysis session used a smaller 25 μm spot size due to the smaller size of the zircon grains (see Table 3). A 5 Hz pulse rate was used with a typical pit depth of 30–50 μm. For further details of the analytical methodology of this laboratory's technique see Payne et al. (2006). The exact fluence settings across the two-year analysis period ranged from 5.6 to 7 J/cm^2. The isotopes measured for all analyses were ^{204}Pb, ^{206}Pb, ^{207}Pb, ^{208}Pb, ^{232}Th and ^{238}U (see Table 3). The GEMOC zircon standard GJ-1 (^{207}Pb/^{206}Pb TIMS age of 607.7 ± 4.3 Ma, ^{206}Pb/^{238}U TIMS age of 600.7 ± 1.1 Ma and ^{207}Pb/^{235}U age of 602.0 ± 1.0 Ma all ages given as 2σ; Jackson et al. 2004) was run as the primary standard every 10–20 unknown analyses, to correct for isotopic drift and down-hole fractionation. The Plešovice zircon standard (^{206}Pb/^{238}U age of 337.13 ± 0.37 Ma (2σ); Sláma et al. 2008) was analysed as a secondary standard to check the accuracy of the technique. Across all analytical sessions, analyses of GJ-1 yielded a ^{206}Pb/^{238}U weighted average age of 601.61 ± 0.47 Ma (n=556, MSWD=1.10, 2σ) and Plešovice yielded a ^{206}Pb/^{238}U weighted average age of 339.55 ± 0.73 (n=243, MSWD=3.7, 2σ). For the later batches analysed in 2017, ^{90}Zr and ^{202}Hg isotopes were measured where possible, see Table 3. For some LA–ICP–MS runs, ^{204}Pb was not measured due to the unresolvable isobaric interference from ^{204}Hg (Schoene 2014). For two of the analysis sessions, the rare earth element suite was also monitored (see Table 3). The 2017 batches were also run with the 91500 zircon as another secondary standard (^{207}Pb/^{206}Pb age of 1065 Ma and ^{206}Pb/^{238}U age of 1062 Ma; Wiedenbeck et al. 1995). During these analyses, 135 analyses of 91500 yielded a ^{206}Pb/^{238}U age of 1036.2 ± 3.3 (MSWD=4.2, 2σ). Two different 91500 crystals were used for these analyses, where one crystal gives good reproducibility while the other is more heterogeneous. This heterogeneity accounts for the large MSWD across the three analytic runs monitoring this standard. However, in this study GJ-1 was used as the primary zircon standard so the isotopic drift across the analytic periods in the secondary standards (Plešovice and 91500 was used as one of two secondary standards and was not used as a primary standard to correct for isotopic drift and down-hole fractionation.

The 2015 data were collected, corrected and filtered in the GLITTER version 3.0 software package (Van Achterbergh et al. 2001). The 2017 data were reduced using Iolite software (Paton et al. 2011). All concordia diagrams and weighted averages were calculated using ISOPLOT 4.15 for Excel (Ludwig 1998).

2.3 Zircon Lu–Hf isotope analysis

After the U–Pb zircon geochronology analyses were conducted, ten of these granitoid samples were selected for further zircon Lu–Hf isotope analysis. A subset of the zircon grains for each

sample were then analysed for their hafnium isotopic composition (the specific grains analysed and their concordance percentage are highlighted in Table 4). The number of Hf analyses for each sample was determined by the variability in the age data and the amount of interpreted inheritance. Nine samples used for Hf and Lu isotopic analyses (all samples except KM-20) were analysed using a Resonetics S-155-LR 193nm excimer laser ablation system connected to a Nu Plasma II multi-collector ICP–MS in the GeoHistory Facility, John de Laeter Centre, Curtin University, Perth, Western Australia. Analyses were carried out using a laser beam diameter of 50 μm. After two cleaning pulses and 40s of baseline acquisition, zircon grains were ablated for 35s using a 10 Hz repetition rate, and a laser beam energy of 2 J/cm². All isotopes (^{180}Hf, ^{179}Hf, ^{178}Hf, ^{177}Hf, ^{176}Hf, ^{175}Lu, ^{174}Hf, ^{173}Yb, ^{172}Yb and ^{171}Yb) were counted on the Faraday collector array (see Table 4 and 5 for further details). Time resolved data were baseline subtracted and reduced using Iolite (DRS after Woodhead et al. 2004) where ^{176}Yb and ^{176}Lu were removed from the 176 mass signal using ^{176}Yb/^{173}Yb = 0.7962 (and ^{176}Lu/^{175}Lu = 0.02655; Chu et al. 2002) with an exponential law mass bias correction assuming ^{172}Yb/^{173}Yb = 1.35274 as per Chu et al. (2002). The interference corrected ^{176}Hf/^{177}Hf was normalised to ^{179}Hf/^{177}Hf = 0.7325 (Patchett and Tatsumoto 1980), for mass bias correction. Mud Tank (^{176}Hf/^{177}Hf of 0.282505 ± 0.000044; Woodhead and Hergt 2005) was used as the primary standard for Hf isotopes and R33 as the primary standard for Lu–Hf analyses (^{176}Hf/^{177}Hf of 0.282764 ± 0.000014; Fisher et al. 2014, Lu/Hf ratios of 0.001989 ± 0.000869; Sláma et al. 2008).

Mudtank analyses yielded ^{176}Hf/^{177}Hf weighted means of 0.2825064 ± 0.0000097 (2σ, n=29, MSWD=0.89, for the first session including all Hf samples except RDT16_053 and KM-20; Table 5) and 0.2825071 ± 0.0000081 (2σ, n=29, MSWD=0.041, for RDT16_053 analysis run). The R33 standard yielded ^{176}Hf/^{177}Hf weighted mean of 0.282718 ± 0.000010 (2σ, n=28, MSWD=1.14) and Lu/Hf ratios of 0.0019903 ± 0.0000097 (2σ, n=28, MSWD=19) for the first session (including all Hf samples except RDT16_053 and KM-20) and for the analyses for RDT16_053 yielded ^{176}Hf/^{177}Hf weighted mean of 0.282708 ± 0.000017 (n=14, MSWD = 3.6) and Lu/Hf ratios of 0.001988 ± 0.000040 (2σ, n=28, MSWD=101). Secondary standards were 91500 (^{176}Hf/^{177}Hf of 0.282306 ± 0.00004; Woodhead et al. 2004), GJ-1 (^{176}Hf/^{177}Hf of 0.282000 ± 0.000005; Morel et al. 2008) and FC-1 (^{176}Hf/^{177}Hf of 0.282172 ± 0.000042; Woodhead and Hergt 2005). Additionally for the first session (March 2017 Table 5, including all Hf samples except RDT16_053 and KM-20), Plešovice was used as a secondary standard (^{176}Hf/^{177}Hf of 0.282482 ± 0.000013 and Lu/Hf ratio of 0.0004–0.0015; Sláma et al. 2008). The ^{176}Hf/^{177}Hf weighted averages for the analysis of the secondary standards are outlined in Table 5. The corrected ^{178}Hf/^{177}Hf ratio was calculated to monitor the accuracy of the mass bias correction and yielded average values of 1.467219 ± 0.000016 (n=214; March 2017) and 1.467117 ± 0.000011 (n=296; July 2017), which are both within the range of values reported by Thirlwall and Anczkiewicz (2004).

Hafnium analysis for one sample (KM-20) was undertaken using a Neptune Plus multi-collector ICP–MS at the University of Wollongong, New South Wales. The dwell time was 50 seconds with 5 Hz

repetition rate and an intensity of 4.4 J/cm². Standards were Mudtank ($^{176}Hf/^{177}Hf$ of 0.282505 ± 0.000044; Woodhead and Hergt 2005) and Plešovice ($^{176}Hf/^{177}Hf$ of 0.282482 ± 0.000013 and Lu/Hf ratio of 0.0004–0.0015; Sláma et al. 2008), yielding $^{176}Hf/^{177}Hf$ weighted averages of 0.282473 ± 0.000023 (2σ, n=2) and 0.282450 ± 0.000018 (2σ, n=2) respectively. The corrected $^{178}Hf/^{177}Hf$ ratio was calculated to monitor the accuracy of the mass bias correction and yielded an average value of 1.467227 ± 0.000012 (n=19), which is within the range of values reported by Thirlwall and Anczkiewicz (2004). All Lu–Hf data was reduced using Iolite software (Paton et al. 2011). Calculation of $\varepsilon Hf_{(t)}$ values employed the decay constant of Scherer et al. (2001) and the Chondritic Uniform Reservoir (CHUR) values of Bouvier et al. (2008), depleted mantle Lu/Hf values of Griffin et al. (2000) and Hf/Hf values of Nowell et al. (1998).

2.4 Sm–Nd, Sr and Pb whole-rock geochemistry

Sm–Nd and Sr isotopic whole-rock analyses were conducted for fourteen granitoid samples and one duplicate run for Sm–Nd analyses (NT-13) at the University of Adelaide's Isotope Geochemistry Facility (see Table 1 of Dew et al. (2018)). Eight samples and one duplicate (NT-13) were used for whole-rock Pb isotope measurements (see Table 1 of Dew et al. (2018)). These samples were chosen due to their spatial distribution across the main tectonic terranes in Thailand and also containing Nd, Sr and Pb elemental concentrations above the detection limits of the X-ray fluorescence spectrometer (XRF) at Franklin and Marshall College, U.S.A. (major and trace element data provided in Table 6). A detailed methodology for the Sr and Sm–Nd whole-rock isotope techniques conducted in the same laboratory are outlined by Arboit et al. (2016).

To minimise error magnification, the optimal spike amount was calculated for each sample (i.e. approximately 0.4 g of Sm–Nd spike H per 2 µg Nd and 0.08 g of Sr spike C per 1 µg Sr). Six of the fourteen samples used for Nd and Sr whole-rock geochemistry contained Pb ppm concentrations below the 1 ppm detection limit of the XRF, therefore, the subsequent whole-rock Pb TIMS analyses were not completed on these samples. The Pb isotopes were corrected for mass fractionation using the Southampton–Brest lead ^{207}Pb–^{204}Pb double spike (SBL74) as outlined by Taylor et al. (2015). This spike was formulated to minimise uncertainty propagation with sample $^{206}Pb/^{204}Pb$ isotope compositions in the range of 14 to 30 (Taylor et al. 2015). SBL74 is calibrated relative to a conventional reference value $^{208}Pb/^{206}Pb$=1.00016 for NIST SRM 982 and has a composition of $^{204}Pb/^{206}Pb$=9.2317, $^{207}Pb/^{206}Pb$=36.6450 and $^{208}Pb/^{206}Pb$=1.8586 (Taylor et al. 2015).

Lead contamination was effectively negated by removing metals and silicates and minimising atmospheric and procedural contamination by conducting analyses in a clean lab setting of the University of Adelaide's Isotope Geochemistry Facility. Lead was isolated from the sample matrix by twice passing each sample through an HBr solution using anion exchange chromatography. For TIMS analysis, each sample was loaded with silicic acid–phosphoric acid emitter onto two zone-refined Re filaments using the double spike procedure outlined by Taylor et al. (2015). The two filament loads consist of: a "natural" run with

sample only and a sample–spike mixture run. The optimum mixture of sample and spike was calculated as $^{204}Pb_{Sample}/^{204}Pb_{Spike}$ (q) = 0.09, with a tolerance range of 0.03–0.65 within which negligible uncertainty magnification was observed.

Sm–Nd, Sr and Pb whole-rock isotopes were measured on the *Isotopix Phoenix* thermal ionization mass spectrometer (TIMS) at the University of Adelaide, South Australia (see Table 7). The total procedural blanks were <475 pg for Sr, <221 pg for Sm, <699 pg for Nd and <74.1 pg for Pb. If the procedural blank is <1/1000th sample then it can be considered negligible (e.g. a procedural blank of 2 ng Nd could be considered not significant for a sample of 2 μg Nd; see Table 7 for elemental concentrations measured by TIMS for individual samples). The mass fractionation for Sm–Nd, Sr and Pb was controlled by the G-2 standard (Flanagan 1976), which yielded average ratios of $^{143}Nd/^{144}Nd$ = 0.512261 ± 0.000002 (2 SE) and $^{87}Sr/^{86}Sr$ = 0.709770 ± 0.000003 (2 SE). For the Pb isotopes the G-2 standard (Flanagan 1976), yielded corrected ratios of 18.3870, 15.6361 and 38.903 for $^{206}Pb/^{204}Pb$, $^{207}Pb/^{204}Pb$ and $^{208}Pb/^{204}Pb$ respectively. A secondary standard, BHVO-2 (Wilson 1997), was also measured for Sm and Nd analyses yielding average ratios of $^{143}Nd/^{144}Nd$ = 0.513034 ± 0.000002 (2 SE). Although none of the samples analysed are basaltic in composition, the Nd ppm value of the BHVO-2 basalt standard was similar to the expected Nd ppm concentration of the unknown granitoid samples. The Nd isotopic reference JNdi-1 (0.512115 ± 0.000007; Tanaka et al. 2000), yielded average ratios of $^{143}Nd/^{144}Nd$ = 0.512100 ± 0.000002 (2 SE) and 0.512103 ± 0.000002 (2 SE). The University of Adelaide Isotope Geochemistry Facility's laboratory average for the JNdi-1 Nd isotopic reference is 0.512106 ± 0.000009 (2σ). During the period of Sr analysis, the two analyses of the Sr isotopic standard SRM987 yielded average ratios of $^{87}Sr/^{86}Sr$ = 0.710246 ± 0.000003 (2 SE) and 0.710243 ± 0.00002 (2 SE). SRM981, the Pb isotopic reference used in this study ($^{206}Pb/^{204}Pb$=16.9412 ± 0.0003; $^{207}Pb/^{204}Pb$=15.4988 ± 0.0006; $^{208}Pb/^{204}Pb$=36.7233 ± 0.0013; Taylor et al. 2015), yielded corrected ratios of 16.9436, 15.5013 and 36.729 for $^{206}Pb/^{204}Pb$, $^{207}Pb/^{204}Pb$ and $^{208}Pb/^{204}Pb$ respectively. The whole-rock measurements from the TIMS analyses and calculated initial isotopic values are displayed in Table 7.

2.5 U–Pb crystallisation and inherited age determination

The crystallisation ages have been interpreted individually for each sample, depending on the nature of the data. This is because different zircons behave differently in the U–Pb isotopic system. The data interpreted to represent the crystallisation age are stated in Dew et al. (2018) with further explanatory information detailed below for each sample (the data are also highlighted in bold in Table 4). Inherited grains are defined as zircons that are older than the crystallisation age of the sample. The associated Concordia curves, regression lines and weighted average age plots are illustrated in Fig. 3 from Dew et al. (2018).

2.5.1 Sibumasu Terrane

While the interpreted crystallisation age for ST-16 was Cambrian, there were also concordant $^{206}Pb/^{238}U$ ages between 371.5 ± 5.81 Ma and 83.7 ± 1.37 Ma, which may have been due to later resetting post-crystallisation (see Table 4). These younger analyses from ST-16 had very low Th:U, suggesting that the large Th ion has diffused from the zircon during a

subsequent thermal event (see Kirkland et al. 2015). The observation that young $^{206}Pb/^{238}U$ age zircons have low Th/U ratios suggests that both Pb and Th have been lost from the zircon. This is supported by petrographic observations of igneous garnet breaking down to muscovite, chlorite and biotite (Fig. 1—mm, nn). Older concordant (±10%) ages were measured from $^{207}Pb/^{206}Pb$ age of 3189.3 ± 17.83 Ma to $^{206}Pb/^{238}U$ age of 710.5 ± 11.63 Ma (Table 1). The older ages analysed were interpreted to be inherited from events prior to the crystallisation of the granite.

NT-17 contained concordant ±5% zircon analyses with ages ranging from 209.7 ± 3.0 Ma and 196.3 ± 2.8 Ma (2σ). The measured dataset included several older analyses with ages of 2755 Ma, 2685 Ma, 1248 Ma, 947 Ma and 836 Ma (see Table 4). The Concordia of NT-17 (Fig. 3 of Dew et al. (2018)) shows that many of the zircons analysed sit off the Concordia line, indicating that the U–Th–Pb system was no longer working as a closed system. A weighted average was first taken from all analyses within ±5% concordance, yielding a $^{206}Pb/^{238}U$ age of 211.2 ± 4.0 Ma (n=17, MSWD=27). This calculated age has a very large Mean Square Weighted Deviation (MSWD) indicating that the data are overdispersed with the observed data scatter exceeding the predicted analytical uncertainties. In attempt to better constrain the crystallisation age, another weighted average age was taken from the cluster of ten concordant (±5%) data analyses, which consequently yielded an age within error of the first weighted average and the data was more closely dispersed within the range of the predicted analytical uncertainties (see Table 4 and Fig. 3 of Dew et al. (2018)).

An Upper Triassic crystallisation age was interpreted for ST-08A (see Table 4). Although the weighted average age MSWD of 3.1 indicates that the data are overdispersed, there are no clear distinguishing factors to filter the data any further. Two interpreted concordant inherited ages were found with a $^{207}Pb/^{206}Pb$ age of 2473 ± 34 Ma and a $^{206}Pb/^{238}U$ age of 393.1 ± 9.3 Ma.

Similar to ST-08A, the crystallisation age of ST-13 was also calculated to be Upper Triassic. Cretaceous aged analyses from ST-13 often had very low Th:U (Table 4, shown in white on Fig. 3 of Dew et al. (2018)), suggesting that the large Th ion has diffused from the zircon during a subsequent thermal event. The observation that young $^{206}Pb/^{238}U$ age zircons have low Th/U ratios suggests that both Pb and Th have been lost from the zircon. Therefore, this younger cluster of Cretaceous data was interpreted to be the age of metamorphic resetting (see Table 4 and text and Fig. 3 of Dew et al. (2018)). There was a prominence of age inheritance for ST-13 ranging from 1736 Ma to 500 Ma. Many of the older ages were taken from cores of zircons with multiple domains. ST-13 often contained up to four CL domains in the one zircon. Often at least one domain was Triassic in age, these inner domains were interpreted to be age of crystallisation.

The majority of zircon analyses for ST-49A were around 80 Ma, with eleven concordant (±5%) zircon analyses, yielding a $^{206}Pb/^{238}U$ age of 79.8 ± 1.6 Ma (n=11, MSWD=3.3; Table 4). This calculated age has a very large MSWD indicating that the data are overdispersed with the observed data scatter exceeding the predicted analytical uncertainties. In attempt to better constrain the crystallisation

age, another weighted average age was taken from the cluster of six concordant (±5%) data analyses yielding a much smaller MSWD of 0.37 ($^{206}Pb/^{238}U$ age of 81.4 ± 1.1 Ma). The lower intercept of a common Pb regression trend of 78.9 ± 1.1 Ma (n=26, MSWD=2.2, Fig. 3 of Dew et al. (2018)). All three of these calculated ages are within error of each other, however, the interpreted crystallisation age was determined to be the cluster of concordant (±5%) data analyses yielding a $^{206}Pb/^{238}U$ age of 81.4 ± 1.1 Ma (n=6, MSWD=0.37, data highlighted in Table 4). One zircon analysis within ±10% concordance gave a $^{206}Pb/^{238}U$ age of 259.8 ± 4.1 Ma, which is interpreted as an inherited grain, possibly reflecting an earlier magmatic event in the region.

Like the crystallisation age of ST-49A, the interpreted crystallisation age for ST-18 was also determined to be Upper Cretaceous (see Table 4 for age data). Zircons from this sample have interpreted age inheritance with concordant ages spanning from 2729 Ma to 524 Ma.

No crystallisation age could be constrained from the zircon analyses conducted on RDT15_076A. It was interpreted that the calculated ages were all inherited zircons (Table 4). Interpreted concordant inherited ages range from $^{207}Pb/^{206}Pb$ age of 2462 ± 21 Ma to $^{206}Pb/^{238}U$ age of 448.1 ± 6.7 Ma (Table 4).

2.5.2 Inthanon Zone

Twenty-two concordant (±5% discordance) magmatic zircon analyses from Th11/02 were used to calculate the weighted average, which yielded an Upper Triassic crystallisation age (Table 4). A discordia line also gives a lower intercept within error of this weighted average at 206.7 ± 1.3 Ma (see Fig. 3 of Dew et al. (2018)). The upper intercept of this regression line gives an age on the boundary of the Eoarchean and the Paleoarchean at 3617 ± 200 Ma. One discordant grain was found at 258.8 Ma, with two older grains within ±10% discordance with $^{206}Pb/^{238}U$ ages of 409.4 ± 6.53 Ma and 304.8 ± 4.99 Ma. There was also a concordant (±5) inherited grain with a $^{206}Pb/^{238}U$ age of 562.9 ± 8.82 Ma.

The interpreted crystallisation age for RDT16_053 is the weighted average of all concordant (±5) analyses with Th:U>0.1, which also yielded an Upper Triassic age like Th11/02 (see Table 4 for reduced data). Analyses younger than 200 Ma were interpreted to have lost Th and Pb from a subsequent thermal event, which was supported by the Th:U and $(^{176}Hf/^{177}Hf)_i$ values. Three older inherited cores are present with Paleoproterozoic–Neoarchean $^{207}Pb/^{206}Pb$ ages ranging from 2746 ± 29 Ma to 2430 ± 27 Ma. The inherited zircon ages found in this sample are similar those found in ST-18 from the Sibumasu Terrane.

The interpreted crystallisation age for RDT16_044 was is Upper Cretaceous in age (Table 4). This age was determined from a singular zircon analysis. The Th:U of this zircon is >0.1 however, the majority of the analyses from this sample have low Th:U indicating that both Pb and Th have been lost from the zircon during subsequent thermal events. Discordia could not be completed with Isoplot software since the youngest cluster of data containing positive and negative rho values.

2.5.3 Sukhothai Terrane

All five samples taken from the Sukhothai Terrane yielded magmatic ages within 13 Ma between 238.6 Ma and 226.5 Ma (data

are displayed in Table 4). No concordant inherited zircons were found from any of these samples (±5% discordant data are coloured yellow in Fig. 3 of Dew et al. (2018)).

The oldest interpreted crystallisation age from the Sukhothai Terrane was interpreted from NT-12 (weighted average age of 238.0 ± 2.9 Ma, see Table 4). The lower concordia intercept of a common Pb regression line for NT-12 is also within error of this weighted average age and yields a $^{206}Pb/^{238}U$ age of 238.6 ± 3.1 Ma (n=12, MSWD=1.03).

The interpreted crystallisation age for NT-10 was Upper Triassic (a weighted average $^{206}Pb/^{238}U$ age of 236.6 ± 2.9 Ma, Table 4). Analyses from NT-10 also form a linear trend with a lower Concordia intercept at 236.2 ± 2.7 Ma and an upper intercept of 5107 ± 750 Ma (n=18, MSWD = 0.84) representing a common Pb component. The lower intercept of this trend is the same age as the weighted average age only the weighted average incorporates 0.2 Ma more uncertainty (at 2σ).

Nineteen concordant (±5%) analyses from NT-11 with Th:U>0.1 yield a $^{206}Pb/^{238}U$ weighted average of 228.7 ± 2.1 Ma (MSWD=0.48; Table 4). No concordant inherited zircons were found, although two very discordant analyses had $^{206}Pb/^{238}U$ ages of 338.8 ± 5.66 Ma and 121.4 ± 2.08 Ma (see Table 4).

The magmatic age of Th11/01 is interpreted to be the weighted average of the ±5% concordant analyses with Th:U>0.1 yielding a $^{206}Pb/^{238}U$ age of 227.9 ± 1.9 Ma (n=23, MSWD=1.2; Table 4). Th11/01 contained two older very discordant analyses with $^{206}Pb/^{238}U$ ages of 455.6 ± 7.64 Ma and 316.1 ± 5.47 Ma (Table 4).

Concordant (±5%) analyses with Th:U>0.1 from sample NT-09 yielded a weighted average $^{206}Pb/^{238}U$ age of 226.5 ± 1.8 Ma (n=18, MSWD=0.48; Table 4). No concordant inherited zircons were found, although one very discordant analysis had a $^{206}Pb/^{238}U$ age of 692.4 ± 10.58 Ma.

2.5.4 Indochina Terrane

KM-20 contains $^{206}Pb/^{238}U$ ages within ±5% discordance for the entire first half of the Triassic period, from 249.4 ± 5.9 Ma to 221.5 ± 5.7 Ma (see Table 4). We interpret that the Lower and Middle Triassic ages are inherited and that crystallisation age of this sample was calculated from the weighted average of all analyses from the youngest to oldest concordant zircon in the Upper Triassic (see Table 4).

The NT-07 quartz diorite sample, was collected further south 60 km east of Nakhon Sawan. The crystallisation age of this sample is interpreted to be Permian (see Table 4). It was very difficult to determine domains from the CL imaging since the majority of zircons from this sample contained dark homogeneous zones, sometimes the whole zircon was dark and homogeneous. Therefore, it was difficult to determine the domain being ablated. This sample yielded a spread of analyses that may suggest limited post-crystallisation disturbance of the isotopic system that is supported by the sericitisation of feldspars seen in thin section (Fig 1—u, v).

Published isotopic data used for comparison

Type and/or location of isotopic data	References for published data
Hafnium (Fig. 4 in Dew *et al.* (2018))	(Cao *et al.* 2018; Chen *et al.* 2014; Deng *et al.* 2017; Gardiner *et al.* 2016; Hieu *et al.* 2016; Jiang *et al.* 2017; Lin *et al.* 2013; Liu *et al.* 2018; Qian *et al.* 2017; Wang *et al.* 2016a; Wang *et al.* 2016b)
$\varepsilon Nd_{(t)}$ against age (Fig. 5a in Dew *et al.* (2018))	(Intasopa and Dunn 1994; Ng *et al.* 2015; Qian *et al.* 2016; Qian *et al.* 2017; Wang *et al.* 2016c).
$\varepsilon Nd_{(t)}$ against initial Sr (Fig. 5c in Dew *et al.* (2018))	Sibumasu (Jiang *et al.* 2017) Indochina (Arboit *et al.* 2015; Intasopa and Dunn 1994; Kamvong *et al.* 2014) Sukhothai including Lincang and Chanthaburi (Barr *et al.* 2006; Deng *et al.* 2017; Hansen *et al.* 2014; Hennig *et al.* 2009; Heppe 2006; Peng *et al.* 2013; Qian *et al.* 2016; Qian *et al.* 2017; Wang *et al.* 2016c; Zhang *et al.* 2016) Inthanon Zone including Bentong Raub (Ng *et al.* 2015; Qian *et al.* 2017; Wang *et al.* 2016c) Lhasa (Ma *et al.* 2017) Truong Son (Hoa *et al.* 2008; Liu *et al.* 2012)
$^{207}Pb/^{204}Pb_{(i)}$ against $^{206}Pb/^{204}Pb_{(i)}$ (Fig. 5d in Dew *et al.* (2018))	(Basori *et al.* 2017; Chen *et al.* 2014; Hoa *et al.* 2008; Meffre *et al.* 2008; Zhou and Mukasa 1997).
Grid of $\varepsilon Nd_{(t)}$ including converted $\varepsilon Hf_{(t)}$ (Fig. 6 in Dew *et al.* (2018))	(Published data from Barr *et al.* 2006; Du *et al.* 2016; Gardiner *et al.* 2018; Gardiner *et al.* 2016; Hansen *et al.* 2014; Hoa *et al.* 2016; Intasopa and Dunn 1994; Jiang *et al.* 2017; Kamvong *et al.* 2014; Lin *et al.* 2013; Liu *et al.* 2012; Ogasawara *et al.* 2017; Qian *et al.* 2016; Qian *et al.* 2017; Wang *et al.* 2016b; Wang *et al.* 2016c).

Acknowledgements

Fieldwork was conducted with the kind assistance of staff and students from Chulalongkorn University and Chiang Mai University. Other field expeditions were conducted with great thanks to Liviu Matenco and Ernst Willingshofer from Utrecht University, Thamfatt Ng and Diew. Pîi Roj from Chiang Mai University Lapidary for training and permission to use facilities. We would like to acknowledge Ann-Eline Debeer

from Ghent University for the zircon mount preparation for the KM, ST and NT samples. Many thanks to David Bruce from the University of Adelaide's Isotope Geochemistry Facility for his support in the whole-rock geochemistry component of this project along with Sarah Gilbert and Aoife McFadden at Adelaide Microscopy for their help with the zircon analyses. Also thanks to Stanley Mertzman at Franklin and Marshall College for analysing the major and trace elements for this research. Thank you to Brad McDonald at the GeoHistory Facility at Curtin University for instrument setup for the Hf analyses. Appreciation to Sheree Armistead for conducting the Hf analysis for the KM-20 sample and assistance with MATLAB.

This is a contribution to IGCP projects #589 (Development of the Asian Tethyan Realm) and #628 (The Gondwana Map). This publication forms TRaX Record #413. This work was supported by Australian Research Council [#DP150101730, #DP120101460 and #FT120100340]. RECD is also funded by a University of Adelaide Research Training Program Stipend and some of the fieldwork conducted was funded on an Endeavour Australia Cheung Kong Fellowship. SN is funded by a PhD fellowship of the Research Foundation Flanders (FWO). PK is funded by the Ratchadaphiseksomphot Endowment Fund, Chulalongkorn University. GeoHistory Facility instruments were funded via an Australian Geophysical Observing System grant provided to AuScope Pty Ltd. by the AQ44 Australian Education Investment Fund program. The NPII multi-collector was obtained via funding from the Australian Research Council LIEF program [#LE150100013].

References

Arboit, F., Amrouch, K., Collins, A.S., King, R. & Morley, C. 2015. Determination of the tectonic evolution from fractures, faults, and calcite twins on the southwestern margin of the Indochina Block. Tectonics, 34, 1576-1599, doi: 10.1002/2015TC003876.

Arboit, F., Collins, A.S., Jourdan, F., King, R., Foden, J. & Amrouch, K. 2016. Geochronological and geochemical study of mafic and intermediate dykes from the Khao Khwang Fold-Thrust Belt: Implications for petrogenesis and tectonic evolution. Gondwana Research, 36, 111-128.

Audley-Charles, M.G., Ballantyne, P.D. & Hall, R. 1988. Mesozoic-Cenozoic rift-drift sequence of Asian fragments from Gondwanaland. Tectonophysics, 155, 317-330.

Barr, S.M., Macdonald, A.S., Ounchanum, P. & Hamilton, M.A. 2006. Age, tectonic setting and regional implications of the Chiang Khong volcanic suite, northern Thailand. Journal of the Geological Society, 163, 1037-1046, doi: 10.1144/0016-76492005-118.

Basori, M.B.I., Zaw, K., Meffre, S., Large, R.R. & Wan Hassan, W.F. 2017. Pb-isotope compositions of the Tasik Chini volcanic-hosted massive sulfide deposit, Central Belt of Peninsular Malaysia: Implication for source region and tectonic setting. Island Arc, e12177-n/a, doi: 10.1111/iar.12177.

Bouvier, A., Vervoort, J.D. & Patchett, P.J. 2008. The Lu–Hf and Sm–Nd isotopic composition of CHUR: Constraints from unequilibrated chondrites and implications for the bulk composition of terrestrial planets. Earth and Planetary Science Letters, 273, 48-57, doi: http://dx.doi.org/10.1016/j.epsl.2008.06.010.

Cao, H.-W., Zhang, Y.-H., Santosh, M., Zhang, S.-T., Tang, L., Pei, Q.-M. & Yang, Q.Y. 2017. Mineralogy, zircon U-Pb-Hf isotopes, and whole-rock geochemistry of Late Cretaceous-Eocene granites from the Tengchong terrane, western Yunnan, China: Record of the closure of the Neo-Tethyan Ocean. Geological Journal, n/a-n/a, doi: 10.1002/gj.2964.

Chen, Z., Lin, W., Faure, M., Lepvrier, C., Van Vuong, N. & Van Tich, V. 2014. Geochronology and isotope analysis of the Late Paleozoic to Mesozoic granitoids from Northeastern Vietnam and implications for the evolution of the South China block. Journal of Southeast Asian Earth Sciences, 86, 131-150.

Chu, N.-C., Taylor, R.N., Chavagnac, V., Nesbitt, R.W., Boella, R.M., Milton, J.A., German, C.R., Bayon, G. & Burton, K. 2002. Hf isotope

ratio analysis using multi-collector inductively coupled plasma mass spectrometry: an evaluation of isobaric interference corrections. Journal of Analytical Atomic Spectrometry, 17, 15967-11574.

Cobbing, E.J., Pitfield, P.E.J., Darbyshire, P.D.F. & Mallick, D.I.J. 1992. Thailand. The granites of the South-east Asian tin belt. HMSO, London, Overseas Memoir of the British Geological Society.

De Clercq, S. 2016. Evolution of the Andaman Basin: constraints from thermochronometry of the Andaman-Nicobar and Peninsular Thai margins. Masters, Ghent University.

De Grave, J., Glorie, S., Charusiri, P. & Kanjanapayont, P. 2015. Thermo-tectonic history of Thailand using zircon U/Pb and apatite fission track constraints: Preliminary results. The 4th Symposium of the International Geosciences Programme (IGCP) 589, Chulalongkorn University, Bangkok, Thailand, 8-13.

Deng, J., Wang, C., Zi, J.-W., Xia, R. & Li, Q. 2017. Constraining subduction-collision processes of the Paleo-Tethys along the Changning–Menglian Suture: New zircon U-Pb ages and Sr–Nd–Pb–Hf–O isotopes of the Lincang Batholith. Gondwana Research, doi: 10.1016/j.gr.2017.10.008.

Dew, R.E.C., Collins, A.S., Glorie, S., Morley, C.K., Blades, M.L., Nachtergaele, S., King, R., Foden, J., De Grave, J., Kanjanapayont, P., Evans, N.J., Alessio, B.L. & Charusiri, P. 2018. Probing into Thailand's basement: New insights from U–Pb geochronology, Sr, Sm–Nd, Pb and Lu–Hf isotopic systems from granitoids. Lithos, 320-321, 332-354, doi: 10.1016/j.lithos.2018.09.019.

Du, B., Wang, C., He, Z., Yang, L., Chen, J., Shi, K., Luo, Z. & Xia, J. 2016. Advances in research of bulk-rock Nd and zircon Hf isotopic mappings: Case study of Sanjiang Tethyan Orogen. Acta Petrologica Sinica, 32, 2555-2570.

Fisher, C.M., Vervoort, J.D. & DuFrane, S.A. 2014. Accurate Hf isotope determinations of complex zircons using the "laser ablation split stream" method. Geochemistry, Geophysics, Geosystems, 15, 121-139, doi: 10.1002/2013GC004962.

Flanagan, F.J. 1976. Descriptions and Analysis of Eight New USGS Rock Standards.

Gardiner, N.J., Searle, M.P., Morley, C.K., Robb, L.J., Whitehouse, M.J., Roberts, N.M.W., Kirkland, C.L. & Spencer, C.J. 2018. The crustal architecture of Myanmar imaged through zircon U-Pb, Lu-Hf and O isotopes: Tectonic and metallogenic implications. Gondwana Research, doi: https://doi.org/10.1016/j.gr.2018.02.008.

Gardiner, N.J., Searle, M.P., Morley, C.K., Whitehouse, M.P., Spencer, C.J. & Robb, L.J. 2016. The closure of Palaeo-Tethys in Eastern Myanmar and Northern Thailand: New insights from zircon U-Pb and Hf isotope data. Gondwana Research, 39, 401-422, doi: 10.1016/j.gr.2015.03.001.

Griffin, W.L., Pearson, N.J., Belousova, E., Jackson, S.E., van Achterbergh, E., O'Reilly, S.Y. & Shee, S.R. 2000. The Hf isotope composition of cratonic mantle: LAM-MC-ICPMS analysis of zircon megacrysts in kimberlites. Geochimica et Cosmochimica Acta, 64, 133-147, doi: https://doi.org/10.1016/S0016-7037(99)00343-9.

Hansen, B.T., Wemmer, K., Putthapiban, P., Kleinhanns, I.C. & Wilsky, F. 2014. Do U/Pb-SHRIMP Dating and Pb Stepwise Leaching (PbSL) Analyses Confirm the Lack of Precambrian Basement Outcrops in Thailand? Open Journal of Geology, Vol.04, No.10, 12pp., doi: 10.4236/ojg.2014.410037.

Hennig, D., Lehmann, B., Frei, D., Belyatsky, B., Zhao, X.F., Cabral, A.R., Zeng, P.S., Zhou, M.F. & Schmidt, K. 2009. Early Permian seafloor to continental arc magmatism in the eastern Paleo-Tethys: U–Pb age and Nd–Sr isotope data from the southern Lancangjiang zone, Yunnan, China. Lithos, 113, 408-422, doi: https://doi.org/10.1016/j.lithos.2009.04.031.

Heppe, K. 2006. Plate Tectonic evolution and mineral resource potential of the Lancang River Zone, southwestern Yunnan, People's Republic of China. Bundesanstalt für Geowissenschaften und Rohstoffe und dem Landesamt für Bergbau, Energie und Geologie, Hanover, Germany.

Hieu, P.T., Dung, N.T., Thuy, N.T.B., Minh, N.T. & Minh, P. 2016. U–Pb ages and Hf isotopic composition of zircon and bulk rock geochemistry of the Dai Loc granitoid complex in Kontum massif: Implications for early Paleozoic crustal evolution in Central Vietnam. Journal of Mineralogical and Petrological Sciences, 111, 326-336, doi: 10.2465/jmps.151229.

Hisada, K.-i., Sugiyama, M., Ueno, K., Charusiri, P. & Arai, S. 2004. Missing ophiolitic rocks along the Mae Yuam Fault as the Gondwana–Tethys divide in north-west Thailand. Island Arc, 13, 119-127, doi: 10.1111/j.1440-1738.2003.00412.x.

Hoa, T.T., Anh, T.T., Phuong, N.T., Dung, P.T.,

Anh, T.V., Izokh, A.E., Borisenko, A.S., Lan, C.Y., Chung, S.L. & Lo, C.H. 2008. Permo-Triassic intermediate–felsic magmatism of the Truong Son belt, eastern margin of Indochina. Comptes Rendus Geoscience, 340, 112-126, doi: https://doi.org/10.1016/j.crte.2007.12.002.

Hoa, T.T., Polyakov, G.V., Tran, T.-A., Borisenko, A.S., Izokh, A.E., Balykin, P.A., Ngo, T.-P. & Pham, T.-D. 2016. Plutonic: Volcanic Associations in the Tu Le Basin and Phan Si Pan Uplift, Northwest Vietnam. In: Tran, H.T., Polyakov, G.V., Tran, A.T., Borisenko, A.S., Izokh, A.E., Balykin, P.A., Ngo, P.T. & Pham, D.T. (eds.) Intraplate Magmatism and Metallogeny of North Vietnam. Springer International Publishing, Cham, 59-101.

Intasopa, S. & Dunn, T. 1994. Petrology and Sr-Nd isotopic systems of the basalts and rhyolites, Loei, Thailand. Journal of Southeast Asian Earth Sciences, 9, 167-180, doi: http://dx.doi.org/10.1016/0743-9547(94)90073-6.

Jackson, S.E., Pearson, N.J., Griffin, W.L. & Belousova, E.A. 2004. The application of laser ablation-inductively coupled plasma-mass spectrometry to in situ U–Pb zircon geochronology. Chemical Geology, 211, 47-69, doi: https://doi.org/10.1016/j.chemgeo.2004.06.017.

Jiang, H., Li, W.-Q., Jiang, S.-Y., Wang, H. & Wei, X.-P. 2017. Geochronological, geochemical and Sr-Nd-Hf isotopic constraints on the petrogenesis of Late Cretaceous A-type granites from the Sibumasu Block, Southern Myanmar, SE Asia. Lithos, 268–271, 32-47, doi: http://dx.doi.org/10.1016/j.lithos.2016.11.005.

Kamvong, T., Khin, Z., Meffre, S., Maas, R., Stein, H. & Lai, C.-K. 2014. Adakites in the Truong Son and Loei fold belts, Thailand and Laos: Genesis and implications for geodynamics and metallogeny. Gondwana Research, 26, 165-184, doi: http://dx.doi.org/10.1016/j.gr.2013.06.011.

Kirkland, C.L., Smithies, R.H., Taylor, R.J.M., Evans, N. & McDonald, B. 2015. Zircon Th/U ratios in magmatic environs. Lithos, 212–215, 397-414, doi: http://dx.doi.org/10.1016/j.lithos.2014.11.021.

Lin, Y.-L., Yeh, M.-W., Lee, T.-Y., Chung, S.-L., Iizuka, Y. & Charusiri, P. 2013. First evidence of the Cambrian basement in Upper Peninsula of Thailand and its implication for crustal and tectonic evolution of the Sibumasu terrane. Gondwana Research, 24, 1031-1037, doi: http://dx.doi.org/10.1016/j.gr.2013.05.014.

Liu, H., Wang, Y., Li, Z., Zi, J.-W. & Huangfu, P. 2018. Geodynamics of the Indosinian orogeny between the South China and Indochina blocks: Insights from latest Permian–Triassic granitoids and numerical modeling. GSA Bulletin, doi: https://doi.org/10.1130/B31904.1.

Liu, J., Tran, M.-D., Tang, Y., Nguyen, Q.-L., Tran, T.-H., Wu, W., Chen, J., Zhang, Z. & Zhao, Z. 2012. Permo-Triassic granitoids in the northern part of the Truong Son belt, NW Vietnam: Geochronology, geochemistry and tectonic implications. Gondwana Research, 22, 628-644, doi: https://doi.org/10.1016/j.gr.2011.10.011.

Ludwig, K.R. 1998. On the Treatment of Concordant Uranium-Lead Ages. Geochimica et Cosmochimica Acta, 62, 665-676, doi: http://dx.doi.org/10.1016/S0016-7037(98)00059-3.

Ma, X., Xu, Z. & Meert, J.G. 2017. Syn-convergence extension in the southern Lhasa terrane: Evidence from late Cretaceous adakitic granodiorite and coeval gabbroic-dioritic dykes. Journal of Geodynamics, 110, 12-30, doi: https://doi.org/10.1016/j.jog.2017.07.004.

Meffre, S., Khin, Z., Khositanont, S., Halpin, J. & Cumming, G. 2008. 'Tectonic evolution of SE Asia', 'Ore Deposits of SE Asia' - Annual Report to Sponsors. CODES.

Metcalfe, I. 1984. Stratigraphy, palaeontology and palaeogeography of the Carboniferous of Southeast Asia. Memoires de la Societe Geologique de France, 147, 107-118.

Morel, M.L.A., Nebel, O., Nebel-Jacobsen, Y.J., Miller, J.S. & Vroon, P.Z. 2008. Hafnium isotope characterisation of the GJ-1 zircon reference material by solution and laser-ablation MC-ICPMS. Chemical Geology, 231-235.

Ng, S.W., Chung, S.L., Robb, L.J., Searle, M.P., Ghani, A.A., Whitehouse, M.J., Oliver, G.J.H., Sone, M., Gardiner, N.J. & Roselee, M.H. 2015. Petrogenesis of Malaysian granitoids in the Southeast Asian tin belt: Part 1. Geochemical and Sr-Nd isotopic characteristics. Bulletin of the Geological Society of America, 127, 1209-1237, doi: 10.1130/B31213.1.

Nowell, G.M., Pearson, D.G., Noble, S.R., Fitton, J.G., Saunders, A.D., Mahoney, J.J. & Taylor, R.N. 1998. High precision Hf isotope measurements of MORB and OIB by thermal ionisation mass spectrometry: insights into the depleted mantle. Chemical Geology, 211-233.

Ogasawara, M., Fukuyama, M. & Tangwattananukul, L. 2017. U-Pb zircon ages and geochemistry of granitic rocks in the Chanthaburi Terrane, Southeast Thailand. The 16th Gondwana International Conference.

Department of Mineral Resources, Bangkok, Thailand, 152.

Patchett, P.J. & Tatsumoto, M. 1980. Hafnium isotope variations in oceanic basalts. Geophysical Research Letters, 7, 1077-1080.

Paton, C., Hellstrom, J., Paul, B., Woodhead, J. & Hergt, J. 2011. Iolite: Freeware for the visualisation and processing of mass spectrometric data. Journal of Analytical Atomic Spectrometry, 26, 2508-2518, doi: 10.1039/c1ja10172b.

Payne, J.L., Barovich, K.M. & Hand, M. 2006. Provenance of metasedimentary rocks in the northern Gawler Craton, Australia: Implications for Palaeoproterozoic reconstructions. Precambrian Research, 148, 275-291, doi: https://doi.org/10.1016/j.precamres.2006.05.002.

Peng, T., Wilde, S.A., Wang, Y., Fan, W. & Peng, B. 2013. Mid-Triassic felsic igneous rocks from the southern Lancangjiang Zone, SW China: Petrogenesis and implications for the evolution of Paleo-Tethys. Lithos, 168-169, 15-32, doi: https://doi.org/10.1016/j.lithos.2013.01.015.

Qian, X., Feng, Q., Wang, Y., Chonglakmani, C. & Monjai, D. 2016. Geochronological and geochemical constraints on the mafic rocks along the Luang Prabang zone: Carboniferous back-arc setting in northwest Laos. Lithos, 245, 60-75, doi: https://doi.org/10.1016/j.lithos.2015.07.019.

Qian, X., Feng, Q., Wang, Y., Zhao, T., Zi, J.-W., Udchachon, M. & Wang, Y. 2017. Late Triassic post-collisional granites related to Paleotethyan evolution in SE Thailand: Geochronological and geochemical constraints. Lithos, 286, 440-453, doi: http://dx.doi.org/10.1016/j.lithos.2017.06.026.

Scherer, E., Münker, C. & Mezger, K. 2001. Calibration of the lutetium-hafnium clock. Science, 293, 683-687.

Schoene, B. 2014. U-Th-Pb Geochronology. In: Rudnick, R. (ed.) Treatise on Geochemistry 2nd Edition. Elsevier, Oxford, U.K., 341-378.

Searle, M.P., Whitehouse, M.J., Robb, L.J., Ghani, A.A., Hutchison, C.S., Sone, M., Ng, S.W.P., Roselee, M.H., Chung, S.L. & Oliver, G.J.H. 2012. Tectonic evolution of the Sibumasu-Indochina terrane collision zone in Thailand and Malaysia: Constraints from new U-Pb zircon chronology of SE Asian tin granitoids. Journal of the Geological Society, 169, 489-500, doi: 10.1144/0016-76492011-107.

Sláma, J., Košler, J., Condon, D.J., Crowley, J.L., Gerdes, A., Hanchar, J.M., Horstwood, M.S.A., Morris, G.A., Nasdala, L., Norberg, N., Schaltegger, U., Schoene, B., Tubrett, M.N. & Whitehouse, M.J. 2008. Plešovice zircon — A new natural reference material for U–Pb and Hf isotopic microanalysis. Chemical Geology, 249, 1-35, doi: https://doi.org/10.1016/j.chemgeo.2007.11.005.

Sone, M. & Metcalfe, I. 2008. Parallel Tethyan sutures in mainland Southeast Asia: New insights for Palaeo-Tethys closure and implications for the Indosinian orogeny. Comptes Rendus - Geoscience, 340, 166-179, doi: 10.1016/j.crte.2007.09.008.

Tanaka, T., Togashi, S., Kamioka, H., Amakawa, H., Kagami, H., Hamamoto, T., Yuhara, M., Orihashi, Y., Yoneda, S., Shimizu, H., Kunimaru, T., Takahashi, K., Yanagi, T., Nakano, T., Fujimaki, H., Shinjo, R., Asahara, Y., Tanimizu, M. & Dragusanu, C. 2000. JNdi-1: a neodymium isotopic reference in consistency with LaJolla neodymium. Chemical Geology, 168, 279-281, doi: https://doi.org/10.1016/S0009-2541(00)00198-4.

Taylor, R.N., Ishizuka, O., Michalik, A., Milton, J.A. & Croudace, I.W. 2015. Evaluating the precision of Pb isotope measurement by mass spectrometry. Journal of Analytical Atomic Spectrometry, 30, 198-213, doi: 10.1039/C4JA00279B.

Thirlwall, M.F. & Anczkiewicz, R. 2004. Multidynamic isotope ratio analysis using MC–ICP–MS and the causes of secular drift in Hf, Nd and Pb isotope ratios. International Journal of Mass Spectrometry, 235, 59-81, doi: https://doi.org/10.1016/j.ijms.2004.04.002.

Van Achterbergh, E., Ryan, C.G., Jackson, S.E. & Griffin, W.L. 2001. Data reduction software for LA-ICP-MS. In: Sylvester, P.J. (ed.) Laser-ablation-ICPMS in the earth sciences; principles and applications. Mineralogical Association of Canada, Ottowa, 239-243.

Wang, L., Long, W., Zhou, D., Xu, W. & Jin, X. 2016a. Late Triassic zircon U-Pb ages and Sr-Nd-Hf isotopes of Darongshan granites in southeastern Guangxi and their geological implications. Geological Bulletin of China, 35, 1291-1303.

Wang, S., Mo, Y., Wang, C. & Ye, P. 2016b. Paleotethyan evolution of the Indochina Block as deduced from granites in northern Laos. Gondwana Research, 38, 183-196, doi: https://doi.org/10.1016/j.gr.2015.11.011.

Wang, Y., He, H., Cawood, P.A., Srithai, B., Feng, Q., Fan, W., Zhang, Y. & Qian, X. 2016c. Geochronological, elemental and Sr-Nd-Hf-O

isotopic constraints on the petrogenesis of the Triassic post-collisional granitic rocks in NW Thailand and its Paleotethyan implications. Lithos, 266-267, 264-286, doi: https://doi.org/10.1016/j.lithos.2016.09.012.

Wiedenbeck, M., AllÉ, P., Corfu, F., Griffin, W.L., Meier, M., Oberli, F., Quadt, A.V., Roddick, J.C. & Spiegel, W. 1995. Three natural zircon standards for U–Th–Pb, Lu–Hf, trace element and REE analyses. Geostandards Newsletter, 19, 1-23, doi: 10.1111/j.1751-908X.1995.tb00147.x.

Wilson, S.A. 1997. Data compilation for USGS reference material BHVO-2, Hawaiian Basalt. U.S. Geological Survey.

Woodhead, J., Hergt, J., Shelley, M., Eggins, S. & Kemp, R. 2004. Zircon Hf-isotope analysis analysis with an excimer laser, depth profiling, ablation of complex geometries and comcomitant age estimation. Chemical Geology, 209, 121-135.

Woodhead, J.D. & Hergt, J.M. 2005. A Preliminary Appraisal of Seven Natural Zircon Reference Materials for In Situ Hf Isotope Determination. Geostandards and Geoanalytical Research, 29, 183-195, doi: 10.1111/j.1751-908X.2005.tb00891.x.

Zhang, Y., Wang, Y., Srithai, B. & Phajuy, B. 2016. Petrogenesis for the Chiang Dao Permian high-iron basalt and its implication on the Paleotethyan Ocean in NW Thailand. Journal of Earth Science, 27, 425-434, doi: 10.1007/s12583-015-0646-4.

Zhou, P. & Mukasa, S.B. 1997. Nd-Sr-Pb isotopic, and major- and trace-element geochemistry of Cenozoic lavas from the Khorat Plateau, Thailand: sources and petrogenesis. Chemical Geology, 137, 175-193.

CHAPTER 3

This chapter is written for *Gondwana Research* as:

Dew, R.E.C., Collins, A.S., Morley, C.K., King, R., Evans, N.J. & Glorie, S. A detrital provenance story from Gondwana to northwest Thailand.

Statement of Authorship

Title of Paper	A detrital provenance story from Gondwana to northwest Thailand
Publication Status	☐ Published ☐ Accepted for Publication ☐ Submitted for Publication ☑ Unpublished and Unsubmitted work written in manuscript style
Publication Details	Dew, R.E.C., Collins, A.S., Morley, C.K., King, R.C., Glorie, S.G. and Evans, N.J. (in prep) A detrital provenance story from Gondwana to northwest Thailand.

Principal Author

Name of Principal Author (Candidate)	Romana E.C. Dew		
Contribution to the Paper	Performed majority of sample analysis, interpreted data, wrote manuscript and acted as corresponding author.		
Overall percentage (%)	80		
Certification:	This paper reports on original research I conducted during the period of my Higher Degree by Research candidature and is not subject to any obligations or contractual agreements with a third party that would constrain its inclusion in this thesis. I am the primary author of this paper.		
Signature		Date	31/12/2018

Co-Author Contributions

By signing the Statement of Authorship, each author certifies that:

i. the candidate's stated contribution to the publication is accurate (as detailed above);

ii. permission is granted for the candidate in include the publication in the thesis; and

iii. the sum of all co-author contributions is equal to 100% less the candidate's stated contribution.

Name of Co-Author	Alan S. Collins		
Contribution to the Paper	Primary supervisorial role, conception and design of the project, helped in data interpretation and manuscript construction and editing		
Signature		Date	31/12/2018

Name of Co-Author	Christopher K. Morley		
Contribution to the Paper	Assistance with data interpretation and manuscript editing		
Signature	Dr. Christopher Morley	Date	31/12/2018

Name of Co-Author	Rosalind King		
Contribution to the Paper	Co-supervisorial role, conception and design of the project, assisted data interpretation, manuscript layout and draft editing		
Signature		Date	28/11/2018

Name of Co-Author	Stijn Glorie		
Contribution to the Paper	Co-supervisorial role, conception and design of the project and manuscript ed		
Signature		Date	30/11/2018

Name of Co-Author	Noreen Evans		
Contribution to the Paper	Hafnium data reduction and manuscript editing		
Signature		Date	28-11-18

ABSTRACT

The evolution of the Sibumasu Terrane forms a principal component in the history of the Tethys Oceans with the northward movement of Gondwana-derived terranes creating the Asian continent that we recognise today. There are various reconstructions for the palaeoposition of the Sibumasu Terrane during the Proterozoic and Paleozoic, with the terrane commonly placed outboard of northwest margin of Australia in the Gondwanan supercontinent. In this study, U–Pb and Lu–Hf isotopic information has been collected from Paleozoic and Mesozoic detrital zircons extracted from the Sibumasu Terrane of northwest Thailand. This new data was also statistically and visually compared to published datasets from Sibumasu, Indochina, Sukhothai, West Burma, China, Tethyan Himalayas, India and Western Australia.

There is a change in source material from the older Paleozoic sedimentary sequences of northwest Thailand (only sourcing zircons from the Sibumasu Terrane and other older "Gondwanan" sources) to the latest Permian–Triassic sedimentary units containing zircons associated with the Indosinian Orogeny. This change is reflected in both the U–Pb ages and Hf signatures with the Proterozoic age peaks characteristic of Gondwana and the younger Indosinian source being consistent with granitoids emplaced throughout Thailand. The temporal changes in the isotopic systems reflects the movement of the Sibumasu Terrane from the northwest Australian margin of Gondwana to its collision with the terranes of present-day Asia.

1. Introduction

Matching detrital zircon age spectra with zircon growth events in potential source regions has been an effective provenance indicator (e.g. Arboit et al., 2016; Spencer et al., 2015; Yang et al., 2018). It has been integral for understanding continental growth history and investigating a region's tectonic evolution and paleogeography (De Pelsmaeker et al., 2018; Glorie et al., 2014; Howard et al., 2009; Spencer et al., 2018). The accessory mineral zircon ($ZrSiO_4$) is highly mechanically and chemically resistant and is common in a multitude of rock types including sandstones, granites and other felsic igneous rocks (Belousova et al., 2002; Bodet and Schärer, 2000). It is also an ideal mineral for geochronology as it readily incorporates U, but takes up minimal to no Pb during crystallisation (Roberts and Spencer, 2015). Zircon U–Pb geochronology clearly demonstrates the existence of age heterogeneities within a single crystal (Košler and Sylvester, 2003). The Lu–Hf isotopic system in zircon can also be measured in conjunction with U–Pb isotopes. Hafnium is geochemically similar to Zr and can replace Zr in the zircon crystal structure, therefore, is also commonly concentrated in crustal rocks such as coarse grained sediments (White, 2013). The Lu–Hf isotopic system can be used to differentiate similarly aged zircon populations by their source characteristics (Griffin et al., 2004; Howard et al., 2009; Patchett and Tatsumoto, 1980). Coupled detrital U–Pb and Lu–Hf zircon analysis has been often correlated to zircon growth events in potential source regions to understand a region's tectonic evolution and palaeogeography (e.g. Arboit et al., 2016; Griffin et al., 2004; Howard et al., 2009; Plavsa et al., 2014; Usuki et al., 2013).

Many details on the evolution of Gondwanan-derived terranes that form Southeast Asia are poorly understood.

The Sibumasu Terrane and its equivalents extend from Tibet and southwest China down through northwest Thailand and eastern Myanmar into Malaysia and eastern Sumatra (Fig. 1; Ali et al., 2013; Cai et al., 2017; Ghani et al., 2013; Metcalfe, 2013). In northwest Thailand, there are some problems relating the stratigraphy of the Sibumasu Terrane to the overall tectonic development of the northwest Thailand. Geological concepts that are poorly understood from the Sibumasu Terrane include:

- stratigraphic variations of Paleozoic and Triassic units and the factors controlling the variations
- the age and stratigraphic relationships between lithologies in Sibumasu
- the tectonic location of some formations
- the paucity/lack of reliable palaeomagnetic data
- the palaeoposition of Sibumasu (and neighbouring terranes) within the Gondwana supercontinent
- the tectonic development of Sibumasu during the Indosinian orogeny
- the exact boundaries of the Sibumasu Terrane

To better constrain the evolution of this region, we conducted the first coupled U–Pb geochronology and Lu–Hf detrital study on Paleozoic and Mesozoic zircons from northwest Thailand. Geological evidence, geochemical signatures, and the detrital age populations are combined in order to reconstruct the evolution of the Sibumasu Terrane. In an attempt to resolve existing arguments about the Sibumasu Terrane, we have compared our new coupled U–Pb and Lu–Hf zircon data to those published from other Southeast Asian terranes (Arboit et al., 2015; Hara et al., 2017), China (Xu et al., 2014; Zhang et al., 2016), the Indian subcontinent (Kaur et al., 2011; Plavsa et al., 2014), and Australia (Cawood and Nemchin, 2000; Kirkland et al., 2011; Yang et al., 2018).

2. Geology of the Sibumasu Terrane

The Sibumasu Terrane is a ribbon continent that is correlated to the South Qiangtang Terrane in Tibet, and the Baoshan and Tengchong terranes in southwest China (Ali et al., 2013; Jiang et al., 2017; Li et al., 2018). Despite the zircon U–Pb and Lu–Hf evidence for an ancient source terrain in the Sibumasu Terrane (Burrett et al., 2014; Dew et al., 2018a), no extensive exposure of Precambrian high grade metamorphic basement has been conclusively identified (e.g. Hansen and Wemmer, 2011). The outcrop geology of Sibumasu is almost entirely composed of Phanerozoic sedimentary, metasedimentary, igneous and metamorphic rocks (Gardiner et al., 2016b; Ridd, 2011; Schwartz et al., 1995; Searle et al., 2012; Ueno and Charoentitirat, 2011).

2.1 Tectonic evolution of the Sibumasu Terrane

The northward movement of terranes from Gondwana throughout the Phanerozoic and the progressive development and destruction of the Tethys Oceans formed the landmasses of Southeast Asia that we recognise today (Audley-Charles et al., 1988; Gardiner et al., 2016a; Metcalfe, 2013).

The Gondwanan supercontinent included much of the present day Asia, Australia, Antarctica, India, Arabia and South America and amalgamated in the late Neoproterozoic to Cambrian (Kelsey et al., 2008; Merdith et al., 2017). Cambrian Gondwana was characterised by subduction and collision with the

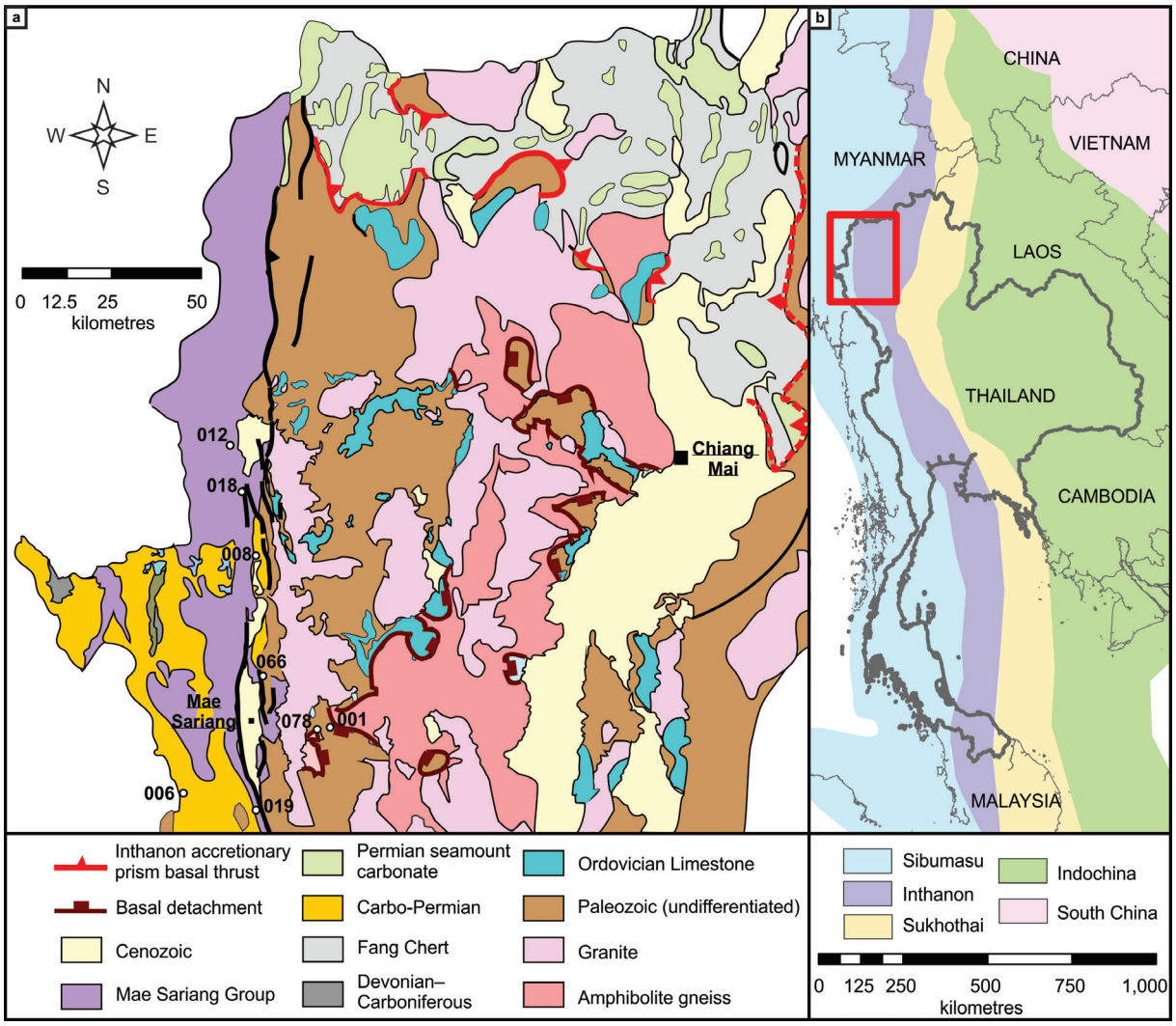

Fig. 1. a (left): Geological map of northwest Thailand with sample localities (sample names are shortened to numerals). Modified from Gardiner et al. (2016a) and Morley (2018), after Baum et al. (1981), von Braun et al. (1981) and DMR (1999). **b** (right): Regional map showing the major tectonic subdivisions, red rectangle indicates the extent of Fig. 1a. Tectonic boundaries adjusted from Metcalfe (2013) and Dew et al. (2018a).

East African Orogen between east Africa, Antarctica, and India (Blades et al., 2015; Fitzsimons, 2003; Kelsey et al., 2008), the Pinjarra—Kuunga Orogen between southwestern Australia, northeastern India and Antarctica (Collins, 2003; Fitzsimons, 2003; Fletcher and Libby, 1993; Ghosh et al., 2005) and the Terra-Australis Orogen along the margins of Australia, Antarctica, and South America (Cawood, 2005). However, the position of the terranes that form the northern Gondwanan margin, including Sibumasu, Lhasa, West Burma and Qiangtang, is still widely debated (Burrett et al., 2014; Cocks and Torsvik, 2013; Hu et al., 2015; Zhang et al., 2018c) and therefore often omitted from global palaeogeographic models (Merdith et al., 2017). However, most terranes of the northern Gondwana margin contain Cambro-Ordovician magmatism (Dew et al., 2018a; Hu et al., 2015; Saki, 2010; Zhang et al., 2018b).

Sibumasu, Baoshan, North China, Tarim, Tibet and South China have

palaeobiogeographic and stratigraphic links to Gondwanan Australia in the early Ordovician (Fang et al., 2018a; Li et al., 2004; Metcalfe, 2013). Silurian graptolites indicate that Sibumasu has affinities with both (peri-) Gondwana and South China, suggesting that a locality between the two is reasonable (Loydell and Aung, 2017).

Upper Devonian vertebrates connect Sibumasu with South China and Australia at this time (Long and Burrett, 1989). The Nd isotopic composition of seawater from western Thailand provides further evidence that during the Upper Devonian Sibumasu was located near the Archean cratons of Western Australia (e.g. Pilbara and Yilgarn), presumably adjacent to the Carnarvon intracratonic basin (Dopieralska et al., 2012).

It is commonly agreed that the Palaeo-Tethys Ocean was initiated in the Lower Devonian (Cocks and Torsvik, 2013; Hara et al., 2012; Metcalfe, 2013; Zhu et al., 2011). This ocean covered the equatorial region from the Devonian to the Triassic, where carbonates and pelagic chert were deposited (Cocks and Torsvik, 2013; Hara et al., 2012; Metcalfe, 2013). However, there are differing models on the timing of separation between Sibumasu, Lhasa, Indochina from Gondwana (Audley-Charles et al., 1988; Li et al., 2004; Loydell and Aung, 2017; Zhang et al., 2018c; Zhu et al., 2011).

Previously published plate-tectonic models (e.g. Li et al. 2004; Metcalfe 2013) suggest that by the Carboniferous, the South China and Indochina terranes were located in equatorial to low northern palaeolatitudes. In contrast, Paleozoic palaeomagnetic data indicate southern palaeolatitudes consistent with Sibumasu being positioned off northwest Australian Gondwana in the Devonian, Carboniferous and Early Permian (Ali et al. 2013; Fang et al. 1989; Huang and Opdyke 1991; Metcalfe 2013). The presence of Gondwana-derived icebergs depositing glacial-marine sediments in rift grabens is frequently used as evidence for Sibumasu's palaeoposition in Carbo-Permian Gondwana (Burrett et al. 2014; Metcalfe 2013; Ridd 2015; Sevastjanova et al. 2011).

The latest projections show that by the early Permian, the Sibumasu Terrane rifted northwards away from the Gondwana margin (as per Burrett et al., 2014). By the middle to late Permian, the widespread Ratburi, Thitsipin and Moulmein limestones indicate that Sibumasu was almost entirely submerged with little topographic relief (Morley, 2018; Ueno and Charoentitirat, 2011).

Present day Thailand is composed of four main components from west to east: the Sibumasu Terrane, the Inthanon Zone (remnants of the Palaeo-Tethys Ocean), the Sukhothai Terrane (known as the Chanthaburi Terrane in southeastern Thailand) and the Indochina Terrane. In the past, there has been much debate on the origin of Sukhothai Terrane, however, it is now acknowledged to be an arc system built on older continental material (Dew et al., 2018a; Hara et al., 2017; Sevastjanova et al., 2011). The exact timing of the collision between the components of present-day Thailand is yet to be identified, current constraints range from latest Permian to late Triassic (Barber et al., 2011; Cai et al., 2017; Hara et al., 2012; Metcalfe, 2013; Morley, 2018; Morley et al., 2013; Searle et al., 2012; Wakita and Metcalfe, 2005).

2.2 Stratigraphy of northwest Thailand

Throughout most of Thailand younger sedimentary sequences, extensive jungle cover and deep lateritic weathering prevent the exposure of older basement sequences. The 'basement' rocks in Thailand, most of which are medium to high-grade regional metamorphic rocks, have been traditionally regarded as Precambrian (Baum et al., 1970; Javanaphet, 1969), although the gneisses and schists of northwest Thailand were described as 'Pre-Permian' by Javanaphet (1969). Dew et al. (2018a) did not find any Precambrian crystallisation ages from the Mae Sariang region, although Precambrian inherited zircon ages were present.

Much of the lower Paleozoic sedimentary sequences have been folded, metamorphosed and are now phyllites, schists, marbles and quartzites (Baum et al., 1970; DMR, 2014). The oldest Paleozoic sequences are well bedded sandstones to quartzites ranging in colour from white to violet-red (e.g. samples RDT16_001 and RDT15_078, see below). These predominantly metasedimentary rocks are commonly cross-bedded and have rare intercalated conglomerates with clast compositions predominantly of quartz pebbles and sporadic black chert (Baum et al. 1970). The Cambro-Ordovician sediments were originally deposited in a shallow marine environment (Baum et al. 1970). Generally the Cambrian to Lower Ordovician strata in Thailand are characterised by clastic deposits, particularly hundreds of meters of very well cemented sandstones, together with some slates (see review in Morley 2018). During the Ordovician, extensive shallow marine carbonates and some shales and greywackes were deposited (e.g. Aye Ko Aung and Cocks 2017; Koch 1973; Ridd 2011; Thein 1973).

Carboniferous-aged sedimentary sequences in northwestern Thailand include thickly-bedded sandstone, conglomeratic arkose, greywacke and shale, with minor intercalations of limestone and chert (Baum et al., 1970; Bunopas, 1981; DMR, 2014; Ingavat et al., 1980; Toriyama, 1975). The Carboniferous clastic sequences in northern Thailand have been previously separated as the Carboniferous sandstones and mélange accretionary sequences of the Inthanon Zone and the Carboniferous–Permian sediments assigned to the Sibumasu Terrane (Baum et al., 1970; Hara et al., 2012). Their petrography and geochemistry is detailed in Hara et al. (2012). The distinction between the two groups of sedimentary sequences was based on their geochemical composition which indicated variable tectonic settings; mélange lithic sequences from a recycled orogen compared to the Sibumasu quartzose sandstones which display characteristics of the craton interior and recycled quartzose types (Hara et al., 2012). West of Mae Sariang, the early Permian clastic sediments have been described as sandstones, greywackes, shales and cherts (Baum et al., 1970; Kamata et al., 2009). Detrital zircons from pre-Triassic sedimentary and meta-sedimentary rocks indicate they have been sourced from Proterozoic and Archean basement (Burrett et al., 2014; Cai et al., 2017). Middle Permian limestones, containing fusulinids, conodonts, brachiopods and corals, are also found across northwest Thailand (Bunopas, 1981; Ingavat et al., 1980). Detrital zircons from Paleozoic sedimentary and meta-sedimentary clastic rocks indicate they have been sourced from Proterozoic and Archean

Table 1. Sample localities, lithologies and published ages. Previous ages taken from Kohn and Unger (1981) map and Baum et al. (1970).

Sample	*Location*	*Lithology*	*Previously estimated age*	*Pre or Syn-collisional*
RDT16_001	18° 8'34.00"N 98° 6'31.00"E	sandstone to quartzite	Cambrian	Pre-collisional
RDT16_006	17°59'13"N 97°44'41"E	argillaceous sandstone (weathered)	middle Permian (Upper Carboniferous to Lower Permian – map)	Pre-collisional
RDT16_008	18°09'47"N 97°55'51"E	lithic wackestone (weathered)	Carboniferous to Permian	Pre-collisional
RDT16_012	18°48'34.36"N 97°51'38.00"E	sublitharenite	middle Triassic	Syn-collisional
RDT16_018	18°41'56.00"N 97°53'25.00"E	sub to litharenite	Silurian-Carboniferous	Pre-collisional
RDT16_019	17°56'48"N 97°55'29"E	litharenite	Carboniferous to Triassic	Pre-collisional
RDT15_066	18°15'54.00"N 97°56'34.00"E	coarse grained subarkose with minor lithics	Permian	Pre-collisional
RDT15_078	18° 8'19.00"N 98° 4'33.00"E	micaceous lithic subarkose	Paleozoic	Pre-collisional

basement (Burrett et al., 2014; Cai et al., 2017).

The Triassic Mae Sariang Group (Bunopas, 1981; Chonglakmani, 2011; DMR, 1999), composed of sandstone, conglomerate, shale and limestone with subordinate bedded chert, is widely distributed in the Mae Hong Son–Mae Sariang region (Baum et al., 1970; Chaodumrong, 2013; Hisada et al., 2004; Srinak et al., 2007). Middle to Upper Triassic bivalves and radiolarian faunas have been reported in the cherts and associated thin-bedded limestone filaments of the Mae Sariang Group (Baum et al., 1970; Chonglakmani, 2011; Kamata et al., 2002; Saesaengseerung et al., 2008). The clastic rocks of the Mae Sariang Group contain oriented pebbles of metamorphic rocks and flute casts, which suggest a transport direction parallel to the strike of mountain belt (Tofke et al., 1993). The Upper Triassic continental sequences indicate uplift, folding and orogenesis (Baum et al., 1970; Hara et al., 2012), and it was therefore proposed by Hara et al. (2012) that these sediments were deposited during, or after, the collision of the Sibumasu, Sukhothai and Indochina terranes (the Indosinian Orogeny).

2.3 Tectono-stratigraphy of northwest Thailand

Northwest Thailand is part of a geologically complex region with Mesozoic–Cenozoic subduction, accretion and orogenesis being further complicated by later Cenozoic extensional reactivation (Gardiner et al., 2016a). Many Phanerozoic collisional and contractional events have obscured the exact location of the tectonic domain boundaries (Gardiner et al., 2016a; Li et al., 2017). The extent of the Sibumasu

Terrane has been variably defined in the past (Audley-Charles et al., 1988; Domeier and Torsvik, 2014; Gardiner et al., 2016b). The Mae Yuam Fault is often used as the boundary between the Sibumasu Terrane and the Inthanon Zone (Gardiner et al., 2016a; Hisada et al., 2004; Morley, 2018). However, this contact is controversial since this is a Cenozoic strike-slip fault in a N–S trending valley (Dopieralska et al., 2012; Hisada et al., 2004; Metcalfe and Isozaki, 2009). A large proportion of the sedimentary sequences east of this fault have provincial affinity to the Sibumasu Terrane rather than being representative of an oceanic suture zone (see discussion in Morley, 2018).

The Triassic rocks of the Mae Sariang Group sit either side of the Mae Yuam Fault, although they extend further on the western side (Fig. 1; Gardiner et al., 2016a; Hisada et al., 2004; Morley, 2018). However, it has been suggested that a thrust, referred to as the Mae Sariang Thrust Zone, which is geographical close to the Mae Yuam Fault, is the real reason for the abrupt lithological change (Gardiner et al., 2016a; Morley, 2018).

In this study, we will define the boundaries of the Sibumasu Terrane as the basement of Peninsula Thailand, which extends north into eastern–central Myanmar, east to the Chiang Rai Line and south through the western Malay Peninsula as defined by Gardiner et al. (2016b). Many of the pre-Indosinian "Inthanon Zone" sequences have long been regarded as part of the Sibumasu Terrane derived from Gondwana (Bunopas 1981; Hada et al. 1997; Metcalfe 1998). Therefore, the pre-Indosinian sedimentary rocks east of the Mae Yuam Fault and the Mae Sariang Thrust Zone in this study are regarded as sequences of the Sibumasu Terrane (see Fig. 1).

3. Methodology

3.1 Sample preparation

Eight detrital samples were taken from northwest Thailand using regional geology maps (Baum et al., 1981; DMR, 1999; von Braun et al., 1981), to target the Cambrian through to the Triassic units. Samples were then crushed and sieved to collect zircon grains using the conventional magnetic and heavy liquid separation procedures (see Fig. 1, Table 1 and Supplementary Fig. 1). Approximately 200 zircon grains per sample, where yields permitted, were handpicked to obtain a pure zircon separate, cast in epoxy resin and polished for U–Pb zircon age determinations. In order to characterise the textural and chemical-zoning features within each zircon, cathodoluminescence (CL) images for zircon were obtained (Fig. 2), using the FEI Quanta 600 (Mineral Liberation Analysis) Scanning Electron Microscope with energy-dispersive x-ray (EDX) and Gatan CL detectors at Adelaide Microscopy.

3.2 U–Pb geochronology

Where zircon yields allowed, 120 zircon grains were selected from each sample for laser ablation inductively coupled plasma mass spectrometry (LA–ICP–MS). The LA–ICP–MS method is particularly useful as specific textural and temporal domains within zircons can be targeted as illustrated in Fig. 2. The majority of LA–ICP–MS analyses were conducted on an Agilent 7900x coupled to a New Wave NW213 laser ablation system with a TwoVol2 sample chamber at Adelaide Microscopy, Adelaide, South Australia (see Supplementary Table 1 and 2). Some U–Pb zircon analyses, detailed in Supplementary Tables 1 and 2, were conducted simultaneously with the zircon

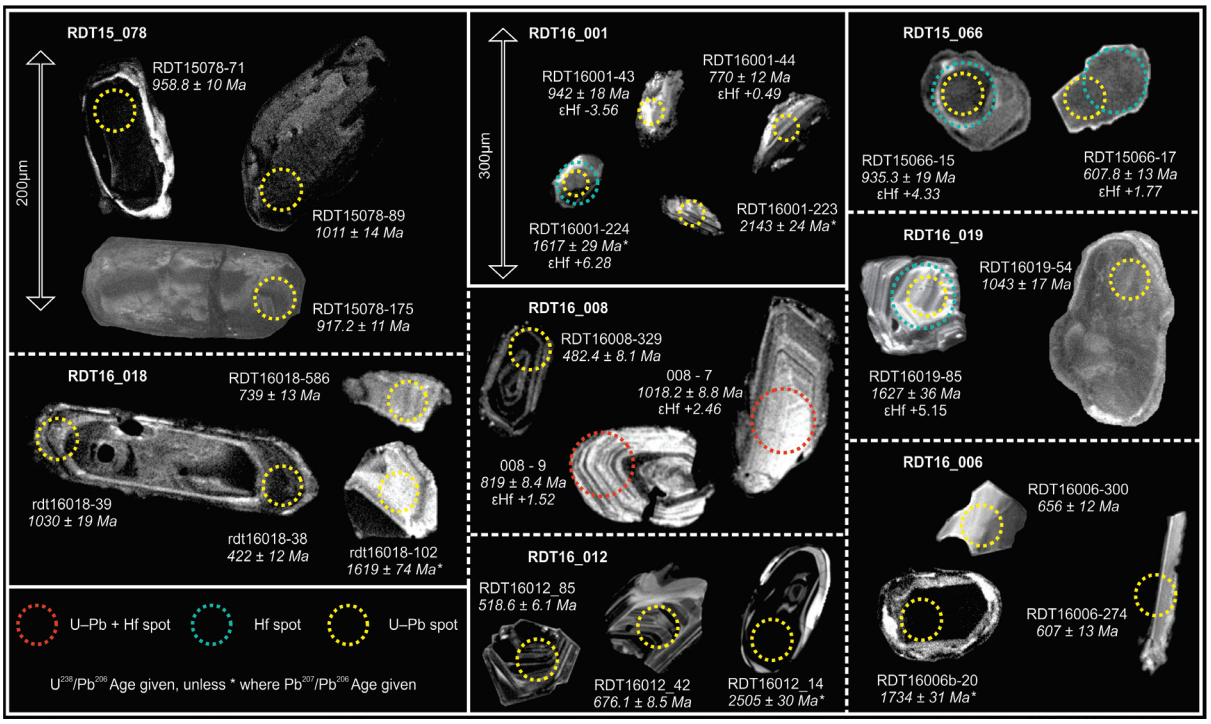

Fig. 2. Cathodoluminescence (CL) images for representative zircon from northwest Thailand. U–Pb laser, Hf spots shown, values are given with two standard deviation error. All images displayed relative to the 200 µm scale bar, except RDT16_001 shown with 300 µm scale bar. The age for each spot is the $^{238}U/^{206}Pb$ age, unless marked with an asterisk (*) where the $^{207}Pb/^{206}Pb$ age is used.

Lu–Hf isotope analyses using a Resonetics S-155-LR 193nm excimer laser ablation system connected via split stream to an Agilent 7700x quadrupole ICP–MS and a Nu Plasma II multi-collector in the GeoHistory Facility, John de Laeter Centre, Curtin University, Perth, Western Australia.

Many of the detrital zircons collected in this study were relatively small, often only 50 µm zircon grains containing multiple textural domains (see Fig. 2 and Table 2). Therefore, to incorporate data from these smaller zircons, spot sizes of 25, 30 and 50 µm were used depending on the zircon grain size (see Supplementary Table 2). Elemental fractionation is extremely sensitive to laser pulse energy (Jackson et al., 2004), and the nature of a laser ablation system means that its energy output varies over time. Therefore, the laser intensity was set at the beginning of each analytical session to maintain the optimal operating conditions and the energy output required for zircon ablation. The set intensity at the beginning of each analytical session varied from 2 to 3 J/cm² at Curtin University and 5.6 to 6.6 J/cm² at Adelaide Microscopy.

Each LA–ICP–MS analysis was bracketed by zircon standard blocks (every 10–16 unknowns) containing GEMOC GJ-1 ($^{207}Pb/^{206}Pb$ TIMS age of 607.7 ± 4.3 Ma, $^{206}Pb/^{238}U$ TIMS age of 600.7 ± 1.1 Ma and $^{207}Pb/^{235}U$ age of 602.0 ± 1.0 Ma; Jackson et al., 2004) as the primary zircon standard with 91500 ($^{207}Pb/^{206}Pb$ age of 1065 Ma and $^{206}Pb/^{238}U$ age of 1062 Ma; Wiedenbeck et al., 1995) and at Adelaide Microscopy also Plešovice ($^{206}Pb/^{238}U$ age of 337.13 ± 0.37 Ma (2σ); Sláma et al., 2008) to monitor drift and down-hole

fractionation. Further information on the analytical methodology is given in Dew et al. (2018b), and for detailed analytical methodology see Payne et al. (2006).

Across all analytical sessions, analyses of GJ-1 yielded a $^{206}Pb/^{238}U$ weighted average age of 601.67 ± 0.39 Ma (n=575, MSWD=0.77, see Supplementary Table 2 for individual standard measurements). All data were reduced using the UPbGeochron4 data reduction scheme in Iolite (Paton et al., 2011).

3.3 Lu–Hf isotopic system

Zircon grains that had less than ±10% discordance (using the ($^{206}Pb/^{238}U$ age)/ $^{207}Pb/^{235}U$ age) calculation; individual analyses are outlined in Supplementary Table 1) were analysed for Hf isotopes. The number of Hf analyses for each sample was determined by the number and variability of the zircon U–Pb age populations. The Hf and Lu isotopic analyses were completed using a Resonetics S-155-LR 193nm excimer laser ablation system connected to a Nu Plasma II multi-collector ICP–MS at the John de Laeter Centre at Curtin University in Perth, Western Australia.

All isotopes (^{180}Hf, ^{179}Hf, ^{178}Hf, ^{177}Hf, ^{176}Hf, ^{175}Lu, ^{174}Hf, ^{173}Yb, ^{172}Yb and ^{171}Yb) were counted on the Faraday collector array. Analyses were carried out using a beam diameter of 50 μm. Typical ablation times were 20s with 40s baseline at front and two cleaning pulses using a 10 Hz repetition rate, a 4 ns pulse rate, and an intensity of 2.8-3 J/cm^2. Time resolved data were baseline subtracted and reduced using Iolite (DRS after Woodhead et al., 2004), where ^{176}Yb and ^{176}Lu were removed from the 176 mass signal using $^{176}Yb/^{173}Yb$ = 0.7962 (Chu et al., 2002) and $^{176}Lu/^{175}Lu$ = 0.02655 (Chu et al., 2002) with an exponential law mass bias correction assuming $^{172}Yb/^{173}Yb$ = 1.35274 (Chu et al., 2002). The interference corrected $^{176}Hf/^{177}Hf$ was normalized to $^{179}Hf/^{177}Hf$ = 0.7325 (Patchett and Tatsumoto, 1980) for mass bias correction.

Mud Tank ($^{176}Hf/^{177}Hf$ of 0.282505 ± 0.000044; Woodhead and Hergt, 2005) was used as the primary standard for Hf isotopes, and R33 the primary standard for Lu–Hf analyses (Lu/Hf ratios of 0.001989 ± 0.000869; Sláma et al., 2008). In each batch of samples several secondary reference material zircons (including GJ-1, FC-1, 91500 and OG-1; Woodhead and Hergt 2005; Morel et al. 2008) were interspersed as a check on data quality. Mudtank analyses yielded $^{176}Hf/^{177}Hf$ weighted-means of 0.2825070±0.0000088 (2σ, n=24, for RDT16_006, RDT16_008 and RDT16_018) and 0.2825071±0.0000081 (2σ, n=13 for RDT16_001, RDT16_019 and RDT15_066 analysis run). The corrected $^{178}Hf/^{177}Hf$ ratio was calculated to monitor the accuracy of the mass bias correction and yielded average values of 1.467069 ± 0.0000071 (n=685; for RDT16_006, RDT16_008 and RDT16_018) and 1.467117 ± 0.000011 (n=296; for RDT16_001, RDT16_019 and RDT15_066), which are both within the range of values reported by Thirlwall and Anczkiewicz (2004).

3.4 Age determination and illustration

The relative values of the uncertainties for $^{206}Pb/^{238}U$, $^{207}Pb/^{235}U$, and $^{207}Pb/^{206}Pb$ systems vary as a function of age: for "young" samples, $^{206}Pb/^{238}U$ age is the most precise and $^{207}Pb/^{206}Pb$ age is the least precise, whereas for "old" samples the values are reversed (Gehrels 2012). Because of these variations, the age resolution of the U–Pb system is less

precise than using $^{207}Pb/^{206}Pb$ older than ca. 1.4 Ga (Gehrels 2012). To determine the most appropriate and precise zircon U–Pb ages for this study's dataset, the kernel density estimate of all the ±10% discordant data were used to determine the minima of the data (1350-1383 Ma). It was then decided that all $^{206}Pb/^{238}U$ ages ≤1351 Ma would be used for age determination, utilising the $^{207}Pb/^{206}Pb$ age for all older grains (interpreted ages are highlighted in Supplementary Table 1).

To visualise the detrital age distributions the Kernel Density Estimation (KDE) was employed. This is a robust statistical method that stacks a Gaussian 'bell curve' on top of each measurement, whose standard deviation is determined by the local probability density (Silverman 1986; Vermeesch 2012). The KDE plots for this study were created using the Java-based DensityPlotter program outlined by Vermeesch (2012).

Multidimensional scaling (MDS) was used to compare the age distribution and hafnium characteristics of the eight samples in this study and then to compare to published data from potential source regions or neighbouring terranes that could have the same source regions to northwest Thailand. MDS is a robust and flexible application of Principal Components Analysis, which uses the Kolmogorov-Smirnov (K-S) test, a calculation of the maximum probability dissimilarity between two or more cumulative distribution functions (Vermeesch 2013).

4. Results

4.1 U–Pb geochronology

Eight samples were used for U–Pb zircon geochronology analyses. The physical structures of the analysed zircons are summarised in Table 2. The U–Pb ages are displayed as kernel density estimations in Fig. 3 and are listed in Supplementary Table 1. Primarily, the ages are interpreted from data within ±10% discordance using the ($^{206}Pb/^{238}U$ age)/$^{207}Pb/^{235}U$ age) calculation. Some analyses clearly show the effects of radiogenic lead loss with anomalously young apparent $^{206}Pb/^{238}U$ ages. Outlier data were rejected after subsequent examination, if the laser beam traversed cracks or overlapped with multiple zircon domains within the grain (see Supplementary Table 1).

Two methods of maximum depositional age calculations were used as presented in Fig. 4; Firstly, the youngest single grain zircon ages within ±12% (within ±5% where possible) discordance (YSG) and, secondly, the weighted mean age of the youngest cluster that overlap in age at 1σ uncertainty values (YC1σ) were taken, following the quantitative interpretation approach for detrital zircon U–Pb age data of Dickinson and Gehrels (2009). YC1 was calculated using ages within ±10% discordance of the ($^{206}Pb/^{238}U$ age)/ $^{207}Pb/^{235}U$ age) discordance calculation. Interestingly, six of the eight samples yielded YC1σ ages between ca. 552 Ma and ca. 505 Ma (see Fig. 4).

RDT15_078 (previously mapped as Paleozoic in age) shows a detrital zircon age distribution that is dominated by ca. 1050 Ma to ca. 900 Ma zircons, but also has significant contributions of zircons with age peaks at ca. 2480 Ma, ca. 1857 Ma and ca. 650 Ma (see Fig. 3). This sample has the oldest interpreted maximum depositional age, yielding a YSG of 472.7 ± 6.9 Ma (Fig. 4).

RDT16_001 also contains similar aged

Table 2. Description of zircon morphologies and cathodoluminescence (CL) interpretations for the eight samples in this study.

Sample	*Zircon Morphology*		*Cathodoluminescence (CL) interpretation*
	Size	*Shape*	
RDT16_001	~100-200 μm	Rounded, in many cases in the original crystal shape has been destroyed, and the final product being smooth sub-rounded grains	Grains are commonly cracked. Some zoning, some or homogeneous. Multiple domains are common. Mottled appearance
RDT16_006	50-200 μm	Sub-rounded. Frequently fragmented or broken grains	Zonation, both oscillatory and diffuse, are common. Some dark grains. Multiple domains are common.
RDT16_008	100-300 μm	Sub-rounded, euhedral to subhedral grains. Rarely broken.	Well-developed oscillatory zoning with multiple domains common.
RDT16_012	~50-150 μm	Rounding of the crystal edges whereas in others the original crystal shape has been destroyed, and the final product being smooth sub to well-rounded grains	Well rounded detrital zircon grains. Well-developed oscillatory zoning. Some grains preserve zoning with convolute boundaries. Inherited cores common. Quartz and white mica inclusions. Some metamictisation. Grains are commonly cracked.
RDT16_018	~50-300 μm	Some grains only have minor rounding of the crystal edges, some are very fragmented and broken	Zonation, both oscillatory and diffuse, are common. Some dark grains.
RDT16_019	~50-300 μm	Sub-rounded to rounded Some euhedral but fragmented or broken	Multiple domains are common. Some grains contain cracks.
RDT15_066	100-200 μm	Smooth sub to well-rounded grains	Well rounded detrital zircon grains. Inherited cores common. Some grains preserve zoning or are homogeneous. Grains are commonly cracked.
RDT15_078	50-200 μm	Sub-rounded subhedral grains	Oscillatory zoning, some diffuse zoning and dark homogeneous grains present. Some grains contain multiple domains.

zircons to RDT15_078 with a large proportion of the zircons analysed aged between ca. 1050 Ma to ca. 900 Ma and peak contributions ca. 1864 Ma and ca. 2474 Ma. However in RDT16_001, there are a greater variety of ages recorded, with peaks also at ca. 2919 Ma, ca. 1604 Ma, ca. 1244 Ma, ca. 1135 Ma and ca. 537 Ma (see Fig. 3). The YSG of RDT16_001 of 471.1 ± 7.8 Ma is within 1σ error of the YSG from RDT15_078.

RDT15_066 has a large age peaks from 927 Ma, 635 Ma and 560 Ma with minor peaks estimated at 3393 Ma, 3071 Ma, 2625 Ma, 2460 Ma, 1835 Ma, 1572 Ma, ca. 1390 Ma and 1152 Ma. The YSG for RDT15_066 yielded an early Carboniferous age of 355.7 ± 8 Ma (this zircon analysis was within 15% ($^{206}Pb/^{238}U$ age)/ $^{207}Pb/^{206}Pb$ age) discordance and 12% ($^{206}Pb/^{238}U$ age)/ $^{207}Pb/^{235}U$ age) discordance.

RDT16_018 has a large proportion of zircons with ages between 1000 and 900 Ma. There are multiple smaller age peaks at 3220 Ma, 2680 Ma, 2473 Ma, 1884 Ma, 1700 Ma, 1490 Ma, 1155 Ma and 536 Ma (see Fig. 3). The YSG of RDT16_018 is 322.9 ± 8 Ma (Fig. 4).

RDT16_008 has a large proportion of ages

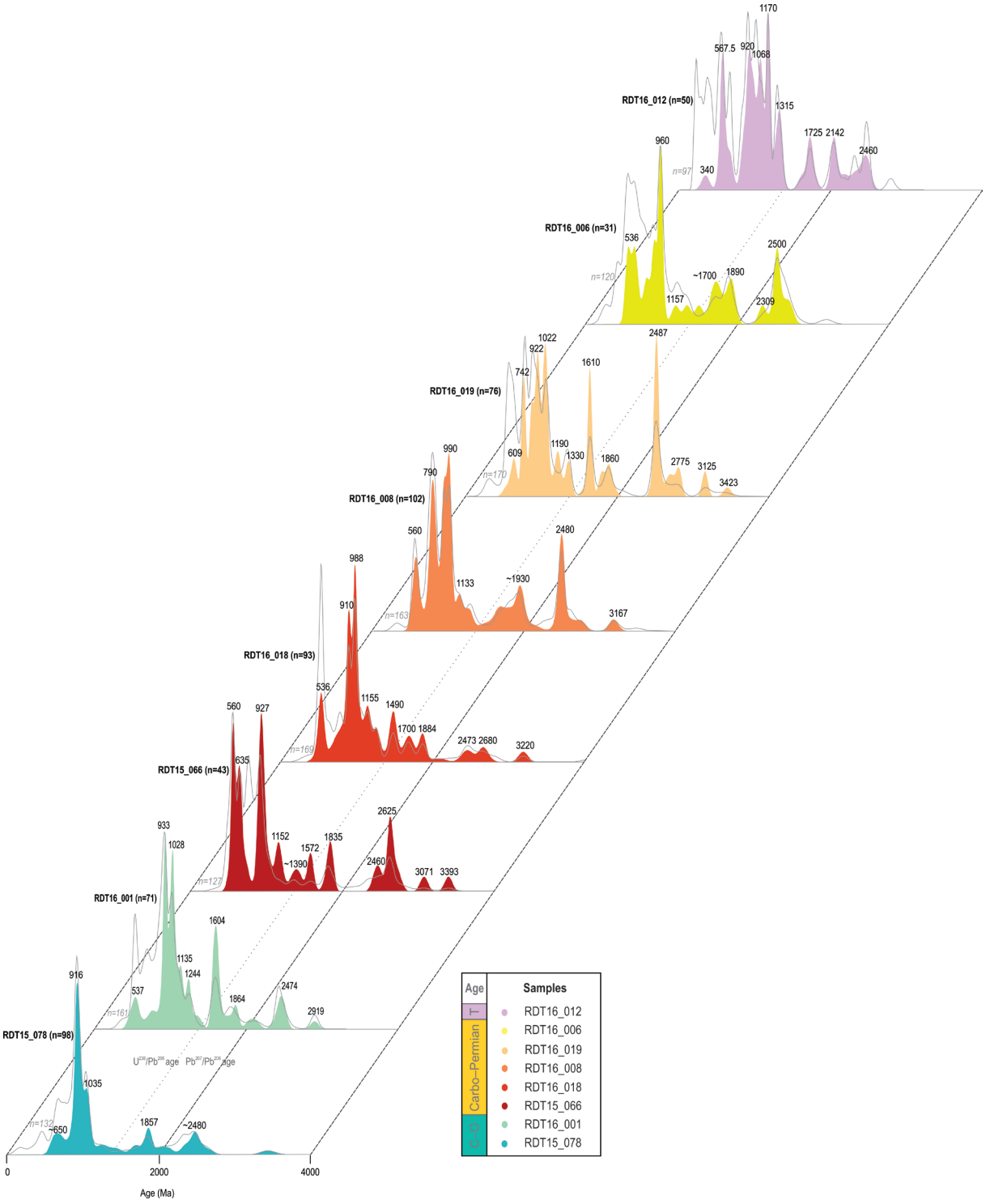

Fig. 3. Kernel Density Estimate (KDE) for each U–Pb sample. Each coloured plot illustrates the kernel density estimate of data with ±10% ($^{206}Pb/^{238}U$ age)/ $^{207}Pb/^{206}Pb$ age) discordance, age peaks of the concordant data are labelled in Ma, the grey line on each plot indicates kernel density plot of all data. Parameters in DensityPlotter 20 Ma bandwidth, 50 Ma bins and the adaptive function.

younger than 1000 Ma, with age peaks at 990 Ma, 790 Ma and 560 Ma. There is also a major peak at 2480 Ma and minor age peaks at 3167 Ma, ca. 1930 Ma and 1133

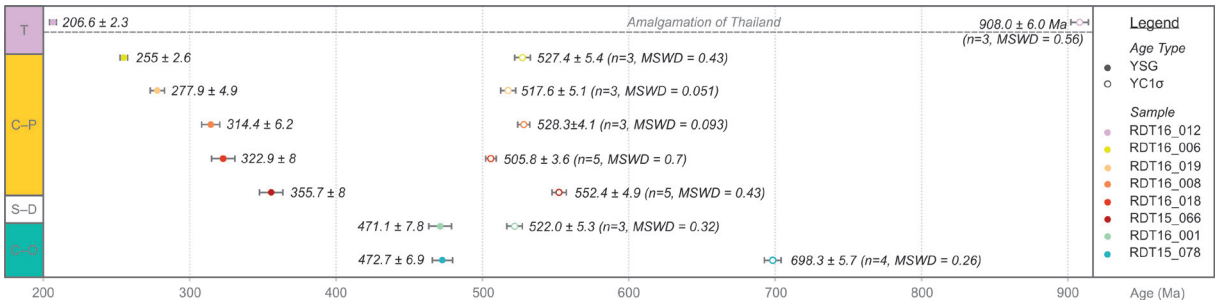

Fig. 4. Age constraints for the stratigraphy of the study area (error bars are of 2 sigma error). The youngest concordant single grain zircon ages (YSG) and the weighted mean age of the youngest cluster that overlap in age at 1σ uncertainty values (YC1σ) for each sample are shown.

Ma (see Fig. 3). The YSG of RDT16_008 is 314.4 ± 6.2 Ma (Fig. 4).

For RDT16_019, there is an abundance of age data at ca. 2487 Ma, 1610 Ma and between ca. 1022 and ca. 740 Ma (see Fig. 3). This sample contains a variety of ages with smaller peaks at 3423 Ma, 3125 Ma, ca. 2775 Ma, ca. 1860 Ma, 1330 Ma, 1190 Ma and 609 Ma (see Fig. 3). Absence of ages 2250–1900 Ma. The YSG of RDT16_019 from the middle Permian at 277.9 ± 4.9 Ma (Fig. 4).

RDT16_006 contained a large proportion of discordant zircon analyses. The concordant data was skewed to the older U–Pb ages. The major age peak was ca. 960 Ma in both the concordant and total U–Pb ages analysed (Fig. 3). The other concordant age peaks were 2500 Ma, 2309 Ma, 1890 Ma, ca. 1700 Ma, ca. 1550–1150 Ma and 600–500 Ma. The YSG of RDT16_006 is 255 ± 2.6 Ma (Fig. 4).

There is a major age contribution for RDT16_012 of ages between ca. 920 and ca. 1330 Ma and also ca. 567.5 Ma. Other ages are ca. 2460–2142 Ma, 1725 Ma and 340 Ma. RDT16_012 has the youngest YSG in this study at 206.6 ± 2.3 Ma (see Fig. 4).

4.2 Lu–Hf isotopic analyses

In total, 299 concordant zircon grains were analysed for Lu–Hf isotopes, and the results show $\varepsilon Hf_{(t)}$ values in the range of −29.58 to +10.24 and Hf depleted mantle model ages (T_{DM}) in the range of 4.36 Ga to 1.01 Ga (illustrated in Fig. 5).

The analysis of 35 zircons from RDT16_001 yielded $\varepsilon Hf_{(t)}$ values between -23.47 and +8.83 (Fig. 5). The prominent age population between 1255–750 Ma record a large variation in $\varepsilon Hf_{(t)}$ values between -23.47 and +8.14, which corresponds to depleted mantle model ages of 3.21 Ga and 1.30 Ga (Fig. 5). The younger $\varepsilon Hf_{(t)}$ values are less varied and all indicate evolved signatures between -21.19 and -11.36, with T_{DM} from 2.73 Ga to 2.18 Ga (Fig. 5). Hf analyses from the earlier Proterozoic zircons show a more juvenile pattern with εHf(t) values ranging from -4.58 to +8.83, which corresponds to depleted mantle model ages of 2.92 Ga and 1.75 Ga (Fig. 5).

Thirty-one zircons from RDT15_066 yielded $\varepsilon Hf_{(t)}$ values between -15.70 and +9.12 (Fig. 5). The late Neoproterozoic to Cambrian age population between 735–500 Ma shows a relatively restricted pattern with $\varepsilon Hf_{(t)}$ values between -7.52 and +1.77, corresponding to depleted mantle model ages of 2.94 Ga and 1.77 Ga (Fig. 5). The other prominent age

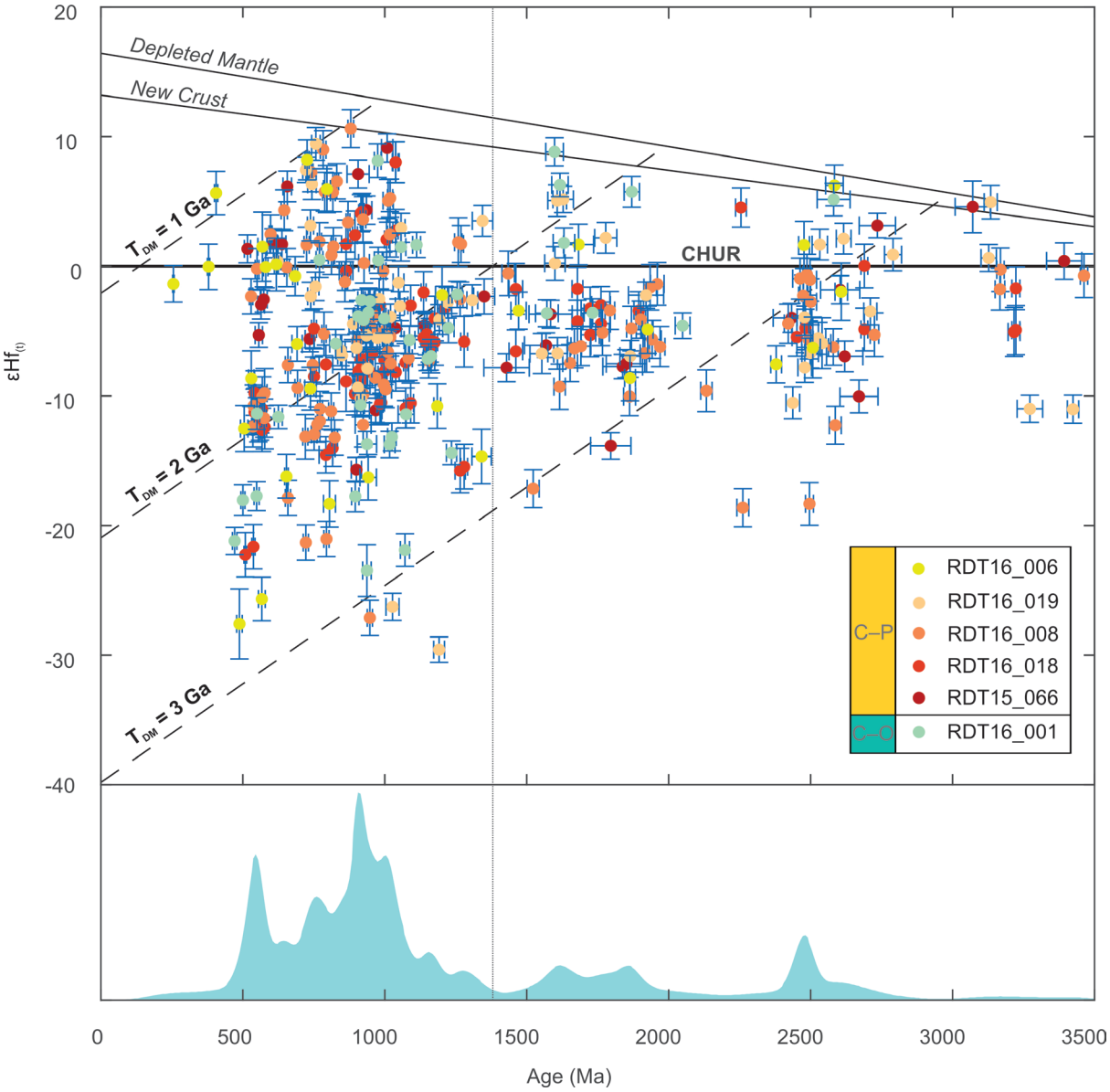

Fig. 5. Plot of $\varepsilon Hf_{(t)}$ versus age for all detrital samples collected from northwest Thailand. The T_{DM} Hf crustal evolution lines are based on a $^{176}Lu/^{177}Hf$ ratio of 0.015 (Griffin et al. 2004). Kernel density estimate of all ±10% ($^{206}Pb/^{238}U$ age)/ $^{207}Pb/^{235}U$ age) discordance ages found in these samples (n=876), peaks show the relative number of zircons.

population (1140–900 Ma) records a larger variation in $\varepsilon Hf_{(t)}$ values (-15.70 to +9.12), which corresponds to depleted mantle model ages of 2.71 Ga and 1.27 Ga (Fig. 5). The $\varepsilon Hf_{(t)}$ values from zircons between 2700 Ma and 1140 Ma show a somewhat restricted pattern of moderately recycled signatures ($\varepsilon Hf_{(t)}$ range -13.86 to -1.82). The $\varepsilon Hf_{(t)}$ values of the zircons older than 2.7 Ga are all positive, ranging from +4.58 to +0.40 and giving T_{DM} between 3.68 Ga to 3.00 Ga (Fig. 5).

The analysis of 40 zircons from RDT16_018 yielded $\varepsilon Hf_{(t)}$ values between -23.47 and +8.83 (Fig. 5). The late Neoproterozoic to Cambrian age population of RDT16_018 (570–500 Ma) primarily shows a restricted pattern with $\varepsilon Hf_{(t)}$ values between -12.62 and +10.80, which corresponds to depleted

mantle model ages of 2.27 Ga and 2.15 Ga (Fig. 5). However, the youngest zircon analysed from this population (also used for YC1σ) has a low $\varepsilon Hf_{(t)}$ at -22.25 and an older T_{DM} of 2.82 Ga. In this sample, the zircons aged between 1200–800 Ma had less variation in these Hf signatures compared to other samples in this study (see Fig. 5). The $\varepsilon Hf_{(t)}$ values taken from zircons older than 1460 Ma show little variation between -6.55 and -1.69, which corresponds to depleted mantle model ages of 3.86 Ga and 2.58 Ga (Fig. 5).

One hundred and twelve zircons from RDT16_008 yielded $\varepsilon Hf_{(t)}$ values between -27.13 and +10.24 (Fig. 5). The 1500–500 Ma age population all have a similar spread of $\varepsilon Hf_{(t)}$ values between -27.13 and +10.24. In comparison, the older 2000–1600 Ma ages record a more restricted $\varepsilon Hf_{(t)}$ pattern with values ranging from -9.79 to -1.36 and associated T_{DM} between 3.09 Ga and 2.65 Ga. The zircon age populations from 3–2 Ga show a greater variance in their hafnium signatures with $\varepsilon Hf_{(t)}$ values between -18.34 and +4.91 and corresponding depleted mantle model age range of 4.07 Ga and 2.52 Ga (Fig. 5). Zircon analyses older than 3 Ga have a more consistent signature, with $\varepsilon Hf_{(t)}$ values ranging from -1.77 to -0.26 and T_{DM} 3.81 to 3.54 Ga.

The analysis of 50 zircons from RDT16_019 yielded $\varepsilon Hf_{(t)}$ values between -29.58 and +9.44 (Fig. 5). The analysed Neoproterozoic grains are all relatively juvenile ranging in $\varepsilon Hf_{(t)}$ values from -2.32 to +9.44, indicating that they grew in a magma derived from a late Paleoproterozoic–Mesoproterozoic source (Fig. 5). In contrast, the 1310–840 Ma population is quite evolved with two grains with very evolved signatures of -29.58 and -26.58. Only one grain within this population has a positive $\varepsilon Hf_{(t)}$ value (+2.96). The 1870-1340 Ma aged grains yield $\varepsilon Hf_{(t)}$ values between -6.94 and +5.15, with corresponding T_{DM} ranging from 2.92 Ga to 1.88 Ga (Fig. 5). Older Archaean grains have $\varepsilon Hf_{(t)}$ values that range from -11.03 to +4.94 with corresponding depleted mantle model ages between 4.36 Ga and 2.92 Ga (Fig. 5).

Thirty-one zircons from RDT16_006 yielded $\varepsilon Hf_{(t)}$ values ranging from -27.61 to +8.14 (Fig. 5). The prominent Neoproterozoi to Cambrian zircon age population records a large variation in $\varepsilon Hf_{(t)}$ values between -27.61 and +8.14, which corresponds to depleted mantle model ages of 3.13 Ga and 1.10 Ga (Fig. 5). In contrast, the younger $\varepsilon Hf_{(t)}$ values are less varied (-1.41 to +5.58; Fig. 5). The Mesoproterozoic grains are evolved, with $\varepsilon Hf_{(t)}$ values ranging from -14.71 to -2.26. Further, their negative $\varepsilon Hf_{(t)}$ values show enrichment away from typical mantle compositions, with significant crustal reworking and model ages between 2.98 Ga and 2.12 Ga. The Neoarchean to Paleoproterozoic zircons have $\varepsilon Hf_{(t)}$ values that range from -8.67 to +6.17 with corresponding depleted mantle model ages between 3.37 Ga and 2.26 Ga (Fig. 5).

5. Discussion

5.1 Changes in provenance over time in northwest Thailand

Prominent age populations of 1200–900 Ma, 650–500 Ma and 2500–2460 Ma are present in each of the eight detrital samples analysed from northwest Thailand (Fig. 3). Therefore, the MDS comparison of the eight samples in this study does not show a significant change in the age of the source region from the Cambrian to the Permian (see Fig. 6a). However, the Triassic sample, RDT16_012 also contains significant component of

younger Paleozoic–Triassic zircons.

Concordant Archean zircon ages were observed in five of the Cambrian–Permian detrital samples. For the Lower Ordovician RDT16_001 sample, no concordant zircon ages greater than 3 Ga were analysed. In contrast to the other six older samples, no zircon domains older than 2.6 Ga were analysed in the two younger Latest Permian to Triassic samples (RDT15_066 and RDT16_012). A younger 340 Ma age peak is present in the Upper Triassic RDT16_012 sample (Fig. 3).

When comparing the $\varepsilon Hf_{(t)}$ values of the zircons older than 1.5 Ga, the older Cambro-Ordovician detrital data (taken from RDT16_001) appears to be more juvenile compared to the more evolved data observed from similar aged zircons from the Carbo-Permian samples (Fig. 5). In stark contrast to this trend, the late Neoproterozoic to Cambrian age population in the older Cambro-Ordovician sample (RDT16_001) contains only evolved signatures with $\varepsilon Hf_{(t)}$ values ranging from -21.19 to -11.36. All five Carbo-Permian detrital samples contain a larger variety of $\varepsilon Hf_{(t)}$ values for the Neoproterozoic–Cambrian aged zircons, including both juvenile and evolved signatures (ranging from -22.25 to +10.80). Lu–Hf isotopes in younger Paleozoic zircons were only analysed from RDT16_006, which yielded $\varepsilon Hf_{(t)}$ values between -1.41 and +5.58 (Fig. 5).

5.2 Correlation across Thailand

The range of ages found in the Cambrian–Permian detrital zircons does not suggest any sedimentary connection with the other Thai terranes at this time. Additionally, the paucity of younger Paleozoic zircon ages suggests that these sediments were not sourcing material from the nearby Paleozoic granites and metamorphic rocks (Bunopas 1981; Dew et al. 2018a; Hansen and Wemmer 2011; Kawakami et al. 2014; Stokes 1988), possibly because the granites were not exposed at the time the sediments were deposited (see Fig. 1 and Fig. 3).

Deformed granitoids and orthogneisses with Cambro-Ordovician crystallisation ages have been previously documented within the Sibumasu Terrane on the Thai Peninsula and were interpreted to be products of arc-related magmatism along the Gondwanan Indo-Australian margin (Dew et al. 2018a; Kawakami et al. 2014; Lin et al. 2013). The detrital zircon ages found in this study are also consistent with inherited zircon analyses from Sibumasu granitoids in Thailand. For example, Dew et al. (2018a) quoted inherited zircon ages ranging from $^{207}Pb/^{206}Pb$ age of 3189.3 ± 17.8 Ma to $^{206}Pb/^{238}U$ age of 371.5 ± 5.8 Ma, with age peaks at 2725 Ma, 2491 Ma, 1360 Ma, 1090 Ma, 940 Ma, 840 Ma, 700 Ma and 500 Ma.

In a detrital zircon study of northern Thailand from the Inthanon Zone by Hara et al. (2013), the youngest zircons in upper Permian sequences (Type 1 sandstones) were late Carboniferous in age (308 ± 14 and 300 ± 16 Ma). In the Triassic sequence (Type 2 sandstone) of Hara et al. (2013) the youngest zircon U–Pb ages of 238 ± 10 and 236 ± 15 Ma, suggests a middle Triassic maximum depositional age. The youngest zircons were proposed to be sourced from a missing arc such as the Sukhothai arc system. This is consistent with the Triassic detrital data in our detrital study, where RDT16_012 indicates a significant change in zircon source. By this time, the Indosinian Orogeny was underway (Arboit et al. 2016; Hansberry et al. 2017; Morley et al.

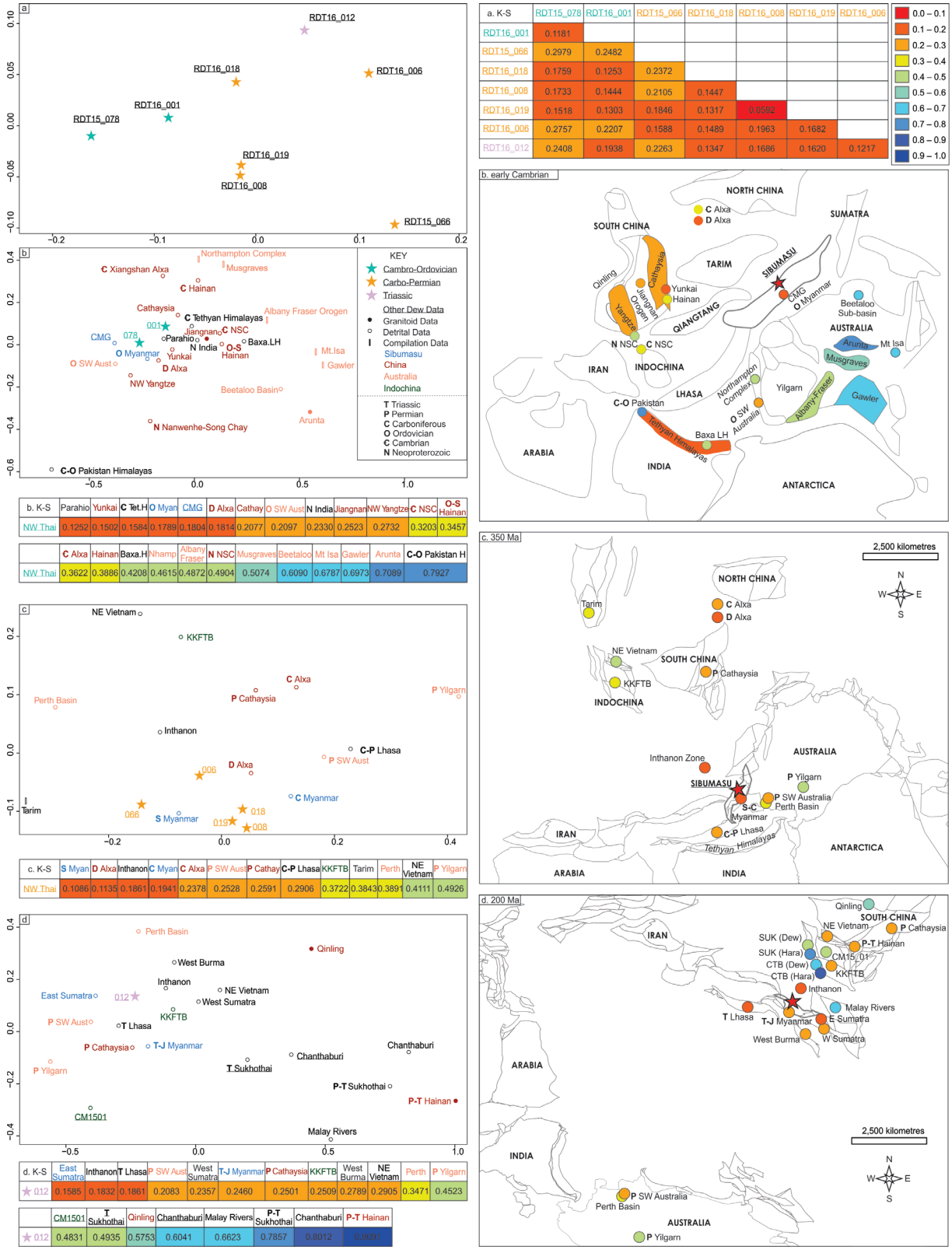

a. K-S	RDT15_078	RDT16_001	RDT15_066	RDT16_018	RDT16_008	RDT16_019	RDT16_006
RDT16_001	0.1181						
RDT15_066	0.2979	0.2482					
RDT16_018	0.1759	0.1253	0.2372				
RDT16_008	0.1733	0.1444	0.2105	0.1447			
RDT16_019	0.1518	0.1303	0.1846	0.1317	0.0592		
RDT16_006	0.2757	0.2207	0.1588	0.1489	0.1963	0.1682	
RDT16_012	0.2408	0.1938	0.2263	0.1347	0.1686	0.1620	0.1217

0.0 – 0.1
0.1 – 0.2
0.2 – 0.3
0.3 – 0.4
0.4 – 0.5
0.5 – 0.6
0.6 – 0.7
0.7 – 0.8
0.8 – 0.9
0.9 – 1.0

b. K-S	Parahio	Yunkai	C Tet.H	O Myan	CMG	D Alxa	Cathay	O SW Aust	N India	Jiangnan	NW Yangtze	C NSC	O-S Hainan
NW Thai	0.1252	0.1502	0.1584	0.1789	0.1804	0.1814	0.2077	0.2097	0.2330	0.2523	0.2732	0.3203	0.3457

	C Alxa	Hainan	Baxa.H	Nhamp	Albany Fraser	N NSC	Musgraves	Beetaloo	Mt Isa	Gawler	Arunta	C-O Pakistan H
NW Thai	0.3622	0.3886	0.4208	0.4615	0.4872	0.4904	0.5074	0.6090	0.6787	0.6973	0.7089	0.7927

c. K-S	S Myan	D Alxa	Inthanon	C Myan	C Alxa	P SW Aust	P Cathay	C-P Lhasa	KKFTB	Tarim	Perth	NE Vietnam	P Yilgarn
NW Thai	0.1086	0.1135	0.1861	0.1941	0.2378	0.2528	0.2591	0.2906	0.3722	0.3843	0.3891	0.4111	0.4926

d. K-S	East Sumatra	Inthanon	T Lhasa	P SW Aust	West Sumatra	T-J Myanmar	P Cathaysia	KKFTB	West Burma	NE Vietnam	Perth	P Yilgarn
★ 012	0.1585	0.1832	0.1861	0.2083	0.2357	0.2460	0.2501	0.2509	0.2789	0.2905	0.3471	0.4523

	CM1501	T Sukhothai	Qinling	Chanthaburi	Malay Rivers	P-T Sukhothai	Chanthaburi	P-T Hainan
★ 012	0.4831	0.4935	0.5753	0.6041	0.6623	0.7857	0.8012	0.8094

Fig. 6. Multidimensional scaling (MDS) plots, associated Kolmogorov–Smirnov (K–S) statistics in relation to the northwest Thai samples in this study and paleogeographic reconstructions highlighting K–S statistics in relation to this study's samples. **a**. The northwest Thai samples from this study. MDS plot of detrital sample U–Pb age distributions from the Sibumasu Terrane in northwest Thailand. Samples with lowest dissimilarity values plot closest to one another (see Vermeesch 2013; 2016).

Fig. 6. (continued) b. Multidimensional scaling (MDS) plot of this study's Cambro-Ordovician samples and potential source areas. Table of K–S statistics in relation to this study's Cambro-Ordovician samples. Palaeogeographic reconstruction of Greater Gondwana for the early Cambrian (modified from Burrett et al. 2014) with key regions coloured according to their K–S statistics relative to this study's Cambro-Ordovician samples. **c**. MDS plot of this study's Carbo-Permian samples and potential source areas. Table of K–S statistics in relation to this study's Carbo-Permian samples, least dissimilar (0) to most dissimilar (1). 350 Ma paleogeographic reconstruction adjusted from Young et al. (2018) with key regions coloured according to their K–S statistics relative to this study's Carbo-Permian samples. **d**. MDS plot of this study's Triassic sample (RDT16_012) and potential source areas. Table of K–S statistics in relation to this study's Triassic sample (RDT16_012), least dissimilar (0) to most dissimilar (1). 200 Ma paleogeographic reconstruction adjusted from Young et al. (2018) with key regions coloured according to their K–S statistics relative to this study's Triassic sample (RDT16_012). Published data sources referenced in supplementary material.

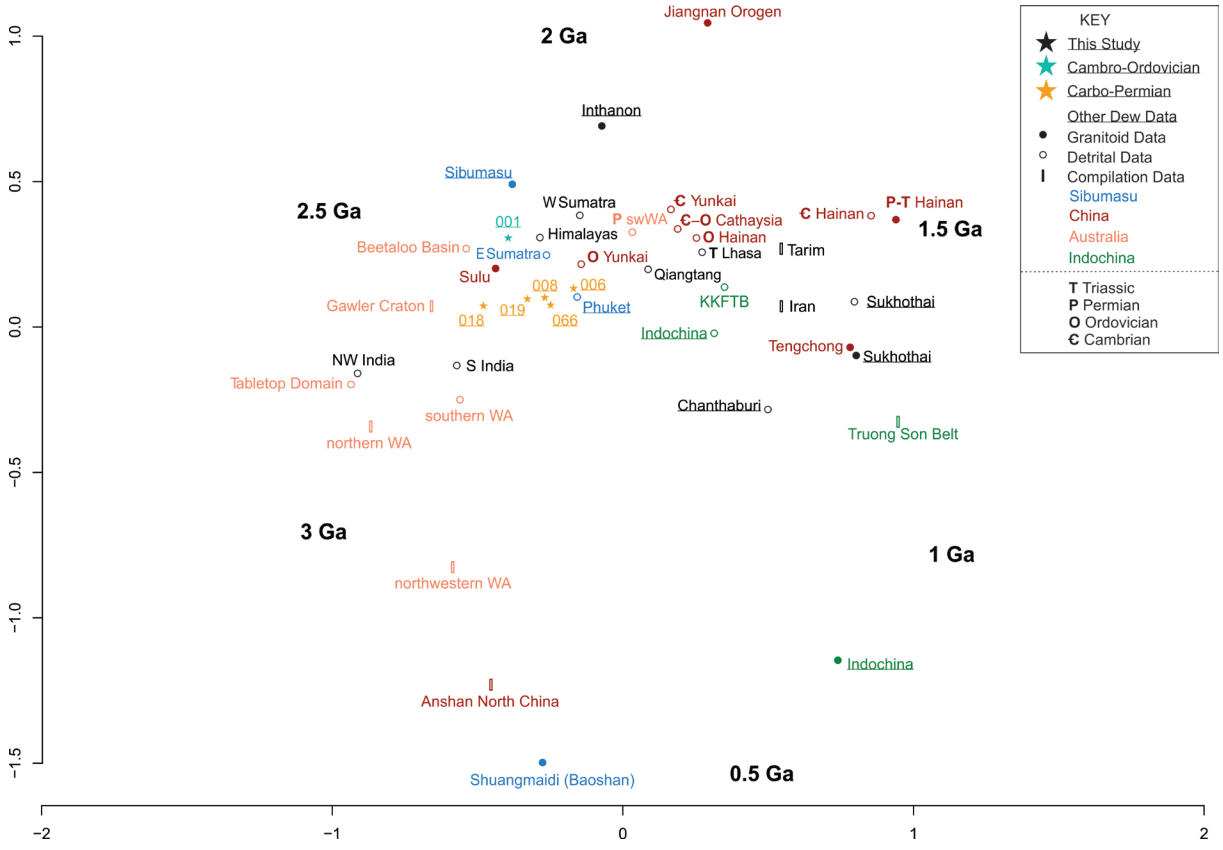

Fig. 7. Multidimensional scaling (MDS) plot of hafnium crustal depleted mantle model ages (T_{DM}) for the detrital samples from the Sibumasu Terrane in northwest Thailand and potential source areas. Synthetic source ages (in bold) were created using the Excel NORMINV function. Samples with lowest dissimilarity values are plotted closest to one another (see Vermeesch 2013; Vermeesch et al. 2016). Published data sources referenced in supplementary material.

2013), creating the potential for zircons to be sourced from the Sukhothai Terrane as suggested by Hara et al. (2013), further to the northeast in Thailand.

5.3 Correlation of age peaks

Broadly speaking, all samples from northwest Thailand yield detrital zircon U–Pb age spectra that are typical of provenance within Gondwana (see Fig. 3 and Supplementary Figure 2 (Burrett et al. 2014; Fitzsimons 2003; Flowerdew et al. 2007; Xu et al. 2013). The following discussion aims to address regions

that contain similar-aged zircon peak populations to those observed in the Cambrian–Triassic strata in northwest Thailand and to propose potential sources. This discussion considers both multi-dimensional scaling of the detrital age distributions and the Hf depleted mantle model ages in order to compare the age and characteristics of the basement sources for our data to published models from Sibumasu, China, Australia and Indochina amongst others (Figs. 6 and 7).

The major age peak at 910 Ma in the cumulative age data of the northwest Thai samples is present in regions that were once part of Gondwana. Abundant 950-900 Ma populations are present in the Tethyan and High Himalayas (Ding et al., 2016; McQuarrie et al., 2008; Myrow et al., 2010; DeCelles et al., 2000; Myrow et al., 2003, 2010; Gehrels et al., 2011), Qiangtang (Dong et al. 2011; Wang et al. 2015), Lhasa (Zhu et al. 2011), Yangtze, East Sumatra (Zhang et al. 2018c), Phuket (Burrett et al. 2014), Antarctica (Fitzsimons 2000; Flowerdew et al. 2007; Kelsey et al. 2008), Indochina (Arboit et al. 2016; Usuki et al. 2013) and the Permian–Jurassic strata from northeast India (Veevers and Saeed, 2009). It is proposed that the 910 Ma detritus from northwest Thailand was likely derived from circa 990–900 Ma Rayner-Eastern Ghats, which is one of the few proximal regions in eastern Gondwana where protoliths of this age occur (Fitzsimons 2000).

Sequences that also contain ca. 1000 Ma zircons are the early Paleozoic sedimentary rocks, Ellsworth-Whitmore Mountains block, Antarctica (Flowerdew et al. 2007), the Dabure Neoproterozoic clastic strata from southern Qiangtang Tibet (Wang et al. 2015), Ordovician and Devonian sediments from NE Iran (Moghadam et al. 2017), detrital zircons from Sumatra (Zhang et al. 2018c) and the Cambrian–Ordovician strata across the Himalayas (Myrow et al. 2010).

Zircon ages similar to major 545 Ma age peak in the northwest Thai samples are found in many regions that were once part of Gondwana (Cai et al. 2017; Ghosh et al. 2005; Moghadam et al. 2017; Myrow et al. 2010). This detrital age population in northwest Thailand is conceivably sourced from the Neoproterozoic–Cambrian Kuunga–Pinjarra Orogen (ages between 600–500 Ma (Collins 2003; Fitzsimons 2000; Veevers et al. 2006), an orogenic belt from Western Australia to eastern Antarctica, which reflects one of the final events in Gondwana amalgamation (Schmitt et al. 2018).

Another large age peak at ca. 749 Ma is observed in the cumulative age data of the northwest Thai samples. These peaks are especially dominant in the two late Carboniferous and early Permian samples; RDT16_008 (790 Ma) and RDT16_019 (742 Ma) (see Fig. 3 and Supplementary Fig. 2). Other similar-aged late Tonian ages are found in the Malani Igneous Suite in northern India (850-700 Ma) and granitoid rocks from Madagascar (Archibald et al. 2016; Archibald et al. 2017; Kroener et al. 2000).

Age populations with maxima ranging from 2500 to 2460 Ma are seen in each analysed northwest Thai sample (Fig. 3). This population may be sourced from ca. 2560–2470 Ma magmatism and orogenesis seen in Australia (Hand et al. 2007; Nordsvan et al. 2018), India (Clark et al. 2009; Collins et al. 2014) and/or central Madagascar (Archibald et al. 2016; Kroener et al. 2000).

Large age peaks between 650 Ma and 600 Ma are seen in RDT15_078, RDT15_066 and RDT16_019 (Fig. 3). This age population could correspond to the 650 Ma granites that intruded the Lamil Group of the Paterson Orogen, Western Australia (Bagas and Nelson 2007).

The 1275 Ma and 1155 Ma ages seen in all of the northwest Thai samples are commonly found in Australian detrital sequences, such as the Late Ordovician Tumblagooda sandstone in the Perth Basin (Cawood and Nemchin 2000; Kettanah et al. 2015). A probable source of these zircons is the Albany–Fraser orogeny in southwest Australia, which records two pulses of magmatism at 1330–1280 Ma and 1200–1130 Ma (Clark et al., 2000; Fitzsimons, 2000).

The 1600 Ma population is also present in Sumatra (Zhang et al. 2018c), Mesoproterozoic–Permian WA, India, Tethyan and High Himalayas (Myrow et al. 2010), and Inorunie Group of the Georgetown Inlier (Nordsvan et al. 2018). This population may correspond to the ca. 1600 Ma magmatic event from the Mount Isa Inlier (Betts et al. 2006; Neumann et al. 2006).

The ca. 1855 Ma age peak seen the northwest Thailand detrital samples is also seen in other parts of Sibumasu (Burrett et al. 2014; Cai et al. 2017). Burrett et al. (2014) proposed that 1860 Ma zircons from quartzite clasts in the Permian Kaeng Krachan Group of the Sibumasu Terrane, were sourced from the Barramundi and Hooper orogens of northwest Australia. Another potential source is the Kimberley and Pine Creek cratons of northern Australia that also contain 1.9–1.8 Ga magmatic rocks (e.g. Cawood and Korsch 2008).

5.4 Correlation of comparable sedimentary sequences

All the samples were compared with compatible published databases of zircon ages from potential source regions that were in proximity to northwest Thailand during the Cambro-Ordovician, Carbo-Permian and Triassic (see Figs. 6 and 7). These possible detrital source regions are widespread across Australasia and vary following the movement of Sibumasu from Gondwana to its amalgamation with SE Asia (Fig. 7). The comparison was statistically modelled across the three time slices (Cambro-Ordovician, Carbo-Permian and Triassic) using MDS (Fig. 6; see Vermeesch 2013). The data are also compared to regions that could be sourcing zircons from similar potential source regions. Comparative regions were selected from various palaeogeographic reconstructions (Burrett et al. 2014; Young et al. 2018).

The potential source regions of the Cambro-Ordovician samples in northwest Thailand are Australia (predominantly northern and western regions), China (including regions of both the North and South China Cratons), the Tethyan Himalayas (northern India, Pakistan and Tibet) and other parts of the Sibumasu Terrane as illustrated in Fig. 6b. From the U–Pb age distribution MDS plot in Fig. 6b, sample RDT15_078 is shown to be least dissimilar to the Chaung Magyi Group of Myanmar (Dew et al. in review). This is unsurprising as both sedimentary packages are Neoproterozoic–Cambrian in age, belong to the Sibumasu Terrane, and are relatively geographically close to each other. It is likely that both regions were sourcing zircons from similar sources.

Both RDT15_078 and RDT16_001 have similarities with the Parahio Formation of northern India and southern Tibet (Myrow et al. 2010 and references therein). RDT16_001 also plots in MDS space close to Cambrian strata from Cathaysia, South China (Xu et al. 2013). The evolved Hf signatures observed in the Neoproterozoic zircons of the Cambro-Ordovician detritus from northwest Thailand are mirrored in the Ordovician sandstones of Cathaysia, South China (Yao et al. 2014). These similarities suggest that, in the Ediacaran–Cambrian, Sibumasu lay close to these regions along the northern Gondwana margin (see Fig. 6). Northern India and South China have been previously recognised as near neighbours in Paleozoic Gondwana (as shown in Fig. 6; Burrett et al. 2014; Cocks and Torsvik, 2013; Yao et al. 2014). Yao et al. (2014) suggested that they collided sometime in the Ediacaran–Ordovician, although more recently, others have argued that South China and India were part of the same Neoproterozoic continent prior to Gondwana (Cawood et al. 2013; Merdith et al. 2017; Wang et al. 2017).

The MDS plot of the Carbo-Permian detrital samples of northwest Thailand (Fig. 6c) shows that the oldest Carboniferous YSG sample, RDT15_066 has a close affinity to the Silurian detrital zircons from Myanmar (Cai et al. 2017) and also from Tarim (Ge et al. 2012; He et al. 2014; Long et al. 2011; Ma et al. 2012), the Perth Basin (Cawood and Nemchin 2000). This affinity may demonstrate similar sediment sources in these regions as Gondwana begins to break up with the development of the Palaeo-Tethys Ocean (Cocks and Torsvik 2013; Hara et al. 2012; Metcalfe 2013; Zhu et al. 2011).

Carbo-Permian samples RDT16_019, RDT16_018 and RDT16_008 cluster together in MDS space, which may be due to the small 45 Ma range in their maximum depositional ages. These three samples are most similar to Carboniferous strata from Myanmar (Cai et al. 2017) and Devonian detrital data from the Alxa Block of northern China (Zhang et al. 2016). The latest Permian sample (RDT16_006) also plots close to the older RDT15_066 sample, suggesting a temporal continuity of source region during the Carboniferous and Permian. The RDT16_006 sample also shows similarities with Silurian strata from Myanmar (Cai et al. 2017) and detrital material from the Inthanon Zone (Hara et al. 2013). These similarities, and the dissimilarity of Sibumasu detritus from South China and Indochina through the later Paleozoic points to the detrital isolation of the Sibumasu Terrane from South China and Indochina terranes during this time. The large range of Hf signatures seen in the Neoproterozoic zircons of all the Carbo-Permian detrital samples from northwest Thailand is also seen in similar-aged zircons from the Permian sediments of the Perth Basin (Cawood and Nemchin 2000; Veevers et al. 2005), indicating that the Sibumasu Terrane still sat outboard on the northwestern margin of Australia at this time.

The Triassic sample from this study, RDT16_012 plots close to East Sumatra in Fig. 6d., which is also interpreted as a part of the Sibumasu Terrane (Zhang et al. 2018c). Other datasets neighbouring RDT16_012 in Fig. 6d include detrital material from the Inthanon Zone (Hara et al. 2013), Triassic–Jurassic sediments from Sibumasu in Myanmar (Cai et al. 2017) and Triassic detrital zircons from Lhasa (Li et al. 2014). This change indicates the separation of the Sibumasu Terrane from Gondwana along with other

terranes in present-day Southeast Asia (Lhasa, West Burma etc.; Fig. 6d).

6. Conclusion

This study used detrital zircon U–Pb and Lu–Hf isotopic systems to elucidate the tectonic history of northwest Thailand. From this analysis, we determined:

- Ordovician to Triassic maximum depositional ages (YSG) of the clastic stratigraphy of Sibumasu in northwest Thailand
- In order of prominence, 1200–900 Ma, 650–500 Ma and 2500–2460 Ma age populations are present in all eight northwest Thai detrital samples
- Hf signatures of the Carbo-Permian samples show an injection of juvenile material in the 1000 and 500 Ma zircons, whereas the Cambro-Ordovician samples show a predominance of evolved zircons of the same age

In this study, the age distributions (Fig. 3 and 6) and Hf signatures of Cambro-Ordovician sediments from northwest Thailand (Fig. 4 and 7) point to affinities with northwestern Australia, the Himalayas, India and South China. Often in palaeogeographic models, Sibumasu is connected to Western Australia before its breakup from Gondwana (Audley-Charles et al. 1988; Burrett et al. 2014; Cocks and Torsvik 2013). The Carbo-Permian Hf signatures indicate a change in provenance away from characteristics of South Chinese detritus towards the variation in Hf signatures found in the Perth Basin. This suggests the separation of South China from Gondwana where the Sibumasu Terrane and Perth Basin were still sharing sediment sources. The Triassic sample from northwest Thailand (RDT16_012) still demonstrates the Australian-Gondwanan sources in addition to an influence of the Permo-Triassic Sukhothai arc system and the amalgamation of Thailand.

Acknowledgements

All field work was conducted with the kind assistance of staff and students of Chiang Mai University. We would like to especially thank Mr Piyanat Viriyasuksing, Dr Niti Mankhemthong and Dr Kannipa Motanated. Many thanks to Sarah Gilbert at Adelaide Microscopy and to Pîi Roj from Chiang Mai University Lapidary for training and permission to use facilities. Thank you to Brad McDonald at the GeoHistory Facility at Curtin University for instrument setup for the Hf analyses. To Dr Morgan Blades for her multidisciplinary advice. To Jarred Lloyd for help using R software and to Sheree Armistead for providing MATLAB script for the hafnium plots. Teagan Romyn for assistance in preliminary editing.

This is a contribution to IGCP projects #589 (Development of the Asian Tethyan Realm) and #628 (The Gondwana Map). This work was supported by Australian Research Council [#DP150101730, #DP120101460 and #FT120100340].
RECD is also funded by a University of Adelaide Research Training Program Stipend and some of the fieldwork conducted was funded on an Endeavour Australia Cheung Kong Fellowship. GeoHistory Facility instruments were funded via an Australian Geophysical Observing System grant provided to AuScope Pty Ltd. by the AQ44 Australian Education Investment Fund program. The NPII multi-collector was obtained via funding from the Australian Research Council LIEF program [#LE150100013].

References

Ali, J.R., Cheung, H.M.C., Aitchison, J.C. & Sun, Y. 2013. Palaeomagnetic re-investigation of Early Permian rift basalts from the Baoshan Block, SW China: constraints on the site-of-origin of the Gondwana-derived eastern Cimmerian terranes. Geophysical Journal International, 193, 650-663, doi: 10.1093/gji/ggt012.

Arboit, F., Amrouch, K., Collins, A.S., King, R. & Morley, C. 2015. Determination of the tectonic evolution from fractures, faults, and calcite twins on the southwestern margin of the Indochina Block. Tectonics, 34, 1576-1599, doi: 10.1002/2015TC003876.

Arboit, F., Collins, A.S., Morley, C.K., King, R. & Amrouch, K. 2016. Detrital zircon analysis of the southwest Indochina terrane, central Thailand: Unravelling the Indosinian orogeny. Geological Society of America Bulletin,, 128, 1024-1043.

Archibald, D.B., Collins, A.S., Foden, J.D., Payne, J.L., Holden, P., Razakamanana, T., De Waele, B., Thomas, R.J. & Pitfield, P.E.J. 2016. Genesis of the Tonian Imorona–Itsindro magmatic Suite in central Madagascar: Insights from U–Pb, oxygen and hafnium isotopes in zircon. Precambrian Research, 281, 312-337, doi: https://doi.org/10.1016/j.precamres.2016.05.014.

Archibald, D.B., Collins, A.S., Foden, J.D. & Razakamanana, T. 2017. Tonian Arc Magmatism in Central Madagascar: The Petrogenesis of the Imorona-Itsindro Suite. The Journal of Geology, 125, 271-297, doi: 10.1086/691185.

Audley-Charles, M.G., Ballantyne, P.D. & Hall, R. 1988. Mesozoic-Cenozoic rift-drift sequence of Asian fragments from Gondwanaland. Tectonophysics, 155, 317-330.

Aye Ko Aung & Cocks, L.R.M. 2017. Chapter 14 Cambrian–Devonian stratigraphy of the Shan Plateau, Myanmar (Burma). Geological Society, London, Memoirs, 48, 317-342, doi: 10.1144/m48.14.

Bagas, I. & Nelson, D.R. 2007. Provenance of Neoproterozoic sedimentary rocks in the northwest Paterson Orogen, Western Australia.

Barber, A.J., Ridd, M.F. & Crow, M.J. 2011. The origin, movement and assembly of the pre-Tertiary tectonic units of Thailand. In: Ridd, M.F., Barber, A.J. & Crow, M.J. (eds.) The Geology of Thailand. The Geological Society, London, 507-537.

Baum, F., von Braun, E., Hahn, L., Hess, A., Koch, K.E., Kruse, G., Quarch, H. & Siebenhüner, M. 1970. On the Geology of Northern Thailand. Beihefte zum Geologischen Jahrbuch, 102, 1-23. 11.

Baum, F., Von Braun, E., Hess, A., Koch, K., 1981. Geological Map of Northern Thailand, 1: 250,000. Sheet 5: Chiang Mai. Federal Institute for Geosciences and Natural Resources of Germany, Hanover, Germany.

Belousova, E.A., Griffin, W.L., O'Reilly, S.Y., Fisher, N.I., 2002. Igneous zircon: trace element composition as an indicator of source rock type. Contrib Mineral Petrol 143, 602–622.

Betts, P.G., Giles, D., Mark, G., Lister, G.S., Goleby, B.R. & Aillères, L. 2006. Synthesis of the proterozoic evolution of the Mt Isa Inlier. Australian Journal of Earth Sciences, 53, 187-211, doi: 10.1080/08120090500434625.

Blades, M.L., Collins, A.S., Foden, J., Payne, J.L., Xu, X., Alemu, T., Woldetinsae, G., Clark, C. & Taylor, R.J.M. 2015. Age and hafnium isotopic evolution of the Didesa and Kemashi Domains, western Ethiopia. Precambrian Research, 270, 267-284, doi: https://doi.org/10.1016/j.precamres.2015.09.018.

Bodet, F. & Schärer, U. 2000. Evolution of the SE-Asian continent from U-Pb and Hf isotopes in single grains of zircon and baddeleyite from large rivers. Geochimica et Cosmochimica Acta, 64, 2067-2091, doi: http://dx.doi.org/10.1016/S0016-7037(00)00352-5.

Bunopas, S. 1981. Paleogeographic history of western Thailand and adjacent parts of Southeast Asia - A plate tectonics interpretation. Paleogeographic History of Western Thailand and Adjacent Parts of Southeast Asia - A Plate Tectonics Interpretation.

Burrett, C., Khin, Z., Meffre, S., Lai, C.K., Khositanont, S., Chaodumrong, P., Udchachon, M., Ekins, S. & Halpin, J. 2014. The configuration of Greater Gondwana—Evidence from LA ICPMS, U–Pb geochronology of detrital zircons from the Palaeozoic and Mesozoic of Southeast Asia and China. Gondwana Research, 26, 31-51, doi: http://dx.doi.org/10.1016/j.gr.2013.05.020.

Cai, F., Ding, L., Yao, W., Laskowski, A.K., Xu, Q., Zhang, J.e. & Sein, K. 2017. Provenance and tectonic evolution of Lower Paleozoic–Upper Mesozoic strata from Sibumasu terrane, Myanmar. Gondwana Research, 41, 325-336, doi: 10.1016/j.gr.2015.03.005.

Cawood, P.A. 2005. Terra Australis Orogen: Rodinia breakup and development of the Pacific and Iapetus margins of Gondwana during the Neoproterozoic and Paleozoic. Earth-Science

Reviews, 69, 249-279, doi: https://doi.org/10.1016/j.earscirev.2004.09.001.

Cawood, P.A. & Korsch, R.J. 2008. Assembling Australia: Proterozoic building of a continent. Precambrian Research, 166, 1-35, doi: https://doi.org/10.1016/j.precamres.2008.08.006.

Cawood, P.A. & Nemchin, A.A. 2000. Provenance record of a rift basin: U/Pb ages of detrital zircons from the Perth Basin, Western Australia. Sedimentary Geology, 134, 209-234, doi: https://doi.org/10.1016/S0037-0738(00)00044-0.

Cawood, P.A., Wang, Y., Xu, Y. & Zhao, G. 2013. Locating South China in Rodinia and Gondwana: A fragment of greater India lithosphere? Geology, 41, 903-906, doi: 10.1130/G34395.1.

Cherry, A.R., McPhie, J., Kamenetsky, V.S., Ehrig, K., Keeling, J.L., Kamenetsky, M.B., Meffre, S. & Apukhtina, O.B. 2017. Linking Olympic Dam and the Cariewerloo Basin: Was a sedimentary basin involved in formation of the world's largest uranium deposit? Precambrian Research, 300, 168-180, doi: https://doi.org/10.1016/j.precamres.2017.08.002.

Chonglakmani, C., 2011. Triassic, In: Ridd, M.F., Barber, A.J., Crow, M.J. (Eds.), The Geology of Thailand. The Geological Society, London, pp. 137-150.

Chu, N.-C., Taylor, R.N., Chavagnac, V., Nesbitt, R.W., Boella, R.M., Milton, J.A., German, C.R., Bayon, G. & Burton, K. 2002. Hf isotope ratio analysis using multi-collector inductively coupled plasma mass spectrometry: an evaluation of isobaric interference corrections. Journal of Analytical Atomic Spectrometry, 17, 15967-11574.

Clark, C., Collins, A.S., Timms, N.E., Kinny, P.D., Chetty, T.R.K. & Santosh, M. 2009. SHRIMP U–Pb age constraints on magmatism and high-grade metamorphism in the Salem Block, southern India. Gondwana Research, 16, 27-36, doi: https://doi.org/10.1016/j.gr.2008.11.001.

Cocks, L.R.M. & Torsvik, T.H. 2013. The dynamic evolution of the Palaeozoic geography of eastern Asia. Earth-Science Reviews, 117, 40-79, doi: http://dx.doi.org/10.1016/j.earscirev.2012.12.001.

Collins, A.S. 2003. Structure and age of the northern Leeuwin Complex, Western Australia: Constraints from field mapping and U–Pb isotopic analysis. Australian Journal of Earth Sciences, 50, 585-599, doi: 10.1046/j.1440-0952.2003.01014.x.

Collins, A.S., Clark, C. & Plavsa, D. 2014. Peninsular India in Gondwana: The tectonothermal evolution of the Southern Granulite Terrain and its Gondwanan counterparts. Gondwana Research, 25, 190-203, doi: https://doi.org/10.1016/j.gr.2013.01.002.

Curtis, S., Wade, C. & Reid, A. 2018. Sedimentary basin formation associated with a silicic large igneous province: stratigraphy and provenance of the Mesoproterozoic Roopena Basin, Gawler Range Volcanics. Australian Journal of Earth Sciences, 65, 447-463, doi: 10.1080/08120099.2018.1460398.

De Pelsmaeker, E., Jolivet, M., Laborde, A., Poujol, M., Robin, C., Zhimulev, F.I., Nachtergaele, S., Glorie, S., De Clercq, S., Batalev, V.Y. & De Grave, J. 2018. Source-to-sink dynamics in the Kyrgyz Tien Shan from the Jurassic to the Paleogene: Insights from sedimentological and detrital zircon U-Pb analyses. Gondwana Research, 54, 180-204, doi: https://doi.org/10.1016/j.gr.2017.09.004.

Department of Mineral Resources (DMR) 1999. Geological Map of Thailand, Scale 1: 1,000,000. Geological Survey Division, Department of Mineral Resources, Bangkok, Thailand.

Department of Mineral Resources (DMR) 2014. Geology of Thailand. Department of Mineral Resources, Ministry of Natural Resources and Environment, Bangkok, Thailand.

Dew, R.E.C., Collins, A.S., Glorie, S., Morley, C.K., Blades, M.L., Nachtergaele, S., King, R., Foden, J., De Grave, J., Kanjanapayont, P., Evans, N.J., Alessio, B.L. & Charusiri, P. 2018a. Probing into Thailand's basement: New insights from U–Pb geochronology, Sr, Sm–Nd, Pb and Lu–Hf isotopic systems from granitoids. Lithos, 320-321, 332-354, doi: 10.1016/j.lithos.2018.09.019.

Dew, R.E.C., Nachtergaele, S., Collins, A.S., Glorie, S., Foden, J., De Grave, J., Blades, M.L., Morley, C.K., Evans, N.J., Alessio, B.L., Kanjanapayont, P., King, R. & Charusiri, P. 2018b. Data analysis of the U–Pb geochronology and Lu–Hf system in zircon and whole-rock Sr, Sm–Nd and Pb isotopic systems for the granitoids of Thailand. Data in Brief, 21, 1794-1809, doi: https://doi.org/10.1016/j.dib.2018.10.176.

Dew, R.E.C., Morley, C.K., Collins, A.S. & Tin Aung Myint. (in review). Age and provenance of the Chaung Magyi Group, Yeywa Dome, Myanmar, based on U–Pb dating of detrital zircons. Journal of Asian Earth Sciences.

Dickinson, W.R. & Gehrels, G.E. 2009. Use of U–Pb ages of detrital zircons to infer maximum depositional ages of strata: A test against a

Colorado Plateau Mesozoic database. Earth and Planetary Science Letters, 288, 115-125, doi: https://doi.org/10.1016/j.epsl.2009.09.013.

Domeier, M. & Torsvik, T.H. 2014. Plate tectonics in the late Paleozoic. Geoscience Frontiers, 5, 303-350, doi: http://dx.doi.org/10.1016/j.gsf.2014.01.002.

Dong, C., Li, C., Wan, Y., Wang, W., Wu, Y., Xie, H. & Liu, D. 2011. Detrital zircon age model of Ordovician Wenquan quartzite south of Lungmuco-Shuanghu Suture in the Qiangtang area, Tibet: Constraint on tectonic affinity and source regions. Science China Earth Sciences, 54, 1034-1042, doi: 10.1007/s11430-010-4166-x.

Dopieralska, J., Belka, Z., Königshof, P., Racki, G., Savage, N., Lutat, P. & Sardsud, A. 2012. Nd isotopic composition of Late Devonian seawater in western Thailand: Geotectonic implications for the origin of the Sibumasu terrane. Gondwana Research, 22, 1102-1109, doi: http://dx.doi.org/10.1016/j.gr.2012.01.009.

Fang, W., Van Der Voo, R. & Liang, Q. 1989. Devonian palaeomagnetism of Yunnan province accross the Shan Thai-South China suture. Tectonics, 8, 939-952.

Fang, X., Chen, T., Burrett, C., Wang, Y., Qu, Y., Zheng, C., Zhang, Y., Zhang, Y. & Li, W. 2018a. Middle Ordovician actinocerid nautiloids (Cephalopoda) from Xainza County, Tibet, western China, and their paleogeographic implications. Journal of Paleontology, 92, 398-411, doi: 10.1017/jpa.2017.152.

Fang, Y., Zhang, Y.-H., Zhang, S.-T., Cao, H.-W., Zou, H. & Dong, J.-H. 2018b. Early Cretaceous I-type granites in the Tengchong terrane: New constraints on the late Mesozoic tectonic evolution of southwestern China. Geoscience Frontiers, 9, 459-470, doi: https://doi.org/10.1016/j.gsf.2017.04.007.

Fergusson, C., Nutman, A.P., Mohajjel, M. & Bennett, V. 2016. The Sanandaj-Sirjan Zone in the Neo-Tethyan suture, western Iran: Zircon U-Pb evidence of late Palaeozoic rifting of northern Gondwana and mid-Jurassic orogenesis. Gondwana Research, 40, 43-57.

Fitzsimons, I.C.W. 2000. Grenville-age basement provinces in East Antarctica: Evidence for three separate collisional orogens. Geology, 28, 879-882, doi: 10.1130/0091-7613(2000)28<879:GBPIEA>2.0.CO;2.

Fitzsimons, I.C.W. 2003. Proterozoic basement provinces of southern and southwestern Australia, and their correlation with Antarctica. Geological Society, London, Special Publications, 206, 93-130, doi: 10.1144/gsl.sp.2003.206.01.07.

Fletcher, I.R. & Libby, W.G. 1993. Further isotopic evidence for the existence of two distinct terranes in the southern Pinjarra Orogen, Western Australia. Geological Survey, Western Australia.

Flowerdew, M.J., Millar, I.L., Curtis, M.L., Vaughan, A.P.M., Horstwood, M.S.A., Whitehouse, M.J. & Fanning, C.M. 2007. Combined U-Pb geochronology and Hf isotope geochemistry of detrital zircons from early Paleozoic sedimentary rocks, Ellsworth-Whitmore Mountains block, Antarctica. Geological Society of America Bulletin, 119, 275-288, doi: 10.1130/b25891.1.

Gardiner, N.J., Hickman, A.H., Kirkland, C.L., Lu, Y., Johnson, T. & Zhao, J.-X. 2017. Processes of crust formation in the early Earth imaged through Hf isotopes from the East Pilbara Terrane. Precambrian Research, 297, 56-76, doi: https://doi.org/10.1016/j.precamres.2017.05.004.

Gardiner, N.J., Roberts, N.M.W., Morley, C.K., Searle, M.P. & Whitehouse, M.J. 2016a. Did Oligocene crustal thickening precede basin development in northern Thailand? A geochronological reassessment of Doi Inthanon and Doi Suthep. Lithos, 240–243, 69-83, doi: http://dx.doi.org/10.1016/j.lithos.2015.10.015.

Gardiner, N.J., Searle, M.P., Morley, C.K., Whitehouse, M.P., Spencer, C.J. & Robb, L.J. 2016b. The closure of Palaeo-Tethys in Eastern Myanmar and Northern Thailand: New insights from zircon U-Pb and Hf isotope data. Gondwana Research, 39, 401-422, doi: 10.1016/j.gr.2015.03.001.

Ge, R., Zhu, W., Zheng, B., Wu, H., He, J. & Zhu, X. 2012. Early Pan-African magmatism in the Tarim Craton: Insights from zircon U–Pb–Lu–Hf isotope and geochemistry of granitoids in the Korla area, NW China. Precambrian Research, 212-213, 117-138, doi: https://doi.org/10.1016/j.precamres.2012.05.001.

Gehrels, G. 2012. Detrital Zircon U-Pb Geochronology: Current Methods and New Opportunities. In: Busby, C. & Azor, A. (eds.) Tectonics of Sedimentary Basins: Recent Advances. Wiley, Online Library, 45-62.

Ghani, A.A., Lo, C.-H. & Chung, S.-L. 2013. Basaltic dykes of the Eastern Belt of Peninsular Malaysia: The effects of the difference in crustal thickness of Sibumasu and Indochina. Journal of Asian Earth Sciences, 77, 127-139, doi:

https://doi.org/10.1016/j.jseaes.2013.08.004.

Ghosh, S., Fallick, A.E., Paul, D.K. & Potts, P.J. 2005. Geochemistry and Origin of Neoproterozoic Granitoids of Meghalaya, Northeast India: Implications for Linkage with Amalgamation of Gondwana Supercontinent. Gondwana Research, 8, 421-432, doi: 10.1016/S1342-937X(05)71144-8.

Glorie, S., De Grave, J., Buslov, M.M., Zhimulev, F.I. & Safonova, I.Y. 2014. Detrital zircon provenance of early Palaeozoic sediments at the southwestern margin of the Siberian Craton: Insights from U–Pb geochronology. Journal of Asian Earth Sciences, 82, 115-123, doi: https://doi.org/10.1016/j.jseaes.2013.12.007.

Griffin, W.L., Belousova, E.A., Shee, S.R., Pearson, N.J. & O'Reilly, S.Y. 2004. Archean crustal evolution in the northern Yilgarn Craton: U–Pb and Hf-isotope evidence from detrital zircons. Precambrian Research, 131, 231–282.

Halpin, J.A., Tran, H.T., Lai, C.-K., Meffre, S., Crawford, A.J. & Zaw, K. 2016. U–Pb zircon geochronology and geochemistry from NE Vietnam: A 'tectonically disputed' territory between the Indochina and South China blocks. Gondwana Research, 34, 254-273, doi: https://doi.org/10.1016/j.gr.2015.04.005.

Hand, M., Reid, A. & Jagodzinski, L. 2007. Tectonic Framework and Evolution of the Gawler Craton, Southern Australia. Economic Geology, 102, 1377-1395, doi: 10.2113/gsecongeo.102.8.1377.

Hansberry, R.L., Zwingmann, H., Loehr, S., Collins, A.S., King, R.C., Morley, C.K. & Drysdale, R.N. 2017. Constraining the timing of shale detachment faulting: A geochemical approach. Lithosphere, 9, 431-440, doi: 10.1130/L612.1.

Hansen, B.T. & Wemmer, K. 2011. Age and evolution of the basement in Thailand. In: Ridd, M.F., Barber, A.J. & Crow, M.J. (eds.) The Geology of Thailand. The Geological Society, London, 19-32.

Hara, H., Kon, Y., Usuki, T., Lan, C.Y., Kamata, Y., Hisada, K.I., Ueno, K., Charoentitirat, T. & Charusiri, P. 2013. U-Pb ages of detrital zircons within the Inthanon Zone of the Paleo-Tethyan subduction zone, northern Thailand: New constraints on accretionary age and arc activity. Journal of Asian Earth Sciences, 74, 50-61, doi: 10.1016/j.jseaes.2013.06.006.

Hara, H., Kunii, M., Hisada, K., Kamata, Y., Ueno, K., Kon, Y., Assavapatchara, S., Treerotchananon, A., Charoentitirat, T. & Charusiri, P. 2015. Provenance and detrital zircon U–Pb ages from Permo-Triassic marine sediments in Northern Thailand: Records of the Sukhothai Arc evolution and the Paleo-Tethys subduction. The 4th Symposium of the International Geosciences Programme (IGCP) 589, Chulalongkorn University, Bangkok, Thailand, 20-23.

Hara, H., Kunii, M., Hisada, K.I., Ueno, K., Kamata, Y., Srichan, W., Charusiri, P., Charoentitirat, T., Watarai, M., Adachi, Y. & Kurihara, T. 2012. Petrography and geochemistry of clastic rocks within the Inthanon zone, northern Thailand: Implications for Paleo-Tethys subduction and convergence. Journal of Asian Earth Sciences, 61, 2-15, doi: 10.1016/j.jseaes.2012.06.012.

Hara, H., Kunii, M., Miyake, Y., Hisada, K.I., Kamata, Y., Ueno, K., Kon, Y., Kurihara, T., Ueda, H., Assavapatchara, S., Treerotchananon, A., Charoentitirat, T. & Charusiri, P. 2017. Sandstone provenance and U–Pb ages of detrital zircons from Permian–Triassic forearc sediments within the Sukhothai Arc, northern Thailand: Record of volcanic-arc evolution in response to Paleo-Tethys subduction. Journal of Asian Earth Sciences, 146, 30-55, doi: 10.1016/j.jseaes.2017.04.021.

Hara, H., Tokiwa, T., Kurihara, T., Charoentitirat, T., Ngamnithiporn, A., Visetnat, K., Tominaga, K., Kamata, Y. & Ueno, K. 2018. Permian–Triassic back-arc basin development in response to Paleo-Tethys subduction, Sa Kaeo–Chanthaburi area in Southeastern Thailand. Gondwana Research, 64, 50-66, doi: https://doi.org/10.1016/j.gr.2018.06.007.

He, J., Zhu, W., Ge, R., Zheng, B. & Wu, H. 2014. Detrital zircon U–Pb ages and Hf isotopes of Neoproterozoic strata in the Aksu area, northwestern Tarim Craton: Implications for supercontinent reconstruction and crustal evolution. Precambrian Research, 254, 194-209, doi: https://doi.org/10.1016/j.precamres.2014.08.016.

Hisada, K.-i., Sugiyama, M., Ueno, K., Charusiri, P. & Arai, S. 2004. Missing ophiolitic rocks along the Mae Yuam Fault as the Gondwana–Tethys divide in north-west Thailand. Island Arc, 13, 119-127, doi: 10.1111/j.1440-1738.2003.00412.x.

Howard, K.E., Hand, M., Barovich, K.M., Reid, A., Wade, B.P. & Belousova, E.A. 2009. Detrital zircon ages: Improving interpretation via Nd and Hf isotopic data. Chemical Geology, 262, 277-292, doi: http://dx.doi.org/10.1016/j.chemgeo.2009.01.029.

Hu, P.-y., Zhai, Q.-g., Jahn, B.-m., Wang, J., Li, C., Lee, H.-y. & Tang, S.-h. 2015. Early Ordovician granites from the South Qiangtang

terrane, northern Tibet: Implications for the early Paleozoic tectonic evolution along the Gondwanan proto-Tethyan margin. Lithos, 220-223, 318-338, doi: https://doi.org/10.1016/j.lithos.2014.12.020.

Huang, K. & Opdyke, N.D. 1991. Paleomagnetic results from the Upper Carboniferous of the Shan-Thai-Malay block of western Yunnan, China. Tectonophysics, 192, 333-344, doi: https://doi.org/10.1016/0040-1951(91)90107-4.

Ingavat, R., Toriyama, R., Pitakpaivan, K., 1980. Fusuline zonation and faunal characteristics of the Ratburi Limestone in Thailand and its equivalents in Malaysia, Geology and Palaeontology of Southeast Asia, pp. 43-62.

Jackson, S.E., Pearson, N.J., Griffin, W.L. & Belousova, E.A. 2004. The application of laser ablation-inductively coupled plasma-mass spectrometry to in situ U–Pb zircon geochronology. Chemical Geology, 211, 47-69, doi: https://doi.org/10.1016/j.chemgeo.2004.06.017.

Javanaphet, C. 1969. Geological Map of Thailand; Scale 1 : 1 000 000, with explanation.

Jiang, H., Li, W.-Q., Jiang, S.-Y., Wang, H. & Wei, X.-P. 2017. Geochronological, geochemical and Sr-Nd-Hf isotopic constraints on the petrogenesis of Late Cretaceous A-type granites from the Sibumasu Block, Southern Myanmar, SE Asia. Lithos, 268–271, 32-47, doi: http://dx.doi.org/10.1016/j.lithos.2016.11.005.

Johnson, S.P., Sheppard, S., Rasmussen, B., Wingate, M.T.D., Kirkland, C.L., Muhling, J.R., Fletcher, I.R. & Belousova, E.A. 2011. Two collisions, two sutures: Punctuated pre-1950Ma assembly of the West Australian Craton during the Ophthalmian and Glenburgh Orogenies. Precambrian Research, 189, 239-262, doi: https://doi.org/10.1016/j.precamres.2011.07.011.

Kamata, Y., Sashida, K., Ueno, K., Hisada, K., Nakornsri, N., Charusiri, P., 2002. Triassic radiolarian faunas from the Mae Sariang area, northern Thailand and their palaeogeographic significance. Journal of Asian Earth Sciences 20, 491-506.

Kamata, Y., Ueno, K., Hara, H., Ichise, M., Charoentitirat, T., Charusiri, P., Sardsud, A., Hisada, K.-i., 2009. Classification of the Sibumasu and Paleo-Tethys tectonic division in Thailand using chert lithofacies. Island Arc 18, 21-31.

Kaur, P., Zeh, A., Chaudhri, N., Gerdes, A. & Okrusch, M. 2011. Archaean to Palaeoproterozoic crustal evolution of the Aravalli mountain range, NW India, and its hinterland: The U–Pb and Hf isotope record of detrital zircon. Precambrian Research, 187, 155-164, doi: https://doi.org/10.1016/j.precamres.2011.03.005.

Kawakami, T., Nakano, N., Higashino, F., Hokada, T., Osanai, Y., Yuhara, M., Charusiri, P., Kamikubo, H., Yonemura, K. & Hirata, T. 2014. U-Pb zircon and CHIME monazite dating of granitoids and high-grade metamorphic rocks from the Eastern and Peninsular Thailand — A new report of Early Paleozoic granite. Lithos, 200–201, 64-79, doi: http://dx.doi.org/10.1016/j.lithos.2014.04.012.

Kelsey, D.E., Wade, B.P., Collins, A.S., Hand, M., Sealing, C.R. & Netting, A. 2008. Discovery of a Neoproterozoic basin in the Prydz belt in East Antarctica and its implications for Gondwana assembly and ultrahigh temperature metamorphism. Precambrian Research, 161, 355-388, doi: https://doi.org/10.1016/j.precamres.2007.09.003.

Kemp, A.I.S., Hickman, A.H., Kirkland, C.L. & Vervoort, J.D. 2015. Hf isotopes in detrital and inherited zircons of the Pilbara Craton provide no evidence for Hadean continents. Precambrian Research, 261, 112-126, doi: https://doi.org/10.1016/j.precamres.2015.02.011.

Kettanah, Y.A., Mory, A.J., Wach, G.D. & Wingate, M.T.D. 2015. Provenance of the Ordovician–lower Silurian Tumblagooda Sandstone, Western Australia. Australian Journal of Earth Sciences, 62, 817-830, doi: 10.1080/08120099.2015.1117020.

Kirkland, C., Spaggiari, C., Wingate, M.T.D., Smithies, R.H., Belousova, E., Murphy, R. & Pawley, M. 2011. Inferences on crust-mantle interaction from Lu-Hf isotopes: a case study from the Albany-Fraser Orogen.

Koch, K. 1973. Geology of the region Sri Sawat-Thong Pha Phum-Sangklaburi, Kanchanaburi province, Thailand. Conf. Geology S.E. Asia Proc, 177-185.

Košler, J. & Sylvester, P.J. 2003. Present Trends and the Future of Zircon in Geochronology: Laser Ablation ICPMS. In: Hanchar, J.M. & Hoskin, P.W.O. (eds.) Zircon. Mineralogical Society of America, Washington, D.C., 243-271.

Kroener, A., Hegner, E., Collins, A.S., Windley, B.F., Brewer, T.S., Razakamanana, T. & Pidgeon, R.T. 2000. Age and magmatic history of the Antananarivo Block, central Madagascar, as derived from zircon geochronology and Nd isotopic systematics. American Journal of Science, 300, 251-288, doi: 10.2475/

ajs.300.4.251.

Ksienzyk, A.K., Jacobs, J., Boger, S.D., Košler, J., Sircombe, K.N. & Whitehouse, M.J. 2012. U–Pb ages of metamorphic monazite and detrital zircon from the Northampton Complex: evidence of two orogenic cycles in Western Australia. Precambrian Research, 198-199, 37-50, doi: https://doi.org/10.1016/j.precamres.2011.12.011.

Li, G., Sandiford, M., Liu, X., Xu, Z., Wei, L. & Li, H. 2014. Provenance of Late Triassic sediments in central Lhasa terrane, Tibet and its implication. Gondwana Research, 25, 1680-1689, doi: https://doi.org/10.1016/j.gr.2013.06.019.

Li, P., Rui, G., Junwen, C. & Ye, G. 2004. Paleomagnetic analysis of eastern Tibet: implications for the collisional and amalgamation history of the Three Rivers Region, SW China. Journal of Asian Earth Sciences, 24, 291-310, doi: http://dx.doi.org/10.1016/j.jseaes.2003.12.003.

Li, S.H., Advokaat, E.L., van Hinsbergen, D.J.J., Koymans, M., Deng, C.L. & Zhu, R.X. 2017. Paleomagnetic constraints on the Mesozoic-Cenozoic paleolatitudinal and rotational history of Indochina and South China: Review and updated kinematic reconstruction. Earth-Science Reviews, 171, 58-77, doi: 10.1016/j.earscirev.2017.05.007.

Li, S.H., van Hinsbergen, D.J.J., Deng, C.L., Advokaat, E.L. & Zhu, R.X. 2018. Paleomagnetic Constraints From the Baoshan Area on the Deformation of the Qiangtang-Sibumasu Terrane Around the Eastern Himalayan Syntaxis. Journal of Geophysical Research-Solid Earth, 123, 977-997, doi: 10.1002/2017jb015112.

Li, X.-H., Li, Z.-X., He, B., Li, W.-X., Li, Q.-L., Gao, Y. & Wang, X.-C. 2012. The Early Permian active continental margin and crustal growth of the Cathaysia Block: In situ U–Pb, Lu–Hf and O isotope analyses of detrital zircons. Chemical Geology, 328, 195-207, doi: https://doi.org/10.1016/j.chemgeo.2011.10.027.

Lin, Y.-L., Yeh, M.-W., Lee, T.-Y., Chung, S.-L., Iizuka, Y. & Charusiri, P. 2013. First evidence of the Cambrian basement in Upper Peninsula of Thailand and its implication for crustal and tectonic evolution of the Sibumasu terrane. Gondwana Research, 24, 1031-1037, doi: http://dx.doi.org/10.1016/j.gr.2013.05.014.

Long, J. & Burrett, C. 1989. Fish from the Upper Devonian of the Shan-Thai terrane indicate proximity to East Gondwana and south China terranes. Geology, 17, 811-813, doi: 10.1130/0091-7613(1989)017<0811:FFTUDO>2.3.CO;2.

Long, X., Yuan, C., Sun, M., Kröner, A., Zhao, G., Wilde, S. & Hu, A. 2011. Reworking of the Tarim Craton by underplating of mantle plume-derived magmas: Evidence from Neoproterozoic granitoids in the Kuluketage area, NW China. Precambrian Research, 187, 1-14, doi: https://doi.org/10.1016/j.precamres.2011.02.001.

Loydell, D.K. & Aung, K.P. 2017. The "Panghkawkwo graptolite bed" (Llandovery, Silurian), Myanmar and the location of the Sibumasu (or Sibuma) Terrane in the Silurian. Palaeogeography, Palaeoclimatology, Palaeoecology, 469, 1-17, doi: https://doi.org/10.1016/j.palaeo.2016.12.028.

Ma, X., Shu, L., Santosh, M. & Li, J. 2012. Detrital zircon U–Pb geochronology and Hf isotope data from Central Tianshan suggesting a link with the Tarim Block: Implications on Proterozoic supercontinent history. Precambrian Research, 206-207, 1-16, doi: https://doi.org/10.1016/j.precamres.2012.02.015.

McQuarrie, N., Robinson, D., Long, S., Tobgay, T., Grujic, D., Gehrels, G. & Ducea, M. 2008. Preliminary stratigraphic and structural architecture of Bhutan: Implications for the along strike architecture of the Himalayan system. Earth and Planetary Science Letters, 272, 105-117, doi: https://doi.org/10.1016/j.epsl.2008.04.030.

Merdith, A.S., Collins, A.S., Williams, S.E., Pisarevsky, S., Foden, J.D., Archibald, D.B., Blades, M.L., Alessio, B.L., Armistead, S., Plavsa, D., Clark, C. & Müller, R.D. 2017. A full-plate global reconstruction of the Neoproterozoic. Gondwana Research, 50, 84-134, doi: https://doi.org/10.1016/j.gr.2017.04.001.

Metcalfe, I. 1998. Palaeozoic and Mesozoic geological evolution of the SE Asian region: multidisciplinary constraints and implications for biogeography. In: Hall, R. & Holloway, J.D. (eds.) Biogeography and Geological Evolution of SE Asia. Backhuys Publishers, Amsterdam, The Netherlands, 25-41.

Metcalfe, I. 2013. Gondwana dispersion and Asian accretion: Tectonic and palaeogeographic evolution of eastern Tethys. Journal of Asian Earth Sciences, 66, 1-33, doi: http://dx.doi.org/10.1016/j.jseaes.2012.12.020.

Metcalfe, I. & Isozaki, Y. 2009. Current perspectives on the Permian-Triassic boundary and end-Permian mass extinction: Preface. Journal of Asian Earth Sciences, 36, 407-412.

Moghadam, H.S., Li, X.-H., Griffin, W.L., Stern, R.J., Thomsen, T.B., Meinhold, G., Aharipour, R. & O'Reilly, S.Y. 2017. Early Paleozoic tectonic reconstruction of Iran: Tales from detrital zircon geochronology. Lithos, 268-271, 87-101, doi: https://doi.org/10.1016/j.lithos.2016.09.008.

Morel, M.L.A., Nebel, O., Nebel-Jacobsen, Y.J., Miller, J.S. & Vroon, P.Z. 2008. Hafnium isotope characterisation of the GJ-1 zircon reference material by solution and laser-ablation MC-ICPMS. Chemical Geology, 231-235.

Morley, C.K. 2018. Understanding Sibumasu in the context of ribbon continents. Gondwana Research, 64, 184-215, doi: https://doi.org/10.1016/j.gr.2018.07.006.

Morley, C.K., Ampaiwan, P., Thanudamrong, S., Kuenphan, N. & Warren, J. 2013. Development of the Khao Khwang fold and thrust belt; implications for the geodynamic setting of Thailand and Cambodia during the Indosinian Orogeny. Journal of Asian Earth Sciences, 62, 705-719, doi: http://dx.doi.org/10.1016/j.jseaes.2012.11.021.

Myrow, P.M., Hughes, N.C., Goodge, J.W., Fanning, C.M., Williams, I.S., Peng, S., Bhargava, O.N., Parcha, S.K. & Pogue, K.R. 2010. Extraordinary transport and mixing of sediment across Himalayan central Gondwana during the Cambrian–Ordovician. GSA Bulletin, 122, 1660-1670, doi: 10.1130/B30123.1.

Neumann, N.L., Southgate, P.N., Gibson, G.M. & McIntyre, A. 2006. New SHRIMP geochronology for the Western Fold Belt of the Mt Isa Inlier: developing a 1800 – 1650 Ma event framework. Australian Journal of Earth Sciences, 53, 1023-1039, doi: 10.1080/08120090600923287.

Nordsvan, A.R., Collins, W.J., Li, Z.-X., Spencer, C.J., Pourteau, A., Withnall, I.W., Betts, P.G. & Volante, S. 2018. Laurentian crust in northeast Australia: Implications for the assembly of the supercontinent Nuna. Geology, 46, 251-254, doi: 10.1130/G39980.1.

Patchett, P.J. & Tatsumoto, M. 1980. Hafnium isotope variations in oceanic basalts. Geophysical Research Letters, 7, 1077-1080.

Paton, C., Hellstrom, J., Paul, B., Woodhead, J. & Hergt, J. 2011. Iolite: Freeware for the visualisation and processing of mass spectrometric data. Journal of Analytical Atomic Spectrometry, 26, 2508-2518, doi: 10.1039/c1ja10172b.

Payne, J.L., Barovich, K.M. & Hand, M. 2006. Provenance of metasedimentary rocks in the northern Gawler Craton, Australia: Implications for Palaeoproterozoic reconstructions. Precambrian Research, 148, 275-291, doi: https://doi.org/10.1016/j.precamres.2006.05.002.

Plavsa, D., Collins, A.S., Payne, J.L., Foden, J.D., Clark, C. & Santosh, M. 2014. Detrital zircons in basement metasedimentary protoliths unveil the origins of southern India. Geological Society of America Bulletin, 126, 791-811, doi: 10.1130/b30977.1.

Reid, A.J. & Payne, J.L. 2017. Magmatic zircon Lu–Hf isotopic record of juvenile addition and crustal reworking in the Gawler Craton, Australia. Lithos, 292-293, 294-306, doi: https://doi.org/10.1016/j.lithos.2017.08.010.

Ridd, M.F. 2011. Lower Palaeozoic. In: Ridd, M.F., Barber, A.J. & Crow, M.J. (eds.) The Geology of Thailand. The Geological Society, London, 33-51.

Ridd, M.F. 2015. Should Sibumasu be renamed Sibuma? The case for a discrete Gondwana-derived block embracing western Myanmar, upper Peninsular Thailand and NE Sumatra. Journal of the Geological Society, doi: 10.1144/jgs2015-065.

Roberts, N.M.W. & Spencer, C.J. 2015. The zircon archive of continent formation through time. Geological Society, London, Special Publications, 389, 197-225, doi: 10.1144/sp389.14.

Saesaengseerung, D., Sashida, K., Sardsud, A., 2008. Discovery of Middle Triassic radiolarian fauna from the Nan area along the Nan-Uttaradit suture zone, northern Thailand. Paleontological Research 12, 397-409.

Saki, A. 2010. Proto-Tethyan remnants in northwest Iran: Geochemistry of the gneisses and metapelitic rocks. Gondwana Research, 17, 704-714, doi: https://doi.org/10.1016/j.gr.2009.08.008.

Schmitt, R.d.S., Fragoso, R.d.A. & Collins, A.S. 2018. Suturing Gondwana in the Cambrian: The Orogenic Events of the Final Amalgamation. In: Siegesmund, S., Basei, M.A.S., Oyhantçabal, P. & Oriolo, S. (eds.) Geology of Southwest Gondwana. Springer International Publishing, Cham, 411-432.

Schwartz, M.O., Rajah, S.S., Askury, A.K., Putthapiban, P. & Djaswadi, S. 1995. The Southeast Asian tin belt. Earth-Science Reviews, 38, 95-293, doi: https://doi.org/10.1016/0012-8252(95)00004-T.

Searle, M.P., Whitehouse, M.J., Robb, L.J., Ghani, A.A., Hutchison, C.S., Sone, M., Ng, S.W.P., Roselee, M.H., Chung, S.L. & Oliver, G.J.H.

2012. Tectonic evolution of the Sibumasu-Indochina terrane collision zone in Thailand and Malaysia: Constraints from new U-Pb zircon chronology of SE Asian tin granitoids. Journal of the Geological Society, 169, 489-500, doi: 10.1144/0016-76492011-107.

Sevastjanova, I., Clements, B., Hall, R., Belousova, E.A., Griffin, W.L. & Pearson, N. 2011. Granitic magmatism, basement ages, and provenance indicators in the Malay Peninsula: Insights from detrital zircon U–Pb and Hf-isotope data. Gondwana Research, 19, 1024-1039, doi: 10.1016/j.gr.2010.10.010.

Sevastjanova, I., Hall, R., Rittner, M., Paw, S.M.T.L., Naing, T.T., Alderton, D.H. & Comfort, G. 2016. Myanmar and Asia united, Australia left behind long ago. Gondwana Research, 32, 24-40, doi: https://doi.org/10.1016/j.gr.2015.02.001.

Shen, L., Yu, J.-H., O'Reilly, S.Y., Griffin, W.L. & Zhou, X. 2018. Subduction-related middle Permian to early Triassic magmatism in central Hainan Island, South China. Lithos, 318-319, 158-175, doi: https://doi.org/10.1016/j.lithos.2018.08.009.

Silverman, B.W. 1986. Density Estimation for Statistics and Data Analysis. Monographs on Statistics and Applied Probability. Chapman and Hall, London.

Sircombe, K.N. & Freeman, M.J. 1999. Provenance of detrital zircons on the Western Australia coastline—Implications for the geologic history of the Perth basin and denudation of the Yilgarn craton. Geology, 27, 879-882, doi: 10.1130/0091-7613(1999)027<0879:PODZOT>2.3.CO;2.

Sláma, J., Košler, J., Condon, D.J., Crowley, J.L., Gerdes, A., Hanchar, J.M., Horstwood, M.S.A., Morris, G.A., Nasdala, L., Norberg, N., Schaltegger, U., Schoene, B., Tubrett, M.N. & Whitehouse, M.J. 2008. Plešovice zircon — A new natural reference material for U–Pb and Hf isotopic microanalysis. Chemical Geology, 249, 1-35, doi: https://doi.org/10.1016/j.chemgeo.2007.11.005.

Spencer, C.J., Cawood, P.A., Hawkesworth, C.J., Prave, A.R., Roberts, N.M.W., Horstwood, M.S.A. & Whitehouse, M.J. 2015. Generation and preservation of continental crust in the Grenville Orogeny. Geoscience Frontiers, 6, 357-372, doi: http://dx.doi.org/10.1016/j.gsf.2014.12.001.

Spencer, C.J., Dyck, B., Mottram, C.M., Roberts, N.M.W., Yao, W.-H. & Martin, E.L. 2018. Deconvolving the pre-Himalayan Indian margin – Tales of crustal growth and destruction. Geoscience Frontiers, doi: https://doi.org/10.1016/j.gsf.2018.02.007.

Srinak, N., Hisada, K., Kamata, Y., Charusiri, P., 2007. Stratigraphy of the Mae Sariang Group of Northwestern Thailand: Implication for Paleoenvironments and Tectonic Setting. The Natural History Journal of Chulalongkorn University 7, 87-108.

Stokes, R.B. 1988. A review of the geology of Myanmar.

Szpunar, M., Hand, M., Barovich, K., Jagodzinski, E. & Belousova, E. 2011. Isotopic and geochemical constraints on the Paleoproterozoic Hutchison Group, southern Australia: Implications for Paleoproterozoic continental reconstructions. Precambrian Research, 187, 99-126, doi: https://doi.org/10.1016/j.precamres.2011.02.006.

Thein, M.L. 1973. The Lower Palaeozoic stratigraphy of western part of the Southern Shan States, Burma. Geological Society of Malaysia Bulletin, 6.

Thirlwall, M.F. & Anczkiewicz, R. 2004. Multidynamic isotope ratio analysis using MC–ICP–MS and the causes of secular drift in Hf, Nd and Pb isotope ratios. International Journal of Mass Spectrometry, 235, 59-81, doi: https://doi.org/10.1016/j.ijms.2004.04.002.

Tofke, T., Lumijuan, A. & Helmcke, D. 1993. Triassic syn-orogenic siliciclastics from the area of Mae Sariang (northwestern Thailand). In: T., T. (ed.) International Biostratigraphy of Mainland Southeast Asia: Facies and Paleontology Symposium, Chiang Mai University, Chiang Mai, 391-400.

Ueno, K. & Charoentitirat, T. 2011. Carboniferous and Permian. In: Ridd, M.F., Barber, A.J. & Crow, M.J. (eds.) The Geology of Thailand. The Geological Society, London, 71-136.

Usuki, T., Lan, C.-Y., Wang, K.-L. & Chiu, H.-Y. 2013. Linking the Indochina block and Gondwana during the Early Paleozoic: Evidence from U–Pb ages and Hf isotopes of detrital zircons. Tectonophysics, 586, 145-159, doi: http://dx.doi.org/10.1016/j.tecto.2012.11.010.

Veevers, J.J., Belousova, E.A., Saeed, A., Sircombe, K., Cooper, A.F. & Read, S.E. 2006. Pan-Gondwanaland detrital zircons from Australia analysed for Hf-isotopes and trace elements reflect an ice-covered Antarctic provenance of 700–500 Ma age, TDM of 2.0–1.0 Ga, and alkaline affinity. Earth-Science Reviews, 76, 135-174, doi: https://doi.org/10.1016/j.earscirev.2005.11.001.

Veevers, J.J., Saeed, A., Belousova, E.A. & Griffin, W.L. 2005. U–Pb ages and source

composition by Hf-isotope and trace-element analysis of detrital zircons in Permian sandstone and modern sand from southwestern Australia and a review of the paleogeographical and denudational history of the Yilgarn Craton. Earth-Science Reviews, 68, 245-279, doi: https://doi.org/10.1016/j.earscirev.2004.05.005.

Vermeesch, P. 2012. On the visualisation of detrital age distributions. Chemical Geology, 312-313, 190-194, doi: https://doi.org/10.1016/j.chemgeo.2012.04.021.

Vermeesch, P. 2013. Multi-sample comparison of detrital age distributions. Chemical Geology, 341, 140-146, doi: 10.1016/j.chemgeo.2013.01.010.

Vermeesch, P., Resentini, A. & Garzanti, E. 2016. An R package for statistical provenance analysis. Sedimentary Geology, 336, 14-25, doi: http://dx.doi.org/10.1016/j.sedgeo.2016.01.009.

von Braun, E., Hahn, L., Maronde, H., 1981. Geological Map of Northern Thailand 1: 250,000, Sheet 6, Li, Bundesanstalt fiir Geowissenschanen und Rohstoffe. Federal Institute for Geosciences and Natural Resources of Germany, Hanover, Germany.

Wakita, K. & Metcalfe, I. 2005. Ocean Plate Stratigraphy in East and Southeast Asia. Journal of Asian Earth Sciences, 24, 679-702, doi: http://dx.doi.org/10.1016/j.jseaes.2004.04.004.

Wang, M., Li, C. & Ming-Xie, C. 2015. Dating of detrital zircons from the Dabure clastic rocks: the discovery of Neoproterozoic strata in southern Qiangtang, Tibet. International Geology Review, 1-12, doi: 10.1080/00206814.2015.1065207.

Wang, W., Cawood, P.A., Zhou, M.-F., Pandit, M.K., Xia, X.-P. & Zhao, J.-H. 2017. Low-δ18O Rhyolites From the Malani Igneous Suite: A Positive Test for South China and NW India Linkage in Rodinia. Geophysical Research Letters, 44, 10,298-210,305, doi: 10.1002/2017GL074717.

White, W.M. 2013. Geochemistry. Wiley-Blackwell.

Wiedenbeck, M., AllÉ, P., Corfu, F., Griffin, W.L., Meier, M., Oberli, F., Quadt, A.V., Roddick, J.C. & Spiegel, W. 1995. Three natural zircon standards for U–Th–Pb, Lu–Hf, trace element and REE analyses. Geostandards Newsletter, 19, 1-23, doi: 10.1111/j.1751-908X.1995.tb00147.x.

Woodhead, J.D. & Hergt, J.M. 2005. A Preliminary Appraisal of Seven Natural Zircon Reference Materials for In Situ Hf Isotope Determination. Geostandards and Geoanalytical Research, 29, 183-195, doi: 10.1111/j.1751-908X.2005.tb00891.x.

Xu, X., O'Reilly, S.Y., Griffin, W.L., Wang, X., Pearson, N.J. & He, Z. 2007. The crust of Cathaysia: Age, assembly and reworking of two terranes. Precambrian Research, 158, 51-78, doi: https://doi.org/10.1016/j.precamres.2007.04.010.

Xu, Y., Cawood, P.A., Du, Y., Hu, L., Yu, W., Zhu, Y. & Li, W. 2013. Linking south China to northern Australia and India on the margin of Gondwana: Constraints from detrital zircon U-Pb and Hf isotopes in Cambrian strata. Tectonics, 32, 1547-1558, doi: doi:10.1002/tect.20099.

Xu, Y., Cawood, P.A., Du, Y., Zhong, Z. & Hughes, N.C. 2014. Terminal suturing of Gondwana along the southern margin of South China Craton: Evidence from detrital zircon U-Pb ages and Hf isotopes in Cambrian and Ordovician strata, Hainan Island. Tectonics, 33, 2490-2504, doi: doi:10.1002/2014TC003748.

Yang, B., Smith, T.M., Collins, A.S., Munson, T.J., Schoemaker, B., Nicholls, D., Cox, G., Farkas, J. & Glorie, S. 2018. Spatial and temporal variation in detrital zircon age provenance of the hydrocarbon-bearing upper Roper Group, Beetaloo Sub-basin, Northern Territory, Australia. Precambrian Research, 304, 140-155, doi: https://doi.org/10.1016/j.precamres.2017.10.025.

Yao, J., Shu, L., Cawood, P.A. & Li, J. 2016. Delineating and characterizing the boundary of the Cathaysia Block and the Jiangnan orogenic belt in South China. Precambrian Research, 275, 265-277, doi: https://doi.org/10.1016/j.precamres.2016.01.023.

Yao, J., Shu, L. & Santosh, M. 2011. Detrital zircon U–Pb geochronology, Hf-isotopes and geochemistry—New clues for the Precambrian crustal evolution of Cathaysia Block, South China. Gondwana Research, 20, 553-567, doi: https://doi.org/10.1016/j.gr.2011.01.005.

Yao, W.-H., Li, Z.-X., Li, W.-X., Li, X.-H. & Yang, J.-H. 2014. From Rodinia to Gondwanaland: A tale of detrital zircon provenance analyses from the southern Nanhua Basin, South China. American Journal of Science, 314, 278-313, doi: 10.2475/01.2014.08.

Young, A., Flament, N., Maloney, K., Williams, S., Matthews, K., Zahirovic, S. & Müller, R.D. 2018. Global kinematics of tectonic plates and subduction zones since the late Paleozoic

Era. Geoscience Frontiers, doi: https://doi.org/10.1016/j.gsf.2018.05.011.

Yu, J.-H., O'Reilly, S.Y., Wang, L., Griffin, W.L., Zhang, M., Wang, R., Jiang, S. & Shu, L. 2008. Where was South China in the Rodinia supercontinent?: Evidence from U–Pb geochronology and Hf isotopes of detrital zircons. Precambrian Research, 164, 1-15, doi: https://doi.org/10.1016/j.precamres.2008.03.002.

Yu, J.-H., O'Reilly, S.Y., Wang, L., Griffin, W.L., Zhou, M.-F., Zhang, M. & Shu, L. 2010. Components and episodic growth of Precambrian crust in the Cathaysia Block, South China: Evidence from U–Pb ages and Hf isotopes of zircons in Neoproterozoic sediments. Precambrian Research, 181, 97-114, doi: https://doi.org/10.1016/j.precamres.2010.05.016.

Zhang, J., Peng, T., Fan, W., Zhao, G., Dong, X., Gao, J., Peng, B., Wei, C., Xia, X., Chen, L. & Liang, X. 2018a. Petrogenesis of the Early Cretaceous granitoids and its mafic enclaves in the Northern Tengchong Terrane, southern margin of the Tibetan Plateau and its tectonic implications. Lithos, 318-319, 283-298, doi: https://doi.org/10.1016/j.lithos.2018.08.017.

Zhang, J., Zhang, B. & Zhao, H. 2016. Timing of amalgamation of the Alxa Block and the North China Block: Constraints based on detrital zircon U–Pb ages and sedimentologic and structural evidence. Tectonophysics, 668-669, 65-81, doi: https://doi.org/10.1016/j.tecto.2015.12.006.

Zhang, L.K., Li, G.M., Santosh, M., Cao, H.W., Dong, S.L., Zhang, Z., Fu, J.G., Xia, X.B., Huang, Y., Liang, W., Zhang, S.T. & Li, S. 2018b. Cambrian magmatism in the Tethys Himalaya and implications for the evolution of the Proto-Tethys along the northern Gondwana margin: A case study and overview. Geological Journal, 0, doi: 10.1002/gj.3311.

Zhang, X., Chung, S.-L., Lai, Y.-M., Ghani, A.A., Murtadha, S., Lee, H.-Y. & Hsu, C.-C. 2018c. Detrital Zircons Dismember Sibumasu in East Gondwana. Journal of Geophysical Research: Solid Earth, 123, doi: 10.1029/2018jb015780.

Zhou, X., Yu, J.-H., O'Reilly, S.Y., Griffin, W.L., Sun, T., Wang, X., Tran, M. & Nguyen, D. 2018. Component variation in the late Neoproterozoic to Cambrian sedimentary rocks of SW China – NE Vietnam, and its tectonic significance. Precambrian Research, 308, 92-110, doi: 10.1016/j.precamres.2018.02.003.

Zhu, D.-C., Zhao, Z.-D., Niu, Y., Dilek, Y. & Mo, X.-X. 2011. Lhasa terrane in southern Tibet came from Australia. Geology, 39, 727-730.

CHAPTER 4

This chapter is written for *Geological Magazine* as:

Dew, R.E.C., Collins, A.S., King, R., Morley, C.K., Evans, N.J. & Glorie, S. The Permo-Triassic tectonic geography of Thailand deduced from terrane-based sediment provenance.

Statement of Authorship

Title of Paper	The Permo-Triassic tectonic geography of Thailand deduced from terrane-based sediment provenance.
Publication Status	☐ Published ☐ Accepted for Publication ☐ Submitted for Publication ☑ Unpublished and Unsubmitted w ork w ritten in manuscript style
Publication Details	Dew, R.E.C., Collins, A.S., Morley, C.K., King, R., Glorie, S. and Evans, N.J. (in prep). The Permo-Triassic tectonic geography of Thailand deduced from terrane-based sediment provenance.

Principal Author

Name of Principal Author (Candidate)	Romana E.C. Dew		
Contribution to the Paper	Performed majority of sample analysis, interpreted data, wrote manuscript and acted as corresponding author.		
Overall percentage (%)	80		
Certification:	This paper reports on original research I conducted during the period of my Higher Degree by Research candidature and is not subject to any obligations or contractual agreements with a third party that would constrain its inclusion in this thesis. I am the primary author of this paper.		
Signature		Date	31/12/2018

Co-Author Contributions

By signing the Statement of Authorship, each author certifies that:

i. the candidate's stated contribution to the publication is accurate (as detailed above);

ii. permission is granted for the candidate in include the publication in the thesis; and

iii. the sum of all co-author contributions is equal to 100% less the candidate's stated contribution.

Name of Co-Author	Alan S. Collins		
Contribution to the Paper	Primary supervisorial role, conception and design of the project, helped in data interpretation and manuscript construction and editing		
Signature		Date	31/12/2018

Name of Co-Author	Christopher K. Morley		
Contribution to the Paper	Assistance with data interpretation and manuscript editing		
Signature	Dr. Christopher Morley	Date	31/12/2018

Name of Co-Author	Rosalind King		
Contribution to the Paper	Co-supervisorial role, conception and design of the project, assisted data interpretation, manuscript layout and draft editing		
Signature		Date	28/11/2018

Name of Co-Author	Stijn Glorie		
Contribution to the Paper	Co-supervisorial role, conception and design of the project and manuscript evaluation		
Signature		Date	30/11/2018

Name of Co-Author	Noreen Evans		
Contribution to the Paper	Hafnium data reduction and manuscript editing		
Signature		Date	28-11-18

ABSTRACT

The northward movement of terranes from Gondwana throughout the Phanerozoic and the progressive development and destruction of the Tethys Oceans formed the landmasses of Southeast Asia that we recognise today. As the detail of these Asian accretions is still widely debated, this work investigates the origin, relative position and separation/collision of the terranes. In particular, the timing and nature of the Indochina and Sibumasu collision and the nature and timing of the Palaeo-Tethys Ocean closure are addressed.

New provenance information (U–Pb geochronology and Lu–Hf isotopic signatures) has been collected using the detrital zircon record in Permo-Triassic sandstones from all three major terranes in Thailand. The comparison of the three terranes' detrital zircon population spectra provides evidence for the shared and separate parts of their tectonic histories. Zircon age peaks at 487–390 Ma, 1000–900 Ma, 1900–1725 Ma and 2572–2425 Ma are present in the Permo-Triassic sediments in all three tectonic terranes in Thailand. Primarily, the ages found in the Sibumasu Terrane are typical of provenance within Gondwana and contain both juvenile and evolved Hf signatures. In contrast, in the Sukhothai Terrane, the predominant age peak is 296–207 Ma and contains $\varepsilon Hf_{(t)}$ values that correspond to the isotopic signatures of the synchronous Sukhothai granitoids. Detrital data from the Huai Hin Lat Formation in Indochina Terrane contain zircon age populations and isotopic characteristics similar to the South China Terrane. These results have implications for research on the Tethys Oceans, not only within Thailand but also for research conducted on greater Southeast Asian tectonics. Additionally, this study unearths information about Indochina, Sibumasu and northern Australia during the Proterozoic to early Paleozoic.

1. Introduction

Southeast Asia is composed of continental fragments that rifted away from the Gondwanan supercontinent during the Paleozoic and Mesozoic (Audley-Charles et al. 1988; Burrett et al. 2014; Cocks and Torsvik 2013). The complex tectonic history of the region has led to controversy over when and where fragments separated from Gondwana and when and where they docked in Southeast Asia (Domeier and Torsvik 2014; Li et al. 2004; Loydell and Aung 2017; Seton et al. 2012; Yan et al. 2018; Zhang et al. 2018).

Mainland Southeast Asia, mostly equivalent to Sundaland or Greater Gondwana, is a significant area for understanding the Indosinian Orogeny (Fontaine 2002; Gardiner et al. 2016; Sone and Metcalfe 2008). This event includes all late Paleozoic to early Mesozoic orogenic phases throughout eastern Asia: from Korea (Cho et al. 2008), China (Hu et al. 2015; Li et al. 2004) and Vietnam (Halpin et al. 2015; Lepvrier et al. 2004), to Thailand (Arboit et al. 2014; Hansberry et al. 2015; Hansberry et al. 2017; Metcalfe 2013; Morley et al. 2013; Warren et al. 2014). The exact timing of the individual collisional events that make up the Indosinian Orogeny remains largely uncertain. Thailand is made up of three terranes: Sibumasu, which has an early Proterozoic isotopic basement, Indochina, which is the most juvenile and lastly the isotopically intermediate Sukhothai (Dew et al. 2018a; Dew et al. 2018b; Dew et al. 2018c). These three terranes that make up the basement of

Thailand are essential to understanding the Indosinian Orogeny. The earliest events of the Indosinian Orogeny are latest Permian to early Triassic in age, and include the collision of South China with Indochina (e.g. Faure et al., 2014). However, the collision of Indochina and Sukhothai terranes with Sibumasu is controversial, and may possibly have been diachronous, with the current proposed timing of collision ranging from the latest Permian to Upper Triassic (e.g. Barber et al. 2017; Barber et al. 2011; Faure et al. 2014; Hara et al. 2013; Metcalfe 2000; Morley et al. 2013; Ridd 2013; Rossignol et al. 2016; Sone and Metcalfe 2008).

To better constrain the evolution of this region, we conducted the first regional-scale, coupled U–Pb geochronology and Lu–Hf detrital study on Permo-Triassic samples across Thailand. Geological evidence, geochemical signatures, and the detrital age populations are combined in order to reconstruct the history of Permo-Triassic Thailand and provide further refine our understanding of the Indosinian Orogeny. In an attempt to resolve existing arguments about the tectonic evolution of Thailand, we have compared our new data to those published from Indochina, Sukhothai, Sibumasu, Lhasa, West Burma, South China and Western Australia (e.g. Arboit et al. 2016; Burrett et al. 2014; Cai et al. 2017; Hara et al. 2013; Hu et al. 2015; Sevastjanova et al. 2016).

2. Geology of Permo-Triassic Thailand

The Sibumasu Terrane and its boundaries have been inconsistently defined (Audley-Charles et al. 1988; Hisada et al. 2004; Metcalfe 1984), but is herein considered as per Gardiner et al. (2016) and illustrated in Fig. 1, to be the basement of Peninsula Thailand, which extends north into eastern–central Myanmar, east to the Chiang Rai Line and south through the western Malay Peninsula. The name Sibumasu is a combination of its constituents: *Si*am-Thailand and *Si*no-China-*Bu*rma-*Ma*laysia-*Su*matra. The Sibumasu Terrane is a ribbon continent that is equivalent to the South Qiangtang Terrane in Tibet, and the Baoshan and Tengchong terranes in southwest China (Ali et al. 2013; Jiang et al. 2017). It contains Sn-bearing, continental collision S-type granites emplaced between 220–200 Ma (Dew et al. 2018a; Gardiner et al. 2016; Schwartz et al. 1995; Searle et al. 2012). Paleozoic sedimentary rocks, including lower Permian glaciomarine diamictites, from the Sibumasu Terrane show Gondwanan biogeographic affinities (Ampaiwan et al. 2009; Metcalfe 2013). The Triassic sediments of the Sibumasu Terrane are composed of marine sandstones, shales, cherts and limestones (Chonglakmani 2011; Kamata et al. 2009; Morley 2018; Ridd 2015).

The Inthanon Zone is commonly acknowledged as the main Palaeo-Tethyan suture marking the convergence between the Sukhothai, Indochina and Sibumasu terranes (Hara et al. 2013; Sone and Metcalfe 2008). It contains deep-water sequences that have been caught up in an accretionary prism that was subsequently thrust westwards onto the eastern margin of the Sibumasu Terrane (Barber et al. 2011; Barr and Macdonald 1991; Hara et al. 2012). The Inthanon Zone also contains deformed continental sequences from the Sibumasu Terrane including metamorphic rocks of unknown age, Cambrian sandstone, Ordovician limestone and various Silurian–Carboniferous sedimentary rocks (Hara et al. 2012; Ueno and Charoentitirat 2011).

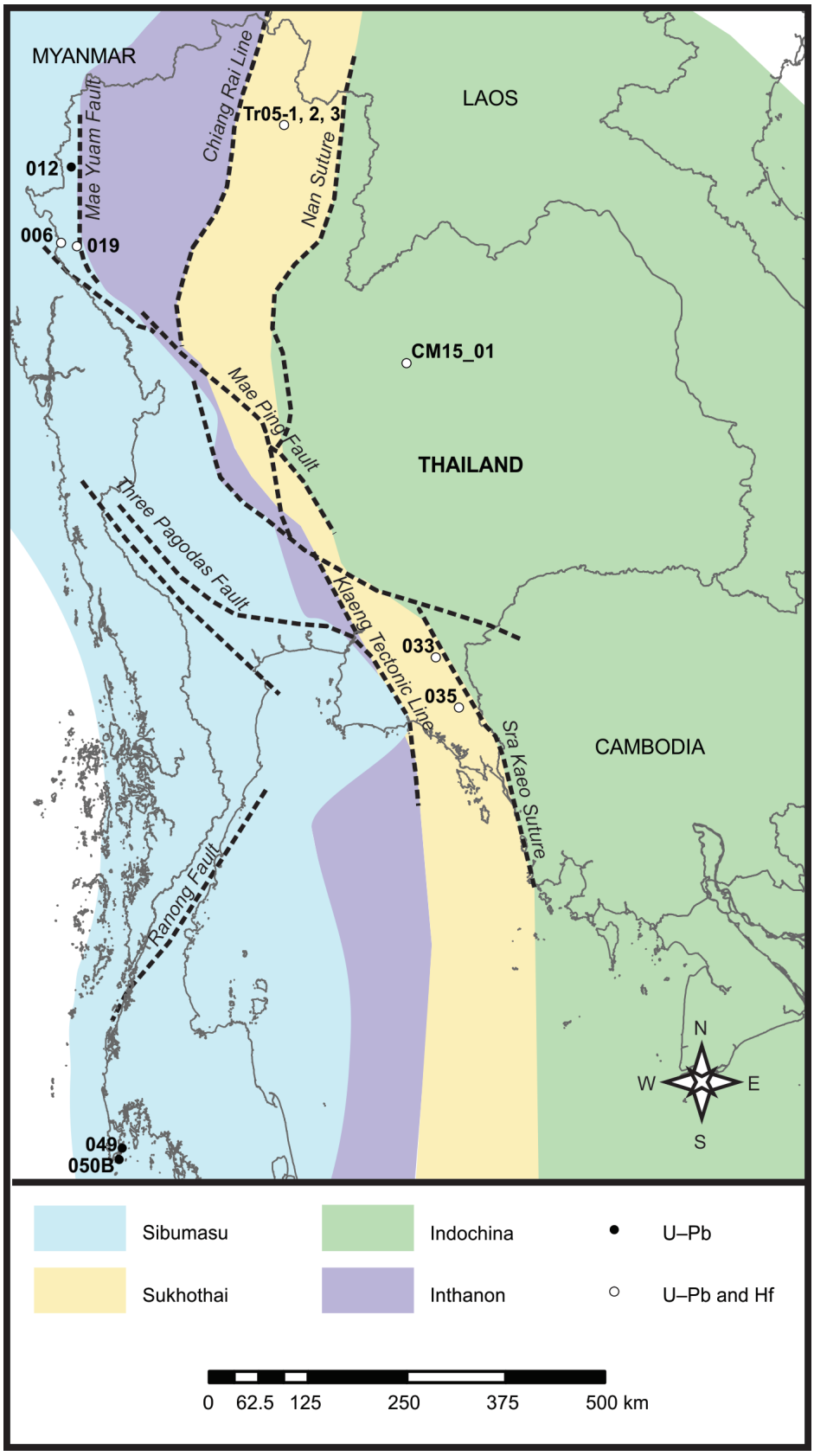

Fig. 1. Geological map of Thailand showing sample localities and major tectonic subdivisions. Tectonic boundaries adjusted from Metcalfe (2013) and Dew et al. (2018a).

The Sukhothai Terrane is thought to be equivalent to the Chanthaburi Terrane in southeast Thailand and the Lincang Terrane of southern China (Fig. 1; Sone and Metcalfe, 2008). This region contains the remnants of an arc system and its associated short-lived basin (e.g. Sone and Metcalfe, 2008; Metcalfe, 2013). The Sukhothai Terrane is dominated by a Permo-Triassic deformed fore-arc basin sequence and overlying late Permian–Triassic shallow marine molasse-type sedimentary rocks (Chaodumrong 1992; Hara et al. 2017). Permo-Triassic granitoids are also emplaced within the Sukhothai Terrane and are predominantly metaluminous granitoids with I-type affinities (Dew et al. 2018a; Sone and Metcalfe 2008; Sone et al. 2012). Indosinian-aged deformation occurred in the "Sukhothai Fold Belt" yielding a K–Ar age between 220–188 Ma (Ahrendt et al. 1993). The Carbo-Permian back-arc basin, that separated the Sukhothai and Indochina terranes, is preserved as a narrow discontinuous ophiolite belt (Fig. 1; Barr and Macdonald 1987; Qian et al. 2016; Sone and Metcalfe 2008; Ueno and Hisada 2001). This suture zone, known as the Nan–Uttaradit Suture in northern Thailand and the Sa Kaeo Suture in the southeast of Thailand, is a mélange complex of gabbro (zircon U–Pb age of 311 ± 10 Ma), tholeiitic meta-basalt (zircon U–Pb age of 316 ± 3 Ma), andesite and radiolarian chert lithologies (Barr and Macdonald 1987; Sone et al. 2012).

The Indochina Terrane incorporates large areas of Laos, Vietnam, Cambodia, Malaysia and Thailand (Fig. 1). There is evidence that it is likely to be a composite terrane containing multiple micro-terranes, potential sutures, metamorphic complexes and mylonitic fault zones (Arboit et al. 2016b; Lepvrier et al. 2004; Sone and Metcalfe 2008). Within Thailand, the Indochina Terrane encompasses all of Thailand east of the Sukhothai Terrane. The granitoids from the Indochina Terrane are mostly metaluminous I-type granitoids that are related to Cu–Fe–Au–Sb mineralisation (Charusiri et al. 1993; Dew et al. 2018a; Salam et al. 2014; Zaw et al. 2014). Mesozoic and Cenozoic sediments cover the Indochina Terrane throughout most of Thailand (Chonglakmani 2011; Minezaki et al. 2018), however basement rocks, up to granulite-facies, are exposed in Vietnam, Laos and Cambodia (Nakano et al. 2018; Shi et al. 2015; Wang et al. 2016a). Inherited zircons and model ages suggest that Indochina Terrane formed between the Paleoproterozoic and the Cambrian (Dew et al. 2018a; Lan et al. 2003; Shi et al. 2015; Wang et al. 2016a). There is evidence that the high grade metamorphism of basement rocks such as the Kontum Massif and the Truong Son Belt were caused by the multi-phased Indosinian Orogeny, often specifically attributed to the oblique collision of the Indochina and South China terranes (see Faure et al. 2018; Halpin et al. 2016; Lan et al. 2003; Lepvrier et al. 2004; Nagy et al. 2001; Nakano et al. 2018).

2.1 Tectonic evolution

It is well established that the Indochina and Sibumasu terranes were once part of the Gondwana supercontinent (Audley-Charles et al. 1988; Burrett et al. 2014; Cocks and Torsvik 2013). However, there are various models on their placement within this supercontinent and the timing of separation (Li et al. 2004; Loydell and Aung 2017; Yan et al. 2018; Zhang et al. 2018). The Sukhothai Terrane is rarely included in models of Gondwana since there has been much historical debate on its origins, however, it is now

acknowledged to be an arc system built on older continental material (Dew et al. 2018a; Hara et al. 2017; Qian et al. 2016; Sevastjanova et al. 2011). It has been suggested that the Sukhothai arc was constructed on the margin of the Indochina Terrane during the late Carboniferous to earliest Permian (Sone and Metcalfe 2008).

Previously published plate-tectonic models (e.g. Li et al. 2004) suggest that by the Carboniferous, South China and Indochina had separated from Gondwana and were located in equatorial to low northern palaeolatitudes. Whereas, a recent palaeomagnetic study by Yan et al. (2018) suggests that Indochina transitioned an estimated 5000 kilometres northwards from Gondwana in the early to middle Permian (ca. 280 Ma), to the southern margin of Eurasia by the late Triassic (ca. 220 Ma). However, it is known that by the late Carboniferous, two elongate tropical carbonate platforms: the Khao Khwang and Pha Nok Khao platforms, developed along the margin of the Indochina Terrane (Dew et al. 2018b; Ueno and Charoentitirat 2011). During the late Carboniferous to early Permian, the Sibumasu Terrane was still on the Indian–Australian margin of Gondwana and Gondwana-derived icebergs dumped glacial-marine sediments in rift grabens at this time (Burrett et al. 2014; Metcalfe 2013). The northward subduction of the main Palaeo-Tethys Ocean commenced in the latest Carboniferous to early Permian (Metcalfe 2013).

Previous studies have proposed separating the Indosinian Orogeny into two stages (e.g. Lepvrier et al. 2004; Morley et al. 2013). The latest Permian to early Triassic (Lopingian–Carnian) first stage Indosinian I is thought to be driven by the collision of the northern margin of Indochina with South China (Arboit et al. 2014; Lepvrier et al. 2004; Metcalfe 2013; Morley et al. 2013). Contemporaneously, or following the South China-Indochina collision, the Sukhothai back arc closed and was subsequently thrust over Indochina (Lepvrier et al. 2004; Morley et al. 2013). On the southern margin of the Khorat continental fragment of the Indochina Terrane, the Khao Khwang Platform was deformed, resulting in the Khao Khwang Fold-Thrust Belt (Arboit et al. 2015; Dew et al. 2018b; Morley et al. 2013; Sone and Metcalfe 2008). The termination of this Indosinian I event is identified as an unconformity in the Khorat Plateau whereby the deformed Permian and older units are overlain by late Triassic rift-related sediments (Kuchinarai Group) (Morley et al. 2013). The late Triassic to early Jurassic Indosinian II is said to mark the closure of the Palaeo-Tethys Ocean (Inthanon Zone) with the collision of the Sibumasu and Sukhothai/Indochina terranes (Searle et al. 2012; Morley et al. 2013).

2.2 Stratigraphy of Permo-Triassic Thailand

Carbonate sequences are characteristic of the Permian stratigraphy in Thailand with the Ratburi Group in Sibumasu, Doi Chiang Dao Limestone in Sukhothai and the Saraburi Group in Indochina (Chonglakmani 2001; Dew et al. 2018b; Toriyama 1967). However, Permo-Triassic clastic sequences are still present across all three terranes. A comparison of the tectono-stratigraphy in the three main tectonic terranes in Thailand was constructed by Sone et al. (2012; Fig. 10). The stratigraphy of the Sukhothai Terrane has since been amended in light of new detrital zircon U–Pb ages presented in Hara et al. (2017; Fig. 15). In addition,

detrital zircon evidence from Arboit et al. (2016b) demonstrates that some formations of the Saraburi Group in the Indochina Terrane, previously considered to be of Middle–Late Permian age, are no older than Late Triassic (Saraburi Group stratigraphy illustrated in Fig. 2 of Arboit et al. (2016b)).

2.3 Permo-Triassic stratigraphy and samples from the Sibumasu Terrane

The outcrop geology of Sibumasu is almost entirely composed of Phanerozoic sedimentary, metasedimentary, igneous and metamorphic rocks (Gardiner et al. 2016; Ridd 2011; Schwartz et al. 1995; Searle et al. 2012; Ueno and Charoentitirat 2011). West of Mae Sariang in northern Thailand, the Permian sedimentary sequences have been described as sandstones, greywackes, limestones, shales and cherts (Baum et al. 1970; Bunopas 1981). Detrital zircons from pre-Triassic sedimentary and meta-sedimentary rocks indicate a Proterozoic and Archean basement source (Arboit et al. 2016b; Burrett et al. 2014; Cai et al. 2017).

The Triassic Mae Sariang Group (Bunopas 1981), composed of sandstone, conglomerate, shale and limestone with subordinate bedded chert, is widely distributed in the Mae Hong Son–Mae Sariang region (Baum et al. 1970; Hisada et al. 2004). Triassic clastic rocks contain oriented pebbles of metamorphic rocks and flute casts, which suggest a transport direction parallel to the strike of mountain belt (Tofke et al. 1993). Based upon stratigraphic and palaeontological evidence (Kamata et al. 2009; Srinak et al. 2007), the age of the Mae Sariang Group is considered to be Middle to Upper Triassic. The Upper Triassic continental sequences indicate uplift, folding and orogenesis (Baum et al. 1970; Hara et al. 2012), and therefore, Hara et al. (2012) proposed that these sediments were deposited during or after the collision of the Sibumasu, Sukhothai and Indochina terranes (the Indosinian Orogeny).

Sample RDT16_019 (Fig. 1 and Table 1) is a poorly to moderately well sorted subarkose sampled from a locality on the margin of Carbo-Permian and Triassic sedimentary units by von Braun et al. (1981). Sample RDT16_006 (Fig. 1 and Table 1) is a well sorted laminated sandstone which has been previously mapped by von Braun et al. (1981) as Triassic sediment. Sample RDT16_012 (Fig. 1 and Table 1) is a well sorted quartz arenite from the Triassic Mae Sariang Group.

Carbo-Permian pebbly mudstone sequences are observed in Sumatra, Malaysia, Peninsula Thailand and Myanmar (Ampaiwan et al. 2004; Ridd 2015; Ueno and Charoentitirat 2011). In Peninsula Thailand, this pebbly mudstone–diamictite unit is known as the Kaeng Krachan Group and is divided into two formations: Ko Sire and Ko He (Chaodumrong et al. 2007, Ridd 2009, Ampaiwan et al. 2009; Raksaskulwong and Wongwanich 1993). Both these formations contain three principal lithofacies: diamictite, sandstone, and fine-grained facies. The low-lying Ko Sire Formation is up to 400 m thick and is characterised by laminated mudstones and dropstones, and dump structures associated with *Cruziana* ichnofacies indicating a glacially influenced offshore environment (Ampaiwan et al. 2009). The Ko Sire Formation is overlain by a 125–400m thick diamictite sequence of the Ko He Formation. It consists of mainly pebbly rocks or diamictite with subordinate, intercalated mudstone and

Table 1. Description of sample localities, associated formations and terranes and interpreted depositional ages.

Sample Name	*Terrane*	*Formation or Group*	*Sample Location*		*Previously Published Age*	*Youngest single concordant grain - YSG*	*Interpreted Maximum Depositional Age*
			Latitude	*Longitude*			
RDT16_006	Sibumasu	undefined	17°59'13"N	97°44'41"E	middle Permian Upper Carboniferous to Lower Permian Kohn and Unger (1981)	255 ± 2.6 Ma	255 ± 2.6 Ma
RDT16_012	Sibumasu	Mae Sariang Group	18°48'34"N	97°51'38"E	middle Triassic (Baum et al. 1970; Hara et al. 2012), Middle to Upper Triassic (Srinak et al. 2007)	206.6 ± 2.3 Ma	206.6 ± 2.3 Ma
RDT16_019	Sibumasu	undefined	17°56'48"N	97°55'29"E	Carboniferous to Triassic	277.9 ± 4.9 Ma	277.9 ± 4.9 Ma
RDT16_049	Sibumasu	Ko He Formation (Kaeng Krachan Group)	7°52'19"N	98°25'56"E	early Permian (Palaeontological evidence: Chaodamrong et al. 2007; Shi et al 2001; Fujikawa et al 2005; Ueno et al. 2002).	415.1 ± 13 Ma	early Permian
RDT16_050B	Sibumasu	Kaeng Krachan Group	7°50'32"N	98°23'18"E	early Permian (Palaeontological evidence: Chaodamrong et al. 2007; Shi et al 2001; Fujikawa et al 2005; Ueno et al. 2002).	508.6 ± 14 Ma	early Permian
RDT16_033	Chanthaburi	Pong Nam Ron Formation	13°25'01"N	102° 0'33"E	Pre-Jurassic, intruded by latest Triassic-early Jurassic Khao Soi Dao pluton	235.8 ± 2.8 Ma	235.8 ± 2.8 Ma
RDT16_035	Chanthaburi	Pong Nam Ron Formation	12°51'22"N	102°16'09"E	Pre-Jurassic, intruded by latest Triassic-early Jurassic Khao Soi Dao pluton	222.5 ± 3.8 Ma	222.5 ± 3.8 Ma
TR_05-1	Sukhothai	Song Group	19°15'55"N	100°16'49"E	Upper Triassic (Hara et al. 2017)	231.9 ± 4.9 Ma	231.9 ± 4.9 Ma
TR_05-2	Sukhothai	Song Group	19°15'58"N	100°16'46"E	Upper Triassic (Hara et al. 2017)	211.8 ± 3.7 Ma	211.8 ± 3.7 Ma
TR_05-3	Sukhothai	Song Group	19°15'58"N	100°17'08"E	Upper Triassic (Hara et al. 2017)	207.8 ± 2.6 Ma	207.8 ± 2.6 Ma
CM15_01	Indochina	Huai Hin Lat Formation	16°40'12"N	101°41'34"E	Upper Triassic (early–middle Norian) based on diverse and abundant flora and fauna (Chonglakmani 2011 and references therein)	226.2 ± 4.6 Ma	226.2 ± 4.6 Ma

Table 1: Description of sample localities, associated formations and terranes and interpreted depositional ages.

sandstone (Chaodumrong et al. 2007). Palaeontological evidence (brachiopods, corals, bryozoans, fusulinids and foraminifera) from the Kaeng Krachan Group constrains the age of deposition as early Permian (Chaodumrong et al. 2007; Shi et al 2001; Fujikawa et al 2005; Ueno et al. 2002).

The pebbly mudstone "diamictite" section of the Kaeng Krachan Group and its glacial sedimentary structures are commonly used as evidence for Sibumasu's position on the northwest margin of Gondwanan Australia during the Permian Period. It is thought that these sediments are diamictites formed when Gondwana-derived icebergs dumped glacial-marine sediments in rift grabens (Ampaiwan et al. 2009; Burrett et al. 2014; Metcalfe 2013).

Samples RDT16_049 and RDT16_050 (Fig. 1 and Table 1) were both taken from the early Permian Kaeng Krachan Group. Sample RDT16_049 is a very to poorly sorted diamictite of the Ko He Formation sampled from the Stop 1 locality of Ampaiwan et al. (2004). Sample RDT16_050 is a poorly sorted conglomerate (suspected diamictite), taken from a construction site near the intersection of the Kao Khad Views Tower road and Highway 4023.

2.4 Permo-Triassic stratigraphy and samples from the Sukhothai Terrane

The Sukhothai Terrane is dominated by deformed shallow marine sedimentary and igneous sequences including the widely distributed Permo-Triassic marine sediments (Hara et al. 2017; Kamata et al. 2016; Sone and Metcalfe 2008). The Permian sediments are classified into the correlative Ngao and Uttaradit Groups (Hara et al. 2017; Ueno and Charoentitirat 2011). The Triassic sediments in the Sukhothai Terrane are divided into the Lower–Upper Triassic Lampang Group and the Upper Triassic temporal equivalent Song and Nam Pat Groups (Bunopas et al. 2001; Chaodumrong 1992; Chonglakmani 2011; Hara et al. 2017). A zircon U–Pb (no Lu–Hf) detrital provenance study has already been conducted on the Ngao, Lampang and Song Groups in the Lampang–Ngao–Phrae area of northern Thailand (Hara et al. 2017). The active Sukhothai arc system has been shown previously to have strongly influenced the deposition of the Permo-Triassic clastic sequences in the Sukhothai Terrane (Chaodumrong and Burrett 1997; Hara et al. 2017).

The samples from the Sukhothai Terrane (TR_05-1, TR_05-2 and TR_05-3) were obtained from the Song Group, further north of the region studied by Hara et al. (2017), in the Phayao region of northern Thailand. The Song Group includes three formations in ascending order: the Pha Daeng, Kang Pla and Wang Chin (Chonglakmani 2011). The Pha Daeng Formation consists of red micaceous sandstones, siltstones, shales and conglomerates with a minor basal limestone-conglomerate (Chaodumrong and Burrett 1997; Chonglakmani 2011). Fossil evidence from directly overlying beds indicate the Pha Daeng Formation was deposited in the Lower-Middle Carnian (Chonglakmani 2011) and the Hara et al. (2017) detrital U–Pb zircon study determined a depositional age of 237–232 Ma for the Pha Daeng Formation. The Kang Pla Formation consists of limestone of variable thickness, with palaeontological evidence constraining the depositional age as middle Carnian to early Norian (Chonglakmani 2011). The Wang Chin Formation contains turbiditic mudstones with interbedded sandstones

and limestones, with fossil evidence indicating it was deposited in the middle Carnian to early Norian (Chonglakmani 2011; Hara et al. 2017). Hara et al. (2017) determined a depositional age of 232–201 Ma from detrital U–Pb zircons.

2.5 Permo-Triassic stratigraphy and samples from the Chanthaburi Terrane

The Chanthaburi Terrane is the southern equivalent of the Sukhothai Terrane and contains comparable Permo-Triassic mixed lithology of siliciclastics and carbonates, with common inclusion of volcanic clasts and tuff (Sone et al. 2012). The late Permian–Middle Triassic succession appears equivalent to the correlated section of the upper Ngao Group to the lower Lampang Group in the Sukhothai terrane (Sone et al. 2012). Both terranes' Permian–Triassic marine stratigraphy reveal lithologically changing sedimentary environments that are typical of arc settings (Sone et al. 2012).

In this southeastern region of Thailand, Triassic clastic sequences have been long identified (e.g. Hughes and Bateson 1967). Both RDT16_033 and RDT16_035 were sampled from the Pong Nam Ron Formation, a feldspathic to lithic greywacke sandstone interbedded with mudstones and conglomerates (Chonglakmani 2011; Sone et al. 2012). Although the formation is widely distributed, until recently it was poorly understood given limited exposure and lack of age constraints (Sone et al. 2012). However, Hara et al. (2018a) conducted a zircon U–Pb detrital provenance analysis of the Pong Nam Ron Formation (three samples yielding a total of 171 detrital zircons) and "the Thung Kabin Mélange". The U–Pb ages of detrital zircons from both units present similar age distributions: the youngest single-grain zircon (YSG) is early Late Triassic in age, the youngest cluster of zircons (YC1σ) is latest Permian to earliest Triassic in age, and there is a range of other Paleozoic and Proterozoic zircons (Hara et al. 2018a). The Pong Nam Ron Formation has been described as a deeper-water turbidite deposit (Sone et al. 2012). Varying theories exist on the tectonic setting associated with the formation of the Pong Nam Ron Formation (Hara et al. 2018b; Sone et al. 2012; Ueno and Charoentitirat 2011).

2.6 Permo-Triassic stratigraphy and samples from the Indochina Terrane

The Permian sequences throughout the Indochina Terrane are shallow marine carbonate dominated with lesser marine clastic sedimentary rocks and deep water conodont-bearing limestones (Arboit et al. 2016b; Burrett et al. 2014b; Dew et al. 2018b; Ueno and Charoentitirat 2011). In contrast, the Triassic sequences of the Indochina Terrane are wholly continental clastic sediments, and in some regions, are fragmented by unconformities from the Indosinian Orogeny (Booth and Sattayarak 2011; Morley et al. 2013).

The Huai Hin Lat Formation, from which sample CM15_01 was taken (Fig. 1 and Table 1), is part of the Kuchinarai Group (Chaodumrong 2013). This formation consists of conglomerate, limestone conglomerate, grey to dark grey sandstone, siltstone, volcaniclastics, black shale and marl containing plant fossils, *Neocalamites* sp., *Clathropteris* sp. that constrain the depositional age to the Upper Triassic (Booth and Sattayarak 2011; Chaodumrong 2013). The Huai Hin Lat Formation is divided into five members: Pho Hai, Sam Khaen Conglomerate, Dat Fa, Phu Hi and I Mo (Chonglakmani and Sattayarak, 1978). A recent combined palaeomagnetic and

zircon U–Pb study of the Huai Hin Lat Formation by Yan et al. (2017) estimated the maximum depositional age to be 227 Ma. This formation was deposited during fault-controlled extension, followed by widespread fluvio-lacustrine conditions (Booth and Sattayarak 2011; Minezaki et al. 2018; Racey et al. 1996). The continental rift basin sediments of the Huai Hin Lat Formation were deposited between Indosinian I and Indosinian II (Booth and Sattayarak 2011; Morley et al. 2013). Much of the Huai Hin Lat Formation was buried by later sedimentary sequences in the Khorat Plateau so most of the information comes from wells or localities where this formation crops out (e.g. locality of CM15_01 sample).

3. Methodology

3.1 Sample preparation

Samples were selected so that Permian and Triassic sediments from each of the three major tectonic terranes in Thailand were included, and to yield full spatial coverage from northern and southern Thailand (see Fig. 1). Samples were crushed, sieved and zircons were concentrated using conventional magnetic and heavy liquid separation procedures. About 200 grains of randomly selected zircon were cast in epoxy resin and polished for U–Pb zircon age determinations. In order to characterise the textural and chemical-zoning features within each zircon, cathodoluminescence (CL) images for zircon were obtained using the FEI Quanta 600 (Mineral Liberation Analysis) Scanning Electron Microscope with energy-dispersive x-ray (EDX) and Gatan CL detectors at Adelaide Microscopy.

3.2 Zircon U–Pb isotopic system

The majority of U–Pb analyses were conducted on an Agilent 7900x with a New Wave NW213 laser ablation system with a TwoVol2 sample chamber at Adelaide Microscopy, Adelaide, South Australia (see Supplementary Tables 1 and 2). Each analysis was bracketed by zircon standard blocks (every 10-16 unknowns) containing GEMOC GJ-1 ($^{207}Pb/^{206}Pb$ TIMS age of 607.7 ± 4.3 Ma, $^{206}Pb/^{238}U$ TIMS age of 600.7 ± 1.1 Ma and $^{207}Pb/^{235}U$ age of 602.0 ± 1.0 Ma; Jackson et al., 2004) as the primary standard for age calculation, drift correction and down-hole fractionation correction, Plešovice ($^{206}Pb/^{238}U$ age of 337.13 ± 0.37 Ma (2σ); Sláma et al. 2008) and 91500 ($^{206}Pb/^{238}U$ age of 1062 Ma; Wiedenbeck et al. 1995). The exact fluence settings varied depending on the energy output of the laser and ranged from 5.6 to 6.58 J/cm^2. The standard measurements for the analytical runs in this study are stated in Supplementary Table 2. Further information on the analytical methodology is given in Dew et al. (2018c), and for detailed analytical methodology of this laboratory's technique see Payne et al. (2006).

Some U–Pb zircon analyses, detailed in Supplementary Table 2, were obtained using laser ablation split stream methods at the GeoHistory Facility, John de Laeter Centre, Curtin University, Perth, Western Australia. A Resonetics S-155-LR 193nm excimer laser ablation system coupled to an Agilent 7700s quadrupole ICP-MS was used for age determination with approximately half the ablation stream directed to a Nu Plasma II multi-collector for Hf isotope determination (see below for analytical detail). Analyses were carried out using a laser beam diameter of 50 μm. After two cleaning pulses and 40s of baseline acquisition, zircon grains were ablated for 35s using a 10 Hz repetition rate, and an on-sample beam energy of 2-3 J/cm^2. The sample cell was flushed

with ultrahigh purity He (320 mL min^{-1}) and N2 (1.2 mL min^{-1}) and high purity Ar was employed as the plasma carrier gas, split to each mass spectrometer.

The U–Pb analyses were conducted over a number of analytical sessions and therefore the standard measurements for each separate analytical run are included in supplementary Table 2. Across all analytical sessions, analyses of GJ-1 yielded a $^{206}Pb/^{238}U$ weighted average age of 601.63 ± 0.40 Ma (n=607, MSWD=0.85). All age data were reduced using the UPbGeochron4 data reduction scheme in Iolite (Paton et al. 2011).

The relative uncertainties for $^{206}Pb/^{238}U$, $^{207}Pb/^{235}U$, and $^{207}Pb/^{206}Pb$ vary as a function of age: for "young" samples, $^{206}Pb/^{238}U$ age is the most precise and $^{207}Pb/^{206}Pb$ age is the least precise, whereas for "old" samples the values are reversed (Gehrels 2012). Because of these variations, the age resolution of the U–Pb system is poorest at 1.4 Ga (Gehrels 2012). To determine the most appropriate and precise age for this work, the kernel density estimate of all the ±10% discordant data was used to determine the minima of the data (1350–1383 Ma). $^{206}Pb/^{238}U$ ages were chosen for grains ≤1351 Ma while $^{207}Pb/^{206}Pb$ ages was used for older zircon grains (interpreted ages are highlighted in Supplementary Table 1).

3.2 Zircon Lu–Hf isotopic system

Zircon grains less than ±10% discordant (using the ($^{206}Pb/^{238}U$ age)/ $^{207}Pb/^{235}U$ age) calculation, individual analyses are outlined in Supplementary Table 1) were analysed for their Hf isotopic composition. The number of Hf analyses was determined by the number and variability in the zircon U–Pb age distribution in each sample. The Hf and Lu isotopic analyses were conducted in split stream with the U–Pb analytic runs stated above, using a Resonetics S-155-LR 193nm excimer laser ablation system connected to a Nu Plasma II multi-collector ICP–MS in the GeoHistory Facility at the John de Laeter Centre at Curtin University in Perth, Western Australia.

All isotopes (^{180}Hf, ^{179}Hf, ^{178}Hf, ^{177}Hf, ^{176}Hf, ^{175}Lu, ^{174}Hf, ^{173}Yb, ^{172}Yb and ^{171}Yb) were counted on the Faraday collector array. Time resolved data was baseline subtracted and reduced using Iolite (DRS after Woodhead et al., 2004), where ^{176}Yb and ^{176}Lu were removed from the 176 mass signal using $^{176}Yb/^{173}Yb$ = 0.7962 (Chu et al., 2002) and $^{176}Lu/^{175}Lu$ = 0.02655 (Chu et al., 2002) with an exponential law mass bias correction assuming $^{172}Yb/^{173}Yb$ = 1.35274 (Chu et al., 2002). The interference corrected $^{176}Hf/^{177}Hf$ was normalised to $^{179}Hf/^{177}Hf$ = 0.7325 (Patchett and Tatsumoto, 1980) for mass bias correction.

Mud Tank was used as the primary standard for Hf isotopes (Woodhead and Hergt 2005), and R33 the primary standard for Lu–Hf analyses (Fisher et al. 2014). Mudtank analyses yielded $^{176}Hf/^{177}Hf$ weighted-means of 0.2825070 ± 0.0000088 (2σ, n=24, for RDT16_006, TR_05-1, TR_05-2, TR_05-3, RDT16_033 and RDT16_035) and 0.2825071 ± 0.0000081 (2σ, n=13 for RDT16_019 and CM15_01 analysis run). The R33 standard yielded $^{176}Hf/^{177}Hf$ weighted-means of 0.282697 ± 0.000011 (2σ, n=24, for RDT16_006, TR_05-1, TR_05-2, TR_05-3, RDT16_033 and RDT16_035) and 0.282708 ± 0.000017 (2σ, n=14 for RDT16_019 and CM15_01 analysis run). In each batch of samples several secondary reference material zircons (including GJ-1, FC-1, 91500 and

OG-1; Woodhead and Hergt 2005; Morel et al. 2008) were interspersed to monitor data quality. The corrected $^{178}Hf/^{177}Hf$ ratio was calculated to monitor the accuracy of the mass bias correction and yielded average values of 1.467069 ± 0.0000071 (n=685; for RDT16_006, TR_05-1, TR_05-2, TR_05-3, RDT16_033 and RDT16_035) and 1.467117 ± 0.000011 (n=296; for RDT16_019 and CM15_01), which are both within the range of values reported by Thirlwall and Anczkiewicz (2004). The weighted averages for the secondary reference materials are quoted in Supplementary Table 3.

4. Results

4.1 Zircon U–Pb geochronology

Eleven samples were used for U–Pb zircon geochronology analyses. CL images for the analysed zircons are given in Fig. 2 and data are summarised in Table 2. The U–Pb ages are displayed as kernel density estimations in Fig. 3 and further details are listed in Supplementary Table 1. Primarily, the ages are interpreted from data within ±10% discordance using the ($^{206}Pb/^{238}U$ age)/ $^{207}Pb/^{235}U$) calculation. Some analyses clearly show the effects of radiogenic lead loss with anomalously young apparent $^{206}Pb/^{238}U$ ages. Outlier data were rejected after examination of the laser log and CL images (e.g., if the laser beam traversed cracks or overlapped multiple zircon domains within the grain; see Supplementary Table 1).

In this study, the maximum depositional age of each sample was determined by calculating the youngest single grain (YSG) zircon ages within ±10% (within ±5% where possible) ($^{206}Pb/^{238}U$ age)/ $^{207}Pb/^{235}U$ age) discordance calculation in conjunction with available palaeontological and stratigraphic evidence. This follows the quantitative interpretation approach for detrital zircon U–Pb age data of Dickinson and Gehrels (2009). The interpreted maximum depositional ages for each sample, incorporating YSG, palaeontological and stratigraphic evidence are detailed in Table 1.

4.1.1 Sibumasu Terrane

Prominent age populations of 2572–2472 Ma, 1200–900 Ma and 585–525 Ma are present in each of the Permo-Triassic detrital samples analysed from the Sibumasu Terrane (Fig. 3). The 1744–1725 Ma age peak is observed in RDT16_012, RDT16_049 and RDT16_050, and is less pronounced in RDT16_019 and RDT16_006 (Fig. 3).

For RDT16_019, there is an abundance of age data between 1022 and 544 Ma and another major peak at 2488 Ma (see Fig. 3). This sample contains a large variety of ages with smaller peaks, from most to least prominent: 1330 Ma, 1610 Ma, 1850 Ma and 3130 Ma (see Fig. 3). There is an absence of analysed zircon ages between 2250–1900 Ma. The YSG of RDT16_019 yielded a $^{206}Pb/^{238}U$ age of 277.9 ± 4.9 Ma (within ±10% discordance).

RDT16_006 contained major age peaks at ca. 960 Ma and 585–530 Ma with other peaks at 2569 Ma, 2488 Ma, 2338 Ma, 1868 Ma, 1685 Ma, 1322 Ma, 1180 Ma and 390 Ma. The YSG of RDT16_006 is 255 ± 2.6 Ma (within ±10% discordance).

For RDT16_012, there are major age peaks between 905 and 1330 Ma and also 240 Ma, 550 Ma, 1330 Ma and 2472 Ma in RDT16_012. Other minor age peaks are 1725 Ma, 2030 Ma and 2800 Ma. The YSG for RDT16_012 is 206.6 ± 2.3 Ma (within ±5% discordance). This age is consistent with the evidence from the

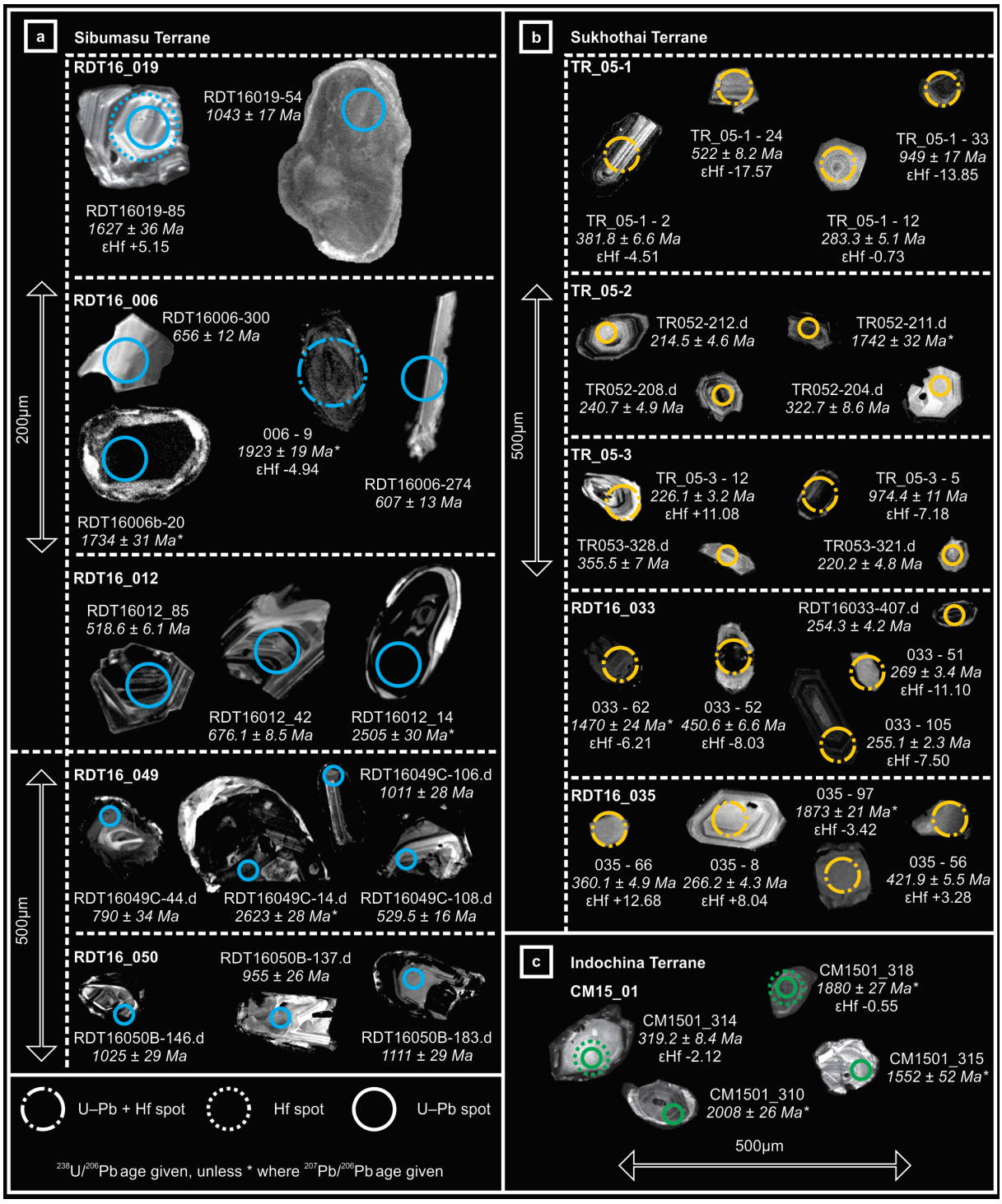

Fig. 2. Cathodoluminescence (CL) images for representative zircons from Permo-Triassic sandstones in Thailand. U-Pb and Hf laser spots shown. Values are given with two standard deviation error. The age for each spot is the $^{238}U/^{206}Pb$ age, unless marked with an asterisk (*) where the $^{207}Pb/^{206}Pb$ age is used.

palaeontology and regional stratigraphic relationships (e.g. Kamata et al. 2009; Srinak et al. 2007).

The detrital zircon age distribution of RDT16_049 exhibits a typical Gondwana

Table 2. Description of zircon morphologies and cathodoluminescence (CL) interpretations for the detrital samples in this study.

Sample Number	*Zircon Morphology*			*Cathodoluminescence (CL) interpretation*
	Size	*Colour*	*Shape*	
RDT16_019	~50-300 µm	White, yellow, orange, brown and rare pinks	Sub-rounded to rounded Some euhedral but fragmented or broken	Multiple domains are common. Some grains contain cracks.
RDT16_006	50-200 µm	Colourless, yellow, orange, pale pink	Sub-rounded. Frequently fragmented or broken grains	Zonation, both oscillatory and diffuse, are common. Some dark grains. Multiple domains are common.
RDT16_012	~50-150 µm	White to pale pinks and yellows	Rounding of the crystal edges whereas in others the original crystal shape has been destroyed, and the final product being smooth sub to well-rounded grains	Well rounded detrital zircon grains. Well-developed oscillatory zoning. Some grains preserve zoning with convolute boundaries. Inherited cores common. Quartz and white mica inclusions. Some metamictisation. Grains are commonly cracked.
RDT16_049	100-400 µm	Mostly pink to purple, some white or colourless	Smooth sub-rounded to well rounded, euhedral-subhedral grains, some are fragmented or broken	Grains can preserve zoning, although some are homogeneous without zonation. Inclusions and inherited domains are common.
RDT16_050B	100-200 µm	Mostly pink to purple, some white or colourless	Sub-rounded euhedral to subhedral grains, some are fragmented or broken	Well rounded detrital zircon grains. Large inclusions are common. Some grains preserve zoning.
TR_05-1	50-300 µm	White, yellow and pale pink	Some euhedral grains, others are fragmented or broken. Varying degrees of rounding from angular to rounded.	Most grains have well-developed oscillatory zoning.
TR_05-2	~75-300 µm	Colourless, white, yellow and orange	Most grains are euhedral, others are fragmented or broken. Angular to sub-rounded.	Most grains have well-developed oscillatory zoning. Some grains have inherited domains.
TR_05-3	50-250 µm	White, colourless, orange, yellow, pale pink and purple	Some grains are euhedral, others are fragmented or broken. Varying degrees of rounding from angular to rounded.	Zonation, both oscillatory and diffuse, are common. Some dark grains. Some grains have multiple domains.
RDT16_033	50-250 µm	Colourless, white, brown and purple	Varying degrees of rounding from angular to rounded. Some grains are fragmented or broken. Rare euhedral grains	Most grains have well-developed oscillatory zoning. Some grains have inherited domains.
RDT16_035	50-300 µm	Colourless and yellow	Varying degrees of rounding from angular to rounded. Some grains are fragmented or broken. Rare euhedral grains.	Most grains do not contain well-developed oscillatory zoning, diffuse zoning is more common. Rarely grains have multiple domains. Some grains have no zonation.
CM15-01	150-300 µm	Colourless, white, grey and rare orange or brown	Some euhedral but fragmented or broken. Varying degrees of rounding from angular to rounded.	Luminescent and preserve well-defined oscillatory zoning.

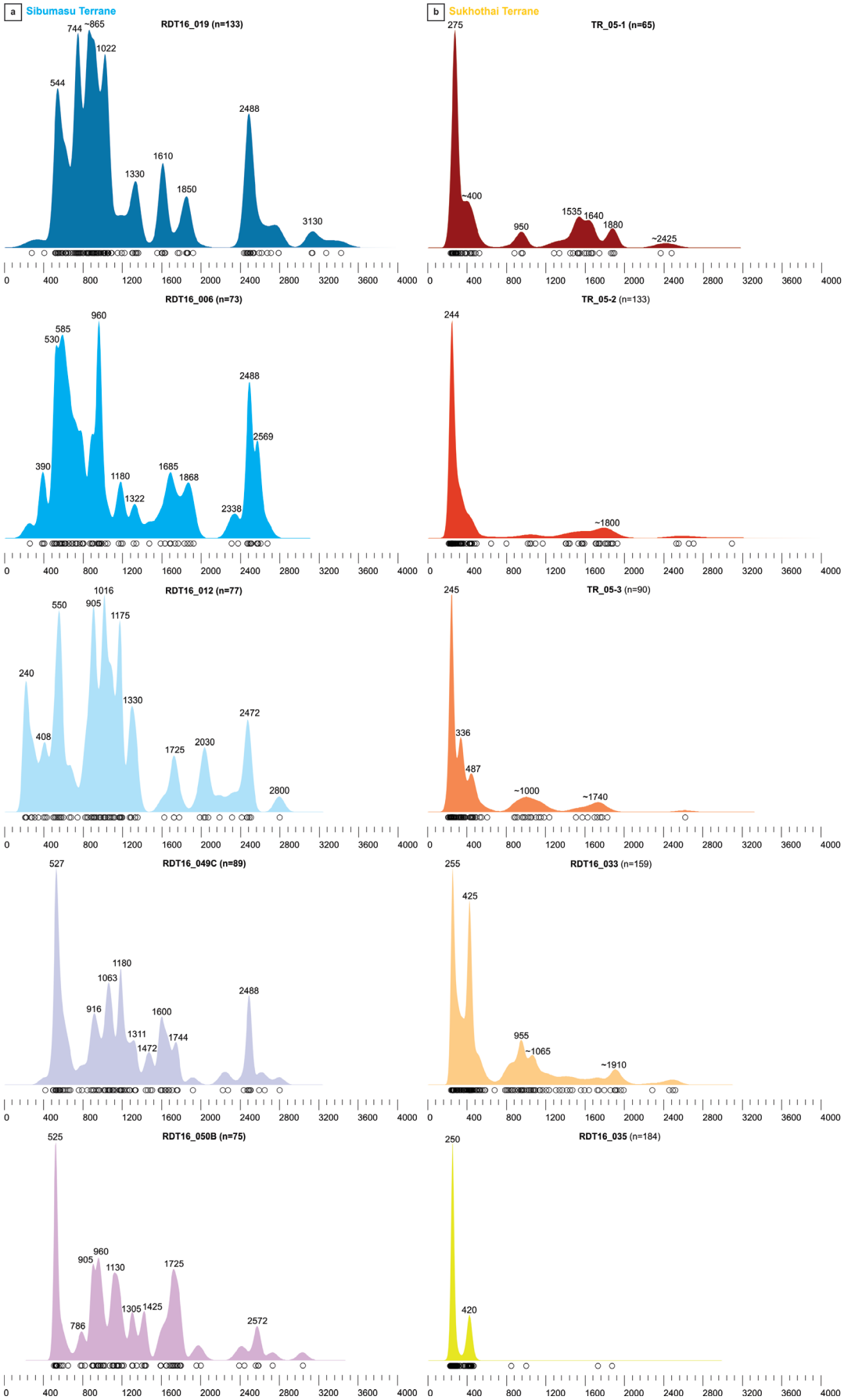
a Sibumasu Terrane
RDT16_019 (n=133)
744 ~865 1022 544 2488 1610 1330 1850 3130
RDT16_006 (n=73)
960 585 530 2488 2569 390 1180 1685 1868 1322 2338
RDT16_012 (n=77)
1016 550 905 1175 240 1330 2472 408 1725 2030 2800
RDT16_049C (n=89)
527 1180 1063 2488 916 1600 1311 1744 1472
RDT16_050B (n=75)
525 960 905 1130 1725 1305 1425 786 2572
b Sukhothai Terrane
TR_05-1 (n=65)
275 ~400 1535 1640 950 1880 ~2425
TR_05-2 (n=133)
244 ~1800
TR_05-3 (n=90)
245 336 487 ~1000 ~1740
RDT16_033 (n=159)
255 425 955 ~1065 ~1910
RDT16_035 (n=184)
250 420
0 400 800 1200 1600 2000 2400 2800 3200 3600 4000

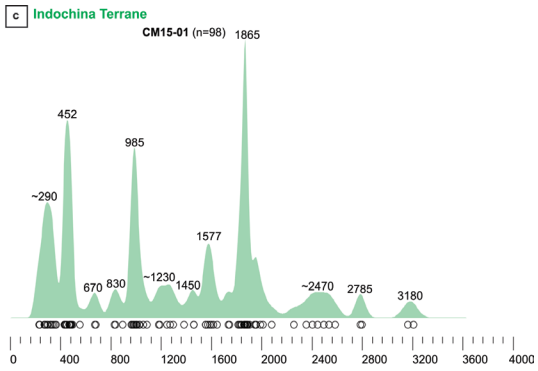

Fig. 3. Kernel Density Estimate (KDE) for each U–Pb sample with age in million years (Ma) along the x axis. Each coloured plot illustrates the kernel density estimate of data with ±10% ($^{206}Pb/^{238}U$ age)/ $^{207}Pb/^{235}U$ age) discordance, Age peaks of the concordant data are labelled in Ma. Plots were created in the Java-based DensityPlotter program outlined by Vermeesch (2012). The parameters used in DensityPlotter are as follows, 20 Ma bandwidth, 50 Ma bins and the adaptive function.

signature with a dominant 527 Ma age peak and minor peaks from 2488 Ma to 916 Ma (Fig. 3). The YSG of RDT16_049 yielded a $^{206}Pb/^{238}U$ age of 415.1 ± 13 Ma (within ±5% discordance, analysis spot RDT16049C-60.d). This zircon age is older than that suggested from Kaeng Krachan Group palaeontological evidence that yields an early Permian depositional age (Chaodumrong et al. 2007; Shi et al 2001; Fujikawa et al 2005; Ueno et al. 2002).

The detrital zircon age distribution and kernel density estimation plot for RDT16_050B (Fig. 3) has a predominant age cluster at ca. 525 Ma. The YSG of RDT16_050B yielded a $^{206}Pb/^{238}U$ age of 508.6 ± 14 Ma (within ±5% discordance, analysis spot RDT16050B-181.d). This YSG is older than the palaeontological evidence from the Kaeng Krachan Group that yields an early Permian depositional age (Chaodumrong et al. 2007; Shi et al 2001; Fujikawa et al 2005; Ueno et al. 2002).

4.1.2 Sukhothai and Chanthaburi terranes
Samples TR_05-1, TR_05-2, TR_05-3, RDT16_033 and RDT16_035 are all Triassic sandstones from the Sukhothai Terrane or southern equivalent Chanthaburi Terrane. Samples TR_05-2, TR_05-3, RDT16_033 and RDT16_035 all have a dominant Permian zircon population at 255–244 Ma and TR_05-1 has a slightly older dominant peak at 275 Ma (Fig. 3). Lesser age population peaks from the detrital Sukhothai samples ranged from 487 to 336 Ma, ca. 1000 Ma, ca. 1910–1535 Ma (Fig. 3). In addition, TR_05-1, TR_05-2, TR_05-3 and RDT16_033 contain several Paleoproterozoic zircon ages (see Supplementary Table 1). TR_05-2 also yielded one Mesoarchean $^{207}Pb/^{206}Pb$ zircon age of 3094.4 ± 8.5 Ma (analysis spot TR_05-2 – 48).

The YSG of TR_05-1 yielded a 206Pb/238U age of 231.9 ± 4.9 Ma (within ±5% discordance, analysis spot TR051-12.d). The YSG of TR_05-2 yielded a $^{206}Pb/^{238}U$ age of 211.8 ± 3.7 Ma (within ±5% discordance). The YSG of TR_05-3 yielded a $^{206}Pb/^{238}U$ age of 207.8 ± 2.6 Ma (within ±5% discordance, TR_05-3 - 17). For RDT16_033, the YSG within ±5% discordance is 235.8 ± 2.8 Ma. For RDT16_035, the YSG within ±5% discordance is 222.5 ± 3.8 Ma (analysis spot 035 – 94).

4.1.3 Indochina Terrane
There are multiple age peaks (~290 Ma, 452 Ma, 965 Ma and 1865 Ma) in the CM15_01 dataset (Fig. 3). For CM15_01, the YSG within ±5% discordance is 226.2 ± 4.6 Ma (analysis spot CM1501-209).

4.2 Zircon Lu–Hf isotopic analyses

In total, 409 concordant zircon grains were analysed from eight samples for Hf isotopic characteristics, and the results show $\varepsilon Hf_{(t)}$ values in the range of –32.17 (analysis spot CM1501-140.d) to +13.66 (analysis spot 035 – 46) and Hf depleted mantle model ages (T_{DM}) from 4.36 Ga to 0.39 Ga (Fig. 4 and supplementary Table 1).

4.2.1 Sibumasu Terrane

Eighty-one zircons were analysed for Hf isotopic characteristics from two samples from the Sibumasu Terrane, yielding $\varepsilon Hf_{(t)}$ values from between -29.58 and +9.44 (Fig. 4) and corresponding depleted mantle model (T_{DM}) ages 4.36 Ga to 1.01 Ga (Supplementary Table 1).

Fifty zircons from RDT16_019 yielded $\varepsilon Hf_{(t)}$ values between -29.58 and +9.44 (Fig. 4). The analysed Neoproterozoic grains are all relatively juvenile ranging in $\varepsilon Hf_{(t)}$ values from -2.32 to +9.44 (Fig. 4). In contrast, the 1310–840 Ma population is quite evolved with values between -29.58 and +2.96. The 1870–1340 Ma aged grains yield $\varepsilon Hf_{(t)}$ values between -6.94 and +5.15, with corresponding T_{DM} values ranging from 2.92 Ga to 1.88 Ga (Fig. 4). Older Archean grains have $\varepsilon Hf_{(t)}$ values that range from -11.03 to +4.94 with corresponding depleted mantle model ages between 4.36 Ga and 2.92 Ga (Fig. 4).

Thirty-one zircons from RDT16_006 yielded $\varepsilon Hf_{(t)}$ values ranging from -27.61 to +8.14 (Fig. 4). The prominent Neoproterozoic–Cambrian zircon age population records a large variation in $\varepsilon Hf_{(t)}$ values between -27.61 and +8.14, which corresponds to depleted mantle model ages of 3.13 Ga and 1.10 Ga (Fig. 4). In contrast, the younger $\varepsilon Hf_{(t)}$ values are less varied between -1.41 and +5.58 (Fig. 4). The Mesoproterozoic grains are evolved with $\varepsilon Hf_{(t)}$ values ranging from -14.71 to -2.26. Further, their negative $\varepsilon Hf_{(t)}$ values show enrichment away from typical mantle compositions, with significant crustal reworking and model ages between 2.98 Ga and 2.12 Ga. The Neoarchean to Paleoproterozoic zircons have $\varepsilon Hf_{(t)}$ values that range from -8.67 to +6.17 with corresponding depleted mantle model ages between 3.37 Ga and 2.26 Ga (Fig. 4).

4.2.2 Sukhothai and Chanthaburi terranes

Three hundred and one zircons from five Sukhothai samples yielded $\varepsilon Hf_{(t)}$ values between -15.70 and +13.66, which corresponds to depleted mantle model ages between 3.66 Ga and 0.39 Ga.

The analysis of 30 zircons from TR_05-1 yielded $\varepsilon Hf_{(t)}$ values between -22.74 and +8.83, with T_{DM} ranging from 2.74 Ga to 0.76 Ga (Fig. 4). The Triassic–Paleozoic zircon population primarily shows a restricted pattern with $\varepsilon Hf_{(t)}$ values between -5.70 and +8.61, which corresponds to depleted mantle model ages of 2.55 Ga and 0.76 Ga (Fig. 5). However, there are two analyses with much more evolved signatures yielding $\varepsilon Hf_{(t)}$ values of -17.57 (522 Ma zircon) and -15.23 (350.6 Ma zircon). These values are more akin to the two $\varepsilon Hf_{(t)}$ values from the 950 Ma age peak (-15.41 and -13.85). The hafnium signatures taken from zircons older than 1445 Ma show more juvenile $\varepsilon Hf_{(t)}$ values between -2.80 and +6.74, which corresponds to depleted mantle model ages of 2.40 Ga and 1.80 Ga (Fig. 4).

The analysis of 47 zircons from TR_05-2 yielded $\varepsilon Hf_{(t)}$ values between -15.43 and +13.44, with T_{DM} ranging from 3.66 Ga to

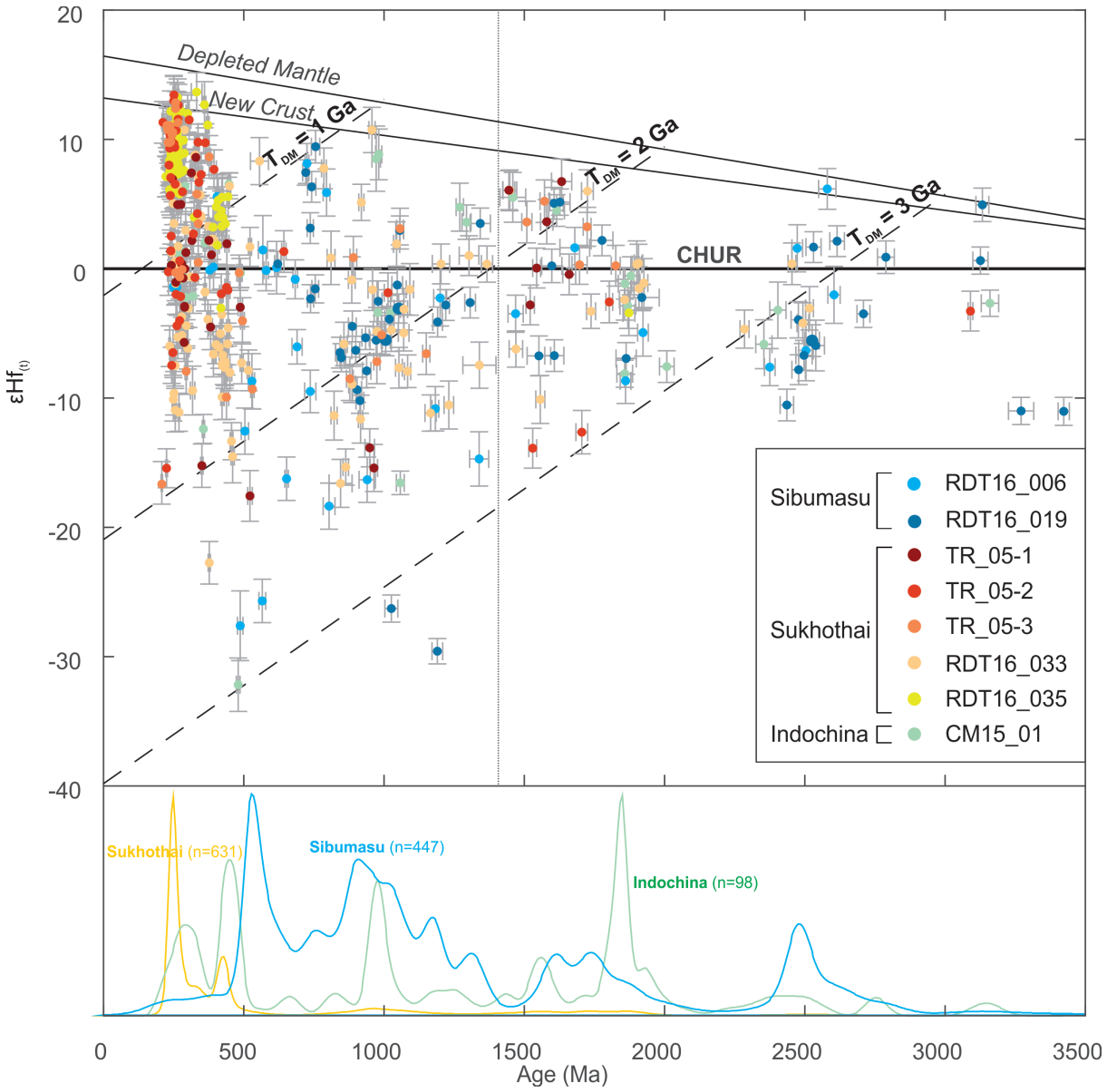

Fig. 4. Plot of $\varepsilon Hf_{(t)}$ versus age for all detrital samples collected from Permo-Triassic sandstones in Thailand. The T_{DM} crustal evolution lines are based on a $^{176}Lu/^{177}Hf$ ratio of 0.015 (Griffin et al. 2004). Kernel density estimate of all ±10% ($^{206}Pb/^{238}U$ age)/ $^{207}Pb/^{235}U$ age) discordance ages found in these samples.

0.39 Ga. Only 12 of 41 Triassic–Paleozoic analyses yield negative $\varepsilon Hf_{(t)}$ values, three of these negative $\varepsilon Hf_{(t)}$ values are taken from zircons older than 420 Ma. One Ediacaran zircon yielded a CHUR-like εHf(t) value of +1.33. All the hafnium signatures taken from zircons older than 1000 Ma are negative with $\varepsilon Hf_{(t)}$ values between -13.88 and -1.86, which corresponds to depleted mantle model ages of 3.66 Ga and 1.95 Ga (Fig. 4).

Thirty-five zircons from TR_05-3 yielded $\varepsilon Hf_{(t)}$ values between -16.56 and +12.83, with T_{DM} ranging from 2.46 Ga to 0.44 Ga (Fig. 4). The 1150.6–207.8 Ma zircons have a variance in their $\varepsilon Hf_{(t)}$ values ranging between -16.56 (from the YSG) and +8.61, which corresponds to depleted mantle model ages of 2.35 Ga and 0.44

Ga (Fig. 5). The hafnium signatures taken from zircons older than 1500 Ma all contain positive $\varepsilon Hf_{(t)}$ values between +0.30 and +5.22, which corresponds to depleted mantle model ages of 2.46 Ga and 1.95 Ga (Fig. 4).

Ninety-six zircons from RDT16_033 yielded $\varepsilon Hf_{(t)}$ values between -22.74 and +10.73, with T_{DM} ranging from 3.24 Ga to 0.58 Ga (Fig. 4). There is a large proportion of juvenile $\varepsilon Hf_{(t)}$ values within the 255 Ma age peak, but still with a wide total range of $\varepsilon Hf_{(t)}$ values (e.g. analysis spot 033 – 51 $\varepsilon Hf_{(t)}$ = -11.10). This variation in $\varepsilon Hf_{(t)}$ values is seen in all age populations <1600 Ma. One zircon with a $^{207}Pb/^{206}Pb$ age of 1725 ± 21 Ma yielded a juvenile $\varepsilon Hf_{(t)}$ value of +6.00. Zircons older than 1730 Ma show less variation in $\varepsilon Hf_{(t)}$ values (-4.67 to +0.42).

The analysis of 93 zircons from RDT16_035 yielded $\varepsilon Hf_{(t)}$ values between -3.42 and +13.66, with corresponding TDM between 2.71 Ga to 0.42 Ga (Fig. 4). The predominant 250 Ma age peak in RDT16_035 yielded exclusively juvenile $\varepsilon Hf_{(t)}$ values ranging from +13.24 to +3.97 (Fig. 4). Only two of the 93 Hf analyses from RDT16_035 yielded $\varepsilon Hf_{(t)}$ values less than 0.

4.2.3 Indochina Terrane

The analysis of 27 zircons from CM15_01 yielded $\varepsilon Hf_{(t)}$ values between -32.17 and +8.84, with T_{DM} from 3.40 Ga to 0.52 Ga (Fig. 4). The $\varepsilon Hf_{(t)}$ values from the middle Carboniferous–Triassic analyses only range between -2.23 and +6.37 (Fig. 4). The 1058–972 Ma age population records a large variation in $\varepsilon Hf_{(t)}$ values between -16.56 and +8.84, which corresponds to depleted mantle model ages of 2.88 Ga and 1.26 Ga (Fig. 4). 1615–1270 Ma zircons record only positive $\varepsilon Hf_{(t)}$ values between +3.60 and +5.52. In contrast, the Paleoproterozoic and Archean grains all yielded negative $\varepsilon Hf_{(t)}$ values (-8.12 to -0.55; Fig. 4).

5. Discussion

5.1 The provenance of the Sibumasu Terrane

In order of prominence, age populations of 1200–900 Ma, 585–525 Ma and 2572–2472 Ma are present in each of the Permo-Triassic detrital samples analysed from the Sibumasu Terrane (Fig. 3).

To compare this study's detrital datasets to published data from potential source regions or neighbouring terranes, we used multidimensional scaling (MDS) (Vermeesch 2013). MDS is a robust and flexible application of Principal Components Analysis, which uses the Kolmogorov-Smirnov (K-S) test, a calculation of the maximum probability dissimilarity between two or more cumulative distribution functions (Vermeesch 2013). The resultant MDS plots for this study are illustrated in Fig. 5. From Fig. 5a it can be seen that the samples in this study from the Sibumasu Terrane plot close together in MDS space, forming two geographically distinct clusters: one from northwestern Thailand with RDT16_019, RDT16_006 and RDT16_012 and the second cluster containing the two samples from Phuket, RDT16_049 and RDT16_050 (Fig. 5a).

The age peaks found in the Sibumasu samples of this study are also observed in other parts of the Sibumasu Terrane (Burrett et al. 2014; Cai et al. 2017; Zhang et al. 2018). The early Triassic 240 Ma age peak from RDT16_012 overlaps with published magmatic data from Sibumasu and Inthanon terranes ranging from 240–200 Ma (Ahrendt et al. 1993; Charusiri

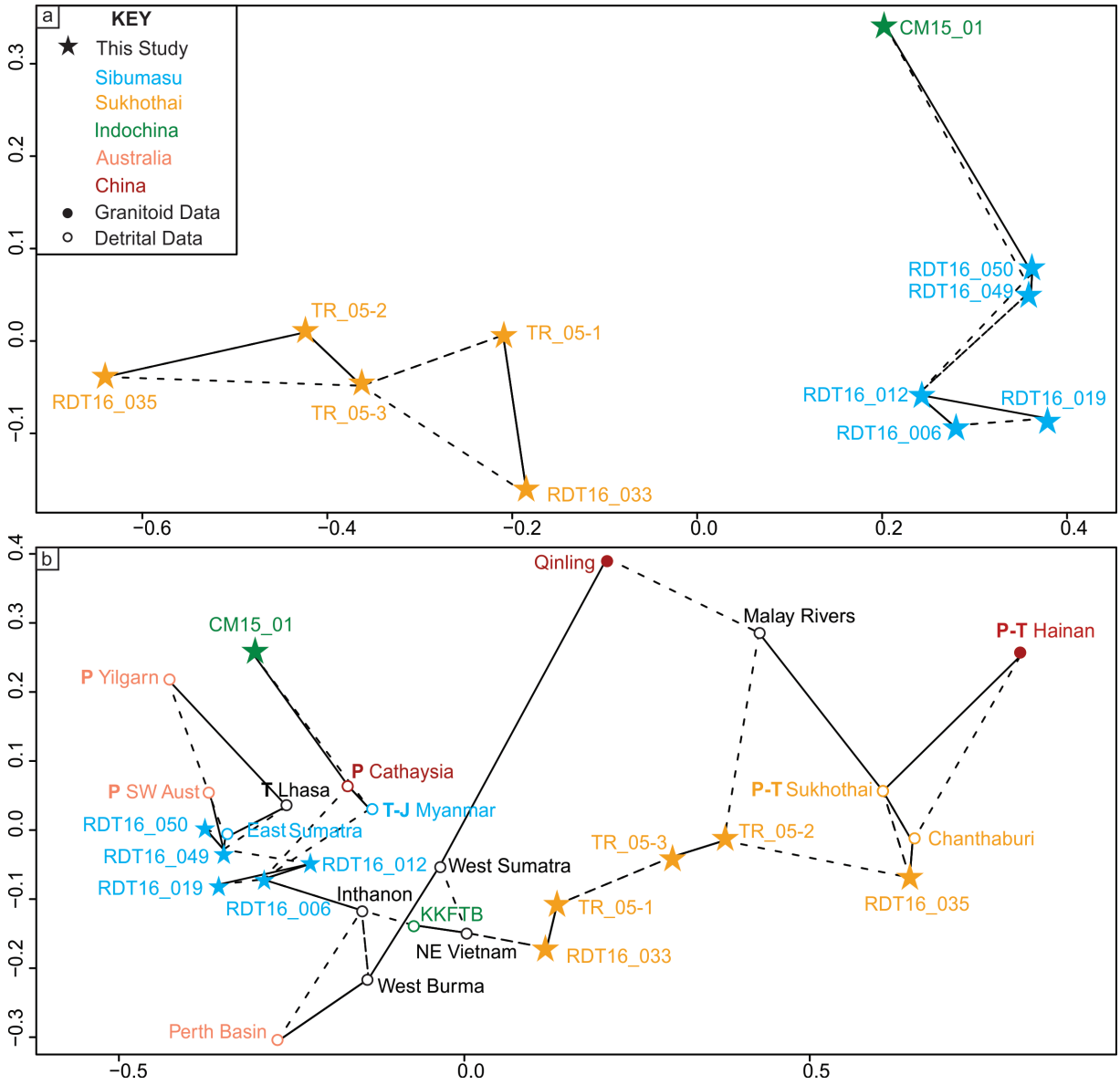

Fig. 5. a: Permo-Triassic samples across Thailand from this study. Multidimensional scaling (MDS) plot of detrital sample U–Pb age distributions from the Permo-Triassic samples in Thailand. Samples with lowest dissimilarity values are plotted closest to one another; solid lines and dashed lines indicate closest and second-closest neighbours respectively (see Vermeesch 2013; Vermeesch et al. 2016). **b:** MDS plot of this study's Permo-Triassic samples and potential source areas. Published data: Triassic–Jurassic (T-J) Myanmar (Cai et al. 2017), East Sumatra and West Sumatra (Zhang et al. 2018), Inthanon Zone (Hara et al. 2013), NE Vietnam (Halpin et al. 2016), Khao Khwang Fold-Thrust Belt (KKFTB) (Arboit et al. 2016b), Permian (P) Cathaysia (Li et al. 2012), Permian (P) SW Australia (Veevers et al. 2005), Perth Basin (Cawood and Nemchin 2000; Sircombe and Freeman 1999), Permian (P) Yilgarn WA (Veevers et al. 2005), Lhasa (Li et al. 2014), Malay Rivers (Sevastjanova et al. 2011), West Burma (Sevastjanova et al. 2016), Permo-Triassic (P-T) Sukhothai (Hara et al. 2017), Chanthaburi (Hara et al. 2018b), Qinling Granite and Permo-Triassic (P-T) Granite from Hainan Island (Shen et al. 2018).

et al. 1993; Dew et al. 2018a; Gardiner et al. 2016; Kawakami et al. 2014; Ng et al. 2015a; Searle et al. 2012; Wang et al. 2016b). These granitoids are thought to be supra-subduction zone granitoids that formed during the closure of the Palaeo-

Tethys Ocean (i.e. the older granites from the Sukhothai Terrane) and the subsequent collision of Sibumasu with the Sukhothai and Indochina terranes during the Upper Triassic (Searle et al. 2012).

Precambrian zircons from the Sibumasu Terrane show a large variation in $\varepsilon Hf_{(t)}$ values, with both juvenile and evolved signatures (ranging from -22.25 to +10.80). Lu–Hf isotopes in younger Paleozoic zircons were only analysed from RDT16_006, which yielded $\varepsilon Hf_{(t)}$ values between -1.41 and +5.58 (Fig. 5). Magmatic isotopic studies have also shown that the Sibumasu Terrane contains evolved recycled crust that has undergone multiple recycling events, with a wide range of $\varepsilon Hf_{(t)}$ signatures observed in inherited zircon grains (Dew et al. 2018a).

5.2 The provenance of the Sukhothai and Chanthaburi terranes

The MDS comparison between the Permo-Triassic samples in this study shows that the samples from the Sukhothai Terrane are least dissimilar to each other and cluster separately from the Sibumasu and Indochina detrital samples (Fig. 5). Unlike the Permo-Triassic Sibumasu samples, the Permo-Triassic data from the Sukhothai Terrane do not show a distinct geographical trend between the samples from northern Sukhothai (TR_05-1, TR_05-2 and TR_05-3) and the southern equivalent, Chanthaburi (RDT16_033 and RDT16_035). There is also no clear change in provenance from oldest to youngest sample (Fig. 5 and Table 1).

All five of the samples from the Sukhothai Terrane have a dominant Permian zircon age populations (Fig. 3). These age peaks are consistent with magmatic ages documented in the Sukhothai Terrane, ranging from 296 to 200 Ma (Beckinsale et al. 1979; Charusiri et al. 1993; Cobbing 2011; Dew et al. 2018a; Hansen and Wemmer 2011; Meffre et al. 2008; Ng et al. 2015b; Qian et al. 2017; Singharajwarapan and Berry 2000; Sone et al. 2012; Wang et al. 2016b; Zaw et al. 2014).

The older Paleozoic zircon age population spanning from 487–400 Ma, is also documented by Carter and Bristow (2003) within the Khorat Group recognising a pervasive zircon formation event at 470–430 Ma. The detrital U–Pb data from the Khorat Group of the Indochina Terrane also contains the 1065–950 Ma zircons observed in the Sukhothai samples of this study (see Carter and Bristow 2003).

The 296–207 Ma detrital data from the Sukhothai Terrane show variation in their Hf isotopic signatures, with $\varepsilon Hf_{(t)}$ values ranging from -16.56 to +13.44. A similar range of zircon-Hf and whole-rock-Nd isotopic signatures were observed for the 296–200 Ma granitoids in the Sukhothai Terrane (Dew et al. 2018a; Qian et al. 2017; Wang et al. 2016b). The whole-rock Nd isotopic signatures of the Permo-Triassic granitoids display a similar trend, forming a continuum from more juvenile metaluminous I-type granitoids in the east of the Sukhothai Terrane through to more evolved granitoids in the west (Dew et al. 2018a). This provides further evidence that the sediments are being sourced locally from the active Sukhothai arc system.

5.3 The provenance of the Indochina Terrane

The MDS comparison between the Permo-Triassic samples in this study in Fig. 5a shows that the sample from the Indochina Terrane (CM15_01) plots closest to the two Sibumasu samples from the Phuket

region.

The CM15_01 age peak of 452 Ma is also observed in all the Permo-Triassic units of the Khao Khwang Fold-Thrust Belt on the southern margin of the Indochina Terrane (Arboit et al. 2016b). However, the middle Carboniferous–Triassic analyses from sample CM15_01 of the Huai Hin Lat Formation are more evolved than the detrital Hf isotopic signatures found in the Khao Khwang Fold-Thrust Belt by Arboit et al. (2016b). A pervasive zircon formation event from 470–430 Ma was also recognised by Carter and Bristow (2003) within the Khorat Group of the Indochina Terrane. Many of the zircon age peaks distinguished in CM15_01 are also seen in the late Cretaceous–early Paleogene Phu Khat Formation further north in the Nakhon Thai region of the Indochina Terrane (see Nulay et al. 2016).

The ~290 Ma age peak in the CM15_01 dataset (Fig. 3) is consistent with crystallisation ages from granitoids within the Indochina Terrane that span from 310 to 203 Ma (Arboit et al. 2016a; Charusiri et al. 1993; Halpin et al. 2016; Kamvong et al. 2014; Ng et al. 2015b; Salam et al. 2014; Zaw et al. 2014). These ages may be associated with Late Carboniferous to end Guadalupian subduction-related volcanic arc activity as a result of the early stages of the South China and Cathaysia collision with Vietnam and Indochina (Halpin et al. 2016; Lepvrier et al. 2004), or the similarly timed collision between Indochina and Sukhothai (Morley et al. 2013).

5.4 Correlation across Thailand and to comparable sedimentary sequences

Some of the zircon forming events in the Indochina Terrane are also seen in the Sukhothai Terrane, such as 290–244 Ma, 487–400 Ma, 1000–950 Ma, 1910–1740 Ma and 2470–2425 Ma (Fig. 3), suggesting similar sources, possibly due to a shared history as suggested by Sone and Metcalfe (2008). However, stratigraphically, the late Permian–Triassic sequences of the Chanthaburi and Sukhothai terranes are clearly distinct from those of the Indochina or Sibumasu terranes. The late Permian–Triassic is largely absent from the western region of the Indochina Terrane due to the Indosinian I unconformity and in the Sibumasu Terrane the late Permian–Triassic sequences are dominantly calcareous with little terrigenous clastic input (Sone et al. 2012).

Many of the age peaks in the Indochina and Sukhothai terranes are also shared with the Permo-Triassic samples from the Sibumasu Terrane (Fig. 3). The following zircon age populations are found in each of the three terranes of Thailand: 487–390 Ma, 900–1000 Ma, 1900–1725 Ma and 2572–2425 Ma (Fig. 3).

The 487–390 Ma age peak is also seen in Permian sedimentary sequences from Cathaysia (Li et al. 2012). These Cathaysian detrital zircons also have a wide range of Hf and O isotope signatures, indicating a binary mixing of melts derived from a depleted mantle source and from continental crustal materials ($\varepsilon Hf_{(t)}$ values mostly between −5.4 and +14.1 and $\delta^{18}O$ values between 5.0‰ and 8.1‰ (Li et al. 2012)). It was proposed by Li et al. (2012) that this detritus was sourced from early Paleozoic granites that formed as part of the Wuyi–Yunkai Orogeny in southeastern China. Dominant Paleozoic zircon ages are also found in detrital material from Kyrgyz Tien Shan (De Pelsmaeker et al. 2018) and at the southwestern Siberian margin (Glorie et al. 2014). The older ages in the 487–390 Ma age population from this work may indicate the closure

of the Proto-Tethys Ocean in the early Paleozoic (500–420 Ma), leading to the collision of South China, North China, Qaidam, Indochina and Tarim with other East Asian blocks at the northern margin of Gondwana (Zhao et al. 2018).

Age peaks with maxima ranging from 2572 to 2425 Ma are seen in Permo-Triassic samples from each of the three terranes in Thailand (Fig. 3). Similar age peaks are observed in many detrital datasets that were once part of Gondwana (e.g. Burrett et al. 2014; Cawood and Nemchin 2000; Condie et al. 2009; Dong et al. 2011; Flowerdew et al. 2007; Li et al. 2012; Moghadam et al. 2017; Wang et al. 2015). This population may be sourced from ca. 2560–2470 Ma magmatism and orogenesis seen in Australia (Betts et al. 2006; Hand et al. 2007; Nordsvan et al. 2018), India (Armistead et al. 2018; Clark et al. 2009; Collins et al. 2014) and Madagascar (Armistead et al. 2018; Kroener et al. 2000).

Age peaks between 1000–900 Ma are observed in detrital samples from each of the Thai terranes in this study. Similar age populations are present in Tethyan and High Himalayas (Ding et al., 2016; McQuarrie et al., 2008; Myrow et al., 2010; DeCelles et al., 2000; Myrow et al., 2003, 2010; Gehrels et al., 2011), Qiangtang (Dong et al. 2011; Wang et al. 2015), Lhasa (Zhu et al. 2011), East Sumatra (Zhang et al. 2018), Yangtze, Phuket, NE Vietnam and Ailaoshan (see Burrett et al. 2014 and references therein), Antarctica (Fitzsimons 2000; Flowerdew et al. 2007; Kelsey et al. 2008), Indochina (Arboit et al. 2016b; Usuki et al. 2013) and the Permian–Jurassic strata from northeast India (Veevers and Saeed, 2009). It is proposed that the 1000–900 Ma detritus from Permo-Triassic sediments in Thailand was likely derived from c.990–900 Ma Rayner-Eastern Ghats, which is one of the few proximal regions in Gondwana where protoliths of this age occur (Fitzsimons 2000).

Some zircon age peaks are only observed in the Sibumasu Terrane (1330–1305 Ma, 1180–1130 Ma, 585–525 Ma), but are common in other parts of Gondwana (Burrett et al. 2014; Cai et al. 2017; Cawood and Nemchin 2000; Fitzsimons 2003; Flowerdew et al. 2007; Li et al. 2014; Veevers et al. 2005; Xu et al. 2013). All of the Permo-Triassic samples from the Sibumasu Terrane record the two peaks at 1330–1305 Ma and 1180–1130 Ma. This detritus is likely to be sourced from the Albany–Fraser Orogen in southwest Australia, or its continuation in the western Musgraves, which records two pulses of magmatism at 1330–1280 Ma and 1200–1130 Ma (Clark et al., 2000; Fitzsimons, 2000). The detrital age population at 585–525 Ma is conceivably part of the Neoproterozoic–Cambrian Kuunga–Pinjarra Orogen (ages between 600–500 Ma (Collins 2003; Fitzsimons 2000; Veevers et al. 2006)), an orogenic belt from Western Australia to eastern Antarctica, which reflects one of the final events in Gondwana amalgamation (Schmitt et al. 2018).

The MDS comparison between this study and published datasets (Fig. 5b) illustrates the geographic distinctions within individual terranes. As discussed above for this study's samples in Fig. 5a, Fig. 5b similarly reflects the distinction between the northern (RDT16_019, RDT16_006, RDT16_012 and Triassic–Jurassic sandstones; Cai et al. 2017) and southern regions of the Sibumasu Terrane (RDT16_049, RDT16_050 and East Sumatra sandstones; Zhang et al. 2018).

The K-S and MDS statistical analysis in Fig. 5b also highlights the mismatch within Indochina between sediments from the northern Thailand (e.g. sample CM15_01) and those from Arboit et al. (2016b) in the Khao Khwang Fold-Thrust Belt. While both datasets are from Indochina, they plot distinct in MDS space, with CM15_01 close to the Permian sediments of Cathaysia (Li et al. 2012), and the Permian sandstones of the Yilgarn Craton in Australia (Veevers et al. 2005). The detrital data from the Khao Khwang Fold-Thrust Belt (Arboit et al. 2016b) are most similar to samples from northeast Vietnam (Halpin et al. 2016), West Sumatra (Zhang et al. 2018), the Inthanon Zone (Hara et al. 2013) and West Burma (Fig. 5). This when combined with the difference in Hf signatures, strengthens the idea, already advocated by Lepvrier et al. (2004) and Morley et al. (2013), of a more complicated geometry for the Indochina Terrane. It is possible to speculate about the presence of a provenance boundary, which may be an intra-continental basin, or even an additional ocean basin along the Siem Reap–Stung Treng line.

5.5 Tectonic implications

This study is significant for understanding the Indosinian Orogeny as the Permian and Triassic datasets span the pre-, syn- and post-collisional settings. Previous studies (Morley et al. 2013; Arboit et al. 2014), suggest that the Indosinian Orogeny had two major peaks of collision: latest Permian to early Triassic and late Triassic to early Jurassic. However, these two separate events are only distinguishable in the Khorat Plateau located in the Indochina Terrane, where after the Indosinian I event there was a short period of extensional tectonics during the Norian (middle Upper Triassic 227–208.5 Ma) that formed a series of half grabens in which thick sequences of Kuchinarai Group sediments were deposited along the main faults (Minezaki et al. 2018). At the end of the Triassic, the collision of the Sibumasu Terrane with the Sukhothai arc system during the Indosinian II event marked the final event of the Indosinian Orogeny in mainland Southeast Asia (Minezaki et al. 2018). From the results of this study, we suggest that RDT16_019, RDT16_049 and RDT16_050 from the Sibumasu Terrane were deposited prior to the amalgamation of Thailand in the Indosinian Orogeny. These three samples exclusively contain age distributions and isotopic signatures characteristic of the Sibumasu Terrane and neighbouring regions within Gondwana (Burrett et al. 2014; Kettanah et al. 2015; Li et al. 2014; Vermeesch et al. 2016; Zhang et al. 2018).

In stark contrast, the detrital zircon age distribution and Hf characteristics of the Sukhothai Terrane illustrates the strong influence of proximal synchronous Sukhothai arc magmatism (Fig. 3 and 4). Detrital data collected within this study show that the collision between Indochina—South China and Sukhothai occurred prior to the deposition of the Triassic sediments in the Sukhothai Terrane. This is supported by the presence of ages (ca. 1860 Ma and ca. 950 Ma) common to both Indochina and South China (Carter and Bristow 2003; Li et al. 2012), suggesting that these were depositionally connected prior to the Upper Triassic.

It is difficult to delineate the two stages of the Indosinian Orogeny within CM15_01 of the Huai Hin Lat Formation. The collisional magmatic ages found in the Sukhothai and Indochina terranes are also present in the latest Permian and Triassic sequences of the Sibumasu Terrane

(RDT16_006 and RDT16_012). This suggests that these samples were sourcing material from Sukhothai or Indochina, and were therefore were deposited after Sibumasu collided with Sukhothai and Indochina. These ages inferred for the collisional history of Thailand are consistent with the published ages for the Indosinian Orogeny, latest Permian to Upper Triassic (e.g. Barber et al. 2017; Barber et al. 2011; Faure et al. 2014; Hara et al. 2013; Metcalfe 2000; Morley et al. 2013; Ridd 2013; Rossignol et al. 2016; Sone and Metcalfe 2008).

The CM15_01 sample from the Indochina Terrane contains Proterozoic age populations that are more commonly found in the Sibumasu Terrane and are characteristic of material sourced from India or northern Australia (Myrow et al. 2010; Veevers et al. 2005). This detritus observed in CM15_01 may be reworked sediment from the Indo-Australian margin of Gondwana (Burrett et al. 2014; Cocks and Torsvik 2013) or sourced from the Sibumasu Terrane during the Indochina—Sibumasu collision, however we cannot distinguish between these two potential detrital origins.

6. Conclusion

This study used detrital zircon U–Pb and Lu–Hf isotopic systems to elucidate the Permo-Triassic tectonic history of Thailand. From this analysis, we determined:

- 487–390 Ma, 1000–900 Ma, 1900–1725 Ma and 2572–2425 Ma zircon age populations are present in the Permo-Triassic sediments across all three tectonic terranes in Thailand
- Detrital samples from the Sibumasu Terrane contain a large variation in their $\varepsilon Hf_{(t)}$ values including both juvenile and evolved signatures (ranging from -22.25 to +10.80)
- The predominant 296–207 Ma detrital age data from the Sukhothai Terrane have $\varepsilon Hf_{(t)}$ values ranging from -16.56 to +13.44, which correspond to the isotopic signatures of the synchronous Sukhothai granitoids
- CM15_01 of the Indochina Terrane contains zircon age populations characteristics similar to South China

The influence of the Indosinian Orogeny and associated magmatism is detected in the latest Permian and Triassic sequences across Thailand. These results have implications for future investigations on the palaeogeographic evolution of Thailand and also broader research conducted on greater Southeast Asian tectonics.

Acknowledgements

All field work was conducted with the kind assistance of staff and students of Chiang Mai University. We would like to especially thank Dr. Rattanaporn Fongngern for collecting Tr05-1, Tr05-2 and Tr05-3 samples, and also Mr Piyanat Viriyasuksing, Dr Niti Mankhemthong and Dr Kannipa Motanated. Other field work was aided by Liviu Matenco, Ernst Willingshofer from Utrecht University and Thamfatt Ng, Diew.

Kind thanks to Dr Morgan L Blades for her assistance in this research. Appreciation to Sheree Armistead for providing MATLAB scripts. A big thanks to Sarah Gilbert at Adelaide Microscopy and Pîi Roj from Chiang Mai University Lapidary.

This is a contribution to IGCP projects #589 (Development of the Asian Tethyan Realm) and #628 (The Gondwana Map). This work was funded by Australian Research Council through projects #DP

120101460 and #FT120100340. RECD is also funded by a University of Adelaide Research Training Program Stipend and much of the field work made possible by an Endeavour Cheong Kong Fellowship.

GeoHistory Facility instruments in the John de Laeter Centre, Curtin University were funded via an Australian Geophysical Observing System grant provided to AuScope Pty Ltd. by the AQ44 Australian Education Investment Fund program. The NPII multi-collector was obtained via funding from the Australian Research Council LIEF program (LE150100013).

References

Ahrendt, H., Chonglakmani, C., Hansen, B.T. & Helmcke, D. 1993. Geochronological cross section through northern Thailand. Journal of Southeast Asian Earth Sciences, 8, 207-217, doi: http://dx.doi.org/10.1016/0743-9547(93)90022-H.

Ali, J.R., Cheung, H.M.C., Aitchison, J.C. & Sun, Y. 2013. Palaeomagnetic re-investigation of Early Permian rift basalts from the Baoshan Block, SW China: constraints on the site-of-origin of the Gondwana-derived eastern Cimmerian terranes. Geophysical Journal International, 193, 650-663, doi: 10.1093/gji/ggt012.

Ampaiwan, T., Charusiri, P. & Hisada, K. 2004. Early Permian Gondwana Sequence in Phuket Peninsular Thailand. International Symposium on the Geologic Evolution of East and Southeast Asia, Bangkok, Thailand, 51-73.

Ampaiwan, T., Hisada, K.-I. & Charusiri, P. 2009. Lower Permian glacially influenced deposits in Phuket and adjacent islands, peninsular Thailand. Island Arc, 18, 52-68, doi: 10.1111/j.1440-1738.2008.00653.x.

Arboit, F., Amrouch, K., Collins, A.S., King, R. & Morley, C. 2015. Determination of the tectonic evolution from fractures, faults, and calcite twins on the southwestern margin of the Indochina Block. Tectonics, 34, 1576-1599, doi: 10.1002/2015TC003876.

Arboit, F., Collins, A.S., Jourdan, F., King, R., Foden, J. & Amrouch, K. 2016a. Geochronological and geochemical study of mafic and intermediate dykes from the Khao Khwang Fold-Thrust Belt: Implications for petrogenesis and tectonic evolution. Gondwana Research, 36, 111-128.

Arboit, F., Collins, A.S., King, R., Morley, C.K. & Hansberry, R. 2014. Structure of the Sibumasu–Indochina collision, central Thailand: A section through the Khao Khwang Fold and thrust belt. Journal of Asian Earth Sciences, 95, 182-191, doi: http://dx.doi.org/10.1016/j.jseaes.2014.06.016.

Arboit, F., Collins, A.S., Morley, C.K., King, R. & Amrouch, K. 2016b. Detrital zircon analysis of the southwest Indochina terrane, central Thailand: Unravelling the Indosinian orogeny. Geological Society of America Bulletin,, 128, 1024-1043.

Armistead, S.E., Collins, A.S., Payne, J.L., Foden, J.D., De Waele, B., Shaji, E. & Santosh, M. 2018. A re-evaluation of the Kumta Suture in western peninsular India and its extension into Madagascar. Journal of Asian Earth Sciences, 157, 317-328, doi: https://doi.org/10.1016/j.jseaes.2017.08.020.

Audley-Charles, M.G., Ballantyne, P.D. & Hall, R. 1988. Mesozoic-Cenozoic rift-drift sequence of Asian fragments from Gondwanaland. Tectonophysics, 155, 317-330.

Barber, A.J., Khin Zaw & Crow, M.J. 2017. Chapter 31 The pre-Cenozoic tectonic evolution of Myanmar. Geological Society, London, Memoirs, 48, 687-712, doi: 10.1144/m48.31.

Barber, A.J., Ridd, M.F. & Crow, M.J. 2011. The origin, movement and assembly of the pre-Tertiary tectonic units of Thailand. In: Ridd, M.F., Barber, A.J. & Crow, M.J. (eds.) The Geology of Thailand. The Geological Society, London, 507-537.

Barr, S.M. & Macdonald, A.S. 1987. Nan River suture zone, northern Thailand. Geology, 15, 907-910, doi: 10.1130/0091-7613(1987)15<907:nrsznt>2.0.co;2.

Barr, S.M. & Macdonald, A.S. 1991. Toward a late Palaeozoic–early Mesozoic tectonic model for Thailand. Journal of Thai Geoscience, 1, 11-22.

Baum, F., von Braun, E., Hahn, L., Hess, A., Koch, K.E., Kruse, G., Quarch, H. & Siebenhüner, M. 1970. On the Geology of Northern Thailand. Beihefte zum Geologischen Jahrbuch, 102, 1-23.

Beckinsale, R.D., Suensilpong, S., Nakapadungrat, S. & Walsh, J.N. 1979. Geochronology and geochemistry of granite magmatism in Thailand in relation to a plate tectonic model. Journal of the Geological Society, 136, 529-537, doi: 10.1144/gsjgs.136.5.0529.

Betts, P.G., Giles, D., Mark, G., Lister, G.S., Goleby, B.R. & Aillères, L. 2006. Synthesis of the proterozoic evolution of the Mt Isa Inlier.

Australian Journal of Earth Sciences, 53, 187-211, doi: 10.1080/08120090500434625.

Booth, J. & Sattayarak, N. 2011. Subsurface Carboniferous - Cretaceous geology of NE Thailand. In: Ridd, M.F., Barber, A.J. & Crow, M.J. (eds.) The Geology of Thailand. The Geological Society, London, 185-222.

Bunopas, S. 1992. Regional Stratigraphic Correlation in Thailand. Geologic Resources of Thailand: Potential for Future Development, 189-208.

Bunopas, S., Vella, P., Fontaine, H., Hada, S., Burrett, C., Haines, P., Potisat, S., Wongwanich, T., Chaodamrong, P., Howard, K.T. & Khositanont, S. 2001. Growth of Asia in the Late Triassic Continent-Continent Collision of Shan-Thai and Indochina Against South China. Gondwana Research, 4, 584-585, doi: http://dx.doi.org/10.1016/S1342-937X(05)70388-9.

Burrett, C., Khin, Z., Meffre, S., Lai, C.K., Khositanont, S., Chaodumrong, P., Udchachon, M., Ekins, S. & Halpin, J. 2014a. The configuration of Greater Gondwana—Evidence from LA ICPMS, U–Pb geochronology of detrital zircons from the Palaeozoic and Mesozoic of Southeast Asia and China. Gondwana Research, 26, 31-51, doi: http://dx.doi.org/10.1016/j.gr.2013.05.020.

Burrett, C., Udchachon, M., Thassanapak, H. & Chitnarin, A. 2014b. Conodonts, radiolarians and ostracodes in the Permian E-Lert Formation, Loei Fold Belt, Indochina Terrane, Thailand. Geological Magazine, 152, 106-142, doi: 10.1017/S001675681400017X.

Cai, F., Ding, L., Yao, W., Laskowski, A.K., Xu, Q., Zhang, J.e. & Sein, K. 2017. Provenance and tectonic evolution of Lower Paleozoic–Upper Mesozoic strata from Sibumasu terrane, Myanmar. Gondwana Research, 41, 325-336, doi: 10.1016/j.gr.2015.03.005.

Carter, A. & Bristow, C.S. 2003. Linking hinterland evolution and continental basin sedimentation by using detrital zircon thermochronology: a study of the Khorat Plateau Basin, eastern Thailand. Basin Research, 15, 271-285, doi: doi:10.1046/j.1365-2117.2003.00201.x.

Cawood, P.A. & Nemchin, A.A. 2000. Provenance record of a rift basin: U/Pb ages of detrital zircons from the Perth Basin, Western Australia. Sedimentary Geology, 134, 209-234, doi: https://doi.org/10.1016/S0037-0738(00)00044-0.

Chaodumrong, P. 1992. Stratigraphy, sedimentology and tectonic implications of the Lampang Group, central north Thailand. Doctorate of Philosophy, University of Tasmania.

Chaodumrong, P. 2013. Lexicon of Stratigraphic Names of Thailand. Geological Standard Division, Bureau of Geological Survey and Department of Mineral Resources.

Chaodumrong, P. & Burrett, C. 1997. Early Late Triassic continental colliding between Shan-Thai and Indochina terranes as indicated by occurrences pf fan delta red beds of Pha Daeng Formation, central north Thailand. The International Conference on Startigraphy and Tectonic Evolution of Southeast Asia and the South Pacific, Bangkok, Thailand, 143-157.

Chaodumrong, P., Xiangdong, W. & Shuzhong, S. 2007. Permian lithostratigraphy of the Shan-Thai Terrane in Thailand: Revision of the Kaeng Krachan and Ratburi Groups. GEOTHAI'07 International Conference on Geology of Thailand: Towards Sustainable Development and Sufficiency Economy, 229-236.

Charusiri, P., Clark, A.H., Farrar, E., Archibald, D. & Charusiri, B. 1993. Granite belts in Thailand: evidence from the 40Ar/39Ar geochronological and geological syntheses. Journal of Southeast Asian Earth Sciences, 8, 127-136, doi: http://dx.doi.org/10.1016/0743-9547(93)90014-G.

Chonglakmani, C. 2001. The Saraburi Group of North-Central Thailand: Implication for Geotectonic Evolution. Gondwana Research, 4, 597-598, doi: http://dx.doi.org/10.1016/S1342-937X(05)70400-7.

Chonglakmani, C. 2011. Triassic. In: Ridd, M.F., Barber, A.J. & Crow, M.J. (eds.) The Geology of Thailand. The Geological Society, London, 137-150.

Clark, C., Collins, A.S., Timms, N.E., Kinny, P.D., Chetty, T.R.K. & Santosh, M. 2009. SHRIMP U–Pb age constraints on magmatism and high-grade metamorphism in the Salem Block, southern India. Gondwana Research, 16, 27-36, doi: https://doi.org/10.1016/j.gr.2008.11.001.

Cobbing, E.J. 2011. Granitic Rocks. In: Ridd, M.F., Barber, A.J. & Crow, M.J. (eds.) The Geology of Thailand. The Geological Society, London, 443-457.

Cocks, L.R.M. & Torsvik, T.H. 2013. The dynamic evolution of the Palaeozoic geography of eastern Asia. Earth-Science Reviews, 117, 40-79, doi: http://dx.doi.org/10.1016/j.earscirev.2012.12.001.

Collins, A.S. 2003. Structure and age of the northern Leeuwin Complex, Western Australia: Constraints from field mapping and U–Pb isotopic analysis. Australian Journal of Earth

Sciences, 50, 585-599, doi: 10.1046/j.1440-0952.2003.01014.x.

Collins, A.S., Clark, C. & Plavsa, D. 2014. Peninsular India in Gondwana: The tectonothermal evolution of the Southern Granulite Terrain and its Gondwanan counterparts. Gondwana Research, 25, 190-203, doi: https://doi.org/10.1016/j.gr.2013.01.002.

Condie, K.C., Belousova, E., Griffin, W.L. & Sircombe, K.N. 2009. Granitoid events in space and time: Constraints from igneous and detrital zircon age spectra. Gondwana Research, 15, 228-242, doi: https://doi.org/10.1016/j.gr.2008.06.001.

De Pelsmaeker, E., Jolivet, M., Laborde, A., Poujol, M., Robin, C., Zhimulev, F.I., Nachtergaele, S., Glorie, S., De Clercq, S., Batalev, V.Y. & De Grave, J. 2018. Source-to-sink dynamics in the Kyrgyz Tien Shan from the Jurassic to the Paleogene: Insights from sedimentological and detrital zircon U-Pb analyses. Gondwana Research, 54, 180-204, doi: https://doi.org/10.1016/j.gr.2017.09.004.

Dew, R.E.C., Collins, A.S., Glorie, S., Morley, C.K., Blades, M.L., Nachtergaele, S., King, R., Foden, J., De Grave, J., Kanjanapayont, P., Evans, N.J., Alessio, B.L. & Charusiri, P. 2018a. Probing into Thailand's basement: New insights from U–Pb geochronology, Sr, Sm–Nd, Pb and Lu–Hf isotopic systems from granitoids. Lithos, 320-321, 332-354, doi: 10.1016/j.lithos.2018.09.019.

Dew, R.E.C., King, R., Collins, A.S., Morley, C.K., Arboit, F. & Glorie, S. 2018b. Stratigraphy of deformed Permian carbonate reefs in Saraburi Province, Thailand. Journal of the Geological Society, 175, 163-175, doi: 10.1144/jgs2017-035.

Dew, R.E.C., Nachtergaele, S., Collins, A.S., Glorie, S., Foden, J., De Grave, J., Blades, M.L., Morley, C.K., Evans, N.J., Alessio, B.L., Kanjanapayont, P., King, R. & Charusiri, P. 2018c. Data analysis of the U–Pb geochronology and Lu–Hf system in zircon and whole-rock Sr, Sm–Nd and Pb isotopic systems for the granitoids of Thailand. Data in Brief, 21, 1794-1809, doi: https://doi.org/10.1016/j.dib.2018.10.176.

Dickinson, W.R. & Gehrels, G.E. 2009. Use of U–Pb ages of detrital zircons to infer maximum depositional ages of strata: A test against a Colorado Plateau Mesozoic database. Earth and Planetary Science Letters, 288, 115-125, doi: https://doi.org/10.1016/j.epsl.2009.09.013.

Domeier, M. & Torsvik, T.H. 2014. Plate tectonics in the late Paleozoic. Geoscience Frontiers, 5, 303-350, doi: http://dx.doi.org/10.1016/j.gsf.2014.01.002.

Dong, C., Li, C., Wan, Y., Wang, W., Wu, Y., Xie, H. & Liu, D. 2011. Detrital zircon age model of Ordovician Wenquan quartzite south of Lungmuco-Shuanghu Suture in the Qiangtang area, Tibet: Constraint on tectonic affinity and source regions. Science China Earth Sciences, 54, 1034-1042, doi: 10.1007/s11430-010-4166-x.

Faure, M., Lepvrier, C., Nguyen, V.V., Vu, T.V., Lin, W. & Chen, Z. 2014. The South China block-Indochina collision: Where, when, and how? Journal of Asian Earth Sciences, 79, 260-274, doi: https://doi.org/10.1016/j.jseaes.2013.09.022.

Faure, M., Nguyen, V.V., Hoai, L.T.T. & Lepvrier, C. 2018. Early Paleozoic or Early-Middle Triassic collision between the South China and Indochina Blocks: The controversy resolved? Structural insights from the Kon Tum massif (Central Vietnam). Journal of Asian Earth Sciences, 166, 162-180, doi: https://doi.org/10.1016/j.jseaes.2018.07.015.

Fisher, C.M., Vervoort, J.D. & DuFrane, S.A. 2014. Accurate Hf isotope determinations of complex zircons using the "laser ablation split stream" method. Geochemistry, Geophysics, Geosystems, 15, 121-139, doi: 10.1002/2013GC004962.

Fitzsimons, I.C.W. 2000. Grenville-age basement provinces in East Antarctica: Evidence for three separate collisional orogens. Geology, 28, 879-882, doi:10.1130/0091-7613(2000)28<879:GBPIEA>2.0.CO;2.

Fitzsimons, I.C.W. 2003. Proterozoic basement provinces of southern and southwestern Australia, and their correlation with Antarctica. Geological Society, London, Special Publications, 206, 93-130, doi: 10.1144/gsl.sp.2003.206.01.07.

Flowerdew, M.J., Millar, I.L., Curtis, M.L., Vaughan, A.P.M., Horstwood, M.S.A., Whitehouse, M.J. & Fanning, C.M. 2007. Combined U-Pb geochronology and Hf isotope geochemistry of detrital zircons from early Paleozoic sedimentary rocks, Ellsworth-Whitmore Mountains block, Antarctica. Geological Society of America Bulletin, 119, 275-288, doi: 10.1130/b25891.1.

Fontaine, H. 2002. Permian of Southeast Asia: An overview. Journal of Asian Earth Sciences, 20, 567-588, doi: 10.1016/S1367-9120(01)00076-1.

Gardiner, N.J., Searle, M.P., Morley, C.K.,

Whitehouse, M.P., Spencer, C.J. & Robb, L.J. 2016. The closure of Palaeo-Tethys in Eastern Myanmar and Northern Thailand: New insights from zircon U-Pb and Hf isotope data. Gondwana Research, 39, 401-422, doi: 10.1016/j.gr.2015.03.001.

Gehrels, G. 2012. Detrital Zircon U-Pb Geochronology: Current Methods and New Opportunities. In: Busby, C. & Azor, A. (eds.) Tectonics of Sedimentary Basins: Recent Advances. Wiley, Online Library, 45-62.

Glorie, S., De Grave, J., Buslov, M.M., Zhimulev, F.I. & Safonova, I.Y. 2014. Detrital zircon provenance of early Palaeozoic sediments at the southwestern margin of the Siberian Craton: Insights from U–Pb geochronology. Journal of Asian Earth Sciences, 82, 115-123, doi: https://doi.org/10.1016/j.jseaes.2013.12.007.

Halpin, J.A., Tran, H.T., Lai, C.-K., Meffre, S., Crawford, A.J. & Zaw, K. 2016. U–Pb zircon geochronology and geochemistry from NE Vietnam: A 'tectonically disputed' territory between the Indochina and South China blocks. Gondwana Research, 34, 254-273, doi: https://doi.org/10.1016/j.gr.2015.04.005.

Hand, M., Reid, A. & Jagodzinski, L. 2007. Tectonic Framework and Evolution of the Gawler Craton, Southern Australia. Economic Geology, 102, 1377-1395, doi: 10.2113/gsecongeo.102.8.1377.

Hansberry, R.L., Collins, A.S., King, R.C., Morley, C.K., Giże, A.P., Warren, J., Löhr, S.C. & Hall, P.A. 2015. Syn-deformation temperature and fossil fluid pathways along an exhumed detachment zone, khao khwang fold-thrust belt, Thailand. Tectonophysics, 655, 73-87, doi: http://dx.doi.org/10.1016/j.tecto.2015.05.012.

Hansberry, R.L., Zwingmann, H., Loehr, S., Collins, A.S., King, R.C., Morley, C.K. & Drysdale, R.N. 2017. Constraining the timing of shale detachment faulting: A geochemical approach. Lithosphere, 9, 431-440, doi: 10.1130/L612.1.

Hansen, B.T. & Wemmer, K. 2011. Age and evolution of the basement in Thailand. In: Ridd, M.F., Barber, A.J. & Crow, M.J. (eds.) The Geology of Thailand. The Geological Society, London, 19-32.

Hara, H., Hirano, M., Kurihara, T., Takahashi, T. & Ueda, H. 2018a. Permian arc evolution associated with Panthalassa subduction along the eastern margin of the South China block, based on sandstone provenance and U–Pb detrital zircon ages of the Kurosegawa belt, Southwest Japan. Journal of Asian Earth Sciences, 151, 112-130, doi: 10.1016/j.jseaes.2017.10.025.

Hara, H., Kon, Y., Usuki, T., Lan, C.Y., Kamata, Y., Hisada, K.I., Ueno, K., Charoentitirat, T. & Charusiri, P. 2013. U-Pb ages of detrital zircons within the Inthanon Zone of the Paleo-Tethyan subduction zone, northern Thailand: New constraints on accretionary age and arc activity. Journal of Asian Earth Sciences, 74, 50-61, doi: 10.1016/j.jseaes.2013.06.006.

Hara, H., Kunii, M., Hisada, K.I., Ueno, K., Kamata, Y., Srichan, W., Charusiri, P., Charoentitirat, T., Watarai, M., Adachi, Y. & Kurihara, T. 2012. Petrography and geochemistry of clastic rocks within the Inthanon zone, northern Thailand: Implications for Paleo-Tethys subduction and convergence. Journal of Asian Earth Sciences, 61, 2-15, doi: 10.1016/j.jseaes.2012.06.012.

Hara, H., Kunii, M., Miyake, Y., Hisada, K.I., Kamata, Y., Ueno, K., Kon, Y., Kurihara, T., Ueda, H., Assavapatchara, S., Treerotchananon, A., Charoentitirat, T. & Charusiri, P. 2017. Sandstone provenance and U–Pb ages of detrital zircons from Permian–Triassic forearc sediments within the Sukhothai Arc, northern Thailand: Record of volcanic-arc evolution in response to Paleo-Tethys subduction. Journal of Asian Earth Sciences, 146, 30-55, doi: 10.1016/j.jseaes.2017.04.021.

Hara, H., Tokiwa, T., Kurihara, T., Charoentitirat, T., Ngamnithiporn, A., Visetnat, K., Tominaga, K., Kamata, Y. & Ueno, K. 2018b. Permian–Triassic back-arc basin development in response to Paleo-Tethys subduction, Sa Kaeo–Chanthaburi area in Southeastern Thailand. Gondwana Research, 64, 50-66, doi: https://doi.org/10.1016/j.gr.2018.06.007.

Hisada, K.-i., Sugiyama, M., Ueno, K., Charusiri, P. & Arai, S. 2004. Missing ophiolitic rocks along the Mae Yuam Fault as the Gondwana–Tethys divide in north-west Thailand. Island Arc, 13, 119-127, doi: 10.1111/j.1440-1738.2003.00412.x.

Hu, L., Cawood, P.A., Du, Y., Xu, Y., Xu, W. & Huang, H. 2015. Detrital records for Upper Permian-Lower Triassic succession in the Shiwandashan Basin, South China and implication for Permo-Triassic (Indosinian) orogeny. Journal of Asian Earth Sciences, 98, 152-166, doi: http://dx.doi.org/10.1016/j.jseaes.2014.11.007.

Hughes, I.G. & Bateson, J.H. 1967. Reconnaissance geological and mineral survey of the Chanthaburi area of South-east Thailand. Institute of Geological Sciences Report 7.

Jackson, S.E., Pearson, N.J., Griffin, W.L. & Belousova, E.A. 2004. The application of laser ablation-inductively coupled plasma-

mass spectrometry to in situ U–Pb zircon geochronology. Chemical Geology, 211, 47-69, doi: https://doi.org/10.1016/j.chemgeo.2004.06.017.

Jiang, H., Li, W.-Q., Jiang, S.-Y., Wang, H. & Wei, X.-P. 2017. Geochronological, geochemical and Sr-Nd-Hf isotopic constraints on the petrogenesis of Late Cretaceous A-type granites from the Sibumasu Block, Southern Myanmar, SE Asia. Lithos, 268–271, 32-47, doi: http://dx.doi.org/10.1016/j.lithos.2016.11.005.

Kamata, Y., Ueno, K., Hara, H., Ichise, M., Charoentitirat, T., Charusiri, P., Sardsud, A. & Hisada, K.-i. 2009. Classification of the Sibumasu and Paleo-Tethys tectonic division in Thailand using chert lithofacies. Island Arc, 18, 21-31, doi: doi:10.1111/j.1440-1738.2008.00652.x.

Kamata, Y., Ueno, K., Miyahigashi, A., Hara, H., Hisada, K.-i., Charoentitirat, T. & Charusiri, P. 2016. Geological significance of the discovery of Middle Triassic (Ladinian) radiolarians from the Hong Hoi Formation of the Lampang Group, Sukhothai Zone, northern Thailand. Revue de Micropaléontologie, 59, 347-358, doi: 10.1016/j.revmic.2016.08.002.

Kamvong, T., Khin, Z., Meffre, S., Maas, R., Stein, H. & Lai, C.-K. 2014. Adakites in the Truong Son and Loei fold belts, Thailand and Laos: Genesis and implications for geodynamics and metallogeny. Gondwana Research, 26, 165-184, doi: http://dx.doi.org/10.1016/j.gr.2013.06.011.

Kawakami, T., Nakano, N., Higashino, F., Hokada, T., Osanai, Y., Yuhara, M., Charusiri, P., Kamikubo, H., Yonemura, K. & Hirata, T. 2014. U-Pb zircon and CHIME monazite dating of granitoids and high-grade metamorphic rocks from the Eastern and Peninsular Thailand — A new report of Early Paleozoic granite. Lithos, 200–201, 64-79, doi: http://dx.doi.org/10.1016/j.lithos.2014.04.012.

Kelsey, D.E., Wade, B.P., Collins, A.S., Hand, M., Sealing, C.R. & Netting, A. 2008. Discovery of a Neoproterozoic basin in the Prydz belt in East Antarctica and its implications for Gondwana assembly and ultrahigh temperature metamorphism. Precambrian Research, 161, 355-388, doi: https://doi.org/10.1016/j.precamres.2007.09.003.

Kettanah, Y.A., Mory, A.J., Wach, G.D. & Wingate, M.T.D. 2015. Provenance of the Ordovician–lower Silurian Tumblagooda Sandstone, Western Australia. Australian Journal of Earth Sciences, 62, 817-830, doi: 10.1080/08120099.2015.1117020.

Kroener, A., Hegner, E., Collins, A.S., Windley, B.F., Brewer, T.S., Razakamanana, T. & Pidgeon, R.T. 2000. Age and magmatic history of the Antananarivo Block, central Madagascar, as derived from zircon geochronology and Nd isotopic systematics. American Journal of Science, 300, 251-288, doi: 10.2475/ajs.300.4.251.

Lan, C.Y., Chung, S.L., Van Long, T., Lo, C.H., Lee, T.-Y., Mertzman, S.A. & Shen, J.J.-S. 2003. Geochemical and Sr–Nd isotopic constraints from the Kontum massif, central Vietnam on the crustal evolution of the Indochina block. Precambrian Research, 7-27.

Lepvrier, C., Maluski, H., Van Tich, V., Leyreloup, A., Truong Thi, P. & Van Vuong, N. 2004. The Early Triassic Indosinian orogeny in Vietnam (Truong Son Belt and Kontum Massif); implications for the geodynamic evolution of Indochina. Tectonophysics, 393, 87-118, doi: http://dx.doi.org/10.1016/j.tecto.2004.07.030.

Li, G., Sandiford, M., Liu, X., Xu, Z., Wei, L. & Li, H. 2014. Provenance of Late Triassic sediments in central Lhasa terrane, Tibet and its implication. Gondwana Research, 25, 1680-1689, doi: https://doi.org/10.1016/j.gr.2013.06.019.

Li, P., Rui, G., Junwen, C. & Ye, G. 2004. Paleomagnetic analysis of eastern Tibet: implications for the collisional and amalgamation history of the Three Rivers Region, SW China. Journal of Asian Earth Sciences, 24, 291-310, doi: http://dx.doi.org/10.1016/j.jseaes.2003.12.003.

Li, X.-H., Li, Z.-X., He, B., Li, W.-X., Li, Q.-L., Gao, Y. & Wang, X.-C. 2012. The Early Permian active continental margin and crustal growth of the Cathaysia Block: In situ U–Pb, Lu–Hf and O isotope analyses of detrital zircons. Chemical Geology, 328, 195-207, doi: https://doi.org/10.1016/j.chemgeo.2011.10.027.

Loydell, D.K. & Aung, K.P. 2017. The "Panghkawkwo graptolite bed" (Llandovery, Silurian), Myanmar and the location of the Sibumasu (or Sibuma) Terrane in the Silurian. Palaeogeography, Palaeoclimatology, Palaeoecology, 469, 1-17, doi: https://doi.org/10.1016/j.palaeo.2016.12.028.

Meffre, S., Khin, Z., Khositanont, S., Halpin, J. & Cumming, G. 2008. 'Tectonic evolution of SE Asia', 'Ore Deposits of SE Asia' - Annual Report to Sponsors. CODES.

Metcalfe, I. 1984. Stratigraphy, palaeontology

and palaeogeography of the Carboniferous of Southeast Asia. Memoires de la Societe Geologique de France, 147, 107-118.

Metcalfe, I. 2000. The Bentong–Raub Suture Zone. Journal of Asian Earth Sciences, 18, 691-712, doi: https://doi.org/10.1016/S1367-9120(00)00043-2.

Metcalfe, I. 2013. Gondwana dispersion and Asian accretion: Tectonic and palaeogeographic evolution of eastern Tethys. Journal of Asian Earth Sciences, 66, 1-33, doi: http://dx.doi.org/10.1016/j.jseaes.2012.12.020.

Minezaki, T., Hisada, K.-i., Hara, H. & Kamata, Y. 2018. Tectono-stratigraphy of Late Carboniferous to Triassic successions of the Khorat Plateau Basin, Indochina Block, northeastern Thailand: Initiation of the Indosinian Orogeny by collision of the Indochina and South China blocks. Journal of Asian Earth Sciences, doi: https://doi.org/10.1016/j.jseaes.2018.10.020.

Moghadam, H.S., Li, X.-H., Griffin, W.L., Stern, R.J., Thomsen, T.B., Meinhold, G., Aharipour, R. & O'Reilly, S.Y. 2017. Early Paleozoic tectonic reconstruction of Iran: Tales from detrital zircon geochronology. Lithos, 268-271, 87-101, doi: https://doi.org/10.1016/j.lithos.2016.09.008.

Morel, M.L.A., Nebel, O., Nebel-Jacobsen, Y.J., Miller, J.S. & Vroon, P.Z. 2008. Hafnium isotope characterisation of the GJ-1 zircon reference material by solution and laser-ablation MC-ICPMS. Chemical Geology, 231-235.

Morley, C.K. 2018. Understanding Sibumasu in the context of ribbon continents. Gondwana Research, 64, 184-215, doi: https://doi.org/10.1016/j.gr.2018.07.006.

Morley, C.K., Ampaiwan, P., Thanudamrong, S., Kuenphan, N. & Warren, J. 2013. Development of the Khao Khwang fold and thrust belt; implications for the geodynamic setting of Thailand and Cambodia during the Indosinian Orogeny. Journal of Asian Earth Sciences, 62, 705-719, doi: http://dx.doi.org/10.1016/j.jseaes.2012.11.021.

Myrow, P.M., Hughes, N.C., Goodge, J.W., Fanning, C.M., Williams, I.S., Peng, S., Bhargava, O.N., Parcha, S.K. & Pogue, K.R. 2010. Extraordinary transport and mixing of sediment across Himalayan central Gondwana during the Cambrian–Ordovician. GSA Bulletin, 122, 1660-1670, doi: 10.1130/B30123.1.

Nagy, E.A., Maluski, H., Lepvrier, C., Schärer, U., Truong Thi, P., Leyreloup, A. & Van Thich, V. 2001. Geodynamic Significance of the Kontum Massif in Central Vietnam: Composite 40Ar/39Ar and U-Pb Ages from Paleozoic to Triassic. The Journal of Geology, 109, 755-770.

Nakano, N., Osanai, Y., Nam, N.V. & Tri, T.V. 2018. Bauxite to eclogite: Evidence for late Permian supracontinental subduction at the Red River shear zone, northern Vietnam. Lithos, 302-303, 37-49, doi: https://doi.org/10.1016/j.lithos.2017.12.023.

Ng, S.W., Chung, S.L., Robb, L.J., Searle, M.P., Ghani, A.A., Whitehouse, M.J., Oliver, G.J.H., Sone, M., Gardiner, N.J. & Roselee, M.H. 2015a. Petrogenesis of Malaysian granitoids in the Southeast Asian tin belt: Part 1. Geochemical and Sr-Nd isotopic characteristics. Bulletin of the Geological Society of America, 127, 1209-1237, doi: 10.1130/B31213.1.

Ng, S.W., Whitehouse, M.J., Searle, M.P., Robb, L.J., Ghani, A.A., Chung, S.L., Oliver, G.J.H., Sone, M., Gardiner, N.J. & Roselee, M.H. 2015b. Petrogenesis of Malaysian granitoids in the Southeast Asian tin belt: Part 2. U-Pb zircon geochronology and tectonic model. Bulletin of the Geological Society of America, 127, 1238-1258, doi: 10.1130/B31214.1.

Nordsvan, A.R., Collins, W.J., Li, Z.-X., Spencer, C.J., Pourteau, A., Withnall, I.W., Betts, P.G. & Volante, S. 2018. Laurentian crust in northeast Australia: Implications for the assembly of the supercontinent Nuna. Geology, 46, 251-254, doi: 10.1130/G39980.1.

Nulay, P., Chonglakmani, C. & Feng, Q. 2016. Petrography, geochemistry and U-Pb detrital zircon dating of the clastic Phu Khat Formation in the Nakhon Thai region, Thailand: Implications for provenance and geotectonic setting. Journal of Earth Science, 27, 329-349, doi: 10.1007/s12583-016-0667-7.

Paton, C., Hellstrom, J., Paul, B., Woodhead, J. & Hergt, J. 2011. Iolite: Freeware for the visualisation and processing of mass spectrometric data. Journal of Analytical Atomic Spectrometry, 26, 2508-2518, doi: 10.1039/c1ja10172b.

Payne, J.L., Barovich, K.M. & Hand, M. 2006. Provenance of metasedimentary rocks in the northern Gawler Craton, Australia: Implications for Palaeoproterozoic reconstructions. Precambrian Research, 148, 275-291, doi: https://doi.org/10.1016/j.precamres.2006.05.002.

Qian, X., Feng, Q., Wang, Y., Chonglakmani, C. & Monjai, D. 2016. Geochronological and geochemical constraints on the mafic rocks

along the Luang Prabang zone: Carboniferous back-arc setting in northwest Laos. Lithos, 245, 60-75, doi: https://doi.org/10.1016/j.lithos.2015.07.019.

Qian, X., Feng, Q., Wang, Y., Zhao, T., Zi, J.-W., Udchachon, M. & Wang, Y. 2017. Late Triassic post-collisional granites related to Paleotethyan evolution in SE Thailand: Geochronological and geochemical constraints. Lithos, 286, 440-453, doi: http://dx.doi.org/10.1016/j.lithos.2017.06.026.

Racey, A., Love, M.A., Canham, A.C., Goodall, J.G.S., Polachan, S. & Jones, P.D. 1996. Stratigraphy and reservoir potential of the Mesozoic Khorat Group, NE Thailand: Part 1: Stratigraphy and Sedimentary Evolution. Journal of Petroleum Geology, 19, 5-40, doi: doi:10.1111/j.1747-5457.1996.tb00511.x.

Ridd, M.F. 2011. Lower Palaeozoic. In: Ridd, M.F., Barber, A.J. & Crow, M.J. (eds.) The Geology of Thailand. The Geological Society, London, 33-51.

Ridd, M.F. 2013. A Middle Permian–Middle Triassic accretionary complex and a Late Triassic foredeep basin: Forerunners of an Indosinian (Late Triassic) thrust complex in the Thailand–Malaysia border area. Journal of Asian Earth Sciences, 76, 99-114, doi: https://doi.org/10.1016/j.jseaes.2012.09.030.

Ridd, M.F. 2015. Should Sibumasu be renamed Sibuma? The case for a discrete Gondwana-derived block embracing western Myanmar, upper Peninsular Thailand and NE Sumatra. Journal of the Geological Society, doi: 10.1144/jgs2015-065.

Rossignol, C., Bourquin, S., Poujol, M., Hallot, E., Dabard, M.-P. & Nalpas, T. 2016. The volcaniclastic series from the Luang Prabang Basin, Laos: A witness of a triassic magmatic arc? Journal of Asian Earth Sciences, 120, 159-183, doi: https://doi.org/10.1016/j.jseaes.2016.02.001.

Salam, A.A., Zaw, K., Meffre, S., McPhie, J. & Lai, C.-K. 2014. Geochemistry and geochronology of the Chatree epithermal gold-silver deposit: Implications for the tectonic setting of the Loei Fold Belt, central Thailand. Gondwana Research, 26, 198-217.

Schmitt, R.d.S., Fragoso, R.d.A. & Collins, A.S. 2018. Suturing Gondwana in the Cambrian: The Orogenic Events of the Final Amalgamation. In: Siegesmund, S., Basei, M.A.S., Oyhantçabal, P. & Oriolo, S. (eds.) Geology of Southwest Gondwana. Springer International Publishing, Cham, 411-432.

Schwartz, M.O., Rajah, S.S., Askury, A.K., Putthapiban, P. & Djaswadi, S. 1995. The Southeast Asian tin belt. Earth-Science Reviews, 38, 95-293, doi: https://doi.org/10.1016/0012-8252(95)00004-T.

Searle, M.P., Whitehouse, M.J., Robb, L.J., Ghani, A.A., Hutchison, C.S., Sone, M., Ng, S.W.P., Roselee, M.H., Chung, S.L. & Oliver, G.J.H. 2012. Tectonic evolution of the Sibumasu-Indochina terrane collision zone in Thailand and Malaysia: Constraints from new U-Pb zircon chronology of SE Asian tin granitoids. Journal of the Geological Society, 169, 489-500, doi: 10.1144/0016-76492011-107.

Seton, M., Müller, R.D., Zahirovic, S., Gaina, C., Torsvik, T., Shephard, G., Talsma, A., Gurnis, M., Turner, M., Maus, S. & Chandler, M. 2012. Global continental and ocean basin reconstructions since 200 Ma. Earth-Science Reviews, 113, 212-270, doi: http://dx.doi.org/10.1016/j.earscirev.2012.03.002.

Sevastjanova, I., Clements, B., Hall, R., Belousova, E.A., Griffin, W.L. & Pearson, N. 2011. Granitic magmatism, basement ages, and provenance indicators in the Malay Peninsula: Insights from detrital zircon U–Pb and Hf-isotope data. Gondwana Research, 19, 1024-1039, doi: 10.1016/j.gr.2010.10.010.

Sevastjanova, I., Hall, R., Rittner, M., Paw, S.M.T.L., Naing, T.T., Alderton, D.H. & Comfort, G. 2016. Myanmar and Asia united, Australia left behind long ago. Gondwana Research, 32, 24-40, doi: https://doi.org/10.1016/j.gr.2015.02.001.

Shen, L., Yu, J.-H., O'Reilly, S.Y., Griffin, W.L. & Zhou, X. 2018. Subduction-related middle Permian to early Triassic magmatism in central Hainan Island, South China. Lithos, 318-319, 158-175, doi: https://doi.org/10.1016/j.lithos.2018.08.009.

Shi, M.F., Lin, F.C., Fan, W.Y., Deng, Q., Cong, F., Tran, M.D., Zhu, H.P. & Wang, H. 2015. Zircon U-Pb ages and geochemistry of granitoids in the Truong Son terrane, Vietnam: Tectonic and metallogenic implications. Journal of Asian Earth Sciences, 101, 101-120, doi: 10.1016/j.jseaes.2015.02.001.

Singharajwarapan, S. & Berry, R. 2000. Tectonic implications of the Nan Suture Zone and its relationship to the Sukhothai Fold Belt, Northern Thailand. Journal of Asian Earth Sciences, 18, 663-673, doi: http://dx.doi.org/10.1016/S1367-9120(00)00017-1.

Sircombe, K.N. & Freeman, M.J. 1999. Provenance of detrital zircons on the Western Australia

coastline—Implications for the geologic history of the Perth basin and denudation of the Yilgarn craton. Geology, 27, 879-882, doi: 10.1130/0091-7613(1999)027<0879:PODZOT>2.3.CO;2.

Sláma, J., Košler, J., Condon, D.J., Crowley, J.L., Gerdes, A., Hanchar, J.M., Horstwood, M.S.A., Morris, G.A., Nasdala, L., Norberg, N., Schaltegger, U., Schoene, B., Tubrett, M.N. & Whitehouse, M.J. 2008. Plešovice zircon — A new natural reference material for U–Pb and Hf isotopic microanalysis. Chemical Geology, 249, 1-35, doi: https://doi.org/10.1016/j.chemgeo.2007.11.005.

Sone, M. & Metcalfe, I. 2008. Parallel Tethyan sutures in mainland Southeast Asia: New insights for Palaeo-Tethys closure and implications for the Indosinian orogeny. Comptes Rendus - Geoscience, 340, 166-179, doi: 10.1016/j.crte.2007.09.008.

Sone, M., Metcalfe, I. & Chaodumrong, P. 2012. The Chanthaburi terrane of southeastern Thailand: Stratigraphic confirmation as a disrupted segment of the Sukhothai Arc. Journal of Asian Earth Sciences, 61, 16-32, doi: 10.1016/j.jseaes.2012.08.021.

Srinak, N., Hisada, K., Kamata, Y. & Charusiri, P. 2007. Stratigraphy of the Mae Sariang Group of Northwestern Thailand: Implication for Paleoenvironments and Tectonic Setting. The Natural History Journal of Chulalongkorn University, 7, 87-108.

Thirlwall, M.F. & Anczkiewicz, R. 2004. Multidynamic isotope ratio analysis using MC–ICP–MS and the causes of secular drift in Hf, Nd and Pb isotope ratios. International Journal of Mass Spectrometry, 235, 59-81, doi: https://doi.org/10.1016/j.ijms.2004.04.002.

Tofke, T., Lumijuan, A. & Helmcke, D. 1993. Triassic syn-orogenic siliciclastics from the area of Mae Sariang (northwestern Thailand). In: T., T. (ed.) International Biostratigraphy of Mainland Southeast Asia: Facies and Paleontology Symposium, Chiang Mai University, Chiang Mai, 391-400.

Toriyama, R. 1967. The Rat Buri Limestone of Thailand. 13-20.

Ueno, K. & Charoentitirat, T. 2011. Carboniferous and Permian. In: Ridd, M.F., Barber, A.J. & Crow, M.J. (eds.) The Geology of Thailand. The Geological Society, London, 71-136.

Ueno, K. & Hisada, K. 2001. The Nan-Uttaradit-Sa Kaeo Suture as a main Paleo-Tethyan suture in Thailand: Is it real? . Gondwana Research, 804-805.

Usuki, T., Lan, C.-Y., Wang, K.-L. & Chiu, H.-Y. 2013. Linking the Indochina block and Gondwana during the Early Paleozoic: Evidence from U–Pb ages and Hf isotopes of detrital zircons. Tectonophysics, 586, 145-159, doi: http://dx.doi.org/10.1016/j.tecto.2012.11.010.

Veevers, J.J., Belousova, E.A., Saeed, A., Sircombe, K., Cooper, A.F. & Read, S.E. 2006. Pan-Gondwanaland detrital zircons from Australia analysed for Hf-isotopes and trace elements reflect an ice-covered Antarctic provenance of 700–500 Ma age, TDM of 2.0–1.0 Ga, and alkaline affinity. Earth-Science Reviews, 76, 135-174, doi: https://doi.org/10.1016/j.earscirev.2005.11.001.

Veevers, J.J., Saeed, A., Belousova, E.A. & Griffin, W.L. 2005. U–Pb ages and source composition by Hf-isotope and trace-element analysis of detrital zircons in Permian sandstone and modern sand from southwestern Australia and a review of the paleogeographical and denudational history of the Yilgarn Craton. Earth-Science Reviews, 68, 245-279, doi: https://doi.org/10.1016/j.earscirev.2004.05.005.

Vermeesch, P. 2012. On the visualisation of detrital age distributions. Chemical Geology, 312-313, 190-194, doi: https://doi.org/10.1016/j.chemgeo.2012.04.021.

Vermeesch, P. 2013. Multi-sample comparison of detrital age distributions. Chemical Geology, 341, 140-146, doi: 10.1016/j.chemgeo.2013.01.010.

Vermeesch, P., Resentini, A. & Garzanti, E. 2016. An R package for statistical provenance analysis. Sedimentary Geology, 336, 14-25, doi: http://dx.doi.org/10.1016/j.sedgeo.2016.01.009.

von Braun, E., Hahn, L. & Maronde, H.-D. 1981. Sheet 6 (Amphoe Li). Geological Map of Northern Thailand Sheet 6.

Wang, M., Li, C. & Ming-Xie, C. 2015. Dating of detrital zircons from the Dabure clastic rocks: the discovery of Neoproterozoic strata in southern Qiangtang, Tibet. International Geology Review, 1-12, doi: 10.1080/00206814.2015.1065207.

Wang, S., Mo, Y., Wang, C. & Ye, P. 2016a. Paleotethyan evolution of the Indochina Block as deduced from granites in northern Laos. Gondwana Research, 38, 183-196, doi: https://doi.org/10.1016/j.gr.2015.11.011.

Wang, Y., He, H., Cawood, P.A., Srithai, B., Feng, Q., Fan, W., Zhang, Y. & Qian, X. 2016b. Geochronological, elemental and Sr-Nd-Hf-O isotopic constraints on the petrogenesis of the

Triassic post-collisional granitic rocks in NW Thailand and its Paleotethyan implications. Lithos, 266-267, 264-286, doi: https://doi.org/10.1016/j.lithos.2016.09.012.

Warren, J., Morley, C.K., Charoentitirat, T., Cartwright, I., Ampaiwan, P., Khositchaisri, P., Mirzaloo, M. & Yingyuen, J. 2014. Structural and fluid evolution of Saraburi Group sedimentary carbonates, central Thailand: A tectonically driven fluid system. Marine and Petroleum Geology, 55, 100-121, doi: http://dx.doi.org/10.1016/j.marpetgeo.2013.12.019.

Wiedenbeck, M., AllÉ, P., Corfu, F., Griffin, W.L., Meier, M., Oberli, F., Quadt, A.V., Roddick, J.C. & Spiegel, W. 1995. Three natural zircon standards for U–Th–Pb, Lu–Hf, trace element and REE analyses. Geostandards Newsletter, 19, 1-23, doi: 10.1111/j.1751-908X.1995.tb00147.x.

Woodhead, J.D. & Hergt, J.M. 2005. A Preliminary Appraisal of Seven Natural Zircon Reference Materials for In Situ Hf Isotope Determination. Geostandards and Geoanalytical Research, 29, 183-195, doi: 10.1111/j.1751-908X.2005.tb00891.x.

Xu, Y., Cawood, P.A., Du, Y., Hu, L., Yu, W., Zhu, Y. & Li, W. 2013. Linking south China to northern Australia and India on the margin of Gondwana: Constraints from detrital zircon U-Pb and Hf isotopes in Cambrian strata. Tectonics, 32, 1547-1558, doi: doi:10.1002/tect.20099.

Yan, Y., Huang, B., Zhang, D., Charusiri, P. & Veeravinantanakul, A. 2018. Paleomagnetic Study on the Permian Rocks of the Indochina Block and Its Implications for Paleogeographic Configuration and Northward Drifting of Cathaysialand in the Paleo-Tethys. Journal of Geophysical Research: Solid Earth, 0, doi: 10.1029/2018jb015511.

Yan, Y., Huang, B., Zhao, J., Zhang, D., Liu, X., Charusiri, P. & Veeravinantanakul, A. 2017. Large southward motion and clockwise rotation of Indochina throughout the Mesozoic: Paleomagnetic and detrital zircon U–Pb geochronological constraints. Earth and Planetary Science Letters, 459, 264-278, doi: https://doi.org/10.1016/j.epsl.2016.11.035.

Zaw, K., Meffre, S., Lai, C.-K., Burrett, C., Santosh, M., Graham, I., Manaka, T., Salam, A., Kamvong, T. & Cromie, P. 2014. Tectonics and metallogeny of mainland Southeast Asia — A review and contribution. Gondwana Research, 26, 5-30, doi: http://dx.doi.org/10.1016/j.gr.2013.10.010.

Zhang, X., Chung, S.-L., Lai, Y.-M., Ghani, A.A., Murtadha, S., Lee, H.-Y. & Hsu, C.-C. 2018. Detrital Zircons Dismember Sibumasu in East Gondwana. Journal of Geophysical Research: Solid Earth, 123, doi: 10.1029/2018jb015780.

Zhao, G., Wang, Y., Huang, B., Dong, Y., Li, S., Zhang, G. & Yu, S. 2018. Geological reconstructions of the East Asian blocks: From the breakup of Rodinia to the assembly of Pangea. Earth-Science Reviews, 186, 262-286, doi: https://doi.org/10.1016/j.earscirev.2018.10.003.

Zhu, D.-C., Zhao, Z.-D., Niu, Y., Dilek, Y. & Mo, X.-X. 2011. Lhasa terrane in southern Tibet came from Australia. Geology, 39, 727-730.

CHAPTER 5

This chapter is in review with the *Journal of Asian Earth Sciences* as:

Dew, R.E.C., Morley, C.K., Tin Aung Myint & Collins, A. Age and provenance of the Chaung Magyi Group, Yeywa Dome, Myanmar, based on U–Pb dating of detrital zircons. *Journal of Asian Earth Sciences*.

Research data related to this submission is held within Mendeley Data Repositiory
https://data.mendeley.com/datasets/phnnnvv4gs/draft?a=ade12e75-5b7f-470fb761-d6c06841e358

Statement of Authorship

Title of Paper	Age and provenance of the Chaung Magyi Group, Yewa Dome, Myanmar, based on U-Pb dating of detrital zircons
Publication Status	☐ Published ☐ Accepted for Publication ☐ Submitted for Publication ☐ Unpublished and Unsubmitted w ork w ritten in manuscript style
Publication Details	Dew, R.E.C., Morley, C.K., Tin Aung Myint and Collins, A.S. (in review). Age and provenance of the Chaung Magyi Group, Yewa Dome, Myanmar, based on U-Pb dating of detrital zircons, *Journal of Asian Earth Sciences*.

Principal Author

Name of Principal Author (Candidate)	Romana E.C. Dew		
Contribution to the Paper	Performed all sample preparation and analysis, interpreted data and created resultant figures, wrote methodology and results sections of manuscript, provided comparison data for discussion and edited full manuscript.		
Overall percentage (%)	55		
Certification:	This paper reports on original research I conducted during the period of my Higher Degree by Research candidature and is not subject to any obligations or contractual agreements with a third party that would constrain its inclusion in this thesis. I am the primary author of this paper.		
Signature		Date	31/12/2018

Co-Author Contributions

By signing the Statement of Authorship, each author certifies that:

i. the candidate's stated contribution to the publication is accurate (as detailed above);
ii. permission is granted for the candidate in include the publication in the thesis; and
iii. the sum of all co-author contributions is equal to 100% less the candidate's stated contribution.

Name of Co-Author	Christopher K. Morley		
Contribution to the Paper	Acted as corresponding author, wrote introductory and discussion material for the manuscript.		
Signature	Dr. Christopher Morley	Date	02/01/2019

Name of Co-Author	Tin Aung Myint		
Contribution to the Paper	Assisted with sample collection, prepared thin sections and wrote background geology of Myanmar.		
Signature		Date	11/06/2019

Name of Co-Author	Alan S. Collins		
Contribution to the Paper	Assisted with manuscript editing.		
Signature		Date	31/12/2018

ABSTRACT

The unfossiliferous Chaung Magyi Group of the Northern Shan Plateau of Myanmar, comprises metasedimentary rocks, in particular greywackes, slates, phyllites and schists, of inferred Proterozoic age that unconformably underlie the late Cambrian Pangyun Formation. To address the problem of the youngest stratigraphic extent of the group, four samples from the Yeywa Dome, east of Kyaukse, Mandalay Division, were collected for U–Pb dating of detrital zircons. Based on the youngest detrital zircons present in sandstone samples from the western Yeywa Dome area, at least the upper part of the Chaung Magyi Group is of latest Proterozoic to late Cambrian age (~500 Ma). Comparison of detrital zircon age frequency histogram distributions show only slight differences in distributions of detrital zircons in the Cambrian of NW Thailand and the Chaung Magyi Group samples (both from the Sibumasu Terrane), with a concentration of ages between 1300 Ma to 820 Ma, with two major peaks at 1086 Ma and 1022 Ma. A younger Cryogenian age peak at 647 Ma is also observed. A spread of older concordant ages ranges from 3093 Ma to 1406 Ma. The minimum depositional age for the Chaung Magyi Group of the west of the Bawdwin Mine (982 Ma) based on ages of cross-cutting dykes (reported in Mitchell, 2018), and the maximum depositional age for Yeywa Dome (~600-500 Ma) based on detrital zircons suggest the age difference (~> 400 Ma) is too great for the Chaung Magyi Group to be considered a single group, the dyke ages require re-investigation.

1. Introduction

The Chaung Magyi Group is a thick metasedimentary sequence that outcrops extensively in a number of areas in the Northern and Southern Shan States (Fig. 1). The type section is exposed along the Chaung Magyi river valley, north of Sedawgyi dam, about 37 km NE of Mandalay (La Touche, 1913). To the east the group is unconformably overlain by late Cambrian sedimentary units (Pangyun Formation), and to the west it is in fault contact with the Mogok Metamorphic Belt (Mitchell, 2018; Ayke Ko Aung and Cocks 2017). Mitchell (2018) states that the Chaung Magyi Group lacks fossils, and hence was assigned a Precambrian age (La Touche, 1913; Brown and Heron, 1923). Conversely Hobson (1941) suggested that the Group was equivalent to the (largely unfossiliferous) Mergui Series, hence was predominantly Carboniferous in age. West of the Bawdwin Mine in the Northern Shan State whole rock K–Ar ages of 834 ± 15 Ma and 982 ± 20 Ma on dolerite and diorite intrusions within the Chaung Magyi are reported, which suggest at least part of the group is at a minimum of Neoproterozoic age (Mitchell et al., 1977; Mitchell, 2018). U–Pb ages from 72 detrital zircons from schists in the Yeywa Dome exhibited zircons with strong are frequency peaks around 955 Ma, with lesser peaks at 1050 and 650 Ma are mentioned in Mitchell (2018), who concluded the data was compatible with deposition in the Neoproterozoic.

The Chaung Magyi Group was excluded from the Paleozoic by Ayke Ko Aung and Cocks (2017) in their review of the Paleozoic units of Myanmar, and assigned an entirely late Precambrian age. The Bawdwin Mine in the northern Shan Plateau of Myanmar is described as being located in late Precambrian–Cambrian shales, slates, greywackes and phyllites of the Chaung Maygi Group (Hopwood, 1985) that are unconformably overlain by Cambrian volcaniclastic agglomerates,

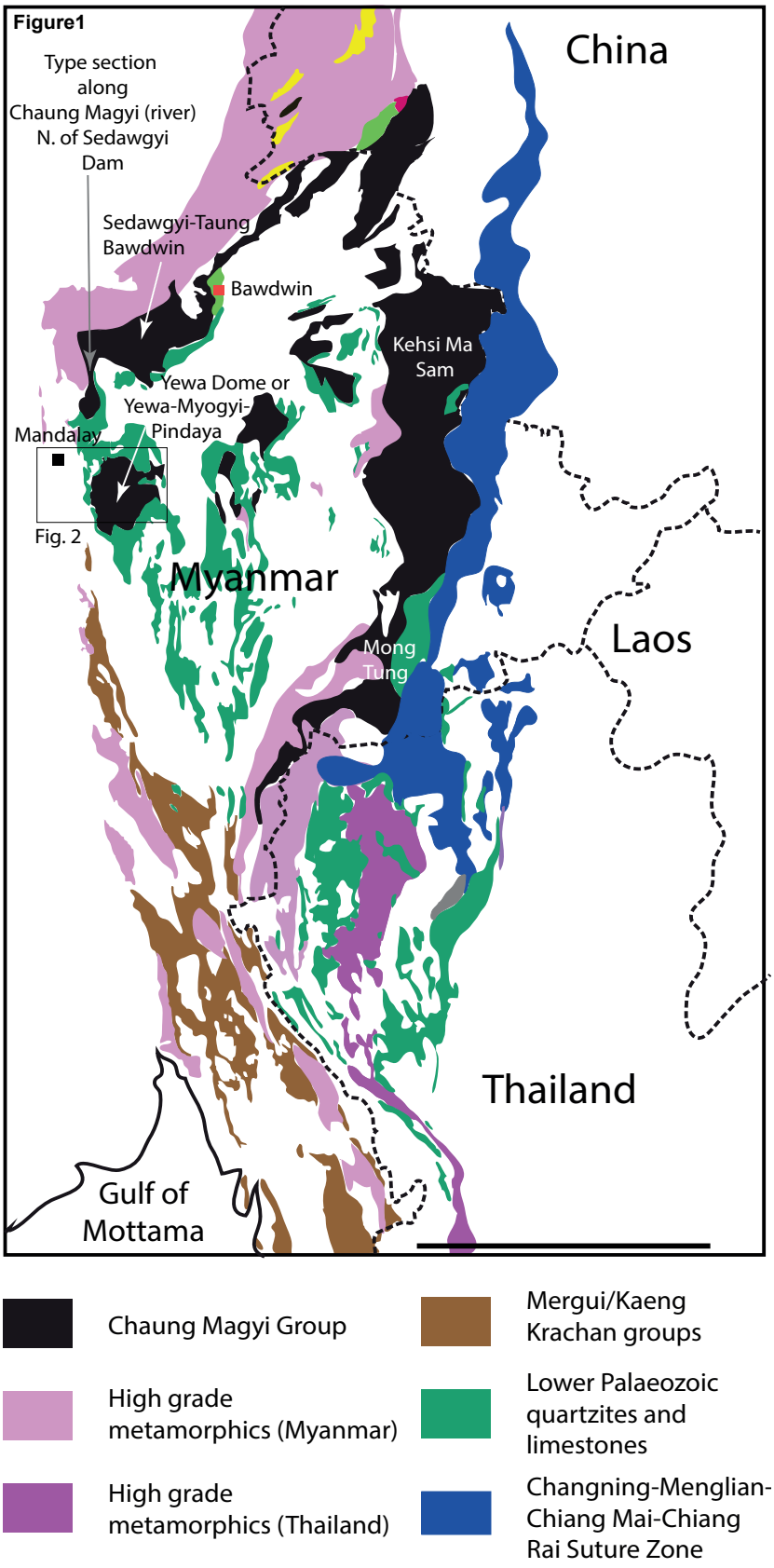

Fig. 1. Location map for Sibumasu-related pre-Permian Paleozoic units, high-grade metamorphics, and the Chaung Magyi Group, modified from Morley (2018).

arkosic and volcanic greywackes, tuffs of the Bawdin Volcanic Formation, and more regionally by Cambrian–Ordovician volcanics and metasediments of the Pangyun Formation. The Chaung Magyi Group in the Bawdwin Mine area comprises rhyolite porphyry intrusives and purple conglomerates, purple and white sandstones, green siltstones, sandstones and occasional dolomites (BGR, 1976; Brinckmann and Hinze, 1981; Hopwood, 1985; Gardiner et al. 2017). The Group is largely undated, and the Cambrian age for the upper part of the sequence largely inferred in the Bawdwin Mine area, but is supported by the U–Pb dating of zircon (499.2 ± 2.1 Ma) in a meta-basic rock from the Gongyanghe Group by Yang et al. (2012), which is thought to be the equivalent formation in Yunnan of the Chaung Magyi Group. Garson et al. (1976) also reported a trilobite and trace fossils from the Chaung Magyi Group. Consequently, either the Chaung Magyi Group has been mis-identified in some areas (Mitchell pers. comm, 2018 indicates this is a likely possibility), or the upper part of the Chaung Magyi Group is Cambrian in age.

In this study, four samples of the Chaung Magyi Group from the Yeywa Dome (Fig. 1 and 2) were collected in order to date any detrital zircons present. The aim was to better constrain the age of the Group from one of its key localities and to address the controversy as to whether the sequence is entirely of Precambrian age, or whether it extends into the Cambrian. The Yeywa Dome is 50 km wide broad dome, with Chaung Magyi Group occupying much the centre (Fig. 1 and 2), with the highest grade rocks, biotite and garnet schists. Unconformably overlying, and surrounding the Chang Magyi outcrops are Paleozoic rocks (Mitchell, 2018).

2. Geological background

The Chaung Magyi Group is found within the continental terrane known as Sibumasu (Metcalfe, 1984). Sibumasu extends through China (Baoshan Block in Yunnan), Myanmar, Thailand, Malaysia and Sumatra, and is a ribbon continent rifted from northern Gondwana in the early Permian, that subsequently collided with the Indochina and Sukhothai terranes to form the core of SE Asia during the Triassic (e.g. Metcalfe 2002, 2017; Sone and Metcalfe, 2008; Morley, 2018; Dew et al. 2018). The outcrop geology of Sibumasu is almost entirely composed of Phanerozoic sedimentary, metasedimentary, igneous and metamorphic rocks (e.g. Metcalfe, 2011; Morley, 2018). Although studies of igneous and detrital zircons point to the presence of Precambrian basement dating back to the Archean (e.g. Burrett et al., 2014; Dew et al., 2018), there are no extensive outcrop examples of Precambrian high-grade rocks in Sibumasu (e.g. Hansen et al., 2014; Mitchell, 2018). The Chaung Maygi Group is the one unit that represents the Precambrian of Sibumasu (Fig. 3), but it is poorly dated, and appears to be confined only to the northern part of Sibumasu in the Shan Plateau of Myanmar and Yunnan (Baoshan Block) (Fig. 1). More typically Cambrian quartzites are the oldest units present in Sibumasu, but the stratigraphic base of the Cambrian is unknown (Ridd, 2011).

The most complete recent published description of the Chaung Magyi Group is given by Mitchell (2018). In the Shan State, the Chaung Magyi Group has been mapped in four large areas: Sedawgyi-Taung-Bawdwin; Yeywa Dome (Yeywa-Myogyi-Pindaya) of the Loi Ling Range area; Mong Tung and north of Kehsi Ma Sam (Fig. 1). Good exposures are present

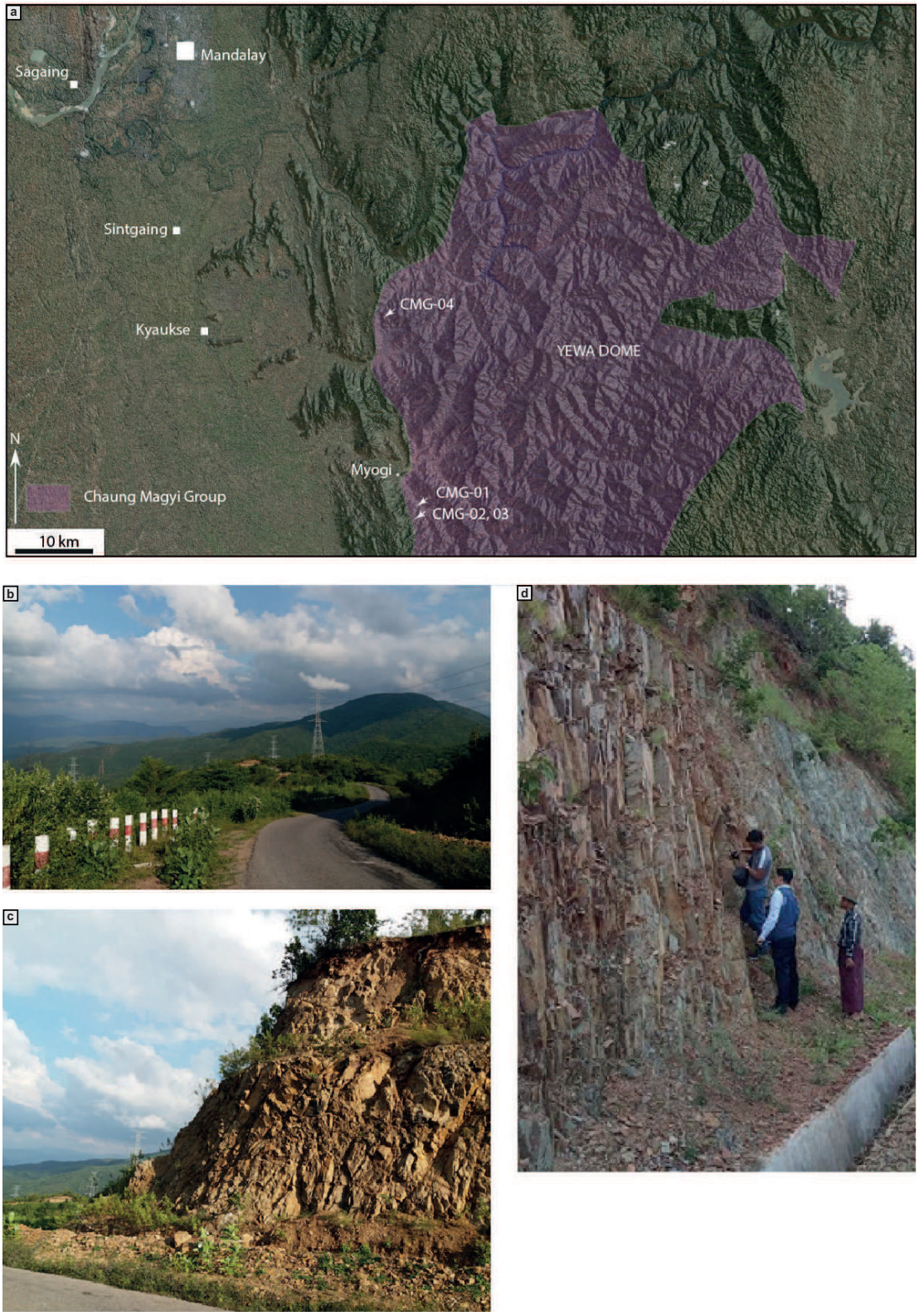

Fig. 2. a. Digital elevation model with semi-transparent satellite image overlay of the NW Shan Plateau area in Myanmar, showing the sample areas. **b.** Yeywa Dome area, panoramic view from Baw Daung (21.637062 N, 96.354916E). **c.** Yeywa Dome area, Chaung Magyi metagreywacke, exposed at Baw Daung (21.637062 N 96.354916E), (in area of CMG-04). **d.** Slate, phyllite and metagreywacke of Chaung Magyi Group, Myogyi area (21.40942 N, 96.39466 E) (in area of CMG 01-03).

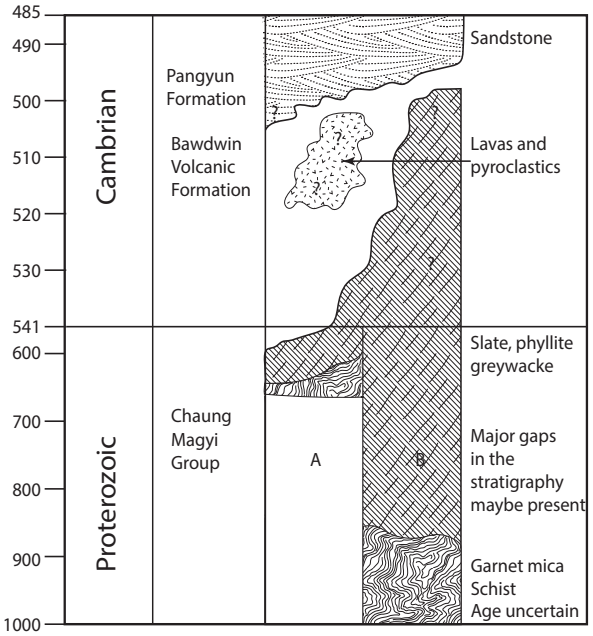

Fig. 3. Stratigraphic column for the Chaung Magyi Formation and overlaying units, age scale is Ma. A) Preferred stratigraphic range for the Chaung Magyi Formation in the Precambrian as discussed in this study. B) Possibly stratigraphic range based on ages of dykes cross-cutting the Chaung Magyi Formation based on data in Mitchell (2018).

in the first three areas. In the area south of Myogyi (Fig. 2), within the Yeywa Dome unpublished notes by Maung Thein (1971) describe the Chaung Magyi as being split into upper and lower groups. The Lower Chaung Magyi Group comprises garnet-mica schists, while the Upper Chaung Magyi Group comprises schists and phyllites, slates and metagreywackes, phyllites and slates, and thin bedded silty limestone. The general descriptions of the Chaung Magyi Group are that it comprises in order of abundance phyllite, slate (often pyrite-rich), metagreywacke, sandy phyllite, mica schist, calc-phyllite, graphite schist and laminated marble. The (arkosic) metagreywackes sometimes exhibit graded bedding, sole markings and slump structures indicative of a deepwater turbidite origin (Garson et al., 1976; Mitchell, 2018). The thickness of the turbidite facies was estimated at over 8000 ft by Garson et al. (1976). Detrital minerals in the greywackes include microcline, sodic plagioclaise, quartzite, tourmaline, zircon, leucoxene, magnetite and hypersthene, detrital mica is often abundant (Mitchell, 2018). Distinctively green-coloured chlorite schists comprise the upper part of the group on the west side of the Yeywa Dome and overlie sericite schists (Mitchell, 2018). Numerous quartz and quartzo-feldspathic veins cross-cut the group. A distinguishing characteristic of the Chaung Magyi Group is that both the shales and the sandstones are very micaceous, unlike the overlying Paleozoic units (Garson et al., 1976).

The four rock samples were collected from section in the upper part of the Chaung Magyi Group in two sand-prone sections (Fig. 2; Table 1) where the University of Mandalay regularly run excursions. In the sample locations steeply dipping to vertical beds of fine-grained greywacke sandstones are the dominant lithology, stacked in predominantly thin beds 10–30 cm thick separated by thin shales and siltstones (Fig. 2). The greywackes are composed of quartz (40%), feldspar (25%), plagioclase (10%), mica (20%) and others (5%). Quartz grains are angular to sub-angular with undulatory extinction. Maximum grain size as 1 mm. Feldspars, including plagioclase, are mostly untwinned, and some are altered to sericite, with grain sizes between 0.05–1mm in diameter. A significant cleavage is present in the samples with the widespread presence of parallel aligned, detrital (and some authigenic) biotite and muscovite flakes. Indications of low-grade metamorphism are the presence of cleavage grading into schistosity in places, the preferred orientation of flattened quartz grains, and the bands of mica and sericite that wrap around such grains (Fig.

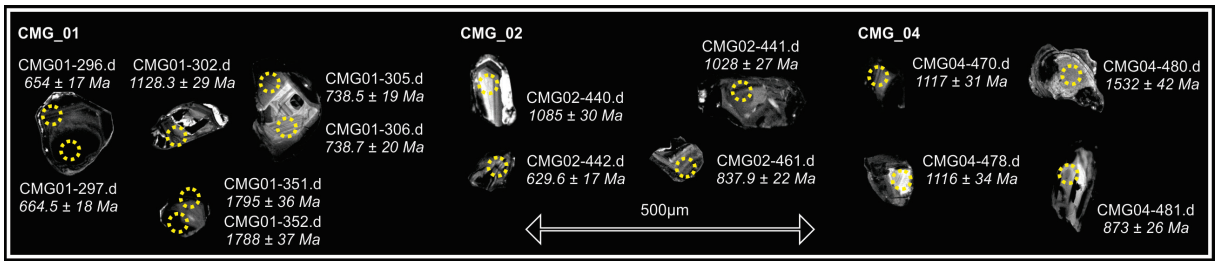

Fig. 4. Cathodoluminescence (CL) images for representative zircons from the Chaung Magyi Group of Myanmar. U–Pb laser spots are shown and values are given with two standard deviation error. All images displayed relative to the 500 µm scale bar the cut off from $^{206}Pb/^{238}U$ age to $^{207}Pb/^{206}Pb$ age is 1500 Ma.

Table 1. Description of zircon morphologies and cathodoluminescence (CL) interpretations for the analysed Chaung Magyi Group samples.

Sample Number	*Zircon Morphology*			*Cathodoluminescence (CL) interpretation*
	Size	*Colour*	*Shape*	
CMG-01	100-300 µm	Silver, white, grey, pink	Original crystal shape mostly destroyed, producing smooth sub to well-rounded grains	Grains preserve oscillatory zoning, rare homogeneous or dark grains. Multiple CL domains commonly present in each zircon. Some grains are cracked.
CMG-02	50-250 µm	Yellow and blue-green. Purple zircons very small.	Some rounded crystal edges or fragmented into pieces whereas in others the original crystal shape has been destroyed, and the final product being smooth sub to well-rounded grains.	Grains preserve oscillatory zoning, rare homogeneous or dark grains. Multiple CL domains commonly present in each zircon. Some grains are cracked.
CMG-04	50-250 µm	Light pink, purple, white, yellow	Very fragmented, some broken grains, the original crystal shape mostly destroyed.	Oscillatory zoning, some diffuse zoning and dark homogeneous grains present. Some grains have a mottled appearance or preserve zoning with convolute boundaries.

2).

3. Methodology

The four collected rock samples (CMG 01–04) were crushed and sieved for zircon grain collection through the conventional magnetic and heavy liquid separation procedures. Where yields permitted (in CMG_01 and CMG_02), about 200 randomly selected zircon grains were cast in epoxy resin and polished for U–Pb zircon age determinations. In the two other samples, all potential zircon grains were separated for age determinations. Cathodoluminescence (CL) images were obtained to identify and characterise the various chemical and textural zones within individual zircons using the FEI Quanta600 Scanning Electron Microscope with the Mineral Liberation Analysis (MLA) at Adelaide Microscopy, Adelaide, South Australia. The resultant CL images are displayed in Fig. 4. The characteristics of the zircons are summarised in Table 1.

Grains that were identified to be zircon and

without metamictisation were selected for laser ablation inductively coupled plasma mass spectrometry (LA–ICP–MS). These analyses were conducted on an Agilent 7900x with a New Wave NW213 laser ablation system with a TwoVol2 sample chamber at Adelaide Microscopy. The spot size was 30 µm with an ablation duration of 30 seconds, fluence of 5.52 J/cm² and a repetition rate of 5 Hz. The isotopes measured with the LA–ICP–MS were ^{90}Zr, ^{201}Hg, ^{204}Pb, ^{206}Pb, ^{207}Pb, ^{208}Pb, ^{232}Th and ^{238}U.

The GEMOC GJ-1 ($^{207}Pb/^{206}Pb$ TIMS age of 607.7 ± 4.3 Ma, $^{206}Pb/^{238}U$ TIMS age of 600.7 ± 1.1 Ma and $^{207}Pb/^{235}U$ age of 602.0 ± 1.0 Ma; Jackson et al., 2004) was run repeatedly as the primary zircon normalising standard every 10–14 unknown analyses, to correct for isotopic drift and down-hole fractionation. The Plešovice zircon standard ($^{206}Pb/^{238}U$ age of 337.13 ± 0.37 Ma (2σ); Sláma et al., 2008) and 91500 ($^{207}Pb/^{206}Pb$ age of 1065 Ma and $^{206}Pb/^{238}U$ age of 1062 Ma; Wiedenbeck et al., 1995) were analysed as secondary standards to check the accuracy of the technique. Across the analytical session, the analyses of GJ-1 yielded a $^{206}Pb/^{238}U$ weighted average age of 601.3 ± 2.2 Ma (n = 57, MSWD = 1.00). The secondary standards: Plešovice and 91500 yielded $^{206}Pb/^{238}U$ weighted average ages of 335.4 ± 1.2 Ma (n = 56, MSWD = 1.08) and 1058.9 ± 7.1 Ma (n = 28, MSWD = 1.5)

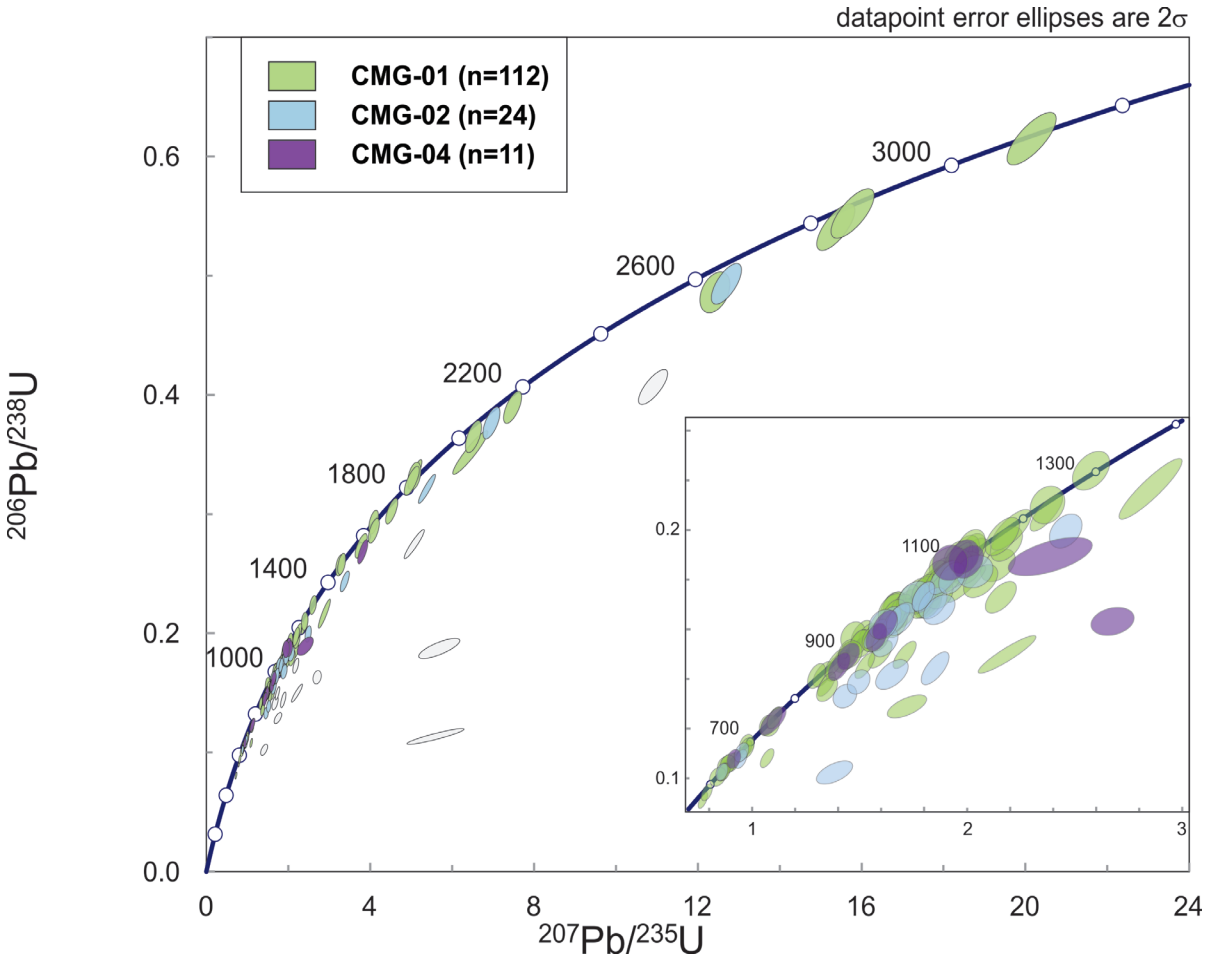

Fig. 5. Concordia diagram displaying age data from the Chaung Magyi Group. Data that is within ±10% discordance is coloured to highlight the three U–Pb samples (CMG-01, CMG-01 and CMG-04).

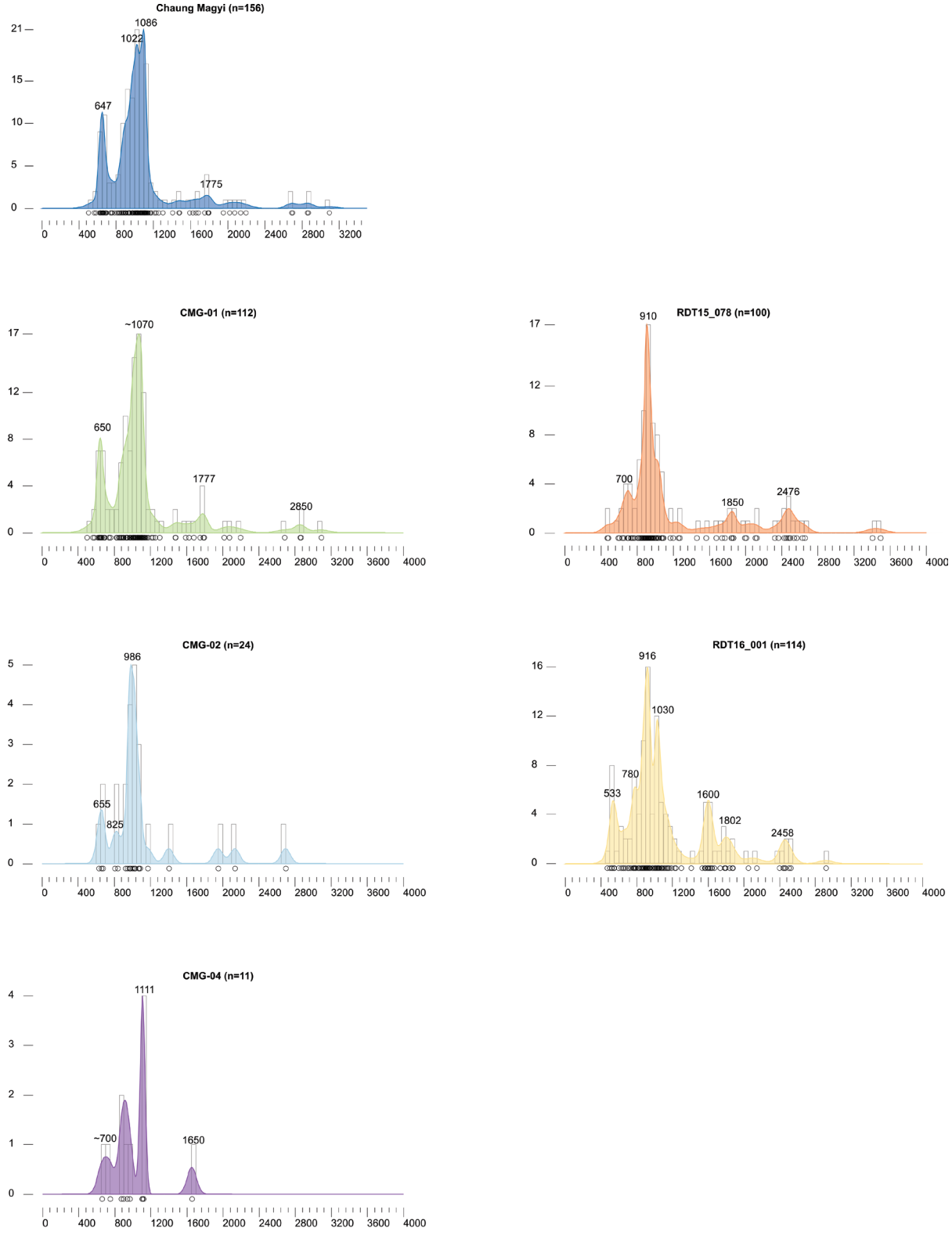

Fig. 6. Kernel Density Estimate (KDE) and histograms for all concordant data from the Chaung Magyi Group and individual KDE plots for each sample (CMG-01, CMG-02 and CMG-04). Samples RDT15_078 and RDT16_001 are comparative detrital data from Cambro-Ordovician sediments in northwest Thailand. Each coloured plot illustrates the KDE of data with ±10% discordance ($^{206}Pb/^{238}U$ age)/ $^{207}Pb/^{235}$ U age calculation), x axis denotes age in million years (Ma) and y axis shows frequency (*n*) of the data. $^{206}Pb/^{238}U$ age to $^{207}Pb/^{206}Pb$ age cut off was 1500 Ma.

respectively. The raw data were reduced using Iolite software (Paton et al., 2011).

Concordia diagrams were created using ISOPLOT 4.15 for Excel (Ludwig, 2009). The kernel density estimate plots were generated using the Java application, DensityPlotter (Vermeesch, 2012). Supplementary data of the analysis is provided in an Excel Spreadsheet (see Appendix V).

4. Results

Concordia plots are displayed in Fig. 5, with the coloured data indicating data within ±10% ($^{206}Pb/^{238}U$ age)/ $^{207}Pb/^{235}$ U age) discordance. Kernel density estimate (KDE) plots for each sample are illustrated in Fig. 6, only data within ±10% ($^{206}Pb/^{238}U$ age)/ $^{207}Pb/^{235}$ U age) discordance is included. The KDE plots were created using the adaptive function in DensityPlotter with a 20 Ma bandwidth and 50 Ma bins. To compensate for the variations of the relative values of the uncertainties for the U–Pb system and the associated resolution issues with the calculated ages (see Gehrels, 2012), the $^{206}Pb/^{238}U$ age was quoted for data younger than 1500 Ma, and the $^{207}Pb/^{206}Pb$ age was used for any data with a $^{206}Pb/^{238}U$ age > 1500 Ma.

Two methods of maximum depositional age calculations are used in this study. Firstly the youngest single grain zircon ages are calculated from ages within ±10% discordance (YSG) and the weighted mean age of the youngest cluster within ±10% discordance that overlap in age at 1σ uncertainty values (YC1σ) following the quantitative interpretation approach for detrital zircon U–Pb age data of Dickinson and Gehrels (2009). YC1σ was calculated using ±10% discordance from the ($^{206}Pb/^{238}U$ age)/ $^{207}Pb/^{235}$ U age) calculation.

CMG_01 shows a detrital zircon age distribution that is dominated by a ca. 1070 Ma age peak, but also has important contributions of zircons with age peaks at ca. 2850 Ma, ca. 1777 Ma and ca. 650 Ma (see Fig. 6). The interpreted maximum depositional ages for CMG_01 are 626.8 ± 8.4 Ma (YC1σ, n = 4, MSWD = 0.39) and a YSG of 500.1 ± 14 Ma.

CMG_02 also contains similar aged zircons to CMG_01 with a large age peak at 986 Ma and other significant contributions from ca. 825 Ma and ca. 655 Ma aged zircons (see Fig. 6). The YSG of CMG_02 yielded a $^{206}Pb/^{238}U$ age of 629.6 ± 17 Ma is within 1σ error of the YC1σ from CMG_01. With a small sample size of 24 concordant zircons, it is unlikely that the YC1σ of CMG_02, yielding a $^{206}Pb/^{238}U$ age of 975 ± 14 Ma (n = 4, MSWD = 0.12), is representative of the maximum depositional age of this unit.

CMG_04 has a large proportion of the concordant age data measured between 1120 Ma and 660 Ma (n = 10, Fig. 6). There is only one older age peak at 1650 Ma (see Fig. 6). The YSG of CMG_04 is 660.3 ± 18 Ma, the YC1σ yields a $^{206}Pb/^{238}U$ age of 1110 ± 15 Ma (n = 4, 181 MSWD = 0.20).

The combined concordant age populations of all three samples from the Chaung Magyi Group show the dominance of zircon ages from 1300 Ma to 820 Ma, with two major peaks at 1086 Ma and 1022 Ma (Fig. 6). A younger Cryogenian age peak at 647 Ma is also observed along with a spread of older concordant ages from 3093 Ma to 1406 Ma (see Table. 2). The YC1σ when incorporating all three samples yields a $^{206}Pb/^{238}U$ of 627.4 ± 7.5 Ma (n = 5, MSWD = 0.32).

5. Discussion

Samples from the upper parts of two sections that are routinely used for geological excursions to demonstrate the stratigraphy of the Chaung Magyi Group are shown in this study, on the basis of detrital zircon ages, to be either of Neoproterozoic or Cambrian age. Two of the youngest zircon grains from CMG-01 indicate end Neoproterozoic (562.2 ± 16 Ma) and Cambrian (500.1 ± 14 Ma) ages. Mitchell (2018) cites a conference abstract (Mitchell et al. 2012) as the reference for analysis of 72 detrital zircons from a schist in the Yeywa Dome. This sample yielded U–Pb ages from that yielded zircons between 1200 and 500 Ma, with a strong peak at ca. 955 Ma and lesser peaks at ca. 1050 Ma and ca. 650 Ma, which Mitchell (2018) states as being compatible with deposition during the late Proterozoic. These results are similar to ours (Fig. 6), although the zircon sample described by Mitchell (2018) is statistically too small. It is curious that Mitchell (2018) notes an upper limit on zircon ages of ~500 Ma, yet chose to place the age of the formation within the late Proterozoic. Presumably this is related to application of conservative statistics to the samples. However, the occurrence of 500 Ma zircons in two separate samples suggests that analysis of larger samples may more reliably establish a Cambrian age. Mitchell (pers. comm. 2018) stated that the schist sample underlies the flysch-type Chaung Magyi, and there is some uncertainty as to whether the metamorphics are actually metamorphosed Chaung Magyi formation or not.

Dating of the Chaung Magyi Group from the west of the Bawdwin Mine based on whole-rock K–Ar ages (834 ± 15 Ma and 982 ± 20 Ma) from cross-cutting dolerite and diorite intrusions (Mitchell et al., 1977; Mitchell, 2018) indicates a minimum age of 982 ± 20 Ma for the Chaung Magyi Group in this locality. The implications of the results from the Yeywa Dome and the Pindaya Range suggest one of the following: 1) The Chaung Magyi Group covers least 500 Ma of geological time, 2) The Chaung Magyi Group needs to be split into separate Groups to reflect a older sequence (~> 982 Ma) and a younger one (~600-500 Ma). Given how much tectonic activity can occur in a 500 Ma time-span, it seems unreasonable to consider the Chaung Magyi Group as a single stratigraphic entity if the dates from the Yeywa Dome and west of the Bawdwin Mine are viable. However, the 1970's vintage of the K–Ar ages from intrusions indicates the dating is highly suspect, and it seems unreasonable that the flyschoid-type of Chaung Magyi would span 500 Ma. While the evidence for a Cambrian age in the Yeywa Dome is limited, evidence that the three samples represent deposition younger than 600 Ma is strong. Hence we prefer to view the Chaung Magyi as late Neoproterozoic to possibly Cambrian in age.

Comparison of the zircons from the Chaung Magyi Group with two Cambro-Ordovician sandstone samples from NW Thailand, reveal only slight differences in distributions of detrital zircons compared with the Chaung Magyi Group samples (Fig. 6). Both the Cambro-Ordovician of NW Thailand and the Chaung Magyi Group show the majority of detrital zircon ages are focused between about 1100 and 600 Ma, with a secondary peak around 650 Ma and the major peak between 1000–900 Ma. A tail of data with minor peaks and troughs stretches back to about 3000 Ma. The pattern of detrital ages seen in Fig. 6 is typical for Sibumasu, and exhibits significant similarities with parts

of NW and SW Australia (Burrett et al., 2014).

The Chaung Magyi Group is considered as being unconformably overlain by the Pangyun Formation (Fig. 3), which forms major cliffs of quartzites above the Chaung Magyi Group in the Bawdwin mine area (La Touche, 1913). The Pangyun Formation is up to 2000 m thick, and comprises quartzites, conglomerates, minor cross-bedded dolomites, siltstones and tuffs, the detrital minerals present are strikingly similar to those of the Chaung Magyi Group (Mitchell, 2018). Trilobites of late Cambrian age are present (Mitchell, 2018). Since part of the Chaung Magyi Group has now been dated as late Cambrian, it is necessary to consider whether the upper part of the group is coeval with the Pangyun Formation, and its deeper water equivalent. While an unconformable relationship between the Pangyun Formation and the older parts of the Chaung Magyi Group remains entirely feasible, we need to reconsider whether this is the only possible relationship. Perhaps in places the shallower marine Pangyun Formation has been thrust over the late Cambrian part of the Chaung Magyi Group.

The latest Proterozoic to Cambrian ages for the samples from the Yeywa Dome, discussed in this study, indicates that the tectonics that affected the upper part of the Chaung Magyi Group must be seen in continuity with those of the Paleozoic succession. In particular, the late Cambrian–Ordovician igneous activity in the Bawdwin area and in the adjacent Baoshan Block (the Yunnan portion of Sibumasu) indicates the presence of an Andean-type belt on the northern margin of Gondwana, (Zhu et al., 2012; Li et al., 2016; Morley, 2018). A Neoproterozoic to early Paleozoic mélange, related to subduction has also been identified along the NW margin of the Baoshan Block by Mao et al. (2014). Consequently, the Chaung Magyi Group can be envisioned as composed of sediments sourced from the Australian part of Gondwana that were deposited on part of the Gondwana continental margin that extended into a deep marine environment. At times during the Neoproterozoic and Cambro-Ordovician, there was subduction along the margin that resulted in deformation and metamorphism of the sedimentary rocks in the accretionary prism and forearc basin settings, and also in volcanic arc activity.

6. Conclusion

Based on the youngest detrital zircons present in sandstone samples from the western Yeywa Dome area, at least the upper part of the Chaung Magyi Group is of latest Proterozoic to late Cambrian age (~500 Ma), which agrees with Garson et al. (1976) and a verbal report that Cambrian trilobites have been found in some areas of the eastern and western Shan Plateau mapped as Chaung Magyi Group. Comparison of detrital zircon age-frequency histogram distributions show only slight differences in distributions of detrital zircons in the Cambro-Ordovician of NW Thailand and the Chaung Magyi Group samples (Fig. 6). These findings have considerable implications for the tectonic history of northern Sibumasu, for the stratigraphic relationships with other lower Paleozoic stratigraphic units, and for the nature of contacts in the field (are they structural or stratigraphic). Further detailed work is needed to better constrain stratigraphic, metamorphic and igneous ages associated with the Chaung Magyi Group.

References

Aye Ko Aung and Cocks, L.R.M., 2017. Chapter 14. Cambrian-Devonian stratigraphy of the Shan Plateau, Myanmar. In: Barber, A.J., Khin Zaw, and Crow M.J., (eds.), Myanmar: Geology, Resources and Tectonics, Geological Society London, Memoir, 48, 319-344.

Bundesanstalt fur Geowissenschaften und Rohstoffe (BGR), 1976. Concluding report on lead/silver/zinc ore exploration in the vicinity of the Bawdwin Mine, Shan State (North East Burma). Bundesanstalt fur Geowissenschaften und Rohstoffe, Hanover.

Brinckmann, J. and Hinze, C., 1981. On the Geology of the Bawdwin Lead-Zin Mine, Northern Shan State, Burma. Geologisches Jahrbuch, D43, 7-45.

Brown, J.C. and Heron, A.M., 1923. The geology and ore deposits of the Tavoy district. Memoir Geological Survey of India, 44, 167-394.

Burrett, C., Khin, Z., Meffre, S., Lai, C.K., Khositanont, S., Chaodumrong, P., Udchachon, M., Ekins, S. & Halpin, J. 2014. The configuration of Greater Gondwana—Evidence from LA ICPMS, U–Pb geochronology of detrital zircons from the Palaeozoic and Mesozoic of Southeast Asia and China. Gondwana Research, 26, 31-51, doi: http://dx.doi.org/10.1016/j.gr.2013.05.020.

Dew, R.E.C., Collins, A.S., Glorie, S., Morley, C.K., Blades, M.L., Nachtergaele, S., King, R., Foden, J., De Grave, J., Kanjanapayont, P., Evans, N.J., Alessio, B.L. & Charusiri, P. 2018. Probing into Thailand's basement: New insights from U–Pb geochronology, Sr, Sm–Nd, Pb and Lu–Hf isotopic systems from granitoids. Lithos, 320-321, 332-354, doi: 10.1016/j.lithos.2018.09.019.

Dickinson, W.R., Gehrels, G.E., 2009. Use of U–Pb ages of detrital zircons to infer maximum depositional ages of strata: A test against a Colorado Plateau Mesozoic database. Earth and Planetary Science Letters 288, 115-125.

Gardiner, N.J., Robb, L.J., Searle, M.P., Kyi Htun, and Khin Zaw. 2017. Chapter 30. The Bawdwin Mine, Myanmar: a review of its geological setting and genesis. In: Barber, A.J., Khin Zaw, and Crow M.J., (eds.), Myanmar: Geology, Resources and Tectonics, Geological Society London, Memoir, 48, 671-688.

Garson, M.S., Amos, B.J., Mitchell, A.H.G., 1976. The geology of the country around the Neyaungga and Ye-ngan, Southern Shan States, Burma. London Institute of Geological Sciences, Overseas Division, Memoir, 2, 70 pp.

Gehrels, G., 2012. Detrital Zircon U-Pb Geochronology: Current Methods and New Opportunities, In: Busby, C., Azor, A. (Eds.), Tectonics of Sedimentary Basins: Recent Advances. Wiley, Online Library, pp. 45-62.

La Touche, T.H.D., 1913. Geology of the Northern Shan States. Memoir of the Geological Society of India, 39, 1-379.

Li, G.-J., Wang, Q.-F., Huang, Y.-H., Gao, L. and Yu, L., 2016. Petrogenesis of middle Ordovicia peraluminous granites in the Baoshan block: implications for the early Paleozoic tectonic evolution along East Gondwana. Lithos, 245, 76-92.

Hansen, B.T., Wemmer, K., Putthapiban, P., Kleinhanns, I.C. & Wilsky, F. 2014. Do U/Pb-SHRIMP Dating and Pb Stepwise Leaching (PbSL) Analyses Confirm the Lack of Precambrian Basement Outcrops in Thailand? Open Journal of Geology, **4**, 10, 12pp., doi: 10.4236/ojg.2014.410037.

Hobson, G.V., 1941. Report on a Geological Survey in Part of Karenni and Southern Shan State. Memoir of the Geological Survey of India, 74, Part 2, 103-209.

Hopwood, T., 1985. Exploration potential of the Bawdwin Silver-Lead Mine, Northern Shan States, Burma. Australian Mineral Development Laboratories, Adelaide, TH Report.

Jackson, S.E., Pearson, N.J., Griffin, W.L., Belousova, E.A., 2004. The application of laser ablation-inductively coupled plasma-mass spectrometry to in situ U–Pb zircon geochronology. Chemical Geology 211, 47-69.

Li, G.-J., Wang, Q.-F., Huang, Y.-H., Gao, L. & Yu, L. 2016. Petrogenesis of middle Ordovician peraluminous granites in the Baoshan block: Implications for the early Paleozoic tectonic evolution along East Gondwana. Lithos, 245, 76-92, doi: https://doi.org/10.1016/j.lithos.2015.10.012.

Mao, X., Yin, F., Tang, Y., Wang, D., Liao, S., Xiong, C., 2014. Early Paleozoic accretionary orogenesis on western margin of Baosha Block. Diqiu Kexue-Zhongguo Dizhi Daxue Xuebao/ Earth Science – Journal of China University of Geoscience 39, 1129-1139.

Metcalfe, I., 1984. Stratigraphy, palaeontology and palaeogeography of the Carboniferous of Southeast Asia. Memoirs of the Geological Society of France, 147, 107-118.

Metcalfe, I., 2002. Permian tectonic framework and palaeogeography of SE Asia. Journal of Asian Earth Sciences 20, 551-566.

Metcalfe, I., 2017. Tectonic evolution of Sundaland.

Bulletin Geological Society of Malaysia, 63, 27-60.

Mitchell, A.H.G., Marshall, T.R., Skinner, A.C., Baker, M.D., Amos, B.J., and Bateson, J.H., 1977. Geology and Exploration Geochemisry of the Yadanatheingi and Kyaukme-Longtawkno Areas, Northern Shan States, Burma. Overseas Geology and Mineral Resources, 51, London: Institute of Geological Sciences, HMSO, 35 pp.

Mitchell, A.H.G., Tin Hlaing, Nyunt Htay, 2012. Mesozoic orogenies along the Mandalay-Yango margin of the Shan Plateau. In: Mantajit, N., and Potisat, S., eds. Proceedings of the Symposium on Geology of Thailand, Bangkok, Thailand, 136-149.

Mitchell, A. H. G., 2018. Geological Belts, Plate Boundaries and Mineral Deposits in Myanmar. Elsevier, Amsterdam, 524 pp.

Morley, C.K. 2018. Understanding Sibumasu in the context of ribbon continents. Gondwana Research, 64, 184-215, doi: https://doi.org/10.1016/j.gr.2018.07.006.

Paton, C., Hellstrom, J., Paul, B., Woodhead, J., Hergt, J., 2011. Iolite: Freeware for the visualisation and processing of mass spectrometric data. Journal of Analytical Atomic Spectrometry 26, 2508-2518.

Ridd, M.F. 2011. Lower Palaeozoic. In: Ridd, M.F., Barber, A.J. & Crow, M.J. (eds.) The Geology of Thailand. The Geological Society, London, 33-51.

San San Win, 2014. Petrology and characterization of the copper and base metals occurrence in the Pein Ye-Taung Le Lon Taung area, Mandalay Region. MSc. Thesis, Department of Geology, University of Mandalay.

Sláma, J., Košler, J., Condon, D.J., Crowley, J.L., Gerdes, A., Hanchar, J.M., Horstwood, M.S.A., Morris, G.A., Nasdala, L., Norberg, N., Schaltegger, U., Schoene, B., Tubrett, M.N., Whitehouse, M.J., 2008. Plešovice zircon — A new natural reference material for U–Pb and Hf isotopic microanalysis. Chemical Geology 249, 1-35.

Sone, M., and Metcalfe, I., 2008. Parallel Tethyan sutures in mainland SE Asia: New insights for Palaeo-Tethys closure. Compte Rendus Geoscience, 340, 166-179.

Vermeesch, P., 2012. On the visualization of detrital age distributions. Chemical Geology, 312-313, 190-194.

Wiedenbeck, M., AllÉ, P., Corfu, F., Griffin, W.L., Meier, M., Oberli, F., Quadt, A.V., Roddick, J.C., Spiegel, W., 1995. Three natural zircon standards for U–Th–Pb, Lu–Hf, trace element and REE analyses. Geostandards Newsletter 19, 1-23.

Yang, X.-J., Jia, X.-C., Xiong, C.-L., Bai, X.-Z., Huang, B.-X., Luo, G., and Yang, C.-B., 2012. LA-ICP-MS zircon U-Pb age of metamorphic basic volcanic rock in Gongyanghe Group of Southern Gaoligong Mountains western Yunnan Province, and its geological significance. Geological Bulletin of China, 31, 264-276.

Zhu, D.C., Zhao, Z.D., Niu, Y.L., Dilek, Y., Wang, Q., Ji,W.H., Dong. G.C., Sui, Q.L., Liu, Y.S., Yuan, H.L., and Mo, X.X., 2012. Cambrian bimodal volcanism in the Lhasa Terrane, southern Tibet: record of an early Paleozoic Andean-type magmatic arc in the Australian proto-Tethyan margin. Chemical Geology, 328, 290-308.

CHAPTER 6

This chapter is published as:

Dew, R.E.C., King, R., Collins, A.S., Morley, C.K., Arboit, F.A. & Glorie, S. 2018. Stratigraphy of deformed Permian carbonate reefs in Saraburi Province, Thailand. *Journal of the Geological Society*, **175**, 163-175, doi: 10.1144/jgs2017-035.

Statement of Authorship

Title of Paper	Stratigraphy of deformed Permian carbonate reefs in Saraburi Province
Publication Status	☑ Published ☐ Accepted for Publication ☐ Submitted for Publication ☐ Unpublished and Unsubmitted w ork w ritten in manuscript style
Publication Details	Dew, R.E.C., King, R., Collins, A.S., Morley, C.K., Arboit, F.A. & Glorie, S. 2018. Stratigraphy of deformed Permian carbonate reefs in Saraburi Province, Thailand. *Journal of the Geological Society*, **175**, 163-175, doi: 10.1144/jgs2017-035.

Principal Author

Name of Principal Author (Candidate)	Romana E.C. Dew		
Contribution to the Paper	Collected samples, logged all 11 stratigraphic sections, identified the majority of the foraminifera and other fossils present, interpreted data, wrote manuscript and acted as corresponding author.		
Overall percentage (%)	80		
Certification:	This paper reports on original research I conducted during the period of my Higher Degree by Research candidature and is not subject to any obligations or contractual agreements with a third party that would constrain its inclusion in this thesis. I am the primary author of this paper.		
Signature		Date	31/12/2018

Co-Author Contributions

By signing the Statement of Authorship, each author certifies that:

i. the candidate's stated contribution to the publication is accurate (as detailed above);

ii. permission is granted for the candidate in include the publication in the thesis; and

iii. the sum of all co-author contributions is equal to 100% less the candidate's stated contribution.

Name of Co-Author	Rosalind King		
Contribution to the Paper	Supervisorial role, conception and design of the project, assisted in field, data interpretation, manuscript construction and editing		
Signature		Date	28/11/2018

Name of Co-Author	Alan S. Collins		
Contribution to the Paper	Supervisorial role, conception and design of the project, helped in data interpretation and manuscript construction and editing		
Signature		Date	31/12/2018

Name of Co-Author	Christopher K. Morley		
Contribution to the Paper	Assistance with field work, data interpretation and manuscript editing		
Signature	Dr. Christopher Morley	Date	31/12/2018

Name of Co-Author	Francesco Arboit		
Contribution to the Paper	Conception of the project, primary assistant in field component of study and aided with data interpretation		
Signature		Date	14/12/2018

Name of Co-Author	Stijn Glorie		
Contribution to the Paper	Co-supervisorial role, manuscript evaluation		
Signature		Date	30/11/2018

ABSTRACT

Kilometre-scale thrusts affect the stratigraphic order of the sedimentary rocks that form the Khao Khwang Platform in central Thailand. The effect of these thrusts requires detailed analysis to unravel the original distribution of the sedimentary units and their associated facies. The Khao Khwang Platform comprises three carbonate dominated units identified previously as the Phu Phe, Khao Khad and Khao Khwang Formations. These carbonates are intercalated with clastic, mixed siliciclastic and carbonate sequences: the Sap Bon, Pang Asok and Nong Pong Formations. The palaeogeography of the area prior to the Indosinian Orogeny is poorly known and has herein been investigated by combining structural reconstructions, microfacies and biostratigraphy in the Saraburi area.

A stratigraphic model for the Yakhtashian–Midian carbonate platform palaeogeography using the well-developed exposed sections of the Khao Khwang Platform, located in the Saraburi Province of Thailand, is presented. This has revealed the presence of several separate carbonate platforms dominated by four major Middle Permian facies: peritidal, platform interior, algal reef and basin slope which are dated using foraminifera and algae. This model integrates recent structural studies and considers their impact on the present day distribution of the facies in terms of platform development using biostratigraphy and detailed microfacies analysis.

1. Introduction

Two carbonate platforms are generally identified on the Thai part of the Indochina Terrane: The Khao Khwang, and Pha Nok Khao Platforms which are separated by the deep-water deposits of the Nam Duk Formation (Wielchowsky and Young 1985). These platforms form part of the Saraburi Group (Fig. 1). The carbonate-dominated late Carboniferous–middle Permian Si That Formation and the Pha Nok Khao Platform are known from outcrops on the western side of the Khorat Plateau, and extend under the Mesozoic deposits of the Khorat Group in the main area of the plateau (Booth and Sattayarak 2011). Two-dimensional seismic reflection data have demonstrated that the Pha Nok Khao 'Platform' comprises a series of small carbonate platforms on structural highs, with deeper water clastic rocks in between (Booth and Sattayarak 2011). Normal faults associated with rifting are responsible for the formation of these small platforms and associated basins and have a strong structural control on subsequent sedimentary facies distribution (Booth and Sattayarak 2011). In the Khao Khwang Platform area (Fig. 2), some Permian clastic units (Pang Asok, Nong Pong and Sap Bon Formations) have been identified as the lateral equivalents of the Permian limestones (Khao Khad, Khao Khwang and Phu Phe Formations) (Chonglakmani 2001; Chutakositkanon et al. 2000; Hinthong et al. 1985; see review in Ueno and Charoentitirat 2011). Given the example of the fault-controlled Pha Nok Khao Platform facies distribution, a similar interpretation may explain the control on clastic and carbonate facies distribution in the Khao Khwang Platform (Fig. 1 and 2), but this cannot be confirmed at present due to the absence of seismic reflection data coverage in the area. However, the outcrop studies to date have not previously demonstrated the presence of large normal faults. Recent surface mapping focussed on understanding the structural geology in parts of the Khao

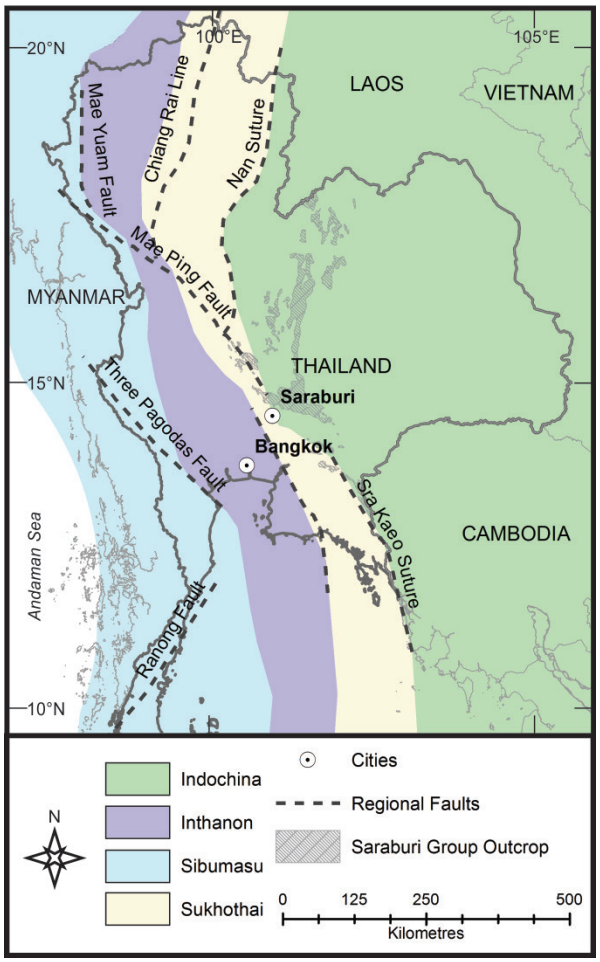

Fig. 1. Regional location map showing the major terranes in Thailand and their relationship with the Khao Khwang Fold–Thrust Belt and Saraburi region. The country boundaries are outlined, with the Thai border in bold.

Khwang Platform indicates that a number of carbonate platforms are present which are separated by time-equivalent deep-water facies. Thrusting has in places juxtaposed different small carbonate platforms giving the impression that one larger platform is present (see Fig. 2–4, Arboit et al. 2014; Morley et al. 2013; Warren et al. 2014).

The carbonate sequences that form the hills of central Thailand's Saraburi Province are also the location of internationally important biostratigraphic studies of Tethyan realm Permian faunas (e.g. Toriyama and Kanmera 1979), yet these karst towers are now far from their original shallow marine setting. These sequences belong to the "Khao Khwang Platform" *sensu* Wielchowsky and Young (1985) were deposited in a tropical shallow marine carbonate platform of late Pennsylvanian to Permian age along the western and possibly southern edge of the Indochina Terrane. Soon after deposition, the Khao Khwang Platform was deformed within the Khao Khwang Fold-Thrust Belt during various stages of the Indosinian Orogeny (Lower–Upper Triassic) (Arboit et al. in press; Arboit et al. 2014; Arboit et al. 2016b; Morley et al. 2013). However, the effect of this deformation is rarely acknowledged when discussing the sedimentology and stratigraphy of this sequence (e.g. Chutakositkanon et al. 2000, Thambunya et al. 2007). Dawson & Racey (1993) introduced the possibility of structural complications during their stratigraphic analysis of the Khao Khwang Platform in the Saraburi Province. The structure of the region has recently been refined with studies showing that the area has undergone extensive shortening and repetition by a series of low angle kilometre-scale thrusts which affect the stratigraphic order of the facies (Arboit et al. in press; Arboit et al. 2014; Morley et al. 2013). This new structural data necessitates a reassessment of the Saraburi Group stratigraphy across this region. One area where thrusting of these separate platforms can be demonstrated is along Highway 21 area north of Saraburi city centre (Fig. 1 and 2). This area was originally described in Dawson and Racey (1993) although the profusion of quarries now present in the area were absent at the time of their study. These new 3D outcrops allow the structural geology of the area to be studied in more detail (Arboit et al. 2014; Morley et al. 2013; Warren et al. 2014).

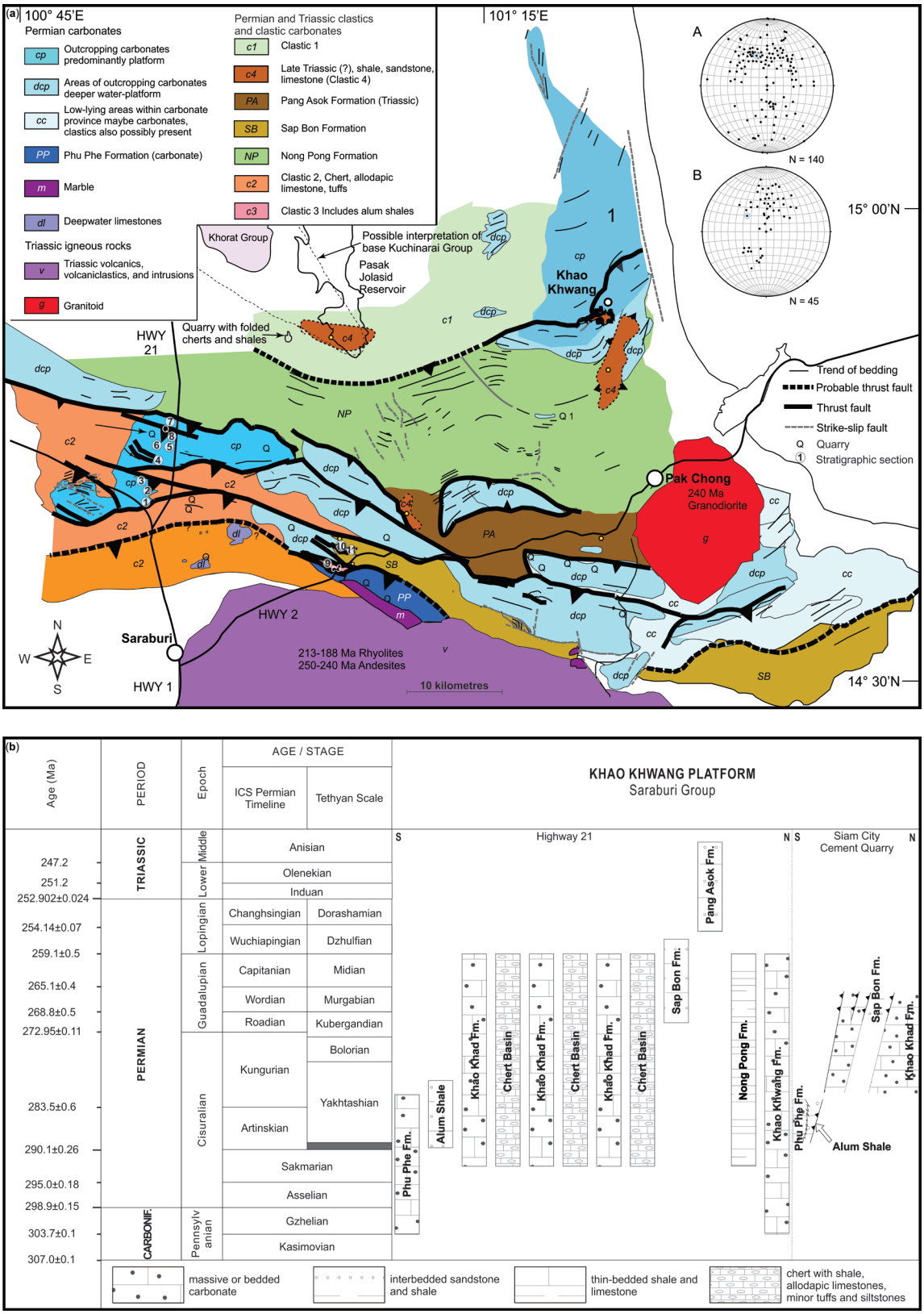

Fig. 2. Locations and ages of the regional Saraburi geology (a) Location map illustrating the regional stratigraphy (b) Stratigraphic model of the Khao Khwang Platform in the Saraburi Province; modified from Menning et al. (2006), Ueno and Charoentitirat (2011), Morley et al. (2013), Hansberry et al. (2015) and Arboit et al. (2016b).

In this paper we attempt to reconstruct the original distribution of the facies by integrating new biostratigraphic studies with the structural analysis of Arboit et al. (2014) to interpret the palaeogeography and palaeoecology of the platform sequences. This was done using new sedimentological logs from 11 field locations along Highway 21 and from the Siam City Cement Quarry along Highway 2 (Fig. 2 and 3, Supplementary Fig. 1 and 2). Following the recent structural reconstructions in the region (i.e. Arboit et al. 2014; Arboit et al. 2016b; Hansberry et al. 2015) the facies distribution and biostratigraphic correlations were reviewed and reinterpreted to develop a revised model for the platform.

2. Geological setting of the Saraburi region of Thailand

2.1 Carbonates and their Permian Depositional Environments

The Permian Period was a time of major global reef building which is also evident in the Permian carbonates of Thailand including the Saraburi Group (Udchachon et al. 2014; Weidlich 2002). The climax of Permian reef development in terms of diversity, abundance and extent occurred in the Guadalupian (Weidlich 2002). At the end of the Guadalupian, a combination of decreasing global sea level, regional salinity fluctuations and micro-continent collision led to a loss of >89% of reef related carbonate production (Udchachon et al. 2014; Weidlich 2002; Wright and Burchette 1998) and this terminated reef development within the Indochina Terrane (Weidlich 2002). This event is marked by an abrupt decline in large fusulinids, and also reef builders such as algae, coral, bryozoans and sponges (BouDagher-Fadel 2008; Davydov 2013; Kawamura and Machiyama 1995).

2.2 The Saraburi Group of the Khao Khwang Platform

In the Saraburi region, the carbonates of the Khao Khwang Platform are situated within the Khao Khwang Fold-Thrust Belt along the western edge of the Indochina Terrane along the eastern side of the Chao Phraya central plain and the western margin of Khorat Plateau (Fig. 1, Chutakositkanon et al. 2000; Ueno and Charoentitirat 2011; Ueno et al. 2012). These sequences were once considered part of the Ratburi Limestone (Dawson and Racey 1993; Sresthaputra et al. 1951), although subsequently they have been separated into the Saraburi Group (Bunopas 1992; Ueno and Charoentitirat 2011). Hinthong et al. (1985) identified three main carbonate sequences of the Saraburi Group: the Phu Phe, Khao Khad and Khao Khwang Formations. These platform units are interbedded with mixed siliciclastic and carbonate sequences, known as the Sap Bon, Pang Asok and Nong Pong Formations (Fig. 1; Chonglakmani 2001; Chutakositkanon et al. 2000).

Structural mapping of the Saraburi area undertaken by one of the authors (CKM) and various MSc and PhD projects was most recently discussed in Arboit et al. (2014) with the current version of the resultant cross-section shown in Fig. 4. The presence of many quarries allows the structural geology of the area to be studied in some detail, in a region where outcrops are generally sparse. The highest density of quarries is in the area north of Saraburi between Highways 1 and 21 and this was the focus area for detailed mapping (Fig. 2) with the aim of producing a regional structural cross-section through the fold-thrust belt. For basic descriptions of the structural geology see Morley et al. (2013), Arboit et al. (2014) and Warren et al.

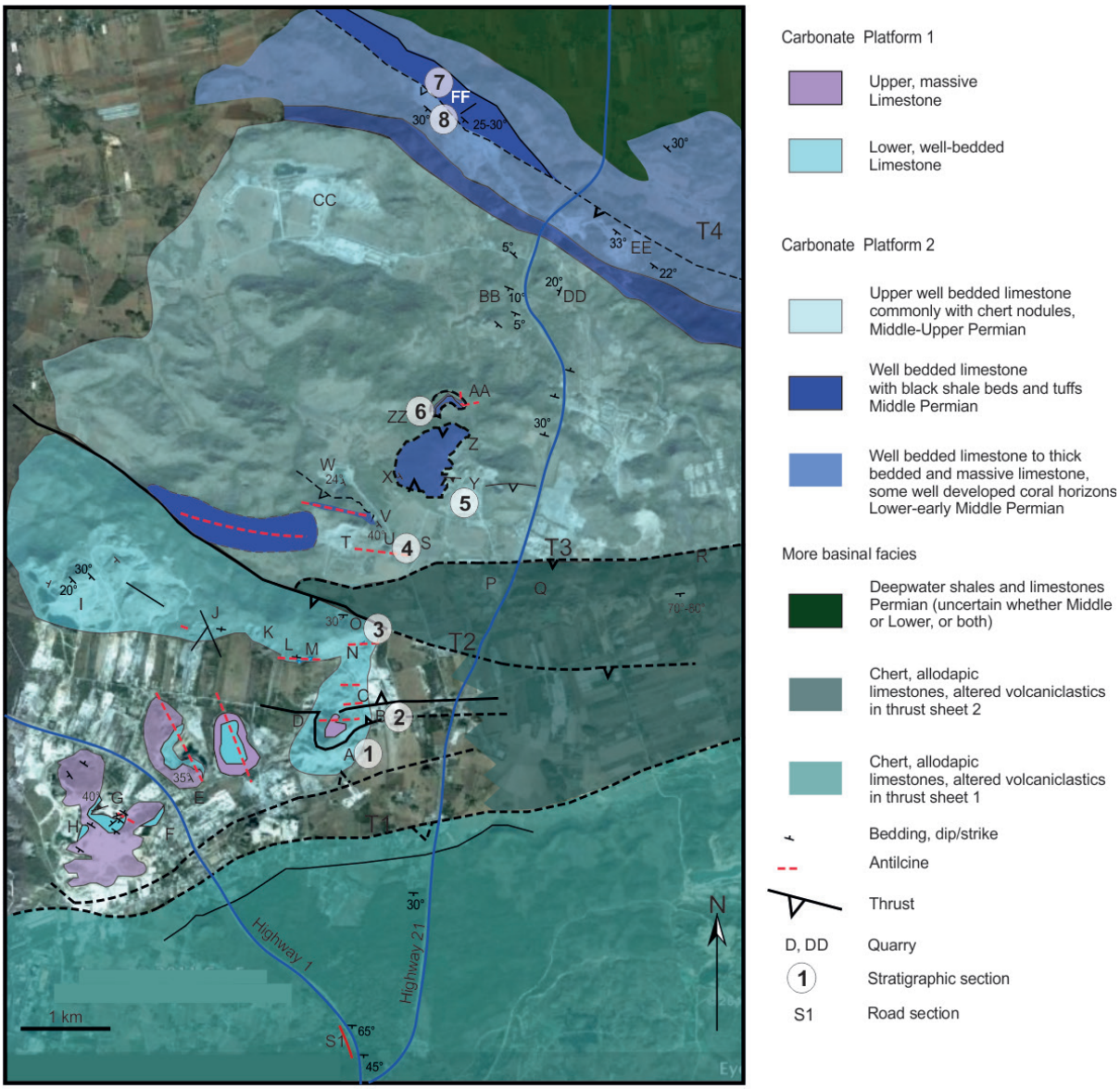

Fig. 3. Highway 21 location map portraying the quarries, stratigraphic section locations and detailed structural data; modified from Warren et al. (2014).

(2015). There are no wells or seismic data to constrain the subsurface interpretation although the surface geology does provide a good constraint for the shallow structure (see Fig. 4). The structure can be broadly interpreted in terms of classic thrust belt with fault bend, fault propagation and detachment folds being present at various scales (Morley et al. 2013; Arboit et al. 2014). However, there are significant lateral and vertical stratigraphic changes with different carbonate platforms separated by intervening shale-chert-allodapic limestone deeper marine deposits in between. Although classic section balancing methods can be used to draw a cross section through the carbonates (see Fig. 4b), there are a number of unknown factors that make such creating a balanced reconstruction difficult. These include a poor constraint on the depth to detachment and the fact that the original width of the deep water basins between the platforms are

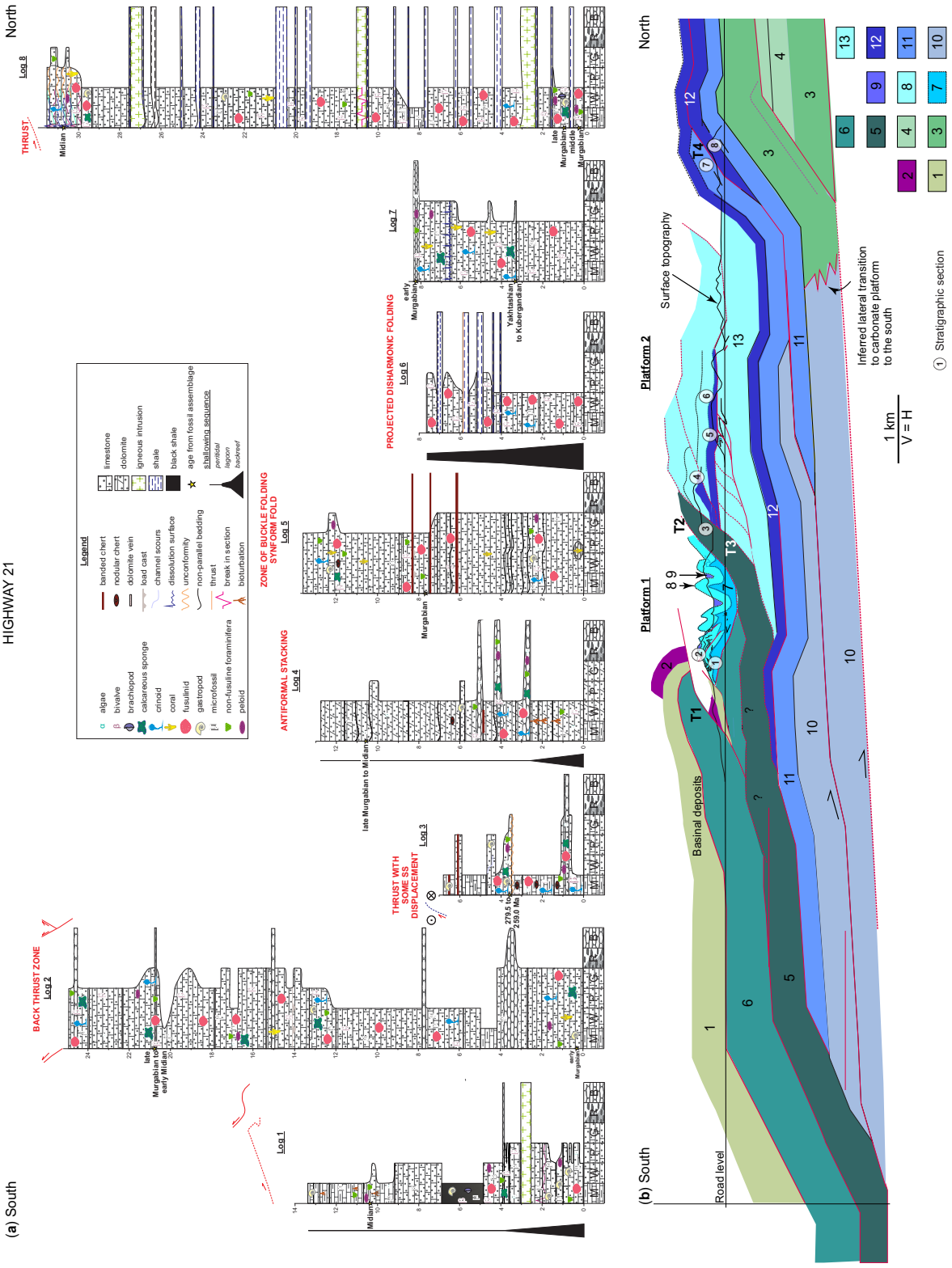
(a) South
North
HIGHWAY 21
THRUST
BACK THRUST ZONE
Log 2
THRUST WITH
SOME SS
DISPLACEMENT
Log 3
ANTIFORMAL STACKING
Log 4
ZONE OF BUCKLE FOLDING
SYNFORM FOLD
Log 5
PROJECTED DISHARMONIC FOLDING
Log 6
Log 7
Log 8
Log 1
Legend
banded chert
nodular chert
dolomite vein
load cast
channel scours
dissolution surface
unconformity
non-parallel bedding
thrust
break in section
bioturbation
limestone
dolomite
igneous intrusion
shale
black shale
age from fossil assemblage
shallowing sequence
algae
bivalve
brachiopod
calcareous sponge
crinoid
coral
fusulinid
gastropod
microfossil
non-fusuline foraminifera
peloid
(b) South
North
Platform 1
Platform 2
Surface topography
Basinal deposits
Road level
T1
T2
T3
T4
Inferred lateral transition
to carbonate platform
to the south
1 km
V = H
Stratigraphic section

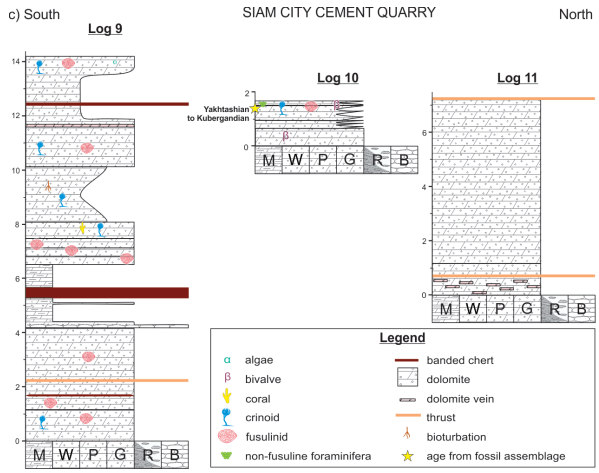

Fig. 4 Stratigraphic log and structural sections (a) Stratigraphic sections from Highway 21 showing some key fossil assemblage interpreted ages, where M is Mudstone, W is Wackestone, P is Packstone, G is Grainstone, R is Rudstone, B is Boundstone, scale is in metres. The star symbol indicates the location of samples containing an age diagnostic fossil assemblage. (b) Regional cross-section through the southern portion of the Saraburi Region with the Khao Khwang Fold-Thrust Belt, extensively modified from Arboit et al. (2014), where 1) Shale underlying marble unit, 2) Marble, inferred from platform to the south of platform 1. Basinal units comprising cherts, shale and allodapic limestone: 3) Early Permian Nong Pong Formation (north of platform 2), 4) Middle-late Permian Nong Pong Formation (north of platform 2. 5) Unnamed formation that lies between platforms 1 and 2, and laterally equivalent to platform 1. 6) Unnamed formation that is equivalent to 4, but is in a separate thrust sheet. Platform 1: 7) Well bedded commonly dark grey limestone, with some black shale layers, 8) Well bedded limestone dark-medium grey, 9) Massive limestone. Platform 2: 10) Hypothetical early Permian carbonate underlying the outcropping middle Permian units, lateral equivalent to deep water early Permian deposits north of the main hills. 11) Early middle Permian carbonates, commonly with reefal build-ups or mounds (Kubergandian-Murgabian). 12) Murgabian dark grey limestones with tuffaceous layers, and distinctive numerous, thin black shale layers, commonly with well-preserved bivalves including alatoconchids (Udchachon et al. 2014). 13) Middle to early late Permian carbonates, well bedded to massive, commonly with extensive diagenetic nodular chert (c) Stratigraphic sections from the Siam City Cement Quarry, scale is in metres and abbreviations same as (a).

unknown and could be tens or over a hundred kilometres. These basins must have been wide enough to accommodate coarse reefal detritus, debris flows, and proximal turbidite deposits, to chert and shale dominated sequences, with thin, fine grained turbidite beds i.e. slope and basinal sediments. The thinner bedded basinal sequences are disharmonically folded and thrusted by tight chevron and kink folds, and are poorly exposed except where they have been rarely quarried for road aggregate. Consequently, estimates of the internal deformation of the sequences can only be roughly estimated. In Fig. 4b, the amount of thrusting that caused platform 1 to converge with platform 2 and the amount of shortening of the basinal deposits between thrusts T2 and T3 is the main unknown factor in estimating the original length of the section. Although the platforms are in close proximity to each other in the present day they were originally separated by a considerable distance at their time of deposition. In the cross-section (Fig. 4b), the transition from the carbonate platforms to the basinal deposits is shown simplistically as it is not clear whether the transition is fault controlled as observed in the Khorat Plateau area (Booth and Sattayarak 2011) or, is represented by an originally gradual lateral lithological transition.

2.3 Dating the Saraburi Group

Paleozoic palaeomagnetic data indicate that the Saraburi Group was deposited at a palaeolatitude of nearly 10° south of the Permian equator from the Upper Pennsylvanian to the late Permian (El Tabakh and Utha-Aroon 1998; Metcalfe 2013; Thambunya et al. 2007). Marine deposition of the Saraburi Group was followed by clastic deposition in some areas (e.g. upper part of the Sap Bon Formation, Ueno and Charoentitirat 2011), and by

Lower Triassic clastic sedimentation in a fore deep marine setting (Pang Asok Formation, Arboit et al. 2016b). This was followed by uplift and deformation in the Indosinian Orogeny, which created the Khao Khwang Fold-Thrust Belt during the Triassic (Fig. 2 and 4, Arboit et al. 2016b; Morley et al. 2013). The Saraburi Group contains a diverse algal and foraminiferal fauna, which has been studied taxonomically by Dawson (1993); Dawson and Racey (1993); Toriyama (1975) and Udchachon et al. (2014). Although often interpreted as a vertical stratigraphic succession, recent fossil and radiometric data demonstrate that these carbonate sequences are mostly contemporaneous (Ueno and Charoentitirat 2011).

The Khao Khad Formation of the Saraburi Group has been previously dated as middle Guadalupian and on the Tethyan Scale, predominantly Murgabian with limited extension into the overlying Midian (Fig. 2b, Baird and Bosence 1993; Dawson and Racey 1993; Ueno and Charoentitirat 2011). The Tethyan Scale is zoned using fusulinids, a foraminiferal fossil group widely studied and observed within the Saraburi Group sequences (Dawson and Racey 1993; Toriyama and Kanmera 1979). In contrast, the primary fossils used for biostratigraphic correlation in the International Commission on Stratigraphy (ICS) Permian timeline are conodonts (Shen et al. 2013). Conodonts are insufficiently studied in the Tethys and therefore fusulinids and to a lesser extent ammonoids are used here to subdivide the Permian (see Fig. 5 and Supplementary Fig. 3, Leven 2003; Ueno and Charoentitirat 2011; Wardlaw et al. 2004). Although the ICS and Tethyan scales in Supplementary Fig. 3 are broadly equivalent the use of different fossil groups does lead to differences in the exact ages (Henderson et al. 2012; Leven 2003; Menning et al. 2006) e.g. in the Tethyan scheme the Murgabian ranges older than the Wordian and has an older top since the Murgabian lacks the conodonts to establish a strong correlation (Menning et al. 2006). Dating in this study therefore uses the Tethyan stages where possible.

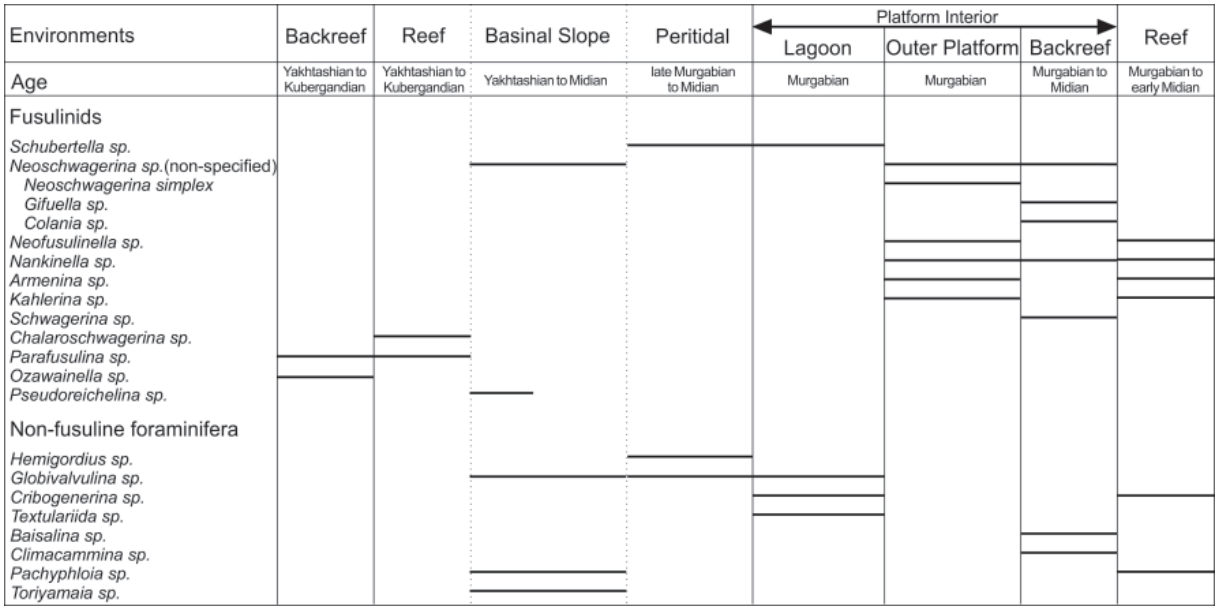

Fig. 5. Distribution of the principal foraminifera and their associated facies during the Yakhtashian to Midian in the Saraburi area.

3. The Saraburi locality and methodology

Fieldwork was carried out along Highway 21 and in Siam City Cement Quarry along Highway 2 in the Saraburi Province of Thailand, approximately 100 kilometres NNE of Bangkok (see Fig. 1). The Saraburi Province was chosen because it has exceptionally well-exposed sections of the Saraburi Group including the platform and basinal sediments. It is also an area of ongoing structural research work where a better understanding of the area's biostratigraphy will assist in unravelling the structure of the area (Arboit et al. in press; Arboit et al. 2014; Hansberry et al. 2015; Morley et al. 2013).

Stratigraphic logs were taken from 11 field locations and these form the basis of facies interpretations and biostratigraphic correlation. The stratigraphic sections were numbered from south to north with: Logs 1 to 8 taken along Highway 21 (Fig. 2 and 4a) and Logs 9 to 11 from the Siam City Cement quarry (Table 1; Fig. 4c). Thirty two samples were studied using thin sections to infer facies and to constrain the ages of the sequences. These data were then used to interpret the depositional setting for the Permian sequences.

4. Fauna of the Khao Khwang carbonate platform

The microfaunas are dominated by foraminifera (see Fig. 5; Fig. 6 and Supplementary Table 1) including fusulinids which help constrain the ages of the sections (see Fig. 5; Supplementary Table 1). The ages for sections (Logs 1 and 4) that lack fusuline foraminifera are harder to constrain and therefore, were based mainly on longer ranging smaller benthic foraminifera. The degree of fossil preservation also varies and is sometimes poor, making identification of the fossils and dating difficult e.g. in Logs 5 and 9 (Fig. 2).

Other commonly identified fossils are described in Supplementary Table 1 and illustrated in Fig. 7. The Guadalupian–Lopingian coral, *Waagenophyllum* sp. (Fig. 7), appear throughout the stratigraphic sections, as both solitary forms and as parts of larger dendroid colonies. Specimens of the large bivalve *Alatoconchia* also occur and are well preserved in Log 6 where they are up to up to 30 cm long, whilst brachiopods are rarely preserved e.g. in Logs 1 and 8. The gastropods identified in the stratigraphic section are mostly composed of recrystallised calcite although in some instances they are replaced with chert.

Table 1. Location of the stratigraphic sections and thin section sites

Location Number	*Latitude*	*Longitude*	*Locality*	*Formation*	*Log Length (m)*	*Average bed thickness (m)*
1	14°41'57.6"N	100°53'00.5"E	Quarry A, Highway 21	Khao Khad	13.3	0.7774
2	14°42'0.70"N	100°53'10.09"E	Quarry B, Highway 21	Khao Khad	24.9	1.5625
3	14°42'50.6"N	100°53'06.0"E	Quarry O, Highway 21	Khao Khad	6.78	0.8475
4	14°43'17.4"N	100°53'25.4"E	Quarry SS, Highway 21	Khao Khad	12.85	0.9179
5	14°43'43.4"N	100°54'02.9"E	Quarry Y, Highway 21	Khao Khad	13.7	1.1399
6	14°44'56.94"N	100°53'04.55"E	Quarry ZZ, Highway 21	Khao Khad	7.74	0.645
7	14°46'06.70"N	100°53'46.90"E	Quarry FF, Highway 21	Khao Khad	8.25	1.625
8	14°46'06.70"N	100°53'46.90"E	Quarry FF, Highway 21	Khao Khad	31.79	0.8129
9	14°37'37.7"N	101°04'24.5"E	Shale Quarry, Siam City Cement	Phu Phe	13.41	1.49
10	14°38'08.9"N	101°04'48.9"E	Middle Ridge, Siam City Cement	Khao Khad	1.67	0.4175
11	14°38'08.9"N	101°04'48.9"E	Middle Ridge, Siam City Cement	Khao Khad	7.21	2.4033
Y	14°43'26.9"N	100°52'57.5"N	Quarry N, Highway 21	Khao Khad	-	-

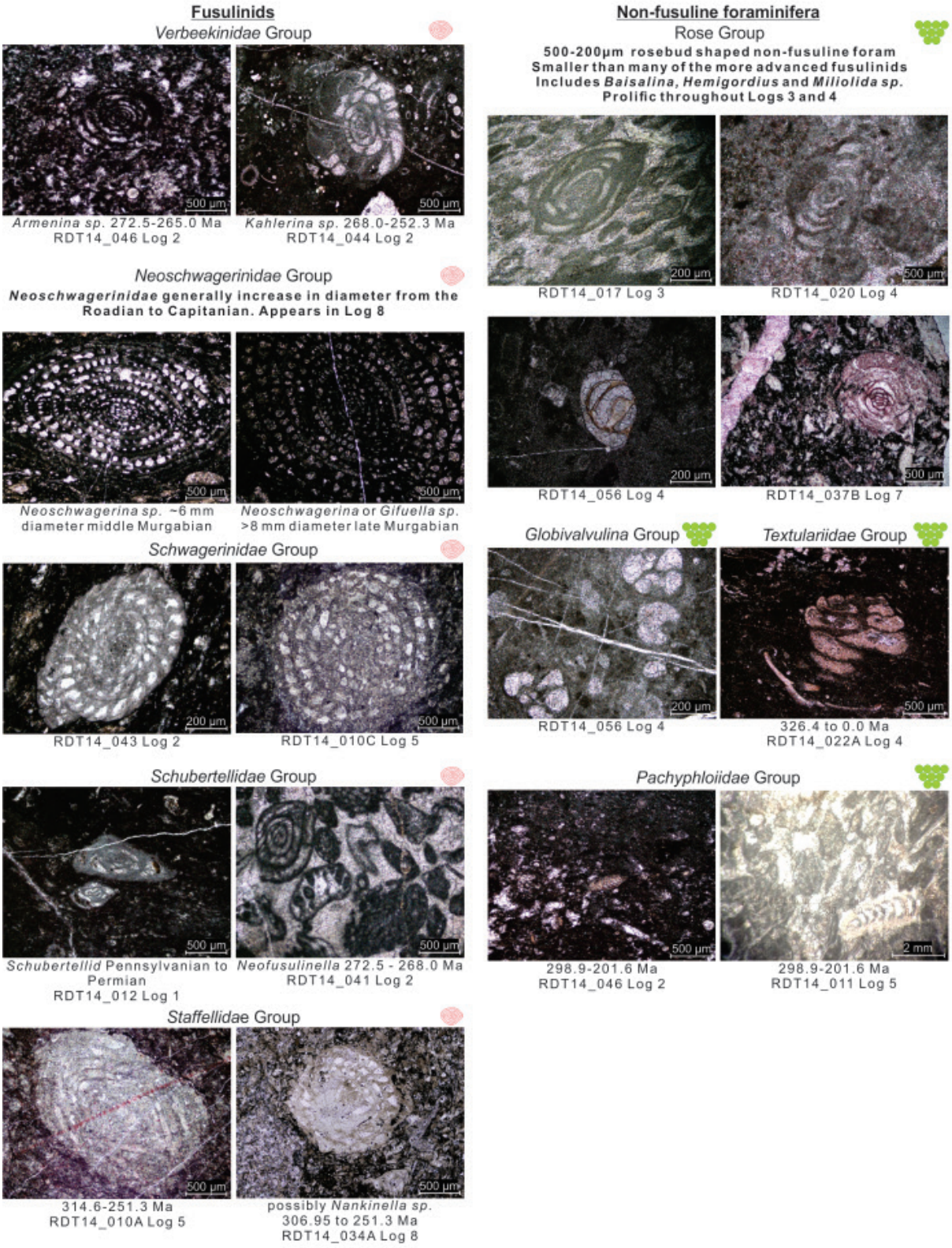

Fig. 6. Foraminiferal groups used to determine age, distinguishes fusuline and non-fusuline foraminifera.

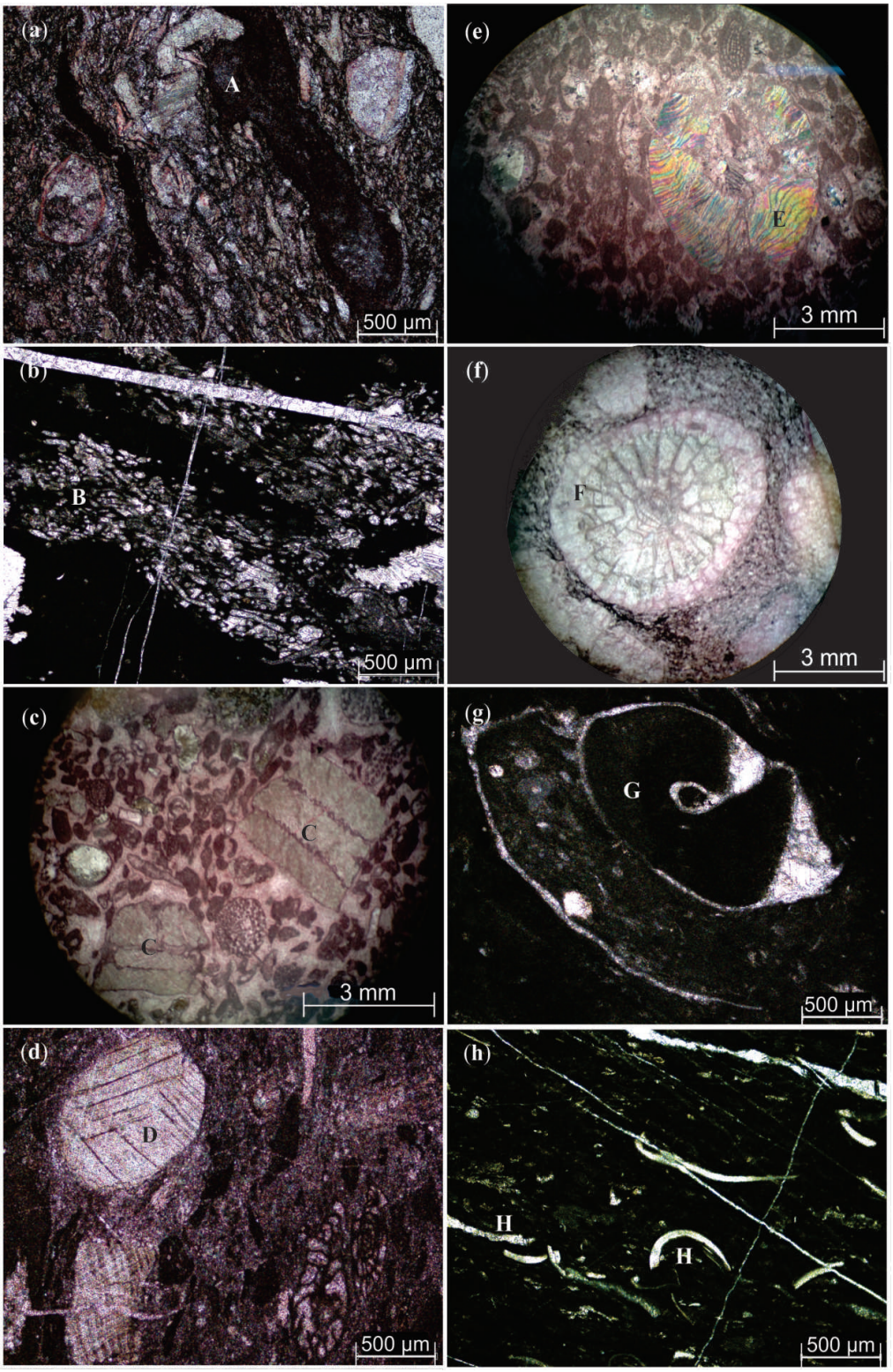

Fig. 7. Other common fossils seen in thin section and in the field (a) *Tubiphytes obscurus* (A) Log 5 RDT14_006B (b) *Girvanella* sp. (B) Log 1 RDT14_015 (c) Three crinoid columnals that clearly show crenulae which connect the plates (C) Log 2 RDT14_041 (d) Crinoid fragments that are more abraded (D) Log 9 RDT14_051 (e) crinoid columnal close to the cup in cross-polarised light (E) Log 2 RDT14_041 (f) Permian rugose coral *Waagenophyllum* sp. (F) Log 5 RDT14_005 (g) Gastropod fragment (G) Log 1 RDT14_012 (h) Bivalve fragments (H) Log 4 RDT14_022A

5. Facies of the Permian Saraburi carbonate sequence

5.1 Peritidal Facies

Peritidal deposits are composed of dark carbonaceous mudstones-wackestones and dolomitised laminated algal boundstones. The mudstone lithologies are dark grey to black and contain rare fusulinids and brachiopods, whereas the wackestones often contain a variety of fossils. Secondary Fe-calcite obscures the original depositional texture in some parts. Peritidal settings were interpreted for the upper sections of Logs 1 and 4. Algae are abundant in the boundstone units and include *Girvanella* (Fig. 7b) whilst foraminifera include *Hemigordius* and *Globivalvulina* with sparse fusulinids (*Schubertella*). The fusulinids present in these sections indicate ages between the late Murgabian to Midian (Fig. 4 and 6). This peritidal setting is similar to the peritidal environment (Unit B: Algal biolithite) described by Thambunya et al. (2007) within central Thailand.

5.2 Platform Interior Facies

The platform interior facies contain three sub-environments: lagoon, outer platform and higher energy backreef. The low-energy lagoon comprises bioturbated skeletal and peloidal wackestones and packstones with localised interbedded shales. Wackestones display a diverse fossil assemblage. Packstones often grade into wackestones or grainstonse within a single bed. A lagoonal environment is interpreted for the lower parts of Logs 1 and 4 and the upper part of Log 6. The fauna comprised abundant algae including *Girvanella*, bivalves (including *Alatoconchidae*), fusulinids (*Neoschwagerina simplex*) and non-fusuline foraminifera (*Globivalvulina*, *Schubertella*, *Cribogenerina* and *Textulariida*, see Fig. 5 and 6). *Alatoconchidae* bivalves preferred a soft muddy substrate according to Udchachon et al. (2014). The fossil assemblages present within the lagoonal environment of this study suggest a Murgabian age. The fauna and facies observed are similar to the subtidal lagoon environment (Unit A: Calcilutite with nodular chert) described by Thambunya et al. (2007) within central Thailand. The peritidal units conformably overlie the lagoonal facies in the work by Thambunya et al. (2007) which is also the case of the peritidal and lagoonal facies in Logs 1 and 4 (see Fig. 4).

The outer platform sequences consist of bedded bioclastic wackestones to grainstones with some algal boundstone interbeds. Isolated coral framestones are present within the bioclastic grainstone-dominated stratigraphic sections. Outer platform settings were interpreted within Logs 1, 2, 5, 7 and 8 (Fig. 4). A variety of foraminifera are present in these sections: *Neoschwagerina simplex*, other *Neoschwagerina* species, *Neofusulinella* sp., *Nankinella* sp., *Kahlerina* sp., and *Armenina* sp. (shown in Fig. 5 and 6). The fossil assemblages constrains a Murgabian age. A similar outer platform environment with bioclastic limestones containing small boundstone patches is described by Kołodziej et al. (2012) in Bulgaria.

The backreef facies comprise parallel bedded bioclastic wackestones and packstones. Packstones often grade into a wackestones within a single bed. This environment is best developed in Logs 5, 6 and 8 from Highway 21. The fauna in the backreef facies comprises crinoids, fusulinids (*Nankinella*, *Schwagerina*, *Colania*, *Neoschwagerina* and *Gifuella* see Fig. 5 and 6), bivalves (*Alatoconchidae*), non-fusuline foraminifera (*Baisalina* and

Climacammina), algae (*Tubiphytes*), gastropods and coral (*Waagenophyllum* in Fig. 7f). Brachiopods, calcareous sponges and peloidal matter are also present. The fusulines indicate a Murgabian to Midian age. Further south in the Log 9 section fossils are replaced by chert. The presence of the foraminifera *Parafusulina* sp. and *Ozawainella* sp. in this section indicate a Yakhtashian to Kubergandian age. These units follow the backreef facies described by Tucker (2001); Wright and Burchette (1996).

5.3 Reef Facies

Reef facies are dominated by algal boundstones and the adjacent marginal shoals comprise fusuline packstones and grainstones. Reef builders were mostly algae and corals. The boundstones along Highway 21 (within Logs 2 and 8) are dominated by encrusting *Archaeolithoporella* and *Tubiphytes* with calcisponges and abundant syndepositional marine cements as described by Dawson and Racey (1993) and Dawson et al. (1993). Within the fusuline packstones to grainstones are abundant bivalves and fusulinids (including *Neofusulinella*, *Nankinella*, *Kahlerina*, and *Armenina*) together with crinoids, corals and the non-fusuline foraminifera *Cribrogenerina* and *Pachyphloia* (Fig. 5 and 6). Algal reef of Murgabian age was interpreted in Log 2. A late Murgabian to Midian algal reef is found at the top of Log 8. The algal reefs of Logs 7, 10 and 11 commonly have sparry calcite cement and pervasive dolomitisation. The fusulinid assemblages in these sections include *Chalaroschwagerina* and *Parafusulina* sp., which indicate an older Bolorian–Kubergandian to possible early Murgabian age. The bivalve and fusulinid-rich grainstones with rarer coral lenses in Log 7 pass westwards into reef mounds. The section is dated as Yakhtashian–Kubergandian. Both the platform margin environments interpreted for the Murgabian–early Midian aged Log 2 and top of Log 8 and the older Yakhtashian–Kubergandian assemblages of Logs 7, 10 and 11 were not entirely rimmed with reef builders, but instead were sites of small isolated biostromes (as concluded by Dawson et al., 1993 prior to the profileration of quarries in the study area).

5.4 Basinal Slope Facies

The basinal slope sediments comprises thinly bedded mudstones with rarer allodapic packstone-grainstone-boundstone beds. Multiple chert nodules and lenses also occur with some bioclasts replaced by chert. The fauna comprises fragmented and abraded crinoids, fusulinids (*Neoschwagerina*, *Pseudoreichelina*), non-fusuline foraminifera (*Toriyamaia* sp., *Pachyphloia* sp., and *Globivalvulina cyprica*) and gastropods. Log 3 is the only section containing basinal slope sediments (Fig. 4). This fossil assemblage indicates an age between the Kubergandian and Midian. Our lithological observations are consistent with the descriptions of Facies 1 Siliceous microcrystalline limestone: Turbidite and basin slope deposits of Dawson (1993).

6. Correlation of the stratigraphic sections from the Khao Khwang Platform

In this work, it is assumed that the Tethyan Murgabian and Midian are broadly equivalent to the ICS Wordian and Capitanian respectively as used previously by Wardlaw et al. (2004), Menning et al. (2006) and Kobayashi et al. (2010) (Fig. 2 and Supplementary Fig. 3). The fossils identified in thin section were correlated

using the Tethyan fusulinid zonations (Fig. 2 and 4 and Supplementary Fig. 3). The Tethyan Scale provides a higher resolution fossil zonation for the Saraburi Group as it represents the currently most appropriate regional timescale for the Indochina Terrane (Fig. 2, Menning et al. 2006; Ueno and Charoentitirat 2011).

The fusulinids identified are mostly representative of the *N. simplex*, *N. craticulifera* and *N. margaritae* Biozones of the Murgabian (Fig. 6, Supplementary Fig. 3 and Supplementary Table 1), which are further described by Menning et al. (2006). The *Neoschwagerinidae* present are not as evolved as *Yabeina* sp., which is characteristic of the overlying Midian discussed by Kobayashi et al. (2010). Log 4 and the upper section of Log 1 lack fusulinids and are therefore tentatively assigned to the early Midian. Stratigraphic sections containing only non-fusuline foraminifera (Logs 1 and 4) were harder to date as many of these taxa are relatively long ranging compared to the fusulines.

The fossil assemblages from Log 7 along Highway 21 and from the Siam City Cement Quarry (Logs 9 to 11) contain Kubergandian aged fossils. The sequences in Logs 1 to 6 and 8 all contain Murgabian aged fossil assemblages whilst the fusuline assemblages in Logs 1, 2, 4 and 8 indicate deposition extending into the Midian. Ages of Kubergandian to Midian are supported by the previous work of Baird and Bosence (1993), Dawson and Racey (1993) and Thambunya et al. (2007).

Hornblende is present in the thin sections of Logs 3 and 9 indicating local syndepositional volcanism. The grey-green dykes and sills of andesitic composition noted in Logs 1 and 8 (Fig. 4) form part of the contemporaneous volcanism recently described by Arboit et al. (2016a). These sills may be associated with the Permo-Triassic Phra Ngam Diorite and Khao Yai Volcanics, which are known to be coeval with the Saraburi Group (Chutakositkanon et al. 2000; Ueno et al. 2012).

7. Tectonic juxtaposition of facies

Deformation related to the Indosinian Orogeny had a large impact on the topography and stratigraphy of the Saraburi Province. The original relationships between the facies and their spatial variations across the three modelled carbonate platforms have been modified as a result of regional scale deformation by thrusting and folding, with Cenozoic strike-slip deformation superimposed. This has led to displacement of the originally geographically adjacent facies as shown by the fossil assemblages and ages recorded herein.

Within the southern platform of Highway 21 (Logs 1 and 2), the facies exhibit rapid vertical and lateral changes (Fig. 4). These lateral changes are at least partially the result of shortening associated with the extensive folding and backthrusting within this region (Fig. 4). The facies in the northern platform (Logs 4 to 8) have a wider lateral extent and variation compared to the southern platform. However, there is less vertical facies variation in some of the sequences in the northern platform. For example, Log 8 contains 30 metres of predominantly highly bioclastic wackestones of the outer platform/back reef (Fig. 4) before changing to a marginal platform with algal patch reefs. The comparatively drawn-out facies variation of the northern platform may be due to the original depositional environment being more stable than in the

southern platform. Alternatively, folding and faulting may have caused repetition or stratigraphic omission in the platform facies in the northern platform (Fig. 4). The two discrete carbonate platforms are separate from each other, with the southern carbonate platform having been transported from the area south of the cherts observed in Log 3 (see Fig. 2, 3 and 4). This separation is justified by the presence of a thrust fault with a component of oblique displacement, which is very close to the locality of Log 3 and divides the southern platform containing Logs 1 and 2 from the northern platform including Logs 4 to 8 (see Fig. 4). Much of the fauna within the turbidite deposits in the interpreted basinal slope facies were derived from the shallow marine environment. The basinal slope environment on Log 3 is dominated by chert along with thinly bedded mudstones, lesser shale and allodapic limestone beds and minimal tuffaceous sandstones. The diverse fossil assemblage observed in Log 3 includes abraded and fragmented *Neoschwagerina* sp., *Toriyamaia* sp., *Pachyphloia* sp., gastropods and *Globivalvulina cyprica*, which can broadly constrain the likely age between the Kubergandian and Midian. This cherty section is quite distinct from the thickly bedded limestone sequences that dominate most of the Khao Khad Formation (Fig 2 and 4) and therefore a separate formation name may be merited for the chert-dominant basins along Highway 21.

It is unclear whether Log 3 represents a narrow restricted break in the carbonate platforms; a deep water channel between two platforms (especially as the facies has a lot of debris flows within it suggesting proximity to a carbonate platform) or, a more extensive deep water basin between isolated platform carbonates. The displacement is unquantified and the original extent of the basinal slope is difficult to determine and was therefore excluded in recent reconstructions (e.g. Arboit et al. 2014). These authors favoured an original 10 to 20 kilometres wide deep water basin. The cherty basinal facies change laterally into carbonate facies within a couple of kilometres from east to west. It is therefore plausible that the facies may also change at a similar rate in a north to south direction.

Another possible explanation is that the cherty slope facies belongs to the Nong Pong Formation. Our descriptions of the basinal slope are consistent with Dawson (1993) Facies 1 Basin Slope (turbidites). Although, Dawson's Facies 1 are north of our Log 3 location, they are similar to the location of the Nong Pong Formation (Unit 3) on the cross-section in Fig. 4. If the sediments in the study region were originally deposited in several carbonate platforms then other formations within the Saraburi Group especially the Nong Pong Formation may also be structurally repeated.

Quarry FF, displayed on Fig. 3, provides an exposure of a carbonate sequence across a major thrust (Quarry FF is imaged in Supplementary Fig. 1g and 1i). The thrust is well exposed in the quarry and forms a zone about 20 m thick of sheared shales with well-developed S-C fabrics, and graphitic slip surfaces, together with sheared lenses of carbonates and igneous rocks. This is thrust T4 in Fig. 4. The section above the thrust is a carbonate, with small build-ups or mounds that are described in Log 7. The footwall section is composed of dark grey to black carbonates with interbedded black shales, and in a number of places contains well-preserved

bivalves, including alatochonchids. The section is described in Log 8. The thrust relationships indicate that the section in Log 7 (hanging wall) should be older than the footwall section (Log 8), and indeed the age for Log 8 based on fusulinids is estimated to be middle to late Murgabian, while Log 7 is Yakhtashian to early Murgabian.

The fossil assemblage in Log 7 that sits above the large thrust in the north provides evidence that this section is older than the assemblage within Log 8 that sits immediately below this thrust structure (see Fig. 4). The foraminifera identified in Log 7 include *Chalaroschwagerina* sp., *Parafusulina* sp. and *Climacammina* sp. indicating a Yakhtashian to Bolorian age that may extend into the Kubergandian. Many of these fossils were also identified in the region by Dawson and Racey (1993) who interpreted this assemblage to be Yakhtashian to late Bolorian (Artinskian). These units are also outlined as *Archaeolithoporella–Tubiphytes* organic build-ups by Dawson et al. (1993) who constrain the boundstones to be early Permian in age. The 2 to 3 metre thick build-ups described by Dawson et al. (1993) are estimated to extend 30 to 45 metres laterally. These stratigraphic sections described by Dawson et al. (1993) are from a similar locale and biostratigraphy to the units described in this paper, further confirming our interpretation. However, the large *Neoschwagerina* sp. and *Gifuella* sp. in Log 8 below the thrust are distinctively younger in age, as they are characteristic of the middle and late Murgabian (see Fig. 5 and 6). The stark contrast in age determined through biostratigraphy confirms the presence of the thrust structure identified by Arboit et al. (2014).

8. Palaeogeography

Recent structural analysis has demonstrated the, previously underappreciated, allochtonous nature of the Saraburi area (Arboit et al. in press; Arboit et al. 2014; Hansberry et al. 2015; Morley et al. 2013). This forces a reinterpretation of this classic Tethyan margin sequence (*cf.* Dawson and Racey 1993). In the new structural framework, the facies variations within the stratigraphic sections require three middle Permian carbonate platforms, recorded in Logs 1–3, 4–8 and 9–11. Each of these platforms deepens northwards, although deformation has obscured the facies' original position and thickness. The four main carbonate facies, described above, are identified in the logged sequences and the following section discusses how these facies may relate to each other and how they change through the Permian.

8.1 Yakhtashian to Kubergandian palaeogeography

The backreef sequences of Log 9 were deposited in the Yakhtashian to Kubergandian (Fig. 8a) whilst on Logs 10 and 11 they comprise algal boundstones and fusuline packstone-grainstones of deposited in a marginal platform environment in the Bolorian to Kubergandian. The marginal reef facies of Log 7 was deposited between the Yakhtashian and the Kubergandian. We interpret that the platform margin was not entirely rimmed with reef builders but was the site of formation of small algal biostromes, this is consistent with the conclusions of Dawson et al. (1993); Dawson and Racey (1993).

8.2 Early to middle Murgabian palaeogeography

The deposition of small algal biostromes continued during the early Murgabian

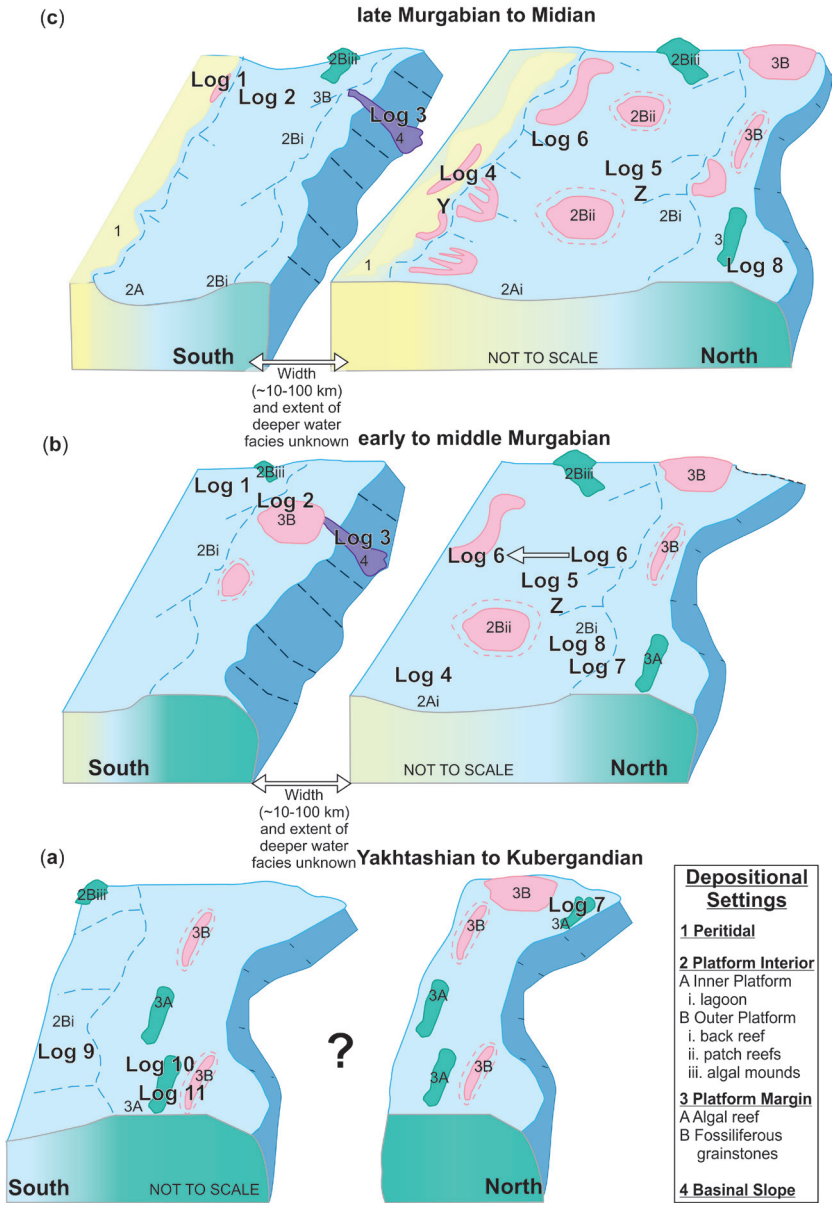

Fig. 8. Interpreted Permian palaeogeography younging from (a) to (c). (a) Yakhtashian to Kubergandian (b) early to middle Murgabian (c) late Murgabian to Midian sequences

on Log 7 whilst a similar biostrome was deposited on the southern platform of Highway 21 (Log 2; Fig. 8b). Also in the early Murgabian, the backreef facies of Log 6 was deposited. The depositional environment for Log 6 shallowed during the middle Murgabian to produce bioturbated skeletal and peloidal wackestones and packstones in a lagoonal environment. Bioturbated lagoonal wackestones accumulated at the location of Log 4 at this time. Outer platform environs are inferred from the middle Murgabian as shown on Logs 1, 2, 5 and 8 (Fig. 8b).

8.3 Late Murgabian to Midian palaeogeography

The vertical change in facies indicates the sequences are predominantly shallowing upwards during the Murgabian and Midian (shown in Fig. 4). The environment on

Log 4 shallowed between the middle and late Murgabian, indicated by the presence of dolomitised peritidal flats (Fig. 4 and 8c). During the late Murgabian, the backreef sediments of Logs 5 and 8 were deposited. Igneous activity evidenced by the presence of contemporaneous andesitic sills in the Log 1 and 8 sections. This interpreted timing of the intrusion is consistent with mid-Permian to Triassic ages of the Khao Khwang Fold-Thrust Belt volcanic suite discussed in Arboit et al. (2016a). The peritidal carbonaceous mudstones-wackestones and dolomitised laminated algal boundstone beds of Logs 1 and 4 were deposited (Fig. 8c). The platform interior setting in Log 8 is topped by Midian-aged packstone and grainstone with algal boundstone interbeds (Fig. 8c).

9. Conclusion

Palaeoenvironmental inferences and fossil identification allow for section correlation and assist in unravelling the structure of this deformed platform. The sequences range from Yakhtashian to Midian in age with much of the assemblage dated as Murgabian. The fossil assemblages were deposited in a shallow marine platform setting. The environments form a continuum, but can be grouped into peritidal, low-energy lagoon, outer platform, backreef, algal biostrome reef and slope to basin (Fig. 5 and Fig. 8). It is possible that there are remnants from three middle Permian platforms within the Saraburi study area. Each of these platforms deepens northwards although deformation has obscured the facies' original position and thickness of the sequence. Particulars on their width, displacement and origin are still largely unknown with further extensive sedimentological studies required to determine the dimensions of the Saraburi carbonate platforms and their associated deeper water areas. This study's interdisciplinary approach of analysing the biostratigraphy in the context of the newly derived allochtonous framework of the region provides a unique perspective on fold-thrust belts and carbonate stratigraphy, which is applicable to many other structurally complicated regions around the world.

Acknowledgements

The authors would like to thank Mr Yot from Siam City Cement Public Company Limited and Laainam Chaipornkaew of Petroleum Authority of Thailand (PTT) for access to the field sites and their friendly assistance in Thailand. Andrew Racey and Anthony Barber are gratefully acknowledged for their helpful and constructive reviews of this manuscript. Vladimir Davydov from Boise State University is thanked for his assessment of the authors' foraminifera identification. George Morgan from Adelaide Petrographic Laboratories Pty Ltd is cordially acknowledged for creating the thin sections for analysis.

This is a contribution to IGCP projects #589 (Development of the Asian Tethyan Realm) and #628 (The Gondwana Map). This publication forms TRaX Record #377. This work was funded by Australian Research Council through projects #DP 120101460 and #FT120100340.

References

Arboit, F., Amrouch, K., Morley, C., Collins, A.S. & King, R. in press. Palaeostress magnitudes in the Khao Khwang fold-thrust belt, new insights into the tectonic evolution of the Indosinian orogeny in central Thailand. Tectonophysics, doi: http://dx.doi.org/10.1016/j.tecto.2017.01.008.

Arboit, F., Collins, A.S., Jourdan, F., King, R., Foden, J. & Amrouch, K. 2016a. Geochronological and geochemical study of mafic and intermediate dykes from the Khao Khwang Fold-Thrust

Belt: Implications for petrogenesis and tectonic evolution. Gondwana Research, 36, 111-128.

Arboit, F., Collins, A.S., King, R., Morley, C.K. & Hansberry, R. 2014. Structure of the Sibumasu–Indochina collision, central Thailand: A section through the Khao Khwang Fold and thrust belt. Journal of Asian Earth Sciences, 95, 182-191, doi: http://dx.doi.org/10.1016/j.jseaes.2014.06.016.

Arboit, F., Collins, A.S., Morley, C.K., King, R. & Amrouch, K. 2016b. Detrital zircon analysis of the southwest Indochina terrane, central Thailand: Unravelling the Indosinian orogeny. Geological Society of America Bulletin,, 128, 1024-1043.

Ayan, T. 1965. Chemical staining methods used in the identification of carbonate minerals. Bulletin of the Mineral Research and Exploration Institute of Turkey, 133-147.

Baird, A. & Bosence, D. 1993. The sedimentological and diagenetic evolution of the Ratburi Limestone, Peninsular Thailand. Journal of Southeast Asian Earth Sciences, 8, 173-180, doi: http://dx.doi.org/10.1016/0743-9547(93)90018-K.

Beavington-Penney, S.J. & Racey, A. 2004. Ecology of extant nummulitids and other larger benthic foraminifera: applications in palaeoenvironmental analysis. Earth-Science Reviews, 67, 219-265, doi: http://dx.doi.org/10.1016/j.earscirev.2004.02.005.

Booth, J. & Sattayarak, N. 2011. Subsurface Carboniferous - Cretaceous geology of NE Thailand. In: Ridd, M.F., Barber, A.J. & Crow, M.J. (eds.) The Geology of Thailand. The Geological Society, London, 185-222.

BouDagher-Fadel, M.K. 2008. The Palaeozoic larger benthic foraminifera: the Carboniferous and Permian. In: Boudagher-Fadel, M.K. (ed.) Developments in Palaeontology and Stratigraphy. Elsevier, 39-118.

Bunopas, S. 1992. Regional Stratigraphic Correlation in Thailand. Geologic Resources of Thailand: Potential for Future Development, 189-208.

Chonglakmani, C. 2001. The Saraburi Group of North-Central Thailand: Implication for Geotectonic Evolution. Gondwana Research, 4, 597-598, doi: http://dx.doi.org/10.1016/S1342-937X(05)70400-7.

Chutakositkanon, V., Charusiri, P. & Sashida, K. 2000. Lithostratigraphy of permian marine sequences. The Island Arc, 9, 173-187.

Davydov, V.I. 2013. Climate fluctuations within the western Pangean tropical shelves - the Pennsylvannian/Permian record from benthic foraminifera. In: Lucas, S.G., DiMichele, W.A., Barrick, J.E., Schneider, J.W. & Spielmann, J.A. (eds.) Part of The Carboniferous-Permian Transition. New Mexico Museum of Natural History, Albuquerque, 73-78.

Dawson, O. 1993. Fusiline foraminiferal biostratigraphy and carbonate facies of the Permian Ratburi Limestone, Saraburi, central Thailand. Journal of Micropalaeontology, 12, 9-33, doi: 10.1144/jm.12.1.9.

Dawson, O., Baird, A. & Bosence, D. 1993. No reef-rimmed margins to the Permian carbonate platforms of Thailand. Journal of Southeast Asian Earth Sciences, 8, 181-186, doi: http://dx.doi.org/10.1016/0743-9547(93)90019-L.

Dawson, O. & Racey, A. 1993. Fusuline-calcareous algal biofacies of the Permian Ratburi Limestone, Saraburi, Central Thailand. Journal of Southeast Asian Earth Sciences, 8, 49-65.

Dunham, R.J. 1962. Classification of carbonate rocks according to depositional texture. In: Ham, W.E. (ed.) Classification of Carbonate Rocks. American Association of Petroleum Geologists Memoir, 108-121.

El Tabakh, M. & Utha-Aroon, C. 1998. Evolution of a Permian carbonate platform to siliciclastic basin: Indochina Plate, Thailand. Sedimentary Geology, 121, 97-119.

Flügel, E. 2010. Microfacies of Carbonates Rocks. Springer, London.

Folk, R.L. 1962. Spectral subdivision of limestone types. Classification of Carbonate Rocks, 1, 62-84.

Hansberry, R.L., Collins, A.S., King, R.C., Morley, C.K., Giże, A.P., Warren, J., Löhr, S.C. & Hall, P.A. 2015. Syn-deformation temperature and fossil fluid pathways along an exhumed detachment zone, khao khwang fold-thrust belt, Thailand. Tectonophysics, 655, 73-87, doi: http://dx.doi.org/10.1016/j.tecto.2015.05.012.

Henderson, C.M., Davydov, V.I. & Wardlaw, B.R. 2012. The Permian Period. In: Gradstein, F.M., Ogg, J., Schmitz, M. & Ogg, G. (eds.) The Geologic Time Scale 2012. Elsevier, 653-679.

Hinthong, C., Chuaviroj, S., Kaewyana, W., Srisukh, S., Oholprasit, C. & Pholachan, S. 1985. Geologic Map of Changwat Pranakhon Si Ayutthaya.

Hornibrook, N.d.B. 1950. Permian Fusulinid Foraminifera from the North Auckland Peninsula, New Zealand. Transactions and Proceedings of the Royal Society of New Zealand, 79, 319-321.

Jin-Zhang, S. 1990. Development of fusuline foraminifera in China. Stud. Benthic Foraminifera, Benthos,, 90, 11-22.

Kawamura, T. & Machiyama, H. 1995. A Late Permian coral reef complex, South Kitakami Terrane, Japan. Sedimentary Geology, 99, 135-150, doi: http://dx.doi.org/10.1016/0037-0738(95)00040-F.

Kobayashi, F., Ross, C.A. & Ross, J.R.P. 2010. Classification, phylogeny, and paleobiogeography of the new subfamily Gifuellinae and a revision of the family Neoschwagerinidae (superorder Fusulinoida); Guadalupian (Middle Permian). The Journal of Foraminiferal Research, 40, 283-300, doi: 10.2113/gsjfr.40.3.283.

Kołodziej, B., Ivanov, M. & Idakieva, V. 2012. Prolific development of pachythecaliines in Late Barremian, Bulgaria: coral taxonomy and sedimentary environment. Annales Societatis Geologorum Poloniae, 82, 291-330.

Leven, E.J. 2003. The Permian Stratigraphy and Fusulinids of the Tethys. Rivista di Paleontologia e Stratigrafia, 109, 267-280.

Loeblich, A.R. & Tappan, H. 1964. Protista 2 (Sarcodina, chiefly "Thecamoebians" and Foraminiferida). The Geological Society of America and The University of Kansas Press, U.S.A.

Menning, M., Alekseev, A.S., Chuvashov, B.I., Davydov, V.I., Devuyst, F.X., Forke, H.C., Grunt, T.A., Hance, L., Heckel, P.H., Izokh, N.G., Jin, Y.G., Jones, P.J., Kotlyar, G.V., Kozur, H.W., Nemyrovska, T.I., Schneider, J.W., Wang, X.D., Weddige, K., Weyer, D. & Work, D.M. 2006. Global time scale and regional stratigraphic reference scales of Central and West Europe, East Europe, Tethys, South China, and North America as used in the Devonian–Carboniferous–Permian Correlation Chart 2003 (DCP 2003). Palaeogeography, Palaeoclimatology, Palaeoecology, 240, 318-372, doi: http://dx.doi.org/10.1016/j.palaeo.2006.03.058.

Metcalfe, I. 2013. Gondwana dispersion and Asian accretion: Tectonic and palaeogeographic evolution of eastern Tethys. Journal of Asian Earth Sciences, 66, 1-33, doi: http://dx.doi.org/10.1016/j.jseaes.2012.12.020.

Morley, C.K., Ampaiwan, P., Thanudamrong, S., Kuenphan, N. & Warren, J. 2013. Development of the Khao Khwang fold and thrust belt; implications for the geodynamic setting of Thailand and Cambodia during the Indosinian Orogeny. Journal of Asian Earth Sciences, 62, 705-719, doi: http://dx.doi.org/10.1016/j.jseaes.2012.11.021.

Shen, S.-Z., Schneider, J.W., Angiolini, L. & Henderson, C.M. 2013. The International Permian Timescale: March 2013 Update. In: Lucas, S.G., DiMichele, W.A., Barrick, J.E., Schneider, J.W. & Spielmann, J.A. (eds.) Part of The Carboniferous-Permian Transition. New Mexico Museum of Natural History, Albuquerque.

Sresthaputra, V., Buravas, S. & Brown, G.F. 1951. Geology. In: Brown, G.F., Buravas, S., Charaljavanaphet, J., Jalichandra, N., Johnston, W.D.J., Sresthaputra, V. & Taylor, G.C. (eds.) Geologic reconnaissance of the mineral deposits of Thailand. United States Geological Survey, Bulletin, Washington, 33-36.

Thambunya, S., Pisutha-Arnond, V. & Khantaprab, C. 2007. Depositional Environments of Permian Rocks of the Khao Khad Formation in Central Thailand. ScienceAsia, 33, 371-381, doi: 10.2306/scienceasia1513-1874.2007.33.371.

Toriyama, R. 1975. Fusuline Fossils from Thailand, Part IX, Permian fusulines from the Rat Buri Limestone in the Khao Phlong Phrab Area, Sara Buri, Central Thailand.

Toriyama, R. & Kanmera, K. 1979. Permian fusulines from the Ratburi Limestone in the Khao Khao area, Sara Buri, Central Thailand. In: Kobayashi, T., Toriyama, R. & Hashimoto, W. (eds.) Geology and Palaeontology of Southeast Asia. University of Tokyo Press, Tokyo, 23-93.

Tucker, M.E. 2001. Limestones. Sedimentary petrology: an introduction to the origin of sedimentary rocks. Blackwell Publishing, United Kingdom, 110-165.

Udchachon, M., Burrett, C., Thassanapak, H., Chonglakmani, C., Campbell, H. & Feng, Q. 2014. Depositional setting and paleoenvironment of an alatoconchid-bearing Middle Permian carbonate ramp sequence in the Indochina Terrane. Journal of Asian Earth Sciences, 87, 37-55, doi: http://dx.doi.org/10.1016/j.jseaes.2014.02.012.

Ueno, K. & Charoentitirat, T. 2011. Carboniferous and Permian. In: Ridd, M.F., Barber, A.J. & Crow, M.J. (eds.) The Geology of Thailand. The Geological Society, London, 71-136.

Ueno, K., Miyahigashi, A., Kamata, Y., Kato, M., Charoentitirat, T. & Limruk, S. 2012. Geotectonic implications of Permian and Triassic carbonate successions in the Central Plain of Thailand. Journal of Asian Earth Sciences, 61, 33-50, doi: http://dx.doi.org/10.1016/j.jseaes.2012.04.015.

Wardlaw, B.R., Davydov, V.I. & Gradstein, F.M. 2004. The Permian Period. In: Gradstein, F.M., Ogg, J.G. & Smith, A.G. (eds.) A Geologic

Time Scale 2004. Cambridge University Press, United Kingdom, 249-270.

Warren, J., Morley, C.K., Charoentitirat, T., Cartwright, I., Ampaiwan, P., Khositchaisri, P., Mirzaloo, M. & Yingyuen, J. 2014. Structural and fluid evolution of Saraburi Group sedimentary carbonates, central Thailand: A tectonically driven fluid system. Marine and Petroleum Geology, 55, 100-121, doi: http://dx.doi.org/10.1016/j.marpetgeo.2013.12.019.

Weidlich, O. 2002. Permian reefs re-examined: Extrinsic control mechanisms of gradual and abrupt changes during 40 my of reef evolution. Geobios, 35, 287-294, doi: 10.1016/S0016-6995(02)00066-9.

Wielchowsky, C.C. & Young, J.D. 1985. Regional facies variations in Permian rocks of the Phetchabun fold and thrust belt, Thailand. In: Thanvarachorn, P., Hokjaroen, S. & Youngme, W. (eds.) Conference on Geology and Mineral Resources Development of the North-east Thailand, Khon Kaen, 41-55.

Wright, V.P. & Burchette, T.P. 1998. Carbonate ramps: an introduction. Geological Society, London, Special Publications, 149, 1-5.

Wright, V.P. & Burchette, T.P. 1996. Shallow-water carbonate environments. In: Reading, H.G. (ed.) Sedimentary Environments: Processes, Facies and Stratigraphy. Blackwell Publishing, Victoria, 325-395.

CHAPTER 7

Discussion and Conclusion

Updated Tectonic Evolution and Palaeogeography of Thailand

Thesis Summary

Three distinct tectonic domains, each with a complex tectonic history filled with multiple rifting and collisional events, amalgamated to form present day Thailand. This thesis endeavours to better unravel the tectonic evolution and palaeogeography of these major Thai terranes: Indochina, Sukhothai and Sibumasu. But, it aims to do this by coupling disparate geological disciplines from palaeontology and sedimentology of the SW margin of Indochina to igneous geochemistry and detrital geochronology. The three Thai terranes all have not always been connected, therefore; each chapter in this thesis provides further information on their origin, relative position, separation/collision with other blocks and past environments. This thesis used zircon isotopic systematics in detrital and granitoid rocks in conjunction with whole-rock granitoid geochemistry and biostratigraphy to characterise the nature of Thailand's development from Gondwana to Southeast Asia today. Understanding the evolution of the terranes of Thailand not only has implications for the palaeogeographic history of Southeast Asia, but also can provide information on the formation of petroleum-hosted basins to the genesis of arc-related mineral resources.

In Chapter 2, I used granites as a probe to further develop our understanding of the unexposed basement in Thailand. From the investigation of zircon U–Pb geochronology and Lu–Hf isotopic systems and whole-rock Sm–Nd, Sr and Pb geochemistry of granitoids, I was able to better characterise the underlying basement and highlight the variance in the history of the three tectonic domains. Magmatic zircon Lu–Hf and whole-rock Sm–Nd data and model ages from granitoids in this study illustrate that the Indochina Terrane is isotopically juvenile and distinct from the Sibumasu Terrane and associated Inthanon Zone, which are composed of considerable recycled Archean–Paleoproterozoic components. The Sukhothai Terrane has a hybridised isotopic signature that indicates juvenile material was contaminated with evolved continental crust. Our $\varepsilon Hf–Nd_{(t)}$ model highlights a trend from evolved granitoid source material in the west of Thailand (Sibumasu and Inthanon) through to juvenile affinities in the east (Indochina). This result was surprisingly different from many existing studies demonstrating that the Indochina Terrane has an ancient basement (Lan et al. 2000; Nagy et al. 2000; Şengör et al. 1988). Instead, my results are more consistent with reports of a composite Indochina Terrane (Arboit et al. 2016b; Lepvrier et al. 2004; Sone and Metcalfe 2008), with little evidence of Precambrian material within western Indochina (as suggested by Ridd 2011), which can reconcile the disparate isotopic characteristics across this terrane.

In Chapter 3, I analysed detrital zircon U–Pb and Lu–Hf isotopic systems of Cambrian–Triassic detrital samples to elucidate the tectonic history of northwest Thailand. From this analysis, I determined Ordovician to Triassic maximum depositional ages (YSG) of the clastic stratigraphy of the Sibumasu Terrane in northwest Thailand. In order of prominence, 1200–900 Ma, 650–500 Ma and 2500–2460 Ma age populations were present in all eight northwest Thai detrital samples. The Hf signatures of the Cambro-Ordovician detrital samples show a predominance of evolved material for 1000–500 Ma zircons. In contrast, the Hf signatures of the Carbo-Permian samples show an injection of juvenile

material in the zircons of the same age. The age distributions and associated Hf signatures indicate that the Sibumasu Terrane has affinities to northwestern Australia, the Himalayas, India and South China. Influence of the Sukhothai arc system and the Indosinian Orogeny can be observed in the Triassic sediments.

Chapter 4 compared detrital zircon U–Pb and Lu–Hf isotopic systems to unravel the Permo-Triassic tectonic history of Thailand. From this analysis, I observed 487–390 Ma, 1000–900 Ma, 1900–1725 Ma and 2572–2425 Ma zircon age populations in the Permo-Triassic sediments across all three tectonic terranes in Thailand. Detrital samples from the Sibumasu Terrane contain a large variation in their $\varepsilon Hf_{(t)}$ values including both juvenile and evolved signatures (ranging from -22.25 to +10.80). The predominant 296–207 Ma detrital ages from the Sukhothai Terrane have $\varepsilon Hf_{(t)}$ values ranging from -16.56 to +13.44, which correspond to the isotopic signatures of the synchronous Sukhothai granitoids. The >Silurian-aged peaks and associated isotopic signatures observed in the detrital data from the Sukhothai Terrane are also seen in sample CM15_01 of the Indochina Terrane. The influence of the Indosinian Orogeny and associated magmatism, including the granitoid crystallisation ages identified in Chapter 2, was detected in the latest Permian and Triassic sequences across Thailand. These results have implications for research on the Tethys Oceans demonstrating the separate sediment sources in the early Permian through to the latest Permian to Triassic amalgamation of the Thai terranes with consumption of the Palaeo-Tethys Ocean.

Chapter 5 analysed detrital zircons from the Chaung Magyi Group in Myanmar. The age populations of this Burmese region of the Sibumasu Terrane were then compared to the age distributions analysed in similar aged units in northwest Thailand. Comparison of the detrital zircon age distributions show only slight differences in between the Cambro-Ordovician of northwest Thailand and the Chaung Magyi Group samples. These findings have considerable implications for the tectonic history of northern Sibumasu, for the stratigraphic relationships with other lower Paleozoic stratigraphic units, and for the nature of contacts in the field. From these new geochronological data, the minimum depositional age for the Chaung Magyi Group of the Pindaya Range (982 Ma) and the maximum depositional age for Yeywa Dome (c.600–500 Ma) suggests the age difference is too great for the Chaung Magyi Group to be considered a single stratigraphic group.

Chapter 6 was the first study to incorporate the effect of structural compilations on the biostratigraphy of the Khao Khwang Platform, southwest Indochina, a section that forms the location for a number of classic palaeontological studies (Ingavat et al. 1980; Toriyama 1967; Toriyama and Kanmera 1979). Through this study, palaeoenvironmental inferences and fossil identification allowed for section correlation and assisted in unravelling the structure of this deformed platform. From this analysis, I constrained the Yakhtashian to Midian age range of the Khao Khad Formation with much of the assemblage dated as Murgabian. Six facies were identified: peritidal, low-energy lagoon, outer platform, backreef, algal biostrome reef and slope to basin. The Khao Khwang Platform has historically been interpreted as a singular carbonate platform forming a continuous

stratigraphic section. However, this study uncovered remnants of potentially three middle Permian platforms within the Saraburi study area. Each of these platforms deepens northwards although deformation has obscured the facies' original position and thickness of the sequence. Nevertheless, the particulars on their width, displacement and origin are still largely unknown, and further extensive sedimentological studies are required to determine the dimensions of the Saraburi carbonate platforms and their associated deeper water areas.

Tectonic and palaeogeographic evolution of Thailand

The palaeogeography of Asia has long been constructed by the use of palaeomagnetic and palaeontological data (Audley-Charles et al. 1988; Burrett 1974; Fang et al. 1989; Huang and Opdyke 1991; Li et al. 2004; Metcalfe 1984). In more recent years, geochronology, especially age distributions and other isotopic signatures (e.g. Arboit et al. 2016b; Dopieralska et al. 2012; Li et al. 2012; Sevastjanova et al. 2016), have also been incorporated to further characterise the provenance and palaeogeography of the Asian terranes.

Precambrian – Origin of Thai terranes

The Gondwanan supercontinent incorporated much of the present day Asia, Australia, Antarctica, India, Arabia and South America and amalgamated in the late Neoproterozoic to Cambrian (Kelsey et al. 2008; Merdith et al. 2017). It is well established that the Indochina and Sibumasu terranes were once part of Gondwana (Audley-Charles et al. 1988; Burrett et al. 2014; Cocks and Torsvik 2013). However, there are various models on their placement within this supercontinent and the timing of separation (Li et al. 2004; Loydell and Aung 2017; Yan et al. 2018; Zhang et al. 2018b). The Sukhothai Terrane is rarely included in models of Gondwana, since there has been much historical debate on its origins, however, it is now acknowledged to be an arc system integrating older continental material (Dew et al. 2018a; Hara et al. 2017; Qian et al. 2016; Sevastjanova et al. 2011).

Chapters 2, 3, 4 and 5 demonstrate that the Sibumasu Terrane contains ancient recycled crustal material within the range of values also seen in cratonic western Australia (Cawood and Nemchin 2000; Fitzsimons 2003; Hand et al. 2007; Ivanic et al. 2012; Kettanah et al. 2015; Kirkland et al. 2011; Ksienzyk et al. 2012; Li et al. 2015; Lin et al. 2013; McCulloch 1987; Tucker et al. 2018; Wilde 1999). Chapter 3 illustrates that although the sedimentary packages of northwest Thailand were deposited in the Phanerozoic, they are dominated by Proterozoic zircon sources.

The Chaung Magyi Group of the Sibumasu Terrane in Myanmar has detrital zircon U–Pb ages constraining deposition within the Yeywa Dome from latest Proterozoic to late Cambrian age as detailed in Chapter 5. The Proterozoic age populations found in Neoproterozoic–Ordovician sediments from the Sibumasu Terrane in northwest Thailand (Chapter 3) and in northern Shan Plateau of Myanmar (Chapter 5) are likely to be sourced from similar-aged magmatism and orogenesis seen in other regions once part of eastern Gondwana including Australia, India and Antarctica (Dawson et al. 2002; Fitzsimons 2000; Fletcher and Libby 1993; Hand et al. 2007; Kirkland et al. 2011; Xu et al. 2014). These data further consolidate the Sibumasu Terrane's palaeoposition outboard of northwestern Australia (Ali et al. 2013; Bunopas 1981; Burrett et al. 2014; Cocks

et al. 2005; Hutchison 2014; McCulloch 1987; Sevastjanova et al. 2016).

There is some disparity on the exact position on the Sibumasu Terrane in relation to the Australian margin. Some authors suggesting a location on the periphery of the Canning Basin (Hutchison 2014), whereas others suggest outboard of the offshore northwest Australian Carnarvon Basin (e.g. Dopieralska et al. 2012; Sevastjanova et al. 2016). Other authors combine Sibumasu with West Burma (Barber and Crow 2009; Gardiner et al. 2018; Morley and Searle 2017), or divide Sibumasu into several sections (Mitchell et al. 2015; Ridd 2015; Zhang et al. 2018b), which are modelled in Gondwana outboard of northwest Australia and Lhasa (Ridd 2015; Zhang et al. 2018b) or with the northern section (Sibusima) outboard of the Greater India and Himalayas (Zhang et al. 2018b). Regardless of when any putative terrane components might have assembled into Sibumasu, and depending on their origin, they may alternately be expected to have similar or different isotopic profiles across the current definition of Sibumasu. Figure 6 in Chapter 2 demonstrates the uniformity of the isotopic signature across the Sibumasu Terrane. Furthermore, the similarity in some of the detrital ages between the northwest Thai detrital data (Chapter 3) and the Burmese Chaung Magyi Group (Chapter 5) implies a contiguous Sibumasu Terrane, at least during the Neoproterozoic and early Paleozoic. Much of the variation in palaeoposition may be due to the different localities of these studies within the elongate ribbon-like Sibumasu Terrane, which extends several 1000km from Yunnan to Sumatra. My data from northwest Thailand and Phuket shows slight geographical variation in age distributions throughout Sibumasu (e.g. see MDS analyses in Chapters 2 and 3), however, these slight variations in age peaks, do not indicate entirely separate zircon source regions. My data and its comparison with published datasets support a continuous Sibumasu Terrane, sharing Proterozoic Gondwanan detrital sources from western Australia, South China and India.

In contrast to the ancient isotopic signatures found in the Sibumasu Terrane and contrary to a number of previous hypotheses (Lan et al. 2000; Metcalfe 1988; Nagy et al. 2000; Şengör et al. 1988), Chapter 2 demonstrates that the Indochina Terrane is built on relatively juvenile crust that formed primarily in the Neoproterozoic. There is no evidence for older crust in the western part of the Indochina Terrane. However, the comparison of data from Chapter 2 with published granitoid studies, highlights a distinct isotopic contrast between juvenile western Indochina and the evolved Truong Son Belt, which are both part of the Indochina Terrane. Differences within the Indochina Terrane are further highlighted in detrital data demonstrating the mismatch within Indochina between sediments from northern Thailand (e.g. sample CM15_01) and the Khorat Plateau and those from Arboit et al. (2016b) in the Khao Khwang Fold-Thrust Belt. This is consistent with previously published evidence (e.g. Arboit et al. 2016b; Faure et al. 2018; Lepvrier et al. 2004; Sone and Metcalfe 2008), that the Indochina Terrane is a composite terrane containing multiple micro-terranes, potential sutures, metamorphic complexes and mylonitic fault zones. It is possible to speculate about the presence of a provenance boundary (Arboit et al. 2016b; Hutchison 1975; Udchachon et al. 2017; Zaw et al. 2014), which may be an intra-continental

basin, or even an additional ocean basin. A more comprehensive study of Indochina, its western margin, the Truong Son Belt and the regions through Cambodia and Laos, is required to further understand this relationship.

It is possible that the Sukhothai Terrane formed with the western margin of the Indochina Terrane during the Neoproterozoic. In Chapter 3, I proposed three hypotheses for the tectonic development of the isotopic hybrid granitoids analysed from the Sukhothai Terrane. 1) The Sukhothai arc would have been located outboard of Sibumasu on the northwest Australian margin of Gondwana (see Fig. 7 of Chapter 2). In this model, the Inthanon Zone would represent the back-arc basin between the Sibumasu and Sukhothai terranes and the main Palaeo-Tethys suture would separate Sukhothai and Indochina (the Nan Suture). However, this explanation is contrary to popular models where the Inthanon Zone represents the main Palaeo-Tethys suture (e.g. Sone and Metcalfe 2008). These models are based on the presence of long-lived Devonian–Triassic highly condensed deep marine cherts, allochthonous limestone-capped seamounts and the continuation of the zone into the Changning–Menglian zone of Yunnan (see reviews in Sone and Metcalfe, 2008; Metcalfe 2013; Gardiner et al., 2015). 2) The Sukhothai arc was derived from the Indochina Terrane, but contains relict Precambrian signatures, similar to those signatures observed in the Truong Son Belt to the northeast (Hoa et al. 2008; Liu et al. 2012; Nagy et al. 2000; Shi et al. 2015). This would require a zone of weakness between the more juvenile western Thai Indochina Terrane and the evolved Sukhothai Terrane crust to have been exploited by the back-arc extension that separated these terranes (see Fig. 1 and Fig. 7 of Chapter 2). For example, analogue modelling by Corti et al. (2013) has shown how the boundary zone between colder, more rigid cratonic (i.e. Archean-type) crust, and less rigid mobile belts tends to localise rifting. (3) The hybridised nature of the mid-Triassic granitoids in the Sukhothai Terrane may be due to the incorporation of evolved distal passive margin sequences of the Sibumasu Terrane as they approached the subduction zone (see Fig. 1 and Fig. 7 of Chapter 2). A similar manner of arc contamination is observed in the Sunda Arc (Handley et al. 2011). In this third model, the Sukhothai Terrane could still be part of the Indochina Terrane and the Inthanon Zone could still represent the major Palaeo-Tethys suture, as shown in Fig. 1, coinciding with the evidence from the long-lived deep basin sedimentary sequences. It also broadly follows the geochemical data from the Sukhothai Terrane that appears to spatially distinguish between the I-type and hybrid granites, with more juvenile granitoids closer to the margin with Indochina and more crustal contamination in the granites further west, closer to the Inthanon Zone boundary. In this third scenario, the more evolved signatures observed in Chapter 2, may have been due to the incorporation of distal sediments of the ancient Sibumasu Terrane, rather than indicating that components of the Sukhothai arc system itself being older than Neoproterozoic.

Regions that conceivably have similar-aged basement material to the Indochina Terrane are the west coast of Australia (Collins 2003), and northeast margin of India (Ghosh et al. 2005), both are locations where the Pinjarra Orogen crops out. The Neoproterozoic–Cambrian Pinjarra Orogen forms part of a much

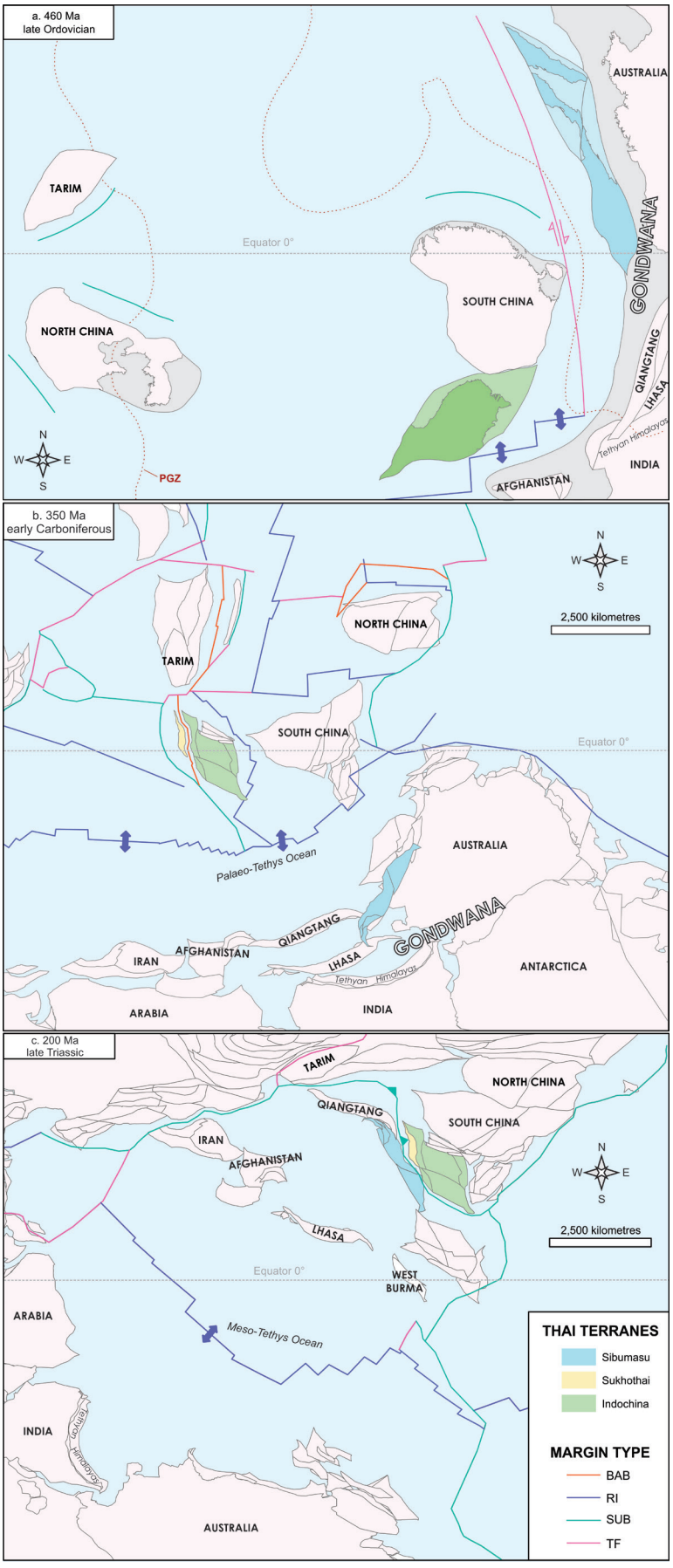
a. 460 Ma
late Ordovician
AUSTRALIA
TARIM
Equator 0°
GONDWANA
SOUTH CHINA
NORTH CHINA
QIANGTANG
LHASA
Tethyan Himalayas
INDIA
AFGHANISTAN
PGZ
N
W
E
S
b. 350 Ma
early Carboniferous
NORTH CHINA
TARIM
SOUTH CHINA
Equator 0°
2,500 kilometres
AUSTRALIA
Palaeo-Tethys Ocean
QIANGTANG
GONDWANA
AFGHANISTAN
IRAN
LHASA
Tethyan Himalayas
ANTARCTICA
ARABIA
INDIA
c. 200 Ma
late Triassic
TARIM
NORTH CHINA
QIANGTANG
SOUTH CHINA
IRAN
AFGHANISTAN
LHASA
2,500 kilometres
Equator 0°
WEST
BURMA
ARABIA
Meso-Tethys Ocean
INDIA
Tethyan Himalayas
AUSTRALIA
THAI TERRANES
Sibumasu
Sukhothai
Indochina
MARGIN TYPE
BAB
RI
SUB
TF

Fig. 1 (previous page). Palaeogeographic reconstructions of Thailand and surrounding regions. Plate margin acronyms are as follows: BAB is back-arc-basin, RI is rift, SUB is subduction zone and TF is transform fault. Plate motion directions are given for key margin boundaries. (a) late Ordovician (460 Ma) paleogeographic reconstruction adjusted from Cocks and Torsvik (2013). Plume generation zones (PGZs) at the core–mantle boundary. (b) early Carboniferous (350 Ma) palaeogeographic reconstruction adjusted from Young et al. (2018). (c) late Triassic (200 Ma) palaeogeographic reconstruction modified from Young et al. (2018) and Golonka et al. (2018).

larger orogenic belt that can be traced along Western Australia and through eastern Antarctica (Burrett et al. 2014; Collins 2003; Ghosh et al. 2005). Published $^{Nd}T_{DM}$ ages of 1.18 to 1.08 Ga from southwestern Australia are consistent with the older Mesoproterozoic model ages for the Indochina Terrane in Chapter 2 (Fletcher and Libby 1993; McCulloch 1987; Wilde 1999). Other possible neighbouring domains could be northwest India (Wang et al. 2017), along with other localities where the East African Orogen intersects the northern Gondwanan margin i.e. the Arabian Nubian Shield and Oman (Blades et al. 2015).

There are multiple published studies illustrating similarities (including common sediment sources, palaeo-proximity, age distribution profiles and isotopic characteristics) between the Indochina and South China terranes (Burrett et al. 2014; Cocks and Torsvik 2013; Gao et al. 2017; Yao et al. 2014). The Sibumasu Terrane also shows affinities to the South China Terrane. The evolved Hf signatures observed in the Neoproterozoic zircons of the Cambro-Ordovician detritus from northwest Thailand in Chapter 3 are mirrored in the Ordovician sandstones of Cathaysia, South China (Yao et al. 2014). These similarities suggest that, in the Ediacaran–Cambrian, Sibumasu lay close to these regions along the northern Gondwana margin (see Chapter 3). Northern India and South China have been previously recognised as near neighbours in the Gondwana supercontinent (Burrett et al. 2014; Cocks and Torsvik, 2013; Yao et al. 2014). Yao et al. (2014) suggested that they collided sometime in the Ediacaran–Ordovician, although more recently, others have argued that South China and India were part of the same Neoproterozoic continent prior to Gondwana (Cawood et al. 2013; Merdith et al. 2017; Wang et al. 2017).

Cambrian to Ordovician

Cambrian Gondwana was characterised by subduction and collision with the East African Orogen between east Africa, Antarctica, and India (Blades et al. 2015; Fitzsimons 2003; Kelsey et al. 2008), Pinjarra—Kuunga Orogen between southwestern Australia, northeastern India and Antarctica (Collins 2003; Fitzsimons 2003; Fletcher and Libby 1993; Ghosh et al. 2005) and the Terra-Australis Orogen along the margins of Australia, Antarctica, and South America (Cawood 2005). However, the position of the terranes that form the northern Gondwanan margin, including Sibumasu, Lhasa, West Burma and Qiangtang, is still widely debated (Burrett et al. 2014; Cocks and Torsvik 2013; Hu et al. 2015; Zhang et al. 2018b) and therefore often omitted from global palaeogeographic models (Merdith et al. 2017). However, most terranes of the northern Gondwana margin contain Cambro-Ordovician magmatism (Dew et al. 2018a; Hu et al. 2015; Saki 2010; Zhang et al. 2018a).

The northern Gondwana margin was tectonically dynamic in the Cambro-Ordovician, when strike-slip faulting caused Indochina and South China to

begin moving eastwards (Fig. 1a; Cocks and Torsvik 2013). Nevertheless, early Ordovician faunas indicate that the Chinese Simao sector of the Indochina Terrane was near Gondwana at this time (Cocks and Torsvik 2013). Components of the Indochina Terrane continued to have Gondwanan biogeographic affinities up until the Silurian (Li et al. 2004).

Sibumasu is commonly modelled close to northwestern Australia in Gondwana during the Cambrian (e.g. Aye Ko Aung and Cocks 2017; Burrett et al. 2014). The Burmese sector of the Sibumasu Terrane contains some Cambrian volcanics (including the Bawdwin Volcanics), they are acidic in composition and apparently peri-continental (Aye Ko Aung and Cocks 2017; Morley 2018). Perhaps then, and certainly from the early Ordovician onwards until the end of the Carboniferous, the Sibumasu edge of Gondwana was a passive margin throughout (Aye Ko Aung and Cocks 2017), a conclusion reinforced by the neodymium isotopic composition of late Devonian seawater in western Thailand (Dopieralska et al.2012).

Chapters 3 and 4 illustrated that although the sedimentary packages of the Sibumasu Terrane were deposited in the Phanerozoic, they are dominated by Proterozoic sources. The dominant Proterozoic sources are consistent with previous models of widespread sedimentation across Gondwana during the Cambrian and Ordovician (Burrett et al. 2014; Myrow et al. 2010; Squire et al. 2006).

Sibumasu, Baoshan, West Burma, North China, Tarim, Tibet and South China have palaeobiogeographic and stratigraphic links to Gondwanan Australia in the early Ordovician (Aye Ko Aung and Cocks 2017; Cocks et al. 2005; Fang et al. 2018; Li et al. 2004; Metcalfe 2013a; Sevastjanova et al. 2016).

Silurian to Devonian

Stratigraphic and palaeontological evidence suggests that Sibumasu and Indochina still had affinities with regions of Gondwana, including Australia, India, South America and China until the late Devonian (Cocks et al. 2005; Faure et al. 2018; Long and Burrett 1989; Loydell and Aung 2017; Wongwanich and Boucot 2011).

The Nd isotopic composition of seawater from western Thailand provides further evidence that during the Upper Devonian the Sibumasu Terrane was located near the Archean cratons of Western Australia (e.g. Pilbara and Yilgarn), suggested by Dopieralska et al. (2012) to be adjacent to the Carnarvon intracratonic basin. Sevastjanova et al. (2016) also proposed, based on Archean Yilgarn and Pilbara zircon populations, that until the Devonian Sibumasu and West Burma were outboard from Western Australia. Additionally, U–Pb zircon analyses by Sevastjanova et al. (2016) suggest that the Indochina Terrane was not close to Sibumasu or West Burma, prior to its separation from Gondwana. Based on faunal similarities it has been suggested that the South China and Indochina terranes were joined during the Devonian (Janvier et al., 1989, Janvier et al., 1996, Janvier et al., 1997, Tong-Dzuy et al., 1996; Racheboeuf et al., 2005, Racheboeuf et al., 2006).

Previous studies (e.g. Cocks and Torsvik 2013; Ridd 2011), have highlighted that there is little evidence of the existence of the western Thai sector of the Indochina Terrane prior to the middle Silurian. The model ages calculated for the western

Indochina Terrane in Chapter 2 are much younger than the previous published source estimates from equivalent regions in Vietnam and Malaysia of greater than 3.7 Ga to 1.88 Ga (Sevastjanova et al. 2011; Usuki et al. 2013). Qian et al. (2017) identified model ages as young as late Silurian from the granitoids in the Chanthaburi Terrane, the southern equivalent of the Sukhothai Terrane. This suggests that the western margin of the Indochina Terrane and possibly the Sukhothai Terrane may have been part of an early Paleozoic arc system, which are consistent with the prominence of early Paleozoic zircons observed in the detrital record of this thesis e.g. 452 Ma age peak in sample CM15_01 from the Huai Hin Lat Formation, 490–400 Ma detrital ages in Sukhothai sandstones (see Chapter 4). A pervasive zircon formation event (470–430 Ma) was also recognised by Carter and Bristow (2003) within the overlying Khorat Group and is also seen in the late Cretaceous–early Paleogene Phu Khat Formation further north in the Nakhon Thai region of the Indochina Terrane (see Nulay et al. 2016). This suggests the western Indochina–Sukhothai may be floored with an Ediacaran–early Paleozoic arc system possibly related to the closure of the Proto-Tethys Ocean in the early Paleozoic (500–420 Ma), leading to the collision of South China, North China, Qaidam, Indochina and Tarim with other East Asian blocks at the northern margin of Gondwana (Zhao et al. 2018).

It is commonly agreed that the Palaeo-Tethys Ocean was initiated in the Lower Devonian (Cocks and Torsvik 2013; Hara et al. 2012; Metcalfe 2013a; Zhu et al. 2011). This ocean covered the equatorial region from the Devonian to the Triassic, where carbonates and pelagic chert were deposited (Cocks and Torsvik 2013; Hara et al. 2012; Metcalfe 2013a). However, there are differing models on the timing of separation between Sibumasu, Lhasa, Indochina from Gondwana (Audley-Charles et al. 1988; Li et al. 2004; Loydell and Aung 2017; Zhang et al. 2018b; Zhu et al. 2011).

Carboniferous to Permian

It is recognised that by the late Carboniferous, two elongate tropical carbonate platforms: the Khao Khwang and Pha Nok Khao platforms, developed along the margin of the Indochina Terrane (Dew et al. 2018b; Ueno and Charoentitirat 2011). Chapter 6 reconstructed the original facies distribution of the Khao Khwang Platform prior to its Triassic deformation into the Khao Khwang Fold-Thrust Belt. This was done using new sedimentological logs from 11 localities within the fold-thrust belt and correlating their biostratigraphy primarily based on the fusuline foraminifera present. Previously the Khao Khad Formation of the Khao Khwang Platform was dated as middle Guadalupian and on the Tethyan Scale, predominantly Murgabian with limited extension into the overlying Midian (Baird and Bosence 1993; Dawson and Racey 1993; Ueno and Charoentitirat 2011). This study outlined in Chapter 6, improved the age constraints of the Khao Khad Formation to span from the Yakhtashian to Midian (Tethyan equivalents to middle Cisuralian to late Guadalupian). The fauna observed in the Khao Khwang sections (Chapter 6), provide evidence for the region's tropical shallow marine location during the middle Cisuralian to late Guadalupian. Palaeomagnetic data (e.g. Li et al. 2004; McElhinny and Lock 1996; Yan et al. 2018; Yan et al. 2017), indicate that the by the Carboniferous, the South China and Indochina terranes

were located in equatorial to low tropical palaeolatitudes, however Li et al. (2004) proposes the northern tropics whereas Yan et al. (2018) suggests southern tropical palaeolatitudes. Nevertheless, both Yan et al. (2018) and Li et al. (2004) acknowledge that the Indochina and South China terranes moved very rapidly northwards during the Permian.

While the origins of the Sukhothai Terrane have not been finely constrained, it is known that it had formed prior to the Carboniferous, as during the Carboniferous and Permian, the Nan basin separated the Sukhothai and Indochina terranes (Fig. 1b; Barr and Macdonald 1987; Qian et al. 2016; Sone and Metcalfe 2008; Ueno and Hisada 2001). This supposedly short-lived back-arc basin, is preserved as a narrow N–S trending and discontinuous ophiolite belt known as the Nan–Uttaradit Suture in northern Thailand and the Sa Kaeo Suture in the southeast of the country (Fig. 1; Sone and Metcalfe 2008; Ueno and Hisada 2001). A variety of geochronological data from various deep marine lithologies constrain the Carbo-Permian age of this back-arc basin (Barr and Macdonald 1987; Sone et al. 2012).

In contrast to the Indochina and South China terranes, Paleozoic palaeomagnetic data indicates southern palaeolatitudes consistent with the tectonic inactivity of the Sibumasu Terrane still located off NW Australian passive margin in Gondwana during the Carboniferous and early Permian (Fig. 1b; Fang et al., 1989; Bunopas, 1982; Bunopas et al., 1989; Metcalfe, 1990; Huang and Opdyke, 1991). Moreover, the presence of Gondwana-derived icebergs depositing glacio-marine sediments in rift grabens is frequently used as evidence for Sibumasu's palaeoposition in Carbo-Permian Gondwana (Burrett et al. 2014; Metcalfe 2013a, b; Ridd 2015; Sevastjanova et al. 2011). Further evidence for this palaeoproximity is the similar-aged and comparative isotopic characteristics of zircons from the Carbo-Permian sediments from the Sibumasu Terrane, described in Chapters 3 and 4, and the Permian sediments of the Perth Basin (Cawood and Nemchin 2000; Veevers et al. 2005).

The latest projected time of the northwards rifting of Sibumasu away from Gondwana is the early Permian (as per Burrett et al. 2014). By the middle to late Permian, the widespread Ratburi, Thitsipin and Moulmein limestones indicate that Sibumasu was almost entirely submerged with little topographic relief (Baird and Bosence 1993; Bunopas 1992; Grant 1976; Morley 2018; Ueno and Charoentitirat 2011). This northward movement of the Sibumasu Terrane is thought to have opened the Meso-Tethys Ocean (Burrett et al. 2014). The late Carboniferous–early Permian sparked the start of the destruction of the main Palaeo-Tethys Ocean, with subduction northwards beneath the Indochina Terrane (Li et al. 2004; Metcalfe 2013a; Sone et al. 2012). As subduction continued, slab rollback caused the Nan back-arc basin to open between the Indochina and the Sukhothai terranes (Metcalfe 2013). Subduction of the Palaeo-Tethys Ocean formed an accretionary wedge of "ocean plate stratigraphy" and caused the arc magmatism of the Sukhothai Terrane (Barr et al. 2006; Qian et al. 2016).

Triassic – Amalgamation of Thailand

Previous studies (e.g. Arboit et al. 2014; Morley et al. 2013) have proposed separating the Indosinian Orogeny into two stages. The latest Permian to early

Triassic (Lopingian–Carnian) first stage Indosinian I is thought to be driven by the collision of the northern margin of Indochina with South China (Arboit et al. 2014; Lepvrier et al. 2004; Metcalfe 2013a; Morley et al. 2013). It has been suggested that it was an oblique collision, with a strong component of right-lateral translation (Lepvrier et al., 2008; Van Vuong et al., 2012). However, based on the stratigraphy and radiometric dates of the plutonic and metamorphic rocks, Faure et al. (2014) argue for a middle Triassic collision of the South China and Indochina terranes. Contemporaneously, or following the South China–Indochina collision, the Sukhothai back arc closed and was subsequently thrust over the Indochina Terrane (Fig. 1c; Lepvrier et al. 2004; Morley et al. 2013). On the southern margin of the Khorat continental fragment of the Indochina Terrane, the Khao Khwang Platform was deformed, resulting in the Khao Khwang Fold-Thrust Belt (Arboit et al. 2014; Morley et al. 2013; Sone and Metcalfe 2008). The termination of this Indosinian I event is identified as an unconformity in the Khorat Plateau whereby the deformed Permian and older units are overlain by late Triassic rift-related sediments of the Kuchinarai Group, including the Huai Hin Lat Formation (Morley et al. 2013). The late Triassic to early Jurassic Indosinian II is said to mark the closure of the Palaeo-Tethys Ocean (Inthanon Zone) with the collision of the Sibumasu and Sukhothai/Indochina terranes (shown in Fig. 1c; Searle et al. 2012; Morley et al. 2013). Detrital data from the Huai Hin Lat Formation (sample CM15_01) in Chapter 4 can not distinguish the two stages of the Indosinian Orogeny. Nevertheless, Chapter 4 illustrates the influence of the Indosinian Orogeny and associated magmatism in the Sukhothai and Indochina terranes is detected in the latest Permian and Triassic sequences across Thailand.

The age and isotopic characteristics of the magmatism associated with the amalgamation of Thailand was further constrained in Chapter 2. The granitoids Sibumasu and Inthanon terranes are shown in Chapter 2, to exhibit similar age patterns and isotopic characteristics, suggesting a similar history. Both terranes generally contain evolved recycled crust, which is a consistent feature of the Hf, Sm–Nd, Sr and Pb isotopic signatures of all granitoids analysed. The Triassic magmatic ages from Sibumasu and Inthanon terranes range from 240–200 Ma (Ahrendt et al. 1993; Charusiri et al. 1993; Dew et al. 2018a; Gardiner et al. 2016; Kawakami et al. 2014; Ng et al. 2015a; Searle et al. 2012; Wang et al. 2016). These granitoids are thought to be supra-subduction zone granitoids that formed during the closure of the Palaeo-Tethys Ocean and the subsequent collision of Sibumasu with the Sukhothai and Indochina terranes during the Upper Triassic (Searle et al. 2012). The Triassic granitoid ages seen in Sibumasu–Inthanon (Chapter 2) are not observed in any of the Permo-Triassic sandstones across Thailand. This may be due to this magmatism being younger or coeval to sediment deposition, alternatively the granitoids were not elevated as a sediment source.

Hybridised zircon-Hf and whole-rock-Nd isotopic signatures were determined in Chapter 2 for Sukhothai granitoids. The whole-rock Nd isotopic signatures of the Permo-Triassic Sukhothai granitoids in Chapter 2 form a continuum from more juvenile metaluminous I-type granitoids in the east of the terrane through to more

evolved granitoids in the west (Dew et al. 2018a). In Chapter 2, I suggest that the hybridised isotopic nature of the mid-Triassic granitoids in the Sukhothai Terrane is due to the integration of evolved material from the Sibumasu Terrane during the progressive subduction of the Palaeo-Tethys Ocean.

The ages and Hf signatures of sediments from the Sukhothai Terrane shown in Chapter 4 to be sourcing detritus from Permo-Triassic Sukhothai arc magmatism. Additionally, the Triassic sample from the Sibumasu Terrane, RDT16_012, discussed in Chapters 3 and 4, is dominated by Australian-Gondwanan sources however, the 240 Ma age peak demonstrates the influence of the Permo-Triassic Sukhothai arc system and the amalgamation of Thailand.

Crystallisation ages from granitoids within the Indochina Terrane that span from 310 to 203 Ma (Arboit et al. 2016a; Charusiri et al. 1993; Dew et al. 2018a; Halpin et al. 2016; Kamvong et al. 2014; Ng et al. 2015b; Salam et al. 2014; Zaw et al. 2014). These ages may be associated with Late Carboniferous to end Guadalupian subduction-related volcanic arc activity as a result of the early stages of the South China and Cathaysia collision with Vietnam and Indochina (Halpin et al. 2016; Lepvrier et al. 2004), the closure of a small ocean basin between several Indochinese fragments (Meffre et al. 2008), or the similarly timed collision between Indochina and Sukhothai (Morley et al. 2013).

Understanding the terranes that make up Thailand are critical to understanding the tectono-geographical link between Southeast Asia and Australia. These data provide a comprehensive investigation on the geochemical signatures of Thai granitoids and implications for basement characteristics, Cambrian–Triassic sedimentary record in the Sibumasu Terrane, Permo-Triassic detritus from Sukhothai and Indochina and the biostratigraphy of the middle Permian Khao Khwang Platform of the Indochina Terrane. Previously some areas have been the subject of few, or no, coupled geochronological and/or isotopic studies. The evolution of the Sibumasu, Sukhothai and Indochina terranes is a symphony through time choreographing a ballet across the globe to form modern-day Thailand (Appendix I – The Conversation). These terranes document the consumption and closure of the Tethys Oceans illustrating the effect of multi-staged separation and collision events. The contribution of these data and the collation of previously published data have allowed for the further development of the palaeogeographic models constructed by Cocks and Torsvik (2013), Young et al. (2018) and Golonka et al. (2018) to better constrain the terranes of Thailand.

References

Ahrendt, H., Chonglakmani, C., Hansen, B.T. & Helmcke, D. 1993. Geochronological cross section through northern Thailand. Journal of Southeast Asian Earth Sciences, 8, 207-217, doi: http://dx.doi.org/10.1016/0743-9547(93)90022-H.

Ali, J.R., Cheung, H.M.C., Aitchison, J.C. & Sun, Y. 2013. Palaeomagnetic re-investigation of Early Permian rift basalts from the Baoshan Block, SW China: constraints on the site-of-origin of the Gondwana-derived eastern Cimmerian terranes. Geophysical Journal International, 193, 650-663, doi: 10.1093/gji/ggt012.

Arboit, F., Collins, A.S., Jourdan, F., King, R., Foden, J. & Amrouch, K. 2016a. Geochronological and geochemical study of mafic and intermediate dykes from the Khao Khwang Fold-Thrust Belt: Implications for petrogenesis and tectonic evolution. Gondwana Research, 36, 111-128.

Arboit, F., Collins, A.S., King, R., Morley, C.K. & Hansberry, R. 2014. Structure of the Sibumasu–

Indochina collision, central Thailand: A section through the Khao Khwang Fold and thrust belt. Journal of Asian Earth Sciences, 95, 182-191, doi: http://dx.doi.org/10.1016/j.jseaes.2014.06.016.

Arboit, F., Collins, A.S., Morley, C.K., King, R. & Amrouch, K. 2016b. Detrital zircon analysis of the southwest Indochina terrane, central Thailand: Unravelling the Indosinian orogeny. Geological Society of America Bulletin,, 128, 1024-1043.

Audley-Charles, M.G., Ballantyne, P.D. & Hall, R. 1988. Mesozoic-Cenozoic rift-drift sequence of Asian fragments from Gondwanaland. Tectonophysics, 155, 317-330.

Aye Ko Aung & Cocks, L.R.M. 2017. Chapter 14 Cambrian–Devonian stratigraphy of the Shan Plateau, Myanmar (Burma). Geological Society, London, Memoirs, 48, 317-342, doi: 10.1144/m48.14.

Baird, A. & Bosence, D. 1993. The sedimentological and diagenetic evolution of the Ratburi Limestone, Peninsular Thailand. Journal of Southeast Asian Earth Sciences, 8, 173-180, doi: http://dx.doi.org/10.1016/0743-9547(93)90018-K.

Barber, A.J. & Crow, M.J. 2009. Structure of Sumatra and its implications for the tectonic assembly of Southeast Asia and the destruction of Paleotethys. Island Arc, 18, 3-20, doi: 10.1111/j.1440-1738.2008.00631.x.

Barr, S.M. & Macdonald, A.S. 1987. Nan River suture zone, northern Thailand. Geology, 15, 907-910, doi: 10.1130/0091-7613(1987)15<907:nrszt>2.0.co;2.

Barr, S.M., Macdonald, A.S., Ounchanum, P. & Hamilton, M.A. 2006. Age, tectonic setting and regional implications of the Chiang Khong volcanic suite, northern Thailand. Journal of the Geological Society, 163, 1037-1046, doi: 10.1144/0016-76492005-118.

Blades, M.L., Collins, A.S., Foden, J., Payne, J.L., Xu, X., Alemu, T., Woldetinsae, G., Clark, C. & Taylor, R.J.M. 2015. Age and hafnium isotopic evolution of the Didesa and Kemashi Domains, western Ethiopia. Precambrian Research, 270, 267-284, doi: https://doi.org/10.1016/j.precamres.2015.09.018.

Bunopas, S. 1981. Paleogeographic history of western Thailand and adjacent parts of Southeast Asia - A plate tectonics interpretation. Paleogeographic History of Western Thailand and Adjacent Parts of Southeast Asia - A Plate Tectonics Interpretation.

Bunopas, S. 1992. Regional Stratigraphic Correlation in Thailand. Geologic Resources of Thailand: Potential for Future Development, 189-208.

Burrett, C., Khin, Z., Meffre, S., Lai, C.K., Khositanont, S., Chaodumrong, P., Udchachon, M., Ekins, S. & Halpin, J. 2014. The configuration of Greater Gondwana—Evidence from LA ICPMS, U–Pb geochronology of detrital zircons from the Palaeozoic and Mesozoic of Southeast Asia and China. Gondwana Research, 26, 31-51, doi: http://dx.doi.org/10.1016/j.gr.2013.05.020.

Burrett, C.F. 1974. Plate tectonics and the fusion of Asia. Earth and Planetary Science Letters, 21, 181-189, doi: https://doi.org/10.1016/0012-821X(74)90052-1.

Carter, A. & Bristow, C.S. 2003. Linking hinterland evolution and continental basin sedimentation by using detrital zircon thermochronology: a study of the Khorat Plateau Basin, eastern Thailand. Basin Research, 15, 271-285, doi: doi:10.1046/j.1365-2117.2003.00201.x.

Cawood, P.A. 2005. Terra Australis Orogen: Rodinia breakup and development of the Pacific and Iapetus margins of Gondwana during the Neoproterozoic and Paleozoic. Earth-Science Reviews, 69, 249-279, doi: https://doi.org/10.1016/j.earscirev.2004.09.001.

Cawood, P.A. & Nemchin, A.A. 2000. Provenance record of a rift basin: U/Pb ages of detrital zircons from the Perth Basin, Western Australia. Sedimentary Geology, 134, 209-234, doi: https://doi.org/10.1016/S0037-0738(00)00044-0.

Cawood, P.A., Wang, Y., Xu, Y. & Zhao, G. 2013. Locating South China in Rodinia and Gondwana: A fragment of greater India lithosphere? Geology, 41, 903-906, doi: 10.1130/G34395.1.

Charusiri, P., Clark, A.H., Farrar, E., Archibald, D. & Charusiri, B. 1993. Granite belts in Thailand: evidence from the 40Ar/39Ar geochronological and geological syntheses. Journal of Southeast Asian Earth Sciences, 8, 127-136, doi: http://dx.doi.org/10.1016/0743-9547(93)90014-G.

Cocks, L.R.M., Fortey, R.A. & Lee, C.P. 2005. A review of Lower and Middle Palaeozoic biostratigraphy in west peninsular Malaysia and southern Thailand in its context within the Sibumasu Terrane. Journal of Asian Earth Sciences, 24, 703-717, doi: https://doi.org/10.1016/j.jseaes.2004.05.001.

Cocks, L.R.M. & Torsvik, T.H. 2013. The dynamic evolution of the Palaeozoic geography of eastern Asia. Earth-Science Reviews, 117, 40-79, doi: http://dx.doi.org/10.1016/j.earscirev.2012.12.001.

Collins, A.S. 2003. Structure and age of the northern Leeuwin Complex, Western Australia: Constraints from field mapping and U–Pb isotopic analysis. Australian Journal of Earth Sciences, 50, 585-599, doi: 10.1046/j.1440-0952.2003.01014.x.

Corti, G., Iandelli, I. & Cerca, M. 2013. Experimental modeling of rifting at craton margins. Geosphere, 9, 138-154, doi: 10.1130/GES00863.1.

Dawson, G.C., Krapež, B., Fletcher, I.R., McNaughton, N.J. & Rasmussen, B. 2002. Did late Palaeoproterozoic assembly of proto-Australia involve collision between the Pilbara, Yilgarn and Gawler Cratons? Geochronological evidence from the Mount Barren Group in the Albany–Fraser Orogen of Western Australia. Precambrian Research, 118, 195-220, doi: https://doi.org/10.1016/S0301-9268(02)00110-9.

Dawson, O. & Racey, A. 1993. Fusuline-calcareous algal biofacies of the Permian Ratburi Limestone, Saraburi, Central Thailand. Journal of Southeast Asian Earth Sciences, 8, 49-65.

Dew, R.E.C., Collins, A.S., Glorie, S., Morley, C.K., Blades, M.L., Nachtergaele, S., King, R., Foden, J., De Grave, J., Kanjanapayont, P., Evans, N.J., Alessio, B.L. & Charusiri, P. 2018a. Probing into Thailand's basement: New insights from U–Pb geochronology, Sr, Sm–Nd, Pb and Lu–Hf isotopic systems from granitoids. Lithos, 320-321, 332-354, doi: 10.1016/j.lithos.2018.09.019.

Dew, R.E.C., King, R., Collins, A.S., Morley, C.K., Arboit, F. & Glorie, S. 2018b. Stratigraphy of deformed Permian carbonate reefs in Saraburi Province, Thailand. Journal of the Geological Society, 175, 163-175, doi: 10.1144/jgs2017-035.

DMR. 2014. Geology of Thailand. Department of Mineral Resources, Ministry of Natural Resources and Environment, Bangkok, Thailand.

Dopieralska, J., Belka, Z., Königshof, P., Racki, G., Savage, N., Lutat, P. & Sardsud, A. 2012. Nd isotopic composition of Late Devonian seawater in western Thailand: Geotectonic implications for the origin of the Sibumasu terrane. Gondwana Research, 22, 1102-1109, doi: http://dx.doi.org/10.1016/j.gr.2012.01.009.

Fang, W., Van Der Voo, R. & Liang, Q. 1989. Devonian palaeomagnetism of Yunnan province accross the Shan Thai-South China suture. Tectonics, 8, 939-952.

Fang, X., Chen, T., Burrett, C., Wang, Y., Qu, Y., Zheng, C., Zhang, Y., Zhang, Y. & Li, W. 2018. Middle Ordovician actinocerid nautiloids (Cephalopoda) from Xainza County, Tibet, western China, and their paleogeographic implications. Journal of Paleontology, 92, 398-411, doi: 10.1017/jpa.2017.152.

Faure, M., Lepvrier, C., Nguyen, V.V., Vu, T.V., Lin, W. & Chen, Z. 2014. The South China block-Indochina collision: Where, when, and how? Journal of Asian Earth Sciences, 79, 260-274, doi: https://doi.org/10.1016/j.jseaes.2013.09.022.

Faure, M., Nguyen, V.V., Hoai, L.T.T. & Lepvrier, C. 2018. Early Paleozoic or Early-Middle Triassic collision between the South China and Indochina Blocks: The controversy resolved? Structural insights from the Kon Tum massif (Central Vietnam). Journal of Asian Earth Sciences, 166, 162-180, doi: https://doi.org/10.1016/j.jseaes.2018.07.015.

Fitzsimons, I.C.W. 2000. Grenville-age basement provinces in East Antarctica: Evidence for three separate collisional orogens. Geology, 28, 879-882, doi:10.1130/0091-7613(2000)28<879:GBPIEA>2.0.CO;2.

Fitzsimons, I.C.W. 2003. Proterozoic basement provinces of southern and southwestern Australia, and their correlation with Antarctica. Geological Society, London, Special Publications, 206, 93-130, doi: 10.1144/gsl.sp.2003.206.01.07.

Fletcher, I.R. & Libby, W.G. 1993. Further isotopic evidence for the existence of two distinct terranes in the southern Pinjarra Orogen, Western Australia. Geological Survey, Western Australia.

Gao, P., Zheng, Y.-F. & Zhao, Z.-F. 2017. Triassic granites in South China: A geochemical perspective on their characteristics, petrogenesis, and tectonic significance. Earth-Science Reviews, 173, 266-294, doi: https://doi.org/10.1016/j.earscirev.2017.07.016.

Gardiner, N.J., Searle, M.P., Morley, C.K., Robb, L.J., Whitehouse, M.J., Roberts, N.M.W., Kirkland, C.L. & Spencer, C.J. 2018. The crustal architecture of Myanmar imaged through zircon U-Pb, Lu-Hf and O isotopes: Tectonic and metallogenic implications. Gondwana Research, doi: https://doi.org/10.1016/j.gr.2018.02.008.

Gardiner, N.J., Searle, M.P., Morley, C.K., Whitehouse, M.P., Spencer, C.J. & Robb, L.J. 2016. The closure of Palaeo-Tethys in Eastern Myanmar and Northern Thailand: New insights from zircon U-Pb and Hf isotope data. Gondwana Research, 39, 401-422, doi: 10.1016/j.gr.2015.03.001.

Ghosh, S., Fallick, A.E., Paul, D.K. & Potts, P.J. 2005. Geochemistry and Origin of Neoproterozoic Granitoids of Meghalaya, Northeast India: Implications for Linkage with Amalgamation of Gondwana Supercontinent. Gondwana Research, 8, 421-432, doi: 10.1016/S1342-937X(05)71144-8.

Golonka, J., Embry, A. & Krobicki, M. 2018. Late Triassic Global Plate Tectonics. In: Tanner, L.H. (ed.) The Late Triassic World: Earth in a Time of Transition. Springer International Publishing, Cham, 27-57.

Grant, R.E. 1976. Permian Brachiopods from Southern Thailand. Memoir (The Paleontological Society), 9, 1-269.

Halpin, J.A., Tran, H.T., Lai, C.-K., Meffre, S., Crawford, A.J. & Zaw, K. 2016. U–Pb zircon geochronology and geochemistry from NE Vietnam: A 'tectonically disputed' territory between the Indochina and South China blocks. Gondwana Research, 34, 254-273, doi: https://doi.org/10.1016/j.gr.2015.04.005.

Hand, M., Reid, A. & Jagodzinski, L. 2007. Tectonic Framework and Evolution of the Gawler Craton, Southern Australia. Economic Geology, 102, 1377-1395, doi: 10.2113/gsecongeo.102.8.1377.

Handley, H.K., Turner, S., Macpherson, C.G., Gertisser, R. & Davidson, J.P. 2011. Hf–Nd isotope and trace element constraints on subduction inputs at island arcs: Limitations of Hf anomalies as sediment input indicators. Earth and Planetary Science Letters, 304, 212-223, doi: https://doi.org/10.1016/j.epsl.2011.01.034.

Hara, H., Kunii, M., Hisada, K.I., Ueno, K., Kamata, Y., Srichan, W., Charusiri, P., Charoentitirat, T., Watarai, M., Adachi, Y. & Kurihara, T. 2012. Petrography and geochemistry of clastic rocks within the Inthanon zone, northern Thailand: Implications for Paleo-Tethys subduction and convergence. Journal of Asian Earth Sciences, 61, 2-15, doi: 10.1016/j.jseaes.2012.06.012.

Hara, H., Kunii, M., Miyake, Y., Hisada, K.I., Kamata, Y., Ueno, K., Kon, Y., Kurihara, T., Ueda, H., Assavapatchara, S., Treerotchananon, A., Charoentitirat, T. & Charusiri, P. 2017. Sandstone provenance and U–Pb ages of detrital zircons from Permian–Triassic forearc sediments within the Sukhothai Arc, northern Thailand: Record of volcanic-arc evolution in response to Paleo-Tethys subduction. Journal of Asian Earth Sciences, 146, 30-55, doi: 10.1016/j.jseaes.2017.04.021.

Hoa, T.T., Anh, T.T., Phuong, N.T., Dung, P.T., Anh, T.V., Izokh, A.E., Borisenko, A.S., Lan, C.Y., Chung, S.L. & Lo, C.H. 2008. Permo-Triassic intermediate–felsic magmatism of the Truong Son belt, eastern margin of Indochina. Comptes Rendus Geoscience, 340, 112-126, doi: https://doi.org/10.1016/j.crte.2007.12.002.

Hu, P.-y., Zhai, Q.-g., Jahn, B.-m., Wang, J., Li, C., Lee, H.-y. & Tang, S.-h. 2015. Early Ordovician granites from the South Qiangtang terrane, northern Tibet: Implications for the early Paleozoic tectonic evolution along the Gondwanan proto-Tethyan margin. Lithos, 220-223, 318-338, doi: https://doi.org/10.1016/j.lithos.2014.12.020.

Huang, K. & Opdyke, N.D. 1991. Paleomagnetic results from the Upper Carboniferous of the Shan-Thai-Malay block of western Yunnan, China. Tectonophysics, 192, 333-344, doi: https://doi.org/10.1016/0040-1951(91)90107-4.

Hutchison, C.S. 1975. Ophiolite in Southeast Asia. GSA Bulletin, 86, 797-806, doi: 10.1130/0016-7606(1975)86<797:oisa>2.0.co;2.

Hutchison, C.S. 2014. Tectonic evolution of Southeast Asia. Bulletin of the Geological Society of Malaysia, 60, 1-18.

Ingavat, R., Toriyama, R. & Pitakpaivan, K. 1980. Fusuline zonation and faunal characteristics of the Ratburi Limestone in Thailand and its equivalents in Malaysia. Geology and Palaeontology of Southeast Asia, 43-62.

Ivanic, T.J., Van Kranendonk, M.J., Kirkland, C.L., Wyche, S., Wingate, M.T.D. & Belousova, E.A. 2012. Zircon Lu–Hf isotopes and granite geochemistry of the Murchison Domain of the Yilgarn Craton: Evidence for reworking of Eoarchean crust during Meso-Neoarchean plume-driven magmatism. Lithos, 148, 112-127, doi: https://doi.org/10.1016/j.lithos.2012.06.006.

Kamvong, T., Khin, Z., Meffre, S., Maas, R., Stein, H. & Lai, C.-K. 2014. Adakites in the Truong Son and Loei fold belts, Thailand and Laos: Genesis and implications for geodynamics and metallogeny. Gondwana Research, 26, 165-184, doi: http://dx.doi.org/10.1016/j.gr.2013.06.011.

Kawakami, T., Nakano, N., Higashino, F., Hokada, T., Osanai, Y., Yuhara, M., Charusiri, P., Kamikubo, H., Yonemura, K. & Hirata, T. 2014. U-Pb zircon and CHIME monazite dating of granitoids and high-grade metamorphic rocks from the Eastern and Peninsular Thailand — A new report of Early Paleozoic granite. Lithos, 200–201, 64-79, doi: http://dx.doi.org/10.1016/j.lithos.2014.04.012.

Kelsey, D.E., Wade, B.P., Collins, A.S., Hand, M.,

Sealing, C.R. & Netting, A. 2008. Discovery of a Neoproterozoic basin in the Prydz belt in East Antarctica and its implications for Gondwana assembly and ultrahigh temperature metamorphism. Precambrian Research, 161, 355-388, doi: https://doi.org/10.1016/j.precamres.2007.09.003.

Kettanah, Y.A., Mory, A.J., Wach, G.D. & Wingate, M.T.D. 2015. Provenance of the Ordovician–lower Silurian Tumblagooda Sandstone, Western Australia. Australian Journal of Earth Sciences, 62, 817-830, doi: 10.1080/08120099.2015.1117020.

Kirkland, C., Spaggiari, C., Wingate, M.T.D., Smithies, R.H., Belousova, E., Murphy, R. & Pawley, M. 2011. Inferences on crust-mantle interaction from Lu-Hf isotopes: a case study from the Albany-Fraser Orogen.

Ksienzyk, A.K., Jacobs, J., Boger, S.D., Košler, J., Sircombe, K.N. & Whitehouse, M.J. 2012. U–Pb ages of metamorphic monazite and detrital zircon from the Northampton Complex: evidence of two orogenic cycles in Western Australia. Precambrian Research, 198-199, 37-50, doi: https://doi.org/10.1016/j.precamres.2011.12.011.

Lan, C.-Y., Chung, S.-L., Shen, J.J.-S., Lo, C.-H., Wang, P.-L., Hoa, T.T., Thanh, H.H. & Mertzman, S.A. 2000. Geochemical and Sr–Nd isotopic characteristics of granitic rocks from northern Vietnam. Journal of Asian Earth Sciences, 18, 267-280, doi: https://doi.org/10.1016/S1367-9120(99)00063-2.

Lepvrier, C., Maluski, H., Van Tich, V., Leyreloup, A., Truong Thi, P. & Van Vuong, N. 2004. The Early Triassic Indosinian orogeny in Vietnam (Truong Son Belt and Kontum Massif); implications for the geodynamic evolution of Indochina. Tectonophysics, 393, 87-118, doi: http://dx.doi.org/10.1016/j.tecto.2004.07.030.

Li, G., Wang, Q., Huang, Y., Chen, F. & Dong, P. 2015. Discovery of Hadean–Mesoarchean crustal materials in the northern Sibumasu block and its significance for Gondwana reconstruction. Precambrian Research, 271, 118-137, doi: https://doi.org/10.1016/j.precamres.2015.10.003.

Li, P., Rui, G., Junwen, C. & Ye, G. 2004. Paleomagnetic analysis of eastern Tibet: implications for the collisional and amalgamation history of the Three Rivers Region, SW China. Journal of Asian Earth Sciences, 24, 291-310, doi: http://dx.doi.org/10.1016/j.jseaes.2003.12.003.

Li, X.-H., Li, Z.-X., He, B., Li, W.-X., Li, Q.-L., Gao, Y. & Wang, X.-C. 2012. The Early Permian active continental margin and crustal growth of the Cathaysia Block: In situ U–Pb, Lu–Hf and O isotope analyses of detrital zircons. Chemical Geology, 328, 195-207, doi: https://doi.org/10.1016/j.chemgeo.2011.10.027.

Lin, Y.-L., Yeh, M.-W., Lee, T.-Y., Chung, S.-L., Iizuka, Y. & Charusiri, P. 2013. First evidence of the Cambrian basement in Upper Peninsula of Thailand and its implication for crustal and tectonic evolution of the Sibumasu terrane. Gondwana Research, 24, 1031-1037, doi: http://dx.doi.org/10.1016/j.gr.2013.05.014.

Liu, J., Tran, M.-D., Tang, Y., Nguyen, Q.-L., Tran, T.-H., Wu, W., Chen, J., Zhang, Z. & Zhao, Z. 2012. Permo-Triassic granitoids in the northern part of the Truong Son belt, NW Vietnam: Geochronology, geochemistry and tectonic implications. Gondwana Research, 22, 628-644, doi: https://doi.org/10.1016/j.gr.2011.10.011.

Long, J. & Burrett, C. 1989. Fish from the Upper Devonian of the Shan-Thai terrane indicate proximity to East Gondwana and south China terranes. Geology, 17, 811-813, doi: 10.1130/0091-7613(1989)017<0811:FFTUDO>2.3.CO;2.

Loydell, D.K. & Aung, K.P. 2017. The "Panghkawkwo graptolite bed" (Llandovery, Silurian), Myanmar and the location of the Sibumasu (or Sibuma) Terrane in the Silurian. Palaeogeography, Palaeoclimatology, Palaeoecology, 469, 1-17, doi: https://doi.org/10.1016/j.palaeo.2016.12.028.

McCulloch, M.T. 1987. Sm-Nd isotopic constraints on the evolution of Precambrian crust in the Australian continent. In: Kröner, A. (ed.) Proterozoic lithospheric evolution. American Geophysical Union, Washington, D.C., Geodynamics, 115-130.

McElhinny, M.W. & Lock, J. 1996. Iaga Paleomagnetic Databases with access. Surveys in Geophysics, 17, 575-591, doi: 10.1007/BF01888979.

Meffre, S., Khin, Z., Khositanont, S., Halpin, J. & Cumming, G. 2008. 'Tectonic evolution of SE Asia', 'Ore Deposits of SE Asia' - Annual Report to Sponsors. CODES.

Merdith, A.S., Collins, A.S., Williams, S.E., Pisarevsky, S., Foden, J.D., Archibald, D.B., Blades, M.L., Alessio, B.L., Armistead, S., Plavsa, D., Clark, C. & Müller, R.D. 2017. A full-plate global reconstruction of the Neoproterozoic. Gondwana Research, 50, 84-134, doi: https://doi.org/10.1016/j.gr.2017.04.001.

Metcalfe, I. 1984. Stratigraphy, palaeontology

and palaeogeography of the Carboniferous of Southeast Asia. Memoires de la Societe Geologique de France, 147, 107-118.

Metcalfe, I. 1988. Origin and assembly of South-east Asian continental terranes. In: Audley-Charles, M.G. & Hallam, A. (eds.) Gondwana and Tethys. Geological Society of London Special Publication 37, London, 101-118.

Metcalfe, I. 2013a. Gondwana dispersion and Asian accretion: Tectonic and palaeogeographic evolution of eastern Tethys. Journal of Asian Earth Sciences, 66, 1-33, doi: http://dx.doi.org/10.1016/j.jseaes.2012.12.020.

Metcalfe, I. 2013b. Tectonic evolution of the Malay Peninsula. Journal of Asian Earth Sciences, 76, 195-213, doi: https://doi.org/10.1016/j.jseaes.2012.12.011.

Mitchell, A.H.G., Myint Thein, H. & Kyaw Min, H. 2015. The medial Myanmar suture zone and the western Myanmar-Mogok foreland. J. Myanmar Geosci. Soc., 6, 73-88.

Morley, C.K. 2018. Understanding Sibumasu in the context of ribbon continents. Gondwana Research, 64, 184-215, doi: https://doi.org/10.1016/j.gr.2018.07.006.

Morley, C.K., Ampaiwan, P., Thanudamrong, S., Kuenphan, N. & Warren, J. 2013. Development of the Khao Khwang fold and thrust belt; implications for the geodynamic setting of Thailand and Cambodia during the Indosinian Orogeny. Journal of Asian Earth Sciences, 62, 705-719, doi: http://dx.doi.org/10.1016/j.jseaes.2012.11.021.

Morley, C.K. & Searle, M. 2017. Chapter 5 Regional tectonics, structure and evolution of the Andaman–Nicobar Islands from ophiolite formation and obduction to collision and back-arc spreading. Geological Society, London, Memoirs, 47, 51-74, doi: 10.1144/m47.5.

Myrow, P.M., Hughes, N.C., Goodge, J.W., Fanning, C.M., Williams, I.S., Peng, S., Bhargava, O.N., Parcha, S.K. & Pogue, K.R. 2010. Extraordinary transport and mixing of sediment across Himalayan central Gondwana during the Cambrian–Ordovician. GSA Bulletin, 122, 1660-1670, doi: 10.1130/B30123.1.

Nagy, E.A., Schärer, U. & Minh, N.T. 2000. Oligo-Miocene granitic magmatism in central Vietnam and implications for continental deformation in Indochina. Terra Nova, 12, 67-76, doi: doi:10.1111/j.1365-3121.2000.00274.x.

Ng, S.W., Chung, S.L., Robb, L.J., Searle, M.P., Ghani, A.A., Whitehouse, M.J., Oliver, G.J.H., Sone, M., Gardiner, N.J. & Roselee, M.H. 2015a. Petrogenesis of Malaysian granitoids in the Southeast Asian tin belt: Part 1. Geochemical and Sr-Nd isotopic characteristics. Bulletin of the Geological Society of America, 127, 1209-1237, doi: 10.1130/B31213.1.

Ng, S.W., Whitehouse, M.J., Searle, M.P., Robb, L.J., Ghani, A.A., Chung, S.L., Oliver, G.J.H., Sone, M., Gardiner, N.J. & Roselee, M.H. 2015b. Petrogenesis of Malaysian granitoids in the Southeast Asian tin belt: Part 2. U-Pb zircon geochronology and tectonic model. Bulletin of the Geological Society of America, 127, 1238-1258, doi: 10.1130/B31214.1.

Nulay, P., Chonglakmani, C. & Feng, Q. 2016. Petrography, geochemistry and U-Pb detrital zircon dating of the clastic Phu Khat Formation in the Nakhon Thai region, Thailand: Implications for provenance and geotectonic setting. Journal of Earth Science, 27, 329-349, doi: 10.1007/s12583-016-0667-7.

Qian, X., Feng, Q., Wang, Y., Chonglakmani, C. & Monjai, D. 2016. Geochronological and geochemical constraints on the mafic rocks along the Luang Prabang zone: Carboniferous back-arc setting in northwest Laos. Lithos, 245, 60-75, doi: https://doi.org/10.1016/j.lithos.2015.07.019.

Qian, X., Feng, Q., Wang, Y., Zhao, T., Zi, J.-W., Udchachon, M. & Wang, Y. 2017. Late Triassic post-collisional granites related to Paleotethyan evolution in SE Thailand: Geochronological and geochemical constraints. Lithos, 286, 440-453, doi: http://dx.doi.org/10.1016/j.lithos.2017.06.026.

Ridd, M.F. 2011. Lower Palaeozoic. In: Ridd, M.F., Barber, A.J. & Crow, M.J. (eds.) The Geology of Thailand. The Geological Society, London, 33-51.

Ridd, M.F. 2015. Should Sibumasu be renamed Sibuma? The case for a discrete Gondwana-derived block embracing western Myanmar, upper Peninsular Thailand and NE Sumatra. Journal of the Geological Society, doi: 10.1144/jgs2015-065.

Saki, A. 2010. Proto-Tethyan remnants in northwest Iran: Geochemistry of the gneisses and metapelitic rocks. Gondwana Research, 17, 704-714, doi: https://doi.org/10.1016/j.gr.2009.08.008.

Salam, A.A., Zaw, K., Meffre, S., McPhie, J. & Lai, C.-K. 2014. Geochemistry and geochronology of the Chatree epithermal gold-silver deposit: Implications for the tectonic setting of the Loei Fold Belt, central Thailand. Gondwana Research, 26, 198-217.

Searle, M.P., Whitehouse, M.J., Robb, L.J., Ghani, A.A., Hutchison, C.S., Sone, M., Ng, S.W.P., Roselee, M.H., Chung, S.L. & Oliver, G.J.H.

2012. Tectonic evolution of the Sibumasu-Indochina terrane collision zone in Thailand and Malaysia: Constraints from new U-Pb zircon chronology of SE Asian tin granitoids. Journal of the Geological Society, 169, 489-500, doi: 10.1144/0016-76492011-107.

Şengör, A.M.C., Altıner, D., Cin, A., Ustaömer, T. & Hsü, K.J. 1988. Origin and assembly of the Tethyside orogenic collage at the expense of Gondwana Land. Geological Society, London, Special Publications, 37, 119-181, doi: 10.1144/gsl.sp.1988.037.01.09.

Sevastjanova, I., Clements, B., Hall, R., Belousova, E.A., Griffin, W.L. & Pearson, N. 2011. Granitic magmatism, basement ages, and provenance indicators in the Malay Peninsula: Insights from detrital zircon U–Pb and Hf-isotope data. Gondwana Research, 19, 1024-1039, doi: 10.1016/j.gr.2010.10.010.

Sevastjanova, I., Hall, R., Rittner, M., Paw, S.M.T.L., Naing, T.T., Alderton, D.H. & Comfort, G. 2016. Myanmar and Asia united, Australia left behind long ago. Gondwana Research, 32, 24-40, doi: https://doi.org/10.1016/j.gr.2015.02.001.

Shi, M.F., Lin, F.C., Fan, W.Y., Deng, Q., Cong, F., Tran, M.D., Zhu, H.P. & Wang, H. 2015. Zircon U-Pb ages and geochemistry of granitoids in the Truong Son terrane, Vietnam: Tectonic and metallogenic implications. Journal of Asian Earth Sciences, 101, 101-120, doi: 10.1016/j.jseaes.2015.02.001.

Sone, M. & Metcalfe, I. 2008. Parallel Tethyan sutures in mainland Southeast Asia: New insights for Palaeo-Tethys closure and implications for the Indosinian orogeny. Comptes Rendus - Geoscience, 340, 166-179, doi: 10.1016/j.crte.2007.09.008.

Sone, M., Metcalfe, I. & Chaodumrong, P. 2012. The Chanthaburi terrane of southeastern Thailand: Stratigraphic confirmation as a disrupted segment of the Sukhothai Arc. Journal of Asian Earth Sciences, 61, 16-32, doi: 10.1016/j.jseaes.2012.08.021.

Squire, R.J., Campbell, I.H., Allen, C.M. & Wilson, C.J.L. 2006. Did the Transgondwanan Supermountain trigger the explosive radiation of animals on Earth? Earth and Planetary Science Letters, 250, 116-133, doi: https://doi.org/10.1016/j.epsl.2006.07.032.

Toriyama, R. 1967. The Rat Buri Limestone of Thailand. 13-20.

Toriyama, R. & Kanmera, K. 1979. Permian fusulines from the Ratburi Limestone in the Khao Khao area, Sara Buri, Central Thailand. In: Kobayashi, T., Toriyama, R. & Hashimoto, W. (eds.) Geology and Palaeontology of Southeast Asia. University of Tokyo Press, Tokyo, 23-93.

Tucker, N.M., Morrissey, L.J., Payne, J.L. & Szpunar, M. 2018. Genesis of the Archean–Paleoproterozoic Tabletop Domain, Rudall Province, and its endemic relationship to the West Australian Craton. Australian Journal of Earth Sciences, 65, 739-768, doi: 10.1080/08120099.2018.1479307.

Udchachon, M., Thassanapak, H. & Burrett, C. 2017. Early Permian radiolarians from the extension of the Sa Kaeo Suture in Cambodia – tectonic implications. Geological Magazine, 155, 1449-1464, doi: 10.1017/S0016756817000322.

Ueno, K. & Charoentitirat, T. 2011. Carboniferous and Permian. In: Ridd, M.F., Barber, A.J. & Crow, M.J. (eds.) The Geology of Thailand. The Geological Society, London, 71-136.

Ueno, K. & Hisada, K. 2001. The Nan-Uttaradit-Sa Kaeo Suture as a main Paleo-Tethyan suture in Thailand: Is it real? . Gondwana Research, 804-805.

Usuki, T., Lan, C.-Y., Wang, K.-L. & Chiu, H.-Y. 2013. Linking the Indochina block and Gondwana during the Early Paleozoic: Evidence from U–Pb ages and Hf isotopes of detrital zircons. Tectonophysics, 586, 145-159, doi: http://dx.doi.org/10.1016/j.tecto.2012.11.010.

Veevers, J.J., Saeed, A., Belousova, E.A. & Griffin, W.L. 2005. U–Pb ages and source composition by Hf-isotope and trace-element analysis of detrital zircons in Permian sandstone and modern sand from southwestern Australia and a review of the paleogeographical and denudational history of the Yilgarn Craton. Earth-Science Reviews, 68, 245-279, doi: https://doi.org/10.1016/j.earscirev.2004.05.005.

Wang, W., Cawood, P.A., Zhou, M.-F., Pandit, M.K., Xia, X.-P. & Zhao, J.-H. 2017. Low-δ18O Rhyolites From the Malani Igneous Suite: A Positive Test for South China and NW India Linkage in Rodinia. Geophysical Research Letters, 44, 10,298-210,305, doi: 10.1002/2017GL074717.

Wang, Y., He, H., Cawood, P.A., Srithai, B., Feng, Q., Fan, W., Zhang, Y. & Qian, X. 2016. Geochronological, elemental and Sr-Nd-Hf-O isotopic constraints on the petrogenesis of the Triassic post-collisional granitic rocks in NW Thailand and its Paleotethyan implications. Lithos, 266-267, 264-286, doi: https://doi.org/10.1016/j.lithos.2016.09.012.

Wilde, S.A. 1999. Evolution of the Western Margin of Australia during the Rodinian and Gondwanan Supercontinent Cycles. Gondwana

Research, 2, 481-499, doi: https://doi.org/10.1016/S1342-937X(05)70287-2.

Wongwanich, T. & Boucot, A.J. 2011. Devonian. In: Ridd, M.F., Barber, A.J. & Crow, M.J. (eds.) The Geology of Thailand. The Geological Society, London, 53-70.

Xu, Y., Cawood, P.A., Du, Y., Zhong, Z. & Hughes, N.C. 2014. Terminal suturing of Gondwana along the southern margin of South China Craton: Evidence from detrital zircon U-Pb ages and Hf isotopes in Cambrian and Ordovician strata, Hainan Island. Tectonics, 33, 2490-2504, doi: doi:10.1002/2014TC003748.

Yan, Y., Huang, B., Zhang, D., Charusiri, P. & Veeravinantanakul, A. 2018. Paleomagnetic Study on the Permian Rocks of the Indochina Block and Its Implications for Paleogeographic Configuration and Northward Drifting of Cathaysialand in the Paleo-Tethys. Journal of Geophysical Research: Solid Earth, 0, doi: 10.1029/2018jb015511.

Yan, Y., Huang, B., Zhao, J., Zhang, D., Liu, X., Charusiri, P. & Veeravinantanakul, A. 2017. Large southward motion and clockwise rotation of Indochina throughout the Mesozoic: Paleomagnetic and detrital zircon U–Pb geochronological constraints. Earth and Planetary Science Letters, 459, 264-278, doi: https://doi.org/10.1016/j.epsl.2016.11.035.

Yao, W.-H., Li, Z.-X., Li, W.-X., Li, X.-H. & Yang, J.-H. 2014. From Rodinia to Gondwanaland: A tale of detrital zircon provenance analyses from the southern Nanhua Basin, South China. American Journal of Science, 314, 278-313, doi: 10.2475/01.2014.08.

Young, A., Flament, N., Maloney, K., Williams, S., Matthews, K., Zahirovic, S. & Müller, R.D. 2018. Global kinematics of tectonic plates and subduction zones since the late Paleozoic Era. Geoscience Frontiers, doi: https://doi.org/10.1016/j.gsf.2018.05.011.

Zaw, K., Meffre, S., Lai, C.-K., Burrett, C., Santosh, M., Graham, I., Manaka, T., Salam, A., Kamvong, T. & Cromie, P. 2014. Tectonics and metallogeny of mainland Southeast Asia — A review and contribution. Gondwana Research, 26, 5-30, doi: http://dx.doi.org/10.1016/j.gr.2013.10.010.

Zhang, L.K., Li, G.M., Santosh, M., Cao, H.W., Dong, S.L., Zhang, Z., Fu, J.G., Xia, X.B., Huang, Y., Liang, W., Zhang, S.T. & Li, S. 2018a. Cambrian magmatism in the Tethys Himalaya and implications for the evolution of the Proto-Tethys along the northern Gondwana margin: A case study and overview. Geological Journal, 0, doi: 10.1002/gj.3311.

Zhang, X., Chung, S.-L., Lai, Y.-M., Ghani, A.A., Murtadha, S., Lee, H.-Y. & Hsu, C.-C. 2018b. Detrital Zircons Dismember Sibumasu in East Gondwana. Journal of Geophysical Research: Solid Earth, 123, doi: 10.1029/2018jb015780.

Zhao, G., Wang, Y., Huang, B., Dong, Y., Li, S., Zhang, G. & Yu, S. 2018. Geological reconstructions of the East Asian blocks: From the breakup of Rodinia to the assembly of Pangea. Earth-Science Reviews, 186, 262-286, doi: https://doi.org/10.1016/j.earscirev.2018.10.003.

Zhu, D.-C., Zhao, Z.-D., Niu, Y., Dilek, Y. & Mo, X.-X. 2011. Lhasa terrane in southern Tibet came from Australia. Geology, 39, 727-730.

APPENDIX I

Other publications during the course of this thesis

Land Use Policy 61 (2017) 368–378

Contents lists available at ScienceDirect

Land Use Policy

journal homepage: www.elsevier.com/locate/landusepol

Rapid land use change by coastal wind farm development: Australian policies, politics and planning

Nick Harvey[a,b,*], Romana E.C. Dew[a], Sarah Hender[c]

[a] The University of Adelaide, Adelaide, South Australia 5005, Australia
[b] James Cook University of North Queensland, Townsville, Queensland 4811, Australia
[c] Department of Environment, Water and Natural Resources, Keswick, South Australia 5000, Australia

ARTICLE INFO

Article history:
Received 25 May 2016
Accepted 21 November 2016

keywords:
Coastal management
Wind farms
Rural coasts
Coastal impact
Rapid land use change
Coastal policy
Environmental management

ABSTRACT

The siting of both onshore and offshore wind farms has caused controversy in a number of countries, particularly in Europe, which currently has the world's largest array of offshore wind turbines. Like the rest of the world there has been a dramatic increase in wind farm development In Australia over the last two decades but none of this has occurred in the offshore environment. Australian wind farms are predominantly located onshore around the southern part of the continent where wind energy is high. This has specifically affected rural coasts where it has created planning and land use policy issues along with environmental impacts and associated public and political reaction. This paper examines the geographic spread, timing and concentration of Australian wind farms around the coast. It also examines the extent to which scientific knowledge on wind farm impacts is incorporated into different state and federal land use and environmental policy and legislative frameworks. The paper concludes that the rapidity in the expansion of the Australian wind energy sector has outpaced strategic land use planning resulting in a piece-meal and cumulative wind farm development on rural coasts.

© 2016 Published by Elsevier Ltd.

1. Introduction

The rapid expansion of wind-generated power has risen from a global cumulative installed capacity of 6100 MW in 1996 to 369, 553 MW at the end of 2014 (GWEC, 2015). Driven by an increasing emphasis on low-emission technologies and government policies directed to meet carbon abatement targets, wind energy has become one of the fastest growing sources of renewable energy worldwide. In order to meet this demand, arrays of wind turbines referred to as wind farms have been built around the globe. Technological change has resulted in an increase in the size and efficiency of turbines, which increased from 10 to 20 m diameter units generating 25–100 kW to megawatt units with rotor diameters of over 100 m installed on towers exceeding 100 m in height (Nelson, 2013, p.11). This has had consequent changes in the impact of individual wind farms. According to Nelson (2013) the US was an important player in the early development of wind farms but by the 1990s was overtaken by Europe, which had significant contributions from Germany. The Global Wind Energy Council estimates that Europe contains 36.25% of the installed capacity worldwide, North America 21.09% and Asia 38.45% with the majority of global growth since 2009 particularly in China (GWEC, 2015).

The growth in the wind energy industry worldwide has seen a simultaneous increase in the number of coastal wind farm developments. This increased capacity for electricity generation is due to the higher wind speeds associated with coastal areas and the potential for wind farms to be in close proximity to human settlements. Consequently, there has been a rapid expansion of both onshore and offshore wind farm developments. There is, however, a trade-off in between the benefits of increased energy efficiencies for offshore wind farms set against the reduced siting, installation and repair costs of coastal onshore wind farms. In Europe, due to the inherent difficulties in finding suitable onshore open spaces in coastal areas, offshore wind energy is becoming a much more viable option (Diesendorf, 2011; EWEA, 2012).

In Australia, recent wind farm development has mirrored the global experience with a rapid increase in output capacity, particularly over the last decade with about half of the wind farms now located around the coast. This is due to a reliable wind environment with coastal sites in close proximity to population centres and electricity grids, mostly on the southeast coast. Unlike Europe, due to Australia's abundance of open spaces and most of its coastal waters being too deep for offshore wind farm technology, all

* Corresponding author at: The University of Adelaide, Adelaide, South Australia 5005, Australia.
E-mail address: nick.harvey@adelaide.edu.au (N. Harvey).

http://dx.doi.org/10.1016/j.landusepol.2016.11.031
0264-8377/© 2016 Published by Elsevier Ltd.

current wind farm developments are land-based (Diesendorf, 2011). Over a decade ago, Mercer (2003) noted this rapid development and potential impact on the Australian coast. Since then there have been a number of site-specific coastal wind farm studies and papers on planning approvals and legal issues but there is a gap in the literature relating to the national impact of this form of coastal development or its broader implications for coastal management.

This paper provides a global context for Australian coastal wind farm development using international examples from the literature of both offshore and onshore coastal wind farm development but focusing on onshore farms, which are of more relevance in Australia. The paper analyses the nature, growth and distribution of the Australian wind farm industry illustrating the extent, timing and impact of wind farm development on the coast. In particular, this paper examines the various issues associated with coastal wind farm development and the extent to which these have been addressed in coastal and planning legislation and policies. This is linked to broader theoretical aspects of the uptake of science into environmental policy. The paper concludes that the rapidity of this form of development has largely moved ahead of specific policies and development controls regulating the industry and this has created a significant land use change around the southern half of the Australian coast.

2. Methodology

Methods for the analysis of Australian wind farm distribution are outlined in a related paper by Harvey and Dew (2016) and summarised here. First, wind farm geo-referenced location data were obtained for all Australian wind farms installed up to mid-2015. These data where then compiled and digitized into an ArcGIS shapefile in order to examine the geographic distribution of all Australian wind farms, which as noted by Harvey and Dew indicated an apparent coastal concentration. In order to quantify this relative concentration a Euclidean distance was calculated between each wind farm and its nearest coastline and the total Australian wind farms were then grouped according to their distance from the coast. Based on these data, 'coastal wind farms' were defined by Harvey and Dew (2016) as being within 25 km of the Australian coastline. Data on the number of wind turbines and their installed wind generating capacity have also been recorded for each wind farm, since individual farms may have a larger number of wind turbines or a greater total generating capacity than the cumulative output of a number of smaller wind farms.

The current research paper builds on the initial assessment of coastal wind farm impacts (Harvey and Dew, 2016) by conducting an analysis of the regulatory planning and policy background, which led to this significant change in coastal land use. In order to do this an extensive review was undertaken for all government policies, legislation and political influences relating to the facilitation or control of coastal wind farm development and siting. The policy analysis required examining both federal and state policies relating to renewable energy matters but the review of legislation primarily focused on an analysis of state-based planning and environmental regulations relating to wind farm development approvals. The reason for this is that the Australian constitution gives individual states the powers to regulate resource use and each state has created its own separate planning and/or environmental legislation. Federal environmental legislation is generally not involved unless a specific wind farm development can be demonstrated to be of 'national' significance.

The research on policy and legislation was supplemented by a document analysis of what has happened 'in practice' through examination of government reports such as planning documents, conditions of approval and environmental impact assessment (EIA) documents. These were analysed to determine issues relating to wind farm development approvals resulting in land use changes.

In addition to a detailed examination of government policy and legislation, the paper uses industry and government statistics on wind farm development to analyse the patterns in the growth of the industry over the last 25 years, with specific focus on differences in the scale and timing of development within and between state jurisdictions resulting in consequent different levels of land use change. These statistical data are then discussed in the context of the geographic spread of wind farms around the coast and linkages to renewal energy policies and planning regulations.

3. Siting issues for coastal wind farm development, the global context

As of early 2015, total global wind power capacity sits at 370 GW increasingly rapidly from 48 GW in 2004 (REN21, 2014). In 2014, 1.3% of the estimated global energy consumption was collectively from wind/solar/geothermal power (REN21, 2014). The rapidity of wind power is shown through its average annual global growth rate of 18% from 2009 to 2014 (REN21, 2014). During 2014, wind generated more than 20% of electricity in several countries, including: Denmark, Nicaragua, Portugal and Spain (REN21, 2014). China was leading in wind power investment and total capacity for 2014, wind with installations rising a record 38 per cent, or 20.7 GW, from a year earlier (REN21, 2014). As of December 2014, 144 countries around the world have renewable energy targets (Climate Change Council, 2014).

In Europe, due to the inherent difficulties in finding suitable onshore open spaces in coastal areas, offshore wind energy is becoming a much more viable option, with the Europe containing the majority of the large offshore wind farms and 6 out of the top 10 are in the UK (Diesendorf, 2011; EWEA, 2012). This phenomenon in Europe has also resulted in reduced siting and environmental issues typically associated with the objections to onshore wind farm developments (Diesendorf, 2011; EWEA, 2012). Six out of the 10 of the world's largest wind farms are in the United Kingdom which now contains 3.4% of the overall global installed wind capacity (GWEC, 2015). In the UK, the siting of onshore wind farms is deliberated in some cases entirely by the local government; in contrast, offshore farms fall within the central government's jurisdiction (Jay, 2012). Toke et al. (2008) state that around 60% of all wind power planning applications are rejected by local councils in England and Wales. The degree of centralised control differs across Europe, for example in Sweden and Denmark, the consensus between local and national government is an important dimension of the authorisation process (Jay, 2012). Globally, the acceptability of onshore wind projects is strongly influenced by the institutional fit to policies and politics, market sectors, intra-firm acceptance and community involvement (Depellegrin et al., 2014; Toke et al., 2008; Wolsink, 2007).

Concerns about impacts of windfarms are often focused on their visual and aesthetic qualities, land-use impacts, wildlife especially aviary mortalities and community health (see Table 1). Additionally, offshore wind farms produce a set of specific marine impacts including marine ecosystem disturbance and navigational safety. Offshore wind farms make up a comparatively small percentage of the global grid-connected capacity only exceeding 8.5 GW across 14 countries (REN21, 2014). The majority of the large offshore wind farms are in Europe and 6 out of the top 10 are in the UK whose waters contain 51.24% of the global cumulative offshore capacity (GWEC, 2015; REN21, 2014). There has been a variety of factors discussed in Jay (2012) that have contributed to the success of offshore wind energy in the UK. Given a lack of such offshore developments in Australia this paper will only focus on issues associated

Table 1
Coastal impacts of wind farms (Harvey and Dew, 2016).

Type of Impact	Examples	References
Socio-cultural	Aesthetics and visual amenity; cultural heritages and norms; *wind turbine syndrome*	Lothian (2008); Chapman et al. (2013); Crichton et al. (2014)
Environmental	Landscape scarring & erosion; biota danger especially bird and bat; water contamination; habitat loss; life-cycle global warming emissions	Mercer (2003); Lothian (2008); Pasqualetti (2012)
Economic/ Technological	Property loss; navigational safety; mechanical and aerodynamic noise	Pasqualetti (2012); Firestone et al. (2015)

with the siting of onshore wind farms such as socio-cultural and environmental impacts and technological factors.

Results from the GIS-based model for visual impact assessment conducted by Depellegrin et al. (2014) indicate that the coastal zone's geomorphological features including beaches, dune ridges and cliffs, act as a natural visibility barrier and absorb the visual impacts of offshore wind arrays.

Firestone et al. (2015) comment on the socio-cultural impacts of wind farms based on a University of Delaware Coastal Campus Wind Project. They concluded that public opinions reflect socially and culturally constructed aspects of the wind turbine rather than based on physical attributes of the turbines (Firestone et al., 2015). Wind turbines may disrupt the residents' cultural connection to the landscape and their community as some in the survey perceived that the turbines do not fit the landscape (Firestone et al., 2015). Firestone et al. (2015) found that some positive attitudes within the community with the turbines being a symbolic representation of progress to cleaner energy. The overall findings of Firestone et al. (2015) could be applicable and have resonance for other rural coastal communities worldwide.

Stemming from these issues are also economic concerns about decreased land values and increased electricity prices. Whilst the majority of studies of long term negative net effects of wind farms on local property values have been inconclusive or without supporting evidence (e.g. Firestone et al., 2015; Hoen et al., 2013; Lang et al., 2014; Vyn and McCullough, 2014), they have played a substantial secondary role in arguments against wind farm developments. In regard to land values, similar to the case of landscape and visual amenity, the issue stems from whether or not the wind farm, and any ancillary services or structures, represents a positive enhancement or negative impact on the visual amenity of the landscape. Again, this is often a subjective assessment of amenity dependent on the particular stakeholder or group of stakeholders. A similar issue stems from the notion that the potential value of the rural land is affected if it were to be subdivided at some future point.

In an American technical report, Erickson et al. (2005, p. 1037) estimate that, "*buildings, power lines and cats comprise approximately 82 percent of the [annual bird] mortality*", compared to wind turbines, which comprise only 0.003 percent. Nevertheless, there is no doubt that in some locations, such as Altamont Pass in California, the incidence of wind-related bird fatalities is unacceptably high, especially of 'charismatic birds', such as falcons and eagles (Pasqualetti, 2012).

From a technological perspective, wind turbines emit a mechanical sound from their gearbox and an aerodynamic noise from the rotation of the blades (Firestone et al., 2015). Turbines have been under past scrutiny due to purported problems including a variety of alleged interference (noise, electromagnetic, electrical, radar and navigation), the blade glint and flicker, stray voltage, oil leaks, fires, ice toss and collapse (Pasqualetti, 2012). There has been a recent increase in the attribution of symptoms and diseases to wind turbine exposure and sub-audible sound for humans and animals, coined the 'wind turbine syndrome' (Crichton et al., 2014).

The continuing evolution of turbine designs is moving towards larger machines with longer blades, higher hub height to reach stronger winds and greater nameplate capacity (REN21, 2014). Current developments aim to reduce operations and maintenance costs with shifts in technologies and strategies to improve wind's economics in a wider range of wind regimes and operating conditions (REN21, 2014). Wind turbine blades have become an area of strategic innovation including recent progress with substantial alterations in the design, materials and manufacturing processes (REN21, 2014).

4. Expansion of the Australian wind power industry on the coast

Due to Australia's relatively low electricity prices and abundance of coal resources (Garnaut, 2011), most land-based wind farm developments need to be of a more significant scale than those in Europe, in order for the electricity generated to be cost-effective. Nevertheless, the scale of wind farm developments has increased dramatically over the last 20 years. As the technology evolves for larger output capacities, the number of turbines constructed per wind farm also increases. The increases in turbine number and output capacity are occurring simultaneously as the demand and need for transitioning towards greater proportions of renewable energy sources develops societally (Hall et al., 2013).

The advent and growth of onshore coastal wind farm developments, here defined as within <25 km of the coastline, represents a significant land-use change within the Australian coastal zone, producing an array of related impacts. As of August 2015, there were 73 wind farms operating in Australia incorporating a total of 2022 turbines with a capacity to produce an output of approximately 4135 MW of electricity. Nationally, wind farms constituted 30.9% of the total clean energy and 4.2% of the electricity generated in 2014. The total Australian installed capacity as of December 2015 is estimated to be nearly 4200 MW (Fig. 1).

Almost 75% of this electricity generation takes place in South Australia and Victoria. A map constructed from the wind farm locational GIS data-base (Fig. 2) illustrates that 64 percent of the nation's wind farms are located near the coast. The coastal zone also is home to half (50%) of the total number of the country's installed wind turbines. Similarly, coastal regions also contain about half (51%) of the total national installed capacity of 4135 MW, indicating that output capacity is more closely aligned with the number of turbines, rather than the number of wind farms. The extent of Australia's coastal wind farm developments also varies considerably on a state-by-state basis reflecting the varying social, economic and environmental conditions that are conducive to wind energy generation.

Since the first wind turbine was installed in South Australia in 1991, at 0.15 MW, wind energy represents the fastest growing source of renewable energy in Australia with an overall 47% compound annual national growth rate over the last 25 years (Fig. 1b). South Australia's coastline extends 3700 kilometres fringing the Southern Ocean (Fig. 2) making it a prime candidate for wind

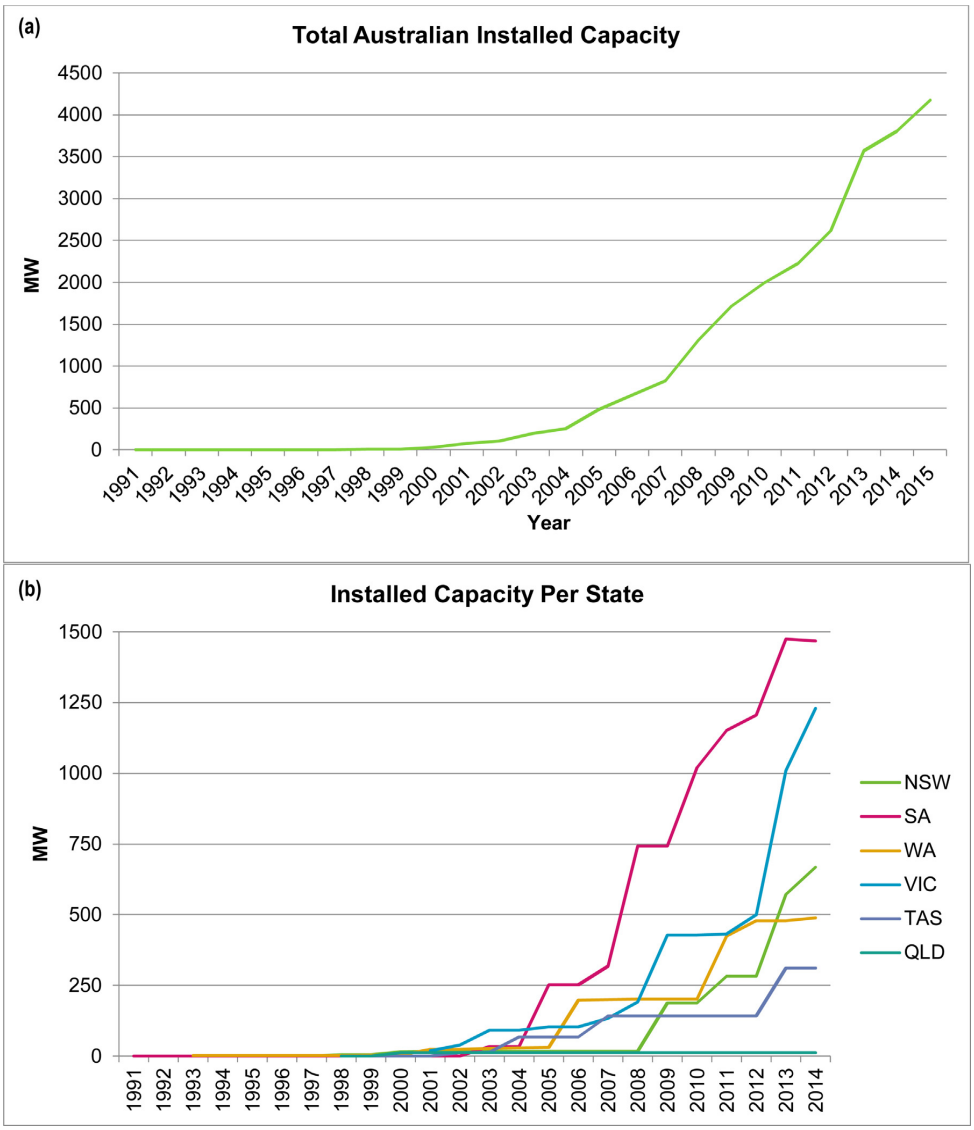

Fig. 1. a) Total Australian Wind Energy Capacity since 1991 b) Total Australian Installed Wind Energy Capacity by State since 1991. Sources: GWEC (2015)

developments. By far the largest capacity of any state (Fig. 3), South Australia generated well over 1400 MW annually for the last three years. Additionally, wind capacity supplied 35 per cent of electricity generated in South Australia for 2013–14 (AER, 2014). On 8 September 2014, wind output accounted for 76 per cent of South Australian electricity generation (AER, 2014). Of the nation's coastal wind farms, South Australia contains over half of the total installed capacity (54%) and number of turbines (50%). Examples of aesthetic impacts on rural coastal South Australian landscapes are described in Harvey and Dew (2016).

After South Australia, Victoria, Tasmania and Western Australia make up the greater proportion of the rest of the Australian coastal capacity (Fig. 3). Similar to the installed capacity, South Australia leads in the number of coastal wind turbines at 446 turbines followed by Victoria (198), Tasmania (124) and Western Australia (122). However, Western Australia, with 15 wind farms, has the highest number of coastal farms in the country.

5. Public controversy, social and environmental issues in Australia

Development of wind power projects has not been without controversy and criticism. Despite well-documented high levels of public support for low emission technologies worldwide, recent opposition and low acceptance of wind farms has also seen rejection rates increase for a growing number of new developments (Smith and Prosser, 2011). Indeed, whilst public support at national levels is needed in terms of successfully implementing policies for

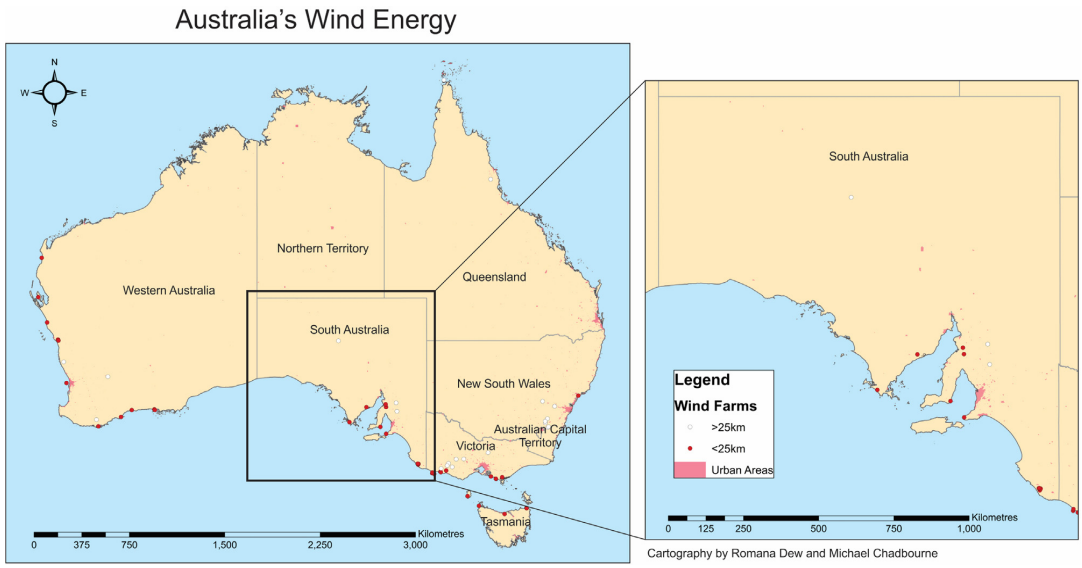

Fig. 2. Map of Australian coastal wind farms. Inset of South Australia.

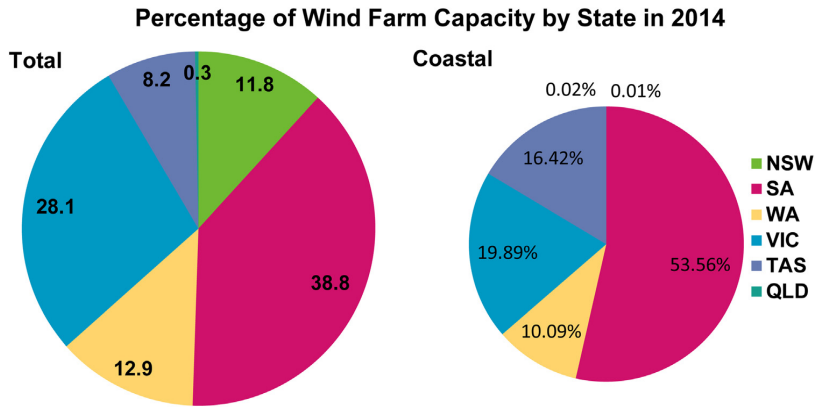

Fig. 3. Pie chart illustrating the percentage of the national wind farm capacity by state for the total and coastal. Source: Authors.

increased renewable energy developments, the role of local acceptance is paramount in determining this success due to the fact that it is the individual wind farm development, not the overall policy, which needs to be accepted at local scales (Wolsink, 2007, p. 2695). Nevertheless, 2015 research from the Climate Institute indicates that public support is increasing within Australia. A total 65 per cent of Australians believe that investment in wind farms and householder solar power should increase (Connor, 2015).

There are a number of well-documented Australian wind farm developments that have caused considerable controversy and criticism in recent years. This growth in opposition has in many cases, been contradictory to the many simultaneous claims of growth in support for renewable energy and, more broadly, climate change mitigation strategies. This 'social gap', between stated support and individual local acceptance may, in part, be explained by the trade-off between the local 'costs' of wind farm development and the national and global 'benefits' of action on climate change (Hall et al., 2013; Huber and Horbaty, 2012). Such a 'social gap' is not unique to wind farm developments, but is common in many new energy and technological developments whereby the local burden of 'costs' and 'risks' are deemed unacceptable in relation to the diffuse 'benefits' to the world at large (Schenk and Stokes, 2013). These 'costs' are typically associated with social, environmental and economic concerns as illustrated in Table 2.

5.1. Socio-cultural

The socio-cultural components of wind farm impacts are primarily subjective psychological effects and examples are shown in Table 1. The inherent rurality implied by the term "wind farm" does correlate with the largely rural coastal landscapes where wind developments are sited. This is certainly the case for wind developments within Australia as depicted in Fig. 2. In regard to land values, the issue stems from whether or not the wind farm, and any ancillary services or structures, represents a positive enhancement or negative impact on the visual amenity of the landscape. Studies by

Table 2
Coastal Impacts and Issues at different stages of Wind farm development.

	Planning	Construction	Connection	Operation
Social	• Landscape & Amenity Perceptions • Winners versus Losers (Hosts)	• Audible Noise • Traffic • Landscapes	• EM Fields • Landscapes	• Sub-audible Noise • Flicker & Glint • EM Fields • Aviation • Landscapes
Environmental	• EPBC issues	• Road construction • Land clearance • Run off • Erosion & Storm Surges • Habitat disturbance	• Cable installations • Erosion & Storm Surges	• Bird & Bat Strikes • Erosion & Storm Surges
Economic	• Winners versus Losers (Hosts) • Property Sub division • Land Values	• Agriculture • Road construction • Land Values	• Cable installations • Land Values	• Tourism • Land Values

Source: Compiled by Authors.

Lothian (2008) indicate that wind farms that are less than three kilometres away have a higher negative effect on the scenic quality of the landscape. Again, this is often a subjective assessment of amenity dependent on the particular stakeholder or group of stakeholders.

As Hindmarsh and Matthews (2008) point out, as of late 2007, there was one coast or landscape guardian group for every second wind farm built (at that time there were 42 wind farms – with 69 from 2015 data analysed in this study). Whilst many of these landscape guardian groups have been accused of holding a 'NIMBY-ist' attitude towards wind farm development, which contrasts with the wider public support for renewable energy, there are more embedded concepts of a 'sense of place' that motivate their opposition (for example, see Hindmarsh, 2010).

There has been a recent increase in the attribution of symptoms and diseases to wind turbine exposure and sub-audible sound for humans and animals, coined the 'wind turbine syndrome' (Crichton et al., 2014). The pilot study conducted by researchers, commissioned by Pacific Hydro considered wind farm noise and residents' reactions near the Cape Bridgewater wind farm in southwestern Victoria. The study has not been validated due to enormous selection bias, unrepresentative sample size, misinformation, blatant leading questions, post-hoc rationalisations leading to unfalsifiable information and rejection of 84.48% of the recorded data (Joshi, 2015). Chapman (2011) describes that the growth in reports of 'wind turbine syndrome', attributed with 216 different diseases and symptoms, appear to be 'contagious' and "spread by the vector of anti-wind farm activist groups". In February 2014, the National Health and Medical Research Council stated there is no reliable or consistent evidence that wind farms are directly responsible for negative health effects in humans. Despite the lack of evidence, however, health concerns attributed to 'wind turbine syndrome' have played, and continue to play, a substantial role in recent arguments in opposition to wind farm proposals (*The Social and Economic Impact of Rural Wind Farms*, Senate Inquiry June 2011, *Select Committee on Wind Turbines*, Final report August 2015).

5.2. Environmental

Environmental impacts that have been discussed in previous literature are highlighted in Table 1. Unlike for the aesthetic issues, mitigation is possible for the majority of the environmental issues (Lothian, 2008). Impacts on any wildlife are assessed by the proponent/developer during initial environmental impacts assessment stages. During this process, if any species are identified that constitute a matter of 'national significance', this triggers a formal EIA process under the Federal *Environment Protection and Biodiversity Conservation Act 1999* (*EPBC Act*). Typically, arguments against wind farm proposals have been utilised by landscape guardian groups which often cite the number of bird and bat fatalities. In terms of the number of wind farm fatalities relative to other structures, such as power lines and buildings, wind farms are responsible for only a fraction (NWCC, 2001). Tarwin Valley Coastal Guardians in southern Victoria stated that four dead koalas were found over 4 to 6 weeks as a result of land clearing to install a transmission line for a nearby wind development (Madigan et al., 2015).

6. Wind farm policy development: the role of science, politics and planning

Despite the rapid expansion of Australian wind energy, there appears to be a lag in policy and development controls to appropriately/adequately manage this land use change and subsequent impacts in a strategic manner (Hall and Harvey, 2006). Additionally, coastal wind farms have not traditionally been viewed as coastal development *per se*. As a result, the extent to which coastal management issues and coastal science have been considered in the planning process for wind farms remains limited.

6.1. Science in wind policy formulation

Over the past three decades there have been consistent calls for greater incorporation of science within environmental policy development and more policy relevant science (UNCED, 1992; OECD, 2002; WCED, 1987; Lalor and Hickey, 2013; Banks, 2009), highlighting the importance of the science-policy nexus. Yet repeated calls indicate that an "increased" or "effective" utilisation of science is not yet occurring, with the barriers to science uptake forming recent focus of research (McNie 2007; Juntti et al., 2009; Lalor and Hickey, 2013; Head et al., 2014). Indeed achieving policy relevant science and science-based policy is immensely complex "it needs to be the right evidence; it needs to occur at the right time and be seen by the right people" (Banks 2009, p. 8). In a study of former environmental Ministers and Senior Public Servants in the Australian and Canadian Governments, Lalor and Hickey (2013, p. 770) found that whilst, the value of science as the foundation of executive decision-making was supported in principle, it was most instrumental when there was "a relatively high degree of certainty about the social, environmental and political outcomes of the decision." Other factors influencing the use of science by policy makers include time constraints to read information, a lack of opportunity to build relationships with academic

researchers and inability to translate science information into policy (Head et al., 2014). Hence it remains that science continues to be over-looked in policy-making. A recent survey of Australian State and Federal Government officials reveals that the key drivers for policy development are budgetary considerations followed by politically acceptability of decisions and short-term considerations (Head et al., 2014).

As the above discussion indicates it is difficult to separate policy making from political contexts. This is even more so the case in Australia, where policy development is strongly influenced by Australia's federated system of governance and the existence of historic conflict between State and Federal government roles and jurisdictions for resource use and environmental controls (Buhrs and Christoff, 2006; Doyle and Kellow, 1995). Despite recent Commonwealth attempts to strengthen its position regarding environmental protection powers, the responsibility of implementing policy, and power, remains with State governments (Buhrs and Christoff, 2006). Presently, each state is responsible for developing its own environmental legislation and environmental policy-making processes which has created inconsistent approaches.

In addition, there are varying drivers behind environmental policy development in Australia, ranging from political party ideology, agendas of particular political leaders and decision-makers, events such as drought and waves of social activism (Dovers, 2013). Although Dovers (2013) finds Australian governments (State and Federal) use varying policy instruments to manage unpredictably changing policy topics, significant moments of change in the environmental policy agenda can be associated with particular governments of the day. Buhrs and Christoff (2006, p. 239) draw a strong link arguing "political-ideological orientations, in particular, appear to play a dominant role . . . in determining environmental policy and outcomes." Even the electoral system has "influenced the potential for environmental issues to become more prominent on the national and State policy agendas" (Buhrs & Christoff, 2006, p. 236) Consequently, the use of science in policy-making is affected by former senior government environment ministers determining "credible science" to be ". . .inclusive of a range of policy options that were suitably matched to the prevailing political and socioeconomic context" (Lalor & Hickey, 2013, p. 771).

Development and management of the Australian coast is one area of environmental policy that has continually lacked a consistent national approach, a victim of the federated system of government (Wescott, 2011). Presently coastal policy remains the jurisdiction of State governments, despite four separate national inquiries since the 1980s proposing the establishment of a national coastal policy (Harvey, 2016). Hence, a range of coastal planning and development issues have been treated according to state-based responses and type of coastal development. For example, coastal canal estate policy has evolved over a period of 5 decades, with varying levels of science and political inputs informing policy between states spanning from politically driven bans, scientifically-specific development control regulations or generic development assessment processes (Harvey and Stocker, 2015). Thus far, the development of coastal wind farms has been considered as a development issue rather than a coastal land use issue. Other than a Federal EPBC Act, coastal wind farms are primarily assessed on a state-by-state basis according to relevant state planning and development processes, legislation and controls. We evaluate the extent to which coastal management issues and coastal science have been considered in the policy-making process for coastal wind farms.

6.2. Socio-political influences

Hindmarsh and Matthews (2008) describe the key problem for wind energy expansion, worldwide, as being primarily a socio-political one. In Australia, despite the rapid rate of growth in wind farm developments, the industry has been hindered by the multiple and often inconsistent Federal, State and Local government policy positions and planning approval processes. In 2006 Hall and Harvey identified inconsistencies in EIA procedures for wind farms in South Australia compared to a more strategic planning approach to wind farm development in Victoria (Hall and Harvey, 2006). More recently in 2014 wind energy provided 4% of Australia's electricity but because of Federal policy uncertainty, most investment and projects were on hold (REN21, 2014).

The conflicting Federal, State and Local government policy positions and planning approval processes have not helped community consultation processes. The consultation process, or lack thereof, has often been a key issue of opposition from both a social and governance perspective. In these instances, opponents regularly state the insufficiency of public engagement by the wind farm developer early-on in the project's planning and proposal period as a major criticism. In many cases, it has also been reported that consultation has taken place after the particular proposal's announcement (Hindmarsh and Matthews, 2008). It has been established in the literature that low levels of social acceptance of wind farms can typically be the result of a perceived unfairness in terms of both procedural processes and outcomes (Gross, 2007). Consequently, this low level of acceptance appears to have contributed to slower development approval processes (Hall et al., 2013).

Stemming from the above consultation issues are also planning and siting issues. Hall et al. (2013) found that wind turbine 'hosts', whose land had at least one wind turbine located on it and who received an annual income from the wind farm developer for hosting turbines, supported wind farms and generally did not hold any visual, noise or other negative concerns. This contrasts with those in the community who were not turbine 'hosts'. Whereas turbine 'hosts' would typically be contacted initially by the developer well before the announcement of the wind farm proposal, for instance, for setting up air-speed monitoring stations, other landowners were not contacted. Ultimately, since the processes of consultation with those who would become turbine 'hosts' was quite often different from those who were not 'hosts', it created a division within the community due to a perceived sense of 'secrecy' or unfairness whereby there were 'winners and losers'. As Gross (2007, p. 2727) describes, "outcomes that are perceived to be unfair can result in protests, damaged relationships and divided communities particularly when decisions are made which benefit some sections of the community at the perceived expense of others". Consultation, as such, needs to extend beyond those that would become turbine 'hosts' in order to foster willing community members.

6.3. Government response

The socio-political issues discussed above when compounded through highly vocal and organized public contestation, have strong potential to significantly reduce wind power's contribution to mitigation targets, pollution reduction and energy security (Hall et al., 2013; Hindmarsh, 2010; Hindmarsh and Matthews, 2008; Huber and Horbaty, 2012). Many of these issues have been addressed in Australia at the national level plus a raft of additions at the state level as discussed below. To date, however, there has been very little consideration in terms of coastal management issues within the planning process of wind farm developments.

6.3.1. Federal government response and environmental impact assessment

Given the rapid rate of growth in the wind farm industry over the past 20 years in Australia, the Federal Government, through the former Federal Department for Environment and Heritage and Australian (DEH) Office, proposed the National Code for Wind Farms.

Table 3
Australian wind farm legislation, regulations, policies and planning guidelines.

Legislation, regulations, policies and planning guidelines	
2015	Renewable Energy Target (RET) reforms
2013	CEC Community Engagement Guidelines
2012	Clean Energy Finance Corporation Act
2010	Renewable Energy (Electricity) (Small-scale Technology Shortfall Charge) Act
	EPHC National Wind Farm Development Guidelines DRAFT
2009	EPBC Act Policy Statement: Wind Farms
2008	CEC Accreditation: Certified Wind Farms Australia (CWFA)
2006	AusWind Best Practice for Implementation of Wind Energy Projects in Australia
2006	DEH and AGO National Code For Wind Farms: A Discussion Paper
2004	AusWEA and ACNT Wind farms and Landscape Values
2000	National Assessment Methodology
	Renewable Energy (Electricity) Regulations
	Renewable Energy (Electricity) Act (Large-scale Generation Shortfall Charge) Act

Source: Compiled by Authors.

The 2006 national code, developed as a discussion paper, particularly focused on the inclusion of a 'consensus building' approach. This style of approach had been developed and applied to a number of different local environmental conflicts in the past where competing interests tended to stall progress of particular development. Despite support from the wind energy industry, local governments and key community representatives, all of the state governments rejected the proposed national code for wind farms (Hindmarsh and Matthews, 2008).

Climate change policies have altered the composition of electricity generation in the National Electricity Market (AER, 2014). Federally, the renewable energy target (RET) originally set the target of 20% of the nation's energy to be generated from renewable energy sources by 2020. This target assisted in providing a stable environment for investment in wind energy across Australia, thus driving wind energy developments. However, the election of the Abbott Coalition Federal Government in 2013 and review of the RET in February 2014 (compiled into the Warburton report) created significant policy uncertainty and subsequent negative impact on investment, causing an 88 per cent reduction in new large-scale renewable energy investment compared to 2013 (Bloomberg New Energy Finance, 2015). In 2014 the Treasurer, Joe Hockey was on record describing wind farms as "utterly offensive" and then in early 2015 the Prime Minister, Tony Abbott described them as "visually awful". Furthermore in July 2015, the $10 billion Clean Energy Finance Corporation (CEFC), the government-owned organisation previously created to catalyse and leverage an increased flow of funds for the commercialisation and deployment of Australian renewable energy, was told by the Treasurer and Finance Minister to stop investing in wind power projects, in a move the Federal Opposition described at the time to be a "dramatic escalation" in the Government's war on wind farms (Norman, 2015). In December 2015 the Turnbull-led Federal Government lifted the ban on the CEFC for wind farm investment, which was introduced by former Prime Minister Tony Abbott (Norman, 2015).

At a national level, whilst the Commonwealth does not have explicit constitutional powers for environmental regulation, certain developments do trigger the process for an EIA if they are deemed to affect matters of national significance through the *Environment Protection and Biodiversity Conservation Act 1999* (*EPBC Act*). In one instance this was triggered because of the potential impact of a proposed wind farm on nationally threatened and migratory bird species (Hall and Harvey, 2006). More recently, this triggering process is assisted through the 2009 EPBC Act policy statement on the wind farm industry (EPBC, 2009). Specific coastal issues are not mentioned in the EPBC Act policy statement beyond the scope of mortality of seabirds or loss of coastal scenic value. Similarly, there are no specific discussions of coastal issues in the 2010 EPHC Draft National Wind Farm Development Guidelines or the 2006 AusWind best practice for implementation guidelines.

The Clean Energy Council (CEC), operating as part of the Australian Government, launched the 2008 certified wind farms Australia (CWFA) accreditation system based on the Auswind, 2006 best practice for implementation guidelines and the international environmental standard ISO 14001. The CWFA includes an auditable framework for managing the environmental impacts, the process of stakeholder consultation, and visual amenity aspects of wind farms both during development and operation. Again, however, there is no specific mention of coastal issues.

The 2006 DEH and the Australian Greenhouse Office (AGO) discussion paper on the proposed National Code for Wind Farms, on the other hand, specifically mentions that the "spectacular beauty of parts of Australia's coastline needs to be preserved" (DEH and AGO, 2006, p. 18) and that such a code, if introduced, would need to ensure that a consistent approach is taken on such issues. The 2006 federal discussion paper also specified that developers should consult with, among others, coastal management authorities as soon as possible to preserve coastlines that are 'unspoiled'. As mentioned previously, the national code, which was supported by the wind energy industry, local governments and key community representatives, was rejected by all state governments (Hindmarsh and Matthews, 2008). As illustrated in Table 3, the national code is only one of a number of key changes which have occurred in legislation, policies and planning guidelines for wind farms since 2000.

In November 2014, the Senate resolved to establish the Select Committee on Wind Turbines to inquire into and report on the application of regulatory governance and economic impact of wind turbines. The committee completed its work on 3 August 2015 with the submission of their final report and recommendations (Madigan et al., 2015). Madigan et al. (2015, p. 3–4) highlight that the Federal Minister for the Environment has committed to a number of matters including:

- establishing an Independent Expert Scientific Committee (IESC) on Industrial Sound to examine (among other matters) the impact of wind turbines on human health;
- publish research on options for wind farm operators to maximise transparency by providing information on wind speed, operational statistics, operating hours and sound monitoring;
- establish a National Wind Farm Commissioner to resolve complaints from concerned residents about the operation of wind farm facilities.
- to seek agreement from the States and Territories to implement National Wind Farm Guidelines as recommended by the IESC which each state and territory government should reflect in their relevant planning and environmental frameworks; and

Table 4
Australian state wind farm legislation, regulations, policies and planning guidelines.

State	Year	Legislation, regulations, policies and planning guidelines
New South Wales	2011	DP&I NSW Planning Guidelines: Wind Farms
	2007	State Environmental Planning Policy (Infrastructure)
South Australia	2012	DPLG Statewide Wind Farms Development Plan Amendment
Western Australia	2011	WAPC Planning Bulletin 67 Guidelines for Wind Farm Development
	2004	WAPC Guidelines for Wind Farm Development
Victoria	2015	Victoria's Renewable Energy Roadmap
	2012	DPCD Policy and planning guidelines for development of wind energy facilities in Victoria
	2003	Victorian Wind Atlas
Tasmania		No policy (the Tasmanian EPA follows the National EPHC Guidelines)
Queensland	2014	Draft Wind Farm State Code[a]

Source: Compiled by Authors

[a] The Queensland Department of Infrastructure, Local Government and Planning released its draft wind farm state code and planning guideline for a second round of public consultation in late 2015 and expects to incorporate the code and guideline into the State Development Assessment Provisions (SDAP) in mid-2016.

6.3.2. State-level government response: legislation, regulations, policies and planning guidelines

The influence of stable and consistent policy on wind energy development and investment is more clearly seen at the state level. Whilst New South Wales has planning guidelines for wind farms, they do not specifically mention coastal issues (Table 4). The New South Wales wind farm located within 10 km of the coastline is, in fact, located near deep-water coal export facilities on the Hunter River in Newcastle. Neither Tasmania nor Queensland have a specific policy for wind farms. Queensland is in the process of implementing specific wind power guidelines in 2016 and the Tasmanian EPA currently endorses the national EPHC guidelines, which do not specifically mention coastal issues. Nevertheless, Tasmania aims to generate 100% of its electricity from renewable sources by 2010 (REN21, 2014). Whilst Queensland has only one wind farm consisting of two turbines within 1 km of the coast on Thursday Island, all of Tasmania's wind electricity is generated less than 15 km from the coast on existing cleared pastoral and grazing land. As for the Australian Capital Territory, Chief Minister Andrew Barr pledges to commit to a target of 100 per cent renewable energy for the territory by 2025, which would make Canberra the first Australian capital to be entirely powered by renewables (Lawson, 2015).

South Australia's Department of Planning in conjunction with local government has established a development amendment plan, which deems that wind farms are an acceptable development in areas with relatively low population densities zoned coastal. This includes a setback distance of between 1 km and 2 km the acceptance of this plan is highlighted in Fig. 2, with few developments within urban regions. South Australia also has a draft consultation plan from 2002 which acknowledges the potential coastal visual impacts due to design issues related to supply and demand. Additionally, this plan acknowledges the risks and vulnerability in siting turbines in areas where there are issues arising from potential coastal erosion and inundation during storm surges. The plan also acknowledges the need to preserve habitats, wetlands, dune systems, lakes, native vegetation and other items of natural significance for aesthetic and biodiversity reasons. South Australia also has a renewable energy target of 33% of the electricity generation by 2020 (REN21, 2014).

Western Australia utilizes its state planning commission guidelines which focus on minimizing coastal visual impacts and the consequences of coastal vegetation removal. These guidelines include a 1 km setback distance from 'noise-sensitive buildings', which was based on South Australian EPA noise guidelines for wind farms. In minimizing visual impacts, the wind turbines within 5 km of the coastline have typically been placed linearly along coastal ridgelines to reflect and complement landscape and topographical features. The majority of such wind farms are also located amongst low lying native scrubland and stabilised sand dunes, and utilised existing roads to reduce vegetation clearance. The more sizeable wind farms in Western Australia are located on existing cleared pastoral and grazing land less than 25 km from the coast.

Victoria's Department of Planning and Community Development has produced guidelines which focus on coastal siting issues related to minimizing the impacts on primarily 'visually significant' landscapes (Table 4). This includes a turbine setback distance of 2 km from dwellings. Victoria's largest wind farms located within 5 km of the coast are positioned linearly behind vegetated dunes on existing cleared pastoral land in order to complement the landscape. With the RET now resolved, the Victorian Government has announced they'd like to back that with further, as yet unspecified, policies to ensure the state had at least 20% of its power from renewable energy by 2020, up from 12% in 2014 (ClimateSpectator, 2015). On August 21st 2015, the Victorian state government released *Renewable Energy Roadmap* and considering feedback from the public consultation on the Roadmap, the Victorian Government will release the Renewable Energy Action Plan.

7. Discussion and conclusion

There has clearly been a dramatic increase in wind farm development. In Australia over the last two decades but unlike Europe all of this development has taken place onshore thus impacting on land use. This paper demonstrates that the most significant area affected has been the rural coasts where wind farm developments have created planning and land use policy issues along with environmental impacts and associated public and political reaction.

Of the total Australian wind farms, 64 percent are located near the coast although the coastal wind farms collectively contain a smaller proportion (50%) of the total number of the country's wind turbines. This is closely linked to the coastal proportion (51%) of national installed wind generated capacity. Over half (54%) of this coastal installed capacity occurs in one state, South Australia. The rapid national expansion of this industry has created a largely unpredicted land use change for many parts of the Australian coast.

A major reason for the high proportion of coastal wind farms around the southern parts of the Australian coast is linked to the high wind energy resource, however, the reasons for the scale and rapidity of this land use change and the geographic variation in development between states are more complex. In large part this is related to separate planning and/or environmental legislation for approval of wind farm developments in each state as a result of Australia's federated system of governance. In addition the speed of the wind farm industry expansion over the last 20 years has largely outpaced a mostly re-active state-based development control planning system rather than a national strategic plan for wind farm development. Early state-based attempts at strategic planning to assist the industry occurred in Victoria but subsequent controls were introduced in recognition of the aesthetic importance of some

coastal landscapes. The fact that South Australia has over half of the nation's coastal wind farm capacity is directly linked to that state having some of the most proactive renewable energy policies, which have encouraged increased development.

At a national level there has been far less certainty for the industry with a recent debate over the RET, negative comments on wind farms from the government and a 2015 directive for the Clean Energy Finance Corporation to stop investing in wind power projects. An earlier attempt to develop a national code for wind farms in 2006 was rejected by all state governments. The proposed national code, however, did recognise the need to address siting issues such as preserving spectacular parts of the Australian coastline.

The public acceptance for renewable energy has not removed the problem of where to site individual wind farms which have encountered environmental and social issues often fuelled by local community concern feeding into local and state politics. In addition, there has been uncertainty with the science around health related and noise issues making it difficult to develop comprehensive policies. A recent national government inquiry resolved to investigate these matters further. Another major issue has been related to the impact of wind farms on landscape aesthetics. Limited scientific empirical studies have identified the importance of coastal landscape aesthetics in wind farm development approvals. Collectively, the political debate and scientific uncertainty has restricted scientific input to government guidelines and policies.

The national result has been an uncoordinated approach to wind farm development with large differences between states in terms of the number of farms and their location. The paper concludes that this lack of coordination occurred at a time of rapid expansion of the wind farm industry particularly over the last 20 years. During this time neither federal nor state governments appeared to be aware that wind farms were gradually creating a nationally site specific land use change. Consequently half of the country's wind turbines and nearly two thirds of its wind farms are now located on rural coasts.

Acknowledgements

We acknowledge the funding of the CSIRO Flagship Collaboration Fund (coastalcluster.org.au) and contributions to an earlier version of the manuscript from Chris Button and to Michael Chadbourne who assisted in constructing wind farm maps from GIS databases.

References

Australian Energy Regulator (AER), 2014. State of the Energy Market 2014. Australian Energy Regulator, Melbourne, pp. 144.
Auswind, 2006. Best Practice Guidelines for Implementation Of Wind Energy Projects In Australia. Auswind and Clean Energy Corporation (CEC).
Banks, G., 2009. Evidence-Based Policy Making: What Is It? How Do We Get It? (ANU Public Lecture Series, Presented by ANZSOG, 4 February). Productivity Commission, Canberra, pp. 27.
Bloomberg New Energy Finance, Rebound in clean energy investment in 2014 beats expectations, 9 January 2015.
Buhrs, T., Christoff, P., 2006. Greening the antipodes?: environmental policy and politics in Australia and New Zealand. Aust. J. Political Sci. 41, 225–240.
Chapman, S., St George, A., Waller, K., 2013. Spatio-temporal Differences in the History of Health and Noise Complaints About Australian Wind Farms: Evidence for the Psychogenic, Communicated Disease Hypothesis. SCPD FASSA.
Chapman, S., 2011. Much angst over wind turbines is just hot air. Sydney Morning Herald, December 21. http://www.smh.com.au/federal-politics/political-opinion/much-angst-over-wind-turbines-is-just-hot-air-20111220-1p3sb.html#ixzz2d8YVpcNi (accessed 27.08.13.).
Climate Change Council, 2014. The Australian Renewable Energy Race: Which States Are Winning or Losing? The Climate Council of Australia Ltd., Australia, pp. 47.
ClimateSpectator, 2015. Wind tower manufacturer to boost staff numbers. Aust. Bus. Rev.
Connor, J., 2015. Public want more solar, wind and action on climate—are politicians listening? Clim. Spectator.
Crichton, F., Dodd, G., Schmid, G., Gamble, G., Petrie, K.J., 2014. Can expectations produce symptoms from infrasound associated with wind turbines? Health Psychol. 33 (4), 360–364.
DEH, AGO, 2006. National Code for Wind Farms: A Discussion Paper. Department of the Environment and Heritage and Australian Greenhouse Office, Australian Government.
Depellegrin, D., Blažauskas, N., Egarter-Vigl, L., 2014. An integrated visual impact assessment model for offshore windfarm development. Ocean Coast. Manage. 98, 95–110.
Diesendorf, M., 2011, (October 6). Europe has offshore wind farms. . . why can't Australia? *The Conversation*, http://theconversation.edu.au/europe-has-offshore-wind-farms-why-cant-australia-3574 (accessed 11.5.13.).
Doyle, T., Kellow, A., 1995. Environmental Politics and Policy Making in Australia. Macmillan, Melbourne, pp. 296.
Dovers, S., 2013. The Australian environmental policy agenda. Aust. J. Public Adm., 114e128.
EPBC, 2009. Wind Farm Industry. EPBC Act Policy Statement 2.3. Environment Protection and Biodiversity Conservation Act 1999. Department of the Environment, Water, Heritage and the Arts, Australian Government.
EPHC, 2010. National Wind Farm Development Guidelines: Draft – July 2010. Environment Protection and Heritage Council.
EWEA, 2012. Maritime Spatial Planning: Supporting Offshore Wind and Grid Development. The European Wind Energy Association, Brussels, Belgium, pp. 3.
Erickson, W.P., Johnson, G.D., Young, D.P., 2005. A Summary and Comparison of Bird Mortality Form Anthropogenic Causes with an Emphasis on Collisions. U.S. Department of Agriculture Forest Service General Technical Report PSW-GTR-191, Albany, California, USA.
Firestone, J., Bates, A., Knapp, L.A., 2015. See me, Feel me, Touch me, Heal me: wind turbines, culture, landscapes, and sound impressions. Land Use Policy 46, 241–249.
GWEC, 2015. Global Wind Statistics 2014. Global Wind Energy Council, Brussels, Belgium.
Garnaut, R., 2011. The Garnaut Review 2011: Australia in the Global Response to Climate Change. Cambridge University Press, Port Melbourne.
Gross, C., 2007. Community perspectives of wind energy in Australia: the application of a justice and community fairness framework to increase social acceptance. Energy Policy 35, 2727–2736.
Hall, A., Harvey, N., 2006. Environmental assessment procedures of wind power projects in Australia. Energy Environ. 17, 715–733.
Hall, N., Ashworth, P., Devine-Wright, P., 2013. Societal acceptance of wind farms: analysis of four common themes across Australian case studies. Energy Policy 58, 200–208.
Harvey, N., Dew, R.E.C., 2016. Coastal Impact of Onshore Wind Farms in Australia, In: Vila-Concejo, A., Bruce, E., Kennedy, D.M., McCarroll, R.J. (Eds.), Proceedings of the 14th International Coastal Symposium. Journal of Coastal Research, Sydney, Australia.
Harvey, N., Stocker, L., 2015. Coastal residential waterways, science and policy-making: the Australian experience. Estuarine Coast. Shelf Sci. 155, A1–A13.
Harvey, N., 2016. The combination-lock effect blocking integrated coastal zone management in Australia: the role of governance and politics. Ocean Yearbook 30, 1–31.
Head, B., Ferguson, M., Cherney, A., Boreham, P., 2014. Are policy-makers interested in social research?: Exploring the sources and uses of valued information among public servants in Australia. Policy Soc. 33, 89–101.
Hindmarsh, R., Matthews, C., 2008. Deliberate speak at the turbine face: community engagement, wind farms, and renewable energy transitions, in Australia. J. Environ. Policy Plann. 10 (3), 217–232.
Hindmarsh, R., 2010. Wind farms and community engagement in Australia: a critical analysis for policy learning. East Asian Sci. Technol. Soc.: Int. J. 4, 541–563.
Hoen, B., Brown, J.P., Jackson, T., Wiser, R., Thayer, M., Cappers, P., 2013. A Spatial Hedonic Analysis of the Effects of Wind Energy Facilities on Surrounding Property Values in the United States. Ernest Orlando Lawrence Berkeley National Laboratory, pp. 51.
Huber, S., Horbaty, R., 2012. Final Report IEA Wind Task 28 on Social Acceptance of Wind Energy Projects Winning Hearts and Minds. International Energy Agency, Switzerland.
Jay, S., 2012. From laggard to world leader: the united kingdoms adoptions of marine wind energy. In: Szarka, J., Cowell, R., Ellis, G., Strachan, P., Warren, C. (Eds.), Learning from Wind Power: Governance, Societal and Policy Perspectives on Sustainable Energy. Palgrave Macmillan, New York, pp. 85–107.
Joshi, K., 2015. You can now get 'wind turbine syndrome' from solar panels and batteries. http://reneweconomy.com.au/2015/you-can-now-get-wind-turbine-syndrome-from-solar-panels-and-batteries-60497#disqus_thread.
Juntti, M., Russel, D., Turnpenny, J., 2009. Evidence: politics and power in public policy for the environment. Environ. Sci. Policy 12, 207–215.
Lalor, B.M., Hickey, G.M., 2013. Environmental science and public policy in Executive government: insights from Australia and Canada. Sci. Public Policy 40, 767–778.
Lang, C., Opaluch, J.J., Sfinarolakis, G., 2014. The windy city: property value impacts of wind turbines in an urban setting. Energy Econ. 44, 413–421.

Lawson, K., 2015. ACT Chief Minister Andrew Barr Pledges 100 Per Cent Renewables by 2025. The Canberra Times, Fairfax Media, Canberra.
Lothian, A., 2008. Scenic perceptions of the visual effects of wind farms on south Australian landscapes. Geog. Res. 46, 196–207.
Madigan, J., Day, B., Back, C., Canavan, M., Leyonhjelm, D., Urquhart, A., Marshall, G., Xenophon, N., Cameron, D., 2015. In: Radcliffe, J., Morris, J., Grant, R., Gauthier, K., Carling, T., Larnach, T., Forkert, J., Stewart, C., Balaga, K., Batts, S. (Eds.), The Senate Select Committee on Wind Turbines Final Report. Commonwealth of Australia, Canberra, Australia.
McNie, E., 2007. Reconciling the supply of scientific information with user demands: an analysis of the problem and review of the literature. Environ. Sci. Policy 10, 17–38.
Mercer, D., 2003. The great Australian wind rush and the devaluation of landscape amenity. Aust. Geog. 34, 91–121.
NWCC (National Wind Coordinating Committee), 2001. Resource Document: Avian collisions with wind turbines: A summary of existing studies and comparisons to other sources of avian collision mortality in the United States.
Nelson, V., 2013. Wind Energy: Renewable Energy and the Environment, 2nd ed. Taylor & Francis, pp. 459.
Norman, J., 2015. Clean Energy Finance Corporation Directed by Government to Stop Funding Wind Farms. Australian Broadcasting Corporation (12-Jul-2015 ed).
OECD (Organization for Economic Cooperation and Development), 2002. Improving Policy Coherence and Integration for Sustainable Development. OECD, Paris.
Pasqualetti, M.J., 2012. The misdirected opposition to wind power. In: Szarka, J., Cowell, R., Ellis, G., Strachan, P., Warren, C. (Eds.), Learning from Wind Power: Governance, Societal and Policy Perspectives on Sustainable Energy. Palgrave Macmillan, New York, pp. 133–152.
REN21, 2014. Renewables 2014 Global Status Report. REN21 Secretariat, Paris216.
Schenk, T., Stokes, L.C., 2013. The Power of Collaboration: engaging all parties in renewable energy infrastructure development. IEEE Power Energy Mag. (may/june 2013).
Smith, L., Prosser, D., 2011. Half of planned wind farms blown away by force of local protests. *The Independent*, July 11, http://www.independent.co.uk/environment/green-living/half-of-plannedwind-farms-blown-away-by-force-of-local-protests-2311645.html (accessed 11.5.13.).
Toke, D., Breukers, S., Wolsink, M., 2008. Wind power deployment outcomes: how can we account for the differences? Renew. Sustain. Energy Rev. 12, 1129–1147.
UNCED United Nations Conference on Environment and Development, 1992. 'Agenda 21: programme of action for sustainable development'. In: United Nations Conference on Environment and Development, Held 3–14 June 1992, Rio de Janeiro, Brazil.
Vyn, R.J., McCullough, R.M., 2014. The effects of wind turbines on property values in Ontario: does public perception match emipirical evidence? Can. J. Agric. Econ. 62, 365–392.
WCED (The World Commission on Environment and Development), 1987. Our Common Future. Oxford University Press, Oxford.
Wescott, G., 2011. Disintegration or disinterest? Coastal and marine policy in Australia. In: Crowley, K., Walker, K.J. (Eds.), Environmental Policy Failure: The Australian Story. Tilde University Press, Melbourne, pp. 88–101 (Chapter 7).
Wolsink, M., 2007. Wind power implementation: the nature of public attitudes: equity and fairness instead of 'backyard motives'. Renew. Sustain. Energy Rev. 11, 1188–1207.

Journal of Coastal Research	SI	75	992 - 996	Coconut Creek, Florida	2016

Coastal Impact of Onshore Wind Farms in Australia

Nick Harvey [†§*] and Romana E.C. Dew[†]

[†]Centre for Coastal Research
The University of Adelaide
South Australia, 5005

[§]College of Marine and Environmental Sciences
James Cook University
Townsville, North Queensland, Australia 4811

www.cerf-jcr.org

www.JCRonline.org

ABSTRACT

Harvey N. and Dew, R.E.C. 2016. Coastal Impacts of Onshore Wind Farms in Australia *In:* Vila-Concejo, A.; Bruce, E.; Kennedy, D.M., and McCarroll, R.J. (eds.), *Proceedings of the 14th International Coastal Symposium* (Sydney, Australia). *Journal of Coastal Research*, Special Issue, No. 75, pp. 992 - 996. Coconut Creek (Florida), ISSN 0749-0208.

The global expansion of wind-generated power has resulted in a rapid proliferation of both onshore and offshore wind farms, particularly in Europe. Australia like the rest of the world has experienced a rapid increase in wind power over the last decade but unlike Europe, its coastal wind farms are all located onshore mostly in the southern part of the country where wind energy resources are high. Around half of the wind farms are located in rural coastal locations. This paper discusses the various environmental, social and political issues associated with coastal wind farm development in Australia by assessing the coastal impact of wind farms and the adequacy of coastal management strategies for dealing with such impacts. The paper concludes that the technological pace of coastal wind farm development has outstripped the development control process, which has resulted in a largely unforeseen cumulative impact on the Australian coast.

ADDITIONAL INDEX WORDS: *Coastal Management, wind farms, aesthetics, coastal landscapes*

INTRODUCTION

There has been a rapid global expansion of wind-generated power, which has risen from a global cumulative installed capacity of 6,100 MW in 1996 to 369,553 MW at the end of 2014 (GWEC, 2015). This demand has been met by the installation of wind turbine arrays referred to as wind farms around the globe. The growth in the wind energy industry worldwide has seen a simultaneous increase in the number of coastal wind farm developments. This increased capacity for electricity generation is due to the higher wind speeds associated with coastal areas and the potential for wind farms to be in close proximity to human settlements. Consequently, there has been a rapid expansion of both onshore and offshore wind farm developments. In Europe, due to the inherent difficulties in finding suitable onshore open spaces in coastal areas, offshore wind energy is becoming a much more viable option (Diesendorf, 2011). This phenomenon in Europe has also resulted in reduced siting and environmental issues typically associated with the objections to onshore wind farm developments (Diesendorf, 2011).

In Australia, recent wind farm development has mirrored the global experience with a rapid increase in output capacity, particularly over the last decade (Figure 1). As of August 2015, there were 73 wind farms operating in Australia incorporating a total of 2,022 turbines with a capacity to produce an output of approximately 4,135 MW of electricity. This rapid development of Australian wind farms includes a significant proportion located around the coast due to a reliable wind environment. This has resulted in wind farm sites in close proximity to population centers and electricity grids, mostly on the southeast coast.

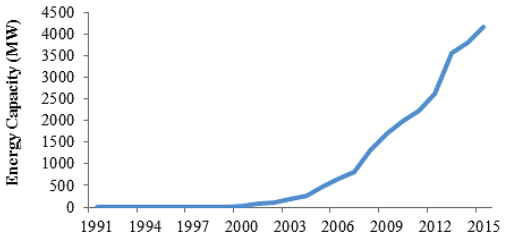

Figure 1. Graph illustrating the total Australian installed capacity of wind energy since 1991. Source: GWEC (2015).

Unlike Europe, due to Australia's abundance of open spaces and most of its coastal waters being too deep for offshore wind farm technology, all current wind farm developments are land-based (Diesendorf, 2011). Over a decade ago, Mercer (2003) noted the start of this rapid development and potential impact on the Australian coast. Since then there have been a number of site-specific coastal wind farm studies and papers on planning approvals and legal issues but there is a gap in the literature relating to the national impact of this form of coastal development or its broader implications for coastal management.

Concerns about impacts of windfarms are often focused on their visual and aesthetic qualities, land-use impacts, community

DOI: 10.2112/SI75-199.1 received received 15 October 2015
accepted in revision 15 January 2016
*Corresponding author: nick.harvey@adelaide.edu.au
©Coastal Education and Research Foundation, Inc. 2016

health and wildlife especially bird mortalities. In addition, offshore wind farms produce a set of specific marine impacts including marine ecosystem disturbance and navigational safety (REN 21, 2014). Given a lack of such offshore developments in Australia this paper focuses on issues associated with the siting of onshore wind farms such as socio-cultural and environmental impacts and technological factors.

Visual impacts are among the most commonly expressed concerns about wind energy development projects in the United States and Europe, in both onshore and offshore settings (Diesendorf, 2011; Firestone *et al.* 2015; Pasqualetti, 2012). Pasqualetti (2012) addressed the criticisms and future potential for wind power within the context of the UK, USA and Mexico. This study concluded that objections to wind farms can be largely reduced to their effects on the community's quality of life and it is not simply the landscape, but rather the cultural connection that individuals have with it (Pasqualetti 2012). Erickson *et al.* (2005) estimate in an American study that, wind turbines, comprise only 0.003 percent of bird fatalities. Nevertheless, there is no doubt that in some locations, such as Altamont Pass in California, the incidence of wind-related bird fatalities is unacceptably high, especially of 'charismatic birds', such as falcons and eagles (Pasqualetti, 2012). From a technological perspective, wind turbines emit a mechanical sound from their gearbox and an aerodynamic noise from the rotation of the blades (Firestone *et al.* 2015). Turbines have been under past scrutiny due to purported problems including a variety of alleged interference (noise, electromagnetic, electrical, radar and navigation), the blade glint and flicker, stray voltage, oil leaks, fires, ice toss and collapse (Pasqualetti, 2012). There has also been a recent increase in the attribution of symptoms and diseases to wind turbine exposure and sub-audible sound for humans and animals, coined the 'wind turbine syndrome' (Crichton *et al.*, 2014).

This paper focuses on coastal impacts from onshore wind farms, which are of relevance in Australia. The paper analyses the nature, growth and distribution of the Australian wind farm industry illustrating the extent, timing and impact of wind farm development on the coast. In particular, this paper examines the various issues associated with coastal wind farm development and the extent to which these have been addressed in coastal management and planning legislation and policies. This is linked in general to the uptake of science into environmental policy. The paper concludes that the rapidity of this form of development has largely moved ahead of specific policies and development controls regulating the industry and this has created a significant impact around the southern half of the Australian coast.

METHODS

Wind farm geo-referenced location data were obtained predominantly from the Wind Energy Market Intelligence for all Australian wind farms installed as of mid-2015 and compiled and digitized into an ArcGIS shapefile in order to examine the geographic distribution of all Australian wind farms. From this information, a Euclidean distance between each wind farm and its nearest coastline was calculated and grouped into farms less than 5 km, 10 km, 25 km and 50 km or greater from the coast.

These data were then used to determine the relative concentration of wind farms near the Australian coast. Data on the number of wind turbines and their installed wind generating capacity was also recorded for each wind farm. This was important as an individual wind farm may have a larger number of wind turbines or a greater total generating capacity than the cumulative output of a number of smaller wind farms.

In addition, government reports such as planning documents, conditions of approval and any environmental impact assessment (EIA) documents were examined to identify potential impacts and proposed mitigation measures for all coastal wind farms. These impacts were categorized and comparisons made with examples from the international wind farm literature. Site visits were also conducted to selected coastal wind farms.

Following the assessment of coastal wind farm impacts, a brief review was undertaken of government policies and legislation, which relate to the facilitation or control of coastal wind farm development and mitigation of any impacts. It is likely that variable state coastal management and planning policies will influence the siting of wind farms and in a more general sense variable state and federal renewable energy policies will influence the extent of wind farm development.

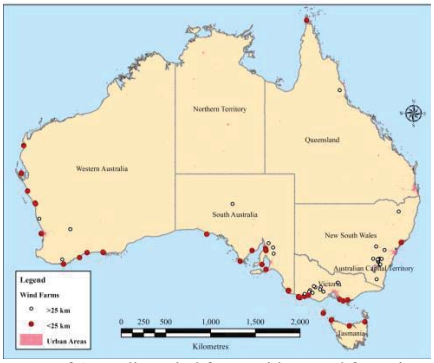

Figure 2. Map of Australian wind farms with coastal farms in red

RESULTS

In this study, coastal wind farms have been defined as being within 25 km of the coast. A map constructed from the wind farm locational GIS data-base (Figure 2) illustrates the distribution of all constructed wind farms in Australia revealing that nearly two thirds (64%) of these are located near the coast. Each wind farm contains a different number of wind turbines. There is also a variation in the energy output of the turbines depending on the type and make of the turbine. In general, there has been an increase in the size and efficiency of turbines over time.

Wind energy represents the fastest growing source of renewable energy in Australia with an overall 47% compound annual growth rate from 1991 to 2015. Analysis of the Australian wind farm data shows that the coastal zone not only contains the majority of wind farms but also half (50%) of the total number of the country's installed wind turbines. Similarly,

coastal regions also contain about half (51%) of the total national installed capacity of 4,135 MW since the MW output capacity is more closely aligned with the number of turbines, rather than the number of wind farms. The extent of Australia's coastal wind farm developments also varies considerably on a state-by-state basis.

An analysis of government reports, EIA statements and planning approvals indicates a number of impacts associated with coastal wind farms although many non-coastal wind farms have similar impacts. These coastal impacts have been categorized in Table 1 according to; a) socio-cultural impacts, in particular aesthetic impacts on landscapes, visual and amenity impacts; b) biophysical impacts such as construction impacts, ecological impacts and bird and bat strikes, and; c) economic and technological impacts.

Table 1. *Coastal impacts of wind farms tabulated from literature*

Wind Farm Impacts	References
a) Aesthetics and visual amenity; cultural heritages and norms; wind turbine syndrome	Lothian 2008; Chapman 2015; Crichton *et al.* 2014
b) Landscape scarring & erosion; biota danger especially bird and bat; water contamination; habitat loss; life-cycle global warming emissions	Mercer 2003; Lothian 2008; Pasqualetti, 2012; Arnett *et al.* 2010
c) Property loss; navigational safety; noise	Pasqualetti, 2012

An Australian study (Lothian 2008) provides empirical evidence to demonstrate the aesthetic impacts of wind farms on the landscape and specifically coastal landscapes of high scenic value. He concluded that wind farms had a greater negative impact on coastal landscapes of high scenic quality compared to lower rated coasts. The aesthetic impact on coastal landscapes is identified as a major impact, particularly given the predominantly unspoiled rural coastal locations of many wind farms sites.

Examples of aesthetic impacts on rural coastal landscapes can be seen in South Australia, which has the highest proportion of the country's wind farms.

Figure 3. Starfish Hill windfarm, Fleurieu Peninsula, South Australia (illustrating visual impact on rural cliffed-coastal landscape)

The Starfish Hill wind farm (Figure 3) near Cape Jervis south of Adelaide comprises 23 wind turbines built on Starfish and Salt Creek Hills where folded meta-sedimentary rocks of the Adelaide Geosyncline are exposed in the coastal cliffs at the southern end of the Fleurieu Peninsula. Environmental impacts, including visual impacts were assessed prior to approval as a Crown Development in 2002.

A second example comes from the Wattle Point wind farm on Yorke Peninsula comprising 55 turbines located across an area of 17.5 km^2. Apart from the illustrated visual impacts on the low-lying sandy coast, there were also impacts on indigenous heritage issues, which required the re-positioning of a number of the turbine locations.

Figure 4. Wattle Point wind farm, Yorke Peninsula, South Australia (illustrating visual impact from nearby beaches)

A third example (Figure 5) comes from the southeast coast of South Australia where there are 23 wind turbines in the Canunda wind farm plus 112 wind turbines in the adjacent Lake Bonney wind farm complex stretching across 24 km^2 of the Woakwine Range formed from older Pleistocene coastal dunes. The total of 135 turbines create a significant visual impact on the rolling dune landscape as shown in Figure 5 where the turbines stand out against the backdrop of the adjacent Lake Bonney and the coastal Canunda National Park.

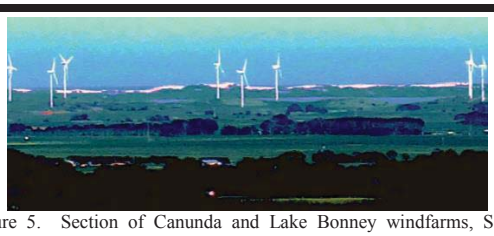

Figure 5. Section of Canunda and Lake Bonney windfarms, South Australia (illustrating visual impact on the coastal dune landscape)

A fourth example (Figure 6) comes from the southwest coast of South Australia where the Cathedral Rocks wind farm contains 33 wind turbines stretching over an area of 29 km^2 above the scenic Pleistocene aeolianite coastal cliffs of the Coffin Bay Peninsula. This aerial view demonstrates the aesthetic impact on a relatively pristine section of coast, which has restricted access for the general public because the wind farm has been built on private farming land.

These four examples of wind farm development, including one of Australia's largest wind farm developments at Canunda/Lake Bonney, illustrate significant visual changes to rural coastal landscapes. In Lothian's empirical study he demonstrated a negative impact of wind farms on perception of

South Australian coastal landscape quality, although it is noted that there are also anecdotal reports in the international literature of positive visual impacts (Firestone *et al.* 2015).

Figure 6. Aerial view of Cathedral Rocks wind farm, Eyre Peninsula, South Australia (illustrating visual impact on a relatively pristine coastal landscape: Photo Coast Protection Board of South Australia)

A perhaps unforeseen impact is the potential for turbine failure to initiate bushfires in the summer months. So far there have been turbine fires in South Australia at the Lake Bonney complex in January 2006; in the Wattle Point wind farm in February 2009; and then a major fire and destruction of one of the Starfish Hill turbines in October 2010. In the latter instance fire crews had major difficulties in getting close to the fire.

Another potential impact is for bird strikes on coastal species of raptors or migratory birds. The Bald Hills wind farm development in Victoria had potential impact on a rare and endangered species of coastal migratory bird, the orange-bellied parrot. This triggered the national environmental legislation (the Environmental Protection and Biodiversity Act, EPBC) causing the federal Environment Minister to stop the project in 2006, although his decision was subsequently overturned.

There have also been reports of the wind turbine syndrome, although this is not specifically a coastal issue. Reviews of the medical literature by Chapman *et al.* (2013) found the evidence for attribution was very poor and conclude that sub-audible, low-frequency sound and infrasound does not pose a direct risk to human health. Chapman, who has been critical of Australian claims of ill-effects from wind turbine syndrome has himself been criticized by the Senate Committee on Wind Turbines (2015; p18-22) which questioned a number of Chapman's assertions. The committee called for further high-quality research on this issue to determine cause and effect.

Development and management of the Australian coast lacks a consistent national policy approach, a victim of the federated system of government (Wescott, 2012). Coastal policy remains the jurisdiction of state governments, despite four separate national inquiries since the 1980s recommending a national coastal policy. Hence, coastal wind farms are assessed on a state-by-state basis according to relevant state planning and development processes, legislation and controls rather than as a coastal management issue.

The influence of wind energy policy is an important factor in the extent of wind farm development, particularly at the state level. South Australia (SA) has ambitious targets and supporting policies, which have resulted in the highest number of wind farms in Australia and 40 percent of the nation's wind capacity (Climate Council, 2014).

In contrast, Victoria which previously had strong support for renewable energy and wind farms with development of its WindAtlas in 2001, changed its policy and planning regulations to restrict wind farm development (Climate Council, 2014). Victorian guidelines now focus on coastal siting issues related to minimizing the impacts on primarily 'visually significant' landscapes. This includes a turbine setback distance of 2 km from dwellings. Victoria's largest wind farms located within 5 km of the coast are positioned linearly behind vegetated dunes on existing cleared pastoral land in order to complement the landscape. These planning changes protect the state's key tourist and coastal regions such as the Great Ocean Road and Mornington Peninsula.

New South Wales planning guidelines for wind farms do not specifically mention coastal issues whereas Queensland does not have specific policies for wind farms. Similarly Tasmania has no wind farm policies, although it is of note that all of Tasmania's wind farms have coastal locations.

Western Australia planning guidelines focus on minimizing coastal visual impacts and coastal vegetation removal. The guidelines include a 1 km setback distance from 'noise-sensitive buildings', based on SA noise guidelines for wind farms. Wind turbines within 5 km of the coastline have typically been placed linearly along coastal ridgelines to reflect and complement landscape and topographical features. The more sizeable coastal wind farms in Western Australia are located on existing cleared pastoral and grazing land less than 25 km from the coast.

The relatively low level of environmental impact of wind energy developments together with favorable planning and policy frameworks has been a major factor in their rapid introduction in rural coastal areas. Notwithstanding this, they have attracted criticism particularly related to aesthetics and siting issues, noise pollution and well as the impacts on local bird and bat populations.

DISCUSSION

The advent and rapid growth of onshore wind farm development in Australia, represents a significant impact on the Australian coast. Coastal wind farms have generally not been classified as coastal development limiting the extent to which coastal management issues have been considered in the planning process.

The major impact of wind farms appears to be the aesthetic impact on the visual quality of coastal landscapes as demonstrated by Lothian (2008). It is interesting to note that Victoria has introduced planning restrictions to protect highly valued coastal landscapes such as the Great Ocean Road, whereas the Cathedral Rocks coastal landscape in SA (Figure 6) for example has comparable landscape qualities but was subject to a routine local government approval process as it was on private land and not visible to the general public. There is clearly a need to incorporate aesthetic impact guidelines into coastal policies to allow for the assessment of different levels of visibility based on location and population.

Unlike the aesthetic issues, mitigation is possible for the many of the environmental issues (Mercer 2003; Lothian 2008; Pasqualetti, 2012) include scarring and erosion, biota danger (especially birds), water contamination and habitat loss. Negative impacts on flora and fauna, namely through land clearance, as well as bird and bat strikes have been a common factor in arguments against wind farm developments (Arnett *et al.*, 2010). These are usually assessed through a formal state-based EIA process unless any species of flora and fauna constitutes a matter of 'national significance', which could trigger the federal EPBC legislation.

One impact identified in the current paper, but not apparent in the general wind farm literature, is the risk of coastal wind turbine failure and its potential to trigger summer bushfires.

CONCLUSIONS

The rapid growth rate in the Australian wind farm industry over the last 25 years has led to half of the wind farms being located around southern coasts where wind energy resources are high. These developments have been assessed on a case-by-case basis under separate state planning legislation. There does not appear to be any national strategic approach to the siting of wind farms and nor has it been treated as a coastal management issue. The result has been a largely unforeseen and unplanned cumulative impact on the visual quality of many Australian rural coastal landscapes.

ACKNOWLEDGMENTS

The authors acknowledge research funding of the CSIRO Flagship Collaboration Fund (coastalcluster.org.au). Photographs were taken by the authors unless otherwise stated.

LITERATURE CITED

Arnett, E.B.; Huso, M.M.P.; Hayes, J.P., and Schirmacher, M., 2010. *Effectiveness of changing wind turbine cut-in speed to reduce bat fatalities at wind facilities.* A final report submitted to the Bats and Wind Energy Cooperative. Austin, Texas: Bat Conservation International.

Chapman, S.; St. George, A.; Waller, K., and Cakic, V., 2013. The Pattern of Complaints about Australian Wind Farms Does Not Match the Establishment and Distribution of Turbines: Support for the Psychogenic, 'Communicated Disease' Hypothesis. *PLoS ONE* 8(10), 1-11.

Crichton, F.; Dodd, G.; Schmid, G.; Gamble, G.; Petrie, K.J., 2014. Can expectations produce symptoms from infrasound associated with wind turbines? *Health Psychology*, 33(4), 360-364.

Climate Council, 2014. *The Australian Renewable Energy Race: Which States Are Winning or Losing?* Climate Council of Australia Limited, 47p.

Diesendorf, M., 2011. *Europe has offshore wind farms ... why can't Australia?* https://theconversation.com/europe-has-offshore-wind-farms-why-cant-australia-3574

Erickson, W.P; Johnson, G. D., and Young, D. P., 2005. *A summary and comparison of bird mortality form anthropogenic causes with an emphasis on collisions*. Albany, California: U.S. Department of Agriculture Forest Service, *General Technical Report PSW-GTR-191*, pp. 1029-1042.

Firestone J.; Bates, A., and Knapp, L.A., 2015. See me, Feel me, Touch me, Heal me: Wind turbines, culture, landscapes, and sound impressions. *Land Use Policy*, 46, 241-249.

Global Wind Energy Council (GWEC) Staff, 2015. *Global Wind Statistics 2014*. Brussels, Belgium: Global Wind Energy Council, 4p.

Hindmarsh, R., 2010. Wind farms and community engagement in Australia: a critical analysis for policy learning. *East Asian Science, Technology and Society: An International Journal*, 4, 541–563.

Hindmarsh, R. and Matthews, C., 2008. Deliberate Speak at the Turbine face: Community Engagement, Wind Farms, and Renewable Energy Transitions, in Australia. *Journal of Environmental Policy & Planning*, 10(3), 217–232.

Lothian, A., 2008. Scenic Perceptions of the Visual Effects of Wind Farms on South Australian Landscapes. *Geographical Research*, 46(2), 196-207.

Mercer, D., 2003. The great Australian wind rush and the devaluation of landscape amenity. *Australian Geographer*, 34, 91–121.

Pasqualetti, M.J., 2012. The Misdirected Opposition to Wind Power. *In*: Szarka, J.; Cowell, R.; Ellis, G.; Strachan, P.A., and Warren, C. (eds.), *Learning from Wind Power*. Hampshire, England: Palgrave Macmillan, pp.133-152.

Senate Select Committee on Wind Turbines, 2015 *Final Report of Senate Select Committee on Wind Turbines*, August 2015, Australian Government, 350p.

Wescott, G., 2012. Disintegration or disinterest? Coastal and marine policy in Australia. *In:* Crowley, K., and Walker, K. (eds.), *Environmental Policy Failure: the Australian story*. Victoria, Australia: Tilde University Press, pp. 88-101.

THE CONVERSATION
Academic rigour, journalistic flair

When Thailand and Australia were closer neighbours, tectonically speaking

October 19, 2018 12.50pm AEDT

The beaches of Koh Phangan are set within rocky crags made of granites, the type of rocks studied to piece Thailand to Australia. Romana Dew, Author provided

Thousands of Australians travel to Thailand each year to lie on a beach at Phuket, meditate at a Buddhist temple in Ayutthaya, spot wild elephants at Khao Yai National Park, or go on some other adventure.

But how many realise that beneath their feet, the framework of the country once formed part of the same continent as Australia?

Our new research, published in Lithos, uncovered the deep links between Australia and Thailand, rebuilding the geography of this part of the ancient supersized continent Gondwana.

Authors

Alan Collins
Professor of Geology, University of Adelaide

Romana Dew
Geology PhD Candidate, University of Adelaide

Read more:* *A map that fills a 500-million year gap in Earth's history

This was a time before the dinosaurs, when the first forests turned the land green and giant dragonflies tracked airways through the vegetation.

Our work suggests that some fictional time-travelling Phuket beach-lover could have walked to the Pilbara in Western Australia. A pre-Jurassic culture vulture in Ayutthaya could have trekked over an

ancient Indonesian-like volcanic island chain, and some Khao Yai elephant-ancestor could have rampaged through the site of the Perth CBD.

On the move

Tracking these bits of continents and their dance across the globe is part of a large effort to map our planet through its history. Last year we published a map of half a billion years of Earth history.

This was one of the first forays into mapping Earth in deep time. But putting the details on these maps is far from straightforward.

To do this, scientists first try to find geological hints in the rocks of two regions to suggest they are related to each other and have similar histories.

The problem with much of Southeast Asia is that the rocks on the surface are too young – they left Gondwana between 400 million and 300 million years ago, and the rocks we need to see are now buried.

Our research gets around this by using some of these young rocks – granites that formed the roots of old volcanoes – as upside-down probes to fingerprint the deeper Earth.

The idea is that the granite magma mixed a little with the older rocks below as it worked its way up in the crust, forming a unique molten rock soup with subtle chemical differences that can help map the geological basement.

Our study in Thailand used granites, between 500 million and 80 million years old, to discover these characteristics of the older underlying basement rocks. These granites contained chemical markers from the magma that can date when it formed and separated from the mantle. In some cases, these date back nearly 3 billion years.

The three blocks of Thailand

Thailand may be one country now, but it is made up of three distinct geological regions: Sibumasu, Sukhothai, and Indochina.

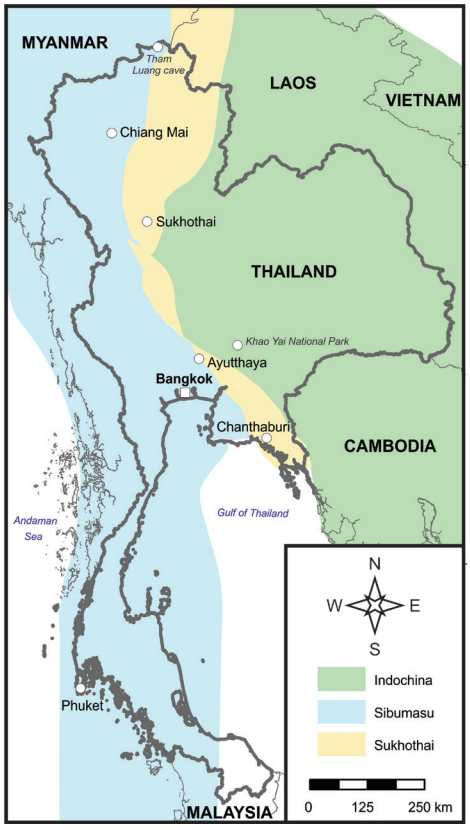

Map of Thailand including the three main blocks (Sibumasu, Sukhothai and Indochina), major cities and landmarks.

Romana Dew

These three blocks all originated in different parts of Gondwana and collided about 200 million years ago. That is a long time ago, but geologically not so old when you consider that the planet is 4,650 million years old.

Sibumasu makes up most of the Thai peninsula and follows north into northwestern Thailand past Tham Luang cave – where the young soccer team and coach were rescued earlier this year – and into Myanmar.

Sukhothai is a volcanic arc system like modern Indonesia or Japan. It cuts through the middle of Thailand past the historic city of Sukhothai, extending southeast to the ruby and sapphire market town of Chanthaburi.

Indochina includes everything in Thailand east of the Sukhothai block, and extends into Cambodia and Vietnam.

Three blocks, three different fingerprints

Although these three blocks form one country today, their telltale chemical fingerprints show a varied history. Sibumasu has very ancient isotopic markers, similar to parts of northwestern Australia.

***Read more:* What's Australia made of? Geologically, it depends on the state you're in**

But the granites from Indochina tell a different, shorter story. The chemical fingerprints from this block show that it formed from melting of the deep Earth much more recently than Sibumasu.

This eastern region formed only between 1.28 billion and 500 million years ago – still very old, granted, but not nearly as old as the Thai Peninsula and Sibumasu. Similar compositions of rocks occurred smeared along the west coast of Australia, and especially in the Margaret River wine region of Western Australia.

The Sukhothai block is chemically somewhere between Sibumasu and Indochina, with separation from the deep earth mantle modelled between 1.74 billion and 850 million years ago.

These intermediate values from the Sukhothai granites are probably a result of mixing of the more youthful Indochina with ancient recycled Sibumasu when the blocks collided and one was pushed over the other.

Thai-Australian reunion?

Australia is currently moving north by up to seven centimetres per year. As we creep towards Asia, like it or lump it, Australia's future really is with Asia.
So Australians, just hang on, enjoy the ride, in a few tens of million years the southern Thai beaches will be a short drive away.

Australia Geology Thailand Gondwana Plate tectonics

https://theconversation.com/when-thailand-and-australia-were-closer-neighbours-tectonically-speaking-100824

ISC2018, Québec City

A DETRITAL PROVENANCE STORY FROM GONDWANA TO NORTHWEST THAILAND

Romana E C Dew[1]*, Alan S Collins[1], Rosalind King[1], Christopher K Morley[2], Noreen J Evans[3] and Stijn Glorie[1]

[1]*Centre for Tectonics, Resources and Exploration, Department of Earth Sciences, The University of Adelaide, Adelaide, South Australia 5005, Australia*

[2]*Department of Geological Sciences, Chiang Mai University, Chiang Mai 50200, Thailand*

[3] *John De Laeter Centre, Department of Applied Geology, Curtin University, Perth, Western Australia, 6102, Australia*

**e-mail: romana.dew@adelaide.edu.au*

The evolution of the Sibumasu Terrane forms a principal component in the history of the Tethys and the development of Southeast Asia. The Sibumasu Terrane is a ribbon continent that is often oversimplified in palaeogeographic reconstructions [1, 2]. During the Proterozoic to early Paleozoic, previous studies have located the Sibumasu Terrane off the northwest margin of Australia in the Gondwanan supercontinent [2]. Sibumasu rifted northwards away from the Gondwana margin in the early Permian, and subsequently collided with the other terranes that make up Thailand during the Triassic Indosinian Orogeny [1, 2]. Overall, there is little specific information known about the older palaeogeographic setting of Sibumasu and its neighbouring terranes. However, analysis of detrital age populations, geochemical signatures and statistical evidence can help us better understand the evolution of the Sibumasu Terrane. Therefore, this study uses U–Pb geochronology and Lu−Hf isotopic information from the Paleozoic and Mesozoic detrital zircon record of the Sibumasu Terrane in northwest Thailand. This study has found a significant change in source material from the older Paleozoic sedimentary sequences sourcing from the Sibumasu Terrane and other older sources, compared to the Permo-Triassic zircon sources associated with the Indosinian Orogeny in the younger sedimentary units. These temporal changes in the isotopic systems reflect the movement of the Sibumasu Terrane from the northwest Australian margin of Gondwana to its collision with the terranes of present-day Asia. In an attempt to better constrain this evolution, we have also compared our new data to those published from Sibumasu, Indochina, Sukhothai, West Burma, South China and Western Australia. These results have implications for understanding Thailand and its present-day neighbours and also their position within the Gondwanan supercontinent.

References

[1] C. Morley, *Puzzling Out Gondwana*, 2017, Department of Mineral Resources, Thailand: Bangkok, 33.

[2] C. Burrett, K. Zaw, S. Meffre, C. Lai, S. Khositanont, P. Chaodumrong, M. Udchachon, S. Elkins, J. Halpin, *Gondwana Research*, 2014, **26**, 31-51.

Acknowledgements

This work was supported by Australian Research Council [#DP120101460 and #FT120100340]. RECD is also funded by an Australian Postgraduate Award and fieldwork was conducted on an Endeavour Cheong Kong Research Fellowship.

Puzzling out Gondwana, Bangkok, Thailand, 7th-21st November 2017

Zircon Probes and Provenance: New insights in the palaeogeography of Southeast Asia

Romana E C Dew[1,*], Alan S Collins[1], Stijn Glorie[1], Rosalind King[1], Christopher K Morley[2, 3], John Foden[1], Johan DeGrave[4], Brandon L Alessio[1], Pitsanupong Kanjanapayont[5], Punya Charusiri[5] and Noreen J Evans[6]

[1] Centre for Tectonics, Resources and Exploration (TRaX), Department of Earth Sciences, The University of Adelaide, Adelaide, South Australia 5005, Australia
[2] PTTEP, EnCo, Soi 11, GGS, Vibhavadi Rangsit Road, Chatuchak, Bangkok 10900, Thailand
[3] Department of Geological Sciences, Chiang Mai University, 239 Huay Kaew Road, Chiang Mai 50200, Thailand
[4] Ghent University, St. Pietersnieuwstraat 33, 9000 Ghent, Belgium
[5] Department of Geology, Faculty of Science, Chulalongkorn University, Bangkok 10330, Thailand
[6] John De Laeter Centre, TIGeR, Department of Applied Geology, Curtin University, Perth, WA, 6102, Australia
* email: romana.dew@adelaide.edu.au

Abstract

The evolution of the Thai terranes: Indochina, Sibumasu and Sukhothai, forms a principal component in the history of the Tethys and the development of Southeast Asia. These terranes have not always been connected, and the premise for this study is to investigate their origin, relative position and separation/collision with other blocks. The thermotectonism and magmatism associated with the Indosinian Orogeny is said to have driven the consecutive accretions of the Indochina, Sukhothai, Sibumasu terranes to the South China terrane (Metcalfe 2013; Morley et al. 2013; Searle et al. 2012). However, the detail of these accretions are still widely debated. In particular, the timing and nature of the Indochina and Sibumasu collision, also the nature and timing of the Palaeo-Tethys closure is still poorly constrained (Gardiner et al. 2015; Morley et al. 2013). Here we present an integrated zircon isotope (U-Pb and Lu-Hf) and whole rock geochemistry (Rb-Sr, Sm-Nd and Pb) dataset from Permo-Triassic granites across Thailand. The U-Pb age, ϵHf and ϵNd signatures assist to characterize the underlying basement and highlight the variance in the history of the three blocks. These signatures indicate that the Sibumasu terrane contains relatively evolved, recycled crust compared to the Sukhothai and Indochina terranes. In comparison, the Sukhothai terrane lies near the CHondritic Uniform Reservoir (CHUR) value. Whereas the variance in the geochemical signature of Inthanon Zone implies the closing of the Palaeo-Tethys Ocean.

In addition, new provenance information has been collected using the detrital zircon record from Permo-Triassic sandstones from all three major terranes in Thailand. The new dataset includes U-Pb geochronology and Lu-Hf isotopes. The comparison of the three terrane's detrital zircon population spectra provides evidence for the shared and separate parts of their tectonic histories. The changes between the Permian and Triassic sandstones from the Sibumasu, Sukhothai and Indochina terranes reflects their amalgamation with mainland Asia. In an attempt to resolve existing arguments about timing of this collision, we have compared our new data to those published from Indochina, Sukhothai, Sibumasu, West Burma, South China and Western Australia (e.g. Arboit et al. 2016; Burrett et al. 2014; Gardiner et al. 2015; Hara et al. 2013).

These results have implications for research on the Tethys Oceans, not only within Thailand but also for research conducted on greater Southeast Asian tectonics. Additionally, this study unearths information on the shared margin of Indochina, Sibumasu and northern Australia during the Proterozoic to early Paleozoic.

References

Arboit, F., Collins, A.S., Morley, C.K., King, R. & Amrouch, K. 2016. Detrital zircon analysis of the southwest Indochina terrane, central Thailand: Unravelling the Indosinian orogeny. Geological Society of America Bulletin,, 128, 1024-1043.

Burrett, C., Khin, Z., Meffre, S., Lai, C.K., Khositanont, S., Chaodumrong, P., Udchachon, M., Ekins, S. & Halpin, J. 2014. The configuration of Greater Gondwana—Evidence from LA ICPMS, U–Pb geochronology of detrital zircons from the Palaeozoic and Mesozoic of Southeast Asia and China. Gondwana Research, 26, 31-51, doi: http://dx.doi.org/10.1016/j.gr.2013.05.020.

Gardiner, N.J., Searle, M.P., Morley, C.K., Whitehouse, M.J., Spencer, C.J. & Robb, L.J.2015. The closure of Palaeo-Tethys in Eastern Myanmar and Northern Thailand: New insights from zircon U–Pb and Hf isotope data. Gondwana Research, doi:10.1016/j.gr.2015.03.001.

Hara, H., Kon, Y., Usuki, T., Lan, C.Y., Kamata, Y., Hisada, K.I., Ueno, K., Charoentitirat, T. & Charusiri, P. 2013. U-Pb ages of detrital zircons within the Inthanon Zone of the Paleo-Tethyan subduction zone, northern Thailand: New constraints on accretionary age and arc activity. Journal of Asian Earth Sciences, 74, 50-61, doi: 10.1016/j.jseaes.2013.06.006.

Metcalfe, I. 2013. Gondwana dispersion and Asian accretion: Tectonic and palaeogeographic evolution of eastern Tethys. Journal of Asian Earth Sciences, 66, 1-33, doi: http://dx.doi.org/10.1016/j.jseaes.2012.12.020.

Morley, C.K., Ampaiwan, P., Thanudamrong, S., Kuenphan, N. & Warren, J. 2013. Development of the Khao Khwang fold and thrust belt; implications for the geodynamic setting of Thailand and Cambodia during the Indosinian Orogeny. Journal of Asian Earth Sciences, 62, 705-719, doi: http://dx.doi.org/10.1016/j.jseaes.2012.11.021.

Searle, M.P., Whitehouse, M.J., Robb, L.J., Ghani, A.A., Hutchison, C.S., Sone, M., Ng, S.W.P., Roselee, M.H., Chung, S.L. & Oliver, G.J.H. 2012. Tectonic evolution of the Sibumasu-Indochina terrane collision zone in Thailand and Malaysia: Constraints from new U-Pb zircon chronology of SE Asian tin granitoids. Journal of the Geological Society, 169, 489-500, doi: 10.1144/0016-76492011-10710.1029/2002TC001398.

Keywords: *Zircon; granite; Thailand; U-Pb geochronology; Hf isotopes; Rb-Sr; Sm-Nd; Pb geochemistry; sandstone; detrital provenance; Sibumasu; Sukhothai; Indochina*

STRATIGRAPHY OF DEFORMED PERMIAN CARBONATES REEFS IN SARABURI PROVINCE OF THAILAND

Dew, Romana E.C.[1], Collins, Alan S.[1], King, Rosalind[1], Arboit, Francesco[1], Glorie, Stijn[1], Morley, Christopher K.[2]

[1] *Centre for Tectonics, Resources and Exploration (TRaX), Department of Earth Sciences, The University of Adelaide, Adelaide, South Australia 5005, Australia*

[2] *Department of Geological Sciences, Chiang Mai University, Chiang Mai, Thailand*

Extended Abstract

The Indosinian Orogeny brought together a number of allochthonous continental blocks and volcanic arcs during the Permian and Triassic periods. Prior to the orogeny, these blocks were dominated by carbonate platforms and minor clastic sediments. One of these platforms—the Asselian-Capitanian Khao Khwang Platform—contains well-bedded platform carbonates along with massive-bedded reef complexes and intervening clastics. Three main depositional environments are found within this platform setting: restricted platform, platform interior and outer platform. Since deposition, the Khao Khwang Platform has been deformed into Khao Khwang Fold-Thrust Belt as part of the Triassic–Lower Jurassic Indosinian Orogeny, along the southern margin of one of the continental fragments of the Indochina Block. Today, the Khao Khwang Platform is commonly exposed through the hills and quarries of the Saraburi Province.

The impact of kilometre-scale thrusts on the sedimentology and stratigraphy of the Permian platform carbonates and basin complexes requires further analysis. The latest Pennsylvanian-Permian Saraburi Group of the Khao Khwang Platform includes six, broadly contemporaneous, sequences. Three of these sequences are massive carbonate dominated units, namely the Phu Phe, Khao Khad and Khao Khwang Formations. These carbonates are divided by clastic, mixed siliciclastic and carbonate sequences: the Sap Bon, Pang Asok and Nong Pong Formations. The palaeogeography of these formations prior to the Indosinian Orogeny is incompletely known, yet it is significant in assisting with structural reconstructions of the Saraburi area and our understanding of Permian fusulinid-dominated habitats.

Here, we present a stratigraphic model for the carbonate reefs and intervening clastic sedimentary rocks using the well-developed exposed sections of the Saraburi Group in the Saraburi Province of Thailand. Unusually, this model acknowledges recent structural studies and considers these controls in accordance with fossil identification, biostratigraphic correlation and palaeoenvironmental analysis. Eleven sections were logged, numbered south to north along Highway 21 Logs 1 to 8 and 9 to 11 within the Siam City Cement quarry along Highway 2. These stratigraphic sections were mostly within the Khao Khad Formation and encompassed units from the three thrust sheets of the deformed platform. As well as stratigraphic logs, field work incorporated fossil identification, sketches, photographs and sample collection. Thin sections were then analysed under transmitted light to validate and add to the field interpretations.

The Saraburi Group sequences studied in this project were deposited in a tropical shallow marine carbonate platform environment. Due to the degree of

deformation in the area, it is uncertain whether they were deposited as two or three platform environments. Overall, textural variations and fossil assemblages indicate the presence of four middle Permian depositional environments. The environments form a continuum but can be grouped into peritidal, platform interior (low-energy lagoon, outer platform and backreef), algal reef and basinal slope environments.

Peritidal zone deposits consist of dark carbonaceous mudstones-wackestones and dolomitised laminated algal boundstone beds. Secondary Fe-calcite camouflaged the original depositional texture in some parts. Fossils include Schubertella, Girvanella and Gyroporella algae, Hemigordius, Globivalvulina sp. along with other microscopic non-fusuline foraminifera. Peritidal settings were interpreted within Logs 1 and 4 with ages constrained between the late Murgabian to Midian.

Platform interior contains three sub-environments: lagoon, the outer platform and the higher energy backreef. The low-energy lagoon is comprised of bioturbated skeletal and peloidal wackestones and packstones with localised interbedded shales. The fossil assemblage contained abundant algae including Girvanella, bivalves (including alatoconchids), fusulinids (N. simplex) and microscopic non-fusuline foraminifera (Globivalvulina, Schubertella, Cribogenerina and Textulariida). The lagoonal environment is interpreted for lower Log 4 and upper Log 6 and deposited in the Murgabian with possible extension into the Midian.

The outer platform sub-environment is a non-parallel bedded bioclastic limestone grading from wackestone through to grainstone with boundstone interbeds. Isolated coral clumps were also observed within the grainstone sections. Inner platform settings were interpreted within Logs 1, 2, 5, 7 and 8. The age of the environment was constrained using the fusuline foraminifera (Neoschwagerina simplex, other Neoschwagerina sp., Neofusulinella, Nankinella, Kahlerina, Armenina). The fossil assemblages gave an age within the Murgabian Stage.

The higher-energy backreef sub-environment is defined by parallel bedded wackestones and packstones. Backreef settings are interpreted within Logs 5, 6 and 8. Each major fossil group is present in the Highway 21 backreefs: crinoids, fusulinids (Nankinella, Schwagerina, Colania, Neoschwagerina and Gifuella see Fig. 3), bivalves (Alatyoconda), non-fusuline foraminifera (Baisalina and Climacammina), algae (Tubiphytes), gastropods and coral (Waagenophyllum). Brachiopods, calcareous sponges and peloidal matter are also observed. The fossil assemblages within the interpreted backreef environment were aged between the Murgabian and Midian. Further south in Log 9, older foraminifera Parafusulina sp. and Ozawainella sp. are also found within the backreef environment. The assemblages in the Siam City Cement Log 9 indicate that this backreef was deposited between the Yahtashian and the Kubergandian.

Reef facies are dominated by algal boundstones and fusuline packstone-grainstone. Reef builders were mostly algae and fusulinids with minor foraminifera and coral building. The boundstones along Highway 21 have a dominant skeletal element of encrusting Archaeolithoporella and Tubiphytes with calcisponges and abundant syndepositional marine cements. The boundstone units lack fusulinids containing rare non-fusuline

foraminifera. Within the fusuline packstone-grainstones, bivalves and fusulinids (including Neofusulinella, Nankinella, Kahlerina, Armenina) are abundant with crinoids, coral and non-fusuline foraminifera (Cribrogenerina and Pachyphloia) commonly occurring. Log 7's bivalve and fusulinid-rich grainstone with coral lenses passes west into a reef mound suggesting lateral facies change. Algal reef depositional environments were interpreted in Log 2 and the top of Log 8 with deposition from the late Murgabian to early Midian. Logs 7, 10 and 11 contained algal reefs with somewhat older fusulinid species Chalaroschwagerina and Parafusulina depicting deposition in the Kubergandian to early Murgabian.

The basinal slope environment comprises of predominantly thinly-bedded mudstones with lesser allodapic packstone-grainstone-boundstone beds. Multiple chert nodules and lenses and some bioclasts have been entirely replaced with chert. This environment can be only found within Log 3. The fossil assemblage includes an eclectic assemblage of fragmented and abraded small crinoid pieces, fusulinids (Neoschwagerina), non-fusuline foraminifera (Toriyamaia, Pachyphloia, Pseudoreichelina and Globivalvulina cyprica) and gastropods. This fossil assemblage indicated a depositional age between the Kubergandian and the Midian.

This shallow marine platform setting was home to diverse fossil assemblages, the foraminifera and algae were analysed to constrain the age of the sections. From the fusuline foraminifera present, the assemblages mostly are within the Neoschwagerina simplex, N. craticulifera and N. margaritae Biozones. The Neoschwagerinidae present in the sections do not appear to be at the complexity of Yabeina sp. characteristic of the Midian Stage. The highest proportion of assemblages classed within the Murgabian Tethyan Stage. The rapid rate of morphological change within the fusulinid taxa usually allows the identification of highly specific ages, although poor preservation due to deformation has made identification more difficult. Overall, the carbonate sequences are mostly contemporaneous with the three southeastern sections appearing slightly older (early middle Permian) than the eight sections taken further north (Kubergandian and Murgabian Stages with some extension into the Midian). Nevertheless, deposition was occurring in the Kubergandian for both the Highway 2 and 21 sequences.

Palaeoenvironmental inferences and fossil identification allow for section correlation and assist in unravelling the structure of this deformed platform. The vertical change in the contemporaneous facies suggests the sequences are predominantly shallowing upwards. Generally, the depositional setting for Logs 1 to 3, 4 to 8 and 9 to 11 appears to be deepening northwards although deformation has obscured the facies' original position and thickness of the sequence. It is suggested that thin-skinned deformation occurred within the mostly contemporaneous sections of the Khao Khad Formation. Nevertheless, additional structural and stratigraphic studies would assist with the further characterisation of the palaeogeography.

KEYWORDS: *Permian biostratigraphy, Khao Khwang Fold-Thrust Belt, Khao Khad Formation, carbonate platform, fusulinid*

Summary of the IGCP 589 Symposium and Field Excursion

The IGCP 589 meeting in Thailand was a thoroughly useful and enjoyable experience. While the technical sessions were very informative and relevant, I found as a first year PhD student that the field excursion and the networking opportunities were very beneficial to make new connections from across the globe. My co-authors and I are preparing the work on the deformed carbonate reefs in Saraburi into a journal article, which will hopefully be submitted later in the year. After presenting my research at the IGCP 589 symposium, I have been given much needed advice on my biostratigraphy and interpretations from experts that were present at the conference. The connections and friendships made during this trip would not have been possible without the support of the Australian IGCP Committee so thank you very much.

In early November 2015, I accepted an Endeavour Australia Cheung Kong Research Fellowship to travel back to Thailand for five months in 2016. I am currently undertaking this fellowship in Thailand and the knowledge gained through the IGCP 589 activities late last year have given me a broad skillset to build upon in this new chapter of my research.

Field expedition with students from Chiang Mai University

Visit to Mae Moh Mine as part of the IGCP 589 Field Excursion

IGCP 589 Field Excursion in northwestern Thailand

Memoirs of Awardees
Endeavour Australia Cheung Kong Research Fellowships

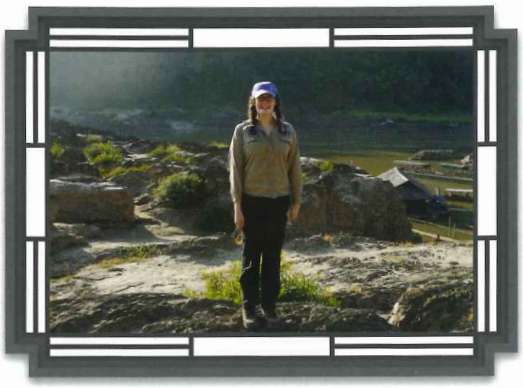

Romana DEW

Student of The University of Adelaide, Australia

Exchange to Chiang Mai University, Thailand

In early November 2015, I accepted an Endeavour Australia Cheung Kong Research Fellowship to travel to Thailand for five months in 2016. I am currently undertaking this fellowship in Thailand as part of my PhD candidature looking at the tectonic evolution of Thailand. This fellowship is integral to my research giving me the time and the funding necessary to collect samples I require from all across Thailand.

For my fellowship I am based in Chiang Mai in northwestern Thailand. My host is Dr. Christopher Morley who is based at Chiang Mai University and has 35 years' experience looking at the geology and tectonics of Southeast Asia. Chris is a principal adviser to my research, so this visit and collaboration with him and his colleagues is highly beneficial to my PhD research. My fellowship begun in January, and I have had great success collecting the required rocks. The plan for second half of my fellowship has been devised to ensure that samples are collected from all necessary areas and can be prepared as much as practicable for geochemical analyses prior to leaving Thailand at the beginning of June.

Through this experience, I have had the opportunity to study a 45-hour Thai language course, attend a ceremony in Bangkok where I was awarded a certificate for this Endeavour Fellowship from the Australian Ambassador to Thailand and also travel all over Thailand and to some neighbouring countries. The experiences from this fellowship have expanded my view of the world and its people's diversity and capabilities. I thank the Cheung Kong Group for the scholarship opportunity, which has broadened and strengthened my PhD research considerably. I look forward to the rest of my Cheung Kong Fellowship and also the rest of my PhD candidature and continuing to delve into and unravel the tectonic evolution of Thailand.

APPENDIX II

Supplementary material for Chapter 2

Table 1. Detailed petrography of analysed granitoid samples

Sample	Texture	Degree of deformation estimation	Quartz? Feldspars?	K-feldspar megacryst	P = perthite O = orthoclase M = microcline	Biotite (colour)	Chlorite	Hornblende	Pyroxene	Muscovite	Sphene	Zircon	Apatite	Other minerals?	Sillimanite needles? Other inherited sedimentary structures? Special textures? Sericitization?
KM-12	Holocrystalline	Weak	Quartz, Plagioclase, Orthoclase	-	P, O	Biotite (dark brown)	Chlorite	Hornblende (green-brown)	-	Muscovite	-	Zircon	-	-	Mafic minerals are metamorphosed to muscovite, epidote, few sericitization, myrmekitic dissolution
KM-18	Holocrystalline	Weak to none	Quartz Plagioclase					Hornblende	Yes						
KM-20	Holocrystalline		Quartz , K-Feldspar, Plagioclase		?							Zircon			
KM-25	Holocrystalline	Weak	Quartz, Plagioclase (zoned), Orthoclase	-	P, O	Biotite (Dark brown)	Chlorite	-		Muscovite	-	Zircon	-	Sillimanite needles Epidote	Medium sericitization
KM-26	Holocrystalline	Weak	Quartz, Plagioclase (zoned)	-	P	Biotite (brown, pink)	Chlorite	-	-	Muscovite (alteration product)	Sphene	Zircon	-	Silimanite, fibrolite	Sillimanite needles associated with biotite Medium sericitization
KM-40A	Holocrystalline	Medium, aligned biotite and quartz recrystallization	Quartz, Plagioclase, Orthoclase	-	P, O	Biotite (red-brown)	Chlorite	-	-	Muscovite (alt. product)	-	-	-		Little sericitization
NT-01	Holocrystalline	Weak	Quartz, Plagioclase, Orthoclase	-	P,O	Biotite (dark brown)	Chlorite	-	-	Muscovite (not alteration product!)	-	Zircon	-		Little sericitization
NT-04	Holocrystalline	Weak	Quartz, Plagioclase, Orthoclase	-	O	-	-	Hornblende	-	-	Sphene	Zircon	-	Tourmaline	Few sericitization
NT-06	Holocrystalline	Weak to moderate (a lot of tapped twins of Pl)	Quartz, Plagioclase, Orthoclase	-	O	-	Chlorite	Hornblende (Tremolite)	-	-	Sphene	-	-	Talc or Calcite (difficult to determine due to crystal size)	No sericitization
NT-07	Holocrystalline	Weak	Quartz, Plagioclase, Orthoclase	-	P, O	-	Chlorite	Brown hornblende + Actinolite	-	Sericite	-	-	-		Strong sericitization
NT-09	Holocrystalline	Weak (difficult to observe due to very strong sericitization)	Quartz, Feldspars difficult to distinguish due to sericitization	-	?	Biotite (brown)	Chlorite	Hornblende (brown)	-	Muscovite (alteration)	-	-	-		Very strong sericitization
NT-10	Holocrystalline	Weak to moderate (curved plagioclase twinning and alignment of the biotites)	Quartz, Orthoclase, Plagioclase	-	P, O	Biotite (brown)	Chlorite	-	-	-	-	Zircon	-		Weak sericitization
NT-11	Holocrystalline	Weak	Quartz, Orthoclase	-	P,O	Biotite (yellow-orange)	-	-	-	-	Sphene	-		Epidote	Recrystallized quartz, weak sericitization Epidote unstable
NT-12	Holocrystalline	Moderate (alignment of mica's)	Quartz, Orthoclase, Plagioclase	-	P, O	Biotite (brown)	Chlorite	-	-	Muscovite	-	-		Garnet	Recrystallized quartz, weak sericitization

Table 1 (continued). Detailed petrography of analysed granitoid samples

Sample	Texture	Degree of deformation estimation	Quartz? Feldspars?	K-feldspar megacryst	P = perthite O = orthoclase M = microcline	Biotite (colour)	Chlorite	Hornblende	Pyroxene	Muscovite	Sphene	Zircon	Apatite	Other minerals?	Sillimanite needles? Other inherited sedimentary structures? Special textures? Sericitization?
NT-13	Holocrystalline	Weak	Quartz, Orthoclase, Plagioclase (sericitized)	-	P, O, M	Biotite (brown)	-	-	-	Muscovite	-	-		Garnet	Strong sericitization
NT-17	Holocrystalline	Weak	Quartz, Orthoclase, Plagioclase	Yes	?		-	-	-	Muscovite	-	Zircon	Apatite		
RDT15_076A	Holocrystalline	Moderate	Quartz, Plagioclase		?		Chlorite					Zircon		Fluorite	
RDT16_044	Holocrystalline	High	Quartz, Plagioclase	-	?	-	Chlorite	Hornblende	-	Muscovite	-	Zircon	-	Garnet	
RDT16_053	Holocrystalline	Weak	Quartz, Plagioclase, Orthoclase	-	?	-	Chlorite	-	-	-	-	Zircon	-	-	
RDGEOCHEM-1	Holocrystalline	Weak	Quartz, Plagioclase, Orthoclase	-	M, P	-	-	-	-	-	-	-	-	-	
ST-03	Holocrystalline	Weak	Quartz, Plagioclase, Orthoclase	-	P, O	-	-	-	-	Muscovite	-	-	-	Tourmaline	Few sericitization
ST-08A	Holocrystalline	Weak to moderate (mica's are bend)	Quartz, Plagioclase, Orthoclase	-	P, O	Biotite (dark brown)	Chlorite	-	-	Muscovite	-	Zircon	Apatite	-	Few sericitization Quartz recrystallization (consertal texture)
ST-13	Holocrystalline		Quartz, Plagioclase, Orthoclase	-	?		-	-	-	-	-	Zircon	-	-	
ST-16	Holocrystalline	Moderate (skewed biotites)	Quartz, Plagioclase (sericitized), Orthoclase	-	O	Biotite (red brown)	Chlorite	-	-	Muscovite	-	Zircon	-	Garnet disintegrates during metamorphic reaction (picture)	Medium sericitization
ST-18	Holocrystalline		Quartz, Plagioclase, Orthoclase	-	?		-	-	-	-	-	Zircon	-		
ST-49A	Holocrystalline	Weak	Quartz, Microcline, Plagioclase, Orthoclase	-	P, O, M	Biotite (dark green to dark grey)	Chlorite	-	-	Muscovite	-	Zircon	-	Garnet	Medium sericitization
Th11/01	Holocrystalline	Weak	Quartz, Microcline, Plagioclase, Orthoclase	-	P, O, M	Biotite (brown)	-	-	-	-	-	Zircon	-		
Th11/02	Holocrystalline	Weak	Quartz, Microcline, Plagioclase, Orthoclase	-	P, O, M	Biotite (brown)	-	-	-	Muscovite	-	Zircon	-		

Table 2. Description of zircon morphologies and cathodoluminescence (CL) interpretations. Fig. 2 of Chapter 2A shows the representative CL images.

Sample Number	Zircon Morphology			Cathodoluminescence (CL) interpretation
	Size	Colour	Shape	
KM-20	100-300 µm	White	Euhedral grains	Lots of bisected zircons with cracks. Quartz inclusion within a zircon. Some homogenously textured zircons. Cores present in several zircons. Oscillatory zoning
NT-07	100-200 µm	White and pale yellow	Subhedral grains	Some homogenously dark cores, homogenous light outer rims
NT-09	200-300 µm	White to pale pink	Euhedral grains, some are broken	Many zircons have large rounded detrital cores and well developed zoned overgrowth. Inclusions are common.
NT-10	100-200 µm	Brown to yellow	Euhedral to subhedral grains	Most zircons have oscillatory zoning. Inclusions are common. Some metamict cores
NT-11	100-200 µm	White to orange	Euhedral grains	Well-developed oscillatory zoning. Lots of inclusions. Cores are often metamict or resorbed.
NT-12	~100-200 µm	White, gold, purple	Euhedral grains	Most grains are oscillatory zoned. Some inclusions. Several homogenous zircons.
NT-17	~100-350 µm	Yellow, orange and pale pink	Euhedral to subhedral grains preserved with prismatic and pyramidal crystal faces. Some grains have rounded edges	Most grains contain oscillatory zoning. Some grains have cracks and diffuse zoning. Inclusions of a Ca-K-Si-Kb mineral present in several grains. Radiation damage present.
RDT15_076A	100-200 µm	Brown, white and orange	Subhedral to anhedral grains. Zircons are well rounded	Poorly-developed zonation present. Some zircons have older inherited cores
RDT16_043	~100-300 µm	White, purple, Yellow, orange and pale pink	Subhedral grains – Most zircon crystals exhibit moderate rounding.	Some zonation present. A few grains have inclusions of quartz or biotite. Some zircons have homogenous domains. Grains are commonly cracked.
RDT16_044	~200-400 µm	White and gold	Euhedral to subhedral grains	Zonation is concentric or oscillatory. Some later zircon overgrowth present.
RDT16_053	200-300 µm	White and yellow	Euhedral to subhedral grains. Some have rounding at the edges	Fine oscillatory zoning. Many zircons are metamict
ST-08A	250-550 µm	White and pale pink	Mostly euhedral grains	Many zircons have large rounded detrital cores and well developed zoned overgrowth. Majority of the zircon cores are metamict, look mottled and cracked. Oscillatory zoning
ST-13	200-350 µm	Yellow, white and pink	Euhedral grains, several subhedral grains	Some cores. Oscillatory zoning present
ST-16	~150-350 µm	White	Subhedral to anhedral grains. Zircons are well rounded	Lots of inherited zircon cores. Multiple domains present in some zircons. Some oscillatory zoning.
ST-18	~150-350 µm	White to grey	Subhedral to anhedral grains. Zircons are well rounded	Some zircons have older rounded inherited cores. Multiple domains present in some zircons. Oscillatory zoning in several zircons.
ST-49A	300-500 µm	Brown	Euhedral to subhedral grains preserved with prismatic and pyramidal crystal faces.	Well-developed oscillatory zoning, some cracks, inclusions and poorly preserved cores
TH11/01	200-400 µm	Pink, yellow and white	Euhedral predominates, some subhedral grains	Well-developed oscillatory zoning, some inclusions and older cores.
TH11/02	250-400 µm	Pink, yellow and white	Euhedral to anhedral grains. Some grains have rounded edges.	Oscillatory zoning present, some inclusions and older cores. Minor metamict cores. Many grains are cracked.

Supplementary Table 3. LA–ICP–MS Analytical Method Information

Analysis Batch Date	Samples Analysed	Spot Size	Isotopes measured	GJ $^{206}Pb/^{238}U$ Weighted Average	Plešovice $^{206}Pb/^{238}U$ Weighted Average	91500 $^{206}Pb/^{238}U$ Weighted Average*
7/09/2015	NT-10	30 µm	^{204}Pb, ^{206}Pb, ^{207}Pb, ^{208}Pb, ^{232}Th, ^{238}U	600.1±5.2 (*n* =12, MSWD=0.23)	337.2±5.8 (*n* =3, MSWD=0.05)	N/A
7/09/2015	NT-09, NT-11, NT-12	30 µm	^{204}Pb, ^{206}Pb, ^{207}Pb, ^{208}Pb, ^{232}Th, ^{238}U	600.2±5.4 (*n* =28, MSWD=2.2)	338.5±6.0 (*n* =11, , MSWD=2.7)	N/A
11/09/2015	ST-16, ST-49A	30 µm	^{204}Pb, ^{206}Pb, ^{207}Pb, ^{208}Pb, ^{232}Th, ^{238}U	600.2±6.2 (*n* =20, MSWD=2.0)	336.3±3.7 (*n* =8, MSWD=0.40)	N/A
11/09/2015	Th11/01, Th11/02	30 µm	^{204}Pb, ^{206}Pb, ^{207}Pb, ^{208}Pb, ^{232}Th, ^{238}U	600.3±8.2 (n=29, MSWD=5.1)	339.7±5.7 (*n* =12, MSWD=2.7)	N/A
25/01/2017	RDT15_076A, RDT16_044, NT-17, NT-07	25 µm	^{90}Zr, ^{202}Hg, ^{204}Pb, ^{206}Pb, ^{207}Pb, ^{208}Pb, ^{232}Th, ^{238}U	601.8±1.0 (*n* =72, MSWD=0.91)	342.8±1.1 (*n* =36, MSWD=2.3)	1033.3±3.2 (*n* =36, MSWD=1.4)
19/05/2017	RDT16_053	30 µm	^{90}Zr,, ^{139}La, ^{140}Ce, ^{141}Pr, ^{146}Nd, ^{146}Sm, ^{153}Eu, ^{157}Gd, ^{159}Tb, ^{163}Dy, ^{165}Ho, ^{166}Er, ^{169}Tm, ^{172}Yb, ^{175}Lu, ^{178}Hf, ^{202}Hg, ^{204}Pb, ^{206}Pb, ^{207}Pb, ^{208}Pb, ^{232}Th, ^{238}U	601.67±0.85 (*n* =112, MSWD=1.04)	330.7±1.5 (*n* =31, MSWD=2.1)	1016.7±4.6 (*n* =28, MSWD=1.7)
21/07/2017	KM-20, KM-21	30 µm	^{90}Zr, ^{139}La, ^{140}Ce, ^{141}Pr, ^{146}Nd, ^{146}Sm, ^{153}Eu, ^{157}Gd, ^{159}Tb, ^{163}Dy, ^{165}Ho, ^{166}Er, ^{169}Tm, ^{172}Yb, ^{175}Lu, ^{178}Hf, ^{202}Hg, ^{204}Pb,	601.72±0.97 (*n* =132, MSWD=0.66)	338.6±1.3 (*n* =66, MSWD=2.4)	1035.2±4.6 (*n* =33, MSWD=1.3)
30/08/2017	ST-08A, ST-13, ST-18	30 µm	^{90}Zr, ^{201}Hg, ^{204}Pb, ^{206}Pb, ^{207}Pb, ^{208}Pb, ^{232}Th, ^{238}U	601.6±1.3 (*n* =99, MSWD=0.89)	338.7±1.0 (*n* =50, MSWD=0.99)	1050.7±5.6 (*n* =25, MSWD=1.4)
28/09/2017	RDT16_043, NT-17	30 µm	^{90}Zr, ^{201}Hg, ^{204}Pb, ^{206}Pb, ^{207}Pb, ^{208}Pb, ^{232}Th, ^{238}U	601.5±1.2 (*n* =52, MSWD=0.76)	343.2±1.3 (*n* =26, MSWD = 1.8)	1067.6±4.4 (*n* =13, MSWD=1.10)

* The use of two different 91500 crystals for these analyses, where one crystal gives good reproducibility while the other is more heterogeneous, accounts for the younger age for the 91500 standard in three of the analysis batches. 91500 was used as one of two secondary standards and was not used as a primary standard to correct for isotopic drift and down-hole fractionation.

Supplementary Table 4. Main isotopes and ratios measured using LA–ICP–MS

Analysis #	Ratios							Ages						Concentrations (ppm)		Th:U	Concordance ($^{206}Pb/^{238}U$ age)/ $^{207}Pb/^{235}U$ age)
	$^{207}Pb/^{235}U$	2σ	$^{206}Pb/^{238}U$	2σ	Rho	$^{207}Pb/^{206}Pb$	2σ	$^{207}Pb/^{235}U$	2σ	Pb^{206}/U^{238}	2σ	$^{207}Pb/^{206}Pb$	2σ	U	Th		
nt-07-333.d	0.3486	0.0071	0.0448	0.0007	0.3720	0.0564	0.0011	302.9	5.4	282.3	4	449	43	1066	1391	1.30	93.20
~~nt-07-334.d~~	~~0.4450~~	~~0.0190~~	~~0.0432~~	~~0.0007~~	~~0.0094~~	0.0744	0.0034	369	13	~~272.8~~	~~4.2~~	~~950~~	~~79~~	684	777	1.14	73.93
nt-07-345.d	0.3560	0.0110	0.0451	0.0006	0.1986	0.0566	0.0016	307.8	8.2	284	3.8	439	64	845	964	1.14	92.27
~~nt-07-354.d~~	~~4.7800~~	~~0.7200~~	~~0.0801~~	~~0.0057~~	~~0.5270~~	0.3630	0.0380	1490	120	~~493~~	~~33~~	~~3310~~	~~190~~	17.5	27.8	1.59	33.09
nt-07-355.d	0.3365	0.0096	0.0440	0.0006	0.0419	0.0554	0.0017	293.1	7.3	277.7	3.8	379	65	626.9	672	1.07	94.75
nt-07-356.d	0.3258	0.0083	0.0442	0.0006	0.1563	0.0534	0.0014	285.3	6.3	278.9	3.4	305	55	763.4	771.8	1.01	97.76
nt-07-357.d	0.3246	0.0076	0.0440	0.0006	0.0947	0.0534	0.0013	284.5	5.8	**277.6**	**3.6**	312	54	838	924	1.10	97.57
~~nt-07-358.d~~	~~0.8040~~	~~0.0980~~	~~0.0398~~	~~0.0014~~	~~0.8860~~	0.1420	0.0110	564	42	~~251.4~~	~~8.5~~	~~2070~~	~~130~~	213.1	323.4	1.52	44.57
~~nt-07-359.d~~	0.7780	0.0760	0.0337	0.0014	0.0203	0.1620	0.0170	574	39	~~213.6~~	~~8.9~~	~~2410~~	~~160~~	311	400	1.29	37.21
nt-07-360.d	0.3100	0.0140	0.0429	0.0008	0.1132	0.0525	0.0024	271	11	**270.9**	**4.9**	227	93	259.5	223.5	0.86	99.96
nt-07-361.d	0.3840	0.0099	0.0494	0.0007	0.1353	0.0566	0.0016	329.4	7.3	310.5	4.3	436	59	784.9	778	0.99	94.26
nt-07-335.d	0.2970	0.0120	0.0428	0.0010	0.2636	0.0509	0.0022	264	9.9	**270.2**	**6**	191	88	616	704	1.14	102.35
nt-07-362.d	0.3216	0.0073	0.0436	0.0006	0.1037	0.0536	0.0013	282.9	5.5	**274.9**	**3.4**	318	53	875	1010	1.15	97.17
nt-07-363.d	0.3389	0.0093	0.0425	0.0006	0.2448	0.0578	0.0015	295.8	6.9	268.5	3.5	475	58	950	1211	1.27	90.77
~~nt-07-364.d~~	0.3303	0.0098	0.0291	0.0011	0.1505	0.0870	0.0045	288.3	7.6	~~184.5~~	~~6.6~~	~~1240~~	~~88~~	992	2590	2.61	64.00
~~*nt-07-365.d*~~	0.5410	0.0350	0.0476	0.0009	0.3063	0.0821	0.0049	429	22	~~*299.9*~~	~~*5.4*~~	~~*1060*~~	~~*110*~~	201.8	123.3	0.61	69.91
nt-07-366.d	0.3335	0.0089	0.0433	0.0006	0.3403	0.0556	0.0014	291	6.8	272.9	3.5	405	54	898	1117	1.24	93.78
~~*nt-07-336.d*~~	0.5230	0.0180	0.0470	0.0009	0.0931	0.0813	0.0031	428	12	~~*295.8*~~	~~*5.4*~~	~~*1169*~~	~~*72*~~	763	1153	1.51	69.11
nt-07-338.d	0.3242	0.0062	0.0430	0.0005	0.1151	0.0548	0.0011	284.6	4.8	**271.2**	**3.2**	381	45	1264	1671	1.32	95.29
nt-07-339.d	0.3366	0.0069	0.0448	0.0006	0.2941	0.0543	0.0011	294.6	5.3	282.4	3.8	369	46	1200	1733	1.44	95.86
nt-07-340.d	0.3536	0.0088	0.0424	0.0007	0.1561	0.0602	0.0015	306.6	6.6	267.9	4.2	583	57	1494	2770	1.85	87.38
nt-07-341.d	0.3371	0.0075	0.0445	0.0006	0.2336	0.0550	0.0012	294.1	5.7	280.5	3.5	378	49	916.2	979	1.07	95.38
nt-07-342.d	0.3304	0.0069	0.0453	0.0006	0.2439	0.0527	0.0011	289.1	5.3	285.7	3.8	296	47	1173	1409	1.20	98.82
nt-07-343.d	0.3890	0.0110	0.0483	0.0007	0.1091	0.0583	0.0017	331.9	8.2	304.1	4.4	493	63	535	519	0.97	91.62

Data in **bold** used for crystallisation weighted average age

Analysis #	Ratios							Ages						Concentrations (ppm)		Th:U	Concordance ($^{206}Pb/^{238}U$ age)/ ($^{207}Pb/^{235}U$ age)
	$^{207}Pb/^{235}U$	2σ	$^{206}Pb/^{238}U$	2σ	Rho	$^{207}Pb/^{206}Pb$	2σ	$^{207}Pb/^{235}U$	2σ	Pb^{206}/U^{238}	2σ	$^{207}Pb/^{206}Pb$	2σ	U	Th		
RDT16053-092.d	0.3470	0.0240	0.0344	0.0011	0.6298	0.0727	0.0046	298	17	218	6.9	890	120	810	283	0.35	73.15
RDT16053-094.d	13.1900	0.2500	0.5005	0.0070	0.5769	0.1907	0.0033	2692	19	2614	30	2746	29	101.6	77.3	0.76	97.10
RDT16053-095.d	0.2264	0.0047	0.0321	0.0004	0.2193	0.0512	0.0012	207.1	3.9	**203.6**	**2.7**	236	50	2601	1378	0.53	98.31
RDT16053-096.d	0.0778	0.0020	0.0113	0.0002	0.5864	0.0495	0.0010	76	1.8	72.1	1.1	174	49	8040	108.2	0.01	94.87
RDT16053-097.d	0.2219	0.0036	0.0320	0.0003	0.4813	0.0502	0.0008	203.4	3	**202.8**	**2.1**	199	35	7138	200.5	0.03	99.71
RDT16053-098.d	0.2214	0.0045	0.0318	0.0004	0.4983	0.0503	0.0009	202.9	3.7	**201.8**	**2.4**	202	42	6790	202	0.03	99.46
RDT16053-099.d	0.2397	0.0100	0.0330	0.0005	0.0410	0.0527	0.0023	217.3	8.2	209.4	3.4	268	94	410.1	232.7	0.57	96.36
RDT16053-100.d	11.3100	0.1700	0.4615	0.0048	0.7120	0.1774	0.0024	2548.2	14	2445	21	2626	22	495	210.3	0.42	95.95
RDT16053-101.d	0.2311	0.0055	0.0317	0.0005	0.3948	0.0527	0.0012	210.9	4.5	**201.3**	**2.9**	303	50	3440	206	0.06	95.45
RDT16053-102.d	0.2184	0.0041	0.0310	0.0003	0.4458	0.0513	0.0010	200.8	3.6	196.8	2.1	247	43	3667	115.5	0.03	98.01
RDT16053-103.d	0.2194	0.0038	0.0314	0.0003	0.5519	0.0505	0.0008	201.4	3.2	**199.5**	**2**	210	36	7490	372	0.05	99.06
RDT16053-104.d	0.2267	0.0061	0.0324	0.0005	0.4358	0.0503	0.0012	207.4	5	**205.6**	**3**	208	55	2130	113.3	0.05	99.13
RDT16053-112.d	0.2248	0.0039	0.0315	0.0004	0.5693	0.0516	0.0008	205.8	3.2	**199.7**	**2.2**	261	34	11170	350.2	0.03	97.04
RDT16053-113.d	0.1834	0.0073	0.0255	0.0010	0.8897	0.0521	0.0011	170.6	6.3	162.4	6.2	278	45	6090	158.5	0.03	95.19
RDT16053-114.d	0.1950	0.0038	0.0278	0.0004	0.6289	0.0507	0.0009	180.8	3.2	177	2.3	218	38	6288	186.9	0.03	97.90
RDT16053-115.d	0.2229	0.0055	0.0308	0.0004	0.5068	0.0522	0.0011	204.7	4.7	195.8	2.7	282	47	3266	71.8	0.02	95.65
RDT16053-117.d	0.2408	0.0058	0.0321	0.0004	0.5304	0.0544	0.0012	218.8	4.7	203.6	2.4	372	47	3873	87.1	0.02	93.05
RDT16053-118.d	0.2190	0.0040	0.0310	0.0003	0.3438	0.0511	0.0009	201	3.3	197	1.9	235	41	5980	236.9	0.04	98.01
RDT16053-119.d	0.2262	0.0050	0.0324	0.0006	0.6855	0.0505	0.0009	206.9	4.1	**205.7**	**3.6**	212	41	5030	639	0.13	99.42
RDT16053-120.d	0.2125	0.0043	0.0305	0.0004	0.3975	0.0505	0.0009	195.5	3.6	193.7	2.3	210	41	3444	15.54	0.00	99.08
RDT16053-121.d	0.2202	0.0077	0.0315	0.0009	0.6586	0.0515	0.0011	203.7	6.9	**199.7**	**5.8**	255	49	3630	1020	0.28	98.04
RDT16053-123.d	0.2262	0.0046	0.0320	0.0003	0.3929	0.0513	0.0010	206.9	3.8	**202.8**	**2**	247	41	3870	103.8	0.03	98.02
RDT16053-124.d	0.1623	0.0040	0.0235	0.0005	0.8052	0.0500	0.0009	152.6	3.5	149.8	3	188	39	14900	378	0.03	98.17
RDT16053-125.d	8.2100	0.1500	0.3743	0.0045	0.6392	0.1578	0.0025	2252	16	2049	21	2430	27	323.7	260	0.80	90.99
RDT16053-126.d	0.2044	0.0041	0.0297	0.0004	0.5802	0.0497	0.0008	188.7	3.5	188.7	2.4	172	38	5960	129	0.02	100.00
RDT16053-127.d	0.2253	0.0048	0.0315	0.0004	0.3046	0.0518	0.0011	206.2	4	**199.8**	**2.6**	266	49	3000	92.8	0.03	96.90
RDT16053-128.d	0.2370	0.0091	0.0323	0.0005	0.1788	0.0535	0.0021	215.3	7.4	**204.8**	**2.9**	307	84	578.7	325.1	0.56	95.12

Data in **bold** used for crystallisation weighted average age, data in **red and bold** used for crystallisation weighted average age in the inset of Fig. 3

Supplementary Table 4 (continued). Main isotopes and ratios measured using LA–ICP–MS

Analysis #	Ratios							Ages						Concentrations (ppm)		Th:U	Concordance ($^{206}Pb/^{238}U$ age)/ $^{207}Pb/^{235}U$ age)
	$^{207}Pb/^{235}U$	2σ	$^{206}Pb/^{238}U$	2σ	Rho	$^{207}Pb/^{206}Pb$	2σ	$^{207}Pb/^{235}U$	2σ	Pb^{206}/U^{238}	2σ	$^{207}Pb/^{206}Pb$	2σ	U	Th		
RDT16053-092.d	0.3470	0.0240	0.0344	0.0011	0.6298	0.0727	0.0046	298	17	218	6.9	890	120	810	283	0.35	73.15
RDT16053-094.d	13.1900	0.2500	0.5005	0.0070	0.5769	0.1907	0.0033	2692	19	2614	30	2746	29	101.6	77.3	0.76	97.10
RDT16053-095.d	0.2264	0.0047	0.0321	0.0004	0.2193	0.0512	0.0012	207.1	3.9	**203.6**	**2.7**	236	50	2601	1378	0.53	98.31
RDT16053-096.d	0.0778	0.0020	0.0113	0.0002	0.5864	0.0495	0.0010	76	1.8	72.1	1.1	174	49	8040	108.2	0.01	94.87
RDT16053-097.d	0.2219	0.0036	0.0320	0.0003	0.4813	0.0502	0.0008	203.4	3	**202.8**	**2.1**	199	35	7138	200.5	0.03	99.71
RDT16053-098.d	0.2214	0.0045	0.0318	0.0004	0.4983	0.0503	0.0009	202.9	3.7	**201.8**	**2.4**	202	42	6790	202	0.03	99.46
RDT16053-099.d	0.2397	0.0100	0.0330	0.0005	0.0410	0.0527	0.0023	217.3	8.2	209.4	3.4	268	94	410.1	232.7	0.57	96.36
RDT16053-100.d	11.3100	0.1700	0.4615	0.0048	0.7120	0.1774	0.0024	2548.2	14	2445	21	2626	22	495	210.3	0.42	95.95
RDT16053-101.d	0.2311	0.0055	0.0317	0.0005	0.3948	0.0527	0.0012	210.9	4.5	**201.3**	**2.9**	303	50	3440	206	0.06	95.45
RDT16053-102.d	0.2184	0.0041	0.0310	0.0003	0.4458	0.0513	0.0010	200.8	3.6	196.8	2.1	247	43	3667	115.5	0.03	98.01
RDT16053-103.d	0.2194	0.0038	0.0314	0.0003	0.5519	0.0505	0.0008	201.4	3.2	**199.5**	**2**	210	36	7490	372	0.05	99.06
RDT16053-104.d	0.2267	0.0061	0.0324	0.0005	0.4358	0.0503	0.0012	207.4	5	**205.6**	**3**	208	55	2130	113.3	0.05	99.13
RDT16053-112.d	0.2248	0.0039	0.0315	0.0004	0.5693	0.0516	0.0008	205.8	3.2	**199.7**	**2.2**	261	34	11170	350.2	0.03	97.04
RDT16053-113.d	0.1834	0.0073	0.0255	0.0010	0.8897	0.0521	0.0011	170.6	6.3	162.4	6.2	278	45	6090	158.5	0.03	95.19
RDT16053-114.d	0.1950	0.0038	0.0278	0.0004	0.6289	0.0507	0.0009	180.8	3.2	177	2.3	218	38	6288	186.9	0.03	97.90
RDT16053-115.d	0.2229	0.0055	0.0308	0.0004	0.5068	0.0522	0.0011	204.7	4.7	195.8	2.7	282	47	3266	71.8	0.02	95.65
RDT16053-117.d	0.2408	0.0058	0.0321	0.0004	0.5304	0.0544	0.0012	218.8	4.7	203.6	2.4	372	47	3873	87.1	0.02	93.05
RDT16053-118.d	0.2190	0.0040	0.0310	0.0003	0.3438	0.0511	0.0009	201	3.3	197	1.9	235	41	5980	236.9	0.04	98.01
RDT16053-119.d	0.2262	0.0050	0.0324	0.0006	0.6855	0.0505	0.0009	206.9	4.1	**205.7**	**3.6**	212	41	5030	639	0.13	99.42
RDT16053-120.d	0.2125	0.0043	0.0305	0.0004	0.3975	0.0505	0.0009	195.5	3.6	193.7	2.3	210	41	3444	15.54	0.00	99.08
RDT16053-121.d	0.2202	0.0077	0.0315	0.0009	0.6586	0.0515	0.0011	203.7	6.9	**199.7**	**5.8**	255	49	3630	1020	0.28	98.04
RDT16053-123.d	0.2262	0.0046	0.0320	0.0003	0.3929	0.0513	0.0010	206.9	3.8	**202.8**	**2**	247	41	3870	103.8	0.03	98.02
RDT16053-124.d	0.1623	0.0040	0.0235	0.0005	0.8052	0.0500	0.0009	152.6	3.5	149.8	3	188	39	14900	378	0.03	98.17
RDT16053-125.d	8.2100	0.1500	0.3743	0.0045	0.6392	0.1578	0.0025	2252	16	2049	21	2430	27	323.7	260	0.80	90.99
RDT16053-126.d	0.2044	0.0041	0.0297	0.0004	0.5802	0.0497	0.0008	188.7	3.5	188.7	2.4	172	38	5960	129	0.02	100.00
RDT16053-127.d	0.2253	0.0048	0.0315	0.0004	0.3046	0.0518	0.0011	206.2	4	**199.8**	**2.6**	266	49	3000	92.8	0.03	96.90
RDT16053-128.d	0.2370	0.0091	0.0323	0.0005	0.1788	0.0535	0.0021	215.3	7.4	**204.8**	**2.9**	307	84	578.7	325.1	0.56	95.12

Analysis #	Ratios							Ages						Concentrations (ppm)		Th:U	Concordance ($^{206}Pb/^{238}U$ age)/ $^{207}Pb/^{235}U$ age)
	$^{207}Pb/^{235}U$	2σ	$^{206}Pb/^{238}U$	2σ	Rho	$^{207}Pb/^{206}Pb$	2σ	$^{207}Pb/^{235}U$	2σ	Pb^{206}/U^{238}	2σ	$^{207}Pb/^{206}Pb$	2σ	U	Th		
nt-07-333.d	0.3486	0.0071	0.0448	0.0007	0.3720	0.0564	0.0011	302.9	5.4	282.3	4	449	43	1066	1391	1.30	93.20
~~nt-07-334.d~~	~~0.4450~~	~~0.0190~~	~~0.0432~~	~~0.0007~~	~~0.0094~~	0.0744	0.0034	369	13	~~272.8~~	~~4.2~~	~~950~~	~~79~~	684	777	1.14	73.93
nt-07-345.d	0.3560	0.0110	0.0451	0.0006	0.1986	0.0566	0.0016	307.8	8.2	284	3.8	439	64	845	964	1.14	92.27
~~nt-07-354.d~~	~~4.7800~~	~~0.7200~~	~~0.0801~~	~~0.0057~~	~~0.5270~~	0.3630	0.0380	1490	120	~~493~~	~~33~~	~~3310~~	~~190~~	17.5	27.8	1.59	33.09
nt-07-355.d	0.3365	0.0096	0.0440	0.0006	0.0419	0.0554	0.0017	293.1	7.3	277.7	3.8	379	65	626.9	672	1.07	94.75
nt-07-356.d	0.3258	0.0083	0.0442	0.0006	0.1563	0.0534	0.0014	285.3	6.3	278.9	3.4	305	55	763.4	771.8	1.01	97.76
nt-07-357.d	0.3246	0.0076	0.0440	0.0006	0.0947	0.0534	0.0013	284.5	5.8	**277.6**	**3.6**	312	54	838	924	1.10	97.57
~~nt-07-358.d~~	~~0.8040~~	~~0.0980~~	~~0.0398~~	~~0.0014~~	~~0.8860~~	0.1420	0.0110	564	42	~~251.4~~	~~8.5~~	~~2070~~	~~130~~	213.1	323.4	1.52	44.57
~~nt-07-359.d~~	0.7780	0.0760	0.0337	0.0014	0.0203	0.1620	0.0170	574	39	~~213.6~~	~~8.9~~	~~2410~~	~~160~~	311	400	1.29	37.21
nt-07-360.d	0.3100	0.0140	0.0429	0.0008	0.1132	0.0525	0.0024	271	11	**270.9**	**4.9**	227	93	259.5	223.5	0.86	99.96
nt-07-361.d	0.3840	0.0099	0.0494	0.0007	0.1353	0.0566	0.0016	329.4	7.3	310.5	4.3	436	59	784.9	778	0.99	94.26
nt-07-335.d	0.2970	0.0120	0.0428	0.0010	0.2636	0.0509	0.0022	264	9.9	**270.2**	**6**	191	88	616	704	1.14	102.35
nt-07-362.d	0.3216	0.0073	0.0436	0.0006	0.1037	0.0536	0.0013	282.9	5.5	**274.9**	**3.4**	318	53	875	1010	1.15	97.17
nt-07-363.d	0.3389	0.0093	0.0425	0.0006	0.2448	0.0578	0.0015	295.8	6.9	268.5	3.5	475	58	950	1211	1.27	90.77
~~nt-07-364.d~~	0.3303	0.0098	0.0291	0.0011	0.1505	0.0870	0.0045	288.3	7.6	~~184.5~~	~~6.6~~	~~1240~~	~~88~~	992	2590	2.61	64.00
~~nt-07-365.d~~	0.5410	0.0350	0.0476	0.0009	0.3063	0.0821	0.0049	429	22	~~299.9~~	~~5.4~~	~~1060~~	~~110~~	201.8	123.3	0.61	69.91
nt-07-366.d	0.3335	0.0089	0.0433	0.0006	0.3403	0.0556	0.0014	291	6.8	272.9	3.5	405	54	898	1117	1.24	93.78
~~nt-07-336.d~~	0.5230	0.0180	0.0470	0.0009	0.0931	0.0813	0.0031	428	12	~~295.8~~	~~5.4~~	~~1169~~	~~72~~	763	1153	1.51	69.11
nt-07-338.d	0.3242	0.0062	0.0430	0.0005	0.1151	0.0548	0.0011	284.6	4.8	**271.2**	**3.2**	381	45	1264	1671	1.32	95.29
nt-07-339.d	0.3366	0.0069	0.0448	0.0006	0.2941	0.0543	0.0011	294.6	5.3	282.4	3.8	369	46	1200	1733	1.44	95.86
nt-07-340.d	0.3536	0.0088	0.0424	0.0007	0.1561	0.0602	0.0015	306.6	6.6	267.9	4.2	583	57	1494	2770	1.85	87.38
nt-07-341.d	0.3371	0.0075	0.0445	0.0006	0.2336	0.0550	0.0012	294.1	5.7	280.5	3.5	378	49	916.2	979	1.07	95.38
nt-07-342.d	0.3304	0.0069	0.0453	0.0006	0.2439	0.0527	0.0011	289.1	5.3	285.7	3.8	296	47	1173	1409	1.20	98.82
nt-07-343.d	0.3890	0.0110	0.0483	0.0007	0.1091	0.0583	0.0017	331.9	8.2	304.1	4.4	493	63	535	519	0.97	91.62

Data in **bold** used for crystallisation weighted average age, concordance calculation using ($^{206}Pb/^{238}U$ age)/ $^{207}Pb/^{235}U$ age), concordant data in green.

Supplementary Table 4 (continued). Main isotopes and ratios measured using LA–ICP–MS

Analysis #	Ratios							Ages						Concentrations (ppm)		Th:U	Concordance
	$^{207}Pb/^{235}U$	2σ	$^{206}Pb/^{238}U$	2σ	Rho	$^{207}Pb/^{206}Pb$	2σ	$^{207}Pb/^{235}U$	2σ	Pb^{206}/U^{238}	2σ	$^{207}Pb/^{206}Pb$	2σ	U	Th		
KM20-172.d	0.2700	0.0220	0.0376	0.0010	0.1373	0.0527	0.0044	239	18	237.6	6.2	250	170	107.6	65	0.60	99.41
KM20-173.d	0.2540	0.0160	0.0360	0.0010	0.0001	0.0512	0.0034	229	13	**227.8**	**5.9**	220	140	180.9	167.3	0.92	99.48
KM20-174.d	0.2510	0.0200	0.0350	0.0009	0.2587	0.0517	0.0039	224	16	221.5	5.7	210	150	144.8	85.5	0.59	98.88
KM20-175.d	0.2410	0.0200	0.0357	0.0010	0.0174	0.0474	0.0040	216	16	**225.8**	**5.9**	50	160	119	97	0.82	104.54
KM20-176.d	0.2290	0.0190	0.0349	0.0009	0.0927	0.0477	0.0038	210	15	221.4	5.6	100	150	141	98.6	0.70	105.43
KM20-177.d	0.2450	0.0180	0.0355	0.0010	0.1541	0.0503	0.0037	220	15	**224.9**	**6**	130	150	130.7	77.37	0.59	102.23
KM20-178.d	0.2750	0.0230	0.0384	0.0012	0.1074	0.0511	0.0040	243	18	243	7.3	220	160	85.9	52.3	0.61	100.00
KM20-179.d	0.2550	0.0190	0.0369	0.0010	0.2187	0.0509	0.0039	231	15	**233.5**	**6.3**	220	150	112.6	70.73	0.63	101.08
KM20-180.d	0.2640	0.0210	0.0342	0.0011	0.1676	0.0569	0.0044	238	16	216.9	6.9	440	150	117.9	79.3	0.67	91.13
KM20-181.d	0.2970	0.0200	0.0373	0.0011	0.0904	0.0565	0.0041	264	15	236	6.8	460	140	105.4	65.2	0.62	89.39
KM20-182.d	0.3840	0.0260	0.0374	0.0008	-0.0577	0.0739	0.0050	~~327~~	~~19~~	~~236.6~~	~~5~~	~~1010~~	~~140~~	~~207.4~~	~~112.3~~	0.54	~~72.35~~
KM20-183.d	0.2470	0.0180	0.0367	0.0011	0.3622	0.0488	0.0034	225	16	**232.5**	**7.1**	170	140	117.1	55.9	0.48	103.33
KM20-184.d	0.2450	0.0160	0.0365	0.0010	0.2518	0.0488	0.0029	224	13	**230.8**	**6.1**	140	120	249.8	139.7	0.56	103.04
KM20-185.d	0.2530	0.0170	0.0359	0.0010	0.1469	0.0517	0.0036	229	13	**228.1**	**6.2**	230	140	156.3	143.6	0.92	99.61
KM20-186.d	0.2370	0.0190	0.0355	0.0009	0.1467	0.0484	0.0037	215	15	**225.1**	**5.7**	110	150	128.4	83.1	0.65	104.70
KM20-194.d	0.2890	0.0200	0.0359	0.0009	0.1649	0.0593	0.0039	259	15	227.3	5.8	520	140	131.8	86.1	0.65	87.76
KM20-195.d	0.2760	0.0170	0.0369	0.0008	0.1313	0.0536	0.0032	248	13	233.2	5.1	360	120	190	134	0.71	94.03
KM20-196.d	0.2730	0.0180	0.0371	0.0009	0.2216	0.0539	0.0034	243	14	**235**	**5.7**	330	130	159	145.3	0.91	96.71
KM20-197.d	0.2890	0.0230	0.0376	0.0009	0.1766	0.0576	0.0043	258	18	238.1	5.7	480	150	132.1	89.9	0.68	92.29
~~KM20-198.d~~	0.3550	0.0240	0.0360	0.0010	-0.0090	0.0719	0.0050	~~310~~	~~18~~	~~228.2~~	~~6.1~~	~~950~~	~~140~~	~~99.7~~	~~61.5~~	0.62	~~73.61~~
~~KM20-199.d~~	0.2640	0.0180	0.0364	0.0009	-0.0318	0.0526	0.0035	239	14	**230.5**	**5.3**	290	140	~~173.8~~	~~125.4~~	0.72	96.44
KM20-200.d	0.3090	0.0160	0.0374	0.0008	0.3723	0.0606	0.0028	273	13	236.7	5	602	98	556	356	0.64	86.70
KM20-201.d	0.2720	0.0160	0.0359	0.0008	0.3584	0.0548	0.0029	243.8	13	227.3	4.8	409	110	305	305	1.00	93.23
KM20-202.d	0.2730	0.0170	0.0357	0.0008	0.0002	0.0560	0.0034	246	14	225.9	4.9	450	140	243.7	162	0.66	91.83
KM20-203.d	0.2580	0.0150	0.0362	0.0008	0.2184	0.0540	0.0031	235.5	12	**229.3**	**5.1**	310	120	231.2	193	0.83	97.37
KM20-204.d	0.2640	0.0140	0.0358	0.0006	0.1239	0.0540	0.0027	238.8	11	226.7	3.9	375	110	248.5	286.2	1.15	94.93
~~KM20-212.d~~	0.3850	0.0280	0.0369	0.0009	-0.0114	0.0759	0.0054	~~329~~	~~21~~	~~233.4~~	~~5.9~~	~~1080~~	~~140~~	~~140.6~~	~~110.6~~	0.79	~~70.94~~
KM20-213.d	0.2640	0.0160	0.0363	0.0007	0.0617	0.0537	0.0032	237	13	**229.6**	**4.4**	340	130	302.5	179.2	0.59	96.88
KM20-214.d	0.3020	0.0200	0.0376	0.0009	0.0224	0.0592	0.0039	269	15	237.6	5.3	550	130	200.7	112.9	0.56	88.33
KM20-215.d	0.2620	0.0160	0.0372	0.0007	0.1491	0.0513	0.0031	236	13	**235.3**	**4.6**	260	130	258	123	0.48	99.70
KM20-216.d	0.2760	0.0210	0.0359	0.0008	0.0181	0.0556	0.0041	246	17	227.6	5.1	450	160	164.1	103.2	0.63	92.52
KM20-217.d	0.2410	0.0160	0.0355	0.0008	0.0080	0.0505	0.0034	219	14	**225**	**4.9**	160	140	176.2	123.1	0.70	102.74

Data in **bold** used for crystallisation weighted average age, concordance calculation using ($^{206}Pb/^{238}U$ age)/ $^{207}Pb/^{235}U$ age), concordant data in green.

Analysis #	Ratios							Ages						Concentrations (ppm)		Th:U	Concordance
	$^{207}Pb/^{235}U$	2σ	$^{206}Pb/^{238}U$	2σ	Rho	$^{207}Pb/^{206}Pb$	2σ	$^{207}Pb/^{235}U$	2σ	Pb^{206}/U^{238}	2σ	$^{207}Pb/^{206}Pb$	2σ	U	Th		
KM20-218.d	0.2590	0.0220	0.0360	0.0009	0.0770	0.0518	0.0044	231	18	**228.1**	**5.7**	220	170	157	116.2	0.74	98.74
KM20-219.d	0.2430	0.0150	0.0368	0.0009	0.1795	0.0490	0.0031	220	12	232.6	5.6	120	130	204.4	150.5	0.74	105.73
KM20-220.d	0.2800	0.0230	0.0395	0.0010	0.0155	0.0531	0.0046	247	18	249.4	5.9	260	170	147	81.7	0.56	100.97
KM20-221.d	0.5950	0.0360	0.0411	0.0010	0.3534	0.1049	0.0057	473	23	259.3	5.9	1694	110	181.2	74.4	0.41	54.82
KM20-222.d	0.2640	0.0230	0.0357	0.0009	0.2571	0.0537	0.0042	237	18	**226.2**	**5.3**	340	160	122.8	71.01	0.58	95.44
~~KM20-223.d~~	~~0.2500~~	~~0.0190~~	~~0.0369~~	~~0.0009~~	~~0.0746~~	~~0.0493~~	~~0.0038~~	~~226~~	~~15~~	**233.6**	**5.4**	~~180~~	~~160~~	~~154.7~~	~~115.8~~	0.75	~~103.36~~
KM20-224.d	0.2570	0.0170	0.0372	0.0008	0.2470	0.0508	0.0032	232	13	**235.5**	**5.2**	210	130	229	223	0.97	101.51
KM20-225.d	0.4530	0.0380	0.0377	0.0010	0.0370	0.0845	0.0070	374	26	238.6	6.2	1290	160	144.9	79.2	0.55	63.80
NT17-158.d	0.4100	0.0190	0.0487	0.0014	0.5169	0.0602	0.0017	306.3	8.6	306.3	8.6	567	61	605	32.6	0.05	100.00
NT17-159.d	0.3730	0.0250	0.0372	0.0006	0.6149	0.0724	0.0041	319	17	235.2	3.8	861	92	1790	350.8	0.20	73.73
NT17-160.d	0.3580	0.0280	0.0348	0.0006	0.7556	0.0726	0.0043	302	18	220.6	3.8	940	110	535	228	0.43	73.05
NT17-161.d	0.3040	0.0120	0.0348	0.0005	0.0838	0.0637	0.0025	267.6	9.3	220.2	3.2	641	81	308.1	210.2	0.68	82.29
NT17-162.d	0.2698	0.0071	0.0353	0.0005	0.2505	0.0553	0.0013	242.5	5.8	223.8	2.9	404	55	1258	569.1	0.45	92.29
NT17-163.d	0.2431	0.0051	0.0337	0.0004	0.5282	0.0522	0.0009	221	4.1	**213.6**	**2.2**	288	40	4120	414	0.10	96.65
NT17-164.d	11.0600	0.2600	0.4341	0.0078	0.7625	0.1840	0.0034	2525	22	2321	35	2685	30	204.9	110.3	0.54	91.92
NT17-165.d	1.5890	0.0580	0.1584	0.0035	0.5584	0.0727	0.0021	960	23	947	19	966	58	135.5	95.7	0.71	98.65
NT17-167.d	0.2412	0.0061	0.0340	0.0005	0.4495	0.0515	0.0011	219.4	5.1	**215.7**	**2.8**	245	49	1238	811	0.66	98.31
NT17-168.d	0.2355	0.0055	0.0339	0.0005	0.4355	0.0504	0.0011	214.8	4.6	**214.7**	**2.8**	201	46	1738	431	0.25	99.95
NT17-169.d	0.5980	0.0310	0.0529	0.0021	0.9093	0.0809	0.0021	470	19	332	13	1197	52	990	718	0.73	70.64
NT17-170.d	0.2582	0.0069	0.0348	0.0006	0.6451	0.0538	0.0012	232.8	5.5	220.3	3.8	343	47	2360	495	0.21	94.63
NT17-171.d	0.2423	0.0059	0.0337	0.0005	0.5327	0.0520	0.0011	220	4.8	**213.5**	**2.8**	274	46	2680	740	0.28	97.05
NT17-180.d	0.2384	0.0082	0.0340	0.0005	0.1722	0.0510	0.0017	216.2	6.7	**215.4**	**2.9**	208	70	428	207.4	0.48	99.63
NT17-181.d	0.2369	0.0100	0.0338	0.0006	0.1387	0.0514	0.0022	214.3	8.5	**213.9**	**3.5**	193	89	240.9	203	0.84	99.81
NT17-182.d	0.2964	0.0073	0.0337	0.0005	0.3896	0.0642	0.0014	263.1	5.7	213.6	3.1	725	48	1819	1329	0.73	81.19
NT17-183.d	0.2608	0.0057	0.0335	0.0005	0.6119	0.0567	0.0010	235.1	4.6	212.3	2.8	471	40	4860	2390	0.49	90.30
NT17-184.d	0.2376	0.0055	0.0335	0.0005	0.5963	0.0517	0.0010	216.2	4.5	**212.1**	**3.1**	263	43	2371	495	0.21	98.10
NT17-185.d	0.2355	0.0054	0.0334	0.0005	0.6524	0.0511	0.0010	214.5	4.4	**211.9**	**2.9**	233	42	3350	576	0.17	98.79
NT17-186.d	0.2429	0.0053	0.0339	0.0004	0.6978	0.0518	0.0009	220.6	4.4	**215**	**2.7**	268	39	4740	378.7	0.08	97.46
NT17-187.d	0.2396	0.0078	0.0346	0.0005	0.1268	0.0503	0.0016	217.9	6.5	219.2	3	182	68	409.3	229.2	0.56	100.60
NT17-188.d	0.2592	0.0065	0.0334	0.0005	0.1579	0.0568	0.0015	233.7	5.3	211.6	2.9	456	57	1169	845	0.72	90.54
NT17-189.d	0.2408	0.0053	0.0340	0.0005	0.7766	0.0512	0.0009	218.9	4.3	**215.5**	**2.9**	241	38	6856	418	0.06	98.45
NT17-190.d	0.2609	0.0057	0.0331	0.0004	0.5352	0.0569	0.0011	235.2	4.6	209.7	2.6	476	41	4584	828	0.18	89.16

Data in **bold** used for crystallisation weighted average age, concordance calculation using ($^{206}Pb/^{238}U$ age)/ $^{207}Pb/^{235}U$ age), concordant data in green.

Analysis #	Ratios						Ages						Concentrations (ppm)		Th:U	Concordance
	$^{207}Pb/^{235}U$	2σ	$^{206}Pb/^{238}U$	2σ	Rho	$^{207}Pb/^{206}Pb$	2σ	$^{207}Pb/^{235}U$	2σ	Pb^{206}/U^{238}	2σ	$^{207}Pb/^{206}Pb$	2σ	U	Th		
NT17-191.d	0.3500	0.0140	0.0302	0.0005	0.3248	0.0852	0.0032	304.5	11	191.7	3	1246	68	9170	4880	0.53	62.96
NT17-192.d	0.2941	0.0099	0.0332	0.0004	0.1655	0.0638	0.0019	260.8	7.7	210.2	2.5	700	68	764	488	0.64	80.60
NT17-193.d	0.4160	0.0130	0.0372	0.0005	0.5187	0.0804	0.0021	351.2	9.5	235.5	3.4	1175	52	1713	852	0.50	67.06
NT17-194.d	0.2499	0.0057	0.0336	0.0005	0.5178	0.0537	0.0011	226.3	4.6	212.7	2.8	340	45	2276	387.3	0.17	93.99
NT17-202.d	0.2346	0.0065	0.0331	0.0005	0.2947	0.0510	0.0013	213.6	5.3	209.7	3	218	55	1095	600	0.55	98.17
NT17-203.d	0.2862	0.0069	0.0331	0.0006	0.5893	0.0625	0.0013	256.2	5.4	209.9	3.5	676	42	4870	1307	0.27	81.93
NT17-204.d	1.4170	0.0350	0.1387	0.0017	0.5411	0.0733	0.0015	895	15	836.9	9.5	1006	41	753	386	0.51	93.51
nt-17-257.d	0.2980	0.0140	0.0381	0.0009	0.2146	0.0577	0.0028	262	11	240.9	5.3	397	99	257.7	152.6	0.59	91.95
nt-17-258.d	0.8810	0.0280	0.0938	0.0016	0.3249	0.0681	0.0021	639	15	577.7	9.5	836	66	425	189	0.44	90.41
nt-17-259.d	0.2699	0.0077	0.0349	0.0005	0.1375	0.0561	0.0016	241.6	6.1	220.9	3	410	59	1042	433	0.42	91.43
nt-17-260.d	0.3750	0.0180	0.0363	0.0006	0.6809	0.0739	0.0028	319	13	229.9	4	961	75	1145	1674	1.46	72.07
nt-17-261.d	0.2514	0.0076	0.0323	0.0004	0.1274	0.0567	0.0017	227.5	6.2	204.6	2.5	443	65	764.2	481.3	0.63	89.93
nt-17-270.d	0.2220	0.0038	0.0312	0.0004	0.3203	0.0515	0.0009	203.4	3.1	197.9	2.5	249	39	3621	704	0.19	97.30
nt-17-271.d	0.2240	0.0110	0.0325	0.0005	0.0024	0.0509	0.0027	203.7	9.5	205.9	3.3	130	100	258.7	237.7	0.92	101.08
nt-17-272.d	0.2501	0.0040	0.0333	0.0004	0.1955	0.0542	0.0009	226.4	3.3	211.1	2.4	370	38	2830	892	0.32	93.24
nt-17-273.d	3.1920	0.0740	0.2139	0.0036	0.3021	0.1086	0.0026	1449	18	1248	19	1755	44	114.8	173.1	1.51	86.13
nt-17-274.d	0.2662	0.0078	0.0351	0.0005	0.1528	0.0550	0.0016	239.3	6.4	222.5	3.3	366	65	803	820	1.02	92.98
nt-17-275.d	0.3120	0.0092	0.0369	0.0006	0.2179	0.0612	0.0017	275.2	7.2	233.4	3.5	588	59	1386	564	0.41	84.81
nt-17-276.d	0.3720	0.0250	0.0403	0.0010	0.6163	0.0676	0.0038	316	18	254.5	6.2	720	110	280.1	223.2	0.80	80.54
nt-17-277.d	3.3390	0.0690	0.1475	0.0028	0.8582	0.1639	0.0019	1487	16	886	16	2492	20	524	85.2	0.16	59.58
nt-17-278.d	12.7000	0.1900	0.4766	0.0073	0.4851	0.1921	0.0025	2655	14	2511	32	2755	22	140.2	83.7	0.60	94.58
nt-17-279.d	0.2457	0.0055	0.0325	0.0004	0.1550	0.0550	0.0013	223	4.6	206.2	2.6	373	51	1370	1610	1.18	92.47
nt-17-280.d	0.2560	0.0110	0.0329	0.0006	0.2554	0.0571	0.0024	231.9	9	208.6	3.4	435	90	381	294	0.77	89.95
nt-17-281.d	0.2428	0.0086	0.0363	0.0006	0.3254	0.0483	0.0016	219.5	7	229.6	3.9	105	70	490	291	0.59	104.60
nt-17-282.d	0.2562	0.0060	0.0337	0.0004	0.2686	0.0551	0.0013	231	4.8	213.9	2.7	380	50	1488	1503	1.01	92.60
nt-17-291.d	0.2636	0.0047	0.0318	0.0004	0.4398	0.0602	0.0010	237.2	3.8	201.6	2.5	600	35	3460	540	0.16	84.99
nt-17-292.d	0.2665	0.0061	0.0333	0.0004	0.3332	0.0578	0.0012	239.4	4.9	210.9	2.8	498	48	2481	504	0.20	88.10
nt-17-293.d	0.2252	0.0034	0.0309	0.0005	0.5285	0.0527	0.0007	206.1	2.8	196.3	2.8	303	29	7580	1478	0.19	95.25
nt-17-294.d	0.3186	0.0077	0.0274	0.0006	0.5275	0.0845	0.0017	280.5	6	174.5	3.9	1292	40	2632	1367	0.52	62.21
nt-17-295.d	0.3040	0.0110	0.0258	0.0005	0.1001	0.0859	0.0033	268.5	8.7	163.9	3	1289	70	7860	10860	1.38	61.04
nt-17-296.d	0.2372	0.0064	0.0331	0.0005	0.2506	0.0520	0.0014	215.6	5.2	209.6	2.9	258	57	1053	407.5	0.39	97.22
nt-17-297.d	0.2384	0.0038	0.0265	0.0004	0.1876	0.0653	0.0012	217	3.1	168.5	2.3	768	37	5060	2448	0.48	77.65
nt-17-298.d	0.3480	0.0250	0.0344	0.0005	0.4998	0.0732	0.0049	298	18	218.3	3.2	810	120	1001	909	0.91	73.26
nt-17-299.d	0.2940	0.0140	0.0314	0.0006	0.3767	0.0682	0.0030	262	11	199.1	3.9	792	94	570.2	377.2	0.66	75.99
nt-17-300.d	0.2253	0.0097	0.0321	0.0006	0.0804	0.0507	0.0022	204.6	8	203.6	3.5	174	90	349	533	1.53	99.51
nt-17-301.d	0.2490	0.0051	0.0348	0.0006	0.4797	0.0519	0.0009	225.5	4.1	220.6	3.7	266	41	2786	1119	0.40	97.83

Analysis #	Ratios							Ages						Concentrations (ppm)		Th:U	Concordance
	$^{207}Pb/^{235}U$	2σ	$^{206}Pb/^{238}U$	2σ	Rho	$^{207}Pb/^{206}Pb$	2σ	$^{207}Pb/^{235}U$	2σ	Pb^{206}/U^{238}	2σ	$^{207}Pb/^{206}Pb$	2σ	U	Th		
RDT16043-205.d	1.6210	0.0380	0.1582	0.0023	0.5763	0.0735	0.0014	977	15	946	13	1019	41	389.5	195.1	0.50	96.83
RDT16043-206.d	0.6840	0.0240	0.0819	0.0021	0.8301	0.0598	0.0013	525	14	507	13	576	47	640	178.9	0.28	96.57
RDT16043-207.d	2.1000	0.0530	0.1937	0.0032	0.6535	0.0778	0.0016	1145	17	1140	17	1133	39	278	135.4	0.49	99.56
RDT16043-208.d	11.2100	0.2400	0.4884	0.0070	0.6805	0.1650	0.0029	2538	20	2560	30	2504	29	118.6	50.8	0.43	100.87
RDT16043-209.d	1.2240	0.0320	0.1209	0.0021	0.6353	0.0727	0.0016	808	15	735	12	989	45	265.6	155.2	0.58	90.97
RDT16043-210.d	0.9400	0.0280	0.0996	0.0021	0.7543	0.0677	0.0014	669	15	612	12	839	45	518	251	0.48	91.48
RDT16043-211.d	3.2340	0.0710	0.1791	0.0027	0.8068	0.1297	0.0021	1464	17	1061	14	2089	29	1756	197	0.11	72.47
RDT16043-212.d	0.5780	0.0180	0.0681	0.0016	0.8777	0.0611	0.0011	461.9	12	424.2	9.6	635	39	2116	101	0.05	91.84
RDT16043-213.d	3.1160	0.0740	0.2417	0.0043	0.8309	0.0931	0.0016	1433	19	1394	22	1484	32	1059	224	0.21	97.28
RDT16043-214.d	1.5390	0.0420	0.1562	0.0027	0.5111	0.0713	0.0017	943	17	935	15	951	47	298	384.7	1.29	99.15
RDT16043-222.d	11.0000	0.2500	0.4836	0.0075	0.5525	0.1653	0.0032	2518	21	2539	33	2506	33	62.14	48.25	0.78	100.83
RDT16043-223.d	1.3510	0.0380	0.1336	0.0023	0.7322	0.0737	0.0015	865	16	808	13	1018	42	441	485	1.10	93.41
RDT16043-224.d	1.7380	0.0410	0.1633	0.0026	0.6601	0.0777	0.0015	1020	15	975	14	1130	37	836	320	0.38	95.59
RDT16043-225.d	1.4810	0.0490	0.1544	0.0042	0.8155	0.0703	0.0015	915	21	924	23	919	44	232	74.5	0.32	100.98
RDT16043-226.d	1.8720	0.0420	0.1819	0.0029	0.7369	0.0749	0.0013	1068.8	15	1076	16	1062	36	603	131.2	0.22	100.67
RDT16043-227.d	2.6130	0.0860	0.1895	0.0053	0.9228	0.1008	0.0018	1293	25	1116	28	1632	32	919	246	0.27	86.31
RDT16043-228.d	8.7200	0.2700	0.3561	0.0087	0.9611	0.1782	0.0028	2294	30	1957	42	2633	26	965	387	0.40	85.31
RDT16043-229.d	0.9900	0.0410	0.1009	0.0037	0.9608	0.0714	0.0012	689	21	618	21	962	35	2051	208	0.10	89.70
RDT16043-230.d	3.1280	0.0820	0.2473	0.0046	0.3769	0.0923	0.0019	1437	19	1425	23	1461	37	449	80	0.18	99.16
RDT16043-231.d	10.4700	0.2400	0.4715	0.0080	0.8576	0.1622	0.0027	2473	21	2486	35	2474	28	240.7	243.1	1.01	100.53
RDT16043-232.d	0.9340	0.0300	0.0964	0.0026	0.9123	0.0704	0.0012	665	16	593	16	932	35	1915	497	0.26	89.17
RDT16043-233.d	3.9760	0.0970	0.2949	0.0051	0.7009	0.0981	0.0019	1625	20	1664	25	1582	37	191.3	101.3	0.53	102.40
RDT16043-234.d	9.4000	0.3300	0.3840	0.0120	0.9437	0.1774	0.0031	2362	34	2088	54	2624	29	537	169.2	0.32	88.40
RDT16043-235.d	1.4760	0.0470	0.1407	0.0024	0.3928	0.0761	0.0021	916	19	848	14	1070	52	284	115.3	0.41	92.58
RDT16043-236.d	1.7300	0.0590	0.1647	0.0035	0.8613	0.0760	0.0016	1013	21	981	19	1080	41	608	62.6	0.10	96.84
RDT16043-244.d	1.1520	0.0290	0.1176	0.0022	0.7161	0.0709	0.0014	776	14	716	13	940	40	630	94.4	0.15	92.27
RDT16043-245.d	26.2000	1.3000	0.6600	0.0190	0.9295	0.2784	0.0086	3288	57	3245	73	3313	54	238.7	86.6	0.36	98.69
RDT16043-246.d	9.7200	0.3100	0.4200	0.0120	0.9084	0.1667	0.0030	2404	30	2262	51	2526	33	427	173.8	0.41	94.09
RDT16043-247.d	1.1140	0.0340	0.1188	0.0025	0.6178	0.0679	0.0017	755	17	723	15	837	53	231.4	121.7	0.53	95.76
RDT16043-248.d	0.7630	0.0240	0.0884	0.0020	0.5860	0.0626	0.0016	574	13	547	12	658	57	304.4	1079	3.54	95.30
RDT16043-249.d	1.7750	0.0460	0.1747	0.0032	0.6262	0.0736	0.0016	1032	17	1037	17	1017	43	229.3	136.4	0.59	100.48
RDT16043-250.d	1.4010	0.0340	0.1401	0.0022	0.5987	0.0722	0.0014	887.1	14	844	13	981	41	457.1	143.6	0.31	95.14

Data in **bold** used for crystallisation weighted average age, concordance calculation using ($^{206}Pb/^{238}U$ age)/ $^{207}Pb/^{235}U$ age), concordant data in green.

Supplementary Table 4 (continued). Main isotopes and ratios measured using LA–ICP–MS

Analysis #	Ratios							Ages						Concentrations (ppm)		Th:U	Concordance
	$^{207}Pb/^{235}U$	2σ	$^{206}Pb/^{238}U$	2σ	Rho	$^{207}Pb/^{206}Pb$	2σ	$^{207}Pb/^{235}U$	2σ	Pb^{206}/U^{238}	2σ	$^{207}Pb/^{206}Pb$	2σ	U	Th		
RDT16043-251.d	4.1690	0.0900	0.2833	0.0043	0.7927	0.1064	0.0018	1665	18	1606	22	1732	31	545	126.3	0.23	96.46
RDT16043-252.d	6.9400	0.2100	0.3232	0.0082	0.8901	0.1546	0.0028	2095	28	1801	40	2395	31	491.1	120.6	0.25	85.97
RDT16043-253.d	1.7480	0.0420	0.1679	0.0025	0.6570	0.0752	0.0014	1025	15	1000	14	1062	39	463.8	228.3	0.49	97.56
RDT16043-254.d	12.6300	0.3100	0.4083	0.0074	0.7424	0.2243	0.0042	2647	23	2204	34	3010	29	169.6	197	1.16	83.26
RDT16043-255.d	1.6790	0.0430	0.1669	0.0026	0.5752	0.0728	0.0015	998	16	994	14	994	43	209.1	160.6	0.77	99.60
RDT16043-256.d	0.7820	0.0270	0.0800	0.0024	0.9421	0.0706	0.0012	582	15	495	14	938	35	2767	496	0.18	85.05
RDT16043-257.d	3.3500	0.1200	0.2547	0.0070	0.6453	0.0955	0.0026	1486	28	1461	36	1523	51	215.4	119.1	0.55	98.32
RDT16043-258.d	2.3380	0.0560	0.2115	0.0030	0.6166	0.0799	0.0016	1222	18	1237	16	1180	39	242.9	165.1	0.68	101.23
RDT16043-259.d	2.2340	0.0510	0.1991	0.0031	0.6035	0.0816	0.0016	1190	15	1169	17	1226	38	594.9	242.4	0.41	98.24
rdt16_044-215.d	0.3200	0.0390	0.0431	0.0013	0.0889	0.0568	0.0077	262	29	271.8	8.3	150	230	0.32	0.039	0.12	103.7405
rdt16_044-216.d	1.9900	0.1000	0.0238	0.0013	0.3911	0.6440	0.0400	1089	35	151.4	8.2	4550	100	1.99	0.1	0.05	13.90266
~~rdt16_044-217.d~~	~~no value~~	~~NAN~~	~~no value~~	~~NAN~~	~~NaN~~	~~no value~~	~~NAN~~	~~no value~~	~~NAN~~	~~no value~~	~~NAN~~	~~no value~~	~~NAN~~	~~no value~~	~~NAN~~	~~#VALUE!~~	~~#VALUE!~~
rdt16_044-218.d	0.2910	0.0220	0.0085	0.0003	0.3916	0.2460	0.0170	254	17	54.3	1.9	3040	110	0.291	0.022	0.08	21.37795
rdt16_044-219.d	0.5080	0.0240	0.0098	0.0004	0.4452	0.3750	0.0160	410	16	63.1	2.2	3744	70	0.508	0.024	0.05	15.39024
~~rdt16_044-220.d~~	~~no value~~	~~NAN~~	~~no value~~	~~NAN~~	~~NaN~~	~~no value~~	~~NAN~~	~~no value~~	~~NAN~~	~~no value~~	~~NAN~~	~~no value~~	~~NAN~~	~~no value~~	~~NAN~~	~~#VALUE!~~	~~#VALUE!~~
rdt16_044-229.d	7.2800	0.4300	0.0712	0.0046	0.2651	0.8290	0.0630	2112	51	441	28	4990	150	7.28	0.43	0.06	20.88068
~~rdt16_044-230.d~~	~~no value~~	~~NAN~~	~~no value~~	~~NAN~~	~~NaN~~	~~no value~~	~~NAN~~	~~no value~~	~~NAN~~	~~no value~~	~~NAN~~	~~no value~~	~~NAN~~	~~no value~~	~~NAN~~	~~#VALUE!~~	~~#VALUE!~~
~~rdt16_044-231.d~~	~~no value~~	~~NAN~~	~~no value~~	~~NAN~~	~~NaN~~	~~no value~~	~~NAN~~	~~no value~~	~~NAN~~	~~no value~~	~~NAN~~	~~no value~~	~~NAN~~	~~no value~~	~~NAN~~	~~#VALUE!~~	~~#VALUE!~~
rdt16_044-232.d	0.0840	0.0063	0.0117	0.0003	-0.0216	0.0530	0.0041	81	5.8	74.9	1.8	150	140	0.084	0.0063	0.08	92.46914
rdt16_044-233.d	0.0846	0.0082	0.0105	0.0004	0.1127	0.0619	0.0066	81	7.6	67.6	2.3	270	190	0.0846	0.0082	0.10	83.45679
rdt16_044-234.d	0.0920	0.0100	0.0105	0.0004	-0.0018	0.0652	0.0078	88.3	9.4	67.5	2.6	320	230	0.092	0.01	0.11	76.44394
~~rdt16_044-235.d~~	~~no value~~	~~NAN~~	~~no value~~	~~NAN~~	~~NaN~~	~~no value~~	~~NAN~~	~~no value~~	~~NAN~~	~~no value~~	~~NAN~~	~~no value~~	~~NAN~~	~~no value~~	~~NAN~~	~~#VALUE!~~	~~#VALUE!~~
rdt16_044-237.d	0.3470	0.0190	0.0459	0.0010	-0.0226	0.0551	0.0032	297	14	288.9	6	280	120	0.347	0.019	0.05	97.27273
rdt16_044-238.d	0.3130	0.0210	0.0441	0.0010	0.1591	0.0513	0.0034	273	17	278.1	6.1	180	140	0.313	0.021	0.07	101.8681
rdt16_044-239.d	0.0780	0.0140	0.0114	0.0006	0.0882	0.0510	0.0100	73	13	73.3	3.7	-230	310	0.078	0.014	0.18	100.411
rdt16_044-240.d	4.5200	0.2000	0.0425	0.0023	0.1600	0.8290	0.0530	1711	37	268	14	5000	130	4.52	0.2	0.04	15.66335
rdt16_044-249.d	0.3340	0.0170	0.0453	0.0009	0.0901	0.0535	0.0028	288	13	285.7	5.3	280	110	0.334	0.017	0.05	99.20139
rdt16_044-250.d	2.4900	0.1200	0.0257	0.0012	0.2313	0.7620	0.0460	1247	35	163.2	7.6	4830	110	2.49	0.12	0.05	13.08741
rdt16_044-252.d	0.3760	0.0200	0.0463	0.0011	0.0633	0.0599	0.0032	320	15	291.5	6.7	470	110	0.376	0.02	0.05	91.09375
rdt16_044-253.d	0.2900	0.0230	0.0404	0.0012	0.1618	0.0522	0.0042	252	18	254.9	7.1	170	160	0.29	0.023	0.08	101.1508
rdt16_044-254.d	0.3230	0.0140	0.0433	0.0009	0.0501	0.0546	0.0026	283	11	273.2	5.5	323	97	0.323	0.014	0.04	96.5371

Data in **bold** used for crystallisation weighted average age, concordance calculation using ($^{206}Pb/^{238}U$ age)/ $^{207}Pb/^{235}U$ age), concordant data in green.

Analysis #	Ratios							Ages						Concentrations (ppm)		Th:U	Concordance
	$^{207}Pb/^{235}U$	2σ	$^{206}Pb/^{238}U$	2σ	Rho	$^{207}Pb/^{206}Pb$	2σ	$^{207}Pb/^{235}U$	2σ	Pb^{206}/U^{238}	2σ	$^{207}Pb/^{206}Pb$	2σ	U	Th		
rdt15_076-10.d	1.6360	0.0460	0.1610	0.0029	0.2051	0.0741	0.0022	979	18	962	16	1004	61	150.9	48.68	0.32	98.26353
rdt15_076-11.d	1.7680	0.0380	0.1656	0.0028	0.5925	0.0771	0.0013	1030	14	987	15	1109	35	380.8	90.8	0.24	95.82524
rdt15_076-12.d	4.0500	0.1200	0.2678	0.0055	0.3962	0.1097	0.0028	1639	24	1532	27	1780	46	399	364	0.91	93.47163
rdt15_076-13.d	1.8950	0.0450	0.1742	0.0034	0.4930	0.0789	0.0017	1076	16	1034	19	1149	44	373.8	95	0.25	96.09665
rdt15_076-14.d	2.1520	0.0430	0.1746	0.0034	0.4905	0.0894	0.0017	1163	14	1039	19	1399	37	515	404	0.78	89.33792
rdt15_076-15.d	1.0840	0.0400	0.1137	0.0021	0.1628	0.0696	0.0026	739	19	693	12	842	78	154.3	78.8	0.51	93.77537
rdt15_076-16.d	6.5440	0.0880	0.3183	0.0051	0.6667	0.1493	0.0017	2049	12	1780	25	2331	20	401.1	252.4	0.63	86.87164
rdt15_076-17.d	9.5500	0.1400	0.4289	0.0065	0.5963	0.1612	0.0020	2387	14	2298	29	2462	21	181.6	205	1.13	96.27147
rdt15_076-18.d	2.1960	0.0610	0.1874	0.0030	0.2075	0.0849	0.0025	1173	19	1106	16	1272	56	124.7	75.58	0.61	94.28815
rdt15_076-19.d	1.8090	0.0280	0.1718	0.0024	0.5135	0.0758	0.0010	1046	10	1022	13	1082	28	503.8	72.3	0.14	97.70554
rdt15_076-20.d	7.3300	0.1000	0.3474	0.0047	0.5090	0.1534	0.0020	2150	12	1921	22	2377	22	303	117.7	0.39	89.34884
rdt15_076-21.d	4.3020	0.0690	0.2930	0.0046	0.5136	0.1068	0.0015	1691	13	1655	23	1734	26	216.2	97.8	0.45	97.87108
rdt15_076-30.d	3.2670	0.0960	0.2327	0.0058	0.8146	0.1017	0.0017	1462	23	1346	30	1640	31	302	98.1	0.32	92.06566
rdt15_076-31.d	1.2350	0.0400	0.1324	0.0024	0.2718	0.0680	0.0023	810	19	801	14	816	70	112.6	89.1	0.79	98.88889
rdt15_076-32.d	1.3030	0.0410	0.1298	0.0024	0.3354	0.0727	0.0022	841	18	786	13	969	62	129.1	113.4	0.88	93.46017
rdt15_076-33.d	0.6610	0.0200	0.0822	0.0013	0.2899	0.0584	0.0017	514	12	509	7.7	514	63	359	309	0.86	99.02724
rdt15_076-35.d	no value	NAN	no value	NAN	NaN	no value	NAN	no value	NAN	no value	NAN	no value	NAN	0.0079	0.054	6.84	#VALUE!
rdt15_076-36.d	no value	NAN	no value	NAN	NaN	no value	NAN	no value	NAN	no value	NAN	no value	NAN	0.0059	0.125	21.19	#VALUE!
rdt15_076-37.d	0.9470	0.0310	0.0900	0.0018	0.3029	0.0770	0.0026	671	17	555.3	11	1056	67	157.6	77.5	0.49	82.75708
rdt15_076-38.d	0.9420	0.0280	0.0953	0.0018	0.4097	0.0717	0.0019	669	15	586.8	11	936	58	323	19.3	0.06	87.713
rdt15_076-39.d	0.8790	0.0320	0.1033	0.0026	0.4930	0.0617	0.0020	637	17	634	15	632	67	350	36.2	0.10	99.52904
rdt15_076-40.d	2.2930	0.0350	0.1427	0.0019	0.4505	0.1165	0.0016	1208	11	859.9	11	1894	25	444.2	132.5	0.30	71.18377
rdt15_076-41.d	1.5320	0.0270	0.1524	0.0026	0.4854	0.0729	0.0012	942	10	914	14	994	34	484	89.7	0.19	97.0276
rdt15_076-42.d	1.2980	0.0380	0.1385	0.0029	0.5183	0.0679	0.0016	841	17	836	16	865	46	317.9	162.9	0.51	99.40547
rdt15_076-43.d	1.5430	0.0270	0.1550	0.0022	0.4403	0.0723	0.0012	947	11	929	12	981	34	387	213	0.55	98.09926
rdt15_076-44.d	0.6660	0.0190	0.0805	0.0014	0.2904	0.0602	0.0017	517	12	499.9	8.2	572	60	268.7	535.9	1.99	96.69246
rdt15_076-45.d	1.5130	0.0490	0.1345	0.0024	0.1814	0.0820	0.0027	931	19	813	14	1207	65	416	59.8	0.14	87.32546
rdt15_076-46.d	0.5570	0.0130	0.0720	0.0011	0.2291	0.0561	0.0013	448.4	8.4	448.1	6.7	429	53	874	470	0.54	99.9331
rdt15_076-55.d	1.4600	0.0600	0.1499	0.0032	0.1813	0.0708	0.0029	903	25	899	18	864	91	78.3	27.36	0.35	99.55703
rdt15_076-56.d	1.6370	0.0440	0.1549	0.0028	0.3843	0.0768	0.0020	980	16	928	15	1075	53	189.1	63.2	0.33	94.69388
rdt15_076-57.d	1.4090	0.0330	0.1376	0.0024	0.3914	0.0739	0.0015	890	13	831	14	1030	41	469	204.7	0.44	93.37079
rdt15_076-58.d	1.4760	0.0320	0.1481	0.0025	0.3728	0.0727	0.0016	921	14	890	14	984	45	397.9	147.4	0.37	96.63409

Data in **bold** used for crystallisation weighted average age, concordance calculation using ($^{206}Pb/^{238}U$ age)/ $^{207}Pb/^{235}U$ age), concordant data in green.

Supplementary Table 4 (continued). Main isotopes and ratios measured using LA–ICP–MS

Analysis #	Ratios							Ages						Concentrations (ppm)		Th:U	Concordance
	$^{207}Pb/^{235}U$	2σ	$^{206}Pb/^{238}U$	2σ	Rho	$^{207}Pb/^{206}Pb$	2σ	$^{207}Pb/^{235}U$	2σ	Pb^{206}/U^{238}	2σ	$^{207}Pb/^{206}Pb$	2σ	U	Th		
rdt15_076-10.d	1.6360	0.0460	0.1610	0.0029	0.2051	0.0741	0.0022	979	18	962	16	1004	61	150.9	48.68	0.32	98.26353
rdt15_076-11.d	1.7680	0.0380	0.1656	0.0028	0.5925	0.0771	0.0013	1030	14	987	15	1109	35	380.8	90.8	0.24	95.82524
rdt15_076-12.d	4.0500	0.1200	0.2678	0.0055	0.3962	0.1097	0.0028	1639	24	1532	27	1780	46	399	364	0.91	93.47163
rdt15_076-13.d	1.8950	0.0450	0.1742	0.0034	0.4930	0.0789	0.0017	1076	16	1034	19	1149	44	373.8	95	0.25	96.09665
rdt15_076-14.d	2.1520	0.0430	0.1746	0.0034	0.4905	0.0894	0.0017	1163	14	1039	19	1399	37	515	404	0.78	89.33792
rdt15_076-15.d	1.0840	0.0400	0.1137	0.0021	0.1628	0.0696	0.0026	739	19	693	12	842	78	154.3	78.8	0.51	93.77537
rdt15_076-16.d	6.5440	0.0880	0.3183	0.0051	0.6667	0.1493	0.0017	2049	12	1780	25	2331	20	401.1	252.4	0.63	86.87164
rdt15_076-17.d	9.5500	0.1400	0.4289	0.0065	0.5963	0.1612	0.0020	2387	14	2298	29	2462	21	181.6	205	1.13	96.27147
rdt15_076-18.d	2.1960	0.0610	0.1874	0.0030	0.2075	0.0849	0.0025	1173	19	1106	16	1272	56	124.7	75.58	0.61	94.28815
rdt15_076-19.d	1.8090	0.0280	0.1718	0.0024	0.5135	0.0758	0.0010	1046	10	1022	13	1082	28	503.8	72.3	0.14	97.70554
rdt15_076-20.d	7.3300	0.1000	0.3474	0.0047	0.5090	0.1534	0.0020	2150	12	1921	22	2377	22	303	117.7	0.39	89.34884
rdt15_076-21.d	4.3020	0.0690	0.2930	0.0046	0.5136	0.1068	0.0015	1691	13	1655	23	1734	26	216.2	97.8	0.45	97.87108
rdt15_076-30.d	3.2670	0.0960	0.2327	0.0058	0.8146	0.1017	0.0017	1462	23	1346	30	1640	31	302	98.1	0.32	92.06566
rdt15_076-31.d	1.2350	0.0400	0.1324	0.0024	0.2718	0.0680	0.0023	810	19	801	14	816	70	112.6	89.1	0.79	98.88889
rdt15_076-32.d	1.3030	0.0410	0.1298	0.0024	0.3354	0.0727	0.0022	841	18	786	13	969	62	129.1	113.4	0.88	93.46017
rdt15_076-33.d	0.6610	0.0200	0.0822	0.0013	0.2899	0.0584	0.0017	514	12	509	7.7	514	63	359	309	0.86	99.02724
rdt15_076-35.d	no value	NAN	no value	NAN	NaN	no value	NAN	no value	NAN	no value	NAN	no value	NAN	0.0079	0.054	6.84	#VALUE!
rdt15_076-36.d	no value	NAN	no value	NAN	NaN	no value	NAN	no value	NAN	no value	NAN	no value	NAN	0.0059	0.125	21.19	#VALUE!
rdt15_076-37.d	0.9470	0.0310	0.0900	0.0018	0.3029	0.0770	0.0026	671	17	555.3	11	1056	67	157.6	77.5	0.49	82.75708
rdt15_076-38.d	0.9420	0.0280	0.0953	0.0018	0.4097	0.0717	0.0019	669	15	586.8	11	936	58	323	19.3	0.06	87.713
rdt15_076-39.d	0.8790	0.0320	0.1033	0.0026	0.4930	0.0617	0.0020	637	17	634	15	632	67	350	36.2	0.10	99.52904
rdt15_076-40.d	2.2930	0.0350	0.1427	0.0019	0.4505	0.1165	0.0016	1208	11	859.9	11	1894	25	444.2	132.5	0.30	71.18377
rdt15_076-41.d	1.5320	0.0270	0.1524	0.0026	0.4854	0.0729	0.0012	942	10	914	14	994	34	484	89.7	0.19	97.0276
rdt15_076-42.d	1.2980	0.0380	0.1385	0.0029	0.5183	0.0679	0.0016	841	17	836	16	865	46	317.9	162.9	0.51	99.40547
rdt15_076-43.d	1.5430	0.0270	0.1550	0.0022	0.4403	0.0723	0.0012	947	11	929	12	981	34	387	213	0.55	98.09926
rdt15_076-44.d	0.6660	0.0190	0.0805	0.0014	0.2904	0.0602	0.0017	517	12	499.9	8.2	572	60	268.7	535.9	1.99	96.69246
rdt15_076-45.d	1.5130	0.0490	0.1345	0.0024	0.1814	0.0820	0.0027	931	19	813	14	1207	65	416	59.8	0.14	87.32546
rdt15_076-46.d	0.5570	0.0130	0.0720	0.0011	0.2291	0.0561	0.0013	448.4	8.4	448.1	6.7	429	53	874	470	0.54	99.9331
rdt15_076-55.d	1.4600	0.0600	0.1499	0.0032	0.1813	0.0708	0.0029	903	25	899	18	864	91	78.3	27.36	0.35	99.55703
rdt15_076-56.d	1.6370	0.0440	0.1549	0.0028	0.3843	0.0768	0.0020	980	16	928	15	1075	53	189.1	63.2	0.33	94.69388
rdt15_076-57.d	1.4090	0.0330	0.1376	0.0024	0.3914	0.0739	0.0015	890	13	831	14	1030	41	469	204.7	0.44	93.37079
rdt15_076-58.d	1.4760	0.0320	0.1481	0.0025	0.3728	0.0727	0.0016	921	14	890	14	984	45	397.9	147.4	0.37	96.63409

Data in **bold** used for crystallisation weighted average age, concordance calculation using ($^{206}Pb/^{238}U$ age)/ $^{207}Pb/^{235}U$ age), concordant data in green.

Analysis #	Ratios							Ages						Concentrations (ppm)		Th:U	Concordance
	$^{207}Pb/^{235}U$	2σ	$^{206}Pb/^{238}U$	2σ	Rho	$^{207}Pb/^{206}Pb$	2σ	$^{207}Pb/^{235}U$	2σ	Pb^{206}/U^{238}	2σ	$^{207}Pb/^{206}Pb$	2σ	U	Th		
ST08A-499.d	3.1500	0.6000	0.0594	0.0051	0.9934	0.2580	0.0300	1030	120	368	30	2600	180	1011.7	376	0.37	35.72816
ST08A-500.d	0.3820	0.0320	0.0356	0.0010	0.5479	0.0784	0.0058	320	22	225.6	5.9	920	140	141.6	175.5	1.24	70.5
ST08A-501.d	0.2412	0.0086	0.0334	0.0007	0.2077	0.0524	0.0017	219.1	6.9	**212**	**4.4**	274	67	307.1	132.7	0.43	96.75947
ST08A-502.d	0.2358	0.0079	0.0341	0.0007	0.1527	0.0504	0.0015	214.3	6.4	**215.9**	**4.2**	183	63	525.9	124.5	0.24	100.7466
ST08A-503.d	10.2700	0.2600	0.4582	0.0089	0.3165	0.1628	0.0032	2455	24	2432	38	2473	34	49.67	252.5	5.08	99.06314
ST08A-504.d	0.3540	0.0260	0.0339	0.0008	0.5463	0.0750	0.0046	305	19	214.8	5.2	880	120	221.4	40.15	0.18	70.42623
ST08A-505.d	0.5020	0.0180	0.0629	0.0015	0.5206	0.0577	0.0017	410	12	393.1	9.3	477	63	315.3	128.5	0.41	95.87805
ST08A-506.d	0.3010	0.0160	0.0340	0.0008	0.0742	0.0652	0.0034	264	12	215.2	4.9	640	100	177.6	149.3	0.84	81.51515
ST08A-507.d	0.5810	0.0520	0.0388	0.0009	0.7212	0.1041	0.0078	446	32	245.6	5.5	1400	140	471	285	0.61	55.06726
ST08A-508.d	0.2730	0.0120	0.0330	0.0007	0.2117	0.0608	0.0024	243.6	9.3	209.2	4.4	542	85	266.7	136.9	0.51	85.87849
ST08A-509.d	0.2494	0.0110	0.0333	0.0008	0.1823	0.0548	0.0023	224.5	8.9	211	4.7	320	87	194.9	201.9	1.04	93.98664
ST08A-510.d	0.3640	0.0240	0.0366	0.0010	0.2616	0.0718	0.0046	312	17	231.8	6.4	880	120	340.9	112.2	0.33	74.29487
ST08A-511.d	0.3315	0.0100	0.0333	0.0007	0.1921	0.0724	0.0020	289.8	7.7	210.9	4.2	962	57	472	521.1	1.10	72.77433
ST08A-512.d	0.2384	0.0082	0.0345	0.0007	0.3516	0.0504	0.0014	216.4	6.7	**218.3**	**4.5**	183	61	485	94.2	0.19	100.878
ST08A-513.d	0.2690	0.0160	0.0331	0.0008	0.1635	0.0589	0.0032	241	13	210.1	5.1	490	120	184.6	99.9	0.54	87.17842
~~ST08A-521.d~~	~~0.2376~~	~~0.0096~~	~~0.0339~~	~~0.0008~~	~~0.0146~~	~~0.0514~~	~~0.0021~~	215.3	7.9	**214.7**	**4.7**	209	83	~~257~~	~~107.5~~	~~0.42~~	99.72132
ST08A-522.d	0.4050	0.0390	0.0349	0.0010	0.2781	0.0791	0.0059	333	26	221.2	6.4	970	140	381.9	148.3	0.39	66.42643
ST08A-523.d	0.2379	0.0062	0.0320	0.0006	0.4698	0.0539	0.0011	216.4	5.1	203.2	3.9	348	43	1925	229.5	0.12	93.90018
ST08A-524.d	1.3310	0.0690	0.0932	0.0024	0.6943	~~0.1053~~	~~0.0040~~	856	29	574	14	1690	62	359.1	223.3	0.62	67.05607
ST08A-525.d	0.2580	0.0160	0.0337	0.0009	0.1201	0.0569	0.0034	230	12	213.5	5.4	330	120	112.6	136.9	1.22	92.82609
ST08A-526.d	0.2329	0.0088	0.0340	0.0007	0.0611	0.0501	0.0019	212.2	7.4	**215.4**	**4.4**	162	77	303.1	92.3	0.30	101.508
ST08A-527.d	0.2930	0.0130	0.0333	0.0007	0.0814	0.0637	0.0024	259	9.7	211.1	4.3	657	75	389.7	154.8	0.40	81.50579
ST08A-528.d	0.2354	0.0087	0.0329	0.0007	0.3290	0.0522	0.0016	213.7	7.1	**208.4**	**4.1**	260	66	399.5	221.2	0.55	97.51989
ST08A-529.d	0.2920	0.0150	0.0332	0.0007	0.3663	0.0633	0.0028	257	11	210.6	4.5	608	93	366.4	124.9	0.34	81.94553
ST08A-530.d	0.2464	0.0082	0.0335	0.0007	0.1335	0.0538	0.0016	223.4	6.8	**212.1**	**4.2**	323	67	422.5	148	0.35	94.94181
ST08A-531.d	0.2912	0.0100	0.0332	0.0007	0.2197	0.0642	0.0020	259.2	8.1	210.8	4.3	691	67	451.3	1054	2.34	81.32716
ST08A-532.d	0.2370	0.0078	0.0329	0.0007	0.2794	0.0522	0.0015	215.3	6.4	**208.8**	**4.1**	264	61	518.2	121.4	0.23	96.98096
ST08A-533.d	0.2486	0.0081	0.0346	0.0008	0.1806	0.0522	0.0016	225	6.6	**219**	**4.8**	264	67	782	233.3	0.30	97.33333
ST08A-534.d	0.2800	0.0110	0.0345	0.0007	0.3537	0.0592	0.0021	249	8.8	218.4	4.5	517	75	355.7	106.1	0.30	87.71084
ST08A-535.d	0.2606	0.0080	0.0329	0.0007	0.3680	0.0572	0.0014	234.7	6.4	208.4	4	469	54	2150	203	0.09	88.79421
ST08A-536.d	0.2681	0.0100	0.0337	0.0007	0.1750	0.0579	0.0021	240.6	8.3	213.7	4.6	464	76	329.8	140.9	0.43	88.81962
ST18-339.d	2.0360	0.0520	0.1859	0.0041	0.6338	0.0795	0.0014	1124	18	1098	22	1171	35	417	268	0.64	97.68683

Data in **bold** used for crystallisation weighted average age, concordance calculation using ($^{206}Pb/^{238}U$ age)/ $^{207}Pb/^{235}U$ age), concordant data in green.

Supplementary Table 4 (continued). Main isotopes and ratios measured using LA–ICP–MS

Analysis #	Ratios							Ages						Concentrations (ppm)		Th:U	Concordance
	$^{207}Pb/^{235}U$	2σ	$^{206}Pb/^{238}U$	2σ	Rho	$^{207}Pb/^{206}Pb$	2σ	$^{207}Pb/^{235}U$	2σ	Pb^{206}/U^{238}	2σ	$^{207}Pb/^{206}Pb$	2σ	U	Th		
ST18-340.d	8.6300	0.2700	0.3643	0.0097	0.8666	0.1711	0.0027	2288	28	1997	46	2563	27	206	166.8	0.81	87.28147
ST18-341.d	0.0810	0.0023	0.0119	0.0003	0.5163	0.0495	0.0011	79	2.2	76.1	1.7	153	49	4049	216.8	0.05	96.32911
ST18-342.d	0.1729	0.0073	0.0237	0.0009	0.8339	0.0526	0.0012	161.2	6.3	150.6	5.4	302	52	1603	723	0.45	93.42432
ST18-343.d	0.0845	0.0067	0.0122	0.0004	0.1124	0.0507	0.0040	81.4	6.2	**78.2**	**2.2**	100	150	218.2	163.7	0.75	96.0688
ST18-344.d	0.0797	0.0024	0.0119	0.0003	0.2831	0.0488	0.0013	77.8	2.3	**76**	**1.7**	124	56	2606	773	0.30	97.68638
ST18-345.d	9.9300	0.2400	0.4409	0.0094	0.8166	0.1632	0.0023	2424	23	2351	42	2484	24	272.1	553	2.03	96.98845
ST18-346.d	0.0832	0.0046	0.0122	0.0003	0.1425	0.0497	0.0027	80.8	4.3	**78.4**	**2.1**	110	110	416.6	312.9	0.75	97.0297
ST18-347.d	0.0847	0.0027	0.0127	0.0003	0.5027	0.0483	0.0012	82.5	2.5	81.5	1.8	106	50	2578	146	0.06	98.78788
ST18-350.d	0.0948	0.0046	0.0120	0.0003	0.2904	0.0572	0.0026	91.5	4.2	77.1	2	408	94	538	309	0.57	84.2623
ST18-351.d	0.0803	0.0021	0.0118	0.0003	0.5337	0.0494	0.0010	78.3	2	75.6	1.6	160	44	7184	540	0.08	96.55172
ST18-352.d	0.7050	0.0220	0.0848	0.0019	0.3977	0.0604	0.0015	541.1	13	524.6	11	586	55	251	315.8	1.26	96.95066
ST18-353.d	8.7400	0.2100	0.3803	0.0082	0.8141	0.1663	0.0023	2307	22	2074	38	2521	24	404.3	103	0.25	89.9003
ST18-354.d	0.0793	0.0038	0.0121	0.0003	0.2366	0.0473	0.0022	77.7	3.5	**77.5**	**2**	52	89	862	670	0.78	99.7426
ST18-363.d	0.0940	0.0032	0.0119	0.0003	0.4846	0.0573	0.0016	91	3	76.3	1.7	457	61	3793	671	0.18	83.84615
ST18-364.d	0.0887	0.0025	0.0120	0.0003	0.4962	0.0536	0.0012	86.2	2.4	76.9	1.8	330	50	4626	385.4	0.08	89.21114
ST18-365.d	4.4200	0.2700	0.0487	0.0028	0.7120	0.6620	0.0250	1659	52	~~305~~	~~17~~	4631	61	54.6	42.6	0.78	18.38457
ST18-366.d	8.1100	1.0000	0.0741	0.0081	0.9365	0.7470	0.0320	2021	100	~~453~~	~~47~~	4827	76	33.6	24.8	0.74	22.41465
ST18-367.d	6.7900	0.5100	0.0684	0.0043	0.8277	0.6970	0.0250	2016	65	~~425~~	~~26~~	4720	60	41	31.9	0.78	21.08135
ST18-368.d	0.1043	0.0071	0.0126	0.0003	0.1506	0.0606	0.0039	99.8	6.4	80.4	2.1	460	120	441.1	447.4	1.01	80.56112
ST18-369.d	0.0861	0.0026	0.0122	0.0003	0.4687	0.0516	0.0012	83.8	2.4	77.8	1.6	243	50	3871	359.7	0.09	92.8401
ST18-370.d	0.1146	0.0084	0.0129	0.0004	0.3063	0.0659	0.0046	109.7	7.7	82.7	2.2	580	140	263.3	254.5	0.97	75.38742
ST18-371.d	0.0822	0.0024	0.0122	0.0003	0.4919	0.0488	0.0011	80.1	2.2	**78.2**	**1.7**	131	48	3209	350.2	0.11	97.62797
ST18-372.d	0.0797	0.0022	0.0120	0.0003	0.4683	0.0483	0.0010	77.8	2.1	76.6	1.6	107	46	4070	366	0.09	98.45758
ST18-373.d	0.0973	0.0050	0.0124	0.0003	0.2680	0.0577	0.0028	94.3	4.7	79.2	1.9	425	100	567	799	1.41	83.98727
ST18-376.d	0.0821	0.0026	0.0122	0.0003	0.4454	0.0486	0.0012	80	2.5	**78**	**1.7**	119	54	2829	284.9	0.10	97.5
ST18-377.d	0.0845	0.0045	0.0130	0.0004	0.0875	0.0478	0.0026	82	4.2	83.2	2.3	40	100	340.7	269.7	0.79	101.4634
ST18-378.d	0.0867	0.0039	0.0125	0.0003	0.2261	0.0506	0.0021	84.1	3.7	79.8	1.9	182	87	787	322.2	0.41	94.88704
ST18-379.d	1.0460	0.0270	0.1153	0.0025	0.6481	0.0658	0.0011	726.1	13	703	14	785	36	720.9	810	1.12	96.81862
ST18-380.d	0.0989	0.0052	0.0133	0.0004	0.2628	0.0545	0.0026	95.3	4.7	84.9	2.2	305	99	587	519.1	0.88	89.08709
ST18-381.d	0.0840	0.0024	0.0122	0.0003	0.5279	0.0499	0.0010	81.8	2.3	78.1	1.6	184	45	3856	355	0.09	95.47677
ST18-392.d	0.0803	0.0048	0.0122	0.0004	0.1381	0.0483	0.0028	77.9	4.5	**78.2**	**2.3**	60	110	397	428	1.08	100.3851
ST18-393.d	2.9560	0.0830	0.2339	0.0051	0.5514	0.0919	0.0020	1390	22	1353	27	1448	40	115.1	61.25	0.53	97.33813

Data in **bold** used for crystallisation weighted average age, concordance calculation using ($^{206}Pb/^{238}U$ age)/ $^{207}Pb/^{235}U$ age), concordant data in green.

Analysis #	Ratios							Ages						Concentrations (ppm)		Th:U	Concordance
	$^{207}Pb/^{235}U$	2σ	$^{206}Pb/^{238}U$	2σ	Rho	$^{207}Pb/^{206}Pb$	2σ	$^{207}Pb/^{235}U$	2σ	Pb^{206}/U^{238}	2σ	$^{207}Pb/^{206}Pb$	2σ	U	Th		
ST18-394.d	2.7450	0.0820	0.1903	0.0053	0.8130	0.1049	0.0019	1338	23	1121	29	1702	33	446	206.7	0.46	83.78176
ST18-395.d	0.0808	0.0022	0.0120	0.0003	0.4864	0.0486	0.0010	78.9	2	77.2	1.6	120	42	5691	297.7	0.05	97.84537
ST18-396.d	0.0900	0.0039	0.0122	0.0003	0.2899	0.0537	0.0021	87.3	3.6	78.2	1.8	288	82	889	755	0.85	89.57617
ST18-397.d	0.0989	0.0043	0.0144	0.0005	0.3770	0.0502	0.0019	95.4	3.9	92.2	2.9	174	78	1037	576	0.56	96.6457
ST18-398.d	0.1285	0.0054	0.0119	0.0003	0.4026	0.0792	0.0030	122.3	4.7	76	1.7	1101	68	5355	3080	0.58	62.14227
ST18-399.d	4.9850	0.1200	0.3192	0.0071	0.7995	0.1134	0.0017	1812	21	1783	35	1850	27	381	266	0.70	98.39956
ST18-400.d	0.0956	0.0041	0.0134	0.0004	0.7768	0.0514	0.0013	92.8	3.8	~~85.6~~	~~2.4~~	243	58	2628	208	0.08	92.24138
ST18-401.d	0.0807	0.0031	0.0125	0.0003	0.2951	0.0466	0.0016	78.6	2.9	**80.2**	**1.9**	31	70	1124	348.5	0.31	102.0356
ST18-402.d	0.0803	0.0022	0.0122	0.0003	0.4405	0.0476	0.0010	78.4	2.1	78.4	1.6	79	45	4877	315.3	0.06	100
ST18-410.d	1.9550	0.0490	0.1844	0.0041	0.6561	0.0773	0.0014	1098	17	1090	22	1118	35	470	154.8	0.33	99.2714
ST18-411.d	0.0909	0.0051	0.0128	0.0004	0.1691	0.0526	0.0028	87.9	4.7	82	2.3	210	110	492.8	504.3	1.02	93.28783
ST18-412.d	0.4200	0.0270	0.0144	0.0004	0.6369	0.2070	0.0110	348	19	92.2	2.2	2749	87	2161	860	0.40	26.49425
ST18-413.d	1.4270	0.0460	0.1225	0.0031	0.6556	0.0853	0.0020	896	20	744	18	1298	45	238.4	179.2	0.75	83.03571
ST18-414.d	0.0806	0.0023	0.0123	0.0003	0.3655	0.0476	0.0011	78.6	2.2	**79**	**1.7**	73	50	3416	1570	0.46	100.5089
ST18-415.d	0.0848	0.0024	0.0124	0.0003	0.2049	0.0499	0.0010	82.5	2.2	**79.1**	**1.7**	177	44	4349	665.7	0.15	95.87879
ST18-416.d	13.2900	0.3400	0.5104	0.0120	0.8340	0.1890	0.0027	2696	25	2652	51	2729	24	209.7	107.6	0.51	98.36795
ST18-417.d	10.5300	0.4600	0.1018	0.0044	0.1398	0.7710	0.0330	2459	41	~~623~~	~~25~~	4903	80	41.6	23.79	0.57	25.3355
ST18-418.d	1.0630	0.0300	0.1086	0.0024	0.5799	0.0710	0.0014	733	15	664	14	944	41	605.2	87.5	0.14	90.58663
ST18-419.d	0.1184	0.0057	0.0131	0.0003	0.2335	0.0652	0.0028	113.1	5.1	84.1	1.9	706	87	2762	31400	11.37	74.35897
ST18-420.d	0.1008	0.0046	0.0126	0.0003	0.4476	0.0578	0.0022	98	4.3	80.6	1.8	454	77	3073	288.5	0.09	82.2449
ST18-421.d	0.4180	0.0310	0.0454	0.0032	0.9806	0.0656	0.0014	342	23	285	20	780	44	1980	444	0.22	83.33333
ST18-422.d	0.0857	0.0037	0.0130	0.0003	0.2246	0.0479	0.0019	83.3	3.5	83.5	2	68	81	849	133.7	0.16	100.2401
ST18-423.d	0.0977	0.0070	0.0132	0.0004	0.4108	0.0559	0.0039	94.6	6.5	84.3	2.3	300	130	363.4	269.2	0.74	89.11205
ST18-424.d	0.3905	0.0110	0.0133	0.0003	0.5298	0.2130	0.0044	334	8.1	~~85.4~~	~~1.9~~	2914	33	4850	1892	0.39	25.56886
ST18-425.d	0.0934	0.0031	0.0134	0.0003	0.3538	0.0507	0.0013	90.5	2.9	85.7	2	201	57	2500	286	0.11	94.69613
ST13-433.d	0.2405	0.0075	0.0338	0.0008	0.4723	0.0518	0.0013	218.8	6	**214.3**	**4.7**	249	54	831	197.8	0.24	97.94
ST13-434.d	0.2330	0.0064	0.0332	0.0007	0.4562	0.05105	0.0011	212.3	5.2	**210.8**	**4.6**	232	48	1554	262.9	0.17	99.29
ST13-435.d	0.2333	0.0079	0.0333	0.0008	0.3720	0.051	0.0014	212.2	6.5	**211.1**	**4.8**	215	61	610.3	160.2	0.26	99.48
ST13-436.d	0.2359	0.0067	0.0331	0.0007	0.5771	0.05177	0.001	214.6	5.5	**210**	**4.5**	257	45	1796	195.5	0.11	97.86
ST13-437.d	0.2290	0.0062	0.0328	0.0007	0.5382	0.05085	0.001	209.1	5.1	**208.2**	**4.6**	217	44	1678	193.9	0.12	99.57
ST13-438.d	0.2289	0.0064	0.0327	0.0007	0.5327	0.05101	0.0011	208.9	5.3	**207.2**	**4.4**	223	46	1761	256.8	0.15	99.19
ST13-439.d	4.0900	0.1000	0.2789	0.0061	0.7401	0.1067	0.0017	1650	20	1584	31	1736	29	304.1	215	0.71	96.00

Data in **bold** used for crystallisation weighted average age, concordance calculation using ($^{206}Pb/^{238}U$ age)/ $^{207}Pb/^{235}U$ age), concordant data in green.

Supplementary Table 4 (continued). Main isotopes and ratios measured using LA–ICP–MS, bold data are used for weighted averages (**magmatic** and **metamorphic**).

Analysis #	Ratios							Ages						Concentrations (ppm)		Th:U	Concordance
	$^{207}Pb/^{235}U$	2σ	$^{206}Pb/^{238}U$	2σ	Rho	$^{207}Pb/^{206}Pb$	2σ	$^{207}Pb/^{235}U$	2σ	Pb^{206}/U^{238}	2σ	$^{207}Pb/^{206}Pb$	2σ	U	Th		
ST13-440.d	0.7180	0.0220	0.0879	0.0021	0.5934	0.0593	0.0013	548	13	542.9	12	554	49	426.8	96.9	0.23	99.07
ST13-441.d	0.2332	0.0062	0.0331	0.0007	0.4867	0.05133	0.001	212.5	5.1	**209.9**	**4.4**	241	45	1790	205.5	0.11	98.78
ST13-442.d	0.1368	0.0048	0.0198	0.0006	0.6456	0.0501	0.0013	130	4.3	126.1	3.8	183	57	2346	217.4	0.09	97.00
ST13-443.d	0.2344	0.0069	0.0336	0.0007	0.4174	0.0506	0.0012	213.3	5.7	**212.9**	**4.6**	212	52	1351	657	0.49	99.81
ST13-444.d	0.2266	0.0063	0.0324	0.0007	0.5751	0.05078	0.00097	207	5.2	**205.4**	**4.4**	223	44	1576	318.7	0.20	99.23
ST13-445.d	0.2286	0.0067	0.0335	0.0007	0.4897	0.04952	0.0011	208.6	5.5	**212.5**	**4.6**	161	49	1093	113.7	0.10	101.87
ST13-446.d	0.0919	0.0034	0.0137	0.0003	0.3801	0.049	0.0015	89.1	3.1	87.8	2.1	127	66	1479	115.1	0.08	98.54
ST13-447.d	0.2322	0.0065	0.0330	0.0007	0.6059	0.05123	0.001	211.6	5.4	**209.5**	**4.6**	234	44	2048	230.6	0.11	99.01
ST13-455.d	1.7400	0.0450	0.1716	0.0038	0.5699	0.0738	0.0014	1020	17	1020	21	1021	38	345.9	158.6	0.46	100.00
ST13-456.d	0.0928	0.0026	0.0120	0.0003	0.3471	0.05653	0.0011	90	2.4	76.7	1.6	452	44	6978	399	0.06	85.22
ST13-457.d	0.2371	0.0075	0.0338	0.0008	0.4479	0.0513	0.0013	215.5	6.1	**213.9**	**4.9**	224	57	743.3	209.1	0.28	99.26
ST13-458.d	0.2374	0.0098	0.0334	0.0008	0.3378	0.052	0.0019	215	8	**211.7**	**5.2**	240	76	312.8	164.4	0.53	98.47
ST13-459.d	1.0000	0.0470	0.1160	0.0040	0.5144	0.0638	0.0025	701	26	706	23	649	84	67.3	23.32	0.35	100.71
ST13-460.d	2.9690	0.0740	0.2381	0.0050	0.5680	0.0905	0.0015	1396	19	1376	26	1428	33	342.2	169.5	0.50	98.57
ST13-461.d	0.2285	0.0078	0.0332	0.0007	0.3552	0.0499	0.0014	208.2	6.5	**210.7**	**4.6**	172	62	496.7	151.2	0.30	101.20
ST13-462.d	0.2543	0.0091	0.0331	0.0008	0.3189	0.0557	0.0016	229.1	7.3	209.8	4.7	404	64	800	205.5	0.26	91.58
ST13-463.d	0.0834	0.0026	0.0125	0.0003	0.4355	0.0489	0.0013	81.3	2.4	***80***	***1.8***	126	54	2339	172.1	0.07	98.40
ST13-464.d	0.2359	0.0084	0.0335	0.0008	0.4516	0.0512	0.0015	214.4	6.9	**212**	**5.1**	222	61	899	413.3	0.46	98.88
ST13-465.d	0.0826	0.0024	0.0125	0.0003	0.4694	0.04807	0.0011	80.5	2.3	***80.2***	***1.7***	93	49	3553	237.7	0.07	99.63
ST13-466.d	0.0854	0.0033	0.0127	0.0003	0.2566	0.0489	0.0017	83.3	3	***81.2***	***1.9***	126	73	1157	160.5	0.14	97.48
ST13-467.d	0.2750	0.0140	0.0376	0.0013	0.7796	0.0522	0.0016	243.9	11	237.6	7.9	264	69	449	178.5	0.40	97.42
ST13-468.d	0.2460	0.0120	0.0333	0.0008	0.1953	0.054	0.0025	221.9	9.7	**211.2**	**5.2**	288	95	214	89.8	0.42	95.18
ST13-469.d	0.0860	0.0032	0.0128	0.0003	0.3327	0.0489	0.0016	83.6	3	***81.7***	***1.9***	115	66	1262	187.6	0.15	97.73
ST13-477.d	1.2250	0.0350	0.1186	0.0029	0.7528	0.0751	0.0013	809	16	722	17	1058	36	653.7	142.3	0.22	89.25
ST13-478.d	0.2415	0.0062	0.0347	0.0008	0.5548	0.05057	0.00092	219.4	5.1	219.6	4.6	215	40	2410	199.2	0.08	100.09
ST13-479.d	0.2354	0.0083	0.0334	0.0008	0.3396	0.0517	0.0016	214.4	7	**211.8**	**4.9**	229	67	476	242.5	0.51	98.79
ST13-480.d	0.2400	0.0120	0.0334	0.0009	0.1828	0.0528	0.0025	216.3	9.8	**211.4**	**5.5**	235	97	195.8	83.7	0.43	97.73
ST13-481.d	0.2291	0.0059	0.0325	0.0007	0.6368	0.05117	0.00085	209.2	4.9	**206.2**	**4.3**	243	38	2742	170.2	0.06	98.57
ST13-482.d	0.2339	0.0084	0.0342	0.0008	0.3748	0.0495	0.0015	212.5	6.9	217	4.9	147	63	584.1	159.1	0.27	102.12
ST13-483.d	0.2403	0.0110	0.0336	0.0008	0.2393	0.0521	0.0021	217.1	8.6	**212.8**	**5.1**	230	85	265	103	0.39	98.02
ST13-484.d	0.0892	0.0040	0.0133	0.0003	0.2021	0.0491	0.002	86.5	3.7	85.1	2.1	111	83	658	148.9	0.23	98.38

Supplementary Table 4 (continued). Main isotopes and ratios measured using LA–ICP–MS, bold data are used for weighted averages (**magmatic** and **metamorphic**).

Analysis #	Ratios							Ages						Concentrations (ppm)		Th:U	Concordance
	$^{207}Pb/^{235}U$	2σ	$^{206}Pb/^{238}U$	2σ	Rho	$^{207}Pb/^{206}Pb$	2σ	$^{207}Pb/^{235}U$	2σ	Pb^{206}/U^{238}	2σ	$^{207}Pb/^{206}Pb$	2σ	U	Th		
ST13-485.d	0.2379	0.0100	0.0339	0.0008	0.3394	0.051	0.002	216	8.6	**215**	**5**	193	80	315.7	146.5	0.46	99.54
ST13-486.d	0.2369	0.0075	0.0345	0.0008	0.4134	0.0505	0.0014	216.3	6.4	218.5	4.7	191	57	695	147.3	0.21	101.02
ST13-487.d	0.3860	0.0340	0.0419	0.0022	0.9483	0.0626	0.0027	319	24	264	14	580	92	600	183.7	0.31	82.76
ST13-488.d	0.2366	0.0073	0.0335	0.0008	0.4922	0.0515	0.0013	215.1	6	**212.4**	**4.8**	241	53	903	162.6	0.18	98.74
ST13-489.d	0.0836	0.0025	0.0126	0.0003	0.5227	0.04819	0.0011	81.4	2.3	***80.7***	***1.7***	103	48	2973	304.2	0.10	99.14
ST13-490.d	0.1470	0.0110	0.0139	0.0004	0.6913	0.0753	0.0048	137.3	9.8	88.7	2.3	870	130	1539	136.5	0.09	64.60
ST13-491.d	0.2366	0.0099	0.0339	0.0008	0.3204	0.0515	0.0019	215.1	8	**214.6**	**5.1**	210	77	338.9	126.7	0.37	99.77

Data in **bold** used for crystallisation weighted average age, concordance calculation using ($^{206}Pb/^{238}U$ age)/ $^{207}Pb/^{235}U$ age), concordant data in green.

Supplementary Table 4 (continued). Main isotopes and ratios measured using LA–ICP–MS (GLITTER reduction).

Analysis #	Ratios							Ages						Concentrations (CPU)		Th:U	Concordance
	$^{207}Pb/^{235}U$	1σ	U	U	Rho	$^{207}Pb/^{206}Pb$	1σ	Pb^{207}/Pb^{206}	1σ	Pb^{206}/U^{238}	1σ	Pb^{207}/U^{235}	1σ	U	Th		
NT10_01	0.2609	0.0087	0.0374	0.0007	0.3188	0.0506	0.0016	221.3	73.52	**236.9**	**4.2**	235.4	6.99	152673	60159	0.39	100.64
NT10_02	0.2655	0.0063	0.0368	0.0006	0.4817	0.0523	0.0011	298.3	48.25	**233.2**	**3.8**	239.1	5.06	366599	227569	0.62	97.53
NT10_03	0.3368	0.0059	0.0383	0.0006	0.6899	0.0638	0.0008	733.5	27.59	242.4	3.77	294.7	4.45	2083001	1189634	0.57	82.25
NT10_04	0.4012	0.0071	0.0393	0.0006	0.6786	0.0741	0.0010	1045.1	27.32	248.2	3.89	342.5	5.15	1356621	339868	0.25	72.47
NT10_05	0.3222	0.0057	0.0380	0.0006	0.6788	0.0614	0.0008	654.8	28.87	240.7	3.75	283.6	4.37	1725050	632866	0.37	84.87
NT10_06	0.2631	0.0048	0.0367	0.0006	0.6439	0.0521	0.0008	287.8	32.84	**232.2**	**3.63**	237.2	3.88	1723306	588609	0.34	97.89
NT10_07	0.3847	0.0070	0.0384	0.0006	0.6536	0.0728	0.0011	1007	28.95	242.7	3.82	330.5	5.14	1087284	354576	0.33	73.43
NT10_08	0.4317	0.0078	0.0385	0.0006	0.6597	0.0815	0.0012	1232.6	27.72	243.2	3.84	364.4	5.55	1125997	370710	0.33	66.74
NT10_09	0.2758	0.0057	0.0371	0.0006	0.5625	0.0539	0.0010	366.5	39.2	**235.1**	**3.74**	247.3	4.52	1365819	439098	0.32	95.07
NT10_10	0.3940	0.0068	0.0372	0.0006	0.7096	0.0768	0.0010	1116.6	24.94	235.5	3.7	337.3	4.92	2274859	221313	0.10	69.82
NT10_11	0.2940	0.0057	0.0375	0.0006	0.6170	0.0569	0.0009	485.1	34.97	237.5	3.76	261.7	4.47	1124189	409907	0.36	90.75
NT10_12	0.2802	0.0055	0.0377	0.0006	0.6136	0.0539	0.0009	367.1	35.53	**238.7**	**3.79**	250.8	4.33	1008124	339216	0.34	95.18
NT10_13	0.2784	0.0052	0.0377	0.0006	0.6453	0.0536	0.0008	355.3	33.31	**238.4**	**3.78**	249.4	4.15	1310387	490891	0.37	95.59
~~NT10_14~~	~~1.2039~~	~~0.0208~~	~~0.0463~~	~~0.0007~~	0.7052	~~0.1888~~	~~0.0024~~	~~2731.4~~	~~20.99~~	~~291.6~~	~~4.56~~	~~802.4~~	~~9.57~~	~~3673102~~	~~1328572~~	~~0.36~~	36.34
NT10_15	0.4557	0.0085	0.0386	0.0006	0.6465	0.0856	0.0013	1328.8	28.5	244.4	3.89	381.3	5.92	1316631	486704	0.37	64.10
NT10_16	0.3481	0.0074	0.0375	0.0006	0.5545	0.0674	0.0012	850.6	37.71	237.1	3.88	303.3	5.6	856199	292173	0.34	78.17
NT10_17	0.2847	0.0077	0.0384	0.0007	0.4277	0.0538	0.0014	361.8	56.08	**243**	**4.19**	254.4	6.11	905358	214435	0.24	95.52
~~NT10_18~~	~~23.3450~~	~~560.4082~~	~~0.0785~~	~~0.0750~~	12.5445	~~0.2500~~	~~0.2775~~	~~3184.6~~	~~1135.34~~	~~486.9~~	~~448.48~~	~~3241.4~~	~~*******~~	~~773~~	~~748~~	~~0.97~~	15.02
~~NT10_19~~	~~Inf~~	~~NaN~~	~~Inf~~	~~NaN~~	~~NaN~~	~~0.0478~~	~~0.0688~~	~~0.1~~	~~0~~	~~NaN~~	~~NaN~~	~~Inf~~	~~NaN~~	~~0~~	~~0~~	~~#DIV/0!~~	~~NaN~~
NT10_20	0.3407	0.0066	0.0382	0.0006	0.6347	0.0647	0.0010	766	32.34	241.6	3.87	297.7	4.98	1352117	578693	0.43	81.16
~~NT10_21~~	~~2.3939~~	~~0.0637~~	~~0.0550~~	~~0.0011~~	0.4221	~~0.3160~~	~~0.0080~~	~~3550.6~~	~~38.55~~	~~345~~	~~6.43~~	~~1240.8~~	~~19.06~~	~~1352954~~	~~587394~~	~~0.43~~	27.80
NT10_22	0.4678	0.0083	0.0393	0.0006	0.7033	0.0863	0.0011	1344.6	25.35	248.7	3.96	389.7	5.77	4393392	1554487	0.35	63.82
~~NT10_23~~	~~2.9611~~	~~0.0537~~	~~0.1521~~	~~0.0025~~	0.6883	~~0.1412~~	~~0.0019~~	~~2242.5~~	~~23.49~~	~~912.8~~	~~13.98~~	~~1397.7~~	~~13.76~~	~~502784~~	~~338990~~	~~0.67~~	65.31
NT09_01	0.2750	0.0074	0.0363	0.0006	0.4176	0.0549	0.0014	407.4	54.42	230.1	3.93	246.7	5.88	336181	209971	0.62	93.27
NT09_02	0.2575	0.0067	0.0352	0.0006	0.4378	0.0531	0.0013	332.7	53.17	**222.9**	**3.75**	232.6	5.37	290672	109805	0.38	95.83
NT09_03	0.2652	0.0095	0.0359	0.0007	0.2894	0.0537	0.0019	356.8	77.28	**227.1**	**4.21**	238.9	7.59	123998	52126	0.42	95.06
NT09_04	0.2484	0.0092	0.0350	0.0007	0.2762	0.0515	0.0019	261.4	82.01	**221.8**	**4.19**	225.3	7.49	263966	103865	0.39	98.45
NT09_05	0.2485	0.0062	0.0364	0.0006	0.4633	0.0496	0.0011	174.4	51.75	**230.3**	**3.82**	225.3	5.01	356200	196266	0.55	102.22
NT09_06	0.2548	0.0066	0.0360	0.0006	0.4428	0.0513	0.0012	253.9	54.25	**228.2**	**3.84**	230.5	5.36	284835	147889	0.52	99.00
NT09_07	0.2423	0.0076	0.0361	0.0007	0.3517	0.0487	0.0015	133.3	69.44	**228.5**	**4.02**	220.3	6.21	179896	74667	0.42	103.72
NT09_08	0.2363	0.0066	0.0362	0.0006	0.4146	0.0474	0.0012	69.1	61.38	229	3.9	215.4	5.39	275418	141548	0.51	106.31

Data in **bold** used for crystallisation weighted average age, concordance calculation using ($^{206}Pb/^{238}U$ age)/ ($^{207}Pb/^{235}U$ age), concordant data within ±5% in green.

Supplementary Table 4 (continued). Main isotopes and ratios measured using LA–ICP–MS (GLITTER reduction).

Analysis #	Ratios							Ages						Concentrations (CPU)		Th:U	Concordance
	$^{207}Pb/^{235}U$	1σ	U	U	Rho	$^{207}Pb/^{206}Pb$	1σ	Pb^{207}/Pb^{206}	1σ	Pb^{206}/U^{238}	1σ	Pb^{207}/U^{235}	1σ	U	Th		
NT09_09	0.2443	0.0066	0.0357	0.0006	0.4288	0.0496	0.0012	177.3	57.32	**226.2**	**3.83**	221.9	5.36	277669	102759	0.37	101.94
NT09_10	0.2580	0.0070	0.0357	0.0006	0.4213	0.0525	0.0013	305.7	56.04	**225.9**	**3.86**	233.1	5.61	291245	110276	0.38	96.91
NT09_11	0.3227	0.0075	0.0359	0.0006	0.5016	0.0653	0.0014	783.7	43.22	227.1	3.8	284	5.76	319625	174861	0.55	79.96
NT09_12	0.2568	0.0058	0.0358	0.0006	0.5276	0.0521	0.0010	290	44.59	**226.5**	**3.71**	232.1	4.68	478097	320367	0.67	97.59
NT09_13	0.2578	0.0074	0.0362	0.0006	0.3996	0.0517	0.0014	272.6	60.49	**229.1**	**3.96**	232.9	5.93	213271	82795	0.39	98.37
NT09_14	0.2615	0.0068	0.0353	0.0006	0.4464	0.0537	0.0013	358.5	52.98	223.7	3.79	235.8	5.44	274805	162956	0.59	94.87
NT09_15	0.2570	0.0063	0.0357	0.0006	0.4802	0.0522	0.0012	293.4	50.14	**226.3**	**3.78**	232.3	5.11	341105	141029	0.41	97.42
NT09_16	0.2484	0.0064	0.0355	0.0006	0.4507	0.0507	0.0012	227.8	53.81	**225**	**3.8**	225.3	5.21	284038	146317	0.52	99.87
NT09_17	0.2463	0.0063	0.0354	0.0006	0.4509	0.0505	0.0012	217.9	53.49	**224.2**	**3.77**	223.6	5.14	333031	212172	0.64	100.27
NT09_18	0.2788	0.0085	0.0361	0.0007	0.3654	0.0561	0.0016	456	63.35	228.3	4.06	249.7	6.71	163234	75455	0.46	91.43
NT09_19	0.2452	0.0066	0.0352	0.0006	0.4240	0.0505	0.0013	218.5	57	**223.1**	**3.81**	222.7	5.4	270146	168818	0.62	100.18
~~NT09_20~~	~~1.9248~~	~~0.0323~~	~~0.1134~~	~~0.0018~~	~~0.7416~~	~~0.1231~~	~~0.0015~~	~~2002.1~~	~~20.92~~	~~692.4~~	~~10.58~~	~~1089.7~~	~~11.23~~	~~1095133~~	~~286378~~	~~0.26~~	~~63.54~~
NT09_21	0.2633	0.0075	0.0366	0.0007	0.4030	0.0521	0.0014	290.9	59.68	**231.9**	**4.02**	237.3	5.99	211560	90574	0.43	97.72
NT09_22	0.2564	0.0077	0.0360	0.0006	0.3689	0.0517	0.0015	271.2	64.11	**228**	**4.01**	231.8	6.21	190206	80165	0.42	98.36
NT09_23	0.2490	0.0071	0.0353	0.0006	0.3945	0.0512	0.0014	247.7	60.73	**223.7**	**3.89**	225.8	5.78	217601	129029	0.59	99.07
NT09_24	0.2427	0.0073	0.0361	0.0006	0.3756	0.0488	0.0014	136.9	65.54	**228.7**	**4**	220.7	5.94	205017	104604	0.51	103.62
NT11_01	0.2554	0.0053	0.0364	0.0006	0.5899	0.0509	0.0009	234.1	39.59	**230.7**	**3.76**	230.9	4.3	893969	510343	0.57	99.91
NT11_02	0.2536	0.0047	0.0365	0.0006	0.6666	0.0504	0.0007	213.2	33.06	**231.1**	**3.71**	229.5	3.84	1583645	1075636	0.68	100.70
NT11_03	0.2605	0.0058	0.0361	0.0006	0.5421	0.0524	0.0010	300.9	43.19	**228.6**	**3.77**	235.1	4.67	804879	372289	0.46	97.24
NT11_04	0.2550	0.0056	0.0359	0.0006	0.5553	0.0516	0.0010	268.5	42.5	**227**	**3.74**	230.7	4.52	663697	353663	0.53	98.40
NT11_05	0.2660	0.0056	0.0364	0.0006	0.5896	0.0531	0.0009	331	39.27	**230.3**	**3.78**	239.5	4.48	599571	336961	0.56	96.16
NT11_06	0.2479	0.0055	0.0352	0.0006	0.5568	0.0510	0.0010	242.4	42.77	**223.2**	**3.69**	224.8	4.43	610822	405799	0.66	99.29
NT11_07	0.2574	0.0049	0.0364	0.0006	0.6539	0.0513	0.0008	255.1	34.02	**230.4**	**3.72**	232.6	3.98	1499538	885230	0.59	99.05
NT11_08	0.2496	0.0069	0.0363	0.0006	0.4327	0.0498	0.0013	186.4	58.5	**230.1**	**3.98**	226.2	5.59	287021	190725	0.66	101.72
NT11_09	0.2560	0.0061	0.0352	0.0006	0.5056	0.0528	0.0011	319.5	47.46	**222.9**	**3.75**	231.4	4.95	433107	260672	0.60	96.33
NT11_10	0.2615	0.0061	0.0366	0.0006	0.5154	0.0518	0.0011	277.8	46.43	**231.7**	**3.88**	235.8	4.93	504844	302736	0.60	98.26
NT11_11	0.2576	0.0050	0.0344	0.0006	0.6550	0.0544	0.0008	386.2	33.53	217.8	3.54	232.7	4.01	1293685	1051763	0.81	93.60
NT11_12	0.2787	0.0061	0.0383	0.0007	0.5649	0.0528	0.0010	319.4	41.4	**242.3**	**4.01**	249.6	4.82	780692	500249	0.64	97.08
~~NT11_13~~	~~0.1602~~	~~0.0038~~	~~0.0190~~	~~0.0003~~	~~0.5008~~	~~0.0611~~	~~0.0013~~	~~643.3~~	~~45.35~~	~~121.4~~	~~2.08~~	~~150.8~~	~~3.36~~	~~807317~~	~~408421~~	~~0.51~~	~~80.50~~
NT11_14	0.2572	0.0058	0.0360	0.0006	0.5414	0.0519	0.0010	280.9	44.23	**227.7**	**3.8**	232.4	4.71	552499	291491	0.53	97.98
NT11_15	0.2655	0.0073	0.0368	0.0007	0.4373	0.0523	0.0013	297.9	56.69	**233.2**	**4.05**	239.1	5.83	259309	135991	0.52	97.53

Data in **bold** used for crystallisation weighted average age, concordance calculation using ($^{206}Pb/^{238}U$ age)/ $^{207}Pb/^{235}U$ age), concordant data within ±5% in green.

Supplementary Table 4 (continued). Main isotopes and ratios measured using LA–ICP–MS (GLITTER reduction).

Analysis #	Ratios							Ages						Concentrations (CPU)		Th:U	Concordance
	$^{207}Pb/^{235}U$	1σ	U	U	Rho	$^{207}Pb/^{206}Pb$	1σ	Pb^{207}/Pb^{206}	1σ	Pb^{206}/U^{238}	1σ	Pb^{207}/U^{235}	1σ	U	Th		
NT11_17	0.2627	0.0057	0.0362	0.0006	0.5699	0.0527	0.0010	315	41.07	**229.1**	**3.81**	236.9	4.59	579311	373965	0.65	96.71
NT11_18	0.2552	0.0052	0.0360	0.0006	0.6121	0.0514	0.0009	259.6	37.95	**228**	**3.75**	230.8	4.23	820310	350107	0.43	98.79
NT11_19	0.2614	0.0058	0.0354	0.0006	0.5597	0.0536	0.0010	352.8	42.74	**224.2**	**3.75**	235.8	4.7	528236	254960	0.48	95.08
NT11_20	0.2609	0.0068	0.0354	0.0006	0.4633	0.0535	0.0013	348	53	**224.3**	**3.87**	235.4	5.48	282139	171439	0.61	95.28
NT11_21	0.2465	0.0055	0.0355	0.0006	0.5650	0.0504	0.0010	212.9	43.64	**224.8**	**3.77**	223.7	4.5	591538	428390	0.72	100.49
NT11_22	0.2574	0.0057	0.0361	0.0006	0.5671	0.0518	0.0010	275.7	42.71	**228.3**	**3.83**	232.5	4.63	575069	329900	0.57	98.19
NT12_01	0.2678	0.0051	0.0375	0.0006	0.6834	0.2678	0.0051	279	32.36	**237**	**3.88**	240.9	4.05	1628806	900577	0.55	98.38
NT12_02	0.2768	0.0048	0.0374	0.0006	0.7471	0.2768	0.0048	354.9	26.9	**237**	**3.84**	248.1	3.84	8357772	849169	0.10	95.53
NT12_03	0.2923	0.0053	0.0390	0.0007	0.7221	0.2923	0.0053	388	29.04	246.4	4.02	260.3	4.16	3619378	539753	0.15	94.66
NT12_04	0.2612	0.0049	0.0372	0.0006	0.7008	0.2612	0.0049	235.6	31.36	**235.6**	**3.87**	235.7	3.91	3226508	524629	0.16	99.96
NT12_05	0.3233	0.0056	0.0379	0.0006	0.7596	0.3233	0.0056	671.3	25.05	239.6	3.89	284.4	4.3	12409518	1121413	0.09	84.25
NT12_06	0.2925	0.0050	0.0387	0.0006	0.7605	0.2925	0.0050	402.9	25.65	245	3.97	260.5	3.95	20552478	1258316	0.06	94.05
NT12_07	0.3082	0.0056	0.0381	0.0006	0.7398	0.3082	0.0056	555.7	27.36	240.9	3.95	272.8	4.31	16613185	1372436	0.08	88.31
NT12_08	0.2915	0.0057	0.0380	0.0006	0.6682	0.2915	0.0057	435.4	32.45	240.6	3.97	259.7	4.45	1376661	490030	0.36	92.65
NT12_09	0.2712	0.0048	0.0383	0.0006	0.7451	0.2712	0.0048	259.9	28.05	**242**	**3.94**	243.6	3.84	7734532	1856029	0.24	99.34
NT12_10	0.2701	0.0048	0.0384	0.0006	0.7495	0.2701	0.0048	241.8	27.59	**242.9**	**3.96**	242.8	3.79	12170251	1397713	0.11	100.04
NT12_11	0.2735	0.0059	0.0379	0.0007	0.6046	0.2735	0.0059	300.1	39.57	**239.8**	**4.03**	245.4	4.67	979453	214275	0.22	97.72
NT12_12	0.2547	0.0057	0.0366	0.0006	0.5915	0.2547	0.0057	215.9	42.01	**231.8**	**3.97**	230.4	4.58	2649860	448677	0.17	100.61
ST16_01	0.2769	0.0053	0.0356	0.0006	0.6166	0.0563	0.0009	464.9	34.36	225.4	3.58	248.2	4.17	1077470	193347	0.18	90.81
ST16_02	1.3825	0.0231	0.1469	0.0023	0.7153	0.0682	0.0008	873.2	25.34	883.5	13.15	881.5	9.83	675963	360024	0.53	100.23
ST16_03	1.9460	0.0422	0.1872	0.0032	0.5243	0.0752	0.0015	1075	38.16	1106.4	17.2	1097.1	14.53	94091	111410	1.18	100.85
ST16_04	1.5743	0.0272	0.1583	0.0025	0.6885	0.0720	0.0010	987.2	26.28	947.1	14.12	960.1	10.71	428663	164618	0.38	98.65
ST16_05	1.2881	0.0214	0.1387	0.0022	0.7207	0.0673	0.0008	846	25.2	837.2	12.53	840.4	9.51	668993	167038	0.25	99.62
ST16_06	0.6307	0.0127	0.0827	0.0014	0.5813	0.0552	0.0009	420.5	37.3	**512.4**	**8.07**	496.5	7.89	331160	255298	0.77	103.20
ST16_07	0.6276	0.0118	0.0799	0.0013	0.6287	0.0569	0.0009	485.5	33.86	**495.7**	**7.74**	494.6	7.37	518496	193271	0.37	100.22
~~ST16_08~~	~~*********~~	~~*********~~	~~49.2480~~	~~15.4537~~	#VALUE!	~~0.8538~~	~~0.0568~~	~~5014.2~~	~~91.15~~	~~******~~	~~1982.6~~	~~8801.1~~	~~316.62~~	~~9~~	~~33~~	~~3.67~~	-
ST16_09	3.8735	0.0631	0.2298	0.0037	0.7408	0.1221	0.0014	1986.8	20.6	1333.6	19.28	1608.2	13.15	449818	67181	0.15	82.93
ST16_10	1.5492	0.0250	0.0987	0.0016	0.7494	0.1137	0.0013	1859.8	20.39	606.6	9.24	950.2	9.95	1419898	162391	0.11	63.84
ST16_11	0.4493	0.0080	0.0593	0.0010	0.6759	0.0549	0.0008	407.1	29.99	371.5	5.81	376.8	5.57	1185078	382385	0.32	98.59
ST16_12	3.4456	0.0564	0.2607	0.0042	0.7398	0.0958	0.0011	1543.5	21.87	1493.1	21.39	1514.9	12.88	370583	133683	0.36	98.56
ST16_13	0.0830	0.0018	0.0131	0.0002	0.5594	0.0460	0.0008	0.1	40.52	83.7	1.37	81	1.65	2116068	127870	0.06	103.33

Data in **bold** used for crystallisation weighted average age, concordance calculation using ($^{206}Pb/^{238}U$ age)/ $^{207}Pb/^{235}U$ age), concordant data within ±5% in green.

Supplementary Table 4 (continued). Main isotopes and ratios measured using LA–ICP–MS (GLITTER reduction).

Analysis #	Ratios							Ages						Concentrations (CPU)		Th:U	Concordance
	$^{207}Pb/^{235}U$	1σ	U	U	Rho	$^{207}Pb/^{206}Pb$	1σ	Pb^{207}/Pb^{206}	1σ	Pb^{206}/U^{238}	1σ	Pb^{207}/U^{235}	1σ	U	Th		
ST16_14	1.0512	0.0216	0.1116	0.0019	0.5701	0.0682	0.0012	875.7	35.94	682.2	10.8	729.5	10.69	187845	50709	0.27	93.52
ST16_15	0.3153	0.0063	0.0405	0.0007	0.5950	0.0564	0.0009	465.9	36.76	256.1	4.13	278.3	4.85	795026	52768	0.07	92.02
ST16_16	0.6263	0.0120	0.0792	0.0013	0.6215	0.0573	0.0009	503.6	33.97	**491.2**	**7.74**	493.8	7.51	449520	230944	0.51	99.47
ST16_17	1.0141	0.0296	0.1186	0.0022	0.3810	0.0620	0.0017	673.1	58.76	722.5	12.49	710.9	14.92	54777	71500	1.31	101.63
ST16_18	0.6298	0.0108	0.0814	0.0013	0.6979	0.0561	0.0007	453.9	28.29	**504.6**	**7.84**	496	6.75	836366	390655	0.47	101.73
ST16_19	8.7675	0.1407	0.4116	0.0066	0.7488	0.1543	0.0018	2394.5	19.23	2222.3	30.34	2314.1	14.62	169321	109637	0.65	96.03
ST16_20	1.0454	0.0248	0.1165	0.0020	0.4863	0.0650	0.0014	775.2	44.68	710.5	11.63	726.6	12.33	91094	26203	0.29	97.78
ST16_21	0.3883	0.0091	0.0465	0.0008	0.4680	0.0605	0.0013	621.7	46.12	293	4.91	333.1	6.66	202847	137240	0.68	87.96
ST16_22	21.9048	0.3582	0.6335	0.0103	0.7587	0.2507	0.0028	3189.3	17.83	3163.5	40.64	3179.5	15.88	215953	61231	0.28	99.50
ST16_23	9.8746	0.1622	0.3157	0.0051	0.7591	0.2268	0.0026	3029.7	18.03	1768.8	25.09	2423.1	15.15	776664	38606	0.05	73.00
ST16_24	0.7237	0.0141	0.0785	0.0013	0.6297	0.0668	0.0011	832.1	32.51	487.4	7.8	552.9	8.29	377626	91907	0.24	88.15
ST16_25	1.8036	0.0330	0.1815	0.0030	0.6735	0.0721	0.0010	987.6	28.38	1075.3	16.34	1046.7	11.94	253797	140168	0.55	102.73
ST16_26	0.1446	0.0029	0.0206	0.0003	0.6024	0.0509	0.0009	237.5	37.95	131.4	2.16	137.2	2.59	1648384	12868	0.01	95.77
ST16_27	0.6195	0.0110	0.0738	0.0012	0.6991	0.0609	0.0008	633.9	28.35	459.3	7.27	489.5	6.9	1325745	95422	0.07	93.83
ST16_28	0.6951	0.0135	0.0756	0.0013	0.6301	0.0667	0.0011	828.3	32.43	469.8	7.55	535.9	8.11	405241	96577	0.24	87.67
ST49A_01	0.0842	0.0015	0.0128	0.0002	0.7062	0.0478	0.0006	86.1	32.16	**81.9**	**1.33**	82	1.41	8453616	625369	0.07	99.88
ST49A_02	0.0812	0.0018	0.0120	0.0002	0.5432	0.0493	0.0010	161.3	44.27	76.6	1.3	79.3	1.7	3528351	548877	0.16	96.60
ST49A_03	0.0790	0.0015	0.0126	0.0002	0.6520	0.0457	0.0007	0.1	15.52	**80.4**	**1.32**	77.2	1.42	3764066	678494	0.18	104.15
ST49A_04	0.0917	0.0017	0.0126	0.0002	0.6735	0.0528	0.0008	321.4	32.36	**80.7**	**1.32**	89.1	1.59	4504674	625384	0.14	90.57
ST49A_05	0.1999	0.0036	0.0136	0.0002	0.6857	0.1068	0.0015	1746	24.74	86.9	1.43	185	3.05	3074368	775177	0.25	46.97
ST49A_06	0.2696	0.0049	0.0066	0.0001	0.6574	0.2967	0.0043	3452.9	22.32	42.4	0.73	242.4	3.92	2366887	888877	0.38	17.49
ST49A_07	0.0919	0.0016	0.0125	0.0002	0.7220	0.0531	0.0007	334.5	28.49	**80.4**	**1.31**	89.3	1.5	11399266	985889	0.09	90.03
ST49A_08	0.5601	0.0101	0.0501	0.0008	0.6927	0.0810	0.0011	1222.2	26.39	315.4	5.06	451.6	6.58	2187646	853627	0.39	69.84
ST49A_09	0.0839	0.0016	0.0129	0.0002	0.6590	0.0470	0.0007	49.7	33.97	**82.9**	**1.36**	81.8	1.48	4877865	671654	0.14	101.34
ST49A_10	0.7090	0.0123	0.0158	0.0003	0.7211	0.3253	0.0041	3595	19.33	101.1	1.67	544.2	7.32	3022646	1466666	0.49	18.58
ST49A_11	0.6214	0.0108	0.0175	0.0003	0.7317	0.2573	0.0032	3230	19.48	112	1.84	490.7	6.75	4910135	1353380	0.28	22.82
ST49A_12	1.5405	0.0296	0.0177	0.0003	0.5897	0.6312	0.0110	4581.4	24.95	113.2	2.13	946.7	11.83	331059	237492	0.72	11.96
ST49A_13	0.1924	0.0034	0.0139	0.0002	0.7176	0.1001	0.0013	1626	23.71	89.3	1.46	178.6	2.9	7143984	1299171	0.18	50.00
ST49A_14	0.1286	0.0044	0.0128	0.0003	0.3037	0.0730	0.0025	1013.6	67.66	81.9	1.62	122.9	4	276858	232668	0.84	66.64
ST49A_15	0.0832	0.0019	0.0127	0.0002	0.5634	0.0474	0.0009	70.5	45.24	**81.5**	**1.38**	81.1	1.74	1702476	656164	0.39	100.49
ST49A_16	0.0841	0.0016	0.0127	0.0002	0.6825	0.0480	0.0007	99.1	34.42	**81.4**	**1.34**	82	1.47	6263415	979421	0.16	99.27

Data in **bold** used for crystallisation weighted average age, concordance calculation using ($^{206}Pb/^{238}U$ age)/ $^{207}Pb/^{235}U$ age), concordant data within ±5% in green.

Supplementary Table 4 (continued). Main isotopes and ratios measured using LA–ICP–MS (GLITTER reduction).

Analysis #	Ratios							Ages						Concentrations (CPU)		Th:U	Concordance
	$^{207}Pb/^{235}U$	1σ	U	U	Rho	$^{207}Pb/^{206}Pb$	1σ	Pb^{207}/Pb^{206}	1σ	Pb^{206}/U^{238}	1σ	Pb^{207}/U^{235}	1σ	U	Th		
ST49A_17	0.0887	0.0023	0.0124	0.0002	0.4680	0.0518	0.0012	278.3	52.38	79.5	1.39	86.3	2.12	879552	477369	0.54	92.12
ST49A_18	0.0900	0.0033	0.0123	0.0002	0.2999	0.0533	0.0019	342.4	79.28	78.5	1.52	87.5	3.07	320682	434279	1.35	89.71
ST49A_19	0.1082	0.0017	0.0130	0.0002	0.7631	0.0602	0.0006	609.6	22.87	83.3	1.3	104.3	1.54	20327612	2398055	0.12	79.87
ST49A_20	0.0831	0.0015	0.0127	0.0002	0.6579	0.0474	0.0007	68.9	34.11	**81.3**	**1.29**	81.1	1.4	3343201	671123	0.20	100.25
ST49A_21	0.3096	0.0058	0.0411	0.0007	0.6247	0.0545	0.0008	389.8	33.71	259.8	4.1	273.9	4.49	710919	207699	0.29	94.85
ST49A_22	0.1092	0.0017	0.0129	0.0002	0.7529	0.0611	0.0007	640.9	23.28	82.9	1.3	105.2	1.57	14538256	3402101	0.23	78.80
ST49A_23	0.1046	0.0020	0.0123	0.0002	0.6246	0.0614	0.0009	652.9	32.5	79	1.27	101	1.8	2099980	581853	0.28	78.22
ST49A_24	0.0780	0.0014	0.0122	0.0002	0.6744	0.0462	0.0006	6.6	32.9	78.3	1.24	76.2	1.31	3957549	676193	0.17	102.76
ST49A_25	0.0800	0.0015	0.0127	0.0002	0.6197	0.0458	0.0007	0.1	21.8	**81.1**	**1.3**	78.2	1.44	2648928	895237	0.34	103.71
ST49A_26	0.1000	0.0016	0.0128	0.0002	0.7564	0.0564	0.0006	467.4	24.47	82.2	1.29	96.8	1.46	12804619	1254642	0.10	84.92
ST49A_27	0.1119	0.0025	0.0124	0.0002	0.5113	0.0656	0.0013	794.4	41.78	79.1	1.33	107.7	2.3	967890	300731	0.31	73.44
ST49A_28	0.0805	0.0015	0.0121	0.0002	0.5840	0.0480	0.0008	101.1	37.27	77.6	1.24	78.6	1.43	1987873	488773	0.25	98.73
ST49A_29	0.1056	0.0021	0.0126	0.0002	0.6014	0.0608	0.0010	630.5	34.97	80.7	1.31	101.9	1.91	1877908	744987	0.40	79.20
ST49A_30	0.1019	0.0027	0.0126	0.0002	0.4214	0.0587	0.0015	555.2	52.94	80.5	1.4	98.5	2.47	605368	362917	0.60	81.73
ST49A_31	0.0770	0.0015	0.0119	0.0002	0.6335	0.0469	0.0007	45	35.39	76	1.23	75.3	1.36	4978989	909817	0.18	100.93
ST49A_32	0.0951	0.0016	0.0123	0.0002	0.7322	0.0558	0.0007	442.6	26.02	79.1	1.25	92.3	1.46	8334582	1087678	0.13	85.70
TH112_01	0.2212	0.0050	0.0325	0.0005	0.5163	0.0493	0.0010	161.4	45.66	**206.2**	**3.39**	202.9	4.13	489601	369993	0.76	101.63
TH112_02	0.2196	0.0050	0.0321	0.0005	0.5109	0.0495	0.0010	173.4	46.25	**203.6**	**3.35**	201.6	4.14	445760	117084	0.26	100.99
TH112_03	0.2279	0.0049	0.0327	0.0005	0.5466	0.0505	0.0009	216.7	42.43	**207.4**	**3.39**	208.4	4.05	563931	291825	0.52	99.52
TH112_04	0.6211	0.0112	0.0410	0.0007	0.6608	0.1098	0.0016	1795.3	25.78	258.8	4.18	490.5	7	557686	176210	0.32	52.76
TH112_05	0.2190	0.0040	0.0327	0.0005	0.6590	0.0485	0.0007	121.5	33.92	**207.6**	**3.31**	201.1	3.37	1250999	111042	0.09	103.23
TH112_06	0.2400	0.0060	0.0325	0.0006	0.4547	0.0536	0.0012	352.2	51.03	205.8	3.48	218.4	4.9	294362	179337	0.61	94.23
TH112_07	0.2232	0.0051	0.0328	0.0006	0.5219	0.0494	0.0010	165.1	46.39	**207.8**	**3.43**	204.6	4.22	468053	159543	0.34	101.56
TH112_08	0.2180	0.0050	0.0324	0.0005	0.5109	0.0488	0.0010	136.8	46.88	**205.4**	**3.4**	200.2	4.16	471454	140675	0.30	102.60
TH112_09	0.2353	0.0049	0.0333	0.0006	0.5838	0.0513	0.0009	252.9	39.65	**210.9**	**3.43**	214.5	4	748756	132073	0.18	98.32
TH112_10	0.2274	0.0041	0.0332	0.0005	0.6758	0.0496	0.0007	177.3	31.98	210.4	3.36	208	3.39	1537575	117928	0.08	101.15
TH112_11	0.2304	0.0048	0.0327	0.0005	0.5771	0.0511	0.0009	246.8	40.12	**207.1**	**3.38**	210.6	3.96	673401	74695	0.11	98.34
TH112_12	0.2306	0.0042	0.0326	0.0005	0.6647	0.0512	0.0007	250.8	32.57	**206.7**	**3.31**	210.7	3.47	1224589	1024180	0.84	98.10
TH112_13	0.2227	0.0044	0.0323	0.0005	0.6117	0.0500	0.0008	192.5	37.07	**204.9**	**3.34**	204.2	3.65	857604	136763	0.16	100.34
TH112_14	0.2258	0.0056	0.0327	0.0006	0.4768	0.0500	0.0011	194.8	51.69	**207.6**	**3.54**	206.8	4.66	447537	295504	0.66	100.39
TH112_15	0.2168	0.0056	0.0319	0.0006	0.4572	0.0493	0.0012	161.4	54.26	**202.2**	**3.46**	199.2	4.66	339090	159415	0.47	101.51

Data in **bold** used for crystallisation weighted average age, concordance calculation using ($^{206}Pb/^{238}U$ age)/ $^{207}Pb/^{235}U$ age), concordant data within ±5% in green.

Supplementary Table 4 (continued). Main isotopes and ratios measured using LA–ICP–MS (GLITTER reduction).

Analysis #	Ratios							Ages						Concentrations (CPU)		Th:U	Concordance
	$^{207}Pb/^{235}U$	1σ	U	U	Rho	$^{207}Pb/^{206}Pb$	1σ	Pb^{207}/Pb^{206}	1σ	Pb^{206}/U^{238}	1σ	Pb^{207}/U^{235}	1σ	U	Th		
TH112_16	0.2385	0.0076	0.0327	0.0006	0.3558	0.0529	0.0016	325.2	67.8	**207.2**	**3.77**	217.2	6.19	177257	87892	0.50	95.40
TH112_17	0.2179	0.0057	0.0330	0.0006	0.4532	0.0478	0.0012	90	57.07	**209.4**	**3.59**	200.1	4.76	328316	177981	0.54	104.65
TH112_18	0.2249	0.0041	0.0329	0.0005	0.6824	0.0495	0.0007	170.7	32.26	**208.9**	**3.38**	206	3.41	1602559	371834	0.23	101.41
TH112_19	0.2524	0.0055	0.0319	0.0005	0.5522	0.0573	0.0011	503.4	41.27	202.5	3.39	228.5	4.47	534447	214047	0.40	88.62
TH112_20	0.2948	0.0051	0.0346	0.0006	0.7268	0.0617	0.0008	662.4	26.48	219.5	3.53	262.3	3.99	2246645	140972	0.06	83.68
TH112_21	0.7550	0.0129	0.0912	0.0015	0.7285	0.0600	0.0007	601.8	26.32	562.9	8.82	571.1	7.47	938163	253055	0.27	98.56
TH112_22	0.3935	0.0079	0.0484	0.0008	0.6184	0.0589	0.0010	563.8	35.06	304.8	4.99	336.9	5.73	595482	192766	0.32	90.47
TH112_23	0.2380	0.0047	0.0331	0.0006	0.6213	0.0521	0.0008	289.9	36.18	**210**	**3.45**	216.7	3.87	936231	155234	0.17	96.91
TH112_24	0.2459	0.0072	0.0332	0.0006	0.3889	0.0538	0.0015	361.5	61.62	210.3	3.76	223.3	5.89	201914	149234	0.74	94.18
TH112_25	0.2275	0.0046	0.0324	0.0005	0.6096	0.0509	0.0009	237.4	38.03	**205.4**	**3.39**	208.1	3.83	831435	181146	0.22	98.70
TH112_26	0.2252	0.0045	0.0326	0.0006	0.6191	0.0501	0.0008	198.1	37.46	**206.8**	**3.41**	206.2	3.74	876232	281269	0.32	100.29
TH112_27	0.2268	0.0045	0.0320	0.0005	0.6271	0.0514	0.0008	257.4	36.88	**203**	**3.35**	207.5	3.75	851914	107253	0.13	97.83
TH112_28	0.2235	0.0043	0.0331	0.0006	0.6520	0.0489	0.0007	144.9	34.97	209.9	3.44	204.8	3.56	1202843	89143	0.07	102.49
TH112_29	0.5434	0.0094	0.0656	0.0011	0.7354	0.0601	0.0007	606.8	26.34	409.4	6.53	440.7	6.19	2317146	365950	0.16	92.90
TH112_30	0.2565	0.0048	0.0337	0.0006	0.6829	0.0552	0.0008	419.3	31.2	213.7	3.5	231.9	3.86	1426684	179125	0.13	92.15
TH112_31	0.2795	0.0078	0.0331	0.0006	0.4172	0.0611	0.0016	644.3	55.55	210.2	3.78	250.2	6.21	373013	221761	0.59	84.01
TH112_32	0.2159	0.0043	0.0321	0.0005	0.6386	0.0487	0.0008	133.5	36.93	203.9	3.37	198.5	3.58	1060789	87939	0.08	102.72
TH112_33	0.2181	0.0052	0.0320	0.0006	0.5211	0.0495	0.0010	172.2	47.93	**202.7**	**3.45**	200.4	4.31	480007	82462	0.17	101.15
TH112_34	0.2284	0.0056	0.0321	0.0006	0.4926	0.0515	0.0011	264	49.99	**203.9**	**3.51**	208.9	4.66	384087	163299	0.43	97.61
TH112_35	0.2622	0.0060	0.0340	0.0006	0.5304	0.0560	0.0011	450.1	43.82	215.4	3.67	236.4	4.86	421139	97584	0.23	91.12
TH112_36	0.2463	0.0046	0.0326	0.0006	0.6823	0.0547	0.0008	400.1	31.41	207	3.4	223.5	3.75	1286648	235314	0.18	92.62
TH112_37	0.2338	0.0044	0.0333	0.0006	0.6848	0.0509	0.0007	234.9	32.4	211.3	3.47	213.4	3.58	1444003	102445	0.07	99.02
TH112_38	0.2224	0.0044	0.0325	0.0006	0.6375	0.0496	0.0008	174.7	36.83	**206.4**	**3.43**	203.9	3.69	1052491	106619	0.10	101.23
TH111_01	0.2469	0.0062	0.0351	0.0006	0.5023	0.0510	0.0011	239.2	50.5	**222.6**	**3.87**	224	5.01	363709	99563	0.27	99.38
TH111_02	0.2591	0.0090	0.0355	0.0007	0.3261	0.0530	0.0018	329.2	75.22	**224.6**	**4.28**	234	7.29	123127	63106	0.51	95.98
TH111_03	0.2482	0.0055	0.0354	0.0006	0.5774	0.0508	0.0009	232.7	42.07	**224.3**	**3.81**	225.1	4.43	569514	137461	0.24	99.64
TH111_04	0.2524	0.0070	0.0361	0.0007	0.4385	0.0508	0.0013	231.2	58.35	**228.3**	**4.08**	228.5	5.7	312788	50870	0.16	99.91
TH111_05	0.2550	0.0073	0.0355	0.0007	0.4242	0.0520	0.0014	286.8	59.5	**225.1**	**4.05**	230.6	5.88	212966	69942	0.33	97.61
TH111_06	0.2978	0.0076	0.0366	0.0007	0.4850	0.0590	0.0014	567.1	49.55	231.8	4.1	264.7	5.96	262733	56588	0.22	87.57
TH111_07	0.2930	0.0077	0.0378	0.0007	0.4674	0.0563	0.0014	463.1	52.83	238.8	4.24	260.9	6.06	280087	47995	0.17	91.53
TH111_08	0.2426	0.0051	0.0355	0.0006	0.6159	0.0496	0.0009	177.7	39.66	**224.6**	**3.8**	220.5	4.18	733478	142689	0.19	101.86

Data in **bold** used for crystallisation weighted average age, concordance calculation using ($^{206}Pb/^{238}U$ age)/ $^{207}Pb/^{235}U$ age), concordant data within ±5% in green.

Supplementary Table 4 (continued). Main isotopes and ratios measured using LA–ICP–MS (GLITTER reduction).

Analysis #	Ratios							Ages						Concentrations (CPU)		Th:U	Concordance
	$^{207}Pb/^{235}U$	1σ	U	U	Rho	$^{207}Pb/^{206}Pb$	1σ	Pb^{207}/Pb^{206}	1σ	Pb^{206}/U^{238}	1σ	Pb^{207}/U^{235}	1σ	U	Th		
TH111_09	0.2665	0.0080	0.0356	0.0007	0.4025	0.0543	0.0015	384.3	61.93	225.5	4.13	239.9	6.4	190849	84067	0.44	94.00
TH111_10	0.2746	0.0072	0.0373	0.0007	0.4765	0.0535	0.0013	348.9	53.1	**235.8**	**4.17**	246.4	5.75	281083	94244	0.34	95.70
TH111_11	0.2329	0.0101	0.0346	0.0007	0.2519	0.0489	0.0021	140.6	97.72	**219.2**	**4.53**	212.6	8.27	153714	70856	0.46	103.10
TH111_12	0.2131	0.0080	0.0363	0.0007	0.3178	0.0425	0.0015	0.1	0	230.1	4.26	196.1	6.68	175351	65130	0.37	117.34
TH111_13	0.2473	0.0075	0.0358	0.0007	0.3975	0.0501	0.0014	199.6	65.35	**226.8**	**4.15**	224.4	6.13	189305	93860	0.50	101.07
TH111_14	0.2553	0.0049	0.0367	0.0006	0.6794	0.0504	0.0007	215	33.47	**232.4**	**3.89**	230.8	3.97	1299193	319518	0.25	100.69
TH111_15	0.2636	0.0051	0.0367	0.0006	0.6846	0.0521	0.0008	291.1	33.07	**232.3**	**3.9**	237.6	4.07	1314595	160480	0.12	97.77
TH111_16	0.2493	0.0047	0.0362	0.0006	0.6928	0.0500	0.0007	195.7	32.48	**229**	**3.83**	226	3.82	1557280	201632	0.13	101.33
TH111_17	0.2568	0.0076	0.0358	0.0007	0.4111	0.0520	0.0015	285.2	62.63	**226.9**	**4.16**	232.1	6.18	186547	74414	0.40	97.76
TH111_18	0.2509	0.0083	0.0356	0.0007	0.3625	0.0512	0.0016	249.8	71.36	**225.2**	**4.24**	227.3	6.74	148745	63609	0.43	99.08
TH111_19	0.3021	0.0067	0.0370	0.0007	0.5776	0.0592	0.0011	575.8	40.07	234.2	4.05	268.1	5.23	476598	110412	0.23	87.36
TH111_20	0.2440	0.0061	0.0360	0.0006	0.5074	0.0492	0.0011	158.6	50.91	**227.8**	**4**	221.7	4.98	359852	93543	0.26	102.75
TH111_21	0.2380	0.0080	0.0354	0.0007	0.3591	0.0488	0.0016	135.8	74.18	**224.4**	**4.23**	216.8	6.57	149774	76126	0.51	103.51
TH111_22	0.2428	0.0066	0.0360	0.0007	0.4606	0.0489	0.0012	145.2	56.92	**228**	**4.07**	220.7	5.38	268988	130708	0.49	103.31
~~TH111_23~~	~~1.0331~~	~~0.0204~~	~~0.0503~~	~~0.0009~~	~~0.6578~~	~~0.1491~~	~~0.0023~~	~~2336.1~~	~~26.57~~	~~316.1~~	~~5.47~~	~~720.5~~	~~10.21~~	~~370271~~	~~183963~~	~~0.50~~	~~43.87~~
TH111_24	0.2501	0.0071	0.0365	0.0007	0.4359	0.0497	0.0013	180.9	60.29	**231.2**	**4.19**	226.7	5.8	226090	41108	0.18	101.99
TH111_25	0.2595	0.0062	0.0363	0.0007	0.5405	0.0519	0.0011	280.2	46.94	**229.8**	**4.02**	234.3	5.03	451678	156723	0.35	98.08
TH111_26	0.2580	0.0051	0.0369	0.0006	0.6747	0.0508	0.0008	231.8	34.42	**233.3**	**3.95**	233	4.12	1422959	171501	0.12	100.13
TH111_27	0.2439	0.0078	0.0353	0.0007	0.3885	0.0501	0.0015	201.1	68.61	**223.6**	**4.21**	221.6	6.34	302933	72953	0.24	100.90
TH111_28	0.2953	0.0084	0.0368	0.0007	0.4437	0.0582	0.0015	536.6	56.99	233.1	4.27	262.7	6.56	218971	104534	0.48	88.73
TH111_29	0.2750	0.0092	0.0366	0.0007	0.3615	0.0545	0.0018	392.6	69.58	231.7	4.46	246.7	7.32	224816	33561	0.15	93.92
TH111_30	0.2636	0.0055	0.0377	0.0007	0.6347	0.0508	0.0009	229.3	38.25	**238.5**	**4.09**	237.5	4.44	931079	309594	0.33	100.42
~~TH111_31~~	~~0.8332~~	~~0.0160~~	~~0.0732~~	~~0.0013~~	~~0.7034~~	~~0.0826~~	~~0.0012~~	~~1258.7~~	~~27.4~~	~~455.6~~	~~7.64~~	~~615.4~~	~~8.85~~	~~668075~~	~~105302~~	~~0.16~~	~~74.03~~
TH111_32	0.2414	0.0070	0.0356	0.0007	0.4259	0.0492	0.0013	157.2	61.42	**225.6**	**4.11**	219.5	5.69	214718	73008	0.34	102.78

Data in **bold** used for crystallisation weighted average age, concordance calculation using ($^{206}Pb/^{238}U$ age)/ $^{207}Pb/^{235}U$ age), concordant data within ±5% in green.

Supplementary Table 4 (continued). Main isotopes and ratios measured using Multicollector (Hf analyses)

Analysis #	Age Used for Hf	Type of age	$^{176}Hf/^{177}Hf$	2σ	$^{176}Lu/^{177}Hf$	$^{176}Yb/^{177}Hf$	$(^{176}Hf/^{177}Hf)_i$	$\varepsilon Hf_{(t)}$	2s	$^{Hf}T_{DM}$(Ga)	$^{Hf}T_{NC}$ (Ga)
RDT16053-097.d	204.1	Pb^{206}/U^{238} weighted average age	0.282333	0.000038	0.002949	0.0903	0.282322	-11.8556	1.33	1.955476	1.757386
RDT16053-099.d	204.1	Pb^{206}/U^{238} weighted average age	0.282211	0.000029	0.00125	0.0467	0.282206	-15.9425	1.015	2.20948	2.012328
RDT16053-101.d	204.1	Pb^{206}/U^{238} weighted average age	0.282169	0.000045	0.00283	0.0975	0.282158	-17.6416	1.575	2.314724	2.11796
RDT16053-103.d	204.1	Pb^{206}/U^{238} weighted average age	0.282362	0.000049	0.004	0.1142	0.282347	-10.9714	1.715	1.900366	1.702072
RDT16053-113.d	204.1	Pb^{206}/U^{238} weighted average age	0.28225	0.000042	0.00418	0.1355	0.282234	-14.9581	1.47	2.148407	1.95103
RDT16053-114.d	204.1	Pb^{206}/U^{238} weighted average age	0.282145	0.000041	0.003622	0.1215	0.282131	-18.5975	1.435	2.373847	2.1773
RDT16053-115.d	204.1	Pb^{206}/U^{238} weighted average age	0.282372	0.000059	0.00307	0.0764	0.28236	-10.4921	2.065	1.87047	1.672065
RDT16053-119.d	204.1	Pb^{206}/U^{238} weighted average age	0.282206	0.000037	0.002776	0.08751	0.282195	-16.3253	1.295	2.233208	2.036144
RDT16053-121.d	204.1	Pb^{206}/U^{238} weighted average age	0.282173	0.000024	0.003752	0.1135	0.282159	-17.6245	0.84	2.313665	2.116897
RDT16053-123.d	204.1	Pb^{206}/U^{238} weighted average age	0.282207	0.000025	0.002582	0.0718	0.282197	-16.2638	0.875	2.229393	2.032315
KM20-177.d	229.9	Pb^{206}/U^{238} weighted average age	0.282852	0.000033	0.000645		0.282849	7.38042	1.155	0.76371	0.561878
KM20-178.d	229.9	Pb^{206}/U^{238} weighted average age	0.282813	0.000039	0.000607		0.28281	6.006413	1.365	0.851128	0.649625
KM20-179.d	229.9	Pb^{206}/U^{238} weighted average age	0.282759	0.000047	0.00084		0.282755	4.060438	1.645	0.974692	0.773654
KM20-185.d	229.9	Pb^{206}/U^{238} weighted average age	0.282842	0.000043	0.000852		0.282838	6.995175	1.505	0.788235	0.586495
KM20-215.d	229.9	Pb^{206}/U^{238} weighted average age	0.282798	0.000041	0.000842		0.282794	5.439978	1.435	0.887125	0.685757
KM20-218.d	229.9	Pb^{206}/U^{238} weighted average age	0.282956	0.000069	0.001134		0.282951	10.98572	2.415	0.533652	0.33095
KM20-224.d	229.9	Pb^{206}/U^{238} weighted average age	0.282833	0.000059	0.000875		0.282829	6.673283	2.065	0.808718	0.607055
rdt15_076-10.d	962	***Pb^{206}/U^{238} zircon age***	0.282421	0.000072	0.001825	0.04668	0.282388	7.485719	2.52	1.332069	1.152453
rdt15_076-13.d	1034	***Pb^{206}/U^{238} zircon age***	0.282033	0.000064	0.000715	0.01532	0.282019	-3.95874	2.24	2.096396	1.921267
rdt15_076-19.d	1022	***Pb^{206}/U^{238} zircon age***	0.281975	0.000046	0.00132	0.0279	0.28195	-6.6929	1.61	2.254888	2.079954
rdt15_076-43.d	929	***Pb^{206}/U^{238} zircon age***	0.282247	0.000054	0.00201	0.0375	0.282212	0.499385	1.89	1.740378	1.561231
rdt15_076-45.d	813	***Pb^{206}/U^{238} zircon age***	0.282396	0.000049	0.00067	0.0132	0.282386	4.042346	1.715	1.429893	1.246535
rdt15_076-55.d	899	***Pb^{206}/U^{238} zircon age***	0.28236	0.000045	0.00241	0.0417	0.282319	3.626678	1.575	1.522959	1.342265
NT10_01	236.6	Pb^{206}/U^{238} weighted average age	0.282496	0.000039	0.003186	0.0786	0.282482	-5.47	1.365	1.58	1.38
NT10_02	236.6	Pb^{206}/U^{238} weighted average age	0.282517	0.000059	0.001077	0.02614	0.282512	-4.39	2.065	1.51	1.31
NT10_12	236.6	Pb^{206}/U^{238} weighted average age	0.282606	0.000064	0.001983	0.04823	0.282597	-1.39	2.24	1.32	1.12
NT10_13	236.6	Pb^{206}/U^{238} weighted average age	0.282572	0.000032	0.002254	0.05453	0.282562	-2.63	1.12	1.40	1.20
NT10_17	236.6	Pb^{206}/U^{238} weighted average age	0.282631	0.000049	0.002668	0.0659	0.282619	-0.61	1.715	1.28	1.08
NT09_05	226.5	Pb^{206}/U^{238} weighted average age	0.282519	0.000052	0.001216	0.03748	0.282514	-4.56	1.82	1.52	1.32
NT09_06	226.5	Pb^{206}/U^{238} weighted average age	0.282531	0.000041	0.0018	0.05385	0.282523	-4.22	1.435	1.49	1.30
NT09_09	226.5	Pb^{206}/U^{238} weighted average age	0.282441	0.000054	0.001115	0.03566	0.282436	-7.31	1.89	1.69	1.49

Analysis #	Age Used for Hf	Type of age	$^{176}Hf/^{177}Hf$	2σ	$^{176}Lu/^{177}Hf$	$^{176}Yb/^{177}Hf$	$(^{176}Hf/^{177}Hf)_i$	$\varepsilon Hf_{(t)}$	2s	$^{Hf}T_{DM}$(Ga)	$^{Hf}T_{NC}$ (Ga)
NT09_12	226.5	Pb^{206}/U^{238} weighted average age	0.282550	0.00005	0.00089	0.02758	0.282546	-3.42	1.75	1.44	1.24
NT09_13	226.5	Pb^{206}/U^{238} weighted average age	0.282494	0.000066	0.001061	0.0352	0.282490	-5.42	2.31	1.57	1.37
NT09_16	226.5	Pb^{206}/U^{238} weighted average age	0.282503	0.000058	0.001396	0.04814	0.282497	-5.15	2.03	1.55	1.35
NT09_17	226.5	Pb^{206}/U^{238} weighted average age	0.282482	0.000053	0.001361	0.04941	0.282476	-5.89	1.855	1.60	1.40
NT09_21	226.5	Pb^{206}/U^{238} weighted average age	0.282555	0.000042	0.000864	0.02941	0.282551	-3.23	1.47	1.43	1.23
NT09_23	226.5	Pb^{206}/U^{238} weighted average age	0.282503	0.000059	0.000945	0.0344	0.282499	-5.09	2.065	1.55	1.35
NT11_01	228.7	Pb^{206}/U^{238} weighted average age	0.282785	0.000052	0.00197	0.0456	0.282777	4.78	1.82	0.93	0.73
NT11_02	228.7	Pb^{206}/U^{238} weighted average age	0.282778	0.000049	0.001594	0.0385	0.282771	4.59	1.715	0.94	0.74
NT11_06	228.7	Pb^{206}/U^{238} weighted average age	0.282752	0.000052	0.001547	0.03743	0.282745	3.68	1.82	1.00	0.80
NT11_07	228.7	Pb^{206}/U^{238} weighted average age	0.282817	0.00005	0.002435	0.05988	0.282807	5.85	1.75	0.86	0.66
NT11_14	228.7	Pb^{206}/U^{238} weighted average age	0.282419	0.000071	0.001659	0.0409	0.282412	-8.12	2.485	1.74	1.54
NT11_15	228.7	Pb^{206}/U^{238} weighted average age	0.282756	0.000044	0.00202	0.0512	0.282728	3.05	1.61	1.04	0.84
NT11_18	228.7	Pb^{206}/U^{238} weighted average age	0.282731	0.000046	0.000798	0.0215	0.282728	3.05	1.61	1.04	0.84
NT11_21	228.7	Pb^{206}/U^{238} weighted average age	0.282743	0.000047	0.00226	0.0658	0.282733	3.25	1.645	1.02	0.82
NT11_22	228.7	Pb^{206}/U^{238} weighted average age	0.282735	0.000052	0.000787	0.02135	0.282732	3.19	1.82	1.03	0.83
ST16_02	883.5	Pb^{206}/U^{238} zircon age	0.282044	0.000051	0.000844	0.0332	0.282030	-6.97	1.785	2.17	1.99
ST16_03	1106.4	Pb^{206}/U^{238} zircon age	0.282124	0.000043	0.000568	0.0206	0.282112	0.98	1.505	1.85	1.67
ST16_04	947.1	Pb^{206}/U^{238} zircon age	0.281434	0.000048	0.000736	0.02823	0.281421	-27.12	1.68	3.44	3.26
ST16_05	837.2	Pb^{206}/U^{238} zircon age	0.282018	0.000045	0.000401	0.01466	0.282012	-8.66	1.575	2.24	2.06
ST16_16	491.2	Pb^{206}/U^{238} zircon age	0.282343	0.000048	0.000371	0.01349	0.282340	-4.82	1.68	1.73	1.54
ST16_17	722.5	Pb^{206}/U^{238} zircon age	0.281745	0.000046	0.000422	0.01598	0.281739	-20.89	1.61	2.90	2.72
ST16_19	2394.5	Pb^{207}/Pb^{206} zircon age	0.280927	0.000054	0.000349	0.01389	0.280911	-12.07	1.89	3.63	3.49
ST16_20	710.5	Pb^{206}/U^{238} zircon age	0.281964	0.000037	0.000839	0.03305	0.281953	-13.60	1.295	2.44	2.26
ST49A_01	81.4	Pb^{206}/U^{238} weighted average age	0.282379	0.000065	0.001408	0.0514	0.282377	-12.63	2.275	1.91	1.71
ST49A_02	81.4	Pb^{206}/U^{238} weighted average age	0.282387	0.000051	0.000661	0.02658	0.282386	-12.31	1.785	1.89	1.69
ST49A_16	81.4	Pb^{206}/U^{238} weighted average age	0.282334	0.000045	0.001966	0.0818	0.282331	-14.25	1.575	2.01	1.81
ST49A_20	81.4	Pb^{206}/U^{238} weighted average age	0.282329	0.000055	0.00172	0.085	0.282326	-14.42	1.925	2.02	1.82
ST49A_28	81.4	Pb^{206}/U^{238} weighted average age	0.282337	0.000089	0.00075	0.0351	0.282336	-14.08	3.115	2.00	1.80
ST49A_30	81.4	Pb^{206}/U^{238} weighted average age	0.282403	0.000064	0.000463	0.01961	0.282402	-11.73	2.24	1.86	1.65
TH112_02	206.4	Pb^{206}/U^{238} weighted average age	0.282323	0.000058	0.00229	0.08595	0.282314	-12.07	2.03	1.97	1.77
TH112_07	206.4	Pb^{206}/U^{238} weighted average age	0.282239	0.000045	0.001299	0.0493	0.282234	-14.91	1.575	2.15	1.95
TH112_10	206.4	Pb^{206}/U^{238} weighted average age	0.282110	0.000054	0.002062	0.07188	0.282102	-19.58	1.89	2.44	2.24

Supplementary Table 4 (continued). Main isotopes and ratios measured using Multicollector (Hf analyses)

Analysis #	Age Used for Hf	Type of age	$^{176}Hf/^{177}Hf$	2σ	$^{176}Lu/^{177}Hf$	$^{176}Yb/^{177}Hf$	$(^{176}Hf/^{177}Hf)_i$	$\varepsilon Hf_{(t)}$	2s	$^{Hf}T_{DM}$(Ga)	$^{Hf}T_{NC}$ (Ga)
TH112_15	206.4	Pb^{206}/U^{238} weighted average age	0.282330	0.000058	0.000807	0.02874	0.282327	-11.62	2.03	1.94	1.74
TH112_26	206.4	Pb^{206}/U^{238} weighted average age	0.282330	0.000074	0.001732	0.0587	0.282323	-11.75	2.59	1.95	1.75
TH112_37	206.4	Pb^{206}/U^{238} weighted average age	0.282255	0.000039	0.003336	0.1069	0.282242	-14.61	1.365	2.13	1.93
TH111_01	227.9	Pb^{206}/U^{238} weighted average age	0.282687	0.000047	0.00466	0.1182	0.282667	0.89	1.645	1.17	0.973262
TH111_03	227.9	Pb^{206}/U^{238} weighted average age	0.282739	0.00005	0.002397	0.06569	0.282729	3.07	1.75	1.04	0.83
TH111_04	227.9	Pb^{206}/U^{238} weighted average age	0.282742	0.000055	0.00116	0.03237	0.282737	3.37	1.925	1.02	0.82
TH111_13	227.9	Pb^{206}/U^{238} weighted average age	0.282716	0.000048	0.001882	0.0542	0.282708	2.34	1.68	1.082241	0.88
TH111_14	227.9	Pb^{206}/U^{238} weighted average age	0.282732	0.000063	0.00379	0.111	0.282716	2.62	2.205	1.064606	0.86
TH111_18	227.9	Pb^{206}/U^{238} weighted average age	0.282719	0.000055	0.00174	0.05102	0.282712	2.47	1.925	1.07	0.87
TH111_26	227.9	Pb^{206}/U^{238} weighted average age	0.282695	0.000041	0.004471	0.1374	0.282676	1.21	1.435	1.15	0.95

Supplementary Table 5. Lu–Hf Standards and Analytical Parameters

Analysis Date	Samples Analysed	MT $^{176}Hf/^{177}Hf$ Weighted Average	R33 $^{176}Hf/^{177}Hf$ Weighted Average	R33 Lu Hf ratio Weighted Average	FC $^{176}Hf/^{177}Hf$ Weighted Average	GJ-1 $^{176}Hf/^{177}Hf$ Weighted Average	Plešovice $^{176}Hf/^{177}Hf$ Weighted Average	91500 $^{176}Hf/^{177}Hf$ Weighted Average
10/03/2017 to 11/03/2017 (Curtin University)	NT-09, NT-10, NT-11, NT-12, RDT15_076A, ST-16, ST-49A, Th11/01, Th11/02	0.2825064±0.0000097 (*n* =29, MSWD=0.89)	0.282718±0.000010 (*n* =28, MSWD=1.14)	0.0019903±0.0000097 (*n* =28, MSWD=19)	0.282173±0.000022 (*n* =12, MSWD=2.3)	0.2820093±0.0000089 (*n* =28, MSWD=0.92)	0.282471±0.000013 (*n* =12, MSWD=0.54)	0.282299±0.000011 (*n* =29, MSWD=1.16)
11/07/2017 (Curtin University)	RDT16_053	0.2825071±0.0000081 (*n* =29, MSWD=0.041)	0.282708±0.000017 (*n* =14, MSWD = 3.6)	0.001988±0.000040 (*n* =14, MSWD=101)	0.282159±0.000019 (*n* =15, MSWD=4.9)	0.282001±0.000019 (*n* =10, MSWD=2.7)	N/A	0.282291±0.000011 (*n* =9, MSWD=0.16)
30/01/2018 (University of Wollongong)	KM-20	0.282473±0.000023 (n=2, MSWD =0.0117)	N/A	N/A	N/A	N/A	0.282450±0.000018 (n=2, MSWD=0.14)	N/A

Supplementary Table 6. Whole-rock major and trace elements

Sample #	KM 12	KM 18	KM 25	KM 26	KM 40A	NT-01	NT-04	NT-06	NT-07	NT-13	NT-17	ST-03	RDGEOCHEM1	RDT16_053
SiO2	71.77	57.01	61.68	67.12	75.38	74.77	63.29	40.46	62.28	77.10	74.75	75.93	80.73	76.33
TiO2	0.24	0.91	0.79	0.43	0.10	0.14	0.39	1.17	1.53	0.10	0.11	0.02	0.54	0.02
Al2O3	14.37	15.92	15.86	16.60	13.67	14.24	16.63	20.71	14.85	13.01	13.89	14.23	14.37	13.44
Fe2O3T	2.73	8.59	7.80	3.39	0.89	1.43	4.08	14.61	7.40	1.37	1.40	0.68	3.10	0.44
MnO	0.06	0.15	0.18	0.06	0.03	0.05	0.09	0.18	0.11	0.03	0.05	0.04	0.02	0.03
MgO	0.42	4.84	2.22	1.62	0.22	0.25	2.51	5.57	1.93	0.29	0.28	0.11	0.10	0.15
CaO	1.70	7.47	5.16	4.08	0.87	0.41	5.33	14.49	3.41	0.30	0.57	0.31	0.06	1.15
Na2O	4.76	2.94	4.09	4.46	2.95	2.99	5.25	1.68	5.37	3.43	3.17	4.65	0.09	3.90
K2O	3.52	2.21	1.92	2.05	5.76	5.45	1.75	0.23	2.43	4.33	5.22	3.85	0.74	4.58
P2O5	0.09	0.21	0.20	0.15	0.08	0.26	0.14	0.51	0.26	0.05	.0.15	0.35	0.08	0.15
Total	**99.66**	**100.25**	**99.90**	**99.96**	**99.95**	**99.99**	**99.46**	**99.61**	**99.57**	**100.01**	**99.44**	**100.17**	**99.83**	**100.19**
LOI	0.62	1.20	1.06	1.10	0.65	1.74	0.64	0.94	1.30	0.92	1.13	0.45	5.19	0.49
Rb	148.6	70.4	48.8	83.2	390.7	753.8	34.7	2.6	44.5	223.6	561.7	904.4	14.5	422.1
Sr	126	367	288	442	105	52	935	861	183	85	82	23	298	108
Y	38.5	26.1	44.5	17.1	37.7	46.4	14.9	23.8	187.9	75.4	43.7	32.5	66.1	33.5
Zr	271	129	231	178	111	127	139	42	331	117	106	45	431	53
V	14	188	103	38	6	9	99	410	175	12	9	3	39	4
Ni	3	47	4	9	6	4	36	8	10	7	4	4	4	4
Cr	8	89	18	30	26	19	68	16	27	26	30	28	34	23
Nb	7.5	5.0	5.5	6.1	20.7	46.6	0.7	<0.5	11.9	7.6	32.7	44.9	11.5	6.0
Ga	21.8	17.3	19.8	20.1	19.5	32.9	20.3	20.0	21.5	17.4	23.3	30.0	15.8	15.7
Cu	21	61	18	65	10	11	109	90	26	12	11	11	25	10
Zn	63	79	90	36	24	45	64	113	31	21	46	32	30	17
Co	52	49	38	39	33	57	55	53	47	53	52	28	12	19
Ba	616	374	364	245	463	180	423	60	418	298	223	16	56	469
La	31	20	24	28	30	26	20	10	85	46	31	14	35	20
Ce	58	38	41	46	50	55	26	17	72	94	50	18	55	24
U	<0.5	0.5	0.5	1.5	10.1	5.4	<0.5	<0.5	0.5	1.9	9.1	5.1	1.6	<0.5
Th	19.2	5.9	4.9	12.1	35.8	51.1	<0.5	<0.5	4.0	11.2	30.9	1.6	3.5	1.1
Sc	3	20	18	4	<1	1	8	37	11	<1	<1	<1	2	<1
Pb	22	<1	4	6	65	9	<1	<1	<1	18	50	<1	<1	22

Supplementary Table 7. Whole-rock TIMS analysis and initial isotopic models

Sample	Age (Ga)	Rb (ppm)	Sr (ppm)	$^{87}Sr/^{86}Sr$ (measured)	2 standard error (2SE)	$^{87}Sr/^{86}Sr_{(t)}$	Sm (ppm)	Nd (ppm)	$^{143}Nd/^{144}Nd$ (measured)	2 standard error (2SE)	$^{143}Nd/^{144}Nd_{(t)}$	$^{Nd}T_{DM}$ (Ga)	$\varepsilon Nd_{(t)}$
KM-12	217	148.6	126	.716038	.000002	0.705499	6.1	24.0	.512634	.000009	0.512359	1.42	0.00
KM-18	229.9	70.4	367	.706306	.000003	0.704491	4.4	19.2	0.512731	0.000002	0.512450	1.00	2.11
KM-25	296	48.8	288	.706240	.000003	0.704176	5.8	23.8	0.512804	0.000002	0.512468	0.90	4.11
KM-26	296	83.2	442	.706376	.000003	0.704083	3.7	20.1	0.512632	0.000002	0.512358	0.85	1.97
KM-40A	238	390.7	105	.731233	.000003	0.694704	5.6	22.4	0.512166	0.000005	0.511817	2.57	-10.04
NT-01	229	753.8	52	.793133	.000004	0.655385	5.8	27.6	0.511907	0.000003	0.511677	2.24	-13.01
NT-04	241	34.7	935	.704771	.000002	0.704403	2.5	11.6	0.512817	0.000003	0.512556	0.70	4.45
NT-06	241	2.6	861	.704208	.000003	0.704178	3.9	14.1	0.512809	0.000001	0.512503	1.28	3.42
NT-07	273.5	44.5	183	.705940	.000004	0.703203	25.4	104.7	0.512953	0.000041	0.512663	0.50	7.36
NT-13	227.9	223.6	85	.726062	.000002	0.701347	(A) 10.7	41.4	.512549	0.000002	0.512259	1.71	-1.66
							(B) 1.0	4.1	0.512552	0.000002	0.512271	1.68	-1.45
NT-17	214.15	561.7	82	.800166	.000004	0.739261	5.7	25.2	0.511978	0.000029	0.511707	2.41	-12.80
ST-03	213.6	904.4	23	1.860644	.000007	1.476070	0.6	1.4	0.512484	0.000003	0.511662		-13.69
RDGEOCHEM_1	203	14.5	298	.704662	.000003	0.704255	7.8	28.9	0.512986	0.000002	0.512722	0.62	6.73

Sample	Pb ppm	U ppm	Th ppm	206/204 Pb (double spike corrected)	207/204 Pb (double spike corrected)	208/204 Pb (double spike corrected)	$206/204Pb_{(i)}$	$207/204\ Pb_{(i)}$	$208/204\ Pb_{(i)}$
KM-12	22	0.5	19.2	18.8521	15.6720	39.0184	18.8019	15.6695	38.391
KM-18	<1	0.5	5.9	Not measured	Not measured	Not measured	-	-	-
KM-25	4	0.5	4.9	18.6389	15.5992	38.6546	18.2638	15.5796	37.462
KM-26	6	1.5	12.1	18.9255	15.6536	38.9766	18.1686	15.6140	36.996
KM-40A	65	10.1	35.8	19.0222	15.7815	39.4380	18.6422	15.7622	39.000
NT-01	9	5.4	51.1	19.5566	15.8514	39.7958	18.1276	15.7789	35.393
NT-04	<1	<0.5	<0.5	Not measured	Not measured	Not measured	-	-	-
NT-06	<1	<0.5	<0.5	Not measured	Not measured	Not measured	-	-	-
NT-07	<1	0.5	4.0	Not measured	Not measured	Not measured	-	-	-
NT-13	18	1.9	11.2	19.3038	15.6977	39.0812	19.0573	15.6852	38.608
	18	1.9	11.2	19.3047	15.7045	39.0973	19.0581	15.6920	38.624
NT-17	50	9.1	30.9	19.1229	15.7977	39.2611	18.7235	15.7776	38.819
ST-03	<1	5.1	1.6	Not measured	Not measured	Not measured	-	-	-
RDGEOCHEM_1	<1	1.6	3.5	Not measured	Not measured	Not measured	-	-	-
RDT16_053	22	0.5	1.1	19.0263	15.8018	39.4318	19.0261	15.7995	39.398

Nd Model assumptions		
Lambda	6.54E-12	a^{-1}
143Nd/144Nd CHUR T=0	.512638	Goldstein et al (1984)
147Sm/144Nd CHUR T=0	.1966	Goldstein et al (1984)
143Nd/144Nd DM T=0	.513150	Goldstein et al (1984)
147Sm/144Nd DM T=0	.2145	Goldstein et al (1984)
Earth Age	4.615E+09	a

Sukhothai
Indochina
Inthanon
Sibumasu

APPENDIX III

Supplementary material for Chapter 3

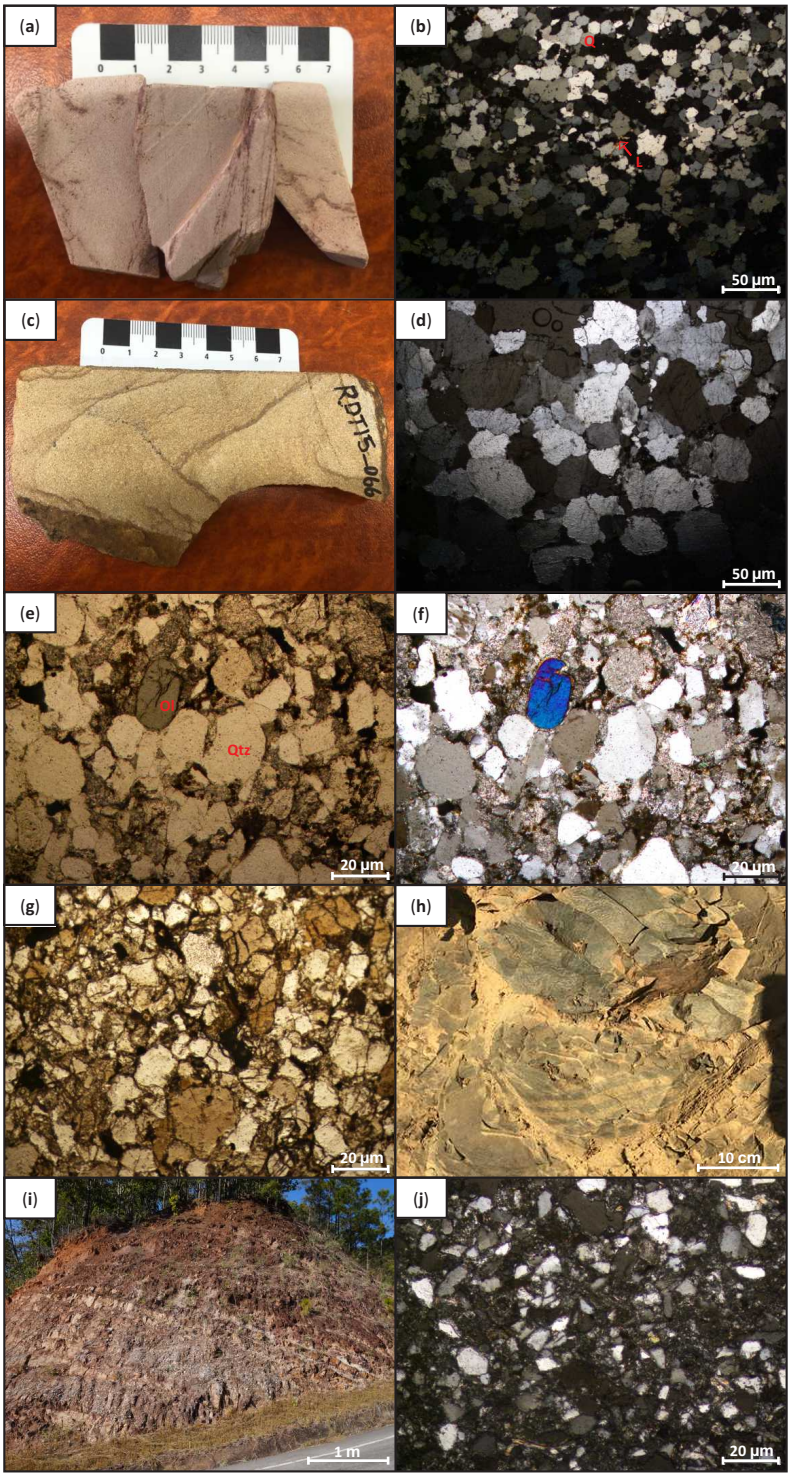

Supplementary Fig. 1. Thin sections,outcrop and hand specimens of samples. Minerals present are labelled where: Qtz is quartz; Ol is olvine; L is undifferentiated lithic fragments; Bt is biotite; Mu is muscovite; Am is amphibole mainly hornblende in these samples); Pl is plagioclase; Mc is microcline and Px is pyroxene. (a) Hand specimen of RDT15_078 (b) RDT16_001 thin section image in Cross Polarised Light (XPL), (c) Hand specimen of RDT15_066, (d) RDT16_018 overview thin section image in Cross Polarised Light (XPL), (e) RDT16_008 thin section image illustrating olivine (Ol) detritus in Plane Polarised Light (PPL) (f) RDT16_008 thin section image showing olivine (Ol) detritus in XPL, (g) RDT16_019 overview thin section image in XPL, (h) RDT16_006 field location, (i) RDT16_012 field locality (j) RDT16_012 overview thin section image in XPL.

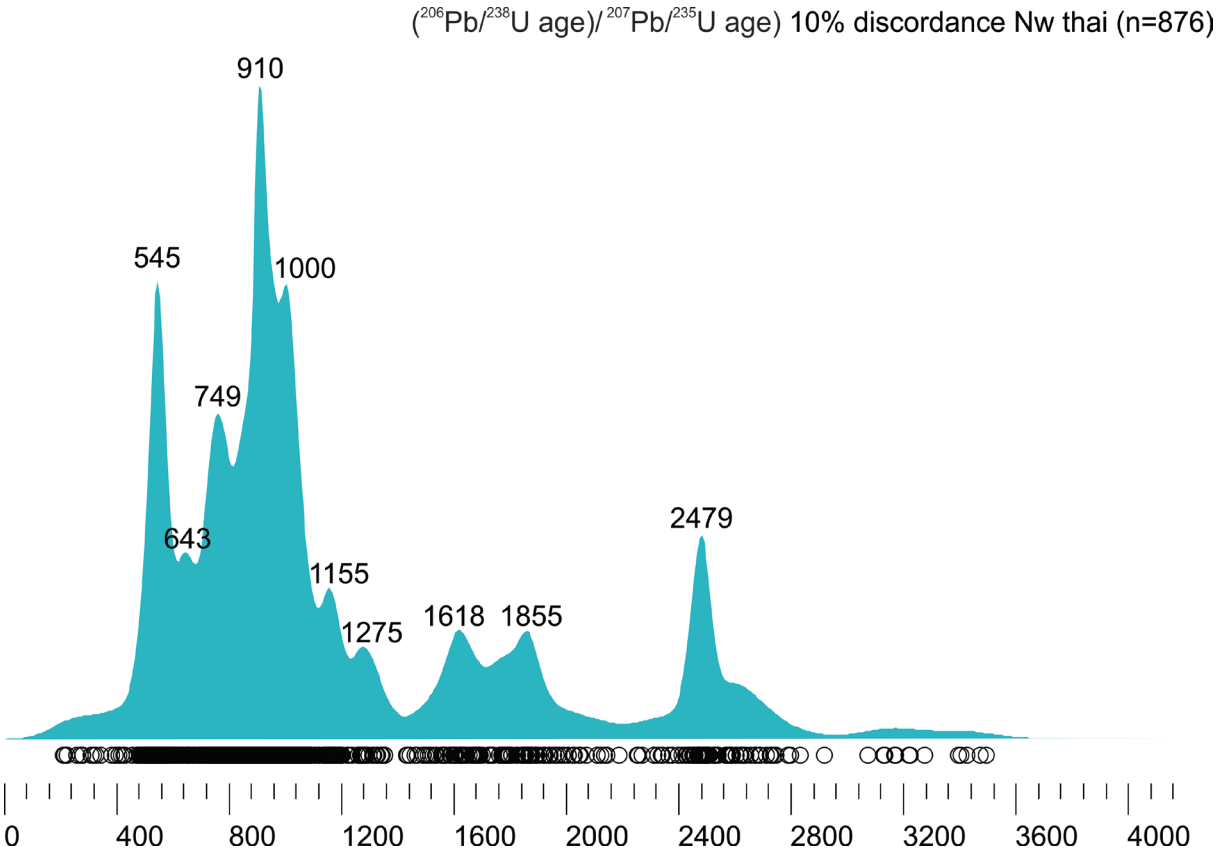

Supplementary Fig. 2. Cumulative Kernel Density Estimate of all eight northwest Thai age distributions

Fig. 6 Data References

b. Cambro-Ordovician. Other Sibumasu data: Chaung Magyi Group (CMG) Myanmar (Dew et al. submitted) and Ordovician (O) Myanmar (Cai et al. 2017). Australian potential sources: Albany-Fraser Orogen (Kirkland et al. 2011), Arunta, Beetaloo Basin (Yang et al. in prep), Gawler Craton (Cherry et al. 2017; Curtis et al. 2018; Reid and Payne 2017; Szpunar et al. 2011), Mt Isa, Musgraves, Northampton Complex (Ksienzyk et al. 2012) and Ordovician (O) SW Australia (Cawood and Nemchin 2000; Kettanah et al. 2015). Chinese potential sources or potential regions sourcing similar zircon distributions: Yunkai (Yu et al. 2008; Yu et al. 2010), Cambrian and Devonian Alxa (Zhang et al. 2016), Cambrian, Ordovician and Silurian Hainan Island (Xu et al. 2014 and references therein), Neoproterozoic and Cambrian Nanwenhe-Song Chay tectonic junction (N-S-C) (Zhou et al. 2018), Jiangnan Orogen (Yao et al. 2016), Cathaysia (Xu et al. 2007; Xu et al. 2013; Xu et al. 2014). NW Yangtze Lei and Shu (2010),Wu et al. (2010), Xiang and Shu (2010) and Duan et al. (2011). Other sources or regions sourcing similar sources (references therein McQuarrie et al. 2008; Myrow et al. 2010; Xu et al. 2014).

c. Carbo-Permian. Published data sources: Silurian (S) Myanmar and Carboniferous (C) Myanmar (Cai et al. 2017), Inthanon Zone (Hara et al. 2013), NE Vietnam (Halpin et al. 2016), Khao Khwang Fold-Thrust Belt (KKFTB) (Arboit et al. 2016), Permian (P) Cathaysia (Li et al. 2012), Devonian (D) and Carboniferous (C) Alxa (Zhang et al. 2016), Permian (P) SW Australia Perth Basin (Cawood and Nemchin 2000; Sircombe and Freeman 1999), Tarim (Ge et al. 2012; He et al. 2014; Long et al. 2011; Ma et al. 2012), Permian (P) Yilgarn WA (Veevers et al. 2005), Carboniferous–Permian (C-P) Lhasa (Zhu et al. 2011).

d. Triassic. Other Dew detrital data (in prep, Chapter 4) are underlined, Triassic (T) Sukhothai, Chanthaburi, CM1501 (Indochina). Other published data: Triassic–Jurassic (T-J) Myanmar (Cai et al. 2017), East Sumatra and West Sumatra (Zhang et al. 2018c), Inthanon Zone (Hara et al. 2013), NE Vietnam (Halpin et al. 2016), Khao Khwang Fold-Thrust Belt (KKFTB) (Arboit et al. 2016), Permian (P) Cathaysia (Li et al. 2012), Permian (P) SW Australia (Veevers et al. 2005), Perth Basin (Cawood and Nemchin 2000; Sircombe and Freeman 1999), Lhasa (Li et al. 2014), Malay Rivers (Sevastjanova et al. 2011), West Burma (Sevastjanova et al. 2016), Permo-Triassic (P-T) Sukhothai (Hara et al. 2015; Hara et al. 2017), Chanthaburi (Hara et al. 2018), Hainan Permo-Triassic granites (Shen et al. 2018).

Fig. 7 Data References

References for published Hf model age ($^{Hf}T_{DM}$) data: Iran compilation of detrital, magmatic and metamorphic data (Fergusson et al. 2016; Moghadam et al. 2017), Tengchong data from the Banwa Granite (Zhang et al. 2018a) and Cretaceous Laoxiangkeng pluton (Fang et al. 2018b), Hainan Permo-Triassic granites (Shen et al. 2018), NW Australia (includes Pilbara craton and Capricorn Orogen) (Gardiner et al. 2017; Johnson et al. 2011; Kemp et al. 2015) Cambrian and Ordovician Yunkai (Yu et al. 2008; Yu et al. 2010), Cathaysia sedimentary rocks (Xu et al. 2007; Xu et al. 2013; Xu et al. 2014; Yao et al. 2011; Yao et al. 2014).

Supplementary Data 1. Published U–Pb age data for multidimensional scaling (MDS) comparison.

Supplementary Table 1. Main isotopes and ratios measured using LA–ICP–MS. Concordance 1 ($^{206}Pb/^{238}U$/ $^{207}Pb/^{206}Pb$) and 2 ($^{206}Pb/^{238}U/^{207}Pb/^{235}U$)

Analysis Spot	U	Th	Th:U	Ratios							Ages						Concordance Calculations	
				$^{207}Pb/^{235}U$	2σ	$^{206}Pb/^{238}U$	2σ	Rho	$^{207}Pb/^{206}Pb$	2σ	$^{207}Pb/^{235}U$	2σ	$^{206}Pb/^{238}U$	2σ	$^{207}Pb/^{206}Pb$	2σ	1	2
rdt15_078-65.d	713.9	374.5	0.52	3.202	0.038	0.2524	0.0029	0.42395	0.0918	0.0011	1456	9.4	1451	15	1457	22	99.59	99.66
rdt15_078-66.d	537	349	0.65	2.819	0.039	0.2179	0.0027	0.52919	0.0934	0.0011	1358	10	1271	14	1490	23	85.30	93.59
rdt15_078-67.d	939	482.2	0.51	1.657	0.036	0.1659	0.0026	0.63369	0.0721	0.0012	990	14	989	14	981	34	100.82	99.90
rdt15_078-68.d	912.4	850.6	0.93	0.935	0.016	0.1034	0.0014	0.36887	0.0657	0.0011	670.5	7.9	633.9	8.4	789	34	80.34	94.54
rdt15_078-69.d	1100	235	0.21	1.568	0.022	0.1596	0.0024	0.58126	0.07099	0.00087	956.2	8.7	954	13	952	26	100.21	99.77
rdt15_078-70.d	865	23.12	0.03	1.956	0.038	0.1803	0.0025	0.54372	0.0785	0.0013	1099	13	1069	13	1157	34	92.39	97.27
rdt15_078-71.d	459	146.5	0.32	1.608	0.024	0.1604	0.0018	0.12805	0.0723	0.0011	973.1	8.8	958.8	10	987	32	97.14	98.53
rdt15_078-72.d	47.33	72.4	1.53	11.65	0.37	0.4637	0.0086	0.642	0.1802	0.0041	2555	29	2455	38	2629	38	93.38	96.09
rdt15_078-73.d	155.6	115.8	0.74	9.42	0.2	0.4057	0.007	0.60394	0.1685	0.0028	2378	19	2193	32	2535	28	86.51	92.22
rdt15_078-74.d	758	336	0.44	1.64	0.03	0.1582	0.0024	0.34097	0.075	0.0014	984	11	946	14	1056	37	89.58	96.14
rdt15_078-75.d	366	149.2	0.41	1.596	0.027	0.1599	0.002	0.11282	0.0726	0.0014	966	10	956	11	986	37	96.96	98.96
rdt15_078-76.d	517	117.5	0.23	1.623	0.028	0.1555	0.0018	0.30088	0.0758	0.0013	979	11	931.8	10	1071	35	87.00	95.18
rdt15_078-77.d	184.9	117.5	0.64	1.79	0.052	0.1727	0.0029	0.44042	0.0754	0.0022	1037	19	1029	17	1049	62	98.09	99.23
rdt15_078-78.d	1001	289.8	0.29	1.456	0.026	0.1503	0.0024	0.51302	0.0704	0.0012	912	11	902	13	928	34	97.20	98.90
rdt15_078-87.d	437	216.8	0.50	10.33	0.1	0.457	0.0055	0.51636	0.1636	0.0015	2463.6	9.1	2426	24	2491	16	97.39	98.47
rdt15_078-88.d	224.5	183.9	0.82	29.96	0.26	0.7115	0.0086	0.57983	0.3049	0.0026	3484.4	8.5	3462	32	3492	13	99.14	99.36
rdt15_078-89.d	419.4	30.12	0.07	1.755	0.038	0.1695	0.0025	0.33788	0.075	0.0016	1030	14	1011	14	1059	43	95.47	98.16
rdt15_078-90.d	592.7	86.9	0.15	1.683	0.028	0.1593	0.0021	0.37853	0.0763	0.0012	1002	11	952.7	12	1094	33	87.08	95.08
rdt15_078-91.d	0.017	0.05	2.94	no value	NAN	no value	NAN	NaN	no value	NAN	no value	NAN	no value	NAN	no value	NAN	#VALUE!	#VALUE!
rdt15_078-92.d	781.6	75.9	0.10	1.48	0.019	0.1492	0.0018	0.3594	0.07171	0.00091	920.8	7.8	896.5	9.8	968	26	92.61	97.36
rdt15_078-93.d	250	198	0.79	8.7	0.1	0.3997	0.0056	0.53232	0.1577	0.0017	2304	10	2166	26	2425	19	89.32	94.01
rdt15_078-94.d	311	185.7	0.60	2.301	0.042	0.1983	0.003	0.50485	0.0838	0.0014	1208	13	1165	16	1272	33	91.59	96.44
rdt15_078-103.d	600	664	1.11	1.803	0.029	0.1745	0.0026	0.36596	0.0753	0.0012	1044	10	1036	14	1067	33	97.09	99.23
rdt15_078-104.d	1832	1254	0.68	1.076	0.018	0.104	0.0016	0.59054	0.0751	0.0011	740.8	8.7	637.6	9.4	1065	28	59.87	86.07
rdt15_078-105.d	578	392.9	0.68	1.931	0.03	0.1803	0.0023	0.34893	0.0775	0.0012	1090	10	1068	13	1125	32	94.93	97.98
rdt15_078-106.d	391.6	119.9	0.31	5.109	0.074	0.2644	0.0039	0.3734	0.14	0.0022	1836	12	1512	20	2220	27	68.11	82.35
rdt15_078-107.d	489.8	197.3	0.40	6.749	0.084	0.3279	0.004	0.51159	0.149	0.0017	2077	11	1828	19	2332	19	78.39	88.01
rdt15_078-108.d	911	969	1.06	1.359	0.021	0.1338	0.0019	0.38611	0.0736	0.0011	870.4	9	809.2	11	1024	31	79.02	92.97
rdt15_078-109.d	455	270	0.59	1.65	0.031	0.1604	0.0021	0.21111	0.0742	0.0014	988	12	958.8	11	1039	39	92.28	97.04
rdt15_078-110.d	0.002	0.051	25.50	no value	NAN	no value	NAN	NaN	no value	NAN	no value	NAN	no value	NAN	no value	NAN	#VALUE!	#VALUE!
rdt15_078-111.d	0.012	0.223	18.58	no value	NAN	no value	NAN	NaN	no value	NAN	no value	NAN	no value	NAN	no value	NAN	#VALUE!	#VALUE!
rdt15_078-112.d	978	293	0.30	3.194	0.083	0.1761	0.0033	0.83658	0.1308	0.0021	1451	21	1045	18	2101	28	49.74	72.02
rdt15_078-113.d	282.1	228.7	0.81	1.866	0.04	0.159	0.0024	0.3761	0.0849	0.0017	1064	14	951	13	1307	40	72.76	89.38
rdt15_078-114.d	0.0054	0.0184	3.41	no value	NAN	no value	NAN	NaN	no value	NAN	no value	NAN	no value	NAN	no value	NAN	#VALUE!	#VALUE!
rdt15_078-115.d	328	190.7	0.58	1.661	0.025	0.1625	0.002	0.31095	0.0741	0.0011	993.2	9.7	970.1	11	1041	30	93.19	97.67
rdt15_078-116.d	161	22.82	0.14	8.21	0.34	0.386	0.012	0.94309	0.1517	0.0032	2249	40	2091	57	2360	37	88.60	92.97
rdt15_078-125.d	543	181.7	0.33	1.456	0.025	0.1484	0.0021	0.42145	0.071	0.0011	910	10	891.8	12	948	34	94.07	98.00
rdt15_078-126.d	375.8	209.7	0.56	1.484	0.025	0.1412	0.0017	0.22052	0.076	0.0013	922	11	851.5	9.8	1087	36	78.33	92.35
rdt15_078-127.d	378	178.8	0.47	1.51	0.028	0.1548	0.0023	0.36643	0.0708	0.0013	932	12	928	13	933	39	99.46	99.57
rdt15_078-128.d	1255	305	0.24	1.506	0.026	0.1497	0.0025	0.24862	0.073	0.001	931	11	899	14	1004	29	89.54	96.56
rdt15_078-129.d	2920	186	0.06	2.688	0.084	0.1539	0.0044	0.8629	0.1264	0.002	1322	23	922	24	2045	28	45.09	69.74
rdt15_078-130.d	479	172.4	0.36	6.842	0.075	0.3305	0.0043	0.47767	0.1501	0.0017	2089.4	9.7	1840	21	2341	19	78.60	88.06
rdt15_078-131.d	1027	24.1	0.02	1.971	0.026	0.183	0.0024	0.47061	0.0776	0.00095	1105.5	8.7	1083	13	1136	25	95.33	97.96
rdt15_078-132.d	3080	1241	0.40	0.6	0.014	0.0567	0.0013	0.6611	0.0773	0.0015	476.5	8.6	355.4	7.8	1122	39	31.68	74.59
rdt15_078-133.d	722	167.7	0.23	1.455	0.023	0.1448	0.002	0.54177	0.0725	0.001	910.6	9.5	873.4	11	986	28	88.58	95.91
rdt15_078-134.d	519	36.7	0.07	0.925	0.021	0.1061	0.0016	0.31445	0.0632	0.0015	664	11	650	9.4	702	47	92.59	97.89
rdt15_078-135.d	1783	273	0.15	1.025	0.021	0.1064	0.002	0.70515	0.0699	0.001	715	10	651	12	914	31	71.23	91.05
rdt15_078-136.d	1630	226	0.14	1.059	0.06	0.1146	0.0052	0.97558	0.065	0.0011	710	30	696	30	750	36	92.80	98.03

Supplementary Table 1. Main isotopes and ratios measured using LA–ICP–MS. Concordance 1 ($^{206}Pb/^{238}U$/ $^{207}Pb/^{206}Pb$) and 2 ($^{206}Pb/^{238}U/^{207}Pb/^{235}U$)

Analysis Spot	U	Th	Th:U	Ratios							Ages						Concordance Calculations	
				$^{207}Pb/^{235}U$	2σ	$^{206}Pb/^{238}U$	2σ	Rho	$^{207}Pb/^{206}Pb$	2σ	$^{207}Pb/^{235}U$	2σ	$^{206}Pb/^{238}U$	2σ	$^{207}Pb/^{206}Pb$	2σ	1	2
rdt15_078-137.d	1259	491	0.39	0.8027	0.0099	0.09615	0.0011	0.42939	0.06039	0.0007	597.6	5.6	591.7	6.6	611	25	96.84	99.01
rdt15_078-138.d	483.4	187	0.39	0.836	0.016	0.0984	0.0013	0.29935	0.0615	0.0012	616	8.6	605.1	7.4	634	40	95.44	98.23
rdt15_078-140.d	330	87.7	0.27	4.483	0.065	0.299	0.004	0.55165	0.1085	0.0013	1725	12	1685	20	1767	22	95.36	97.68
rdt15_078-149.d	165	75.5	0.46	1.1	0.032	0.124	0.0018	0.031773	0.0649	0.0021	750	16	753.2	11	723	69	104.18	100.43
rdt15_078-152.d	223	87	0.39	25.91	0.24	0.6536	0.0078	0.62062	0.287	0.0022	3342.3	8.9	3240	31	3400	12	95.29	96.94
rdt15_078-153.d	755	393	0.52	1.878	0.02	0.1734	0.0019	0.41028	0.07846	0.0008	1072.7	7.2	1030.6	10	1155	20	89.23	96.08
rdt15_078-154.d	0.067	0.23	3.43	no value	NAN	no value	NAN	NaN	no value	NAN	no value	NAN	no value	NAN	no value	NAN	#VALUE!	#VALUE!
rdt15_078-155.d	618	315	0.51	1.779	0.026	0.169	0.002	0.66434	0.07628	0.00089	1037.6	9.3	1006.3	11	1095	23	91.90	96.98
rdt15_078-156.d	561	200	0.36	1.779	0.023	0.1686	0.0019	0.39157	0.07641	0.00096	1035.8	8.5	1004.3	11	1097	25	91.55	96.96
rdt15_078-157.d	331.2	165.9	0.50	0.679	0.02	0.0761	0.0012	0.30469	0.0643	0.0018	522	12	472.7	6.9	705	63	67.05	90.56
rdt15_078-158.d	2417	2956	1.22	2.805	0.089	0.1359	0.0038	0.97322	0.1485	0.0012	1343	23	820	22	2325	14	35.27	61.06
rdt15_078-159.d	170.8	80.1	0.47	1.534	0.036	0.1527	0.0021	0.2161	0.0729	0.0017	940	14	915.7	11	982	48	93.25	97.41
rdt15_078-160.d	172.6	64.1	0.37	1.708	0.042	0.1503	0.0021	0.07507	0.0826	0.0022	1005	16	902.5	12	1231	49	73.31	89.80
rdt15_078-169.d	2067	1066	0.52	0.897	0.012	0.0863	0.0013	0.24662	0.0756	0.0012	650.1	6.3	533.4	7.5	1068	33	49.94	82.05
rdt15_078-170.d	505	216.2	0.43	1.524	0.027	0.1479	0.0024	0.43399	0.0747	0.0013	937	11	889	13	1050	36	84.67	94.88
rdt15_078-171.d	807	210.9	0.26	1.38	0.019	0.1404	0.0018	0.257	0.0714	0.0011	879.5	8.1	846.9	10	956	31	88.59	96.29
rdt15_078-172.d	917	141	0.15	1.052	0.024	0.1149	0.0022	0.59018	0.0665	0.0013	730	12	701	13	810	40	86.54	96.03
rdt15_078-173.d	695	240.5	0.35	1.414	0.02	0.1448	0.0018	0.43074	0.07073	0.00093	894.1	8.5	871.6	9.9	939	28	92.82	97.48
rdt15_078-174.d	345	305	0.88	1.001	0.022	0.1147	0.0016	0.22426	0.0635	0.0014	703	11	700	9	688	48	101.74	99.57
rdt15_078-175.d	534	220.3	0.41	1.563	0.022	0.153	0.0019	0.35105	0.0743	0.0011	953.8	8.7	917.2	11	1045	29	87.77	96.16
rdt15_078-176.d	690	370	0.54	1.861	0.027	0.1732	0.0022	0.48478	0.0778	0.001	1065.5	9.4	1029.6	12	1137	25	90.55	96.63
rdt15_078-177.d	397	76.7	0.19	6.087	0.082	0.3341	0.0048	0.4869	0.1322	0.0017	1986	12	1857	23	2121	23	87.55	93.50
rdt15_078-178.d	497.4	173.8	0.35	4.739	0.053	0.3008	0.0036	0.49043	0.1141	0.0011	1772.6	9.3	1695	18	1864	18	90.93	95.62
rdt15_078-179.d	5380	6280	1.17	0.462	0.014	0.02617	0.0007	0.72236	0.1284	0.0024	387	10	166.5	4.4	2071	34	8.04	43.02
rdt15_078-180.d	248	73.5	0.30	1.679	0.041	0.1639	0.0029	0.485	0.0748	0.0016	994	16	977	16	1034	44	94.49	98.29
rdt15_078-189.d	1153	128.5	0.11	1.2	0.023	0.12	0.0017	0.55484	0.0721	0.0011	799	10	730.3	10	977	33	74.75	91.40
rdt15_078-190.d	818	90.2	0.11	4.481	0.064	0.2878	0.0042	0.58599	0.1127	0.0013	1726	12	1630	21	1842	22	88.49	94.44
rdt15_078-191.d	738	138.5	0.19	4.738	0.044	0.3001	0.0037	0.56073	0.1142	0.001	1772.8	7.7	1691	18	1864	16	90.72	95.39
rdt15_078-192.d	904	445.1	0.49	1.522	0.019	0.1538	0.0019	0.44124	0.07166	0.00087	937.5	7.8	922	11	968	25	95.25	98.35
rdt15_078-193.d	838	105.3	0.13	1.502	0.019	0.1519	0.0017	0.22746	0.07158	0.00091	929.8	7.6	911.2	9.7	968	27	94.13	98.00
rdt15_078-194.d	0.0049	0.039	7.96	no value	NAN	no value	NAN	NaN	no value	NAN	no value	NAN	no value	NAN	no value	NAN	#VALUE!	#VALUE!
rdt15_078-195.d	1194	681	0.57	0.65	0.014	0.0771	0.0012	0.32625	0.0609	0.0013	507.3	8.3	478.5	7.5	621	44	77.05	94.32
rdt15_078-196.d	374.1	128.6	0.34	1.556	0.028	0.1544	0.002	0.39257	0.073	0.0012	950	11	925	11	993	35	93.15	97.37
rdt15_078-197.d	1679	57.2	0.03	4.872	0.046	0.3113	0.0039	0.69733	0.11325	0.00084	1795.9	8	1746	19	1848	13	94.48	97.22
rdt15_078-198.d	0.0082	0.043	5.24	no value	NAN	no value	NAN	NaN	no value	NAN	no value	NAN	no value	NAN	no value	NAN	#VALUE!	#VALUE!
rdt15_078-199.d	558	369	0.66	1.42	0.026	0.1473	0.0021	0.43096	0.0698	0.0012	895	11	885.3	12	914	35	96.86	98.92
rdt15_078-200.d	1945	280	0.14	1.68	0.1	0.1301	0.0033	0.47871	0.093	0.0049	988	37	788	19	1425	92	55.30	79.76
rdt15_078-209.d	756	139.8	0.18	3.758	0.085	0.2646	0.0052	0.78649	0.103	0.0015	1583	19	1512	27	1672	27	90.43	95.51
rdt15_078-210.d	372.4	115.6	0.31	4.676	0.064	0.3176	0.004	0.38205	0.1068	0.0015	1761	11	1777	20	1739	25	102.19	100.91
rdt15_078-211.d	1145	681	0.59	1.392	0.029	0.1359	0.0023	0.65644	0.0741	0.0012	884	12	821	13	1040	33	78.94	92.87
rdt15_078-212.d	1739	136.9	0.08	1.299	0.016	0.1331	0.0018	0.49568	0.07097	0.00086	844.5	7	805.1	10	949	25	84.84	95.33
rdt15_078-214.d	168.8	78.7	0.47	1.968	0.068	0.158	0.0026	0.17413	0.0905	0.0029	1088	21	945	15	1373	58	68.83	86.86
RDT15078-9.d	269.1	177.1	0.66	1.936	0.043	0.1844	0.0023	0.41387	0.0755	0.0016	1091	15	1091	12	1074	41	101.58	100.00
RDT15078-10.d	2536	1662	0.66	0.934	0.067	0.0575	0.0012	0.8539	0.1146	0.0061	654	33	360.1	7.6	1798	87	20.03	55.06
RDT15078-11.d	335	190.2	0.57	1.296	0.032	0.127	0.0021	0.3671	0.0736	0.0018	842	14	770	12	1022	52	75.34	91.45
RDT15078-12.d	609.7	381.9	0.63	10.03	0.18	0.4252	0.0059	0.85765	0.1707	0.0022	2435	17	2282	26	2562	21	89.07	93.72
RDT15078-15.d	159.7	71.9	0.45	1.488	0.043	0.1507	0.0023	0.20141	0.0717	0.0021	922	18	904	13	953	60	94.86	98.05
RDT15078-16.d	603	469	0.78	1.74	0.13	0.1266	0.002	0.6602	0.0989	0.0067	1006	49	768	11	1480	120	51.89	76.34

Supplementary Table 1. Main isotopes and ratios measured using LA–ICP–MS. Concordance 1 ($^{206}Pb/^{238}U$/ $^{207}Pb/^{206}Pb$) and 2 ($^{206}Pb/^{238}U/^{207}Pb/^{235}U$)

Analysis Spot	U	Th	Th:U	Ratios							Ages						Concordance Calculations	
				$^{207}Pb/^{235}U$	2σ	$^{206}Pb/^{238}U$	2σ	Rho	$^{207}Pb/^{206}Pb$	2σ	$^{207}Pb/^{235}U$	2σ	$^{206}Pb/^{238}U$	2σ	$^{207}Pb/^{206}Pb$	2σ	1	2
RDT15078-17.d	90.8	158.5	1.75	9.2	0.18	0.4066	0.0051	0.49322	0.1633	0.003	2355	18	2198	23	2486	30	88.42	93.33
RDT15078-18.d	55.8	43.8	0.78	2.51	0.16	0.1786	0.0034	0.52368	0.1036	0.0066	1253	46	1059	19	1580	120	67.03	84.52
RDT15078-19.d	709	579	0.82	1.82	0.032	0.1733	0.0021	0.45565	0.076	0.0014	1053	12	1030	12	1087	36	94.76	97.82
RDT15078-27.d	48.1	102.1	2.12	10.77	0.32	0.433	0.011	0.72408	0.1809	0.0041	2497	29	2311	52	2653	38	87.11	92.55
RDT15078-28.d	720	135	0.19	1.625	0.043	0.1531	0.003	0.617	0.0771	0.0018	978	17	918	17	1120	47	81.96	93.87
RDT15078-29.d	175.1	147.3	0.84	1.656	0.043	0.1601	0.0024	0.28006	0.0753	0.0021	989	17	957	13	1053	54	90.88	96.76
RDT15078-30.d	87.3	10.02	0.11	1.468	0.051	0.143	0.0028	0.13226	0.0751	0.0029	912	21	861	16	1019	78	84.49	94.41
RDT15078-31.d	134.8	120.7	0.90	5.73	0.19	0.3343	0.0086	0.13768	0.1234	0.0048	1931	27	1857	41	1993	68	93.18	96.17
RDT15078-32.d	184.8	184	1.00	9.34	0.17	0.4217	0.0063	0.6952	0.1599	0.0026	2369	17	2266	29	2449	27	92.53	95.65
RDT15078-33.d	1373	753	0.55	1.25	0.071	0.1087	0.005	0.86574	0.0821	0.0022	813	33	664	29	1231	52	53.94	81.67
RDT15078-34.d	1829	981	0.54	1.109	0.022	0.0969	0.0016	0.27383	0.0831	0.0018	756.6	10	596.3	9.2	1262	41	47.25	78.81
RDT15078-35.d	863	102.8	0.12	1.318	0.026	0.1384	0.0017	0.56495	0.0691	0.0013	852.5	11	835.2	9.5	897	39	93.11	97.97
RDT15078-36.d	297	212	0.71	6.23	0.53	0.344	0.02	0.23987	0.133	0.011	1997	67	1902	97	2110	130	90.14	95.24
RDT15078-37.d	750	796	1.06	1.571	0.052	0.1451	0.003	0.10277	0.0783	0.0021	954	20	873	17	1131	52	77.19	91.51
RDT15078-38.d	698	155.3	0.22	1.589	0.041	0.1509	0.002	0.2839	0.0765	0.002	963	16	906	11	1087	51	83.35	94.08
RDT15078-39.d	242	40.9	0.17	1.49	0.14	0.1078	0.0048	0.2964	0.105	0.012	918	57	659	28	1640	200	40.18	71.79
~~RDT15078-40.d~~	~~300~~	~~142~~	~~0.47~~	~~5.5~~	~~2~~	~~0.195~~	~~0.06~~	~~0.071059~~	~~0.24~~	~~0.11~~	~~1820~~	~~250~~	~~1130~~	~~310~~	~~2810~~	~~530~~	~~40.21~~	62.09
RDT15078-41.d	282	161.5	0.57	7.62	0.19	0.3516	0.0067	0.65967	0.1568	0.003	2185	24	1941	32	2420	34	80.21	88.83
RDT15078-42.d	904	677	0.75	1.202	0.034	0.1224	0.0032	0.83214	0.0711	0.0013	799	16	743	18	951	37	78.13	92.99
RDT15078-51.d	3010	445	0.15	0.811	0.053	0.0712	0.0037	0.98553	0.0818	0.0016	600	29	442	22	1238	40	35.70	73.67
RDT15078-54.d	856	479	0.56	5.379	0.097	0.2743	0.0037	0.66255	0.1415	0.0021	1880	16	1562	19	2243	26	69.64	83.09
RDT15078-55.d	1880	410	0.22	0.64	0.017	0.0714	0.0025	0.54562	0.0654	0.002	501.4	11	444	15	773	61	57.44	88.55
RDT15078-56.d	892	287	0.32	1.481	0.055	0.139	0.0039	0.83998	0.077	0.0015	917	22	838	22	1114	41	75.22	91.38
RDT15078-57.d	289.5	152.2	0.53	5.63	0.11	0.3304	0.0051	0.66564	0.1237	0.0022	1918	17	1839	25	2004	32	91.77	95.88
RDT15078-58.d	91.1	235	2.58	1.936	0.069	0.1795	0.0036	0.4386	0.078	0.0025	1089	24	1066	20	1128	65	94.50	97.89
RDT15078-59.d	943	501	0.53	1.196	0.037	0.1103	0.0017	0.24224	0.0784	0.0024	796	16	675	10	1129	56	59.79	84.80
RDT15078-60.d	203.6	187.8	0.92	1.63	0.039	0.1527	0.0022	0.25981	0.0777	0.0021	981	16	916	12	1131	52	80.99	93.37
RDT15078-61.d	1124	1413	1.26	1.337	0.047	0.1223	0.0025	0.23718	0.0782	0.0023	858	19	743	15	1144	61	64.95	86.60
RDT15078-62.d	237.2	145.1	0.61	1.322	0.061	0.1246	0.0032	0.49813	0.0765	0.0025	847	25	756	18	1073	66	70.46	89.26
RDT15078-70.d	237	167	0.70	2.37	0.14	0.1762	0.0041	0.47914	0.0966	0.0052	1228	42	1046	22	1506	91	69.46	85.18
RDT15078-71.d	42.2	49.2	1.17	7.51	0.35	0.362	0.013	0.80103	0.1499	0.0043	2149	44	1991	59	2322	51	85.75	92.65
RDT15078-72.d	170.6	147.3	0.86	1.739	0.053	0.156	0.0026	0.22817	0.0808	0.0024	1019	19	934	14	1187	59	78.69	91.66
RDT15078-73.d	6750	1.12E+04	1.66	0.583	0.036	0.02439	0.00094	-0.44494	0.178	0.015	463	23	155.3	5.9	2530	150	6.14	33.54
RDT15078-74.d	510	515	1.01	1.122	0.029	0.114	0.0018	0.6153	0.0709	0.0015	762	14	695	10	942	42	73.78	91.21
RDT15078-75.d	3770	1440	0.38	0.495	0.019	0.0431	0.0013	0.777	0.0851	0.003	407	12	271.8	7.7	1298	59	20.94	66.78
RDT15078-76.d	246.4	269	1.09	10.2	0.18	0.456	0.0063	0.68056	0.1616	0.0025	2451	16	2420	28	2471	26	97.94	98.74
RDT15078-77.d	654	417	0.64	1.597	0.031	0.1574	0.0023	0.4891	0.0737	0.0013	967.6	12	942	13	1024	36	91.99	97.35
RDT15078-78.d	882	729	0.83	6.08	0.14	0.3068	0.0058	0.83474	0.1431	0.0021	1984	19	1723	28	2262	25	76.17	86.84
RDT15078-79.d	595	613	1.03	1.497	0.032	0.1506	0.0018	0.48894	0.072	0.0014	929	13	904	10	979	42	92.34	97.31
RDT15078-80.d	266.4	69.4	0.26	3.167	0.072	0.2361	0.0031	0.32908	0.0974	0.0021	1446	18	1366	16	1562	40	87.45	94.47
RDT15078-81.d	2187	1872	0.86	0.727	0.018	0.0742	0.0013	0.83683	0.0708	0.0011	553.7	10	461.2	7.6	945	33	48.80	83.29
RDT15078-82.d	908	607	0.67	2.434	0.055	0.2042	0.004	0.83445	0.0863	0.0013	1250	17	1197	22	1343	30	89.13	95.76
RDT15078-83.d	662	1307	1.97	2.523	0.045	0.215	0.0027	0.67766	0.0851	0.0013	1277	13	1255	14	1312	31	95.66	98.28
RDT16019-416.d	1108	750	0.68	0.786	0.022	0.0809	0.0018	0.68617	0.0706	0.0016	589	13	501	10	930	46	53.87	85.06
RDT16019-424.d	340	295.3	0.87	1.702	0.04	0.1714	0.003	0.65744	0.0718	0.0013	1007	15	***1019***	***16***	969	38	105.16	101.19
RDT16019-425.d	971	665	0.68	1.47	0.029	0.1475	0.0025	0.7267	0.07224	0.0012	916.9	12	***887***	***14***	986	33	89.96	96.74
RDT16019-426.d	371.1	184.8	0.50	1.865	0.043	0.1765	0.0034	0.4953	0.0768	0.0017	1066	15	***1047***	***19***	1099	46	95.27	98.22
RDT16019-427.d	46.23	68.2	1.48	1.421	0.078	0.1323	0.0032	0.28646	0.0783	0.0043	888	33	800	18	1060	120	75.47	90.09

Supplementary Table 1. Main isotopes and ratios measured using LA–ICP–MS. Concordance 1 ($^{206}Pb/^{238}U$/ $^{207}Pb/^{206}Pb$) and 2 ($^{206}Pb/^{238}U/^{207}Pb/^{235}U$)

Analysis Spot	U	Th	Th:U	Ratios							Ages						Concordance Calculations	
				$^{207}Pb/^{235}U$	2σ	$^{206}Pb/^{238}U$	2σ	Rho	$^{207}Pb/^{206}Pb$	2σ	$^{207}Pb/^{235}U$	2σ	$^{206}Pb/^{238}U$	2σ	$^{207}Pb/^{206}Pb$	2σ	1	2
RDT16019-428.d	68.1	71.3	1.05	10.5	0.26	0.4627	0.0097	0.59547	0.1648	0.0036	2479	23	2447	43	***2499***	***38***	97.92	98.71
RDT16019-429.d	947	614.7	0.65	1.418	0.031	0.1424	0.0025	0.76657	0.07187	0.0012	895	13	858	14	975	34	88.00	95.87
RDT16019-431.d	268.4	109.8	0.41	2.669	0.059	0.1935	0.0034	0.63548	0.1	0.0019	1317	16	1140	18	1615	36	70.59	86.56
RDT16019-432.d	113.5	124.1	1.09	1.084	0.042	0.1222	0.0026	0.34909	0.0653	0.0026	746	22	***742***	***15***	725	84	102.34	99.46
RDT16019-433.d	723	262	0.36	0.713	0.023	0.0835	0.0021	0.64402	0.062	0.0016	544	13	516	12	649	57	79.51	94.85
RDT16019-434.d	130.4	96.9	0.74	1.802	0.057	0.1685	0.003	0.34811	0.0776	0.0024	1041	20	***1006***	***16***	1113	63	90.39	96.64
RDT16019-435.d	72	58.8	0.82	1.321	0.059	0.1281	0.0029	0.13155	0.0746	0.0035	846	26	777	16	977	98	79.53	91.84
RDT16019-436.d	502.9	56.5	0.11	1.107	0.026	0.1213	0.0019	0.34124	0.0662	0.0015	755	12	***738***	***11***	796	49	92.71	97.75
RDT16019-437.d	295.3	165.6	0.56	0.336	0.015	0.04406	0.0008	0.18656	0.0562	0.0026	296	12	277.9	4.9	405	100	68.62	93.89
RDT16019-445.d	151	51.6	0.34	1.634	0.056	0.1574	0.0039	0.52132	0.0754	0.0023	977	22	942	21	1047	62	89.97	96.42
RDT16019-446.d	722	124.7	0.17	9.46	0.16	0.4328	0.007	0.81865	0.1585	0.0023	2382	16	2316	32	***2436***	***24***	95.07	97.23
RDT16019-447.d	120.8	86.9	0.72	1.417	0.051	0.1255	0.0023	0.18501	0.0821	0.003	890	21	762	13	1222	69	62.36	85.62
RDT16019-448.d	355.8	450	1.26	3.435	0.073	0.2517	0.0049	0.64123	0.0991	0.0019	1510	17	1446	25	***1598***	***36***	90.49	95.76
RDT16019-449.d	245.5	225.1	0.92	3.897	0.085	0.2837	0.0046	0.65331	0.0995	0.0018	1610	18	1609	23	***1607***	***34***	100.12	99.94
RDT16019-450.d	522.3	346.5	0.66	0.863	0.022	0.1011	0.0018	0.52857	0.0619	0.0014	630	12	***621***	***11***	652	50	95.25	98.57
RDT16019-451.d	706	604	0.86	1.576	0.035	0.1471	0.0024	0.57283	0.0777	0.0015	959	14	884	14	1128	39	78.37	92.18
RDT16019-452.d	1175	448.3	0.38	1.503	0.029	0.1498	0.0024	0.60624	0.07262	0.0012	930.3	12	***899***	***14***	997	33	90.17	96.64
RDT16019-453.d	613.7	291.9	0.48	1.053	0.023	0.1183	0.0019	0.43095	0.0646	0.0014	729	12	***721***	***11***	745	46	96.78	98.90
RDT16019-454.d	567	603	1.06	3.325	0.085	0.2354	0.0053	0.87337	0.1023	0.0016	1482	20	1361	28	1661	29	81.94	91.84
RDT16019-455.d	238	205	0.86	0.826	0.029	0.0949	0.0017	0.41763	0.063	0.0019	608	16	584.2	9.9	693	66	84.30	96.09
RDT16019-456.d	1732	1268	0.73	1.041	0.03	0.0943	0.0023	0.88509	0.0805	0.0014	724	15	581	14	1210	31	48.02	80.25
RDT16019-457.d	447.8	458.3	1.02	1.571	0.034	0.1566	0.0026	0.48723	0.0726	0.0015	957	13	***938***	***15***	993	42	94.46	98.01
RDT16019-458.d	155.4	16	0.10	1.26	0.11	0.1008	0.0036	0.65299	0.0874	0.0056	804	46	618	21	1290	130	47.91	76.87
RDT16019-466.d	161.6	111.9	0.69	4.546	0.11	0.3021	0.005	0.46638	0.1091	0.0023	1737	21	1700	25	***1777***	***39***	95.67	97.87
RDT16019-467.d	352	131.4	0.37	1.684	0.043	0.1641	0.0026	0.44756	0.0744	0.0016	1000	16	***979***	***14***	1038	45	94.32	97.90
RDT16019-468.d	531	372	0.70	4.81	0.14	0.2708	0.0064	0.84317	0.1284	0.0024	1780	26	1543	32	2069	34	74.58	86.69
RDT16019-469.d	115.3	93.7	0.81	9.82	0.25	0.4219	0.0096	0.77233	0.1689	0.0031	2412	24	2265	44	***2539***	***31***	89.21	93.91
RDT16019-470.d	996	379	0.38	0.942	0.022	0.1058	0.0018	0.64419	0.0646	0.0013	674	12	648	11	750	43	86.40	96.14
RDT16019-471.d	137	100	0.73	1.539	0.083	0.1335	0.0023	0.21103	0.0837	0.0045	940	33	807	13	1220	100	66.15	85.85
RDT16019-472.d	176.7	117.8	0.67	1.326	0.049	0.1324	0.0023	0.31923	0.0721	0.0026	851	21	801	13	951	73	84.23	94.12
RDT16019-473.d	736	314.2	0.43	12.93	0.21	0.5026	0.0081	0.83007	0.1866	0.0026	2673	16	2622	34	***2709***	***23***	96.79	98.09
RDT16019-474.d	198.1	172.4	0.87	4.88	0.1	0.3092	0.0053	0.54868	0.1143	0.0022	1796	18	1735	26	***1863***	***36***	93.13	96.60
RDT16019-475.d	282	194.7	0.69	1.338	0.034	0.1407	0.0026	0.36656	0.0695	0.0018	860	15	***848***	***15***	891	54	95.17	98.60
RDT16019-476.d	380	552	1.45	3.619	0.074	0.2637	0.0043	0.65684	0.0995	0.0017	1551	16	1508	22	1607	32	93.84	97.23
RDT16019-477.d	142.7	52.5	0.37	1.658	0.092	0.1453	0.0033	0.27225	0.0827	0.0042	985	35	874	19	1203	100	72.65	88.73
RDT16019-478.d	187.8	96.6	0.51	1.9	0.046	0.1781	0.0025	0.46573	0.0771	0.0017	1078	16	***1056***	***14***	1109	42	95.22	97.96
RDT16019-479.d	195.3	203.4	1.04	0.5	0.027	0.04847	0.00098	0.22908	0.0747	0.004	408	18	305.1	6	980	120	31.13	74.78
RDT16019-480.d	2076	481	0.23	0.556	0.014	0.0648	0.0014	0.71987	0.06205	0.0012	447.8	9.3	404.4	8.4	664	41	60.90	90.31
RDT16019-489.d	65.8	77.4	1.18	4.77	0.15	0.3011	0.0059	0.45336	0.1153	0.0034	1774	27	1695	29	1861	53	91.08	95.55
RDT16019-490.d	426.6	300.7	0.70	0.878	0.024	0.1019	0.0018	0.39069	0.0625	0.0016	638	13	625	10	666	56	93.84	97.96
RDT16019-491.d	227.1	402	1.77	1.139	0.032	0.1211	0.002	0.18248	0.0684	0.002	769	15	***737***	***11***	849	62	86.81	95.84
RDT16019-492.d	184.8	171	0.93	13.15	0.24	0.4871	0.007	0.67381	0.1957	0.0031	2688	17	2556	30	2786	26	91.74	95.09
RDT16019-493.d	402.6	160	0.40	4.421	0.095	0.2326	0.0038	0.74728	0.1376	0.0023	1715	17	1347	20	2195	28	61.37	78.54
RDT16019-494.d	221.9	279	1.26	1.118	0.041	0.1137	0.0019	0.43157	0.0719	0.0026	760	20	694	11	936	73	74.15	91.32
RDT16019-495.d	150.1	117.6	0.78	1.065	0.038	0.1195	0.002	0.14602	0.0642	0.0024	732	19	727	11	718	80	101.25	99.32
RDT16019-496.d	193.8	74.2	0.38	1.451	0.038	0.1453	0.0018	0.21121	0.0726	0.0019	908	16	874	10	986	52	88.64	96.26
RDT16019-497.d	258	211.5	0.82	2.6	0.12	0.1841	0.0067	0.77255	0.1011	0.0031	1284	35	1086	37	1633	59	66.50	84.58

Supplementary Table 1. Main isotopes and ratios measured using LA–ICP–MS. Concordance 1 ($^{206}Pb/^{238}U$/ $^{207}Pb/^{206}Pb$) and 2 ($^{206}Pb/^{238}U/^{207}Pb/^{235}U$)

Analysis Spot	U	Th	Th:U	Ratios							Ages						Concordance Calculations	
				$^{207}Pb/^{235}U$	2σ	$^{206}Pb/^{238}U$	2σ	Rho	$^{207}Pb/^{206}Pb$	2σ	$^{207}Pb/^{235}U$	2σ	$^{206}Pb/^{238}U$	2σ	$^{207}Pb/^{206}Pb$	2σ	1	2
RDT16019-498.d	244.7	321	1.31	8.82	0.16	0.3988	0.0054	0.67885	0.1598	0.0024	2317	17	2162	25	2453	26	88.14	93.31
RDT16019-499.d	139.3	83.1	0.60	0.749	0.037	0.0837	0.0013	0.06204	0.0659	0.0036	562	21	518.3	8	720	110	71.99	92.22
RDT16019-500.d	397.5	120.9	0.30	4.541	0.078	0.2903	0.0038	0.62653	0.1134	0.0018	1737	14	1642	19	1850	29	88.76	94.53
RDT16019-501.d	808	256	0.32	1.978	0.052	0.1445	0.0025	0.74194	0.0991	0.0019	1107	18	869	14	1602	36	54.24	78.50
RDT16019-509.d	626	506	0.81	3.246	0.073	0.2355	0.0046	0.58984	0.0998	0.0015	1465	18	1362	24	1620	30	84.07	92.97
RDT16019-510.d	405	284.6	0.70	1.151	0.025	0.1258	0.0017	0.41605	0.0666	0.0014	776	12	763.6	9.7	812	45	94.04	98.40
RDT16019-511.d	285.6	224.6	0.79	1.473	0.035	0.143	0.002	0.37	0.0747	0.0018	919	15	861	11	1047	48	82.23	93.69
RDT16019-512.d	127.6	179.9	1.41	10.06	0.17	0.4514	0.0056	0.56285	0.1614	0.0025	2438	16	2400	25	2466	27	97.32	98.44
RDT16019-513.d	360.9	233.1	0.65	3.515	0.059	0.2542	0.0028	0.42149	0.1004	0.0017	1531	14	1459	14	1628	31	89.62	95.30
RDT16019-514.d	441.9	182.6	0.41	13.25	0.21	0.5243	0.0066	0.7629	0.1823	0.0025	2696	15	2716	28	2671	22	101.68	100.74
RDT16019-515.d	714	1106	1.55	7.062	0.12	0.3233	0.0042	0.80466	0.1581	0.0021	2117	16	1805	21	2433	23	74.19	85.26
RDT16019-516.d	320.2	314.2	0.98	3.815	0.073	0.2734	0.0037	0.53781	0.1009	0.0018	1594	15	1557	18	1635	32	95.23	97.68
RDT16019-517.d	142.8	66	0.46	1.8	0.3	0.1276	0.004	0.85863	0.098	0.012	982	82	774	23	1450	210	53.38	78.82
RDT16019-518.d	47.38	37.2	0.79	2.48	0.19	0.155	0.0054	0.66976	0.1158	0.0068	1250	57	927	30	1810	120	51.22	74.16
RDT16019-519.d	246.2	114.6	0.47	0.895	0.032	0.0937	0.001	0.16876	0.0691	0.0024	646	17	577.6	6.1	856	73	67.48	89.41
RDT16019-520.d	509	491	0.96	2.967	0.063	0.2229	0.0026	0.45328	0.0964	0.0019	1397	16	1297	14	1551	37	83.62	92.84
RDT16019-521.d	368.3	62.33	0.17	1.543	0.03	0.1539	0.0017	0.29281	0.0729	0.0015	946.5	12	922.3	9.8	1004	42	91.86	97.44
RDT16019-522.d	212.2	81	0.38	1.398	0.038	0.1436	0.0026	0.25084	0.0706	0.002	885	16	864	15	924	60	93.51	97.63
RDT16019-530.d	697.7	302.2	0.43	2.891	0.051	0.2305	0.0026	0.50531	0.0907	0.0015	1378	14	1339	14	1434	32	93.38	97.17
RDT16019-531.d	171.9	82.3	0.48	1.794	0.047	0.1688	0.0023	0.14781	0.0772	0.0021	1042	18	1005	13	1107	56	90.79	96.45
RDT16019-532.d	586	116.6	0.20	1.801	0.077	0.1587	0.0053	0.93439	0.0816	0.0016	1035	29	948	30	1225	39	77.39	91.59
RDT16019-533.d	807	360	0.45	24.65	0.4	0.6118	0.0065	0.81155	0.2915	0.0037	3293	16	3075	26	***3423***	***20***	89.83	93.38
RDT16019-534.d	261.8	123	0.47	2.198	0.05	0.1953	0.0024	0.18242	0.0812	0.0018	1178	16	1149	13	1227	45	93.64	97.54
RDT16019-535.d	188.7	265.4	1.41	10.71	0.18	0.4622	0.0043	0.41341	0.1678	0.0027	2496	15	2448	19	***2531***	***27***	96.72	98.08
RDT16019-536.d	131	127	0.97	1.671	0.053	0.1601	0.004	0.31883	0.0767	0.0026	993	20	956	22	1075	68	88.93	96.27
RDT16019-537.d	65.14	95.4	1.46	1.186	0.058	0.1246	0.0026	0.098538	0.0691	0.0035	784	27	***756***	***15***	810	110	93.33	96.43
RDT16019-538.d	261	26	0.10	1.246	0.043	0.1233	0.0038	0.54352	0.0734	0.0023	817	20	748	22	1016	67	73.62	91.55
RDT16019-539.d	307.7	241.2	0.78	3.655	0.065	0.2658	0.0032	0.45133	0.0992	0.0016	1560	14	1519	16	***1606***	33	94.58	97.37
RDT16019-540.d	2551	2491	0.98	0.763	0.016	0.0785	0.0012	0.74774	0.0701	0.001	574.9	9.2	487.3	7.4	929	29	52.45	84.76
RDT16019-541.d	379.4	284.3	0.75	3.851	0.075	0.226	0.0031	0.61363	0.1232	0.0021	1601	16	1313	16	1996	30	65.78	82.01
RDT16019-542.d	332	208.8	0.63	0.97	0.03	0.1025	0.0013	0.28052	0.069	0.0022	688	16	629.1	7.4	875	64	71.90	91.44
RDT16019-543.d	57.3	115	2.01	4.98	0.17	0.3058	0.0052	0.23197	0.1186	0.004	1815	29	1719	26	***1919***	62	89.58	94.71
RDT16019-544.d	369.8	198.7	0.54	2.457	0.052	0.2084	0.0024	0.35289	0.0853	0.0017	1257	15	***1220***	13	1316	38	92.71	97.06
RDT16019-545.d	228.5	150.9	0.66	1.03	0.036	0.1064	0.0017	0.1904	0.0702	0.0025	715	18	651	10	900	70	72.33	91.05
RDT16019-546.d	221	102.5	0.46	0.653	0.035	0.0664	0.0013	0.55763	0.0711	0.0032	510	22	414	8.2	916	93	45.20	81.18
RDT16019-547.d	886	44.1	0.05	1.486	0.036	0.1507	0.0028	0.7681	0.0714	0.0013	922	15	***904***	***16***	961	36	94.07	98.05
RDT16019-548.d	1239	508	0.41	1.061	0.028	0.1104	0.0017	0.50934	0.07	0.0017	732	14	674.7	9.7	911	47	74.06	92.17
RDT16019-556.d	159	140.2	0.88	10.61	0.21	0.4685	0.0075	0.64673	0.1646	0.0028	2488	19	2474	33	***2497***	29	99.08	99.44
RDT16019-557.d	182.6	257	1.41	3.577	0.095	0.2695	0.0054	0.65542	0.0969	0.0022	1545	22	1537	27	***1552***	42	99.03	99.48
RDT16019-558.d	322.6	545	1.69	4.219	0.099	0.2511	0.005	0.75596	0.1216	0.002	1676	20	1442	26	1974	30	73.05	86.04
RDT16019-559.d	527.4	137.5	0.26	2.474	0.052	0.1868	0.003	0.64484	0.096	0.0017	1262	15	1104	16	1539	34	71.73	87.48
RDT16019-560.d	240.2	122.9	0.51	1.648	0.058	0.163	0.004	0.69754	0.0732	0.0019	982	22	***972***	***22***	997	54	97.49	98.98
RDT16019-42.d	109.1	155.7	1.43	10.15	0.22	0.4545	0.0073	0.56635	0.1612	0.0027	2445	20	2413	33	2463	29	97.97	98.69
RDT16019-43.d	298	129.8	0.44	3.296	0.079	0.229	0.0037	0.59843	0.1038	0.0018	1477	19	1328	19	1685	33	78.81	89.91
RDT16019-44.d	606	210	0.35	1.757	0.04	0.1709	0.0027	0.60031	0.07443	0.0013	1027.9	15	1017	15	1044	34	97.41	98.94
RDT16019-45.d	139.7	61.45	0.44	4.922	0.13	0.3295	0.0066	0.68847	0.1083	0.0021	1804	23	1833	32	1762	35	104.03	101.61
RDT16019-53.d	857	201.7	0.24	1.55	0.034	0.1596	0.0026	0.63344	0.07036	0.0012	949.1	14	954	14	931	34	102.47	100.52

Supplementary Table 1. Main isotopes and ratios measured using LA–ICP–MS. Concordance 1 ($^{206}Pb/^{238}U$/ $^{207}Pb/^{206}Pb$) and 2 ($^{206}Pb/^{238}U/^{207}Pb/^{235}U$)

Analysis Spot	U	Th	Th:U	Ratios							Ages						Concordance Calculations	
				$^{207}Pb/^{235}U$	2σ	$^{206}Pb/^{238}U$	2σ	Rho	$^{207}Pb/^{206}Pb$	2σ	$^{207}Pb/^{235}U$	2σ	$^{206}Pb/^{238}U$	2σ	$^{207}Pb/^{206}Pb$	2σ	1	2
RDT16019-54.d	155.2	143.3	0.92	1.733	0.048	0.1758	0.0031	0.29412	0.0715	0.0018	1017	18	1043	17	952	51	109.56	102.56
RDT16019-55.d	505	31.1	0.06	0.684	0.017	0.0836	0.0014	0.25304	0.0594	0.0013	528.1	10	517.7	8.2	559	51	92.61	98.03
RDT16019-56.d	353	406	1.15	1.042	0.048	0.0836	0.0015	0.61887	0.0893	0.0032	716	23	517.6	9.1	1359	68	38.09	72.29
RDT16019-57.d	152	135.8	0.89	2.075	0.057	0.178	0.0039	0.41894	0.0843	0.002	1135	19	1055	22	1284	48	82.17	92.95
RDT16019-58.d	5223	7380	1.41	0.423	0.029	0.03951	0.00081	0.56344	0.0769	0.0044	353	19	249.8	5	1053	88	23.72	70.76
RDT16019-59.d	126	182	1.44	1.815	0.057	0.1648	0.0032	0.18858	0.0803	0.0025	1044	21	983	18	1156	63	85.03	94.16
RDT16019-60.d	473.9	52	0.11	1.393	0.033	0.1416	0.0024	0.42517	0.0712	0.0014	884	14	853	13	960	40	88.85	96.49
RDT16019-61.d	123.9	88.2	0.71	0.555	0.037	0.04539	0.00096	0.18367	0.0895	0.0059	439	24	286.1	5.9	1160	130	24.66	65.17
RDT16019-62.d	329	198.7	0.60	1.114	0.031	0.1241	0.0021	0.39511	0.0652	0.0015	759	15	**754.7**	**12**	748	51	100.90	99.43
RDT16019-63.d	135	84.2	0.62	20.99	0.92	0.563	0.015	0.91233	0.2657	0.0073	3112	48	2870	62	**3271**	**45**	87.74	92.22
RDT16019-64.d	1934	529.1	0.27	1.525	0.056	0.1056	0.0021	0.58613	0.1044	0.003	931	22	647	12	1663	54	38.91	69.50
RDT16019-65.d	711	898	1.26	9.53	0.27	0.3975	0.0095	0.94995	0.1732	0.0025	2380	26	2151	44	2590	24	83.05	90.38
RDT16019-66.d	354	148.9	0.42	1.738	0.053	0.1728	0.0043	0.64972	0.0733	0.0016	1020	20	**1026**	**23**	1014	44	101.18	100.59
RDT16019-74.d	420	177.2	0.42	1.955	0.044	0.1771	0.0032	0.55821	0.0803	0.0015	1098.1	15	1050	18	1202	38	87.35	95.62
RDT16019-75.d	88.3	51.1	0.58	13.25	0.34	0.4903	0.0099	0.73306	0.1961	0.0035	2696	24	2568	43	**2789**	**30**	92.08	95.25
RDT16019-76.d	88.3	64	0.72	1.503	0.056	0.1246	0.0023	0.089421	0.0882	0.0033	923	23	757	13	1302	75	58.14	82.02
RDT16019-77.d	244.1	35.62	0.15	1.045	0.032	0.0967	0.0015	0.026697	0.0783	0.0022	722	16	594.8	9.1	1108	57	53.68	82.38
RDT16019-78.d	59	75.8	1.28	1.161	0.092	0.0864	0.0021	0.40359	0.0989	0.0069	757	38	533	12	1400	130	38.07	70.41
RDT16019-79.d	261	244	0.93	1.186	0.039	0.117	0.0021	0.37846	0.0737	0.0021	788	17	712.7	12	988	55	72.14	90.44
RDT16019-80.d	51.37	31.78	0.62	1.966	0.075	0.1698	0.0033	0.057302	0.0851	0.0033	1093	26	1010	18	1231	77	82.05	92.41
RDT16019-81.d	1016	7.74	0.01	0.818	0.019	0.0962	0.0015	0.52486	0.06165	0.0011	606	10	591.8	9	652	38	90.77	97.66
RDT16019-82.d	103.9	82.66	0.80	1.56	0.046	0.1525	0.0025	0.20307	0.0741	0.002	949	18	**914**	**14**	1007	56	90.76	96.31
RDT16019-83.d	307	52.3	0.17	0.792	0.025	0.0872	0.0015	0.25105	0.0659	0.0019	590	14	539	9.1	777	60	69.37	91.36
RDT16019-84.d	362.7	222.4	0.61	1.558	0.035	0.156	0.0023	0.39675	0.07225	0.0013	952.6	14	**934.3**	**13**	985	38	94.85	98.08
RDT16019-85.d	141.3	86.9	0.62	3.73	0.088	0.2685	0.0043	0.40208	0.1009	0.0019	1574	19	1532	22	**1627**	**36**	94.16	97.33
RDT16019-86.d	72.61	29.96	0.41	18.54	0.41	0.5563	0.0097	0.62808	0.242	0.0041	3014	22	2847	40	**3126**	**27**	91.07	94.46
RDT16019-94.d	135.4	170	1.26	4.547	0.11	0.2893	0.0047	0.36021	0.1143	0.0023	1737	20	1637	23	1856	36	88.20	94.24
RDT16019-95.d	162.3	98.1	0.60	1.916	0.053	0.1726	0.0029	0.13361	0.0806	0.0021	1083	18	1026	16	1179	52	87.02	94.74
RDT16019-96.d	563	86.7	0.15	2.96	0.33	0.181	0.014	0.9892	0.0999	0.005	1205	88	1049	77	1460	100	71.85	87.05
RDT16019-98.d	664	136.3	0.21	1.884	0.042	0.1774	0.0029	0.54983	0.07672	0.0013	1074.8	14	**1052**	**16**	1109	34	94.86	97.88
RDT16019-99.d	254.3	143.9	0.57	9.462	0.2	0.4212	0.0063	0.64519	0.1622	0.0024	2381.5	19	2264	29	**2477**	**26**	91.40	95.07
RDT16019-100.d	270.3	178.9	0.66	1.216	0.038	0.1208	0.002	0.37189	0.0726	0.0019	804	17	734.9	11	974	55	75.45	91.41
RDT16019-101.d	515.6	129.3	0.25	1.238	0.032	0.1275	0.0022	0.60836	0.0701	0.0014	816	14	773	13	922	39	83.84	94.73
RDT16019-103.d	27.52	9.2	0.33	2.43	0.19	0.112	0.0029	0.27355	0.157	0.011	1178	55	683	17	2110	150	32.37	57.98
RDT16019-104.d	46.5	100.6	2.16	1.358	0.068	0.1398	0.0029	0.034546	0.071	0.0035	857	29	**843**	**16**	830	100	101.57	98.37
RDT16019-105.d	574	147.9	0.26	10.91	0.28	0.4697	0.0085	0.86865	0.1672	0.0026	2508	24	2479	37	**2526**	**26**	98.14	98.84
RDT16019-106.d	203.2	94.1	0.46	1.381	0.039	0.1373	0.0022	0.16343	0.0727	0.0018	877	17	829.3	12	979	53	84.71	94.56
RDT16019-107.d	295.2	33.8	0.11	0.897	0.027	0.1004	0.0018	0.2422	0.0649	0.0018	647	15	616.4	10	738	60	83.52	95.27
RDT16019-108.d	648	366	0.56	0.746	0.021	0.0871	0.0015	0.47567	0.0618	0.0014	564.5	12	538.5	9.1	648	48	83.10	95.39
RDT16019-109.d	220.1	89.4	0.41	2.293	0.057	0.1842	0.0029	0.43499	0.09	0.0019	1206	18	1089	16	1407	41	77.40	90.30
RDT16019-110.d	1511	98.3	0.07	1.429	0.036	0.1411	0.0026	0.7561	0.07368	0.0012	902	16	850	15	1026	34	82.85	94.24
RDT16019-121.d	469	174.7	0.37	20.42	0.48	0.6102	0.011	0.82018	0.2424	0.0036	3109	24	3070	44	**3133**	**23**	97.99	98.75
RDT16019-122.d	244	86.1	0.35	2.864	0.074	0.2395	0.0045	0.69476	0.0865	0.0016	1369	20	1383	23	***1343***	***36***	102.98	101.02
RDT16019-123.d	593	57.4	0.10	0.816	0.022	0.091	0.0017	0.45765	0.0649	0.0015	603.7	12	561.4	9.8	758	47	74.06	92.99
RDT16019-124.d	148.8	171.2	1.15	2.382	0.065	0.2029	0.0035	0.3136	0.0854	0.0021	1233	20	**1190**	**19**	1300	46	91.54	96.51
RDT16019-125.d	218.2	132.7	0.61	9.75	0.21	0.4274	0.0069	0.69898	0.1651	0.0026	2408	20	2292	31	2505	26	91.50	95.18
RDT16019-126.d	1738	443.9	0.26	1.135	0.061	0.0966	0.0034	0.95433	0.0831	0.002	757	28	593	20	1244	49	47.67	78.34

Supplementary Table 1. Main isotopes and ratios measured using LA–ICP–MS. Concordance 1 ($^{206}Pb/^{238}U$/ $^{207}Pb/^{206}Pb$) and 2 ($^{206}Pb/^{238}U/^{207}Pb/^{235}U$)

Analysis Spot	U	Th	Th:U	Ratios							Ages						Concordance Calculations	
				$^{207}Pb/^{235}U$	2σ	$^{206}Pb/^{238}U$	2σ	Rho	$^{207}Pb/^{206}Pb$	2σ	$^{207}Pb/^{235}U$	2σ	$^{206}Pb/^{238}U$	2σ	$^{207}Pb/^{206}Pb$	2σ	1	2
RDT16019-127.d	302.4	271.2	0.90	2.677	0.06	0.2248	0.0036	0.53299	0.0861	0.0015	1319.5	17	**1307**	**19**	1333	34	98.05	99.05
RDT16019-128.d	382.2	332.2	0.87	0.733	0.019	0.08557	0.0013	0.23984	0.0622	0.0015	557.2	12	529.1	7.8	659	54	80.29	94.96
RDT16019-129.d	58.8	53.4	0.91	1.719	0.099	0.1284	0.0028	0.32366	0.0966	0.005	1003	37	778	16	1458	99	53.36	77.57
RDT16019-130.d	243	104.8	0.43	1.308	0.036	0.1392	0.0025	0.54245	0.0681	0.0015	846	16	840	14	856	45	98.13	99.29
RDT16019-131.d	167.5	323	1.93	10.29	0.22	0.4536	0.0073	0.63729	0.1642	0.0026	2458	20	2409	32	2497	27	96.48	98.01
RDT16019-134.d	1077	56	0.05	2.037	0.044	0.1838	0.003	0.70561	0.0802	0.0012	1127.1	15	1087	16	1200	31	90.58	96.44
RDT16019-142.d	448.9	56.2	0.13	0.761	0.02	0.08951	0.0014	0.26449	0.0615	0.0014	573.7	11	552.5	8	636	48	86.87	96.30
RDT16019-143.d	12.42	0.138	0.01	3.16	0.28	0.1384	0.0048	0.44477	0.167	0.014	1346	68	833	27	2150	170	38.74	61.89
RDT16019-144.d	440	3.26	0.01	0.76	0.022	0.0873	0.0015	0.36957	0.0628	0.0015	571	13	539.3	9.1	674	53	80.01	94.45
RDT16019-145.d	1136	139.3	0.12	0.795	0.021	0.0881	0.0019	0.68323	0.06537	0.0013	592	12	543.9	11	772	41	70.45	91.88
RDT16019-146.d	757	180.2	0.24	1.364	0.037	0.1308	0.0023	0.6416	0.0754	0.0015	871	16	792	13	1062	39	74.58	90.93
~~RDT16019-147.d~~	~~43.94~~	~~Below LOD~~	~~#VALUE!~~	~~1.297~~	~~0.099~~	~~0.0987~~	~~0.0026~~	~~0.013656~~	~~0.0971~~	~~0.0074~~	~~801~~	~~36~~	~~606~~	~~15~~	~~1280~~	~~130~~	~~47.34~~	75.66
RDT16019-148.d	651	167.5	0.26	1.299	0.033	0.1377	0.0025	0.67082	0.06814	0.0013	843	15	831	14	861	39	96.52	98.58
RDT16019-149.d	200.1	136.3	0.68	4.44	0.14	0.2157	0.0041	0.80089	0.1473	0.0031	1710	26	1260	22	2306	36	54.64	73.68
RDT16019-150.d	611	651	1.07	10.005	0.21	0.4462	0.0068	0.78566	0.162	0.0023	2433.1	19	2377	30	**2478**	**24**	95.92	97.69
RDT16019-151.d	388	45.8	0.12	1.257	0.051	0.1264	0.004	0.88236	0.0714	0.0016	815	24	765	23	944	47	81.04	93.87
RDT16019-152.d	194	178.8	0.92	0.808	0.031	0.093	0.0019	0.3534	0.0631	0.0021	596	17	572.8	11	644	74	88.94	96.11
RDT16019-153.d	478.7	202.7	0.42	1.621	0.04	0.1537	0.0026	0.45704	0.0762	0.0015	976	15	921	14	1091	41	84.42	94.36
RDT16019-154.d	1521	167.3	0.11	3.212	0.072	0.2203	0.004	0.84619	0.10544	0.0016	1458.6	17	1283	21	1718	27	74.68	87.96
RDT16019-162.d	133.5	57.22	0.43	11.58	0.24	0.4747	0.0072	0.6336	0.1765	0.0028	2569.3	20	2502	32	**2615**	**26**	95.68	97.38
RDT16019-163.d	246.6	74.1	0.30	2.222	0.054	0.203	0.0032	0.46299	0.0792	0.0015	1186	17	**1191**	**17**	1167	39	102.06	100.42
RDT16019-164.d	62.6	39.5	0.63	0.887	0.045	0.0897	0.0019	0.0062059	0.0723	0.0038	636	25	553.3	11	890	110	62.17	87.00
RDT16019-165.d	354.9	155.5	0.44	1.572	0.041	0.1522	0.0024	0.40552	0.0749	0.0016	958	17	912.7	13	1048	44	87.09	95.27
~~RDT16019-166.d~~	~~0.148~~	~~0.141~~	~~0.95~~	~~no value~~	~~NAN~~	~~no value~~	~~NAN~~	~~NaN~~	~~no value~~	~~NAN~~	~~no value~~	~~NAN~~	~~no value~~	~~NAN~~	~~no value~~	~~NAN~~	~~#VALUE!~~	#VALUE!
RDT16019-167.d	863.5	559.6	0.65	1.53	0.034	0.1493	0.0023	0.57086	0.07408	0.0013	940.7	14	896.7	13	1034	34	86.72	95.32
RDT16018-568.d	122.1	149.8	1.23	1.173	0.084	0.0901	0.0023	0.35812	0.0926	0.0059	773	38	556	13	1370	130	40.58	71.93
RDT16018-569.d	225.8	144.3	0.64	2.28	0.048	0.1988	0.0036	0.57495	0.0833	0.0017	1204	15	1168	19	1265	39	92.33	97.01
RDT16018-573.d	271.6	40.81	0.15	3.117	0.068	0.2467	0.0044	0.5899	0.0914	0.0019	1434	17	1420	23	1443	40	98.41	99.02
RDT16018-574.d	228.9	68.9	0.30	1.682	0.044	0.1629	0.0028	0.47882	0.0746	0.0018	999	17	972	16	1047	49	92.84	97.30
RDT16018-575.d	186.8	126.1	0.68	2.795	0.065	0.2186	0.0045	0.57148	0.0933	0.0021	1351	17	1273	24	1480	42	86.01	94.23
RDT16018-576.d	816	105.7	0.13	12.62	0.24	0.4852	0.0086	0.85764	0.1882	0.0026	2649	18	2547	37	2724	22	93.50	96.15
RDT16018-577.d	2720	1103	0.41	1.271	0.025	0.1044	0.0018	0.8267	0.0881	0.0013	831.6	11	640	11	1383	28	46.28	76.96
RDT16018-578.d	720	184	0.26	1.917	0.043	0.1677	0.0041	0.78893	0.0832	0.0015	1084	15	999	22	1269	36	78.72	92.16
RDT16018-579.d	2169	1663	0.77	0.554	0.017	0.0579	0.0014	0.73778	0.0689	0.0014	446.4	11	362.5	8.7	885	41	40.96	81.21
RDT16018-581.d	232.1	242.4	1.04	5.333	0.11	0.3341	0.0063	0.65796	0.1157	0.0021	1871	17	1856	30	1887	33	98.36	99.20
RDT16018-582.d	311.6	489	1.57	1.763	0.056	0.1638	0.003	0.57377	0.0783	0.0021	1030	21	977	17	1132	53	86.31	94.85
RDT16018-583.d	1249	542	0.43	1.5	0.16	0.1003	0.0039	0.78953	0.108	0.0081	892	48	615	23	1660	110	37.05	68.95
RDT16018-584.d	210.5	130.5	0.62	1.668	0.05	0.1547	0.0028	0.40939	0.0786	0.0023	992	19	927	16	1136	57	81.60	93.45
RDT16018-585.d	142	127	0.89	2.694	0.073	0.2186	0.0044	0.56191	0.0895	0.0021	1322	20	1273	24	1397	46	91.12	96.29
RDT16018-586.d	122.5	89.1	0.73	1.144	0.054	0.1215	0.0023	0.3938	0.0689	0.0031	770	26	739	13	845	98	87.46	95.97
018 - 1	131.6	215	1.63	0.76	0.021	0.0918	0.0009	0.22758	0.0603	0.0017	573	12	***566.1***	***5.3***	608	62	93.11	98.80
018 - 2	264	298	1.13	0.736	0.018	0.08955	0.00088	0.42934	0.06	0.0014	560.8	10	***552.8***	***5.2***	602	50	91.83	98.57
018 - 3	70.2	115.7	1.65	23.39	0.29	0.6652	0.0074	0.76987	0.256	0.0023	3244	12	3287	29	***3221.4***	***14***	102.04	101.33
018 - 4	57.2	111.6	1.95	0.834	0.042	0.0934	0.0011	0.613	0.0653	0.0034	613	22	575.5	6.7	742	99	77.56	93.88
018 - 5	61.5	57.5	0.93	4.498	0.079	0.3009	0.0039	0.49831	0.1074	0.0018	1730	15	1696	20	***1760***	***33***	96.36	98.03
018 - 6	171	191	1.12	3.24	0.047	0.2579	0.0025	0.58442	0.0918	0.0012	1466	11	1479	13	***1460***	***24***	101.30	100.89
018 - 7	377	445	1.18	1.92	0.02	0.1809	0.0013	0.3716	0.07719	0.00083	1088.7	7.3	***1071.9***	***7.2***	1129	21	94.94	98.46

Supplementary Table 1. Main isotopes and ratios measured using LA–ICP–MS. Concordance 1 ($^{206}Pb/^{238}U$/ $^{207}Pb/^{206}Pb$) and 2 ($^{206}Pb/^{238}U/^{207}Pb/^{235}U$)

Analysis Spot	U	Th	Th:U	Ratios							Ages						Concordance Calculations	
				$^{207}Pb/^{235}U$	2σ	$^{206}Pb/^{238}U$	2σ	Rho	$^{207}Pb/^{206}Pb$	2σ	$^{207}Pb/^{235}U$	2σ	$^{206}Pb/^{238}U$	2σ	$^{207}Pb/^{206}Pb$	2σ	1	2
018 - 8	148.3	70.3	0.47	2.217	0.032	0.1998	0.0019	0.34324	0.0803	0.0011	1185.8	10	***1174.4***	***10***	1200	28	97.87	99.04
018 - 9	117.9	170	1.44	0.948	0.073	0.0906	0.0014	0.77708	0.0745	0.0045	669	35	558.9	8.1	1000	110	55.89	83.54
018 - 10	291	449	1.54	0.64	0.012	0.08184	0.00079	0.15851	0.0575	0.0011	503.4	7.9	***507.1***	***4.7***	524	41	96.77	100.74
018 - 11	81.9	240	2.93	0.849	0.034	0.08843	0.0011	0.30494	0.07	0.0025	622	19	547.2	6.6	948	68	57.72	87.97
018 - 12	134.4	183.8	1.37	1.553	0.03	0.1581	0.0017	0.39847	0.0709	0.0013	951	12	***946.3***	***9.2***	953	38	99.30	99.51
018 - 13	269	143	0.53	1.318	0.057	0.1432	0.0043	0.93549	0.0669	0.0013	849	26	***862***	***24***	827	40	104.23	101.53
018 - 14	275	270	0.98	0.708	0.013	0.08731	0.00078	0.12211	0.0589	0.0012	542.9	8	***539.6***	***4.6***	568	45	95.00	99.39
018 - 15	43.3	33.1	0.76	2.077	0.061	0.1965	0.0027	0.054656	0.0784	0.0025	1142	21	***1157***	***14***	1150	67	100.61	101.31
018 - 16	213	226	1.06	6.65	0.11	0.341	0.0043	0.86315	0.1422	0.0016	2065	15	1891	21	2253	19	83.93	91.57
018 - 17	86	40.8	0.47	1.347	0.045	0.1431	0.0028	0.60059	0.0684	0.0019	864	20	***862***	***16***	891	58	96.75	99.77
018 - 18	701	462	0.66	13.987	0.12	0.5527	0.0047	0.85158	0.18393	0.0013	2748.6	8.1	2838	19	***2687.7***	***12***	105.59	103.25
018 - 19	97	150.7	1.55	10.25	0.15	0.4718	0.0061	0.80377	0.1594	0.0017	2457	14	2491	27	***2450***	***17***	101.67	101.38
018 - 20	175	190.2	1.09	8.31	0.34	0.3031	0.0064	0.50346	0.2019	0.0078	2258	36	1706	32	2824	62	60.41	75.55
018 - 21	113	280	2.48	0.723	0.021	0.08666	0.00097	0.13872	0.0608	0.0019	555	13	535.7	5.8	644	64	83.18	96.52
018 - 22	132.4	241	1.82	2.127	0.035	0.1925	0.0016	0.047826	0.0805	0.0014	1157	11	***1135.1***	***8.7***	1210	33	93.81	98.11
018 - 23	186	105	0.56	1.507	0.028	0.1521	0.0016	0.37065	0.0725	0.0012	932	11	***912.6***	***9.2***	1003	32	90.99	97.92
018 - 24	35.3	38.4	1.09	22.49	0.31	0.6447	0.0083	0.6315	0.2548	0.0034	3204	13	3207	32	***3215***	***21***	99.75	100.09
018 - 25	135.9	184.1	1.35	1.79	0.032	0.1746	0.0022	0.43495	0.0749	0.0013	1041	12	***1037***	***12***	1066	33	97.28	99.62
018 - 26	168.3	179.6	1.07	1.495	0.028	0.1531	0.0013	0.52572	0.071	0.0012	928	11	***918.2***	***7.5***	958	34	95.85	98.94
018 - 27	718	250	0.35	1.483	0.035	0.151	0.0034	0.9405	0.07159	0.00068	922	15	***906***	***19***	972	19	93.21	98.26
018 - 28	534.8	111.3	0.21	1.197	0.057	0.1298	0.0044	0.96618	0.0674	0.0012	803	26	***791***	***24***	843	38	93.83	98.51
018 - 29	300	214	0.71	3.543	0.097	0.2065	0.0047	0.94373	0.1256	0.0014	1534	21	1209	25	2038	19	59.32	78.81
018 - 30	208	198	0.95	1.677	0.049	0.1652	0.0021	0.57414	0.0742	0.0015	1002	16	***986***	***11***	1040	39	94.81	98.40
018 - 31	106.7	126.5	1.19	1.278	0.034	0.1347	0.0016	0.3749	0.0696	0.0019	835	15	814.5	8.9	921	55	88.44	97.54
018 - 32	158.3	81.05	0.51	5.595	0.058	0.3513	0.0032	0.46321	0.11581	0.0012	1915	9	1941	15	***1893***	***17***	102.54	101.36
018 - 33	167.9	111.5	0.66	10.617	0.11	0.4793	0.0045	0.70628	0.1624	0.0015	2489.7	10	2524	20	***2480***	***16***	101.77	101.38
018 - 34	118.7	183.9	1.55	2.109	0.034	0.1947	0.0017	0.11505	0.0785	0.0013	1151	11	***1146.8***	***9.4***	1170	33	98.02	99.64
018 - 35	371	278	0.75	1.705	0.025	0.1687	0.0014	0.3359	0.07391	0.00097	1013.9	8.5	***1004.8***	***7.7***	1039	28	96.71	99.10
018 - 36	162	104	0.64	1.489	0.021	0.1524	0.0014	0.073375	0.0712	0.0011	925.5	8.5	***914.3***	***7.7***	965	30	94.75	98.79
018 - 37	577.5	657	1.14	2.613	0.05	0.2168	0.0035	0.94266	0.08784	0.00082	1303	14	***1264***	***18***	1382	18	91.46	97.01
018 - 38	111	87.9	0.79	2.626	0.041	0.2193	0.0023	0.35527	0.0872	0.0013	1307	12	***1278***	***12***	1366	29	93.56	97.78
018 - 39	217.8	308.8	1.42	1.58	0.057	0.1599	0.0045	0.85579	0.0723	0.0013	962	22	***956***	***25***	989	37	96.66	99.38
018 - 40	213.9	137.9	0.64	1.664	0.036	0.1645	0.002	0.62543	0.0737	0.0012	996	13	***981.5***	***11***	1030	33	95.29	98.54
018 - 41	141.7	167.5	1.18	0.716	0.018	0.0876	0.00084	0.28921	0.0601	0.0016	547	11	542.1	4.7	609	60	89.01	99.10
018 - 42	176.7	187	1.06	0.717	0.013	0.08913	0.00097	0.36883	0.05921	0.00096	548.7	7.7	550.4	5.7	575	37	95.72	100.31
018 - 43	81	254	3.14	4.213	0.083	0.2894	0.0025	0.33941	0.1057	0.0018	1675	16	1638.5	13	***1722***	***32***	95.15	97.82
018 - 44	276	393	1.42	1.658	0.021	0.1673	0.0013	0.37445	0.07226	0.00091	992.5	8	997.2	6.9	990	26	100.73	100.47
018 - 45	106.7	172.1	1.61	1.104	0.028	0.1232	0.0015	0.37354	0.0654	0.0015	754	13	749	8.7	785	47	95.41	99.34
018 - 46	254	77	0.30	1.883	0.025	0.1842	0.0019	0.38898	0.0747	0.0011	1074.8	8.6	1089.6	10	1064	30	102.41	101.38
018 - 47	153	344	2.25	0.758	0.022	0.09074	0.001	0.47012	0.0611	0.0017	572	13	559.9	6.1	630	59	88.87	97.88
018 - 48	79.7	87.6	1.10	1.798	0.044	0.1744	0.0017	0.27822	0.0752	0.0018	1043	16	1036.3	9.1	1072	49	96.67	99.36
018 - 49	251	98.1	0.39	1.421	0.023	0.1487	0.0015	0.59153	0.0697	0.00096	898.7	9.5	893.4	8.7	924	28	96.69	99.41
018 - 50	222	68.6	0.31	4.072	0.06	0.2892	0.0032	0.77259	0.10299	0.001	1649	12	1637	16	1677	19	97.61	99.27
rdt16018-9.d	286.6	185.4	0.65	0.969	0.046	0.1097	0.0022	0.38027	0.0631	0.0027	685	24	671	12	689	91	97.39	97.96
rdt16018-10.d	152.1	121.6	0.80	2.181	0.095	0.2042	0.0049	0.60688	0.077	0.0028	1173	30	1197	26	1129	79	106.02	102.05
rdt16018-12.d	174	156	0.90	1.667	0.076	0.166	0.004	0.58378	0.0714	0.0027	996	28	989	22	969	78	102.06	99.30

Supplementary Table 1. Main isotopes and ratios measured using LA–ICP–MS. Concordance 1 ($^{206}Pb/^{238}U$/ $^{207}Pb/^{206}Pb$) and 2 ($^{206}Pb/^{238}U/^{207}Pb/^{235}U$)

Analysis Spot	U	Th	Th:U	Ratios							Ages						Concordance Calculations	
				$^{207}Pb/^{235}U$	2σ	$^{206}Pb/^{238}U$	2σ	Rho	$^{207}Pb/^{206}Pb$	2σ	$^{207}Pb/^{235}U$	2σ	$^{206}Pb/^{238}U$	2σ	$^{207}Pb/^{206}Pb$	2σ	1	2
rdt16018-13.d	587	194.5	0.33	2.636	0.11	0.1997	0.004	0.71338	0.0941	0.0032	1309	30	1177	21	1512	63	77.84	89.92
rdt16018-14.d	350.8	94.4	0.27	6.68	0.28	0.3646	0.0091	0.80491	0.1308	0.0045	2068	37	2000	43	2106	59	94.97	96.71
rdt16018-15.d	434.8	289.6	0.67	1.075	0.046	0.1211	0.0025	0.56104	0.063	0.0024	741	22	736	15	712	80	103.37	99.33
rdt16018-16.d	85.8	56.9	0.66	1.395	0.087	0.1071	0.0026	0.3799	0.0935	0.0053	878	37	655	15	1479	110	44.29	74.60
rdt16018-17.d	200.5	154.3	0.77	2.124	0.096	0.198	0.0048	0.70094	0.0765	0.0027	1154	31	1164	26	1096	72	106.20	100.87
rdt16018-18.d	755	278.2	0.37	0.679	0.029	0.0819	0.0019	0.53508	0.059	0.0022	525.3	17	507	11	568	79	89.26	96.52
rdt16018-19.d	163.6	112.6	0.69	1.461	0.068	0.1516	0.0037	0.6138	0.0693	0.0027	914	28	909	21	905	78	100.44	99.45
rdt16018-20.d	141.7	124.3	0.88	0.725	0.036	0.0875	0.0021	0.37963	0.0592	0.0027	552	21	540	12	566	100	95.41	97.83
rdt16018-21.d	206.3	128.9	0.62	3.527	0.15	0.2644	0.0059	0.61995	0.0953	0.0034	1533	34	1511	30	1537	71	98.31	98.56
rdt16018-29.d	292.6	61.6	0.21	0.87	0.041	0.0972	0.0025	0.42918	0.0668	0.0027	634	22	598	14	821	84	72.84	94.32
rdt16018-30.d	139.7	71.5	0.51	1.337	0.068	0.1301	0.0033	0.45085	0.0749	0.0034	858	30	788	19	1093	88	72.10	91.84
rdt16018-31.d	238.1	148.3	0.62	0.803	0.036	0.0916	0.002	0.23874	0.0648	0.0027	598	20	565	12	774	86	73.00	94.48
rdt16018-32.d	144	93.5	0.65	23.8	1.2	0.391	0.011	0.75792	0.4475	0.016	3259	48	2125	49	4071	57	52.20	65.20
rdt16018-33.d	172.3	129	0.75	3.228	0.14	0.2587	0.006	0.65191	0.0934	0.0034	1467	33	1484	31	1488	69	99.73	101.16
rdt16018-34.d	76	54.7	0.72	12.06	0.51	0.4344	0.01	0.58298	0.2041	0.0073	2613	37	2322	45	2852	58	81.42	88.86
rdt16018-35.d	163.8	183.1	1.12	1.717	0.076	0.1675	0.0038	0.53099	0.0755	0.0029	1013	28	998	21	1071	77	93.18	98.52
rdt16018-36.d	53.8	77.9	1.45	9.84	0.56	0.413	0.017	0.8397	0.1734	0.0066	2412	53	2225	78	2582	64	86.17	92.25
rdt16018-37.d	136.4	146.9	1.08	1.196	0.058	0.1359	0.0034	0.298	0.0645	0.003	798	28	820	19	750	99	109.33	102.76
rdt16018-38.d	834	983	1.18	0.589	0.028	0.0678	0.002	0.81087	0.0635	0.0023	469	18	422	12	712	78	59.27	89.98
rdt16018-39.d	354.7	317.9	0.90	1.83	0.075	0.1734	0.0034	0.6116	0.0765	0.0027	1055	27	1030	19	1099	70	93.72	97.63
rdt16018-40.d	142.1	155	1.09	0.814	0.044	0.0893	0.0021	0.097808	0.0658	0.0034	601	23	552	12	783	100	70.50	91.85
rdt16018-41.d	880	370	0.42	4.021	0.16	0.2746	0.0052	0.76851	0.1057	0.0035	1639	32	1565	26	1724	62	90.78	95.49
rdt16018-43.d	215.1	134.7	0.63	1.781	0.081	0.1676	0.0039	0.57864	0.0757	0.0029	1038	30	1002	22	1088	79	92.10	96.53
rdt16018-44.d	122.5	86.7	0.71	0.828	0.048	0.0938	0.0023	0.20199	0.0647	0.0034	607	27	578	13	734	120	78.75	95.22
rdt16018-52.d	70.3	45	0.64	1.519	0.079	0.1499	0.004	0.39081	0.0713	0.0034	936	31	902	23	947	110	95.25	96.37
rdt16018-53.d	796	143.7	0.18	5.4	0.22	0.3347	0.0073	0.74397	0.1158	0.0039	1886	34	1859	35	1889	61	98.41	98.57
rdt16018-54.d	752	364	0.48	2.117	0.087	0.1805	0.0041	0.74099	0.0838	0.0029	1155	29	1069	22	1292	69	82.74	92.55
rdt16018-55.d	283	47.78	0.17	1.726	0.074	0.1656	0.004	0.49608	0.0752	0.0029	1016	28	987	22	1085	75	90.97	97.15
rdt16018-56.d	230.5	120.9	0.52	2.016	0.087	0.1843	0.0041	0.45085	0.0787	0.003	1122	30	1089	22	1176	73	92.60	97.06
rdt16018-58.d	316.2	119.6	0.38	3.127	0.13	0.2397	0.0052	0.64688	0.0935	0.0033	1438	31	1386	27	1490	66	93.02	96.38
rdt16018-59.d	204.1	276.5	1.35	1.909	0.088	0.1672	0.004	0.50851	0.0811	0.0033	1082	32	998	22	1212	81	82.34	92.24
rdt16018-60.d	371	252.4	0.68	1.752	0.078	0.1627	0.0041	0.63404	0.0783	0.0029	1026	28	971	23	1150	76	84.43	94.64
rdt16018-61.d	324.5	87.4	0.27	1.816	0.1	0.1631	0.0052	0.76129	0.0793	0.003	1046	35	972	29	1173	77	82.86	92.93
rdt16018-62.d	222.9	424	1.90	0.793	0.038	0.0819	0.0019	0.33228	0.0703	0.0032	592	22	507	11	922	97	54.99	85.64
rdt16018-63.d	422.8	229.6	0.54	1.676	0.07	0.1628	0.0036	0.61644	0.0742	0.0026	999	27	972	20	1043	72	93.19	97.30
rdt16018-71.d	3212	258.7	0.08	0.405	0.019	0.0514	0.0013	0.88545	0.05872	0.0021	345.5	14	322.9	8	546	77	59.14	93.46
rdt16018-72.d	85.2	131.6	1.54	0.714	0.04	0.0821	0.0022	0.13377	0.0642	0.0035	543	24	509	13	706	120	72.10	93.74
rdt16018-73.d	941	304	0.32	1.685	0.066	0.1671	0.0032	0.70813	0.07322	0.0025	1002.8	25	996	17	1016	70	98.03	99.32
rdt16018-74.d	88.8	130.5	1.47	0.84	0.11	0.0851	0.0026	0.58582	0.0701	0.007	575	38	528	16	730	150	72.33	91.83
rdt16018-75.d	308.7	392.1	1.27	1.74	0.073	0.1684	0.0038	0.51903	0.0748	0.0028	1021	27	1004	21	1056	77	95.08	98.33
rdt16018-76.d	544.4	140.4	0.26	2.778	0.12	0.2276	0.0053	0.78969	0.0877	0.003	1348	32	1321	28	1376	66	96.00	98.00
rdt16018-77.d	124.7	81.9	0.66	8.3	1.2	0.2404	0.0097	0.81669	0.224	0.026	2050	140	1384	50	2600	220	53.23	67.51
rdt16018-78.d	396	63.26	0.16	1.261	0.057	0.1311	0.0032	0.1801	0.0693	0.0027	829	25	794	18	895	78	88.72	95.78
rdt16018-79.d	2527	1085	0.43	0.796	0.036	0.0747	0.0024	0.89287	0.077	0.0026	593	20	464	14	1113	69	41.69	78.25
rdt16018-80.d	618	218	0.35	0.822	0.035	0.0946	0.002	0.60157	0.0625	0.0023	609	20	583	12	684	76	85.23	95.73
rdt16018-81.d	427.6	246.3	0.58	0.747	0.034	0.0846	0.002	0.36871	0.0631	0.0026	567	20	523	12	719	86	72.74	92.24
rdt16018-82.d	48.3	22.28	0.46	3.12	0.18	0.265	0.01	0.60216	0.0844	0.0041	1421	44	1507	53	1285	97	117.28	106.05

Supplementary Table 1. Main isotopes and ratios measured using LA–ICP–MS. Concordance 1 ($^{206}Pb/^{238}U$/ $^{207}Pb/^{206}Pb$) and 2 ($^{206}Pb/^{238}U/^{207}Pb/^{235}U$)

Analysis Spot	U	Th	Th:U	Ratios							Ages						Concordance Calculations	
				$^{207}Pb/^{235}U$	2σ	$^{206}Pb/^{238}U$	2σ	Rho	$^{207}Pb/^{206}Pb$	2σ	$^{207}Pb/^{235}U$	2σ	$^{206}Pb/^{238}U$	2σ	$^{207}Pb/^{206}Pb$	2σ	1	2
rdt16018-84.d	202.5	13.26	0.07	0.822	0.042	0.0902	0.0022	0.36592	0.065	0.003	609	23	556	13	774	98	71.83	91.30
rdt16018-85.d	232	66.2	0.29	1.035	0.05	0.1141	0.003	0.57351	0.0645	0.0027	720	25	696	17	760	90	91.58	96.67
rdt16018-93.d	180.6	179	0.99	1.21	0.057	0.1248	0.0032	0.38338	0.0715	0.0031	802	26	759	19	971	89	78.17	94.64
rdt16018-94.d	353.4	212.7	0.60	1.148	0.056	0.1066	0.0024	0.29792	0.079	0.0035	776	26	653	14	1168	88	55.91	84.15
rdt16018-95.d	291.7	290.5	1.00	1.564	0.066	0.1521	0.0031	0.37497	0.0764	0.0029	955	26	916	17	1101	79	83.20	95.92
rdt16018-96.d	47	25.65	0.55	5.49	0.27	0.2448	0.007	0.54319	0.1653	0.007	1900	43	1413	37	2501	76	56.50	74.37
rdt16018-97.d	371	237.8	0.64	3.106	0.13	0.2415	0.0055	0.70216	0.0944	0.0033	1434	32	1396	29	1515	65	92.15	97.35
rdt16018-98.d	239.2	146.9	0.61	3.251	0.14	0.2548	0.0061	0.65871	0.0935	0.0034	1465	33	1461	31	1497	69	97.60	99.73
rdt16018-99.d	182.6	42.43	0.23	1.12	0.057	0.1172	0.003	0.4328	0.0692	0.0031	762	28	714	18	905	95	78.90	93.70
rdt16018-100.d	261.1	220.4	0.84	1.529	0.066	0.1532	0.0033	0.40915	0.0732	0.0028	943	25	918	18	1012	77	90.71	97.35
rdt16018-101.d	310.9	137.2	0.44	7.07	0.29	0.3469	0.008	0.80848	0.1487	0.0051	2119	36	1917	38	2337	56	82.03	90.47
rdt16018-102.d	103.8	129.7	1.25	3.534	0.15	0.2583	0.0063	0.51861	0.1004	0.0039	1533	35	1479	32	1619	74	91.35	96.48
rdt16018-103.d	144.8	190.8	1.32	0.633	0.035	0.079	0.0022	0.3993	0.058	0.0029	497	21	491	13	502	110	97.81	98.79
rdt16018-104.d	1085	344	0.32	1.379	0.06	0.1414	0.0042	0.72438	0.0706	0.0026	878	26	852	24	941	76	90.54	97.04
rdt16018-105.d	374.2	934	2.50	0.721	0.036	0.0806	0.002	0.44536	0.0641	0.0026	549	21	499	12	737	87	67.71	90.89
rdt16018-106.d	49.55	22.49	0.45	1.116	0.072	0.103	0.0032	0.083484	0.0798	0.0053	760	33	631	19	1110	130	56.85	83.03
rdt16018-107.d	128.5	138	1.07	1.714	0.092	0.1393	0.0033	0.32027	0.0879	0.0042	1011	33	842	18	1370	94	61.46	83.28
rdt16018-115.d	1825	732	0.40	0.846	0.035	0.0804	0.0018	0.68442	0.0759	0.0027	625	20	498	11	1090	67	45.69	79.68
rdt16018-116.d	331.1	624.1	1.88	0.681	0.032	0.0807	0.002	0.39301	0.0609	0.0027	527	20	500	12	632	94	79.11	94.88
rdt16018-117.d	624.7	216.1	0.35	5.148	0.21	0.3214	0.0074	0.82079	0.1151	0.0039	1846	35	1794	36	1876	60	95.63	97.18
rdt16018-118.d	151.3	241.6	1.60	2.136	0.1	0.1831	0.0046	0.65032	0.0849	0.0034	1157	34	1083	25	1303	77	83.12	93.60
rdt16018-119.d	70.1	28.83	0.41	1.549	0.084	0.1528	0.0038	0.27677	0.0722	0.0037	944	34	918	21	991	110	92.63	97.25
rdt16018-120.d	115	81.9	0.71	9.98	0.42	0.4311	0.0098	0.77633	0.166	0.0057	2430	40	2307	44	2519	59	91.58	94.94
rdt16018-121.d	454.3	127.9	0.28	2.29	0.096	0.1895	0.0037	0.64433	0.0871	0.0031	1208	30	1118	20	1363	67	82.02	92.55
rdt16018-122.d	689	156.3	0.23	1.098	0.051	0.1077	0.003	0.80702	0.0723	0.0025	754	25	659	18	1003	71	65.70	87.40
rdt16018-123.d	304.6	110.3	0.36	1.476	0.063	0.1497	0.0037	0.63551	0.0704	0.0026	921	25	898	21	937	75	95.84	97.50
rdt16018-124.d	598.8	349.4	0.58	1.459	0.061	0.1503	0.0035	0.73632	0.0702	0.0025	911	26	902	20	933	69	96.68	99.01
rdt16018-125.d	624	106	0.17	1.669	0.068	0.1665	0.0036	0.75798	0.0729	0.0025	999	26	992	20	1009	69	98.32	99.30
rdt16018-126.d	445.9	38.6	0.09	2.67	0.11	0.2214	0.0051	0.72441	0.0866	0.0031	1319	33	1288	27	1362	70	94.57	97.65
rdt16018-134.d	379	187	0.49	4.222	0.17	0.2914	0.0065	0.72821	0.1038	0.0036	1675	34	1646	33	1689	63	97.45	98.27
rdt16018-135.d	335.4	352.7	1.05	1.056	0.052	0.0999	0.0034	0.37558	0.0771	0.0036	730	26	613	20	1128	94	54.34	83.97
rdt16018-136.d	459.6	4.98	0.01	0.73	0.033	0.0875	0.002	0.50082	0.0598	0.0024	556	19	541	12	587	84	92.16	97.30
rdt16018-137.d	232.5	300	1.29	0.703	0.035	0.0868	0.0021	0.1843	0.0584	0.0029	541	20	536	13	517	110	103.68	99.08
rdt16018-138.d	99.9	201.7	2.02	0.843	0.05	0.0876	0.0025	0.13147	0.0695	0.004	619	27	541	15	850	120	63.65	87.40
rdt16018-139.d	272.5	197.4	0.72	2.938	0.13	0.2075	0.005	0.6524	0.1019	0.0038	1392	33	1214	27	1661	69	73.09	87.21
rdt16018-140.d	93	127	1.37	1.737	0.11	0.165	0.0044	0.29278	0.0765	0.0042	1026	36	986	25	1085	100	90.88	96.10
rdt16018-141.d	113.4	43.68	0.39	1.817	0.085	0.1749	0.004	0.40598	0.0746	0.0031	1051	31	1038	22	1048	83	99.05	98.76
rdt16018-142.d	90	126.5	1.41	0.796	0.042	0.0885	0.0023	0.16327	0.0641	0.0034	592	24	546	13	746	110	73.19	92.23
rdt16018-143.d	894	343.2	0.38	1.195	0.05	0.1319	0.003	0.75201	0.06475	0.0022	798	24	798	17	762	74	104.72	100.00
rdt16018-144.d	171	160.2	0.94	2.43	0.15	0.182	0.0045	0.62089	0.096	0.005	1238	44	1077	25	1521	97	70.81	87.00
rdt16018-145.d	124.6	97.5	0.78	13.23	0.57	0.518	0.015	0.71888	0.1836	0.0068	2698	41	2686	65	2683	62	100.11	99.56
rdt16018-153.d	1901	2110	1.11	0.977	0.066	0.0829	0.0045	0.97637	0.0854	0.0029	682	32	512	26	1318	65	38.85	75.07
rdt16018-154.d	157.8	87.6	0.56	3.204	0.14	0.2435	0.0055	0.61122	0.0946	0.0036	1456	34	1403	28	1508	71	93.04	96.36
rdt16018-155.d	172.1	192.6	1.12	1.594	0.074	0.157	0.0034	0.44658	0.0736	0.0031	967	29	941	19	1036	81	90.83	97.31
rdt16018-156.d	514	103.6	0.20	1.502	0.063	0.1503	0.0033	0.62853	0.0728	0.0026	932	26	902	19	1016	72	88.78	96.78
rdt16018-157.d	187.2	100.7	0.54	4.8	0.22	0.2909	0.0057	0.37681	0.1196	0.0048	1781	39	1645	29	1953	74	84.23	92.36
rdt16018-158.d	222	42.5	0.19	1.5	0.089	0.1309	0.0037	0.56184	0.0817	0.0037	928	36	792	21	1225	89	64.65	85.34
rdt16018-159.d	745	241	0.32	2.464	0.1	0.1944	0.0041	0.8315	0.0907	0.0031	1258	31	1144	22	1443	68	79.28	90.94

Supplementary Table 1. Main isotopes and ratios measured using LA–ICP–MS. Concordance 1 ($^{206}Pb/^{238}U$/ $^{207}Pb/^{206}Pb$) and 2 ($^{206}Pb/^{238}U/^{207}Pb/^{235}U$)

Analysis Spot	U	Th	Th:U	Ratios							Ages						Concordance Calculations	
				$^{207}Pb/^{235}U$	2σ	$^{206}Pb/^{238}U$	2σ	Rho	$^{207}Pb/^{206}Pb$	2σ	$^{207}Pb/^{235}U$	2σ	$^{206}Pb/^{238}U$	2σ	$^{207}Pb/^{206}Pb$	2σ	1	2
rdt16018-160.d	306	267	0.87	2.199	0.092	0.1793	0.0039	0.42032	0.0876	0.0032	1178	29	1062	21	1374	74	77.29	90.15
rdt16018-161.d	326.7	64.1	0.20	1.707	0.071	0.1595	0.0037	0.52143	0.0761	0.0029	1013	27	953	21	1091	77	87.35	94.08
rdt16018-162.d	1139	908	0.80	3.68	0.18	0.2508	0.0085	0.79146	0.1037	0.0037	1570	38	1441	44	1686	66	85.47	91.78
rdt16018-163.d	430	231.5	0.54	8.31	0.37	0.3686	0.01	0.8818	0.1602	0.0054	2265	41	2018	49	2455	58	82.20	89.09
rdt16018-164.d	406	78.3	0.19	1.83	0.076	0.1705	0.0036	0.583	0.0775	0.0028	1057	27	1014	20	1139	69	89.03	95.93
008 - 1	5.82	0.616	0.11	2.73	0.26	0.176	0.0078	0.45164	0.1133	0.0091	1338	69	1043	43	1850	150	56.38	77.95
008 - 2	488	461	0.94	1.597	0.034	0.1591	0.0024	0.89191	0.07298	0.00075	968	13	952	13	1011	21	94.16	98.35
008 - 3	207.2	391.5	1.89	1.588	0.021	0.1598	0.0015	0.35771	0.07206	0.001	965	8.4	955.7	8.1	992	29	96.34	99.04
008 - 4	87.4	81.4	0.93	10.99	0.16	0.4386	0.0039	0.36084	0.1824	0.0025	2521	14	2344	18	2672	22	87.72	92.98
008 - 5	399	178.7	0.45	7.14	0.17	0.3635	0.0053	0.97863	0.1421	0.0018	2126	23	1998	25	2251	23	88.76	93.98
008 - 6	493	208.4	0.42	0.689	0.012	0.08557	0.001	0.57515	0.05817	0.00096	531.9	7.1	529.2	6	541	36	97.82	99.49
008 - 7	129.6	63.6	0.49	1.767	0.032	0.1711	0.0016	0.4434	0.0741	0.0012	1033	12	1018.2	8.8	1050	33	96.97	98.57
008 - 8	30	38.2	1.27	1.163	0.052	0.1292	0.0018	0.072749	0.066	0.0029	783	24	783.1	10	784	95	99.89	100.01
008 - 9	186	157.4	0.85	1.266	0.023	0.1355	0.0015	0.24451	0.068	0.0013	832	11	819	8.4	860	40	95.23	98.44
008 - 10	293	289	0.99	25.54	0.41	0.6165	0.0092	0.96816	0.3004	0.0022	3331	15	3095	37	3471.4	11	89.16	92.92
008 - 11	142	85.8	0.60	1.725	0.029	0.1716	0.0017	0.28943	0.0731	0.0012	1017	11	1020.7	9.3	1012	34	100.86	100.36
008 - 12	212.9	231.9	1.09	0.949	0.018	0.1075	0.0012	0.81682	0.06418	0.0011	677	9.6	657.9	7	752	37	87.49	97.18
008 - 13	358	244.3	0.68	1.674	0.024	0.1669	0.0017	0.61813	0.07219	0.00085	998.5	8.9	994.9	9.5	992	25	100.29	99.64
008 - 14	254	207	0.81	1.813	0.024	0.1713	0.0016	0.25171	0.07662	0.0011	1049.7	8.8	1019	9.1	1112	29	91.64	97.08
008 - 15	25.2	24.91	0.99	10.06	0.17	0.4578	0.0055	0.51807	0.1604	0.0025	2442	16	2430	24	2463	26	98.66	99.51
008 - 16	22.31	62.7	2.81	1.582	0.066	0.161	0.0024	0.28393	0.0703	0.0028	959	26	964	13	907	85	106.28	100.52
008 - 17	155	86.5	0.56	11.8	0.21	0.4924	0.0052	0.83695	0.1726	0.0021	2595	17	2584	23	2587	21	99.88	99.58
008 - 18	299	116	0.39	2.585	0.035	0.2169	0.0019	0.76849	0.08625	0.00093	1295.9	9.9	1265.5	10	1342	21	94.30	97.65
008 - 19	103.2	61.2	0.59	4.485	0.064	0.2986	0.0033	0.5595	0.1078	0.0013	1727	12	1684	16	1767	24	95.30	97.51
008 - 20	303	233	0.77	1.715	0.022	0.1714	0.0017	0.23336	0.07278	0.00091	1014	8.1	1019.5	9.4	1009	26	101.04	100.54
008 - 21	270	291	1.08	0.703	0.014	0.08707	0.00071	0.12148	0.0584	0.0012	540.1	8.5	538.2	4.2	538	45	100.04	99.65
008 - 22	222	163	0.73	2.543	0.029	0.2175	0.0017	0.28132	0.08489	0.0011	1284.2	8.4	1268.6	8.9	1313	25	96.62	98.79
008 - 23	266.4	161.7	0.61	2.587	0.037	0.2157	0.0025	0.6384	0.08689	0.001	1296.3	10	1259	13	1359	22	92.64	97.12
008 - 24	43.7	83.9	1.92	1.891	0.058	0.1832	0.0024	0.47949	0.0753	0.002	1078	20	1084	13	1063	54	101.98	100.56
008 - 25	45.29	71.8	1.59	10.68	0.16	0.4695	0.0058	0.71537	0.1642	0.0019	2495	14	2481	26	2500	21	99.24	99.44
008 - 26	290	49.4	0.17	1.771	0.031	0.1699	0.0022	0.81665	0.07579	0.00087	1034	12	1011	12	1087	23	93.01	97.78
008 - 27	152.5	134.1	0.88	1.334	0.027	0.1427	0.0017	0.45255	0.0675	0.0012	860	12	859.8	9.5	852	37	100.92	99.98
008 - 28	584	36.55	0.06	0.788	0.012	0.09719	0.00093	0.61643	0.05863	0.00075	590.7	6.6	597.9	5.4	558	28	107.15	101.22
008 - 29	428	521	1.22	5.07	0.12	0.3208	0.0061	0.9557	0.11443	0.0011	1829	20	1793	30	1869	17	95.93	98.03
008 - 30	113	66	0.58	1.686	0.041	0.1672	0.0021	0.64395	0.0732	0.0015	1002	15	997	11	1020	41	97.75	99.50
008 - 31	163.9	384	2.34	3.687	0.044	0.2669	0.0023	0.44661	0.09966	0.0011	1568.2	9.5	1525	12	1616	20	94.37	97.25
008 - 32	205	78	0.38	3.198	0.045	0.2567	0.0028	0.67705	0.0904	0.001	1456	11	1473	14	1435	22	102.65	101.17
008 - 33	222	647	2.91	4.022	0.065	0.2835	0.0023	0.5329	0.1026	0.0014	1638	13	1608.7	12	1668	25	96.44	98.21
008 - 34	93.2	173	1.86	1.174	0.031	0.1297	0.0013	0.084139	0.0662	0.0019	789	15	786.1	7.7	797	62	98.63	99.63
008 - 35	255.3	152.5	0.60	4.353	0.073	0.2755	0.0034	0.88095	0.1142	0.0013	1703	14	1569	17	1865	21	84.13	92.13
008 - 36	183.4	157.6	0.86	0.406	0.015	0.04879	0.00052	0.19302	0.0603	0.0021	347	11	307.1	3.2	600	80	51.18	88.50
008 - 37	566	212.2	0.37	1.753	0.045	0.1685	0.0037	0.93878	0.07566	0.00077	1026	17	1003	21	1084	20	92.53	97.76
008 - 38	208.8	183.1	0.88	1.05	0.017	0.12189	0.001	0.33916	0.0628	0.0011	728.3	8.2	741.4	6	701	36	105.76	101.80
008 - 39	206.8	92.6	0.45	3.833	0.096	0.2529	0.0039	0.86647	0.1115	0.0015	1597	20	1453	20	1821	24	79.79	90.98
008 - 40	106	290	2.74	0.655	0.021	0.08527	0.0011	-0.10068	0.056	0.002	512	13	527.5	6.4	428	80	123.25	103.03
008 - 41	209	17.7	0.08	0.756	0.026	0.0868	0.0017	0.73928	0.063	0.0015	572	15	536.7	9.9	698	51	76.89	93.83
008 - 42	86.6	167	1.93	7.25	0.34	0.3656	0.0097	0.96065	0.1433	0.0034	2137	42	2007	46	2265	41	88.61	93.92
008 - 43	134.8	43.1	0.32	8.2	0.49	0.348	0.015	0.98833	0.174	0.0032	2235	53	1921	70	2592	30	74.11	85.95

Supplementary Table 1. Main isotopes and ratios measured using LA–ICP–MS. Concordance 1 ($^{206}Pb/^{238}U$/ $^{207}Pb/^{206}Pb$) and 2 ($^{206}Pb/^{238}U/^{207}Pb/^{235}U$)

Analysis Spot	U	Th	Th:U	Ratios							Ages						Concordance Calculations	
				$^{207}Pb/^{235}U$	2σ	$^{206}Pb/^{238}U$	2σ	Rho	$^{207}Pb/^{206}Pb$	2σ	$^{207}Pb/^{235}U$	2σ	$^{206}Pb/^{238}U$	2σ	$^{207}Pb/^{206}Pb$	2σ	1	2
008 - 44	111.3	80.9	0.73	1.547	0.032	0.1584	0.0016	0.15944	0.0713	0.0016	948	13	947.6	9.1	957	45	99.02	99.96
008 - 45	521	285	0.55	0.916	0.019	0.107	0.0015	0.69905	0.06231	0.00088	659.8	9.9	655.2	8.6	681	30	96.21	99.30
008 - 46	111	140.6	1.27	1.251	0.033	0.1343	0.0019	0.31218	0.0672	0.0017	825	14	812.3	11	834	52	97.40	98.46
008 - 47	378	512	1.35	1.619	0.022	0.155	0.0016	0.42371	0.07543	0.00096	977.2	8.5	928.9	9	1077	26	86.25	95.06
008 - 48	87.1	81	0.93	1.471	0.038	0.1453	0.0016	0.29092	0.0738	0.0018	917	16	874.7	8.9	1048	50	83.46	95.39
008 - 49	427.4	262.7	0.61	2.751	0.08	0.1961	0.0045	0.96792	0.10224	0.001	1346	21	1154	24	1666	19	69.27	85.74
008 - 50	384	109.8	0.29	1.125	0.038	0.1184	0.0028	0.94257	0.06891	0.001	766	18	721	16	900	30	80.11	94.13
008 - 51	135.9	110.6	0.81	13.78	0.14	0.5307	0.0051	0.71477	0.188	0.0017	2734.3	9.7	2744	21	2725	15	100.70	100.35
008 - 52	103.3	115.5	1.12	1.601	0.026	0.1562	0.002	0.39946	0.0741	0.0013	973.2	10	937	12	1039	37	90.18	96.28
008 - 53	125.3	69.2	0.55	1.437	0.029	0.1503	0.0014	0.19895	0.0692	0.0015	904	12	902.8	8	908	44	99.43	99.87
008 - 54	34.7	52.2	1.50	6.61	0.16	0.364	0.0043	0.64167	0.1332	0.0031	2058	21	2001	20	2133	39	93.81	97.23
008 - 55	126.8	193.8	1.53	0.759	0.024	0.08899	0.00082	0.44832	0.0618	0.0018	574	13	549.5	4.8	680	62	80.81	95.73
008 - 56	99	174	1.76	1.77	0.18	0.1526	0.003	0.73107	0.0846	0.0085	1015	53	915	17	1200	140	76.25	90.15
008 - 57	218.2	72.6	0.33	3.277	0.093	0.225	0.0049	0.95745	0.10585	0.0012	1476	23	1307	26	1730	21	75.55	88.55
008 - 58	76.3	122.9	1.61	0.746	0.029	0.0936	0.0015	0.45918	0.0585	0.002	566	17	576.7	8.6	537	73	107.39	101.89
008 - 59	209	132	0.63	5.528	0.051	0.3445	0.0031	0.59714	0.11653	0.0011	1904.8	8	1908	15	1902	17	100.32	100.17
008 - 60	267	270	1.01	10.572	0.089	0.4699	0.0034	0.64605	0.16314	0.0014	2486.9	8	2483.1	15	2487.3	14	99.83	99.85
008 - 61	255	187	0.73	4.93	0.089	0.3058	0.0062	0.92382	0.11739	0.001	1808	16	1719	31	1916	16	89.72	95.08
008 - 62	83	120	1.45	5.92	0.088	0.3565	0.004	0.77551	0.1204	0.0016	1965	13	1966	19	1960	24	100.31	100.05
008 - 63	157	187.5	1.19	1.736	0.049	0.17	0.0033	0.81757	0.0737	0.0012	1020	18	1012	18	1029	34	98.35	99.22
008 - 64	52	91.2	1.75	4.301	0.078	0.3028	0.0032	0.21832	0.1037	0.002	1692	15	1705	16	1691	35	100.83	100.77
008 - 65	135.8	141	1.04	3.162	0.049	0.2412	0.0023	0.28889	0.0949	0.0014	1447	12	1392.8	12	***1522***	***29***	91.51	96.25
008 - 66	159.2	66.4	0.42	1.652	0.039	0.1669	0.0025	0.71003	0.072	0.0014	989	15	995	14	986	38	100.91	100.61
008 - 67	49	73.2	1.49	1.021	0.035	0.1182	0.0015	0.025552	0.0624	0.0022	713	18	720.3	8.8	666	77	108.15	101.02
008 - 68	163.4	263	1.61	9.696	0.099	0.4374	0.0034	0.51199	0.1617	0.0015	2407.2	9.6	2339	15	2474	16	94.54	97.17
008 - 69	343.2	55.4	0.16	1.227	0.022	0.1342	0.0016	0.68399	0.06634	0.00091	814	9.8	811.4	9	814	29	99.68	99.68
008 - 70	89.5	92.9	1.04	3.969	0.054	0.2846	0.0027	0.23118	0.1011	0.0014	1629	11	1615	14	1653	26	97.70	99.14
008 - 71	64.5	181	2.81	1.611	0.038	0.1618	0.0019	0.44858	0.0736	0.0016	975	14	966.5	11	1022	43	94.57	99.13
008 - 72	235.7	158	0.67	5.792	0.063	0.3477	0.0032	0.6496	0.12091	0.0012	1944.8	9.5	1923	15	1970	17	97.61	98.88
008 - 73	111.7	135.9	1.22	10.373	0.097	0.4588	0.0034	0.44254	0.1638	0.0015	2468.4	8.7	2434.1	15	2494	15	97.60	98.61
008 - 74	112.1	97.3	0.87	1.261	0.029	0.1352	0.0015	0.22393	0.0684	0.0015	829	14	817.3	8.6	872	46	93.73	98.59
008 - 75	90.4	90.9	1.01	1.144	0.032	0.1272	0.0015	0.047436	0.0647	0.0019	773	15	772	8.6	760	60	101.58	99.87
008 - 76	105.5	76.6	0.73	1.572	0.053	0.1542	0.0033	0.6423	0.0732	0.0018	957	21	927	19	1016	48	91.24	96.87
008 - 77	285	224	0.79	0.921	0.021	0.1055	0.0018	0.72778	0.063	0.0011	662	11	646	11	713	36	90.60	97.58
008 - 78	137	109	0.80	1.519	0.031	0.154	0.0017	0.26374	0.0709	0.0014	937	12	923.5	9.7	954	41	96.80	98.56
008 - 79	271	148.7	0.55	0.769	0.017	0.09082	0.00081	0.38672	0.0614	0.0012	578.4	9.6	560.4	4.8	644	43	87.02	96.89
008 - 80	98.6	91.9	0.93	6.8	0.11	0.3254	0.0044	0.76382	0.1512	0.0017	2085	14	1816	21	2357	20	77.05	87.10
008 - 81	119.3	104.7	0.88	5.141	0.085	0.3137	0.0035	0.3872	0.1194	0.0022	1845	15	1759	17	1942	32	90.58	95.34
008 - 82	593	910	1.53	1.541	0.055	0.1543	0.0051	0.95776	0.07281	0.00073	944	22	924	28	1007	20	91.76	97.88
008 - 83	64	141.6	2.21	8.73	0.34	0.398	0.011	0.95909	0.1605	0.0022	2318	33	2157	52	2458	24	87.75	93.05
008 - 84	237	141.2	0.60	1.071	0.025	0.11777	0.0011	0.37119	0.0663	0.0013	740	12	717.7	6.6	807	41	88.93	96.99
008 - 85	141.8	220.6	1.56	1.17	0.026	0.12715	0.0012	0.22159	0.0669	0.0015	788	12	771.6	6.8	835	44	92.41	97.92
008 - 86	189.5	387.9	2.05	0.703	0.014	0.08664	0.00078	0.030519	0.0588	0.0012	541.6	8.3	535.6	4.6	551	47	97.21	98.89
008 - 87	424	414	0.98	1.285	0.022	0.1363	0.0018	0.74907	0.06818	0.00083	840.2	10	823.5	10	871	25	94.55	98.01
008 - 88	88.1	82.8	0.94	19.78	0.27	0.582	0.0059	0.78486	0.2474	0.0026	3080	13	2957	24	3167	17	93.37	96.01
008 - 89	121	84	0.69	19.43	0.33	0.5678	0.0087	0.93695	0.2477	0.0021	3062	16	2898	36	3168.9	13	91.45	94.64
008 - 90	128.4	47.6	0.37	5.695	0.061	0.351	0.0033	0.49651	0.1185	0.0015	1931.6	9.7	1939	16	1935	22	100.21	100.38
008 - 91	592	440	0.74	2.135	0.048	0.1963	0.0039	0.95868	0.07948	0.00079	1162	17	1155	21	1182	20	97.72	99.40

Supplementary Table 1. Main isotopes and ratios measured using LA–ICP–MS. Concordance 1 ($^{206}Pb/^{238}U$/ $^{207}Pb/^{206}Pb$) and 2 ($^{206}Pb/^{238}U/^{207}Pb/^{235}U$)

Analysis Spot	U	Th	Th:U	Ratios							Ages						Concordance Calculations	
				$^{207}Pb/^{235}U$	2σ	$^{206}Pb/^{238}U$	2σ	Rho	$^{207}Pb/^{206}Pb$	2σ	$^{207}Pb/^{235}U$	2σ	$^{206}Pb/^{238}U$	2σ	$^{207}Pb/^{206}Pb$	2σ	1	2
008 - 92	121.3	195.1	1.61	1.53	0.027	0.1542	0.0014	0.35325	0.0718	0.0012	943.8	10	924.3	8	980	34	94.32	97.93
008 - 93	101.5	143	1.41	1.279	0.027	0.13758	0.0011	0.26408	0.0669	0.0015	835	12	831	6.4	834	44	99.64	99.52
008 - 94	302	212.4	0.70	8.71	0.086	0.4032	0.0031	0.74489	0.15689	0.0013	2307.8	9	2184	14	2421.3	14	90.20	94.64
008 - 95	29.63	51.2	1.73	1.25	0.067	0.1298	0.0024	0.4561	0.0702	0.0036	822	31	789	14	920	110	85.76	95.99
008 - 96	166	184	1.11	1.907	0.08	0.1723	0.0016	0.20179	0.081	0.0034	1079	27	1024.6	9	1203	80	85.17	94.96
008 - 97	287.5	249	0.87	7.328	0.066	0.3355	0.0029	0.66467	0.1583	0.0014	2152	8	1865	14	2440	15	76.43	86.66
008 - 98	400	528	1.32	1.152	0.015	0.12556	0.001	0.1354	0.06652	0.00087	778	6.9	762.5	5.8	823	28	92.65	98.01
008 - 99	68.5	60	0.88	1.157	0.035	0.1269	0.0013	0.3853	0.0663	0.0019	779	16	770	7.2	800	60	96.25	98.84
008 - 100	86.7	40.9	0.47	1.156	0.038	0.1187	0.0021	0.64256	0.0712	0.0019	780	18	723	12	958	53	75.47	92.69
008 - 101	232	68.9	0.30	1.348	0.019	0.13398	0.0012	0.43834	0.07303	0.00096	866.2	8.1	810.5	7	1016	25	79.77	93.57
008 - 102	105.8	129.2	1.22	1.22	0.026	0.1302	0.0014	0.26753	0.0685	0.0015	813	12	788.8	7.7	881	43	89.53	97.02
008 - 103	139.3	151.6	1.09	1.242	0.022	0.13078	0.0012	0.11094	0.0689	0.0014	819.3	10	792.3	6.8	888	40	89.22	96.70
008 - 104	109.8	90.2	0.82	6.2	2.1	0.179	0.018	0.99796	0.21	0.045	~~1720~~	~~250~~	~~1054~~	~~95~~	~~2510~~	~~370~~	~~41.99~~	61.28
008 - 105	122	144	1.18	10.59	0.16	0.4698	0.004	0.63192	0.164	0.0021	2489	14	2482	18	2498	23	99.36	99.72
008 - 106	670	191.2	0.29	0.759	0.012	0.09225	0.00092	0.56662	0.05982	0.00075	573.4	6.8	568.8	5.5	594	27	95.76	99.20
008 - 107	546.3	589	1.08	0.7711	0.01	0.0934	0.0013	0.63614	0.05962	0.00075	580.2	5.9	575.4	7.6	586	27	98.19	99.17
008 - 108	53.3	111.1	2.08	3.475	0.092	0.232	0.004	0.58211	0.1076	0.0026	1519	21	1345	21	1769	43	76.03	88.55
008 - 109	401	33.7	0.08	1.127	0.022	0.1236	0.0018	0.84121	0.06533	0.00079	766	11	751.3	10	786	26	95.59	98.08
008 - 110	234	210.4	0.90	10.77	0.1	0.475	0.0044	0.78456	0.16399	0.0014	2504.4	9.3	2505	19	2496.1	14	100.36	100.02
008 - 111	188	230	1.22	1.081	0.031	0.1128	0.0025	0.38251	0.0706	0.002	744	15	689	14	940	58	73.30	92.61
008 - 112	302	248	0.82	1.738	0.034	0.1607	0.0017	0.64063	0.0789	0.0013	1023	13	960.5	9.4	1168	33	82.23	93.89
008 - 113	94.3	210	2.23	1.224	0.047	0.1243	0.0036	0.78675	0.0707	0.0016	809	22	755	20	941	46	80.23	93.33
008 - 114	273	119	0.44	1.19	0.11	0.1219	0.009	0.97849	0.0697	0.0021	782	54	739	52	915	60	80.77	94.50
008 - 115	95.2	154	1.62	1.142	0.029	0.1233	0.0015	0.38425	0.0678	0.0015	774	14	749.7	8.5	853	46	87.89	96.86
008 - 116	281.9	445	1.58	4.431	0.046	0.2926	0.0026	0.62921	0.10957	0.001	1719	8.3	1654	13	1793	17	92.25	96.22
008 - 117	339.6	437	1.29	1.182	0.024	0.1156	0.0032	0.10431	0.0721	0.0019	793	11	705	18	979	50	72.01	88.90
008 - 118	164.1	346	2.11	1.119	0.021	0.12278	0.0011	0.17406	0.0652	0.0013	762	10	746.5	6.6	787	45	94.85	97.97
008 - 119	95.3	92.3	0.97	11.23	0.13	0.475	0.0043	0.50928	0.1722	0.0017	2543.3	10	2505	19	2580	17	97.09	98.49
008 - 120	707	649	0.92	1.373	0.015	0.14461	0.0012	0.64594	0.06876	0.00067	877.1	6.6	870.7	6.7	890	20	97.83	99.27
008 - 121	34.8	28.47	0.82	1.429	0.08	0.1374	0.0041	0.63559	0.0758	0.0031	904	31	834	22	1076	81	77.51	92.26
008 - 122	151	3.57	0.02	0.739	0.017	0.0891	0.0011	0.49191	0.06	0.0012	561.2	9.6	550.3	6.7	603	45	91.26	98.06
RDT16008-297.d	100.1	83.2	0.83	1.483	0.071	0.1381	0.003	0.27135	0.0767	0.0034	923	30	833	17	1094	95	76.14	90.25
RDT16008-298.d	226.5	99.7	0.44	1.788	0.078	0.1823	0.0031	0.4505	0.0701	0.0027	1040	29	1079	17	933	79	115.65	103.75
RDT16008-299.d	284.1	133.4	0.47	1.034	0.048	0.1101	0.0023	0.45328	0.0674	0.0028	718	23	673	13	835	82	80.60	93.73
RDT16008-300.d	314.5	100.8	0.32	18.45	0.72	0.5162	0.0085	0.78516	0.2565	0.0084	3015	38	2681	36	3224	53	83.16	88.92
RDT16008-301.d	77.1	62.7	0.81	1.528	0.11	0.1309	0.0043	0.6277	0.0831	0.0049	923	40	792	24	1220	110	64.92	85.81
RDT16008-302.d	2112	1442	0.68	8.71	0.35	0.3578	0.0069	0.94056	0.1761	0.0057	2306	38	1973	32	2614.9	54	75.45	85.56
RDT16008-303.d	64.3	54.28	0.84	0.643	0.042	0.085	0.0023	0.16616	0.0554	0.0036	502	26	527	14	400	140	131.75	104.98
RDT16008-304.d	517.9	217	0.42	4.408	0.19	0.2755	0.0068	0.89175	0.1157	0.0038	1711	37	1566	34	1888	60	82.94	91.53
RDT16008-305.d	247.1	112.3	0.45	1.255	0.056	0.1315	0.0024	0.16296	0.07	0.0028	821	25	797	14	914	82	87.20	97.08
RDT16008-306.d	70.49	76.7	1.09	1.339	0.069	0.1255	0.003	0.2569	0.0783	0.0038	862	30	761	17	1151	99	66.12	88.28
RDT16008-307.d	1316	269	0.20	7.006	0.27	0.3356	0.0054	0.85658	0.15214	0.0049	2112	35	1864	26	2370	57	78.65	88.26
RDT16008-308.d	123.2	61.1	0.50	3.47	0.16	0.2424	0.0051	0.56319	0.1045	0.0043	1520	37	1398	26	1698	75	82.33	91.97
RDT16008-309.d	159.5	103	0.65	9.1	0.37	0.4169	0.0076	0.46904	0.1605	0.0057	2347	37	2247	34	2453	60	91.60	95.74
RDT16008-310.d	515.5	206.3	0.40	9.14	0.36	0.4202	0.0065	0.7564	0.1595	0.0052	2350	36	2260	30	2449	56	92.28	96.17
RDT16008-311.d	184.7	140.8	0.76	1.633	0.072	0.1617	0.003	0.44455	0.0739	0.0029	980	28	967	16	1040	77	92.98	98.67
RDT16008-319.d	298.2	121.1	0.41	2.677	0.13	0.2041	0.004	0.66975	0.0939	0.0037	1318	36	1196	22	1520	73	78.68	90.74
RDT16008-320.d	608	54	0.09	1.764	0.093	0.1533	0.0033	0.75882	0.0834	0.0033	1033	35	919	19	1284	80	71.57	88.96

Supplementary Table 1. Main isotopes and ratios measured using LA–ICP–MS. Concordance 1 ($^{206}Pb/^{238}U$/ $^{207}Pb/^{206}Pb$) and 2 ($^{206}Pb/^{238}U/^{207}Pb/^{235}U$)

Analysis Spot	U	Th	Th:U	Ratios							Ages						Concordance Calculations	
				$^{207}Pb/^{235}U$	2σ	$^{206}Pb/^{238}U$	2σ	Rho	$^{207}Pb/^{206}Pb$	2σ	$^{207}Pb/^{235}U$	2σ	$^{206}Pb/^{238}U$	2σ	$^{207}Pb/^{206}Pb$	2σ	1	2
RDT16008-321.d	55	73	1.33	1.186	0.071	0.1306	0.003	0.31371	0.0654	0.0036	785	34	791	17	810	120	97.65	100.76
RDT16008-322.d	220	40.24	0.18	1.976	0.091	0.1928	0.0045	0.55675	0.0766	0.0031	1108	30	1136	25	1102	78	103.09	102.53
RDT16008-323.d	90.4	67.8	0.75	1.391	0.073	0.1457	0.0034	0.19072	0.0702	0.0034	885	32	876	19	906	100	96.69	98.98
RDT16008-324.d	327	73.8	0.23	1.501	0.062	0.1533	0.0026	0.35719	0.0714	0.0026	929	25	919	14	974	73	94.35	98.92
RDT16008-325.d	379	99.5	0.26	4.348	0.18	0.289	0.0053	0.64675	0.1104	0.0038	1700	34	1636	27	1804	65	90.69	96.24
RDT16008-326.d	259.1	110.7	0.43	1.648	0.07	0.1687	0.0031	0.42584	0.072	0.0027	986	27	1006	17	980	75	102.65	102.03
RDT16008-327.d	189.8	148.2	0.78	10.2	0.42	0.4583	0.0086	0.83026	0.163	0.0054	2449	38	2429	38	2487	55	97.67	99.18
RDT16008-328.d	429	1.75	0.00	0.746	0.033	0.0933	0.0016	0.48369	0.0586	0.0023	565	19	576	9	554	84	103.97	101.95
RDT16008-329.d	582.4	192.4	0.33	0.616	0.028	0.0777	0.0014	0.56896	0.0592	0.0023	487	18	482.4	8.1	565	85	85.38	99.06
RDT16008-330.d	1294	146.4	0.11	2.064	0.084	0.1781	0.0035	0.83664	0.08508	0.0028	1137	29	1059	19	1320	65	80.23	93.14
RDT16008-338.d	649.6	271	0.42	3.751	0.15	0.2233	0.004	0.66942	0.1167	0.0039	1581	32	1299	21	1901	61	68.33	82.16
RDT16008-339.d	132	147.3	1.12	1.59	0.076	0.154	0.0031	0.41614	0.0727	0.0031	966	30	923	17	998	85	92.48	95.55
RDT16008-340.d	69.65	23.26	0.33	2.007	0.11	0.1795	0.0036	0.073231	0.077	0.0041	1115	38	1065	20	1094	110	97.35	95.52
RDT16008-341.d	47.5	97.1	2.04	6.1	0.27	0.3359	0.0074	0.50515	0.1251	0.005	1984	39	1868	35	2021	73	92.43	94.15
RDT16008-342.d	222.1	130.4	0.59	4.171	0.18	0.2679	0.0051	0.69595	0.1094	0.0039	1670	36	1529	26	1781	64	85.85	91.56
RDT16008-343.d	57	53.9	0.95	1.657	0.1	0.1402	0.0039	0.073872	0.0814	0.0053	982	40	848	22	1230	120	68.94	86.35
RDT16008-344.d	287.5	165.5	0.58	2.308	0.095	0.1946	0.0037	0.56945	0.0833	0.003	1215	29	1146	20	1272	72	90.09	94.32
RDT16008-346.d	109.8	321	2.92	1.772	0.088	0.1667	0.0035	0.38241	0.0748	0.0033	1029	32	994	19	1072	86	92.72	96.60
RDT16008-347.d	327.8	361	1.10	0.392	0.02	0.05	0.001	0.18793	0.0565	0.0027	334	15	314.4	6.2	425	110	73.98	94.13
RDT16008-348.d	61.11	55.09	0.90	1.258	0.074	0.1203	0.0031	0.22753	0.0741	0.0043	824	33	732	18	999	120	73.27	88.83
RDT16008-349.d	1051	417.7	0.40	2.162	0.085	0.1918	0.003	0.67462	0.0805	0.0027	1168.5	28	1131	16	1209	67	93.55	96.79
RDT16008-350.d	251.9	144.7	0.57	13.02	0.51	0.4894	0.0084	0.68432	0.1903	0.0064	2683	38	2566	36	2743	54	93.55	95.64
RDT16008-351.d	525	107.8	0.21	1.726	0.069	0.1631	0.0027	0.46391	0.0768	0.0027	1017.1	26	974	15	1106	71	88.07	95.76
RDT16008-352.d	282.3	248.4	0.88	1.439	0.063	0.141	0.0025	0.3215	0.074	0.0029	906	27	850	14	1039	80	81.81	93.82
006 - 1	419.9	276.8	0.66	2.517	0.038	0.2015	0.0022	0.76802	0.09008	0.001	1276	11	***1183***	***12***	1425	22	83.02	92.71
006 - 2	166.5	271	1.63	0.865	0.02	0.1004	0.0012	0.46618	0.0622	0.0013	632	11	***616.9***	***6.9***	689	41	89.54	97.61
~~006 - 3~~	~~0.028~~	~~0.098~~	~~3.50~~	~~no value~~	~~NAN~~	~~no value~~	~~NAN~~	~~NaN~~	~~no value~~	~~NAN~~	~~no value~~	~~NAN~~	~~no value~~	~~NAN~~	~~no value~~	~~NAN~~	#VALUE!	#VALUE!
006 - 4	46.12	45.43	0.99	0.315	0.023	0.03514	0.00068	0.23894	0.0655	0.0049	279	18	222.6	4.2	800	170	27.83	79.78
006 - 5	592	96	0.16	12.83	0.73	0.375	0.017	0.99461	0.245	0.0038	2647	57	2047	80	3150	25	64.98	77.33
006 - 6	97	91.7	0.95	9.86	0.31	0.42	0.012	0.90283	0.1749	0.0023	2424	30	2256	56	***2604***	***22***	86.64	93.07
006 - 7	215	380	1.77	4.36	0.15	0.2645	0.0072	0.8668	0.1192	0.002	1702	28	1518	35	***1942***	***29***	78.17	89.19
006 - 8	81.4	102	1.25	1.03	0.03	0.1041	0.0022	0.43935	0.0707	0.0019	718	15	638	13	937	56	68.09	88.86
006 - 9	316.1	128.9	0.41	5.032	0.092	0.3088	0.0041	0.85651	0.1179	0.0013	1824	16	1738	21	***1923***	***19***	90.38	95.29
006 - 10	224	312	1.39	8.6	0.15	0.3792	0.0036	0.48193	0.1648	0.0025	2296	16	2073	17	***2504***	***26***	82.79	90.29
006 - 11	175	143	0.82	0.488	0.014	0.06051	0.00067	0.13587	0.0585	0.0018	404.8	9.7	378.7	4.1	532	65	71.18	93.55
006 - 12	213	94.5	0.44	1.188	0.051	0.1212	0.0034	0.91127	0.0709	0.0014	792	24	737	20	948	40	77.74	93.06
006 - 13	494	154	0.31	0.812	0.024	0.0922	0.0027	0.58429	0.0638	0.0014	603	13	568	16	731	45	77.70	94.20
006 - 14	67.7	49.5	0.73	1.52	0.066	0.1373	0.0025	0.48145	0.0797	0.0029	946	24	829	14	1202	72	68.97	87.63
006 - 15	183	109.5	0.60	0.761	0.025	0.0855	0.0016	0.57978	0.0642	0.0018	573	14	528.9	9.6	735	57	71.96	92.30
006 - 16	300	251	0.84	3.91	0.082	0.2501	0.0046	0.9275	0.11316	0.0011	1614	17	1438	24	1849	18	77.77	89.10
006 - 17	212	318	1.50	0.771	0.028	0.0757	0.0013	0.45208	0.072	0.0023	579	16	470.1	7.8	978	65	48.07	81.19
006 - 18	250	276	1.10	3.21	0.11	0.2309	0.0065	0.85404	0.1001	0.0015	1457	26	***1339***	***34***	1623	28	82.50	91.90
006 - 19	522	227	0.43	0.662	0.021	0.0813	0.0022	0.86684	0.05897	0.00099	515	13	504	13	568	38	88.73	97.86
006 - 20	380	222	0.58	8.141	0.11	0.3852	0.0034	0.74779	0.1528	0.0017	2246	12	2101	16	2375	19	88.46	93.54
006 - 21	683	582	0.85	1.71	0.08	0.1571	0.0053	0.97646	0.078	0.0012	1007	30	940	29	1143	31	82.24	93.35
006 - 22	790	1115	1.41	8.1	0.75	0.1849	0.0076	0.74776	0.315	0.021	2246	91	1093	41	3530	100	30.96	48.66
006 - 23	160.5	226	1.41	1.069	0.027	0.1118	0.0014	0.44414	0.0688	0.0016	737	13	683.2	8.4	888	49	76.94	92.70

Supplementary Table 1. Main isotopes and ratios measured using LA–ICP–MS. Concordance 1 ($^{206}Pb/^{238}U$/ $^{207}Pb/^{206}Pb$) and 2 ($^{206}Pb/^{238}U/^{207}Pb/^{235}U$)

Analysis Spot	U	Th	Th:U	Ratios							Ages						Concordance Calculations	
				$^{207}Pb/^{235}U$	2σ	$^{206}Pb/^{238}U$	2σ	Rho	$^{207}Pb/^{206}Pb$	2σ	$^{207}Pb/^{235}U$	2σ	$^{206}Pb/^{238}U$	2σ	$^{207}Pb/^{206}Pb$	2σ	1	2
006 - 24	153.6	95.6	0.62	3.318	0.059	0.2602	0.0036	0.78855	0.0919	0.0013	1484	14	1490	18	***1469***	***27***	101.43	100.40
006 - 25	265	64.5	0.24	0.973	0.018	0.10653	0.0011	0.35023	0.0666	0.0012	689.6	9.4	652.6	6.3	817	39	79.88	94.63
~~006 - 26~~	~~0.046~~	~~0.161~~	~~3.50~~	~~no value~~	~~NAN~~	~~no value~~	~~NAN~~	~~NaN~~	~~no value~~	~~NAN~~	~~no value~~	~~NAN~~	~~no value~~	~~NAN~~	~~no value~~	~~NAN~~	#VALUE!	#VALUE!
006 - 27	127	117.4	0.92	0.522	0.019	0.06271	0.00075	0.15028	0.0604	0.0022	425	13	392.1	4.6	607	80	64.60	92.26
006 - 28	99	108.2	1.09	1.249	0.036	0.1313	0.0021	0.63464	0.07	0.0016	825	15	***795***	***12***	920	48	86.41	96.36
006 - 29	689	345	0.50	2.48	0.28	0.1508	0.0046	0.35723	0.126	0.015	1243	79	905	26	1870	190	48.40	72.81
006 - 30	63.1	42.5	0.67	0.36	0.028	0.03986	0.00081	0.59085	0.0656	0.0046	316	22	252	5	750	150	33.60	79.75
006 - 31	577	162.5	0.28	3.47	0.21	0.2386	0.009	0.9739	0.1038	0.003	1504	50	1377	47	***1680***	***53***	81.96	91.56
006 - 32	123.7	97	0.78	8.3	0.12	0.3729	0.0047	0.70934	0.1618	0.0018	2265	14	2042	22	***2473***	***19***	82.57	90.15
006 - 33	176	31.4	0.18	0.84	0.019	0.0941	0.0013	0.41166	0.064	0.0013	619	11	579.7	7.7	732	44	79.19	93.65
006 - 34	394.8	167.7	0.42	2.13	0.19	0.161	0.011	0.99275	0.0946	0.0027	1130	66	957	59	1518	54	63.04	84.69
006 - 35	414	158.5	0.38	4.14	0.12	0.2609	0.0057	0.94092	0.11393	0.0012	1660	23	1494	29	1861	19	80.28	90.00
006 - 36	107	105	0.98	1.203	0.033	0.11908	0.0012	0.23549	0.0729	0.0021	801	15	***725.2***	***6.9***	1004	61	72.23	90.54
006 - 37	154	164	1.06	10.57	0.3	0.4421	0.0067	0.6708	0.1728	0.0034	2482	25	2359	30	***2580***	***31***	91.43	95.04
006 - 38	181.3	82.5	0.46	1.35	0.025	0.127	0.0015	0.58929	0.077	0.0012	867	11	770.7	8.4	1122	31	68.69	88.89
006 - 39	1199	613	0.51	1.051	0.034	0.113	0.0031	0.97421	0.0672	0.00073	728	17	***690***	***18***	845	23	81.66	94.78
006 - 40	882	484	0.55	1.99	0.25	0.1275	0.0099	0.86789	0.1133	0.0073	1112	94	772	56	1920	110	40.21	69.42
006 - 41	337	220	0.65	1.371	0.046	0.1324	0.0038	0.85287	0.0745	0.0012	877	19	804	21	1060	33	75.85	91.68
006 - 42	187	44.3	0.24	0.662	0.021	0.0785	0.0016	0.22429	0.0616	0.0021	515	13	487.3	9.8	662	70	73.61	94.62
006 - 43	237	421	1.78	2.593	0.064	0.2046	0.0043	0.74918	0.0909	0.0012	1301	17	***1200***	***23***	1442	26	83.22	92.24
006 - 44	150	67.8	0.45	0.521	0.022	0.06488	0.001	0.61108	0.0586	0.0019	425	15	405.2	6	541	73	74.90	95.34
006 - 45	422	465	1.10	0.3053	0.0085	0.04035	0.00042	0.12335	0.0539	0.0015	271.2	6.5	255	2.6	353	63	72.24	94.03
006 - 46	362	300	0.83	1.851	0.047	0.1403	0.0037	0.39834	0.0952	0.0023	1062	17	846	21	1523	45	55.55	79.66
006 - 47	111	116	1.05	2.49	0.13	0.1622	0.0054	0.70444	0.1122	0.004	1266	38	968	30	1827	64	52.98	76.46
006 - 48	918	930	1.01	0.807	0.03	0.0833	0.0015	0.54955	0.0694	0.0017	600	17	515.9	9	905	50	57.01	85.98
006 - 49	241	285	1.18	2.7	0.051	0.1929	0.0038	0.80571	0.101	0.0014	1330	14	1136	21	1639	25	69.31	85.41
006 - 50	203	211	1.04	1.118	0.033	0.103	0.0019	0.542	0.0786	0.0021	760	16	632	11	1149	53	55.00	83.16
006 - 51	451.7	98.7	0.22	0.773	0.03	0.0917	0.0021	0.88399	0.0614	0.0011	580	17	***566***	***12***	650	38	87.08	97.59
~~006 - 52~~	~~0.0101~~	~~0.061~~	~~6.04~~	~~no value~~	~~NAN~~	~~no value~~	~~NAN~~	~~NaN~~	~~no value~~	~~NAN~~	~~no value~~	~~NAN~~	~~no value~~	~~NAN~~	~~no value~~	~~NAN~~	~~#VALUE!~~	#VALUE!
RDT16006-273.d	108.2	91.2	0.84	1.33	0.053	0.1217	0.0022	0.32997	0.003	0.0031	852	24	740	13	1103	83	67.09	86.85
RDT16006-274.d	112.2	144.3	1.29	0.897	0.04	0.0989	0.0022	0.023882	0.0034	0.0035	638	22	607	13	700	110	86.71	95.14
RDT16006-275.d	564	121.5	0.22	5.137	0.1	0.3299	0.0058	0.77912	0.0013	0.0016	1836	17	1835	28	1826	25	100.49	99.95
RDT16006-276.d	1228	883	0.72	6.47	0.22	0.2615	0.0094	0.65461	0.0042	0.0045	2029	31	1490	48	2626	42	56.74	73.44
RDT16006-277.d	773	183	0.24	0.877	0.021	0.0991	0.0016	0.25143	0.0016	0.0017	639	11	609.1	9.6	711	53	85.67	95.32
RDT16006-278.d	334.6	44	0.13	1.208	0.032	0.1299	0.0023	0.48273	0.0016	0.0017	801	14	788	13	816	51	96.57	98.38
RDT16006-279.d	767	279	0.36	1.612	0.024	0.1605	0.0024	0.49793	0.00097	0.0011	975	9.4	959	13	1003	32	95.61	98.36
RDT16006-280.d	565	255.3	0.45	11.53	0.17	0.5024	0.0079	0.79513	0.0013	0.0019	2563	14	2621	34	2507	19	104.55	102.26
RDT16006-281.d	2050	5190	2.53	1.052	0.052	0.0678	0.0025	0.94455	0.0022	0.0023	714	25	422	15	1773	40	23.80	59.10
RDT16006-290.d	503	279	0.55	0.855	0.038	0.075	0.0017	-0.073093	0.0049	0.0049	617	20	465.5	10	1158	95	40.20	75.45
RDT16006-291.d	930	337	0.36	1.665	0.032	0.161	0.003	0.70734	0.00098	0.0012	994	12	962	17	1035	32	92.95	96.78
RDT16006-292.d	1383	1350	0.98	10.35	0.14	0.4513	0.0073	0.8209	0.0013	0.0019	2465	13	2398	33	2502	20	95.84	97.28
RDT16006-293.d	424	504	1.19	9.54	0.24	0.4046	0.01	0.8678	0.0021	0.0025	2383	25	2185	48	2572	24	84.95	91.69
RDT16006-294.d	226	195.9	0.87	1.636	0.039	0.1613	0.0028	0.33076	0.0017	0.0018	982	15	965	15	1010	50	95.54	98.27
~~RDT16006-295.d~~	~~327.7~~	~~385~~	~~1.17~~	1.769	0.059	0.1639	0.0028	0.59583	0.0018	0.0019	1024	19	979	16	1107	52	88.44	95.61
RDT16006-299.d	260	193.5	0.74	1.129	0.029	0.1179	0.0022	0.37458	0.0018	0.0019	762	14	719	13	881	56	81.61	94.36
RDT16006-300.d	98.9	33.4	0.34	1	0.043	0.1072	0.002	0.12876	0.003	0.0031	691	22	656	12	735	96	89.25	94.93
RDT16006-301.d	1120	87.4	0.08	2	0.22	0.1456	0.0096	0.98288	0.0038	0.0039	993	67	865	53	1230	82	70.33	87.11

Supplementary Table 1. Main isotopes and ratios measured using LA–ICP–MS. Concordance 1 ($^{206}Pb/^{238}U$/ $^{207}Pb/^{206}Pb$) and 2 ($^{206}Pb/^{238}U/^{207}Pb/^{235}U$)

Analysis Spot	U	Th	Th:U	Ratios							Ages						Concordance Calculations	
				$^{207}Pb/^{235}U$	2σ	$^{206}Pb/^{238}U$	2σ	Rho	$^{207}Pb/^{206}Pb$	2σ	$^{207}Pb/^{235}U$	2σ	$^{206}Pb/^{238}U$	2σ	$^{207}Pb/^{206}Pb$	2σ	1	2
RDT16006-302.d	177.6	217.9	1.23	4.17	0.088	0.2881	0.005	0.5149	0.0018	0.002	1662	17	1630	25	1689	35	96.51	98.07
RDT16006-303.d	803	92.6	0.12	0.692	0.015	0.0827	0.0013	0.40285	0.0012	0.0013	533	8.8	511.9	7.8	616	47	83.10	96.04
RDT16006-312.d	125.2	82.4	0.66	9.95	0.2	0.4207	0.008	0.61903	0.0028	0.0031	2425	19	2260	36	2567	31	88.04	93.20
RDT16006-313.d	234.9	114.4	0.49	0.867	0.028	0.1014	0.0017	0.34517	0.002	0.002	631	15	622.4	10	635	69	98.02	98.64
RDT16006-314.d	396.6	174.9	0.44	3.877	0.072	0.2768	0.0047	0.65754	0.0014	0.0016	1606	15	1574	24	1632	30	96.45	98.01
RDT16006-315.d	665.7	179.4	0.27	5.214	0.078	0.3261	0.0055	0.76828	0.0012	0.0015	1852	13	1817	27	1890	24	96.14	98.11
RDT16006-316.d	658.1	37.5	0.06	1.521	0.043	0.1499	0.0029	0.72941	0.0013	0.0014	934	17	900	16	1019	40	88.32	96.36
RDT16006-317.d	366	176.4	0.48	1.426	0.089	0.0988	0.0017	0.49119	0.0053	0.0054	869	34	607	10	1518	91	39.99	69.85
RDT16006-318.d	42.5	12.23	0.29	0.829	0.063	0.0903	0.0027	0.17747	0.0053	0.0053	585	37	556	16	590	160	94.24	95.04
RDT16006-319.d	1154	89	0.08	1.382	0.02	0.1441	0.0022	0.58221	0.00083	0.001	879.8	8.6	867	12	904	30	95.91	98.55
RDT16006-320.d	1272	214.1	0.17	4.25	0.16	0.2247	0.006	0.91247	0.0022	0.0025	1658	33	1303	32	2136	34	61.00	78.59
RDT16006-322.d	761	520	0.68	0.776	0.03	0.0788	0.0014	0.44995	0.0025	0.0026	580	17	489.7	8.3	928	71	52.77	84.43
RDT16006-323.d	1697	81.6	0.05	8.1	0.28	0.3896	0.0095	0.93839	0.0022	0.0025	2215	34	2114	44	2309	30	91.55	95.44
RDT16006-324.d	422	107.6	0.25	2.867	0.1	0.2263	0.0056	0.86526	0.0015	0.0017	1355	27	1312	29	1419	36	92.46	96.83
RDT16006-325.d	424.9	210.5	0.50	12.49	0.2	0.5006	0.0094	0.72439	0.0022	0.0026	2640	16	2612	40	2672	24	97.75	98.94
RDT16006-326.d	254	117.9	0.46	3.711	0.072	0.2464	0.0044	0.62162	0.0017	0.0019	1568	15	1418	23	1767	33	80.25	90.43
RDT16006-327.d	622	176.9	0.28	9.32	0.18	0.4098	0.0074	0.82498	0.0016	0.0021	2363	18	2213	35	2487	21	88.98	93.65
RDT16006-328.d	481	106	0.22	1.95	0.051	0.1721	0.0034	0.65764	0.0015	0.0016	1093	18	1022	19	1226	40	83.36	93.50
RDT16006-338.d	612	187	0.31	1.654	0.031	0.1655	0.0027	0.63048	0.001	0.0012	988	12	987	15	982	34	100.51	99.90
RDT16006-339.d	314.3	127.9	0.41	0.84	0.021	0.0954	0.0017	0.22738	0.0016	0.0017	617	12	586.8	9.8	695	60	84.43	95.11
RDT16006-340.d	199.8	212.4	1.06	1.433	0.038	0.147	0.0025	0.28695	0.0018	0.0019	897	16	884	14	906	57	97.57	98.55
RDT16006-341.d	80	134.4	1.68	1.951	0.073	0.1599	0.0032	0.2403	0.0033	0.0034	1089	25	955	18	1326	80	72.02	87.70
RDT16006-342.d	1344	146.3	0.11	5.21	0.22	0.2208	0.0081	0.96538	0.0022	0.0026	1818	40	1279	43	2529	26	50.57	70.35
RDT16006-343.d	190	66.2	0.35	0.902	0.035	0.107	0.0021	0.30761	0.0023	0.0024	644	18	655	12	572	83	114.51	101.71
RDT16006-344.d	605.9	92.7	0.15	3.745	0.061	0.2372	0.0037	0.69979	0.0013	0.0016	1577	13	1371	19	1860	26	73.71	86.94
RDT16006-345.d	91.6	115.4	1.26	2.139	0.056	0.1972	0.004	0.31243	0.0022	0.0023	1155	18	1159	21	1135	56	102.11	100.35
RDT16006-346.d	82.8	35.89	0.43	1.252	0.053	0.1163	0.0025	-0.083785	0.0038	0.0039	812	24	709	14	1040	100	68.17	87.32
RDT16006-347.d	331	237.3	0.72	3.294	0.06	0.2413	0.0041	0.60951	0.0014	0.0016	1477	14	1392	21	1584	30	87.88	94.25
RDT16006-348.d	352	679	1.93	0.961	0.047	0.0882	0.0015	0.14142	0.004	0.0041	677	23	545.6	9.2	1070	94	50.99	80.59
RDT16006-349.d	109.1	154.7	1.42	0.698	0.036	0.0846	0.0018	0.13381	0.0031	0.0032	528	22	523	11	490	110	106.73	99.05
RDT16006-359.d	538.9	317.9	0.59	0.701	0.016	0.0855	0.0014	0.36185	0.0012	0.0013	537.5	9.3	528.9	8.5	556	49	95.13	98.40
RDT16006b-10.d	734.1	73	0.10	1.608	0.035	0.1402	0.0022	0.49947	0.00098	0.0014	972.2	14	845.5	12	1264	34	66.89	86.97
RDT16006b-14.d	379.1	237.3	0.63	1.191	0.035	0.1263	0.0019	0.28405	0.0016	0.0018	793	16	766.4	11	857	52	89.43	96.65
RDT16006b-15.d	1158	1278	1.10	3.36	0.17	0.1722	0.0072	0.98023	0.0017	0.0025	1458	40	1018	39	2209	31	46.08	69.82
RDT16006b-16.d	2372	1497	0.63	0.871	0.028	0.06192	0.0011	0.26383	0.0029	0.0032	634	15	387.2	6.7	1635	55	23.68	61.07
RDT16006b-17.d	604	431	0.71	11.09	0.52	0.417	0.018	0.97909	0.0014	0.0028	2497	40	2222	81	2760	24	80.51	88.99
RDT16006b-18.d	504.6	33.1	0.07	2.509	0.065	0.1761	0.0035	0.79315	0.0011	0.0017	1271	19	1044	19	1680	31	62.14	82.14
RDT16006b-19.d	384	186.5	0.49	3.81	0.2	0.204	0.0087	0.96964	0.0019	0.0026	1556	41	1189	46	2119	34	56.11	76.41
RDT16006b-20.d	280.4	235.7	0.84	4.534	0.1	0.3075	0.0045	0.45245	0.0012	0.0018	1734	18	1728	22	1734	31	99.65	99.65
RDT16006b-21.d	1597	889	0.56	2.13	0.18	0.1083	0.0027	0.85113	0.0082	0.0084	1122	52	666	17	2085	92	31.94	59.36
RDT16006b-22.d	2264	1116	0.49	0.634	0.02	0.0625	0.0014	0.79038	0.0011	0.0014	497	12	390.7	8.5	1009	43	38.72	78.61
RDT16006b-23.d	907	483	0.53	9.84	0.3	0.392	0.01	0.96477	0.0011	0.0026	2408	29	2125	48	2664	24	79.77	88.25
RDT16006b-24.d	145	124.6	0.86	3	0.13	0.16	0.0029	0.53637	0.0046	0.0049	1387	33	956	16	2101	65	45.50	68.93
RDT16006b-25.d	108.1	128.8	1.19	1.298	0.061	0.093	0.0017	0.33405	0.0042	0.0044	833	25	573.7	10	1610	80	35.63	68.87
RDT16006b-26.d	219	121.8	0.56	2.25	0.19	0.1652	0.005	0.3403	0.0071	0.0072	1139	45	986	27	1403	92	70.28	86.57
RDT16006b-34.d	383	281	0.73	10.41	0.22	0.4654	0.0074	0.78327	0.0012	0.0024	2470	20	2461	32	2468	25	99.72	99.64
RDT16006b-35.d	502.8	89.7	0.18	1.665	0.039	0.1599	0.0024	0.57613	0.00093	0.0013	992.8	15	955.8	13	1069	35	89.41	96.27
RDT16006b-36.d	2073	1288	0.62	1.389	0.051	0.1146	0.0035	0.95105	0.00086	0.0014	875	22	698	20	1361	31	51.29	79.77

Supplementary Table 1. Main isotopes and ratios measured using LA–ICP–MS. Concordance 1 ($^{206}Pb/^{238}U$/ $^{207}Pb/^{206}Pb$) and 2 ($^{206}Pb/^{238}U/^{207}Pb/^{235}U$)

Analysis Spot	U	Th	Th:U	Ratios							Ages						Concordance Calculations	
				$^{207}Pb/^{235}U$	2σ	$^{206}Pb/^{238}U$	2σ	Rho	$^{207}Pb/^{206}Pb$	2σ	$^{207}Pb/^{235}U$	2σ	$^{206}Pb/^{238}U$	2σ	$^{207}Pb/^{206}Pb$	2σ	1	2
RDT16006b-37.d	86.1	46.4	0.54	1.994	0.076	0.1441	0.0028	0.12227	0.0035	0.0037	1103	25	869	16	1581	71	54.97	78.79
RDT16006b-38.d	317	45.8	0.14	1.474	0.044	0.1487	0.0029	0.69352	0.0012	0.0015	914	18	893	16	958	42	93.22	97.70
RDT16006b-39.d	141.9	57.9	0.41	1.167	0.048	0.0852	0.0017	0.15731	0.0036	0.0038	775	22	526.8	10	1546	70	34.08	67.97
RDT16006b-40.d	987	207	0.21	6.66	0.38	0.304	0.016	0.98347	0.0022	0.003	1985	65	1686	83	2407	34	70.05	84.94
RDT16006b-41.d	164.8	115.7	0.70	2.084	0.058	0.177	0.0036	0.27222	0.002	0.0023	1142	18	1050	20	1310	53	80.15	91.94
RDT15066-9.d	63.4	44.8	0.71	12.38	0.52	0.5189	0.012	0.38191	0.1753	0.0073	2633	39	2696	50	***2604***	***69***	103.53	102.39
RDT15066-10.d	187.8	106.2	0.57	13.39	0.55	0.5202	0.011	0.68653	0.1894	0.0075	2706	39	2699	48	***2735***	***64***	98.68	99.74
RDT15066-11.d	414.6	255.8	0.62	11.89	0.48	0.4968	0.01	0.68826	0.1765	0.0069	2595.4	38	2603	45	***2620***	***64***	99.35	100.29
RDT15066-12.d	139.9	14.43	0.10	1.668	0.082	0.1334	0.0032	-0.20846	0.0912	0.0048	994	31	808	18	1437	99	56.23	81.29
RDT15066-13.d	1921	1465	0.76	1.405	0.066	0.1417	0.0039	0.92817	0.07284	0.0029	893	28	854	22	1007	80	84.81	95.63
RDT15066-14.d	1081	74.3	0.07	0.779	0.04	0.0919	0.0025	0.8228	0.0628	0.0027	583	22	567	15	695	91	81.58	97.26
RDT15066-15.d	396.8	431.8	1.09	1.517	0.064	0.1562	0.0033	0.34153	0.072	0.003	937	26	***935.3***	***19***	982	85	95.24	99.82
RDT15066-17.d	979	362	0.37	0.805	0.034	0.0989	0.0022	0.46679	0.06017	0.0024	599.1	19	***607.8***	***13***	601	88	101.13	101.45
RDT15066-18.d	732	319	0.44	18.63	0.76	0.5898	0.013	0.81216	0.233	0.0091	3022	40	2987	51	***3071***	***62***	97.26	98.84
RDT15066-19.d	131.1	68.4	0.52	1.375	0.065	0.1448	0.0034	0.25062	0.0712	0.0034	879	27	873	19	950	99	91.89	99.32
RDT15066-20.d	420	113.1	0.27	1.169	0.076	0.125	0.006	0.93293	0.068	0.0028	777	37	757	35	879	94	86.12	97.43
RDT15066-21.d	80.4	35.17	0.44	1.459	0.098	0.1211	0.0031	0.20405	0.0861	0.0055	899	39	737	18	1310	130	56.26	81.98
RDT15066-22.d	209.8	109.9	0.52	1.754	0.079	0.1745	0.0038	0.40337	0.0743	0.0032	1031	28	***1037***	***21***	1039	88	99.81	100.58
RDT15066-30.d	741	83.2	0.11	0.482	0.021	0.05673	0.0013	0.45515	0.0555	0.0024	399.7	14	355.7	8	420	95	84.69	88.99
RDT15066-31.d	85.1	69.8	0.82	11.63	0.49	0.4704	0.011	0.52533	0.1788	0.0074	2579	41	2487	48	2635	68	94.38	96.43
RDT15066-32.d	358	280.4	0.78	1.73	0.073	0.1693	0.0035	0.44132	0.0738	0.003	1020	28	***1008.3***	***20***	1038	86	97.14	98.85
RDT15066-33.d	159.3	284.7	1.79	0.89	0.055	0.0781	0.0021	0.23004	0.0826	0.005	644	29	484.7	12	1248	120	38.84	75.26
RDT15066-35.d	1933	1020	0.53	0.676	0.029	0.0772	0.0018	0.71717	0.06335	0.0025	523.4	18	479.2	11	722	84	66.37	91.56
RDT15066-36.d	190.2	116.6	0.61	2.443	0.12	0.2043	0.0053	0.72535	0.085	0.0038	1256	36	1197	28	1332	85	89.86	95.30
RDT15066-37.d	639.2	125.9	0.20	2.129	0.087	0.1934	0.0039	0.46784	0.07991	0.0032	1157.4	28	***1139.7***	***21***	1192	81	95.61	98.47
RDT15066-38.d	569	145	0.25	1.418	0.069	0.1394	0.0043	0.82807	0.0736	0.003	896	29	843	25	1033	83	81.61	94.08
RDT15066-39.d	65.1	38.8	0.60	1.044	0.058	0.1157	0.0029	0.11409	0.0662	0.0037	731	28	705	17	795	120	88.68	96.44
RDT15066-40.d	340.8	140.4	0.41	3.833	0.16	0.2838	0.0061	0.4563	0.0978	0.0039	1599.6	32	1611	30	***1584***	***76***	101.70	100.71
RDT15066-41.d	87.8	93.5	1.06	0.792	0.049	0.0894	0.0026	0.13037	0.0644	0.0041	591	28	553	16	700	130	79.00	93.57
RDT15066-49.d	165.4	66.8	0.40	13.09	0.54	0.4729	0.011	0.72363	0.2006	0.008	2689	39	2495	47	2829	64	88.19	92.79
RDT15066-50.d	747	103.6	0.14	2.1	0.094	0.1323	0.0037	0.87668	0.1016	0.004	1146	31	801	21	1651	74	48.52	69.90
RDT15066-51.d	684	267	0.39	1.566	0.065	0.151	0.0033	0.37396	0.0748	0.0031	957.5	26	906.2	18	1061	83	85.41	94.64
RDT15066-52.d	467	124.4	0.27	1.1	0.06	0.1081	0.0042	0.85398	0.0725	0.0031	748	29	661	25	1000	89	66.10	88.37
RDT15066-53.d	279	168.9	0.61	1.54	0.088	0.1176	0.0029	-0.29092	0.0962	0.0065	938	34	716	17	1470	120	48.71	76.33
RDT15066-54.d	16.21	0.025	0.00	3.05	0.34	0.1086	0.0046	0.40497	0.206	0.022	1343	80	663	27	2700	170	24.56	49.37
RDT15066-55.d	222.4	118.8	0.53	1.612	0.083	0.142	0.0033	0.25974	0.081	0.0042	974	30	855	19	1217	100	70.25	87.78
RDT15066-56.d	1223	88.1	0.07	1.469	0.06	0.1498	0.0032	0.74432	0.06991	0.0028	917.9	24	***899.9***	***18***	928	82	96.97	98.04
RDT15066-57.d	252.2	294	1.17	0.897	0.043	0.102	0.0022	0.1504	0.0625	0.003	648	23	626	13	673	110	93.02	96.60
RDT15066-58.d	109	88.8	0.81	1.453	0.082	0.13	0.0032	0.33238	0.0791	0.0043	906	34	788	18	1163	110	67.76	86.98
RDT15066-59.d	87.5	70.2	0.80	1.449	0.074	0.1504	0.0036	0.18233	0.0689	0.0034	907	30	904	20	925	100	97.73	99.67
RDT15066-60.d	379	76.7	0.20	1.229	0.057	0.1195	0.0027	0.48802	0.0739	0.0033	816	25	727.7	15	1035	90	70.31	89.18
RDT15066-68.d	802	228.2	0.28	1.013	0.052	0.1025	0.0031	0.79642	0.0711	0.0032	707	26	629	18	942	87	66.77	88.97
RDT15066-69.d	334	94	0.28	0.919	0.043	0.1072	0.0026	0.45168	0.0617	0.0028	664	24	***656.4***	***15***	653	100	100.52	98.86
RDT15066-70.d	516	233.6	0.45	9.67	0.4	0.4186	0.0093	0.72204	0.163	0.0064	2404	38	2253	42	2487	66	90.59	93.72
RDT15066-71.d	544	205	0.38	0.778	0.036	0.0915	0.002	0.34052	0.0598	0.0027	583	20	***564.1***	***12***	591	92	95.45	96.76
RDT15066-72.d	223	206	0.92	1.015	0.064	0.0893	0.0023	0.56735	0.079	0.0044	706	31	551.4	13	1165	110	47.33	78.10
RDT15066-73.d	101.9	201.2	1.97	1.023	0.064	0.0868	0.0025	0.2516	0.0828	0.0051	711	31	537	15	1241	110	43.27	75.53

Supplementary Table 1. Main isotopes and ratios measured using LA–ICP–MS. Concordance 1 ($^{206}Pb/^{238}U$/ $^{207}Pb/^{206}Pb$) and 2 ($^{206}Pb/^{238}U/^{207}Pb/^{235}U$)

Analysis Spot	U	Th	Th:U	Ratios							Ages						Concordance Calculations	
				$^{207}Pb/^{235}U$	2σ	$^{206}Pb/^{238}U$	2σ	Rho	$^{207}Pb/^{206}Pb$	2σ	$^{207}Pb/^{235}U$	2σ	$^{206}Pb/^{238}U$	2σ	$^{207}Pb/^{206}Pb$	2σ	1	2
RDT15066-74.d	557	75.6	0.14	1.014	0.049	0.1049	0.0023	0.43997	0.0669	0.003	710	24	643.2	13	840	94	76.57	90.59
RDT15066-75.d	872	33.3	0.04	0.753	0.032	0.08864	0.0019	0.40038	0.06	0.0025	570.8	19	547.4	11	594	91	92.15	95.90
RDT15066-76.d	619	245.2	0.40	1.613	0.073	0.1555	0.0043	0.77225	0.07365	0.003	976	28	***935***	***23***	1030	84	90.78	95.80
RDT15066-77.d	609	307	0.50	1.599	0.07	0.1523	0.0038	0.65825	0.0746	0.0031	971	28	914	22	1061	87	86.15	94.13
RDT15066-79.d	1913	451.4	0.24	2.215	0.09	0.1573	0.0033	0.62859	0.10059	0.004	1185.9	28	941.4	19	1635	74	57.58	79.38
RDT15066-89.d	248	81.2	0.33	1.308	0.064	0.1292	0.0031	0.48462	0.0736	0.0034	849	28	783	18	1019	94	76.84	92.23
RDT15066-90.d	270.9	137.8	0.51	1.067	0.077	0.079	0.002	0.55276	0.0981	0.0064	722	32	490	12	1513	110	32.39	67.87
RDT15066-91.d	229.8	226	0.98	1.247	0.059	0.1292	0.0031	0.35298	0.0711	0.0033	823	26	783	18	960	95	81.56	95.14
RDT15066-92.d	681	104.4	0.15	4.159	0.17	0.276	0.0062	0.73757	0.1094	0.0043	1664	34	1571	31	1788	72	87.86	94.41
RDT15066-93.d	108.4	93.6	0.86	7.48	0.33	0.3647	0.0092	0.69031	0.1495	0.0062	2168	39	2003	44	2339	70	85.63	92.39
RDT15066-94.d	216.5	195.4	0.90	1.178	0.054	0.123	0.0027	0.18285	0.0693	0.0031	791	24	748.5	16	908	90	82.43	94.63
RDT15066-95.d	575	205	0.36	1.557	0.066	0.1619	0.0039	0.59907	0.0699	0.0029	952	26	***968***	***22***	935	85	103.53	101.68
RDT15066-96.d	308	230	0.75	1.24	0.054	0.1268	0.0028	0.38294	0.0714	0.003	819	24	769.6	16	964	84	79.83	93.97
RDT15066-97.d	228.7	251.7	1.10	1.368	0.061	0.1391	0.0031	0.43417	0.0716	0.0031	873	26	839.1	18	976	84	85.97	96.12
RDT15066-98.d	1578	449	0.28	7.69	0.39	0.3001	0.0095	0.97112	0.1683	0.0067	2188	46	1693	46	2538	67	66.71	77.38
RDT15066-99.d	900	76.6	0.09	0.829	0.036	0.0931	0.0021	-0.47105	0.065	0.0028	612.3	20	573.7	13	759	89	75.59	93.70
RDT15066-107.d	893	279	0.31	8.3	0.35	0.336	0.0079	0.89577	0.1622	0.0063	2261	39	1866	38	2478	65	75.30	82.53
RDT15066-109.d	673	142	0.21	0.945	0.041	0.1135	0.0025	0.44324	0.05976	0.0025	674.6	21	693.1	15	589	88	117.67	102.74
RDT15066-110.d	286.8	335	1.17	3.521	0.15	0.2622	0.0057	0.47754	0.0973	0.004	1535	33	1502	30	***1568***	***76***	95.79	97.85
RDT15066-111.d	501	451	0.90	8.79	0.36	0.4015	0.009	0.84714	0.1578	0.0062	2315	38	2178	42	***2433***	***65***	89.52	94.08
RDT15066-112.d	307	201.2	0.66	5.159	0.21	0.3403	0.0071	0.43277	0.1098	0.0044	1847	35	1888	34	***1796***	***71***	105.12	102.22
RDT15066-113.d	1241	361.5	0.29	0.891	0.038	0.1062	0.0024	0.664	0.06114	0.0025	646.4	20	***650.3***	***14***	640	85	101.61	100.60
RDT15066-114.d	529	218.8	0.41	0.866	0.038	0.104	0.0024	0.26992	0.0615	0.0026	634.3	21	***637.8***	***14***	646	93	98.73	100.55
RDT15066-115.d	1351	264	0.20	0.785	0.033	0.09308	0.002	0.35963	0.06085	0.0025	588.1	18	***573.6***	***12***	629	87	91.19	97.53
RDT15066-116.d	432	268	0.62	0.712	0.033	0.0829	0.0019	0.0027108	0.062	0.003	544	20	513.3	11	672	99	76.38	94.36
RDT15066-117.d	1148	378	0.33	0.732	0.035	0.0901	0.0023	0.88168	0.0597	0.0025	556	20	***556.2***	***13***	584	92	95.24	100.04
RDT15066-118.d	913	509	0.56	0.846	0.051	0.0912	0.0022	0.60689	0.0675	0.0036	617	24	562.3	13	803	81	70.02	91.13
RDT15066-127.d	2190	182.8	0.08	12.02	0.49	0.4731	0.01	0.78689	0.1818	0.0071	2605.1	38	2496	44	***2670.3***	***67***	93.47	95.81
RDT15066-128.d	423	415.1	0.98	0.676	0.032	0.07602	0.0017	0.27253	0.0645	0.003	523	19	472.3	10	752	95	62.81	90.31
RDT15066-129.d	308	112.8	0.37	0.974	0.043	0.1078	0.0025	0.24187	0.0652	0.0029	689	22	659.8	15	775	89	85.14	95.76
RDT15066-130.d	262.9	107.6	0.41	1.466	0.086	0.1428	0.0056	0.88905	0.0737	0.0032	909	36	864	31	1031	86	83.80	95.05
RDT15066-131.d	867	631	0.73	4.672	0.19	0.3005	0.0062	0.72488	0.11243	0.0044	1761.5	34	1693	31	***1838***	***70***	92.11	96.11
RDT15066-132.d	144.1	113	0.78	1.695	0.082	0.1537	0.0038	-0.13961	0.0799	0.004	1008	29	923	21	1173	95	78.69	91.57
RDT15066-133.d	71.7	45.3	0.63	25.47	1.1	0.644	0.016	0.69177	0.2849	0.012	3325	42	3200	62	***3393***	***62***	94.31	96.24
RDT15066-134.d	211.6	156.9	0.74	1.027	0.048	0.1144	0.0027	0.4364	0.0653	0.003	718	24	698.3	15	776	95	89.99	97.26
RDT15066-135.d	271	89.5	0.33	0.853	0.039	0.0945	0.0021	0.23416	0.0655	0.003	626	22	581.9	12	794	100	73.29	92.96
RDT15066-136.d	205.2	106.2	0.52	2.921	0.12	0.2331	0.0051	0.42677	0.0925	0.0038	1388	32	***1350***	***27***	1469	78	91.90	97.26
RDT15066-137.d	593	1267	2.14	0.642	0.028	0.0793	0.002	0.51704	0.0604	0.0026	502.7	17	491.8	12	610	94	80.62	97.83
RDT15066-138.d	646	124.9	0.19	1.576	0.065	0.1608	0.0034	0.51885	0.07204	0.0029	959.8	26	960.8	19	984	80	97.64	100.10
RDT15066-139.d	183	228	1.25	1.713	0.078	0.1655	0.0037	0.31978	0.077	0.0035	1019	31	987	20	1108	92	89.08	96.86
RDT15066-147.d	181	96.4	0.53	1.887	0.095	0.1751	0.0048	0.67095	0.0813	0.0037	1071	33	1040	26	1224	88	84.97	97.11
RDT15066-148.d	242	197.2	0.81	0.796	0.04	0.085	0.0019	0.091428	0.0693	0.0035	595	22	525.6	12	913	100	57.57	88.34
RDT15066-149.d	342	96	0.28	1.671	0.081	0.1514	0.0044	0.83006	0.0813	0.0034	993	31	911	24	1225	83	74.37	91.74
RDT15066-150.d	205.8	186.6	0.91	9.17	0.39	0.3843	0.0089	0.6711	0.174	0.007	2354	39	2095	41	2595	66	80.73	89.00
RDT15066-151.d	635.3	2580	4.06	0.809	0.034	0.08913	0.0019	0.34803	0.0664	0.0028	601.4	19	550.3	11	806	88	68.28	91.50
RDT15066-152.d	219	139	0.63	1.739	0.1	0.1293	0.0039	0.36999	0.0971	0.0057	1019	38	783	22	1560	110	50.19	76.84
RDT15066-152.d	374	84.5	0.23	3.44	0.18	0.2334	0.0072	0.88265	0.1051	0.0045	1507	43	**1351**	38	1719	78	78.59	89.65

Supplementary Table 1. Main isotopes and ratios measured using LA–ICP–MS. Concordance 1 ($^{206}Pb/^{238}U$/ $^{207}Pb/^{206}Pb$) and 2 ($^{206}Pb/^{238}U/^{207}Pb/^{235}U$)

Analysis Spot	U	Th	Th:U	Ratios							Ages						Concordance Calculations	
				$^{207}Pb/^{235}U$	2σ	$^{206}Pb/^{238}U$	2σ	Rho	$^{207}Pb/^{206}Pb$	2σ	$^{207}Pb/^{235}U$	2σ	$^{206}Pb/^{238}U$	2σ	$^{207}Pb/^{206}Pb$	2σ	1	2
RDT15066-153.d	726	136	0.19	5.92	0.28	0.2822	0.0078	0.9587	0.1502	0.006	1958	40	1600	39	2347	68	68.17	81.72
RDT15066-154.d	386	115	0.30	1.479	0.096	0.1514	0.0069	0.84185	0.071	0.0032	911	40	***906***	***39***	945	94	95.87	99.45
RDT15066-155.d	211	126	0.60	1.664	0.081	0.1513	0.0033	0.43569	0.0787	0.0038	992	30	909	18	1161	91	78.29	91.63
RDT15066-156.d	333	102	0.31	0.931	0.065	0.0859	0.0026	0.51148	0.0773	0.005	664	33	531	15	1150	130	46.17	79.97
RDT15066-156.d	126	137	1.09	4.21	0.21	0.2515	0.0069	0.68783	0.1182	0.0053	1671	40	1445	36	1920	79	75.26	86.48
RDT15066-157.d	170.9	166.4	0.97	1.681	0.074	0.1512	0.0035	0.25669	0.0801	0.0036	1004	28	908	20	1191	89	76.24	90.44
RDT15066-158.d	370.8	218.4	0.59	0.677	0.03	0.07922	0.0018	0.25965	0.0613	0.0027	526.9	19	491.4	10	646	99	76.07	93.26
RDT15066-159.d	117.6	183	1.56	1.58	0.11	0.1237	0.0032	0.45552	0.0925	0.0062	946	42	751	18	1404	120	53.49	79.39
RDT15066-160.d	204.2	112.9	0.55	1.41	0.064	0.1385	0.003	0.38603	0.0723	0.0031	891	27	836	17	1002	90	83.43	93.83
RDT15066-168.d	24.04	9.81	0.41	3.55	0.28	0.1248	0.0043	0.37596	0.213	0.016	1530	64	757	25	2920	120	25.92	49.48
RDT15066-169.d	316	53	0.17	2.114	0.1	0.1733	0.0048	0.78306	0.0887	0.0038	1152	33	1030	26	1393	81	73.94	89.41
RDT15066-170.d	234	128.8	0.55	1.089	0.05	0.1076	0.0024	0.21771	0.0747	0.0035	747	25	659.3	14	1064	91	61.96	88.26
RDT15066-171.d	172	79.5	0.46	1.132	0.058	0.1169	0.003	0.18434	0.0703	0.0036	771	28	713	17	965	100	73.89	92.48
RDT15066-172.d	148.6	129.8	0.87	1.783	0.081	0.1611	0.0038	0.1773	0.0814	0.0037	1040	29	963	21	1244	84	77.41	92.60
RDT15066-173.d	451.2	197.6	0.44	0.919	0.04	0.0999	0.0021	0.29959	0.0673	0.0029	661.7	21	613.6	12	838	87	73.22	92.73
RDT15066-174.d	658	195	0.30	1.193	0.051	0.1246	0.0029	0.65588	0.06987	0.0028	796.2	24	758	17	921	85	82.30	95.20
RDT15066-175.d	886	238	0.27	1.033	0.052	0.1055	0.0037	0.88677	0.07103	0.0029	718	26	646	21	960	81	67.29	89.97
RDT15066-176.d	67.21	143.7	2.14	10.23	0.44	0.4229	0.0095	0.36316	0.177	0.0075	2457	39	2272	43	2626	70	86.52	92.47
RDT15066-177.d	96.8	161.2	1.67	3.554	0.16	0.2483	0.0057	0.24942	0.1033	0.0046	1535	35	1431	29	1691	81	84.62	93.22
RDT15066-178.d	282	229	0.81	1.465	0.088	0.1328	0.0035	0.3181	0.0809	0.0042	903	33	803	20	1187	96	67.65	88.93
RDT15066-179.d	42.65	441.4	10.35	68.6	3	0.585	0.017	0.89776	0.8489	0.034	4302	44	2963	70	5073	76	58.41	68.87
RDT15066-180.d	500	409	0.82	1.21	0.065	0.1236	0.0046	0.87614	0.0711	0.003	803	31	750	26	952	85	78.78	93.40
RDT15066-181.d	200.7	128.7	0.64	4.111	0.17	0.2717	0.0058	0.3472	0.1105	0.0046	1656	34	1549	29	1802	75	85.96	93.54
RDT15066-189.d	303	161.9	0.53	1.555	0.072	0.1448	0.0039	0.62341	0.0762	0.0033	949	29	871	22	1097	87	79.40	91.78
RDT15066-190.d	801	94.1	0.12	0.811	0.035	0.0916	0.002	0.38797	0.06139	0.0026	602	20	564.8	12	648	90	87.16	93.82
RDT15066-191.d	421	216.2	0.51	2.292	0.099	0.1965	0.0048	0.71093	0.0813	0.0033	1209	30	1156	26	1226	81	94.29	95.62
RDT15066-192.d	32.61	572.2	17.55	80.6	3.4	0.708	0.018	0.71053	0.8002	0.032	4470	42	3460	67	4963	73	69.72	77.40
RDT15066-194.d	166.9	122.8	0.74	1.109	0.054	0.1209	0.0027	0.2621	0.0652	0.0031	758	26	***735.5***	***16***	761	100	96.65	97.03
RDT15066-195.d	812	615	0.76	0.63	0.029	0.0728	0.0021	0.75894	0.0613	0.0026	494.6	18	452.6	13	642	92	70.50	91.51
RDT15066-196.d	234.6	142	0.61	0.893	0.069	0.0882	0.0035	0.79199	0.0717	0.0042	641	36	545	21	1004	120	54.28	85.02
RDT15066-197.d	157	92.3	0.59	3.252	0.15	0.2548	0.0067	0.60647	0.0903	0.0038	1470	36	1462	34	***1429***	***80***	102.31	99.46
RDT15066-198.d	885	231	0.26	4.82	0.22	0.3025	0.0081	0.95305	0.11334	0.0045	1785	39	1707	38	***1851***	***71***	92.22	95.63
RDT15066-199.d	93.5	55.1	0.59	1.695	0.094	0.1409	0.0034	0.44882	0.0873	0.0046	1009	36	849	19	1355	110	62.66	84.14
RDT15066-200.d	289.3	212.7	0.74	1.541	0.067	0.1576	0.0034	0.48443	0.0714	0.003	945	27	***943***	***19***	972	87	97.02	99.79
RDT15066-201.d	542	34.1	0.06	0.663	0.029	0.0834	0.0018	0.24106	0.0577	0.0025	515.7	18	***516.3***	***11***	518	92	99.67	100.12
RDT15066-202.d	114.1	94.9	0.83	1.278	0.061	0.1317	0.0029	0.2606	0.0693	0.0033	834	28	798.6	17	897	100	89.03	95.76
RDT15066-203.d	948	142.8	0.15	0.743	0.032	0.0903	0.0019	0.44099	0.06044	0.0025	564.1	18	557.4	11	611	90	91.23	98.81
RDT15066-204.d	605	178	0.29	5.26	0.24	0.2893	0.0078	0.90414	0.1309	0.0052	1859	39	1637	39	2107	70	77.69	88.06
RDT15066-205.d	688	135	0.20	0.87	0.069	0.1019	0.0052	0.9301	0.0632	0.003	635	39	624	30	705	100	88.51	98.27
RDT15066-205.d	310	189	0.61	6.15	0.31	0.3099	0.01	0.90665	0.1411	0.0059	2002	48	1740	49	2238	72	77.75	86.91
RDT16012_0	220.6	60.9	0.28	2.061	0.064	0.1706	0.0037	0.81535	0.0887	0.0018	1130	21	1016	20	1388	39	73.20	89.91
RDT16012_1	1011	401	0.40	0.56	0.018	0.0489	0.0011	0.74712	0.0834	0.0019	449	12	307.8	6.9	1277	45	24.10	68.55
RDT16012_2	444	311.1	0.70	1.292	0.029	0.1384	0.0016	0.5061	0.06839	0.0013	840.4	13	835.2	9	870	39	96.00	99.38
RDT16012_3	211.4	92.1	0.44	6.236	0.13	0.3643	0.004	0.63291	0.1251	0.0021	2007.4	18	2001	19	2026	30	98.77	99.68
RDT16012_4	359	370	1.03	0.739	0.019	0.08931	0.001	0.31946	0.0604	0.0014	560.7	11	551.3	6.1	599	50	92.04	98.32
RDT16012_5	166	105.66	0.64	0.776	0.023	0.0937	0.0012	0.28176	0.0605	0.0016	581	13	577.1	7.2	590	57	97.81	99.33
RDT16012_6	759.9	69.8	0.09	0.809	0.018	0.0971	0.0011	0.4114	0.06056	0.0012	601.2	10	597.3	6.3	616	42	96.96	99.35
RDT16012_7	689	26.43	0.04	1.51	0.033	0.1515	0.0017	0.49128	0.07236	0.0013	933	13	908.9	9.3	986	37	92.18	97.42

Supplementary Table 1. Main isotopes and ratios measured using LA–ICP–MS. Concordance 1 ($^{206}Pb/^{238}U/^{207}Pb/^{206}Pb$) and 2 ($^{206}Pb/^{238}U/^{207}Pb/^{235}U$)

Analysis Spot	U	Th	Th:U	Ratios							Ages						Concordance Calculations	
				$^{207}Pb/^{235}U$	2σ	$^{206}Pb/^{238}U$	2σ	Rho	$^{207}Pb/^{206}Pb$	2σ	$^{207}Pb/^{235}U$	2σ	$^{206}Pb/^{238}U$	2σ	$^{207}Pb/^{206}Pb$	2σ	1	2
RDT16012_8	456.5	192.4	0.42	1.616	0.036	0.1605	0.0019	0.61614	0.07298	0.0013	975.4	14	959.1	11	1004	36	95.53	98.33
RDT16012_9	2833	2845	1.00	5.565	0.12	0.1591	0.0024	0.92505	0.2522	0.0038	1908	19	951	13	3196.5	24	29.75	49.84
RDT16012_10	129	142.8	1.11	1.252	0.043	0.1095	0.0019	0.48589	0.082	0.0024	819	19	669	11	1216	59	55.02	81.68
RDT16012_11	259.2	103.4	0.40	3.45	0.39	0.1651	0.0031	0.85855	0.14	0.013	1349	77	984	17	1800	150	54.67	72.94
RDT16012_12	243.8	45.08	0.18	1.619	0.037	0.1623	0.0018	0.27367	0.072	0.0015	975.4	14	969.2	9.7	970	43	99.92	99.36
RDT16012_13	81.5	29.93	0.37	0.581	0.025	0.0661	0.0011	0.005255	0.0635	0.0028	461	16	412.3	6.8	640	95	64.42	89.44
RDT16012_14	76.42	107.72	1.41	9.9	0.23	0.4317	0.0057	0.64968	0.1652	0.003	2424	21	2311	26	2505	30	92.26	95.34
RDT16012_15	71.9	26.61	0.37	1.744	0.054	0.1687	0.0023	0.25109	0.0756	0.0022	1022	20	1004	12	1044	59	96.17	98.24
RDT16012_16	36.08	23.36	0.65	1.072	0.086	0.0577	0.0013	0.26887	0.1332	0.01	701	42	361.4	7.9	1830	150	19.75	51.55
RDT16012_17	934	517	0.55	1.477	0.031	0.147	0.0017	0.74586	0.07289	0.0012	919.7	13	884	9.6	1009	33	87.61	96.12
RDT16012_18	451.8	118.1	0.26	1.892	0.041	0.177	0.0023	0.53423	0.07752	0.0014	1076.7	14	1050	13	1126	37	93.25	97.52
RDT16012_19	26.11	18.85	0.72	2.7	0.11	0.1986	0.0033	0.11461	0.0998	0.0043	1314	32	1166	18	1523	84	76.56	88.74
RDT16012_20	65.7	27.66	0.42	4.941	0.13	0.2926	0.0053	0.54147	0.1227	0.0028	1804	22	1652	26	1983	41	83.31	91.57
RDT16012_21	969	277.6	0.29	0.5059	0.012	0.0632	0.001	0.57497	0.05824	0.0012	414.8	8.3	395	6.3	527	47	74.95	95.23
RDT16012_22	770	848	1.10	1.988	0.096	0.1485	0.006	0.959	0.0959	0.0017	1087	33	888	34	1538	34	57.74	81.69
RDT16012_23	53.17	36.21	0.68	1.622	0.057	0.1502	0.0024	0.14116	0.0788	0.0028	969	22	902	13	1092	73	82.60	93.09
RDT16012_24	346.2	223.8	0.65	1.06	0.12	0.0571	0.0011	0.85804	0.127	0.012	675	51	358.1	6.8	1670	140	21.44	53.05
RDT16012_25	624.6	408	0.65	1.505	0.046	0.1353	0.0016	0.33774	0.0806	0.0022	931	18	817.6	9.3	1194	52	68.48	87.82
RDT16012_26	246.2	139.2	0.57	0.808	0.031	0.07222	0.001	0.48842	0.0807	0.0027	595	18	450	6	1161	69	38.76	75.63
RDT16012_27	50	25.34	0.51	12.97	0.38	0.475	0.011	0.85082	0.197	0.0036	2664	29	2498	47	2796	31	89.34	93.77
RDT16012_28	1121	247	0.22	0.2394	0.0059	0.03257	0.00037	0.21967	0.05345	0.0012	217.6	4.8	206.6	2.3	329	51	62.80	94.94
RDT16012_29	477.1	130.9	0.27	0.2709	0.011	0.03398	0.00039	0.12033	0.0586	0.0023	242	8.2	***215.4***	***2.4***	494	81	43.60	89.01
RDT16012_30	451.3	81.6	0.18	0.2637	0.009	0.03494	0.00044	0.23819	0.0552	0.0018	237.4	7.3	***221.4***	***2.7***	380	70	58.26	93.26
RDT16012_31	299.7	38.43	0.13	2.184	0.048	0.1991	0.0024	0.48229	0.0799	0.0015	1174.8	15	1170	13	1183	37	98.90	99.59
RDT16012_32	516	184.4	0.36	8.36	0.23	0.3758	0.0073	0.93984	0.1611	0.0025	2261	26	2052	34	2466	26	83.21	90.76
RDT16012_33	200	104.67	0.52	4.375	0.094	0.3002	0.0033	0.51385	0.1058	0.0019	1705	18	1691	16	1723	33	98.14	99.18
RDT16012_34	291.2	132.7	0.46	0.936	0.023	0.1073	0.0012	0.34635	0.0634	0.0014	670.7	12	656.6	7	702	49	93.53	97.90
RDT16012_35	570	183	0.32	0.2499	0.0076	0.03477	0.00045	0.24923	0.0518	0.0015	226.3	6.3	***220.3***	***2.8***	250	62	88.12	97.35
RDT16012_36	305.3	96.59	0.32	1.463	0.035	0.1517	0.0017	0.44146	0.0699	0.0014	912.7	14	910.3	9.7	912	42	99.81	99.74
RDT16012_37	120.5	102.1	0.85	8.04	0.18	0.3949	0.0054	0.7447	0.1475	0.0026	2231	21	2143	25	2311	30	92.73	96.06
RDT16012_38	686	245.5	0.36	2.201	0.046	0.201	0.0022	0.69281	0.07926	0.0013	1179.8	15	1180	12	1173	33	100.60	100.02
RDT16012_39	127.7	87.4	0.68	4.718	0.11	0.3146	0.004	0.52213	0.1086	0.0021	1766	19	1762	20	1773	34	99.38	99.77
RDT16012_40	224.3	124.6	0.56	0.34	0.013	0.04283	0.0006	0.25609	0.0576	0.0021	294.9	10	270.3	3.7	454	79	59.54	91.66
RDT16012_41	261.2	178.8	0.68	0.243	0.009	0.03373	0.00048	0.17974	0.0523	0.0019	220.5	7.6	***213.8***	***3***	253	78	84.51	96.96
RDT16012_42	192	75.2	0.39	0.976	0.027	0.1106	0.0015	0.16052	0.0636	0.0016	691	14	676.1	8.5	715	58	94.56	97.84
RDT16012_43	199.9	121.2	0.61	2.904	0.065	0.2407	0.0025	0.42334	0.0869	0.0017	1380	17	1390	13	1352	38	102.81	100.72
RDT16012_44	617	897	1.45	0.63	0.036	0.04293	0.0008	0.1619	0.1028	0.0049	485	22	270.9	5	1555	87	17.42	55.86
RDT16012_45	75.81	66.89	0.88	6.796	0.15	0.3815	0.0045	0.57074	0.1284	0.0024	2086	21	2082	21	2071	33	100.53	99.81
RDT16012_46	417.5	64.1	0.15	6.366	0.13	0.3606	0.0041	0.69962	0.1262	0.0021	2025.7	18	1984	20	2043	29	97.11	97.94
RDT16012_47	309	327	1.06	2.648	0.057	0.2201	0.0024	0.43777	0.0862	0.0016	1313.9	16	1282	13	1335	36	96.03	97.57
RDT16012_48	360.5	219.6	0.61	7.638	0.15	0.3997	0.0042	0.7198	0.13693	0.0022	2188.2	18	2166	19	2185	28	99.13	98.99
RDT16012_49	145.9	170.2	1.17	4.094	0.091	0.292	0.0036	0.41905	0.1007	0.002	1655	19	1650	18	1624	37	101.60	99.70
RDT16012_50	283.1	235.6	0.83	1.95	0.043	0.1836	0.0019	0.40703	0.0757	0.0015	1096.3	15	1086.4	10	1077	40	100.87	99.10
RDT16012_51	160.5	84.6	0.53	3.52	0.12	0.2218	0.0029	0.29313	0.1136	0.0037	1523	26	1292	15	1819	55	71.03	84.83
RDT16012_52	384.5	72.1	0.19	2.533	0.055	0.2181	0.0028	0.67643	0.08296	0.0015	1281.3	16	1271	15	1264	35	100.55	99.20
RDT16012_53	94.2	153.3	1.63	2.428	0.066	0.2041	0.0029	0.13155	0.0852	0.0023	1247	19	1196	16	1291	53	92.64	95.91
RDT16012_54	757	146	0.19	1.924	0.046	0.1806	0.003	0.82068	0.0755	0.0013	1087	16	1070	16	1078	35	99.26	98.44
RDT16012_55	487	395	0.81	2.031	0.05	0.1722	0.003	0.78463	0.08413	0.0015	1124	17	1023	17	1286	35	79.55	91.01

Supplementary Table 1. Main isotopes and ratios measured using LA–ICP–MS. Concordance 1 ($^{206}Pb/^{238}U/^{207}Pb/^{206}Pb$) and 2 ($^{206}Pb/^{238}U/^{207}Pb/^{235}U$)

Analysis Spot	U	Th	Th:U	Ratios							Ages						Concordance Calculations	
				$^{207}Pb/^{235}U$	2σ	$^{206}Pb/^{238}U$	2σ	Rho	$^{207}Pb/^{206}Pb$	2σ	$^{207}Pb/^{235}U$	2σ	$^{206}Pb/^{238}U$	2σ	$^{207}Pb/^{206}Pb$	2σ	1	2
RDT16012_56	320.4	391.3	1.22	0.587	0.017	0.06887	0.0009	0.30312	0.0607	0.0016	467.7	11	429.2	5.4	608	56	70.59	91.77
RDT16012_57	821.4	222.7	0.27	0.7471	0.016	0.09166	0.00099	0.39762	0.05826	0.0011	565.7	9.4	565.2	5.8	532	41	106.24	99.91
RDT16012_58	94.82	21.4	0.23	1.588	0.048	0.1638	0.0022	0.26317	0.0718	0.0021	961	19	980	13	952	59	102.94	101.98
RDT16012_59	67.9	88	1.30	1.164	0.056	0.1107	0.0017	0.21346	0.0789	0.0037	774	26	676.1	10	1046	95	64.64	87.35
RDT16012_60	479.5	302.9	0.63	0.4042	0.01	0.05456	0.00062	0.2514	0.0547	0.0013	343.9	7.5	342.4	3.8	373	52	91.80	99.56
RDT16012_61	214.9	145.1	0.68	2.155	0.049	0.1987	0.0025	0.44804	0.0799	0.0016	1165	16	1168	14	1189	40	98.23	100.26
RDT16012_62	127	150.4	1.18	2.147	0.056	0.1981	0.0025	0.38048	0.0802	0.0019	1159	18	1164	13	1175	48	99.06	100.43
RDT16012_63	217.5	161.6	0.74	1.909	0.045	0.1792	0.0022	0.30101	0.0785	0.0016	1081	16	1063	12	1162	43	91.48	98.33
RDT16012_64	440.2	439	1.00	0.703	0.017	0.08635	0.00089	0.43393	0.06001	0.0012	539	10	533.8	5.3	595	46	89.71	99.04
RDT16012_65	452.3	243.5	0.54	8.135	0.16	0.3668	0.0039	0.77431	0.1636	0.0025	2244.4	18	2013	18	2490	26	80.84	89.69
RDT16012_66	639	373	0.58	5.35	0.21	0.2661	0.0083	0.95907	0.1478	0.0025	1858	32	1514	42	2316	29	65.37	81.49
RDT16012_67	206	178.7	0.87	3.991	0.097	0.2795	0.0047	0.79671	0.106	0.0019	1632	19	1587	24	1723	33	92.11	97.24
RDT16012_68	187.4	194.1	1.04	0.743	0.022	0.0933	0.0012	0.20415	0.059	0.0017	563	13	574.7	7	524	62	109.68	102.08
RDT16012_69	179.2	197	1.10	1.93	0.054	0.1707	0.0024	0.52112	0.0833	0.0019	1086	19	1015	13	1259	45	80.62	93.46
RDT16012_70	807	233.9	0.29	1.306	0.045	0.1359	0.0036	0.90673	0.07009	0.0013	840	20	820	20	918	39	89.32	97.62
RDT16012_71	149.5	96.7	0.65	10.62	0.23	0.4709	0.0056	0.62716	0.1611	0.0028	2487	20	2485	25	2464	28	100.85	99.92
RDT16012_72	153.8	115.9	0.75	1.797	0.048	0.172	0.002	0.35508	0.0747	0.0017	1041	17	1022	11	1047	49	97.61	98.17
RDT16012_73	277.1	80.7	0.29	1.375	0.039	0.1405	0.0023	0.76602	0.0699	0.0014	875	17	847	13	913	42	92.77	96.80
RDT16012_74	166.5	121.4	0.73	2.245	0.052	0.2022	0.0023	0.26757	0.0795	0.0017	1192	16	1186	12	1169	43	101.45	99.50
RDT16012_75	45.86	56.73	1.24	0.734	0.041	0.0816	0.0015	0.055931	0.0649	0.0037	546	24	505.4	9.2	610	120	82.85	92.56
RDT16012_76	320.2	176.4	0.55	1.48	0.035	0.153	0.0017	0.44055	0.0692	0.0014	919.9	14	917.5	9.7	887	43	103.44	99.74
RDT16012_77	417.3	117.44	0.28	9.067	0.18	0.4165	0.0044	0.7061	0.1559	0.0024	2344.7	18	2243	20	2409	27	93.11	95.66
RDT16012_78	265.1	66.83	0.25	0.352	0.013	0.04387	0.00059	0.11835	0.058	0.0021	305.6	9.7	276.7	3.6	470	78	58.87	90.54
RDT16012_79	476.2	448	0.94	2.881	0.077	0.2289	0.0037	0.89321	0.08989	0.0015	1372	21	1327	20	1418	33	93.58	96.72
RDT16012_80	1026	762	0.74	1.229	0.034	0.1217	0.0025	0.87672	0.07262	0.0013	810	15	739	15	995	35	74.27	91.23
RDT16012_81	101.9	137.7	1.35	0.786	0.03	0.0895	0.0014	0.15051	0.0629	0.0023	583	17	552.3	8.5	653	79	84.58	94.73
RDT16012_82	1073	188.7	0.18	0.787	0.018	0.0838	0.0013	0.68561	0.0676	0.0012	588.1	10	518.7	7.9	845	38	61.38	88.20
RDT16012_83	158.5	151	0.95	1.47	0.041	0.1461	0.002	0.43437	0.0727	0.0017	916	16	879	11	982	50	89.51	95.96
RDT16012_84	1175	1372	1.17	0.516	0.015	0.05845	0.001	0.71885	0.06356	0.0013	422.1	9.5	366	6.2	715	41	51.19	86.71
RDT16012_85	270.7	169.2	0.63	0.731	0.021	0.08379	0.001	0.15721	0.0627	0.0017	554.6	12	518.6	6.1	660	60	78.58	93.51
RDT16012_86	716	118.4	0.17	1.132	0.079	0.1004	0.0031	0.94694	0.077	0.0031	737	35	616	18	1024	79	60.16	83.58
RDT16012_87	266	208	0.78	1.974	0.044	0.1866	0.0023	0.48239	0.0763	0.0015	1105.5	15	1102	12	1093	39	100.82	99.68
RDT16012_88	150.2	74.84	0.50	0.631	0.024	0.08	0.0011	0.15808	0.0575	0.0022	494	15	495.7	6.7	435	80	113.95	100.34
RDT16012_89	619.9	12.2	0.02	2.718	0.055	0.2289	0.0025	0.61074	0.0855	0.0014	1333.6	15	1328	13	1323	33	100.38	99.58
RDT16012_90	338.5	497.7	1.47	1.552	0.037	0.1561	0.0021	0.66088	0.07194	0.0014	948	15	934	12	981	36	95.21	98.52
RDT16012_91	519	306	0.59	3.074	0.074	0.2213	0.0034	0.84345	0.10007	0.0017	1422	19	1287	18	1619	32	79.49	90.51
RDT16012_92	732	108.1	0.15	0.3838	0.0094	0.04881	0.0005	0.32021	0.05674	0.0012	329.2	6.9	307.2	3.1	459	48	66.93	93.32
RDT16012_93	301	244	0.81	0.529	0.016	0.0663	0.00089	0.20173	0.058	0.0017	429	11	413.7	5.4	490	62	84.43	96.43
RDT16012_94	53.06	57.3	1.08	2.141	0.069	0.1889	0.0028	0.17017	0.0823	0.0026	1155	23	1115	15	1216	64	91.69	96.54
RDT16012_95	462.4	403.9	0.87	2.255	0.052	0.1896	0.0022	0.51345	0.0858	0.0016	1197	16	1119	12	1328	37	84.26	93.48
RDT16012_96	207	222.2	1.07	1.57	0.072	0.1066	0.0032	-0.41424	0.1127	0.0081	945	27	651	18	1680	110	38.75	68.89
RDT16001-12.d	211.9	82.2	0.39	1.5	0.04	0.147	0.0022	0.31728	0.0739	0.002	926	16	884	12	1005	54	87.96	95.46
RDT16001-13.d	175.6	62	0.35	1.871	0.051	0.1737	0.0026	0.27768	0.0784	0.0023	1065	18	1032	15	1104	58	93.48	96.90
RDT16001-14.d	61.6	61.8	1.00	8.6	0.22	0.3967	0.0072	0.50824	0.1559	0.0034	2283	23	2150	33	2396	39	89.73	94.17
RDT16001-15.d	704.3	36.67	0.05	1.096	0.017	0.12	0.0017	0.24249	0.0662	0.0013	749.7	8.4	730.4	9.8	794	40	91.99	97.43
RDT16001-16.d	811	130.4	0.16	4.305	0.068	0.2828	0.0047	0.82024	0.11	0.0014	1692	13	1604	24	1794	23	89.41	94.80
RDT16001-17.d	170.8	52.3	0.31	6.39	0.12	0.3627	0.0055	0.44488	0.1274	0.0024	2026	17	1993	26	***2049***	***34***	97.27	98.37
RDT16001-18.d	54.8	34.21	0.62	12.38	0.36	0.428	0.011	0.44783	0.2137	0.0062	2628	26	2293	50	2919	50	78.55	87.25

Supplementary Table 1. Main isotopes and ratios measured using LA–ICP–MS. Concordance 1 ($^{206}Pb/^{238}U$/ $^{207}Pb/^{206}Pb$) and 2 ($^{206}Pb/^{238}U/^{207}Pb/^{235}U$)

Analysis Spot	U	Th	Th:U	Ratios							Ages						Concordance Calculations	
				$^{207}Pb/^{235}U$	2σ	$^{206}Pb/^{238}U$	2σ	Rho	$^{207}Pb/^{206}Pb$	2σ	$^{207}Pb/^{235}U$	2σ	$^{206}Pb/^{238}U$	2σ	$^{207}Pb/^{206}Pb$	2σ	1	2
RDT16001-19.d	185.6	224.6	1.21	3.765	0.07	0.2754	0.0042	0.53376	0.099	0.0018	1580	15	1567	21	1589	34	98.62	99.18
RDT16001-20.d	491	77.9	0.16	1.756	0.033	0.1675	0.0027	0.46682	0.0758	0.0014	1027	13	***998***	***15***	1081	37	92.32	97.18
RDT16001-21.d	1152	157.7	0.14	0.987	0.018	0.0959	0.0016	0.49954	0.0737	0.0013	695.5	8.9	590.2	9.2	1023	35	57.69	84.86
RDT16001-22.d	468	110.2	0.24	1.283	0.035	0.1258	0.0021	0.070137	0.0737	0.002	834	15	764	12	999	50	76.48	91.61
RDT16001-23.d	113.2	56.6	0.50	9.65	0.17	0.4191	0.0069	0.49353	0.1659	0.003	2398	17	2254	32	2505	31	89.98	93.99
RDT16001-24.d	181.4	162.5	0.90	1.249	0.038	0.1148	0.0019	-0.0078852	0.0785	0.0026	818	17	700	11	1110	72	63.06	85.57
RDT16001-25.d	193	127.6	0.66	3.35	0.1	0.2474	0.006	0.7049	0.0976	0.0022	1487	25	1422	31	1564	44	90.92	95.63
RDT16001-26.d	766	75.4	0.10	1.047	0.081	0.1065	0.0052	0.96659	0.0668	0.0019	694	36	649	30	779	60	83.31	93.52
RDT16001-35.d	394.9	115.5	0.29	1.355	0.027	0.1307	0.002	0.28242	0.0751	0.0017	868	12	791.3	11	1044	46	75.80	91.16
RDT16001-36.d	593	209.4	0.35	1.6	0.046	0.1366	0.0027	0.7357	0.0846	0.0019	962	18	825	15	1283	42	64.30	85.76
RDT16001-37.d	362	79.6	0.22	1.697	0.047	0.1697	0.0035	0.63755	0.0724	0.0016	1000	18	1009	19	973	44	103.70	100.90
RDT16001-38.d	383	115.2	0.30	1.442	0.047	0.1429	0.0034	0.75865	0.072	0.0015	897	20	860	19	973	44	88.39	95.88
RDT16001-39.d	845	195.7	0.23	3.898	0.078	0.2542	0.0048	0.78648	0.1096	0.0016	1609	16	1459	25	1785	27	81.74	90.68
RDT16001-40.d	301.5	126	0.42	6.8	0.12	0.3119	0.0055	0.75313	0.1586	0.0023	2080	16	1748	27	2435	24	71.79	84.04
RDT16001-41.d	604.4	257.2	0.43	1.545	0.031	0.1566	0.0025	0.61415	0.0705	0.0012	946	12	938	14	933	37	100.54	99.15
RDT16001-42.d	311.2	109	0.35	1.285	0.034	0.1032	0.0029	0.50666	0.091	0.0027	833	15	632	17	1396	56	45.27	75.87
RDT16001-43.d	165	63	0.38	1.555	0.052	0.1576	0.0032	0.34741	0.0721	0.0023	944	21	***942***	***18***	934	69	100.86	99.79
RDT16001-44.d	217	238	1.10	1.133	0.036	0.1269	0.0021	0.25345	0.0647	0.0021	764	17	***770***	***12***	711	69	108.30	100.79
RDT16001-45.d	1481	604	0.41	3.57	0.14	0.1948	0.0063	0.9611	0.1303	0.002	1519	34	1144	34	2093	27	54.66	75.31
RDT16001-46.d	625	373	0.60	0.729	0.017	0.0839	0.0014	0.2972	0.0635	0.0016	554.2	10	***519.4***	***8.4***	697	54	74.52	93.72
RDT16001-47.d	400.1	228.3	0.57	1.521	0.029	0.1531	0.0024	0.3988	0.0722	0.0015	936	12	***918***	***13***	966	42	95.03	98.08
RDT16001-48.d	790	88.5	0.11	2.27	0.094	0.1835	0.0049	0.92357	0.0873	0.0018	1181	30	1083	27	1344	41	80.58	91.70
RDT16001-57.d	798	173.7	0.22	1.602	0.044	0.1387	0.0027	0.78466	0.0829	0.0014	964	17	836	15	1251	34	66.83	86.72
RDT16001-58.d	448	221.7	0.49	0.72	0.019	0.0848	0.0018	0.42022	0.0614	0.0016	550	11	***524.1***	***10***	617	57	84.94	95.29
RDT16001-59.d	1255	172	0.14	3.019	0.077	0.1561	0.0041	0.93945	0.1394	0.0017	1410	20	934	23	2217	22	42.13	66.24
RDT16001-60.d	713	493	0.69	0.647	0.015	0.0807	0.0012	0.31974	0.0581	0.0013	504.6	9.1	***500.2***	***7.1***	499	51	100.24	99.13
RDT16001-61.d	160.2	30.6	0.19	2.005	0.071	0.1595	0.0042	0.594	0.0907	0.0027	1105	24	952	23	1409	57	67.57	86.15
RDT16001-62.d	340.4	135.8	0.40	2.125	0.044	0.1884	0.0025	0.31469	0.0808	0.0017	1157	13	***1112***	***14***	1201	42	92.59	96.11
RDT16001-63.d	473	5.77	0.01	1.73	0.11	0.1574	0.0063	0.9455	0.0762	0.0021	990	39	938	35	1069	56	87.75	94.75
RDT16001-64.d	269.9	206.5	0.77	1.924	0.039	0.1767	0.0025	0.34112	0.0788	0.0016	1085	14	1048	13	1145	42	91.53	96.59
RDT16001-65.d	381.3	30.39	0.08	1.487	0.03	0.1527	0.0023	0.44024	0.0706	0.0014	924	12	***915***	***13***	930	40	98.39	99.03
RDT16001-66.d	323.2	288.4	0.89	1.005	0.025	0.1053	0.0018	0.30374	0.0696	0.0018	703	13	645.2	11	889	55	72.58	91.78
RDT16001-67.d	548.9	93.6	0.17	9.86	0.16	0.3355	0.0056	0.6384	0.2124	0.0031	2418	15	1863	27	2919	24	63.82	77.05
RDT16001-68.d	527	117.8	0.22	1.153	0.023	0.1145	0.0017	0.29278	0.0729	0.0015	777	11	698.4	10	989	42	70.62	89.88
RDT16001-69.d	58.4	82.2	1.41	15.22	0.29	0.5167	0.0085	0.4807	0.2132	0.0039	2821	18	2681	36	2917	29	91.91	95.04
RDT16001-70.d	316	105.7	0.33	1.993	0.049	0.1834	0.0035	0.59278	0.0774	0.0016	1108	17	***1087***	***19***	1113	44	97.66	98.10
RDT16001-71.d	1157	146.7	0.13	2.142	0.032	0.1956	0.0028	0.72071	0.07915	0.00097	1160.2	10	***1151***	***15***	1172	25	98.21	99.21
RDT16001-72.d	44.81	47.32	1.06	8.11	0.31	0.3389	0.009	0.547	0.176	0.0059	2230	35	1874	43	***2581***	***58***	72.61	84.04
RDT16001-81.d	370	95.3	0.26	4.024	0.084	0.2156	0.0041	0.71873	0.1342	0.0023	1635	17	1257	22	2147	30	58.55	76.88
RDT16001-82.d	626	356	0.57	1.476	0.027	0.1492	0.0023	0.50644	0.0716	0.0013	919	11	***896***	***13***	961	36	93.24	97.50
RDT16001-83.d	895	456	0.51	3.958	0.055	0.2824	0.0041	0.71354	0.10132	0.0013	1624	11	1602	21	***1642***	***23***	97.56	98.65
RDT16001-84.d	154.2	105.8	0.69	4.008	0.085	0.2911	0.0051	0.49846	0.0992	0.002	1633	17	1645	25	***1603***	***37***	102.62	100.73
RDT16001-85.d	360.7	161.4	0.45	1.861	0.042	0.1735	0.0027	0.32665	0.0772	0.0018	1062	15	1032	15	1109	45	93.06	97.18
RDT16001-86.d	441.3	307	0.70	0.546	0.019	0.0575	0.0011	0.18546	0.0694	0.0026	440	13	360	6.9	850	79	42.35	81.82
RDT16001-87.d	570	372	0.65	1.368	0.083	0.0843	0.0025	0.68244	0.1145	0.0049	852	34	521	15	1789	72	29.12	61.15
RDT16001-88.d	311	409	1.32	0.764	0.023	0.0883	0.0017	0.26276	0.0633	0.0019	574	13	545.1	9.9	671	66	81.24	94.97
RDT16001-89.d	610.4	241.4	0.40	3.731	0.058	0.2632	0.004	0.59084	0.1012	0.0015	1577	12	1505	21	1640	27	91.77	95.43

Supplementary Table 1. Main isotopes and ratios measured using LA–ICP–MS. Concordance 1 ($^{206}Pb/^{238}U/^{207}Pb/^{206}Pb$) and 2 ($^{206}Pb/^{238}U/^{207}Pb/^{235}U$).

Analysis Spot	U	Th	Th:U	Ratios							Ages						Concordance Calculations	
				$^{207}Pb/^{235}U$	2σ	$^{206}Pb/^{238}U$	2σ	Rho	$^{207}Pb/^{206}Pb$	2σ	$^{207}Pb/^{235}U$	2σ	$^{206}Pb/^{238}U$	2σ	$^{207}Pb/^{206}Pb$	2σ	1	2
RDT16001-90.d	791	46.2	0.06	2.146	0.035	0.1978	0.0032	0.56389	0.0793	0.0013	1161	11	1163	17	1168	32	99.57	100.17
RDT16001-92.d	318	258	0.81	1.613	0.036	0.1638	0.0026	0.39255	0.0715	0.0016	972	14	977	14	944	45	103.50	100.51
RDT16001-93.d	556.2	152.7	0.27	0.882	0.02	0.0973	0.0016	0.35033	0.0657	0.0015	640	11	598.3	9.2	776	51	77.10	93.48
RDT16001-102.d	162.3	299.6	1.85	0.902	0.036	0.0874	0.0017	0.075779	0.0756	0.0034	647	20	539.5	10	968	93	55.73	83.38
RDT16001-103.d	328	247	0.75	4.053	0.09	0.2905	0.0059	0.71868	0.1006	0.0016	1638	18	1641	30	***1624***	***30***	101.05	100.18
RDT16001-104.d	464	226.1	0.49	2.526	0.048	0.2148	0.0034	0.63879	0.0848	0.0014	1280	13	***1255***	***18***	1298	32	96.69	98.05
RDT16001-105.d	430	163.9	0.38	1.994	0.072	0.1586	0.0045	0.7946	0.0898	0.002	1101	24	946	25	1404	43	67.38	85.92
RDT16001-106.d	512	300.9	0.59	1.313	0.045	0.1351	0.0042	0.81695	0.0702	0.0014	843	21	814	24	921	42	88.38	96.56
RDT16001-107.d	425.9	295	0.69	1.273	0.034	0.1273	0.0029	0.65317	0.0717	0.0016	831	15	772	16	963	45	80.17	92.90
RDT16001-108.d	54.9	36.7	0.67	1.909	0.097	0.1475	0.0052	0.18388	0.0979	0.0055	1066	34	884	29	1440	120	61.39	82.93
RDT16001-109.d	325	58.2	0.18	1.671	0.041	0.1496	0.0025	0.28183	0.0812	0.0023	994	15	898	14	1194	53	75.21	90.34
RDT16001-110.d	166	104.1	0.63	1.215	0.069	0.0874	0.0043	0.74368	0.1016	0.0038	787	33	538	26	1594	73	33.75	68.36
RDT16001-111.d	194	198.7	1.02	1.922	0.049	0.175	0.0037	0.45037	0.0789	0.002	1084	18	1038	20	1159	52	89.56	95.76
RDT16001-112.d	741	162.2	0.22	0.927	0.035	0.0951	0.0034	0.88511	0.0701	0.0013	657	18	584	20	913	40	63.96	88.89
RDT16001-113.d	270.8	210.1	0.78	1.829	0.047	0.1691	0.0038	0.53914	0.0786	0.0019	1049	17	1006	21	1127	48	89.26	95.90
RDT16001-114.d	272.5	205	0.75	4.888	0.1	0.3059	0.006	0.77548	0.1155	0.0018	1795	17	1717	30	1877	28	91.48	95.65
RDT16001-123.d	629	81.6	0.13	1.726	0.03	0.1507	0.0023	0.50717	0.0829	0.0014	1016	11	904	13	1255	35	72.03	88.98
RDT16001-124.d	1151	59.8	0.05	1.484	0.021	0.1425	0.0023	0.54254	0.0753	0.0012	922.3	8.5	858	13	1066	33	80.49	93.03
RDT16001-125.d	109.2	107.1	0.98	0.978	0.042	0.0909	0.0025	0.16969	0.0794	0.0039	682	22	560	15	1056	99	53.03	82.11
RDT16001-126.d	411	164	0.40	1.909	0.038	0.1753	0.0032	0.5648	0.0785	0.0015	1083	13	1040	18	1150	41	90.43	96.03
RDT16001-127.d	198.3	189.4	0.96	1.689	0.046	0.1636	0.003	0.33852	0.0747	0.0021	998	17	976	17	1021	57	95.59	97.80
RDT16001-128.d	405.9	46.2	0.11	1.527	0.031	0.1568	0.0026	0.47904	0.0705	0.0014	937	13	938	15	924	40	101.52	100.11
RDT16001-129.d	233	29.2	0.13	1.439	0.036	0.1457	0.0024	0.22968	0.0714	0.0019	900	15	876	14	931	56	94.09	97.33
RDT16001-130.d	621	191	0.31	1.819	0.038	0.1677	0.003	0.66004	0.078	0.0014	1049	14	1000	16	1132	35	88.34	95.33
RDT16001-132.d	72.5	45.8	0.63	3.06	0.2	0.1691	0.0041	0.34251	0.1314	0.0083	1378	49	1006	23	1960	120	51.33	73.00
RDT16001-133.d	155.9	105.7	0.68	1.526	0.046	0.1465	0.0029	0.35175	0.0752	0.0022	933	19	880	16	1040	61	84.62	94.32
RDT16001-134.d	168	139.5	0.83	0.753	0.03	0.0846	0.0017	0.22244	0.0655	0.0028	566	18	***523.4***	***9.9***	691	92	75.75	92.47
RDT16001-135.d	265	178	0.67	3.36	0.11	0.2275	0.007	0.87527	0.1063	0.002	1475	29	1316	37	1720	35	76.51	89.22
RDT16001-136.d	978	261	0.27	1.388	0.038	0.1372	0.0032	0.89356	0.07308	0.001	877	17	828	18	1011	28	81.90	94.41
RDT16001-137.d	183.7	58.8	0.32	4.24	0.12	0.2778	0.007	0.64318	0.1099	0.0024	1677	22	1577	35	1781	39	88.55	94.04
RDT16001-138.d	897	406	0.45	1.632	0.032	0.1544	0.0031	0.76112	0.07616	0.0012	979	12	925	17	1094	31	84.55	94.48
RDT16001-139.d	2150	792	0.37	1.345	0.095	0.1123	0.0074	0.9857	0.0844	0.0013	819	42	679	42	1289	31	52.68	82.91
RDT16001-140.d	1684	606	0.36	5.2	0.15	0.2195	0.0066	0.96148	0.1711	0.002	1837	25	1275	35	2564	19	49.73	69.41
RDT16001-149.d	649.6	260.3	0.40	1.282	0.025	0.1292	0.0022	0.55889	0.072	0.0014	836	12	783	12	968	38	80.89	93.66
RDT16001-150.d	156	43.8	0.28	1.295	0.054	0.1179	0.0038	0.51828	0.0805	0.0029	834	24	717	22	1161	72	61.76	85.97
RDT16001-151.d	548.9	382.2	0.70	0.893	0.031	0.087	0.0015	0.071438	0.0745	0.0029	642	16	537.4	8.8	989	77	54.34	83.71
RDT16001-152.d	687	190.5	0.28	4.225	0.062	0.2476	0.0039	0.63005	0.123	0.0017	1676	12	1425	20	1993	25	71.50	85.02
RDT16001-153.d	82	48.4	0.59	6.23	0.35	0.278	0.014	0.90276	0.1594	0.0041	1951	56	1564	74	2434	44	64.26	80.16
RDT16001-154.d	459	39.57	0.09	1.507	0.033	0.1471	0.0023	0.14276	0.0742	0.0018	927	13	884	13	1013	45	87.27	95.36
RDT16001-155.d	1817	753	0.41	1.373	0.047	0.1037	0.0029	0.9281	0.0951	0.0016	869	20	635	17	1521	32	41.75	73.07
RDT16001-156.d	164.3	123.5	0.75	1.598	0.044	0.1587	0.0031	0.43654	0.0729	0.0019	966	17	***948***	***17***	974	53	97.33	98.14
RDT16001-157.d	138.5	95.7	0.69	9.87	0.24	0.4237	0.0099	0.8287	0.1677	0.0026	2419	22	2271	45	2526	27	89.90	93.88
RDT16001-158.d	442.1	111.6	0.25	4.528	0.093	0.2873	0.006	0.75566	0.1133	0.0018	1734	17	1625	30	1842	29	88.22	93.71
RDT16001-159.d	751	75.9	0.10	1.7	0.043	0.1711	0.0035	0.75286	0.0719	0.0013	1004	16	***1017***	***19***	971	36	104.74	101.29
RDT16001-160.d	405	377	0.93	1.973	0.08	0.1821	0.0051	0.88158	0.0771	0.0017	1087	27	***1075***	***28***	1106	42	97.20	98.90
RDT16001-161.d	487	51.3	0.11	5.366	0.083	0.3357	0.0055	0.64838	0.1149	0.0017	1878	13	1867	27	***1870***	***27***	99.84	99.41
RDT16001-162.d	356.8	354.6	0.99	0.601	0.021	0.0758	0.0013	0.39969	0.0575	0.0018	475	13	***471.1***	***7.8***	457	70	103.09	99.18

Supplementary Table 1. Main isotopes and ratios measured using LA–ICP–MS. Concordance 1 ($^{206}Pb/^{238}U$/ $^{207}Pb/^{206}Pb$) and 2 ($^{206}Pb/^{238}U/^{207}Pb/^{235}U$)

Analysis Spot	U	Th	Th:U	Ratios							Ages						Concordance Calculations	
				$^{207}Pb/^{235}U$	2σ	$^{206}Pb/^{238}U$	2σ	Rho	$^{207}Pb/^{206}Pb$	2σ	$^{207}Pb/^{235}U$	2σ	$^{206}Pb/^{238}U$	2σ	$^{207}Pb/^{206}Pb$	2σ	1	2
RDT16001-163.d	193.7	124.5	0.64	2.865	0.066	0.2287	0.0042	0.46344	0.0901	0.002	1366	17	1326	22	1408	43	94.18	97.07
RDT16001-173.d	258	185.5	0.72	4.721	0.072	0.3188	0.0051	0.52513	0.1066	0.0017	1768	13	1782	25	***1732***	***30***	102.89	100.79
RDT16001-174.d	757	219.7	0.29	2.553	0.046	0.1699	0.0033	0.75549	0.1084	0.0017	1285	13	1010	18	1766	28	57.19	78.60
RDT16001-175.d	186	46.3	0.25	1.308	0.052	0.1292	0.0035	0.628	0.0734	0.0023	839	23	782	20	966	65	80.95	93.21
RDT16001-176.d	244	95.7	0.39	1.843	0.069	0.1586	0.0053	0.79363	0.0837	0.002	1046	26	946	30	1258	48	75.20	90.44
RDT16001-177.d	124.5	54.3	0.44	9.72	0.19	0.4322	0.0074	0.48034	0.1623	0.0031	2402	18	2312	33	2465	33	93.79	96.25
RDT16001-178.d	388	64.1	0.17	1.317	0.045	0.1373	0.0038	0.75035	0.0692	0.0016	848	20	***827***	***21***	870	48	95.06	97.52
RDT16001-179.d	595	81.8	0.14	2.272	0.037	0.1868	0.0028	0.53143	0.0874	0.0014	1201	12	1103	15	1361	31	81.04	91.84
RDT16001-180.d	359	37.3	0.10	2.414	0.045	0.2113	0.0033	0.55474	0.0826	0.0014	1244	13	***1235***	***18***	1244	34	99.28	99.28
RDT16001-181.d	666	237.3	0.36	1.586	0.031	0.1507	0.0027	0.62951	0.0764	0.0014	963	12	904	15	1087	36	83.16	93.87
RDT16001-182.d	776	115.8	0.15	1.021	0.021	0.1016	0.0016	0.52835	0.0723	0.0014	711.8	10	623.3	9.3	985	40	63.28	87.57
RDT16001-183.d	110.5	59.3	0.54	6.55	0.27	0.1389	0.0045	0.55885	0.344	0.013	2030	41	836	26	3643	57	22.95	41.18
RDT16001-184.d	1080	24.1	0.02	1.517	0.062	0.1573	0.0062	0.87037	0.0706	0.0012	926	26	***937***	***34***	938	38	99.89	101.19
RDT16001-193.d	261.2	131	0.50	4.982	0.096	0.2624	0.0043	0.60771	0.1362	0.0023	1811	16	1501	22	2175	29	69.01	82.88
RDT16001-194.d	828	53.2	0.06	1.274	0.077	0.0838	0.0039	0.95157	0.1056	0.0025	802	35	517	23	1712	43	30.20	64.46
RDT16001-195.d	1358	420.2	0.31	1.516	0.021	0.1544	0.002	0.64583	0.07099	0.00094	935.5	8.4	***925.4***	***11***	951	27	97.31	98.92
RDT16001-196.d	642	375	0.58	2.392	0.057	0.2147	0.0042	0.70763	0.0799	0.0014	1236	17	1255	22	1188	35	105.64	101.54
RDT16001-197.d	46.8	42.4	0.91	2.084	0.097	0.1737	0.0042	0.19728	0.0865	0.0041	1120	32	1031	23	1230	100	83.82	92.05
RDT16001-198.d	1006	75.6	0.08	1.572	0.052	0.144	0.0029	0.81932	0.0777	0.0016	950	20	867	16	1121	40	77.34	91.26
RDT16001-199.d	212.8	182.7	0.86	2.031	0.048	0.1758	0.003	0.43209	0.0835	0.002	1120	16	1043	16	1249	46	83.51	93.13
RDT16001-200.d	1811	140.5	0.08	1.148	0.016	0.1169	0.0017	0.59723	0.07085	0.001	775.1	7.6	712.6	10	943	29	75.57	91.94
RDT16001-201.d	1817	408	0.22	1.096	0.027	0.1096	0.0024	0.82481	0.0726	0.0011	748	13	670	14	994	31	67.40	89.57
RDT16001-202.d	327.2	189.9	0.58	3.694	0.058	0.2588	0.0038	0.51813	0.1028	0.0016	1567	13	1484	20	1666	29	89.08	94.70
RDT16001-203.d	461.1	93.48	0.20	1.589	0.029	0.1523	0.002	0.12408	0.0761	0.0017	964	11	913.7	11	1068	42	85.55	94.78
RDT16001-204.d	705	67.1	0.10	1.24	0.04	0.1109	0.0031	0.78097	0.0798	0.0017	811	18	677	18	1173	41	57.72	83.48
RDT16001-213.d	236	123.1	0.52	2.052	0.045	0.1921	0.0032	0.31309	0.0771	0.0017	1128	15	***1132***	***17***	1096	47	103.28	100.35
RDT16001-214.d	209.2	234	1.12	1.549	0.041	0.1565	0.0026	0.45273	0.0714	0.0017	945	16	***937***	***15***	949	50	98.74	99.15
RDT16001-215.d	180.3	91.9	0.51	7.41	0.34	0.319	0.014	0.96271	0.1669	0.0025	2111	46	1765	68	2517	25	70.12	83.61
RDT16001-216.d	596	143.6	0.24	1.634	0.03	0.1634	0.0023	0.44931	0.0722	0.0013	980	11	***975***	***12***	975	36	100.00	99.49
RDT16001-217.d	590	53.9	0.09	1.209	0.029	0.1248	0.0025	0.6316	0.0701	0.0014	800	14	758	14	911	41	83.21	94.75
RDT16001-218.d	345	407	1.18	0.712	0.021	0.0888	0.0014	0.22087	0.058	0.0018	543	12	548	8.5	488	66	112.30	100.92
RDT16001-219.d	382	108.9	0.29	2.239	0.088	0.1651	0.0052	0.88191	0.0965	0.0017	1173	29	982	29	1544	35	63.60	83.72
RDT16001-220.d	209.5	51.6	0.25	0.697	0.038	0.0592	0.002	0.25287	0.0881	0.0055	527	22	370	12	1220	110	30.33	70.21
RDT16001-221.d	124.4	104.1	0.84	1.303	0.054	0.1217	0.0031	0.35261	0.0765	0.0029	833	23	739	18	1036	82	71.33	88.72
RDT16001-222.d	365	305	0.84	0.75	0.025	0.0891	0.0016	0.33681	0.0611	0.0019	567	15	***549.7***	***9.4***	590	70	93.17	96.95
RDT16001-223.d	365	262	0.72	6.788	0.091	0.3656	0.0054	0.62709	0.1336	0.0018	2081	12	2009	25	2143	24	93.75	96.54
RDT16001-224.d	257.9	135	0.52	4.065	0.07	0.2929	0.0043	0.58564	0.1003	0.0016	1643	14	1655	21	***1617***	***29***	102.35	100.73
RDT16001-233.d	672	133.1	0.20	0.703	0.021	0.0712	0.0014	0.4223	0.0709	0.0019	537	13	443.4	8.6	909	53	48.78	82.57
RDT16001-234.d	903	384	0.43	1.54	0.038	0.1502	0.0034	0.81543	0.07399	0.0012	941	15	901	19	1034	32	87.14	95.75
RDT16001-235.d	561	389	0.69	1.739	0.036	0.1725	0.0028	0.59539	0.0728	0.0012	1020	13	***1025***	***15***	998	35	102.71	100.49
RDT16001-236.d	392.2	115.9	0.30	7.89	0.16	0.3595	0.007	0.87287	0.1582	0.002	2209	20	1976	34	2431	21	81.28	89.45
RDT16001-237.d	643	82.8	0.13	8.804	0.11	0.4001	0.0058	0.73038	0.1589	0.0018	2315	12	2167	27	2441	20	88.78	93.61
RDT16001-238.d	284.8	248	0.87	2.54	0.11	0.1623	0.0028	-0.10302	0.1151	0.0059	1270	29	969	16	1792	81	54.07	76.30
RDT16001-239.d	1259	64.8	0.05	1.497	0.025	0.1509	0.0025	0.71494	0.07134	0.001	927.1	10	***906***	***14***	961	28	94.28	97.72
RDT16001-240.d	608.9	136.8	0.22	1.969	0.035	0.1809	0.0029	0.62415	0.0786	0.0013	1103	12	***1071***	***16***	1156	35	92.65	97.10
RDT16001-241.d	221.8	75.6	0.34	3.57	0.11	0.2602	0.0061	0.73034	0.0979	0.0021	1532	24	1488	31	***1571***	***40***	94.72	97.13
RDT16001-242.d	315	54.9	0.17	3.754	0.062	0.2747	0.0045	0.60666	0.0992	0.0017	1581	14	1563	23	***1598***	***31***	97.81	98.86

Supplementary Table 1 (continued). Main isotopes and ratios measured using LA–ICP–MS. Concordance calculation 1 ($^{206}Pb/^{238}U/^{207}Pb/^{206}Pb$) and calculation 2 ($^{206}Pb/^{238}U/^{207}Pb/^{235}U$). Age data used for Hf analyses is highlighted in bold.

Analysis Spot	U	Th	Th:U	Ratios							Ages						Concordance Calculations	
				$^{207}Pb/^{235}U$	2σ	$^{206}Pb/^{238}U$	2σ	Rho	$^{207}Pb/^{206}Pb$	2σ	$^{207}Pb/^{235}U$	2σ	$^{206}Pb/^{238}U$	2σ	$^{207}Pb/^{206}Pb$	2σ	1	2
RDT16001-243.d	381.9	627	1.64	0.745	0.02	0.0889	0.0015	0.23025	0.061	0.0018	562	12	***548.5***	***9***	594	64	92.34	97.60
RDT16001-244.d	569	95.7	0.17	2.73	0.05	0.189	0.0037	0.71879	0.1047	0.0017	1332	14	1114	20	1700	30	65.53	83.63
RDT16001-245.d	1329	237.1	0.18	1.263	0.027	0.1147	0.0022	0.7834	0.0797	0.0013	829	13	699	12	1180	31	59.24	84.32
RDT16001-246.d	693	98.5	0.14	3.537	0.062	0.2631	0.0044	0.78707	0.09679	0.0013	1531	14	1506	22	***1560***	***24***	96.54	98.37
RDT16001-247.d	241.3	113.2	0.47	1.287	0.048	0.1151	0.0027	0.60706	0.0805	0.0025	828	21	701	15	1169	62	59.97	84.66
RDT16001-256.d	382	251	0.66	0.855	0.035	0.102	0.0024	0.47281	0.0613	0.0022	622	20	***625***	***14***	604	73	103.48	100.48
RDT16001-257.d	228.5	227	0.99	10.1	0.15	0.4555	0.0067	0.67489	0.1602	0.0022	2439	14	2417	30	***2450***	***23***	98.65	99.10
RDT16001-258.d	697	257	0.37	1.431	0.029	0.1402	0.0022	0.49672	0.0737	0.0014	899	12	845	13	1018	39	83.01	93.99
RDT16001-259.d	503	108.7	0.22	2.336	0.058	0.2093	0.0037	0.73937	0.0801	0.0014	1216	17	***1224***	***20***	1184	34	103.38	100.66
RDT16001-260.d	683	54.51	0.08	2.154	0.035	0.194	0.0028	0.56242	0.0803	0.0013	1165	11	1144	15	1194	32	95.81	98.20
RDT16001-261.d	947	58.7	0.06	1.431	0.023	0.1417	0.0022	0.55451	0.073	0.0012	900.8	9.5	854	12	1001	33	85.31	94.80
RDT16001-262.d	141.1	56.6	0.40	1.873	0.05	0.1783	0.0031	0.36101	0.0758	0.0021	1064	18	***1057***	***17***	1048	56	100.86	99.34
RDT16001-263.d	220.4	189.9	0.86	3.188	0.073	0.2395	0.0043	0.62894	0.096	0.0018	1448	18	1383	22	1532	35	90.27	95.51

Supplementary Table 1. Main isotopes and ratios measured using the Multicollector (Hf analyses).Yellow analyses drilled through small zircons.

Analysis Spot #	Age Used for Hf	Type of age	$^{176}Hf/^{177}Hf$	2σ	$^{176}Lu/^{177}Hf$	$^{176}Yb/^{177}Hf$	$(^{176}Hf/^{177}Hf)_i$	$\varepsilon Hf_{(t)}$	2s	T_{DM}(Hf) (Ga)	T_{NC}(Hf) (Ga)
RDT16019-424.d	1019	$^{206}Pb/^{238}U$ zircon age	0.282053	0.000028	0.001177	0.02568	0.282030	-3.90	0.98	2.08	1.91
RDT16019-425.d	887	$^{206}Pb/^{238}U$ zircon age	0.282179	0.000034	0.00482	0.1084	0.282099	-4.46	1.19	2.01	1.84
RDT16019-426.d	1047	$^{206}Pb/^{238}U$ zircon age	0.282121	0.000036	0.001733	0.03279	0.282087	-1.26	1.26	1.94	1.77
RDT16019-428.d	2499	$^{207}Pb/^{206}Pb$ zircon age	0.281738	0.000034	0.000811	0.01457	0.281699	18.40	1.19	1.90	1.76
RDT16019-432.d	742	$^{206}Pb/^{238}U$ zircon age	0.282556	0.000034	0.00434	0.0933	0.282496	6.33	1.19	1.23	1.05
RDT16019-434.d	1006	$^{206}Pb/^{238}U$ zircon age	0.282134	0.000035	0.00744	0.204	0.281993	-5.51	1.225	2.17	1.99
RDT16019-436.d	738	$^{206}Pb/^{238}U$ zircon age	0.282267	0.000031	0.000951	0.02249	0.282254	-2.32	1.085	1.77	1.58
RDT16019-446.d	2436	$^{207}Pb/^{206}Pb$ zircon age	0.281021	0.000035	0.002026	0.04261	0.280927	-10.54	1.225	3.57	3.44
RDT16019-448.d	1598	$^{207}Pb/^{206}Pb$ zircon age	0.281831	0.000037	0.00186	0.0412	0.281775	0.22	1.295	2.28	2.12
RDT16019-449.d	1607	$^{207}Pb/^{206}Pb$ zircon age	0.281636	0.000035	0.00206	0.0598	0.281573	-6.72	1.225	2.71	2.55
RDT16019-450.d	621	$^{206}Pb/^{238}U$ zircon age	0.282419	0.000028	0.00128	0.037	0.282404	0.37	0.98	1.51	1.32
RDT16019-452.d	899	$^{206}Pb/^{238}U$ zircon age	0.282087	0.000031	0.00285	0.087	0.282039	-6.31	1.085	2.14	1.96
RDT16019-453.d	721	$^{206}Pb/^{238}U$ zircon age	0.282567	0.000028	0.001981	0.06848	0.282540	7.44	0.98	1.15	0.96
RDT16019-457.d	938	$^{206}Pb/^{238}U$ zircon age	0.281998	0.000037	0.00163	0.0584	0.281969	-7.90	1.295	2.26	2.09
RDT16019-466.d	1777	$^{206}Pb/^{238}U$ zircon age	0.281751	0.000034	0.001085	0.0346	0.281714	2.19	1.19	2.30	2.14
RDT16019-467.d	979	$^{206}Pb/^{238}U$ zircon age	0.282125	0.000045	0.001646	0.06086	0.282095	-2.52	1.575	1.97	1.79
RDT16019-469.d	2539	$^{207}Pb/^{206}Pb$ zircon age	0.281029	0.000056	0.00083	0.0292	0.280989	-5.94	1.96	3.38	3.25

Supplementary Table 1. Main isotopes and ratios measured using the Multicollector (Hf analyses). Yellow analyses drilled through small zircons.

RDT16019-473.d	2709	$^{207}Pb/^{206}Pb$ zircon age	0.280983	0.00003	0.000717	0.02574	0.280946	-3.49	1.05	3.37	3.24
RDT16019-474.d	1863	$^{207}Pb/^{206}Pb$ zircon age	0.281416	0.000035	0.0004035	0.01524	0.281402	-6.94	1.225	2.92	2.76
RDT16019-475.d	848	$^{206}Pb/^{238}U$ zircon age	0.282075	0.000031	0.001248	0.0413	0.282055	-6.88	1.085	2.13	1.95
RDT16019-478.d	1056	$^{206}Pb/^{238}U$ zircon age	0.282219	0.000032	0.000948	0.03568	0.282200	2.96	1.12	1.69	1.51
RDT16019-491.d	737	$^{206}Pb/^{238}U$ zircon age	0.282418	0.000034	0.000681	0.0244	0.282409	3.14	1.19	1.43	1.24
RDT16019-533.d	3423	$^{207}Pb/^{206}Pb$ zircon age	0.280428	0.000031	0.002539	0.1156	0.280261	-11.03	1.085	4.36	4.26
RDT16019-535.d	2531	$^{207}Pb/^{206}Pb$ zircon age	0.28123	0.000034	0.000459	0.0174	0.281208	1.67	1.19	2.92	2.79
RDT16019-537.d	756	$^{206}Pb/^{238}U$ zircon age	0.282586	0.000036	0.000817	0.0325	0.282574	9.44	1.26	1.05	0.86
RDT16019-539.d	1606	$^{207}Pb/^{206}Pb$ zircon age	0.281955	0.000035	0.00161	0.059	0.281906	5.06	1.225	1.99	1.83
RDT16019-543.d	1919	$^{207}Pb/^{206}Pb$ zircon age	0.281524	0.000029	0.000715	0.0229	0.281498	-2.23	1.015	2.68	2.53
RDT16019-544.d	1220	$^{206}Pb/^{238}U$ zircon age	0.281959	0.000034	0.001148	0.0325	0.281933	-2.81	1.19	2.17	2.00
RDT16019-547.d	904	$^{206}Pb/^{238}U$ zircon age	0.281954	0.000028	0.000258	0.00818	0.281950	-9.36	0.98	2.33	2.15
RDT16019-556.d	2497	$^{207}Pb/^{206}Pb$ zircon age	0.281069	0.000033	0.001552	0.03083	0.280995	-6.70	1.155	3.39	3.26
RDT16019-557.d	1552	$^{207}Pb/^{206}Pb$ zircon age	0.281652	0.000044	0.001492	0.03597	0.281608	-6.74	1.54	2.66	2.50
RDT16019-560.d	972	$^{206}Pb/^{238}U$ zircon age	0.282073	0.00003	0.00321	0.068	0.282014	-5.53	1.05	2.15	1.97
RDT16019-62.d	754.7	$^{206}Pb/^{238}U$ zircon age	0.282279	0.000031	0.001019	0.0318	0.282265	-1.56	1.085	1.73	1.55
RDT16019-63.d	3271	$^{207}Pb/^{206}Pb$ zircon age	0.280425	0.00003	0.00099	0.0276	0.280363	-11.00	1.05	4.24	4.13
RDT16019-66.d	1026	$^{207}Pb/^{206}Pb$ zircon age	0.281422	0.00003	0.001426	0.0458	0.281394	-26.28	1.05	3.44	3.27
RDT16019-75.d	2789	$^{207}Pb/^{206}Pb$ zircon age	0.281098	0.000036	0.001537	0.0394	0.281016	0.89	1.26	3.17	3.05
RDT16019-82.d	914	$^{206}Pb/^{238}U$ zircon age	0.281922	0.000028	0.00014	0.00442	0.281920	-10.20	0.98	2.39	2.21
RDT16019-84.d	934.3	$^{206}Pb/^{238}U$ zircon age	0.282065	0.000026	0.001212	0.0371	0.282044	-5.34	0.91	2.10	1.93
RDT16019-85.d	1627	$^{207}Pb/^{206}Pb$ zircon age	0.281946	0.000029	0.001658	0.0506	0.281895	5.15	1.015	2.00	1.84
RDT16019-86.d	3126	$^{207}Pb/^{206}Pb$ zircon age	0.280833	0.00003	0.000792	0.0222	0.280785	0.63	1.05	3.46	3.34
RDT16019-98.d	1052	$^{206}Pb/^{238}U$ zircon age	0.282061	0.000032	0.001449	0.04345	0.282032	-3.08	1.12	2.06	1.88
RDT16019-99.d	2477	$^{207}Pb/^{206}Pb$ zircon age	0.281134	0.00004	0.001028	0.03381	0.281085	-3.95	1.4	3.21	3.08
RDT16019-104.d	843	$^{206}Pb/^{238}U$ zircon age	0.282085	0.000034	0.000977	0.03197	0.282070	-6.49	1.19	2.11	1.93
RDT16019-105.d	2526	$^{207}Pb/^{206}Pb$ zircon age	0.281061	0.000035	0.001103	0.0374	0.281008	-5.56	1.225	3.35	3.22
RDT16019-121.d	3133	$^{207}Pb/^{206}Pb$ zircon age	0.280983	0.000037	0.001349	0.04324	0.280902	4.94	1.295	3.21	3.09
RDT16019-122.d	1343	$^{207}Pb/^{206}Pb$ zircon age	0.282057	0.000034	0.00101	0.03653	0.282031	3.50	1.19	1.88	1.71
RDT16019-124.d	1190	$^{206}Pb/^{238}U$ zircon age	0.281207	0.000028	0.0004566	0.01492	0.281197	-29.58	0.98	3.76	3.59
RDT16019-127.d	1307	$^{206}Pb/^{238}U$ zircon age	0.281924	0.000034	0.0017	0.0676	0.281882	-2.62	1.19	2.22	2.06
RDT16019-150.d	2478	$^{207}Pb/^{206}Pb$ zircon age	0.281006	0.000033	0.000633	0.0251	0.280976	-7.81	1.155	3.44	3.31
RDT16019-162.d	2615	$^{207}Pb/^{206}Pb$ zircon age	0.281233	0.000034	0.001346	0.0474	0.281166	2.13	1.19	2.96	2.83

Supplementary Table 1 (continued). Main isotopes and ratios measured using the Multicollector (Hf analyses).

RDT16019-163.d	1191	$^{206}Pb/^{238}U$ zircon age	0.281936	0.000033	0.00097	0.0413	0.281914	-4.12	1.155	2.23	2.06
018 - 1	566.1	$^{206}Pb/^{238}U$ zircon age	0.282078	0.000048	0.0005597	0.01756	0.282072	-12.62	1.68	2.27	2.09
018 - 2	552.8	$^{206}Pb/^{238}U$ zircon age	0.282108	0.00005	0.000433	0.01367	0.282104	-11.80	1.75	2.21	2.03
018 - 3	3221.4	$^{207}Pb/^{206}Pb$ zircon age	0.280896	0.000047	0.0038604	0.12097	0.280657	-1.69	1.645	3.67	3.55
018 - 5	1760	$^{207}Pb/^{206}Pb$ zircon age	0.281596	0.000041	0.0004845	0.01371	0.281580	-2.98	1.435	2.60	2.44
018 - 6	1460	$^{207}Pb/^{206}Pb$ zircon age	0.281701	0.000047	0.001016	0.0262	0.281673	-6.55	1.645	2.58	2.42
018 - 7	1071.9	$^{206}Pb/^{238}U$ zircon age	0.281817	0.000044	0.0009326	0.025488	0.281798	-10.93	1.54	2.55	2.38
018 - 8	1174.4	$^{206}Pb/^{238}U$ zircon age	0.281942	0.000049	0.000644	0.01649	0.281928	-4.01	1.715	2.21	2.04
018 - 10	507.1	$^{206}Pb/^{238}U$ zircon age	0.281847	0.000049	0.0010193	0.02427	0.281837	-22.25	1.715	2.82	2.63
018 - 12	946.3	$^{206}Pb/^{238}U$ zircon age	0.281997	0.00004	0.0002236	0.005047	0.281993	-6.87	1.4	2.21	2.03
018 - 13	862	$^{206}Pb/^{238}U$ zircon age	0.282261	0.000042	0.00192	0.0427	0.282230	-0.38	1.47	1.74	1.56
018 - 14	539.6	$^{206}Pb/^{238}U$ zircon age	0.282137	0.00005	0.000898	0.01932	0.282128	-11.23	1.75	2.17	1.98
018 - 15	1157	$^{206}Pb/^{238}U$ zircon age	0.2819	0.000051	0.001075	0.02144	0.281877	-6.22	1.785	2.33	2.16
018 - 17	862	$^{206}Pb/^{238}U$ zircon age	0.282305	0.000053	0.0009828	0.01912	0.282289	1.72	1.855	1.61	1.43
018 - 18	2687.7	$^{207}Pb/^{206}Pb$ zircon age	0.281183	0.000047	0.005094	0.1028	0.280921	-4.86	1.645	3.43	3.31
018 - 19	2450	$^{207}Pb/^{206}Pb$ zircon age	0.281095	0.000042	0.000733	0.01368	0.281061	-5.45	1.47	3.28	3.15
018 - 22	1135.1	$^{206}Pb/^{238}U$ zircon age	0.281925	0.000045	0.0006625	0.012948	0.281911	-5.51	1.575	2.27	2.10
018 - 23	912.6	$^{206}Pb/^{238}U$ zircon age	0.282022	0.000037	0.00099	0.0216	0.282005	-7.20	1.295	2.20	2.02
018 - 24	3215	$^{207}Pb/^{206}Pb$ zircon age	0.280692	0.000054	0.002027	0.0386	0.280567	-5.06	1.89	3.86	3.74
018 - 25	1037	$^{206}Pb/^{238}U$ zircon age	0.281927	0.000042	0.001455	0.0311	0.281899	-8.16	1.47	2.36	2.18
018 - 26	918.2	$^{206}Pb/^{238}U$ zircon age	0.281977	0.00005	0.001125	0.02409	0.281958	-8.76	1.75	2.30	2.12
018 - 27	906	$^{206}Pb/^{238}U$ zircon age	0.282032	0.000043	0.002775	0.0648	0.281985	-8.07	1.505	2.25	2.07
018 - 28	791	$^{206}Pb/^{238}U$ zircon age	0.281892	0.00004	0.00112	0.0268	0.281875	-14.53	1.4	2.56	2.38
018 - 30	986	$^{206}Pb/^{238}U$ zircon age	0.281944	0.000041	0.000992	0.02529	0.281926	-8.36	1.435	2.33	2.15
018 - 32	1893	$^{207}Pb/^{206}Pb$ zircon age	0.281574	0.000042	0.00258	0.06708	0.281481	-3.42	1.47	2.73	2.58
018 - 33	2480	$^{207}Pb/^{206}Pb$ zircon age	0.281087	0.000048	0.000549	0.014409	0.281061	-4.74	1.68	3.26	3.13
018 - 34	1146.8	$^{206}Pb/^{238}U$ zircon age	0.281921	0.000048	0.001363	0.0412	0.281892	-5.92	1.68	2.30	2.13
018 - 35	1004.8	$^{206}Pb/^{238}U$ zircon age	0.282224	0.000046	0.000846	0.02677	0.282208	2.08	1.61	1.70	1.52
018 - 36	914.3	$^{206}Pb/^{238}U$ zircon age	0.282337	0.000041	0.00081	0.0253	0.282323	4.11	1.435	1.51	1.32
018 - 37	1264	$^{206}Pb/^{238}U$ zircon age	0.281575	0.000049	0.001499	0.0528	0.281539	-15.76	1.715	2.99	2.82
018 - 38	1278	$^{206}Pb/^{238}U$ zircon age	0.281827	0.000056	0.000673	0.02582	0.281811	-5.81	1.96	2.40	2.23
018 - 39	956	$^{206}Pb/^{238}U$ zircon age	0.282096	0.000036	0.000874	0.0323	0.282080	-3.55	1.26	2.01	1.83
018 - 40	981.5	$^{206}Pb/^{238}U$ zircon age	0.281871	0.000046	0.0003204	0.014	0.281865	-10.60	1.61	2.46	2.29

Supplementary Table 1 (continued). Main isotopes and ratios measured using the Multicollector (Hf analyses).

018 - 42	550.4	$^{206}Pb/^{238}U$ zircon age	0.282135	0.000039	0.0001694	0.008	0.282133	-10.80	1.365	2.15	1.96
018 - 43	1722	$^{207}Pb/^{206}Pb$ zircon age	0.281553	0.000048	0.0004165	0.02092	0.281539	-5.29	1.68	2.71	2.55
018 - 44	997.2	$^{206}Pb/^{238}U$ zircon age	0.281959	0.000054	0.00044	0.02236	0.281951	-7.21	1.89	2.27	2.09
018 - 45	749	$^{206}Pb/^{238}U$ zircon age	0.282079	0.000043	0.0004649	0.02538	0.282072	-8.50	1.505	2.16	1.98
018 - 46	1089.6	$^{206}Pb/^{238}U$ zircon age	0.282019	0.000045	0.000432	0.0244	0.282010	-3.02	1.575	2.08	1.91
018 - 48	1036.3	$^{206}Pb/^{238}U$ zircon age	0.282362	0.000045	0.0003178	0.01719	0.282356	8.03	1.575	1.36	1.18
018 - 49	893.4	$^{206}Pb/^{238}U$ zircon age	0.281944	0.000046	0.000086	0.0049	0.281943	-9.85	1.61	2.35	2.17
018 - 50	1677	$^{207}Pb/^{206}Pb$ zircon age	0.281624	0.000047	0.00082	0.04942	0.281598	-4.24	1.645	2.61	2.45
008 - 1	~~1043~~		~~0.296~~	~~0.028~~	~~0.00011~~	~~-0.002~~	~~0.295998~~	~~491.73~~	~~980~~	~~-42.86~~	~~-43.26~~
008 - 2	952	$^{206}Pb/^{238}U$ zircon age	0.28206	0.000047	0.000656	0.0326	0.282048	-4.78	1.645	2.08	1.91
008 - 3	955.7	$^{206}Pb/^{238}U$ zircon age	0.282068	0.000042	0.001188	0.0589	0.282047	-4.75	1.47	2.09	1.91
008 - 4	2672	$^{206}Pb/^{238}U$ zircon age	0.281104	0.000044	0.00128	0.0595	0.281039	-1.05	1.54	3.20	3.07
008 - 5	2251	$^{206}Pb/^{238}U$ zircon age	0.281501	0.000083	0.0005642	0.0224	0.281477	4.71	2.905	2.52	2.38
008 - 6	529.2	$^{206}Pb/^{238}U$ zircon age	0.282391	0.000039	0.000465	0.01842	0.282386	-2.31	1.365	1.61	1.42
008 - 7	1018.2	$^{206}Pb/^{238}U$ zircon age	0.282224	0.00005	0.000717	0.03093	0.282210	2.46	1.75	1.69	1.51
008 - 8	783.1	$^{206}Pb/^{238}U$ zircon age	0.282552	0.000042	0.0004994	0.02098	0.282545	9.00	1.47	1.10	0.91
008 - 9	819	$^{206}Pb/^{238}U$ zircon age	0.282324	0.000042	0.000859	0.03058	0.282311	1.52	1.47	1.59	1.41
008 - 10	3471.4	$^{207}Pb/^{206}Pb$ zircon age	0.280637	0.000061	0.001811	0.0778	0.280516	-0.78	2.135	3.81	3.71
008 - 11	1020.7	$^{206}Pb/^{238}U$ zircon age	0.28194	0.000039	0.000638	0.0259	0.281928	-7.50	1.365	2.30	2.13
008 - 12	657.9	$^{206}Pb/^{238}U$ zircon age	0.28188	0.000047	0.000855	0.03511	0.281869	-17.73	1.645	2.66	2.47
008 - 13	994.9	$^{206}Pb/^{238}U$ zircon age	0.282155	0.000042	0.000532	0.02029	0.282145	-0.38	1.47	1.85	1.67
008 - 14	1019	$^{206}Pb/^{238}U$ zircon age	0.282305	0.000042	0.000847	0.0274	0.282289	5.26	1.47	1.52	1.34
008 - 15	2463	$^{207}Pb/^{206}Pb$ zircon age	0.281187	0.000045	0.0001708	0.005981	0.281179	-0.95	1.575	3.03	2.89
008 - 16	964	$^{206}Pb/^{238}U$ zircon age	0.282082	0.000048	0.000856	0.0319	0.282066	-3.86	1.68	2.04	1.86
008 - 17	2587	$^{207}Pb/^{206}Pb$ zircon age	0.28081	0.000042	0.000619	0.02139	0.280779	-12.26	1.47	3.79	3.66
008 - 18	1265.5	$^{206}Pb/^{238}U$ zircon age	0.281952	0.000038	0.001713	0.0624	0.281911	-2.53	1.33	2.19	2.02
008 - 19	1767	$^{207}Pb/^{206}Pb$ zircon age	0.281541	0.00005	0.000773	0.02799	0.281515	-5.12	1.75	2.73	2.58
008 - 20	1019.5	$^{206}Pb/^{238}U$ zircon age	0.282029	0.000042	0.002219	0.0737	0.281986	-5.44	1.47	2.18	2.00
008 - 21	538.2	$^{206}Pb/^{238}U$ zircon age	0.282146	0.000046	0.0004064	0.01319	0.282142	-10.77	1.61	2.14	1.95
008 - 22	1268.6	$^{206}Pb/^{238}U$ zircon age	0.282042	0.000041	0.00054	0.01402	0.282029	1.72	1.435	1.93	1.76
008 - 23	1259	$^{206}Pb/^{238}U$ zircon age	0.282065	0.000054	0.001091	0.03575	0.282039	1.86	1.89	1.91	1.74
008 - 24	1084	$^{206}Pb/^{238}U$ zircon age	0.281929	0.000049	0.001485	0.0432	0.281899	-7.09	1.715	2.33	2.15
008 - 25	2500	$^{207}Pb/^{206}Pb$ zircon age	0.281126	0.000051	0.0004551	0.01257	0.281104	-2.74	1.785	3.16	3.03

Supplementary Table 1 (continued). Main isotopes and ratios measured using the Multicollector (Hf analyses).

008 - 26	1011	$^{206}Pb/^{238}U$ zircon age	0.281969	0.000045	0.00052	0.0148	0.281959	-6.60	1.575	2.24	2.07
008 - 27	859.8	$^{206}Pb/^{238}U$ zircon age	0.282231	0.000044	0.001412	0.0401	0.282208	-1.19	1.54	1.79	1.61
008 - 28	597.9	$^{206}Pb/^{238}U$ zircon age	0.28249	0.000042	0.001039	0.02059	0.282478	2.48	1.47	1.36	1.17
008 - 29	1869	$^{207}Pb/^{206}Pb$ zircon age	0.281509	0.000049	0.00144	0.0361	0.281458	-4.80	1.715	2.79	2.64
008 - 30	997	$^{206}Pb/^{238}U$ zircon age	0.281934	0.000047	0.00199	0.0532	0.281897	-9.13	1.645	2.39	2.21
008 - 31	1616	$^{207}Pb/^{206}Pb$ zircon age	0.281513	0.00005	0.0005848	0.015119	0.281495	-9.29	1.75	2.87	2.71
008 - 32	1435	$^{206}Pb/^{238}U$ zircon age	0.281906	0.000049	0.00176	0.0467	0.281858	-0.55	1.715	2.20	2.03
008 - 33	1668	$^{207}Pb/^{206}Pb$ zircon age	0.281563	0.000043	0.0005702	0.01493	0.281545	-6.33	1.505	2.73	2.57
008 - 34	786.1	$^{206}Pb/^{238}U$ zircon age	0.282179	0.000048	0.00253	0.061	0.282142	-5.21	1.68	1.98	1.80
008 - 35	1865	$^{207}Pb/^{206}Pb$ zircon age	0.281382	0.000048	0.00175	0.0497	0.281320	-9.79	1.68	3.09	2.94
008 - 36	~~307.1~~		~~0.282528~~	~~0.000046~~	~~0.0015522~~	~~0.04264~~	~~0.282519~~	~~-2.58~~	~~1.61~~	~~1.45~~	~~1.26~~
008 - 37	1003	$^{206}Pb/^{238}U$ zircon age	0.281905	0.00004	0.001196	0.03084	0.281882	-9.50	1.4	2.41	2.24
008 - 38	741.4	$^{206}Pb/^{238}U$ zircon age	0.282528	0.000043	0.000435	0.0113	0.282522	7.25	1.505	1.17	0.99
008 - 39	1821	$^{207}Pb/^{206}Pb$ zircon age	0.281467	0.000042	0.001586	0.04085	0.281412	-7.53	1.47	2.92	2.77
008 - 40	527.5	$^{206}Pb/^{238}U$ zircon age	0.28212	0.000042	0.000641	0.0181	0.282114	-12.01	1.47	2.21	2.02
008 - 41	536.7	$^{206}Pb/^{238}U$ zircon age	0.282479	0.000045	0.001264	0.0237	0.282466	0.68	1.575	1.43	1.23
008 - 42	2265	$^{207}Pb/^{206}Pb$ zircon age	0.280841	0.000051	0.0005018	0.01265	0.280819	-18.34	1.785	3.90	3.76
008 - 43	2592	$^{207}Pb/^{206}Pb$ zircon age	0.280781	0.000042	0.000762	0.01806	0.280743	-13.43	1.47	3.86	3.73
008 - 44	947.6	$^{206}Pb/^{238}U$ zircon age	0.281428	0.000039	0.0004217	0.01083	0.281420	-27.13	1.365	3.44	3.26
008 - 45	655.2	$^{206}Pb/^{238}U$ zircon age	0.282381	0.000042	0.000956	0.02303	0.282369	-0.09	1.47	1.57	1.38
008 - 46	812.3	$^{206}Pb/^{238}U$ zircon age	0.282317	0.000043	0.001352	0.0368	0.282296	0.86	1.505	1.63	1.44
008 - 47	928.9	$^{206}Pb/^{238}U$ zircon age	0.282069	0.000044	0.000966	0.0287	0.282052	-5.16	1.54	2.09	1.91
008 - 48	874.7	$^{206}Pb/^{238}U$ zircon age	0.282562	0.000055	0.002471	0.0528	0.282521	10.24	1.925	1.09	0.91
008 - 49	~~1154~~	$^{206}Pb/^{238}U$ zircon age	~~0.281436~~	~~0.000051~~	~~0.0008194~~	~~0.02375~~	~~0.281418~~	~~-22.54~~	~~1.785~~	~~3.31~~	~~3.15~~
008 - 50	721	$^{206}Pb/^{238}U$ zircon age	0.281749	0.000041	0.000814	0.02258	0.281738	-20.97	1.435	2.90	2.72
008 - 51	2725	$^{207}Pb/^{206}Pb$ zircon age	0.280955	0.000048	0.001347	0.0378	0.280885	-5.28	1.68	3.49	3.36
008 - 52	937	$^{206}Pb/^{238}U$ zircon age	0.281982	0.000044	0.000575	0.0212	0.281972	-7.82	1.54	2.26	2.08
008 - 53	902.8	$^{206}Pb/^{238}U$ zircon age	0.282072	0.00005	0.001064	0.02846	0.282054	-5.69	1.75	2.10	1.92
008 - 54	2133	$^{207}Pb/^{206}Pb$ zircon age	0.281189	0.000046	0.000932	0.02668	0.281151	-9.60	1.61	3.28	3.14
008 - 55	549.5	$^{206}Pb/^{238}U$ zircon age	0.282169	0.00004	0.0009626	0.0264	0.282159	-9.91	1.4	2.09	1.91
008 - 56	915	$^{206}Pb/^{238}U$ zircon age	0.282111	0.000049	0.000764	0.0221	0.282098	-3.86	1.715	2.00	1.82
008 - 57	1307	$^{206}Pb/^{238}U$ zircon age	0.281505	0.00004	0.000913	0.02613	0.281482	-16.79	1.4	3.08	2.92
008 - 58	576.7	$^{206}Pb/^{238}U$ zircon age	0.28215	0.000054	0.000433	0.01237	0.282145	-9.78	1.89	2.11	1.92

Supplementary Table 1 (continued). Main isotopes and ratios measured using the Multicollector (Hf analyses).

008 - 59	1902	$^{207}Pb/^{206}Pb$ zircon age	0.281535	0.000041	0.002186	0.0613	0.281456	-4.11	1.435	2.78	2.63
008 - 60	2487.3	$^{207}Pb/^{206}Pb$ zircon age	0.281212	0.000045	0.000857	0.02302	0.281171	-0.65	1.575	3.03	2.89
008 - 61	1916	$^{207}Pb/^{206}Pb$ zircon age	0.281437	0.000042	0.00173	0.0516	0.281374	-6.70	1.47	2.94	2.79
008 - 62	1960	$^{207}Pb/^{206}Pb$ zircon age	0.28153	0.000047	0.000921	0.02821	0.281496	-1.36	1.645	2.66	2.51
008 - 63	1012	$^{206}Pb/^{238}U$ zircon age	0.282301	0.000047	0.000707	0.01988	0.282288	5.06	1.645	1.52	1.34
008 - 64	1691	$^{207}Pb/^{206}Pb$ zircon age	0.281557	0.000043	0.0006844	0.01841	0.281535	-6.16	1.505	2.74	2.58
008 - 65	1522	$^{207}Pb/^{206}Pb$ zircon age	0.281357	0.000048	0.000496	0.01442	0.281343	-16.85	1.68	3.25	3.09
008 - 66	995	$^{206}Pb/^{238}U$ zircon age	0.282023	0.000038	0.0005	0.0149	0.282014	-5.03	1.33	2.13	1.96
008 - 67	720.3	$^{206}Pb/^{238}U$ zircon age	0.281972	0.000049	0.000931	0.02528	0.281959	-13.15	1.715	2.42	2.24
008 - 68	2474	$^{207}Pb/^{206}Pb$ zircon age	0.281166	0.000045	0.0006571	0.018255	0.281135	-2.25	1.575	3.11	2.98
008 - 69	811.4	$^{206}Pb/^{238}U$ zircon age	0.28196	0.00004	0.000181	0.0052	0.281957	-11.17	1.4	2.37	2.19
008 - 70	1653	$^{207}Pb/^{206}Pb$ zircon age	0.281565	0.000041	0.001351	0.0402	0.281523	-7.47	1.435	2.79	2.63
008 - 71	966.5	$^{206}Pb/^{238}U$ zircon age	0.281951	0.000045	0.001093	0.0332	0.281931	-8.60	1.575	2.33	2.15
008 - 72	1970	$^{207}Pb/^{206}Pb$ zircon age	0.281367	0.000044	0.0003741	0.01296	0.281353	-6.20	1.54	2.95	2.81
008 - 73	2494	$^{207}Pb/^{206}Pb$ zircon age	0.281049	0.000042	0.000491	0.01286	0.281026	-5.68	1.47	3.33	3.20
008 - 74	817.3	$^{206}Pb/^{238}U$ zircon age	0.282443	0.000043	0.0008482	0.02347	0.282430	5.71	1.505	1.33	1.15
008 - 75	772	$^{206}Pb/^{238}U$ zircon age	0.281993	0.000038	0.000387	0.01081	0.281987	-10.99	1.33	2.33	2.15
008 - 76	927	$^{206}Pb/^{238}U$ zircon age	0.282222	0.000044	0.000911	0.02594	0.282206	0.25	1.54	1.75	1.58
008 - 77	646	$^{206}Pb/^{238}U$ zircon age	0.282509	0.000045	0.000761	0.0227	0.282500	4.32	1.575	1.28	1.09
008 - 78	923.5	$^{206}Pb/^{238}U$ zircon age	0.282326	0.00005	0.001294	0.0378	0.282304	3.62	1.75	1.54	1.36
008 - 79	560.4	$^{206}Pb/^{238}U$ zircon age	0.282323	0.000049	0.000078	0.002689	0.282322	-3.89	1.715	1.73	1.54
008 - 80	2357	$^{207}Pb/^{206}Pb$ zircon age	0.281102	0.000048	0.0010672	0.02931	0.281054	-7.86	1.68	3.35	3.21
008 - 81	1942	$^{207}Pb/^{206}Pb$ zircon age	0.281407	0.000042	0.0005434	0.01452	0.281387	-5.64	1.47	2.90	2.75
008 - 82	924	$^{206}Pb/^{238}U$ zircon age	0.281894	0.000049	0.0022	0.071	0.281856	-12.23	1.715	2.52	2.34
008 - 83	2458	$^{207}Pb/^{206}Pb$ zircon age	0.281054	0.000047	0.001281	0.03766	0.280994	-7.64	1.645	3.42	3.28
008 - 84	717.7	$^{206}Pb/^{238}U$ zircon age	0.282403	0.00004	0.001816	0.04877	0.282379	1.64	1.4	1.51	1.32
008 - 85	771.6	$^{206}Pb/^{238}U$ zircon age	0.281968	0.000045	0.000501	0.0139	0.281961	-11.95	1.575	2.39	2.21
008 - 86	535.6	$^{206}Pb/^{238}U$ zircon age	0.282102	0.000045	0.0003737	0.010318	0.282098	-12.37	1.575	2.24	2.05
008 - 87	823.5	$^{206}Pb/^{238}U$ zircon age	0.281919	0.000039	0.001759	0.0533	0.281892	-13.22	1.365	2.50	2.32
008 - 88	3167	$^{207}Pb/^{206}Pb$ zircon age	0.280786	0.000046	0.00156	0.04114	0.280691	-1.77	1.61	3.63	3.51
008 - 89	3168.9	$^{207}Pb/^{206}Pb$ zircon age	0.28082	0.000048	0.001446	0.0398	0.280732	-0.26	1.68	3.54	3.43
008 - 90	1935	$^{207}Pb/^{206}Pb$ zircon age	0.281517	0.00005	0.0003392	0.00883	0.281505	-1.63	1.75	2.65	2.50
008 - 91	1155	$^{206}Pb/^{238}U$ zircon age	0.281873	0.000038	0.001162	0.0348	0.281848	-7.29	1.33	2.39	2.22

Supplementary Table 1 (continued). Main isotopes and ratios measured using the Multicollector (Hf analyses).

008 - 92	924.3	$^{206}Pb/^{238}U$ zircon age	0.281934	0.000046	0.000697	0.02042	0.281922	-9.88	1.61	2.38	2.20
008 - 93	831	$^{206}Pb/^{238}U$ zircon age	0.282462	0.000039	0.001072	0.0295	0.282445	6.56	1.365	1.29	1.10
008 - 94	2421.3	$^{207}Pb/^{206}Pb$ zircon age	0.281122	0.000043	0.000291	0.00692	0.281109	-4.42	1.505	3.20	3.06
008 - 95	789	$^{206}Pb/^{238}U$ zircon age	0.281718	0.000049	0.0009639	0.02723	0.281704	-20.66	1.715	2.93	2.75
008 - 96	1024.6	$^{206}Pb/^{238}U$ zircon age	0.282126	0.000038	0.000874	0.0261	0.282109	-0.98	1.33	1.91	1.73
008 - 97	2440	$^{207}Pb/^{206}Pb$ zircon age	0.281058	0.00004	0.000891	0.02357	0.281017	-7.26	1.4	3.38	3.25
008 - 98	762.5	$^{206}Pb/^{238}U$ zircon age	0.281973	0.000039	0.000974	0.027088	0.281959	-12.21	1.365	2.40	2.21
008 - 99	770	$^{206}Pb/^{238}U$ zircon age	0.282364	0.000042	0.000778	0.0233	0.282353	1.90	1.47	1.53	1.35
008 - 100	723	$^{206}Pb/^{238}U$ zircon age	0.282183	0.000048	0.00063	0.01709	0.282174	-5.47	1.68	1.95	1.77
008 - 101	810.5	$^{206}Pb/^{238}U$ zircon age	0.281901	0.000043	0.000176	0.0061	0.281898	-13.28	1.505	2.50	2.32
008 - 102	788.8	$^{206}Pb/^{238}U$ zircon age	0.282462	0.000043	0.000852	0.02493	0.282449	5.75	1.505	1.30	1.12
008 - 103	792.3	$^{206}Pb/^{238}U$ zircon age	0.282132	0.00004	0.00154	0.0496	0.282109	-6.23	1.4	2.05	1.87
008 - 104	~~1054~~	$^{206}Pb/^{238}U$ zircon age	~~0.282407~~	~~0.000042~~	~~0.001153~~	~~0.0366~~	~~0.282384~~	~~9.43~~	~~1.47~~	~~1.28~~	~~1.11~~
008 - 105	2498	$^{207}Pb/^{206}Pb$ zircon age	0.281205	0.000047	0.001081	0.0335	0.281153	-1.04	1.645	3.06	2.93
008 - 106	568.8	$^{206}Pb/^{238}U$ zircon age	0.282144	0.000044	0.0001672	0.00519	0.282142	-10.07	1.54	2.12	1.93
008 - 107	575.4	$^{206}Pb/^{238}U$ zircon age	0.282097	0.000042	0.000493	0.01551	0.282092	-11.71	1.47	2.22	2.04
008 - 108	1345		**0.281425**	**0.000045**	**0.000882**	**0.0348**	**0.281403**	**-18.76**	**1.575**	**3.23**	**3.07**
008 - 109	751.3	$^{206}Pb/^{238}U$ zircon age	0.281955	0.000035	0.000733	0.0222	0.281945	-12.97	1.225	2.43	2.25
008 - 110	2496.1	$^{207}Pb/^{206}Pb$ zircon age	0.28068	0.000047	0.000242	0.00955	0.280668	-18.33	1.645	4.07	3.94
008 - 111	689	$^{206}Pb/^{238}U$ zircon age	0.282113	0.000058	0.00177	0.0686	0.282090	-9.22	2.03	2.16	1.97
008 - 112	960.5	$^{206}Pb/^{238}U$ zircon age	0.282093	0.000063	0.000648	0.0234	0.282081	-3.42	2.205	2.01	1.83
008 - 113	755	$^{206}Pb/^{238}U$ zircon age	0.282069	0.000044	0.000417	0.0157	0.282063	-8.69	1.54	2.17	1.99
008 - 114	739	$^{206}Pb/^{238}U$ zircon age	0.282022	0.000068	0.000881	0.0341	0.282010	-10.94	2.38	2.30	2.12
008 - 115	749.7	$^{206}Pb/^{238}U$ zircon age	0.282112	0.000044	0.00088	0.0313	0.282100	-7.52	1.54	2.10	1.92
008 - 116	1793	$^{207}Pb/^{206}Pb$ zircon age	0.281579	0.000042	0.0009563	0.0379	0.281546	-3.41	1.47	2.65	2.50
008 - 117	705	$^{206}Pb/^{238}U$ zircon age	0.282367	0.000051	0.00191	0.0789	0.282342	0.05	1.785	1.59	1.41
008 - 118	746.5	$^{206}Pb/^{238}U$ zircon age	0.282101	0.000038	0.0001426	0.00592	0.282099	-7.61	1.33	2.10	1.92
008 - 119	2580	$^{207}Pb/^{206}Pb$ zircon age	0.280971	0.00004	0.0003528	0.0129	0.280954	-6.23	1.4	3.43	3.30
008 - 120	870.7	$^{206}Pb/^{238}U$ zircon age	0.282375	0.000046	0.002709	0.1187	0.282331	3.39	1.61	1.52	1.33
008 - 121	834	$^{206}Pb/^{238}U$ zircon age	0.282468	0.000065	0.000765	0.0275	0.282456	7.00	2.275	1.26	1.08
008 - 122	550.3	$^{206}Pb/^{238}U$ zircon age	0.282433	0.000045	0.0000341	0.00148	0.282433	-0.20	1.575	1.49	1.30
006 - 1	1183	Pb^{206}/U^{238} zircon age	0.281759	0.000049	0.001299	0.0448	0.281730	-10.83	1.715	2.63	2.46
006 - 2	616.9	Pb^{206}/U^{238} zircon age	0.282407	0.000058	0.00075	0.0267	0.282398	0.08	2.03	1.53	1.34

Supplementary Table 1 (continued). Main isotopes and ratios measured using the Multicollector (Hf analyses).

006 - 4	~~222.6~~		~~0.282886~~	~~0.000046~~	~~0.000885~~	~~0.0272~~	~~0.282882~~	~~8.39~~	~~1.61~~	~~0.69~~	~~0.49~~
006 - 5	~~3150~~		~~0.280641~~	~~0.000048~~	~~0.00126~~	~~0.0406~~	~~0.280565~~	~~-6.67~~	~~1.68~~	~~3.90~~	~~3.78~~
006 - 6	2604	Pb^{207}/Pb^{206} zircon age	0.281087	0.000063	0.0006211	0.02088	0.281056	-2.02	2.205	3.20	3.07
006 - 7	1942	Pb^{207}/Pb^{206} zircon age	~~0.281443~~	~~0.000062~~	~~0.00191~~	~~0.0782~~	~~0.281373~~	~~-6.15~~	~~2.17~~	~~2.93~~	~~2.78~~
006 - 8	~~638~~		~~0.281783~~	~~0.000046~~	~~0.0001136~~	~~0.0047~~	~~0.281782~~	~~-21.29~~	~~1.61~~	~~2.86~~	~~2.68~~
006 - 9	1923	Pb^{207}/Pb^{206} zircon age	0.281562	0.000052	0.003917	0.129	0.281419	-4.94	1.82	2.84	2.69
006 - 10	2504	Pb^{207}/Pb^{206} zircon age	0.281079	0.000067	0.00163	0.05375	0.281001	-6.32	2.345	3.37	3.24
006 - 11	378.7	Pb^{206}/U^{238} zircon age	0.282551	0.00005	0.000982	0.03263	0.282544	-0.10	1.75	1.35	1.16
006 - 12	737	Pb^{206}/U^{238} zircon age	0.282064	0.000047	0.000856	0.03043	0.282052	-9.49	1.645	2.21	2.03
006 - 13	568	Pb^{206}/U^{238} zircon age	0.282477	0.000076	0.000826	0.0272	0.282468	1.45	2.66	1.40	1.21
006 - 14	~~829~~		~~0.282005~~	~~0.000076~~	~~0.000933~~	~~0.0283~~	~~0.281990~~	~~-9.60~~	~~2.66~~	~~2.29~~	~~2.11~~
006 - 15	528.9	Pb^{206}/U^{238} zircon age	0.282216	0.000061	0.000982	0.02879	0.282206	-8.70	2.135	2.00	1.81
006 - 16	1849	$^{207}Pb/^{206}Pb$ zircon age	~~0.281458~~	~~0.000045~~	~~0.00213~~	~~0.0667~~	~~0.281383~~	~~-7.91~~	~~1.575~~	~~2.96~~	~~2.81~~
006 - 17	~~470.1~~		~~0.281843~~	~~0.000067~~	~~0.000511~~	~~0.01642~~	~~0.281839~~	~~-23.03~~	~~2.345~~	~~2.84~~	~~2.65~~
006 - 18	1339	Pb^{206}/U^{238} zircon age	0.281549	0.00006	0.00112	0.0407	0.281521	-14.71	2.1	2.98	2.82
006 - 19	504	Pb^{206}/U^{238} zircon age	0.28212	0.000051	0.00075	0.0258	0.282113	-12.56	1.785	2.22	2.03
006 - 20	2375	Pb^{207}/Pb^{206} zircon age	0.281088	0.000041	0.000854	0.0269	0.281049	-7.61	1.435	3.35	3.21
006 - 21	940	Pb^{206}/U^{238} zircon age	0.281778	0.00005	0.0027	0.097	0.281730	-16.32	1.75	2.78	2.60
006 - 22	~~1093~~		~~0.281268~~	~~0.000064~~	~~0.00527~~	~~0.214~~	~~0.281159~~	~~-33.09~~	~~2.24~~	~~3.90~~	~~3.73~~
006 - 23	683.2	Pb^{206}/U^{238} zircon age	0.28236	0.000043	0.00226	0.0723	0.282331	-0.82	1.505	1.63	1.45
006 - 24	1469	Pb^{207}/Pb^{206} zircon age	0.281779	0.000041	0.000916	0.02818	0.281754	-3.48	1.435	2.40	2.24
006 - 25	652.6	Pb^{206}/U^{238} zircon age	0.281928	0.000048	0.001072	0.03052	0.281915	-16.24	1.68	2.56	2.38
006 - 27	392.1	Pb^{206}/U^{238} zircon age	0.282552	0.000052	0.001363	0.0374	0.282542	0.13	1.82	1.35	1.15
006 - 28	795	Pb^{206}/U^{238} zircon age	0.282464	0.000052	0.000974	0.03187	0.282449	5.89	1.82	1.30	1.12
006 - 29	~~905~~		~~0.282224~~	~~0.000049~~	~~0.00136~~	~~0.0483~~	~~0.282201~~	~~-0.43~~	~~1.715~~	~~1.78~~	~~1.60~~
006 - 30	~~252~~		~~0.282578~~	~~0.000048~~	~~0.00147~~	~~0.042~~	~~0.282571~~	~~-1.97~~	~~1.68~~	~~1.37~~	~~1.17~~
006 - 31	1680	Pb^{207}/Pb^{206} zircon age	0.281794	0.000045	0.00103	0.03522	0.281761	1.62	1.575	2.26	2.10
006 - 32	2473	Pb^{207}/Pb^{206} zircon age	0.281263	0.000052	0.0004145	0.0131	0.281243	1.58	1.82	2.88	2.75
006 - 33	579.7	Pb^{206}/U^{238} zircon age	0.282417	0.000045	0.0000788	0.00346	0.282416	-0.13	1.575	1.51	1.32
006 - 34	~~957~~		~~0.281637~~	~~0.000046~~	~~0.000773~~	~~0.0306~~	~~0.281623~~	~~-19.73~~	~~1.61~~	~~3.00~~	~~2.83~~
006 - 35	1861	Pb^{207}/Pb^{206} zircon age	0.28155	0.00005	0.00554	0.207	0.281354	-8.67	1.75	3.02	2.87
006 - 36	725.2	Pb^{206}/U^{238} zircon age	0.282577	0.000044	0.00145	0.0518	0.282557	8.14	1.54	1.10	0.92
006 - 37	2580	Pb^{207}/Pb^{206} zircon age	0.281331	0.000045	0.000586	0.02112	0.281302	6.17	1.575	2.70	2.56

Supplementary Table 1 (continued). Main isotopes and ratios measured using the Multicollector (Hf analyses).

006 - 38	~~770.7~~		~~0.282062~~	~~0.000047~~	~~0.000451~~	~~0.0191~~	~~0.282055~~	~~-8.61~~	~~1.645~~	~~2.18~~	~~2.00~~
006 - 39	690	Pb^{206}/U^{238} zircon age	0.282212	0.000038	0.002524	0.1179	0.282179	-6.04	1.33	1.96	1.78
006 - 40	~~772~~		~~0.281383~~	~~0.000073~~	~~0.00194~~	~~0.084~~	~~0.281355~~	~~-33.40~~	~~2.555~~	~~3.69~~	~~3.51~~
006 - 41	804	Pb^{206}/U^{238} zircon age	0.281778	0.000051	0.001254	0.0528	0.281759	-18.36	1.785	2.80	2.62
006 - 42	487.3	Pb^{206}/U^{238} zircon age	0.281699	0.000077	0.000082	0.00504	0.281698	-27.61	2.695	3.13	2.95
006 - 43	1200	Pb^{206}/U^{238} zircon age	0.281999	0.000062	0.001681	0.0751	0.281961	-2.26	2.17	2.12	1.95
006 - 44	405.2	Pb^{206}/U^{238} zircon age	0.282693	0.000048	0.000688	0.0278	0.282688	5.58	1.68	1.01	0.82
006 - 45	255	Pb^{206}/U^{238} zircon age	0.282593	0.00004	0.001704	0.0842	0.282585	-1.41	1.4	1.34	1.14
006 - 46	~~846~~		~~0.281949~~	~~0.000048~~	~~0.00157~~	~~0.0799~~	~~0.281924~~	~~-11.57~~	~~1.68~~	~~2.42~~	~~2.24~~
006 - 47	~~968~~		~~0.28206~~	~~0.00011~~	~~0.000937~~	~~0.0464~~	~~0.282043~~	~~-4.61~~	~~3.85~~	~~2.09~~	~~1.91~~
006 - 48	~~515.9~~		~~0.282326~~	~~0.000057~~	~~0.00176~~	~~0.1114~~	~~0.282309~~	~~-5.35~~	~~1.995~~	~~1.79~~	~~1.60~~
006 - 49	~~1136~~		~~0.281763~~	~~0.000062~~	~~0.002212~~	~~0.1094~~	~~0.281716~~	~~-12.41~~	~~2.17~~	~~2.69~~	~~2.52~~
006 - 50	~~632~~		~~0.282177~~	~~0.000038~~	~~0.001084~~	~~0.0575~~	~~0.282164~~	~~-7.88~~	~~1.33~~	~~2.03~~	~~1.84~~
006 - 51	566	Pb^{206}/U^{238} zircon age	0.281706	0.000048	0.000291	0.0115	0.281703	-25.69	1.68	3.07	2.89
RDT15066-9.d	2604	Pb^{207}/Pb^{206} zircon age	0.281098	0.000031	0.000727	0.0374	0.281062	-1.82	1.085	3.19	3.06
RDT15066-10.d	2735	Pb^{207}/Pb^{206} zircon age	0.281145	0.000027	0.000576	0.0259	0.281115	3.14	0.945	3.00	2.87
RDT15066-11.d	2620	Pb^{207}/Pb^{206} zircon age	0.280933	0.000034	0.00052	0.0254	0.280907	-6.95	1.19	3.502236492	3.37
RDT15066-15.d	935.3	Pb^{206}/U^{238} zircon age	0.282353	0.000031	0.002112	0.09656	0.282316	4.33	1.085	1.51	1.33
RDT15066-17.d	607.8	Pb^{206}/U^{238} zircon age	0.282462	0.000032	0.000888	0.0447	0.282452	1.77	1.12	1.41	1.22
RDT15066-18.d	3071	Pb^{207}/Pb^{206} zircon age	0.280991	0.000057	0.000985	0.042	0.280933	4.58	1.995	3.18	3.06
RDT15066-22.d	1037	Pb^{206}/U^{238} zircon age	0.282023	0.000028	0.001496	0.0774	0.281994	-4.79	0.98	2.15	1.97
RDT15066-32.d	1008.3	Pb^{206}/U^{238} zircon age	0.282418	0.000031	0.0007079	0.03634	0.282405	9.12	1.085	1.27	1.09
RDT15066-37.d	1139.7	Pb^{206}/U^{238} zircon age	0.28194	0.000031	0.000268	0.0143	0.281934	-4.57	1.085	2.22	2.04
RDT15066-40.d	1584	Pb^{207}/Pb^{206} zircon age	0.281686	0.000031	0.000426	0.02282	0.281673	-3.70	1.085	2.51	2.35
RDT15066-56.d	899.9	Pb^{206}/U^{238} zircon age	0.281774	0.000027	0.0000374	0.00252	0.281773	-15.70	0.945	2.71	2.54
RDT15066-69.d	656.4	Pb^{206}/U^{238} zircon age	0.281432	0.000031	0.00111	0.0425	0.281393	-7.52	1.085	2.94	2.79
RDT15066-71.d	564.1	Pb^{206}/U^{238} zircon age	0.282349	0.000032	0.0002782	0.01285	0.282346	-2.96	1.12	1.67	1.48
RDT15066-76.d	935	Pb^{206}/U^{238} zircon age	0.282065	0.00003	0.0003222	0.01664	0.282059	-4.77	1.05	2.07	1.89
RDT15066-95.d	968	Pb^{206}/U^{238} zircon age	0.281876	0.000027	0.000914	0.0401	0.281859	-11.11	0.945	2.48	2.31
RDT15066-110.d	1568	Pb^{207}/Pb^{206} zircon age	0.281649	0.000027	0.00111	0.0273	0.281616	-6.10	0.945	2.64	2.48
RDT15066-111.d	2433	Pb^{207}/Pb^{206} zircon age	0.281161	0.000032	0.0010347	0.02579	0.281113	-3.99	1.12	3.18	3.05
RDT15066-112.d	1796	Pb^{207}/Pb^{206} zircon age	0.281296	0.000029	0.00135	0.03485	0.281250	-13.86	1.015	3.28	3.13
RDT15066-113.d	650.3	Pb^{206}/U^{238} zircon age	~~0.27~~	~~0.2~~	~~0.0139~~	~~0.451~~					

Supplementary Table 1 (continued). Main isotopes and ratios measured using the Multicollector (Hf analyses).

RDT15066-114.d	637.8	Pb^{206}/U^{238} zircon age	0.282445	0.000033	0.001188	0.0331	0.282431	1.69	1.155	1.44	1.25
RDT15066-115.d	573.6	Pb^{206}/U^{238} zircon age	0.282371	0.000028	0.001845	0.0466	0.282351	-2.57	0.98	1.66	1.47
RDT15066-117.d	556.2	Pb^{206}/U^{238} zircon age	0.282295	0.000027	0.000995	0.0237	0.282285	-5.31	0.945	1.81	1.63
RDT15066-127.d	2670.3	Pb^{207}/Pb^{206} zircon age	0.280809	0.000036	0.000434	0.00871	0.280787	-10.05	1.26	3.72	3.59
RDT15066-131.d	1838	Pb^{207}/Pb^{206} zircon age	0.281436	0.000027	0.00117	0.0296	0.281395	-7.74	0.945	2.94	2.79
RDT15066-133.d	3393	Pb^{207}/Pb^{206} zircon age	0.280724	0.00004	0.001878	0.0426	0.280601	0.40	1.4	3.68	3.57
RDT15066-136.d	1350	Pb^{206}/U^{238} zircon age	0.281897	0.000039	0.00135	0.0331	0.281863	-2.33	1.365	2.24	2.07
RDT15066-154.d	906	Pb^{206}/U^{238} zircon age	0.282458	0.000031	0.002632	0.0699	0.282413	7.11	1.085	1.31	1.13
RDT15066-194.d	735.5	Pb^{206}/U^{238} zircon age	0.282174	0.000028	0.000844	0.033	0.282162	-5.62	0.98	1.97	1.79
RDT15066-197.d	1429	Pb^{207}/Pb^{206} zircon age	0.281675	0.000031	0.000676	0.02097	0.281657	-7.83	1.085	2.64	2.47
RDT15066-198.d	1851	Pb^{207}/Pb^{206} zircon age	0.281432	0.000031	0.00111	0.0425	0.281393	-7.52	1.085	2.94	2.79
RDT15066-200.d	943	Pb^{206}/U^{238} zircon age	0.282138	0.000026	0.001247	0.038	0.282116	-2.59	0.91	1.94	1.76
RDT15066-201.d	516.3	Pb^{206}/U^{238} zircon age	0.282507	0.000031	0.000964	0.0216	0.282498	1.34	1.085	1.37	1.18
RDT16001-17.d	2049	Pb^{207}/Pb^{206} zircon age	0.281438	0.000028	0.002333	0.0561	0.281347	-4.58	0.98	2.92	2.77
RDT16001-20.d	998	Pb^{206}/U^{238} zircon age	0.282063	0.000032	0.001232	0.0308	0.282040	-4.04	1.12	2.07	1.90
RDT16001-43.d	942	Pb^{206}/U^{238} zircon age	0.282104	0.000034	0.000852	0.02237	0.282089	-3.56	1.19	2.00	1.82
RDT16001-44.d	770	Pb^{206}/U^{238} zircon age	0.282343	0.000038	0.00209	0.0586	0.282313	0.49	1.33	1.62	1.43
RDT16001-47.d	918	Pb^{206}/U^{238} zircon age	0.282148	0.000023	0.000965	0.02785	0.282131	-2.60	0.805	1.92	1.74
RDT16001-60.d	500.2	Pb^{206}/U^{238} zircon age	0.281971	0.000034	0.001131	0.03405	0.281960	-18.04	1.19	2.56	2.37
RDT16001-62.d	1112	Pb^{206}/U^{238} zircon age	0.282166	0.000028	0.001835	0.04603	0.282128	1.65	0.98	1.81	1.64
RDT16001-65.d	915	Pb^{206}/U^{238} zircon age	0.281907	0.000026	0.000126	0.00454	0.281905	-10.70	0.91	2.42	2.24
RDT16001-70.d	1087	Pb^{206}/U^{238} zircon age	0.281976	0.00003	0.001935	0.0551	0.281936	-5.69	1.05	2.24	2.07
RDT16001-71.d	1151	Pb^{206}/U^{238} zircon age	0.281912	0.000026	0.002646	0.0766	0.281855	-7.14	0.91	2.38	2.21
RDT16001-72.d	2581	Pb^{207}/Pb^{206} zircon age	0.281291	0.000036	0.0003674	0.010136	0.281273	5.15	1.26	2.76	2.63
RDT16001-82.d	896	Pb^{206}/U^{238} zircon age	0.281736	0.000034	0.001084	0.03041	0.281718	-17.75	1.19	2.83	2.66
RDT16001-83.d	1631 ± 20	weighted average of -83 and -84	0.281825	0.000033	0.000869	0.0265	0.281798	1.81	1.155	2.21	2.05
RDT16001-90.d	1163	Pb^{206}/U^{238} zircon age	0.281863	0.000037	0.000459	0.01124	0.281853	-6.93	1.295	2.38	2.21
RDT16001-92.d	977	Pb^{206}/U^{238} zircon age	0.282207	0.000029	0.001463	0.049	0.282180	0.46	1.015	1.78	1.60
RDT16001-103.d	~~1624~~	Pb^{207}/Pb^{206} zircon age	~~0.282294~~	~~0.000031~~	~~0.001402~~	~~0.0398~~	~~0.282251~~	~~17.71~~	~~1.085~~	~~1.23~~	~~1.06~~
RDT16001-104.d	1255	Pb^{206}/U^{238} zircon age	0.281959	0.000029	0.001299	0.0432	0.281928	-2.17	1.015	2.16	1.99
RDT16001-156.d	948	Pb^{206}/U^{238} zircon age	0.282122	0.000026	0.000685	0.02292	0.282110	-2.69	0.91	1.95	1.77
RDT16001-159.d	1017	Pb^{206}/U^{238} zircon age	0.281774	0.000029	0.001054	0.0331	0.281754	-13.75	1.015	2.68	2.51
RDT16001-160.d	1075	Pb^{206}/U^{238} zircon age	0.281826	0.00003	0.00214	0.07008	0.281783	-11.41	1.05	2.58	2.41

Supplementary Table 1 (continued). Main isotopes and ratios measured using the Multicollector (Hf analyses). Analyses highlighted either drilled through the target or coupled badly. Integrations may have been adjusted

RDT16001-161.d	1870	Pb^{207}/Pb^{206} zircon age	0.281799	0.000034	0.00126	0.03976	0.281754	5.74	1.19	2.16	2.00
RDT16001-162.d	471.1	Pb^{206}/U^{238} zircon age	0.281902	0.00003	0.001361	0.04118	0.281890	-21.19	1.05	2.73	2.54
RDT16001-173.d	1732	Pb^{206}/U^{238} zircon age	0.281614	0.000031	0.001008	0.0308	0.281581	-3.59	1.085	2.61	2.46
RDT16001-178.d	827	Pb^{206}/U^{238} zircon age	0.282113	0.000031	0.001188	0.0399	0.282095	-5.96	1.085	2.06	1.88
RDT16001-180.d	1235	Pb^{206}/U^{238} zircon age	0.281634	0.000026	0.00162	0.0479	0.281596	-14.39	0.91	2.88	2.72
RDT16001-184.d	937	Pb^{206}/U^{238} zircon age	0.281829	0.000028	0.001334	0.041	0.281805	-13.72	0.98	2.62	2.44
RDT16001-195.d	925.4	Pb^{206}/U^{238} zircon age	0.28209	0.000032	0.000424	0.0135	0.282083	-4.16	1.12	2.03	1.85
RDT16001-213.d	1132	Pb^{206}/U^{238} zircon age	~~0.281088~~	~~0.000036~~	~~0.001058~~	0.0341	~~0.281065~~	~~-35.55~~	~~1.26~~	~~4.07~~	~~3.91~~
RDT16001-214.d	937	Pb^{206}/U^{238} zircon age	0.281548	0.000057	0.001003	0.028	0.281530	-23.47	1.995	3.21	3.04
RDT16001-216.d	975	Pb^{206}/U^{238} zircon age	0.282418	0.000037	0.0010759	0.02617	0.282398	8.14	1.295	1.30	1.12
RDT16001-222.d	549.7	Pb^{206}/U^{238} zircon age	0.282125	0.000035	0.000686	0.0212	0.282118	-11.36	1.225	2.18	2.00
RDT16001-224.d	1617	Pb^{207}/Pb^{206} zircon age	0.281954	0.000026	0.00068	0.0219	0.281933	6.28	0.91	1.92	1.76
RDT16001-235.d	1025	Pb^{206}/U^{238} zircon age	0.281794	0.000031	0.001505	0.0456	0.281765	-13.17	1.085	2.65	2.48
RDT16001-239.d	906	Pb^{206}/U^{238} zircon age	0.282129	0.000035	0.001479	0.0454	0.282104	-3.85	1.225	1.99	1.81
RDT16001-240.d	1071	Pb^{206}/U^{238} zircon age	0.28151	0.000036	0.001012	0.0312	0.281490	-21.89	1.26	3.21	3.04
RDT16001-241.d	1571	Pb^{207}/Pb^{206} zircon age	0.281726	0.00003	0.001418	0.0435	0.281684	-3.62	1.05	2.49	2.33
RDT16001-242.d	1598	Pb^{207}/Pb^{206} zircon age	0.282035	0.000031	0.000582	0.01682	0.282017	8.83	1.085	1.75	1.59
RDT16001-243.d	548.5	Pb^{206}/U^{238} zircon age	0.281943	0.000032	0.000414	0.01333	0.281939	-17.73	1.12	2.57	2.39
RDT16001-246.d	1560	Pb^{207}/Pb^{206} zircon age	0.282235	0.000033	0.002138	0.06156	~~0.282172~~	~~13.44~~	~~1.155~~	~~1.44~~	~~1.28~~
RDT16001-256.d	625	Pb^{206}/U^{238} zircon age	0.282075	0.000026	0.001022	0.02751	0.282063	-11.62	0.91	2.26	2.07
RDT16001-257.d	2450	Pb^{207}/Pb^{206} zircon age	0.282135	0.00003	0.0013405	0.03729	0.282072	30.52	1.05	1.12	0.98
RDT16001-259.d	1224	Pb^{206}/U^{238} zircon age	0.281892	0.000032	0.000751	0.0223	0.281875	-4.77	1.12	2.29	2.12
RDT16001-262.d	1057	Pb^{206}/U^{238} zircon age	0.282175	0.000031	0.000862	0.0248	0.282158	1.48	1.085	1.78	1.60

Supplementary Table 2. LA–ICP–MS Analytical Method Information. Errors given as 2σ.

Analysis Batch Date	*Samples Analysed*	*Spot Size*	*Isotopes measured*	*Standard $^{206}Pb/^{238}U$ weighted averages*			
				GJ-1	*Plešovice*	*91500**	*MT*
25/1/2017	RDT15_078	25 µm	^{90}Zr, ^{202}Hg, ^{204}Pb, ^{206}Pb, ^{207}Pb, ^{208}Pb, ^{232}Th, ^{238}U	601.8±1.0 (*n*=72, MSWD=0.91)	342.8±1.1 (*n*=36, MSWD=2.3)	1033.3±3.2 (*n*=36, MSWD=1.4)	Not measured
19/5/2017	RDT15_078, RDT16_018, RDT16_019	30 µm	^{90}Zr, ^{139}La, ^{140}Ce, ^{141}Pr, ^{146}Nd, ^{146}Sm, ^{153}Eu, ^{157}Gd, ^{159}Tb, ^{163}Dy, ^{165}Ho, ^{166}Er, ^{169}Tm, ^{172}Yb, ^{175}Lu, ^{178}Hf, ^{202}Hg, ^{204}Pb, ^{206}Pb, ^{207}Pb, ^{208}Pb, ^{232}Th, ^{238}U	601.67±0.85 (*n*=112, MSWD=1.04)	330.7±1.5 (*n*=31, MSWD=2.1)	1016.7±4.6 (*n*=28, MSWD=1.7)	Not measured
At Curtin University 10/7/17	RDT16_006, RDT16_008, RDT16_018	50 µm	^{90}Zr, ^{202}Hg, ^{204}Pb, ^{206}Pb, ^{207}Pb, ^{208}Pb, ^{232}Th, ^{238}U	601.84 ± 1.28 (*n*=13, MSWD=0.02) Skewness = 0.31	Not measured	1058.03 ± 2.91 (*n*=13, MSWD=2.78) Skewness = 8.83	715.55 ± 3.29 (*n*=24, MSWD = 1.68, over dispersion) Skewness = 10.20
21/07/2017	RDT16_008, RDT16_018, RDT16_033, RDT16_035	30 µm	^{90}Zr, ^{139}La, ^{140}Ce, ^{141}Pr, ^{146}Nd, ^{146}Sm, ^{153}Eu, ^{157}Gd, ^{159}Tb, ^{163}Dy, ^{165}Ho, ^{166}Er, ^{169}Tm, ^{172}Yb, ^{175}Lu, ^{178}Hf, ^{202}Hg, ^{204}Pb, ^{206}Pb, ^{207}Pb, ^{208}Pb, ^{232}Th, ^{238}U	601.72±0.97 (*n*=132, MSWD=0.66)	338.6±1.3 (*n*=66, MSWD=2.4)	1035.2±4.6 (*n*=33, MSWD=1.3)	Not measured
28/09/2017	RDT16_012	30 µm	^{90}Zr, ^{201}Hg, ^{204}Pb, ^{206}Pb, ^{207}Pb, ^{208}Pb, ^{232}Th, ^{238}U	601.5±1.2 (*n*=52, MSWD=0.76)	343.2±1.3 (*n*=26, MSWD = 1.8)	1067.6±4.4 (*n*=13, MSWD=1.10)	Not measured

* The use of two different 91500 crystals for these analyses, where one crystal gives good reproducibility while the other is more heterogeneous, accounts for the younger age for the 91500 standard in three of the analysis batches. 91500 was used as one of two secondary standards and was not used as a primary standard to correct for isotopic drift and down-hole

Supplementary Table 3. Lu–Hf Standards and Analytical Runs. Errors given as 2σ.

Analysis Date	*Samples Analysed*	*Standard $^{176}Hf/^{177}Hf$ weighted averages*					*Standard Lu:Hf weighted average*
		MT	*R33*	*FC-1*	*GJ-1*	*91500*	*R33*
10/07/2017	RDT16_006, RDT16_008, RDT16_018,	0.2825070 ± 0.0000088 (*n*=24, MSWD=0.84)	0.282697 ± 0.000011 (*n*=24, MSWD=1.3)	0.282145 ± 0.000017 (n=15, MSWD=2.0)	0.282009 ± 0.000013 (n=15, MSWD=0.98)	0.282303 ± 0.000018 (n=15, MSWD=1.6)	0.001990 ± 0.000016 (n=24, MSWD=112)
11/07/2017	RDT15_066, RDT16_001, RDT16_019	0.2825071±0.0000081 (*n*=13, MSWD=0.041)	0.282708±0.000017 (*n*=14, MSWD = 3.6)	0.282159 ± 0.000019 (n=15, MSWD=4.9)	0.282001 ± 0.000019 (n=10, MSWD=2.7)	0.282291 ± 0.000011 (n=9, MSWD=0.16)	0.001988 ± 0.000040 (n=14, MSWD=101)

APPENDIX IV

Supplementary material for Chapter 4

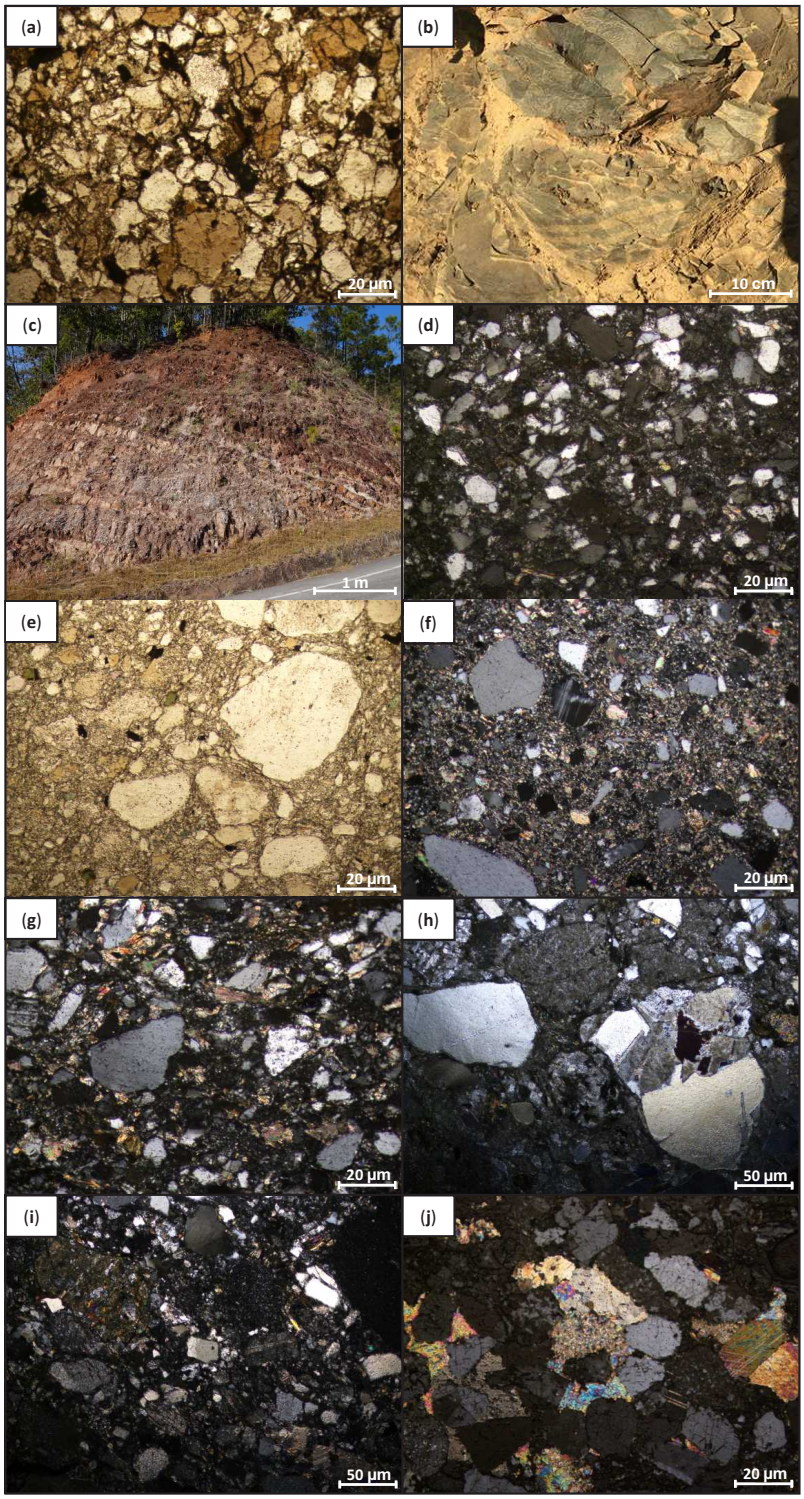

Supplementary Fig. 1. Thin sections, outcrop and hand specimens of samples. (a) RDT16_019 overview thin section image in Cross Polarised Light (XPL) (b) RDT16_006 field outcrop, (c) RDT16_012 field locality, (d) RDT16_012 overview thin section image in XPL, (e) RDT16_049 thin section image illustrating polyminerallic poorly sorted detritus in Plane Polarised Light (PPL) (f) RDT16_049 thin section image illustrating polyminerallic poorly sorted detritus in XPL, (g) RDT16_033 overview thin section image in XPL, (h) RDT16_035 image illustrating polyminerallic poorly sorted detritus in XPL, (i) RDT16_035 image illustrating polyminerallic variation in sorting across the thin section compared to (h) in XPL, (j) CM15_01 overview thin section image in XPL.

Supplementary Table 1. Main isotopes and ratios measured using LA–ICP–MS. Concordance 1 ($^{206}Pb/^{238}U/^{207}Pb/^{235}U$) and 2 ($^{206}Pb/^{238}U/^{207}Pb/^{206}Pb$).

Sample Name	Analysis Spot	U	Th	Th:U	Ratios							Ages						Concordance Calculations		Notes
					$^{207}Pb/^{235}U$	2σ	$^{206}Pb/^{238}U$	2σ	Rho	$^{207}Pb/^{206}Pb$	2σ	$^{207}Pb/^{235}U$	2σ	$^{206}Pb/^{238}U$	2σ	$^{207}Pb/^{206}Pb$	2σ	1	2	
RDT16_006	006 - 1	419.9	276.8	0.66	2.517	0.038	0.2015	0.0022	0.76802	0.09008	0.001	1276	11	1183	12	1425	22	92.71	83.02	
RDT16_006	006 - 10	224	312	1.39	8.6	0.15	0.3792	0.0036	0.48193	0.1648	0.003	2296	16	2073	17	2504	26	90.29	82.79	
RDT16_006	006 - 11	175	143	0.82	0.488	0.014	0.06051	0.00067	0.13587	0.0585	0.002	404.8	9.7	378.7	4.1	532	65	93.55	71.18	
RDT16_006	006 - 12	213	94.5	0.44	1.188	0.051	0.1212	0.0034	0.91127	0.0709	0.001	792	24	737	20	948	40	93.06	77.74	
RDT16_006	006 - 13	494	154	0.31	0.812	0.024	0.0922	0.0027	0.58429	0.0638	0.001	603	13	568	16	731	45	94.20	77.70	
RDT16_006	006 - 14	67.7	49.5	0.73	1.52	0.066	0.1373	0.0025	0.48145	0.0797	0.003	946	24	829	14	1202	72	87.63	68.97	
RDT16_006	006 - 15	183	109.5	0.60	0.761	0.025	0.0855	0.0016	0.57978	0.0642	0.002	573	14	528.9	9.6	735	57	92.30	71.96	YC1σ
RDT16_006	006 - 16	300	251	0.84	3.91	0.082	0.2501	0.0046	0.9275	0.11316	0.001	1614	17	1438	24	1849	18	89.10	77.77	
RDT16_006	006 - 17	212	318	1.50	0.771	0.028	0.0757	0.0013	0.45208	0.072	0.002	579	16	470.1	7.8	978	65	81.19	48.07	
RDT16_006	006 - 18	250	276	1.10	3.21	0.11	0.2309	0.0065	0.85404	0.1001	0.002	1457	26	1339	34	1623	28	91.90	82.50	
RDT16_006	006 - 19	522	227	0.43	0.662	0.021	0.0813	0.0022	0.86684	0.05897	0.001	515	13	504	13	568	38	97.86	88.73	
RDT16_006	006 - 2	166.5	271	1.63	0.865	0.02	0.1004	0.0012	0.46618	0.0622	0.001	632	11	616.9	6.9	689	41	97.61	89.54	
RDT16_006	006 - 20	380	222	0.58	8.141	0.11	0.3852	0.0034	0.74779	0.1528	0.002	2246	12	2101	16	2375	19	93.54	88.46	
RDT16_006	006 - 21	683	582	0.85	1.71	0.08	0.1571	0.0053	0.97646	0.078	0.001	1007	30	940	29	1143	31	93.35	82.24	
RDT16_006	006 - 22	790	1115	1.41	8.1	0.75	0.1849	0.0076	0.74776	0.315	0.021	2246	91	1093	41	3530	100	48.66	30.96	
RDT16_006	006 - 23	160.5	226	1.41	1.069	0.027	0.1118	0.0014	0.44414	0.0688	0.002	737	13	683.2	8.4	888	49	92.70	76.94	
RDT16_006	006 - 24	153.6	95.6	0.62	3.318	0.059	0.2602	0.0036	0.78855	0.0919	0.001	1484	14	1490	18	1469	27	100.40	101.43	
RDT16_006	006 - 25	265	64.5	0.24	0.973	0.018	0.10653	0.0011	0.35023	0.0666	0.001	689.6	9.4	652.6	6.3	817	39	94.63	79.88	
RDT16_006	006 - 27	127	117.4	0.92	0.522	0.019	0.06271	0.00075	0.15028	0.0604	0.002	425	13	392.1	4.6	607	80	92.26	64.60	
RDT16_006	006 - 28	99	108.2	1.09	1.249	0.036	0.1313	0.0021	0.63464	0.07	0.002	825	15	795	12	920	48	96.36	86.41	
RDT16_006	006 - 29	689	345	0.50	2.48	0.28	0.1508	0.0046	0.35723	0.126	0.015	1243	79	905	26	1870	190	72.81	48.40	
RDT16_006	006 - 30	63.1	42.5	0.67	0.36	0.028	0.03986	0.00081	0.59085	0.0656	0.005	316	22	252	5	750	150	79.75	33.60	
RDT16_006	006 - 31	577	162.5	0.28	3.47	0.21	0.2386	0.009	0.9739	0.1038	0.003	1504	50	1377	47	1680	53	91.56	81.96	
RDT16_006	006 - 32	123.7	97	0.78	8.3	0.12	0.3729	0.0047	0.70934	0.1618	0.002	2265	14	2042	22	2473	19	90.15	82.57	
RDT16_006	006 - 33	176	31.4	0.18	0.84	0.019	0.0941	0.0013	0.41166	0.064	0.001	619	11	579.7	7.7	732	44	93.65	79.19	
RDT16_006	006 - 34	394.8	167.7	0.42	2.13	0.19	0.161	0.011	0.99275	0.0946	0.003	1130	66	957	59	1518	54	84.69	63.04	
RDT16_006	006 - 35	414	158.5	0.38	4.14	0.12	0.2609	0.0057	0.94092	0.11393	0.001	1660	23	1494	29	1861	19	90.00	80.28	
RDT16_006	006 - 36	107	105	0.98	1.203	0.033	0.11908	0.0012	0.23549	0.0729	0.002	801	15	725.2	6.9	1004	61	90.54	72.23	
RDT16_006	006 - 37	154	164	1.06	10.57	0.3	0.4421	0.0067	0.6708	0.1728	0.003	2482	25	2359	30	2580	31	95.04	91.43	
RDT16_006	006 - 38	181.3	82.5	0.46	1.35	0.025	0.127	0.0015	0.58929	0.077	0.001	867	11	770.7	8.4	1122	31	88.89	68.69	
RDT16_006	006 - 39	1199	613	0.51	1.051	0.034	0.113	0.0031	0.97421	0.0672	0.001	728	17	690	18	845	23	94.78	81.66	
RDT16_006	006 - 4	46.12	45.43	0.99	0.315	0.023	0.03514	0.00068	0.23894	0.0655	0.005	279	18	222.6	4.2	800	170	79.78	27.83	discordant
RDT16_006	006 - 40	882	484	0.55	1.99	0.25	0.1275	0.0099	0.86789	0.1133	0.007	1112	94	772	56	1920	110	69.42	40.21	
RDT16_006	006 - 41	337	220	0.65	1.371	0.046	0.1324	0.0038	0.85287	0.0745	0.001	877	19	804	21	1060	33	91.68	75.85	
RDT16_006	006 - 42	187	44.3	0.24	0.662	0.021	0.0785	0.0016	0.22429	0.0616	0.002	515	13	487.3	9.8	662	70	94.62	73.61	
RDT16_006	006 - 43	237	421	1.78	2.593	0.064	0.2046	0.0043	0.74918	0.0909	0.001	1301	17	1200	23	1442	26	92.24	83.22	
RDT16_006	006 - 44	150	67.8	0.45	0.521	0.022	0.06488	0.001	0.61108	0.0586	0.002	425	15	405.2	6	541	73	95.34	74.90	
RDT16_006	006 - 45	422	465	1.10	0.3053	0.0085	0.04035	0.00042	0.12335	0.0539	0.002	271.2	6.5	255	2.6	353	63	94.03	72.24	YSG
RDT16_006	006 - 46	362	300	0.83	1.851	0.047	0.1403	0.0037	0.39834	0.0952	0.002	1062	17	846	21	1523	45	79.66	55.55	
RDT16_006	006 - 47	111	116	1.05	2.49	0.13	0.1622	0.0054	0.70444	0.1122	0.004	1266	38	968	30	1827	64	76.46	52.98	
RDT16_006	006 - 48	918	930	1.01	0.807	0.03	0.0833	0.0015	0.54955	0.0694	0.002	600	17	515.9	9	905	50	85.98	57.01	
RDT16_006	006 - 49	241	285	1.18	2.7	0.051	0.1929	0.0038	0.80571	0.101	0.001	1330	14	1136	21	1639	25	85.41	69.31	
RDT16_006	006 - 5	592	96	0.16	12.83	0.73	0.375	0.017	0.99461	0.245	0.004	2647	57	2047	80	3150	25	77.33	64.98	discordant
RDT16_006	006 - 50	203	211	1.04	1.118	0.033	0.103	0.0019	0.542	0.0786	0.002	760	16	632	11	1149	53	83.16	55.00	
RDT16_006	006 - 51	451.7	98.7	0.22	0.773	0.03	0.0917	0.0021	0.88399	0.0614	0.001	580	17	566	12	650	38	97.59	87.08	
RDT16_006	006 - 6	97	91.7	0.95	9.86	0.31	0.42	0.012	0.90283	0.1749	0.002	2424	30	2256	56	2604	22	93.07	86.64	
RDT16_006	006 - 7	215	380	1.77	4.36	0.15	0.2645	0.0072	0.8668	0.1192	0.002	1702	28	1518	35	1942	29	89.19	78.17	
RDT16_006	006 - 8	81.4	102	1.25	1.03	0.03	0.1041	0.0022	0.43935	0.0707	0.002	718	15	638	13	937	56	88.86	68.09	
RDT16_006	006 - 9	316.1	128.9	0.41	5.032	0.092	0.3088	0.0041	0.85651	0.1179	0.001	1824	16	1738	21	1923	19	95.29	90.38	
RDT16_006	RDT16006-273.d	108.2	91.2	0.84	1.33	0.053	0.1217	0.0022	0.32997	0.003	0.003	852	24	740	13	1103	83	86.85	67.09	

Supplementary Table 1. Main isotopes and ratios measured using LA–ICP–MS. Concordance 1 ($^{206}Pb/^{238}U/^{207}Pb/^{235}U$) and 2 ($^{206}Pb/^{238}U/^{207}Pb/^{206}Pb$).

RDT16_006	RDT16006-274.d	112.2	144.3	1.29	0.897	0.04	0.0989	0.0022	0.023882	0.0034	0.004	638	22	607	13	700	110	95.14	86.71	
RDT16_006	RDT16006-275.d	564	121.5	0.22	5.137	0.1	0.3299	0.0058	0.77912	0.0013	0.002	1836	17	1835	28	1826	25	99.95	100.49	
RDT16_006	RDT16006-276.d	1228	883	0.72	6.47	0.22	0.2615	0.0094	0.65461	0.0042	0.005	2029	31	1490	48	2626	42	73.44	56.74	
RDT16_006	RDT16006-277.d	773	183	0.24	0.877	0.021	0.0991	0.0016	0.25143	0.0016	0.002	639	11	609.1	9.6	711	53	95.32	85.67	
RDT16_006	RDT16006-278.d	334.6	44	0.13	1.208	0.032	0.1299	0.0023	0.48273	0.0016	0.002	801	14	788	13	816	51	98.38	96.57	
RDT16_006	RDT16006-279.d	767	279	0.36	1.612	0.024	0.1605	0.0024	0.49793	0.00097	0.001	975	9.4	959	13	1003	32	98.36	95.61	
RDT16_006	RDT16006-280.d	565	255.3	0.45	11.53	0.17	0.5024	0.0079	0.79513	0.0013	0.002	2563	14	2621	34	2507	19	102.26	104.55	
RDT16_006	RDT16006-281.d	2050	5190	2.53	1.052	0.052	0.0678	0.0025	0.94455	0.0022	0.002	714	25	422	15	1773	40	59.10	23.80	
RDT16_006	RDT16006-290.d	503	279	0.55	0.855	0.038	0.075	0.0017	-0.073093	0.0049	0.005	617	20	465.5	10	1158	95	75.45	40.20	
RDT16_006	RDT16006-291.d	930	337	0.36	1.665	0.032	0.161	0.003	0.70734	0.00098	0.001	994	12	962	17	1035	32	96.78	92.95	
RDT16_006	RDT16006-292.d	1383	1350	0.98	10.35	0.14	0.4513	0.0073	0.8209	0.0013	0.002	2465	13	2398	33	2502	20	97.28	95.84	
RDT16_006	RDT16006-293.d	424	504	1.19	9.54	0.24	0.4046	0.01	0.8678	0.0021	0.003	2383	25	2185	48	2572	24	91.69	84.95	
RDT16_006	RDT16006-294.d	226	195.9	0.87	1.636	0.039	0.1613	0.0028	0.33076	0.0017	0.002	982	15	965	15	1010	50	98.27	95.54	
RDT16_006	RDT16006-299.d	260	193.5	0.74	1.129	0.029	0.1179	0.0022	0.37458	0.0018	0.002	762	14	719	13	881	56	94.36	81.61	
RDT16_006	RDT16006-300.d	98.9	33.4	0.34	1	0.043	0.1072	0.002	0.12876	0.003	0.003	691	22	656	12	735	96	94.93	89.25	
RDT16_006	RDT16006-301.d	1120	87.4	0.08	2	0.22	0.1456	0.0096	0.98288	0.0038	0.004	993	67	865	53	1230	82	87.11	70.33	
RDT16_006	RDT16006-302.d	177.6	217.9	1.23	4.17	0.088	0.2881	0.005	0.5149	0.0018	0.002	1662	17	1630	25	1689	35	98.07	96.51	
RDT16_006	RDT16006-303.d	803	92.6	0.12	0.692	0.015	0.0827	0.0013	0.40285	0.0012	0.001	533	8.8	511.9	7.8	616	47	96.04	83.10	
RDT16_006	RDT16006-312.d	125.2	82.4	0.66	9.95	0.2	0.4207	0.008	0.61903	0.0028	0.003	2425	19	2260	36	2567	31	93.20	88.04	
RDT16_006	RDT16006-313.d	234.9	114.4	0.49	0.867	0.028	0.1014	0.0017	0.34517	0.002	0.002	631	15	622.4	10	635	69	98.64	98.02	
RDT16_006	RDT16006-314.d	396.6	174.9	0.44	3.877	0.072	0.2768	0.0047	0.65754	0.0014	0.002	1606	15	1574	24	1632	30	98.01	96.45	
RDT16_006	RDT16006-315.d	665.7	179.4	0.27	5.214	0.078	0.3261	0.0055	0.76828	0.0012	0.002	1852	13	1817	27	1890	24	98.11	96.14	
RDT16_006	RDT16006-316.d	658.1	37.5	0.06	1.521	0.043	0.1499	0.0029	0.72941	0.0013	0.001	934	17	900	16	1019	40	96.36	88.32	
RDT16_006	RDT16006-317.d	366	176.4	0.48	1.426	0.089	0.0988	0.0017	0.49119	0.0053	0.005	869	34	607	10	1518	91	69.85	39.99	
RDT16_006	RDT16006-318.d	42.5	12.23	0.29	0.829	0.063	0.0903	0.0027	0.17747	0.0053	0.005	585	37	556	16	590	160	95.04	94.24	
RDT16_006	RDT16006-319.d	1154	89	0.08	1.382	0.02	0.1441	0.0022	0.58221	0.00083	0.001	879.8	8.6	867	12	904	30	98.55	95.91	
RDT16_006	RDT16006-320.d	1272	214.1	0.17	4.25	0.16	0.2247	0.006	0.91247	0.0022	0.003	1658	33	1303	32	2136	34	78.59	61.00	
RDT16_006	RDT16006-322.d	761	520	0.68	0.776	0.03	0.0788	0.0014	0.44995	0.0025	0.003	580	17	489.7	8.3	928	71	84.43	52.77	
RDT16_006	RDT16006-323.d	1697	81.6	0.05	8.1	0.28	0.3896	0.0095	0.93839	0.0022	0.003	2215	34	2114	44	2309	30	95.44	91.55	
RDT16_006	RDT16006-324.d	422	107.6	0.25	2.867	0.1	0.2263	0.0056	0.86526	0.0015	0.002	1355	27	1312	29	1419	36	96.83	92.46	
RDT16_006	RDT16006-325.d	424.9	210.5	0.50	12.49	0.2	0.5006	0.0094	0.72439	0.0022	0.003	2640	16	2612	40	2672	24	98.94	97.75	
RDT16_006	RDT16006-326.d	254	117.9	0.46	3.711	0.072	0.2464	0.0044	0.62162	0.0017	0.002	1568	15	1418	23	1767	33	90.43	80.25	
RDT16_006	RDT16006-327.d	622	176.9	0.28	9.32	0.18	0.4098	0.0074	0.82498	0.0016	0.002	2363	18	2213	35	2487	21	93.65	88.98	
RDT16_006	RDT16006-328.d	481	106	0.22	1.95	0.051	0.1721	0.0034	0.65764	0.0015	0.002	1093	18	1022	19	1226	40	93.50	83.36	
RDT16_006	RDT16006-338.d	612	187	0.31	1.654	0.031	0.1655	0.0027	0.63048	0.001	0.001	988	12	987	15	982	34	99.90	100.51	
RDT16_006	RDT16006-339.d	314.3	127.9	0.41	0.84	0.021	0.0954	0.0017	0.22738	0.0016	0.002	617	12	586.8	9.8	695	60	95.11	84.43	
RDT16_006	RDT16006-340.d	199.8	212.4	1.06	1.433	0.038	0.147	0.0025	0.28695	0.0018	0.002	897	16	884	14	906	57	98.55	97.57	
RDT16_006	RDT16006-341.d	80	134.4	1.68	1.951	0.073	0.1599	0.0032	0.2403	0.0033	0.003	1089	25	955	18	1326	80	87.70	72.02	
RDT16_006	RDT16006-342.d	1344	146.3	0.11	5.21	0.22	0.2208	0.0081	0.96538	0.0022	0.003	1818	40	1279	43	2529	26	70.35	50.57	
RDT16_006	RDT16006-343.d	190	66.2	0.35	0.902	0.035	0.107	0.0021	0.30761	0.0023	0.002	644	18	655	12	572	83	101.71	114.51	
RDT16_006	RDT16006-344.d	605.9	92.7	0.15	3.745	0.061	0.2372	0.0037	0.69979	0.0013	0.002	1577	13	1371	19	1860	26	86.94	73.71	
RDT16_006	RDT16006-345.d	91.6	115.4	1.26	2.139	0.056	0.1972	0.004	0.31243	0.0022	0.002	1155	18	1159	21	1135	56	100.35	102.11	
RDT16_006	RDT16006-346.d	82.8	35.89	0.43	1.252	0.053	0.1163	0.0025	-0.083785	0.0038	0.004	812	24	709	14	1040	100	87.32	68.17	
RDT16_006	RDT16006-347.d	331	237.3	0.72	3.294	0.06	0.2413	0.0041	0.60951	0.0014	0.002	1477	14	1392	21	1584	30	94.25	87.88	
RDT16_006	RDT16006-348.d	352	679	1.93	0.961	0.047	0.0882	0.0015	0.14142	0.004	0.004	677	23	545.6	9.2	1070	94	80.59	50.99	
RDT16_006	RDT16006-349.d	109.1	154.7	1.42	0.698	0.036	0.0846	0.0018	0.13381	0.0031	0.003	528	22	523	11	490	110	99.05	106.73	YC1σ
RDT16_006	RDT16006-359.d	538.9	317.9	0.59	0.701	0.016	0.0855	0.0014	0.36185	0.0012	0.001	537.5	9.3	528.9	8.5	556	49	98.40	95.13	YC1σ
RDT16_006	RDT16006b-10.d	734.1	73	0.10	1.608	0.035	0.1402	0.0022	0.49947	0.00098	0.001	972.2	14	845.5	12	1264	34	86.97	66.89	
RDT16_006	RDT16006b-14.d	379.1	237.3	0.63	1.191	0.035	0.1263	0.0019	0.28405	0.0016	0.002	793	16	766.4	11	857	52	96.65	89.43	
RDT16_006	RDT16006b-15.d	1158	1278	1.10	3.36	0.17	0.1722	0.0072	0.98023	0.0017	0.003	1458	40	1018	39	2209	31	69.82	46.08	
RDT16_006	RDT16006b-16.d	2372	1497	0.63	0.871	0.028	0.06192	0.0011	0.26383	0.0029	0.003	634	15	387.2	6.7	1635	55	61.07	23.68	
RDT16_006	RDT16006b-17.d	604	431	0.71	11.09	0.52	0.417	0.018	0.97909	0.0014	0.003	2497	40	2222	81	2760	24	88.99	80.51	
RDT16_006	RDT16006b-18.d	504.6	33.1	0.07	2.509	0.065	0.1761	0.0035	0.79315	0.0011	0.002	1271	19	1044	19	1680	31	82.14	62.14	
RDT16_006	RDT16006b-19.d	384	186.5	0.49	3.81	0.2	0.204	0.0087	0.96964	0.0019	0.003	1556	41	1189	46	2119	34	76.41	56.11	

Supplementary Table 1. Main isotopes and ratios measured using LA–ICP–MS. Concordance 1 ($^{206}Pb/^{238}U/^{207}Pb/^{235}U$) and 2 ($^{206}Pb/^{238}U/^{207}Pb/^{206}Pb$).

RDT16_006	RDT16006b-20.d	280.4	235.7	0.84	4.534	0.1	0.3075	0.0045	0.45245	0.0012	0.002	1734	18	1728	22	1734	31	99.65	99.65	
RDT16_006	RDT16006b-21.d	1597	889	0.56	2.13	0.18	0.1083	0.0027	0.85113	0.0082	0.008	1122	52	666	17	2085	92	59.36	31.94	
RDT16_006	RDT16006b-22.d	2264	1116	0.49	0.634	0.02	0.0625	0.0014	0.79038	0.0011	0.001	497	12	390.7	8.5	1009	43	78.61	38.72	
RDT16_006	RDT16006b-23.d	907	483	0.53	9.84	0.3	0.392	0.01	0.96477	0.0011	0.003	2408	29	2125	48	2664	24	88.25	79.77	
RDT16_006	RDT16006b-24.d	145	124.6	0.86	3	0.13	0.16	0.0029	0.53637	0.0046	0.005	1387	33	956	16	2101	65	68.93	45.50	
RDT16_006	RDT16006b-25.d	108.1	128.8	1.19	1.298	0.061	0.093	0.0017	0.33405	0.0042	0.004	833	25	573.7	10	1610	80	68.87	35.63	
RDT16_006	RDT16006b-26.d	219	121.8	0.56	2.25	0.19	0.1652	0.005	0.3403	0.0071	0.007	1139	45	986	27	1403	92	86.57	70.28	
RDT16_006	RDT16006b-34.d	383	281	0.73	10.41	0.22	0.4654	0.0074	0.78327	0.0012	0.002	2470	20	2461	32	2468	25	99.64	99.72	
RDT16_006	RDT16006b-35.d	502.8	89.7	0.18	1.665	0.039	0.1599	0.0024	0.57613	0.00093	0.001	992.8	15	955.8	13	1069	35	96.27	89.41	
RDT16_006	RDT16006b-36.d	2073	1288	0.62	1.389	0.051	0.1146	0.0035	0.95105	0.00086	0.001	875	22	698	20	1361	31	79.77	51.29	
RDT16_006	RDT16006b-37.d	86.1	46.4	0.54	1.994	0.076	0.1441	0.0028	0.12227	0.0035	0.004	1103	25	869	16	1581	71	78.79	54.97	
RDT16_006	RDT16006b-38.d	317	45.8	0.14	1.474	0.044	0.1487	0.0029	0.69352	0.0012	0.002	914	18	893	16	958	42	97.70	93.22	
RDT16_006	RDT16006b-39.d	141.9	57.9	0.41	1.167	0.048	0.0852	0.0017	0.15731	0.0036	0.004	775	22	526.8	10	1546	70	67.97	34.08	
RDT16_006	RDT16006b-40.d	987	207	0.21	6.66	0.38	0.304	0.016	0.98347	0.0022	0.003	1985	65	1686	83	2407	34	84.94	70.05	
RDT16_006	RDT16006b-41.d	164.8	115.7	0.70	2.084	0.058	0.177	0.0036	0.27222	0.002	0.002	1142	18	1050	20	1310	53	91.94	80.15	
RDT16_012	RDT16012_0	220.6	60.9	0.28	2.061	0.064	0.1706	0.0037	0.81535	0.0887	0.002	1130	21	1016	20	1388	39	89.91	89.91	
RDT16_012	RDT16012_1	1011	401	0.40	0.56	0.018	0.0489	0.0011	0.74712	0.0834	0.002	449	12	307.8	6.9	1277	45	68.55	68.55	
RDT16_012	RDT16012_10	129	142.8	1.11	1.252	0.043	0.1095	0.0019	0.48589	0.082	0.002	819	19	669	11	1216	59	81.68	81.68	
RDT16_012	RDT16012_11	259.2	103.4	0.40	3.45	0.39	0.1651	0.0031	0.85855	0.14	0.013	1349	77	984	17	1800	150	72.94	72.94	
RDT16_012	RDT16012_12	243.8	45.08	0.18	1.619	0.037	0.1623	0.0018	0.27367	0.072	0.002	975.4	14	969.2	9.7	970	43	99.36	99.36	
RDT16_012	RDT16012_13	81.5	29.93	0.37	0.581	0.025	0.0661	0.0011	0.005255	0.0635	0.003	461	16	412.3	6.8	640	95	89.44	89.44	
RDT16_012	RDT16012_14	76.42	107.72	1.41	9.9	0.23	0.4317	0.0057	0.64968	0.1652	0.003	2424	21	2311	26	2505	30	95.34	95.34	
RDT16_012	RDT16012_15	71.9	26.61	0.37	1.744	0.054	0.1687	0.0023	0.25109	0.0756	0.002	1022	20	1004	12	1044	59	98.24	98.24	
RDT16_012	RDT16012_16	36.08	23.36	0.65	1.072	0.086	0.0577	0.0013	0.26887	0.1332	0.010	701	42	361.4	7.9	1830	150	51.55	51.55	
RDT16_012	RDT16012_17	934	517	0.55	1.477	0.031	0.147	0.0017	0.74586	0.07289	0.001	919.7	13	884	9.6	1009	33	96.12	96.12	
RDT16_012	RDT16012_18	451.8	118.1	0.26	1.892	0.041	0.177	0.0023	0.53423	0.07752	0.001	1076.7	14	1050	13	1126	37	97.52	97.52	
RDT16_012	RDT16012_19	26.11	18.85	0.72	2.7	0.11	0.1986	0.0033	0.11461	0.0998	0.004	1314	32	1166	18	1523	84	88.74	88.74	
RDT16_012	RDT16012_2	444	311.1	0.70	1.292	0.029	0.1384	0.0016	0.5061	0.06839	0.001	840.4	13	835.2	9	870	39	99.38	99.38	
RDT16_012	RDT16012_20	65.7	27.66	0.42	4.941	0.13	0.2926	0.0053	0.54147	0.1227	0.003	1804	22	1652	26	1983	41	91.57	91.57	
RDT16_012	RDT16012_21	969	277.6	0.29	0.5059	0.012	0.0632	0.001	0.57497	0.05824	0.001	414.8	8.3	395	6.3	527	47	95.23	95.23	
RDT16_012	RDT16012_22	770	848	1.10	1.988	0.096	0.1485	0.006	0.959	0.0959	0.002	1087	33	888	34	1538	34	81.69	81.69	
RDT16_012	RDT16012_23	53.17	36.21	0.68	1.622	0.057	0.1502	0.0024	0.14116	0.0788	0.003	969	22	902	13	1092	73	93.09	93.09	YC1σ(3+)
RDT16_012	RDT16012_24	346.2	223.8	0.65	1.06	0.12	0.0571	0.0011	0.85804	0.127	0.012	675	51	358.1	6.8	1670	140	53.05	53.05	
RDT16_012	RDT16012_25	624.6	408	0.65	1.505	0.046	0.1353	0.0016	0.33774	0.0806	0.002	931	18	817.6	9.3	1194	52	87.82	87.82	
RDT16_012	RDT16012_26	246.2	139.2	0.57	0.808	0.031	0.07222	0.001	0.48842	0.0807	0.003	595	18	450	6	1161	69	75.63	75.63	
RDT16_012	RDT16012_27	50	25.34	0.51	12.97	0.38	0.475	0.011	0.85082	0.197	0.004	2664	29	2498	47	2796	31	93.77	93.77	
RDT16_012	RDT16012_28	1121	247	0.22	0.2394	0.0059	0.03257	0.00037	0.21967	0.05345	0.001	217.6	4.8	206.6	2.3	329	51	94.94	94.94	YSG
RDT16_012	RDT16012_29	477.1	130.9	0.27	0.2709	0.011	0.03398	0.00039	0.12033	0.0586	0.002	242	8.2	215.4	2.4	494	81	89.01	89.01	
RDT16_012	RDT16012_3	211.4	92.1	0.44	6.236	0.13	0.3643	0.004	0.63291	0.1251	0.002	2007.4	18	2001	19	2026	30	99.68	99.68	
RDT16_012	RDT16012_30	451.3	81.6	0.18	0.2637	0.009	0.03494	0.00044	0.23819	0.0552	0.002	237.4	7.3	221.4	2.7	380	70	93.26	93.26	YC1σ(2+)
RDT16_012	RDT16012_31	299.7	38.43	0.13	2.184	0.048	0.1991	0.0024	0.48229	0.0799	0.002	1174.8	15	1170	13	1183	37	99.59	99.59	
RDT16_012	RDT16012_32	516	184.4	0.36	8.36	0.23	0.3758	0.0073	0.93984	0.1611	0.003	2261	26	2052	34	2466	26	90.76	90.76	
RDT16_012	RDT16012_33	200	104.67	0.52	4.375	0.094	0.3002	0.0033	0.51385	0.1058	0.002	1705	18	1691	16	1723	33	99.18	99.18	
RDT16_012	RDT16012_34	291.2	132.7	0.46	0.936	0.023	0.1073	0.0012	0.34635	0.0634	0.001	670.7	12	656.6	7	702	49	97.90	97.90	
RDT16_012	RDT16012_35	570	183	0.32	0.2499	0.0076	0.03477	0.00045	0.24923	0.0518	0.002	226.3	6.3	220.3	2.8	250	62	97.35	97.35	YC1σ(2+)
RDT16_012	RDT16012_36	305.3	96.59	0.32	1.463	0.035	0.1517	0.0017	0.44146	0.0699	0.001	912.7	14	910.3	9.7	912	42	99.74	99.74	YC1σ(3+)
RDT16_012	RDT16012_37	120.5	102.1	0.85	8.04	0.18	0.3949	0.0054	0.7447	0.1475	0.003	2231	21	2143	25	2311	30	96.06	96.06	
RDT16_012	RDT16012_38	686	245.5	0.36	2.201	0.046	0.201	0.0022	0.69281	0.07926	0.001	1179.8	15	1180	12	1173	33	100.02	100.02	
RDT16_012	RDT16012_39	127.7	87.4	0.68	4.718	0.11	0.3146	0.004	0.52213	0.1086	0.002	1766	19	1762	20	1773	34	99.77	99.77	
RDT16_012	RDT16012_4	359	370	1.03	0.739	0.019	0.08931	0.001	0.31946	0.0604	0.001	560.7	11	551.3	6.1	599	50	98.32	98.32	
RDT16_012	RDT16012_40	224.3	124.6	0.56	0.34	0.013	0.04283	0.0006	0.25609	0.0576	0.002	294.9	10	270.3	3.7	454	79	91.66	91.66	
RDT16_012	RDT16012_41	261.2	178.8	0.68	0.243	0.009	0.03373	0.00048	0.17974	0.0523	0.002	220.5	7.6	213.8	3	253	78	96.96	96.96	YC
RDT16_012	RDT16012_42	192	75.2	0.39	0.976	0.027	0.1106	0.0015	0.16052	0.0636	0.002	691	14	676.1	8.5	715	58	97.84	97.84	
RDT16_012	RDT16012_43	199.9	121.2	0.61	2.904	0.065	0.2407	0.0025	0.42334	0.0869	0.002	1380	17	1390	13	1352	38	100.72	100.72	

Supplementary Table 1. Main isotopes and ratios measured using LA–ICP–MS. Concordance 1 ($^{206}Pb/^{238}U/^{207}Pb/^{235}U$) and 2 ($^{206}Pb/^{238}U/^{207}Pb/^{206}Pb$).

RDT16_012	RDT16012_44	617	897	1.45	0.63	0.036	0.04293	0.0008	0.1619	0.1028	0.005	485	22	270.9	5	1555	87	55.86	55.86	
RDT16_012	RDT16012_45	75.81	66.89	0.88	6.796	0.15	0.3815	0.0045	0.57074	0.1284	0.002	2086	21	2082	21	2071	33	99.81	99.81	
RDT16_012	RDT16012_46	417.5	64.1	0.15	6.366	0.13	0.3606	0.0041	0.69962	0.1262	0.002	2025.7	18	1984	20	2043	29	97.94	97.94	
RDT16_012	RDT16012_47	309	327	1.06	2.648	0.057	0.2201	0.0024	0.43777	0.0862	0.002	1313.9	16	1282	13	1335	36	97.57	97.57	
RDT16_012	RDT16012_48	360.5	219.6	0.61	7.638	0.15	0.3997	0.0042	0.7198	0.13693	0.002	2188.2	18	2166	19	2185	28	98.99	98.99	
RDT16_012	RDT16012_49	145.9	170.2	1.17	4.094	0.091	0.292	0.0036	0.41905	0.1007	0.002	1655	19	1650	18	1624	37	99.70	99.70	
RDT16_012	RDT16012_5	166	105.66	0.64	0.776	0.023	0.0937	0.0012	0.28176	0.0605	0.002	581	13	577.1	7.2	590	57	99.33	99.33	
RDT16_012	RDT16012_50	283.1	235.6	0.83	1.95	0.043	0.1836	0.0019	0.40703	0.0757	0.002	1096.3	15	1086.4	10	1077	40	99.10	99.10	
RDT16_012	RDT16012_51	160.5	84.6	0.53	3.52	0.12	0.2218	0.0029	0.29313	0.1136	0.004	1523	26	1292	15	1819	55	84.83	84.83	
RDT16_012	RDT16012_52	384.5	72.1	0.19	2.533	0.055	0.2181	0.0028	0.67643	0.08296	0.002	1281.3	16	1271	15	1264	35	99.20	99.20	
RDT16_012	RDT16012_53	94.2	153.3	1.63	2.428	0.066	0.2041	0.0029	0.13155	0.0852	0.002	1247	19	1196	16	1291	53	95.91	95.91	
RDT16_012	RDT16012_54	757	146	0.19	1.924	0.046	0.1806	0.003	0.82068	0.0755	0.001	1087	16	1070	16	1078	35	98.44	98.44	
RDT16_012	RDT16012_55	487	395	0.81	2.031	0.05	0.1722	0.003	0.78463	0.08413	0.002	1124	17	1023	17	1286	35	91.01	91.01	
RDT16_012	RDT16012_56	320.4	391.3	1.22	0.587	0.017	0.06887	0.0009	0.30312	0.0607	0.002	467.7	11	429.2	5.4	608	56	91.77	91.77	
RDT16_012	RDT16012_57	821.4	222.7	0.27	0.7471	0.016	0.09166	0.00099	0.39762	0.05826	0.001	565.7	9.4	565.2	5.8	532	41	99.91	99.91	
RDT16_012	RDT16012_58	94.82	21.4	0.23	1.588	0.048	0.1638	0.0022	0.26317	0.0718	0.002	961	19	980	13	952	59	101.98	101.98	
RDT16_012	RDT16012_59	67.9	88	1.30	1.164	0.056	0.1107	0.0017	0.21346	0.0789	0.004	774	26	676.1	10	1046	95	87.35	87.35	
RDT16_012	RDT16012_6	759.9	69.8	0.09	0.809	0.018	0.0971	0.0011	0.4114	0.06056	0.001	601.2	10	597.3	6.3	616	42	99.35	99.35	
RDT16_012	RDT16012_60	479.5	302.9	0.63	0.4042	0.01	0.05456	0.00062	0.2514	0.0547	0.001	343.9	7.5	342.4	3.8	373	52	99.56	99.56	
RDT16_012	RDT16012_61	214.9	145.1	0.68	2.155	0.049	0.1987	0.0025	0.44804	0.0799	0.002	1165	16	1168	14	1189	40	100.26	100.26	
RDT16_012	RDT16012_62	127	150.4	1.18	2.147	0.056	0.1981	0.0025	0.38048	0.0802	0.002	1159	18	1164	13	1175	48	100.43	100.43	
RDT16_012	RDT16012_63	217.5	161.6	0.74	1.909	0.045	0.1792	0.0022	0.30101	0.0785	0.002	1081	16	1063	12	1162	43	98.33	98.33	
RDT16_012	RDT16012_64	440.2	439	1.00	0.703	0.017	0.08635	0.00089	0.43393	0.06001	0.001	539	10	533.8	5.3	595	46	99.04	99.04	
RDT16_012	RDT16012_65	452.3	243.5	0.54	8.135	0.16	0.3668	0.0039	0.77431	0.1636	0.003	2244.4	18	2013	18	2490	26	89.69	89.69	
RDT16_012	RDT16012_66	639	373	0.58	5.35	0.21	0.2661	0.0083	0.95907	0.1478	0.003	1858	32	1514	42	2316	29	81.49	81.49	
RDT16_012	RDT16012_67	206	178.7	0.87	3.991	0.097	0.2795	0.0047	0.79671	0.106	0.002	1632	19	1587	24	1723	33	97.24	97.24	
RDT16_012	RDT16012_68	187.4	194.1	1.04	0.743	0.022	0.0933	0.0012	0.20415	0.059	0.002	563	13	574.7	7	524	62	102.08	102.08	
RDT16_012	RDT16012_69	179.2	197	1.10	1.93	0.054	0.1707	0.0024	0.52112	0.0833	0.002	1086	19	1015	13	1259	45	93.46	93.46	
RDT16_012	RDT16012_7	689	26.43	0.04	1.51	0.033	0.1515	0.0017	0.49128	0.07236	0.001	933	13	908.9	9.3	986	37	97.42	97.42	YC1σ(3+)
RDT16_012	RDT16012_70	807	233.9	0.29	1.306	0.045	0.1359	0.0036	0.90673	0.07009	0.001	840	20	820	20	918	39	97.62	97.62	
RDT16_012	RDT16012_71	149.5	96.7	0.65	10.62	0.23	0.4709	0.0056	0.62716	0.1611	0.003	2487	20	2485	25	2464	28	99.92	99.92	
RDT16_012	RDT16012_72	153.8	115.9	0.75	1.797	0.048	0.172	0.002	0.35508	0.0747	0.002	1041	17	1022	11	1047	49	98.17	98.17	
RDT16_012	RDT16012_73	277.1	80.7	0.29	1.375	0.039	0.1405	0.0023	0.76602	0.0699	0.001	875	17	847	13	913	42	96.80	96.80	
RDT16_012	RDT16012_74	166.5	121.4	0.73	2.245	0.052	0.2022	0.0023	0.26757	0.0795	0.002	1192	16	1186	12	1169	43	99.50	99.50	
RDT16_012	RDT16012_75	45.86	56.73	1.24	0.734	0.041	0.0816	0.0015	0.055931	0.0649	0.004	546	24	505.4	9.2	610	120	92.56	92.56	
RDT16_012	RDT16012_76	320.2	176.4	0.55	1.48	0.035	0.153	0.0017	0.44055	0.0692	0.001	919.9	14	917.5	9.7	887	43	99.74	99.74	
RDT16_012	RDT16012_77	417.3	117.44	0.28	9.067	0.18	0.4165	0.0044	0.7061	0.1559	0.002	2344.7	18	2243	20	2409	27	95.66	95.66	
RDT16_012	RDT16012_78	265.1	66.83	0.25	0.352	0.013	0.04387	0.00059	0.11835	0.058	0.002	305.6	9.7	276.7	3.6	470	78	90.54	90.54	
RDT16_012	RDT16012_79	476.2	448	0.94	2.881	0.077	0.2289	0.0037	0.89321	0.08989	0.002	1372	21	1327	20	1418	33	96.72	96.72	
RDT16_012	RDT16012_8	456.5	192.4	0.42	1.616	0.036	0.1605	0.0019	0.61614	0.07298	0.001	975.4	14	959.1	11	1004	36	98.33	98.33	
RDT16_012	RDT16012_80	1026	762	0.74	1.229	0.034	0.1217	0.0025	0.87672	0.07262	0.001	810	15	739	15	995	35	91.23	91.23	
RDT16_012	RDT16012_81	101.9	137.7	1.35	0.786	0.03	0.0895	0.0014	0.15051	0.0629	0.002	583	17	552.3	8.5	653	79	94.73	94.73	
RDT16_012	RDT16012_82	1073	188.7	0.18	0.787	0.018	0.0838	0.0013	0.68561	0.0676	0.001	588.1	10	518.7	7.9	845	38	88.20	88.20	
RDT16_012	RDT16012_83	158.5	151	0.95	1.47	0.041	0.1461	0.002	0.43437	0.0727	0.002	916	16	879	11	982	50	95.96	95.96	
RDT16_012	RDT16012_84	1175	1372	1.17	0.516	0.015	0.05845	0.001	0.71885	0.06356	0.001	422.1	9.5	366	6.2	715	41	86.71	86.71	
RDT16_012	RDT16012_85	270.7	169.2	0.63	0.731	0.021	0.08379	0.001	0.15721	0.0627	0.002	554.6	12	518.6	6.1	660	60	93.51	93.51	
RDT16_012	RDT16012_86	716	118.4	0.17	1.132	0.079	0.1004	0.0031	0.94694	0.077	0.003	737	35	616	18	1024	79	83.58	83.58	
RDT16_012	RDT16012_87	266	208	0.78	1.974	0.044	0.1866	0.0023	0.48239	0.0763	0.002	1105.5	15	1102	12	1093	39	99.68	99.68	
RDT16_012	RDT16012_88	150.2	74.84	0.50	0.631	0.024	0.08	0.0011	0.15808	0.0575	0.002	494	15	495.7	6.7	435	80	100.34	100.34	
RDT16_012	RDT16012_89	619.9	12.2	0.02	2.718	0.055	0.2289	0.0025	0.61074	0.0855	0.001	1333.6	15	1328	13	1323	33	99.58	99.58	
RDT16_012	RDT16012_9	2833	2845	1.00	5.565	0.12	0.1591	0.0024	0.92505	0.2522	0.004	1908	19	951	13	3196.5	24	49.84	49.84	
RDT16_012	RDT16012_90	338.5	497.7	1.47	1.552	0.037	0.1561	0.0021	0.66088	0.07194	0.001	948	15	934	12	981	36	98.52	98.52	
RDT16_012	RDT16012_91	519	306	0.59	3.074	0.074	0.2213	0.0034	0.84345	0.10007	0.002	1422	19	1287	18	1619	32	90.51	90.51	
RDT16_012	RDT16012_92	732	108.1	0.15	0.3838	0.0094	0.04881	0.0005	0.32021	0.05674	0.001	329.2	6.9	307.2	3.1	459	48	93.32	93.32	

Supplementary Table 1. Main isotopes and ratios measured using LA–ICP–MS. Concordance 1 ($^{206}Pb/^{238}U/^{207}Pb/^{235}U$) and 2 ($^{206}Pb/^{238}U/^{207}Pb/^{206}Pb$).

RDT16_012	RDT16012_93	301	244	0.81	0.529	0.016	0.0663	0.00089	0.20173	0.058	0.002	429	11	413.7	5.4	490	62	96.43	96.43	
RDT16_012	RDT16012_94	53.06	57.3	1.08	2.141	0.069	0.1889	0.0028	0.17017	0.0823	0.003	1155	23	1115	15	1216	64	96.54	96.54	
RDT16_012	RDT16012_95	462.4	403.9	0.87	2.255	0.052	0.1896	0.0022	0.51345	0.0858	0.002	1197	16	1119	12	1328	37	93.48	93.48	
RDT16_012	RDT16012_96	207	222.2	1.07	1.57	0.072	0.1066	0.0032	-0.41424	0.1127	0.008	945	27	651	18	1680	110	68.89	68.89	
RDT16_019	RDT16019-100.d	270.3	178.9	0.66	1.216	0.038	0.1208	0.002	0.37189	0.0726	0.002	804	17	734.9	11	974	55	91.41	75.45	
RDT16_019	RDT16019-101.d	515.6	129.3	0.25	1.238	0.032	0.1275	0.0022	0.60836	0.0701	0.001	816	14	773	13	922	39	94.73	83.84	
RDT16_019	RDT16019-103.d	27.52	9.2	0.33	2.43	0.19	0.112	0.0029	0.27355	0.157	0.011	1178	55	683	17	2110	150	57.98	32.37	
RDT16_019	RDT16019-104.d	46.5	100.6	2.16	1.358	0.068	0.1398	0.0029	0.034546	0.071	0.004	857	29	843	16	830	100	98.37	101.57	
RDT16_019	RDT16019-105.d	574	147.9	0.26	10.91	0.28	0.4697	0.0085	0.86865	0.1672	0.003	2508	24	2479	37	2526	26	98.84	98.14	
RDT16_019	RDT16019-106.d	203.2	94.1	0.46	1.381	0.039	0.1373	0.0022	0.16343	0.0727	0.002	877	17	829.3	12	979	53	94.56	84.71	
RDT16_019	RDT16019-107.d	295.2	33.8	0.11	0.897	0.027	0.1004	0.0018	0.2422	0.0649	0.002	647	15	616.4	10	738	60	95.27	83.52	
RDT16_019	RDT16019-108.d	648	366	0.56	0.746	0.021	0.0871	0.0015	0.47567	0.0618	0.001	564.5	12	538.5	9.1	648	48	95.39	83.10	
RDT16_019	RDT16019-109.d	220.1	89.4	0.41	2.293	0.057	0.1842	0.0029	0.43499	0.09	0.002	1206	18	1089	16	1407	41	90.30	77.40	
RDT16_019	RDT16019-110.d	1511	98.3	0.07	1.429	0.036	0.1411	0.0026	0.7561	0.07368	0.001	902	16	850	15	1026	34	94.24	82.85	
RDT16_019	RDT16019-121.d	469	174.7	0.37	20.42	0.48	0.6102	0.011	0.82018	0.2424	0.004	3109	24	3070	44	3133	23	98.75	97.99	
RDT16_019	RDT16019-122.d	244	86.1	0.35	2.864	0.074	0.2395	0.0045	0.69476	0.0865	0.002	1369	20	1383	23	1343	36	101.02	102.98	/Pb^{206} zircon age b
RDT16_019	RDT16019-123.d	593	57.4	0.10	0.816	0.022	0.091	0.0017	0.45765	0.0649	0.002	603.7	12	561.4	9.8	758	47	92.99	74.06	
RDT16_019	RDT16019-124.d	148.8	171.2	1.15	2.382	0.065	0.2029	0.0035	0.3136	0.0854	0.002	1233	20	1190	19	1300	46	96.51	91.54	
RDT16_019	RDT16019-125.d	218.2	132.7	0.61	9.75	0.21	0.4274	0.0069	0.69898	0.1651	0.003	2408	20	2292	31	2505	26	95.18	91.50	small zircon
RDT16_019	RDT16019-126.d	1738	443.9	0.26	1.135	0.061	0.0966	0.0034	0.95433	0.0831	0.002	757	28	593	20	1244	49	78.34	47.67	
RDT16_019	RDT16019-127.d	302.4	271.2	0.90	2.677	0.06	0.2248	0.0036	0.53299	0.0861	0.002	1319.5	17	1307	19	1333	34	99.05	98.05	
RDT16_019	RDT16019-128.d	382.2	332.2	0.87	0.733	0.019	0.08557	0.0013	0.23984	0.0622	0.002	557.2	12	529.1	7.8	659	54	94.96	80.29	
RDT16_019	RDT16019-129.d	58.8	53.4	0.91	1.719	0.099	0.1284	0.0028	0.32366	0.0966	0.005	1003	37	778	16	1458	99	77.57	53.36	
RDT16_019	RDT16019-130.d	243	104.8	0.43	1.308	0.036	0.1392	0.0025	0.54245	0.0681	0.002	846	16	840	14	856	45	99.29	98.13	
RDT16_019	RDT16019-131.d	167.5	323	1.93	10.29	0.22	0.4536	0.0073	0.63729	0.1642	0.003	2458	20	2409	32	2497	27	98.01	96.48	
RDT16_019	RDT16019-134.d	1077	56	0.05	2.037	0.044	0.1838	0.003	0.70561	0.0802	0.001	1127.1	15	1087	16	1200	31	96.44	90.58	
RDT16_019	RDT16019-142.d	448.9	56.2	0.13	0.761	0.02	0.08951	0.0014	0.26449	0.0615	0.001	573.7	11	552.5	8	636	48	96.30	86.87	
RDT16_019	RDT16019-143.d	12.42	0.138	0.01	3.16	0.28	0.1384	0.0048	0.44477	0.167	0.014	1346	68	833	27	2150	170	61.89	38.74	discordant
RDT16_019	RDT16019-144.d	440	3.26	0.01	0.76	0.022	0.0873	0.0015	0.36957	0.0628	0.002	571	13	539.3	9.1	674	53	94.45	80.01	
RDT16_019	RDT16019-145.d	1136	139.3	0.12	0.795	0.021	0.0881	0.0019	0.68323	0.06537	0.001	592	12	543.9	11	772	41	91.88	70.45	
RDT16_019	RDT16019-146.d	757	180.2	0.24	1.364	0.037	0.1308	0.0023	0.6416	0.0754	0.002	871	16	792	13	1062	39	90.93	74.58	
RDT16_019	RDT16019-148.d	651	167.5	0.26	1.299	0.033	0.1377	0.0025	0.67082	0.06814	0.001	843	15	831	14	861	39	98.58	96.52	
RDT16_019	RDT16019-149.d	200.1	136.3	0.68	4.44	0.14	0.2157	0.0041	0.80089	0.1473	0.003	1710	26	1260	22	2306	36	73.68	54.64	
RDT16_019	RDT16019-150.d	611	651	1.07	10.005	0.21	0.4462	0.0068	0.78566	0.162	0.002	2433.1	19	2377	30	2478	24	97.69	95.92	
RDT16_019	RDT16019-151.d	388	45.8	0.12	1.257	0.051	0.1264	0.004	0.88236	0.0714	0.002	815	24	765	23	944	47	93.87	81.04	
RDT16_019	RDT16019-152.d	194	178.8	0.92	0.808	0.031	0.093	0.0019	0.3534	0.0631	0.002	596	17	572.8	11	644	74	96.11	88.94	
RDT16_019	RDT16019-153.d	478.7	202.7	0.42	1.621	0.04	0.1537	0.0026	0.45704	0.0762	0.002	976	15	921	14	1091	41	94.36	84.42	
RDT16_019	RDT16019-154.d	1521	167.3	0.11	3.212	0.072	0.2203	0.004	0.84619	0.10544	0.002	1458.6	17	1283	21	1718	27	87.96	74.68	
RDT16_019	RDT16019-162.d	133.5	57.22	0.43	11.58	0.24	0.4747	0.0072	0.6336	0.1765	0.003	2569.3	20	2502	32	2615	26	97.38	95.68	
RDT16_019	RDT16019-163.d	246.6	74.1	0.30	2.222	0.054	0.203	0.0032	0.46299	0.0792	0.002	1186	17	1191	17	1167	39	100.42	102.06	
RDT16_019	RDT16019-164.d	62.6	39.5	0.63	0.887	0.045	0.0897	0.0019	0.0062059	0.0723	0.004	636	25	553.3	11	890	110	87.00	62.17	
RDT16_019	RDT16019-165.d	354.9	155.5	0.44	1.572	0.041	0.1522	0.0024	0.40552	0.0749	0.002	958	17	912.7	13	1048	44	95.27	87.09	
RDT16_019	RDT16019-167.d	863.5	559.6	0.65	1.53	0.034	0.1493	0.0023	0.57086	0.07408	0.001	940.7	14	896.7	13	1034	34	95.32	86.72	
RDT16_019	RDT16019-416.d	1108	750	0.68	0.786	0.022	0.0809	0.0018	0.68617	0.0706	0.002	589	13	501	10	930	46	85.06	53.87	
RDT16_019	RDT16019-42.d	109.1	155.7	1.43	10.15	0.22	0.4545	0.0073	0.56635	0.1612	0.003	2445	20	2413	33	2463	29	98.69	97.97	
RDT16_019	RDT16019-424.d	340	295.3	0.87	1.702	0.04	0.1714	0.003	0.65744	0.0718	0.001	1007	15	1019	16	969	38	101.19	105.16	
RDT16_019	RDT16019-425.d	971	665	0.68	1.47	0.029	0.1475	0.0025	0.7267	0.07224	0.001	916.9	12	887	14	986	33	96.74	89.96	
RDT16_019	RDT16019-426.d	371.1	184.8	0.50	1.865	0.043	0.1765	0.0034	0.4953	0.0768	0.002	1066	15	1047	19	1099	46	98.22	95.27	
RDT16_019	RDT16019-427.d	46.23	68.2	1.48	1.421	0.078	0.1323	0.0032	0.28646	0.0783	0.004	888	33	800	18	1060	120	90.09	75.47	
RDT16_019	RDT16019-428.d	68.1	71.3	1.05	10.5	0.26	0.4627	0.0097	0.59547	0.1648	0.004	2479	23	2447	43	2499	38	98.71	97.92	
RDT16_019	RDT16019-429.d	947	614.7	0.65	1.418	0.031	0.1424	0.0025	0.76657	0.07187	0.001	895	13	858	14	975	34	95.87	88.00	
RDT16_019	RDT16019-43.d	298	129.8	0.44	3.296	0.079	0.229	0.0037	0.59843	0.1038	0.002	1477	19	1328	19	1685	33	89.91	78.81	
RDT16_019	RDT16019-431.d	268.4	109.8	0.41	2.669	0.059	0.1935	0.0034	0.63548	0.1	0.002	1317	16	1140	18	1615	36	86.56	70.59	
RDT16_019	RDT16019-432.d	113.5	124.1	1.09	1.084	0.042	0.1222	0.0026	0.34909	0.0653	0.003	746	22	742	15	725	84	99.46	102.34	

Supplementary Table 1. Main isotopes and ratios measured using LA–ICP–MS. Concordance 1 ($^{206}Pb/^{238}U/^{207}Pb/^{235}U$) and 2 ($^{206}Pb/^{238}U/^{207}Pb/^{206}Pb$).

RDT16_019	RDT16019-433.d	723	262	0.36	0.713	0.023	0.0835	0.0021	0.64402	0.062	0.002	544	13	516	12	649	57	94.85	79.51	YC1σ
RDT16_019	RDT16019-434.d	130.4	96.9	0.74	1.802	0.057	0.1685	0.003	0.34811	0.0776	0.002	1041	20	1006	16	1113	63	96.64	90.39	
RDT16_019	RDT16019-435.d	72	58.8	0.82	1.321	0.059	0.1281	0.0029	0.13155	0.0746	0.004	846	26	777	16	977	98	91.84	79.53	
RDT16_019	RDT16019-436.d	502.9	56.5	0.11	1.107	0.026	0.1213	0.0019	0.34124	0.0662	0.002	755	12	738	11	796	49	97.75	92.71	
RDT16_019	RDT16019-437.d	295.3	165.6	0.56	0.336	0.015	0.04406	0.0008	0.18656	0.0562	0.003	296	12	277.9	4.9	405	100	93.89	68.62	YSG
RDT16_019	RDT16019-44.d	606	210	0.35	1.757	0.04	0.1709	0.0027	0.60031	0.07443	0.001	1027.9	15	1017	15	1044	34	98.94	97.41	
RDT16_019	RDT16019-445.d	151	51.6	0.34	1.634	0.056	0.1574	0.0039	0.52132	0.0754	0.002	977	22	942	21	1047	62	96.42	89.97	
RDT16_019	RDT16019-446.d	722	124.7	0.17	9.46	0.16	0.4328	0.007	0.81865	0.1585	0.002	2382	16	2316	32	2436	24	97.23	95.07	
RDT16_019	RDT16019-447.d	120.8	86.9	0.72	1.417	0.051	0.1255	0.0023	0.18501	0.0821	0.003	890	21	762	13	1222	69	85.62	62.36	
RDT16_019	RDT16019-448.d	355.8	450	1.26	3.435	0.073	0.2517	0.0049	0.64123	0.0991	0.002	1510	17	1446	25	1598	36	95.76	90.49	
RDT16_019	RDT16019-449.d	245.5	225.1	0.92	3.897	0.085	0.2837	0.0046	0.65331	0.0995	0.002	1610	18	1609	23	1607	34	99.94	100.12	
RDT16_019	RDT16019-45.d	139.7	61.45	0.44	4.922	0.13	0.3295	0.0066	0.68847	0.1083	0.002	1804	23	1833	32	1762	35	101.61	104.03	
RDT16_019	RDT16019-450.d	522.3	346.5	0.66	0.863	0.022	0.1011	0.0018	0.52857	0.0619	0.001	630	12	621	11	652	50	98.57	95.25	
RDT16_019	RDT16019-451.d	706	604	0.86	1.576	0.035	0.1471	0.0024	0.57283	0.0777	0.002	959	14	884	14	1128	39	92.18	78.37	
RDT16_019	RDT16019-452.d	1175	448.3	0.38	1.503	0.029	0.1498	0.0024	0.60624	0.07262	0.001	930.3	12	899	14	997	33	96.64	90.17	
RDT16_019	RDT16019-453.d	613.7	291.9	0.48	1.053	0.023	0.1183	0.0019	0.43095	0.0646	0.001	729	12	721	11	745	46	98.90	96.78	
RDT16_019	RDT16019-454.d	567	603	1.06	3.325	0.085	0.2354	0.0053	0.87337	0.1023	0.002	1482	20	1361	28	1661	29	91.84	81.94	
RDT16_019	RDT16019-455.d	238	205	0.86	0.826	0.029	0.0949	0.0017	0.41763	0.063	0.002	608	16	584.2	9.9	693	66	96.09	84.30	
RDT16_019	RDT16019-456.d	1732	1268	0.73	1.041	0.03	0.0943	0.0023	0.88509	0.0805	0.001	724	15	581	14	1210	31	80.25	48.02	
RDT16_019	RDT16019-457.d	447.8	458.3	1.02	1.571	0.034	0.1566	0.0026	0.48723	0.0726	0.002	957	13	938	15	993	42	98.01	94.46	
RDT16_019	RDT16019-458.d	155.4	16	0.10	1.26	0.11	0.1008	0.0036	0.65299	0.0874	0.006	804	46	618	21	1290	130	76.87	47.91	
RDT16_019	RDT16019-466.d	161.6	111.9	0.69	4.546	0.11	0.3021	0.005	0.46638	0.1091	0.002	1737	21	1700	25	1777	39	97.87	95.67	
RDT16_019	RDT16019-467.d	352	131.4	0.37	1.684	0.043	0.1641	0.0026	0.44756	0.0744	0.002	1000	16	979	14	1038	45	97.90	94.32	
RDT16_019	RDT16019-468.d	531	372	0.70	4.81	0.14	0.2708	0.0064	0.84317	0.1284	0.002	1780	26	1543	32	2069	34	86.69	74.58	
RDT16_019	RDT16019-469.d	115.3	93.7	0.81	9.82	0.25	0.4219	0.0096	0.77233	0.1689	0.003	2412	24	2265	44	2539	31	93.91	89.21	
RDT16_019	RDT16019-470.d	996	379	0.38	0.942	0.022	0.1058	0.0018	0.64419	0.0646	0.001	674	12	648	11	750	43	96.14	86.40	
RDT16_019	RDT16019-471.d	137	100	0.73	1.539	0.083	0.1335	0.0023	0.21103	0.0837	0.005	940	33	807	13	1220	100	85.85	66.15	
RDT16_019	RDT16019-472.d	176.7	117.8	0.67	1.326	0.049	0.1324	0.0023	0.31923	0.0721	0.003	851	21	801	13	951	73	94.12	84.23	
RDT16_019	RDT16019-473.d	736	314.2	0.43	12.93	0.21	0.5026	0.0081	0.83007	0.1866	0.003	2673	16	2622	34	2709	23	98.09	96.79	
RDT16_019	RDT16019-474.d	198.1	172.4	0.87	4.88	0.1	0.3092	0.0053	0.54868	0.1143	0.002	1796	18	1735	26	1863	36	96.60	93.13	
RDT16_019	RDT16019-475.d	282	194.7	0.69	1.338	0.034	0.1407	0.0026	0.36656	0.0695	0.002	860	15	848	15	891	54	98.60	95.17	
RDT16_019	RDT16019-476.d	380	552	1.45	3.619	0.074	0.2637	0.0043	0.65684	0.0995	0.002	1551	16	1508	22	1607	32	97.23	93.84	
RDT16_019	RDT16019-477.d	142.7	52.5	0.37	1.658	0.092	0.1453	0.0033	0.27225	0.0827	0.004	985	35	874	19	1203	100	88.73	72.65	
RDT16_019	RDT16019-478.d	187.8	96.6	0.51	1.9	0.046	0.1781	0.0025	0.46573	0.0771	0.002	1078	16	1056	14	1109	42	97.96	95.22	
RDT16_019	RDT16019-479.d	195.3	203.4	1.04	0.5	0.027	0.04847	0.00098	0.22908	0.0747	0.004	408	18	305.1	6	980	120	74.78	31.13	
RDT16_019	RDT16019-480.d	2076	481	0.23	0.556	0.014	0.0648	0.0014	0.71987	0.06205	0.001	447.8	9.3	404.4	8.4	664	41	90.31	60.90	
RDT16_019	RDT16019-489.d	65.8	77.4	1.18	4.77	0.15	0.3011	0.0059	0.45336	0.1153	0.003	1774	27	1695	29	1861	53	95.55	91.08	
RDT16_019	RDT16019-490.d	426.6	300.7	0.70	0.878	0.024	0.1019	0.0018	0.39069	0.0625	0.002	638	13	625	10	666	56	97.96	93.84	
RDT16_019	RDT16019-491.d	227.1	402	1.77	1.139	0.032	0.1211	0.002	0.18248	0.0684	0.002	769	15	737	11	849	62	95.84	86.81	
RDT16_019	RDT16019-492.d	184.8	171	0.93	13.15	0.24	0.4871	0.007	0.67381	0.1957	0.003	2688	17	2556	30	2786	26	95.09	91.74	
RDT16_019	RDT16019-493.d	402.6	160	0.40	4.421	0.095	0.2326	0.0038	0.74728	0.1376	0.002	1715	17	1347	20	2195	28	78.54	61.37	
RDT16_019	RDT16019-494.d	221.9	279	1.26	1.118	0.041	0.1137	0.0019	0.43157	0.0719	0.003	760	20	694	11	936	73	91.32	74.15	
RDT16_019	RDT16019-495.d	150.1	117.6	0.78	1.065	0.038	0.1195	0.002	0.14602	0.0642	0.002	732	19	727	11	718	80	99.32	101.25	
RDT16_019	RDT16019-496.d	193.8	74.2	0.38	1.451	0.038	0.1453	0.0018	0.21121	0.0726	0.002	908	16	874	10	986	52	96.26	88.64	
RDT16_019	RDT16019-497.d	258	211.5	0.82	2.6	0.12	0.1841	0.0067	0.77255	0.1011	0.003	1284	35	1086	37	1633	59	84.58	66.50	
RDT16_019	RDT16019-498.d	244.7	321	1.31	8.82	0.16	0.3988	0.0054	0.67885	0.1598	0.002	2317	17	2162	25	2453	26	93.31	88.14	
RDT16_019	RDT16019-499.d	139.3	83.1	0.60	0.749	0.037	0.0837	0.0013	0.06204	0.0659	0.004	562	21	518.3	8	720	110	92.22	71.99	YC1σ
RDT16_019	RDT16019-500.d	397.5	120.9	0.30	4.541	0.078	0.2903	0.0038	0.62653	0.1134	0.002	1737	14	1642	19	1850	29	94.53	88.76	
RDT16_019	RDT16019-501.d	808	256	0.32	1.978	0.052	0.1445	0.0025	0.74194	0.0991	0.002	1107	18	869	14	1602	36	78.50	54.24	
RDT16_019	RDT16019-509.d	626	506	0.81	3.246	0.073	0.2355	0.0046	0.58984	0.0998	0.002	1465	18	1362	24	1620	30	92.97	84.07	
RDT16_019	RDT16019-510.d	405	284.6	0.70	1.151	0.025	0.1258	0.0017	0.41605	0.0666	0.001	776	12	763.6	9.7	812	45	98.40	94.04	
RDT16_019	RDT16019-511.d	285.6	224.6	0.79	1.473	0.035	0.143	0.002	0.37	0.0747	0.002	919	15	861	11	1047	48	93.69	82.23	
RDT16_019	RDT16019-512.d	127.6	179.9	1.41	10.06	0.17	0.4514	0.0056	0.56285	0.1614	0.003	2438	16	2400	25	2466	27	98.44	97.32	
RDT16_019	RDT16019-513.d	360.9	233.1	0.65	3.515	0.059	0.2542	0.0028	0.42149	0.1004	0.002	1531	14	1459	14	1628	31	95.30	89.62	

Supplementary Table 1. Main isotopes and ratios measured using LA–ICP–MS. Concordance 1 ($^{206}Pb/^{238}U/^{207}Pb/^{235}U$) and 2 ($^{206}Pb/^{238}U/^{207}Pb/^{206}Pb$).

																					YC1σ	
RDT16_019	RDT16019-514.d	441.9	182.6	0.41	13.25	0.21	0.5243	0.0066	0.7629	0.1823	0.003	2696	15	2716	28	2671	22	100.74	101.68			
RDT16_019	RDT16019-515.d	714	1106	1.55	7.062	0.12	0.3233	0.0042	0.80466	0.1581	0.002	2117	16	1805	21	2433	23	85.26	74.19			
RDT16_019	RDT16019-516.d	320.2	314.2	0.98	3.815	0.073	0.2734	0.0037	0.53781	0.1009	0.002	1594	15	1557	18	1635	32	97.68	95.23			
RDT16_019	RDT16019-517.d	142.8	66	0.46	1.8	0.3	0.1276	0.004	0.85863	0.098	0.012	982	82	774	23	1450	210	78.82	53.38			
RDT16_019	RDT16019-518.d	47.38	37.2	0.79	2.48	0.19	0.155	0.0054	0.66976	0.1158	0.007	1250	57	927	30	1810	120	74.16	51.22			
RDT16_019	RDT16019-519.d	246.2	114.6	0.47	0.895	0.032	0.0937	0.001	0.16876	0.0691	0.002	646	17	577.6	6.1	856	73	89.41	67.48			
RDT16_019	RDT16019-520.d	509	491	0.96	2.967	0.063	0.2229	0.0026	0.45328	0.0964	0.002	1397	16	1297	14	1551	37	92.84	83.62			
RDT16_019	RDT16019-521.d	368.3	62.33	0.17	1.543	0.03	0.1539	0.0017	0.29281	0.0729	0.002	946.5	12	922.3	9.8	1004	42	97.44	91.86			
RDT16_019	RDT16019-522.d	212.2	81	0.38	1.398	0.038	0.1436	0.0026	0.25084	0.0706	0.002	885	16	864	15	924	60	97.63	93.51			
RDT16_019	RDT16019-53.d	857	201.7	0.24	1.55	0.034	0.1596	0.0026	0.63344	0.07036	0.001	949.1	14	954	14	931	34	100.52	102.47			
RDT16_019	RDT16019-530.d	697.7	302.2	0.43	2.891	0.051	0.2305	0.0026	0.50531	0.0907	0.002	1378	14	1339	14	1434	32	97.17	93.38			
RDT16_019	RDT16019-531.d	171.9	82.3	0.48	1.794	0.047	0.1688	0.0023	0.14781	0.0772	0.002	1042	18	1005	13	1107	56	96.45	90.79			
RDT16_019	RDT16019-532.d	586	116.6	0.20	1.801	0.077	0.1587	0.0053	0.93439	0.0816	0.002	1035	29	948	30	1225	39	91.59	77.39			
RDT16_019	RDT16019-533.d	807	360	0.45	24.65	0.4	0.6118	0.0065	0.81155	0.2915	0.004	3293	16	3075	26	3423	20	93.38	89.83			
RDT16_019	RDT16019-534.d	261.8	123	0.47	2.198	0.05	0.1953	0.0024	0.18242	0.0812	0.002	1178	16	1149	13	1227	45	97.54	93.64			
RDT16_019	RDT16019-535.d	188.7	265.4	1.41	10.71	0.18	0.4622	0.0043	0.41341	0.1678	0.003	2496	15	2448	19	2531	27	98.08	96.72			
RDT16_019	RDT16019-536.d	131	127	0.97	1.671	0.053	0.1601	0.004	0.31883	0.0767	0.003	993	20	956	22	1075	68	96.27	88.93			
RDT16_019	RDT16019-537.d	65.14	95.4	1.46	1.186	0.058	0.1246	0.0026	0.098538	0.0691	0.004	784	27	756	15	810	110	96.43	93.33			
RDT16_019	RDT16019-538.d	261	26	0.10	1.246	0.043	0.1233	0.0038	0.54352	0.0734	0.002	817	20	748	22	1016	67	91.55	73.62			
RDT16_019	RDT16019-539.d	307.7	241.2	0.78	3.655	0.065	0.2658	0.0032	0.45133	0.0992	0.002	1560	14	1519	16	1606	33	97.37	94.58			
RDT16_019	RDT16019-54.d	155.2	143.3	0.92	1.733	0.048	0.1758	0.0031	0.29412	0.0715	0.002	1017	18	1043	17	952	51	102.56	109.56			
RDT16_019	RDT16019-540.d	2551	2491	0.98	0.763	0.016	0.0785	0.0012	0.74774	0.0701	0.001	574.9	9.2	487.3	7.4	929	29	84.76	52.45			
RDT16_019	RDT16019-541.d	379.4	284.3	0.75	3.851	0.075	0.226	0.0031	0.61363	0.1232	0.002	1601	16	1313	16	1996	30	82.01	65.78			
RDT16_019	RDT16019-542.d	332	208.8	0.63	0.97	0.03	0.1025	0.0013	0.28052	0.069	0.002	688	16	629.1	7.4	875	64	91.44	71.90			
RDT16_019	RDT16019-543.d	57.3	115	2.01	4.98	0.17	0.3058	0.0052	0.23197	0.1186	0.004	1815	29	1719	26	1919	62	94.71	89.58			
RDT16_019	RDT16019-544.d	369.8	198.7	0.54	2.457	0.052	0.2084	0.0024	0.35289	0.0853	0.002	1257	15	1220	13	1316	38	97.06	92.71			
RDT16_019	RDT16019-545.d	228.5	150.9	0.66	1.03	0.036	0.1064	0.0017	0.1904	0.0702	0.003	715	18	651	10	900	70	91.05	72.33			
RDT16_019	RDT16019-546.d	221	102.5	0.46	0.653	0.035	0.0664	0.0013	0.55763	0.0711	0.003	510	22	414	8.2	916	93	81.18	45.20			
RDT16_019	RDT16019-547.d	886	44.1	0.05	1.486	0.036	0.1507	0.0028	0.7681	0.0714	0.001	922	15	904	16	961	36	98.05	94.07			
RDT16_019	RDT16019-548.d	1239	508	0.41	1.061	0.028	0.1104	0.0017	0.50934	0.07	0.002	732	14	674.7	9.7	911	47	92.17	74.06			
RDT16_019	RDT16019-55.d	505	31.1	0.06	0.684	0.017	0.0836	0.0014	0.25304	0.0594	0.001	528.1	10	517.7	8.2	559	51	98.03	92.61			
RDT16_019	RDT16019-556.d	159	140.2	0.88	10.61	0.21	0.4685	0.0075	0.64673	0.1646	0.003	2488	19	2474	33	2497	29	99.44	99.08			
RDT16_019	RDT16019-557.d	182.6	257	1.41	3.577	0.095	0.2695	0.0054	0.65542	0.0969	0.002	1545	22	1537	27	1552	42	99.48	99.03			
RDT16_019	RDT16019-558.d	322.6	545	1.69	4.219	0.099	0.2511	0.005	0.75596	0.1216	0.002	1676	20	1442	26	1974	30	86.04	73.05			
RDT16_019	RDT16019-559.d	527.4	137.5	0.26	2.474	0.052	0.1868	0.003	0.64484	0.096	0.002	1262	15	1104	16	1539	34	87.48	71.73			
RDT16_019	RDT16019-56.d	353	406	1.15	1.042	0.048	0.0836	0.0015	0.61887	0.0893	0.003	716	23	517.6	9.1	1359	68	72.29	38.09			
RDT16_019	RDT16019-560.d	240.2	122.9	0.51	1.648	0.058	0.163	0.004	0.69754	0.0732	0.002	982	22	972	22	997	54	98.98	97.49			
RDT16_019	RDT16019-57.d	152	135.8	0.89	2.075	0.057	0.178	0.0039	0.41894	0.0843	0.002	1135	19	1055	22	1284	48	92.95	82.17			
RDT16_019	RDT16019-58.d	5223	7380	1.41	0.423	0.029	0.03951	0.00081	0.56344	0.0769	0.004	353	19	249.8	5	1053	88	70.76	23.72			
RDT16_019	RDT16019-59.d	126	182	1.44	1.815	0.057	0.1648	0.0032	0.18858	0.0803	0.003	1044	21	983	18	1156	63	94.16	85.03			
RDT16_019	RDT16019-60.d	473.9	52	0.11	1.393	0.033	0.1416	0.0024	0.42517	0.0712	0.001	884	14	853	13	960	40	96.49	88.85			
RDT16_019	RDT16019-61.d	123.9	88.2	0.71	0.555	0.037	0.04539	0.00096	0.18367	0.0895	0.006	439	24	286.1	5.9	1160	130	65.17	24.66			
RDT16_019	RDT16019-62.d	329	198.7	0.60	1.114	0.031	0.1241	0.0021	0.39511	0.0652	0.002	759	15	754.7	12	748	51	99.43	100.90			
RDT16_019	RDT16019-63.d	135	84.2	0.62	20.99	0.92	0.563	0.015	0.91233	0.2657	0.007	3112	48	2870	62	3271	45	92.22	87.74			
RDT16_019	RDT16019-64.d	1934	529.1	0.27	1.525	0.056	0.1056	0.0021	0.58613	0.1044	0.003	931	22	647	12	1663	54	69.50	38.91			
RDT16_019	RDT16019-65.d	711	898	1.26	9.53	0.27	0.3975	0.0095	0.94995	0.1732	0.003	2380	26	2151	44	2590	24	90.38	83.05			
RDT16_019	RDT16019-66.d	354	148.9	0.42	1.738	0.053	0.1728	0.0043	0.64972	0.0733	0.002	1020	20	1026	23	1014	44	100.59	101.18			
RDT16_019	RDT16019-74.d	420	177.2	0.42	1.955	0.044	0.1771	0.0032	0.55821	0.0803	0.002	1098.1	15	1050	18	1202	38	95.62	87.35			
RDT16_019	RDT16019-75.d	88.3	51.1	0.58	13.25	0.34	0.4903	0.0099	0.73306	0.1961	0.004	2696	24	2568	43	2789	30	95.25	92.08			
RDT16_019	RDT16019-76.d	88.3	64	0.72	1.503	0.056	0.1246	0.0023	0.089421	0.0882	0.003	923	23	757	13	1302	75	82.02	58.14			
RDT16_019	RDT16019-77.d	244.1	35.62	0.15	1.045	0.032	0.0967	0.0015	0.026697	0.0783	0.002	722	16	594.8	9.1	1108	57	82.38	53.68			
RDT16_019	RDT16019-78.d	59	75.8	1.28	1.161	0.092	0.0864	0.0021	0.40359	0.0989	0.007	757	38	533	12	1400	130	70.41	38.07			
RDT16_019	RDT16019-79.d	261	244	0.93	1.186	0.039	0.117	0.0021	0.37846	0.0737	0.002	788	17	712.7	12	988	55	90.44	72.14			
RDT16_019	RDT16019-80.d	51.37	31.78	0.62	1.966	0.075	0.1698	0.0033	0.057302	0.0851	0.003	1093	26	1010	18	1231	77	92.41	82.05			

Supplementary Table 1. Main isotopes and ratios measured using LA–ICP–MS. Concordance 1 ($^{206}Pb/^{238}U/^{207}Pb/^{235}U$) and 2 ($^{206}Pb/^{238}U/^{207}Pb/^{206}Pb$).

RDT16_019	RDT16019-81.d	1016	7.74	0.01	0.818	0.019	0.0962	0.0015	0.52486	0.06165	0.001	606	10	591.8	9	652	38	97.66	90.77
RDT16_019	RDT16019-82.d	103.9	82.66	0.80	1.56	0.046	0.1525	0.0025	0.20307	0.0741	0.002	949	18	914	14	1007	56	96.31	90.76
RDT16_019	RDT16019-83.d	307	52.3	0.17	0.792	0.025	0.0872	0.0015	0.25105	0.0659	0.002	590	14	539	9.1	777	60	91.36	69.37
RDT16_019	RDT16019-84.d	362.7	222.4	0.61	1.558	0.035	0.156	0.0023	0.39675	0.07225	0.001	952.6	14	934.3	13	985	38	98.08	94.85
RDT16_019	RDT16019-85.d	141.3	86.9	0.62	3.73	0.088	0.2685	0.0043	0.40208	0.1009	0.002	1574	19	1532	22	1627	36	97.33	94.16
RDT16_019	RDT16019-86.d	72.61	29.96	0.41	18.54	0.41	0.5563	0.0097	0.62808	0.242	0.004	3014	22	2847	40	3126	27	94.46	91.07
RDT16_019	RDT16019-94.d	135.4	170	1.26	4.547	0.11	0.2893	0.0047	0.36021	0.1143	0.002	1737	20	1637	23	1856	36	94.24	88.20
RDT16_019	RDT16019-95.d	162.3	98.1	0.60	1.916	0.053	0.1726	0.0029	0.13361	0.0806	0.002	1083	18	1026	16	1179	52	94.74	87.02
RDT16_019	RDT16019-96.d	563	86.7	0.15	2.96	0.33	0.181	0.014	0.9892	0.0999	0.005	1205	88	1049	77	1460	100	87.05	71.85
RDT16_019	RDT16019-98.d	664	136.3	0.21	1.884	0.042	0.1774	0.0029	0.54983	0.07672	0.001	1074.8	14	1052	16	1109	34	97.88	94.86
RDT16_019	RDT16019-99.d	254.3	143.9	0.57	9.462	0.2	0.4212	0.0063	0.64519	0.1622	0.002	2381.5	19	2264	29	2477	26	95.07	91.40
RDT16_049	RDT16049C-10.d	164.6	75.8	2.17	1.441	0.046	0.146	0.0043	0.26026	0.0716	0.002	901	19	878	24	930	60	97.45	94.41
RDT16_049	RDT16049C-100.d	610	129	4.73	5.11	0.22	0.296	0.01	0.90673	0.1227	0.003	1810	37	1667	52	1982	39	92.10	84.11
RDT16_049	RDT16049C-106.d	310.8	129.2	2.41	1.678	0.048	0.1699	0.0051	0.44561	0.0717	0.002	997	19	1011	28	957	47	101.40	105.64
RDT16_049	RDT16049C-107.d	466	357	1.31	3.298	0.11	0.2309	0.0083	0.89292	0.1029	0.002	1468	28	1336	43	1669	35	91.01	80.05
RDT16_049	RDT16049C-108.d	108.6	96.5	1.13	0.676	0.03	0.0857	0.0027	0.048016	0.0581	0.003	519	19	529.5	16	438	96	102.02	120.89
RDT16_049	RDT16049C-109.d	73.8	64.1	1.15	3.747	0.11	0.2803	0.0083	0.23712	0.0968	0.003	1575	25	1591	42	1540	51	101.02	103.31
RDT16_049	RDT16049C-11.d	278.4	228.7	1.22	1.98	0.053	0.1885	0.0053	0.3194	0.0761	0.002	1107	18	1113	29	1082	46	100.54	102.87
RDT16_049	RDT16049C-110.d	727	167.2	4.35	4.165	0.097	0.3026	0.0084	0.51767	0.09987	0.002	1665.5	19	1705	41	1618	32	102.37	105.38
RDT16_049	RDT16049C-111.d	860	863	1.00	1.034	0.079	0.0999	0.0033	0.62231	0.0755	0.005	706	36	613	19	980	110	86.83	62.55
RDT16_049	RDT16049C-112.d	294.2	142.2	2.07	4.947	0.14	0.3146	0.01	0.7699	0.1139	0.002	1807	24	1760	50	1858	35	97.40	94.73
RDT16_049	RDT16049C-113.d	100.8	77.6	1.30	2.226	0.072	0.204	0.0061	0.35502	0.0793	0.002	1183	23	1196	33	1148	57	101.10	104.18
RDT16_049	RDT16049C-114.d	230.6	192.5	1.20	3.885	0.11	0.2836	0.0089	0.61946	0.0996	0.002	1605	23	1607	44	1602	40	100.12	100.31
RDT16_049	RDT16049C-115.d	346	143.8	2.41	13.57	0.44	0.494	0.017	0.88692	0.1969	0.004	2704	35	2589	71	2797	32	95.75	92.56
RDT16_049	RDT16049C-116.d	157.1	234.6	0.67	1.463	0.05	0.1513	0.0047	0.35124	0.0702	0.002	909	20	908	26	886	61	99.89	102.48
RDT16_049	RDT16049C-117.d	679	326.6	2.08	2.199	0.06	0.2022	0.0063	0.52145	0.0788	0.002	1177	19	1186	34	1159	43	100.76	102.33
RDT16_049	RDT16049C-118.d	383.9	190.8	2.01	13.8	0.34	0.5449	0.016	0.78501	0.1839	0.003	2733	24	2801	66	2685	29	102.49	104.32
RDT16_049	RDT16049C-119.d	235.4	196.3	1.20	1.733	0.049	0.1725	0.0049	0.37281	0.0728	0.002	1018	18	1025	27	989	47	100.69	103.64
RDT16_049	RDT16049C-12.d	970	44.3	21.90	0.962	0.066	0.1103	0.0059	0.91857	0.0614	0.002	667	31	671	33	626	57	100.60	107.19
RDT16_049	RDT16049C-120.d	248.6	105.3	2.36	5.52	0.15	0.3473	0.01	0.74142	0.1146	0.002	1898	24	1919	50	1865	34	101.11	102.90
RDT16_049	RDT16049C-126.d	232	232.1	1.00	0.706	0.028	0.0882	0.0027	0.30444	0.0578	0.002	537	17	544.5	16	481	77	101.40	113.20
RDT16_049	RDT16049C-127.d	240.9	130	1.85	1.097	0.034	0.125	0.0037	0.41371	0.0638	0.002	749	17	758.7	21	703	56	101.30	107.92
RDT16_049	RDT16049C-128.d	700	52	13.46	2.517	0.11	0.2201	0.0079	0.89034	0.0817	0.002	1259	30	1279	42	1219	42	101.59	104.92
RDT16_049	RDT16049C-129.d	398	711	0.56	0.664	0.021	0.0842	0.0025	0.14109	0.0572	0.002	516.5	13	521.2	15	472	65	100.91	110.42
RDT16_049	RDT16049C-13.d	178.9	113.3	1.58	1.901	0.059	0.1806	0.0054	0.36302	0.0765	0.002	1078	21	1070	30	1078	54	99.26	99.26
RDT16_049	RDT16049C-130.d	1471	10.51	139.96	0.7254	0.018	0.0909	0.0026	0.50029	0.05787	0.001	553.6	11	561	15	511	43	101.34	109.78
RDT16_049	RDT16049C-131.d	1223	166.1	7.36	0.681	0.018	0.08609	0.0024	0.49645	0.05722	0.001	527.1	11	532.3	14	484	44	100.99	109.98
RDT16_049	RDT16049C-132.d	209.2	261.6	0.80	2.126	0.06	0.1999	0.0059	0.32787	0.0771	0.002	1153	19	1174	32	1100	48	101.82	106.73
RDT16_049	RDT16049C-133.d	599	1118	0.54	1.712	0.056	0.1561	0.0057	0.87316	0.07948	0.002	1008	21	933	32	1173	38	92.56	79.54
RDT16_049	RDT16049C-134.d	406	97.1	4.18	1.83	0.13	0.1626	0.0092	0.95901	0.0776	0.002	1005	48	963	51	1104	58	95.82	87.23
RDT16_049	RDT16049C-14.d	426.6	244.4	1.75	11.64	0.27	0.4747	0.013	0.73833	0.1771	0.003	2573.7	22	2503	58	2623	28	97.25	95.43
RDT16_049	RDT16049C-15.d	224.3	134.7	1.67	10.97	0.26	0.4756	0.014	0.6576	0.167	0.003	2518	22	2506	60	2522	30	99.52	99.37
RDT16_049	RDT16049C-16.d	891	178.9	4.98	0.72	0.02	0.0881	0.0025	0.55135	0.05922	0.001	550.2	12	544.6	15	568	45	98.98	95.88
RDT16_049	RDT16049C-17.d	387	287	1.35	3.554	0.093	0.2631	0.0079	0.58946	0.0988	0.002	1537	21	1504	40	1591	37	97.85	94.53
RDT16_049	RDT16049C-23.d	577.2	879	0.66	0.637	0.018	0.08034	0.0023	0.38353	0.0575	0.001	500.8	12	498	14	487	53	99.44	102.26
RDT16_049	RDT16049C-24.d	647	89.8	7.20	2.355	0.06	0.2088	0.0061	0.54638	0.0818	0.002	1228	19	1223	33	1230	38	99.59	99.43
RDT16_049	RDT16049C-25.d	491	204.8	2.40	0.696	0.022	0.0858	0.0025	0.30754	0.0588	0.002	534.3	13	530.5	15	535	59	99.29	99.16
RDT16_049	RDT16049C-26.d	429	175.9	2.44	11.83	0.38	0.4727	0.015	0.87738	0.1811	0.003	2580	30	2489	67	2657	29	96.47	93.68
RDT16_049	RDT16049C-27.d	335.8	332	1.01	4.538	0.13	0.2972	0.0093	0.71815	0.1107	0.002	1732	24	1675	46	1800	37	96.71	93.06
RDT16_049	RDT16049C-28.d	253	173	1.46	0.671	0.028	0.0838	0.0027	0.36831	0.0583	0.002	520	16	518.2	16	498	75	99.65	104.06
RDT16_049	RDT16049C-29.d	796.5	58.9	13.52	4.105	0.13	0.2804	0.0083	0.75304	0.1058	0.002	1646	26	1592	42	1720	36	96.72	92.56
RDT16_049	RDT16049C-30.d	589	626	0.94	2.736	0.073	0.2288	0.0068	0.60483	0.0865	0.002	1334	20	1327	36	1338	38	99.48	99.18
RDT16_049	RDT16049C-31.d	778.7	95.5	8.15	2.248	0.055	0.2024	0.0057	0.52437	0.08075	0.002	1194.4	17	1188	31	1208	36	99.46	98.34
RDT16_049	RDT16049C-32.d	682	552	1.24	0.642	0.018	0.0799	0.0023	0.199	0.0583	0.001	503.5	11	496	14	520	53	98.51	95.38

Supplementary Table 1. Main isotopes and ratios measured using LA–ICP–MS. Concordance 1 ($^{206}Pb/^{238}U/^{207}Pb/^{235}U$) and 2 ($^{206}Pb/^{238}U/^{207}Pb/^{206}Pb$).

RDT16_049	RDT16049C-33.d	290.6	192.6	1.51	9.33	0.23	0.4237	0.012	0.68784	0.1592	0.003	2368	23	2275	56	2443	29	96.07	93.12	
RDT16_049	RDT16049C-39.d	1430	336.6	4.25	5.062	0.14	0.3128	0.0095	0.73376	0.1185	0.002	1831	24	1753	47	1929	32	95.74	90.88	
RDT16_049	RDT16049C-40.d	237.9	150.7	1.58	10.57	0.27	0.4744	0.014	0.67726	0.1615	0.003	2482	24	2500	61	2464	30	100.73	101.46	
RDT16_049	RDT16049C-41.d	17.02	1.232	13.81	2384	61	20.5	0.62	0.88409	0.8393	0.013	7893	25	19754	190	5051	30	250.27	391.09	
RDT16_049	RDT16049C-42.d	384	249.4	1.54	11.19	0.3	0.4712	0.014	0.79042	0.1722	0.003	2533	26	2486	61	2574	30	98.14	96.58	
RDT16_049	RDT16049C-43.d	440	169	2.60	0.878	0.044	0.0986	0.0041	0.88849	0.0638	0.002	630	23	605	24	695	58	96.03	87.05	
RDT16_049	RDT16049C-44.d	255.5	33.59	7.61	1.27	0.067	0.131	0.0059	0.85728	0.0692	0.002	812	31	790	34	864	63	97.29	91.44	
RDT16_049	RDT16049C-45.d	133.7	95	1.41	2.199	0.069	0.2014	0.0058	0.26685	0.0791	0.002	1176	22	1182	31	1146	57	100.51	103.14	
RDT16_049	RDT16049C-46.d	768	136.3	5.63	0.673	0.02	0.0843	0.0025	0.54236	0.0585	0.001	521.9	12	521.3	15	523	51	99.89	99.67	
RDT16_049	RDT16049C-47.d	1740	142	12.25	0.833	0.034	0.0964	0.0035	0.91341	0.06161	0.001	609	18	594	21	652	43	97.54	91.10	
RDT16_049	RDT16049C-48.d	857	435	1.97	3.711	0.12	0.2546	0.0085	0.82654	0.105	0.002	1563	28	1459	44	1704	38	93.35	85.62	
RDT16_049	RDT16049C-49.d	386.2	309.5	1.25	1.447	0.04	0.1493	0.0043	0.5157	0.07	0.002	906	17	896.8	24	913	44	98.98	98.23	
RDT16_049	RDT16049C-56.d	672.2	292	2.30	2.484	0.069	0.1993	0.0064	0.82198	0.09042	0.002	1263	20	1170	34	1427	34	92.64	81.99	
RDT16_049	RDT16049C-57.d	157.2	449.7	0.35	0.756	0.029	0.0924	0.0028	0.17482	0.0598	0.002	567	17	569.4	17	522	79	100.42	109.08	
RDT16_049	RDT16049C-58.d	465	22.8	20.39	12.81	0.46	0.508	0.017	0.91829	0.1791	0.004	2651	37	2648	76	2635	35	99.89	100.49	
RDT16_049	RDT16049C-59.d	368	48	7.67	1.908	0.058	0.1859	0.0057	0.51978	0.0743	0.002	1081	21	1098	31	1043	45	101.57	105.27	
RDT16_049	RDT16049C-60.d	2903	1335	2.17	0.53	0.016	0.0665	0.0021	0.84849	0.05744	0.001	430.3	11	415.1	13	498	40	96.47	83.35	YSG
RDT16_049	RDT16049C-61.d	170.3	130.6	1.30	10.83	0.27	0.4679	0.013	0.63686	0.1678	0.003	2507	23	2472	59	2529	31	98.60	97.75	
RDT16_049	RDT16049C-62.d	356.2	187	1.90	4.544	0.12	0.2883	0.0088	0.668	0.1142	0.002	1735	22	1633	45	1859	36	94.12	87.84	
RDT16_049	RDT16049C-63.d	1022	278	3.68	3.72	0.13	0.2509	0.0096	0.91078	0.1074	0.002	1563	30	1438	50	1750	34	92.00	82.17	
RDT16_049	RDT16049C-64.d	844	219	3.85	4.534	0.13	0.3129	0.0097	0.76839	0.1052	0.002	1730	25	1752	48	1709	36	101.27	102.52	
RDT16_049	RDT16049C-65.d	232.2	185.4	1.25	8.92	0.25	0.4117	0.013	0.69108	0.157	0.003	2323	26	2222	61	2414	34	95.65	92.05	
RDT16_049	RDT16049C-66.d	1076	68.1	15.80	2.037	0.097	0.1874	0.0074	0.90583	0.077	0.002	1106	32	1104	40	1100	45	99.82	100.36	
RDT16_049	RDT16049C-7.d	289.4	83.3	3.47	2.413	0.062	0.2142	0.0061	0.28435	0.0817	0.002	1244	18	1251	32	1227	42	100.56	101.96	
RDT16_049	RDT16049C-72.d	470	223.7	2.10	1.844	0.051	0.1785	0.0053	0.62441	0.0747	0.002	1059	19	1060	30	1049	39	100.09	101.05	
RDT16_049	RDT16049C-73.d	447	33.2	13.46	1.342	0.074	0.1403	0.0064	0.77517	0.0672	0.002	840	33	843	36	806	59	100.36	104.59	
RDT16_049	RDT16049C-74.d	379	177.4	2.14	2.234	0.059	0.2069	0.006	0.51635	0.0782	0.002	1189	19	1212	32	1139	41	101.93	106.41	
RDT16_049	RDT16049C-75.d	594	54.5	10.90	2.499	0.094	0.2182	0.0075	0.9084	0.0818	0.002	1259	28	1270	40	1238	38	100.87	102.58	
RDT16_049	RDT16049C-76.d	8380	9200	0.91	2.32	0.18	0.17	0.013	0.991	0.0965	0.002	1143	57	995	69	1548	38	87.05	64.28	
RDT16_049	RDT16049C-77.d	855	473	1.81	1.627	0.073	0.1624	0.0065	0.91219	0.0712	0.002	963	31	967	36	948	45	100.42	102.00	
RDT16_049	RDT16049C-78.d	2154	1054	2.04	1.815	0.07	0.1764	0.0064	0.95264	0.07409	0.001	1053	26	1047	35	1042	39	99.43	100.48	
RDT16_049	RDT16049C-79.d	3950	1942	2.03	1.593	0.058	0.1519	0.0056	0.9588	0.07536	0.001	958	24	910	31	1074	34	94.99	84.73	
RDT16_049	RDT16049C-8.d	618	184	3.36	1.903	0.051	0.1794	0.0052	0.63316	0.07653	0.002	1079	18	1063	29	1102	40	98.52	96.46	
RDT16_049	RDT16049C-80.d	950	874	1.09	9.83	0.23	0.4592	0.013	0.7048	0.1549	0.003	2418.8	21	2434	57	2402	30	100.63	101.33	
RDT16_049	RDT16049C-81.d	206.3	228.5	0.90	4.24	0.17	0.291	0.011	0.86537	0.1066	0.002	1670	34	1643	56	1731	42	98.38	94.92	
RDT16_049	RDT16049C-82.d	501	204.3	2.45	3.494	0.089	0.2601	0.0074	0.45151	0.0973	0.002	1522	21	1489	38	1566	34	97.83	95.08	
RDT16_049	RDT16049C-88.d	401.4	131.5	3.05	1.874	0.048	0.182	0.0052	0.30636	0.0748	0.002	1070.7	17	1077	28	1049	40	100.59	102.67	
RDT16_049	RDT16049C-89.d	1214	111.2	10.92	0.68	0.018	0.08563	0.0024	0.42312	0.05735	0.001	525.9	11	529.5	14	492	45	100.68	107.62	
RDT16_049	RDT16049C-9.d	774	310	2.50	0.979	0.026	0.1079	0.0031	0.29593	0.066	0.002	691.6	13	660.3	18	791	47	95.47	83.48	
RDT16_049	RDT16049C-90.d	293.3	146.8	2.00	0.758	0.025	0.0916	0.0027	0.18912	0.0602	0.002	571	14	564.7	16	570	65	98.90	99.07	
RDT16_049	RDT16049C-91.d	2470	2870	0.86	0.771	0.019	0.0889	0.0026	0.61963	0.06248	0.001	579.7	11	549.8	16	682	38	94.84	80.62	
RDT16_049	RDT16049C-92.d	153.4	88.9	1.73	0.841	0.03	0.1014	0.0031	0.4097	0.0604	0.002	616	17	622.5	18	573	69	101.06	108.64	
RDT16_049	RDT16049C-93.d	240.6	229.8	1.05	1.776	0.051	0.173	0.005	0.4837	0.0744	0.002	1034	19	1028	28	1035	45	99.42	99.32	
RDT16_049	RDT16049C-94.d	917	375	2.45	3.773	0.11	0.2799	0.0086	0.89764	0.09679	0.002	1584	25	1589	44	1560	34	100.32	101.86	
RDT16_049	RDT16049C-95.d	1106	96.3	11.48	1.53	0.039	0.1585	0.0045	0.67571	0.0699	0.001	940.6	16	948	25	918	36	100.79	103.27	
RDT16_049	RDT16049C-96.d	31.51	67.16	0.47	0.801	0.055	0.0967	0.0035	0.024778	0.0624	0.005	582	33	594	21	470	150	102.06	126.38	
RDT16_049	RDT16049C-97.d	185.6	169.7	1.09	2.095	0.058	0.1925	0.0056	0.31447	0.0786	0.002	1143	19	1134	30	1144	46	99.21	99.13	
RDT16_049	RDT16049C-98.d	112.9	91.1	1.24	2.596	0.077	0.2294	0.0067	0.13354	0.0821	0.002	1298	21	1331	35	1224	53	102.54	108.74	
RDT16_049	RDT16049C-99.d	1157	418	2.77	0.88	0.022	0.1047	0.003	0.47138	0.06083	0.001	639.8	12	641.9	18	620	42	100.33	103.53	
RDT16_050	RDT16050B-135.d	590	251.7	2.34	3.48	0.13	0.2498	0.0095	0.90854	0.1002	0.002	1504	33	1432	49	1617	37	95.21	88.56	
RDT16_050	RDT16050B-136.d	1062	632	1.68	0.695	0.02	0.087	0.0026	0.55121	0.05819	0.001	534.1	12	537.6	15	519	48	100.66	103.58	
RDT16_050	RDT16050B-137.d	144.7	207.7	0.70	1.531	0.046	0.1599	0.0047	0.40276	0.0693	0.002	939	18	955	26	871	56	101.70	109.64	
RDT16_050	RDT16050B-143.d	270	128.6	2.10	13.11	0.33	0.5281	0.015	0.65848	0.1797	0.003	2684	23	2730	65	2645	29	101.71	103.21	
RDT16_050	RDT16050B-144.d	380.5	327.8	1.16	8.02	0.22	0.3645	0.011	0.80395	0.1593	0.003	2228	26	2000	54	2446	31	89.77	81.77	

Supplementary Table 1. Main isotopes and ratios measured using LA–ICP–MS. Concordance 1 ($^{206}Pb/^{238}U/^{207}Pb/^{235}U$) and 2 ($^{206}Pb/^{238}U/^{207}Pb/^{206}Pb$).

RDT16_050	RDT16050B-145.d	440.7	259.3	1.70	2.047	0.054	0.1959	0.0057	0.49149	0.0757	0.002	1128	18	1152	31	1074	41	102.13	107.26	
RDT16_050	RDT16050B-146.d	378.3	106.9	3.54	1.766	0.053	0.1725	0.0052	0.70516	0.0739	0.002	1028	20	1025	29	1029	42	99.71	99.61	
RDT16_050	RDT16050B-147.d	274	137.5	1.99	1.431	0.043	0.151	0.0044	0.35323	0.0683	0.002	899	18	907	24	866	49	100.89	104.73	
RDT16_050	RDT16050B-148.d	258	200	1.29	2.259	0.063	0.2048	0.0059	0.39733	0.0801	0.002	1195	20	1201	32	1185	47	100.50	101.35	
RDT16_050	RDT16050B-149.d	164.1	119.1	1.38	2.217	0.064	0.2039	0.0061	0.37105	0.0792	0.002	1184	20	1195	33	1151	50	100.93	103.82	
RDT16_050	RDT16050B-150.d	189.2	124.1	1.52	1.582	0.046	0.1599	0.0045	0.23	0.0718	0.002	959	18	956.7	26	961	50	99.76	99.55	
RDT16_050	RDT16050B-151.d	2164	125.1	17.30	2.86	0.078	0.2251	0.0065	0.80406	0.09166	0.002	1367	22	1308	34	1455	33	95.68	89.90	
RDT16_050	RDT16050B-152.d	285.3	210.8	1.35	2.641	0.086	0.2244	0.0069	0.79516	0.0853	0.002	1305	25	1304	37	1314	40	99.92	99.24	
RDT16_050	RDT16050B-153.d	65.74	73.46	0.89	10.09	0.27	0.4609	0.013	0.67068	0.1581	0.003	2439	24	2444	61	2433	34	100.21	100.45	
RDT16_050	RDT16050B-154.d	1606	83.1	19.33	4.523	0.11	0.3054	0.0089	0.79838	0.10702	0.002	1732.7	20	1717	44	1748	30	99.09	98.23	
RDT16_050	RDT16050B-155.d	1517	48.4	31.34	4.757	0.12	0.3207	0.0091	0.75305	0.10739	0.002	1774.9	21	1792	45	1752	30	100.96	102.28	
RDT16_050	RDT16050B-161.d	325.1	202.3	1.61	3.132	0.083	0.2506	0.0075	0.57392	0.0906	0.002	1437	21	1440	38	1425	40	100.21	101.05	
RDT16_050	RDT16050B-162.d	1049	324	3.24	4.788	0.14	0.3198	0.01	0.83688	0.1085	0.002	1775	25	1786	49	1770	31	100.62	100.90	
RDT16_050	RDT16050B-163.d	1220	291	4.19	4.4	0.15	0.3047	0.01	0.93979	0.1036	0.002	1714	27	1714	51	1685	35	100.00	101.72	
RDT16_050	RDT16050B-164.d	425	45.41	9.36	1.967	0.05	0.1895	0.0053	0.53039	0.07506	0.002	1102	17	1118	29	1060	40	101.45	105.47	
RDT16_050	RDT16050B-165.d	465	159.9	2.91	2.37	0.09	0.194	0.0061	0.62475	0.0879	0.002	1223	28	1144	32	1362	50	93.54	83.99	
RDT16_050	RDT16050B-166.d	277	185	1.50	2.311	0.075	0.2083	0.0064	0.50917	0.081	0.002	1212	23	1218	34	1199	51	100.50	101.58	
RDT16_050	RDT16050B-167.d	135.7	289.1	0.47	10.99	0.27	0.4878	0.014	0.46542	0.163	0.003	2519	23	2559	60	2480	31	101.59	103.19	
RDT16_050	RDT16050B-168.d	118.6	223.5	0.53	7.54	0.37	0.3183	0.011	0.6426	0.1719	0.006	2163	39	1781	53	2546	56	82.34	69.95	
RDT16_050	RDT16050B-169.d	56.94	139.3	0.41	0.663	0.04	0.0837	0.0028	0.12411	0.0579	0.004	503	24	518	17	410	130	102.98	126.34	
RDT16_050	RDT16050B-170.d	1332	562	2.37	1.534	0.051	0.1497	0.0052	0.89716	0.07397	0.001	938	20	898	29	1031	37	95.74	87.10	
RDT16_050	RDT16050B-171.d	396.3	267.6	1.48	10.06	0.27	0.45	0.014	0.72378	0.1616	0.003	2435	25	2391	61	2469	31	98.19	96.84	
RDT16_050	RDT16050B-173.d	2.48	14.56	0.17	1042	84	8.98	0.74	0.97068	0.828	0.017	6900	110	14130	580	5026	39	204.78	281.14	
RDT16_050	RDT16050B-174.d	105.5	32.2	3.28	12.07	0.32	0.4931	0.014	0.56896	0.1768	0.004	2604	25	2581	62	2616	34	99.12	98.66	
RDT16_050	RDT16050B-175.d	3.96	0.0048	825.00	479	16	4.26	0.17	0.80201	0.827	0.019	6262	34	10610	200	5024	42	169.43	211.19	
RDT16_050	RDT16050B-181.d	868	741	1.17	0.658	0.019	0.08211	0.0024	0.49916	0.05768	0.001	511.5	12	508.6	14	498	50	99.43	102.13	YSG
RDT16_050	RDT16050B-182.d	419	274	1.53	1.523	0.082	0.1501	0.007	0.94409	0.0713	0.002	913	36	897	39	941	54	98.25	95.32	
RDT16_050	RDT16050B-183.d	255.3	67.3	3.79	1.991	0.054	0.1882	0.0054	0.37792	0.0767	0.002	1113	18	1111	29	1097	44	99.82	101.28	
RDT16_050	RDT16050B-184.d	223.4	162.8	1.37	2.129	0.058	0.197	0.0057	0.36294	0.0786	0.002	1156	19	1159	30	1142	44	100.26	101.49	
RDT16_050	RDT16050B-185.d	115.3	145.1	0.79	1.97	0.065	0.1862	0.0056	0.28583	0.0764	0.002	1098	22	1102	31	1073	58	100.36	102.70	
RDT16_050	RDT16050B-186.d	220	138	1.59	4.454	0.12	0.3081	0.0094	0.59391	0.1052	0.002	1718	24	1729	46	1703	40	100.64	101.53	
RDT16_050	RDT16050B-187.d	1.597	1.267	1.26	326	18	2.87	0.18	0.71944	0.849	0.036	5859	60	8620	300	5071	82	147.12	169.99	
RDT16_050	RDT16050B-188.d	252.8	95.8	2.64	13.27	0.33	0.4936	0.015	0.67165	0.1941	0.003	2695	24	2586	62	2772	29	95.96	93.29	
RDT16_050	RDT16050B-189.d	1290	136	9.49	1.82	0.13	0.1587	0.0091	0.9801	0.0775	0.002	994	51	942	51	1080	66	94.77	87.22	
RDT16_050	RDT16050B-190.d	374	50.9	7.35	1.389	0.088	0.1313	0.0067	0.94211	0.0737	0.002	853	38	791	38	996	60	92.73	79.42	
RDT16_050	RDT16050B-191.d	503	360	1.40	1.805	0.055	0.1642	0.0053	0.70305	0.0793	0.002	1042	20	979	29	1173	42	93.95	83.46	
RDT16_050	RDT16050B-192.d	587	89.1	6.59	2.654	0.091	0.2246	0.0075	0.87959	0.0851	0.002	1307	27	1304	40	1306	39	99.77	99.85	
RDT16_050	RDT16050B-198.d	533	818	0.65	1.249	0.033	0.1362	0.0038	0.4227	0.06629	0.001	820.8	15	822.7	22	808	43	100.23	101.82	
RDT16_050	RDT16050B-200.d	285	192.4	1.48	4.552	0.11	0.3107	0.0088	0.52162	0.106	0.002	1737	21	1743	43	1724	35	100.35	101.10	
RDT16_050	RDT16050B-201.d	505	36.5	13.84	1.886	0.05	0.1813	0.0052	0.53484	0.0753	0.002	1075	17	1074	28	1067	39	99.91	100.66	
RDT16_050	RDT16050B-202.d	452	60.8	7.43	5.54	0.35	0.276	0.015	0.96136	0.1399	0.004	1842	63	1555	77	2217	45	84.42	70.14	
RDT16_050	RDT16050B-203.d	107.8	99.4	1.08	0.656	0.03	0.0844	0.0027	0.17186	0.0572	0.003	507	19	522.2	16	409	93	103.00	127.68	
RDT16_050	RDT16050B-204.d	490	127.5	3.84	5.79	0.33	0.324	0.014	0.93958	0.125	0.004	1906	49	1801	65	2003	51	94.49	89.92	
RDT16_050	RDT16050B-205.d	3.78	4.86	0.78	189.7	8.7	1.634	0.083	0.48469	0.866	0.029	5309	49	6180	200	5110	65	116.41	120.94	
RDT16_050	RDT16050B-206.d	1528	730	2.09	0.673	0.027	0.0743	0.0033	0.92971	0.06568	0.001	517	16	461	20	789	41	89.17	58.43	
RDT16_050	RDT16050B-207.d	389	339	1.15	5.86	0.74	0.277	0.012	0.76636	0.147	0.013	1853	83	1568	64	2150	110	84.62	72.93	
RDT16_050	RDT16050B-208.d	443	231.6	1.91	1.692	0.047	0.1703	0.005	0.42273	0.0721	0.002	1002	18	1013	27	986	45	101.10	102.74	
RDT16_050	RDT16050B-209.d	826	286.7	2.88	4.211	0.12	0.28	0.0085	0.68937	0.1088	0.002	1674	23	1590	43	1774	34	94.98	89.63	
RDT16_050	RDT16050B-210.d	245.5	109.7	2.24	3.153	0.092	0.2427	0.0076	0.48528	0.0935	0.002	1441	23	1399	39	1487	45	97.09	94.08	
RDT16_050	RDT16050B-211.d	156.1	173.9	0.90	4.017	0.11	0.2912	0.0082	0.4069	0.1	0.002	1636	22	1646	41	1624	41	100.61	101.35	
RDT16_050	RDT16050B-212.d	147	154.3	0.95	0.753	0.037	0.0913	0.0029	0.22781	0.0599	0.003	564	21	562.8	17	546	92	99.79	103.08	

Supplementary Table 1. Main isotopes and ratios measured using LA–ICP–MS. Concordance 1 ($^{206}Pb/^{238}U/^{207}Pb/^{235}U$) and 2 ($^{206}Pb/^{238}U/^{207}Pb/^{206}Pb$).

RDT16_050	RDT16050B-213.d	168.9	124.2	1.36	0.67	0.027	0.086	0.0025	0.063329	0.0563	0.002	515	17	532.3	15	402	83	103.36	132.41	
RDT16_050	RDT16050B-219.d	152.9	68.02	2.25	2.699	0.086	0.2324	0.0068	0.45363	0.084	0.002	1320	24	1346	36	1263	50	101.97	106.57	
RDT16_050	RDT16050B-220.d	242.3	194.6	1.25	4.071	0.1	0.2917	0.0084	0.46295	0.1008	0.002	1646	21	1651	41	1630	38	100.30	101.29	
RDT16_050	RDT16050B-221.d	1541	210.4	7.32	5.896	0.15	0.3548	0.01	0.69203	0.1196	0.002	1958	23	1956	49	1947	31	99.90	100.46	
RDT16_050	RDT16050B-222.d	453.7	61.5	7.38	0.924	0.032	0.1061	0.0034	0.62744	0.0629	0.002	660	17	650	20	677	53	98.48	96.01	
RDT16_050	RDT16050B-223.d	627	513	1.22	3.73	0.18	0.25	0.013	0.95101	0.1086	0.002	1546	40	1426	66	1767	35	92.24	80.70	
RDT16_050	RDT16050B-224.d	164.6	95.67	1.72	4.713	0.12	0.3135	0.0092	0.46697	0.1088	0.002	1768	22	1756	45	1770	39	99.32	99.21	
RDT16_050	RDT16050B-225.d	131.6	187.9	0.70	0.677	0.028	0.0846	0.0025	0.14863	0.0582	0.002	521	18	523.3	15	460	86	100.44	113.76	
RDT16_050	RDT16050B-226.d	76.2	56.5	1.35	3.735	0.12	0.2808	0.0086	0.27012	0.0967	0.003	1574	26	1594	43	1533	54	101.27	103.98	
RDT16_050	RDT16050B-227.d	301.4	291.3	1.03	1.215	0.039	0.1285	0.004	0.52911	0.0686	0.002	803	18	779	23	856	54	97.01	91.00	
RDT16_050	RDT16050B-228.d	530	170.9	3.10	1.554	0.051	0.15	0.0046	0.71914	0.0737	0.002	947	20	901	26	1021	46	95.14	88.25	
RDT16_050	RDT16050B-229.d	237	179.5	1.32	2.125	0.059	0.1988	0.0058	0.40454	0.0773	0.002	1154	19	1168	31	1120	46	101.21	104.29	
RDT16_050	RDT16050B-230.d	135.1	222.1	0.61	1.554	0.051	0.1517	0.0046	0.27982	0.0745	0.002	949	19	910	26	1025	61	95.89	88.78	
RDT16_050	RDT16050B-236.d	326.8	211	1.55	0.675	0.021	0.0854	0.0025	0.25174	0.0572	0.002	522.5	13	528.3	15	463	62	101.11	114.10	
RDT16_050	RDT16050B-237.d	185	336	0.55	6.89	0.89	0.1406	0.0091	0.97312	0.302	0.026	1790	130	845	51	2940	210	47.21	28.74	
RDT16_050	RDT16050B-238.d	134	104.2	1.29	4.17	0.13	0.302	0.0092	0.28121	0.1005	0.003	1661	25	1699	46	1603	49	102.29	105.99	
RDT16_050	RDT16050B-239.d	343	193	1.78	1.62	0.047	0.1645	0.0049	0.36673	0.0712	0.002	974	18	981	27	947	51	100.72	103.59	
RDT16_050	RDT16050B-240.d	503	233	2.16	1.652	0.044	0.1682	0.0048	0.43892	0.0711	0.002	989.9	16	1002	27	948	43	101.22	105.70	
RDT16_050	RDT16050B-241.d	222.7	143.2	1.56	1.982	0.053	0.1862	0.0054	0.23002	0.0775	0.002	1106	18	1100	29	1110	46	99.46	99.10	
RDT16_050	RDT16050B-242.d	201	240.7	0.84	0.677	0.025	0.0863	0.0026	0.24653	0.0573	0.002	523	16	533.6	15	447	74	102.03	119.37	
RDT16_050	RDT16050B-243.d	215	182	1.18	0.73	0.029	0.0871	0.0026	0.31653	0.0606	0.002	553	17	538.4	16	562	78	97.36	95.80	
RDT16_050	RDT16050B-244.d	133.4	170.6	0.78	1.597	0.052	0.1609	0.0049	0.2171	0.072	0.002	965	21	961	27	951	62	99.59	101.05	
RDT16_050	RDT16050B-245.d	352	345	1.02	0.802	0.025	0.0978	0.0029	0.25495	0.0597	0.002	596	14	601.4	17	556	59	100.91	108.17	
RDT16_050	RDT16050B-246.d	361	295	1.22	0.796	0.026	0.0953	0.0028	0.35426	0.0605	0.002	593	14	586.6	16	586	60	98.92	100.10	
RDT16_050	RDT16050B-247.d	120.5	70.9	1.70	18.8	0.44	0.6023	0.017	0.58249	0.2261	0.004	3030	23	3037	68	3019	29	100.23	100.60	
RDT16_050	RDT16050B-248.d	425	217.9	1.95	4.638	0.11	0.3147	0.009	0.43799	0.1068	0.002	1753	21	1765	45	1736	35	100.68	101.67	
RDT16_050	RDT16050B-249.d	592	30.4	19.47	4.47	0.22	0.3007	0.012	0.96581	0.1047	0.003	1680	50	1685	64	1694	46	100.30	99.47	
RDT16_050	RDT16050B-250.d	333.4	81.9	4.07	0.695	0.023	0.0853	0.0025	0.22801	0.059	0.002	533	14	527.6	15	524	62	98.99	100.69	
RDT16_033	033 - 1	394	89	4.43	1.31	0.025	0.136	0.0019	0.78904	0.06927	0.0009	849	11	821.9	11	907	27	96.81	90.62	
RDT16_033	033 - 10	625	169.3	3.69	1.778	0.027	0.16	0.002	0.85856	0.08049	0.0007	1036.8	9.9	957	11	1208	17	92.30	79.22	
RDT16_033	033 - 100	1188	1620	0.73	0.5668	0.0076	0.07099	0.00087	0.51647	0.05803	0.0007	455.8	4.9	442.1	5.2	528	28	96.99	83.73	
RDT16_033	033 - 101	248	399	0.62	1.624	0.036	0.1604	0.0028	0.87536	0.07414	0.0009	983	15	959	16	1046	24	97.56	91.68	
RDT16_033	033 - 102	146.4	379	0.39	0.587	0.014	0.07336	0.00086	0.19285	0.0612	0.0014	471.1	9.5	456.4	5.2	638	48	96.88	71.54	
RDT16_033	033 - 103	192.5	229	0.84	0.395	0.012	0.05208	0.00062	0.34479	0.0557	0.0016	338.7	8.8	327.3	3.8	437	61	96.63	74.90	
RDT16_033	033 - 104	55	51.3	1.07	0.298	0.021	0.03957	0.00059	0.08451	0.054	0.0036	266	16	250.1	3.6	360	140	94.02	69.47	
RDT16_033	033 - 105	1860	647	2.87	0.3019	0.0036	0.04037	0.00037	0.41086	0.05423	0.0007	267.9	2.8	255.1	2.3	377	28	95.22	67.67	
RDT16_033	033 - 106	128	159	0.81	0.73	0.097	0.0742	0.004	0.46523	0.0757	0.0059	574	53	461	23	1150	170	80.31	40.09	
RDT16_033	033 - 107	64	63.6	1.01	0.591	0.052	0.05419	0.00098	0.52949	0.0801	0.0065	476	34	340.2	6	1120	150	71.47	30.38	
RDT16_033	033 - 108	187	128.7	1.45	0.524	0.015	0.06758	0.00072	0.37345	0.0564	0.0016	427	10	421.5	4.3	461	66	98.71	91.43	
RDT16_033	033 - 109	487.2	511	0.95	1.944	0.043	0.1775	0.0022	0.85908	0.0799	0.0011	1095	15	1053	12	1192	28	96.16	88.34	
RDT16_033	033 - 11	3.71	12.6	0.29	110.8	7.7	0.949	0.071	0.98471	0.83	0.018	4769	75	4260	250	5029	40	89.33	84.71	
RDT16_033	033 - 110	69.5	142.2	0.49	8.68	0.15	0.3906	0.0049	0.70644	0.1638	0.002	2304	15	2129	22	2493	21	92.40	85.40	
RDT16_033	033 - 111	452	29.5	15.32	1.488	0.019	0.1528	0.0014	0.51003	0.07034	0.0009	925	7.9	916.3	7.9	936	25	99.06	97.90	
RDT16_033	033 - 112	222.5	182	1.22	7.496	0.11	0.3753	0.0043	0.85381	0.14488	0.0013	2172	13	2054	20	2285	16	94.57	89.89	
RDT16_033	033 - 113	213	193	1.10	0.332	0.012	0.03806	0.0005	0.58051	0.0644	0.002	291.8	9.1	240.8	3.1	755	65	82.52	31.89	
RDT16_033	033 - 114	378	205.9	1.84	1.459	0.022	0.1474	0.0022	0.82718	0.07165	0.0008	913.1	9.4	886	12	976	24	97.03	90.78	
RDT16_033	033 - 115	333	218	1.53	0.497	0.011	0.06255	0.00067	0.33463	0.0577	0.0013	409.2	7.7	391.7	4.2	507	51	95.72	77.26	
RDT16_033	033 - 116	161	92.6	1.74	1.368	0.095	0.1403	0.0073	0.95105	0.0694	0.0017	864	41	845	41	915	50	97.80	92.35	
RDT16_033	033 - 117	418	295	1.42	0.5196	0.0097	0.06609	0.00082	0.31388	0.05713	0.001	424.6	6.5	412.5	5	496	40	97.15	83.17	
RDT16_033	033 - 118	555	1250	0.44	0.6294	0.01	0.07942	0.00091	0.52678	0.05796	0.0008	495.5	6.4	492.6	5.5	529	30	99.41	93.12	
RDT16_033	033 - 119	377	326	1.16	2.491	0.045	0.2101	0.0032	0.84605	0.08549	0.0009	1272	12	1231	17	1325	21	96.78	92.91	
RDT16_033	033 - 12	854	578	1.48	0.6828	0.0098	0.0834	0.00074	0.75855	0.05931	0.0007	528.3	5.9	516.4	4.4	576	25	97.75	89.65	
RDT16_033	033 - 120	102.9	88.7	1.16	0.625	0.038	0.04272	0.0007	0.27221	0.1088	0.0063	491	24	269.7	4.3	1750	110	54.93	15.41	
RDT16_033	033 - 13	497	82.2	6.05	3.153	0.061	0.2366	0.0043	0.93999	0.09655	0.0008	1446	14	1369	22	1557	16	94.67	87.93	

Supplementary Table 1. Main isotopes and ratios measured using LA–ICP–MS. Concordance 1 ($^{206}Pb/^{238}U/^{207}Pb/^{235}U$) and 2 ($^{206}Pb/^{238}U/^{207}Pb/^{206}Pb$).

RDT16_033	033 - 14	366	243	1.51	4.208	0.073	0.2858	0.004	0.79825	0.1057	0.0012	1674	14	1620	20	1725	21	96.77	93.91	
RDT16_033	033 - 15	49.3	54.7	0.90	0.854	0.08	0.0903	0.0054	0.85234	0.0683	0.0032	615	44	556	32	840	100	90.41	66.19	
RDT16_033	033 - 16	347.7	88.3	3.94	1.411	0.028	0.1422	0.0022	0.76147	0.07276	0.001	895	12	857	12	1004	29	95.75	85.36	
RDT16_033	033 - 17	131	99	1.32	1.314	0.038	0.1341	0.0025	0.65174	0.0719	0.0016	852	16	811	14	980	47	95.19	82.76	
RDT16_033	033 - 18	407	213.5	1.91	8.718	0.1	0.3957	0.0042	0.8335	0.15997	0.0014	2308.4	11	2149	20	2454.2	14	93.09	87.56	
RDT16_033	033 - 19	2.88	10.3	0.28	32.3	2.2	0.351	0.028	0.80188	0.665	0.029	3544	67	1940	130	4648	69	54.74	41.74	
RDT16_033	033 - 2	72.3	52.9	1.37	1.531	0.055	0.1378	0.0034	0.70361	0.0809	0.0023	947	24	832	19	1206	55	87.86	68.99	
RDT16_033	033 - 20	470	347	1.35	0.521	0.015	0.06206	0.00091	-0.11681	0.061	0.0022	427	11	388.1	5.5	638	78	90.89	60.83	
RDT16_033	033 - 21	1151	879	1.31	0.56	0.012	0.0692	0.0015	0.87642	0.05898	0.0007	451.3	7.7	431.5	9.3	570	27	95.61	75.70	
RDT16_033	033 - 22	1153	743	1.55	0.3663	0.0062	0.04922	0.00039	0.35992	0.0536	0.0009	316.8	4.6	309.7	2.4	348	37	97.76	88.99	
RDT16_033	033 - 23	462	643	0.72	0.631	0.012	0.07402	0.001	0.67417	0.06192	0.0009	496.5	7.4	460.3	6	681	32	92.71	67.59	
RDT16_033	033 - 24	128.7	104.9	1.23	0.397	0.018	0.0505	0.0013	0.71332	0.0573	0.0026	338	13	317.5	7.8	468	96	93.93	67.84	
RDT16_033	033 - 25	239	398	0.60	0.492	0.014	0.05945	0.00066	0.37479	0.0605	0.0015	405.9	9.4	372.2	4	611	54	91.70	60.92	
RDT16_033	033 - 26	141	144	0.98	0.5	0.34	0.0401	0.0037	0.98998	0.061	0.0064	283	29	253	22	530	150	89.40	47.74	
RDT16_033	033 - 27	444	583	0.76	0.2941	0.0055	0.04046	0.00055	0.55481	0.05302	0.0009	261.7	4.4	255.7	3.4	323	41	97.71	79.16	
RDT16_033	033 - 28	610	196	3.11	0.5089	0.0078	0.06683	0.00077	0.56988	0.05754	0.0008	417.6	5.2	417	4.6	513	30	99.86	81.29	
RDT16_033	033 - 29	158	200	0.79	0.313	0.013	0.04093	0.00044	0.2251	0.0552	0.0022	277.7	9.9	258.6	2.7	416	90	93.12	62.16	
RDT16_033	033 - 3	197	144	1.37	0.585	0.016	0.0688	0.00093	0.58322	0.0614	0.0014	467.2	10	428.9	5.6	650	52	91.80	65.98	
RDT16_033	033 - 30	78.7	168.9	0.47	1.993	0.034	0.1846	0.0023	0.24297	0.0785	0.0014	1113	11	1092	13	1153	35	98.11	94.71	
RDT16_033	033 - 31	770	490	1.57	0.5463	0.0073	0.06962	0.00066	0.50646	0.05671	0.0007	442.5	4.8	433.8	4	477	29	98.03	90.94	
RDT16_033	033 - 32	157	196	0.80	0.381	0.018	0.04244	0.00053	-0.21192	0.0649	0.0031	329	12	267.9	3.3	771	98	81.43	34.75	
RDT16_033	033 - 33	222	200	1.11	0.568	0.015	0.07217	0.00074	0.59821	0.0574	0.0014	455.9	9.9	449.2	4.4	492	56	98.53	91.30	
RDT16_033	033 - 34	155	117	1.32	1.431	0.03	0.1473	0.0021	0.58726	0.0694	0.0011	901	12	885	12	913	35	98.22	96.93	
RDT16_033	033 - 35	1147	857	1.34	0.3554	0.0076	0.04806	0.00068	0.72874	0.05347	0.0008	309.4	5.5	302.6	4.2	349	33	97.80	86.70	
RDT16_033	033 - 36	194.1	192.8	1.01	0.322	0.014	0.04068	0.00065	0.555	0.0573	0.0022	283	11	257	4	513	82	90.81	50.10	
RDT16_033	033 - 37	588	141.9	4.14	2.812	0.052	0.2347	0.0031	0.86936	0.08726	0.0009	1358	14	1359	16	**1367**	20	100.07	99.41	
RDT16_033	033 - 38	54.4	73.8	0.74	0.307	0.021	0.03968	0.00064	-0.019191	0.0559	0.0038	271	16	250.8	4	400	150	92.55	62.70	
RDT16_033	033 - 39	102.7	90.5	1.13	0.331	0.014	0.04207	0.00061	0.34302	0.0564	0.0023	291	11	265.7	3.8	465	95	91.31	57.14	
RDT16_033	033 - 4	311	241	1.29	0.2743	0.008	0.03725	0.00044	-0.10318	0.0531	0.0016	245.8	6.4	**235.8**	**2.8**	318	69	95.93	74.15	YSG
RDT16_033	033 - 40	275.7	355.9	0.77	10.955	0.11	0.4788	0.0042	0.80154	0.166	0.0014	2519	9.1	2522	18	**2516.6**	14	100.12	100.21	
RDT16_033	033 - 42	23.12	65.5	0.35	12.22	0.33	0.1338	0.003	0.87638	0.671	0.011	2622	24	809	17	4671	26	30.85	17.32	
RDT16_033	033 - 43	98.6	127	0.78	2.084	0.031	0.1807	0.0024	0.33951	0.0837	0.0014	1143	10	1071	13	1291	36	93.70	82.96	
RDT16_033	033 - 44	1244	533.4	2.33	0.3577	0.0057	0.04694	0.00045	0.44496	0.05565	0.0008	310.4	4.3	295.7	2.8	434	33	95.26	68.13	
RDT16_033	033 - 45	213	224	0.95	2.011	0.051	0.1806	0.0035	0.81875	0.08095	0.0011	1117	17	1070	19	1217	26	95.79	87.92	
RDT16_033	033 - 46	293	209	1.40	5.33	0.058	0.3336	0.0027	0.71745	0.11634	0.0011	1873.2	9.3	1855.9	13	1901	17	99.08	97.63	
RDT16_033	033 - 47	576	641	0.90	1.332	0.019	0.1434	0.0017	0.69316	0.06773	0.0007	859.5	8.1	863.5	9.8	858	23	100.47	100.64	
RDT16_033	033 - 48	304	338	0.90	0.573	0.03	0.06532	0.00079	0.52124	0.0646	0.0032	458	19	407.9	4.8	740	100	89.06	55.12	
RDT16_033	033 - 49	81.2	54.8	1.48	0.321	0.021	0.03849	0.0007	0.42659	0.0598	0.0034	283	16	243.5	4.3	590	130	86.04	41.27	
RDT16_033	033 - 5	128.1	98.8	1.30	0.408	0.018	0.0516	0.00068	0.047912	0.0579	0.0025	347	13	324.3	4.1	505	92	93.46	64.22	
RDT16_033	033 - 50	1456	362	4.02	0.3183	0.0043	0.04425	0.00033	0.4409	0.05247	0.0006	280.6	3.4	279.1	2.1	303	27	99.47	92.11	
RDT16_033	033 - 51	381	233	1.64	0.308	0.0081	0.04261	0.00055	0.57857	0.0526	0.0013	272.4	6.3	269	3.4	310	56	98.75	86.77	
RDT16_033	033 - 52	960	783	1.23	0.5651	0.0094	0.0724	0.0011	0.78574	0.05708	0.0007	454.7	6.1	**450.6**	**6.6**	491	28	99.10	91.77	
RDT16_033	033 - 53	200.9	123.9	1.62	0.443	0.012	0.05494	0.00091	0.49137	0.0585	0.0016	371.9	8.6	344.7	5.5	542	58	92.69	63.60	
RDT16_033	033 - 54	436	349	1.25	1.202	0.021	0.1296	0.0015	0.63498	0.06727	0.0009	801	9.5	785.7	8.4	854	29	98.09	92.00	
RDT16_033	033 - 55	128.4	261.6	0.49	0.64	0.029	0.0604	0.0011	0.62375	0.0774	0.003	503	19	378.3	6.5	1129	82	75.21	33.51	
RDT16_033	033 - 56	177.8	124.7	1.43	3.103	0.041	0.2491	0.0023	0.40364	0.0912	0.0012	1432.9	10	1433.7	12	1448	25	100.06	99.01	
RDT16_033	033 - 57	276.2	253	1.09	0.529	0.012	0.06815	0.00063	0.085851	0.0566	0.0013	430.6	7.8	425	3.8	466	48	98.70	91.20	
RDT16_033	033 - 58	218	165	1.32	1.65	0.031	0.1633	0.0024	0.66276	0.0728	0.0011	989	12	975	13	1005	31	98.58	97.01	
RDT16_033	033 - 59	1950	517	3.77	0.2786	0.01	0.0333	0.0013	0.80634	0.0616	0.0012	249.1	7.9	210.8	8.2	673	41	84.62	31.32	
RDT16_033	033 - 6	623	805	0.77	0.3177	0.0091	0.04185	0.00073	0.80159	0.05523	0.001	279.9	7	264.3	4.5	414	42	94.43	63.84	
RDT16_033	033 - 60	50.9	50	1.02	0.363	0.026	0.04194	0.00074	0.34443	0.0642	0.0044	312	19	264.8	4.6	710	150	84.87	37.30	
RDT16_033	033 - 61	422	338	1.25	0.2917	0.007	0.03976	0.00037	0.19261	0.0538	0.0013	259.7	5.5	251.3	2.3	352	57	96.77	71.39	
RDT16_033	033 - 62	171.7	174.1	0.99	3.157	0.045	0.2497	0.0021	0.49103	0.0923	0.0012	1446	11	1436.8	11	**1470**	24	99.36	97.74	
RDT16_033	033 - 63	138.6	103.3	1.34	0.347	0.012	0.04774	0.00068	0.44765	0.0529	0.0018	302.1	9.1	300.6	4.2	316	78	99.50	95.13	

Supplementary Table 1. Main isotopes and ratios measured using LA–ICP–MS. Concordance 1 ($^{206}Pb/^{238}U/^{207}Pb/^{235}U$) and 2 ($^{206}Pb/^{238}U/^{207}Pb/^{206}Pb$).

RDT16_033	033 - 64	796	445	1.79	0.2748	0.0039	0.0393	0.00038	0.36869	0.05294	0.0008	246.4	3.1	248.5	2.4	322	32	100.85	77.17
RDT16_033	033 - 65	424	397	1.07	0.3311	0.0086	0.04649	0.00063	0.3619	0.0526	0.0012	290.1	6.5	292.9	3.9	317	51	100.97	92.40
RDT16_033	033 - 66	348	200	1.74	4.76	0.055	0.3058	0.0036	0.95013	0.11808	0.0009	1777.4	9.7	1720	18	1926.3	14	96.77	89.29
RDT16_033	033 - 67	366	461	0.79	0.4348	0.0091	0.05773	0.00073	0.32475	0.0569	0.0011	366.4	6.4	361.8	4.5	495	43	98.74	73.09
RDT16_033	033 - 68	358	323	1.11	0.3326	0.0092	0.0443	0.00055	0.34733	0.0544	0.0014	292.2	7.1	279.4	3.4	409	52	95.62	68.31
RDT16_033	033 - 69	87.7	70.5	1.24	0.335	0.017	0.04585	0.00062	0.13516	0.053	0.0027	294	13	289	3.8	310	110	98.30	93.23
RDT16_033	033 - 7	119.5	201	0.59	2.84	0.11	0.2243	0.0065	0.93849	0.0923	0.0015	1367	28	1303	35	1469	31	95.32	88.70
RDT16_033	033 - 70	309.8	241.2	1.28	0.675	0.011	0.08438	0.00093	0.23372	0.05823	0.0009	523.5	6.5	522.2	5.5	539	37	99.75	96.88
RDT16_033	033 - 71	147.9	67.5	2.19	5.628	0.061	0.352	0.003	0.62557	0.11697	0.0011	1920	9.3	1944	14	1909	18	101.25	101.83
RDT16_033	033 - 72	250	152	1.64	0.2661	0.0095	0.03837	0.00059	0.096844	0.0524	0.0018	239.2	7.6	242.7	3.7	309	77	101.46	78.54
RDT16_033	033 - 73	145	226	0.64	0.527	0.039	0.05423	0.00081	0.58903	0.0704	0.0045	426	25	340.4	5	1020	140	79.91	33.37
RDT16_033	033 - 74	597	264	2.26	0.561	0.011	0.07137	0.00089	0.48751	0.0573	0.0009	451.7	6.9	444.4	5.4	504	33	98.38	88.17
RDT16_033	033 - 75	277.3	218.7	1.27	2.371	0.071	0.2053	0.0058	0.94587	0.08437	0.001	1231	22	1203	31	1299	22	97.73	92.61
RDT16_033	033 - 76	533	419	1.27	0.3022	0.0059	0.03937	0.0007	0.20716	0.0565	0.0012	268	4.6	248.9	4.3	464	48	92.87	53.64
RDT16_033	033 - 78	43.9	48.2	0.91	1.935	0.054	0.1759	0.002	0.32057	0.08	0.0022	1097	18	1044.7	11	1200	53	95.23	87.06
RDT16_033	033 - 79	243	405	0.60	0.403	0.01	0.05362	0.00076	0.50589	0.0548	0.0013	343.8	7.5	336.7	4.7	393	53	97.93	85.67
RDT16_033	033 - 8	194	114	1.70	0.335	0.012	0.04142	0.00056	0.22561	0.0589	0.0021	292.8	9	261.6	3.4	548	80	89.34	47.74
RDT16_033	033 - 80	293.1	132	2.22	0.4441	0.01	0.06022	0.00064	0.2729	0.0544	0.0012	372.8	7	377	3.9	384	48	101.13	98.18
RDT16_033	033 - 81	362	593	0.61	0.285	0.0063	0.04008	0.00056	0.37452	0.0522	0.0011	254.5	5	253.3	3.5	284	50	99.53	89.19
RDT16_033	033 - 82	430	316	1.36	3.14	0.2	0.23	0.011	0.98946	0.0995	0.0016	1428	49	1340	59	1611	29	93.84	83.18
RDT16_033	033 - 83	200.5	129.7	1.55	1.685	0.062	0.1532	0.0016	0.50203	0.0808	0.0028	1000	22	919.1	9.1	1200	62	91.91	76.59
RDT16_033	033 - 84	335	388	0.86	0.542	0.012	0.06778	0.00078	0.54905	0.0571	0.0012	440.7	8	422.7	4.7	495	45	95.92	85.39
RDT16_033	033 - 85	74.8	78	0.96	0.5	0.18	0.0438	0.0019	0.98946	0.07	0.014	365	73	276	12	590	170	75.62	46.78
RDT16_033	033 - 86	109.5	146.4	0.75	0.481	0.017	0.06423	0.00065	0.1839	0.0546	0.0019	398	12	401.3	4	397	81	100.83	101.08
RDT16_033	033 - 87	179	182	0.98	0.292	0.014	0.04081	0.00065	0.28614	0.0524	0.0023	259	11	257.8	4	303	97	99.54	85.08
RDT16_033	033 - 88	244	317	0.77	2.144	0.046	0.1984	0.0036	0.80463	0.07901	0.001	1164	15	1166	20	1170	25	100.17	99.66
RDT16_033	033 - 89	384	179	2.15	5.277	0.051	0.3308	0.0027	0.71725	0.11682	0.001	1864.9	8.3	1842.2	13	1907	15	98.78	96.60
RDT16_033	033 - 9	58	59	0.98	0.572	0.093	0.0363	0.0017	0.19679	0.112	0.035	472	57	229	11	1100	950	48.52	20.82
RDT16_033	033 - 90	81	82.2	0.99	0.505	0.021	0.06763	0.00098	0.31433	0.0551	0.002	416	15	421.8	5.9	404	85	101.39	104.41
RDT16_033	033 - 91	315	156.5	2.01	5.212	0.063	0.3562	0.0037	0.85105	0.10645	0.0009	1855.4	10	1964	18	1738	16	105.85	113.00
RDT16_033	033 - 92	0.118	0.074	1.59	31	31	0.31	0.31	NaN	0.74	0.74	3500	3500	1800	1800	4800	4800	51.43	37.50
RDT16_033	033 - 93	201	127.2	1.58	1.921	0.065	0.1727	0.0046	0.93997	0.0814	0.0011	1088	24	1026	25	1232	27	94.30	83.28
RDT16_033	033 - 94	1027	443	2.32	1.984	0.032	0.1831	0.0021	0.80537	0.07938	0.001	1109	11	1084	11	1173	21	97.75	92.41
RDT16_033	033 - 95	130	100	1.30	0.9	0.051	0.07382	0.00091	0.14202	0.0894	0.0052	658	28	459.1	5.5	1390	110	69.77	33.03
RDT16_033	033 - 96	125.9	159	0.79	0.424	0.016	0.05458	0.00064	0.065301	0.0568	0.0023	358	11	342.6	3.9	467	86	95.70	73.36
RDT16_033	033 - 97	160.5	368	0.44	5.091	0.064	0.3249	0.0028	0.66865	0.11375	0.0012	1834.1	11	1814	14	1858	19	98.90	97.63
RDT16_033	033 - 98	43	42.5	1.01	1.09	0.11	0.047	0.0011	0.87976	0.166	0.013	739	48	296.2	6.6	2470	120	40.08	11.99
RDT16_033	033 - 99	145.4	214.7	0.68	0.461	0.013	0.0597	0.0007	0.139	0.0561	0.0016	384.4	9.3	373.8	4.3	460	66	97.24	81.26
RDT16_033	RDT16033-360.d	303.3	92.9	3.26	0.674	0.031	0.0808	0.0018	0.39232	0.0605	0.0025	526	18	500.7	11	614	93	95.19	81.55
RDT16_033	RDT16033-361.d	563	649	0.87	0.2833	0.013	0.03948	0.00075	0.15886	0.0525	0.0023	253.5	11	249.6	4.7	293	95	98.46	85.19
RDT16_033	RDT16033-362.d	478	291	1.64	0.421	0.021	0.0579	0.0012	0.43901	0.0528	0.0023	356	15	362.5	7.2	303	99	101.83	119.64
RDT16_033	RDT16033-363.d	1438	248.2	5.79	2.446	0.097	0.2108	0.0036	0.85996	0.08434	0.0028	1257.1	28	1232	19	1299	64	98.00	94.84
RDT16_033	RDT16033-364.d	329	104.1	3.16	0.2785	0.014	0.03977	0.00077	0.11744	0.0507	0.0026	248.7	11	251.3	4.8	225	110	101.05	111.69
RDT16_033	RDT16033-365.d	605	76.4	7.92	5.073	0.2	0.3347	0.0056	0.78588	0.1098	0.0036	1831	33	1860	27	1793	61	101.58	103.74
RDT16_033	RDT16033-366.d	783	244.5	3.20	1.541	0.061	0.1593	0.0027	0.59012	0.06999	0.0024	948	25	953	15	924	69	100.53	103.14
RDT16_033	RDT16033-367.d	527.5	463	1.14	0.512	0.023	0.0698	0.0012	0.35866	0.0528	0.0021	418.9	15	435.1	7.2	310	89	103.87	140.35
RDT16_033	RDT16033-368.d	138.5	55.7	2.49	0.347	0.024	0.0479	0.0011	0.23177	0.0526	0.0034	300	18	301.7	6.9	280	140	100.57	107.75
RDT16_033	RDT16033-369.d	284	165	1.72	0.393	0.024	0.04396	0.00078	0.26782	0.0645	0.0035	336	18	277.3	4.8	735	120	82.53	37.73
RDT16_033	RDT16033-370.d	277.9	118	2.36	0.556	0.026	0.07009	0.0011	0.15425	0.0567	0.0025	450	17	436.6	6.9	500	100	97.02	87.32
RDT16_033	RDT16033-371.d	2227	1194	1.87	0.2613	0.011	0.03109	0.00049	0.24989	0.0608	0.0023	235.5	8.8	197.4	3.1	629	76	83.82	31.38
RDT16_033	RDT16033-372.d	84.5	46.02	1.84	2.127	0.1	0.1943	0.0035	0.29671	0.0777	0.0034	1158	34	1144	19	1151	89	98.79	99.39
RDT16_033	RDT16033-373.d	221.1	148	1.49	1.573	0.069	0.1599	0.0024	0.2268	0.0705	0.0028	958	27	956	13	966	79	99.79	98.96
RDT16_033	RDT16033-374.d	5500	2263	2.43	0.3888	0.017	0.03649	0.00071	0.7305	0.0769	0.0027	333.3	12	231	4.4	1116	69	69.31	20.70
RDT16_033	RDT16033-374.d	2350	435	5.40	0.539	0.023	0.0699	0.0012	0.44839	0.0553	0.0021	437.3	15	435.7	7.1	431	83	99.63	101.09

Supplementary Table 1. Main isotopes and ratios measured using LA–ICP–MS. Concordance 1 ($^{206}Pb/^{238}U/^{207}Pb/^{235}U$) and 2 ($^{206}Pb/^{238}U/^{207}Pb/^{206}Pb$).

RDT16_033	RDT16033-382.d	828	640	1.29	1.689	0.07	0.1579	0.0029	0.76228	0.0789	0.0027	1004	26	946	16	1167	69	94.22	81.06
RDT16_033	RDT16033-383.d	188.8	123.5	1.53	2.066	0.09	0.1923	0.0032	0.33574	0.0782	0.0031	1139	31	1133	17	1142	78	99.47	99.21
RDT16_033	RDT16033-384.d	292.8	140.4	2.09	0.565	0.028	0.06787	0.0011	0.35516	0.0612	0.0027	456	18	423.2	6.7	621	95	92.81	68.15
RDT16_033	RDT16033-385.d	724	316.3	2.29	0.2992	0.015	0.03934	0.0006	0.1791	0.0556	0.0026	264.9	12	248.7	3.7	415	98	93.88	59.93
RDT16_033	RDT16033-386.d	377.7	125.4	3.01	1.684	0.073	0.1641	0.0035	0.68969	0.0749	0.0027	1001	27	979	19	1062	73	97.80	92.18
RDT16_033	RDT16033-387.d	241.5	163.7	1.48	0.343	0.021	0.03958	0.00072	0.074504	0.0634	0.0038	297	16	250.2	4.5	660	140	84.24	37.91
RDT16_033	RDT16033-388.d	169.6	63.01	2.69	0.415	0.024	0.0526	0.0011	0.14415	0.0587	0.0035	351	17	330.5	6.8	500	130	94.16	66.10
RDT16_033	RDT16033-389.d	1774	1431	1.24	0.5517	0.022	0.0683	0.0012	0.51644	0.05905	0.0021	446.8	14	425.7	7.1	562	77	95.28	75.75
RDT16_033	RDT16033-390.d	216.1	189	1.14	1.735	0.079	0.161	0.0029	0.47814	0.0788	0.0032	1018	29	962	16	1172	76	94.50	82.08
RDT16_033	RDT16033-391.d	429	564	0.76	0.684	0.046	0.0707	0.0014	0.69132	0.0719	0.0042	519	24	440.2	8.7	914	110	84.82	48.16
RDT16_033	RDT16033-392.d	501	258	1.94	0.458	0.023	0.05889	0.0011	0.46873	0.056	0.0024	382	16	368.8	6.7	423	95	96.54	87.19
RDT16_033	RDT16033-393.d	359	170	2.11	0.702	0.032	0.0856	0.0016	0.31207	0.0601	0.0025	540	19	529	9.7	599	92	97.96	88.31
RDT16_033	RDT16033-394.d	1974	1605	1.23	1.266	0.051	0.1221	0.0021	0.71769	0.0755	0.0026	831.6	24	743	12	1078	70	89.35	68.92
RDT16_033	RDT16033-395.d	781.3	1084	0.72	3.793	0.15	0.2723	0.0047	0.7951	0.10098	0.0033	1593	32	1551	24	1640	62	97.36	94.57
RDT16_033	RDT16033-396.d	268.6	155.4	1.73	0.41	0.025	0.04367	0.00086	0.32183	0.0684	0.0037	347	18	275.5	5.3	839	120	79.39	32.84
RDT16_033	RDT16033-404.d	540	552	0.98	0.506	0.022	0.066	0.0012	0.36217	0.0571	0.0022	416.9	15	411.9	7	482	84	98.80	85.46
RDT16_033	RDT16033-405.d	212	137	1.55	3.484	0.15	0.2611	0.0056	0.6593	0.0981	0.0035	1522	33	1494	29	1595	67	98.16	93.67
RDT16_033	RDT16033-406.d	77.3	46.91	1.65	0.269	0.024	0.03966	0.001	0.0096892	0.0522	0.0047	243	20	250.7	6.5	240	180	103.17	104.46
RDT16_033	RDT16033-407.d	597	462	1.29	0.2956	0.013	0.04025	0.00067	0.42643	0.0544	0.0022	262.4	11	254.3	4.2	379	91	96.91	67.10
RDT16_033	RDT16033-408.d	1222	944	1.29	0.5078	0.021	0.06484	0.0011	0.35167	0.0582	0.0022	417.1	14	404.9	6.9	534	82	97.08	75.82
RDT16_033	RDT16033-409.d	841	204.5	4.11	0.39	0.018	0.05082	0.00088	0.42115	0.0573	0.0023	333.7	13	319.5	5.4	493	86	95.74	64.81
RDT16_033	RDT16033-410.d	1413	450	3.14	5.925	0.23	0.3591	0.0059	0.80673	0.1224	0.004	1966	34	1977	28	1990	59	100.56	99.35
RDT16_033	RDT16033-411.d	624	59.8	10.43	4.85	0.21	0.3001	0.0067	0.83939	0.1203	0.0041	1790	36	1690	33	1964	57	94.41	86.05
RDT16_033	RDT16033-412.d	948	334	2.84	0.5277	0.021	0.06756	0.00098	0.16188	0.0575	0.0022	429.8	14	421.4	5.9	519	80	98.05	81.19
RDT16_033	RDT16033-413.d	912	707	1.29	1.82	0.071	0.1739	0.0025	0.64247	0.07692	0.0026	1051.5	26	1033	14	1113	67	98.24	92.81
RDT16_033	RDT16033-414.d	835	215.6	3.87	1.114	0.051	0.111	0.0025	0.80773	0.074	0.0026	757	25	678	15	1041	72	89.56	65.13
RDT16_033	RDT16033-415.d	402	56.92	7.06	0.447	0.02	0.0577	0.001	0.2734	0.0577	0.0024	376.2	15	361.6	6.3	496	93	96.12	72.90
RDT16_033	RDT16033-423.d	380	168.1	2.26	3.36	0.14	0.2673	0.0051	0.72616	0.0891	0.003	1491	33	1526	26	1413	68	102.35	108.00
RDT16_033	RDT16033-424.d	133.1	78.1	1.70	0.636	0.037	0.0694	0.0013	0.041221	0.0651	0.0037	505	23	432.4	7.8	730	120	85.62	59.23
RDT16_033	RDT16033-425.d	593	163.8	3.62	0.4233	0.018	0.057	0.00083	0.26581	0.0532	0.0021	358.6	13	357.3	5.1	341	81	99.64	104.78
RDT16_033	RDT16033-426.d	269.3	159.4	1.69	0.282	0.016	0.03994	0.00081	0.14945	0.0512	0.0028	253.2	12	252.4	5	224	120	99.68	112.68
RDT16_033	RDT16033-427.d	374	275	1.36	0.315	0.017	0.04034	0.00076	-0.034881	0.0568	0.003	277.7	13	254.9	4.7	451	110	91.79	56.52
RDT16_033	RDT16033-428.d	688	568	1.21	0.567	0.026	0.0713	0.0015	0.54683	0.0574	0.0022	456	17	443.8	8.8	496	86	97.32	89.48
RDT16_033	RDT16033-429.d	514.6	378.7	1.36	0.2965	0.014	0.04245	0.00069	0.069518	0.0507	0.0022	263.8	11	268	4.3	209	94	101.59	128.23
RDT16_033	RDT16033-430.d	192.9	19.6	9.84	0.842	0.04	0.095	0.0022	0.19968	0.064	0.0027	619	22	585	13	745	88	94.51	78.52
RDT16_033	RDT16033-431.d	206.6	77.9	2.65	1.551	0.066	0.1573	0.0024	0.3259	0.0709	0.0027	950	26	941	13	945	81	99.05	99.58
RDT16_033	RDT16033-432.d	188.4	224	0.84	0.388	0.035	0.0384	0.00091	0.56014	0.0719	0.0058	326	24	242.8	5.7	870	160	74.48	27.91
RDT16_033	RDT16033-433.d	1200	233.6	5.14	1.317	0.052	0.1319	0.0019	0.69785	0.07309	0.0024	852.2	23	798.5	11	1016	70	93.70	78.59
RDT16_033	RDT16033-434.d	85.9	60.9	1.41	0.513	0.034	0.0445	0.0013	0.28385	0.0842	0.0051	422	22	280.6	7.8	1270	130	66.49	22.09
RDT16_033	RDT16033-435.d	986	464	2.13	0.367	0.024	0.0465	0.0012	0.63039	0.0578	0.0029	313	16	293.1	7.3	468	95	93.64	62.63
RDT16_033	RDT16033-436.d	285.4	356.5	0.80	0.588	0.03	0.0711	0.0012	0.32237	0.0605	0.0028	467	19	442.6	7.4	602	99	94.78	73.52
RDT16_033	RDT16033-437.d	257	174.6	1.47	0.524	0.024	0.069	0.0012	0.19423	0.0549	0.0023	427.8	16	430.1	7	403	94	100.54	106.72
RDT16_033	RDT16033-446.d	602.5	258.3	2.33	0.618	0.028	0.0733	0.0012	0.34314	0.0604	0.0024	488.6	18	456	7.3	610	86	93.33	74.75
RDT16_033	RDT16033-447.d	201.5	124.1	1.62	0.704	0.038	0.0753	0.0016	0.15356	0.0666	0.0036	540	22	467.8	9.7	781	100	86.63	59.90
RDT16_033	RDT16033-448.d	475	231	2.06	3.963	0.16	0.2504	0.0042	0.65439	0.1137	0.0039	1630	34	1440	22	1859	64	88.34	77.46
RDT16_033	RDT16033-449.d	302.8	155	1.95	1.006	0.045	0.1011	0.002	0.31596	0.0722	0.0029	705	22	621	11	974	83	88.09	63.76
RDT16_033	RDT16033-450.d	459.1	153.1	3.00	1.85	0.076	0.1695	0.0029	0.51155	0.0776	0.0028	1063	27	1009	16	1136	73	94.92	88.82
RDT16_033	RDT16033-451.d	211.8	113.8	1.86	0.298	0.018	0.04025	0.00079	0.16609	0.0535	0.003	265	14	254.3	4.9	340	130	95.96	74.79
RDT16_033	RDT16033-452.d	239.9	111.9	2.14	0.317	0.017	0.03991	0.0008	0.081036	0.0567	0.003	277.9	13	252.3	5	429	110	90.79	58.81
RDT16_033	RDT16033-453.d	3284	8100	0.41	0.578	0.029	0.0669	0.0015	0.59417	0.0652	0.0024	466	18	417.4	8.9	768	75	89.57	54.35
RDT16_033	RDT16033-454.d	602	672	0.90	0.749	0.032	0.0864	0.0014	0.49835	0.0625	0.0023	566.4	18	534.1	8.5	687	78	94.30	77.74
RDT16_033	RDT16033-455.d	150.1	224	0.67	0.459	0.035	0.0408	0.0011	0.27237	0.0829	0.006	387	24	257.8	6.6	1190	150	66.61	21.66
RDT16_033	RDT16033-456.d	536.8	227.9	2.36	0.312	0.015	0.04046	0.00065	0.12458	0.0563	0.0026	275.9	12	255.6	4	433	100	92.64	59.03
RDT16_033	RDT16033-457.d	244.3	144.8	1.69	0.564	0.03	0.0673	0.0012	0.14704	0.0589	0.0029	453	19	419.9	7.3	604	110	92.69	69.52

Supplementary Table 1. Main isotopes and ratios measured using LA–ICP–MS. Concordance 1 ($^{206}Pb/^{238}U/^{207}Pb/^{235}U$) and 2 ($^{206}Pb/^{238}U/^{207}Pb/^{206}Pb$).

RDT16_033	RDT16033-458.d	293	260	1.13	0.834	0.038	0.0938	0.0017	0.44867	0.0639	0.0025	614	21	578	9.8	717	84	94.14	80.61	
RDT16_033	RDT16033-459.d	1422	676.1	2.10	0.666	0.027	0.0805	0.0012	0.57906	0.05965	0.0021	517.4	17	499.2	7.4	594	76	96.48	84.04	
RDT16_033	RDT16033-460.d	1074	267.3	4.02	0.5309	0.022	0.0618	0.0012	0.49812	0.062	0.0022	432.6	15	386.3	7.3	665	77	89.30	58.09	
RDT16_033	RDT16033-468.d	685	389	1.76	0.3214	0.015	0.04267	0.00074	0.030844	0.0554	0.0026	282.3	12	269.3	4.5	392	99	95.39	68.70	
RDT16_033	RDT16033-469.d	174.3	52.8	3.30	1.919	0.099	0.1853	0.0039	0.36338	0.0759	0.0035	1086	35	1095	21	1105	92	100.83	99.10	
RDT16_033	RDT16033-470.d	299.1	111.6	2.68	0.535	0.026	0.069	0.0012	0.3043	0.0561	0.0025	434	18	430.2	7.1	469	96	99.12	91.73	
RDT16_033	RDT16033-471.d	239	103.2	2.32	0.337	0.02	0.04639	0.00094	0.1323	0.0536	0.0031	293	15	292.3	5.8	317	120	99.76	92.21	
RDT16_033	RDT16033-472.d	164.8	229.3	0.72	0.618	0.032	0.0777	0.0016	0.14555	0.0586	0.0028	486	20	482	9.3	556	110	99.18	86.69	
RDT16_035	035 - 1	4760	2280	2.09	0.3106	0.0026	0.04366	0.00029	0.40923	0.05156	0.0005	274.6	2	275.49	1.8	264	20	100.32	104.35	
RDT16_035	035 - 10	81	68	1.19	0.353	0.018	0.0435	0.001	0.27578	0.0583	0.003	308	13	274.3	6.4	500	110	89.06	54.86	
RDT16_035	035 - 100	89.5	53.6	1.67	0.325	0.02	0.03895	0.00056	0.14306	0.0614	0.0036	284	16	246.3	3.5	610	130	86.73	40.38	
RDT16_035	035 - 101	376	419	0.90	0.584	0.012	0.07132	0.00078	0.861	0.05948	0.001	466.5	7.6	444.1	4.7	580	35	95.20	76.57	
RDT16_035	035 - 102	110.6	100	1.11	0.271	0.014	0.0393	0.00042	0.14044	0.0514	0.0026	244	11	248.5	2.6	220	110	101.84	112.95	
RDT16_035	035 - 103	154.9	93.2	1.66	0.536	0.015	0.06977	0.00071	0.33895	0.0559	0.0015	435.5	9.9	434.7	4.3	451	61	99.82	96.39	
RDT16_035	035 - 104	111.2	87.8	1.27	0.283	0.014	0.04123	0.00065	0.17878	0.0495	0.0023	252	11	260.4	4	210	100	103.33	124.00	
RDT16_035	035 - 105	306	367	0.83	0.277	0.01	0.03861	0.00055	0.31216	0.0526	0.0019	247.8	8	244.2	3.4	292	78	98.55	83.63	
RDT16_035	035 - 106	9.18	38.6	0.24	6.48	0.23	0.0882	0.0026	0.51347	0.537	0.02	2037	32	547	15	4332	56	~~26.85~~	~~12.63~~	
RDT16_035	035 - 107	84.9	64.7	1.31	0.27	0.014	0.03985	0.00063	0.26675	0.0497	0.0025	242	11	251.9	3.9	170	100	104.09	148.18	
RDT16_035	035 - 108	176	119	1.48	0.313	0.012	0.04204	0.00055	0.036895	0.0545	0.0021	276.4	9	265.5	3.4	390	81	96.06	68.08	
RDT16_035	035 - 109	50.3	40.5	1.24	0.311	0.022	0.03996	0.00077	-0.025388	0.0551	0.0044	276	18	252.6	4.8	420	160	91.52	60.14	
RDT16_035	035 - 11	132	111	1.19	0.284	0.014	0.03964	0.00054	0.20893	0.0521	0.0025	253	11	250.6	3.3	270	110	99.05	92.81	
RDT16_035	035 - 110	53.4	28.06	1.90	0.324	0.019	0.04165	0.00063	0.14286	0.0565	0.0033	283	15	263.1	3.9	430	130	92.97	61.19	
RDT16_035	035 - 111	100.6	72.6	1.39	0.296	0.011	0.04025	0.00047	0.19786	0.0536	0.0021	262.9	8.8	254.4	2.9	329	86	96.77	77.33	
RDT16_035	035 - 112	109.1	58.8	1.86	0.276	0.012	0.03944	0.00054	0.088373	0.051	0.0023	248.3	9.7	249.3	3.4	230	99	100.40	108.39	
RDT16_035	035 - 12	141.7	117.2	1.21	0.526	0.017	0.06566	0.00069	0.090597	0.0573	0.0019	430	11	410	4.2	513	69	95.35	79.92	
RDT16_035	035 - 13	229.3	180.9	1.27	0.534	0.012	0.06706	0.00066	0.18034	0.0579	0.0014	434.2	8.2	418.4	4	514	55	96.36	81.40	
RDT16_035	035 - 14	91.4	74.4	1.23	0.302	0.016	0.03932	0.00058	0.37523	0.0558	0.0028	267	13	248.6	3.6	410	110	93.11	60.63	
RDT16_035	035 - 15	40	40.9	0.98	0.339	0.028	0.04115	0.00097	0.18051	0.0602	0.0049	298	22	259.9	6	560	180	87.21	46.41	
RDT16_035	035 - 16	84.3	95.7	0.88	0.286	0.014	0.03956	0.00047	0.37866	0.0527	0.0025	255	11	250.1	2.9	303	98	98.08	82.54	
RDT16_035	035 - 17	40.81	34.3	1.19	0.409	0.04	0.04114	0.00067	0.10655	0.0732	0.0072	347	29	259.9	4.1	880	210	74.90	29.53	
RDT16_035	035 - 18	77.29	55.3	1.40	0.295	0.015	0.03939	0.00057	0.045583	0.0544	0.0026	262	12	249	3.5	370	110	95.04	67.30	
RDT16_035	035 - 19	24.75	20.84	1.19	2.477	0.076	0.0524	0.0012	0.37196	0.3413	0.01	1262	22	328.9	7.2	3659	45	26.06	8.99	small zircon
RDT16_035	035 - 2	80	37.8	2.12	0.333	0.02	0.04566	0.00087	-0.11763	0.052	0.0036	291	15	287.8	5.4	280	140	98.90	102.79	
RDT16_035	035 - 20	163.8	270	0.61	0.291	0.014	0.03721	0.00041	-0.12379	0.0569	0.0029	259	11	235.5	2.6	440	110	90.93	53.52	
RDT16_035	035 - 21	186.8	150.7	1.24	0.383	0.015	0.0514	0.0016	0.79687	0.0564	0.0015	328	11	322.9	9.7	482	60	98.45	66.99	
RDT16_035	035 - 22	118	67.3	1.75	0.2885	0.01	0.04098	0.00049	0.14984	0.0514	0.0019	257	7.9	258.9	3	252	82	100.74	102.74	
RDT16_035	035 - 23	241.4	163	1.48	0.284	0.011	0.03846	0.00045	0.43969	0.0533	0.0019	253.7	8.6	243.3	2.8	344	83	95.90	70.73	
RDT16_035	035 - 24	72.2	43.5	1.66	0.296	0.016	0.0416	0.00047	0.1495	0.0503	0.0026	262	13	262.7	2.9	250	120	100.27	105.08	
RDT16_035	035 - 25	224.1	238	0.94	0.283	0.011	0.03771	0.00053	0.61068	0.0547	0.0016	252.5	8.6	238.6	3.3	383	67	94.50	62.30	
RDT16_035	035 - 26	58.1	58.2	1.00	0.423	0.053	0.04178	0.001	0.74744	0.0709	0.0073	350	36	263.8	6.2	1000	210	75.37	26.38	
RDT16_035	035 - 27	93	74.4	1.25	0.282	0.013	0.03955	0.00049	0.078593	0.0508	0.0023	252	11	250	3	240	100	99.21	104.17	
RDT16_035	035 - 28	5.39	30.5	0.18	22.5	2.3	0.258	0.021	0.93605	0.629	0.027	3164	97	1470	100	4573	63	46.46	32.15	
RDT16_035	035 - 29	221	105	2.10	0.316	0.013	0.0452	0.001	0.38944	0.0506	0.002	278	10	284.8	6.4	214	84	102.45	133.08	
RDT16_035	035 - 3	129.6	71.6	1.81	0.311	0.013	0.04191	0.0005	0.38914	0.0532	0.0019	274.1	9.7	264.7	3.1	313	81	96.57	84.57	
RDT16_035	035 - 30	153.5	89.7	1.71	0.268	0.013	0.03586	0.00053	0.38823	0.0568	0.003	240	11	227.1	3.3	460	120	94.63	49.37	
RDT16_035	035 - 31	156.6	204.6	0.77	0.293	0.013	0.03838	0.00042	0.15804	0.0557	0.0024	260.3	9.8	242.8	2.6	434	96	93.28	55.94	
RDT16_035	035 - 32	268.7	267	1.01	0.983	0.021	0.1008	0.0014	0.80023	0.0708	0.0012	695	11	619	8.1	947	34	89.06	65.36	
RDT16_035	035 - 33	4.06	12.26	0.33	12.88	0.61	0.1498	0.005	0.1443	0.621	0.031	2665	44	908	26	4541	75	34.07	20.00	
RDT16_035	035 - 34	179	125.9	1.42	0.2815	0.01	0.03983	0.00038	0.19786	0.051	0.0018	251.5	7.9	251.8	2.4	221	79	100.12	113.94	
RDT16_035	035 - 35	49.3	22.4	2.20	0.308	0.023	0.04181	0.00082	0.024074	0.0528	0.0038	271	18	264	5.1	260	150	97.42	101.54	
RDT16_035	035 - 36	8.55	39.1	0.22	9.56	0.36	0.112	0.0033	0.41748	0.609	0.024	2386	35	684	19	4528	62	28.67	15.11	
RDT16_035	035 - 37	94.9	69.1	1.37	0.301	0.014	0.04092	0.0006	0.10475	0.0526	0.0026	266	11	258.5	3.7	342	100	97.18	75.58	
RDT16_035	035 - 38	53.8	25.7	2.09	0.286	0.025	0.03797	0.00095	0.47101	0.0563	0.0042	253	19	240.2	5.9	380	160	94.94	63.21	

Supplementary Table 1. Main isotopes and ratios measured using LA–ICP–MS. Concordance 1 ($^{206}Pb/^{238}U/^{207}Pb/^{235}U$) and 2 ($^{206}Pb/^{238}U/^{207}Pb/^{206}Pb$).

RDT16_035	035 - 39	42.7	29.5	1.45	0.272	0.025	0.04144	0.00064	-0.10977	0.0488	0.0047	248	20	261.8	4	130	190	105.56	201.38
RDT16_035	035 - 4	139.1	69.4	2.00	0.326	0.014	0.04261	0.0006	0.22403	0.0552	0.0021	288	11	269	3.7	438	87	93.40	61.42
RDT16_035	035 - 40	138.4	129	1.07	0.287	0.011	0.039	0.0011	0.37997	0.053	0.0021	256.6	9.1	246.8	6.6	315	89	96.18	78.35
RDT16_035	035 - 41	67.1	55.7	1.20	0.441	0.022	0.05934	0.00084	-0.022989	0.053	0.0027	373	16	371.6	5.1	340	120	99.62	109.29
RDT16_035	035 - 42	186.4	152	1.23	0.331	0.016	0.04051	0.00055	0.22082	0.0592	0.0027	292	12	256	3.4	600	100	87.67	42.67
RDT16_035	035 - 43	78	83.3	0.94	0.286	0.019	0.03984	0.00051	0.070036	0.0522	0.0034	254	15	251.9	3.2	250	140	99.17	100.76
RDT16_035	035 - 44	76.6	58.6	1.31	0.303	0.019	0.04061	0.00067	0.23947	0.0547	0.0034	269	15	256.6	4.2	340	130	95.39	75.47
RDT16_035	035 - 45	189	72	2.63	0.333	0.01	0.04414	0.00056	0.26484	0.055	0.0016	291.6	7.9	278.5	3.5	406	66	95.51	68.60
RDT16_035	035 - 46	54.9	19.11	2.87	0.417	0.036	0.0529	0.0031	0.67383	0.0575	0.0036	357	25	332	19	500	140	93.00	66.40
RDT16_035	035 - 47	57	61.2	0.93	0.298	0.017	0.03962	0.00068	0.20176	0.0558	0.0034	269	15	250.5	4.2	440	140	93.12	56.93
RDT16_035	035 - 48	210.9	141.3	1.49	0.526	0.015	0.06545	0.00082	0.34205	0.0583	0.0016	428.7	9.8	408.7	4.9	543	64	95.33	75.27
RDT16_035	035 - 49	113.8	79.2	1.44	0.289	0.013	0.0383	0.00052	0.33158	0.0552	0.0025	257	10	242.3	3.2	400	98	94.28	60.58
RDT16_035	035 - 5	62.8	33.9	1.85	0.296	0.019	0.04118	0.00067	0.024346	0.0522	0.0034	264	15	260.1	4.1	260	140	98.52	100.04
RDT16_035	035 - 50	48.7	21.7	2.24	0.278	0.018	0.04177	0.00071	-0.12008	0.0486	0.0033	248	14	263.8	4.4	100	140	106.37	263.80
RDT16_035	035 - 51	253.6	186.8	1.36	0.529	0.016	0.0649	0.0012	0.74955	0.0587	0.0013	430	11	405.5	7.3	559	48	94.30	72.54
RDT16_035	035 - 52	161	91.3	1.76	1.79	0.27	0.128	0.016	0.99505	0.0977	0.0045	960	120	770	93	1566	95	80.21	49.17
RDT16_035	035 - 53	91.1	46.2	1.97	0.3	0.017	0.04163	0.00057	0.26884	0.0515	0.0028	265	13	262.9	3.5	280	120	99.21	93.89
RDT16_035	035 - 54	6.96	44	0.16	13.88	0.58	0.15	0.0042	0.49772	0.68	0.026	2739	41	901	23	4688	61	32.90	19.22
RDT16_035	035 - 55	138.8	121.3	1.14	0.316	0.013	0.03946	0.0005	0.24047	0.0577	0.0021	277.8	9.8	249.5	3.1	524	78	89.81	47.61
RDT16_035	035 - 56	207	151	1.37	0.519	0.015	0.06764	0.00091	0.26825	0.0561	0.0015	424.1	9.9	421.9	5.5	453	59	99.48	93.13
RDT16_035	035 - 57	344	315	1.09	0.3262	0.0084	0.04539	0.00043	0.070854	0.0528	0.0014	286.4	6.4	286.1	2.6	316	57	99.90	90.54
RDT16_035	035 - 58	155	133	1.17	0.288	0.012	0.03723	0.00053	0.10416	0.0562	0.0022	257.5	9.1	235.7	3.3	446	88	91.53	52.85
RDT16_035	035 - 59	75.2	78.4	0.96	0.317	0.013	0.03981	0.0006	0.15752	0.0571	0.0027	281	10	251.6	3.7	500	100	89.54	50.32
RDT16_035	035 - 6	77.4	90.4	0.86	0.275	0.016	0.0398	0.00053	0.35609	0.0501	0.0028	246	13	251.6	3.3	190	120	102.28	132.42
RDT16_035	035 - 60	177	228	0.78	0.2689	0.0095	0.03788	0.00057	0.20966	0.0513	0.0016	241.4	7.6	239.6	3.5	250	68	99.25	95.84
RDT16_035	035 - 61	156.6	158.1	0.99	0.298	0.015	0.03767	0.00052	0.30305	0.0577	0.0027	264	12	238.4	3.2	480	100	90.30	49.67
RDT16_035	035 - 62	118.6	96.5	1.23	0.274	0.013	0.03748	0.00047	0.051074	0.053	0.0024	248	10	237.2	2.9	328	98	95.65	72.32
RDT16_035	035 - 63	564	670	0.84	0.489	0.013	0.0624	0.0012	0.080795	0.0594	0.0016	403.9	8.8	390.4	7.4	570	56	96.66	68.49
RDT16_035	035 - 64	8.66	30	0.29	5.16	0.33	0.0784	0.0027	0.39307	0.475	0.028	1826	55	486	16	4146	84	26.62	11.72
RDT16_035	035 - 65	99.7	65.8	1.52	0.285	0.014	0.03906	0.0005	-0.13614	0.053	0.0027	256	11	247	3.1	310	110	96.48	79.68
RDT16_035	035 - 66	170.7	115	1.48	0.41	0.012	0.05745	0.0008	0.19981	0.0545	0.0016	349.8	8.1	360.1	4.9	405	65	102.94	88.91
RDT16_035	035 - 67	129.8	113.3	1.15	0.278	0.01	0.0389	0.00052	0.12398	0.0519	0.002	248.7	8.3	246	3.2	261	85	98.91	94.25
RDT16_035	035 - 68	40.27	26.98	1.49	0.331	0.022	0.04189	0.00064	-0.1555	0.0571	0.0038	289	17	264.5	3.9	450	150	91.52	58.78
RDT16_035	035 - 69	167	151	1.11	0.294	0.013	0.04012	0.00087	0.46049	0.053	0.0019	265	10	253.6	5.4	322	82	95.70	78.76
RDT16_035	035 - 7	119	126	0.94	0.287	0.017	0.04119	0.00065	0.0022027	0.051	0.0031	260	13	260.2	4	210	130	100.08	123.90
RDT16_035	035 - 70	148.6	88	1.69	0.341	0.013	0.04084	0.00058	0.31213	0.0604	0.002	297	9.7	258	3.6	608	75	86.87	42.43
RDT16_035	035 - 71	327	243.2	1.34	0.501	0.014	0.06445	0.001	0.66023	0.0562	0.0013	411.6	9.7	402.6	6.3	466	51	97.81	86.39
RDT16_035	035 - 72	112.6	91.4	1.23	0.297	0.017	0.0375	0.00071	0.20121	0.0573	0.0033	265	14	237.3	4.4	530	130	89.55	44.77
RDT16_035	035 - 73	105.5	87	1.21	0.303	0.016	0.03891	0.00065	0.33981	0.0568	0.0029	268	13	246	4.1	500	110	91.79	49.20
RDT16_035	035 - 74	89.9	84.9	1.06	0.299	0.017	0.03905	0.0006	0.14578	0.0566	0.0031	264	13	246.9	3.7	440	120	93.52	56.11
RDT16_035	035 - 75	192.9	214.3	0.90	0.53	0.011	0.06799	0.0006	0.040432	0.0567	0.0012	431.4	7	424	3.6	488	51	98.28	86.89
RDT16_035	035 - 76	143.5	108.4	1.32	0.283	0.013	0.03689	0.00047	0.22365	0.0557	0.0026	253	10	233.5	2.9	400	100	92.29	58.38
RDT16_035	035 - 77	161.7	119.1	1.36	0.2573	0.0085	0.03659	0.00055	0.55716	0.0533	0.0016	232.2	6.9	231.7	3.4	346	71	99.78	66.97
RDT16_035	035 - 78	80	79.9	1.00	0.29	0.017	0.03774	0.00055	0.034587	0.0562	0.0033	257	13	238.8	3.4	420	130	92.92	56.86
RDT16_035	035 - 79	36.1	32.1	1.12	0.348	0.028	0.03944	0.00067	-0.049859	0.0637	0.0052	300	21	249.4	4.1	640	180	83.13	38.97
RDT16_035	035 - 8	63.5	42.2	1.50	0.325	0.018	0.04217	0.0007	0.020163	0.0559	0.0033	287	13	266.2	4.3	430	130	92.75	61.91
RDT16_035	035 - 80	227.6	327.6	0.69	0.304	0.011	0.0411	0.00039	0.1477	0.0541	0.0019	269.3	8.2	259.6	2.4	364	80	96.40	71.32
RDT16_035	035 - 81	68.4	50.2	1.36	0.291	0.016	0.03989	0.00065	-0.26286	0.0536	0.0033	258	12	252.1	4	340	140	97.71	74.15
RDT16_035	035 - 82	572	237	2.41	0.3108	0.0064	0.04296	0.00047	0.30035	0.05257	0.001	274.6	4.9	271.1	2.9	311	40	98.73	87.17
RDT16_035	035 - 83	114	64.2	1.78	0.267	0.014	0.03813	0.00051	0.15812	0.0511	0.0027	241	11	241.2	3.2	250	110	100.08	96.48
RDT16_035	035 - 84	62.6	41.5	1.51	0.279	0.016	0.04154	0.00056	0.043128	0.0489	0.0028	249	13	262.3	3.4	140	130	105.34	187.36
RDT16_035	035 - 85	190.4	126.5	1.51	0.2858	0.0087	0.04013	0.00046	-0.052923	0.0517	0.0017	254.9	6.9	253.7	2.8	264	75	99.53	96.10
RDT16_035	035 - 86	52.4	53.48	0.98	0.297	0.023	0.03959	0.00059	0.24575	0.0557	0.0044	262	18	250.3	3.7	410	160	95.53	61.05
RDT16_035	035 - 87	86	62.5	1.38	0.303	0.023	0.04027	0.00073	0.30072	0.0548	0.004	267	17	254.5	4.6	390	160	95.32	65.26

Supplementary Table 1. Main isotopes and ratios measured using LA–ICP–MS. Concordance 1 ($^{206}Pb/^{238}U/^{207}Pb/^{235}U$) and 2 ($^{206}Pb/^{238}U/^{207}Pb/^{206}Pb$).

RDT16_035	035 - 88	88	56.3	1.56	0.314	0.019	0.04403	0.00096	0.23714	0.0511	0.0031	276	15	277.7	5.9	230	130	100.62	120.74	
RDT16_035	035 - 89	76.2	78.8	0.97	0.273	0.016	0.0386	0.00058	0.081988	0.0519	0.0031	244	13	244.2	3.6	280	120	100.08	87.21	
RDT16_035	035 - 9	203.6	119	1.71	0.2993	0.0082	0.04133	0.00049	0.29601	0.0526	0.0015	265.6	6.4	261.1	3	295	63	98.31	88.51	
RDT16_035	035 - 90	226.5	170	1.33	0.528	0.013	0.06724	0.00071	0.27466	0.0563	0.0013	430.1	8.7	419.5	4.3	471	53	97.54	89.07	
RDT16_035	035 - 91	110	58.4	1.88	0.382	0.018	0.04145	0.00053	0.10391	0.0666	0.003	327	13	261.8	3.3	834	89	80.06	31.39	
RDT16_035	035 - 92	150.7	139.2	1.08	0.54	0.013	0.06825	0.00063	0.013834	0.0574	0.0015	437.7	8.8	425.6	3.8	492	59	97.24	86.50	
RDT16_035	035 - 93	98.1	78.1	1.26	0.281	0.017	0.03908	0.00065	0.3978	0.0519	0.0028	250	13	247.1	4	280	120	98.84	88.25	
RDT16_035	035 - 94	433	471	0.92	0.2484	0.0065	0.03512	0.0006	0.33829	0.0536	0.0013	225.1	5.3	222.5	3.8	353	56	98.84	63.03	YSG
RDT16_035	035 - 95	69.2	57.7	1.20	0.332	0.02	0.03988	0.00057	0.37302	0.0602	0.0033	290	15	252.1	3.6	610	120	86.93	41.33	
RDT16_035	035 - 96	38.3	21.7	1.76	0.326	0.025	0.04067	0.00081	0.17803	0.0592	0.0045	287	19	257	5	540	160	89.55	47.59	
RDT16_035	035 - 97	124	156	0.79	5.152	0.059	0.3272	0.0029	0.38797	0.1147	0.0014	1845.5	9.5	1828	14	**1873**	21	99.05	97.60	
RDT16_035	035 - 98	87.9	55.7	1.58	0.298	0.016	0.04074	0.00051	0.056193	0.0532	0.003	264	13	257.4	3.2	310	130	97.50	83.03	
RDT16_035	035 - 99	695	362	1.92	0.3506	0.0059	0.04761	0.00088	0.70226	0.05284	0.001	305.9	4.6	299.8	5.4	326	40	98.01	91.96	
RDT16_035	RDT16035-473.d	69.6	38.1	1.83	0.549	0.064	0.0439	0.0014	0.20636	0.0898	0.0098	424	40	276.6	8.4	1240	220	65.24	22.31	
RDT16_035	RDT16035-474.d	234.6	126.4	1.86	0.589	0.03	0.0692	0.0012	0.066999	0.0622	0.003	469	19	431.1	7.5	659	110	91.92	65.42	
RDT16_035	RDT16035-475.d	74	36.3	2.04	0.659	0.051	0.0428	0.0012	0.10498	0.1144	0.0085	500	30	270.1	7.4	1760	140	54.02	15.35	
RDT16_035	RDT16035-476.d	23.74	11.04	2.15	0.46	0.065	0.0396	0.0018	0.088032	0.088	0.012	359	44	250	11	830	300	69.64	30.12	
RDT16_035	RDT16035-477.d	185	105.7	1.75	0.305	0.019	0.03928	0.00086	0.23083	0.057	0.0034	272	15	248.3	5.3	490	120	91.29	50.67	
RDT16_035	RDT16035-478.d	198.1	78.8	2.51	0.576	0.028	0.0672	0.0011	0.15927	0.0629	0.0029	461	19	419.9	6.8	720	95	91.08	58.32	
RDT16_035	RDT16035-479.d	107.3	68.4	1.57	0.29	0.021	0.03961	0.00086	0.093452	0.0543	0.0039	259	16	250.4	5.3	350	140	96.68	71.54	
RDT16_035	RDT16035-480.d	174.9	80.2	2.18	0.583	0.03	0.06721	0.0011	-0.000362	0.0637	0.0031	466	19	419.3	6.5	686	110	89.98	61.12	
RDT16_035	RDT16035-481.d	293.5	116.5	2.52	0.311	0.017	0.04068	0.00075	0.082937	0.0566	0.0031	273	13	257	4.6	451	120	94.14	56.98	
RDT16_035	RDT16035-482.d	1273	1418	0.90	0.3111	0.013	0.03731	0.00049	0.27846	0.0605	0.0023	274.7	10	236.1	3.1	634	78	85.95	37.24	
RDT16_035	RDT16035-490.d	1183	1150	1.03	0.5185	0.021	0.06637	0.00095	0.33922	0.057	0.0021	423.6	14	414.2	5.7	487	77	97.78	85.05	
RDT16_035	RDT16035-491.d	67	46.1	1.45	0.284	0.025	0.0404	0.0011	0.0052728	0.0519	0.0045	253	20	255.6	6.7	220	180	101.03	116.18	
RDT16_035	RDT16035-492.d	102.2	46.3	2.21	0.329	0.029	0.03865	0.00093	0.15368	0.062	0.0054	294	22	244.4	5.8	640	180	83.13	38.19	
RDT16_035	RDT16035-493.d	160.6	67.4	2.38	0.331	0.025	0.03864	0.00094	0.45386	0.0631	0.0043	290	19	244.4	5.8	690	140	84.28	35.42	
RDT16_035	RDT16035-494.d	211	137	1.54	0.809	0.044	0.0686	0.0012	-0.005695	0.086	0.0045	600	24	427.5	7.3	1303	100	71.25	32.81	
RDT16_035	RDT16035-495.d	184.5	113.6	1.62	0.332	0.021	0.03927	0.00085	0.12551	0.0614	0.0038	285	15	248.2	5.3	610	120	87.09	40.69	
RDT16_035	RDT16035-496.d	69.3	41.54	1.67	0.292	0.027	0.0404	0.0011	0.093319	0.0535	0.0049	258	21	255.1	6.9	250	190	98.88	102.04	
RDT16_035	RDT16035-497.d	1554	601	2.59	0.3644	0.016	0.04858	0.00083	0.68898	0.0548	0.0021	315	12	305.8	5.1	398	87	97.08	76.83	
RDT16_035	RDT16035-498.d	222	133	1.67	0.323	0.018	0.0467	0.0011	0.2352	0.0514	0.0027	284	14	294.3	7	240	110	103.63	122.63	
RDT16_035	RDT16035-499.d	162	79	2.05	0.318	0.021	0.0428	0.0011	0.28699	0.0557	0.0036	282	16	270.7	6.9	430	140	95.99	62.95	
RDT16_035	RDT16035-500.d	247.1	94.2	2.62	4.539	0.18	0.3126	0.0047	0.45298	0.1062	0.0037	1739	34	1753	23	1731	63	100.81	101.27	
RDT16_035	RDT16035-501.d	178.8	124.4	1.44	0.315	0.019	0.04109	0.00086	0.11624	0.0552	0.0032	279	15	259.5	5.3	420	130	93.01	61.79	
RDT16_035	RDT16035-502.d	294	128	2.30	0.563	0.028	0.06737	0.001	0.26775	0.0614	0.0028	451	18	420.2	6.3	638	98	93.17	65.86	
RDT16_035	RDT16035-503.d	167.9	77.6	2.16	0.328	0.02	0.04087	0.00081	-0.073058	0.0586	0.0036	286	15	258.2	5	510	130	90.28	50.63	
RDT16_035	RDT16035-504.d	59.9	27.33	2.19	0.292	0.028	0.0406	0.0012	0.15181	0.0518	0.0047	258	22	256.4	7.7	260	190	99.38	98.62	
RDT16_035	RDT16035-512.d	264	175	1.51	0.316	0.018	0.04005	0.00077	0.16727	0.0566	0.003	278	14	253.1	4.8	440	110	91.04	57.52	
RDT16_035	RDT16035-513.d	127.1	53.69	2.37	0.539	0.031	0.0698	0.0015	0.21071	0.057	0.0032	436	20	434.9	8.8	450	120	99.75	96.64	
RDT16_035	RDT16035-514.d	454.8	275.4	1.65	0.541	0.024	0.06961	0.0011	0.23789	0.0566	0.0024	438.1	16	433.8	6.3	453	93	99.02	95.76	
RDT16_035	RDT16035-515.d	298	186.9	1.59	0.427	0.03	0.04471	0.001	0.15179	0.0681	0.004	356	20	281.9	6.5	780	120	79.19	36.14	
RDT16_035	RDT16035-516.d	293.1	132.9	2.21	0.318	0.017	0.03956	0.00069	0.13335	0.0587	0.003	280.2	13	250.1	4.3	541	110	89.26	46.23	
RDT16_035	RDT16035-517.d	161.4	80	2.02	0.561	0.029	0.0695	0.0015	0.11058	0.0577	0.0028	453	19	432.7	9	478	110	95.52	90.52	
RDT16_035	RDT16035-518.d	365	242	1.51	0.558	0.027	0.07142	0.0011	0.43999	0.0565	0.0024	450	17	445.3	7	463	98	98.96	96.18	
RDT16_035	RDT16035-519.d	161.5	77.1	2.09	0.331	0.022	0.04183	0.0009	0.13501	0.0578	0.0036	289	16	264.6	5.6	470	140	91.56	56.30	
RDT16_035	RDT16035-520.d	47.93	25.12	1.91	0.431	0.051	0.0425	0.0014	0.29722	0.0781	0.0093	353	36	269.1	8.7	830	240	76.23	32.42	
RDT16_035	RDT16035-521.d	213.1	102.3	2.08	0.558	0.027	0.0679	0.0013	0.2112	0.0598	0.0027	448	18	423.4	7.8	580	98	94.51	73.00	
RDT16_035	RDT16035-522.d	43.5	23.5	1.85	0.572	0.057	0.0423	0.0015	0.33193	0.1005	0.0093	444	37	266.9	9.1	1550	190	60.11	17.22	
RDT16_035	RDT16035-523.d	69.4	25.48	2.72	0.318	0.028	0.0426	0.0011	0.06138	0.0543	0.0047	281	21	268.8	6.9	350	180	95.66	76.80	
RDT16_035	RDT16035-524.d	132	107.7	1.23	0.386	0.029	0.04058	0.00095	0.34102	0.0703	0.0047	327	21	256.4	5.9	910	150	78.41	28.18	
RDT16_035	RDT16035-525.d	103.2	42.7	2.42	0.376	0.026	0.04601	0.001	-0.005879	0.0599	0.0042	324	19	289.9	6.1	570	140	89.48	50.86	
RDT16_035	RDT16035-533.d	327.5	138.5	2.36	0.322	0.018	0.04109	0.00085	0.015518	0.0569	0.0032	288	14	259.5	5.3	428	120	90.10	60.63	

Supplementary Table 1. Main isotopes and ratios measured using LA–ICP–MS. Concordance 1 ($^{206}Pb/^{238}U/^{207}Pb/^{235}U$) and 2 ($^{206}Pb/^{238}U/^{207}Pb/^{206}Pb$).

RDT16_035	RDT16035-534.d	169.6	138.6	1.22	0.327	0.023	0.03977	0.00091	0.1979	0.0586	0.0038	286	17	251.3	5.6	520	140	87.87	48.33
RDT16_035	RDT16035-535.d	163	68.5	2.38	0.327	0.024	0.0406	0.0014	0.38937	0.0598	0.0039	288	18	256.4	8.8	520	140	89.03	49.31
RDT16_035	RDT16035-536.d	253	161.6	1.57	0.615	0.031	0.071	0.0014	0.21161	0.0617	0.0029	486	19	442.3	8.4	656	100	91.01	67.42
RDT16_035	RDT16035-537.d	52.1	25.18	2.07	0.454	0.051	0.0415	0.0015	0.14979	0.0758	0.0083	371	36	262.3	9.4	870	240	70.70	30.15
RDT16_035	RDT16035-538.d	527	214.6	2.46	0.548	0.024	0.06946	0.0011	0.38356	0.056	0.0022	444	16	432.9	6.5	441	85	97.50	98.16
RDT16_035	RDT16035-539.d	149.7	152	0.98	0.311	0.023	0.03944	0.00091	0.19451	0.0571	0.004	272	17	249.3	5.6	460	150	91.65	54.20
RDT16_035	RDT16035-540.d	327	95.7	3.42	0.33	0.016	0.04465	0.00085	0.19997	0.0522	0.0025	288.4	12	281.6	5.3	285	100	97.64	98.81
RDT16_035	RDT16035-541.d	257	108.7	2.36	0.587	0.028	0.0714	0.0013	0.31843	0.0588	0.0026	467	18	444.6	7.6	536	97	95.20	82.95
RDT16_035	RDT16035-542.d	377.2	161.8	2.33	0.585	0.028	0.06848	0.0011	0.1179	0.0616	0.0028	466	18	426.9	6.9	632	98	91.61	67.55
RDT16_035	RDT16035-543.d	141.9	79.75	1.78	0.665	0.044	0.04395	0.0011	0.26957	0.1123	0.0074	517	25	277.2	6.5	1800	120	53.62	15.40
RDT16_035	RDT16035-544.d	19.33	45.51	0.42	7.39	0.71	0.0971	0.0054	0.7204	0.534	0.035	2080	82	595	32	4303	99	28.61	13.83
RDT16_035	RDT16035-545.d	231.7	87.1	2.66	0.584	0.031	0.0682	0.0012	0.13253	0.0616	0.0031	469	19	425.2	7.3	620	110	90.66	68.58
RDT16_035	RDT16035-546.d	196.7	90	2.19	0.301	0.018	0.03847	0.00082	-0.070904	0.0572	0.0035	267	14	243.3	5.1	470	130	91.12	51.77
RDT16_035	RDT16035-547.d	160.6	128.1	1.25	0.291	0.019	0.03843	0.00087	-0.090165	0.0544	0.0037	258	15	243	5.4	330	140	94.19	73.64
RDT16_035	RDT16035-555.d	326	115.6	2.82	0.306	0.016	0.04126	0.00077	0.26701	0.0521	0.0025	269.6	13	260.6	4.7	271	100	96.66	96.16
RDT16_035	RDT16035-556.d	113.5	68.5	1.66	0.338	0.025	0.0396	0.0011	0.10423	0.0593	0.0044	294	18	250	6.8	570	150	85.03	43.86
RDT16_035	RDT16035-557.d	397.5	288	1.38	0.287	0.015	0.03971	0.00069	0.13435	0.0505	0.0025	256.3	12	251	4.3	217	110	97.93	115.67
RDT16_035	RDT16035-558.d	60.4	41.39	1.46	0.378	0.037	0.0396	0.0012	0.12726	0.0686	0.0071	322	27	250.4	7.6	750	210	77.76	33.39
RDT16_035	RDT16035-559.d	132.1	54.78	2.41	0.358	0.026	0.03956	0.00096	0.16236	0.0642	0.0044	314	19	250	6	690	140	79.62	36.23
RDT16_035	RDT16035-560.d	376	148.6	2.53	0.615	0.032	0.0685	0.0013	0.34123	0.0624	0.0028	484	20	427.1	7.7	675	98	88.24	63.27
RDT16_035	RDT16035-561.d	320	118.1	2.71	0.535	0.025	0.0665	0.0014	0.14109	0.0565	0.0026	435	17	414.9	8.3	443	100	95.38	93.66
RDT16_035	RDT16035-562.d	500	253	1.98	0.601	0.03	0.075	0.0016	0.096683	0.056	0.0024	475	19	465.9	9.3	443	83	98.08	105.17
RDT16_035	RDT16035-563.d	132.1	83.7	1.58	0.403	0.036	0.0419	0.0012	0.30566	0.0682	0.0058	343	25	264.3	7.2	800	170	77.06	33.04
RDT16_035	RDT16035-564.d	75.3	30.22	2.49	0.363	0.031	0.0418	0.0013	0.1554	0.0609	0.0051	311	23	263.5	8.1	540	180	84.73	48.80
RDT16_035	RDT16035-565.d	155.2	121.6	1.28	0.464	0.032	0.0607	0.0015	0.23417	0.0539	0.0032	384	22	379.8	9	320	130	98.91	118.69
RDT16_035	RDT16035-566.d	79.6	67.7	1.18	0.411	0.038	0.0391	0.0012	0.11136	0.0777	0.0074	345	27	247.4	7.5	1000	190	71.71	24.74
RDT16_035	RDT16035-567.d	98.9	39.5	2.50	0.354	0.026	0.0424	0.0011	0.10424	0.06	0.0045	309	20	267.4	7	580	150	86.54	46.10
RDT16_035	RDT16035-568.d	518	140.9	3.68	0.314	0.017	0.0421	0.0011	0.51932	0.0534	0.0026	276.3	13	265.7	6.7	330	110	96.16	80.52
RDT16_035	RDT16035-569.d	515	682	0.76	0.289	0.015	0.03776	0.0008	0.41287	0.0549	0.0026	258	12	238.9	4.9	398	100	92.60	60.03
RDT16_035	RDT16035-577.d	104.96	54.15	1.94	0.303	0.02	0.0389	0.0011	-0.035483	0.0564	0.0041	267	16	245.8	6.8	420	140	92.06	58.52
RDT16_035	RDT16035-578.d	474.7	389.2	1.22	0.56	0.026	0.0675	0.0012	0.34252	0.0606	0.0025	450.4	17	420.8	7	607	91	93.43	69.32
RDT16_035	RDT16035-579.d	351	113	3.11	0.335	0.018	0.03914	0.00083	0.2756	0.0622	0.0031	292.3	13	248.1	5.3	644	110	84.88	38.52
RDT16_035	RDT16035-580.d	313	164.7	1.90	0.564	0.027	0.06679	0.001	0.2064	0.0613	0.0027	452	18	417.3	6.2	631	98	92.32	66.13
RDT16_035	RDT16035-581.d	160.6	120.9	1.33	0.567	0.032	0.0652	0.0013	0.13601	0.0624	0.0033	455	21	407	8.1	657	110	89.45	61.95
RDT16_035	RDT16035-582.d	311.2	147	2.12	0.595	0.03	0.0668	0.0012	0.43695	0.0642	0.0028	473	19	416.7	7.4	734	89	88.10	56.77
RDT16_035	RDT16035-583.d	448	319	1.40	0.367	0.021	0.04444	0.001	0.46788	0.0583	0.0029	315	16	280.2	6.4	519	100	88.95	53.99
RDT16_035	RDT16035-584.d	122	61.1	2.00	0.43	0.035	0.0381	0.0011	0.035578	0.0806	0.0066	357	25	240.9	6.5	1160	160	67.48	20.77
RDT16_035	RDT16035-585.d	133	89.8	1.48	0.781	0.055	0.072	0.0021	0.166	0.0794	0.0056	583	31	448	12	1170	150	76.84	38.29
RDT16_035	RDT16035-586.d	158.4	142.9	1.11	0.349	0.023	0.03953	0.00098	0.27987	0.0622	0.0038	305	17	249.8	6.1	630	130	81.90	39.65
RDT16_035	RDT16035-587.d	62.6	44.4	1.41	0.448	0.038	0.0487	0.0015	0.13771	0.0678	0.0057	377	28	306.4	9.1	760	170	81.27	40.32
RDT16_035	RDT16035-588.d	105.1	44.57	2.36	0.643	0.04	0.0684	0.0015	0.19118	0.0681	0.0041	499	24	426.1	8.9	790	120	85.39	53.94
RDT16_035	RDT16035-589.d	303.9	251	1.21	0.357	0.019	0.04703	0.00083	0.006793	0.0547	0.0028	310	14	296.2	5.1	370	110	95.55	80.05
RDT16_035	RDT16035-590.d	159.7	120.2	1.33	0.317	0.023	0.04009	0.00095	0.22753	0.0569	0.0038	276	18	253.3	5.9	430	140	91.78	58.91
RDT16_035	RDT16035-591.d	296	33	8.97	0.279	0.018	0.03706	0.00076	-0.035345	0.0537	0.0035	250	14	234.5	4.7	320	130	93.80	73.28
RDT16_035	RDT16035-599.d	519	446	1.16	0.316	0.016	0.03984	0.00072	0.10919	0.0571	0.0027	278.6	12	251.8	4.5	479	100	90.38	52.57
RDT16_035	RDT16035-600.d	417	276	1.51	0.516	0.024	0.06742	0.0011	0.067371	0.0555	0.0025	422.1	16	420.5	6.4	404	96	99.62	104.08
RDT16_035	RDT16035-601.d	296	165	1.79	0.583	0.028	0.0693	0.0014	0.1202	0.0601	0.0026	467	17	432	8.2	575	99	92.51	75.13
RDT16_035	RDT16035-602.d	159	37.69	4.22	0.337	0.024	0.04305	0.0011	0.080577	0.0559	0.0038	295	18	272.3	6.4	400	150	92.31	68.08
RDT16_035	RDT16035-603.d	207	128	1.62	0.363	0.022	0.04174	0.00094	0.19946	0.0616	0.0035	314	16	263.5	5.8	630	120	83.92	41.83
RDT16_035	RDT16035-604.d	157.8	46.9	3.36	1.372	0.068	0.1408	0.0024	0.22934	0.0703	0.0032	880	30	849	14	932	91	96.48	91.09
RDT16_035	RDT16035-605.d	231	118.6	1.95	0.355	0.022	0.04295	0.001	0.31488	0.0596	0.0033	308	16	271	6.2	568	110	87.99	47.71
RDT16_035	RDT16035-606.d	181	75.9	2.38	0.528	0.029	0.0686	0.0014	0.20606	0.0551	0.0029	429	19	427.8	8.4	388	110	99.72	110.26
RDT16_035	RDT16035-607.d	236	140.3	1.68	0.541	0.027	0.0692	0.0013	0.19808	0.0565	0.0026	439	18	431.2	7.6	462	100	98.22	93.33
RDT16_035	RDT16035-608.d	80.4	40.93	1.96	0.303	0.027	0.0409	0.0011	0.20435	0.0539	0.0045	267	21	258	6.5	340	170	96.63	75.88

Supplementary Table 1. Main isotopes and ratios measured using LA–ICP–MS. Concordance 1 ($^{206}Pb/^{238}U/^{207}Pb/^{235}U$) and 2 ($^{206}Pb/^{238}U/^{207}Pb/^{206}Pb$).

RDT16_035	RDT16035-609.d	41.92	10.71	3.91	0.283	0.035	0.0417	0.0015	0.19245	0.0493	0.0061	251	28	263	9.1	60	230	104.78	438.33	
RDT16_035	RDT16035-610.d	62.66	48.84	1.28	0.337	0.033	0.0394	0.0012	0.0004163	0.0633	0.0062	292	25	248.8	7.3	560	200	85.21	44.43	
RDT16_035	RDT16035-611.d	602.3	423	1.42	0.3079	0.014	0.0417	0.0007	0.39322	0.0538	0.0023	272	11	263.3	4.3	347	93	96.80	75.88	
RDT16_035	RDT16035-612.d	202.5	101.5	2.00	0.551	0.031	0.0683	0.0014	0.29175	0.0575	0.003	443	20	426.9	8.6	500	110	96.37	85.38	
RDT16_035	RDT16035-613.d	70.5	27.67	2.55	0.296	0.027	0.0416	0.0013	0.13026	0.0519	0.0046	260	21	262.5	8.2	180	170	100.96	145.83	
RDT16_035	RDT16035-621.d	138.2	82.3	1.68	0.355	0.029	0.04222	0.001	0.2338	0.0639	0.0051	310	22	266.5	6.2	690	160	85.97	38.62	
RDT16_035	RDT16035-622.d	100.8	61.2	1.65	0.463	0.043	0.0421	0.0011	0.34159	0.079	0.0065	373	27	265.9	6.8	1060	160	71.29	25.08	
RDT16_035	RDT16035-623.d	87.2	49.82	1.75	0.256	0.021	0.04	0.0011	0.17849	0.0472	0.0038	230	17	252.7	7	90	150	109.87	280.78	
RDT16_035	RDT16035-624.d	55.7	22.1	2.52	0.256	0.027	0.0391	0.0012	0.039538	0.0478	0.0051	230	21	247.2	7.7	110	190	107.48	224.73	
RDT16_035	RDT16035-625.d	91.3	59.3	1.54	0.295	0.027	0.04067	0.00097	-0.009174	0.0522	0.0046	258	21	256.9	6	220	180	99.57	116.77	
RDT16_035	RDT16035-626.d	149.8	41.9	3.58	0.318	0.022	0.0463	0.0011	0.25498	0.0511	0.0033	279	16	291.4	6.9	190	130	104.44	153.37	
RDT16_035	RDT16035-627.d	97.6	33.4	2.92	0.316	0.024	0.0408	0.0011	0.15427	0.0575	0.0042	279	18	257.5	6.9	570	150	92.29	45.18	
RDT16_035	RDT16035-628.d	30.5	12.5	2.44	0.375	0.048	0.0423	0.002	0.016599	0.0659	0.0085	310	37	267	13	570	270	86.13	46.84	
RDT16_035	RDT16035-629.d	168.5	83.9	2.01	0.293	0.019	0.04137	0.00087	-0.014601	0.0524	0.0035	259	15	261.3	5.4	260	130	100.89	100.50	
RDT16_035	RDT16035-630.d	205.1	157.3	1.30	0.553	0.029	0.0699	0.0013	0.24511	0.0584	0.0029	448	19	435.6	7.7	526	110	97.23	82.81	
RDT16_035	RDT16035-631.d	215	91.4	2.35	0.268	0.016	0.03957	0.00077	0.11454	0.0494	0.0029	242	13	250.2	4.7	155	120	103.39	161.42	
RDT16_035	RDT16035-632.d	146.4	88.3	1.66	0.312	0.021	0.04055	0.00096	0.1413	0.0572	0.0038	275	16	256.2	5.9	490	130	93.16	52.29	
RDT16_035	RDT16035-633.d	253.7	123.4	2.06	0.288	0.017	0.04003	0.00082	0.28487	0.054	0.003	256	14	253	5.1	310	120	98.83	81.61	
RDT16_035	RDT16035-634.d	95	77.4	1.23	0.501	0.044	0.0422	0.0011	0.43068	0.0851	0.0066	406	29	266.3	7	1300	170	65.59	20.48	
RDT16_035	RDT16035-635.d	65.8	36.09	1.82	0.352	0.035	0.0411	0.0013	0.30165	0.0626	0.0061	309	26	259.8	7.8	630	200	84.08	41.24	
RDT16_035	RDT16035-643.d	114.4	49.7	2.30	0.298	0.022	0.04014	0.00097	0.040563	0.0544	0.0041	263	18	253.6	6	300	150	96.43	84.53	
RDT16_035	RDT16035-644.d	207.1	107.1	1.93	0.296	0.017	0.03872	0.0008	0.028086	0.056	0.0033	262	14	244.8	4.9	400	130	93.44	61.20	
RDT16_035	RDT16035-645.d	286.1	129.9	2.20	0.527	0.026	0.0686	0.0012	0.46685	0.0565	0.0025	428	17	427.5	7.3	449	97	99.88	95.21	
RDT16_035	RDT16035-646.d	66.97	20.92	3.20	0.275	0.025	0.0402	0.0012	0.19835	0.0495	0.0044	242	20	254.1	7.4	140	180	105.00	181.50	
RDT16_035	RDT16035-647.d	136.4	52.1	2.62	0.281	0.022	0.0418	0.0012	0.080243	0.0505	0.0039	251	17	263.7	7.1	170	160	105.06	155.12	
RDT16_035	RDT16035-648.d	167.9	51.6	3.25	0.565	0.032	0.0734	0.0013	0.15792	0.0566	0.0031	456	21	457.4	7.7	440	110	100.31	103.95	
RDT16_035	RDT16035-649.d	63.7	26.44	2.41	0.308	0.026	0.0416	0.0013	0.2322	0.0559	0.0046	270	20	262.7	7.8	390	160	97.30	67.36	
RDT16_035	RDT16035-650.d	80.3	43.9	1.83	0.297	0.023	0.0402	0.0012	0.29107	0.0546	0.004	269	19	253.8	7.2	380	150	94.35	66.79	
RDT16_035	RDT16035-651.d	63.7	30.16	2.11	0.289	0.024	0.0397	0.0013	0.12478	0.0511	0.004	256	18	250.6	7.9	270	160	97.89	92.81	
RDT16_035	RDT16035-652.d	61.8	34.72	1.78	0.418	0.06	0.043	0.0015	0.74075	0.0682	0.0081	329	35	271.4	9	690	220	82.49	39.33	
RDT16_035	RDT16035-653.d	608	305	1.99	0.431	0.02	0.0581	0.0013	0.48902	0.0539	0.0022	364.4	14	363.9	7.7	358	90	99.86	101.65	
RDT16_035	RDT16035-654.d	165.3	81.7	2.02	0.295	0.019	0.04239	0.00087	0.33666	0.0507	0.003	263	15	267.6	5.4	200	120	101.75	133.80	
RDT16_035	RDT16035-655.d	107.1	46.1	2.32	0.536	0.034	0.0699	0.0014	0.20947	0.056	0.0033	433	22	435.4	8.4	450	130	100.55	96.76	
RDT16_035	RDT16035-656.d	319.3	74.7	4.27	0.2777	0.014	0.03972	0.00083	0.20367	0.051	0.0025	248.1	11	251.1	5.1	207	100	101.21	121.30	
RDT16_035	RDT16035-657.d	102.9	79.3	1.30	0.265	0.022	0.0396	0.0011	0.19716	0.0497	0.004	240	18	250.5	6.5	140	160	104.38	178.93	
RDT16_035	RDT16035-667.d	59.2	44.4	1.33	0.396	0.033	0.0422	0.0013	0.028694	0.0698	0.006	342	24	266.2	8.3	860	180	77.84	30.95	
RDT16_035	RDT16035-668.d	914	370	2.47	0.564	0.023	0.0718	0.0012	0.36298	0.058	0.0021	453.6	15	446.8	7.3	530	79	98.50	84.30	
RDT16_035	RDT16035-669.d	155.8	58.8	2.65	0.309	0.019	0.04189	0.00093	0.16347	0.0539	0.0033	274	15	264.5	5.7	350	130	96.53	75.57	
RDT16_035	RDT16035-670.d	28.02	7.66	3.66	0.282	0.039	0.0404	0.0015	0.18213	0.05	0.0068	250	32	255	9.3	180	260	102.00	141.67	
RDT16_035	RDT16035-671.d	55.2	34.9	1.58	0.263	0.026	0.0388	0.0013	0.14094	0.0514	0.0052	240	22	245	7.8	180	190	102.08	136.11	
RDT16_035	RDT16035-672.d	29.95	20.46	1.46	0.341	0.041	0.0448	0.0018	0.15838	0.0574	0.0074	289	31	282	11	320	240	97.58	88.13	
RDT16_035	RDT16035-673.d	559	355.1	1.57	0.556	0.025	0.06954	0.0011	0.32642	0.0591	0.0023	448.9	16	433.3	6.7	575	82	96.52	75.36	
RDT16_035	RDT16035-674.d	137.8	78.7	1.75	0.594	0.032	0.0677	0.0013	0.24522	0.0659	0.0033	474	20	422.4	7.9	809	100	89.11	52.21	
RDT16_035	RDT16035-675.d	86.9	73.7	1.18	0.328	0.024	0.04035	0.00093	0.02356	0.0593	0.0045	286	18	255	5.8	550	160	89.16	46.36	
RDT16_035	RDT16035-676.d	1165	324.9	3.59	1.757	0.07	0.1674	0.0029	0.76909	0.07759	0.0026	1029	26	999	16	1134	67	97.08	88.10	
RDT16_035	RDT16035-677.d	113.3	57.5	1.97	0.388	0.029	0.0423	0.001	0.0098602	0.0681	0.0054	329	21	267	6.3	760	150	81.16	35.13	
TR_05-1	TR_05-1 - 1	332	198	1.68	3.549	0.039	0.2715	0.0037	0.56103	0.09475	0.0008	1537.8	8.7	1548	19	1521	15	100.66	101.78	
TR_05-1	TR_05-1 - 10	516	261	1.98	0.4097	0.0075	0.0559	0.0007	0.11213	0.0532	0.001	348.4	5.4	350.6	4.3	328	43	100.63	106.89	
TR_05-1	TR_05-1 - 11	164.7	93.5	1.76	0.312	0.013	0.04184	0.00069	0.19639	0.0548	0.0024	275	10	264.2	4.3	377	98	96.07	70.08	
TR_05-1	TR_05-1 - 12	71.7	33.7	2.13	0.317	0.02	0.04493	0.00082	0.14428	0.0521	0.0034	283	16	283.3	5.1	290	140	100.11	97.69	
TR_05-1	TR_05-1 - 13	696	319.1	2.18	0.3491	0.0087	0.04563	0.00063	-0.44623	0.0555	0.0015	303.8	6.5	287.6	3.9	418	57	94.67	68.80	
TR_05-1	TR_05-1 - 15	93.9	73.8	1.27	0.38	0.019	0.04978	0.00084	0.0060706	0.055	0.0028	328	13	313.2	5.2	430	110	95.49	72.84	
TR_05-1	TR_05-1 - 16	155	76	2.04	0.312	0.015	0.04371	0.00068	-0.13768	0.0512	0.0026	275	12	275.8	4.2	230	110	100.29	119.91	
TR_05-1	TR_05-1 - 17	54.1	39	1.39	0.422	0.036	0.05241	0.0011	0.17353	0.0591	0.005	353	26	329.3	6.5	490	170	93.29	67.20	

Supplementary Table 1. Main isotopes and ratios measured using LA–ICP–MS. Concordance 1 ($^{206}Pb/^{238}U/^{207}Pb/^{235}U$) and 2 ($^{206}Pb/^{238}U/^{207}Pb/^{206}Pb$).

TR_05-1	TR_05-1 - 18	317	159.6	1.99	3.583	0.072	0.2579	0.0044	0.74355	0.1021	0.0013	1544	16	1479	23	1660	23	95.79	89.10	
TR_05-1	TR_05-1 - 19	230	241	0.95	3.814	0.078	0.2762	0.004	0.66899	0.1008	0.002	1594	16	1572	20	1633	36	98.62	96.26	
TR_05-1	TR_05-1 - 2	790	338	2.34	0.4594	0.0093	0.06101	0.0011	0.589	0.05411	0.0008	383.5	6.5	381.8	6.6	385	36	99.56	99.17	
TR_05-1	TR_05-1 - 21	178.4	107.4	1.66	0.283	0.011	0.03892	0.00053	0.28965	0.0527	0.0019	252.2	8.6	246.2	3.3	291	82	97.62	84.60	
TR_05-1	TR_05-1 - 22	502	262	1.92	0.3344	0.0083	0.04604	0.00065	0.14304	0.0525	0.0013	292.7	6.3	290.2	4	293	55	99.15	99.04	
TR_05-1	TR_05-1 - 23	205.3	122.7	1.67	0.428	0.012	0.06	0.00086	0.087972	0.052	0.0015	361.2	8.3	375.6	5.2	289	65	103.99	129.97	
TR_05-1	TR_05-1 - 24	507	506	1.00	0.768	0.043	0.0841	0.0015	0.3515	0.0656	0.0034	574	23	522	8.2	708	75	90.94	73.73	
TR_05-1	TR_05-1 - 25	791	465	1.70	0.3738	0.007	0.04586	0.00064	0.0056184	0.0586	0.0011	322.3	5.2	289.1	3.9	555	42	89.70	52.09	
TR_05-1	TR_05-1 - 26	422.6	782	0.54	0.567	0.019	0.0706	0.0012	0.47411	0.0584	0.0016	455	12	439.8	7.5	529	60	96.66	83.14	
TR_05-1	TR_05-1 - 27	303	144.3	2.10	0.351	0.012	0.04659	0.00061	0.27393	0.0548	0.0017	305.4	8.7	293.6	3.8	399	72	96.14	73.58	
TR_05-1	TR_05-1 - 28	204.7	306	0.67	3.121	0.07	0.2304	0.0048	0.83955	0.0978	0.0012	1436	17	1336	25	1580	22	93.04	84.56	
TR_05-1	TR_05-1 - 29	170	176	0.97	3.117	0.05	0.2482	0.0038	0.66286	0.09089	0.001	1436	12	1429	19	1445	21	99.51	98.89	
TR_05-1	TR_05-1 - 3	302.5	118.5	2.55	0.2744	0.0095	0.03822	0.00056	0.052959	0.0519	0.0018	245.8	7.6	241.8	3.5	273	79	98.37	88.57	
TR_05-1	TR_05-1 - 31	764	1170	0.65	0.614	0.012	0.07856	0.0013	0.52226	0.0563	0.0008	485.7	7.2	487.5	7.7	464	32	100.37	105.06	
TR_05-1	TR_05-1 - 32	525	179	2.93	3.4	0.035	0.2578	0.0035	0.75215	0.09578	0.0007	1503.9	8.2	1479	18	1544	14	98.34	95.79	
TR_05-1	TR_05-1 - 33	1039	589	1.76	1.573	0.033	0.1582	0.0031	0.92584	0.07191	0.0006	961	13	949	17	984	17	98.75	96.44	
TR_05-1	TR_05-1 - 4	116.5	129.6	0.90	1.583	0.043	0.1613	0.0023	0.28006	0.0701	0.0018	964	16	963.9	13	935	52	99.99	103.09	
TR_05-1	TR_05-1 - 5	94.7	60.9	1.56	0.329	0.021	0.04415	0.00073	0.28999	0.0545	0.0034	289	16	278.5	4.5	340	140	96.37	81.91	
TR_05-1	TR_05-1 - 6	151.5	57.7	2.63	0.377	0.014	0.05011	0.0008	0.14239	0.0543	0.0021	324	10	315.2	4.9	381	91	97.28	82.73	
TR_05-1	TR_05-1 - 7	216.4	55.6	3.89	0.326	0.012	0.04586	0.00062	0.19057	0.0513	0.0017	285.7	9	289	3.8	248	73	101.16	116.53	
TR_05-1	TR_05-1 - 8	293	200	1.47	0.462	0.015	0.06156	0.0012	0.48883	0.0541	0.0017	385	11	385	7.1	378	71	100.00	101.85	
TR_05-1	TR_05-1 - 9	617	266	2.32	0.2856	0.0063	0.04084	0.0005	0.2762	0.0504	0.0011	254.9	5	258	3.1	213	47	101.22	121.13	
TR_05-1	TR051-10.d	790.6	317.2	2.49	0.2867	0.0082	0.04023	0.00079	0.33297	0.0525	0.0012	255.4	6.5	254.2	4.9	289	51	99.53	97.24	
TR_05-1	TR051-11.d	851	198.5	4.29	4.362	0.099	0.3006	0.0058	0.80513	0.10677	0.0014	1704.3	19	1693	29	1741	24	99.34	76.53	
TR_05-1	TR051-12.d	290.1	101.5	2.86	0.267	0.01	0.03663	0.00078	0.077057	0.0537	0.002	239	8.2	231.9	4.9	303	77	97.03	92.10	YSG
TR_05-1	TR051-13.d	532.8	305.4	1.74	0.596	0.016	0.0756	0.0015	0.37593	0.058	0.0012	473.1	10	469.7	8.8	510	46	99.28	128.55	
TR_05-1	TR051-14.d	105.9	58.79	1.80	0.315	0.016	0.04486	0.0011	0.078976	0.0525	0.0026	277	13	282.8	6.7	220	100	102.09	70.59	
TR_05-1	TR051-15.d	875	422.3	2.07	3.631	0.095	0.2298	0.0052	0.83289	0.1155	0.0016	1555	21	1332	27	1887	26	85.66	59.85	
TR_05-1	TR051-16.d	194.1	73.1	2.66	0.343	0.015	0.04344	0.00095	0.099575	0.0584	0.0025	297	11	274.1	5.9	458	92	92.29	91.94	
TR_05-1	TR051-17.d	126.8	59.84	2.12	3.772	0.12	0.2678	0.0063	0.58334	0.1027	0.0022	1582	24	1528	32	1662	41	96.59	31.67	
TR_05-1	TR051-18.d	690.2	264.1	2.61	1.232	0.038	0.0873	0.0021	0.73837	0.1047	0.0021	813	17	539.4	13	1703	36	66.35	62.23	
TR_05-1	TR051-19.d	323.2	274.9	1.18	0.6	0.018	0.06951	0.0014	0.20238	0.0634	0.0016	475.6	11	433.1	8.6	696	57	91.06	45.65	
TR_05-1	TR051-20.d	312.7	150.8	2.07	0.384	0.014	0.04541	0.00097	0.10919	0.0626	0.0021	327.9	10	286.2	6	627	73	87.28	95.30	
TR_05-1	TR051-28.d	97.4	45.08	2.16	8.74	0.22	0.4191	0.0094	0.59274	0.1525	0.0029	2307	24	2253	43	2364	32	97.66	67.65	
TR_05-1	TR051-29.d	718	272	2.64	3.67	0.15	0.2241	0.0054	0.66405	0.1205	0.0035	1544	25	1301	29	1923	34	84.26	94.59	
TR_05-1	TR051-30.d	318.8	183.3	1.74	3.616	0.086	0.2666	0.0053	0.62124	0.0996	0.0016	1551	19	1522	27	1609	29	98.13	36.20	
TR_05-1	TR051-31.d	342	228	1.50	0.391	0.018	0.04332	0.00097	0.095192	0.0666	0.0029	334	13	273.3	6	755	87	81.83	93.92	
TR_05-1	TR051-32.d	240.9	238.1	1.01	2.623	0.067	0.2202	0.0044	0.52447	0.0874	0.0015	1304	19	1282	23	1365	33	98.31	92.19	
TR_05-1	TR051-33.d	414.5	315.5	1.31	2.956	0.069	0.2347	0.0047	0.67788	0.09254	0.0014	1395	18	1358	25	1473	29	97.35	78.60	
TR_05-1	TR051-34.d	1395	758	1.84	0.596	0.016	0.07304	0.0015	0.61674	0.05946	0.001	474.4	10	454.3	8.8	578	38	95.76	97.36	
TR_05-1	TR051-35.d	276	56.2	4.91	5.261	0.12	0.3313	0.0065	0.69912	0.1162	0.0017	1859	21	1843	32	1893	26	99.14	59.35	
TR_05-1	TR051-36.d	280.2	129.7	2.16	0.2964	0.011	0.03876	0.0008	0.12099	0.056	0.0019	263	8.6	245.1	5	413	74	93.19	74.34	
TR_05-1	TR051-37.d	3036	208.5	14.56	3.699	0.086	0.2381	0.0048	0.84323	0.11333	0.0015	1569	19	1376	25	1851	23	87.70	57.69	
TR_05-1	TR051-38.d	253.8	125.1	2.03	0.372	0.014	0.04643	0.001	0.33778	0.059	0.002	319.3	11	292.5	6.2	507	74	91.61	128.55	
TR_05-1	TR051-39.d	153.8	85.6	1.80	0.326	0.015	0.04633	0.0011	0.184	0.0517	0.0022	285	11	291.8	6.9	227	89	102.39	93.92	
TR_05-1	TR051-40.d	762.2	566	1.35	5.04	0.11	0.3179	0.0059	0.76001	0.116	0.0015	1824.4	18	1778	29	1893	24	97.46	97.26	
TR_05-1	TR051-41.d	392.5	181.4	2.16	0.292	0.01	0.04096	0.00083	0.23984	0.0522	0.0015	259.8	8	258.7	5.1	266	65	99.58	85.81	
TR_05-1	TR051-42.d	168.4	128.6	1.31	0.412	0.016	0.05386	0.0012	0.2598	0.0557	0.002	348	12	338.1	7.6	394	76	97.16	26.34	
TR_05-1	TR051-50.d	106.5	70.3	1.51	0.673	0.087	0.0473	0.0013	0.58211	0.1	0.011	481	45	297.6	8.1	1130	180	61.87	12.11	
TR_05-1	TR051-51.d	35.65	25.63	1.39	1.98	0.23	0.0552	0.0027	0.83157	0.254	0.022	1019	76	345	16	2850	150	33.86	63.13	
TR_05-1	TR051-52.d	265.6	169.5	1.57	0.36	0.02	0.0451	0.0013	0.27287	0.0581	0.0031	310	15	284.1	7.8	450	110	91.65	85.81	
TR_05-1	TR051-53.d	690	164.8	4.19	4.404	0.1	0.2813	0.0058	0.82693	0.11396	0.0015	1712	20	1597	29	1861	25	93.28	95.36	
TR_05-1	TR051-54.d	64.25	47.85	1.34	0.559	0.031	0.0689	0.0017	0.070848	0.06	0.0033	442	20	429.1	10	450	110	97.08	44.96	
TR_05-1	TR051-55.d	206.1	186.3	1.11	0.668	0.025	0.0676	0.0015	0.39312	0.0719	0.0022	517	15	421.3	8.9	937	65	81.49	75.18	

Supplementary Table 1. Main isotopes and ratios measured using LA–ICP–MS. Concordance 1 ($^{206}Pb/^{238}U/^{207}Pb/^{235}U$) and 2 ($^{206}Pb/^{238}U/^{207}Pb/^{206}Pb$).

TR_05-1	TR051-56.d	242.8	232.2	1.05	0.2998	0.011	0.04047	0.00097	0.17266	0.0546	0.0019	264.9	8.6	255.6	6	340	75	96.49	153.00	
TR_05-1	TR051-57.d	79	33.1	2.39	0.348	0.022	0.0486	0.0014	0.045709	0.053	0.0034	297	17	306	8.3	200	130	103.03	43.64	
TR_05-1	TR051-58.d	89	54.1	1.65	0.374	0.022	0.04219	0.0011	0.11058	0.0651	0.0039	319	16	266.2	6.8	610	120	83.45	43.49	
TR_05-1	TR051-59.d	430.5	109.8	3.92	0.57	0.029	0.0593	0.0021	0.84555	0.0688	0.0021	451	19	371	13	853	64	82.26	18.67	
TR_05-1	TR051-60.d	40.37	20.02	2.02	0.965	0.074	0.0557	0.0017	0.2548	0.132	0.01	667	38	349.1	11	1870	140	52.34	13.14	
TR_05-1	TR051-61.d	41.08	39.34	1.04	1	0.12	0.044	0.0016	0.60658	0.165	0.015	652	51	277.3	10	2110	180	42.53	90.44	
TR_05-1	TR051-62.d	479.1	120.4	3.98	1.44	0.035	0.146	0.0028	0.46352	0.07184	0.0012	903.7	15	878.2	16	971	35	97.18	88.78	
TR_05-1	TR051-63.d	1648	104.3	15.80	3.054	0.07	0.2337	0.0046	0.7836	0.09494	0.0013	1419.5	18	1353	24	1524	26	95.32	58.88	
TR_05-1	TR051-64.d	342.3	228.2	1.50	0.544	0.018	0.06332	0.0013	0.19384	0.0632	0.0019	439	12	395.7	7.9	672	64	90.14	35.93	
TR_05-1	TR051-72.d	106.2	41.94	2.53	0.386	0.019	0.04212	0.0011	-0.017183	0.0676	0.0034	330	14	265.9	6.9	740	110	80.58	97.19	
TR_05-1	TR051-73.d	136.6	136.4	1.00	4.084	0.1	0.2876	0.0058	0.42705	0.1034	0.002	1647	21	1628	29	1675	35	98.85	20.44	
TR_05-1	TR051-74.d	274.1	197.5	1.39	0.467	0.017	0.04031	0.00087	0.2713	0.0842	0.0028	386	12	254.7	5.4	1246	69	65.98	45.34	
TR_05-1	TR051-75.d	371.7	179.3	2.07	0.422	0.017	0.04775	0.00098	0.26523	0.064	0.0024	354	12	300.6	6	663	78	84.92	63.63	
TR_05-1	TR051-76.d	170.9	109.9	1.56	0.317	0.014	0.0408	0.00095	0.17271	0.0566	0.0023	278.5	11	257.7	5.9	405	86	92.53	58.72	
TR_05-1	TR051-77.d	403	240	1.68	3.73	0.19	0.2073	0.006	0.68513	0.1299	0.0041	1546	32	1212	32	2064	42	78.40	100.46	
TR_05-1	TR051-78.d	143.7	149.1	0.96	3.575	0.096	0.2703	0.0058	0.4866	0.0962	0.002	1541	22	1541	30	1534	38	100.00	88.64	
TR_05-1	TR051-79.d	352	137.5	2.56	4.669	0.11	0.2944	0.0054	0.51771	0.1152	0.0018	1759.5	19	1662	27	1875	27	94.46	92.04	
TR_05-1	TR051-80.d	270.2	129.1	2.09	9.51	0.27	0.4251	0.011	0.91831	0.1622	0.0023	2382	26	2277	49	2474	23	95.59	99.18	
TR_05-1	TR051-81.d	710.9	221	3.22	3.774	0.089	0.2777	0.0055	0.71898	0.09843	0.0014	1586	19	1578	28	1591	27	99.50	77.81	
TR_05-1	TR051-82.d	466.7	169.2	2.76	1.827	0.049	0.1609	0.0032	0.61502	0.082	0.0015	1051	17	961	18	1235	35	91.44	128.89	
TR_05-2	TR_05-2 - 1	245	105.1	2.33	0.2915	0.0088	0.04226	0.00059	0.1409	0.0504	0.0017	260.6	6.7	266.8	3.7	207	75	102.38	128.89	
TR_05-2	TR_05-2 - 10	58.7	25.04	2.34	0.251	0.024	0.03761	0.00082	0.097358	0.048	0.0046	224	20	238	5.1	70	190	106.25	340.00	
TR_05-2	TR_05-2 - 11	53.21	21.72	2.45	0.383	0.031	0.04852	0.00098	0.075043	0.0571	0.0047	329	22	305.4	6	430	170	92.83	71.02	
TR_05-2	TR_05-2 - 12	282	115	2.45	0.2688	0.0083	0.03814	0.0006	-0.059336	0.0511	0.0017	241.4	6.6	241.3	3.7	239	78	99.96	100.96	
TR_05-2	TR_05-2 - 13	132.7	103.7	1.28	0.278	0.014	0.03973	0.00061	0.038331	0.0504	0.0024	248	11	251.2	3.8	240	110	101.29	104.67	
TR_05-2	TR_05-2 - 14	177	92.6	1.91	0.347	0.024	0.03911	0.00061	0.46681	0.0638	0.004	301	18	247.3	3.8	730	130	82.16	33.88	
TR_05-2	TR_05-2 - 15	198	79.2	2.50	0.76	0.13	0.051	0.0016	0.90058	0.101	0.013	541	65	320.6	9.6	1490	250	59.26	21.52	
TR_05-2	TR_05-2 - 16	239.8	388.5	0.62	0.4	0.012	0.05363	0.00076	0.1621	0.0538	0.0015	341.3	8.5	336.8	4.7	365	67	98.68	92.27	
TR_05-2	TR_05-2 - 17	507	312	1.63	0.2729	0.007	0.03654	0.00054	-0.039131	0.0544	0.0016	244.8	5.6	231.3	3.4	380	62	94.49	60.87	
TR_05-2	TR_05-2 - 18	140.1	106.2	1.32	4.44	0.054	0.3093	0.0041	0.65288	0.1046	0.0012	1720.9	9.7	1737	20	1705	21	100.94	101.88	
TR_05-2	TR_05-2 - 19	210.6	161.9	1.30	0.545	0.016	0.07143	0.001	-0.068267	0.0552	0.0017	441	11	444.8	6	405	67	100.86	109.83	
TR_05-2	TR_05-2 - 2	196	144	1.36	0.373	0.014	0.05097	0.00075	0.12015	0.0526	0.0019	323	10	320.5	4.6	316	79	99.23	101.42	
TR_05-2	TR_05-2 - 20	120.6	109.6	1.10	0.3	0.017	0.0404	0.0007	-0.099649	0.0532	0.0031	266	13	255.3	4.3	320	120	95.98	79.78	
TR_05-2	TR_05-2 - 21	179.3	100.5	1.78	0.297	0.011	0.0402	0.00063	-0.29	0.0539	0.0022	264.9	8.6	254.1	3.9	351	88	95.92	72.39	
TR_05-2	TR_05-2 - 22	1065	492	2.16	0.3087	0.0051	0.04299	0.00055	0.244	0.0521	0.0009	273.7	4.1	271.4	3.4	294	39	99.16	92.31	
TR_05-2	TR_05-2 - 23	280	323.8	0.86	1.638	0.034	0.1704	0.0024	0.68467	0.0692	0.001	984	13	1014.1	13	902	31	103.06	112.43	
TR_05-2	TR_05-2 - 24	141	113.5	1.24	0.386	0.013	0.05418	0.00086	0.12327	0.0516	0.0018	331.1	9.8	340.1	5.3	259	77	102.72	131.31	
TR_05-2	TR_05-2 - 25	257.3	199	1.29	0.519	0.014	0.06733	0.0011	0.13736	0.0552	0.0015	423.9	9.4	420	6.6	415	63	99.08	101.20	
TR_05-2	TR_05-2 - 26	57.5	31.68	1.82	0.272	0.023	0.0396	0.00086	0.095424	0.0503	0.0045	244	18	250.4	5.3	170	180	102.62	147.29	
TR_05-2	TR_05-2 - 27	276	187	1.48	0.2608	0.0089	0.0369	0.00049	-0.043103	0.0512	0.0019	235	7.1	233.6	3.1	241	79	99.40	96.93	
TR_05-2	TR_05-2 - 28	129.3	40.3	3.21	0.309	0.017	0.04462	0.00071	0.17629	0.0508	0.0028	275	12	281.4	4.4	200	120	102.33	140.70	
TR_05-2	TR_05-2 - 29	85	42.9	1.98	0.476	0.088	0.0382	0.0011	0.75394	0.084	0.013	377	54	241.5	6.9	1150	270	64.06	21.00	
TR_05-2	TR_05-2 - 3	141.4	89.6	1.58	0.396	0.016	0.05328	0.00087	0.097447	0.0544	0.0024	339	12	334.6	5.3	364	97	98.70	91.92	
TR_05-2	TR_05-2 - 30	587	168	3.49	0.892	0.012	0.10487	0.0013	0.20218	0.06159	0.0009	647.3	6.6	642.9	7.8	661	31	99.32	97.26	
TR_05-2	TR_05-2 - 31	40.3	20.89	1.93	0.265	0.026	0.0381	0.00089	0.1738	0.0503	0.0048	236	21	241	5.5	150	200	102.12	160.67	
TR_05-2	TR_05-2 - 32	178	129	1.38	0.279	0.01	0.03784	0.00053	-0.08654	0.0531	0.0022	249.6	7.9	239.4	3.3	319	87	95.91	75.05	
TR_05-2	TR_05-2 - 33	69	34.6	1.99	0.43	0.024	0.05791	0.00097	-0.16386	0.0535	0.0033	364	18	362.9	5.9	330	130	99.70	109.97	
TR_05-2	TR_05-2 - 34	434.9	207	2.10	4.879	0.043	0.3201	0.0038	0.67866	0.1103	0.0008	1798.2	7.4	1789.9	19	1803	12	99.54	99.27	
TR_05-2	TR_05-2 - 35	390	164	2.38	0.2707	0.0097	0.0379	0.00052	0.069508	0.0518	0.0019	242.8	7.8	239.8	3.2	266	77	98.76	90.15	
TR_05-2	TR_05-2 - 36	186	179	1.04	0.447	0.017	0.05547	0.00089	0.40564	0.0585	0.002	374	12	348	5.5	557	73	93.05	62.48	
TR_05-2	TR_05-2 - 37	142.9	73.5	1.94	0.275	0.015	0.03971	0.00066	0.13236	0.0502	0.0027	247	11	251.1	4.1	190	120	101.66	132.16	
TR_05-2	TR_05-2 - 38	147	107	1.37	0.24	0.014	0.03341	0.0006	0.1218	0.0519	0.0032	218	12	211.8	3.7	240	130	97.16	88.25	YSG
TR_05-2	TR_05-2 - 39	421.5	242.5	1.74	0.318	0.0098	0.04359	0.00058	0.27229	0.0528	0.0015	280	7.5	275.1	3.6	314	66	98.25	87.61	
TR_05-2	TR_05-2 - 4	700	399	1.75	3.634	0.046	0.2743	0.004	0.74333	0.09521	0.0007	1556	10	1562	20	1530	14	100.39	102.09	

Supplementary Table 1. Main isotopes and ratios measured using LA–ICP–MS. Concordance 1 ($^{206}Pb/^{238}U/^{207}Pb/^{235}U$) and 2 ($^{206}Pb/^{238}U/^{207}Pb/^{206}Pb$).

TR_05-2	TR_05-2 - 40	252	152	1.66	0.237	0.01	0.03549	0.00055	0.39187	0.0479	0.002	216.8	8.5	224.8	3.4	101	90	103.69	222.57
TR_05-2	TR_05-2 - 41	730	374.1	1.95	0.2892	0.0061	0.04091	0.00057	0.19381	0.0509	0.0012	257.8	4.8	258.4	3.5	230	53	100.23	112.35
TR_05-2	TR_05-2 - 42	139.6	48.88	2.86	0.25	0.014	0.03786	0.00062	0.0048356	0.0488	0.0028	227	12	239.6	3.8	130	120	105.55	184.31
TR_05-2	TR_05-2 - 43	211	206.6	1.02	0.273	0.0095	0.03842	0.00062	0.03585	0.0517	0.0019	244.7	7.6	243	3.8	300	78	99.31	81.00
TR_05-2	TR_05-2 - 44	408.1	256	1.59	0.2681	0.0074	0.03764	0.00049	-0.24366	0.0516	0.0016	240.9	6	238.2	3.1	251	69	98.88	94.90
TR_05-2	TR_05-2 - 45	470	371	1.27	0.2652	0.0078	0.03779	0.00055	0.27151	0.0503	0.0015	238.6	6.3	239.4	3.3	207	67	100.34	115.65
TR_05-2	TR_05-2 - 46	54.9	36.8	1.49	0.492	0.034	0.0628	0.0013	0.19967	0.0579	0.0041	403	23	393.8	8.4	470	150	97.72	83.79
TR_05-2	TR_05-2 - 47	349	300	1.16	0.371	0.01	0.05186	0.00069	0.26322	0.0519	0.0013	319.9	7.7	325.9	4.2	290	58	101.88	112.38
TR_05-2	TR_05-2 - 48	970	386	2.51	17.89	0.42	0.543	0.013	0.91172	0.2358	0.0012	2980	23	2805	56	3090.4	8.5	94.13	90.76
TR_05-2	TR_05-2 - 49	160	130	1.23	0.259	0.013	0.03725	0.00057	0.064123	0.0496	0.0025	233	11	235.8	3.5	180	110	101.20	131.00
TR_05-2	TR_05-2 - 5	155.6	111.9	1.39	0.547	0.018	0.07037	0.00096	0.25825	0.0564	0.0019	444	11	438.4	5.8	472	74	98.74	92.88
TR_05-2	TR_05-2 - 50	483	298	1.62	0.288	0.011	0.03918	0.00057	0.35066	0.0532	0.0021	256.3	8.8	247.7	3.6	329	87	96.64	75.29
TR_05-2	TR_05-2 - 6	779	411	1.90	0.3061	0.0067	0.04144	0.0006	0.6565	0.0535	0.0011	271	5.2	261.8	3.7	345	47	96.61	75.88
TR_05-2	TR_05-2 - 7	125.8	66.6	1.89	0.327	0.013	0.04214	0.00075	0.12361	0.0563	0.0025	287	10	266.1	4.7	455	99	92.72	58.48
TR_05-2	TR_05-2 - 8	709	269	2.64	0.338	0.01	0.04304	0.00069	0.31469	0.0569	0.0018	295.3	7.8	271.6	4.3	468	65	91.97	58.03
TR_05-2	TR_05-2 - 9	76.1	41.9	1.82	0.302	0.024	0.04094	0.00079	0.035146	0.0544	0.0044	268	19	258.7	4.9	340	160	96.53	76.09
TR_05-2	TR052-100.d	1426	753	1.89	0.2929	0.0079	0.04018	0.0008	0.2426	0.0527	0.0012	260.5	6.2	253.9	4.9	302	48	97.47	84.07
TR_05-2	TR052-101.d	471.4	1206	0.39	0.2933	0.0097	0.03968	0.00077	0.11389	0.0534	0.0016	260.2	7.6	250.8	4.8	311	64	96.39	80.64
TR_05-2	TR052-102.d	448.1	231.7	1.93	0.3146	0.01	0.04294	0.00086	0.29621	0.0528	0.0015	276.7	8.1	271	5.3	289	62	97.94	93.77
TR_05-2	TR052-103.d	309.2	209	1.48	5.163	0.12	0.3262	0.0061	0.61524	0.1142	0.0017	1844	20	1819	30	1860	28	98.64	97.80
TR_05-2	TR052-104.d	38.64	13.62	2.84	0.38	0.033	0.0496	0.0016	0.13067	0.0558	0.0048	315	24	311.6	9.9	230	170	98.92	135.48
TR_05-2	TR052-105.d	683.5	409.3	1.67	0.3153	0.0096	0.04353	0.00092	0.38452	0.0523	0.0013	277.4	7.4	274.6	5.7	270	54	98.99	101.70
TR_05-2	TR052-106.d	138.1	103.2	1.34	1.248	0.04	0.1314	0.0028	0.24616	0.0682	0.002	817	18	796	16	836	60	97.43	95.22
TR_05-2	TR052-107.d	63.4	74.2	0.85	12.9	0.31	0.5004	0.01	0.5333	0.1861	0.0033	2671	23	2612	44	2700	29	97.79	96.74
TR_05-2	TR052-108.d	201.1	427.5	0.47	5.051	0.12	0.323	0.0064	0.61056	0.1125	0.0018	1826	20	1803	31	1831	29	98.74	98.47
TR_05-2	TR052-116.d	369	65.2	5.66	0.542	0.017	0.068	0.0014	0.30445	0.0573	0.0015	438.7	11	424.2	8.7	473	58	96.69	89.68
TR_05-2	TR052-117.d	204.2	119.9	1.70	0.389	0.015	0.05295	0.0012	0.092443	0.0532	0.002	331.7	11	332.5	7.2	279	79	100.24	119.18
TR_05-2	TR052-118.d	305.9	128.5	2.38	0.326	0.013	0.04553	0.001	0.18434	0.0518	0.0019	285.7	9.8	286.9	6.3	229	76	100.42	125.28
TR_05-2	TR052-119.d	97.4	62.47	1.56	0.538	0.026	0.0696	0.0017	0.14811	0.0556	0.0025	434	17	433.5	10	371	97	99.88	116.85
TR_05-2	TR052-120.d	201.3	98.9	2.04	2.988	0.082	0.2382	0.0053	0.51637	0.0897	0.0019	1401	21	1376	27	1403	39	98.22	98.08
TR_05-2	TR052-121.d	596	309	1.93	0.3387	0.01	0.04479	0.00087	0.14468	0.0546	0.0014	295.3	7.8	282.4	5.4	359	58	95.63	78.66
TR_05-2	TR052-122.d	428.1	474	0.90	0.641	0.019	0.0795	0.0016	0.38439	0.0578	0.0013	501.2	12	493.2	9.5	492	51	98.40	100.24
TR_05-2	TR052-123.d	732.5	219.9	3.33	0.341	0.01	0.04312	0.0009	0.28386	0.0571	0.0014	297	7.8	272.1	5.6	468	54	91.62	58.14
TR_05-2	TR052-124.d	176.3	104.7	1.68	0.55	0.041	0.03819	0.00097	0.18066	0.1015	0.0069	430	24	241.5	6	1430	120	56.16	16.89
TR_05-2	TR052-125.d	629	102.8	6.12	1.905	0.059	0.1769	0.0045	0.8056	0.0769	0.0013	1080	21	1049	25	1108	35	97.13	94.68
TR_05-2	TR052-126.d	136.1	75	1.81	0.399	0.019	0.05275	0.0012	0.17763	0.0545	0.0025	336	14	331.3	7.6	302	95	98.60	109.70
TR_05-2	TR052-127.d	419	340.8	1.23	3.258	0.088	0.2389	0.0052	0.7948	0.0976	0.0015	1466	21	1379	27	1571	29	94.07	87.78
TR_05-2	TR052-128.d	1036	870	1.19	3.114	0.071	0.2504	0.0049	0.77826	0.08916	0.0012	1435.2	18	1439	25	1405	26	100.26	102.42
TR_05-2	TR052-129.d	286.7	156.3	1.83	3.157	0.078	0.2492	0.0049	0.65491	0.0907	0.0015	1445	19	1435	25	1431	31	99.31	100.28
TR_05-2	TR052-137.d	241.4	102.8	2.35	0.28	0.012	0.038	0.00082	0.065573	0.0531	0.0022	250.6	9.1	240.4	5.1	275	85	95.93	87.42
TR_05-2	TR052-138.d	37.97	56.54	0.67	1.835	0.074	0.1747	0.0041	0.26052	0.0749	0.0026	1047	27	1037	22	1011	76	99.04	102.57
TR_05-2	TR052-139.d	89.5	87.9	1.02	0.28	0.018	0.03775	0.00097	0.052775	0.0535	0.0035	246	14	238.8	6	210	130	97.07	113.71
TR_05-2	TR052-140.d	148	137.4	1.08	0.447	0.021	0.05472	0.0012	0.069763	0.0586	0.0026	371	15	343.3	7.2	461	96	92.53	74.47
TR_05-2	TR052-141.d	100.77	36.55	2.76	0.338	0.02	0.03683	0.00089	0.018433	0.0665	0.0039	291	15	233.5	5.6	630	120	80.24	37.06
TR_05-2	TR052-142.d	223.6	131.2	1.70	0.278	0.012	0.03853	0.00083	0.1773	0.052	0.0021	248.3	9.7	243.7	5.1	236	85	98.15	103.26
TR_05-2	TR052-143.d	91.86	55.8	1.65	0.439	0.024	0.0498	0.0012	0.10426	0.0632	0.0033	365	17	313.2	7.1	590	110	85.81	53.08
TR_05-2	TR052-144.d	283.1	246.3	1.15	0.283	0.012	0.03555	0.00072	0.18498	0.0573	0.0023	251.6	9.4	225.1	4.5	431	83	89.47	52.23
TR_05-2	TR052-145.d	136.7	81.1	1.69	0.416	0.025	0.04323	0.001	0.18099	0.0692	0.0038	346	17	272.7	6.4	750	120	78.82	36.36
TR_05-2	TR052-146.d	290.2	191.3	1.52	0.578	0.018	0.06748	0.0013	0.022888	0.0616	0.0018	461.3	12	420.9	7.9	607	63	91.24	69.34
TR_05-2	TR052-147.d	20	10.37	1.93	0.702	0.071	0.0395	0.0018	0.13361	0.132	0.014	502	40	249	11	1540	220	49.60	16.17
TR_05-2	TR052-148.d	896	367.6	2.44	4.432	0.095	0.2834	0.0049	0.65938	0.11144	0.0014	1717.1	18	1608	25	1820	23	93.65	88.35
TR_05-2	TR052-149.d	67.63	21.29	3.18	0.369	0.028	0.03803	0.0011	0.063493	0.0715	0.0055	311	21	240.5	7	710	160	77.33	33.87
TR_05-2	TR052-150.d	134.8	87.8	1.54	0.272	0.015	0.03547	0.00086	0.028749	0.0557	0.0031	243	12	224.6	5.3	310	110	92.43	72.45
TR_05-2	TR052-151.d	106.4	141.2	0.75	0.463	0.031	0.0532	0.0013	0.4319	0.0624	0.0036	377	20	333.8	8.1	570	120	88.54	58.56

Supplementary Table 1. Main isotopes and ratios measured using LA–ICP–MS. Concordance 1 ($^{206}Pb/^{238}U/^{207}Pb/^{235}U$) and 2 ($^{206}Pb/^{238}U/^{207}Pb/^{206}Pb$).

TR_05-2	TR052-159.d	168.1	126.9	1.32	0.31	0.015	0.03944	0.00089	0.059625	0.0566	0.0027	271	12	249.3	5.5	373	100	91.99	66.84
TR_05-2	TR052-160.d	648.2	212	3.06	0.2913	0.009	0.03933	0.00081	0.25381	0.0528	0.0014	258.8	7.1	248.6	5.1	287	57	96.06	86.62
TR_05-2	TR052-161.d	39.74	29.04	1.37	0.28	0.027	0.0369	0.0013	0.092378	0.0567	0.0056	244	21	233.1	7.9	170	180	95.53	137.12
TR_05-2	TR052-162.d	183.2	64.64	2.83	12.7	0.28	0.5034	0.0096	0.69386	0.1803	0.0025	2656.5	21	2626	41	2654	23	98.85	98.94
TR_05-2	TR052-163.d	41.12	27.39	1.50	4.44	0.15	0.2926	0.0067	0.20943	0.1077	0.0034	1713	30	1653	34	1735	61	96.50	95.27
TR_05-2	TR052-164.d	291.8	108.5	2.69	0.2641	0.011	0.03599	0.00077	0.14076	0.053	0.0021	236.5	8.6	227.9	4.8	267	81	96.36	85.36
TR_05-2	TR052-165.d	445.8	87.5	5.09	5.63	0.18	0.3368	0.0074	0.8434	0.119	0.0022	1915	27	1869	36	1928	32	97.60	96.94
TR_05-2	TR052-166.d	5515	519.5	10.62	3.291	0.07	0.2384	0.0041	0.80654	0.09824	0.0012	1477.9	17	1378	22	1588.4	23	93.24	86.75
TR_05-2	TR052-167.d	161.3	74.1	2.18	0.284	0.014	0.03907	0.00091	0.059387	0.0521	0.0026	255	12	247	5.6	234	100	96.86	105.56
TR_05-2	TR052-168.d	225.4	149	1.51	0.314	0.014	0.04228	0.00086	0.079763	0.0534	0.0023	277.3	11	266.9	5.3	283	86	96.25	94.31
TR_05-2	TR052-169.d	186	75.59	2.46	0.429	0.016	0.05686	0.0012	0.09017	0.0541	0.002	359.8	12	356.4	7.1	313	77	99.06	113.87
TR_05-2	TR052-170.d	341.1	238.9	1.43	0.334	0.012	0.04397	0.00093	0.26773	0.0544	0.0017	291.1	9	277.4	5.7	346	68	95.29	80.17
TR_05-2	TR052-171.d	286.9	142.6	2.01	0.358	0.015	0.04362	0.00092	0.14645	0.0589	0.0023	309	11	275.2	5.7	487	84	89.06	56.51
TR_05-2	TR052-172.d	236.8	223.4	1.06	0.352	0.018	0.0363	0.00088	0.26297	0.0694	0.0032	304	14	229.8	5.5	787	99	75.59	29.20
TR_05-2	TR052-173.d	302	200.8	1.50	0.294	0.012	0.03701	0.00085	0.32684	0.0571	0.0021	259.6	9.4	234.2	5.3	438	77	90.22	53.47
TR_05-2	TR052-181.d	245.4	148.1	1.66	0.2654	0.011	0.03698	0.00084	0.10269	0.0518	0.0021	237.4	8.8	234	5.2	218	83	98.57	107.34
TR_05-2	TR052-182.d	501.5	259.9	1.93	0.3	0.0098	0.04082	0.00084	0.22274	0.0527	0.0015	265.4	7.7	257.9	5.2	288	62	97.17	89.55
TR_05-2	TR052-183.d	904.1	1106	0.82	3.727	0.084	0.2721	0.005	0.74586	0.09756	0.0013	1576.2	18	1551	26	1574	25	98.40	98.54
TR_05-2	TR052-184.d	198.8	177.5	1.12	3.568	0.088	0.2606	0.0053	0.53798	0.0972	0.0017	1540	20	1492	27	1559	33	96.88	95.70
TR_05-2	TR052-185.d	214.1	98.3	2.18	0.249	0.012	0.03562	0.00085	0.17367	0.0497	0.0023	223.7	9.9	225.5	5.3	142	94	100.80	158.80
TR_05-2	TR052-186.d	341.5	289.5	1.18	0.2859	0.011	0.03849	0.00084	0.21259	0.0529	0.0018	253.9	8.7	243.4	5.2	284	75	95.86	85.70
TR_05-2	TR052-187.d	109.6	64.9	1.69	0.303	0.018	0.04023	0.0011	0.093961	0.0549	0.0033	264	14	254.2	6.6	260	120	96.29	97.77
TR_05-2	TR052-188a.d	798	68.4	11.67	0.59	0.027	0.0719	0.0019	0.61246	0.0584	0.002	469	17	447.6	11	522	77	95.44	85.75
TR_05-2	TR052-188b.d	447	55	8.13	4.232	0.11	0.2753	0.0061	0.79399	0.1104	0.0017	1680	21	1566	31	1802	28	93.21	86.90
TR_05-2	TR052-189.d	923.9	569	1.62	0.3603	0.0098	0.04852	0.0009	0.46192	0.05283	0.0011	311.8	7.3	305.4	5.6	305	44	97.95	100.13
TR_05-2	TR052-190.d	142.6	152.7	0.93	0.412	0.02	0.05294	0.0012	0.19244	0.0563	0.0026	346	14	332.5	7.3	366	97	96.10	90.85
TR_05-2	TR052-191.d	171.5	195.9	0.88	0.415	0.019	0.05091	0.0011	0.15758	0.0583	0.0024	349	13	320	6.6	462	91	91.69	69.26
TR_05-2	TR052-192.d	19.79	8.2	2.41	11.46	0.37	0.4759	0.011	0.33739	0.1715	0.0047	2548	30	2504	49	2551	48	98.27	98.16
TR_05-2	TR052-193.d	87.7	46	1.91	0.269	0.018	0.03724	0.001	-0.018464	0.0517	0.0036	237	15	235.6	6.5	150	130	99.41	157.07
TR_05-2	TR052-194.d	268.3	218.9	1.23	0.2844	0.011	0.03721	0.00077	0.033925	0.0546	0.0021	252.6	9	235.5	4.8	351	83	93.23	67.09
TR_05-2	TR052-195.d	164.5	113.5	1.45	0.535	0.022	0.06794	0.0014	0.13152	0.0564	0.0022	431	14	423.6	8.6	392	81	98.28	108.06
TR_05-2	TR052-203.d	1453	830	1.75	0.5364	0.013	0.06887	0.0012	0.46147	0.05561	0.0009	435.5	8.4	429.3	7.2	428	35	98.58	100.30
TR_05-2	TR052-204.d	70.5	55.3	1.27	0.403	0.025	0.0514	0.0014	0.059636	0.0569	0.0037	336	18	322.7	8.6	310	130	96.04	104.10
TR_05-2	TR052-205.d	92.4	52.9	1.75	0.314	0.019	0.04131	0.0011	0.15676	0.0544	0.0032	274	14	260.9	6.5	270	120	95.22	96.63
TR_05-2	TR052-206.d	334.5	199.9	1.67	0.299	0.013	0.03988	0.0009	-0.072398	0.054	0.0023	263.7	10	252	5.6	307	92	95.56	82.08
TR_05-2	TR052-207.d	268.2	158.7	1.69	0.2747	0.011	0.03789	0.00082	0.16925	0.0516	0.0018	245	8.6	239.7	5.1	233	76	97.84	102.88
TR_05-2	TR052-208.d	516	427.5	1.21	0.2897	0.0092	0.03805	0.00078	0.22595	0.0546	0.0016	258.1	7.4	240.7	4.9	357	62	93.26	67.42
TR_05-2	TR052-209.d	244.5	149.6	1.63	0.27	0.015	0.03535	0.00086	0.304	0.0544	0.0027	240	12	223.9	5.3	298	100	93.29	75.13
TR_05-2	TR052-210.d	184.1	145.6	1.26	0.412	0.017	0.05344	0.0012	0.11941	0.0557	0.0022	347	12	335.5	7	375	85	96.69	89.47
TR_05-2	TR052-211.d	347.2	297	1.17	4.395	0.11	0.2927	0.0061	0.56148	0.107	0.0019	1710	20	1654	30	1742	32	96.73	94.95
TR_05-2	TR052-212.d	282.3	105.1	2.69	0.2379	0.011	0.03384	0.00074	0.030578	0.0508	0.0026	215.2	9	214.5	4.6	147	93	99.67	145.92
TR_05-2	TR052-213.d	199.5	105.7	1.89	0.274	0.015	0.03754	0.00095	0.15062	0.0527	0.0028	244	12	237.5	5.9	230	110	97.34	103.26
TR_05-2	TR052-214.d	74.52	67.94	1.10	0.395	0.025	0.0532	0.0014	0.12647	0.0533	0.0033	330	18	333.8	8.7	220	120	101.15	151.73
TR_05-2	TR052-215.d	276.6	279.9	0.99	0.297	0.014	0.0367	0.00084	0.20328	0.0584	0.0027	261	11	232.3	5.2	437	94	89.00	53.16
TR_05-2	TR052-216.d	453.1	185.5	2.44	0.617	0.018	0.07647	0.0015	0.30868	0.0579	0.0013	487.4	11	474.9	8.7	497	51	97.44	95.55
TR_05-2	TR052-217.d	127.5	54.7	2.33	0.425	0.031	0.04107	0.0011	0.2298	0.0733	0.0048	351	21	259.3	6.7	800	140	73.87	32.41
TR_05-2	TR052-225.d	328.2	116.4	2.82	5.355	0.13	0.3311	0.0066	0.66795	0.1154	0.0017	1877	19	1842	32	1882	27	98.14	97.87
TR_05-2	TR052-226.d	232.4	121.2	1.92	4.622	0.11	0.3073	0.0057	0.50667	0.1076	0.0017	1751	20	1726	28	1755	28	98.57	98.35
TR_05-2	TR052-227.d	104.4	70.1	1.49	0.287	0.017	0.04026	0.00099	0.070799	0.0516	0.003	252	13	254.4	6.1	170	110	100.95	149.65
TR_05-2	TR052-228.d	35.88	20.5	1.75	0.335	0.036	0.0398	0.0015	0.061205	0.0624	0.0067	281	27	251.6	9.3	360	210	89.54	69.89
TR_05-2	TR052-83.d	998	185	5.39	10.58	0.25	0.4574	0.0089	0.85111	0.1672	0.0023	2485	23	2426	40	2527	23	97.63	96.00
TR_05-2	TR052-84.d	782	585	1.34	3.059	0.068	0.2432	0.0043	0.66569	0.09096	0.0012	1421.8	17	1403	22	1441	25	98.68	97.36
TR_05-2	TR052-85.d	493	164.4	3.00	4.497	0.1	0.3091	0.0059	0.71707	0.10501	0.0015	1728.2	19	1735	29	1711	26	100.39	101.40
TR_05-2	TR052-86.d	85.77	111.1	0.77	2.243	0.068	0.1983	0.0038	0.27298	0.0818	0.0021	1188	21	1166	21	1223	48	98.15	95.34

Supplementary Table 1. Main isotopes and ratios measured using LA–ICP–MS. Concordance 1 ($^{206}Pb/^{238}U/^{207}Pb/^{235}U$) and 2 ($^{206}Pb/^{238}U/^{207}Pb/^{206}Pb$).

TR_05-2	TR052-9.d	152.8	88.5	1.73	4.93	0.12	0.315	0.0058	0.3311	0.115	0.002	1804	20	1764	28	1871	32	97.78	94.28	
TR_05-2	TR052-94.d	688	358.5	1.92	2.071	0.047	0.1853	0.0034	0.70967	0.08046	0.0011	1137.6	16	1095	18	1203	27	96.26	91.02	
TR_05-2	TR052-95.d	198	62.5	3.17	0.286	0.013	0.03951	0.00093	0.1471	0.0524	0.0022	253.6	10	249.7	5.8	252	90	98.46	99.09	
TR_05-2	TR052-96.d	171.5	95.3	1.80	0.357	0.018	0.03845	0.00088	0.0079761	0.0681	0.0034	308	13	243.2	5.4	748	99	78.96	32.51	
TR_05-2	TR052-97.d	1065.2	794.1	1.34	0.348	0.0092	0.04443	0.00082	0.16021	0.0567	0.0012	302.7	6.9	280.2	5.1	455	47	92.57	61.58	
TR_05-2	TR052-98.d	344.1	124.4	2.77	0.338	0.013	0.04643	0.00094	0.19263	0.0528	0.0018	295.4	9.8	292.5	5.8	278	73	99.02	105.22	
TR_05-2	TR052-99.d	120.3	62.3	1.93	0.529	0.025	0.0672	0.0016	0.19267	0.0568	0.0025	428	16	419.3	9.9	409	95	97.97	102.52	
TR_05-3	TR_05-3 - 1	127.7	66.7	1.91	0.264	0.016	0.0386	0.00062	0.085643	0.0499	0.003	237	13	244.2	3.8	170	130	103.04	143.65	
TR_05-3	TR_05-3 - 10	422	335	1.26	3.193	0.037	0.2461	0.003	0.62077	0.09413	0.0009	1455.1	9	1418.2	15	**1509**	**18**	97.46	93.98	
TR_05-3	TR_05-3 - 11	174	140.4	1.24	0.278	0.01	0.04068	0.00064	0.066008	0.0504	0.0021	248.3	8.3	257	3.9	208	93	103.50	123.56	
TR_05-3	TR_05-3 - 12	238.9	211.4	1.13	0.2476	0.0088	0.0357	0.00051	-0.093936	0.0503	0.0019	224.3	7.1	226.1	3.2	190	83	100.80	119.00	
TR_05-3	TR_05-3 - 13	270	146.4	1.84	5.065	0.055	0.3284	0.0043	0.57597	0.11155	0.0009	1829.9	9.3	1830	21	1826	16	100.01	100.22	
TR_05-3	TR_05-3 - 14	176	174	1.01	0.39	0.017	0.05377	0.00084	0.19354	0.0525	0.0022	334	12	337.6	5.1	296	92	101.08	114.05	
TR_05-3	TR_05-3 - 15	222	234	0.95	0.409	0.012	0.05299	0.00089	0.10094	0.056	0.0018	348.6	8.3	332.8	5.5	441	69	95.47	75.46	
TR_05-3	TR_05-3 - 16	531	359	1.48	0.289	0.0074	0.04066	0.00071	0.15731	0.0516	0.0013	259.4	5.8	256.9	4.4	266	59	99.04	96.58	
TR_05-3	TR_05-3 - 17	376	304	1.24	0.2341	0.0064	0.03276	0.00041	0.02751	0.0516	0.0015	213.4	5.2	207.8	2.6	254	63	97.38	81.81	YSG
TR_05-3	TR_05-3 - 18	273	190.6	1.43	0.2528	0.0096	0.03639	0.00053	-0.006218	0.0506	0.002	228.4	7.8	230.4	3.3	215	85	100.88	107.16	
TR_05-3	TR_05-3 - 19	446	257	1.74	0.344	0.011	0.04441	0.00059	0.167	0.0559	0.0017	299.6	8.2	280.1	3.6	440	68	93.49	63.66	
TR_05-3	TR_05-3 - 2	58.5	40	1.46	0.385	0.031	0.05377	0.00089	0.087828	0.052	0.0041	331	23	337.6	5.4	210	160	101.99	160.76	
TR_05-3	TR_05-3 - 20	536	296	1.81	0.684	0.011	0.08581	0.001	0.42691	0.05771	0.0009	529.1	6.6	530.7	6.2	513	34	100.30	103.45	
TR_05-3	TR_05-3 - 21	522	352	1.48	0.479	0.011	0.06018	0.00092	0.39181	0.058	0.0013	397.4	7.2	376.7	5.6	526	48	94.79	71.62	
TR_05-3	TR_05-3 - 22	914	105.6	8.66	1.457	0.028	0.1459	0.0022	0.7716	0.07228	0.0009	914	12	878.1	12	990	26	96.07	88.70	
TR_05-3	TR_05-3 - 23	381	238	1.60	0.262	0.01	0.03743	0.00049	0.15126	0.0507	0.0019	235.9	8.2	236.9	3.1	207	84	100.42	114.44	
TR_05-3	TR_05-3 - 24	651	199	3.27	1.629	0.014	0.1663	0.0021	0.51678	0.07079	0.0006	981.1	5.3	991.8	12	949	17	101.09	104.51	
TR_05-3	TR_05-3 - 25	349	51.25	6.81	1.45	0.027	0.1482	0.0022	0.70353	0.07111	0.001	909	11	890.6	12	962	29	97.98	92.58	
TR_05-3	TR_05-3 - 27	329	247	1.33	0.623	0.014	0.07987	0.0011	0.23871	0.0565	0.0011	490.9	8.9	495.3	6.8	463	44	100.90	106.98	
TR_05-3	TR_05-3 - 28	147	225	0.65	0.315	0.015	0.04309	0.00098	0.51681	0.0535	0.0023	279	12	271.9	6.1	332	94	97.46	81.90	
TR_05-3	TR_05-3 - 29	70.1	48.2	1.45	0.318	0.023	0.04208	0.0007	0.099352	0.0536	0.0038	280	18	265.7	4.3	330	150	94.89	80.52	
TR_05-3	TR_05-3 - 30	508	327	1.55	0.2796	0.0074	0.03905	0.00049	0.028528	0.0517	0.0015	250.1	5.9	247	3	265	66	98.76	93.21	
TR_05-3	TR_05-3 - 31	254	163	1.56	0.271	0.013	0.03785	0.00055	-0.049612	0.0523	0.0025	246.6	9.1	239.5	3.4	290	110	97.12	82.59	
TR_05-3	TR_05-3 - 32	380	175.3	2.17	4.455	0.036	0.3056	0.0035	0.43353	0.10563	0.0008	1722.4	6.8	1718.8	17	1724	14	99.79	99.70	
TR_05-3	TR_05-3 - 33	891	351	2.54	0.619	0.015	0.0779	0.0014	0.75798	0.05702	0.0009	488.7	9.5	483.8	8.6	487	34	99.00	99.34	
TR_05-3	TR_05-3 - 34	492	142.2	3.46	2.057	0.028	0.1954	0.0023	0.38163	0.07602	0.0009	1134.1	9.3	1150.6	13	1096	24	101.45	104.98	
TR_05-3	TR_05-3 - 35	877	364	2.41	0.547	0.011	0.0704	0.0013	0.71347	0.05596	0.0007	442.3	7.3	438.3	7.9	451	29	99.10	97.18	
TR_05-3	TR_05-3 - 36	331	119.3	2.77	1.821	0.031	0.1782	0.0023	0.50448	0.0738	0.001	1052	11	1057	12	1040	29	100.48	101.63	
TR_05-3	TR_05-3 - 37	393	167.9	2.34	0.3308	0.0089	0.04677	0.00064	0.19164	0.0509	0.0013	289.8	6.8	294.7	3.9	238	58	101.69	123.82	
TR_05-3	TR_05-3 - 38	341	222	1.54	3.28	0.047	0.2444	0.0035	0.77167	0.09733	0.0008	1475	11	1409	18	**1572**	**16**	95.53	89.63	
TR_05-3	TR_05-3 - 39	141.3	86.5	1.63	0.279	0.014	0.0406	0.00068	0.039919	0.0503	0.0027	251	11	256.5	4.2	180	110	102.19	142.50	
TR_05-3	TR_05-3 - 40	105.4	58.8	1.79	4.397	0.068	0.3053	0.0039	0.26125	0.104	0.0015	1711	13	1717	19	1697	27	100.35	101.18	
TR_05-3	TR_05-3 - 41	105.5	88.2	1.20	0.283	0.019	0.03614	0.00061	-0.041337	0.0566	0.0037	252	15	228.9	3.8	420	140	90.83	54.50	
TR_05-3	TR_05-3 - 42	207.8	170.5	1.22	0.367	0.022	0.03997	0.00064	0.29076	0.0671	0.004	315	16	252.6	4	830	130	80.19	30.43	
TR_05-3	TR_05-3 - 5	356	262	1.36	1.571	0.022	0.1632	0.002	0.28688	0.0697	0.001	958.1	8.7	974.4	11	913	30	101.70	106.73	
TR_05-3	TR_05-3 - 8	234.9	123.2	1.91	0.256	0.0097	0.0372	0.00056	0.088463	0.0499	0.002	231	7.9	235.4	3.5	173	85	101.90	136.07	
TR_05-3	TR053-229.d	73.3	37.54	1.95	0.463	0.031	0.04469	0.0012	0.042191	0.0749	0.0049	376	21	281.7	7.3	820	140	74.92	34.35	
TR_05-3	TR053-230.d	342.6	222.9	1.54	0.487	0.016	0.0569	0.0011	0.13909	0.0614	0.0019	400.8	11	356.7	6.7	592	64	89.00	60.25	
TR_05-3	TR053-231.d	333.9	249.9	1.34	0.575	0.018	0.07183	0.0014	0.18407	0.0575	0.0015	459	12	447.1	8.1	473	57	97.41	94.52	
TR_05-3	TR053-232.d	283.7	244.4	1.16	0.303	0.012	0.0409	0.00085	0.13667	0.0527	0.0019	267.1	9.2	258.4	5.3	283	78	96.74	91.31	
TR_05-3	TR053-233.d	550.9	506.4	1.09	0.816	0.028	0.0887	0.0017	0.49108	0.0657	0.0018	605	16	547.8	10	766	60	90.55	71.51	
TR_05-3	TR053-234.d	845	1540	0.55	0.3304	0.012	0.03544	0.00068	0.32512	0.0667	0.002	288.5	8.8	224.5	4.2	784	64	77.82	28.64	
TR_05-3	TR053-235.d	228.5	81.15	2.82	0.284	0.012	0.0392	0.00085	0.15945	0.0518	0.0021	253	9.7	247.8	5.3	231	84	97.94	107.27	
TR_05-3	TR053-236.d	54.28	34.78	1.56	2.42	0.086	0.1922	0.0044	0.21219	0.0905	0.0029	1239	25	1132	24	1388	63	91.36	81.56	
TR_05-3	TR053-237.d	77.71	40.07	1.94	0.341	0.023	0.04002	0.0011	0.030827	0.0623	0.0044	291	17	252.8	6.8	460	140	86.87	54.96	
TR_05-3	TR053-238.d	745	193.4	3.85	0.4725	0.013	0.06106	0.0011	0.37922	0.0554	0.0012	392.7	8.7	382	6.8	413	46	97.28	92.49	
TR_05-3	TR053-239.d	318.7	318.1	1.00	0.419	0.015	0.0505	0.00097	0.080005	0.0595	0.002	354.4	11	317.5	6	533	75	89.59	59.57	

Supplementary Table 1. Main isotopes and ratios measured using LA–ICP–MS. Concordance 1 ($^{206}Pb/^{238}U/^{207}Pb/^{235}U$) and 2 ($^{206}Pb/^{238}U/^{207}Pb/^{206}Pb$).

TR_05-3	TR053-247.d	106	138.6	0.76	0.798	0.066	0.04008	0.0012	0.68387	0.144	0.01	577	34	253.2	7.2	2070	120	43.88	12.23
TR_05-3	TR053-248.d	111.8	73.3	1.53	0.461	0.032	0.03943	0.001	0.23761	0.0858	0.0057	376	22	249.2	6.5	1070	130	66.28	23.29
TR_05-3	TR053-249.d	589.1	280.2	2.10	0.36	0.013	0.04026	0.00079	0.29239	0.0637	0.002	310.6	9.6	254.4	4.9	706	67	81.91	36.03
TR_05-3	TR053-250.d	324.8	198.7	1.63	11.644	0.25	0.4724	0.0081	0.51681	0.1764	0.0023	2574.7	20	2493	36	2618	22	96.83	95.23
TR_05-3	TR053-251.d	457.8	100.1	4.57	1.617	0.04	0.1519	0.0028	0.51492	0.07604	0.0013	974.6	15	911.6	16	1092	36	93.54	83.48
TR_05-3	TR053-252.d	82.8	48.99	1.69	1.342	0.062	0.0764	0.002	0.44839	0.1269	0.0054	852	28	474.1	12	1973	80	55.65	24.03
TR_05-3	TR053-253.d	359.6	195.3	1.84	0.429	0.014	0.05463	0.0011	0.10006	0.0567	0.0017	362	10	342.8	6.6	444	65	94.70	77.21
TR_05-3	TR053-254.d	309.8	209.3	1.48	2.044	0.05	0.1862	0.0035	0.57036	0.07855	0.0013	1128	17	1100	19	1152	33	97.52	95.49
TR_05-3	TR053-255.d	75.96	48.56	1.56	0.385	0.021	0.04971	0.0012	0.14217	0.0561	0.003	325	16	312.6	7.5	340	110	96.18	91.94
TR_05-3	TR053-256.d	736.6	223.7	3.29	0.821	0.021	0.0985	0.0018	0.50151	0.05964	0.001	607.2	12	605.4	11	578	39	99.70	104.74
TR_05-3	TR053-257.d	101.9	26.5	3.85	0.599	0.026	0.074	0.0017	0.22595	0.0583	0.0024	472	17	459.9	10	460	88	97.44	99.98
TR_05-3	TR053-258.d	82.9	48.9	1.70	0.298	0.019	0.0369	0.00098	-0.049415	0.0588	0.0039	260	14	233.5	6.1	380	130	89.81	61.45
TR_05-3	TR053-259.d	56.4	28.6	1.97	0.667	0.057	0.0461	0.0014	0.3132	0.1046	0.0082	502	33	290	8.6	1480	150	57.77	19.59
TR_05-3	TR053-260.d	806.6	721	1.12	0.5944	0.015	0.07523	0.0014	0.28104	0.0568	0.0011	472.9	9.4	467.5	8.5	463	43	98.86	100.97
TR_05-3	TR053-261.d	271.3	51.79	5.24	0.432	0.016	0.05696	0.0012	0.029807	0.0544	0.0019	362.9	11	357	7.2	345	78	98.37	103.48
TR_05-3	TR053-262.d	339.6	260.7	1.30	1.793	0.043	0.172	0.003	0.3953	0.07485	0.0013	1040.7	16	1022.6	17	1052	34	98.26	97.21
TR_05-3	TR053-271.d	991.8	444.7	2.23	0.541	0.014	0.0692	0.0013	0.48069	0.05593	0.001	439	9.1	431.2	7.6	437	40	98.22	98.67
TR_05-3	TR053-272.d	946	489	1.93	0.3198	0.0087	0.0443	0.00088	0.39398	0.05192	0.0011	281.3	6.7	279.4	5.4	267	47	99.32	104.64
TR_05-3	TR053-273.d	337.4	203.1	1.66	0.268	0.012	0.0361	0.00079	0.2187	0.0527	0.0021	239.7	9.4	228.6	4.9	276	87	95.37	82.83
TR_05-3	TR053-274.d	464.5	178.4	2.60	0.281	0.01	0.03907	0.00082	0.22246	0.0517	0.0017	250.3	8.2	247	5.1	231	70	98.68	106.93
TR_05-3	TR053-275.d	114.2	56.1	2.04	0.443	0.023	0.05427	0.0013	0.1876	0.059	0.0029	366	16	340.6	7.7	450	100	93.06	75.69
TR_05-3	TR053-276.d	161.5	87.1	1.85	0.281	0.015	0.03753	0.00093	0.20423	0.054	0.0026	248	11	237.4	5.8	282	100	95.73	84.18
TR_05-3	TR053-277.d	143.5	87.4	1.64	0.28	0.015	0.03924	0.00097	0.12767	0.0518	0.0026	248	12	248	6	200	100	100.00	124.00
TR_05-3	TR053-278.d	1872	905.3	2.07	0.3061	0.008	0.03407	0.00064	0.30625	0.0648	0.0013	270.9	6.2	215.9	4	752	43	79.70	28.71
TR_05-3	TR053-279.d	47.5	32.4	1.47	0.49	0.038	0.0392	0.0013	0.19265	0.0913	0.0067	392	25	247.9	8.3	1170	160	63.24	21.19
TR_05-3	TR053-280.d	126.1	97.5	1.29	0.455	0.02	0.05924	0.0013	0.13341	0.0559	0.0023	377	14	370.9	8	363	88	98.38	102.18
TR_05-3	TR053-281.d	529.6	432.2	1.23	0.341	0.014	0.04023	0.00081	0.42528	0.0601	0.002	296	11	254.2	5	557	74	85.88	45.64
TR_05-3	TR053-282.d	223.4	163	1.37	0.289	0.012	0.03898	0.00092	0.1385	0.0541	0.0022	256.5	9.8	246.4	5.7	304	87	96.06	81.05
TR_05-3	TR053-283.d	321.9	478.5	0.67	0.398	0.014	0.05466	0.0012	0.29195	0.0523	0.0016	338.9	10	343	7.1	270	66	101.21	127.04
TR_05-3	TR053-284.d	228.7	108.1	2.12	4.791	0.11	0.3158	0.0061	0.60061	0.1089	0.0017	1780	20	1768	30	1773	29	99.33	99.72
TR_05-3	TR053-285.d	101.5	76.3	1.33	0.45	0.023	0.05814	0.0013	0.08716	0.0555	0.0027	373	16	364.8	8.1	340	100	97.80	107.29
TR_05-3	TR053-293.d	495	93.1	5.32	0.558	0.017	0.07274	0.0014	0.48615	0.0553	0.0012	448.6	11	452.5	8.7	397	50	100.87	113.98
TR_05-3	TR053-294.d	147.6	130.4	1.13	0.397	0.019	0.05165	0.0012	0.23933	0.0551	0.0025	336	14	324.5	7.2	340	95	96.58	95.44
TR_05-3	TR053-295.d	296.6	136.9	2.17	0.296	0.011	0.0394	0.00083	0.14864	0.0544	0.002	261.8	8.9	249.1	5.2	331	76	95.15	75.26
TR_05-3	TR053-296.d	148.4	78.3	1.90	0.32	0.016	0.04106	0.001	0.040196	0.0568	0.0029	279	12	259.3	6.2	370	110	92.94	70.08
TR_05-3	TR053-297.d	2111	980	2.15	0.4629	0.012	0.05547	0.0011	0.53663	0.05985	0.0011	385.8	8	347.9	6.9	591	38	90.18	58.87
TR_05-3	TR053-298.d	268.5	25.27	10.63	3.935	0.094	0.281	0.0052	0.58499	0.1005	0.0015	1618	19	1596	26	1628	29	98.64	98.03
TR_05-3	TR053-299.d	74.4	89.6	0.83	8.75	0.46	0.1136	0.0043	0.79169	0.543	0.017	2270	55	691	25	4353	48	30.44	15.87
TR_05-3	TR053-300.d	194.4	151	1.29	0.284	0.014	0.03849	0.00085	0.13177	0.0541	0.0026	252	11	243.4	5.3	277	97	96.59	87.87
TR_05-3	TR053-301.d	818.4	604.4	1.35	0.3091	0.0087	0.04251	0.00082	0.21763	0.0524	0.0012	272.9	6.7	268.3	5	275	52	98.31	97.56
TR_05-3	TR053-302.d	64.82	35.53	1.82	0.299	0.021	0.0392	0.0012	0.069136	0.0554	0.004	259	16	247.5	7.5	290	140	95.56	85.34
TR_05-3	TR053-303.d	242.1	221.5	1.09	0.299	0.014	0.03631	0.00079	-0.016542	0.0593	0.0027	263	10	229.8	4.9	483	93	87.38	47.58
TR_05-3	TR053-304.d	252	138.7	1.82	4.709	0.11	0.3136	0.0057	0.43057	0.1078	0.0018	1766	20	1757	28	1756	30	99.49	100.06
TR_05-3	TR053-305.d	76.58	80.11	0.96	2.293	0.073	0.2014	0.0042	0.29	0.0823	0.0022	1204	22	1182	22	1222	54	98.17	96.73
TR_05-3	TR053-306.d	205.3	101.2	2.03	0.584	0.021	0.0721	0.0015	0.21885	0.059	0.002	464	13	448.7	9.3	514	73	96.70	87.30
TR_05-3	TR053-307.d	333.4	230.3	1.45	0.535	0.017	0.06911	0.0014	0.12572	0.0563	0.0016	434.2	11	430.7	8.3	425	62	99.19	101.34
TR_05-3	TR053-315.d	335.3	260.8	1.29	0.2747	0.011	0.03842	0.0008	0.29209	0.0519	0.0018	245	8.6	243	5	232	74	99.18	104.74
TR_05-3	TR053-316.d	1011.7	493.8	2.05	1.86	0.043	0.1763	0.0033	0.7171	0.0759	0.0011	1065.5	15	1046	18	1088	28	98.17	96.14
TR_05-3	TR053-317.d	289.1	183.9	1.57	0.28	0.013	0.03447	0.00074	0.27343	0.0583	0.0025	248.3	10	218.4	4.6	453	92	87.96	48.21
TR_05-3	TR053-318.d	281.3	120.8	2.33	0.287	0.012	0.03922	0.00084	0.15865	0.0527	0.0021	255.1	9.8	248	5.2	271	84	97.22	91.51
TR_05-3	TR053-319.d	70.7	45.1	1.57	0.41	0.025	0.052	0.0014	0.030139	0.057	0.0035	343	18	326.5	8.8	370	130	95.19	88.24
TR_05-3	TR053-320.d	325	185.4	1.75	0.287	0.013	0.03833	0.00082	0.12223	0.0542	0.0023	254.8	10	242.5	5.1	323	91	95.17	75.08
TR_05-3	TR053-321.d	314	244.4	1.28	0.2525	0.0099	0.03476	0.00077	0.18295	0.0528	0.0019	227.4	8	220.2	4.8	264	76	96.83	83.41
TR_05-3	TR053-322.d	385.4	162.1	2.38	0.323	0.012	0.04324	0.00097	0.16065	0.0537	0.0019	283.3	9.5	272.8	6	322	77	96.29	84.72

Supplementary Table 1. Main isotopes and ratios measured using LA–ICP–MS. Concordance 1 ($^{206}Pb/^{238}U/^{207}Pb/^{235}U$) and 2 ($^{206}Pb/^{238}U/^{207}Pb/^{206}Pb$).

TR_05-3	TR053-323.d	1302	276.5	4.71	0.3258	0.0088	0.04171	0.00081	0.22454	0.0565	0.0013	286.4	6.8	263.4	5	449	50	91.97	58.66	
TR_05-3	TR053-324.d	101.52	82.86	1.23	0.257	0.015	0.03317	0.00092	0.0012112	0.0567	0.0035	228	12	210.3	5.8	340	130	92.24	61.85	
TR_05-3	TR053-325.d	485.7	290.8	1.67	2.767	0.066	0.2115	0.0038	0.53551	0.094	0.0015	1344.1	18	1236	20	1504	30	91.96	82.18	
TR_05-3	TR053-326.d	196.3	103.3	1.90	0.329	0.015	0.03849	0.00088	0.024181	0.0617	0.0027	286	11	243.4	5.5	567	94	85.10	42.93	
TR_05-3	TR053-327.d	210.2	135.7	1.55	0.78	0.033	0.0769	0.0017	0.6679	0.0726	0.0024	578	19	477.1	10	931	73	82.54	51.25	
TR_05-3	TR053-328.d	223.4	141.4	1.58	0.43	0.016	0.05671	0.0011	0.10118	0.0551	0.0019	362.2	11	355.5	7	364	73	98.15	97.66	
TR_05-3	TR053-329.d	91.87	191.3	0.48	1.578	0.052	0.1611	0.0034	0.1339	0.0714	0.0022	955	20	962	19	917	62	100.73	104.91	
CM15_01	CM1501-181.d	3465	7000	0.51	0.228	0.0054	0.02217	0.00037	0.53447	0.0745	0.0016	208.3	4.5	141.3	2.3	1046	43	67.83	13.51	
CM15_01	CM1501-297.d	237	147.9	1.57	0.52	0.045	0.0352	0.0014	0.3035	0.104	0.008	417	29	222.9	8.5	1600	140	53.45	13.93	
CM15_01	CM1501-253.d	1613	608	2.59	0.312	0.014	0.0352	0.00062	0.38743	0.0637	0.0024	275	10	223	3.9	727	85	81.09	30.67	
CM15_01	CM1501-215.d	2177	1276	1.67	0.2897	0.0062	0.03537	0.00049	0.24805	0.0594	0.0014	258.1	4.9	224.1	3	566	52	86.83	39.59	
CM15_01	CM1501-209.d	224.7	169.9	1.32	0.268	0.014	0.03572	0.00073	0.12131	0.0547	0.003	239	11	226.2	4.6	320	110	94.64	70.69	YC1
CM15_01	CM1501-293.d	68.51	25.62	2.70	0.404	0.041	0.0364	0.0011	0.059999	0.0855	0.0092	337	29	230.1	6.6	970	220	68.28	23.72	
CM15_01	CM1501-319.d	237.6	303.9	0.80	0.26	0.014	0.03649	0.00073	0.075169	0.0523	0.0029	235	11	231	4.5	260	120	98.30	88.85	
CM15_01	CM1501-377.d	976	1060	0.93	0.276	0.0081	0.0365	0.00045	0.050923	0.0549	0.0017	247	6.4	231.1	2.8	374	67	93.56	61.79	
CM15_01	CM1501-415.d	620	279	1.97	0.385	0.039	0.03693	0.00074	0.1867	0.0775	0.009	322	25	233.7	4.6	930	170	72.58	25.13	
CM15_01	CM1501-362.d	765	923	0.83	0.407	0.029	0.0372	0.00073	0.15026	0.0796	0.0053	343	20	235.4	4.5	1100	130	68.63	21.40	
CM15_01	CM1501-378.d	144.6	105.2	1.42	0.43	0.039	0.03807	0.00091	0.38421	0.0801	0.0065	357	27	240.8	5.7	1050	160	67.45	22.93	
CM15_01	CM1501-358.d	146.9	176.6	0.84	0.85	0.18	0.041	0.003	0.69841	0.143	0.023	590	90	259	19	1990	300	43.90	13.02	
CM15_01	CM1501-254.d	1179	549	2.09	0.36	0.022	0.04105	0.00072	0.14956	0.0628	0.0026	310	14	259.3	4.4	665	72	83.65	38.99	
CM15_01	CM1501-225.d	195.7	128.5	1.54	0.347	0.02	0.04218	0.00087	-0.0102	0.0604	0.0038	302	15	266.3	5.4	510	130	88.18	52.22	
CM15_01	CM1501-278.d	173.1	108.8	1.55	0.286	0.017	0.04256	0.00086	0.061678	0.0487	0.003	253	14	268.6	5.4	100	120	106.17	268.60	
CM15_01	CM1501-342.d	439	154	2.88	0.418	0.017	0.04279	0.00081	0.12992	0.0711	0.0029	353	12	270	5	904	80	76.49	29.87	
CM15_01	CM1501-413.d	220.8	190.6	1.17	0.397	0.027	0.04283	0.00078	0.12104	0.0667	0.0044	335	19	270.3	4.8	730	140	80.69	37.03	
CM15_01	CM1501-412.d	285.8	181	1.61	0.55	0.064	0.0431	0.0013	0.4813	0.094	0.01	451	44	272.2	8.2	1360	200	60.35	20.01	
CM15_01	CM1501-405.d	244.5	208.3	1.25	0.421	0.024	0.04316	0.00087	0.18614	0.0711	0.0041	353	17	272.3	5.4	840	120	77.14	32.42	
CM15_01	CM1501-166.d	215.8	60.16	3.60	0.323	0.014	0.0433	0.00075	0.082557	0.0537	0.0024	283	11	273.2	4.6	328	99	96.54	83.29	
CM15_01	CM1501-408.d	214.6	147.3	1.57	0.39	0.022	0.04345	0.00082	0.29153	0.0649	0.0037	331	16	274.1	5.1	690	120	82.81	39.72	
CM15_01	CM1501-376.d	251.6	137.1	1.85	0.343	0.016	0.04406	0.0008	-0.00974	0.0563	0.0027	299	11	277.9	4.9	423	99	92.94	65.70	
CM15_01	CM1501-340.d	871	528	1.66	0.419	0.014	0.04416	0.00079	0.10498	0.0685	0.0023	353.8	9.9	278.5	4.9	855	67	78.72	32.57	
CM15_01	CM1501-165.d	228	97.2	2.37	0.413	0.019	0.04459	0.00081	0.20267	0.0678	0.0032	351	14	281.2	5	794	99	80.11	35.42	
CM15_01	CM1501-347.d	40.9	25.7	1.64	0.437	0.052	0.0447	0.0023	0.11938	0.0734	0.0094	353	36	282	14	740	270	79.89	38.11	f analysis rejected
CM15_01	CM1501-344.d	1141	542	2.12	0.387	0.013	0.0448	0.00067	0.42449	0.0626	0.0019	333.6	9.8	282.5	4.1	679	65	84.68	41.61	
CM15_01	CM1501-410.d	78.8	66.4	1.25	0.576	0.087	0.0456	0.0016	0.69601	0.087	0.011	427	47	287.4	9.6	1000	220	67.31	28.74	
CM15_01	CM1501-184.d	486.9	203.1	2.42	0.422	0.02	0.0459	0.00062	0.14523	0.0663	0.0031	355	14	289.3	3.9	739	96	81.49	39.15	
CM15_01	CM1501-321.d	336.2	100	3.38	0.322	0.014	0.04612	0.00093	0.29049	0.0507	0.0022	282	11	290.6	5.7	190	91	103.05	152.95	
CM15_01	CM1501-213.d	395.8	204.3	1.90	0.433	0.032	0.04615	0.00088	0.40475	0.0677	0.0046	359	21	290.8	5.4	730	130	81.00	39.84	discordant
CM15_01	CM1501-252.d	1474	468.9	3.08	0.3744	0.0097	0.04697	0.00056	0.19456	0.0575	0.0015	322.4	7.2	295.9	3.5	490	57	91.78	60.39	
CM15_01	CM1501-384.d	160.2	163.2	1.06	0.517	0.027	0.0505	0.0013	0.048578	0.0762	0.0045	419	18	317.6	8.2	970	130	75.80	32.74	
CM15_01	CM1501-271.d	102.5	148.2	0.69	0.379	0.024	0.0506	0.001	0.14137	0.0539	0.0034	322	17	318.1	6.3	290	130	98.79	109.69	
CM15_01	CM1501-314.d	66.1	71.8	0.99	0.382	0.031	0.0508	0.0014	-0.07376	0.0551	0.0048	321	23	319.2	8.4	270	170	99.44	118.22	
CM15_01	CM1501-272.d	124.2	102.7	1.19	0.443	0.033	0.0524	0.001	0.19192	0.0631	0.0049	370	23	329.4	6.2	610	150	89.03	54.00	
CM15_01	CM1501-180.d	226.2	312.6	0.74	0.412	0.024	0.0528	0.001	0.084393	0.0566	0.0035	349	17	331.4	6.4	420	130	94.96	78.90	
CM15_01	CM1501-411.d	60	52.4	1.17	0.879	0.064	0.0536	0.0015	0.15131	0.119	0.0087	625	34	336.4	9.1	1820	140	53.82	18.48	
CM15_01	CM1501-146.d	65.5	83.6	0.78	0.769	0.072	0.0541	0.0015	0.24915	0.1036	0.0092	559	37	339.5	9.4	1490	160	60.73	22.79	
CM15_01	CM1501-335.d	103.5	99.3	1.04	0.432	0.027	0.0544	0.0012	0.11096	0.0579	0.0038	360	19	341.4	7.6	410	130	94.83	83.27	
CM15_01	CM1501-346.d	164	188	0.86	0.525	0.03	0.0547	0.0012	0.032084	0.0699	0.0042	423	20	342.9	7.1	850	130	81.06	40.34	
CM15_01	CM1501-183.d	132	167.8	0.80	0.535	0.043	0.0562	0.0016	0.7506	0.0694	0.0046	434	29	352.1	9.6	770	140	81.13	45.73	discordant
CM15_01	CM1501-227.d	1109	968	1.16	0.486	0.016	0.0568	0.0015	0.6378	0.0619	0.0019	402	11	355.9	9	652	65	88.53	54.59	
CM15_01	CM1501-345.d	499.6	132.6	3.80	0.43	0.012	0.05679	0.00067	0.1817	0.0547	0.0015	362.3	8.7	356	4.1	375	62	98.26	94.93	
CM15_01	CM1501-269.d	165.7	123.7	1.35	0.51	0.031	0.0569	0.0012	0.50253	0.0655	0.0037	413	20	356.6	7.6	690	110	86.34	51.68	
CM15_01	CM1501-161.d	366	397	0.99	0.66	0.1	0.0576	0.0014	0.68752	0.0791	0.0094	484	49	361.1	8.6	920	170	74.61	39.25	
CM15_01	CM1501-292.d	1098	757	1.47	0.473	0.013	0.05769	0.00093	0.38042	0.0595	0.0016	392.2	8.8	361.5	5.6	572	59	92.17	63.20	
CM15_01	CM1501-317.d	164.6	187.7	0.91	0.554	0.03	0.0588	0.0011	-0.09611	0.0684	0.0039	443	19	368.3	6.4	780	120	83.14	47.22	

Supplementary Table 1. Main isotopes and ratios measured using LA–ICP–MS. Concordance 1 ($^{206}Pb/^{238}U/^{207}Pb/^{235}U$) and 2 ($^{206}Pb/^{238}U/^{207}Pb/^{206}Pb$).

CM15_01	CM1501-232.d	171	132	1.22	1.23	0.14	0.0592	0.0031	0.39066	0.15	0.015	780	59	370	19	2180	170	47.44	16.97	
CM15_01	CM1501-157.d	223.6	167.2	1.38	0.667	0.045	0.0595	0.0013	0.52159	0.0803	0.0046	510	26	372.2	7.7	1160	120	72.98	32.09	
CM15_01	CM1501-257.d	61.7	47.9	1.29	0.924	0.097	0.0635	0.0018	0.39989	0.1039	0.0097	632	47	397	11	1440	180	62.82	27.57	
CM15_01	CM1501-230.d	69.5	58.4	1.19	1.192	0.093	0.0664	0.0025	0.36011	0.1267	0.0088	773	41	414	15	1960	130	53.56	21.12	
CM15_01	CM1501-145.d	169.5	187	0.92	1.059	0.088	0.0666	0.0019	0.39805	0.1158	0.0086	717	39	415	11	1790	120	57.88	23.18	
CM15_01	CM1501-383.d	944	343	2.84	0.7	0.054	0.0669	0.0028	0.23862	0.0774	0.0072	536	32	417	17	1070	170	77.80	38.97	
CM15_01	CM1501-191.d	259.1	121.5	2.12	0.537	0.024	0.0685	0.0012	0.1232	0.0568	0.0026	433	16	427.2	7.2	440	100	98.66	97.09	
CM15_01	CM1501-179.d	267.1	302.1	0.91	0.575	0.021	0.0686	0.0011	0.039049	0.0609	0.0025	459	14	427.8	6.8	588	87	93.20	72.76	
CM15_01	CM1501-295.d	203.2	192.7	1.05	0.681	0.043	0.0693	0.0016	0.50418	0.0722	0.0044	528	27	431.9	9.5	910	120	81.80	47.46	
CM15_01	CM1501-142.d	529.8	571.5	0.92	0.591	0.017	0.06968	0.00086	0.18914	0.061	0.0016	471.8	10	434.2	5.2	627	62	92.03	69.25	
CM15_01	CM1501-380.d	283	120.2	2.37	1.63	0.45	0.0702	0.0049	0.90657	0.159	0.032	890	140	436	29	1980	290	48.99	22.02	
CM15_01	CM1501-391.d	317	409	0.82	0.558	0.019	0.0701	0.001	0.13797	0.0581	0.0021	450	13	436.5	6.1	497	75	97.00	87.83	
CM15_01	CM1501-403.d	170.3	156	1.17	0.551	0.025	0.0708	0.001	0.12035	0.0565	0.0025	444	16	440.8	6.2	419	98	99.28	105.20	
CM15_01	CM1501-299.d	333	257	1.28	0.715	0.046	0.0712	0.0012	0.014366	0.0736	0.0052	540	24	443.3	7.1	960	120	82.09	46.18	
CM15_01	CM1501-366.d	349.9	348.5	0.98	0.59	0.018	0.07184	0.00094	0.036224	0.0593	0.0019	471	11	447.2	5.7	549	72	94.95	81.46	
CM15_01	CM1501-247.d	537.5	480.9	1.08	0.594	0.017	0.07245	0.00089	0.20749	0.0593	0.0017	472.1	10	450.9	5.3	549	60	95.51	82.13	
CM15_01	CM1501-312.d	251.2	130.7	2.04	0.824	0.069	0.0729	0.0016	0.26064	0.0825	0.0063	599	36	453.3	9.6	1130	150	75.68	40.12	
CM15_01	CM1501-136.d	134.8	124.9	1.08	0.76	0.04	0.0731	0.0014	-0.04732	0.0768	0.0047	573	24	454.6	8.3	1000	120	79.34	45.46	
CM15_01	CM1501-289.d	225.6	219.5	1.07	0.659	0.025	0.0735	0.0011	0.12831	0.0646	0.0024	511	15	457.2	6.6	717	84	89.47	63.77	
CM15_01	CM1501-381.d	350.3	188.4	1.92	0.671	0.026	0.0738	0.0015	0.10404	0.0658	0.0024	518	15	458.6	8.9	774	78	88.53	59.25	
CM15_01	CM1501-162.d	727	387	1.93	0.596	0.014	0.07478	0.00098	0.29977	0.0577	0.0013	473.5	9.1	464.8	5.9	497	51	98.16	93.52	
CM15_01	CM1501-178.d	153.4	106.7	1.47	0.641	0.027	0.0757	0.0014	-0.01552	0.0615	0.0029	499	17	470.5	8.2	579	100	94.29	81.26	
CM15_01	CM1501-235.d	120.8	79.3	1.48	1.1	0.14	0.0765	0.0031	0.19105	0.104	0.013	735	65	475	19	1530	200	64.63	31.05	
CM15_01	CM1501-325.d	158.2	152.1	1.04	0.67	0.031	0.0766	0.0014	0.098334	0.0641	0.0031	518	19	475.6	8.2	660	100	91.81	72.06	
CM15_01	CM1501-360.d	127.8	108.6	1.18	0.806	0.052	0.0769	0.0013	-0.02548	0.0766	0.0052	589	28	477.2	7.5	950	130	81.02	50.23	
CM15_01	CM1501-275.d	447	323	1.36	0.654	0.019	0.0772	0.0012	0.41828	0.0611	0.0016	510	12	479.5	7.2	630	59	94.02	76.11	
CM15_01	CM1501-140.d	270	212.5	1.29	0.638	0.021	0.0773	0.0011	0.33243	0.0593	0.0018	499	13	480.1	6.5	553	68	96.21	86.82	2
CM15_01	CM1501-324.d	255.9	237.5	1.07	0.908	0.046	0.0774	0.0015	0.41737	0.0842	0.0038	649	23	480.7	8.7	1242	89	74.07	38.70	
CM15_01	CM1501-223.d	484.5	266.6	1.84	0.658	0.017	0.0785	0.0011	0.1573	0.0607	0.0017	512.1	11	487.8	6.7	601	60	95.25	81.16	
CM15_01	CM1501-382.d	406	185.6	2.23	0.648	0.021	0.0801	0.0013	0.23747	0.0588	0.002	505	13	496.4	7.6	521	71	98.30	95.28	
CM15_01	CM1501-137.d	111.5	82.4	1.37	0.91	0.066	0.0812	0.0017	0.29426	0.0821	0.006	642	32	503	10	1110	140	78.35	45.32	
CM15_01	CM1501-202.d	36.71	19.44	1.86	0.979	0.068	0.0813	0.0021	-0.04405	0.0917	0.0073	680	37	504	13	1250	170	74.12	40.32	
CM15_01	CM1501-298.d	927	501	1.86	0.736	0.015	0.0893	0.0012	0.35135	0.0598	0.0013	559.3	8.8	551.1	7.4	581	45	98.53	94.85	
CM15_01	CM1501-296.d	459	354	1.28	1.5	0.33	0.0928	0.0068	0.97399	0.122	0.022	920	140	571	39	1840	270	62.07	31.03	
CM15_01	CM1501-226.d	2691	2499	1.08	1.014	0.024	0.0928	0.002	0.68724	0.0792	0.0014	710	12	572	12	1172	34	80.56	48.81	
CM15_01	CM1501-144.d	1423	2193	0.64	1.11	0.18	0.0964	0.0023	0.89578	0.0799	0.0093	715	55	593	14	1050	140	82.94	56.48	
CM15_01	CM1501-301.d	2954	1182	2.48	1.298	0.052	0.1012	0.0018	0.29871	0.0944	0.0038	839	20	621	11	1480	59	74.02	41.96	
CM15_01	CM1501-188.d	2201	1282	1.70	1.035	0.017	0.1018	0.0011	0.66235	0.0736	0.001	721.1	8.4	624.7	6.7	1026	28	86.63	60.89	
CM15_01	CM1501-300.d	637	58.7	10.65	0.984	0.023	0.1099	0.0017	0.39459	0.0649	0.0014	694	12	671.8	9.8	762	49	96.80	88.16	
CM15_01	CM1501-279.d	479.7	517.3	0.90	1.02	0.029	0.1108	0.0018	0.34069	0.0678	0.0021	712	15	677	10	834	62	95.08	81.18	
CM15_01	CM1501-255.d	50.6	40.6	1.30	2.4	0.27	0.1122	0.0062	0.60963	0.149	0.011	1182	70	682	35	2210	120	57.70	30.86	
CM15_01	CM1501-233.d	87	92.3	0.95	6.5	1.5	0.127	0.015	0.74093	0.364	0.055	1920	190	762	86	3550	250	39.69	21.46	
CM15_01	CM1501-341.d	166.9	128.8	1.30	1.43	0.064	0.13	0.0018	0.23987	0.0793	0.0034	892	26	788	10	1136	86	88.34	69.37	
CM15_01	CM1501-148.d	764	124	10.40	1.378	0.045	0.137	0.0037	0.89599	0.073	0.0013	878	20	827	21	1004	36	94.19	82.37	
CM15_01	CM1501-229.d	460.3	83.9	5.62	1.357	0.031	0.1385	0.0023	0.40161	0.0709	0.0016	870	14	836	13	943	48	96.09	88.65	
CM15_01	CM1501-170.d	289.9	57.1	5.02	1.587	0.041	0.1489	0.0024	0.2994	0.0769	0.0019	964	17	894	14	1100	48	92.74	81.27	
CM15_01	CM1501-160.d	113.6	76.4	1.55	1.85	0.1	0.1494	0.0034	0.47299	0.0909	0.0046	1053	36	897	19	1387	96	85.19	64.67	6
CM15_01	CM1501-211.d	1204	548	2.22	2.194	0.063	0.1539	0.0034	0.82561	0.1029	0.0019	1176	20	922	19	1671	34	78.40	55.18	
CM15_01	CM1501-267.d	1038	199.7	5.22	1.582	0.028	0.1608	0.0018	0.60726	0.07108	0.0011	962.1	11	961	10	961	32	99.89	100.00	
CM15_01	CM1501-392.d	354.5	372.6	0.97	1.617	0.037	0.161	0.002	0.35552	0.0728	0.0016	975	15	962	11	991	46	98.67	97.07	
CM15_01	CM1501-316.d	243	105	2.43	3.75	0.55	0.1621	0.0078	0.66908	0.18	0.024	1580	120	967	43	2500	210	61.20	38.68	
CM15_01	CM1501-364.d	1199	202.4	5.81	2.006	0.043	0.1621	0.0026	0.79067	0.0896	0.0014	1116	14	968	15	1411	29	86.74	68.60	
CM15_01	CM1501-143.d	118.2	58	2.19	1.922	0.074	0.1628	0.0026	0.31465	0.0858	0.0031	1080	25	972	15	1291	70	90.00	75.29	

Supplementary Table 1. Main isotopes and ratios measured using LA–ICP–MS. Concordance 1 ($^{206}Pb/^{238}U/^{207}Pb/^{235}U$) and 2 ($^{206}Pb/^{238}U/^{207}Pb/^{206}Pb$).

CM15_01	CM1501-336.d	185.5	135.4	1.37	1.692	0.042	0.164	0.0024	0.26702	0.075	0.0019	1003	16	978	13	1052	53	97.51	92.97	
CM15_01	CM1501-357.d	306	161.5	1.94	1.748	0.05	0.1645	0.0021	0.27963	0.0765	0.0022	1025	19	981	11	1087	59	95.71	90.25	
CM15_01	CM1501-339.d	2103	578	3.72	1.763	0.049	0.1663	0.0028	0.099479	0.0767	0.0024	1030	17	992	15	1096	53	96.31	90.51	
CM15_01	CM1501-274.d	200.3	152.3	1.29	1.796	0.045	0.1676	0.0025	0.51806	0.0776	0.0017	1041	17	998	14	1121	44	95.87	89.03	
CM15_01	CM1501-168.d	235	145.2	1.62	2.04	0.25	0.1684	0.004	0.75901	0.0863	0.0076	1082	49	1002	22	1197	91	92.61	83.71	
CM15_01	CM1501-313.d	487.1	207.2	2.51	1.824	0.034	0.1689	0.0021	0.41051	0.0782	0.0014	1052.8	12	1006	11	1143	36	95.55	88.01	
CM15_01	CM1501-322.d	417	366	1.18	1.721	0.039	0.1721	0.0024	0.44867	0.0722	0.0016	1014	15	1023	13	982	44	100.89	104.18	
CM15_01	CM1501-246.d	539	296.5	1.76	2.059	0.065	0.1731	0.0033	0.2194	0.0873	0.0023	1137	20	1029	18	1358	51	90.50	75.77	
CM15_01	CM1501-311.d	795	156	6.19	1.869	0.035	0.1785	0.0026	0.56203	0.0759	0.0013	1070	13	1058	14	1092	35	98.88	96.89	
CM15_01	CM1501-149.d	57.7	34.4	1.68	2.368	0.1	0.1815	0.0036	0.15361	0.0929	0.0038	1220	31	1074	19	1455	90	88.03	73.81	
CM15_01	CM1501-210.d	148.6	56.8	2.54	2.118	0.068	0.1832	0.0029	0.060044	0.0841	0.003	1152	22	1084	16	1263	67	94.10	85.83	
CM15_01	CM1501-250.d	98.1	86.2	1.10	3.25	0.26	0.1998	0.0043	0.35861	0.1165	0.0086	1444	59	1174	23	1820	130	81.30	64.51	
CM15_01	CM1501-323.d	234.8	238.3	0.99	2.287	0.055	0.2011	0.0025	0.26688	0.0823	0.002	1205	17	1181	14	1234	48	98.01	95.71	
CM15_01	CM1501-234.d	1648	346	4.70	3.163	0.069	0.2024	0.0038	0.88481	0.11295	0.0015	1445	17	1187	20	1847	25	82.15	64.27	
CM15_01	CM1501-249.d	317.6	227.4	1.36	2.235	0.041	0.2023	0.0023	0.37028	0.0802	0.0015	1192	13	1187	12	1192	37	99.58	99.58	
CM15_01	CM1501-201.d	175.8	103.5	1.67	2.821	0.077	0.213	0.0033	0.37444	0.0959	0.0025	1360	21	1244	17	1534	52	91.47	81.10	
CM15_01	CM1501-407.d	443	369	1.24	3.006	0.071	0.2132	0.0036	0.40155	0.102	0.0021	1407	18	1246	19	1654	38	88.56	75.33	
CM15_01	CM1501-236.d	984	596.2	1.62	2.646	0.043	0.2177	0.0025	0.63885	0.08792	0.0013	1312.4	12	1270	13	1376	27	96.77	92.30	
CM15_01	CM1501-337.d	319.2	63.6	5.05	2.619	0.048	0.2224	0.0031	0.45328	0.0856	0.0016	1304	14	1294	16	1319	36	99.23	98.10	
CM15_01	CM1501-248.d	77.7	49.31	1.53	4.004	0.1	0.2249	0.0037	0.15768	0.1292	0.0037	1630	21	1307	20	2070	53	80.18	63.14	discordant
CM15_01	CM1501-268.d	372.8	197.6	1.89	2.826	0.054	0.2317	0.0027	0.48972	0.0883	0.0015	1360	14	1343	14	1380	34	98.75	97.32	
CM15_01	CM1501-214.d	477.2	371.7	1.25	3.067	0.053	0.2414	0.003	0.49594	0.0918	0.0015	1423	13	1393	15	1457	31	97.89	95.61	
CM15_01	CM1501-182.d	818.8	174.2	4.85	3.333	0.063	0.2418	0.0035	0.75011	0.0998	0.0015	1487	15	1395	18	1615	28	93.81	86.38	8
CM15_01	CM1501-315.d	151.1	103.1	1.52	3.281	0.1	0.2452	0.0049	0.51067	0.0973	0.0027	1469	25	1413	26	1552	52	96.19	91.04	
CM15_01	CM1501-359.d	1614	234.6	6.91	3.913	0.071	0.2457	0.0039	0.89798	0.11527	0.0015	1614	15	1415	20	1882	23	87.67	75.19	
CM15_01	CM1501-163.d	167.8	110.3	1.56	3.17	0.076	0.2484	0.0033	0.28045	0.0925	0.0023	1446	19	1430	17	1459	46	98.89	98.01	
CM15_01	CM1501-393.d	461.8	162.1	2.90	3.94	0.16	0.2532	0.0089	0.90422	0.1126	0.0022	1615	33	1453	45	1837	35	89.97	79.10	
CM15_01	CM1501-224.d	473	86	6.17	3.487	0.07	0.2617	0.0046	0.74312	0.0965	0.0016	1522	16	1497	24	1552	31	98.36	96.46	
CM15_01	CM1501-288.d	683	91.4	7.87	4.159	0.092	0.2687	0.0046	0.80622	0.112	0.0017	1663	19	1533	24	1827	28	92.18	83.91	
CM15_01	CM1501-158.d	149	197.5	0.78	3.77	0.08	0.2699	0.0038	0.42177	0.1012	0.0021	1586	17	1539	19	1645	36	97.04	93.56	
CM15_01	CM1501-291.d	191	190.2	1.02	3.68	0.076	0.2701	0.0028	0.28926	0.0983	0.0019	1566	16	1541	14	1587	36	98.40	97.10	
CM15_01	CM1501-363.d	427	539	0.78	3.637	0.058	0.2711	0.0023	0.31028	0.0972	0.0015	1559.2	13	1546	12	1569	30	99.15	98.53	
CM15_01	CM1501-294.d	960	638	1.53	4.39	0.11	0.2797	0.007	0.89646	0.1138	0.0018	1707	20	1588	36	1858	28	93.03	85.47	
CM15_01	CM1501-287.d	589	147.7	4.44	4.153	0.087	0.2831	0.0047	0.81015	0.1064	0.0016	1662	17	1606	24	1735	27	96.63	92.56	
CM15_01	CM1501-270.d	302.5	354.4	0.85	4.355	0.1	0.2839	0.0049	0.63164	0.1111	0.002	1703	18	1609	25	1810	33	94.48	88.90	
CM15_01	CM1501-338.d	295	134	2.37	4.52	0.16	0.2827	0.0084	0.67335	0.1151	0.0029	1739	29	1619	42	1886	45	93.10	85.84	
CM15_01	CM1501-361.d	211.2	207.4	1.04	3.954	0.075	0.2891	0.0033	0.31407	0.0992	0.002	1623	15	1639	17	1599	37	100.99	102.50	
CM15_01	CM1501-277.d	610	80.5	7.99	4.602	0.079	0.2907	0.004	0.67025	0.1146	0.0018	1748	14	1644	20	1869	28	94.05	87.96	
CM15_01	CM1501-169.d	97.2	68.3	1.42	5.37	0.34	0.297	0.011	0.81295	0.1309	0.0048	1874	51	1672	57	2103	68	89.22	79.51	
CM15_01	CM1501-164.d	627	423	1.50	4.686	0.075	0.3043	0.0032	0.53638	0.1116	0.0017	1763.4	13	1712	16	1821	28	97.09	94.01	
CM15_01	CM1501-231.d	680.7	105.9	6.39	4.914	0.084	0.3116	0.0045	0.76026	0.1138	0.0016	1803	15	1747	22	1860	26	96.89	93.92	
CM15_01	CM1501-333.d	268.1	119.1	2.25	4.634	0.082	0.3133	0.0035	0.46483	0.107	0.0018	1755	15	1756	17	1743	30	100.06	100.75	
CM15_01	CM1501-310.d	449	346	1.41	5.38	0.11	0.3152	0.006	0.82611	0.1236	0.0019	1881	18	1764	29	2008	26	93.78	87.85	
CM15_01	CM1501-388.d	244.7	141.3	1.79	5.42	0.15	0.3222	0.0053	0.44748	0.1207	0.0027	1882	23	1799	26	1954	40	95.59	92.07	
CM15_01	CM1501-265.d	840	58.5	15.17	5.019	0.076	0.3225	0.0031	0.62776	0.1126	0.0016	1821.5	13	1802	15	1839	25	98.93	97.99	
CM15_01	CM1501-401.d	132.4	96.3	1.45	5.206	0.11	0.3226	0.0037	0.44351	0.1162	0.0021	1853	17	1802	18	1890	33	97.25	95.34	
CM15_01	CM1501-355.d	236.9	110	2.21	5.174	0.098	0.326	0.0036	0.36497	0.1147	0.002	1846	16	1818	18	1869	31	98.48	97.27	
CM15_01	CM1501-159.d	291.8	281.4	1.07	5.206	0.1	0.3277	0.004	0.39066	0.1151	0.0022	1852	16	1827	20	1876	35	98.65	97.39	
CM15_01	CM1501-404.d	132.7	98.4	1.43	5.298	0.12	0.3279	0.0047	0.54636	0.1167	0.0022	1865	19	1827	23	1902	35	97.96	96.06	
CM15_01	CM1501-245.d	749	186.6	3.90	8.34	0.16	0.3282	0.0042	0.33766	0.1841	0.0036	2267	17	1829	21	2685	32	80.68	68.12	discordant
CM15_01	CM1501-318.d	391.1	164.4	2.45	5.226	0.087	0.3283	0.0041	0.59413	0.1153	0.0018	1855	14	1829	20	1880	27	98.60	97.29	
CM15_01	CM1501-406.d	271.1	157.8	1.81	5.182	0.086	0.3283	0.0033	0.43763	0.1143	0.0018	1848	14	1829	16	1866	28	98.97	98.02	
CM15_01	CM1501-356.d	172.6	97.9	1.85	6.75	0.35	0.3323	0.0079	0.87074	0.1447	0.0047	2051	45	1846	38	2256	55	90.00	81.83	

Supplementary Table 1. Main isotopes and ratios measured using LA–ICP–MS. Concordance 1 ($^{206}Pb/^{238}U/^{207}Pb/^{235}U$) and 2 ($^{206}Pb/^{238}U/^{207}Pb/^{206}Pb$).

CM15_01	CM1501-368.d	1219	336.6	3.55	5.246	0.08	0.3332	0.0031	0.66538	0.11388	0.0015	1859	13	1854	15	1859	24	99.73	99.73
CM15_01	CM1501-138.d	24.07	25.77	0.93	7.56	0.93	0.335	0.011	0.89009	0.157	0.012	2095	70	1859	50	2440	140	88.74	76.19
CM15_01	CM1501-139.d	96.8	151.6	0.64	5.78	0.17	0.3394	0.0064	0.37968	0.1231	0.0037	1938	26	1882	31	1986	53	97.11	94.76
CM15_01	CM1501-185.d	443.9	85.5	5.30	5.731	0.094	0.3445	0.0035	0.66095	0.1198	0.0017	1935	14	1907	17	1950	25	98.55	97.79
CM15_01	CM1501-141.d	263	133.8	2.13	5.57	0.12	0.3494	0.006	0.73417	0.1154	0.0019	1908	19	1930	29	1883	29	101.15	102.50
CM15_01	CM1501-367.d	236.5	150	1.54	5.794	0.099	0.3498	0.0042	0.56944	0.1195	0.0018	1944	15	1933	20	1943	27	99.43	99.49
CM15_01	CM1501-343.d	121.5	162.7	0.75	6.71	0.13	0.3776	0.0044	0.299	0.1288	0.0025	2072	16	2064	21	2078	33	99.61	99.33
CM15_01	CM1501-167.d	18.1	10.7	1.97	15.3	1.4	0.399	0.028	0.87289	0.27	0.011	2767	81	2130	130	3276	64	76.98	65.02
CM15_01	CM1501-276.d	151.3	154.8	0.95	8.4	0.15	0.4023	0.0052	0.54704	0.1512	0.0026	2273	17	2182	23	2354	29	96.00	92.69
CM15_01	CM1501-334.d	157.1	146.1	1.09	9.25	0.16	0.4219	0.0056	0.44525	0.1593	0.0028	2361	16	2268	26	2442	30	96.06	92.87
CM15_01	CM1501-147.d	122.6	126.2	0.96	9.34	0.21	0.4365	0.0076	0.73142	0.1558	0.0027	2370	21	2332	34	2404	29	98.40	97.00
CM15_01	CM1501-212.d	286.8	52.8	5.38	9.95	0.18	0.4386	0.0063	0.6578	0.164	0.0024	2428	16	2343	28	2494	25	96.50	93.95
CM15_01	CM1501-244.d	469.7	84.7	5.38	10.62	0.17	0.457	0.0058	0.74128	0.1677	0.0023	2490.4	14	2425	26	2534	24	97.37	95.70
CM15_01	CM1501-273.d	232.9	117.1	1.95	10.95	0.2	0.4583	0.0055	0.71747	0.1728	0.0025	2516	17	2431	24	2581	25	96.62	94.19
CM15_01	CM1501-251.d	252.8	66.3	4.88	14.05	0.23	0.5158	0.0058	0.72472	0.1964	0.0027	2752	16	2680	25	2794	23	97.38	95.92
CM15_01	CM1501-409.d	152.8	138.8	1.14	14.54	0.25	0.539	0.0051	0.54318	0.1952	0.0029	2784	16	2778	21	2782	25	99.78	99.86
CM15_01	CM1501-385.d	631	182.9	3.57	19.77	0.36	0.5648	0.0091	0.86459	0.2535	0.0034	3077	18	2883	38	3206	20	93.70	89.93
CM15_01	CM1501-256.d	48.06	56.5	0.84	21.26	0.45	0.6226	0.0089	0.55655	0.2467	0.0046	3151	19	3117	35	3160	31	98.92	98.64

Supplementary Table 1 (continued). Main isotopes and ratios measured using the Multicollector (Hf analyses).

Sample Name	Analysis Spot #	Age Used for Hf	Type of age	$^{176}Hf/^{177}Hf$	2σ	$^{176}Lu/^{177}Hf$	$^{176}Yb/^{177}Hf$	$(^{176}Hf/^{177}Hf)_i$	$\varepsilon Hf_{(t)}$	2s	$^{Hf}T_{DM}$ (Ga)	$^{Hf}T_{NC}$ (Ga)
RDT16_006	006 - 1	1183	$^{206}Pb/^{238}U$ zircon age	0.281759	0.000049	0.001299	0.0448	0.281730	-10.83	1.715	2.63	2.46
RDT16_006	006 - 11	378.7	$^{206}Pb/^{238}U$ zircon age	0.282551	0.00005	0.000982	0.03263	0.282544	-0.10	1.75	1.35	1.16
RDT16_006	006 - 12	737	$^{206}Pb/^{238}U$ zircon age	0.282064	0.000047	0.000856	0.03043	0.282052	-9.49	1.645	2.21	2.03
RDT16_006	006 - 13	568	$^{206}Pb/^{238}U$ zircon age	0.282477	0.000076	0.000826	0.0272	0.282468	1.45	2.66	1.40	1.21
RDT16_006	006 - 15	528.9	$^{206}Pb/^{238}U$ zircon age	0.282216	0.000061	0.000982	0.02879	0.282206	-8.70	2.135	2.00	1.81
RDT16_006	006 - 18	1339	$^{206}Pb/^{238}U$ zircon age	0.281549	0.00006	0.00112	0.0407	0.281521	-14.71	2.1	2.98	2.82
RDT16_006	006 - 19	504	$^{206}Pb/^{238}U$ zircon age	0.28212	0.000051	0.00075	0.0258	0.282113	-12.56	1.785	2.22	2.03
RDT16_006	006 - 2	616.9	$^{206}Pb/^{238}U$ zircon age	0.282407	0.000058	0.00075	0.0267	0.282398	0.08	2.03	1.53	1.34
RDT16_006	006 - 21	940	$^{206}Pb/^{238}U$ zircon age	0.281778	0.00005	0.0027	0.097	0.281730	-16.32	1.75	2.78	2.60
RDT16_006	006 - 23	683.2	$^{206}Pb/^{238}U$ zircon age	0.28236	0.000043	0.00226	0.0723	0.282331	-0.82	1.505	1.63	1.45
RDT16_006	006 - 25	652.6	$^{206}Pb/^{238}U$ zircon age	0.281928	0.000048	0.001072	0.03052	0.281915	-16.24	1.68	2.56	2.38
RDT16_006	006 - 27	392.1	$^{206}Pb/^{238}U$ zircon age	0.282552	0.000052	0.001363	0.0374	0.282542	0.13	1.82	1.35	1.15
RDT16_006	006 - 28	795	$^{206}Pb/^{238}U$ zircon age	0.282464	0.000052	0.000974	0.03187	0.282449	5.89	1.82	1.30	1.12
RDT16_006	006 - 33	579.7	$^{206}Pb/^{238}U$ zircon age	0.282417	0.000045	0.0000788	0.00346	0.282416	-0.13	1.575	1.51	1.32
RDT16_006	006 - 36	725.2	$^{206}Pb/^{238}U$ zircon age	0.282577	0.000044	0.00145	0.0518	0.282557	8.14	1.54	1.10	0.92
RDT16_006	006 - 39	690	$^{206}Pb/^{238}U$ zircon age	0.282212	0.000038	0.002524	0.1179	0.282179	-6.04	1.33	1.96	1.78
RDT16_006	006 - 41	804	$^{206}Pb/^{238}U$ zircon age	0.281778	0.000051	0.001254	0.0528	0.281759	-18.36	1.785	2.80	2.62
RDT16_006	006 - 42	487.3	$^{206}Pb/^{238}U$ zircon age	0.281699	0.000077	0.000082	0.00504	0.281698	-27.61	2.695	3.13	2.95
RDT16_006	006 - 43	1200	$^{206}Pb/^{238}U$ zircon age	0.281999	0.000062	0.001681	0.0751	0.281961	-2.26	2.17	2.12	1.95
RDT16_006	006 - 44	405.2	$^{206}Pb/^{238}U$ zircon age	0.282693	0.000048	0.000688	0.0278	0.282688	5.58	1.68	1.01	0.82

Supplementary Table 1 (continued). Main isotopes and ratios measured using the Multicollector.

Sample Name	Analysis Spot #	Age Used	Type of age	$^{176}Hf/^{177}Hf$	2σ	$^{176}Lu/^{177}Hf$	$^{176}Yb/^{177}Hf$	$(^{176}Hf/^{177}Hf)_i$	$\varepsilon Hf_{(t)}$	2s	$^{Hf}T_{DM}$ (Ga)	$^{Hf}T_{NC}$ (Ga)
RDT16_006	006 - 45	255	$^{206}Pb/^{238}U$ zircon age	0.282593	0.00004	0.001704	0.0842	0.282585	-1.41	1.4	1.34	1.14
RDT16_006	006 - 51	566	$^{206}Pb/^{238}U$ zircon age	0.281706	0.000048	0.000291	0.0115	0.281703	-25.69	1.68	3.07	2.89
RDT16_019	RDT16019-104.d	843	$^{206}Pb/^{238}U$ zircon age	0.282085	0.000034	0.000977	0.03197	0.282070	-6.49	1.19	2.11	1.93
RDT16_019	RDT16019-124.d	1190	$^{206}Pb/^{238}U$ zircon age	0.281207	0.000028	0.0004566	0.01492	0.281197	-29.58	0.98	3.76	3.59
RDT16_019	RDT16019-127.d	1307	$^{206}Pb/^{238}U$ zircon age	0.281924	0.000034	0.0017	0.0676	0.281882	-2.62	1.19	2.22	2.06
RDT16_019	RDT16019-163.d	1191	$^{206}Pb/^{238}U$ zircon age	0.281936	0.000033	0.00097	0.0413	0.281914	-4.12	1.155	2.23	2.06
RDT16_019	RDT16019-424.d	1019	$^{206}Pb/^{238}U$ zircon age	0.282053	0.000028	0.001177	0.02568	0.282030	-3.90	0.98	2.08	1.91
RDT16_019	RDT16019-425.d	887	$^{206}Pb/^{238}U$ zircon age	0.282179	0.000034	0.00482	0.1084	0.282099	-4.46	1.19	2.01	1.84
RDT16_019	RDT16019-426.d	1047	$^{206}Pb/^{238}U$ zircon age	0.282121	0.000036	0.001733	0.03279	0.282087	-1.26	1.26	1.94	1.77
RDT16_019	RDT16019-432.d	742	$^{206}Pb/^{238}U$ zircon age	0.282556	0.000034	0.00434	0.0933	0.282496	6.33	1.19	1.23	1.05
RDT16_019	RDT16019-434.d	1006	$^{206}Pb/^{238}U$ zircon age	0.282134	0.000035	0.00744	0.204	0.281993	-5.51	1.225	2.17	1.99
RDT16_019	RDT16019-436.d	738	$^{206}Pb/^{238}U$ zircon age	0.282267	0.000031	0.000951	0.02249	0.282254	-2.32	1.085	1.77	1.58
RDT16_019	RDT16019-450.d	621	$^{206}Pb/^{238}U$ zircon age	0.282419	0.000028	0.00128	0.037	0.282404	0.37	0.98	1.51	1.32
RDT16_019	RDT16019-452.d	899	$^{206}Pb/^{238}U$ zircon age	0.282087	0.000031	0.00285	0.087	0.282039	-6.31	1.085	2.14	1.96
RDT16_019	RDT16019-453.d	721	$^{206}Pb/^{238}U$ zircon age	0.282567	0.000028	0.001981	0.06848	0.282540	7.44	0.98	1.15	0.96
RDT16_019	RDT16019-457.d	938	$^{206}Pb/^{238}U$ zircon age	0.281998	0.000037	0.00163	0.0584	0.281969	-7.90	1.295	2.26	2.09
RDT16_019	RDT16019-467.d	979	$^{206}Pb/^{238}U$ zircon age	0.282125	0.000045	0.001646	0.06086	0.282095	-2.52	1.575	1.97	1.79
RDT16_019	RDT16019-475.d	848	$^{206}Pb/^{238}U$ zircon age	0.282075	0.000031	0.001248	0.0413	0.282055	-6.88	1.085	2.13	1.95
RDT16_019	RDT16019-478.d	1056	$^{206}Pb/^{238}U$ zircon age	0.282219	0.000032	0.000948	0.03568	0.282200	2.96	1.12	1.69	1.51
RDT16_019	RDT16019-491.d	737	$^{206}Pb/^{238}U$ zircon age	0.282418	0.000034	0.000681	0.0244	0.282409	3.14	1.19	1.43	1.24
RDT16_019	RDT16019-537.d	756	$^{206}Pb/^{238}U$ zircon age	0.282586	0.000036	0.000817	0.0325	0.282574	9.44	1.26	1.05	0.86
RDT16_019	RDT16019-544.d	1220	$^{206}Pb/^{238}U$ zircon age	0.281959	0.000034	0.001148	0.0325	0.281933	-2.81	1.19	2.17	2.00
RDT16_019	RDT16019-547.d	904	$^{206}Pb/^{238}U$ zircon age	0.281954	0.000028	0.000258	0.00818	0.281950	-9.36	0.98	2.33	2.15
RDT16_019	RDT16019-560.d	972	$^{206}Pb/^{238}U$ zircon age	0.282073	0.00003	0.00321	0.068	0.282014	-5.53	1.05	2.15	1.97
RDT16_019	RDT16019-62.d	754.7	$^{206}Pb/^{238}U$ zircon age	0.282279	0.000031	0.001019	0.0318	0.282265	-1.56	1.085	1.73	1.55
RDT16_019	RDT16019-66.d	1026	$^{206}Pb/^{238}U$ zircon age	0.281422	0.00003	0.001426	0.0458	0.281394	-26.28	1.05	3.44	3.27
RDT16_019	RDT16019-82.d	914	$^{206}Pb/^{238}U$ zircon age	0.281922	0.000028	0.00014	0.00442	0.281920	-10.20	0.98	2.39	2.21
RDT16_019	RDT16019-84.d	934.3	$^{206}Pb/^{238}U$ zircon age	0.282065	0.000026	0.001212	0.0371	0.282044	-5.34	0.91	2.10	1.93
RDT16_019	RDT16019-98.d	1052	$^{206}Pb/^{238}U$ zircon age	0.282061	0.000032	0.001449	0.04345	0.282032	-3.08	1.12	2.06	1.88
RDT16_033	033 - 1	821.9	$^{206}Pb/^{238}U$ zircon age	0.281946	0.000054	0.000045	0.001976	0.281945	-11.36	1.89	2.39	2.21
RDT16_033	033 - 10	957	$^{206}Pb/^{238}U$ zircon age	0.281984	0.00005	0.001457	0.04135	0.282916	10.73	1.75	0.58	0.38
RDT16_033	033 - 100	442.1	$^{206}Pb/^{238}U$ zircon age	0.282358	0.000046	0.001877	0.0919	0.282342	-5.82	1.61	1.76	1.57
RDT16_033	033 - 101	959	$^{206}Pb/^{238}U$ zircon age	0.282151	0.000046	0.001006	0.0531	0.282133	-1.62	1.61	1.89	1.72
RDT16_033	033 - 102	456.4	$^{206}Pb/^{238}U$ zircon age	0.282126	0.000041	0.0006068	0.03091	0.282121	-13.34	1.435	2.24	2.05
RDT16_033	033 - 103	327.3	$^{206}Pb/^{238}U$ zircon age	0.282839	0.000044	0.001847	0.0823	0.282828	8.79	1.54	0.75	0.55
RDT16_033	033 - 104	250.1	$^{206}Pb/^{238}U$ zircon age	0.282852	0.000039	0.0004771	0.0207	0.282850	7.85	1.365	0.75	0.55
RDT16_033	033 - 105	255.1	$^{206}Pb/^{238}U$ zircon age	0.282424	0.000045	0.002377	0.11297	0.282413	-7.50	1.575	1.72	1.52
RDT16_033	033 - 106	461	$^{206}Pb/^{238}U$ zircon age	0.28241	0.000062	0.000856	0.04278	0.282403	-3.27	2.17	1.61	1.42
RDT16_033	033 - 107	340.2	$^{206}Pb/^{238}U$ zircon age	0.282807	0.000043	0.000747	0.03	0.282802	8.18	1.505	0.80	0.60
RDT16_033	033 - 108	421.5	$^{206}Pb/^{238}U$ zircon age	0.282431	0.000048	0.001404	0.06202	0.282420	-3.54	1.68	1.60	1.41
RDT16_033	033 - 109	1053	$^{206}Pb/^{238}U$ zircon age	0.281913	0.000045	0.000534	0.026	0.281902	-7.66	1.575	2.34	2.16
RDT16_033	033 - 110	2493	$^{207}Pb/^{206}Pb$ zircon age	0.281092	0.000045	0.000515	0.02555	0.281067	-4.21	1.575	3.24	3.11
RDT16_033	033 - 111	916.3	$^{206}Pb/^{238}U$ zircon age	0.281881	0.000053	0.000195	0.00902	0.281878	-11.63	1.855	2.48	2.30
RDT16_033	033 - 112	2285	$^{207}Pb/^{206}Pb$ zircon age	0.281235	0.000042	0.001013	0.047	0.281191	-4.67	1.47	3.11	2.97
RDT16_033	033 - 113	240.8	$^{206}Pb/^{238}U$ zircon age	0.282697	0.000045	0.00106	0.04891	0.282692	2.07	1.575	1.11	0.91
RDT16_033	033 - 114	886	$^{206}Pb/^{238}U$ zircon age	0.281984	0.00004	0.000683	0.0316	0.281973	-8.95	1.4	2.29	2.11
RDT16_033	033 - 115	391.7	$^{206}Pb/^{238}U$ zircon age	0.282365	0.00005	0.00177	0.0777	0.282352	-6.61	1.75	1.77	1.58
RDT16_033	033 - 116	845	$^{206}Pb/^{238}U$ zircon age	0.28179	0.000053	0.0004556	0.01852	0.281783	-16.60	1.855	2.73	2.55
RDT16_033	033 - 117	412.5	$^{206}Pb/^{238}U$ zircon age	0.282366	0.000046	0.001642	0.0717	0.282353	-6.09	1.61	1.75	1.56
RDT16_033	033 - 118	492.6	$^{206}Pb/^{238}U$ zircon age	0.282282	0.000046	0.0014059	0.05667	0.282269	-7.29	1.61	1.89	1.70
RDT16_033	033 - 119	1231	$^{206}Pb/^{238}U$ zircon age	0.28172	0.000053	0.000542	0.0225	0.281707	-10.54	1.855	2.65	2.48
RDT16_033	033 - 12	516.4	$^{206}Pb/^{238}U$ zircon age	0.282253	0.000045	0.001567	0.0431	0.282238	-7.86	1.575	1.94	1.75
RDT16_033	033 - 120	269.7	$^{206}Pb/^{238}U$ zircon age	0.282779	0.000069	0.0005115	0.01765	0.282776	5.69	2.415	0.90	0.70
RDT16_033	033 - 13	1557	$^{207}Pb/^{206}Pb$ zircon age	0.281697	0.000053	0.00255	0.075	0.281631	-10.11	1.855	2.73	2.56
RDT16_033	033 - 14	1725	$^{207}Pb/^{206}Pb$ zircon age	0.281898	0.000047	0.0013	0.0374	0.281855	6.00	1.645	2.03	1.87
RDT16_033	033 - 15	556	$^{206}Pb/^{238}U$ zircon age	0.282688	0.000052	0.001754	0.04618	0.282670	8.32	1.82	0.96	0.77
RDT16_033	033 - 16	857	$^{206}Pb/^{238}U$ zircon age	0.282081	0.000048	0.000108	0.00347	0.282079	-5.82	1.68	2.08	1.90
RDT16_033	033 - 17	811	$^{206}Pb/^{238}U$ zircon age	0.282341	0.000059	0.00291	0.078	0.282297	0.84	2.065	1.63	1.44
RDT16_033	033 - 18	2454.2	$^{207}Pb/^{206}Pb$ zircon age	0.281282	0.000046	0.001282	0.03234	0.281222	0.38	1.61	2.94	2.81
RDT16_033	033 - 19	~~4648~~		~~0.283~~	~~0.011~~	~~0.00539~~	~~0.1729~~	~~0.282512~~	~~99.00~~	~~385~~	~~1.12~~	~~1.20~~
RDT16_033	033 - 2	832	$^{206}Pb/^{238}U$ zircon age	0.282116	0.00009	0.000827	0.0317	0.282103	-5.54	3.15	2.04	1.86
RDT16_033	033 - 20	388.1	$^{206}Pb/^{238}U$ zircon age	0.282616	0.000042	0.00187	0.0444	0.282602	2.18	1.47	1.22	1.02
RDT16_033	033 - 21	431.5	$^{206}Pb/^{238}U$ zircon age	0.282321	0.000046	0.0029	0.07	0.282298	-7.64	1.61	1.86	1.67
RDT16_033	033 - 22	309.7	$^{206}Pb/^{238}U$ zircon age	0.282608	0.000042	0.006064	0.13593	0.282573	-0.62	1.47	1.33	1.13
RDT16_033	033 - 23	460.3	$^{206}Pb/^{238}U$ zircon age	0.282122	0.000058	0.00431	0.102	0.282085	-14.53	2.03	2.31	2.12
RDT16_033	033 - 24	317.5	$^{206}Pb/^{238}U$ zircon age	0.282325	0.000054	0.000988	0.01878	0.282319	-9.42	1.89	1.89	1.69
RDT16_033	033 - 25	372.2	$^{206}Pb/^{238}U$ zircon age	0.282452	0.000043	0.00171	0.0391	0.282440	-3.92	1.505	1.59	1.39
RDT16_033	033 - 26	253	$^{206}Pb/^{238}U$ zircon age	0.28296	0.00005	0.002315	0.0442	0.282949	11.43	1.75	0.52	0.32
RDT16_033	033 - 27	255.7	$^{206}Pb/^{238}U$ zircon age	0.282333	0.000048	0.0037	0.07428	0.282315	-10.94	1.68	1.94	1.74
RDT16_033	033 - 28	417	$^{206}Pb/^{238}U$ zircon age	0.282424	0.000045	0.00551	0.1069	0.282381	-5.02	1.575	1.69	1.50
RDT16_033	033 - 29	258.6	$^{206}Pb/^{238}U$ zircon age	0.282641	0.00004	0.001226	0.02044	0.282635	0.44	1.4	1.23	1.03
RDT16_033	033 - 3	428.9	$^{206}Pb/^{238}U$ zircon age	0.282315	0.000044	0.001168	0.0436	0.282306	-7.42	1.54	1.85	1.66
RDT16_033	033 - 30	1092	$^{206}Pb/^{238}U$ zircon age	0.282083	0.000042	0.001672	0.0325	0.282049	-1.60	1.47	2.00	1.82
RDT16_033	033 - 31	433.8	$^{206}Pb/^{238}U$ zircon age	0.282327	0.000042	0.002243	0.0452	0.282309	-7.20	1.47	1.84	1.65
RDT16_033	033 - 32	267.9	$^{206}Pb/^{238}U$ zircon age	0.282931	0.000055	0.001509	0.02719	0.282923	10.85	1.925	0.57	0.37
RDT16_033	033 - 33	449.2	$^{206}Pb/^{238}U$ zircon age	0.282706	0.000041	0.002717	0.04541	0.282683	6.40	1.435	1.00	0.80
RDT16_033	033 - 34	885	$^{206}Pb/^{238}U$ zircon age	0.282246	0.000047	0.00268	0.0523	0.282201	-0.87	1.645	1.79	1.61
RDT16_033	033 - 35	302.6	$^{206}Pb/^{238}U$ zircon age	0.282535	0.000044	0.004682	0.0902	0.282509	-3.06	1.54	1.48	1.28
RDT16_033	033 - 36	257	$^{206}Pb/^{238}U$ zircon age	0.282604	0.000054	0.0027	0.05486	0.282591	-1.15	1.89	1.33	1.13
RDT16_033	033 - 37	1367	$^{207}Pb/^{206}Pb$ zircon age	0.281998	0.00004	0.002726	0.055	0.281928	0.36	1.4	2.09	1.92

Supplementary Table 1 (continued). Main isotopes and ratios measured using the Multicollector.

RDT16_033	033 - 38	250.8	$^{206}Pb/^{238}U$ zircon age	0.282731	0.000048	0.000992	0.01868	0.282726	3.50	1.68	1.03	0.83
RDT16_033	033 - 39	265.7	$^{206}Pb/^{238}U$ zircon age	0.282673	0.000044	0.001262	0.02524	0.282667	1.72	1.54	1.15	0.95
RDT16_033	033 - 4	235.8	$^{206}Pb/^{238}U$ zircon age	0.282473	0.000045	0.001196	0.04346	0.282468	-5.99	1.575	1.61	1.41
RDT16_033	033 - 40	2516.6	$^{207}Pb/^{206}Pb$ zircon age	0.28123	0.000048	0.00303	0.0583	0.281084	-3.06	1.68	3.19	3.06
RDT16_033	033 - 43	1071	$^{206}Pb/^{238}U$ zircon age	0.28205	0.000046	0.001542	0.0336	0.282019	-3.13	1.61	2.07	1.90
RDT16_033	033 - 44	295.7	$^{206}Pb/^{238}U$ zircon age	0.282489	0.000045	0.002548	0.0496	0.282475	-4.40	1.575	1.56	1.36
RDT16_033	033 - 45	1070	$^{206}Pb/^{238}U$ zircon age	0.282012	0.00004	0.00219	0.0508	0.281968	-4.96	1.4	2.19	2.01
RDT16_033	033 - 46	1901	$^{207}Pb/^{206}Pb$ zircon age	0.28163	0.000052	0.001335	0.0316	0.281582	0.33	1.82	2.51	2.36
RDT16_033	033 - 47	863.5	$^{206}Pb/^{238}U$ zircon age	0.28184	0.00004	0.002055	0.05313	0.281807	-15.34	1.4	2.66	2.49
RDT16_033	033 - 48	407.9	$^{206}Pb/^{238}U$ zircon age	0.28237	0.000042	0.00319	0.0795	0.282346	-6.47	1.47	1.77	1.58
RDT16_033	033 - 49	243.5	$^{206}Pb/^{238}U$ zircon age	0.282873	0.000047	0.0006632	0.01556	0.282870	8.42	1.645	0.71	0.51
RDT16_033	033 - 5	324.3	$^{206}Pb/^{238}U$ zircon age	0.282832	0.000049	0.000662	0.01912	0.282828	8.73	1.715	0.75	0.55
RDT16_033	033 - 50	279.1	$^{206}Pb/^{238}U$ zircon age	0.282514	0.00005	0.001835	0.04442	0.282504	-3.72	1.75	1.50	1.31
RDT16_033	033 - 51	269	$^{206}Pb/^{238}U$ zircon age	0.282316	0.000042	0.00272	0.0685	0.282302	-11.10	1.47	1.96	1.76
RDT16_033	033 - 52	450.6	$^{206}Pb/^{238}U$ zircon age	0.282295	0.00004	0.002407	0.0603	0.282275	-8.03	1.4	1.90	1.71
RDT16_033	033 - 53	344.7	$^{206}Pb/^{238}U$ zircon age	0.282746	0.000044	0.00257	0.0723	0.282729	5.70	1.54	0.96	0.76
RDT16_033	033 - 54	785.7	$^{206}Pb/^{238}U$ zircon age	0.28255	0.000045	0.002844	0.0754	0.282508	7.76	1.575	1.18	0.99
RDT16_033	033 - 55	378.3	$^{206}Pb/^{238}U$ zircon age	0.282663	0.000051	0.003416	0.0958	0.282639	3.25	1.785	1.14	0.95
RDT16_033	033 - 56	1448	$^{207}Pb/^{206}Pb$ zircon age	0.282072	0.000045	0.001314	0.03877	0.282036	6.06	1.575	1.80	1.64
RDT16_033	033 - 57	425	$^{206}Pb/^{238}U$ zircon age	0.282337	0.000042	0.001059	0.02774	0.282329	-6.69	1.47	1.80	1.61
RDT16_033	033 - 58	975	$^{206}Pb/^{238}U$ zircon age	0.282047	0.000053	0.000843	0.0265	0.282032	-4.85	1.855	2.11	1.93
RDT16_033	033 - 59	210.8	$^{206}Pb/^{238}U$ zircon age	0.282413	0.000047	0.00238	0.0728	0.282404	-8.81	1.645	1.77	1.57
RDT16_033	033 - 6	264.3	$^{206}Pb/^{238}U$ zircon age	0.282481	0.000048	0.002305	0.0796	0.282470	-5.28	1.68	1.59	1.39
RDT16_033	033 - 60	264.8	$^{206}Pb/^{238}U$ zircon age	0.282844	0.000045	0.001064	0.0315	0.282839	7.79	1.575	0.77	0.56
RDT16_033	033 - 61	251.3	$^{206}Pb/^{238}U$ zircon age	0.282361	0.000048	0.0013	0.0396	0.282355	-9.63	1.68	1.85	1.66
RDT16_033	033 - 62	1470	$^{207}Pb/^{206}Pb$ zircon age	0.281702	0.00004	0.000929	0.02888	0.281676	-6.21	1.4	2.57	2.41
RDT16_033	033 - 63	300.6	$^{206}Pb/^{238}U$ zircon age	0.282429	0.000046	0.001206	0.0384	0.282422	-6.15	1.61	1.67	1.48
RDT16_033	033 - 64	248.5	$^{206}Pb/^{238}U$ zircon age	0.282777	0.000047	0.001164	0.03392	0.282772	5.05	1.645	0.93	0.73
RDT16_033	033 - 65	292.9	$^{206}Pb/^{238}U$ zircon age	0.282695	0.00005	0.001904	0.0578	0.282685	2.96	1.75	1.09	0.89
RDT16_033	033 - 66	1926.3	$^{207}Pb/^{206}Pb$ zircon age	0.281561	0.000054	0.00099	0.0326	0.281525	-1.11	1.89	2.61	2.47
RDT16_033	033 - 67	361.8	$^{206}Pb/^{238}U$ zircon age	0.282516	0.000042	0.00139	0.0404	0.282507	-1.80	1.47	1.45	1.25
RDT16_033	033 - 68	279.4	$^{206}Pb/^{238}U$ zircon age	0.28247	0.00004	0.001183	0.03784	0.282464	-5.15	1.4	1.59	1.40
RDT16_033	033 - 69	289	$^{206}Pb/^{238}U$ zircon age	0.282913	0.000045	0.0011798	0.03829	0.282907	10.73	1.575	0.60	0.40
RDT16_033	033 - 7	1303	$^{206}Pb/^{238}U$ zircon age	0.282024	0.000044	0.00151	0.0521	0.281987	1.01	1.54	2.00	1.83
RDT16_033	033 - 70	522.2	$^{206}Pb/^{238}U$ zircon age	0.28252	0.000043	0.001643	0.0551	0.282504	1.69	1.505	1.35	1.16
RDT16_033	033 - 71	1909	$^{207}Pb/^{206}Pb$ zircon age	0.281549	0.000048	0.0006847	0.02621	0.281524	-1.53	1.68	2.63	2.48
RDT16_033	033 - 72	242.7	$^{206}Pb/^{238}U$ zircon age	0.282673	0.000043	0.001115	0.0419	0.282668	1.25	1.505	1.16	0.96
RDT16_033	033 - 73	340.4	$^{206}Pb/^{238}U$ zircon age	0.282784	0.000054	0.000664	0.0213	0.282780	7.39	1.89	0.85	0.65
RDT16_033	033 - 74	444.4	$^{206}Pb/^{238}U$ zircon age	0.282386	0.00004	0.001216	0.0501	0.282376	-4.58	1.4	1.68	1.49
RDT16_033	033 - 75	1203	$^{206}Pb/^{238}U$ zircon age	0.282057	0.000044	0.001061	0.051	0.282033	0.37	1.54	1.96	1.79
RDT16_033	033 - 76	248.9	$^{206}Pb/^{238}U$ zircon age	0.282348	0.000048	0.00104	0.0388	0.282343	-10.10	1.68	1.88	1.68
RDT16_033	033 - 78	1044.7	$^{206}Pb/^{238}U$ zircon age	0.282192	0.000049	0.0007229	0.02903	0.282178	1.91	1.715	1.74	1.57
RDT16_033	033 - 79	336.7	$^{206}Pb/^{238}U$ zircon age	0.282782	0.000051	0.00082	0.0296	0.282777	7.20	1.785	0.86	0.66
RDT16_033	033 - 8	261.6	$^{206}Pb/^{238}U$ zircon age	0.282792	0.000054	0.000981	0.03069	0.282787	5.89	1.89	0.88	0.68
RDT16_033	033 - 80	377	$^{206}Pb/^{238}U$ zircon age	0.281916	0.000047	0.001495	0.04852	0.281905	-22.74	1.645	2.76	2.56
RDT16_033	033 - 81	253.3	$^{206}Pb/^{238}U$ zircon age	0.28282	0.000051	0.00217	0.0946	0.282810	6.50	1.785	0.84	0.64
RDT16_033	033 - 82	1340	$^{206}Pb/^{238}U$ zircon age	0.281749	0.000051	0.00097	0.0431	0.281724	-7.46	1.785	2.54	2.38
RDT16_033	033 - 83	919.1	$^{206}Pb/^{238}U$ zircon age	0.28237	0.00004	0.001221	0.0594	0.282349	5.13	1.4	1.45	1.26
RDT16_033	033 - 84	422.7	$^{206}Pb/^{238}U$ zircon age	0.282246	0.00005	0.00092	0.0428	0.282239	-9.92	1.75	2.00	1.81
RDT16_033	033 - 85	276	$^{206}Pb/^{238}U$ zircon age	0.282838	0.000044	0.00086	0.038	0.282834	7.85	1.54	0.77	0.57
RDT16_033	033 - 86	401.3	$^{206}Pb/^{238}U$ zircon age	0.282367	0.000042	0.00002658	0.001723	0.282367	-5.87	1.47	1.73	1.54
RDT16_033	033 - 87	257.8	$^{206}Pb/^{238}U$ zircon age	0.282807	0.000046	0.000745	0.0339	0.282803	6.38	1.61	0.85	0.65
RDT16_033	033 - 88	1166	$^{206}Pb/^{238}U$ zircon age	0.281756	0.00004	0.001112	0.0522	0.281732	-11.16	1.4	2.64	2.47
RDT16_033	033 - 89	1907	$^{207}Pb/^{206}Pb$ zircon age	0.281608	0.000042	0.000767	0.03673	0.281580	0.42	1.47	2.51	2.36
RDT16_033	033 - 9	229	$^{206}Pb/^{238}U$ zircon age	0.282955	0.000074	0.001412	0.0408	0.282949	10.89	2.59	0.54	0.34
RDT16_033	033 - 90	421.8	$^{206}Pb/^{238}U$ zircon age	0.282682	0.000044	0.000771	0.03353	0.282676	5.53	1.54	1.03	0.84
RDT16_033	033 - 91	1738	$^{207}Pb/^{206}Pb$ zircon age	0.281617	0.000038	0.0009576	0.0453	0.281585	-3.29	1.33	2.60	2.44
RDT16_033	033 - 92	~~4800~~		~~0.224~~	~~0.057~~	~~0.0018~~	~~0.14~~	~~0.223831~~	~~-1995.68~~	~~1995~~	~~64.91~~	~~64.88~~
RDT16_033	033 - 93	1026	$^{206}Pb/^{238}U$ zircon age	0.282012	0.000047	0.000525	0.02549	0.282002	-4.75	1.645	2.14	1.96
RDT16_033	033 - 94	1084	$^{206}Pb/^{238}U$ zircon age	0.281907	0.000036	0.001559	0.0737	0.281875	-7.93	1.26	2.38	2.20
RDT16_033	033 - 95	459.1	$^{206}Pb/^{238}U$ zircon age	0.282421	0.000052	0.000758	0.0368	0.282414	-2.89	1.82	1.59	1.40
RDT16_033	033 - 96	342.6	$^{206}Pb/^{238}U$ zircon age	0.28269	0.000045	0.001081	0.0429	0.282683	4.01	1.575	1.07	0.87
RDT16_033	033 - 97	1858	$^{207}Pb/^{206}Pb$ zircon age	0.281572	0.000045	0.001118	0.05401	0.281533	-2.40	1.575	2.64	2.49
RDT16_033	033 - 98	296.2	$^{206}Pb/^{238}U$ zircon age	0.28278	0.000046	0.000832	0.0397	0.282775	6.25	1.61	0.89	0.69
RDT16_033	033 - 99	373.8	$^{206}Pb/^{238}U$ zircon age	0.282653	0.000044	0.001419	0.0641	0.282643	3.30	1.54	1.13	0.94
RDT16_035	035 - 1	275.49	$^{206}Pb/^{238}U$ zircon age	0.28287	0.000044	0.00182	0.06434	0.282861	8.80	1.54	0.71	0.51
RDT16_035	035 - 10	274.3	$^{206}Pb/^{238}U$ zircon age	0.282918	0.00005	0.000395	0.01147	0.282916	10.73	1.75	0.58	0.38
RDT16_035	035 - 100	246.3	$^{206}Pb/^{238}U$ zircon age	0.282859	0.000043	0.000321	0.01251	0.282858	8.04	1.505	0.73	0.53
RDT16_035	035 - 101	444.1	$^{206}Pb/^{238}U$ zircon age	0.282674	0.000043	0.001337	0.0636	0.282663	5.57	1.505	1.05	0.85
RDT16_035	035 - 102	248.5	$^{206}Pb/^{238}U$ zircon age	0.282811	0.000045	0.00122	0.0512	0.282805	6.24	1.575	0.85	0.65
RDT16_035	035 - 103	434.7	$^{206}Pb/^{238}U$ zircon age	0.282617	0.000037	0.0008745	0.04094	0.282610	3.48	1.295	1.17	0.98
RDT16_035	035 - 104	260.4	$^{206}Pb/^{238}U$ zircon age	0.28284	0.000043	0.0005156	0.02147	0.282837	7.64	1.505	0.77	0.57
RDT16_035	035 - 105	244.2	$^{206}Pb/^{238}U$ zircon age	0.282858	0.00004	0.000587	0.0263	0.282855	7.91	1.4	0.74	0.54
RDT16_035	035 - 106	547	$^{206}Pb/^{238}U$ zircon age	~~0.2~~	~~2.1~~	~~0.142~~	~~7.7~~	~~0.201456~~	~~-17132.69~~	~~73500~~	~~164.69~~	~~164.68~~
RDT16_035	035 - 107	251.9	$^{206}Pb/^{238}U$ zircon age	0.282902	0.000044	0.000469	0.01844	0.282900	9.66	1.54	0.64	0.43
RDT16_035	035 - 108	265.5	$^{206}Pb/^{238}U$ zircon age	0.28283	0.000045	0.001116	0.0428	0.282824	7.30	1.575	0.80	0.60
RDT16_035	035 - 109	252.6	$^{206}Pb/^{238}U$ zircon age	0.282907	0.000045	0.000839	0.0367	0.282903	9.79	1.575	0.63	0.43
RDT16_035	035 - 11	250.6	$^{206}Pb/^{238}U$ zircon age	0.282865	0.000047	0.000922	0.02909	0.282861	8.25	1.645	0.72	0.52
RDT16_035	035 - 110	263.1	$^{206}Pb/^{238}U$ zircon age	0.282906	0.000048	0.000796	0.02626	0.282902	9.99	1.68	0.62	0.42
RDT16_035	035 - 111	254.4	$^{206}Pb/^{238}U$ zircon age	0.282845	0.000047	0.0003317	0.01336	0.282843	7.72	1.645	0.76	0.56
RDT16_035	035 - 112	249.3	$^{206}Pb/^{238}U$ zircon age	0.282864	0.000045	0.000296	0.01049	0.282863	8.29	1.575	0.72	0.52
RDT16_035	035 - 12	410	$^{206}Pb/^{238}U$ zircon age	0.282652	0.000042	0.001541	0.0501	0.282640	4.00	1.47	1.12	0.92

Supplementary Table 1 (continued). Main isotopes and ratios measured using the Multicollector.

RDT16_035	035 - 13	418.4	$^{206}Pb/^{238}U$ zircon age	0.282451	0.000042	0.00192	0.0666	0.282436	-3.04	1.47	1.57	1.37
RDT16_035	035 - 14	248.6	$^{206}Pb/^{238}U$ zircon age	0.282881	0.000047	0.000559	0.01593	0.282878	8.83	1.645	0.69	0.48
RDT16_035	035 - 15	259.9	$^{206}Pb/^{238}U$ zircon age	0.282899	0.000056	0.000815	0.0264	0.282895	9.67	1.96	0.64	0.44
RDT16_035	035 - 16	250.1	$^{206}Pb/^{238}U$ zircon age	0.282894	0.000041	0.000943	0.0311	0.282890	9.26	1.435	0.66	0.46
RDT16_035	035 - 17	259.9	$^{206}Pb/^{238}U$ zircon age	0.282932	0.000049	0.000982	0.0275	0.282927	10.81	1.715	0.57	0.37
RDT16_035	035 - 18	249	$^{206}Pb/^{238}U$ zircon age	0.282886	0.000048	0.000742	0.0204	0.282883	8.99	1.68	0.68	0.47
RDT16_035	035 - 19	328.9	$^{206}Pb/^{238}U$ zircon age	~~0.3~~	~~0.17~~	~~0.101~~	~~3.1~~	~~0.299379~~	~~594.54~~	~~5950~~	~~-62.88~~	~~-63.53~~
RDT16_035	035 - 2	287.8	$^{206}Pb/^{238}U$ zircon age	0.282859	0.00004	0.000462	0.01342	0.282857	8.93	1.4	0.71	0.51
RDT16_035	035 - 20	235.5	$^{206}Pb/^{238}U$ zircon age	0.282878	0.000048	0.000825	0.0235	0.282874	8.39	1.68	0.70	0.50
RDT16_035	035 - 21	322.9	$^{206}Pb/^{238}U$ zircon age	0.282704	0.000044	0.001606	0.0473	0.282694	3.97	1.54	1.05	0.85
RDT16_035	035 - 22	258.9	$^{206}Pb/^{238}U$ zircon age	0.282856	0.000044	0.000463	0.01203	0.282854	8.19	1.54	0.74	0.53
RDT16_035	035 - 23	243.3	$^{206}Pb/^{238}U$ zircon age	0.282801	0.000053	0.00105	0.0292	0.282796	5.80	1.855	0.87	0.67
RDT16_035	035 - 24	262.7	$^{206}Pb/^{238}U$ zircon age	0.282854	0.000047	0.0011125	0.02877	0.282849	8.09	1.645	0.74	0.54
RDT16_035	035 - 25	238.6	$^{206}Pb/^{238}U$ zircon age	0.282861	0.000047	0.001084	0.03136	0.282856	7.82	1.645	0.74	0.54
RDT16_035	035 - 26	263.8	$^{206}Pb/^{238}U$ zircon age	0.282922	0.000052	0.00117	0.0357	0.282916	10.51	1.82	0.59	0.39
RDT16_035	035 - 27	250	$^{206}Pb/^{238}U$ zircon age	0.282919	0.000044	0.000677	0.0181	0.282916	10.19	1.54	0.60	0.40
RDT16_035	035 - 29	284.8	$^{206}Pb/^{238}U$ zircon age	0.282894	0.000048	0.001351	0.0342	0.282887	9.93	1.68	0.64	0.44
RDT16_035	035 - 3	264.7	$^{206}Pb/^{238}U$ zircon age	0.282861	0.000043	0.000964	0.0307	0.282856	8.40	1.505	0.73	0.52
RDT16_035	035 - 30	227.1	$^{206}Pb/^{238}U$ zircon age	0.28285	0.000044	0.001564	0.0408	0.282843	7.11	1.54	0.78	0.58
RDT16_035	035 - 31	242.8	$^{206}Pb/^{238}U$ zircon age	0.282906	0.000045	0.001354	0.0439	0.282900	9.46	1.575	0.64	0.44
RDT16_035	035 - 32	619	$^{206}Pb/^{238}U$ zircon age	0.282331	0.000045	0.001699	0.0495	0.282311	-2.96	1.575	1.72	1.53
RDT16_035	035 - 34	251.8	$^{206}Pb/^{238}U$ zircon age	0.282876	0.00004	0.001076	0.0263	0.282871	8.64	1.4	0.70	0.50
RDT16_035	035 - 35	264	$^{206}Pb/^{238}U$ zircon age	0.282998	0.000041	0.000919	0.02087	0.282993	13.24	1.435	0.42	0.21
RDT16_035	035 - 37	258.5	$^{206}Pb/^{238}U$ zircon age	0.282885	0.000044	0.000715	0.01625	0.282882	9.16	1.54	0.67	0.47
RDT16_035	035 - 38	240.2	$^{206}Pb/^{238}U$ zircon age	0.282984	0.000045	0.001286	0.02717	0.282978	12.17	1.575	0.47	0.26
RDT16_035	035 - 39	261.8	$^{206}Pb/^{238}U$ zircon age	0.282898	0.000041	0.000775	0.01994	0.282894	9.68	1.435	0.64	0.44
RDT16_035	035 - 4	269	$^{206}Pb/^{238}U$ zircon age	0.282836	0.000043	0.001059	0.0324	0.282831	7.60	1.505	0.78	0.58
RDT16_035	035 - 40	246.8	$^{206}Pb/^{238}U$ zircon age	0.282875	0.000044	0.000926	0.0212	0.282871	8.52	1.54	0.70	0.50
RDT16_035	035 - 41	371.6	$^{206}Pb/^{238}U$ zircon age	0.282876	0.000044	0.001557	0.0393	0.282865	11.11	1.54	0.64	0.44
RDT16_035	035 - 42	256	$^{206}Pb/^{238}U$ zircon age	0.282822	0.000057	0.00278	0.0627	0.282809	6.53	1.995	0.84	0.64
RDT16_035	035 - 43	251.9	$^{206}Pb/^{238}U$ zircon age	0.282854	0.000046	0.001075	0.0268	0.282849	7.86	1.61	0.75	0.55
RDT16_035	035 - 44	256.6	$^{206}Pb/^{238}U$ zircon age	0.282886	0.00005	0.000767	0.01668	0.282882	9.15	1.75	0.67	0.47
RDT16_035	035 - 45	278.5	$^{206}Pb/^{238}U$ zircon age	0.282823	0.00004	0.0004265	0.008221	0.282821	7.46	1.4	0.80	0.60
RDT16_035	035 - 46	332	$^{206}Pb/^{238}U$ zircon age	0.282969	0.000043	0.001089	0.02037	0.282962	13.66	1.505	0.44	0.24
RDT16_035	035 - 47	250.5	$^{206}Pb/^{238}U$ zircon age	0.282843	0.000042	0.00092	0.0226	0.282839	7.47	1.47	0.77	0.57
RDT16_035	035 - 48	408.7	$^{206}Pb/^{238}U$ zircon age	0.282698	0.000048	0.00268	0.0599	0.282677	5.29	1.68	1.04	0.84
RDT16_035	035 - 49	242.3	$^{206}Pb/^{238}U$ zircon age	0.282868	0.000045	0.0009257	0.02258	0.282864	8.17	1.575	0.72	0.52
RDT16_035	035 - 5	260.1	$^{206}Pb/^{238}U$ zircon age	0.282956	0.000036	0.000841	0.0249	0.282952	11.69	1.26	0.51	0.31
RDT16_035	035 - 50	263.8	$^{206}Pb/^{238}U$ zircon age	0.282966	0.000046	0.001051	0.0199	0.282961	12.08	1.61	0.49	0.29
RDT16_035	035 - 51	405.5	$^{206}Pb/^{238}U$ zircon age	0.282597	0.000042	0.002059	0.0463	0.282581	1.82	1.47	1.25	1.06
RDT16_035	035 - 52	770	$^{206}Pb/^{238}U$ zircon age	0.282681	0.000052	0.001618	0.0342	0.282658	12.70	1.82	0.85	0.67
RDT16_035	035 - 53	262.9	$^{206}Pb/^{238}U$ zircon age	0.282866	0.000048	0.001042	0.01954	0.282861	8.53	1.68	0.72	0.52
RDT16_035	035 - 55	249.5	$^{206}Pb/^{238}U$ zircon age	0.282926	0.000047	0.001764	0.03736	0.282918	10.24	1.645	0.60	0.39
RDT16_035	035 - 56	421.9	$^{206}Pb/^{238}U$ zircon age	0.282627	0.000046	0.00187	0.0432	0.282612	3.28	1.61	1.17	0.98
RDT16_035	035 - 57	286.1	$^{206}Pb/^{238}U$ zircon age	0.282827	0.000047	0.00127	0.0296	0.282820	7.61	1.645	0.79	0.59
RDT16_035	035 - 58	235.7	$^{206}Pb/^{238}U$ zircon age	0.282816	0.000049	0.001449	0.03381	0.282810	6.11	1.715	0.85	0.65
RDT16_035	035 - 59	251.6	$^{206}Pb/^{238}U$ zircon age	0.282849	0.000045	0.000925	0.0244	0.282845	7.70	1.575	0.76	0.56
RDT16_035	035 - 6	251.6	$^{206}Pb/^{238}U$ zircon age	0.282895	0.000043	0.000705	0.02561	0.282892	9.37	1.505	0.65	0.45
RDT16_035	035 - 60	239.6	$^{206}Pb/^{238}U$ zircon age	0.282869	0.000051	0.000967	0.0219	0.282865	8.14	1.785	0.72	0.52
RDT16_035	035 - 61	238.4	$^{206}Pb/^{238}U$ zircon age	0.282912	0.000049	0.000615	0.018242	0.282909	9.69	1.715	0.62	0.42
RDT16_035	035 - 62	237.2	$^{206}Pb/^{238}U$ zircon age	0.282855	0.000049	0.000843	0.02125	0.282851	7.62	1.715	0.75	0.55
RDT16_035	035 - 63	390.4	$^{206}Pb/^{238}U$ zircon age	0.282666	0.000046	0.00489	0.1397	0.282630	3.21	1.61	1.15	0.96
RDT16_035	035 - 65	247	$^{206}Pb/^{238}U$ zircon age	0.28291	0.000045	0.001471	0.0426	0.282903	9.67	1.575	0.63	0.43
RDT16_035	035 - 66	360.1	$^{206}Pb/^{238}U$ zircon age	0.28293	0.000051	0.001936	0.0572	0.282917	12.68	1.785	0.53	0.33
RDT16_035	035 - 67	246	$^{206}Pb/^{238}U$ zircon age	0.282885	0.000053	0.00083	0.0244	0.282881	8.87	1.855	0.68	0.48
RDT16_035	035 - 68	264.5	$^{206}Pb/^{238}U$ zircon age	0.282887	0.000044	0.000747	0.02181	0.282883	9.36	1.54	0.66	0.46
RDT16_035	035 - 69	253.6	$^{206}Pb/^{238}U$ zircon age	0.282867	0.000045	0.000623	0.0177	0.282864	8.43	1.575	0.72	0.51
RDT16_035	035 - 7	260.2	$^{206}Pb/^{238}U$ zircon age	0.282911	0.00005	0.000823	0.0291	0.282907	10.10	1.75	0.61	0.41
RDT16_035	035 - 70	258	$^{206}Pb/^{238}U$ zircon age	0.282979	0.000039	0.001397	0.03975	0.282972	12.36	1.365	0.47	0.27
RDT16_035	035 - 71	402.6	$^{206}Pb/^{238}U$ zircon age	0.282681	0.000044	0.001856	0.0648	0.282667	4.79	1.54	1.06	0.87
RDT16_035	035 - 72	237.3	$^{206}Pb/^{238}U$ zircon age	0.282866	0.000043	0.0006427	0.02402	0.282863	8.04	1.505	0.73	0.53
RDT16_035	035 - 73	246	$^{206}Pb/^{238}U$ zircon age	0.282944	0.000048	0.000583	0.0207	0.282941	11.00	1.68	0.55	0.34
RDT16_035	035 - 74	246.9	$^{206}Pb/^{238}U$ zircon age	0.282836	0.000046	0.000616	0.02532	0.282833	7.19	1.61	0.79	0.59
RDT16_035	035 - 75	424	$^{206}Pb/^{238}U$ zircon age	0.28269	0.000052	0.001985	0.0852	0.282674	5.52	1.82	1.03	0.84
RDT16_035	035 - 76	233.5	$^{206}Pb/^{238}U$ zircon age	0.282843	0.000037	0.000491	0.0187	0.282841	7.16	1.295	0.78	0.58
RDT16_035	035 - 77	231.7	$^{206}Pb/^{238}U$ zircon age	0.28285	0.000049	0.001249	0.0471	0.282845	7.26	1.715	0.77	0.57
RDT16_035	035 - 78	238.8	$^{206}Pb/^{238}U$ zircon age	0.282838	0.000043	0.0003506	0.01595	0.282836	7.13	1.505	0.79	0.59
RDT16_035	035 - 79	249.4	$^{206}Pb/^{238}U$ zircon age	0.28285	0.000046	0.0003947	0.01774	0.282848	7.78	1.61	0.75	0.55
RDT16_035	035 - 8	266.2	$^{206}Pb/^{238}U$ zircon age	0.28285	0.000044	0.001	0.0278	0.282845	8.04	1.54	0.75	0.55
RDT16_035	035 - 80	259.6	$^{206}Pb/^{238}U$ zircon age	0.282902	0.000048	0.000876	0.0435	0.282898	9.76	1.68	0.64	0.43
RDT16_035	035 - 81	252.1	$^{206}Pb/^{238}U$ zircon age	0.282914	0.000045	0.000609	0.0248	0.282911	10.07	1.575	0.61	0.41
RDT16_035	035 - 82	271.1	$^{206}Pb/^{238}U$ zircon age	0.282785	0.000045	0.00135	0.0553	0.282778	5.78	1.575	0.90	0.70
RDT16_035	035 - 83	241.2	$^{206}Pb/^{238}U$ zircon age	0.282891	0.00004	0.000473	0.0192	0.282889	9.03	1.4	0.67	0.47
RDT16_035	035 - 84	262.3	$^{206}Pb/^{238}U$ zircon age	0.282872	0.000051	0.000944	0.03942	0.282867	8.74	1.785	0.70	0.50
RDT16_035	035 - 85	253.7	$^{206}Pb/^{238}U$ zircon age	0.282849	0.000041	0.000993	0.0416	0.282844	7.74	1.435	0.76	0.56
RDT16_035	035 - 86	250.3	$^{206}Pb/^{238}U$ zircon age	0.282877	0.00005	0.000569	0.02558	0.282874	8.72	1.75	0.69	0.49
RDT16_035	035 - 87	254.5	$^{206}Pb/^{238}U$ zircon age	0.282895	0.000046	0.000493	0.0212	0.282893	9.47	1.61	0.65	0.45
RDT16_035	035 - 88	277.7	$^{206}Pb/^{238}U$ zircon age	0.282958	0.000041	0.000696	0.0293	0.282954	12.17	1.435	0.50	0.29
RDT16_035	035 - 89	244.2	$^{206}Pb/^{238}U$ zircon age	0.282842	0.00004	0.000314	0.0158	0.282841	7.39	1.4	0.77	0.57
RDT16_035	035 - 9	261.1	$^{206}Pb/^{238}U$ zircon age	0.282873	0.000046	0.000745	0.022	0.282869	8.79	1.61	0.70	0.50
RDT16_035	035 - 90	419.5	$^{206}Pb/^{238}U$ zircon age	0.282657	0.000044	0.001218	0.0596	0.282647	4.47	1.54	1.10	0.90

Supplementary Table 1 (continued). Main isotopes and ratios measured using the Multicollector.

RDT16_035	035 - 91	261.8	$^{206}Pb/^{238}U$ zircon age	0.282943	0.000044	0.000802	0.0309	0.282939	11.27	1.54	0.54	0.34
RDT16_035	035 - 92	425.6	$^{206}Pb/^{238}U$ zircon age	0.282639	0.000049	0.001215	0.0629	0.282629	3.97	1.715	1.13	0.94
RDT16_035	035 - 93	247.1	$^{206}Pb/^{238}U$ zircon age	0.282883	0.000045	0.000328	0.01384	0.282881	8.91	1.575	0.68	0.48
RDT16_035	035 - 94	222.5	$^{206}Pb/^{238}U$ zircon age	0.282851	0.000045	0.001033	0.0475	0.282847	7.13	1.575	0.77	0.57
RDT16_035	035 - 95	252.1	$^{206}Pb/^{238}U$ zircon age	0.282891	0.000058	0.000487	0.0213	0.282889	9.27	2.03	0.66	0.46
RDT16_035	035 - 96	257	$^{206}Pb/^{238}U$ zircon age	0.282924	0.000042	0.000262	0.00947	0.282923	10.59	1.47	0.58	0.38
RDT16_035	035 - 97	1873	$^{207}Pb/^{206}Pb$ zircon age	0.281513	0.00005	0.00053	0.0282	0.281494	-3.42	1.75	2.71	2.56
RDT16_035	035 - 98	257.4	$^{206}Pb/^{238}U$ zircon age	0.282883	0.000041	0.0002176	0.00835	0.282882	9.15	1.435	0.67	0.47
RDT16_035	035 - 99	299.8	$^{206}Pb/^{238}U$ zircon age	0.282941	0.000041	0.000952	0.0348	0.282936	12.00	1.435	0.52	0.32
TR_05-1	TR_05-1 - 1	1521	$^{207}Pb/^{206}Pb$ zircon age	0.281772	0.000044	0.00114	0.0501	0.281739	-2.80	1.54	2.40	2.24
TR_05-1	TR_05-1 - 10	350.6	$^{206}Pb/^{238}U$ zircon age	0.282141	0.000048	0.001027	0.0387	0.282134	-15.23	1.68	2.27	2.08
TR_05-1	TR_05-1 - 11	264.2	$^{206}Pb/^{238}U$ zircon age	0.282765	0.000043	0.00122	0.04314	0.282759	4.95	1.505	0.94	0.74
TR_05-1	TR_05-1 - 12	283.3	$^{206}Pb/^{238}U$ zircon age	0.282591	0.000043	0.000898	0.0288	0.282586	-0.73	1.505	1.32	1.12
TR_05-1	TR_05-1 - 13	287.6	$^{206}Pb/^{238}U$ zircon age	0.28245	0.000042	0.001261	0.0466	0.282443	-5.70	1.47	1.63	1.44
TR_05-1	TR_05-1 - 14	232.6	$^{206}Pb/^{238}U$ zircon age	0.282697	0.000044	0.001283	0.0465	0.282691	1.86	1.54	1.12	0.92
TR_05-1	TR_05-1 - 15	313.2	$^{206}Pb/^{238}U$ zircon age	0.282804	0.000045	0.001112	0.0379	0.282797	7.41	1.575	0.83	0.63
TR_05-1	TR_05-1 - 16	275.8	$^{206}Pb/^{238}U$ zircon age	0.282759	0.000046	0.00131	0.0392	0.282752	4.97	1.61	0.95	0.75
TR_05-1	TR_05-1 - 17	329.3	$^{206}Pb/^{238}U$ zircon age	0.282828	0.000052	0.001063	0.03258	0.282821	8.61	1.82	0.76	0.56
TR_05-1	TR_05-1 - 18	1660	$^{207}Pb/^{206}Pb$ zircon age	0.281801	0.000045	0.002701	0.0941	0.281716	-0.44	1.575	2.37	2.21
TR_05-1	TR_05-1 - 19	1633	$^{207}Pb/^{206}Pb$ zircon age	0.281971	0.00005	0.001138	0.0377	0.281936	6.74	1.75	1.91	1.75
TR_05-1	TR_05-1 - 2	381.8	$^{206}Pb/^{238}U$ zircon age	0.282425	0.00005	0.00106	0.0417	0.282417	-4.51	1.75	1.63	1.44
TR_05-1	TR_05-1 - 20	300.8	$^{206}Pb/^{238}U$ zircon age	0.282627	0.00005	0.000528	0.01567	0.282624	0.99	1.75	1.22	1.03
TR_05-1	TR_05-1 - 21	246.2	$^{206}Pb/^{238}U$ zircon age	0.282837	0.00005	0.002327	0.07343	0.282826	6.93	1.75	0.80	0.60
TR_05-1	TR_05-1 - 22	290.2	$^{206}Pb/^{238}U$ zircon age	0.282611	0.00005	0.001572	0.0489	0.282602	-0.01	1.75	1.28	1.08
TR_05-1	TR_05-1 - 23	375.6	$^{206}Pb/^{238}U$ zircon age	0.282623	0.000047	0.001743	0.04922	0.282611	2.19	1.645	1.21	1.01
TR_05-1	TR_05-1 - 24	522	$^{206}Pb/^{238}U$ zircon age	0.28197	0.000056	0.00101	0.0345	0.281960	-17.57	1.96	2.55	2.36
TR_05-1	TR_05-1 - 25	289.1	$^{206}Pb/^{238}U$ zircon age	0.28253	0.000047	0.00201	0.0577	0.282519	-2.98	1.645	1.46	1.27
TR_05-1	TR_05-1 - 26	439.8	$^{206}Pb/^{238}U$ zircon age	0.282585	0.000051	0.002711	0.0863	0.282563	1.93	1.785	1.27	1.08
TR_05-1	TR_05-1 - 27	293.6	$^{206}Pb/^{238}U$ zircon age	0.282648	0.000055	0.00221	0.0653	0.282636	1.25	1.925	1.20	1.00
TR_05-1	TR_05-1 - 28	1580	$^{207}Pb/^{206}Pb$ zircon age	0.28191	0.000049	0.000924	0.02613	0.281882	3.63	1.715	2.06	1.90
TR_05-1	TR_05-1 - 29	1445	$^{207}Pb/^{206}Pb$ zircon age	0.282109	0.000043	0.00259	0.077	0.282038	6.07	1.505	1.80	1.64
TR_05-1	TR_05-1 - 3	241.8	$^{206}Pb/^{238}U$ zircon age	0.282646	0.000047	0.001195	0.04705	0.282641	0.26	1.645	1.22	1.02
TR_05-1	TR_05-1 - 31	487.5	$^{206}Pb/^{238}U$ zircon age	0.282414	0.000043	0.002189	0.0653	0.282394	-2.98	1.505	1.62	1.42
TR_05-1	TR_05-1 - 32	1544	$^{206}Pb/^{238}U$ zircon age	0.281837	0.000044	0.001106	0.03044	0.281805	0.05	1.54	2.25	2.09
TR_05-1	TR_05-1 - 33	949	$^{206}Pb/^{238}U$ zircon age	0.281823	0.000042	0.001609	0.04334	0.281794	-13.85	1.47	2.64	2.46
TR_05-1	TR_05-1 - 4	963.9	$^{206}Pb/^{238}U$ zircon age	0.281759	0.000052	0.001003	0.0427	0.281741	-15.41	1.82	2.74	2.57
TR_05-1	TR_05-1 - 5	278.5	$^{206}Pb/^{238}U$ zircon age	0.282626	0.000041	0.000945	0.0376	0.282621	0.39	1.435	1.24	1.05
TR_05-1	TR_05-1 - 6	315.2	$^{206}Pb/^{238}U$ zircon age	0.282651	0.000041	0.0004178	0.013977	0.282649	2.18	1.435	1.16	0.96
TR_05-1	TR_05-1 - 7	289	$^{206}Pb/^{238}U$ zircon age	0.282526	0.000043	0.000875	0.03191	0.282521	-2.91	1.505	1.46	1.26
TR_05-1	TR_05-1 - 8	385	$^{206}Pb/^{238}U$ zircon age	0.28258	0.00005	0.000941	0.0343	0.282573	1.07	1.75	1.28	1.09
TR_05-1	TR_05-1 - 9	258	$^{206}Pb/^{238}U$ zircon age	0.2826	0.000049	0.0014237	0.05096	0.282593	-1.05	1.715	1.32	1.12
TR_05-2	TR_05-2 - 1	266.8	$^{206}Pb/^{238}U$ zircon age	0.282983	0.000046	0.001635	0.00051	0.282975	12.65	1.61	0.46	0.25
TR_05-2	TR_05-2 - 10	238	$^{206}Pb/^{238}U$ zircon age	0.282933	0.00005	0.001805	0.0015	0.282925	10.24	1.75	0.59	0.39
TR_05-2	TR_05-2 - 11	305.4	$^{206}Pb/^{238}U$ zircon age	0.282928	0.000043	0.001673	0.0014	0.282918	11.51	1.505	0.56	0.36
TR_05-2	TR_05-2 - 12	241.3	$^{206}Pb/^{238}U$ zircon age	0.282709	0.000041	0.000945	0.0024	0.282705	2.52	1.435	1.08	0.88
TR_05-2	TR_05-2 - 13	251.2	$^{206}Pb/^{238}U$ zircon age	0.283014	0.000043	0.00146	0.0014	0.283007	13.44	1.505	0.39	0.19
TR_05-2	TR_05-2 - 14	247.3	$^{206}Pb/^{238}U$ zircon age	0.282856	0.000054	0.001969	0.00088	0.282847	7.69	1.89	0.76	0.56
TR_05-2	TR_05-2 - 15	320.6	$^{206}Pb/^{238}U$ zircon age	0.282385	0.000046	0.000954	0.00071	0.282379	-7.23	1.61	1.75	1.56
TR_05-2	TR_05-2 - 16	336.8	$^{206}Pb/^{238}U$ zircon age	0.282861	0.00004	0.001811	0.0019	0.282850	9.78	1.4	0.69	0.50
TR_05-2	TR_05-2 - 17	231.3	$^{206}Pb/^{238}U$ zircon age	0.282638	0.000052	0.001197	0.0013	0.282633	-0.24	1.82	1.25	1.05
TR_05-2	TR_05-2 - 18	1705	$^{207}Pb/^{206}Pb$ zircon age	0.281371	0.000048	0.000856	0.00082	0.281343	-12.64	1.68	3.13	2.98
TR_05-2	TR_05-2 - 19	444.8	$^{206}Pb/^{238}U$ zircon age	0.282469	0.000052	0.001295	0.00047	0.282458	-1.66	1.82	1.50	1.31
TR_05-2	TR_05-2 - 2	320.5	$^{206}Pb/^{238}U$ zircon age	0.282666	0.000044	0.0010817	0.00021	0.282660	2.69	1.54	1.13	0.93
TR_05-2	TR_05-2 - 20	255.3	$^{206}Pb/^{238}U$ zircon age	0.282817	0.000052	0.001605	0.0018	0.282809	6.54	1.82	0.84	0.64
TR_05-2	TR_05-2 - 21	254.1	$^{206}Pb/^{238}U$ zircon age	0.282897	0.000039	0.001289	0.0014	0.282891	9.39	1.365	0.65	0.45
TR_05-2	TR_05-2 - 22	271.4	$^{206}Pb/^{238}U$ zircon age	0.282513	0.000048	0.00231	0.002	0.282501	-4.01	1.68	1.52	1.32
TR_05-2	TR_05-2 - 23	1014.1	$^{206}Pb/^{238}U$ zircon age	0.282114	0.000044	0.001205	0.0012	0.282091	-1.86	1.54	1.95	1.78
TR_05-2	TR_05-2 - 24	340.1	$^{206}Pb/^{238}U$ zircon age	0.282766	0.000042	0.000931	0.0011	0.282760	6.68	1.47	0.89	0.70
TR_05-2	TR_05-2 - 25	420	$^{206}Pb/^{238}U$ zircon age	0.282475	0.000044	0.00114	0.0028	0.282466	-1.94	1.54	1.50	1.31
TR_05-2	TR_05-2 - 26	250.4	$^{206}Pb/^{238}U$ zircon age	0.282997	0.000054	0.000507	0.00073	0.282995	12.98	1.89	0.42	0.22
TR_05-2	TR_05-2 - 27	233.6	$^{206}Pb/^{238}U$ zircon age	0.28287	0.000045	0.0012	0.0023	0.282865	8.01	1.575	0.73	0.52
TR_05-2	TR_05-2 - 28	281.4	$^{206}Pb/^{238}U$ zircon age	0.282783	0.000044	0.001287	0.003	0.282776	5.95	1.54	0.90	0.70
TR_05-2	TR_05-2 - 29	241.5		0.282919	0.000045	0.001135	0.0019	~~0.282914~~	~~9.93~~	~~1.575~~	~~0.61~~	~~0.41~~
TR_05-2	TR_05-2 - 3	334.6	$^{206}Pb/^{238}U$ zircon age	0.2827	0.000047	0.000813	0.00065	0.282695	4.26	1.645	1.04	0.85
TR_05-2	TR_05-2 - 30	642.9	$^{206}Pb/^{238}U$ zircon age	0.282426	0.000046	0.000723	0.0018	0.282417	1.33	1.61	1.47	1.28
TR_05-2	TR_05-2 - 31	241	$^{206}Pb/^{238}U$ zircon age	0.282934	0.000053	0.0006679	0.00017	0.282931	10.52	1.855	0.57	0.37
TR_05-2	TR_05-2 - 32	239.4	$^{206}Pb/^{238}U$ zircon age	0.282931	0.00005	0.002091	0.0026	0.282922	10.15	1.75	0.59	0.39
TR_05-2	TR_05-2 - 33	362.9	$^{206}Pb/^{238}U$ zircon age	0.282836	0.000042	0.0005852	0.00025	0.282832	9.74	1.47	0.72	0.52
TR_05-2	TR_05-2 - 34	1803	$^{207}Pb/^{206}Pb$ zircon age	0.281593	0.000046	0.000862	0.002	0.281564	-2.57	1.61	2.61	2.45
TR_05-2	TR_05-2 - 35	239.8	$^{206}Pb/^{238}U$ zircon age	0.28268	0.000046	0.001472	0.0033	0.282673	1.38	1.61	1.15	0.95
TR_05-2	TR_05-2 - 36	348	$^{206}Pb/^{238}U$ zircon age	0.282776	0.000046	0.000607	0.00072	0.282772	7.28	1.61	0.86	0.66
TR_05-2	TR_05-2 - 37	251.1	$^{206}Pb/^{238}U$ zircon age	0.282908	0.000051	0.001593	0.0017	0.282901	9.67	1.785	0.63	0.43
TR_05-2	TR_05-2 - 38	211.8	$^{206}Pb/^{238}U$ zircon age	0.282975	0.000046	0.000762	0.0012	0.282972	11.32	1.61	0.50	0.29
TR_05-2	TR_05-2 - 39	275.1	$^{206}Pb/^{238}U$ zircon age	0.282554	0.000039	0.0005074	0.00021	0.282551	-2.15	1.365	1.40	1.20
TR_05-2	TR_05-2 - 4	1530	$^{207}Pb/^{206}Pb$ zircon age	0.281447	0.000044	0.000888	0.0015	0.281421	-13.88	1.54	3.08	2.92
TR_05-2	TR_05-2 - 40	224.8	$^{206}Pb/^{238}U$ zircon age	0.28221	0.000043	0.000549	0.00071	0.282208	-15.43	1.505	2.19	2.00
TR_05-2	TR_05-2 - 41	258.4	$^{206}Pb/^{238}U$ zircon age	0.282571	0.000044	0.000902	0.0007	0.282567	-1.98	1.54	1.38	1.18
TR_05-2	TR_05-2 - 42	239.6	$^{206}Pb/^{238}U$ zircon age	0.282922	0.000047	0.001361	0.0025	0.282916	9.96	1.645	0.61	0.40
TR_05-2	TR_05-2 - 43	243	$^{206}Pb/^{238}U$ zircon age	0.282425	0.00004	0.000846	0.0026	0.282421	-7.47	1.4	1.71	1.51
TR_05-2	TR_05-2 - 44	238.2	$^{206}Pb/^{238}U$ zircon age	0.2828	0.000043	0.0010106	0.00027	0.282796	5.66	1.505	0.88	0.68
TR_05-2	TR_05-2 - 45	239.4	$^{206}Pb/^{238}U$ zircon age	0.282839	0.000048	0.001145	0.0017	0.282834	7.05	1.68	0.79	0.59

Supplementary Table 1 (continued). Main isotopes and ratios measured using the Multicollector.

TR_05-2	TR_05-2 - 46	393.8	$^{206}Pb/^{238}U$ zircon age	0.282758	0.000043	0.0004873	0.0003	0.282754	7.68	1.505	0.87	0.68
TR_05-2	TR_05-2 - 47	325.9	$^{206}Pb/^{238}U$ zircon age	0.282566	0.000047	0.000842	0.00065	0.282561	-0.68	1.645	1.35	1.15
TR_05-2	TR_05-2 - 48	3090.4	$^{207}Pb/^{206}Pb$ zircon age	0.280748	0.000044	0.000819	0.0013	0.280699	-3.28	1.54	3.66	3.54
TR_05-2	TR_05-2 - 49	235.8	$^{206}Pb/^{238}U$ zircon age	0.282903	0.000045	0.000636	0.0026	0.282900	9.32	1.575	0.65	0.44
TR_05-2	TR_05-2 - 5	438.4	$^{206}Pb/^{238}U$ zircon age	0.282475	0.00005	0.000874	0.0007	0.282468	-1.46	1.75	1.48	1.29
TR_05-2	TR_05-2 - 50	247.7	$^{206}Pb/^{238}U$ zircon age	0.282449	0.00005	0.000644	0.0049	0.282446	-6.49	1.75	1.65	1.46
TR_05-2	TR_05-2 - 6	261.8	$^{206}Pb/^{238}U$ zircon age	0.282501	0.00005	0.001057	0.00092	0.282496	-4.41	1.75	1.53	1.34
TR_05-2	TR_05-2 - 7	266.1	$^{206}Pb/^{238}U$ zircon age	0.28295	0.000054	0.001075	0.00042	0.282945	11.56	1.89	0.53	0.32
TR_05-2	TR_05-2 - 8	271.6	$^{206}Pb/^{238}U$ zircon age	0.282636	0.00005	0.000879	0.00099	0.282632	0.61	1.75	1.23	1.03
TR_05-2	TR_05-2 - 9	258.7	$^{206}Pb/^{238}U$ zircon age	0.282929	0.000046	0.000827	0.00056	0.282925	10.70	1.61	0.57	0.37
TR_05-3	TR_05-3 - 1	244.2	$^{206}Pb/^{238}U$ zircon age	0.282928	0.000051	0.000662	0.0038	0.282925	10.38	1.785	0.58	0.38
TR_05-3	TR_05-3 - 10	1509	$^{206}Pb/^{238}U$ zircon age	0.281954	0.000046	0.000922	0.00068	0.281928	3.61	1.61	2.00	1.84
TR_05-3	TR_05-3 - 11	257	$^{206}Pb/^{238}U$ zircon age	0.28299	0.000045	0.0008139	0.00037	0.282986	12.83	1.575	0.44	0.23
TR_05-3	TR_05-3 - 12	226.1	$^{206}Pb/^{238}U$ zircon age	0.28296	0.000049	0.00091	0.0014	0.282956	11.08	1.715	0.52	0.32
TR_05-3	TR_05-3 - 13	1826	$^{206}Pb/^{238}U$ zircon age	0.281655	0.000045	0.000795	0.0013	0.281627	0.23	1.575	2.46	2.30
TR_05-3	TR_05-3 - 14	337.6	$^{206}Pb/^{238}U$ zircon age	0.282677	0.000049	0.000916	0.0011	0.282671	3.48	1.715	1.09	0.90
TR_05-3	TR_05-3 - 15	332.8	$^{206}Pb/^{238}U$ zircon age	0.282746	0.000047	0.001142	0.0016	0.282739	5.77	1.645	0.95	0.75
TR_05-3	TR_05-3 - 16	256.9	$^{206}Pb/^{238}U$ zircon age	0.282619	0.000041	0.00082	0.0053	0.282615	-0.30	1.435	1.27	1.07
TR_05-3	TR_05-3 - 17	207.8	$^{206}Pb/^{238}U$ zircon age	0.28219	0.000047	0.000932	0.00079	0.282186	-16.56	1.645	2.25	2.05
TR_05-3	TR_05-3 - 18	230.4	$^{206}Pb/^{238}U$ zircon age	0.28292	0.000046	0.000828	0.00081	0.282916	9.77	1.61	0.61	0.41
TR_05-3	TR_05-3 - 19	280.1	$^{206}Pb/^{238}U$ zircon age	0.282614	0.000043	0.001261	0.0012	0.282607	-0.06	1.505	1.27	1.08
TR_05-3	TR_05-3 - 2	337.6	$^{206}Pb/^{238}U$ zircon age	0.282589	0.000049	0.0004362	0.00019	0.282586	0.48	1.715	1.28	1.09
TR_05-3	TR_05-3 - 20	530.7	$^{206}Pb/^{238}U$ zircon age	0.282188	0.000044	0.0000301	0.00013	0.282188	-9.31	1.54	2.04	1.85
TR_05-3	TR_05-3 - 21	376.7	$^{206}Pb/^{238}U$ zircon age	0.282797	0.000047	0.000618	0.00016	0.282793	8.65	1.645	0.80	0.60
TR_05-3	TR_05-3 - 22	878.1	$^{206}Pb/^{238}U$ zircon age	0.281998	0.000048	0.000477	0.00081	0.281990	-8.51	1.68	2.26	2.08
TR_05-3	TR_05-3 - 23	236.9	$^{206}Pb/^{238}U$ zircon age	0.282953	0.000045	0.001013	0.0036	0.282949	11.05	1.575	0.54	0.33
TR_05-3	TR_05-3 - 24	991.8	$^{206}Pb/^{238}U$ zircon age	0.282022	0.000043	0.000468	0.0018	0.282013	-5.12	1.505	2.14	1.96
TR_05-3	TR_05-3 - 25	890.6	$^{206}Pb/^{238}U$ zircon age	0.282255	0.000047	0.000505	0.00078	0.282247	0.86	1.645	1.69	1.51
TR_05-3	TR_05-3 - 26	208.4		~~0.282185~~	~~0.000041~~	~~0.000657~~	~~0.00083~~	~~0.282182~~	~~-16.69~~	~~1.435~~	~~2.26~~	~~2.06~~
TR_05-3	TR_05-3 - 27	495.3	$^{206}Pb/^{238}U$ zircon age	0.282364	0.000051	0.00051	0.00061	0.282359	-4.03	1.785	1.69	1.50
TR_05-3	TR_05-3 - 28	271.9	$^{206}Pb/^{238}U$ zircon age	0.2826	0.00004	0.000688	0.0017	0.282597	-0.63	1.4	1.30	1.10
TR_05-3	TR_05-3 - 29	265.7	$^{206}Pb/^{238}U$ zircon age	0.282942	0.000045	0.000899	0.0014	0.282938	11.30	1.575	0.54	0.34
TR_05-3	TR_05-3 - 3	297.1		~~0.282875~~	~~0.00005~~	~~0.000954~~	~~0.0015~~	~~0.282870~~	~~9.60~~	~~1.75~~	~~0.67~~	~~0.47~~
TR_05-3	TR_05-3 - 30	247	$^{206}Pb/^{238}U$ zircon age	0.282935	0.00004	0.001439	0.0025	0.282928	10.56	1.4	0.57	0.37
TR_05-3	TR_05-3 - 31	239.5	$^{206}Pb/^{238}U$ zircon age	0.282918	0.000045	0.001232	0.0011	0.282912	9.83	1.575	0.61	0.41
TR_05-3	TR_05-3 - 32	1724	$^{207}Pb/^{206}Pb$ zircon age	0.281824	0.000043	0.001393	0.00091	0.281778	3.24	1.505	2.19	2.04
TR_05-3	TR_05-3 - 33	483.8	$^{206}Pb/^{238}U$ zircon age	0.282478	0.000039	0.000707	0.0012	0.282472	-0.31	1.365	1.45	1.25
TR_05-3	TR_05-3 - 34	1150.6	$^{206}Pb/^{238}U$ zircon age	0.281897	0.000046	0.00121	0.0044	0.281871	-6.57	1.61	2.35	2.17
TR_05-3	TR_05-3 - 35	438.3	$^{206}Pb/^{238}U$ zircon age	0.282236	0.000049	0.0008801	0.00063	0.282229	-9.93	1.715	2.01	1.82
TR_05-3	TR_05-3 - 36	1057	$^{206}Pb/^{238}U$ zircon age	0.282218	0.000045	0.000721	0.0015	0.282204	3.10	1.575	1.68	1.50
TR_05-3	TR_05-3 - 37	294.7	$^{206}Pb/^{238}U$ zircon age	0.282382	0.000051	0.001143	0.0009	0.282376	-7.93	1.785	1.78	1.58
TR_05-3	TR_05-3 - 38	1572	$^{207}Pb/^{206}Pb$ zircon age	0.281983	0.000047	0.001699	0.0013	0.281932	5.22	1.645	1.95	1.79
TR_05-3	TR_05-3 - 39	256.5	$^{206}Pb/^{238}U$ zircon age	0.282979	0.000038	0.001007	0.0014	0.282974	12.39	1.33	0.46	0.26
TR_05-3	TR_05-3 - 4	300		~~0.282963~~	~~0.00005~~	~~0.001019~~	~~0.002~~	~~0.282957~~	~~12.77~~	~~1.75~~	~~0.48~~	~~0.27~~
TR_05-3	TR_05-3 - 40	1697	$^{207}Pb/^{206}Pb$ zircon age	0.281744	0.000043	0.000963	0.0011	0.281713	0.30	1.505	2.35	2.19
TR_05-3	TR_05-3 - 41	228.9	$^{206}Pb/^{238}U$ zircon age	0.282949	0.000048	0.000882	0.00085	0.282945	10.75	1.68	0.55	0.34
TR_05-3	TR_05-3 - 42	252.6		~~0.282872~~	~~0.000046~~	~~0.00145~~	~~0.0031~~	~~0.282865~~	~~8.45~~	~~1.61~~	~~0.71~~	~~0.51~~
TR_05-3	TR_05-3 - 5	974.4	$^{206}Pb/^{238}U$ zircon age	0.281973	0.000049	0.0003687	0.00063	0.281966	-7.18	1.715	2.25	2.07
TR_05-3	TR_05-3 - 6	713		0.282562	0.000057	0.000676	0.00054	0.282553	7.71	1.995	1.12	0.93
TR_05-3	TR_05-3 - 7	255.3		~~0.282706~~	~~0.000038~~	~~0.001101~~	~~0.0029~~	~~0.282701~~	~~2.69~~	~~1.33~~	~~1.08~~	~~0.88~~
TR_05-3	TR_05-3 - 8	235.4	$^{206}Pb/^{238}U$ zircon age	0.282916	0.00004	0.000749	0.0011	0.282913	9.75	1.4	0.62	0.41
CM15_01	CM1501-278.d	268.6	$^{206}Pb/^{238}U$ zircon age	0.282657	0.000026	0.0004114	0.02113	0.282655	1.37	0.91	1.18	0.98
CM15_01	CM1501-376.d	277.9	$^{206}Pb/^{238}U$ zircon age	0.282594	0.000035	0.000558	0.0344	0.282591	-0.68	1.225	1.31	1.11
CM15_01	CM1501-340.d	278.5	$^{206}Pb/^{238}U$ zircon age	0.282476	0.000026	0.0006	0.0438	0.282473	-4.85	0.91	1.57	1.38
CM15_01	CM1501-321.d	290.6	$^{206}Pb/^{238}U$ zircon age	0.282785	0.000036	0.000485	0.03095	0.282782	6.37	1.26	0.88	0.68
CM15_01	CM1501-252.d	295.9	$^{206}Pb/^{238}U$ zircon age	0.28254	0.000049	0.000724	0.0573	0.282536	-2.23	1.715	1.42	1.23
CM15_01	CM1501-314.d	319.2	$^{206}Pb/^{238}U$ zircon age	0.282527	0.000038	0.0004037	0.02158	0.282525	-2.12	1.33	1.43	1.24
CM15_01	CM1501-345.d	356	$^{206}Pb/^{238}U$ zircon age	0.282214	0.000032	0.000459	0.03897	0.282211	-12.39	1.12	2.10	1.91
CM15_01	CM1501-292.d	361.5	$^{206}Pb/^{238}U$ zircon age	0.282625	0.000032	0.001576	0.0872	0.282614	2.00	1.12	1.21	1.01
CM15_01	CM1501-366.d	447.2	$^{206}Pb/^{238}U$ zircon age	0.282694	0.000025	0.0006571	0.0448	0.282688	6.55	0.875	0.99	0.79
CM15_01	CM1501-140.d	480.1	$^{206}Pb/^{238}U$ zircon age	0.281576	0.000059	0.000232	0.00888	0.281574	-32.17	2.065	3.40	3.22
CM15_01	CM1501-223.d	487.8	$^{206}Pb/^{238}U$ zircon age	0.282481	0.000032	0.001347	0.0773	0.282469	-0.33	1.12	1.45	1.26
CM15_01	CM1501-160.d	897	$^{206}Pb/^{238}U$ zircon age	0.282224	0.00003	0.000871	0.03894	0.282209	-0.31	1.05	1.77	1.59
CM15_01	CM1501-143.d	972	$^{206}Pb/^{238}U$ zircon age	0.282516	0.00003	0.000908	0.02066	0.282410	8.51	2.52	1.28	1.10
CM15_01	CM1501-336.d	978	$^{206}Pb/^{238}U$ zircon age	0.282088	0.00005	0.000921	0.0744	0.282071	-3.38	1.75	2.02	1.84
CM15_01	CM1501-357.d	981	$^{206}Pb/^{238}U$ zircon age	0.282434	0.000056	0.001082	0.0863	0.282414	8.84	1.96	1.26	1.08
CM15_01	CM1501-322.d	1023	$^{206}Pb/^{238}U$ zircon age	0.28205	0.000038	0.0004044	0.03249	0.282042	-3.39	1.33	2.05	1.88
CM15_01	CM1501-311.d	1058	$^{206}Pb/^{238}U$ zircon age	0.281676	0.000026	0.00139	0.092	0.281648	-16.56	0.91	2.88	2.71
CM15_01	CM1501-236.d	1270	$^{206}Pb/^{238}U$ zircon age	0.282132	0.000053	0.0007551	0.05973	0.282114	4.76	1.855	1.74	1.57
CM15_01	CM1501-337.d	1294	$^{206}Pb/^{238}U$ zircon age	0.282078	0.000038	0.000499	0.04056	0.282066	3.60	1.33	1.83	1.66
CM15_01	CM1501-214.d	1457	$^{207}Pb/^{206}Pb$ zircon age	~~0.282674~~	~~0.000036~~	~~0.001584~~	~~0.0839~~	~~0.282632~~	~~25.95~~	~~1.26~~	~~0.52~~	~~0.35~~
CM15_01	CM1501-182.d	1615	$^{207}Pb/^{206}Pb$ zircon age	0.281904	0.000035	0.0006425	0.0319	0.281884	4.50	1.225	2.03	1.87
CM15_01	CM1501-163.d	1459	$^{207}Pb/^{206}Pb$ zircon age	0.282027	0.000055	0.0004808	0.022	0.282014	5.52	1.925	1.85	1.68
CM15_01	CM1501-294.d	1858	$^{207}Pb/^{206}Pb$ zircon age	0.281405	0.00003	0.00095	0.05442	0.281372	-8.12	1.05	2.98	2.83
CM15_01	CM1501-277.d	1869	$^{207}Pb/^{206}Pb$ zircon age	0.281532	0.00005	0.0005567	0.02922	0.281512	-2.87	1.75	2.68	2.53
CM15_01	CM1501-310.d	2008	$^{207}Pb/^{206}Pb$ zircon age	0.281313	0.000035	0.000609	0.0385	0.281290	-7.57	1.225	3.06	2.92
CM15_01	CM1501-318.d	1880	$^{207}Pb/^{206}Pb$ zircon age	0.281588	0.000042	0.0004927	0.0342	0.281570	-0.55	1.47	2.55	2.39
CM15_01	CM1501-368.d	1859	$^{207}Pb/^{206}Pb$ zircon age	0.281569	0.000034	0.00005372	0.00591	0.281567	-1.16	1.19	2.57	2.41
CM15_01	CM1501-141.d	1883	$^{207}Pb/^{206}Pb$ zircon age	0.282516	0.00003	0.000908	0.0339	0.282484	~~31.94~~	~~1.05~~	~~0.55~~	~~0.40~~
CM15_01	CM1501-276.d	2354	$^{207}Pb/^{206}Pb$ zircon age	0.281135	0.000054	0.000495	0.02271	0.281113	-5.84	1.89	3.23	3.09
CM15_01	CM1501-147.d	2404	$^{207}Pb/^{206}Pb$ zircon age	0.281236	0.000062	0.001785	0.0952	0.281154	-3.20	2.17	3.11	2.98
CM15_01	CM1501-256.d	3160	$^{207}Pb/^{206}Pb$ zircon age	0.280696	0.000029	0.0004223	0.03003	0.280670	-2.67	1.015	3.68	3.56

Supplementary Table 2. LA–ICP–MS Analytical Method Information. Errors given as 2σ.

Analysis Batch Date	*Samples Analysed*	*Spot Size*	*Isotopes measured*	*Standard $^{206}Pb/^{238}U$ weighted averages*			
				GJ-1	*Plešovice*	*91500**	*MT*
19/5/2017	RDT16_018, RDT16_019	30 µm	^{90}Zr, ^{139}La, ^{140}Ce, ^{141}Pr, ^{146}Nd, ^{146}Sm, ^{153}Eu, ^{157}Gd, ^{159}Tb, ^{163}Dy, ^{165}Ho, ^{166}Er, ^{169}Tm, ^{172}Yb, ^{175}Lu, ^{178}Hf, ^{202}Hg, ^{204}Pb, ^{206}Pb, ^{207}Pb, ^{208}Pb, ^{232}Th, ^{238}U	601.67±0.85 (*n*=112, MSWD=1.04)	330.7±1.5 (*n*=31, MSWD=2.1)	1016.7±4.6 (*n*=28, MSWD=1.7)	Not measured
At Curtin University 10/7/17	RDT16_006, RDT16_033, RDT16_035, TR_05-1, TR_05-2 and TR_05-3	50 µm	^{90}Zr, ^{202}Hg, ^{204}Pb, ^{206}Pb, ^{207}Pb, ^{208}Pb, ^{232}Th, ^{238}U	601.84 ± 1.28 (*n*=13, MSWD=0.02) Skewness = 0.31	Not measured	1058.03 ± 2.91 (*n*=13, MSWD=2.78) Skewness = 8.83	715.55 ± 3.29 (*n*=24, MSWD = 1.68) Skewness = 10.20
21/07/2017	RDT16_033, RDT16_035	30 µm	^{90}Zr, ^{139}La, ^{140}Ce, ^{141}Pr, ^{146}Nd, ^{146}Sm, ^{153}Eu, ^{157}Gd, ^{159}Tb, ^{163}Dy, ^{165}Ho, ^{166}Er, ^{169}Tm, ^{172}Yb, ^{175}Lu, ^{178}Hf, ^{202}Hg, ^{204}Pb, ^{206}Pb, ^{207}Pb, ^{208}Pb, ^{232}Th, ^{238}U	601.72±0.97 (*n*=132, MSWD=0.66)	338.6±1.3 (*n*=66, MSWD=2.4)	1035.2±4.6 (*n*=33, MSWD=1.3)	Not measured
28/09/2017	RDT16_012	30 µm	^{90}Zr, ^{201}Hg, ^{204}Pb, ^{206}Pb, ^{207}Pb, ^{208}Pb, ^{232}Th, ^{238}U	601.5±1.2 (*n*=52, MSWD=0.76)	343.2±1.3 (*n*=26, MSWD = 1.8)	1067.6±4.4 (*n*=13, MSWD=1.10)	Not measured
18/09/2018	RDT16_049C, RDT16_050B	30 µm	^{90}Zr, ^{201}Hg, ^{204}Pb, ^{206}Pb, ^{207}Pb, ^{208}Pb, ^{232}Th, ^{238}U	601.3 ± 2.2 Ma (*n* = 57, MSWD = 1.00)	335.4 ± 1.2 Ma (*n* = 56, MSWD = 1.08)	1058.9 ± 7.1 Ma (*n* = 28, MSWD = 1.5)	Not measured

* The use of two different 91500 crystals for these analyses, where one crystal gives good reproducibility while the other is more heterogeneous, accounts for the younger age for the 91500 standard in three of the analysis batches. 91500 was used as one of two secondary standards and was not used as a primary standard to correct for isotopic drift and down-hole fractionation.

Supplementary Table 3. Lu–Hf Standards and Analytical Runs. Errors given as 2σ.

Analysis Date	*Samples Analysed*	*Standard $^{176}Hf/^{177}Hf$ weighted averages*					*Standard Lu:Hf weighted average*
		MT	*R33*	*FC-1*	*GJ-1*	*91500*	*R33*
10/07/2017	RDT16_006, RDT16_033, RDT16_035, TR_05-1, TR_05-2 and TR_05-3	0.2825070 ± 0.0000088 (*n*=24, MSWD=0.84)	0.282697 ± 0.000011 (*n*=24, MSWD=1.3)	0.282145 ± 0.000017 (n=15, MSWD=2.0)	0.282009 ± 0.000013 (n=15, MSWD=0.98)	0.282303 ± 0.000018 (n=15, MSWD=1.6)	0.001990 ± 0.000016 (n=24, MSWD=112)
11/07/2017	RDT16_019, CM15_01	0.2825071±0.0000081 (*n*=13, MSWD=0.041)	0.282708±0.000017 (*n*=14, MSWD = 3.6)	0.282159 ± 0.000019 (n=15, MSWD=4.9)	0.282001 ± 0.000019 (n=10, MSWD=2.7)	0.282291 ± 0.000011 (n=9, MSWD=0.16)	0.001988 ± 0.000040 (n=14, MSWD=101)

APPENDIX V

Supplementary material for Chapter 5

Supplementary Table 1. Main isotopes and ratios measured using LA–ICP–MS

Analysis #	Ratios							Ages						Concentrations (ppm)			Th:U	Concordance Calculations	
	$^{207}Pb/^{235}U$	2σ	$^{206}Pb/^{238}U$	2σ	Rho	$^{207}Pb/^{206}Pb$	2σ	$^{207}Pb/^{235}U$ Age	2σ	Pb^{206}/U^{238} Age	2σ	$^{207}Pb/^{206}Pb$ Age	2σ	U	Th	Pb		($^{206}Pb/^{238}U$ age)/ $^{207}Pb/^{206}Pb$ age)	($^{206}Pb/^{238}U$ age)/ $^{207}Pb/^{235}U$ age)
CMG01-256.d	1.434	0.043	0.148	0.004	0.411	0.070	0.002	899	18	891	24	901	51	242.1	76.1	335	0.31	99	99
CMG01-257.d	0.978	0.028	0.114	0.003	0.241	0.062	0.002	690	15	694.2	19	652	56	339.4	106.4	343.1	0.31	106	101
CMG01-258.d	2.372	0.062	0.207	0.006	0.776	0.083	0.001	1231	19	1213	33	1256	34	1272	276	1456	0.22	97	99
CMG01-259.d	4.059	0.097	0.294	0.008	0.504	0.100	0.002	1647.1	19	1658	41	1625	33	455.5	337	2560	0.74	102	101
CMG01-260.d	2.146	0.066	0.186	0.005	0.410	0.084	0.002	1161	21	1098	29	1267	49	179.7	43.74	285.3	0.24	87	95
CMG01-261.d	1.967	0.052	0.186	0.005	0.513	0.076	0.002	1101	18	1100	29	1101	39	456	148.7	770	0.33	100	100
CMG01-262.d	2.580	0.071	0.224	0.006	0.418	0.084	0.002	1292	21	1302	34	1275	43	198.5	232.9	1407	1.17	102	101
CMG01-263.d	2.377	0.066	0.210	0.006	0.205	0.082	0.002	1235	21	1229	33	1223	51	171.1	56.43	337	0.33	100	100
CMG01-264.d	2.044	0.056	0.190	0.006	0.402	0.078	0.002	1128	19	1121	30	1136	43	370	123.5	649	0.33	99	99
CMG01-265.d	5.570	0.570	0.114	0.005	0.921	0.327	0.021	1779	88	691	31	3390	120	3330	5520	3.68E+04	1.66	20	39
CMG01-266.d	1.826	0.053	0.171	0.005	0.672	0.078	0.002	1052	19	1016	28	1126	41	330.2	338.9	1152	1.03	90	97
CMG01-267.d	1.332	0.038	0.142	0.004	0.606	0.068	0.001	856	17	857	24	843	43	534	331	1158	0.62	102	100
CMG01-274.d	1.676	0.051	0.169	0.005	0.095	0.072	0.002	995	20	1007	27	948	59	139.9	139.5	666	1.00	106	101
CMG01-275.d	40.500	1.400	0.472	0.018	0.375	0.631	0.018	3767	32	2482	77	4564	46	11.71	0.715	752	0.06	54	66
CMG01-276.d	1.999	0.074	0.178	0.006	0.892	0.081	0.002	1106	25	1056	33	1203	40	2410	254.2	1062	0.11	88	95
CMG01-277.d	1.511	0.040	0.158	0.005	0.546	0.069	0.001	932.5	16	946.6	25	889	43	492	172.7	771	0.35	106	102
CMG01-278.d	1.072	0.026	0.108	0.003	0.630	0.072	0.001	739.3	13	662.1	18	974	38	3317	1989	6760	0.60	68	90
CMG01-279.d	1.838	0.051	0.178	0.005	0.502	0.075	0.002	1059	19	1057	29	1054	44	310.4	194.4	986	0.63	100	100
CMG01-280.d	1.854	0.055	0.179	0.006	0.503	0.075	0.002	1060	20	1060	30	1042	47	328	258	1310	0.79	102	100
CMG01-281.d	1.391	0.037	0.144	0.004	0.469	0.070	0.002	883.7	16	869	24	909	44	586	188.7	806	0.32	96	98
CMG01-282.d	1.472	0.047	0.157	0.005	0.245	0.068	0.002	915	19	942	26	831	58	146.8	113.5	502	0.77	113	103
CMG01-283.d	1.628	0.040	0.163	0.005	0.609	0.072	0.001	979.4	15	972.4	25	987	36	1187	1152	5110	0.97	99	99
CMG01-284.d	15.340	0.380	0.541	0.016	0.720	0.204	0.004	2834	24	2785	67	2857	29	156.8	53.6	489	0.34	97	98
CMG01-285.d	0.700	0.018	0.081	0.002	0.622	0.063	0.001	538.6	11	500.1	14	695	42	2030	828	1900	0.41	72	93

Analysis #	Ratios							Ages						Concentrations (ppm)			Th:U	Concordance Calculations	
	$^{207}Pb/^{235}U$	2σ	$^{206}Pb/^{238}U$	2σ	Rho	$^{207}Pb/^{206}Pb$	2σ	$^{207}Pb/^{235}U$ Age	2σ	Pb^{206}/U^{238} Age	2σ	$^{207}Pb/^{206}Pb$ Age	2σ	U	Th	Pb		($^{206}Pb/^{238}U$ age)/ $^{207}Pb/^{206}Pb$ age)	($^{206}Pb/^{238}U$ age)/ $^{207}Pb/^{235}U$ age)
CMG01-286.d	0.773	0.018	0.091	0.003	0.649	0.062	0.001	582	11	562.2	16	655	38	3890	1198	3000	0.31	86	97
CMG01-287.d	6.420	0.350	0.352	0.015	0.934	0.127	0.004	1977	54	1939	72	2018	53	570	77.8	871	0.14	96	98
CMG01-288.d	1.719	0.047	0.170	0.005	0.527	0.073	0.002	1013	17	1013	27	997	43	364	249	1191	0.68	102	100
CMG01-294.d	1.939	0.092	0.187	0.006	0.234	0.076	0.004	1079	32	1101	33	983	96	39.56	15.55	79	0.39	112	102
CMG01-295.d	1.598	0.046	0.150	0.005	0.645	0.078	0.002	974	18	900	25	1137	44	796	732	2287	0.92	79	92
CMG01-296.d	0.912	0.023	0.107	0.003	0.401	0.062	0.001	656.8	12	654	17	658	43	1119	328	975	0.29	99	100
CMG01-297.d	0.931	0.024	0.109	0.003	0.685	0.062	0.001	666.8	13	664.5	18	658	40	1269	382	1191	0.30	101	100
CMG01-298.d	1.945	0.051	0.186	0.005	0.408	0.076	0.002	1094	18	1098.8	28	1074	41	431	122.6	642	0.28	102	100
CMG01-299.d	2.033	0.048	0.192	0.005	0.323	0.076	0.001	1125.2	16	1133.2	29	1100	35	786	221.6	1197	0.28	103	101
CMG01-300.d	5.067	0.140	0.334	0.010	0.855	0.110	0.002	1824	24	1855	49	1787	31	611	124.6	1090	0.20	104	102
CMG01-301.d	1.956	0.051	0.189	0.005	0.316	0.075	0.002	1100	18	1117.1	29	1056	42	360.1	129.1	664	0.36	106	102
CMG01-302.d	1.996	0.052	0.191	0.005	0.415	0.076	0.002	1112	18	1128.3	29	1070	42	436	175.1	919	0.40	105	101
CMG01-303.d	1.983	0.054	0.188	0.005	0.313	0.077	0.002	1110	19	1110	29	1098	47	225	104	532	0.46	101	100
CMG01-304.d	1.895	0.050	0.183	0.005	0.254	0.075	0.002	1077	18	1081	28	1065	45	323	142.9	735	0.44	102	100
CMG01-305.d	1.072	0.030	0.121	0.003	0.285	0.064	0.002	737	15	738.5	19	709	51	324.6	276.3	937	0.85	104	100
CMG01-306.d	1.086	0.035	0.121	0.004	0.218	0.065	0.002	742	17	738.7	20	723	66	175.4	104	363	0.59	102	100
CMG01-307.d	1.853	0.048	0.181	0.005	0.475	0.074	0.002	1063	17	1074	29	1037	42	452.3	41.11	214.3	0.09	104	101
CMG01-313.d	1.772	0.045	0.175	0.005	0.394	0.073	0.002	1033	17	1037.4	27	1011	41	488.8	2342	10990	4.79	103	100
CMG01-314.d	4.064	0.110	0.286	0.009	0.620	0.104	0.002	1645	21	1622	43	1682	35	754	519	2944	0.69	96	99
CMG01-315.d	1.569	0.056	0.157	0.005	0.131	0.073	0.002	952	23	939	26	949	73	86.7	44.37	200.7	0.51	99	99
CMG01-316.d	0.876	0.024	0.104	0.003	0.495	0.061	0.001	637.1	13	637.7	18	620	45	1152	707	2140	0.61	103	100
CMG01-317.d	2.022	0.053	0.194	0.006	0.348	0.076	0.002	1120	18	1140	30	1071	43	338	182.5	961	0.54	106	102
CMG01-318.d	1.662	0.053	0.164	0.005	0.429	0.074	0.002	988	20	980	28	1011	52	196.3	124.6	563	0.63	97	99
CMG01-319.d	20.120	0.490	0.616	0.018	0.755	0.236	0.004	3094	23	3089	70	3093	26	465	144	2190	0.31	100	100

Supplementary Table 1 (continued). Main isotopes and ratios measured using LA–ICP–MS

Analysis #	Ratios							Ages						Concentrations (ppm)			Th:U	Concordance Calculations	
	$^{207}Pb/^{235}U$	2σ	$^{206}Pb/^{238}U$	2σ	Rho	$^{207}Pb/^{206}Pb$	2σ	$^{207}Pb/^{235}U$ Age	2σ	Pb^{206}/U^{238} Age	2σ	$^{207}Pb/^{206}Pb$ Age	2σ	U	Th	Pb		$(^{206}Pb/^{238}U$ age)/ $^{207}Pb/^{206}Pb$ age)	$(^{206}Pb/^{238}U$ age)/ $^{207}Pb/^{235}U$ age)
CMG01-320.d	0.875	0.028	0.105	0.003	0.202	0.061	0.002	637	15	644	18	580	63	215.7	32.8	93.5	0.15	111	101
CMG01-321.d	0.899	0.034	0.106	0.003	0.240	0.061	0.002	648	18	651.2	18	612	72	188.9	133	395	0.70	106	100
CMG01-322.d	0.888	0.029	0.106	0.003	0.200	0.061	0.002	642	16	647.5	18	614	64	290.7	158.1	474	0.54	105	101
CMG01-323.d	1.712	0.044	0.150	0.005	0.736	0.083	0.002	1010.9	16	899	25	1259	38	719	534	2296	0.74	71	89
CMG01-324.d	10.880	0.290	0.407	0.012	0.764	0.193	0.003	2509	25	2199	56	2758	29	607	552	2856	0.91	80	88
CMG01-330.d	1.965	0.052	0.189	0.006	0.540	0.075	0.002	1102	18	1114	31	1066	41	529.3	261.5	1385	0.49	105	101
CMG01-331.d	1.865	0.049	0.178	0.005	0.652	0.075	0.001	1067	17	1057	28	1074	37	899	30.11	146.1	0.03	98	99
CMG01-332.d	1.898	0.057	0.180	0.006	0.688	0.076	0.002	1075	20	1064	30	1084	43	429	287.4	1271	0.67	98	99
CMG01-333.d	1.946	0.053	0.185	0.006	0.658	0.076	0.001	1095	18	1093	31	1087	39	1005	346	1605	0.34	101	100
CMG01-334.d	1.106	0.029	0.124	0.004	0.578	0.064	0.001	755.5	14	756.1	20	739	41	779	623	2115	0.80	102	100
CMG01-335.d	1.723	0.075	0.129	0.004	0.633	0.098	0.004	1005	24	781.7	22	1523	58	1123	367	2400	0.33	51	78
CMG01-336.d	1.825	0.049	0.171	0.005	0.372	0.077	0.002	1051	18	1017	27	1120	43	385.6	1058	4034	2.74	91	97
CMG01-337.d	6.496	0.160	0.365	0.011	0.603	0.128	0.002	2042	22	2008	50	2074	31	573	161.1	1141	0.28	97	98
CMG01-338.d	2.186	0.061	0.195	0.006	0.466	0.082	0.002	1172	20	1145	31	1224	46	268	21.7	119.5	0.08	94	98
CMG01-339.d	1.794	0.045	0.170	0.005	0.492	0.076	0.001	1041.5	16	1015	27	1090	37	1428	1295	6120	0.91	93	97
CMG01-340.d	1.999	0.060	0.185	0.005	0.302	0.079	0.002	1110	20	1093	29	1131	51	204.9	91.4	479	0.45	97	98
CMG01-341.d	1.702	0.047	0.167	0.005	0.368	0.074	0.002	1006	18	992	27	1024	46	349	180	795	0.52	97	99
CMG01-347.d	5.660	0.410	0.188	0.007	0.772	0.211	0.011	1849	58	1105	37	2805	80	813	2520	13010	3.10	39	60
CMG01-349.d	1.944	0.060	0.188	0.006	0.866	0.075	0.001	1090	21	1108	33	1048	37	1121	70.42	362	0.06	106	102
CMG01-350.d	15.750	0.430	0.553	0.017	0.722	0.206	0.004	2856	26	2832	70	2867	30	316	269.6	3629	0.85	99	99
CMG01-351.d	5.054	0.130	0.332	0.010	0.392	0.110	0.002	1826	22	1848	46	1795	36	246.4	125.3	1087	0.51	103	101
CMG01-352.d	4.990	0.150	0.328	0.010	0.744	0.110	0.002	1814	25	1827	49	1788	37	154	55.3	489	0.36	102	101
CMG01-353.d	1.596	0.043	0.163	0.005	0.629	0.071	0.001	967	17	972	26	939	41	689	98	446	0.14	104	101
CMG01-354.d	2.189	0.110	0.150	0.006	0.920	0.105	0.003	1162	35	901	35	1689	47	1752	612	3850	0.35	53	78

Analysis #	Ratios							Ages						Concentrations (ppm)			Th:U	Concordance Calculations	
	$^{207}Pb/^{235}U$	2σ	$^{206}Pb/^{238}U$	2σ	Rho	$^{207}Pb/^{206}Pb$	2σ	$^{207}Pb/^{235}U$ Age	2σ	Pb^{206}/U^{238} Age	2σ	$^{207}Pb/^{206}Pb$ Age	2σ	U	Th	Pb		$(^{206}Pb/^{238}U$ age)/ $^{207}Pb/^{206}Pb$ age)	$(^{206}Pb/^{238}U$ age)/ $^{207}Pb/^{235}U$ age)
CMG01-355.d	1.108	0.029	0.124	0.004	0.505	0.064	0.001	755.8	14	755.7	20	746	43	801.2	581.2	2028	0.73	101	100
CMG01-356.d	1.657	0.048	0.169	0.005	0.483	0.071	0.002	989	18	1006	28	948	48	251.2	107.3	499	0.43	106	102
CMG01-357.d	1.668	0.046	0.163	0.005	0.332	0.074	0.002	993	18	970	26	1028	46	253.1	115.8	524	0.46	94	98
CMG01-358.d	2.208	0.077	0.200	0.007	0.739	0.079	0.002	1174	25	1175	36	1169	42	396	215.1	1030	0.54	101	100
CMG01-359.d	1.803	0.047	0.175	0.005	0.362	0.074	0.002	1044	17	1041	27	1042	43	441.5	171.6	838	0.39	100	100
CMG01-360.d	1.798	0.046	0.172	0.005	0.641	0.075	0.001	1043.1	17	1025	27	1072	37	706	229.9	1112	0.33	96	98
CMG01-366.d	0.865	0.023	0.103	0.003	0.458	0.061	0.001	632	12	**629.1**	**17**	631	46	821	522.7	1490	0.64	100	100
CMG01-367.d	0.867	0.023	0.102	0.003	0.372	0.062	0.001	634.2	13	**628.5**	**17**	642	47	803	505	1444	0.63	98	99
CMG01-368.d	1.807	0.045	0.173	0.005	0.639	0.075	0.001	1047.2	16	1029.9	27	1070	36	1518	506	2348	0.33	96	98
CMG01-369.d	1.955	0.055	0.183	0.005	0.372	0.077	0.002	1096	19	1085	29	1101	46	257.9	104.7	521	0.41	99	99
CMG01-370.d	2.167	0.065	0.198	0.006	0.590	0.080	0.002	1167	21	1161	34	1165	49	246.5	183.6	1013	0.74	100	99
CMG01-371.d	0.967	0.028	0.111	0.004	0.652	0.063	0.001	685.3	14	679	20	686	47	1110	337.2	1093	0.30	99	99
CMG01-372.d	0.977	0.028	0.112	0.003	0.376	0.063	0.002	690.8	14	685.6	20	696	52	595.7	224.6	643	0.38	99	99
CMG01-373.d	1.388	0.039	0.147	0.005	0.751	0.069	0.001	881	17	881	26	875	40	1622	589	2390	0.36	101	100
CMG01-374.d	1.513	0.045	0.154	0.005	0.332	0.071	0.002	931	18	925	25	931	52	206.5	98.1	418	0.48	99	99
CMG01-375.d	1.807	0.050	0.176	0.005	0.442	0.074	0.002	1046	18	1046	27	1026	45	332.5	40.58	193.1	0.12	102	100
CMG01-376.d	1.875	0.051	0.174	0.005	0.294	0.078	0.002	1069	18	1036	27	1121	45	366	51.9	218	0.14	92	97
CMG01-377.d	12.390	0.300	0.487	0.014	0.376	0.184	0.004	2631	23	2553	62	2686	33	116.5	158.3	1590	1.36	95	97
CMG01-383.d	1.302	0.034	0.141	0.004	0.465	0.067	0.001	844.7	15	851.5	23	816	42	970	142.1	564	0.15	104	101
CMG01-385.d	3.235	0.083	0.257	0.007	0.409	0.091	0.002	1464	20	1475	37	1439	38	210.5	99.2	664	0.47	103	101
CMG01-386.d	1.348	0.034	0.138	0.004	0.680	0.071	0.001	865.3	15	832.8	22	944	36	2621	726	3264	0.28	88	96
CMG01-387.d	7.451	0.180	0.390	0.011	0.657	0.138	0.002	2164	22	2123	52	2196	30	465	183.7	1822	0.40	97	98
CMG01-388.d	1.963	0.053	0.186	0.005	0.087	0.076	0.002	1100	18	1100	29	1090	42	345.4	59.9	304	0.17	101	100
CMG01-389.d	1.861	0.046	0.179	0.005	0.452	0.075	0.001	1066.3	17	1059	28	1066	38	709	362.3	1745	0.51	99	99

Supplementary Table 1 (continued). Main isotopes and ratios measured using LA–ICP–MS

Analysis #	Ratios							Ages						Concentrations (ppm)			Th:U	Concordance Calculations	
	$^{207}Pb/^{235}U$	2σ	$^{206}Pb/^{238}U$	2σ	Rho	$^{207}Pb/^{206}Pb$	2σ	$^{207}Pb/^{235}U$ Age	2σ	Pb^{206}/U^{238} Age	2σ	$^{207}Pb/^{206}Pb$ Age	2σ	U	Th	Pb		($^{206}Pb/^{238}U$ age)/ $^{207}Pb/^{206}Pb$ age)	($^{206}Pb/^{238}U$ age)/ $^{207}Pb/^{206}Pb$ age)
CMG01-390.d	1.668	0.043	0.163	0.005	0.495	0.074	0.001	994.4	16	975.4	25	1030	38	809	418.8	1912	0.52	95	98
CMG01-391.d	2.857	0.120	0.217	0.010	0.909	0.097	0.002	1353	34	1255	57	1554	44	1280	390	2450	0.30	81	93
CMG01-392.d	3.279	0.079	0.258	0.007	0.480	0.092	0.002	1474	19	1481	37	1453	34	633	254.2	1713	0.40	102	100
CMG01-393.d	1.894	0.045	0.182	0.005	0.607	0.075	0.001	1077.6	16	1077.2	27	1066	35	1471	168.7	640	0.11	101	100
CMG01-394.d	1.449	0.038	0.151	0.004	0.305	0.069	0.002	908.1	16	904.9	24	895	48	585	194.9	749	0.33	101	100
CMG01-395.d	1.498	0.037	0.155	0.004	0.487	0.070	0.001	928.7	15	927.2	24	924	38	1182	137	548	0.12	100	100
CMG01-402.d	0.842	0.031	0.101	0.003	0.275	0.061	0.002	617	17	**618.3**	**18**	571	72	185.2	181	509	0.98	108	100
CMG01-403.d	1.649	0.049	0.169	0.005	0.465	0.071	0.002	985	19	1003	27	932	49	262.9	96.1	447	0.37	108	102
CMG01-404.d	1.608	0.042	0.158	0.005	0.623	0.074	0.001	970.8	17	946	26	1018	40	1069	125.3	297	0.12	93	97
CMG01-405.d	5.050	0.200	0.275	0.010	0.933	0.131	0.003	1808	34	1562	50	2108	36	1007	94.7	712	0.09	74	86
CMG01-406.d	1.696	0.043	0.168	0.005	0.427	0.073	0.002	1006.8	16	1002	27	997	42	639	259.8	1185	0.41	101	100
CMG01-407.d	0.791	0.021	0.094	0.003	0.497	0.061	0.001	591.2	12	581.2	16	618	43	1845	518	1327	0.28	94	98
CMG01-408.d	1.728	0.043	0.172	0.005	0.418	0.073	0.001	1017.9	16	1024	27	997	40	775	203.9	908	0.26	103	101
CMG01-409.d	2.066	0.065	0.180	0.005	0.469	0.084	0.002	1134	22	1063	29	1258	49	203.8	210.5	1037	1.03	84	94
CMG01-410.d	1.663	0.045	0.166	0.005	0.411	0.072	0.002	991	17	991	27	980	43	466.5	219	1023	0.47	101	100
CMG01-411.d	2.160	0.059	0.173	0.005	0.593	0.090	0.002	1164	19	1028	28	1418	40	589.8	548	2468	0.93	72	88
CMG01-412.d	1.351	0.040	0.136	0.004	0.490	0.072	0.002	865	17	821	23	992	46	1723	664	1630	0.39	83	95
CMG01-413.d	1.570	0.046	0.157	0.005	0.398	0.073	0.002	956	18	938	26	979	49	285.3	138.9	618	0.49	96	98
CMG01-414.d	1.458	0.046	0.150	0.005	0.280	0.070	0.002	908	19	900	25	914	57	187.5	103.1	422	0.55	98	99
CMG01-415.d	4.500	0.120	0.303	0.009	0.699	0.108	0.002	1728	21	1704	44	1750	34	513	466	3680	0.91	97	99
CMG01-421.d	0.869	0.025	0.103	0.003	0.330	0.061	0.002	632.9	14	**630.3**	**17**	620	52	424	227.1	647	0.54	102	100
CMG01-422.d	1.908	0.057	0.181	0.005	0.291	0.076	0.002	1079	20	1073	29	1068	51	174.6	99.8	481	0.57	100	99
CMG01-423.d	1.527	0.038	0.146	0.004	0.712	0.076	0.001	940.5	16	875	24	1082	36	2232	1109	3820	0.50	81	93

Analysis #	Ratios							Ages						Concentrations (ppm)			Th:U	Concordance Calculations	
	$^{207}Pb/^{235}U$	2σ	$^{206}Pb/^{238}U$	2σ	Rho	$^{207}Pb/^{206}Pb$	2σ	$^{207}Pb/^{235}U$ Age	2σ	Pb^{206}/U^{238} Age	2σ	$^{207}Pb/^{206}Pb$ Age	2σ	U	Th	Pb		($^{206}Pb/^{238}U$ age)/ $^{207}Pb/^{206}Pb$ age)	($^{206}Pb/^{238}U$ age)/ $^{207}Pb/^{206}Pb$ age)
CMG01-424.d	1.879	0.051	0.178	0.005	0.750	0.076	0.001	1071	18	1054	29	1094	36	1414	259	740	0.18	96	98
CMG01-425.d	3.754	0.120	0.274	0.008	0.711	0.099	0.002	1576	25	1557	43	1590	42	242.5	22.62	205	0.09	98	99
CMG02-426.d	6.935	0.170	0.377	0.011	0.647	0.133	0.002	2100	22	2060	51	2137	31	894	510	4850	0.57	96	98
CMG02-428.d	1.854	0.053	0.144	0.005	0.693	0.094	0.003	1062	19	867	31	1475	49	1600	571	3370	0.36	59	82
CMG02-429.d	12.670	0.300	0.494	0.014	0.682	0.186	0.003	2652.9	22	2584	60	2699	27	2179	1452	18060	0.67	96	97
CMG02-430.d	5.360	0.170	0.322	0.010	0.922	0.120	0.002	1871	28	1797	49	1952	30	1472	202.1	1739	0.14	92	96
CMG02-431.d	1.642	0.044	0.164	0.005	0.450	0.073	0.002	985	17	976	26	1001	41	409.4	225.9	1007	0.55	98	99
CMG02-432.d	1.758	0.060	0.173	0.005	0.292	0.074	0.002	1024	22	1029	28	992	62	110.9	123.3	581	1.11	104	100
CMG02-433.d	3.355	0.090	0.244	0.007	0.720	0.099	0.002	1490	21	1406	37	1606	33	561.3	215.9	1444	0.38	88	94
CMG02-434.d	2.462	0.062	0.200	0.006	0.356	0.089	0.002	1258.6	18	1173.3	30	1398	37	572	184.1	1063	0.32	84	93
CMG02-440.d	2.039	0.069	0.183	0.005	0.174	0.081	0.003	1122	23	1085	30	1168	62	119.6	86.7	451	0.72	93	97
CMG02-441.d	1.803	0.045	0.173	0.005	0.453	0.075	0.002	1044.5	16	1028	27	1071	40	640.4	502	2410	0.78	96	98
CMG02-442.d	0.861	0.023	0.103	0.003	0.334	0.061	0.001	629.4	12	**629.6**	**17**	616	46	767	371	1136	0.48	102	100
CMG02-443.d	1.843	0.054	0.171	0.005	0.424	0.079	0.002	1061	19	1015	28	1137	50	245	142.3	724	0.58	89	96
CMG02-444.d	1.386	0.069	0.102	0.004	0.568	0.095	0.004	866	28	628	22	1495	66	1554	1132	2860	0.73	42	73
CMG02-445.d	1.434	0.045	0.133	0.004	0.217	0.078	0.002	898	18	805.7	22	1111	46	894	193.5	845	0.22	73	90
CMG02-446.d	1.653	0.062	0.142	0.005	0.538	0.083	0.002	986	24	854	28	1260	53	1055	1137	3120	1.08	68	87
CMG02-447.d	1.671	0.054	0.164	0.005	0.693	0.074	0.002	991	21	977	30	1028	45	566	175.7	841	0.31	95	99
CMG02-448.d	1.621	0.049	0.155	0.005	0.415	0.076	0.002	975	19	927	26	1066	51	220.3	113.5	498	0.52	87	95
CMG02-450.d	1.897	0.058	0.181	0.006	0.623	0.076	0.002	1075	21	1072	31	1083	46	298	123.1	600	0.41	99	100
CMG02-451.d	1.873	0.060	0.168	0.005	0.385	0.080	0.002	1065	21	1001	27	1182	50	212.6	110.7	557	0.52	85	94
CMG02-452.d	1.692	0.054	0.164	0.005	0.482	0.075	0.002	1000	20	979	30	1041	55	232	161.1	756	0.69	94	98
CMG02-453.d	1.933	0.051	0.181	0.005	0.345	0.078	0.002	1090	17	1070	28	1121	41	519	98.4	476	0.19	95	98
CMG02-459.d	1.575	0.043	0.158	0.005	0.713	0.072	0.001	958	17	947	27	972	39	1492	368	1593	0.25	97	99

Supplementary Table 1 (continued). Main isotopes and ratios measured using LA–ICP–MS

Analysis #	Ratios							Ages						Concentrations (ppm)			Th:U	Concordance Calculations	
	$^{207}Pb/^{235}U$	2σ	$^{206}Pb/^{238}U$	2σ	Rho	$^{207}Pb/^{206}Pb$	2σ	$^{207}Pb/^{235}U$ Age	2σ	Pb^{206}/U^{238} Age	2σ	$^{207}Pb/^{206}Pb$ Age	2σ	U	Th	Pb		($^{206}Pb/^{238}U$ age)/ $^{207}Pb/^{206}Pb$ age)	($^{206}Pb/^{238}U$ age)/ $^{207}Pb/^{206}Pb$ age)
CMG02-460.d	1.612	0.055	0.162	0.005	0.222	0.073	0.002	970	22	968	27	969	65	117.2	95.2	425	0.81	100	100
CMG02-461.d	1.498	0.043	0.139	0.004	0.277	0.078	0.002	927	17	837.9	22	1128	51	1787	915	4030	0.51	74	90
CMG02-462.d	0.949	0.024	0.108	0.003	0.451	0.063	0.001	676.4	12	660.3	18	711	43	1272	370	1089	0.29	93	98
CMG02-463.d	1.799	0.043	0.173	0.005	0.523	0.075	0.001	1043.7	16	1030.3	27	1064	37	998	657	3120	0.66	97	99
CMG02-464.d	0.953	0.027	0.111	0.003	0.389	0.062	0.001	677.3	14	675.3	18	667	51	512	123.1	372	0.24	101	100
CMG04-465.d	0.917	0.026	0.108	0.003	0.276	0.062	0.002	659.5	14	660.3	18	646	50	513	90.9	278.3	0.18	102	100
CMG04-466.d	1.580	0.040	0.157	0.005	0.363	0.073	0.002	960.2	16	939	25	991	44	684	332.7	1492	0.49	95	98
CMG04-467.d	1.100	0.049	0.123	0.005	0.677	0.064	0.002	743	23	748	26	710	50	900	270	1080	0.30	105	101
CMG04-468.d	1.450	0.042	0.149	0.004	0.393	0.071	0.002	906	18	897	24	921	51	319.3	119.9	490	0.38	97	99
CMG04-469.d	2.680	0.082	0.163	0.005	0.238	0.119	0.003	1321	24	974.9	26	1916	48	202.1	102	611	0.50	51	74
CMG04-470.d	1.988	0.058	0.189	0.006	0.231	0.076	0.002	1107	19	1117	31	1070	51	228.9	113.8	589	0.50	104	101
CMG04-476.d	2.009	0.057	0.187	0.005	0.360	0.078	0.002	1116	19	1106	29	1120	47	232.4	259.4	1266	1.12	99	99
CMG04-477.d	1.924	0.067	0.187	0.006	0.075	0.075	0.002	1081	23	1103	31	1021	65	97.7	89.2	445	0.91	108	102
CMG04-478.d	2.390	0.160	0.189	0.006	0.587	0.092	0.005	1203	36	1116	34	1401	92	268.1	106.1	731	0.40	80	93
CMG04-479.d	1.620	0.047	0.162	0.005	0.481	0.073	0.002	978	17	967	27	988	47	277	315.6	1375	1.14	98	99
CMG04-480.d	3.794	0.100	0.269	0.008	0.734	0.102	0.002	1587	21	1532	42	1656	34	975	152.2	893	0.16	93	97
CMG04-481.d	1.408	0.042	0.145	0.005	0.545	0.070	0.002	888	18	873	26	914	50	310	81.1	282	0.26	96	98

Yellow shaded data used for individual sample YC1σ and YSG, data in **bold** used for combined Chaung Magyi Group YC1σ weighted average.

APPENDIX VI

Supplementary material for Chapter 6

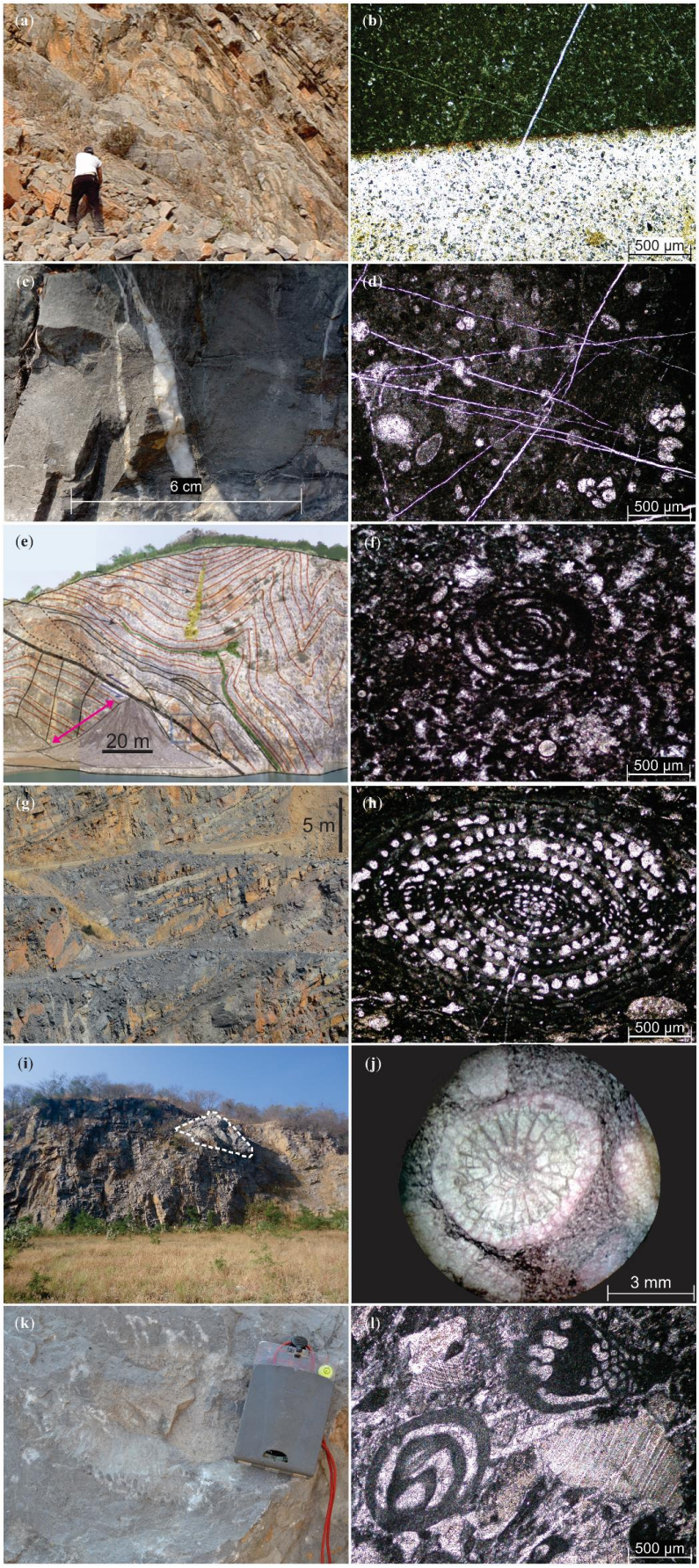
(a)
(b)
500 µm
(c)
6 cm
(d)
500 µm
(e)
20 m
(f)
500 µm
(g)
5 m
(h)
500 µm
(i)
(j)
3 mm
(k)
(l)
500 µm

Supplementary Fig. 1 Characteristic outcrop images and photomicrographs of the six main facies identified (**a**) Outcrop image from Quarry N where the peritidal facies facies were described; (**b**) Photomicrograph from RDT14_057 (Log 4, Quarry SS) illustrating characteristics of the peritidal facies; (**c**) Outcrop image from the location of Log 6 (Quarry ZZ) where lagoonal facies were described; (**d**) Photomicrograph from RDT14_056 (Log 4, Quarry SS) illustrating characteristics of the lagoonal facies; (**e**) Outcrop image from the location of Log 2 indicated by the pink arrow (Quarry B) where outer platform facies were described; (**f**) Photomicrograph from RDT14_046 (Log 2, Quarry B) illustrating characteristics of the lagoonal facies; (**g**) Outcrop image from the location of Log 8 (Quarry FF) where backreef facies were described; (**f**) Photomicrograph from RDT14_023 (Log 8, Quarry FF) illustrating characteristics of the backreef facies; (**i**) Outcrop image from Quarry FF where reef facies were observed; (**j**) Photomicrograph from RDT14_005 (isolated coral clump in a life assemblage, Log 5, Quarry Y) illustrating characteristics of the reef facies; (**k**) Outcrop image from the location of Log 3 (Quarry O) where basinal slope facies were described; (**l**) Photomicrograph from RDT14_018 (allodapic debris flow, Log 3, Quarry O) illustrating characteristics of the basinal slope facies.

Supplementary Fig. 2 Detailed stratigraphic logs with faunal abundances observed from photomicrographs

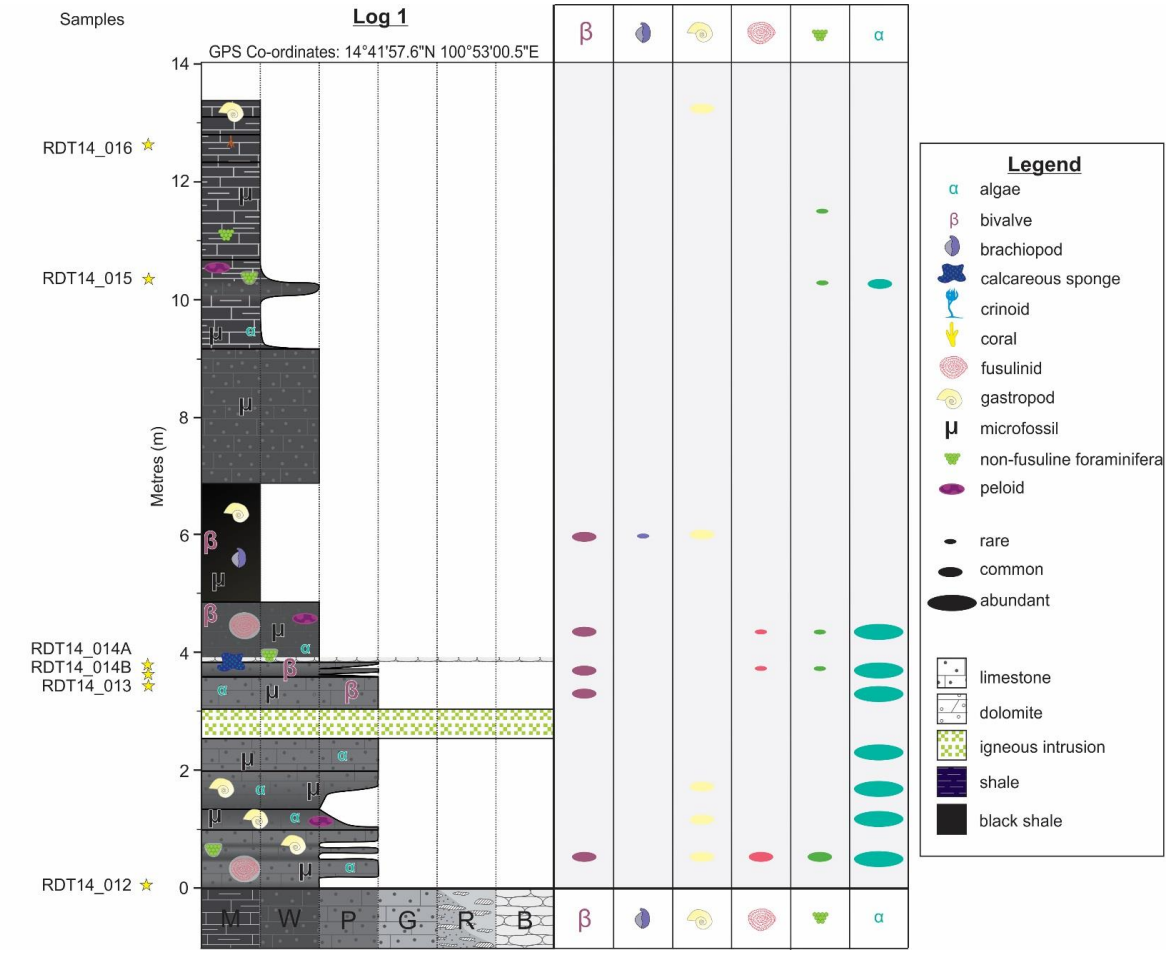

Stratigraphic Log 1: Highway 21 - Quarry A Khao Yai Hill incorporating both macrofacies and microfacies analyses. Where M is Mudstone, W is Wackestone, P is Packstone, G is Grainstone, R is Rudstone and B is Boundstone.

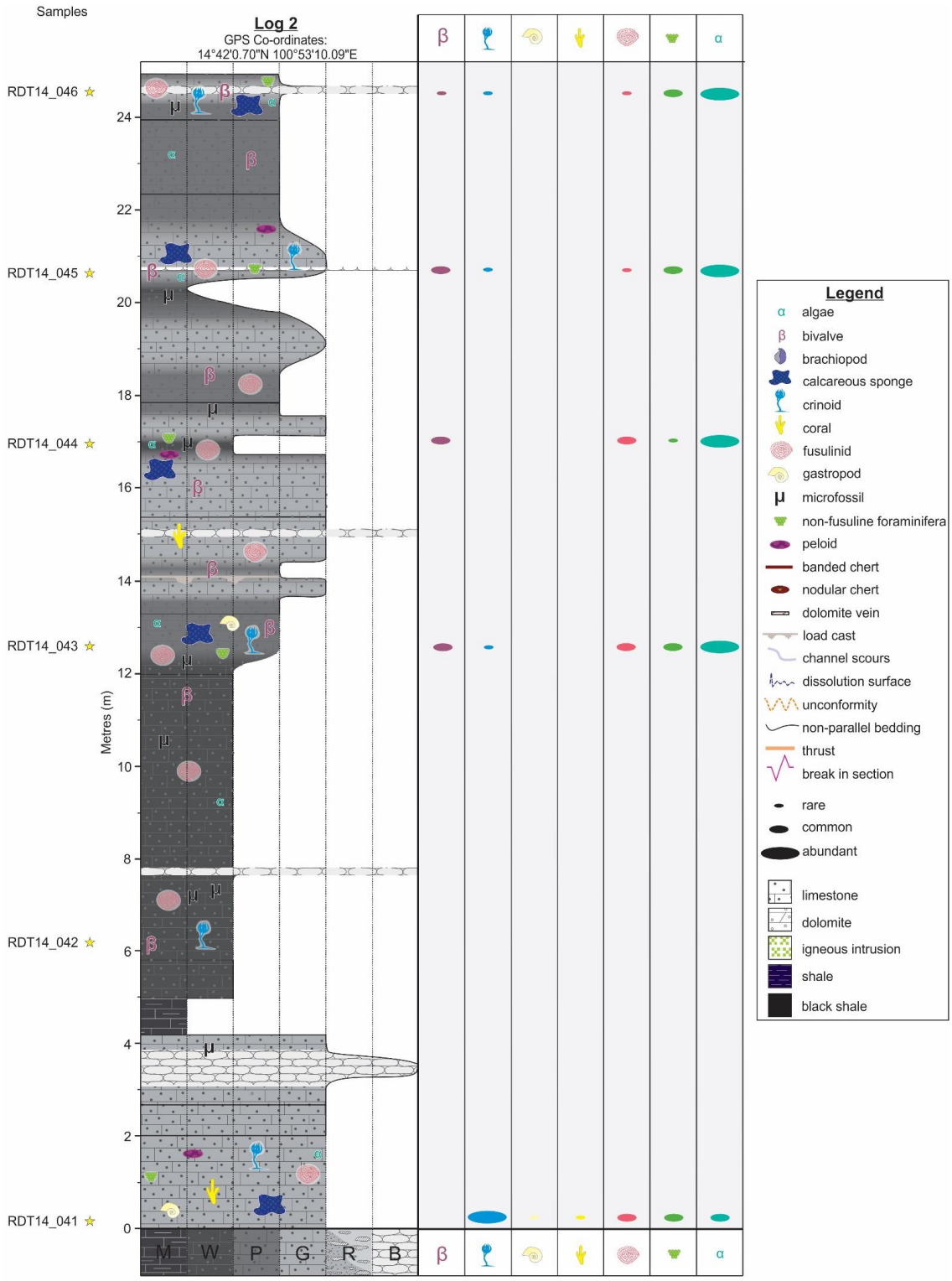

Stratigraphic Log 2: Highway 21 - Quarry B, the Khao Yai Detachment Fold region incorporating both macrofacies and microfacies analyses. Where M is Mudstone, W is Wackestone, P is Packstone, G is Grainstone, R is Rudstone and B is Boundstone.

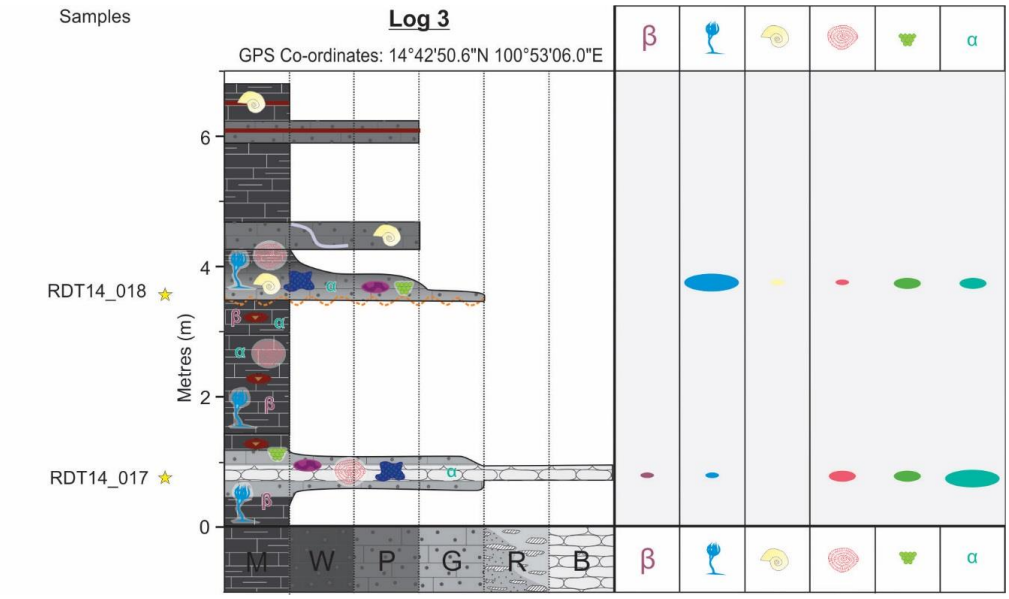

Stratigraphic Log 3: Highway 21 - Quarry O region incorporating both macrofacies and microfacies analyses. Where M is Mudstone, W is Wackestone, P is Packstone, G is Grainstone, R is Rudstone and B is Boundstone.

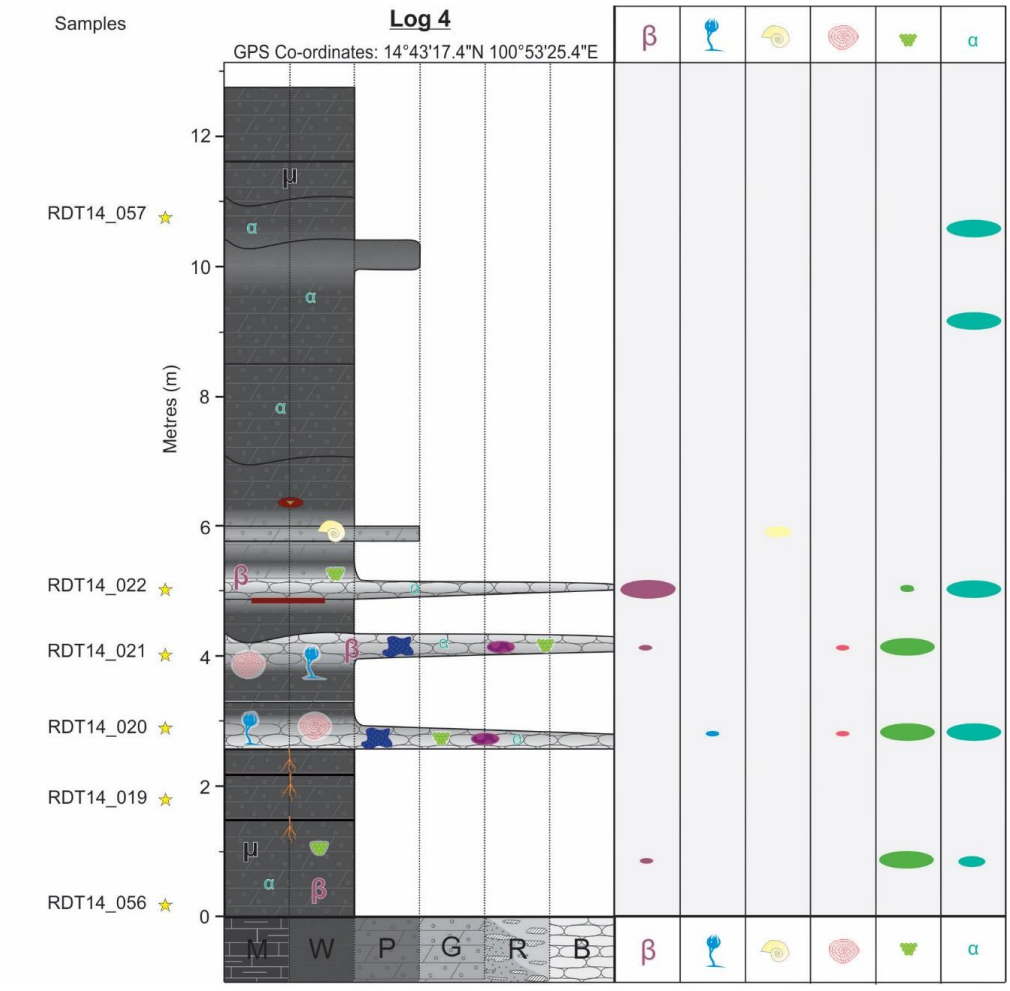

Stratigraphic Log 4: Highway 21 - Quarry SS region incorporating both macrofacies and microfacies analyses. Where M is Mudstone, W is Wackestone, P is Packstone, G is Grainstone, R is Rudstone and B is Boundstone.

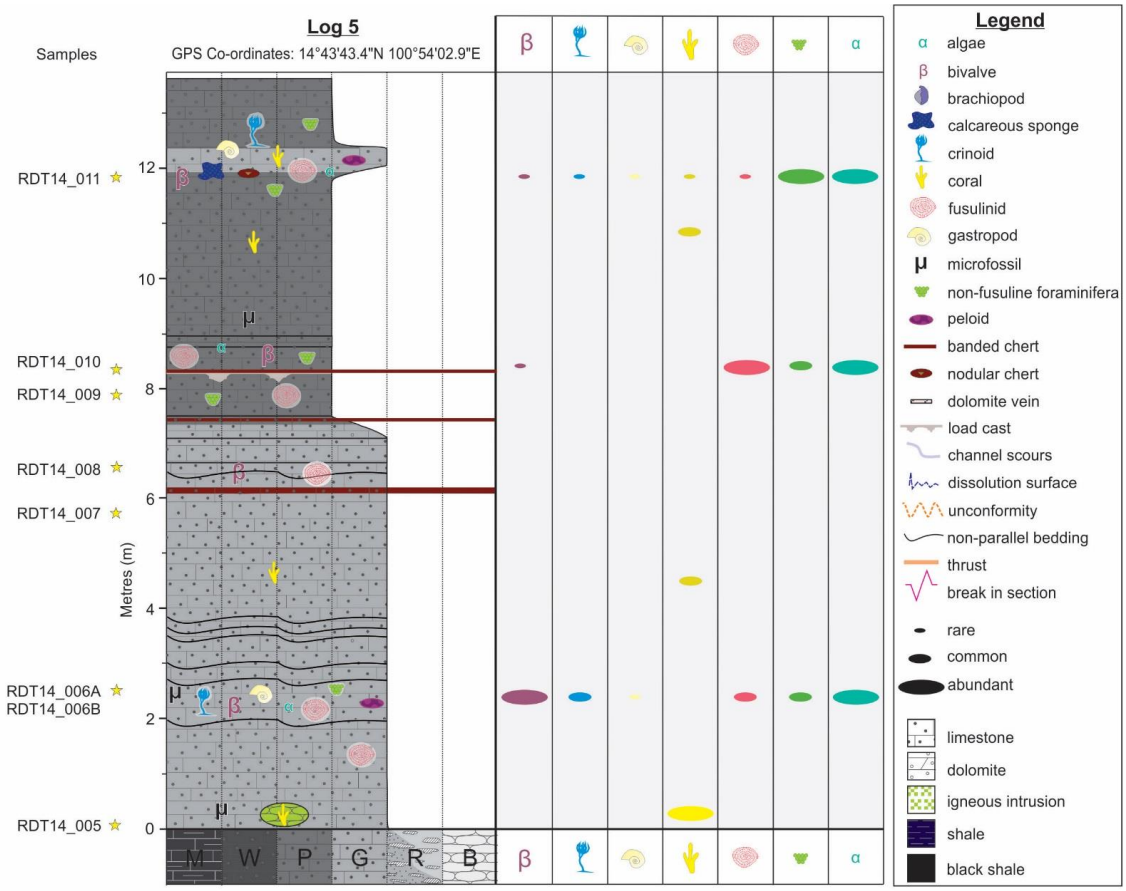

Stratigraphic Log 5: Highway 21 - Quarry Y, the *Synform* region incorporating both macrofacies and microfacies analyses. Where M is Mudstone, W is Wackestone, P is Packstone, G is Grainstone, R is Rudstone and B is Boundstone.

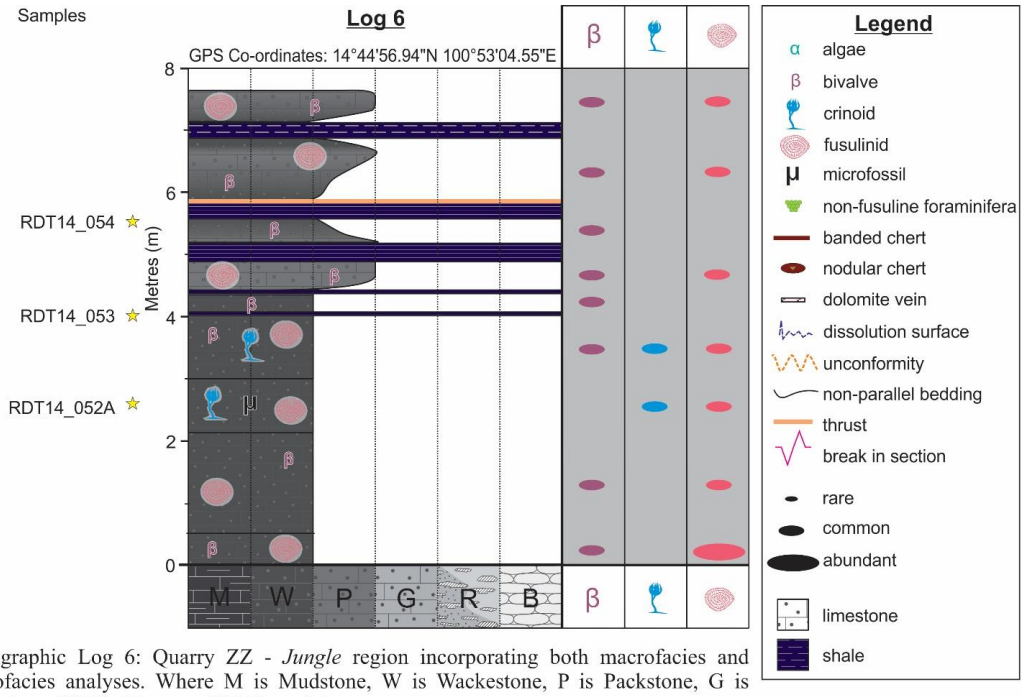

Stratigraphic Log 6: Quarry ZZ - *Jungle* region incorporating both macrofacies and microfacies analyses. Where M is Mudstone, W is Wackestone, P is Packstone, G is Grainstone, R is Rudstone and B is Boundstone.

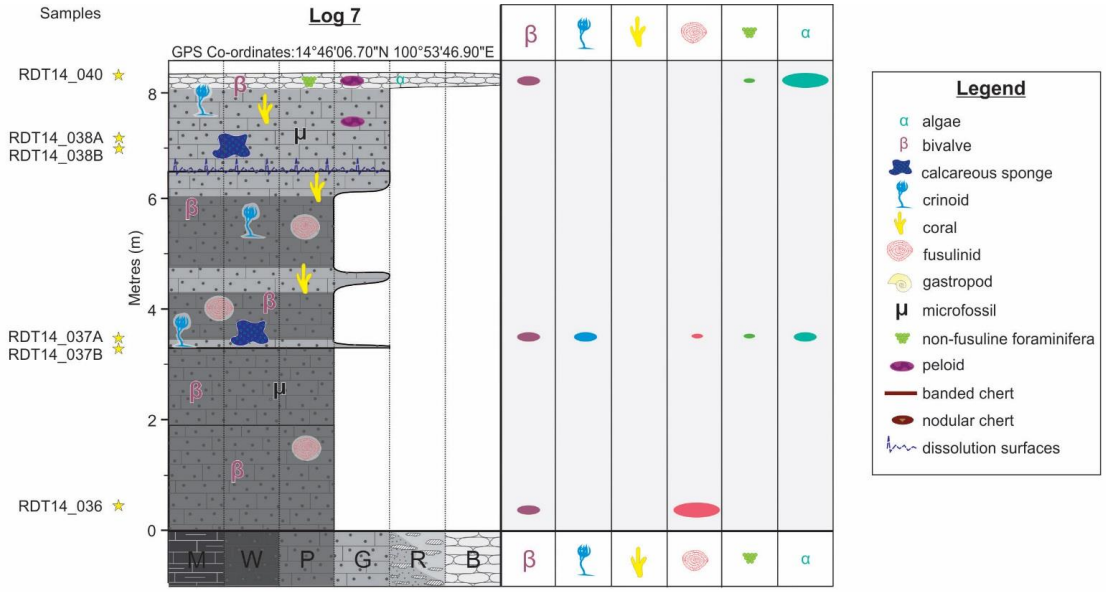

Stratigraphic Log 7: Quarry FF Above the Thrust region incorporating both macrofacies and microfacies analyses. Scale is in metres, where M=Mudstone, W is Wackestone, P is Packstone, G is Grainstone, R is Rudstone, B is Boundstone.

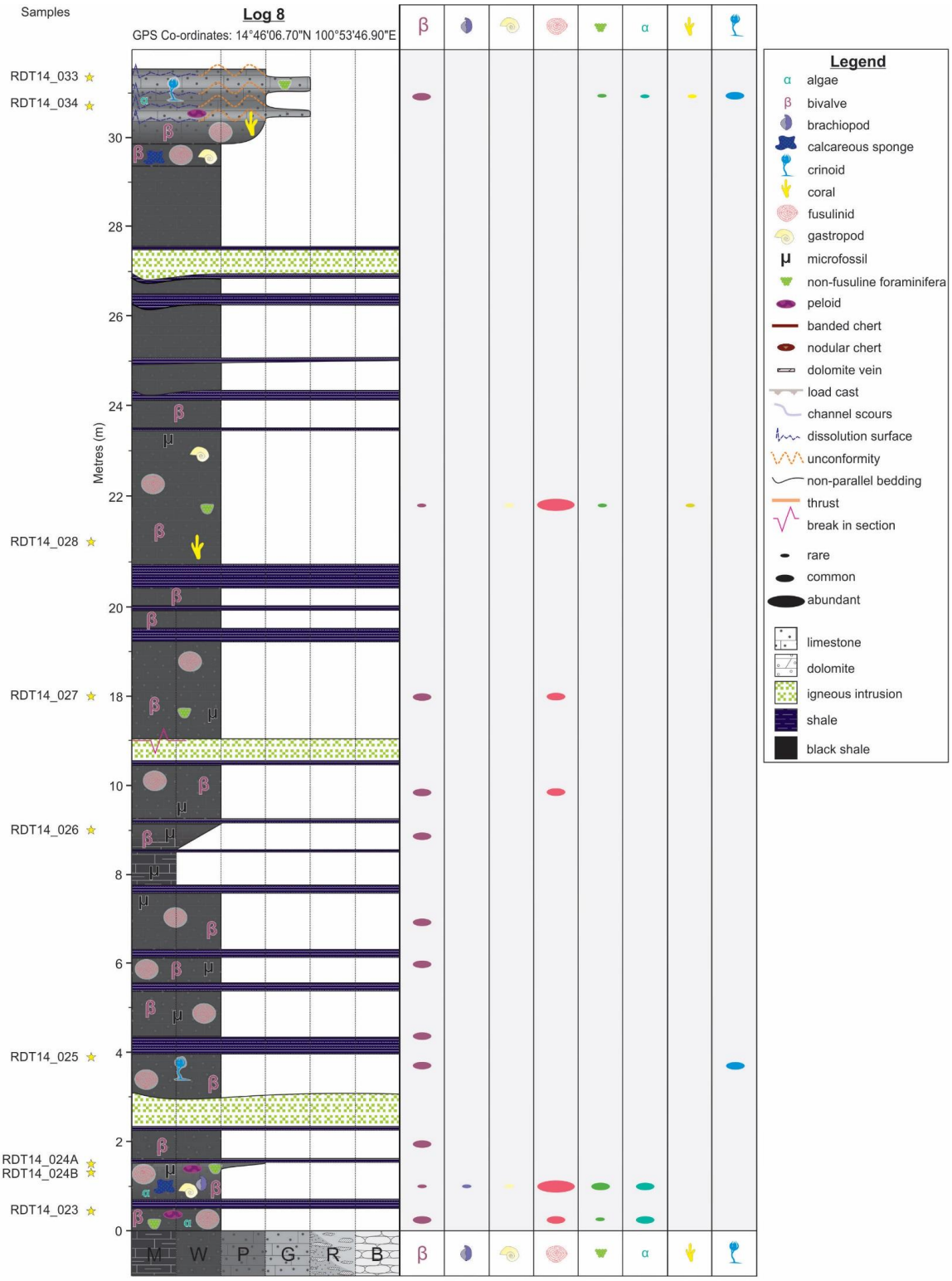

Stratigraphic Log 8: the Quarry FF Below the Thrust region incorporating both macrofacies and microfacies analyses. Scale is in metres, where M=Mudstone, W is Wackestone, P is Packstone, G is Grainstone, R is Rudstone, B is Boundstone.

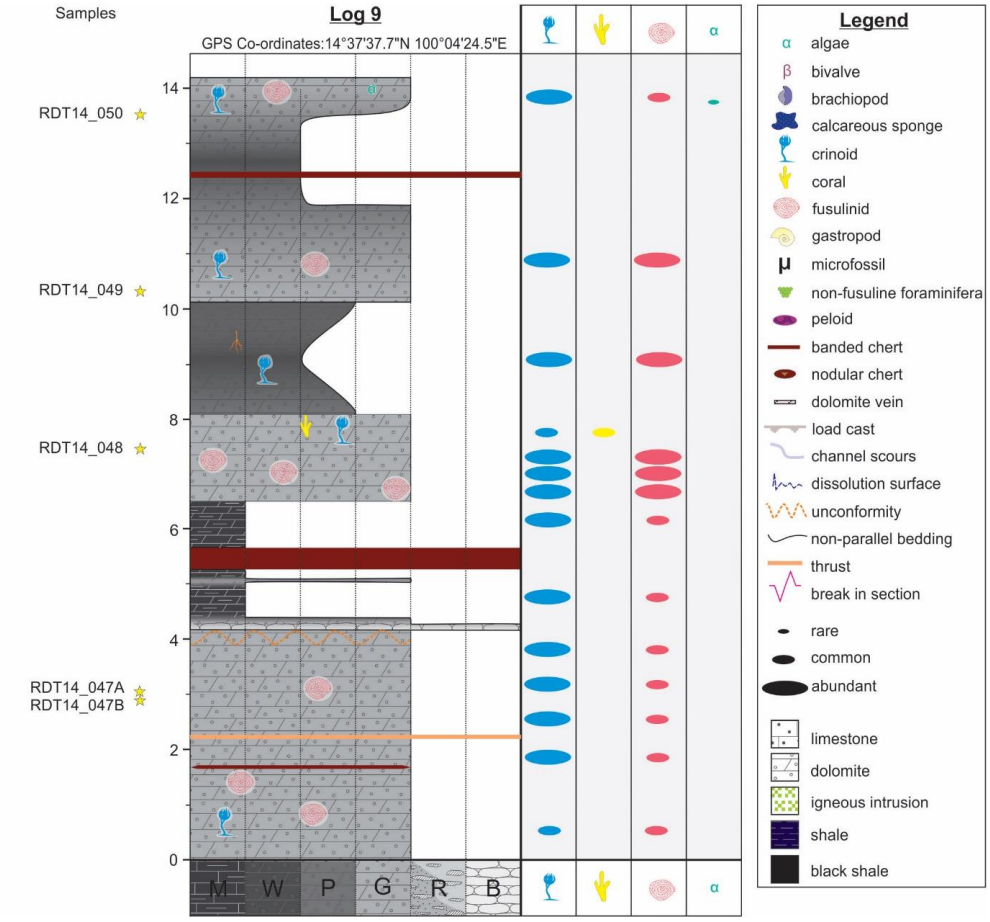

Stratigraphic Log 9: Siam City Cement - *The Trees Ridge* region incorporating both macrofacies and microfacies analyses. Scale is in metres, M is Mudstone, W is Wackestone, P is Packstone, G is Grainstone, R is Rudstone and B is Boundstone

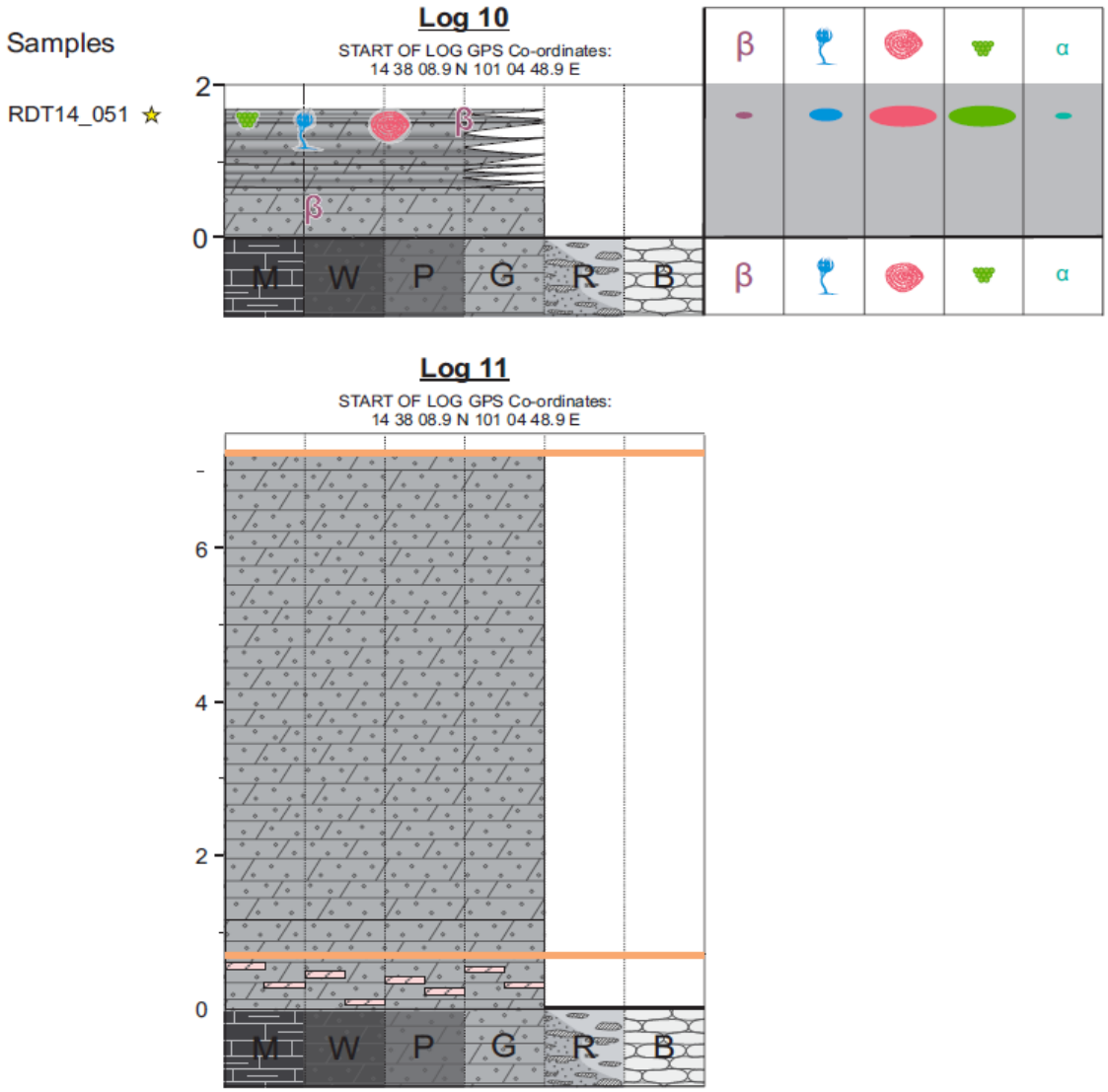

Stratigraphic Logs 11 and 12: the Siam City Cement Middle Ridge regions incorporating both macrofacies and microfacies analyses. M=Mudstone, W=Wackestone, P=Packstone, G=Grainstone, R=Rudstone, B=Boundstone

\

Supplementary Fig. 3 Correlation between the International Permian Timeline and the Tethyan Scale used in this study, dates are determined by the first appearance datum of fossils, Fusulinaceans not to scale, images taken from BouDagher-Fadel (2008); Dawson (1993); Hornibrook (1950); Kobayashi *et al.* (2010); Leven (2003); Toriyama (1975).

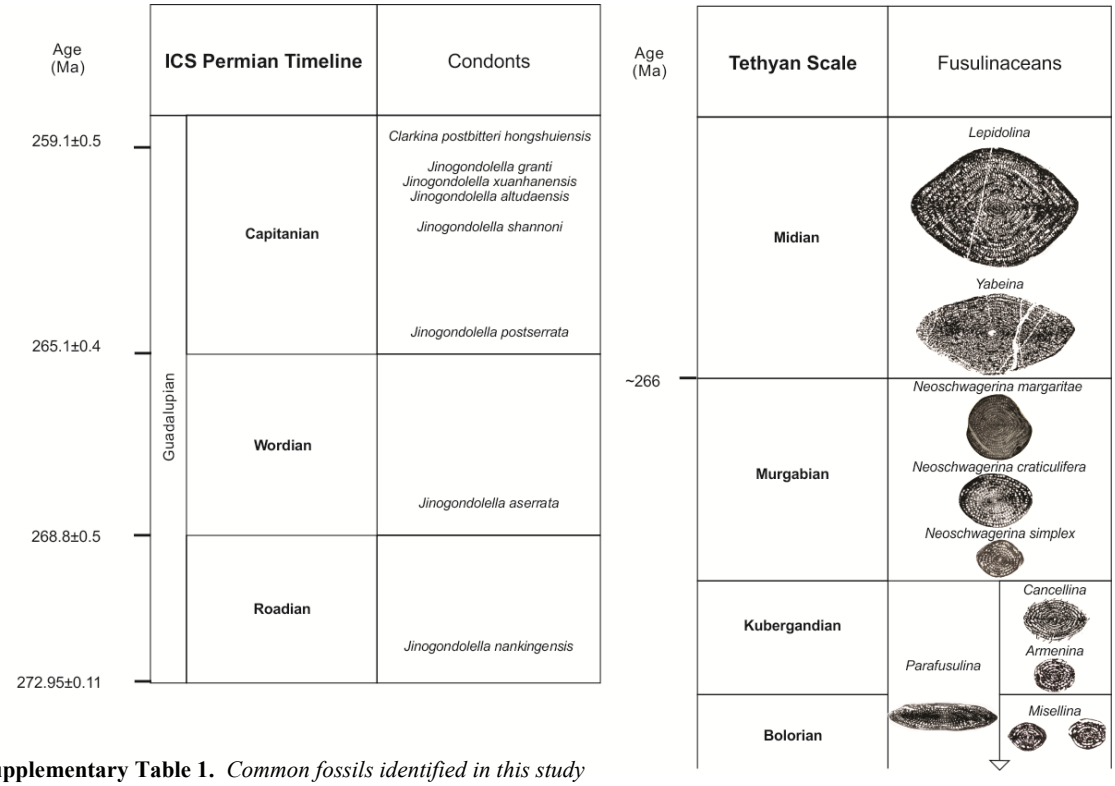

Supplementary Table 1. *Common fossils identified in this study*
Information collated from observations, Beavington-Penney and Racey (2004); Dawson and Racey (1993); Flügel (2010); Loeblich and Tappan (1964). Drawings of foraminifera from Jin-Zhang (1990)

Fossils Identified		Age Range	Description	Presence	Species examples	Used to constrain age
Fusulinids	*Neoschwagerinidae* 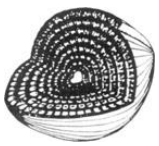	272.5 to 254.0 Ma	Largest fusulinids, generally increasing in diameter through the Permian, thick walls that are coated or encrusted with algae	Logs 2, 3, 4, 5 and 8	*Neoschwagerina sp.* *Gifuella sp.*	X X
	Verbeekinidae	Murgabian	~1 mm-500 µm, dark brown to black test walls and usually light coloured chambers	Log 2	*Kahlerina sp.* *Armenina sp.*	X X

Supplementary Table 1. *Common fossils identified in this study*
Information collated from observations, Beavington-Penney and Racey (2004); Dawson and Racey (1993); Flügel (2010); Loeblich and Tappan (1964). Drawings of foraminifera from Jin-Zhang (1990)

	Schwagerinidae	303.4 to 254.0 Ma	Few mm, light grey test walls and the light coloured chamber interiors	Logs 5, 7, 8, 9, 10	*Parafusulina sp.* *Schwagerina sp.* *Chalaroschwagerina sp.*	X X X
	Schubertellidae	314.6 to 252.3 Ma	Small elongate elliptical fusulinids with dark walls and usually light coloured chambers	Logs 1, 2 and 3	*Schubertella sp.* *Neofusulinella sp.* *Toriyamaia sp.*	*X* *X*
	Staffellidae	314.6 to 251.3 Ma	Small elongate elliptical fusulinids, relatively lighter test walls and chambers compared to the other fusulinids	Logs 2, 4, 5 and 8	*Nankinella sp.*	*X*
Non-fusuline foraminifera	"Rose" Group	varies	500-200 µm rosebud shaped non-fusuline foraminifera	Logs 3, 4 and 7	*Miliolida, Baisalina* and *Hemigordius sp.*	
	Globivalvulina	336.0 to 251.3 Ma	100-500µm popcorn-like non-fusuline foraminifera	Log 4	*Globivalvulina cyprica*	
	Textulariidae	326.4 to 0.0 Ma	Two spirals forming into one spiral non-fusuline foraminifera	Log 4	*Textularia sp.*	
Algae	*Tubiphytes*	342.8 to 145.5 Ma	Irregularly cylindrical tube-like encrusting problematic algae	Logs 4, 5, 7, 10	*Tubiphytes sp.*	
	Dasycladaceae	471.8 to 11.608 Ma	Sponge-like ring structure, green algae	Logs 1, 2, 4 and 8	*Mizzia sp.* *Macroporella sp.*	
	Girvanella	542.0 to 5.332 Ma	Worm-like interwoven cluster, blue green algae	Logs 1 and 4	*Girvanella sp.*	
	Epimastopora	318.1 to 136.4 Ma	0.23-0.55mm thick porous green algae	Log 2	N/A	
	Archaeolithoporella	295.0 to 37.2 Ma	irregularly and complexly stacked lamellar layers, problematic algae	Log 7	*Archaeolithoporella sp.*	
	Phylloid	late Paleozoic	Poorly preserved, leaf-like growth, calcareous algae	Log 10	Hard to distinguish between in thin section	
	Udoteaceae	306.95 to 0.0 Ma	Multiple filaments form a thallus, green algae		Hard to distinguish between in thin section	

Supplementary Table 1. *Common fossils identified in this study*
Information collated from observations, Beavington-Penney and Racey (2004); Dawson and Racey (1993); Flügel (2010); Loeblich and Tappan (1964). Drawings of foraminifera from Jin-Zhang (1990)

	Gymnocodiacean	Permian to Cretaceous	Few mm wide, tubular internal skeleton, red algae	Log 5	Hard to distinguish between in thin section	
Crinoids		Ordovician – 0 Ma	Flowery when whole, cup-like,	Logs 2 to 11	Unidentifiable due to fragmentation	
Coral		Cambrian - 0.0 Ma	Highly variable in size, either as individual rugosans or in a dendroid colony	Logs 2, 5, 7, 8 and 9	*Waagenophyllum sp.*	
Gastropods		Cambrian - 0.0 Ma	Snail-like shell	Logs 1-8, 10	Unidentifiable due to fragmentation	
Bivalves		Cambrian - 0.0 Ma	Shells with two curved valves when whole. Mostly one valve preserved in thin section	Logs 1-8	Members of the *Alatoconchidae* family	

Stratigraphy of deformed Permian carbonate reefs in the Saraburi Province, Thailand

Thesis submitted in accordance with the requirements of the University of Adelaide for an Honours Degree in Geology

Romana Elysium Carthew Dew

November 2014

THE UNIVERSITY of ADELAIDE

Romana Dew
Stratigraphy of deformed Permian carbonate reefs, Thailand

TITLE

Stratigraphy of deformed Permian carbonate reefs in the Saraburi Province, Thailand

RUNNING TITLE

Stratigraphy of deformed Permian carbonate reefs, Thailand

ABSTRACT

The Indosinian Orogeny brought together a number of continental blocks and volcanic arcs during the Permian and Triassic periods. Prior to the orogeny, carbonate platforms and minor clastic sediments were deposited on the margins of these continental blocks. The Khao Khwang Platform formed along the southern margin of one continental fragment of the Indochina Block and was deformed in the early Triassic creating the Khao Khwang Fold-Thrust Belt.

The palaeogeography of the Indochina Block margin prior to this deformation is incompletely known, yet is significant in assisting with structural reconstructions of the area and in assisting with our understanding of the ecology of Permian fusulinid-dominated habitats. The sedimentology and stratigraphy of the Permian platform carbonates and basin complexes require further analysis. Three main carbonate platform dominated facies have been identified previously as the Phu Phe, Khao Khad and Khao Khwang formations. These platform facies are divided by clastic, mixed siliciclastic and carbonate sequences known as the Sap Bon, Pang Asok and Nong Pong formations.

Here, I present a stratigraphic model for the carbonate reefs and intervening clastic sedimentary rocks using the exposed well-developed sections in central Thailand. The model integrates fossil identification, biostratigraphic correlation and palaeoenvironmental analysis, in accordance with structural controls and fieldwork in the Saraburi Province, Thailand. Eleven sections were logged, encompassing units from three thrust sheets. The stratigraphic logs suggest five depositional environments for the middle Permian sequences, dated using foraminifera and algae. Characteristics of mass transport were identified indicating basinal facies receiving turbid debris flows. Furthermore, depositional texture variations indicated energy changes from peritidal, lagoonal through to reef environments. The palaeoenvironmental inferences and fossil identification allow section correlation and assist in unravelling the structure of this fold-thrust belt.

KEYWORDS

Permian biostratigraphy, carbonate stratigraphy, Khao Khwang Fold-Thrust Belt, Khao Khad Formation, carbonate platform, fusulinid.

Romana Dew
Stratigraphy of deformed Permian carbonate reefs, Thailand

LIST OF FIGURES

Figure 1: a) Location map portraying the regional stratigraphy, cross-section and field locations b) Stratigraphic log of the Khao Khwang Platform in the Saraburi Province c) Comparisons between the International Permian Timeline and the Tethyan Scale, dates are determined by the first appearance datum (FAD) of fossils highlighted; modified from Menning et al. (2006) Ueno and Charoentitirat (2011), Morley et al. (2013) and Shen et al. (2013).....5
Figure 2: Regional cross-section through the southern portion of the Saraburi Region, the Khao Khwang Fold-Thrust Belt with stratigraphic sections superimposed scale in metres, M=Mudstone, W=Wackestone, P=Packstone, G=Grainstone, R=Rudstone, B=Boundstone (modified Arboit et al. (in press)).....6
Figure 3: Diagram depicting the characteristics of the six depositional settings of carbonate platforms incorporating information from Wright and Burchette (1996), Wright and Burchette (1998), Chutakositkanon et al. (2000), Tucker (2001), Flügel (2010) and Boggs (2011a). 9
Figure 4: Distinct foraminiferal groups used to determine age distinguishing the fusulinid and non-fusuline foraminifera that are also distinguished in the stratigraphic sections of Figures 2 and 7. Information from Plummer (1948), Loeblich and Tappan (1964), Sartorio and Venturini (1988), Dawson & Racey (1993), Ueno and Sakagami (1993), BouDagher-Fadel (2008), Flügel (2010) and Kobayashi et al. (2010).....16
Figure 5: Distinct algal groups seen in thin section using information from Sano et al. (1990), Dawson & Racey (1993), Wendt (1997) and Flügel (2010) a) Log 5 RDT14_006B *Tubiphytes obscurus, a* cosmopolitan reef builder abundant throughout all Permian (A) b) Log 4 RDT14_057 *Tubiphytes* (B) c) Log 1 RDT14_012 *Mizzia* dasycladean algae common in Guadalupian and Lopingian shelf and back reef environments d) Log 2 RDT14_041 *Mizzia* Dasycladean algae surrounded by calcite cement (D) e) Log 1 RDT14_015 *Girvanella* (E) f) Log 2 RDT14_043 common green dasycladean algae (F1) possibly *Epimastopora* (F2) g) Log 7 RDT14_040A oncoid in an algal boundstone (G) h) Log 7 RDT14_040A algal boundstone textures.....18
Figure 6: Other common fossils seen in thin section and in the field using information from Sorauf (1978), Fontaine et al. (1988), Dawson and Racey (1993) and Scholle and Ulmer-Scholle (2003) a) crinoidal grainstone in outcrop b) Log 2 RDT14_041 crinoid columnal close to the cup in cross-polarised light (B) c) Log 2 RDT14_041 three crinoid columnals (C) clearly shows crenulae which connect the plates d) Log 9 RDT14_051 crinoid fragments that are more abraded (D) e) Log 5 RDT14_005 Permian rugose coral *Waagenophyllum sp*. (E) f) Log 1 RDT14_012 gastropod fragment (F) g) Log 6 30 cm bivalve h) Log 4 RDT14_022A bivalve fragments (H) 19
Figure 7: Fence line diagram correlating the stratigraphic logs along Highway 21 and from the Siam City Cement quarry highlighting some of the general structural trends between logs, scale on stratigraphic logs is in metres.....27
Figure 8: a-c) Interpreted Permian palaeography d) Balanced cross-section through the southern portion of the Saraburi Region, the Khao Khwang Fold-Thrust Belt adjusted from Arboit (pers. data, 2014). 32

Romana Dew
Stratigraphy of deformed Permian carbonate reefs, Thailand

INTRODUCTION

The Khao Khwang Platform is a late Pennsylvanian to Permian carbonate and mixed clastic sequence located in central Thailand (Figure 1). It formed as an elongate carbonate platform along the edge of the Indochina Block (Ueno and Charoentitirat 2011). The Khao Khwang Platform is interpreted to have formed in similar conditions to present-day carbonate platforms in clear, shallow, tropical waters of moderate salinity and little siliciclastic input (Bunopas 1992, Ueno and Charoentitirat 2011). The study area is located primarily within the Khao Khad Formation, an 1800 m thick intercalated carbonate and clastic sequence of the Saraburi Group, which crops out in a WNW to ESE trending belt in the Saraburi Province (Figure 1, Ueno and Charoentitirat 2011).

The Khao Khwang Platform was deformed during the Indosinian Orogeny, between the latest Permian and Lower Triassic, resulting in the Khao Khwang Fold-Thrust Belt (Helmcke 1985, Sone and Metcalfe 2008, Morley et al. 2013). The Permo-Triassic Phra Ngam Diorite and Khao Yai Volcanics were extruded into and intruded within the Saraburi Group coeval with deposition (Chutakositkanon et al. 2000, Ueno et al. 2012).

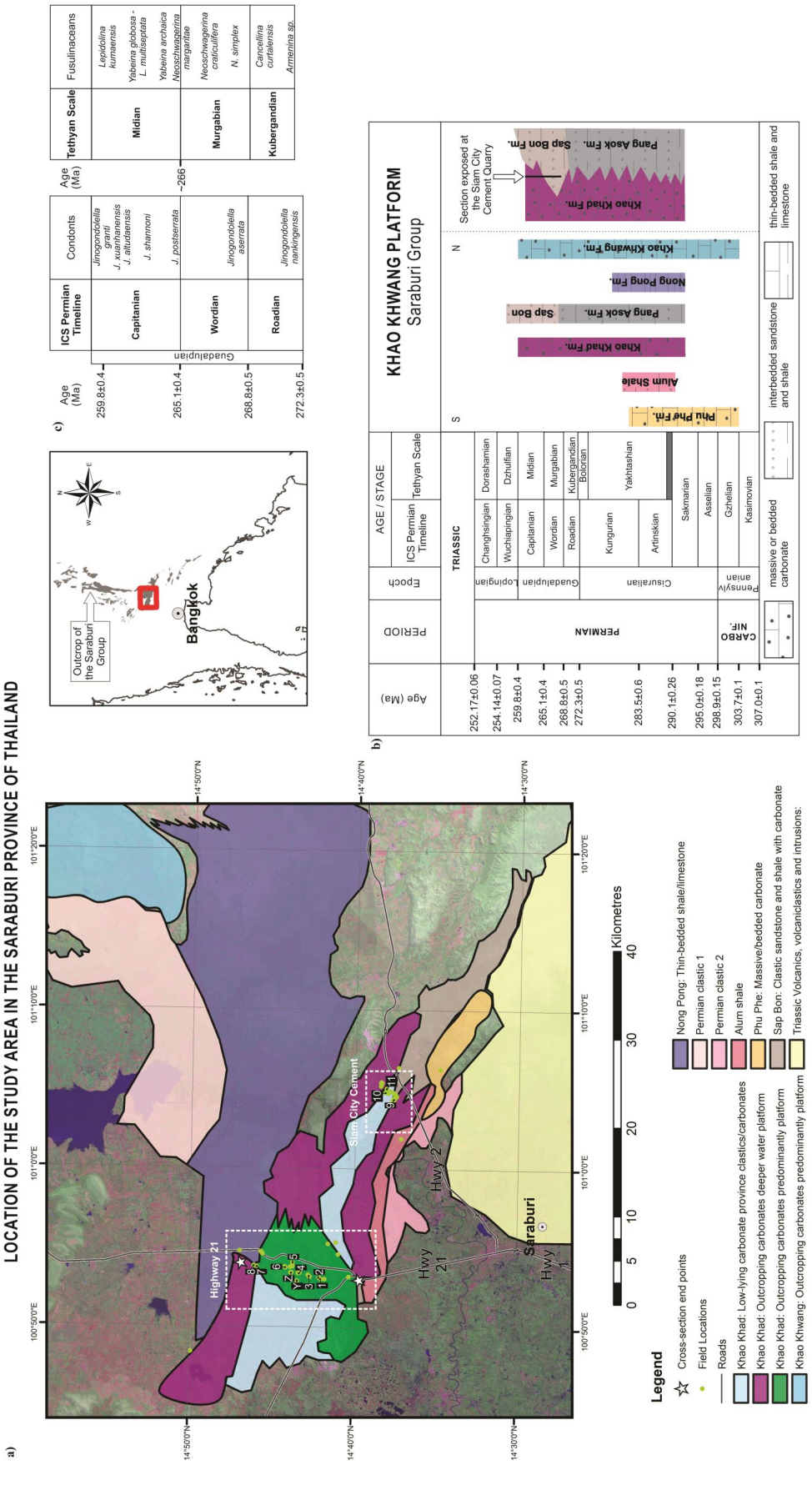

Figure 1: a) Location map portraying the regional stratigraphy, cross-section and field locations b) Stratigraphic log of the Khao Khwang Platform in the Saraburi Province c) Comparisons between the International Permian Timeline and the Tethyan Scale, dates are determined by the first appearance datum (FAD) of fossils highlighted; modified from Menning et al. (2006) Ueno and Charoentitirat (2011), Morley et al. (2013) and Shen et al. (2013)

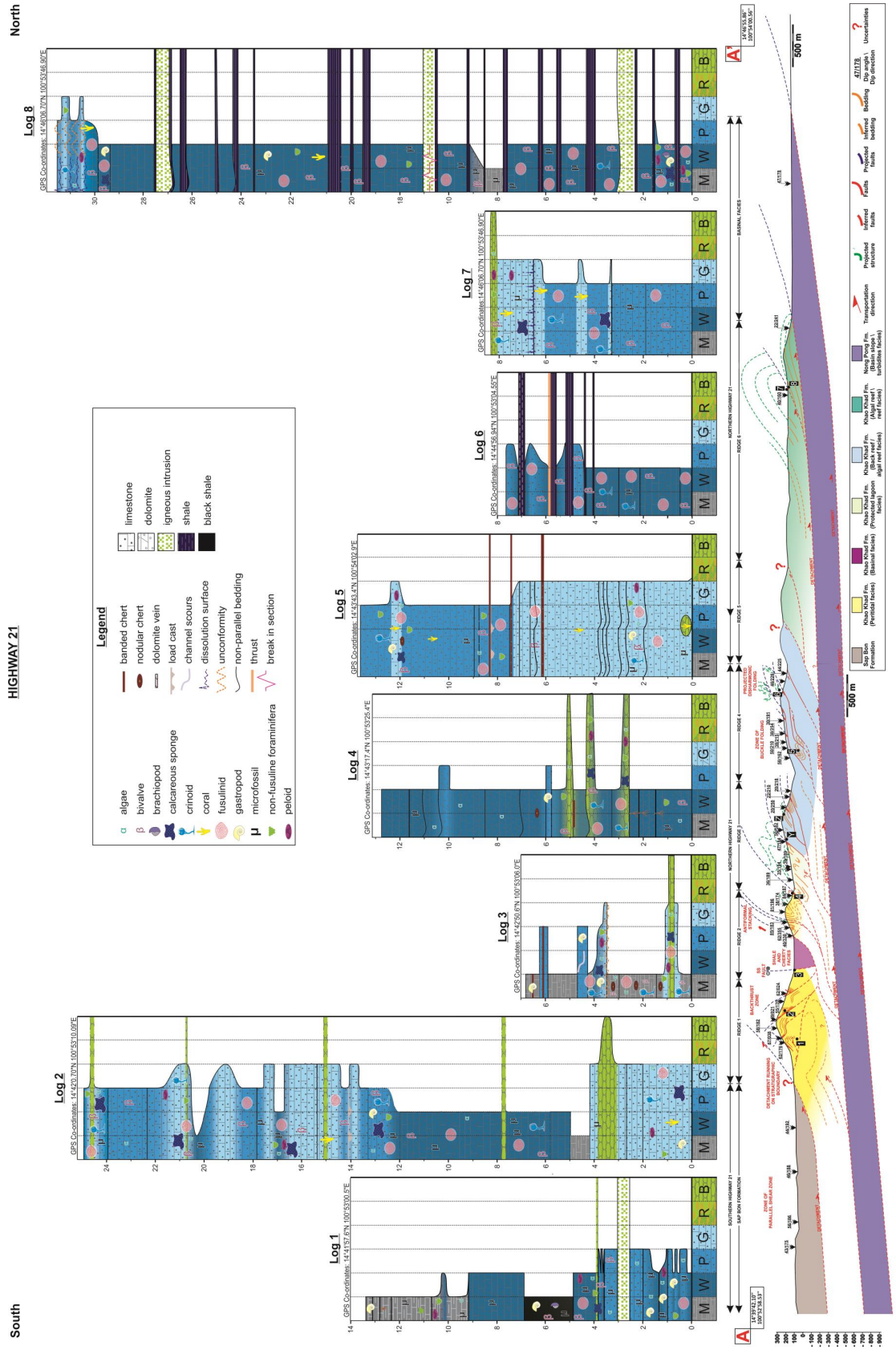

Figure 2: Regional cross-section through the southern portion of the Saraburi Region, the Khao Khwang Fold-Thrust Belt with stratigraphic sections superimposed scale in metres, M=Mudstone, W=Wackestone, P=Packstone, G=Grainstone, R=Rudstone, B=Boundstone (modified Arboit et al. (in press))

The Khao Khwang Platform contains diverse algae and foraminifera, which have been studied taxonomically (Dawson and Racey 1993, Udchachon et al. 2014). Previous sedimentological and stratigraphic studies, however, did not recognise the recently described structural complexity (e.g. Chutakositkanon et al. 2000, Thambunya et al. 2007). Many of the stratigraphic units have been named informally without thorough definitions and descriptions; without comprehensive regional work completed on detailed lithology, depositional environments and diagenetic history (Thambunya et al. 2007, Ueno and Charoentitirat 2011). Furthermore, many stratigraphic works have failed to incorporate the available palaeontological data (Ueno and Charoentitirat 2011). Moreover, Dawson & Racey (1993) is the only study to introduce the possibility of structural complications into their stratigraphic analysis of the Highway 21. Within the last 21 years, the structure of the region has been refined and recent studies have shown that low angle kilometre-scale thrusts deform the stratigraphy (Morley et al. 2013, Arboit et al. in press). Therefore, this study aims to redescribe the sedimentology and interpret the shallow marine depositional environments of the Khao Khad Formation in light of the newly described structural cross-sections published through the region (Arboit et al. in press).

In this paper, I attempt to reconstruct the original distribution of the facies by using the structural balancing presented in Arboit et al. (in press) and from this interpret the palaeogeography and palaeoecology of the platform. In this study, I demonstrate that the Khao Khad Formation formed in a shallow marine carbonate platform setting, using a series of stratigraphic logs from 11 field locations along Highway 21 and from the Siam City Cement Quarry along Highway 2 (Figure 1). I then use macrofacies and

microfacies analysis to create biostratigraphic correlations and facies associations to reconstruct a model for the depositional setting of the Khao Khad Formation.

CARBONATES AND THEIR DEPOSITIONAL ENVIRONMENTS

Carbonates constitute 20-25% of all sedimentary rocks in the global geologic record and are host to about half of the world's major petroleum reservoirs (James 1977, Tucker 2001, Boggs 2011b). Permian carbonates are prolific throughout Thailand and are economically significant for cement and stone production (Thambunya et al. 2007). The carbonate mineral identification is advantageous for economic and palaeoenvironmental applications. Of the sixty carbonate minerals, three are significant for environmental interpretation: calcite, aragonite and dolomite (Boggs 2011b). Ultimately, all aragonite and magnesian calcite marine cements stabilise to calcite and dolomite through dissolution and reprecipitation processes (MacKenzie and Adams 2007, Moore and Wade 2013). The stabilisation process results in a loss of the original geochemical information and textural details, which becomes problematic for recognising ancient marine cements, especially in the aragonite seas of the upper Paleozoic, Paleogene and Neogene (Wright and Burchette 1996, Moore and Wade 2013). Dolomite is predominantly a secondary product of calcite or aragonite transformation, especially prevalent with reef limestones. Although dolomite does occur as a primary mineral in magnesium enriched seawaters and in association with sulphide ore hydrothermal vein systems (Tucker and Wright 1990, Luhr 2003, MacKenzie and Adams 2007). Mineral replacement can occur early in diagenesis, soon after deposition, prior to compaction or later in the burial process (Tucker 2001, MacKenzie and Adams 2007)

Romana Dew
Stratigraphy of deformed Permian carbonate reefs, Thailand

Modern carbonate platforms are often insightful analogues for ancient carbonate environments. Most modern carbonate production occurs in clear, shallow, warm waters of moderate salinity and little siliciclastic input between latitudes of 30°N and 30°S (James 1977, Wright and Burchette 1996, Boggs 2011a). Modern and ancient carbonate platforms occur in six depositional settings (Figure 3) and the type of carbonate platform that develops depends on tectonics and relative sea level change (Tucker and Wright 1990, Wright and Burchette 1998, Tucker 2001, Flügel 2010). The type and amount of carbonate production is influenced partly by the type of carbonate platform, with shallow marine tropical reefs producing the most carbonates (Wright and Burchette 1996, Luhr 2003).

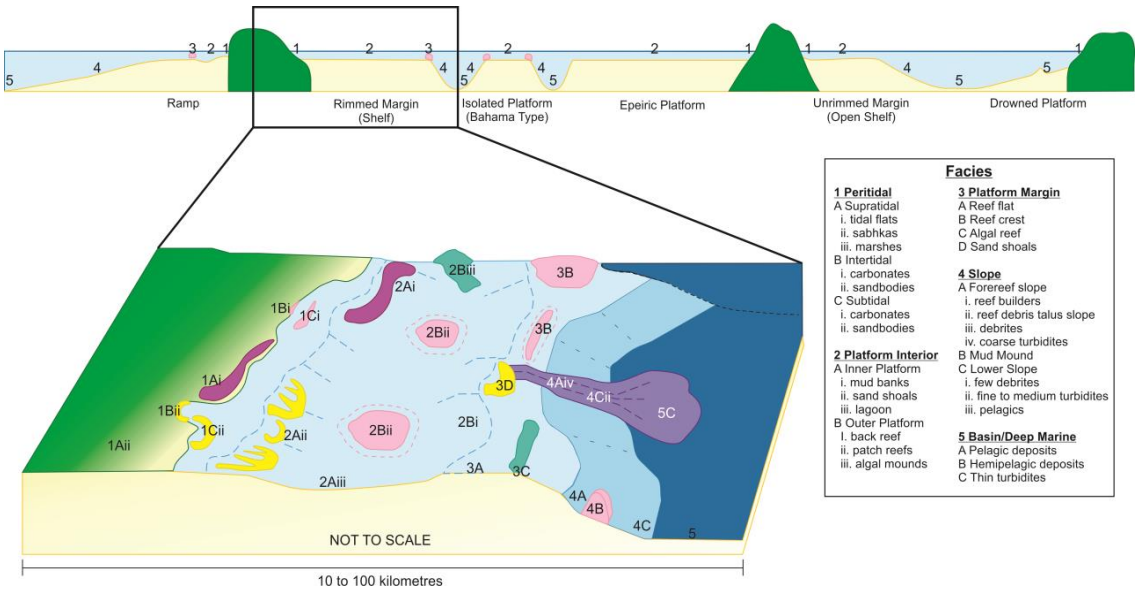

Figure 3: Diagram depicting the characteristics of the six depositional settings of carbonate platforms incorporating information from Wright and Burchette (1996), Wright and Burchette (1998), Chutakositkanon et al. (2000), Tucker (2001), Flügel (2010) and Boggs (2011a).

PERMIAN REEF DEVELOPMENT

The Permian is a time of major reef building as seen throughout Thailand (Weidlich 2002, Kiessling et al. 2003, Udchachon et al. 2014). Reefs at this time have been

divided into three compositional types: microbial reefs, metazoan reefs and calcareous algae reefs (Weidlich 2002). Crinoids and siliceous sponges increased during the Permian indicating a cooling trend from the earlier warmer waters that were conducive to deposition of peloids and aragonitic shells and cements (Kiessling et al. 2003). The climax of Permian reef growth occurred in the Guadalupian Epoch with high reef diversity with all three reef compositional types in addition to the extent, abundance and size of reef localities (Weidlich 2002). At the end of the Guadalupian, a combination of decreasing global sea level, regional salinity fluctuations and micro-continent collision led to a loss of >89% carbonate production (Weidlich 2002, Udchachon et al. 2014). The end-Guadalupian crisis terminated the reef domain of the Indochina Platform (Weidlich 2002). This is indicated in the fossil record with the abrupt decline in large fusulinids, a type of tropical benthic foraminifera, which were major reef builders during the Guadalupian (BouDagher-Fadel 2008, Davydov 2013, Hada et al. in press).

KHAO KHWANG FOLD-THRUST BELT

The carbonate platforms associated with the Khao Khwang Fold-Thrust Belt are situated extensively along the edge of the Indochina Block, on the eastern side of the Chao Phraya central plain and western margin of Khorat Plateau (Chutakositkanon et al. 2000, Ueno and Charoentitirat 2011, Ueno et al. 2012).

In the Saraburi region, the carbonates of the Khao Khwang Platform were deposited between the Upper Pennsylvanian and the late Permian (Ueno and Charoentitirat 2011). These sequences were once considered part of the Ratburi Limestone (Brown et al. 1951, Toriyama and Kanmera 1979, Dawson and Racey 1993) although subsequently they have been separated into the Saraburi Group due to the distinct faunal assemblages

present (Bunopas 1992). Paleozoic palaeomagnetic data indicate that the Saraburi Group was deposited at a palaeolatitude of nearly 10º south of the Permian equator (El Tabakh and Utha-Aroon 1998, Thambunya et al. 2007, Metcalfe 2013). Hinthong et al. (1985) identified three main formations that represented the facies in the carbonate platform. These are the Phu Phe, Khao Khad and Khao Khwang formations. These platform facies are divided by clastic, mixed siliciclastic and carbonate sequences, known as the Sap Bon, Pang Asok and Nong Pong formations (Chutakositkanon et al. 2000, Chonglakmani 2001). Although traditionally interpreted as a vertical stratigraphic succession, recent fossil data demonstrate that the carbonate sequences are mostly contemporaneous (Ueno and Charoentitirat 2011). Marine deposition of the Saraburi Group was terminated by uplift and deformation caused by the Indosinian Orogeny, sometime between the latest Permian and Ladinian (Baird and Bosence 1993, Sone and Metcalfe 2008).

KHAO KHAD FORMATION

The Khao Khad Formation of the Saraburi Group has been previously dated as middle Guadalupian and on the Tethyan Scale, predominantly Murgabian with limited extension into the Midian (Figure 1, Baird and Bosence 1993, Dawson and Racey 1993, Ueno and Charoentitirat 2011). The Tethyan Scale is zoned using fusulinids, in contrast to the conodonts being the primary fossil used for the biostratigraphic correlation for The International Commission on Stratigraphy (ICS) Permian Timeline (Figure 1, Wardlaw et al. 2004, Shen et al. 2013). Conodonts are insufficiently studied in the Tethys, hence fusulinids and to a lesser extent ammonoids are used to subdivide the Permian (Wardlaw et al. 2004). Although the ICS and Tethyan scales are broadly equivalent, as shown in Figure 1, the use of different determinants leads to differences

in the exact ages (Menning et al. 2006, Dickins et al. 2007, Henderson et al. 2012). For example, the Murgabian rocks are only provisionally correlated to the ICS Wordian as they lack the conodonts to establish a strong correlation (Menning et al. 2006).

The fusulinid-brachiopod-gastropod assemblages and overall bioclastic lithology imply that the Khao Khad Formation was deposited in a tropical shallow marine carbonate platform environment (Thambunya et al. 2007, Ueno and Charoentitirat 2011). The facies indicate that there was a transgressive and regressive cycle during the Cisuralian and Guadalupian (Dawson and Racey 1993, Chutakositkanon et al. 2000). These cycles are visible through changes in the lithological and palaeontological characteristics.

Further subdivisions of the Khao Khad Formation have been previously identified through fossil analysis using the abundance and diversity of fusuline and calcareous algal biota. Chutakositkanon et al. (2000) regroup the Khao Khad Formation in the Khao Pun area into two lithostratigraphic units, the Khao Sung and Khao Pun Formations that are subdivided into six members. In contrast, Thambunya et al. (2007) distinguished fifteen rock units of the Khao Khad Formation within their three study areas. Thambunya et al. (2007) also created a depositional model that infers the Khao Khad Formation formed from an inner shelf lagoon with a barrier bar/shallow platform in the outer shelf and foreslope. Dawson and Racey (1993) recognise six main biofacies in their study locations just north of Saraburi. It is also suggested that there was a sedimentary hiatus related to a worldwide marine regression in the early middle Permian, which caused a period of intense dolomitisation in carbonates of the Khao Khad Formation (Dawson and Racey 1993).

Romana Dew
Stratigraphy of deformed Permian carbonate reefs, Thailand

FIELD AND THIN SECTION ANALYSES

Fieldwork was carried out along Highway 21 and in Siam City Cement Quarry in the Saraburi Province of Thailand, approximately 100 kilometres NNE of Bangkok. The Saraburi Province was chosen due to the exceptionally exposed sections of the Permian carbonate reefs and intervening clastic sediments within the region. It is also an area of ongoing structural work and a better understanding of the area's stratigraphy will assist in unravelling the structure of the area.

Stratigraphic logs were constructed along with fossil identification, sketches, photographs and samples taken from the Saraburi Province. The sequences were classified using both the Dunham (1962) and Folk (1962) classification schemes. In total, stratigraphic logs were taken from 11 field locations to form the basis of facies interpretations and biostratigraphic correlation. Sections were numbered from south to north in Highway 21: Logs 1 to 8 and Logs 9 to 11 from Siam City Cement. The logs were digitised using CorelDRAW software (Figure 2).

Thirty-two samples were prepared into thin sections for optical microscopy. All 32 sections were then stained with Alizarin Red and potassium ferricyanide to discriminate calcite and dolomite as per Appendix A. The sections were then analysed under transmitted light to validate and add to the field interpretations as per Appendix A.

The fossil assemblages determined in the field and by thin section analysis were used to infer facies and their associations in addition to the age and timing of the sequences.

The facies and their associations were then used to reconstruct a model for the depositional setting of the Khao Khad Formation during the Permian.

FOSSILS AND LITHOLOGY OF THE KHAO KHAD FORMATION

Fossils from thin section analyses

FORAMINIFERA

Generally, the sequences are highly bioclastic, dominated by a variety of foraminifera. Five groups of fusulinids commonly appear in the thin section and are identified in Figure 4. *Verbeekinidae* are ~1 mm-500 μm in size with dark brown to black test walls and usually light coloured chambers. They are present in the Murgabian assemblage in Log 2 (Figure 2). *Neoschwagerinidae* have thick walls that are coated or encrusted with algae. Many of the larger foraminifera including the *Neoschwagerinidae* have a symbiotic relationship with photosynthetic algae that is indicated by this dark algal coating (Dawson and Racey 1993, Beavington-Penney and Racey 2004). This relationship is suggested to have evolved during the Carboniferous (Beavington-Penney and Racey 2004). *Neoschwagerinidae* are the largest fusulinids, generally increasing in diameter through the Permian. They appear in Log 8 (Figure 2) including the *Neoschwagerina* and *Gifuella sp.* of the middle and late Murgabian. The *Schwagerinidae* are few mm in diameter with strong contrast between the light storm grey of the test walls and the lighter colour of the chamber interiors (see Figure 4).

Schubertellidae are small elongate elliptical fusulinids with dark walls and usually light coloured chambers. They are present in Logs 1 and 2. *Staffellidae* are small elongate elliptical fusulinids that occur within well-agitated marine shoals. They appear taupe in

colour in thin section, lighter than other fusulinid groups. *Nankinella,* a member of this taxa, occur from the Sakmarian to Changhsingian. *Staffellidae* occur in the back reef of Logs 5 and 8 (Figure 2).

Four groups of non-fusuline foraminifera assisted in determining the age of samples (Figure 4). The "rose" group are distinguished as 500-200 µm rosebud shaped non-fusuline foraminifera. They are smaller than many of the more advanced fusulinids and include *Miliolida, Baisalina* and *Hemigordius sp.* This group of non-fusuline foraminifera are prolific throughout Logs 3 and 4 (Figure 2). The *Globivalvulina* group (Figure 4) is characterised by ~200 µm-sized foraminifera that have several chambers that link together to give the appearance of popped corn. Species of *Globivalvulina* are present in the global fossil record between 336.0 to 251.3 Ma. *Globivalvulina* sp. proliferate Log 4 (Figure 2). Other foraminifera are present in the samples but did not occur frequently and were less useful for constraining the age of the sequence, for example, the *Textulariidae* Group that have two columns of chambers that merge into one and still occur today. The ages for sections (1 and 4) that predominantly contain non-fusuline foraminifera were harder to constrain as their morphology changes occur at a slower rate than the rapidly evolving Permian fusulinids.

Varying degrees of preservation are present in the study area affecting the taxonomic identification of the fossils. The fusulinids in Log 5 and 9 (Figure 2) are generally less well preserved and subsequently fossils are harder to identify. Crosscutting veins and compaction are visible in some of the thin sections, particularly for Logs 7 and 10.

Romana Dew
Stratigraphy of deformed Permian carbonate reefs, Thailand

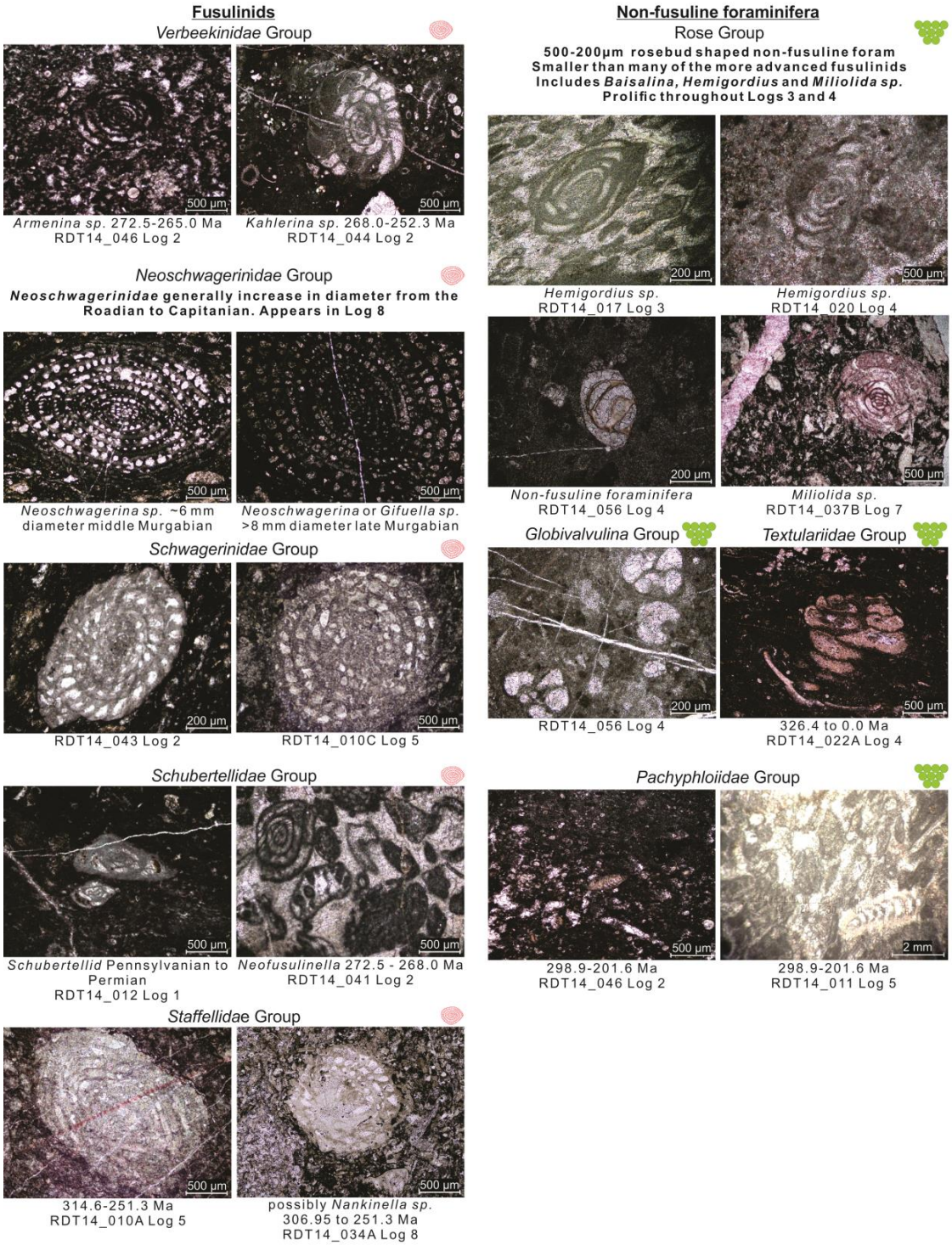

Figure 4: Distinct foraminiferal groups used to determine age distinguishing the fusulinid and non-fusuline foraminifera that are also distinguished in the stratigraphic sections of Figures 2 and 7. Information from Plummer (1948), Loeblich and Tappan (1964), Sartorio and Venturini (1988), Dawson & Racey (1993), Ueno and Sakagami (1993), BouDagher-Fadel (2008), Flügel (2010) and Kobayashi et al. (2010).

Romana Dew
Stratigraphy of deformed Permian carbonate reefs, Thailand

ALGAE

Four algal types: *Tubiphytes*, *Dasycladaceae*, *Girvanella* and *Epimastopora* regularly occurred in thin section (Figure 5). Algal sedimentary structures such as oncoids and boundstone textures were also identified in the thin sections as depicted in Figure 5. *Archaeolithoporella, Phylloid, Udoteacean* and *Gymnocodiacean* algae were occasionally also present. Algae appear in most of the Permian Khao Khad Formation.

CRINOIDS

Large crinoid columnals are present in thin section portray varying degrees of abrasion as shown in Figure 6. Crinoids were identified in both the Highway 21 and Siam City Cement areas. They are present in all sections except Log 1.

CORAL

The coral present in thin section were mostly identified as rugose coral of the *Waagenophyllum sp*. shown in Figure 6. They occurred as both solitary corals and parts of larger dendroid colonies. In colonies, coral are spaced between 1-5 mm apart, each with diameters between 4.5 and 7 mm. Major septa are slightly thicker than other septa and nearly touch the columella (Appendix C). Minor septa are thinner and shorter than the major septa. *Waagenophyllum sp*. occurs in the Guadalupian and Lopingian. Coral was present in Logs 2, 5, 7-9.

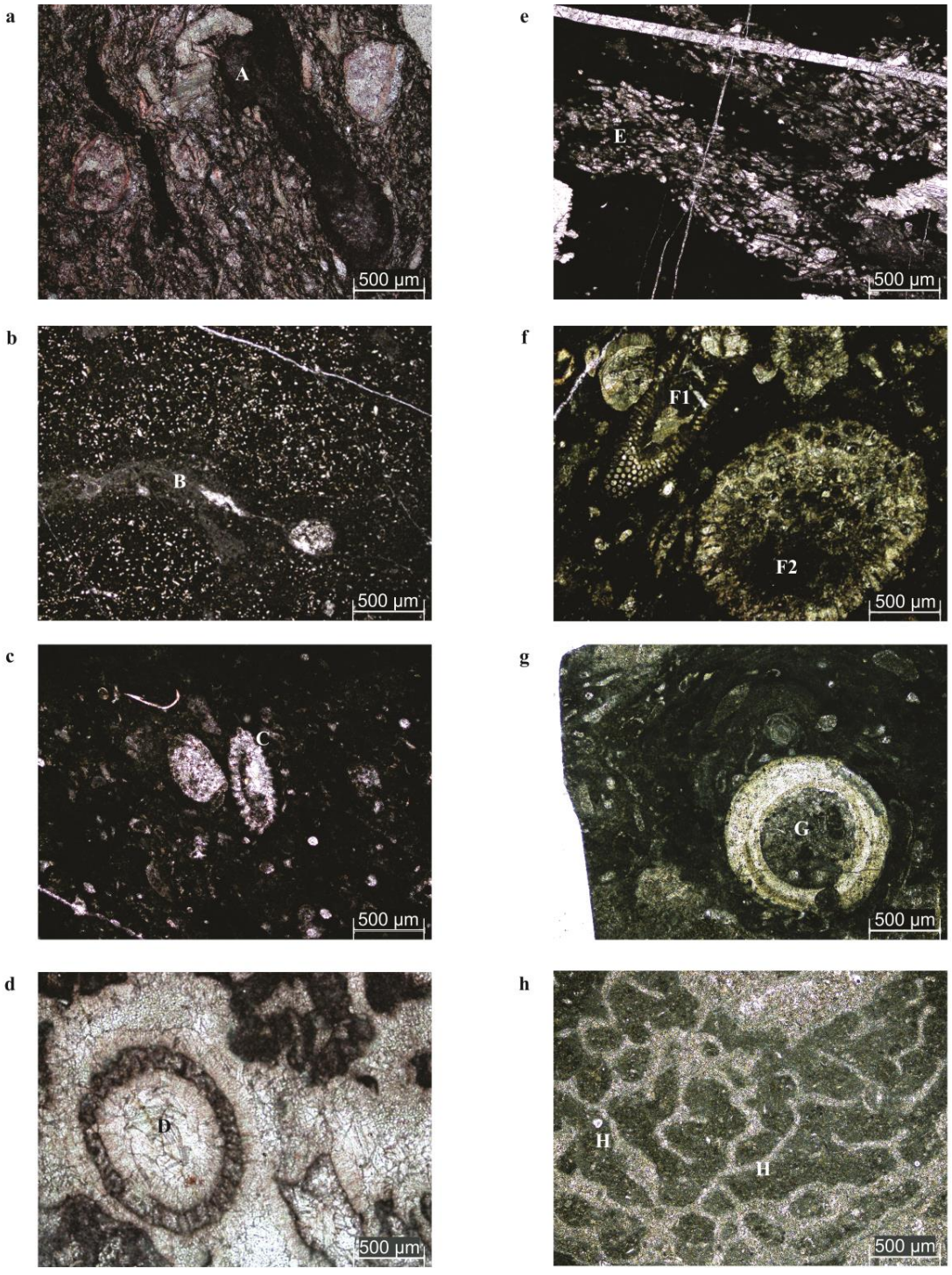

Figure 5: Distinct algal groups seen in thin section using information from Sano et al. (1990), Dawson & Racey (1993), Wendt (1997) and Flügel (2010) a) Log 5 RDT14_006B *Tubiphytes obscurus, a* cosmopolitan reef builder abundant throughout all Permian (A) b) Log 4 RDT14_057 *Tubiphytes* (B) c) Log 1 RDT14_012 *Mizzia* dasycladean algae common in Guadalupian and Lopingian shelf and back reef environments d) Log 2 RDT14_041 *Mizzia* Dasycladean algae surrounded by calcite cement (D) e) Log 1 RDT14_015 *Girvanella* (E) f) Log 2 RDT14_043 common green dasycladean algae (F1) possibly *Epimastopora* (F2) g) Log 7 RDT14_040A oncoid in an algal boundstone (G) h) Log 7 RDT14_040A algal boundstone textures.

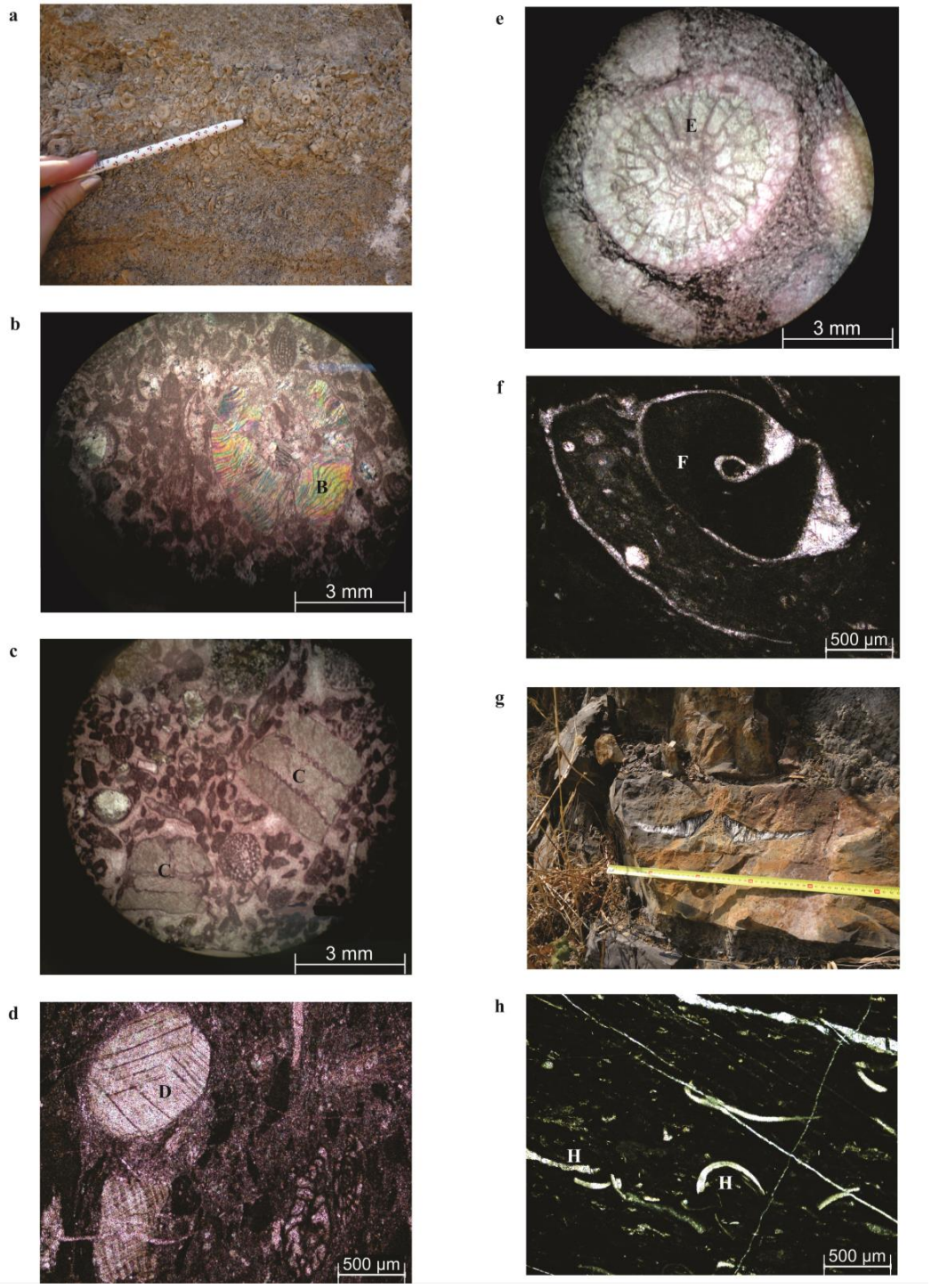

Figure 6: Other common fossils seen in thin section and in the field using information from Sorauf (1978), Fontaine et al. (1988), Dawson and Racey (1993) and Scholle and Ulmer-Scholle (2003) a) crinoidal grainstone in outcrop b) Log 2 RDT14_041 crinoid columnal close to the cup in cross-polarised light (B) c) Log 2 RDT14_041 three crinoid columnals (C) clearly shows crenulae which connect the plates d) Log 9 RDT14_051 crinoid fragments that are more abraded (D) e) Log 5 RDT14_005 Permian rugose coral *Waagenophyllum sp*. (E) f) Log 1 RDT14_012 gastropod fragment (F) g) Log 6 30 cm bivalve h) Log 4 RDT14_022A bivalve fragments (H)

GASTROPODS

Rare fragments of gastropod shells were recognised in most of the thin sections in the Highway 21 region. A typical gastropod fragment is illustrated by the gastropod in Figure 6.

BIVALVES

Bivalves were identified in the Highway 21 sections as illustrated in Figure 6. A large variety of bivalves are present, ranging in preservation from very fragmented to almost complete and vary in size between several 100 μm to 30 cm. They are common in the entire Khao Khad Formation sequence. Gregarious *alatoconchid*-bearing limestones were observed in Log 6 (Figure 6g).

Lithobiofacies of the Permian Saraburi Carbonate Sequence

Platform facies have been interpreted from the examination of logged sections to determine the type of carbonate platform (Figure 3). The environments form a continuum but can be grouped into peritidal, low-energy lagoon, high-energy middle platform to backreef, algal reef and slope to basin illustrated in Figure 3. The relationship between these facies in logged sections allows the classification of several facies associations, which are indicative of broad environments of deposition.

PERITIDAL

The peritidal zones lack coral and fusulinids and are predominantly classed as mudstones and wackestones with abundant algae (*Girvanella*) and microscopic non-fusuline foraminifera. Some algal grainstones were also present within the tidal environments. Peritidal environments occur within Log 1, 2 and the dolomitised Log 4.

Ages range from early middle Permian to middle Murgabian with possible extension into the Midian.

LAGOON

The low-energy lagoonal environment is comprised of bioturbated wackestones predominant with abundant algae including *Girvanella* and microscopic non-fusuline foraminifera (*Globivalvulina* and *Textulariida*). Algal boundstone interbeds sporadically occur along with chert nodules and lenses. The dolomitised bioturbated algal wackestones of Log 4 are characteristic of the lagoonal environment. The fossil assemblage in Log 4 implies deposition after the middle Kungurian.

OUTER PLATFORM

Massive planar-bedded dark-storm-grey wackestone with minor grainstone masses indicate the change from the lagoon and into the higher energy outer platform. Bivalves, crinoids and small foraminifera encompass the majority of the fauna.

In contrast, the backreef frequently includes non-parallel-bedded storm-grey set of wackestones, packstones and grainstones. Isolated boundstone clumps of coral families also occur like in Log 5. Fossils are disarticulated in the back reef and include each major fossil group: crinoids, fusulinids (*Nankinella, Schwagerina, Neoschwagerina* and *Gifuella* see Figure 4), bivalves (including *alatoconchids*), non-fusuline foraminifera (*Baisalina* and *Climacammina*), algae (*Tubiphytes*), coral (*Waagenophyllum* in Figure 6) and gastropods. Brachiopods, calcareous sponges and peloidal matter are also present.

The continuum of the outer platform is the interpreted depositional environment for Logs 5, 6 and 8. Chert lenses are present in the backreef of Log 5 whereas shale interbeds occur in Log 6 and 8. At a similar time to the platform interior setting, igneous activity was occurring nearby, leading to the sills found in Log 1 and 8. The fossil assemblages suggest middle to late Murgabian for the outer platform sequences.

REEF

Reef facies are dominated by algal boundstones and fusuline packstone-grainstone. Reef builders were mostly algae and fusulinids with minor foraminifera and coral building. The boundstones along Highway 21 have a dominant skeletal element of encrusting *Archaeolithoporella* and *Tubiphytes* with calcisponges and abundant syndepositional marine cements. This is consistent with descriptions by Dawson et al. (1993). The boundstone units lack fusulinids containing rare non-fusuline foraminifera. Within the fusuline packstone-grainstones, bivalves and fusulinids (including *Neofusulinella, Nankinella, Kahlerina, Armenina*) are abundant with crinoids, coral and non-fusuline foraminifera (*Cribrogenerina* and *Pachyphloia*) commonly occurring. Log 7's bivalve and fusulinid-rich grainstone with coral lenses passes west into a reef mound suggesting lateral facies change. I interpret that the platform margin was not entirely rimmed with reef builders and the margin was home to small biostromes instead. The algal reefs were identified within Logs 1, 2 and 7 and the fossil assemblages of Logs 2 and 7 depict deposition in the early to late Murgabian.

BASINAL SLOPE

The basinal slope facies are predominantly mudstones with lesser allodapic packstone-grainstone-boundstone beds. Multiple chert nodules and lenses, in addition to beds with

scoured bases along with other characteristics of mass transport are indicative of turbid debris deposits. Log 3 is the only section representative of the basinal slope environment. The fossil assemblage includes an eclectic assemblage of fragmented and abraded fossils including small crinoids pieces, fusulinids (*Neoschwagerina*), non-fusuline foraminifera (*Agathammina, Pachyphloia, Hemigordiopsis* and *Globivalvulina cyprica*) and gastropods. Together this assemblage indicates an age between Murgabian and Dzhulfian Tethyan stages.

PLATFORM (SIAM CITY CEMENT)

Logs 9 to 11 also appear to have been deposited in a platform environment.
The platform margin is characterised by dolomitised light grey grainstone is the major textural classification present in this platform margin although some mudstone and wackestone beds occur sporadically. It lacks fossil diversity with abraded crinoids dominant with minor coral, fusulinids and algae. Log 9 illustrates this platform margin. Hornblende is abundant in thin section with chert lenses appearing in outcrop. Some fossils were observed in the field to be replaced by chert. The age of the sequence could not be constrained due to the lack of fossils present in thin section.

The backreef and reef consists of pervasively dolomitised massive homogenous light pink-grey sequence. It is extremely fossiliferous although fossils were unidentifiable in the field due to the high levels of recrystallisation. The backreef and reef are distinguished within Logs 10 and 11. A diverse array of fusulinids including *Parafusulina*, *Schubertilids, Schwagerina* and *Ozawainella* were identified in thin section. They imply a late Kungurian to Guadalupian age.

Romana Dew
Stratigraphy of deformed Permian carbonate reefs, Thailand

AGE AND BIOSTRATIGRAPHIC CORRELATION

Age

Random errors may have occurred when constraining age as various resources gave ages using the Tethys Scale, ICS Permian Timeline or numerical age ranges. Further errors would be present if the fossil is assigned to an ICS epoch whose boundaries have since changed, i.e. the differences between timelines within Wardlaw et al. (2004), Menning et al. (2006), and Shen et al. (2013). The Tethyan Stages are sometimes referred to as the Transcaucasia or Pamirian whose boundaries between the stages vary further (Nestell and Nestell 2006, Dickins et al. 2007, Ueno and Charoentitirat 2011). For ease in this project, I have assumed that the Tethyan Murgabian and Midian are equivalent to the ICS Wordian and Capitanian respectively as suggested by Menning et al. (2006) and shown in Figure 1. This equivalence has been previously used by Wardlaw et al. (2004), Kobayashi et al. (2010).

The fossils identified in thin section were correlated using the Tethyan fusulinid zonations as no conodonts were present to be confident using the ICS Permian Timeline (Figure 1). The Tethyan Scale gave higher resolution for the fossil zonation of the Khao Khad Formation as it is the correct regional timescale for the Indochina Block (Menning et al. 2006, Ueno and Charoentitirat 2011).

Romana Dew
Stratigraphy of deformed Permian carbonate reefs, Thailand

Biostratigraphic Correlation

The presence of fusulinids is very helpful to recognise Permian aged sedimentary rocks; however, it is harder to establish definitive ages for sequences without prolific fusulinids. Sections (Logs 1 and 4) that predominantly contained non-fusuline foraminifera were harder to constrain ages, as they change in morphology at a slower rate than the fusulinids in the Permian.

From the fusulinids present, the sections mostly appear to be within the *Neoschwagerina simplex, N. craticulifera* and *N. margaritae* zones described in Menning et al. (2006) and depicted in Figure 1c. The *Neoschwagerinidae* present in the sections do not appear to be at the complexity of *Yabeina sp.* that are characteristic of the Capitanian/Midian discussed by Kobayashi et al. (2010) and displayed in Figure 1c. The upper section of Log 1 lacks fusulinids and therefore may still have deposition into the early Capitanian (Midian).

Overall, the fossils, especially the fusulinids, appear older in the Siam City Cement sections than the fossils along Highway 21. Nevertheless, it must be considered that the fossils are not well preserved therefore, the determination of the fossil taxonomy and age is poor.

Scattered dolomite rhombs occur within Log 4 and all three Siam City Cement sections (see Figure 7). The dolomitised peritidal environments of Log 4 and nearby Y sample location are probably the same tidal zone due to their proximity and similarity. It has been suggested that there was a sedimentary hiatus related to a worldwide marine regression in the early middle Permian, which caused a period of intense dolomitisation in the Khao Khad carbonates (Dawson and Racey 1993). This event implies that sections with intense dolomitisation were deposited prior to the early middle Permian. This is consistent with the fossil assemblages that indicate that Log 4 was deposited after the middle Kungurian and loosely constrained late Kungurian-Guadalupian Logs 10 and 11.

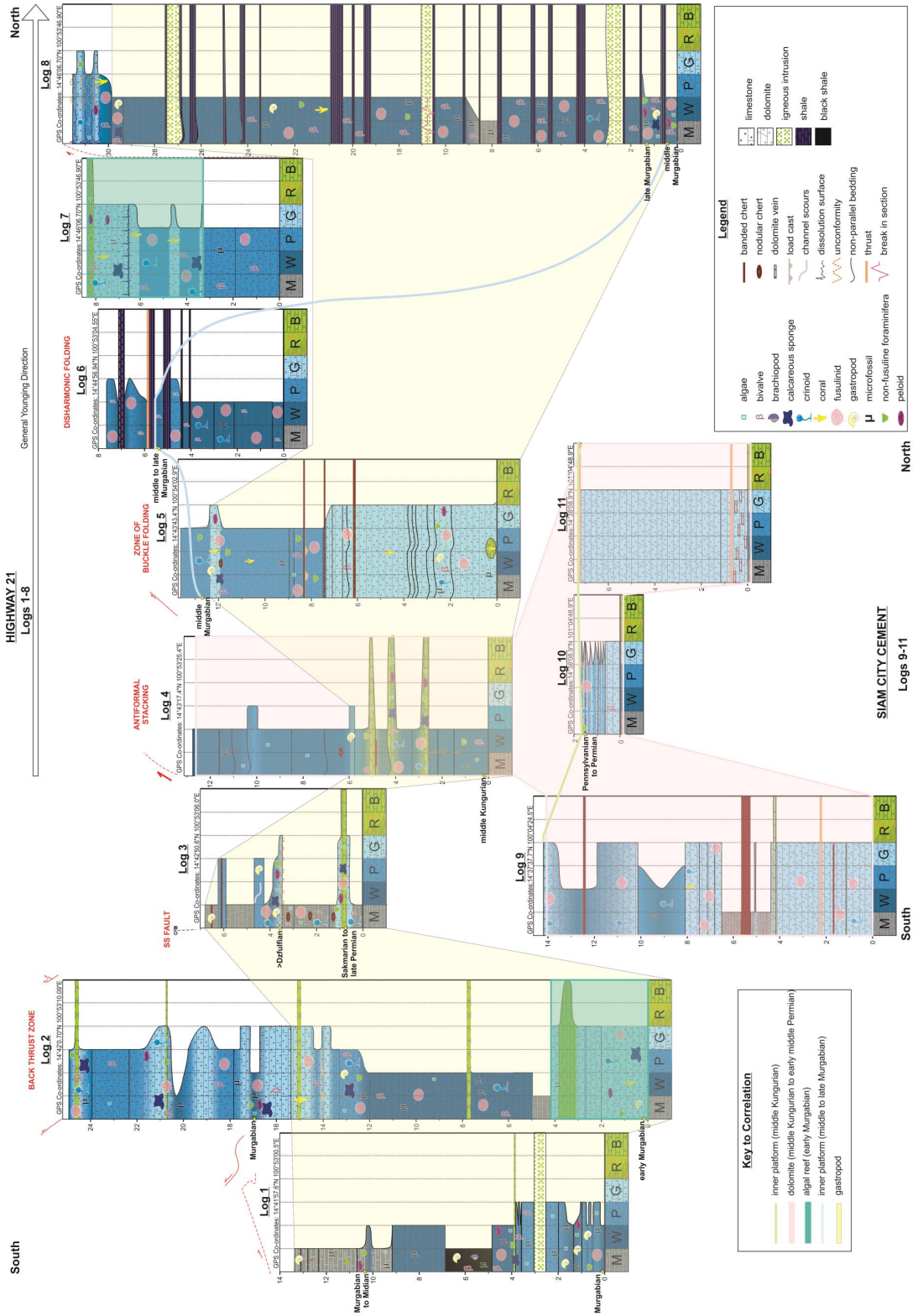

Figure 7: Fence line diagram correlating the stratigraphic logs along Highway 21 and from the Siam City Cement quarry highlighting some of the general structural trends between logs, scale on stratigraphic logs is in metres

The cooling trend throughout the Permian led to the decline of siliceous sponges, peloids and aragonitic shells (Kiessling et al. 2003, Scholle and Ulmer-Scholle 2003). The fossil assemblages indicate that most of the sequences were deposited prior to this cooling trend. Aragonitic-shelled gastropods are present at the least in the bottom of all sections south of Log 6 and 7 (shown in Figure 7). They disappear in middle Murgabian peritidal environment of Log 2, however, are still present in the late Murgabian backreef, which was perhaps warmer and more conducive for gastropods at this later time.

Logs 6 and 7 both grade from a protected inner platform lagoonal environment into an energetic middle platform to backreef. They both are also constrained to the middle to late Murgabian. The backreef environments found in the Log 5 and Z sample location may also be extensions of the same environment. In contrast, the Log 2 and Log 7 are both early Murgabian algal reefs with RDT14_041 and RDT14_038 samples appearing very similar in thin section.

There is little variance between the marginal platform of Log 9 and the backreef of Logs 10 and 11 further north. I interpret the age of these sections to be Murgabian, which is consistent with the age given in Morley et al. (2013). In contrast, the Highway 21 section can be better constrained to sections depicting sections between middle Kungurian through to the Murgabian and Midian. I interpret that the Siam City Cement sections are laterally equivalent or slightly older than the Highway 21 sections. These ages are within the ranges given previously by Baird and Bosence (1993), Dawson and Racey (1993) and Thambunya et al. (2007).

Other correlative relationships

The stratigraphic sections of Highway 21 are dominated by carbonate sequences with chert in Logs 3-5 (Figure 2). The percentage of allochems decreases up section in Log 1 and 5 unlike in Logs 6, 7 and 8 where the percentage increases up section. In contrast, the Siam City Cement sections are predominantly grainstone in composition although some micrite is present in Log 9.

There are a number of sills in the Log 1 and 8 (Figure 2). The andesitic composition of the minor dikes and sills noted in the field is consistent with previous geochemical results (Chutakositkanon, pers. data, 1996). Thin section analysis also depicted volcanic influences with volcanic hornblende occurs within the matrix of samples from Logs 3 and 9. This indicates that these sections were proximal to volcanic activity or more volcanic activity was occurring during deposition of these sequences. The sills in Logs 1 and 8 indicate that at a similar time to the Murgabian platform interior setting, igneous activity was occurring nearby. This could be associated with the Permo-Triassic Phra Ngam Diorite and Khao Yai Volcanics that are coeval with the Saraburi Group (Chutakositkanon et al. 2000, Ueno et al. 2012). As Log 1 was taken from the Khao Yai Hill locality it is probable that it may be proximal to the Khao Yai Volcanics.

PALAEOGRAPHY

Fontaine (2002) states that massive carbonate sequences represent extensive carbonate platforms; this is certainly true for the Khao Khad Formation in the Saraburi Province. The sequences studied in this project were deposited in a tropical shallow marine carbonate platform environment. However, it is difficult to determine whether they were deposited as one singular platform or multiple platform environments due to the

shortening and deformation that has since occurred. However, five carbonate facies can be identified from the examination of logged sections. The relationship between these facies in logged sections allows the classification of a number of facies associations, which are indicative of broad environments of deposition. The environments form a continuum but can be grouped into peritidal, low-energy lagoon, high-energy middle platform to backreef, algal reef and slope to basin highlighted in Figure 3.

The balanced section by Arboit et al. (pers. data, 2014) depicts the position of the facies shown in Figure 1 prior to deformation. The balanced section (Figure 8) was incorporated into my interpretation of the lithobiofacies analysis and biostratigraphy to reconstruct the palaeogeography of the margin. Most of the correlations and facies associations previously discussed were back up by the balanced section (Figure 8).

Kungurian to early middle Permian

Prior to the early middle Permian, the rocks found in Logs 4, 9-11 were deposited in peritidal and backreef environments respectively. The peritidal zones lack fusulinids and are predominantly classed as wackestones with abundant algae and microscopic non-fusuline foraminifera. After this time, there was a sedimentary hiatus and dolomitisation occurred.

Murgabian

Algal reef deposition began in the early Murgabian for Logs 2 and 7. Reef facies are dominated by algal boundstones and fusuline packstone-grainstones. Reef builders were mostly algae and fusulinids with minor foraminifera and coral building. I interpret

that the platform margin was not entirely rimmed with reef builders and the margin was home to small biostromes instead.

The fusulinids of Log 2 portray the evolution through the Murgabian from *Neofusulinella, Nankinella, Kahlerina* to *Armenina*. A Murgabian decrease in sea level is indicated between the back reef seen in RDT14_043 and the peritidal environment of RDT14_044 situated higher in the Log 2 section. The top of Log 2 returns to algal boundstones and fusuline packstone-grainstones.

Platform interior environs are inferred for middle to late Murgabian aged sequences: Logs 6, 8, Jungle and possibly Log 5 and Z sample location. Mudstone and wackestone form the quiet protected lagoon with bivalves and small foraminifera dominating the fauna. The backreef comprises of disarticulated fossils and higher energy wackestone and packstones. At a similar time to the platform interior setting igneous activity was occurring nearby leading to the sills found in Logs 1 and 8. Peritidal algal wackestones and mudstones occurred in Log 1 during this time.

Midian

The peritidal algal wackestones and mudstones of Log 1 extends into the Midian, although is poorly constrained lacking coral and fusulinids. The black shale of Log 1 (Figure 2 and 7) correlates with the Chutakositkanon et al. (2000) description of the late middle Permian transgression where the carbonate and fine-grained clastic sedimentation on the barrier was accompanied by anaerobic-starved conditions.

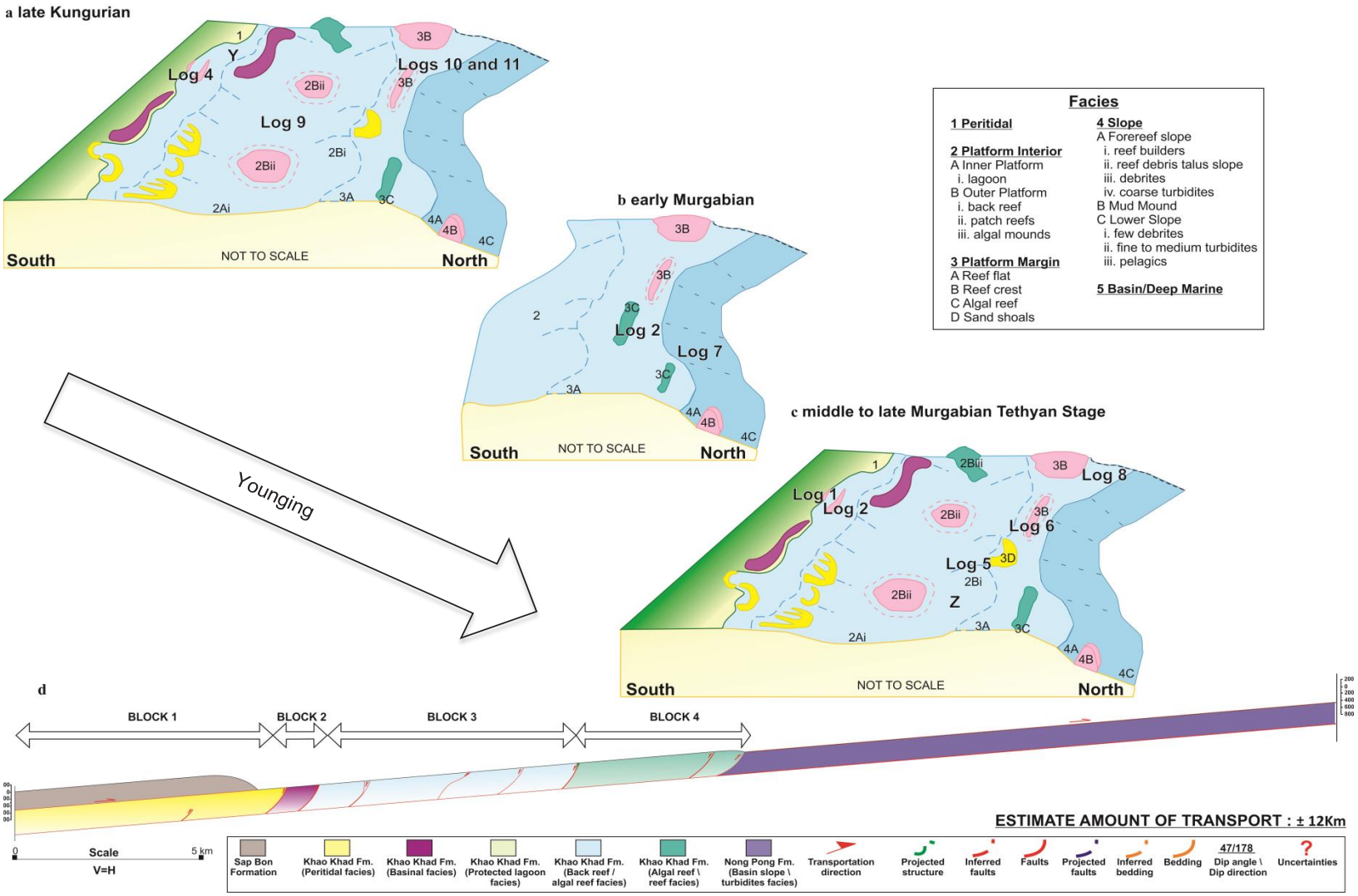

Figure 8: a-c) Interpreted Permian palaeography d) Balanced cross-section through the southern portion of the Saraburi Region, the Khao Khwang Fold-Thrust Belt adjusted from Arboit (pers. data, 2014).

Romana Dew
Stratigraphy of deformed Permian carbonate reefs, Thailand

IMPROVEMENTS

The analyses could be improved by integrating isotope analysis of oxygen and carbon similar to Mirzaloo (2013). Correlations with previous stratigraphic studies such as Chutakositkanon et al. (2000) would be beneficial to understand the biostratigraphic variations within the Saraburi Group at different localities. The three-dimensional simulation of stratigraphic architecture and facies distribution modelling of carbonate sediments (SIMSAFADIM) used by Bitzer and Salas (2002) could be useful to interpret palaeography.

REGIONAL TECTONIC SETTING

From my observations and interpretations, the overall direction and age of the fold-thrust belt indicates that the exposed northern foreland is younger than southern hinterland (Figure 2). Considering that this is a northward-verging fold-thrust belt, this younging down structure is what would be expected of a forward propagating fold-thrust belt. Thrust planes are visible at Logs 6, 9 and 11, which are all proximal to large-scale thrusts depicted in Figure 1. Thin-skinned deformation is suggested to have occurred within the Khao Khad Formation. There are several discrepancies to this general younging to the north trend that may be explained within the structure.

- The ages of Log 2 (early-late Murgabian) and 6 (middle to late Murgabian) appear to illustrate out of sequence thrusting.
- Logs 1 and 2 are south verging and are within the backthrust zone of the hinterland (Arboit et al. in press), which could explain why the southernmost Log 1 contains the youngest assemblages (Murgabian to Midian).

- Although Log 2 does contain some peritidal facies it is mostly part of an algal complex therefore, Figure 2 needs to be modified to indicate this.
- The older age of Log 4 (Kungurian) could be explained by the nearby strike slip fault that may have transported the sequence north. Possibly deposited further south near the late Kungurian Siam City Cement Logs 9-11.

CONCLUSIONS

The Khao Khad Formation of the study area is generally younging northwards in accordance with typical forward propagating fold-thrust belts. However, backthrusting leads to the youngest sequence being in the southern Log 1. The sequences in Logs 1-11 range from late Kungurian to Capitanian (Midian) in age with the highest proportion of assemblages classed within the Murgabian. The rapid rate of morphological change within the fusulinid taxa usually allows the identification of highly specific ages, although in the Khao Khad Formation it is harder to determine as the fossils are generally poorly preserved due to deformation. The diverse fossil assemblages were deposited in shallow marine platform environments. The environments form a continuum but can be grouped into peritidal, low-energy lagoon, high-energy middle platform to backreef, algal reef and slope to basin (Figures 3 and 8). Further structural and stratigraphic studies would assist with the further characterisation of the palaeography.

ACKNOWLEDGEMENTS

I would to formerly acknowledge:

Australian Research Council (ARC)
South Australian Chapter of the Geological Society of Australia

Mr Yot (Siam City Cement Public Company Limited)
Laainam Chaipornkaew (Petroleum Authority of Thailand (PTT))
Vladimir Davydov (Boise State University)
Aaron Hunter (Curtin University)
George Morgan (Adelaide Petrographic Laboratories Pty Ltd)

Alan Collins
Rosalind King
Francesco Arboit
Chris Morley

Morgan Blades
Robert Dew
Trudi Dew
Nicholas Harvey
Katie Howard
Madison White

REFERENCES

ARBOIT F., COLLINS A. S., KING R., MORLEY C. K. & HANSBERRY R. in press. Structure of the Sibumasu–Indochina collision, central Thailand: A section through the Khao Khwang Fold and thrust belt, *Journal of Asian Earth Sciences*.

BAIRD A. & BOSENCE D. 1993. The sedimentological and diagenetic evolution of the Ratburi Limestone, Peninsular Thailand, *Journal of Southeast Asian Earth Sciences* **8**, 173-180.

BEAVINGTON-PENNEY S. J. & RACEY A. 2004. Ecology of extant nummulitids and other larger benthic foraminifera: applications in palaeoenvironmental analysis, *Earth-Science Reviews* **67**, 219-265.

BITZER K. & SALAS R. 2002. SIMSAFADIM: three-dimensional simulation of stratigraphic architecture and facies distribution modeling of carbonate sediments, *Computers & Geosciences* **28**, 1177-1192.

BOGGS S. 2011a Carbonate and Evaporite Environments. Principles of Sedimentology and Stratigraphy: International Edition*.* 308-333, United States of America: Pearson Education, Inc.

--- 2011b Carbonate Sedimentary Rocks. Principles of Sedimentology and Stratigraphy: International Edition*.* 135-167, United States of America: Pearson Education, Inc., 5th ed.

BOUDAGHER-FADEL M. K. 2008 The Palaeozoic larger benthic foraminifera: the Carboniferous and Permian. In BOUDAGHER-FADEL M. K. ed. Developments in Palaeontology and Stratigraphy*.* 39-118: Elsevier.

BROWN G. F., BURAVAS S., CHARALJAVANAPHET J., JALICHANDRA N., JOHNSTON W. D. J., SRESTHAPUTRA V. & TAYLOR G. C. 1951. Geologic reconnaissance of the mineral deposits of Thailand, *United States Geological Survey, Bulletin* **984**, 1-183.

BUNOPAS S. 1992. Regional Stratigraphic Correlation in Thailand, *Geologic Resources of Thailand: Potential for Future Development*, 189-208.

CHONGLAKMANI C. 2001. The Saraburi Group of North-Central Thailand: Implication for Geotectonic Evolution, *Gondwana Research* **4**, 597-598.

CHUTAKOSITKANON V., CHARUSIRI P. & SASHIDA K. 2000. Lithostratigraphy of permian marine sequences, *The Island Arc* **9**, 173-187.

DAVYDOV V. I. 2013 Climate fluctuations within the western Pangean tropical shelves - the Pennsylvannian/Permian record from benthic foraminifera. In LUCAS S. G.*, et al.* eds. Part of The Carboniferous-Permian Transition*.* 73-78, Albuquerque: New Mexico Museum of Natural History.

DAWSON O., BAIRD A. & BOSENCE D. 1993. No reef-rimmed margins to the Permian carbonate platforms of Thailand, *Journal of Southeast Asian Earth Sciences* **8**, 181-186.

DAWSON O. & RACEY A. 1993. Fusuline-calcareous algal biofacies of the Permian Ratburi Limestone, Saraburi, Central Thailand, *Journal of Southeast Asian Earth Sciences* **8**, 49-65.

DICKINS J. M., ZUNYI Y. & HONGFU Y. 2007 Late Palaeozoic and Early Mesozoic Circum-Pacific Events and Their Global Correlation*.* Cambridge University Press.

DUNHAM R. J. 1962 Classification of carbonate rocks according to depositional texture. In HAM W. E. ed. Classification of carbonate rocks*.* 108-121: American Association of Petroleum Geologists Memoir.

EL TABAKH M. & UTHA-AROON C. 1998. Evolution of a Permian carbonate platform to siliciclastic basin: Indochina Plate, Thailand, *Sedimentary Geology* **121**, 97-119.

FLÜGEL E. 2010 Microfacies of Carbonates Rocks. Springer, London.

FOLK R. L. 1962. Spectral subdivision of limestone types, *Classification of Carbonate Rocks* **1**, 62-84.

FONTAINE H., LYS M. & DUC TIEN N. 1988. Some Permian corals from East Peninsular Malaysia: associated microfossils, paleogeographic significance, *Journal of Southeast Asian Earth Sciences* **2**, 65-78.

FONTAINE H. 2002. Permian of Southeast Asia: An overview, *Journal of Asian Earth Sciences* **20**, 567-588.

HADA S., KHOSITHANONT S., GOTO H., FONTAINE H. & SALYAPONGSE S. in press. Evolution and extinction of Permian fusulinid fauna in the Khao Tham Yai Limestone in NE Thailand, *Journal of Asian Earth Sciences*.

HELMCKE D. 1985. The Permo-Triassic "Paleotethys" in mainland Southeast-Asia and adjacent parts of China, *Geologische Rundschau* **74**, 215-228.

HENDERSON C. M., DAVYDOV V. I. & WARDLAW B. R. 2012 The Permian Period. In GRADSTEIN F. M., *et al.* eds. The Geologic Time Scale 2012. 653-679: Elsevier.

JAMES N. P. 1977. Facies Models 8. Shallowing-Upward Sequences in Carbonates, *1977*.

KIESSLING W., FLÜGEL E. & GOLONKA J. 2003. Patterns of phanerozoic carbonate platform sedimentation, *Lethaia* **36**, 195-226.

KOBAYASHI F., ROSS C. A. & ROSS J. R. P. 2010. Classification, phylogeny, and paleobiogeography of the new subfamily Gifuellinae and a revision of the family Neoschwagerinidae (superorder Fusulinoida); Guadalupian (Middle Permian), *The Journal of Foraminiferal Research* **40**, 283-300.

LOEBLICH A. R. & TAPPAN H. 1964 Protista 2 (Sarcodina, chiefly "Thecamoebians" and Foraminiferida). The Geological Society of America and The University of Kansas Press, U.S.A.

LUHR J. F. 2003 Earth. Dorling Kindersley Limited, London.

MACKENZIE W. S. & ADAMS A. E. 2007 A Colour Atlas of Rocks and Minerals in Thin Section. (9th edition). Manson Publishing Ltd, London.

MENNING M., ALEKSEEV A. S., CHUVASHOV B. I., DAVYDOV V. I., DEVUYST F. X., FORKE H. C., GRUNT T. A., HANCE L., HECKEL P. H., IZOKH N. G., JIN Y. G., JONES P. J., KOTLYAR G. V., KOZUR H. W., NEMYROVSKA T. I., SCHNEIDER J. W., WANG X. D., WEDDIGE K., WEYER D. & WORK D. M. 2006. Global time scale and regional stratigraphic reference scales of Central and West Europe, East Europe, Tethys, South China, and North America as used in the Devonian–Carboniferous–Permian Correlation Chart 2003 (DCP 2003), *Palaeogeography, Palaeoclimatology, Palaeoecology* **240**, 318-372.

METCALFE I. 2013. Gondwana dispersion and Asian accretion: Tectonic and palaeogeographic evolution of eastern Tethys, *Journal of Asian Earth Sciences* **66**, 1-33.

MIRZALOO M. 2013. Contrasting depositional and digenetic complexity in deep and shallow water successions in the Permian carbonates of Pak Chong region, Central Thailand. Chulalongkorn University, Bangkok.

MOORE C. H. & WADE W. J. 2013 Marine diagenetic environment. pp. 93-131.

MORLEY C. K., AMPAIWAN P., THANUDAMRONG S., KUENPHAN N. & WARREN J. 2013. Development of the Khao Khwang fold and thrust belt; implications for the geodynamic setting of Thailand and Cambodia during the Indosinian Orogeny, *Journal of Asian Earth Sciences* **62**, 705-719.

NESTELL G. P. & NESTELL M. K. 2006. Middle Permian (Late Guadalupian) foraminifers from Dark Canyon, Guadalupe Mountains, New Mexico, *Micropaleontology* **52**, 1-50.

PLUMMER H. J. 1948. Morphology of Globivalvulina, *American Midland Naturalist* **39**, 169-173.

SANO H., HORIBO K. & KUMAMOTO Y. 1990. Tubiphytes-archaeolithoporella-girvanella reefal facies in Permian buildup, Mino terrane, central Japan, *Sedimentary Geology* **68**, 293-306.

SARTORIO D. & VENTURINI S. 1988 Southern Tethys Biofacies. Azienda Generale Italiana Petroli (AGIP), Italy.

SCHOLLE P. A. & ULMER-SCHOLLE D. S. 2003 A Color Guide to the Petrography of Carbonate Rocks: Grains, Textures, Porosity, Diagenesis, AAPG Memoir 77. American Association of Petroleum Geologists, Tulsa.

SHEN S.-Z., SCHNEIDER J. W., ANGIOLINI L. & HENDERSON C. M. 2013 The International Permian Timescale: March 2013 Update. In LUCAS S. G.*, et al.* eds. Part of The Carboniferous-Permian Transition. Albuquerque: New Mexico Museum of Natural History.

SONE M. & METCALFE I. 2008. Parallel Tethyan sutures in mainland Southeast Asia: New insights for Palaeo-Tethys closure and implications for the Indosinian orogeny, *Comptes Rendus - Geoscience* **340**, 166-179.

SORAUF J. E. 1978. Original Structure and Composition of Permian Rugose and Triassic Scleractinian Corals, *Palaeontology* **21**, 321-339.

THAMBUNYA S., PISUTHA-ARNOND V. & KHANTAPRAB C. 2007. Depositional Environments of Permian Rocks of the Khao Khad Formation in Central Thailand, *ScienceAsia* **33**, 371-381.

TORIYAMA R. & KANMERA K. 1979 Permian fusulines from the Ratburi Limestone in the Khao Khao area, Sara Buri, Central Thailand. In KOBAYASHI T., TORIYAMA R. & HASHIMOTO W. eds. Geology and Palaeontology of Southeast Asia. 23-93, Tokyo: University of Tokyo Press.

TUCKER M. E. & WRIGHT V. P. 1990 Carbonate Sedimentology. Blackwell Publishing Ltd.

TUCKER M. E. 2001 Limestones. Sedimentary petrology: an introduction to the origin of sedimentary rocks. 110-165, United Kingdom: Blackwell Publishing, 3rd ed.

UDCHACHON M., BURRETT C., THASSANAPAK H., CHONGLAKMANI C., CAMPBELL H. & FENG Q. 2014. Depositional setting and paleoenvironment of an alatoconchid-bearing Middle Permian carbonate ramp sequence in the Indochina Terrane, *Journal of Asian Earth Sciences* **87**, 37-55.

UENO K. & SAKAGAMI S. 1993. Middle Permian foraminifers from Ban Nam Suai Tha Sa-at, Changwat Loei, Northeast Thailand, *Transactions and Proceedings of the Palaeontological Society of Japan*, 277-291.

UENO K. & CHAROENTITIRAT T. 2011 Carboniferous and Permian. In RIDD M. F., BARBER A. J. & CROW M. J. eds. The Geology of Thailand. 71-136, London: The Geological Society.

UENO K., MIYAHIGASHI A., KAMATA Y., KATO M., CHAROENTITIRAT T. & LIMRUK S. 2012. Geotectonic implications of Permian and Triassic carbonate successions in the Central Plain of Thailand, *Journal of Asian Earth Sciences* **61**, 33-50.

WARDLAW B. R., DAVYDOV V. I. & GRADSTEIN F. M. 2004 The Permian Period. In GRADSTEIN F. M., OGG J. G. & SMITH A. G. eds. A Geologic Time Scale 2004. 249-270, United Kingdom: Cambridge University Press.

WEIDLICH O. 2002. Permian reefs re-examined: Extrinsic control mechanisms of gradual and abrupt changes during 40 my of reef evolution, *Geobios* **35**, 287-294.

WENDT J. 1997. Aragonitic dasycladalean algae from the Upper Permian of Sichuan, China, *Lethaia* **29**, 361-368.

WRIGHT V. P. & BURCHETTE T. P. 1996 Shallow-water carbonate environments. In READING H. G. ed. Sedimentary Environments: Processes, Facies and Stratigraphy. 325-395, Victoria: Blackwell Publishing, Third ed.

WRIGHT V. P. & BURCHETTE T. P. 1998. Carbonate ramps: an introduction, *Geological Society, London, Special Publications* **149**, 1-5.